THE BEHAVIOUR OF REINFORCED CONCRETE CANTILEVER COLUMNS UNDER LATERAL IMPACT LOAD

by

Matthys Johannes Loedolff

Dissertation presented for the

Degree of Doctor of Philosophy

(Engineering)

at the

University of Stellenbosch

Promoter: Prof. J M Louw

September 1989

Stellenbosch University http://scholar.sun.ac.za

THE BEHAVIOUR OF REINFORCED CONCRETE CANTILEVER COLUMNS UNDER LATERAL IMPACT LOAD

by

Matthys Johannes Loedolff

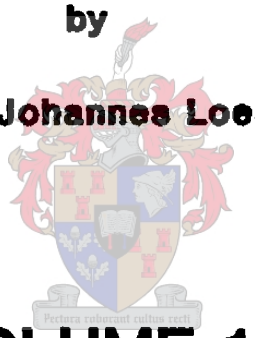

VOLUME 1

University of Stellenbosch

September 1989

Stellenbosch University http://scholar.sun.ac.za

Declaration

I the undersigned declare that the work contained in this dissertation is my own original work and has not previously in its entirety or in part been submitted at any University for a degree.

Signature: MJoedolff Date: 12-02-1990

Stellenbosch University http://scholar.sun.ac.za

ADVANCED COURSEWORK

In preparation for the PhD-candidacy, a number of post-M.Eng courses were completed satisfactorily. These are:

Advanced Structural Design (SB03)

Theory of Elasticity (SM02)

Stochastic Structural Dynamics (SM04)

Introduction to Continuum Mechanics (SM05)

Plates and Shells (SM06)

Energy methods of Continuum Mechanics (SM07)

Applied Mathematics (TW01)

Stellenbosch University http://scholar.sun.ac.za

SYNOPSIS

The behaviour of 28 reinforced concrete cantilever columns subjected to a soft lateral impact load applied at about midheight, were examined through experiments. Eight further columns were subjected to a static lateral load. The pertinent variables considered were the magnitude of the lateral loading, the percentages of longitudinal and shear reinforcement and the concrete strength.

Chapter 2 is a review of available literature, from as early as 1940, on the experimental work done on impact loaded reinforced and prestressed concrete members. The test arrangements used by the different investigators are also discussed.

Chapter 3 gives a state-of-the-art report on the local damage problem of reinforced concrete structures and members subjected to impact loading. A number of solutions to predict the local response are discussed. Different types of local damage are shown in this chapter as well, and the most solutions for the different situations are also given.

In chapter 4 the mechanical properties of concrete and reinforcement are discussed. A brief review of the experimental research, on the different properties of materials used, also follows in this chapter. Formulae to modify and adapt the static material properties to dynamic properties are recommended.

In chapter 5 an analytical model for the dynamic response of a cantilever column is given. The normally used Bernoulli-Euler formulation is extended to the Timoshenko formulation by taking into account additional components for shear deformation, rotatory inertia, an axial load and a lumped mass at the top of the column. A complete solution for the specific column under investigation is given.

Stellenbosch University http://scholar.sun.ac.za

Chapter 6 deals with the correlation between the free and forced vibration theory derived in chapter 5 and the experimental test results. The theory is compared with measured values from the experiments by using a number of graphs. The measured accelerations, measured strain and measured loads transferred to the laboratory floor are compared with the values from the theory.

Chapter 7 discusses the experimental investigations. All the parameters investigated are discussed and the impact test results are compared with the static test results. The influences of the axial load, the concrete strength, the shear reinforcement and the longitudinal reinforcement, as well as the repeatability of these tests, are discussed. A number of graphs are used to illustrate and explain the parameter influences.

In chapter 8 a design method for this specific problem is suggested. The suggested design is based on the modified compression field theory of Collins and Vecchio. A lower bound and a upper bound solution are suggested and shown on a graph. The moment/shear graphs for each series of columns are shown and discussed.

Chapter 9 suggests a number of directions and aspects for further research of this type of problem.

One of the most important parts of this dissertation is Appendix B. This appendix gives a complete and detailed report of the experimental work done in the laboratory. The report discusses not only the experimental arrangement, but also the design of test apparatus and some of the instrumentation. Each test is discussed in detail and photographs show the crack patterns and failure mechanisms for each column. All the original data are displayed in the form of graphs and additional graphs show relevant processed data.

Stellenbosch University http://scholar.sun.ac.za

OPSOMMING.

Die gedrag van 28 gewapende beton kantelkolomme onder laterale skoklaste aangewend in die omgewing van midhoogte, word eksperimenteel ondersoek. Op ag verdere kolomme is 'n statiese laterale las aangewend. Die belangrikste veranderlikes wat ondersoek is, is die grootte van die laterale skoklaste, die persentasies langswapening en skuifwapening en die betonsterktes.

Hoofstuk 2 bespreek die beskikbare literatuur, van so vroeg as 1940, oor die eksperimentele werk wat gedoen is oor botsbelastings op gewapende beton en spanbeton dele. Al die verskillende toetsmetodes word ook bespreek.

Hoofstuk 3 gee 'n literatuuroorsig oor die probleme van lokale skade in gewapendebeton strukture en dele wat onderwerp word aan botsbelastings. 'n Aantal oplossings om die lokale invloed te voorspel word bespreek. Al die verskillende tipes lokale skade word getoon en die beste oplossings vir die verskillende toestande word gegee.

In hoofstuk 4 word die meganiese eienskappe van beton en die wapeningstaal bespreek. 'n Kort oorsig van die eksperimentele ondersoek van die materiaaleienskappe word ook in die hoofstuk behandel. Formules om die statiese waardes van die materiale aan te pas vir dinamiese of impaktoestande word ook gegee.

In hoofstuk 5 word 'n analitiese model vir die dinamiese reaksie van 'n kolom gegee. Die algemeen gebruikte Bernoulli-Euler formule word uitgebrei tot die Timoshenko formule deur additionele terme vir skuifvervorming en rotasietraagheid in berekening te bring, asook die aksiale las op die kolom met die gekonsentreerde massa by die bopunt van die kolom. 'n Volledige oplossing vir die bepaalde kolom wat ondersoek word, word gegee.

Stellenbosch University http://scholar.sun.ac.za

Hoofstuk 6 handel oor die korrelasie tussen die vrye en gedwonge vibrasie teorie, soos afgelei in hoofstuk 5, en die eksperimentele toets resultate. Die teorie word vergelyk met die gemete waardes deur 'n aantal grafieke te gebruik. Die gemete versnellings, betonvervormings en die las oorgedra na die laboratoriumvloer word vergelyk met die berekende waardes van die teorie.

Hoofstuk 7 bespreek die eksperimentele ondersoek. Al die veranderlikes wat ondersoek is word bespreek en die botslasresultate word met die statiese toetsresultate vergelyk. Die invloede van die aksiale las, betonsterktes, skuifwapening en die langswapening asook die herhaalbaarheid van die toetse word bespreek. 'n Aantal grafieke word gebruik om die veranderlikes se invloede te toon.

In hoofstuk 8 word 'n ontwerpmetode vir die spesifieke probleem voorgestel. Die voorgestelde ontwerpmetode is gebaseer op die aangepaste drukveld teorie van Collins and Vecchio. 'n Laer en 'n hoër grens oplossing word voorgestel en op 'n grafiek getoon. Die moment/skuif diagram vir elke reeks toetse word gegee en bespreek.

Hoofstuk 9 stel 'n aantal rigtings vir verdere navorsing voor vir die tipe probleem.

Een van die belangrikste dele van die proefskrif is Byvoegsel B. Dit gee 'n volledige verslag van die eksperimentele werk wat in die laboratorium gedoen is. Die verslag bespreek nie net die eksperimentele opstelling nie, maar ook die ontwerp van die toetsapparaat en sommige instrumente. Elke toets word volledig bespreek en foto's toon die kraak patrone en swig meganismes. Al die oorspronklike data word getoon in die vorm van grafieke en additionele grafieke toon verwerkte data.

Stellenbosch University http://scholar.sun.ac.za

CONTENTS

Stellenbosch University http://scholar.sun.ac.za

Stellenbosch University http://scholar.sun.ac.za

Stellenbosch University http://scholar.sun.ac.za

Stellenbosch University http://scholar.sun.ac.za

Stellenbosch University http://scholar.sun.ac.za

Stellenbosch University http://scholar.sun.ac.za

Stellenbosch University http://scholar.sun.ac.za

Stellenbosch University http://scholar.sun.ac.za

NOTATION

A = Area of column cross-section
A = Constant
A = Cross sectional area of missile
a = Half the concrete aggregate size
a = The vibration frequency coefficient
A_p = The weight of the missile per unit projected area
B = Constant
c = A coefficient depending on the ratio of the target thickness to the diameter of the missile
C_c = Speed of sound in concrete
C_E = Speed of plastic stress wave
C_p = Speed of an elastic stress wave
D = Diameter of the missile
d_p = Perforation thickness
d_p = The penetration depth
d_s = Scabbing thickness
E = Elasticity modulus of concrete
E = Impact elasticity modulus of concrete
E = Modulus of elasticity
E_o = Static elasticity modulus for concrete
E_m = Modulus of elasticity of mild steel
E_s = Secant modulus of elasticity
E_t = Tangent modulus of elasticity
f = Impact tensile strength of concrete
f'_c = Cylinder compressive strength of concrete
f_o = Static tensile strength of concrete
f_c = Impact compressive strength of concrete
f_{co} = Static compressive strength of concrete.
f_{cu} = Compressive cube strength of concrete
f_r = The relative rib surface area of reinforcing bar
f_{tm} = Impact tensile strength of concrete.
f_{to} = Static tensile strength of concrete
g = Acceleration of gravity
G = Modulus of shear

Stellenbosch University http://scholar.sun.ac.za

I = Impact factor

I = Inertia moment of the section

I' = Impact factor

I_a = Average inertia moment of the concrete section

I_{cr} = Moment of inertia of the cracked section

l_{cr} = Second moment of area of cracked column

K = Concrete penetrability factor

K' = Buckling factor

K' = Nose shape factor

L = Span length or length of column

L = The missile length

M = Bending moment

m = Mass of column per unit length

M = Weight of falling mass

M_o = Mass of the concentrated mass at free end of column

ml = Total weight of column

M_n = The generalized mass of the column associated with the n-th mode

M_y = Yield moment

N = Axial load on the column.

N = Missile nose shape factor

n = The ratio of the radius of the nose to the diameter of the missile.

p = Material density

p_c = Density of concrete

P_c = Small deflection static collapse load

$P_n(t)$ = The generalized load associated with the n-th mode

Q = Shear force

R = Pipe radius

R = Radius of ring

r^2 = I/A = radius of gyration of the cross section

S = Strain rate factor

t = Pipe wall thickness

t = Time

V = Missile impact velocity

v = Poissons ratio (pipe: elastic

v_p = Poissons ratio (pipe: plastic

Stellenbosch University http://scholar.sun.ac.za

W = Depth of the ring
w = Total weight of the beam
W = Weight of the falling mass
W = Weight of the missile
x_o = The position of the point load
x_e = Plastic deformation of missile
x_p = Penetration depth
y = Distance from centroid of section to desired position
Y = Random variable for d_s
y = Transverse displacement of column
Z = Random variable for d_p

α = Area reduction factor
α = Virtual angle change
αA = Effective shear area of the section
β = $(E_m/E)^{0.2}$
β = A material parameter varying between 20 and 25
$\dot{\sigma}$ = Impact stress rate
σ = Stress in concrete
σ = Tensile strength of reinforcement
$\dot{\sigma}_o$ = Static stress rate
σ_o = Static yield stress
σ_{cr} = Average critical wrinkling stress of a pipe impactor
τ = Bond strength corresponding with impact rate of loading
τ_o = Bond strength corresponding to the static rate of loading
θ = Natural frequency coefficient
Ω_i = Natural angular frequency of the i-th mode of the column
δ = A variable
δ = Displacement
$\emptyset_n(x)$ = Mode shape function of the n-th mode
ϵ = A variable
ϵ = Strain
ϵ = Strain in concrete
$\dot{\epsilon}$ = Strain rate

Stellenbosch University http://scholar.sun.ac.za

MATHEMATICAL SYMBOLS

Σ = Sum

Δ = Increment

$\emptyset$ = Bar diameter

$\dot{}$ = Derivative with respect to time

$\ddot{}$ = Double derivative with respect to time

$'$ = Derivative with respect to length

$''$ = Double derivative with respect to length

$'''$ = The third derivative with respect to length

$''''$ = The fourth derivative with respect to length

∂ = Partial derivative

Stellenbosch University http://scholar.sun.ac.za

ACKNOWLEDGEMENTS

I wish to express my sincere gratitude to the following people:

My supervisor Prof. J.M. Louw for his inspiration and guidance;

The C.S.I.R. (Council for Scientific and Industrial Research) for financial assistance;

The South African Transport Services for financing some of the apparatus and test materials;

Mr. P.E. Dunaiski for all his help with the instrumentation and for the computer programs used during the experimental phase of this research, which were written by him;

Mr. G. Maritz for the use of his spreadsheet program UMNV;

The personnel from the civil engineering workshop;

Van Wyk and Louw Inc. for the opportunity to do this study as well as for financial support;

My wife for her moral support and encouragement.

Stellenbosch University http://scholar.sun.ac.za

1. INTRODUCTION.

Impulsive or impact loading cases such as vehicle or ship collisions with buildings, bridges or off-shore structures as well as blast waves on civilian and military shelters, missile and aircraft impact on nuclear containments, etc. play an increasing important role in structural design. In an impact, the peak magnitude of the load and its variation with time depend on, among other things, the masses involved (including that of the structure that is set in motion by the impact) and the precise manner in which the energy of the impact is absorbed.

The response of a member or structure to an impact loading can be divided into the local effects and the global effects of the member or structure. The local effects are usually treated by empirical formulae derived from extensive laboratory studies. The global or overall effects are treated in a more analytical manner by taking into account the energy absorption or the momentum and impulse response of a member.

There appears to be a significant difference in the magnitude of the expected quasi-static design impact load on bridge columns as prescribed by the various highway bridge codes. For example, the South African Committee for State Authotities (CSRA) (178), calls for a nominal horizontal concentrated longitudinal force along the weak axis of the pier equal to (3 x the vehicle speed in km/h) kN, subject to a minimum of 200 kN. Simultaneously, 120 kN must be applied transversely. A load factor of 1,25 is prescribed for the ultimate limit state. The corresponding ultimate concentrated load required by the Ontario Bridge Code (186) is 1248 kN as caused by a 450 kN truck and 112 kN caused by a passenger vehicle weiging 20 kN. The numerical values of the latter code are based on the loads used by the West German DIN 1072. The South African Transport Services (187) requires a nominal horizontal longitudinal load of 600 kN applied simultaneously with a transverse load of 200 kN for bridge

Stellenbosch University http://scholar.sun.ac.za

supports adjacent to railway tracks. The recommended maximum load factor is 1,4.

For both economic and safety reasons, it remains imperative to have a clear understanding of the impact load characteristics as well as the column or element behaviour when subjected to such a load.

Up to the early seventies very little reliable experimental work had been done on the global impact response of reinforced concrete members. This was probably due to problems experienced with accurate measuring instruments. Since then small computers and better instruments became more easily available for research.

Recently a number of studies concentrated on the column or beam impact problem (10, 77, 181). All these studies concentrated on columns or beams supported at both ends and most of their column or beam failures were flexural failures. All these tests were also done with the members in a horizontal position. Evidently no tests had been done on cantilevered columns which are strongly influenced by shear actions.

This dissertation contains a number of lateral impact tests executed on reinforced concrete cantilever columns. It appears that this specific type of experimental arrangement to investigate the impact problem of a cantilever column has up to now not been used anywhere else. The fact that the column is a cantilever column and tested in an upright position is thus unique. A complete report of the experimental work done in the laboratory of the University of Stellenbosch, South Africa, is given in Appendix B. This should be very valuable for further research, therefore it was kept as complete as possible.

It is hoped that this work will shed light on not only the problem of lateral impact loads on reinforced cantilever columns, but perhaps also on other related impact problems as well. Thus the purpose of this work was also to lay the foundation for further laboratory and analytical research at the University of

Stellenbosch University http://scholar.sun.ac.za

Stellenbosch on the problem of lateral impact loading on reinforced concrete elements.

Stellenbosch University http://scholar.sun.ac.za

2. REVIEW OF THE AVAILABLE LITERATURE.

2.1 Introduction.

In this section a survey of the available experimental information and literature will be discussed. A brief description will be given of various test series performed by different authors.

This chapter will concentrate on the global influence of the members. The local influences of the projectiles, strikers, impactors, etc. in the contact zones of the member will be discussed in detail in chapter 3 of this study.

2.2 Different types of impact load tests.

Most of the tests differ in the manner in which the impact load was applied to the test specimen. The impact loads were applied in one of the following manners:

- A falling mass
- Servo hydraulic machines
- Projectiles
- The test specimen's own energy
- Air blast loadings
- Spring loading systems
- Deformation controlled impact
- Pendulum applied loads

2.2.1 Falling mass and pendulum applied loads. (125, 77, 181)

The falling mass and the pendulum type load could be classified in one group because their results are very similar. With this group of tests on beams an impact load is produced by a falling mass striking the beam. The impact releases an amount of energy

Stellenbosch University http://scholar.sun.ac.za

which is determined by the mass of the falling body and the falling height. A certain amount of energy can however result in different load time histories. If the impact energy is produced by a heavy body falling a short distance, the peak value will be lower and the duration will be longer than if the same energy is produced by a light body falling a long distance. Similarly the impact load history can be changed by changing the stiffness of the contact zone or the buffer between the striker and the beam or member. A high stiffness will result in a high load with a short duration and vice versa. See figure 2.1.

The pendulum system is exactly the same but for this study it had significant advantages The first and most important advantage was that a horizontal load could be applied to a column standing in a vertical position, as a column is supposed to be. In all the tests previously done on columns, the columns were tested in a horizontal position, like beams. The second important advantage is that the speed of the striker can be controlled much more accurately than that of a falling mass due to uncontrolable friction normally present with the falling mass. The exact impact position and the flight of the pendulum can also be controlled much better than that of the falling mass.

2.2.2 Air blast loading. (10)

This type of loads were primarily used for tests on slabs and walls where a distributed load rather than a point load was required. The air blast is produced by detonating an explosive. The resulting load pulse on the specimen has a very short rise time and a relatively short duration. The load history can be changed by varying the size of the explosive charge and or its relative position to the test specimen.

Stellenbosch University http://scholar.sun.ac.za

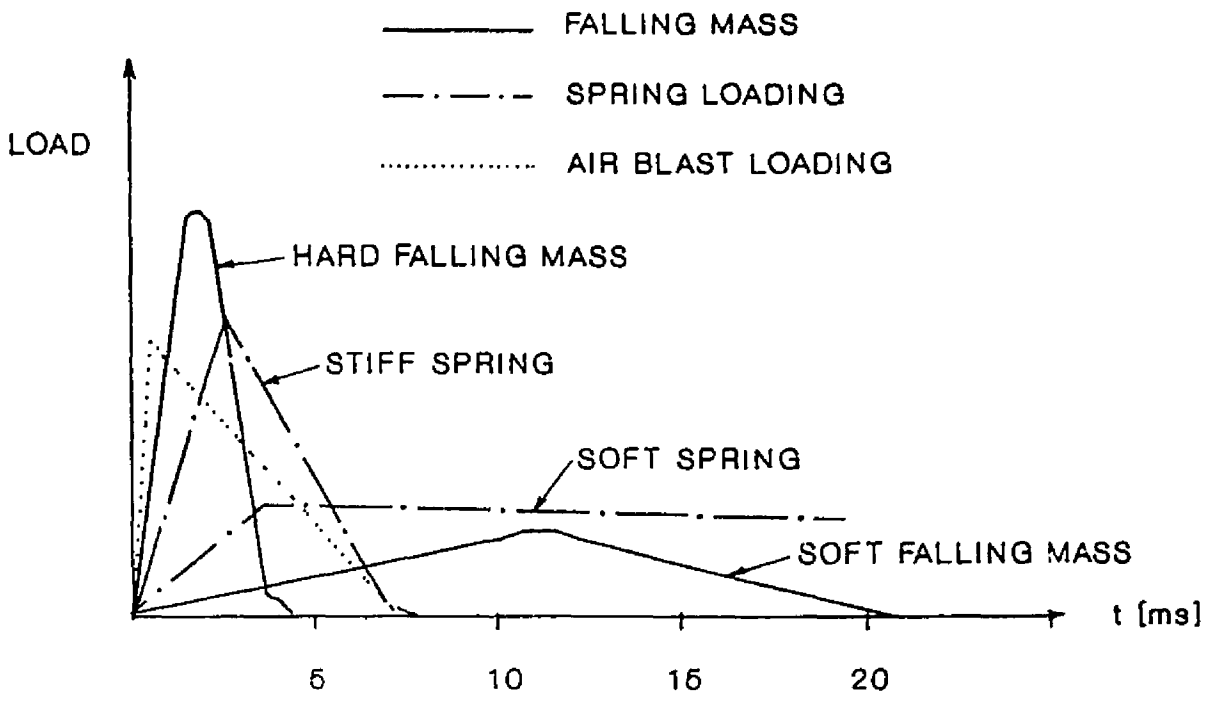

Figure 2.1: Load pulses caused by the different systems.(10)

2.2.3 Spring loading. (24, 105, 106, 107, 122)

With this system a spring is prestressed to a desired force and this force is then suddenly transferred to the test beam which is initially unloaded. As the beam deflects, the original deformation of the spring is changed and the force in the spring is changed accordingly. The shape of the load pulse can be chosen by the choice of the spring characteristics in comparison with the stiffness of the beam. If the spring is very soft, the force in the spring will remain almost constant as the beam deflects and the load pulse then becomes nearly rectangular. If the spring is very stiff, even a small deflection of the beam will almost unload the spring. The load pulse then resembles the one obtained during a stiff impact between a falling mass and a beam.

Stellenbosch University http://scholar.sun.ac.za

2.2.4 Deformation controlled impact.

With this system a special loading device is used in which the beam is given a predetermined deflection within say one tenth of a second. The resulting load pulse on the beam depends on the stiffness of the total set up.

2.2.5 Projectiles. (refer to chapter 3)

Projectiles are normally used to investigate the local effects in the contact zones. Nearly all types of projectiles have been used in tests. The local effects is a study on its own and as indicated earlier this aspect will be discussed in the next chapter.

2.2.6 Test specimen's own energy. (10)

Ammann (10) used this technique in his experiments. This system uses the energy of the specimen itself. A simply supported beam's one is lifted to a certain height and then it is suddenly released allowing the beam to fall rotating around the hinge at the other end of the beam. The falling free end is stopped by a rigid support. Thus the beam uses its own energy. This energy can be controlled by additional distributed loads on the beam and by changing the lifting height of the one end of the beam.

Another way to use this system is to suddenly remove any support of a multi-span beam, allowing that section to fall. This technique has also been used by Ammann (10).

2.3 Test results of different authors.

In this section all the available literature on this subject will be discussed chronologically.

Stellenbosch University http://scholar.sun.ac.za

2.3.1 T.D. Mylrea - 1940 (150)

Mylrea investigated the resistance of various grades of reinforcing steel by means of tests on simply supported reinforced concrete beams. The beams had a width of 250 mm and a depth of 400mm and the span was 2,4 m. Very small reinforcement percentages were used (0,03-0,2%) and the beams had no web reinforcement. The cylinder strength of the concrete was 'lMPa and the yield stress of the steel ranged from 320 to 790 MPa. The weight of the falling mass was either 2,5 or 11 kN and the load was transmitted to the beam through an embedded steel plate.

The only measurement taken was the height required to rupture the steel. This height ranged from 0,23 to 2,3 m, depending on the type and quantity of steel. Photographs indicate shear punching failures during impact loading. The height of fall required to rupture the steel increased drastically as the steel percentage was increased. This can be the result of many factors and thus any evaluation of results can only be tentative.

2.3.2 L.G. Simms - 1945 (150)

Tests were done on two types of simply supported centrally loaded reinforced concrete beams. The cross section of the first type was 100 mm wide and 200 mm deep, with a span length of 1,8 m. In these beams stirrups were provided to avoid shear failure. The longitudinal reinforcement in general consisted of mild steel with a yield stress of 310 MPa. In a few tests a high strength steel, with a yield stress of 625 MPa, was used. The percentage of reinforcement ranged from 0,09 to 3%. The second type had a cross section which was 500 mm wide, 150 mm deep and the span was 1,5 m. The reinforcement consisted of three types of cold-worked steel, ribbed mesh sheet steel, and three types of mild steel. The quantity of reinforcement was 0,28%.

Stellenbosch University http://scholar.sun.ac.za

The average compressive cube strength of the concrete used was 21 MPa for the first type and 27 MPa for the second type of tests. The load was transmitted to the concrete through a steel bearing plate. The weight of the falling mass, W, was equal to that of the test unit, which was 0,9 kN for the first type and 3,2 kN for the second type. The falling height, H, ranged from 0,25 to 3,8 m.

All the failures (under static as well as impact load) were classified as flexural failures.

Simms compares the energy of the blow in each impact test to the strain energy in a static test at a similar deflection. The released impact energy is larger than the absorbed strain energy calculated on the basis of the static load deflection curve and the maximum deflection under impact loading. In his assessment, Simms, assumed that the complete difference could be explained as a loss of energy, and thus ignored that the load deflection curve might depend on the loading rate. Simms calculated the loss of energy by equating the momentum immediately before the impact to that immediately after the impact, assuming that the beam deforms elastically in the same manner under static and impact conditions and that the falling weight remained in contact with the beam throughout the impact period. Simms thus arrived at a calculated value for the reduction factor, α, as follows:

$$\alpha = U_s/(WH) = 1/\{1+(4/5)(w/W)\} \qquad (2.1)$$

Where: w = total weight of the beam
W = weight of the falling mass
With w/W =1 it follows that α = 0,556.

Simms values for α ranged from 0,4 to 0,7 and thus his values compare reasonably with the calculated value.

Stellenbosch University http://scholar.sun.ac.za

2.3.3 J. Penzien and R.J. Hansen - 1954 (122)

In 1947 Penzien and Hansen studied at MIT the behaviour of simple reinforced concrete beams subjected to dynamic loads. They used a high-pressure-gas piston cylinder arrangement to provide the load. They were primarily concerned with the strains occurring in the reinforcement and concrete of a beam loaded impulsively without failure. They introduced the use of a dynamic magnification factor, but the only information about strength characteristics concerns the yield point of standard steel (ASTM Designation A15-48) which is increased with about 35% above the static value at strain rates of $0,7 \times 10^{4}$ - $0,7 \times 10^{7}$ $MN/m^2/s$. This seems to confirm findings by other authors.

2.3.4 F.T. Mavis and F.A. Richards - 1955 (106)

Simply supported reinforced concrete beams without web reinforcement were tested in pairs simultaneously. The beams were 125 mm square with a span of 1,8 m and the depth to the center of the steel was 100 mm. The reinforcement consisted of one 16 mm bar (1,5%). Two types of steel were used, a structural grade steel with a yield strength of 270 MPa and a hard grade steel with a yield strength of 525 Mpa. The concrete had an average cube compressive strength of 33 MPa.

The dynamic load was in the form of a controlled displacement, built up gradually and then decreased again. The built up was between 0,16 and 0,36 seconds. Thus the loading may be considered as a high rate loading rather than an impact load.

The information given in the report is insufficient but it looks as if the strength under a high loading rate was about 35% higher than the ordinary static test. The beams reinforced with the high yield steel performed much better than that with the soft structural steel and the high yield steel beams had a very good rehabilitation, in other words their permanent deflection was very much lower than that of the other beams.

Stellenbosch University http://scholar.sun.ac.za

2.3.5 F.T. Mavis and M.J. Greaves - 1957 (105)

Simply supported reinforced concrete beams without web reinforcement were tested statically and impulsively at mid-span. Loads, reactions and deflections were measured, but only a limited number of results are given. A spring loading system was used to introduce the impulsive load. This loading system contained several heavy beams that were moved and deflected when the spring force was released. Thus an interpretation of the few results given are unreliable.

Mavis and Greaves also found that a high-grade or hard steel used as reinforcement outperformed a soft or mild steel used as reinforcement in all aspects. They found that about 13% more initial load was required to start the damage in a hard-grade beam than in a mild-grade beam. They also suggested that additional reinforcement should be provided in the compression zone of the concrete beam to provide for the tension force generated in that section due to the whiplash effect, as they called it.

2.3.6 F.T. Mavis and J.J. Stewart - 1959 (107)

Tests were performed on simply supported reinforced concrete beams without web reinforcement. Static and impulsive loads were applied at the third-points of the span, which was 2,4 m. The impulsive load was applied with a spring loading system. The beams tested were 280 mm wide and 148 mm deep. The reinforcement, which was placed 120 mm from the compression face, consisted of one or two 16 mm bars corresponding to 0,6 and 1,2% reinforcement respectively. The steel used was structural, intermediate and hard-grade. The concrete had an average cube strength of 40 MPa.

Stellenbosch University http://scholar.sun.ac.za

Twenty seven beams were tested. A motion picture camera operating at approximately 200 frames per second recorded data from an oscilloscope and simultaneously photographed the beam during the test.

One of the most significant conclusions that can be drawn from the results of Mavis and Stewart is that the hard grade bars once again, as in previous studies, out performed the mild reinforcement. They also had the highest residual load capacity after the dynamic test.

2.3.7 J.J. Trott and E.N. Fox - 1959 (160)

Trott and Fox used something close to a falling weight system, but with their system's rebound was prohibited. Five beams with a cross section 64 mm square and length 460 mm were tested to determine whether or not the rate of loading significantly affects the mechanical properties of concrete beams tested in flexure. Two loading rates were used: $5x10^{-7}$/s, the rate used in normal tests and about 0,06/s when the beams were tested under impact conditions. The higher loading rate increased the fracture load with something like 35%. It seems that the higher loading rate increased the strain at which the cracking of the concrete began.

2.3.8 G.K. Wadlin and J.J. Stewart - 1961 (169)

This study of Wadlin and Stewart was an extension of the studies by Mavis and Stewart (discussed earlier) and exactly the same equipment were used as that for the previous studies.

Three prestressed and two reinforced beams were tested statically to destruction and seven prestressed and four reinforced concrete beams were tested dynamically to varying degrees of failure. All the beams were simply supported. They found that with the dynamic tests, the reactions had negative values immediately

Stellenbosch University http://scholar.sun.ac.za

after the initial application of the load. This can be contributed to the vibration of the beam.

When the prestressed concrete beams are compared with the reinforced concrete beams, on the basis of their ultimate strength, the difference in behaviour of the two types under impulsive loading were small. The reinforced concrete beams were slightly superior. The two types of beams absorbed approximately equal amounts of energy before crushing of the concrete occurred. After the concrete began to crush, the prestressed beam failed completely in half the time required for the reinforced beam.

2.3.9 S.C.C. Bate - 1961 (10)

This paper reports a large number of tests carried out as an extension of the investigation by Simms. The test series contained a total of 360 beam tests out of which 306 were tests on prestressed concrete beams and 54 were tests on ordinary reinforced concrete beams.

The impact loading consisted of a blow from a freely falling hammer of the same order of mass as the test beam. This mass struck the simply supported beam at mid-span. Measurements included the maximum deflection during impact and the residual deflection after impact. The impact resistance was assessed by testing enough beams to determine the energy of a single blow just insufficient to cause failure. Beams that did not fail under impact were subsequently tested under static loading. In some cases the effects of repeated blows were examined. The behaviour of beams tested under impact loading were compared to the behaviour of similar beams tested under static loading.

In his assessment of the results, Bate used the same approach as used by Simms except that the calculated α values are determined by equation (2.2):

Stellenbosch University http://scholar.sun.ac.za

$$\alpha = [1+(17/35)(ml/M)]/[1+(5/8)(ml/M)]^2 \qquad (2.2)$$

where: ml = total weight of beam
M = weight of falling mass

Bate found that in some cases shear failure occurred under impact loading while similar beams under static loading failed in flexure. In some other cases failure under static loading was due to crushing of the concrete (perhaps followed by shear) and under impact loading was due to fracture of the wires. Bate's paper provides no information on the contact zone conditions or on the shape of the load pulse.

Bate concluded that for ordinary reinforced concrete beams, stirrup reinforcement increases the static energy of deformations, but under impact loading its function is much more important than such increases would suggests. The presence of shear reinforcement prevents the disruption of the member in shear and is almost as important as the longitudinal steel in developing resistance to impact. He also found that for reinforced and prestressed beams of the same static strength, failing in bending under impact, prestressed concrete beams have a much lower ultimate resistance to the impact of a single blow than ordinary reinforced concrete beams. For blows insufficient to cause failure, prestressed concrete beams suffer less permanent deformation than ordinary reinforced concrete beams.

2.3.10 J.N. Cernica and M.J. Charignon - 1963 (24)

Simply reinforced concrete beams without web reinforcement were centrally loaded with a spring loading system. The beams tested were 125 mm wide, 190 mm deep and 2,65 m long. In general the beams had only tensile reinforcement, which was either two 12,7 mm or two 16 mm bars. Three types of reinforcing steel, structural steel (290 MPa yield), intermediate steel (335 MPa yield) and high strength steel (475 MPa yield), were used. The average cylinder strength of the concrete was 54 MPa.

Stellenbosch University http://scholar.sun.ac.za

A stiff spring was used to apply the loads so that all the beams were completely unloaded at a deflection of 75-100 mm (3-4% of span length).

The information given does not permit any firm conclusions. Although it may be noted that the initial spring force required to obtain failure was in all cases approximately twice the static strength of the beam. This observation has limited value. since this ratio might depend on the stiffness of the spring.

2.3.11 E.S. Perry, N.H. Burns and J.N. Thompson - 1967 (125)

They tested composite reinforced concrete beams, simply supported and centrally loaded by a falling mass. A soft cushion between the falling mass and the beam resulted in a long rise time (nearly 70 ms). No quantitative results are given and thus this paper is not to important.

2.3.12 W.A. Hamilton - 1968 (65)

Nine simply supported pretensioned prestressed concrete beams were tested. Two were tested statically and seven were tested dynamically. The load was applied with a spring loading system, the same type as that used by Mavis et al. All the beams had a span of 2,4 m and a rectangular section of 254 mm deep and 203 mm wide.

Hamilton concludes that the impact strength of the beam is about 35% higher than the static strength of the beam. Unfortunately he does not provide enough information to verify this results and he does not indicate the type of failure of the dynamic tested beams. The number of tests are very small as well.

Stellenbosch University http://scholar.sun.ac.za

2.3.13 C. Popp - 1975 (128)

Popp tested a number of reinforced concrete beams with impact loads applied through a falling weight mechanism. He tested these beams to investigate the influence of the type of steel used as reinforcement and whether it is better to use a softer more ductile reinforcement rather than a harder reinforcing steel, as was commonly believed earlier. After a comprehensive study he found that the softer steel had no advantage above the harder steel and in fact it is better to use the harder steel. By using the harder steel, space inside the beam or member is saved and the massing of reinforcing bars can be avoided.

2.3.14 G. Hughes and D. M. Speirs - 1982 (77)

Hughes and Speirs describes 80 impact tests on pin-ended reinforced concrete beams and 12 test on simply supported reinforced concrete beams. For each test the impact force history and beam displacements were measured. Various models for the impact are discussed. The simple beam vibration model is shown to be applicable over the test range and the importance of two parameters, the mass ratio and the pulse ratio, is recognized. An appendix gives the numerical solution to the impact equation.

They also used a falling mass system to apply the impact load. In the impact zone they used a number of pad systems to provide different K-factors for the Hertz contact law used by them. These pads range from 25 mm rubber to different sections of ply wood to a 30 mm steel plate. The cross section was 200 mm deep and 100 mm wide and had span lengths of 2,7 and 1,6 m. Compression reinforcement as well as tension reinforcement of bars ranging from 6 mm to 16 mm were used. Stirrups were also used in the beams. The average concrete cube strength was 44,4 MPa.

Stellenbosch University http://scholar.sun.ac.za

The simple beam theory gave very good results for the range tested by them but if beams outside these ranges are tested additional provision should be made for shear stiffness and rotational inertia, which is ignored by this simple beam theory described by them.

2.3.15 W. Ammann - 1983 (10)

Ammann investigated the sudden removal of one of the supports of a structure. In one of the chapters he describes the dynamic behaviour of a simply supported beam, one end lifted to a certain height and then released, allowing it to fall onto a shock absorbing element. This beam is investigated analytically by using the extended Timoshenko beam formulation for vibration of the beam. He then also discusses the phenomenon of a travelling plastic hinge in reinforced concrete beams.

He also describes a test set-up for double span beams where one of the three supports is suddenly removed. He also tested a number of these beams.

He found that the mechanisms of load transfer and the deformation characteristics of continuous reinforced concrete beams in the event of support failure can be estimated to a degree with simple rigid-body models. Such models can be bar elements, joined by friction-endowed hinges, provided the approximate location of the plastic hinges constituting the failure mechanism is known. The complex dynamic behaviour of multi-span beams under sudden removal of support can thus be modelled by simple systems of one to two degrees of freedom. In the presence of membrane effects due to restrained longitudinal deformations, these models have to be complicate and thus the applicability to practical cases remains restricted.

Stellenbosch University http://scholar.sun.ac.za

2.3.16 B.P. Hughes and A.T. Mahmood - 1984 (72)

Six series of model prestressed concrete beams, a total of 38 beams, were tested. The beams had a cross section of 50,6 mm wide and 101,6 mm deep and with a clear span of either 916 mm or 1240 mm. They were prestressed with 5 mm Belgian indented wire, or 6,35 mm high-tensile seven-wire stranded or 7 mm high-tensile crimped wire. Hammers weighing 36,7, 26,8 or 19,3 kg, giving mass ratios (beam/hammer) of 0,55, 0,574 or 0,8, were used for impacting the beam at mid-span. The beams had similar concrete strengths and tendon eccentricities but different prestressing indices. A high speed camera was used to record the deflection of the beams.

Hughes and Mahmood conclude by saying that their test results agreed with the predictions of a modal analysis based on a fundamental mode rather than a static mode as used by them. They also found that the inclusion of nominal shear stirrups in some beams nearly doubled the impact capacities of those beams.

2.3.17 H. Ohnuma, C. Ito and S.G. Nomachi - 1985 (118)

Ohnuma, Ito and Nomachi tested 18 reinforced concrete beams and 30 reinforced concrete slabs under impact loading from a falling hammer excelled by compressed N_2 gas. The velocity of the 9,8 cm diameter mass was any velocity lower than 50 m/s. The depths of the beams were 200, 300 or 500 mm with stirrup reinforcement and longitudinal reinforcement ranging from .95% to 1,16%. No further information on the test results of the beams are given and it looks as if they were more interested in the local damage to the slabs. They mentioned that the reinforced concrete beams in the static and low velocity impact tests showed bending failure, while in the case of high velocity they showed shear failure.

Stellenbosch University http://scholar.sun.ac.za

2.3.18 D. Flade, H. Steinhilber and L. Malcher - 1985 (48)

Flade, Steinhilber and Malcher describe impact tests at a HDR-plant, where impulsive loads of 200 kNs and 0,1 s duration have been realized. They describe there test equipment briefly. They used a pendular falling hammer with crash pads in the contact zone to enforce a desired impact load history. They were not interested in the local effects but only in the global effects. No further information is provided in this paper.

2.3.19 M. Feyerabend - 1988 (181)

Feyerabend tested a number of steel and a number of reinforced concrete columns subjected to a horizontal impact load. A total of eight concrete columns were tested. The cross section of all the reinforced concrete columns weas 300 mm square and the span length was 4 m. The concrete cube strength of all the columns was somewhere between 35 and 45 MPa. The columns were reinforced with 4 Ø18, or 4 Ø25 or 4 Ø28 high strength steel bars. Stirrups of 12 mm diameter with a spacing of 150 mm were provided in all the columns. The columns were tested in a horizontal position (like a beam) with an axial load applied to the one end which could slide freely in the horizontal direction except for the inertia of the mass at that end (see figure 2.2).

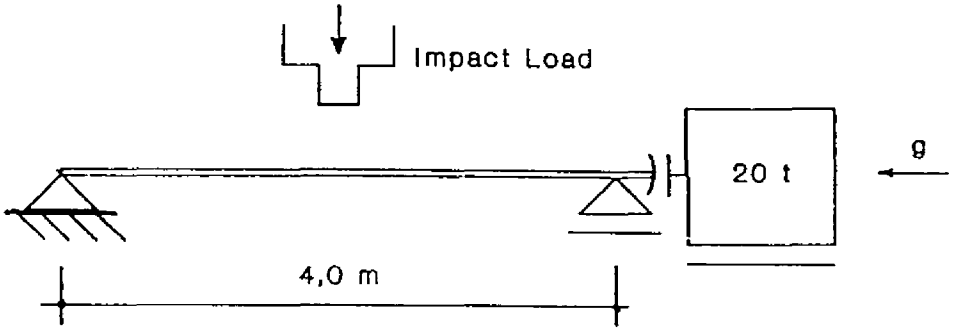

Figure 2.2: Test column set-up as used by Feyerabend.

Stellenbosch University http://scholar.sun.ac.za

The axial load was applied by external prestressed bars pulling the free-sliding end towards the stationary end. The mass was allowed to slide in the horizontal direction

Three axial loads were used. a 245 kN for the column reinforced with 4 Ø18 bars, 197 kN for the column reinforced with 4 Ø25 bars and 201 kN for the column reinforced with 4 Ø28 bars. The lateral impact load was applied with 1,14 ton falling mass. The impact load was changed by changing the falling height and thus the impact velocity was changed. Impact velocities ranging from 0,75 m/s to 6,0 m/s were used.

He provides an approximate analytical solution for the column behaviour and he compares this results with a finite difference analyses based on a self-developed computer program called ACI (Analysis of Columns under Impact loading). The results given compare satisfactorily. Although these comparisons were very good it would have be interesting to see the comparisons of the measured strain and calculated strain as well as the measured support forces and the calculated support forces.

Another very interesting aspect of this study is the influence the lateral impact load has on the axial load of the column. This influence is due to the deflection of the column as well as the cracking of the concrete column and the inertia of the 20 ton mass fixed to the one end of the column. From the results and theory given it is not clear whether he took the crack effect on the axial load into account with his theoretical and computer model. Unfortunately he does not show the comparison between the theoretical values and the experimental values of the axial loads.

The most important differences between the work of Feyerabend and and this study is that he used a column supported at both ends. he used a hard impact and all his columns failed in bending.

Unfortunately he cannot predict the failure of the column subjected to an impact loading

Stellenbosch University http://scholar.sun.ac.za

2.3 Conclusions

In this section only the studies and papers on the impact behaviour of reinforced and prestressed concrete beam and column elements have been briefly reviewed. Although a wide range of studies on reinforced concrete slabs etc. are available, they normally cannot be considered as two dimensional members like columns and beams and thus they were therefore omitted in this section. The local influence, of impactors or strikers, has also not been dealt with in this section but that will be treated in detail in the next chapter. The two fields of local and global effects are normally separated. The local effects are usually approached empirically, whereas the global effects are approached mathematically.

Although a considerable amount of work has been done, there are still a lot of grey areas. One of these is the strain rate effects on especially the concrete. Modelling the behaviour of a material like concrete for finite element analysis with computer programs remains a difficult task, especially when strain rate effects are to be considered as well.

In a number of tests, shear failures occurred under impact loading (Bate - 1961) while similar specimens failed in flexure under static loading. Apparently at this moment no method is available which would reliably predict the resistance of members failing in shear under impact loading.

Stellenbosch University http://scholar.sun.ac.za

3 LOCAL DAMAGE OF CONCRETE STRUCTURES AND MEMBERS DUE TO IMPACT LOADS

3.1 Introduction

The effect of impactors or strikers on reinforced concrete structures or members can be classified into local effects and the global dynamic response of the structure or member. If the kinetic energy transmitted through the zone of impact is considerably smaller than the strain energy capacity of the structure, the local effects will probably be the governing consideration. These local effects are governed by stress wave propagation and the behaviour of sound concrete and cracked concrete under multi-axial, high loading rate conditions. Because of the complexity of especially the local effects impactors or strikers have on reinforced concrete, no complete physical model of the problem has been developed yet.

In recent years the local effects of impactors on reinforced concrete structures have been studied quite extensively and a lot of research has gone into this subject. At present it appears that only empirical and semi empirical equations have been developed for design purposes. Because of all the research that has been done on this particular subject, this study will not pursue the development of yet another design method for this problem of local damage.

The local effects are an integral part of the response of any reinforced concrete member subjected to [illegible] loading. Thus it is necessary to investigate this local damage further. Therefore a state of the art report on the [illegible] of local effects of impactors on reinforced concrete will be given here. This report was [illegible] if and whether local effects would play a significant [illegible] of a soft impact loading on a [illegible]

Stellenbosch University http://scholar.sun.ac.za

From this state-of-the-art report it will be clear that for the investigation in this dissertation, the local effects are very small and the energy dissipated by the local damage is omissible. In fact this report will indicate that no local damage can be expected for the column under such a soft impact loading as was used in this investigation. This was confirmed by the test results given in Appendix B. Both soft and hard impacts are covered in this chapter because this will give a better understanding of the local damage problem and because other studies and investigations related to this dissertation used hard impacts.

3.2 Classifications and definitions

Missiles, impactors or strikers can be classified as being either 'hard' or 'soft' (or deformable) depending on whether they undergo significant deformation during impact.

Local damage is generally classified (90) into the following classes:

1. Penetration: Penetration is the entry of a missile into the target without exiting at the back face. Penetration may be accompanied by peeling off some pieces of concrete from the back face (with a thickness less than the concrete cover).

2. Scabbing: Scabbing is the ejecting of concrete pieces, which have at least the size of the concrete cover, from the back face and are thrown away from the target.

3. Perforation: Perforation is the entry of a missile into the target and its exit at the back face.

4. Spalling: Spalling is the ejecting of concrete pieces from the front face of the target (impact face).

Stellenbosch University http://scholar.sun.ac.za

Penetration and spalling normally goes together and Hughes (75) classified spalling as part of penetration.

For a given impact, the severity of the damage increases as the barrier thickness, d, decreases as shown in fig. 3.1. The scabbing thickness, d_s, is defined as the barrier thickness which is just enough to prevent scabbing. The perforation thickness, d_p, is defined as the barrier thickness which is enough to prevent perforation. These two thicknesses define the bounds between the possible damage of an impact.

For $d > d_s$ the damage is penetration with the missile coming to rest at a penetration depth x_p;

For $d < d_s$ but $d > d_p$ the damage is scabbing;

For $d < d_p$ the damage is perforation.

Impact formulae normally predict x_p, d_s, and d_p for any given impact.

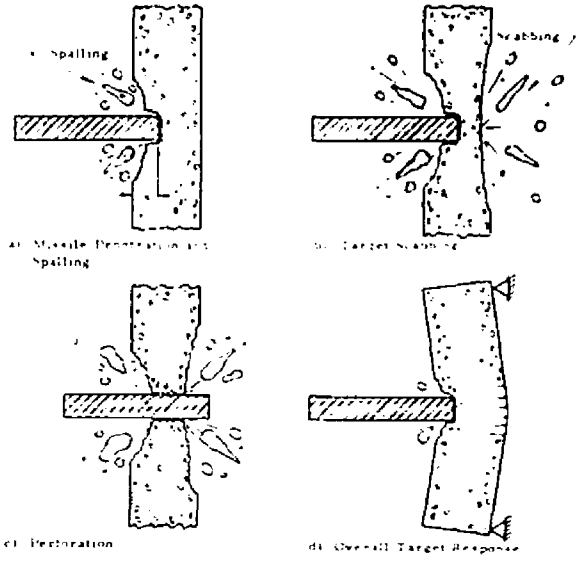

Figure 3.1: Classification of local impact damage.(from Kennedy (90))

Stellenbosch University http://scholar.sun.ac.za

The local damage process is influenced by many parameters. These parameters are classified into two groups: missile parameters and target parameters.(8)

Missile parameters: Mass of missile, M
Size of missile, e.g., the diameter
Velocity of missile, V
Nose shape of missile, N
Deformability of the missile
Inclination of missile.

Target parameters: Target thickness
Concrete strength
Size of aggregate
Amount of reinforcement

First the influence of hard (or solid) missiles will be discussed and then the influence of soft (or deformable) missiles.

3.3 Impact effect of hard or solid missiles on concrete

3.3.1 Available formulae for the prediction of local concrete damage

Unfortunately, nearly all of the available prediction equations are dimensional equations thus necessitating the use of the dimensional units given in their symbol definitions. This means that about all the equations are still in the Imperial and American systems and the compressive strength of concrete is the cylinder strength and not the cube strength.

Stellenbosch University http://scholar.sun.ac.za

3.3.1.1 Modified Petry formula

The Modified Petry formula developed originally in 1910, predicts the penetration depth (x_p) in inches as follows (8,90,170,178):

$$x_p = 12K_pA_p \log_{10}(1,0 + V^2/215000) \quad (3.1)$$

Where: V = Impact velocity, in ft/s

A_p = The weight of the missile per unit projected area, in lb/ft^2

K_p = A coefficient depending on the nature of the concrete and taking into account the effect of reinforcement.

Originally K_p was defined as: 0,00799 for massive concrete; 0,00426 for normal reinforced concrete; and 0,00284 for specially reinforced concrete. Note that these values are independent of the concrete strength (an obvious deficiency) and only dependent on how the concrete is reinforced. For special reinforced concrete in which the front and rear face steel is laced together with special ties, Amirikian (177) has revised K_p to account for the effect of concrete strength. The revised K_p values as a function of concrete strength (f_c') are shown in fig. 3.2. Even though this figure is only applicable for specially reinforced concrete it is sometimes used for normal reinforced concrete as well. When eq. (3.1) is used with the original values of K_p it is defined as the Modified Petry I formula. If eq. (3.1) is use with the values in fig. 3.2 it is called the Modified Petry II formula.

Stellenbosch University http://scholar.sun.ac.za

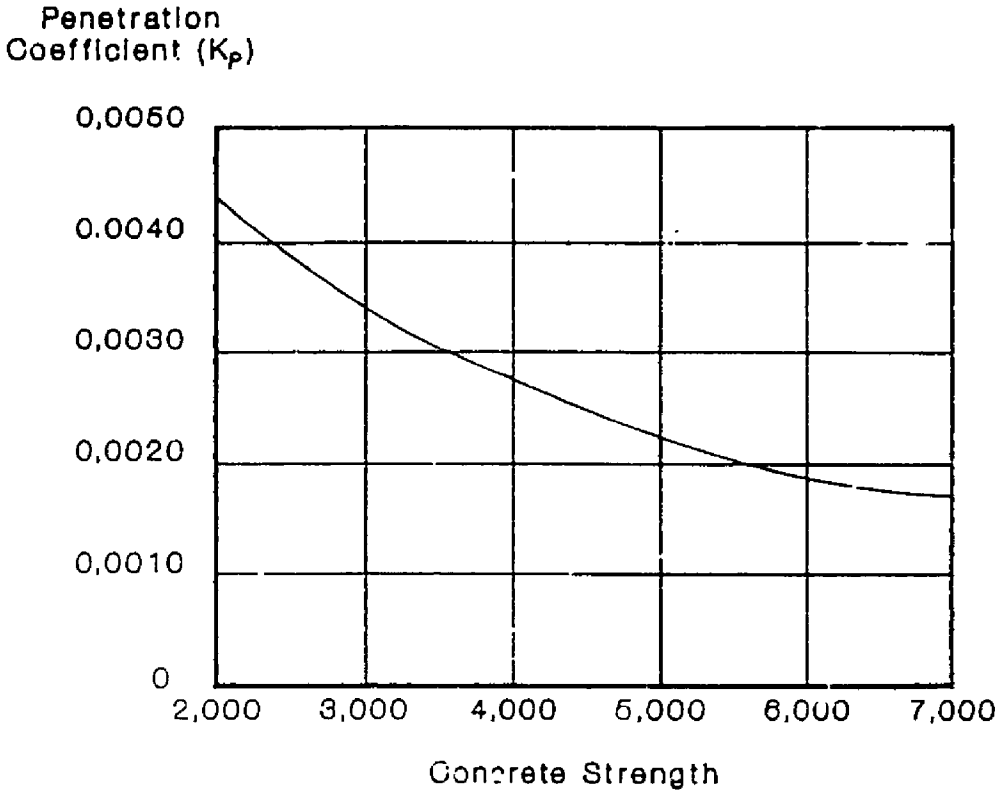

Figure 3.2: Value of Petry penetration coefficient K. for specially reinforced concrete. (from Amirikian (177))

Amirikian (177) suggested that the perforation thickness is determined by:

$$d_p = 2x_p \qquad (3.2$$

and the scabbing thickness is determined by:

$$d_s = 2.2\ x_p \qquad (3.3)$$

where the penetration thickness x_p is given by the Modified Petry formula (eq. (3.1)).

Equation (3.2) is defined as the Modified Petry formula for perforation and equation (3.3) is defined as the Modified Petry formula for scabbing.

Stellenbosch University http://scholar.sun.ac.za

3.3.1.2 Army Corps of Engineers formula

The Army Corps of Engineers developed the following formula in 1946:

$$x_p/D = \{(282WV^{1.8})/(D^{2.76}\, f_c'^{0.5}\, 1000^{1.8})\} + 0,5 \qquad (3.4)$$

Where: D = Diameter of the missile in inches
W = Weight of the missile in pounds
f_c' = Compressive strength of concrete in psi

Eq. (3.4) has been commonly referred to as the Army Corps of Engineers (ACE) formula

In 1943 perforation and scabbing thickness tests were reported for 37 mm, 75mm, and 155 mm projectiles. Regression analysis of these tests led to the following relationships for predicting scabbing and perforation thicknesses:

$$d_s/D = 2,12 = 1,36\, x_p/D\ , \qquad 0,65 \leq x_p/D \leq 11,75 \qquad (3.5)$$

$$d_p/D = 1,32 = 1,24\, x_p/D\ , \qquad 1,35 \leq x_p/D \leq 13,5 \qquad (3.6)$$

These relationships are applicable only within the slab thickness to projectile diameter ratios indicated. According to Kennedy (90) the diameter ratio for eq. (3.5) is ($3 \leq d_s/D \leq 18$) and for eq. (3.6) it is ($3 \leq d_p/D \leq 18$). For ratios (Kennedy's ratios) less than three, these equations will lead to increasingly conservative results.

These formulae are dimensionally incorrect and thus the specified English units must be used.

Stellenbosch University http://scholar.sun.ac.za

3.3.1.3 Modified National Defence Research Committee (NDRC) formula

In 1946 the National Defense Research Committee (NDRC) proposed the following formula for predicting the penetration depth of non-deformable projectiles penetrating a massive concrete target:

$$x_p/D = \{(4KNWV^{1.8})/D(1000D)^{1.8}\}^{1/2} \quad \text{for } x_p/D \leq 2,0 \qquad (3.7)$$

$$x_p/D = 1 + (KNWV^{1.8})/D(1000D)^{1.8} \quad \text{for } x_p/D > 2,0 \qquad (3.8)$$

Where: N = Missile nose shape factor
= 0,72 for flat nose
0,84 for blunt nose
1,00 for spherical nose
1,14 for very sharp nose
W = Weight of missile, in pounds
V = Missile velocity, in ft/s
D = Missile diameter, in inches

K = Concrete penetrability factor and is given by:

$$K = 180/(f'_c)^{1/2} \qquad (3.9)$$

Where: f'_c = Compressive strength of concrete, in psi

The scabbing and perforation thicknesses are predicted by equations (3.5) and (3.6) which were developed by regression analysis for the specific ranges of x_p/D. Equations (3.5) and (3.6) cannot be used for small values of x_p/D. Since the NDRC formula is based upon a theory of penetration it can be extrapolated beyond the range of available test data with greater confidence. Thus for small values of x_p/D (or $d_s/d < 3$, or $d_p/D < 3$) the following curve-fitting extrapolation equations were developed:

Stellenbosch University http://scholar.sun.ac.za

$$d_s/D = 7,91(x_p/D) - 5,06(x_p/D)^2 \quad \text{for} \quad x_p/D \leq 0,65 \tag{3.10}$$

$$d_p/D = 3,19(x_p/D) - 0,718(x_p/D)^2 \quad \text{for} \quad x_p/D \leq 1,35 \tag{3.11}$$

With formulae (3.5) to (3.11) the perforation and scabbing of a very wide range of missiles can be predicted. This is the advantage of the modified NDRC formulae.

3.3.1.4 Ammann and Whitney formula

The following formula has been developed to predict the penetration depth of small explosively generated fragments travelling over 1000 ft/s:

$$x_p/D = (282NWV^{1,8})/(D(f'_c)^{1/2}(1000D)^{1,8}) \tag{3.12}$$

Where: N = Missile nose shape factor
W = Weight of missile, in pounds
V = Impact velocity, in ft/s
D = Missile diameter, in inches

3.3.1.5 The Ballistic Research Laboratory (BRL) formula

The Ballistic Research Laboratory (BRL) have proposed the following formula to predict directly the perforation thickness for concrete walls having an ultimate compressive strength of 3000 psi:

$$d_p/D = 7,8(WV^{1,33})/(D^{2,8}\ 1000^{1,33}) \tag{3.13}$$

Stellenbosch University http://scholar.sun.ac.za

This equation has been extended for other values of the ultimate compressive strength as follows:

$$d_p/D = (427WV^{1.33})/(D^{2.8}\ f'_c{}^{0.5}\ 1000^{1.33}) \qquad (3.14)$$

Where: W = Weight of missile, in pounds
V = Impact velocity, in ft/s
D = Missile diameter, in inches
f'_c = Cylinder Compressive strength of concrete, in psi

The scabbing thickness d_s can be obtained from:

$$d_s = 2d_p \qquad (3.15)$$

where d_p is defined by eq. (3.14). Equation (3.14) is known as the modified BRL formula for perforation and eq. (3.15) is known as the modified BRL formula for scabbing.

3.3.1.6 Bechtel Corporation formula

The Bechtel Corporation has proposed an empirical formula for calculating the scabbing thickness of a concrete panel as follows:

$$d_s = (15,5\ W^{0.4}\ V^{0.5})/(f'_c{}^{0.5}\ D^{0.2}) \qquad (3.16)$$

Where: W = Weight of missile, in pounds
V = Impact velocity, in ft/s
D = Missile diameter, in inches
f'_c = Compressive strength of concrete, in psi

3.3.1.7 Stone and Webster Corporation formula

Stone and Webster have proposed a formula for predicting the scabbing thickness for a concrete panel under the impact of solid missiles as follows:

Stellenbosch University http://scholar.sun.ac.za

$$d_s = (WV^2/c)^{1/3} \qquad (3.17)$$

Where: W = Weight of missile, in pounds

V = Impact velocity, in ft/s

c = A coefficient that depends on the ratio of the target thickness to the diameter of the missile

The ranges of test parameters for this formula were:

3000 psi $\leq f'_c \leq$4500 psi and 1,5 $\leq d/D \leq$ 3,0.

3.3.1.8 Commissariat À L'Energie Atomique-Electricité de France (CEA-EDF)

In 1977 the following empirical formula for calculating the perforation thickness of concrete was proposed on the basis of experiments carried out in France by CEA-EDF:

$$d_p = 0,765(f'_c)^{0.375}\, V^{0.75}\, (W/D)^{1/2} \qquad (3.18)$$

Where: W = Weight of missile, in pounds

V = Impact velocity, in ft/s

D = Missile diameter, in inches

f'_c = Compressive strength of concrete, in psi

The limits for the validity of this formula are:

1. Reinforcing steel = 9,34 - 18,68 lb/ft^3
2. Concrete compressive strength f'_c = 4300 -7300 psi
3. Missile impact velocity V = 82 - 1476 ft/s
4. Ratio of target thickness to missile diameter d/D = 0,349 - 4,17.

Stellenbosch University http://scholar.sun.ac.za

3.3.1.9 Kar formula

By using regression analysis, Kar (88) revised the NDRC formula in 1978 to account for the size of aggregates and the type of missile material. His formula for predicting the penetration depth is as follows:

$$x_p/D = \{(4\alpha N/(f'_c)^{0.5})\ (E/E_m)^{1.25}\ (WV^{1.8}/D(1000D_1)^{1.8})\}^{1/2}$$

for $x_p/D \leq 2$ (3.19)

$$x_p/D = (\alpha N/(f'_c)^{0.5})\ (E/E_m)^{1.25}\ (WV^{1.8}/D(1000D_1)^{1.8}) + 1$$

for $x_p/D > 2$ (3.20)

Where:
- D = Outside diameter of actual missile or inscribed circle
- D_1 = Diameter of projectile, which has same contact area as that of actual missile
- E = Modulus of elasticity of the missile material
- E_m = Modulus of elasticity of mild steel
- f'_c = Compressive strength of concrete, in psi
- W = Weight of missile, in pounds
- V = Impact velocity, in ft/s
- N = Missile shape factor
  = 0,72 for flat nosed hard missiles

For missiles with a special nose, N, the nose shape factor is given by the following:

$$N = 0,72 + 0,25\ (n - 0,25)^{0.5} \leq 1,17 \quad (3.21)$$

Where: n = The ratio of the radius of the nose to the diameter of the missile.

For missiles with a hollow circular section (pipe) or an irregular section, the nose shape factor is given by:

$$N = 0,72 + \{(D/D_1)^2 - 1\}(0,0306) \leq 1,17 \quad (3.22)$$

Stellenbosch University http://scholar.sun.ac.za

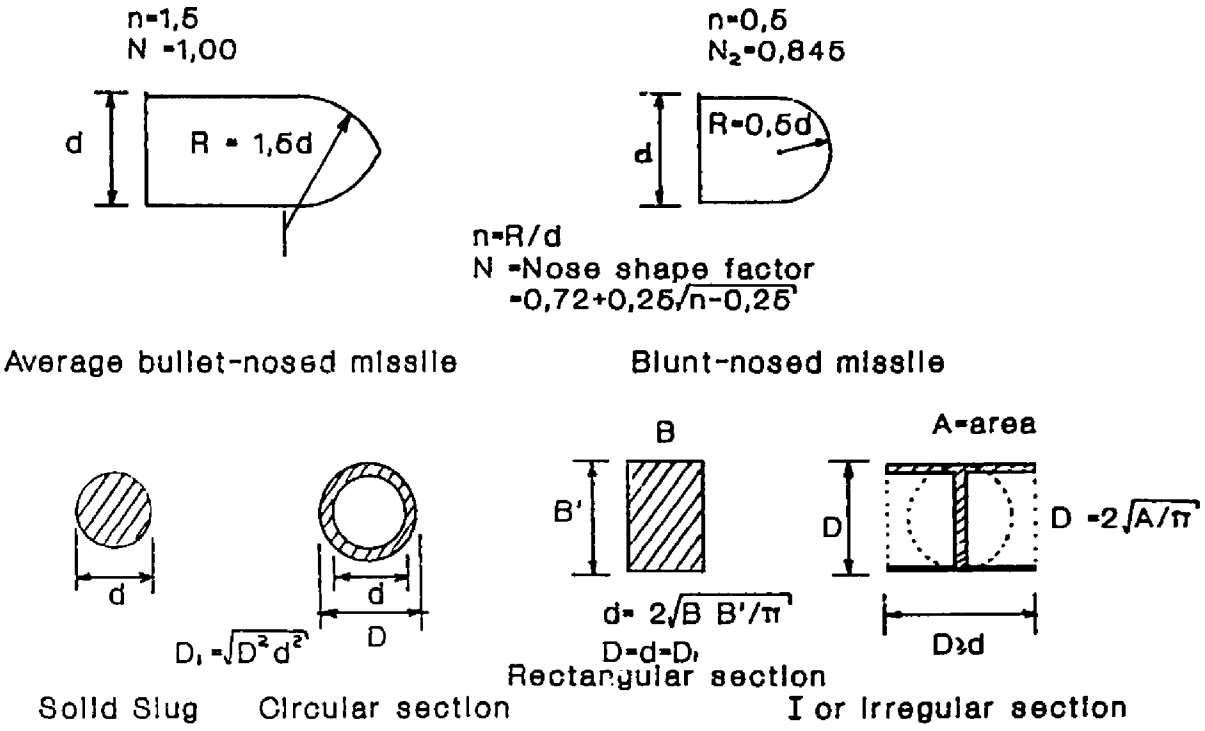

Figure 3.3: Diameters and shapes of projectiles for Kar (88) formula

The value of α is dependent on the dimensional units of equations (3.19) and (3.20). When the different quantities are in the ft, pounds and seconds units, as described earlier, α is equal to 180,0.

When D is expressed in centimeters; D_1 is expressed in centimeters; f'_c is expressed in kilonewtons per square meter; V is expressed in m/s; W is expressed in kilograms and x_p is expressed in centimeters, then the value of α is 120328,0. The following expression was used to calculate this value of α:

$$[\{(kN/m^2)/psi\}^{0.5}\ (cm/in.)^{2.8}]/[(kg/lb)\ (m/ft)^{1.8}] \qquad (3.23)$$

Stellenbosch University http://scholar.sun.ac.za

Kar (88) also proposed the following scabbing and perforation equations:

$$\beta(d_s - a)/D_1 = 7,91(x_p/D_1) - 5,06(x_p/D_1)^2 \quad \text{for} \quad x_p/D_1 \leq 0,65 \tag{3.24}$$

$$\beta(d_s - a)/D_1 = 2,12 + 1,36(x_p/D_1) \quad \text{for } 0,65 \leq x_p/D_1 \leq 11,75 \text{ (or } 3 \leq d_s/D_1 \leq 18) \tag{3.25}$$

$$(d_p - a)/D_1 = 3,19(x_p/D_1) - 0,718(x_p/D_1)^2 \quad \text{for} \quad x_p/D_1 \leq 1,35 \tag{3.26}$$

$$(d_p - a)/D_1 = 1,32 + 1,24(x_p/D_1) \quad \text{for } 1,35 \leq x_p/D_1 \leq 13,5 \text{ (or } 3 \leq d_p/D_1 \leq 18) \tag{3.27}$$

Where: $\beta = (E_m/E)^{0,2}$

a = Half the concrete aggregate size

These formulae can be used to determine the penetration depth and the thickness to prevent perforation and scabbing. From his results it can be seen that the thickness of the test target does not significantly influence the depth of penetration. The aggregate sizes are shown to have effects on the thickness to prevent perforation and back face scabbing.

3.3.1.10 Degen formula

In 1980, based on statistical analysis of the penetration, perforation and residual velocity data presented in refs. (47, 57 and 59), Degen proposed the following perforation formulae (35):

Stellenbosch University http://scholar.sun.ac.za

$$d_p/D = 0,69 + 1,29\ x_p/D \quad \text{for } 2,65 \leq d/D \leq 18 \qquad (3.28)$$

$$d_p/D = 2,2x_p/D - 0,3\ (x_p/D)^2 \quad \text{for } x_p/D \leq 1,52 \qquad (3.29)$$

Where: d_p = Perforation thickness, in inches
D = Missile diameter, in inches
x_p = Penetration depth, in inches

From the interpretation of test data, the following limits for application of this eq. are supposed:

(1) Reinforcing steel is 160 - 350 kg/m^3 (9,97 - 21,8 lb/ft^3),
(2) Striking velocity, V is 20 - 230 m/s (82 -1023 ft/s),
(3) Weight of missile, W is 15 - 343 kg (33 - 756 lb),
(4) Concrete compressive strength, f'$_c$ is 28 - 43 MPa (4113 - 6245 psi),
(5) Barrier thickness, d is 150 - 610 mm (6 - 24 in),
(6) Missile diameter, D is 100 - 305 mm (4 - 12 in),
(7) Ratio of slab thickness to missile diameter, d/D is 0,5 - 27.

3.3.1.11 Chang formula

In 1981, using simplified models, principles of mechanics and Bayesian statistics, Chang (27) proposed the following two formulae for predicting scabbing and perforation thicknesses of a concrete panel:

$$d_s = Y(200/V)^{0.13}\ [(WV^2)^{0.4}]/[D^{0.2}\ f'_c{}^{0.4}] \qquad (3.30)$$

$$d_p = Z(200/V)^{0.25}\ (WV^2/D\ f'_c)^{0.5} \qquad (3.31)$$

Where: d_s = Scabbing thickness, in inches
d_p = Perforation thickness, in inches
V = Impact velocity, in ft/s
W = Weight of missile, in pounds
D = Missile diameter, in inches
f'$_c$ = Compressive strength of concrete in psi

Stellenbosch University http://scholar.sun.ac.za

Y = Random variable for d_s

Z = Random variable for d_p

The values of Y and Z is determined by the Bayesian statistical method and by comparing the calculated values of Y and Z. This values of Y and Z can be adapted as more posterior sample data becomes available. Chang (27) gives more detail on this process. Chang (27) found Y to be equal to 1,84 and Z to be equal to 1,0 for their test data. Thus the formulae is simplified to :

$$d_s = 1{,}84(200/V)^{0.15}\,[(WV^2)^{0.4}]/[D^{0.2}\,f'_c{}^{0.4}] \qquad (3.30a)$$

$$d_p = (200/V)^{0.25}\,(WV^2/D\,f'_c)^{0.5} \qquad (3.31a)$$

The test data from which Chang developed his equations cover the following ranges:

$$55 \leq V \leq 1023 \text{ ft/s},$$
$$0{,}24 \leq W \leq 756 \text{ lb},$$
$$2 \leq d \leq 24 \text{ in},$$
$$0{,}79 \leq D \leq 12 \text{ in},$$
$$3300 \leq f'_c \leq 6600 \text{ psi}.$$

3.3.1.12 Haldar penetration formula

In 1983, Haldar et al. (61) introduced a new dimensionless parameter I, called the impact factor. The impact factor I is defined as:

$$I = (W\,N\,V^2)/(g\,D^3\,f'_c) \qquad (3.32)$$

All the parameters in equation (3.32) are identical to the parameters in the NDRC equations. To be consistent with units, eq. (3.31) can be rewritten as:

Stellenbosch University http://scholar.sun.ac.za

$$I = (12\ N\ W\ V^2)/(32,2\ D^3\ f'_c) \qquad (3.32a)$$

Where:
- I = Impact factor
- N = Nose shape factor (normally 0,72)
- W = Weight of missile, in pounds
- V = Impact velocity, in ft/s
- D = Missile diameter, in inches
- f'_c = Compressive strength of concrete, in psi

In 1984, after plotting several scatter diagrams for several ranges of I values and carrying out linear regression analysis for different ranges of I values, Haldar (61) found that three equations for three different ranges of the impact factor, showed the best fit of the data points. They are:

$$x_p/D = -0,0308 + 0,2251\ I \quad \text{for } 0,3 \leq I \leq 4,0 \qquad (3.33)$$

$$x_p/D = 0,6740 + 0,0567\ I \quad \text{for } 4,0 \leq I \leq 21,0 \qquad (3.34)$$

$$x_p/D = 1,1875 + 0,0299\ I \quad \text{for } 21,0 \leq I \leq 455 \qquad (3.35)$$

Where: x_p = Penetration depth, in inches

Haldar uses the impact factor method as well to predict the scabbing thickness as follows:

$$d_s/D = 3,3437 + 0,0342\ I \quad \text{for } 21 \leq I \leq 385 \qquad (3.36)$$

Where: d_s = Scabbing thickness, in inches

For large missiles where I is smaller than 21 the scabbing formula eq. (3.36) cannot be used. For this larger missiles Haldar did not provide a formula to predict the scabbing thickness.

Stellenbosch University http://scholar.sun.ac.za

3.3.1.13 Hughes formula

In 1984, assuming a parabolic impact force-penetration depth relationship, Hughes (75) formulated formulae to predict penetration depth, scabbing thickness and perforation thickness. He defined an impact factor in terms of the concrete tensile strength, f_r as follows:

$$I' = MV^2/f_r D^3 \qquad (3.37)$$

Where: I' = Impact factor
$f_r = 7,5\ (f'_c)^{0,5}$ with units of psi
$f_r = 0,63\ (f'_c)^{0,5}$ with units of MPa
M = Missile mass = W/g
V = Impact velocity
D = Missile diameter

To be consistent with units equation (3.37) can be rewritten as:

$$I' = (12W/32,2)V^2/f_r D^3 \qquad (3.37a)$$

Where: $f_r = 7,5\ (f'_c)^{0,5}$
W = Weight of missile, in pounds
V = Impact velocity, in ft/s
D = Missile diameter, in inches
f'_c = Compressive strength of concrete, in psi

He proposed the following formula to predict the penetration depth:

$$x_p/D = (0,19\ K'\ I')/S \qquad (3.38)$$

Where: x_p = Penetration depth
K' = Nose shape factor and is equal to 1,0 for flat nosed missiles; 1,12 for blunt nosed missiles; 1,26 for average bullet nose (spherical end); and 1,39 for very sharp nose.
S = Strain rate factor given by:

$$S = 1,0 + 12,3\ \ln(1,0 + 0,03\ I') \qquad (3.39)$$

Stellenbosch University http://scholar.sun.ac.za

Note that the impact factor, I', is dimensionless and therefore consistent units must be used in its computation. Eq. (3.38) is valid so long as neither scabbing nor perforation occurs.

Hughes equations for scabbing and perforation are as follows:

$$d_s/D = 1,74(x_p/D) + 2,3 \qquad (3.40)$$

$$d_p/D = 1,58(x_p/D) + 1,4 \qquad (3.41)$$

Where: d_s = Scabbing thickness
d_p = Perforation thickness

These formulae are valid in the range I' < 3500 which is the range of the available test data of Hughes. The above formulae will be conservative in the range I' < 40, and d/D < 3,5, because the theory used, neglects both elastic and global effects which tend to reduce the severity of local damage. For d/D < 3,5 the global effects seems significant and for I' < 40 the elastic effects seems significant, therefore Hughes gave the following formulae for scabbing and perforation in these ranges:

$$d_s/D = 5,0\ (x_p/D) \qquad (3.42)$$

$$d_p/D = 3,6\ (x_p/D) \qquad (3.43)$$

3.3.1.14 Adeli and Amin formula

In 1985, Adeli and Amin (8) defined the dimensionless impact factor, I, as:

$$I = (N\ W\ V^2)/(g\ D^3\ f'_c) \qquad (3.44)$$

To be consistent with the units given later, eq. (3.44) can be written as:

$$I = (12\ N\ W\ V^2)/(32,2\ D^3\ f'_c) \qquad (3.44a)$$

Stellenbosch University http://scholar.sun.ac.za

By using the least squares technique they found that the relationship between the impact factor, I, and the penetration depth, x_p, is best described as a quadratic and a cubic polynomial. They proposed the following two equations to predict the penetration depth of concrete:

$$x_p/D = 0,0416 + 0,1698\ I - 0,0045\ I^2 \qquad (3.45)$$

$$x_p/D = 0,0123 + 0,196\ I - 0,008\ I^2 + 0,0001\ I^3 \qquad (3.46)$$

Adeli and Amin also proposed the following new formulae for predicting scabbing and perforation thicknesses based on the impact factor:

$$d_s/D = 1,8685 + 0,4035\ I - 0,0114\ I^2 \qquad (3.47)$$

$$d_p/D = 0,906 + 0,3214\ I - 0,0106\ I^2 \qquad (3.48)$$

Where:
- x_p = Penetration depth, in inches
- D = Missile diameter, in inches
- I = Impact factor
- N = Nose shape factor defined by NDRC
  = 0,72; 1,0; 0,84; 1,14; for flat, bullet, blunt and very sharp nose respectively
- W = Weight of missile, in pounds
- V = Impact velocity, in ft/s
- f'_c = Compressive strength of concrete, in psi
- g = The gravity acceleration, in ft/s^2
- d_s = Scabbing thickness, in inches
- d_p = Perforation thickness, in inches

Adeli and Amin's proposed formulae have been developed within the following range of applicability:

$$89 \leq V \leq 1023 \text{ ft/s}$$
$$0,7 \leq d/D \leq 18$$
$$0,24 \leq W \leq 756 \text{ lb}$$
$$0,3 \leq I \leq 21$$
$$D \leq 12$$
$$x_p/D \leq 2,0$$

Stellenbosch University http://scholar.sun.ac.za

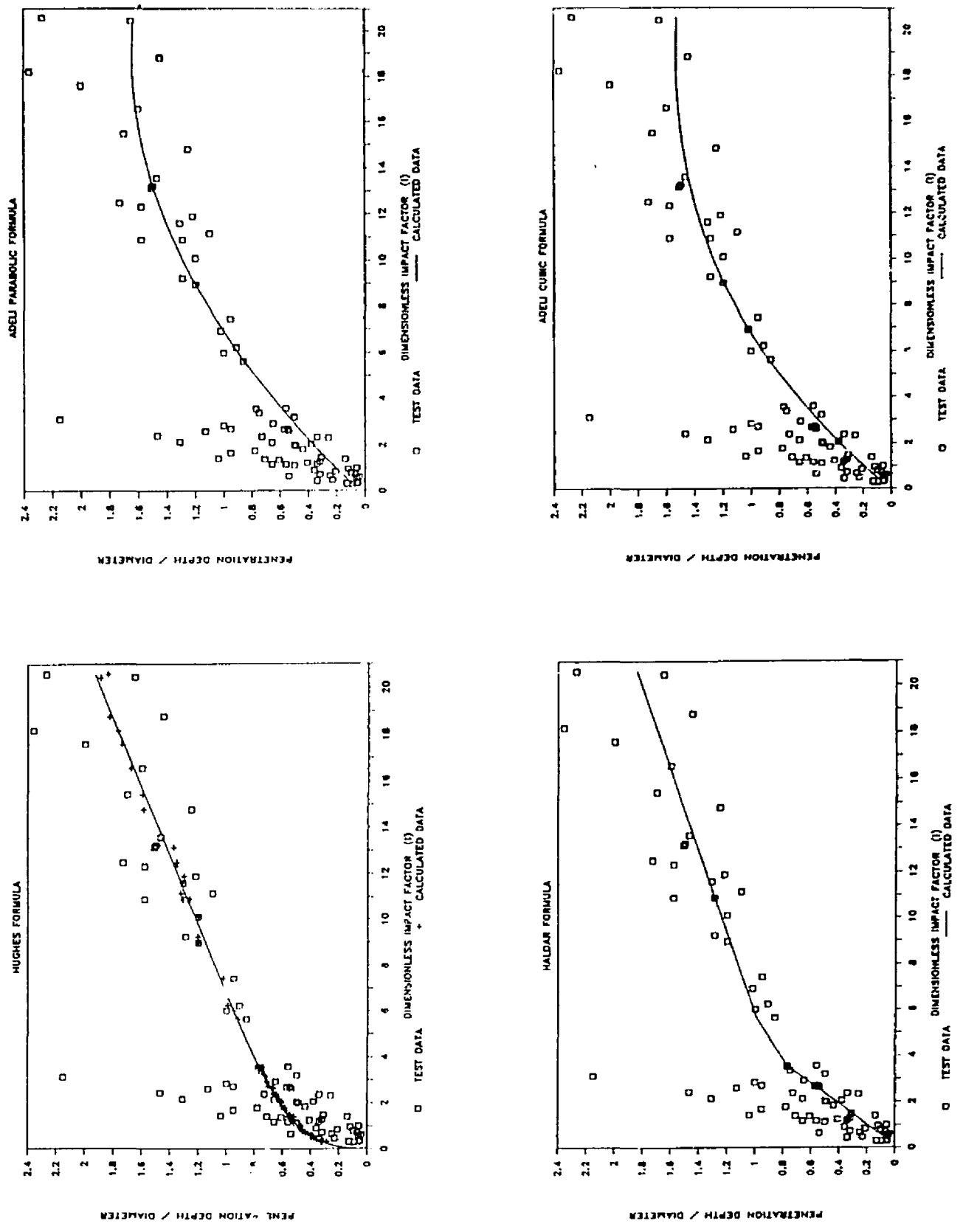

Figure 3.4: Comparison of recent penetration formulae with test data.

Stellenbosch University http://scholar.sun.ac.za

3.3.2 Comparison of formulae

Based on the excellent study by Adeli and Amin (8) the penetration, scabbing and perforation formulae will be compared.

3.3.2.1 Comparison of penetration formulae

Using the updated test data summarized by Sliter (152), the formulae for predicting local effects of hard or solid missiles can be evaluated. It is interesting to note that all the recent formulae are based on a dimensionless impact factor. Figure 3.4 shows the recent penetration formulae (Haldar, Hughes, Adeli parabolic and Adeli cubic) along with the available test data. After drawing scatter diagrams of available penetration formulae for x_p/x (x is the experimentally observed depth) versus x/D, Adeli and Amin (8) made the following observations:

(1) For $x/D \geq 0,6$, Modified NDRC, Haldar, Hughes and the Parabolic and Cubic Adeli formulae tend to agree with experimental results within ± 25%.

(2) For $x/D \leq 0,6$, Modified Petry II, Haldar and the Parabolic and Cubic Adeli formulae agree with experimental results better than the other ones.

(3) ACE and the Petry I formulae over predict the penetration depth with a big margin.

Generally, Hughes, Haldar and the Parabolic and Cubic Adeli formulae predict the penetration depth better than the other ones. Therefore Adeli and Amin carried out two statistical comparisons on these formulae. In each comparison they calculated the variance and the coefficient of variation. The results are given in tables 3.1 and 3.2.

Stellenbosch University http://scholar.sun.ac.za

Table 3.1: A statistical comparison of penetration formulae with all available data points.

Penetration Formula	Variance	Coefficient of Variation
NDRC	0,03607	0,18035
Haldar	0,02515	0,15061
Hughes	0,04242	0,19560
Parabolic Adeli	0,02280	0,14339
Cubic Adeli	0,02315	0,14449

Table 3.2: A statistical comparison of penetration formulae with data points of velocity > 475 ft/s

Penetration Formula	Variance	Coefficient of Variation
NDRC	0,02229	0,12037
Haldar	0,03353	0,14761
Hughes	0,03378	0,14818
Parabolic Adeli	0,02598	0,12994
Cubic Adeli	0,02650	0,13124

3.3.2.2 Comparison of scabbing formulae

After comparing the results of nine of the available scabbing formulae (NDRC, Petry I, Petry II, ACE, BRL, Bechtel, Chang, Hughes and the Adeli formula), Adeli and Amin (8) made the following observations:

(1) The Adeli, Chang and Bechtel formulae predict the scabbing thickness better than the other formulae and they are in general the least conservative formulae among all the formulae. NDRC and ACE formulae agree with the experimental data quite well but they are somewhat more conservative than the Chang and Bechtel formulae.

Stellenbosch University http://scholar.sun.ac.za

(2) The Hughes formula is the most conservative in predicting the scabbing thickness. This might be expected since it was originally developed from a physical model of unreinforced concrete barriers, while the tests were performed on reinforced barriers.

(3) Modified Petry I and II and BRL formulae are the poorest in predicting the scabbing thickness.

3.3.2.3 Comparison of perforation formulae

After similar comparisons, to those for scabbing, were performed by Adeli and Amin (8), they made the following observations:

(1) The Adeli perforation formula, Chang , Degen and CEA-EDF formulae predict the perforation thickness better than the other ones. In general, they are the least conservative formulae and could be used reliably to calculate the perforation thickness for situations similar to those of the tests. NDRC and Petry I also show good agreement with the experimental results but not as good as those of the Adeli, Chang, Degen and CEA-EDF formulae.

(2) Hughes formula predicted that perforation occurred in 41 tests out of 87 tests where perforation actually did not occur. This conservatism might be expected since the physical model from which the formula was developed was based on unreinforced concrete barriers.

(3) Petry II and BRL formulae predicted that perforation did not occur in 14 and 13 tests, respectively, out of 16 tests where perforation actually occurred. Therefore, they are not recommended to be used to calculate the perforation thickness for situations similar to those of the tests.

(4) The ACE formula has the smallest range of applicability and does not show good agreement with the experimental results.

Stellenbosch University http://scholar.sun.ac.za

3.3.3 Conclusions on impact effect of hard (or so) missiles

Since all the formulae were basically developed empirically or semi-empirically for the concrete impact problem, more experiments should be conducted. In these experiments the amount of reinforcing steel, the aggregate size, and the inclination of the missile on the target surface need to be considered. The amount of reinforcement seems to have a considerable influence on the perforation of concrete walls. Eibl (41) found that stirrups or shear reinforcement increase the resistance to punching considerably because the shear reinforcement is activated soon after contact. On the other hand the bending reinforcement has no significant influence to the punching problem, because it is activated only after large deformations of the punching cone occurred.

A study by Haldar (61), using the energy approach, confirms that for smaller non-deformable missiles the energy dissipation due to the overall structural response is very small compared to the local effects and can for most cases be neglected.

The following recommendations are suggested for design engineers:

(1) For non-deformable missiles with velocities lower than 475 ft/s, the Adeli Parabolic formula is recommended for calculating the penetration depth.

(2) For non-deformable missiles of velocity higher than 475 ft/s and lower than 1000 ft/s, the Adeli Parabolic or Modified NDRC formula is recommended for calculating the penetration depth.

(3) For non-deformable missiles with velocities less than 1020 ft/s, the Adeli, Chang or Bechtel formula is recommended for computing the scabbing thickness.

Stellenbosch University http://scholar.sun.ac.za

(4) For non-deformable missiles of velocity less than 1020 ft/s, the Adeli, Chang, Degen, or CEA-EDF formula is recommended for computing the perforation thickness.

3.4 Impact effect of soft or deformable missiles on concrete

Deformable missiles or impactors can be divided into two categories: (a) intermediately deformable - subject to plastic deformation upon impact;

and (b) highly deformable - missile or impactor destroyed upon impact.

Once again two modes of failure can be considered in design:

(1) local effects; and

(2) global effects.

Where the literature is replete with methods to analyze the impact effects of non-deformable missiles on concrete, there are very little information available for the analysis of the effects of deformable missiles on concrete. The first step in analyzing the effect of deformable missiles or impactors on concrete is to determine the impactive load or to find a simplified force-time history model for the impact of deformable missiles.

3.4.1 Method of McMahon, Meyers and Buchert

3.4.1.1 McMahon's force-time history

McMahon, et al. (108) developed a shape for the force-time history for a pipe missile that resembles that of missile decelerations as observed in tests. The simplified force-time history model suggested for the impact of deformable missiles is shown in figure 3.5.

Stellenbosch University http://scholar.sun.ac.za

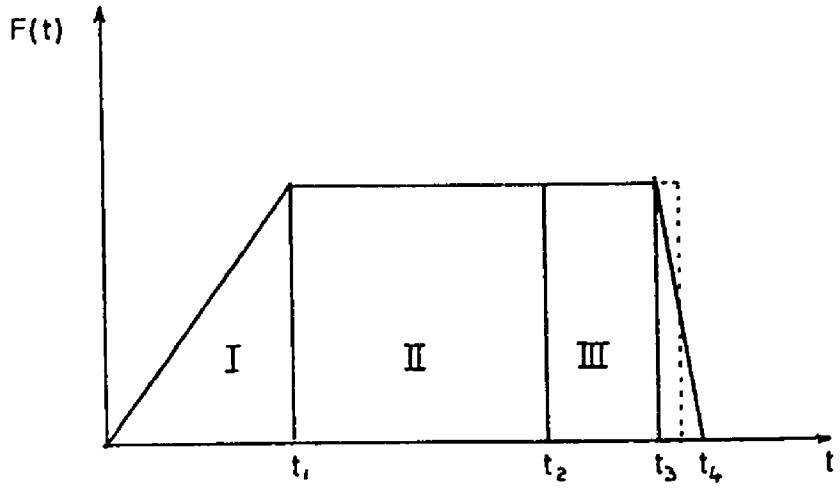

t_1 is the time it takes to develop maximum stress in the missile.
t_2 is the time that the missile is in a compressed plastic state.
t_3 is the time that the stress in the missile starts to decrease.
t_4 is the time at which the stress in the missile is reduced to zero.

Figure 3.5: Force-time history model (108)

The following assumptions was made by McMahon, et al. in their derivations:

1. Local effects damage is completely dependent on momentum and the missile kinetic energy that must be dissipated by missile and barrier deformation.

2. Kinetic energy can be absorbed by: (a) Energy of the missile penetrating the barrier = E_p; (b) strain energy of the missile = SE_m; (c) strain energy of the target = SE_t.

3. For local effects, $E_p + SE_m >>> SE_t$.

Stellenbosch University http://scholar.sun.ac.za

Therefore, SE_t can be conservatively neglected when considering local effects damage by assuming the missile kinetic energy, KE, to be absorbed by missile deformation and penetration ($KE = E_p + SE_m$).

The time period $t < t_1$ represents a linear stress increase after impact as well as a time delay prior to initiating plastic deformation. During this time it is assumed that energy is absorbed by penetration only. The time period $t_2 < t < t_3$ represents missile penetration after the tension wave returns from the free end. During the interval $t_1 < t < t_2$, it is assumed that the missile deforms plastically by wrinkling. The interval $t_3 - t_4$ is extremely small and can be accounted for by averaging t_3 and t_4. McMahon Approximated t_1 by:

$$t_1 = (3,2 \times 10^{-6})\sigma_{cr} \qquad (3.49)$$

Where: σ_{cr} = The average critical wrinkling stress of the pipe impacting the barrier, given by eq. (3.50).

$$\sigma'_{cr} = K' \{(1-v^2)/(1-v_p^2)\}^{0,5} (E_t/E)^{0,5} E_m (t/R) \qquad (3.50)$$

Where:
- E_t = Tangent modulus of elasticity
- E_s = Secant modulus of elasticity
- E = Modulus of elasticity
- t = Pipe wall thickness
- R = Pipe radius
- v = Poissons ratio (pipe) elastic
- v_p = Poissons ratio (pipe) plastic
- K' = Buckling factor dependent on R/t
  ($K' = 0,52$ for $R/t = 20$)

The propagated interface stress is continually decreasing with time. There is also a drop in stress after wrinkling. To account for these variations the average interface stress assumed for a bilinear stress-time diagram is:

$$\sigma_{cr} = 0,90\ \sigma'_{cr} \qquad (3.51)$$

Stellenbosch University http://scholar.sun.ac.za

The time during which the pipe is compressed plastically is the time it takes the initially propagated stress wave to return as a reflected tension wave and is:

$$t_2 = L/C_p + L/C_e \qquad (3.52)$$

Where: L = The missile length
C_p = Speed of an elastic stress wave
C_e = Speed of plastic stress wave

$$C_p = (E/p)^{0.5} \qquad (3.53)$$

$$C_e = (E_t/p)^{0.5} \qquad (3.54)$$

Where: E = Modulus of elasticity
E_t = Tangent modulus of elasticity
p = Material density

The final time, t_3, can be evaluated from the impulse-momentum relationship:

$$t_3 = (-m\ V_2)/F + t_2 \qquad (3.55)$$

Where: m = The missile mass
V_2 = The missile velocity at t_2
F = The interface force

3.4.1.2 Penetration according to McMahon, et al. (108)

Penetration and missile deformation can now be calculated from the time history shown in figure 3.5. Areas I and III represent penetration and Area II represents plastic missile deformation. Therefore for Area I:

$F(t) = Ft/t_1$ and $a(t)$(acceleration) $= Ft/mt_1$

integrating to obtain velocity. Thus:

Stellenbosch University http://scholar.sun.ac.za

$$v(t) = \int a(t)\,dt = Ft^2/2mt_1 + C_1 \quad ; \quad C_1 = V_o$$

and $$x(t) = \int v(t)\,dt = Ft^3/6mt_1 + V_o t + C_2 \quad ; \quad C_2 = 0$$

Thus the penetration during time t_1 is:

$$x_1 = Ft_1^2/6m + V_o t_1 \qquad (3.56)$$

Similarly the plastic missile deformation during t_1 to t_2 is:

$$x_c = x_2 - x_1 = (m/2F)(V_2-V_1)^2 + (mV_1/F)(V_2-V_1)$$

$$= (m/2F)(V_2^2-V_1^2) \qquad (3.57)$$

And the penetration during t_2 to t_3 is:

$$x_3 - x_2 = -(mV_2^2)/2F \qquad (3.58)$$

The total penetration is therefore:

$$x_p = x_1 + x_3 - x_2 \qquad (3.59)$$

Where: x_p = Penetration depth
x_1 = Penetration during time t_1
x_c = Plastic deformation of missile
F = The interface force
V_o = Missile velocity at time t_o

The preceding solution assumes that the missile deforms plastically until the tension wave is reflected back to the impact end from the free end of the missile ($t_2 < t < t_1$).

3.4.1.3 Spalling thickness according to McMahon, et al. (108)

McMahon, et al. suggested the following procedure to determine a specific concrete spalling thickness: (In all formulae, subscripts 0, 1, 2, and 3 are used to indicate values at t_o, t_1, t_2, and t_3.)

Stellenbosch University http://scholar.sun.ac.za

1. Determine critical pipe stress, eq. (3.50) and eq. (3.51).
2. Determine pipe force: $F = -\sigma_{cr} A$
3. Determine rise time: $t_1 = 3{,}2 \times 10^{-6} F$ (F in kips)
4. Determine wrinkling duration, eq. (3.52)
5. Determine intermediate pipe velocities:

$$V_1 = Ft_1/2m + V_0 \qquad (3.60)$$

$$V_2 = (F/m)(t_2 - t_1) + V_1 \qquad (3.61)$$

6. Determine final impact duration, eq. (3.55)
7. Determine penetration distance, eq. (3.59)
8. Determine crushing length,

$$x_c = (m/F)[(V_2 - V_1)^2/2 + V_1(V_2 - V_1)] \qquad (3.62)$$

9. Find R_2

$$R_2 = [f'_c/(p\ V)]\ t_3 \qquad (3.63)$$

10. Use spalling equation:

$$(x + r)^2\ x > [(6W_m KE_m/\pi R_2 M_u r_u) - W_m][1{,}728/\theta_c''] - R_2^2 t_c \qquad (3.64)$$

Where:
- $x = h - x_p - t_c$
- x_p = Penetration depth in inches
- r = Pipe radius in inches
- W_m = Missile weight in kips
- $KE_m = (W_m V_m^2)/(2g)$ in kip-ft
- R_2 = As defined by eq. (3.63)
- M_u = Ultimate moment capacity at hinge in inch-kips per inch
- r_u = Ultimate rotational capacity at hinge in radians
- θ_c = 0,15 kcf
- t_c = Concrete cover in inches

Solution of the spalling equation is a rapidly converging iterative procedure. A barrier thickness h is assumed, and if the spalling equation is satisfied, the thickness is sufficient. Unfortunately this spalling equation is limited in its application and does not apply to thin barriers, h < 12 inches (300 mm). The equation is not valid for lower thicknesses because the failure mechanism for such slabs can be different.

Stellenbosch University http://scholar.sun.ac.za

For highly deformable missiles there is no penetration, since the missile is destroyed during impact. This means that the missile momentum is entirely dissipated before the reflected stress wave returns. Therefore a constant time history for the impact can be assumed.

3.4.2 Kar method (88)

In 1979, Kar investigated all the available methods for analyzing the effect of deformable missiles impacting concrete structures. He also commented on the assumed force-time history as developed by McMahon, et al. (108). His objection against McMahon's theory is that McMahon's deceleration-time history is dependent on an assumed contact pressure at the interface of the missile and the barrier, and sufficient verification with test results have not been provided. Therefore Kar modified the originally proposed time history based on the principle of colliding elastic bodies and available test data. Once again the load-time history has to be developed before the structural resistance can be evaluated.

3.4.2.1 Load-time history according to Kar

From the principle of colliding elastic bodies, the velocity, V, of the missile at time, t, can be obtained from:

$$V = V_o \exp(-\rho_c A C_c t/M) \qquad (3.65)$$

Where:
- V = Missile velocity
- V_o = Normal impact velocity
- ρ_c = Density of concrete
- A = Cross sectional area of missile
- C_c = Speed of sound in concrete
- M = Mass of missile
- t = Time

Stellenbosch University http://scholar.sun.ac.za

By differentiating equation (3.65) with respect to time, the deceleration, a, of the missile is given by:

$$a = V_o(-p_c AC_c/M)\exp(-p_c AC_c t/M) \qquad (3.66)$$

Because of the limited rigidity of the barrier, effective deceleration a_{eff} is assumed to be given by:

$$a_{eff} = a\delta \qquad (3.67)$$

Where:

$$\delta = 0,63(k_{barrier}/k_{missile})^{0.10} \leq 1,0 \qquad (3.68)$$

Where the stiffness of the missile $k_{missile}$ is given by:

$$k_{missile} = AE/L \qquad (3.69)$$

Where: L = Length of missile

In eq.(3.68) $k_{barrier}$ = Stiffness of the barrier acting as a spring. In determining $k_{barrier}$, the uncracked properties of the barrier are considered.

Kar (88) proposed a theory that the magnitude of the deceleration starts from zero at t = 0, linearly increases, and peaks at time t' given by:

$$t' = 0,0464\{(\text{depth of penetration in feet})/(V_o)^{0.3}\} \qquad (3.70)$$

Where V_o is in feet per second and all the other parameters are in the Fps units.

After reaching the peak at time t = t', The missile decelerates linearly and stops at time t = 2t'. A triangular deceleration function with equal rise and decay times is thus obtained (see fig. 3.6). To find the load-time history the following equation can be used:

$$F = M\,a \qquad (3.71)$$

Stellenbosch University http://scholar.sun.ac.za

From equation (3.70), a triangular load time history with equal rise and decay times, is thus obtained.

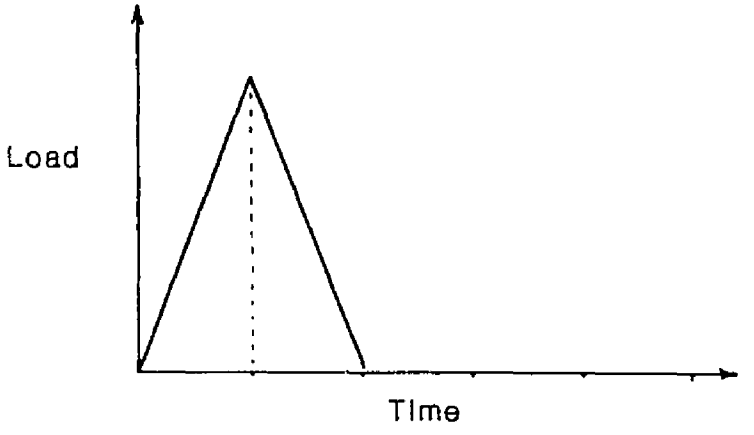

Figure 3.6: Deceleration-time history according to Kar (88).

3.4.2.2 Penetration depth according to Kar

By using eq. (3.66), the time t = 2t' can be found because the deceleration at that time is zero (a = 0) and all the other parameters are known. Thus, t' is known, and from eq. (3.70) the penetration depth, x_p, can be found.

3.4.2.3 Scabbing and perforation thicknesses according to Kar

To find the scabbing and perforation thicknesses it is suggested that Kar's formulae for hard or non-deformable missiles (eq.'s (3.24) - (3.27)) are used. The only difference is that the penetration depth, x_p, is changed.

Stellenbosch University http://scholar.sun.ac.za

3.4.3 Sliter method (152)

In 1980, Sliter evaluated the method that the NDRC formula for penetration of hard missiles (eq.'s (3.7) and (3.8)) is used for deformable missiles as well. To account for the deformability of the missiles, especially pipe missiles, the nose shape factor, N, is adjusted or an "equivalent" diameter for D in the formulae is used.

A conservative estimate of penetration has been obtained by assuming an effective diameter, D_e, as the diameter of a solid cylinder having the same cross-sectional area (metal) as the pipe. Since this assumption effectively concentrates the impact area and prescribes non-deformability of the missile, an upper-bound estimate of penetration results. An appropriate choice for the nose shape factor N is 0,72 corresponding to the flat-nosed effective missile.

A lower estimate (not a lower bound) can be obtained by taking the diameter, D, to be the outside diameter, D_o, and perhaps give the nose shape factor a bigger value than 0,72 to account for the sharp edges of the pipe.

Comparisons by Sliter show that the best overall agreement between the measured and calculated penetration depths is obtained using the outside diameter, D_o, of the pipes in the NDRC formulae. He also found that the formulae with N = 0,72 gives somewhat better agreement than that with N = 1,0. Use of the equivalent diameter, D_e, clearly gives a conservatively high prediction.

If the NDRC formulae for scabbing and perforation (eq.'s (3.10) and (3.11)) is used to estimate the scabbing and perforation thicknesses for deformable missiles, the same reasoning, as for penetration depth, applies.

In conclusion Sliter said that the sparsity of data makes it difficult to decide whether the method investigated by him is adequate for design purposes.

Stellenbosch University http://scholar.sun.ac.za

3.4.4 Conclusions on the impact effect of deformable missiles

Due to the little data available on the impact damage effects of deformable missiles on concrete, it is at this stage very difficult to compare the three methods discussed in this study. All three methods have their shortcomings and their fields of applicability.

The method discussed by Sliter is once again an empirical method and what is worse is that this method was developed for hard missiles. Attempts are now made to fit it onto data of deformable missiles. The results of this method does not compare well with the little available data. Therefore this method is definitely not recommended.

McMahon, et al. and Kar tried to develop a complete different approach than the empirical approach, although they still use some empirical values. The main difference between their approaches is the assumption of the load-time histories. This means that their fields of applicability is totally different and therefore their methods are very difficult to compare. Due to this difference and the scarcity of available data, these two methods will not be compared. The reader can decide which one is preferable or which one compares most favourably with his available test data.

Stellenbosch University http://scholar.sun.ac.za

4. MECHANICAL PROPERTIES OF CONCRETE AND REINFORCING STEEL SUBJECTED TO IMPACT.

4.1 Introduction

The influence of high stress or strain rates upon the mechanical properties of materials is considered in this chapter. The high stress rates or loading rates, associated with impact loads, have a significant influence on properties like the compressive strength, tensile strength, stress-strain behaviour and bond between steel and concrete. Insufficient insight into the behaviour of materials at higher rates of loading may lead to overestimating safety of structures and to uneconomical design.

4.2 Strain rates

The loading rates (increase in stress per unit time) and strain rates of typical impact conditions encountered in practice are given in table 4.1. These figures (134, 173) are very approximate and subject to considerable scatter, because not only the mass and stiffness of the structure itself determine the loading rate, but also the stiffness of the striker.

Table 4.1: Loading rate and strain rate categories

Load category	Loading case	Loading rate $\dot{\sigma}$ (N/mm^2ms)	Strain rate $\dot{\epsilon}$ ($1/s$)
Quasi-static			$<10^{-4}$
	Vessel collision	10^{-4} to 10^{-3}	10^{-5}
Intermediate			10^{-4} to 10^{-2}
	Vehicle collision	10^{-3} to 10^{-2}	10^{-4}
	Gas explosion	10^{-3} to 10^{-2}	10^{-4}
	Crashing aircraft	10^{-1} to 10^{0}	10^{-2}
High			10^{-2} to 10^{1}
	Earthquake	5.10^{-1} to 10^{2}	10^{-2} to 3.10^{0}
	Pile-driving	10^{0} to 3.10^{1}	3.10^{-2} to 10^{0}
Shock waves			$>10^{1}$

Stellenbosch University http://scholar.sun.ac.za

4.3 Concrete

Experimental investigations showed that concrete is a rate sensitive material.

4.3.1 Tension

The effect the loading rate has upon the tensile strength of concrete has been dealt with in a limited number of publications (183, 134). Typical results are shown in figure 4.1, with the stress or strain rate on the horizontal axis and the impact tensile strength normalized by the static strength along the vertical axis. Evident from this figure is that the direct tensile strength increases with higher loading rates.

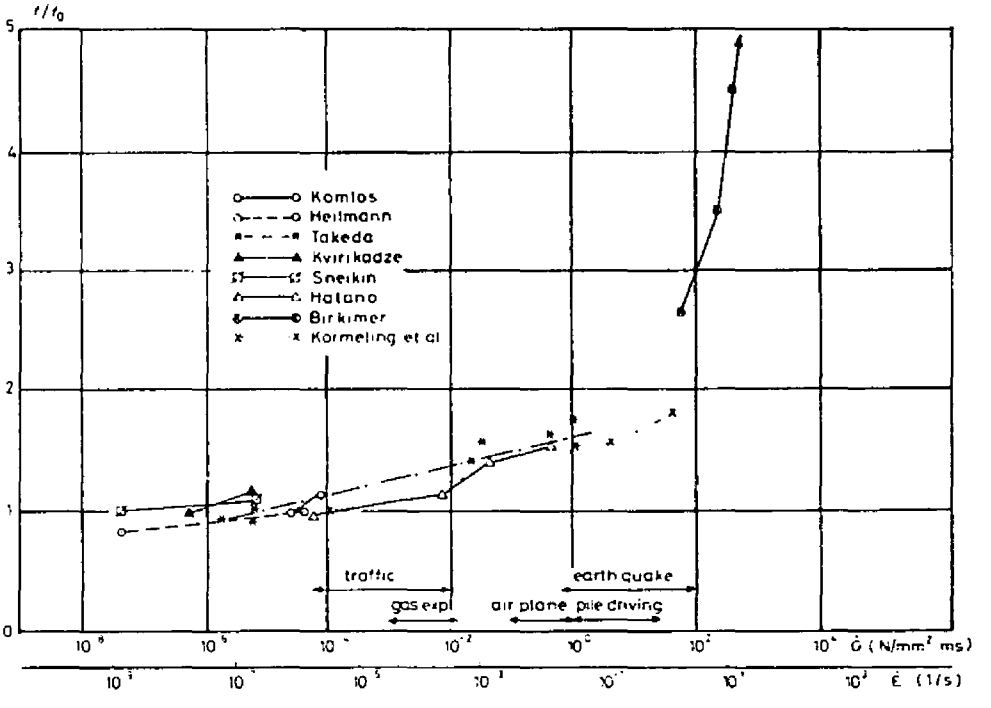

Figure 4.1: Influence of the stress rate on the uniaxial tensile strength of concrete (183).

A relationship between tensile strength and stress rate was derived by Mihashi and Izumi (179) as follows:

Stellenbosch University http://scholar.sun.ac.za

$$(f/f_o) = (\dot{\sigma}/\dot{\sigma}_o)^{(1/(1+\beta))} \qquad (4.1)$$

Where: f = Impact tensile strength of concrete
f_o = Static tensile strength of concrete
$\dot{\sigma}$ = Impact stress rate
$\dot{\sigma}_o$ = Static stress rate
β = A material parameter varying between 20 and 25

Zielinski linked the results of an extensive experimental program, carried out on 26 concrete mixes in the Stevin laboratory (180), to equation 4.1. With the exponent $1/(1+\beta)$ equal to 0.042 and $\dot{\sigma}_o = 10^{-4}$ N/mm² per ms and f_o = 3,1 N/mm², the results of 323 tests are shown in figure 4.2.

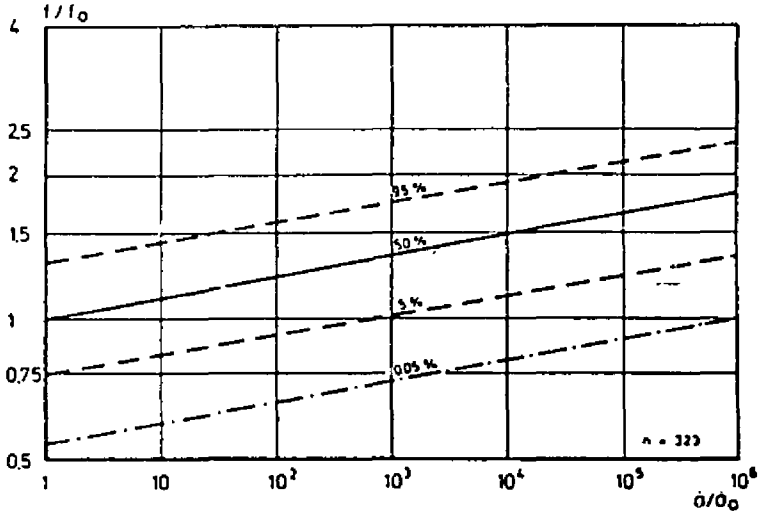

Figure 4.2: Increase of tensile strength of concrete with increasing stress rate (173).

In figure 4.2 the values on the horizontal axis begins with 1 (unity), corresponding to the static test. With increasing rate, the strength also increases and attains at 10^6 a mean value of 1,8 times the static strength. The value which 5% of the results will reach is 1,35 and the value which will be exceeded by 5% of the results is 2,37. From the figure it also emerges that for a loading rate ratio of 10^3 the 5% lower limit just coincides with unity. It can also be shown statistically that in only 0,05% of cases there will be no increase in strength at all if the loading rate ratio is increased to 10^6. The general conclusion is that

Stellenbosch University http://scholar.sun.ac.za

higher loading rates result in an increase of tensile strength of concrete. This increase may be influenced by some factors such as the composition and the properties of the constituents of the concrete.

Figure 4.3 shows stress-strain relationships (173, 134) determined in uniaxial impact and static tensile tests respectively. It indicates that not only the tensile strength but also the corresponding strains are greater under impact than under static loading conditions.

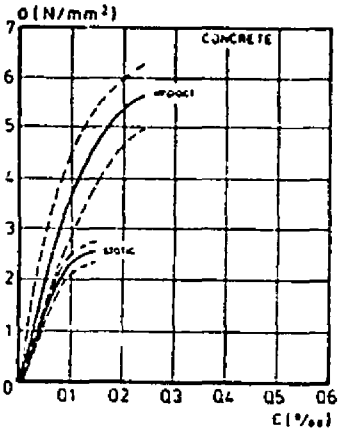

Figure 4.3: Static and Impact stress-strain diagram (173, 134).

While the static modulus of elasticity (secant modulus determined at the origin of the diagram) was 25500 N/mm² at σ=2 N/mm²; in the impact test it was 39500 N/mm² at the same level of stress. At σ=5N/mm² this latter value decreased to 30000 N/mm². The strain associated with the highest stress is 0,014% in the static test and 0,024% in the impact test. These results therefore show that the concrete behaves in a more rigid, but not in a more brittle manner when subjected to impact loading.

A model for tensile fracture of concrete at high rates of loading explains the above mentioned phenomena by considering the amount of simultaneous cracking of concrete and the paths of single cracks as being stress rate dependent. At high stress rates more extensive cracking takes place and cracks are forced to propagate

Stellenbosch University http://scholar.sun.ac.za

through tough aggregate particles instead of along weak interfaces between the particles and the matrix.

This model predicts higher tensile strength and fracture energy for concretes made with tough well-bonded aggregate particles, which is in fair agreement with experimental results showing higher tensile strength of concretes with low water-cement ratios and relatively small aggregate particles. The properties of interfaces are essential to the tensile behaviour of concrete at low loading rates, whereas the properties of aggregate are essential to the behaviour at high rates of loading.

4.3.2 Compression

Figure 4.4 shows results of compressive tests conducted by several researchers (179) on various concretes. Despite the considerable scatter exhibited by the experimental results it can be concluded that the compressive strength of concrete increases with the rate of loading, especially when the strain rate exceeds ten mm/mm per second.

This increase is less than in the case of tensile strength. At high loading rates ($\dot{\epsilon} > 0,2/s$) the compressive strength increases very rapidly. A similar effect can be observed for tensile strength (see fig. 4.1).

Dargel (179) suggested the following relationships:

$$f_c/f_{co} = 1,10 + 9,06.10^{-3} \ln(\dot{\epsilon}) \qquad \text{for } \dot{\epsilon} \leq 0,191\ s^{-1}$$

$$f_c/f_{co} = 1,30 + 13 \ln(\dot{\epsilon}) \qquad \text{for } \dot{\epsilon} > 0,191\ s^{-1} \qquad (4.2)$$

Where: f_c = Impact compressive strength of concrete
f_{co} = Static compressive strength of concrete

It fits the experimental results rather well, as shown in figure 4.4. Note that the relationship between $\dot{\sigma}$ and $\dot{\epsilon}$ involves the E-modulus which is rate dependent. Here again the increase in

Stellenbosch University http://scholar.sun.ac.za

strength depends on the composition and the properties of the constituents of the concrete. It was observed (74) that under impact loading conditions, more aggregate particles were fractured than under static compressive loading. Concretes with a smaller maximum size of aggregate particles and a better interfacial bond with the cement matrix, exhibited higher strengths but were less affected by high rates of loading. This indicates that impact compressive loading forced cracks to undergo rapid extension through tougher material zones.

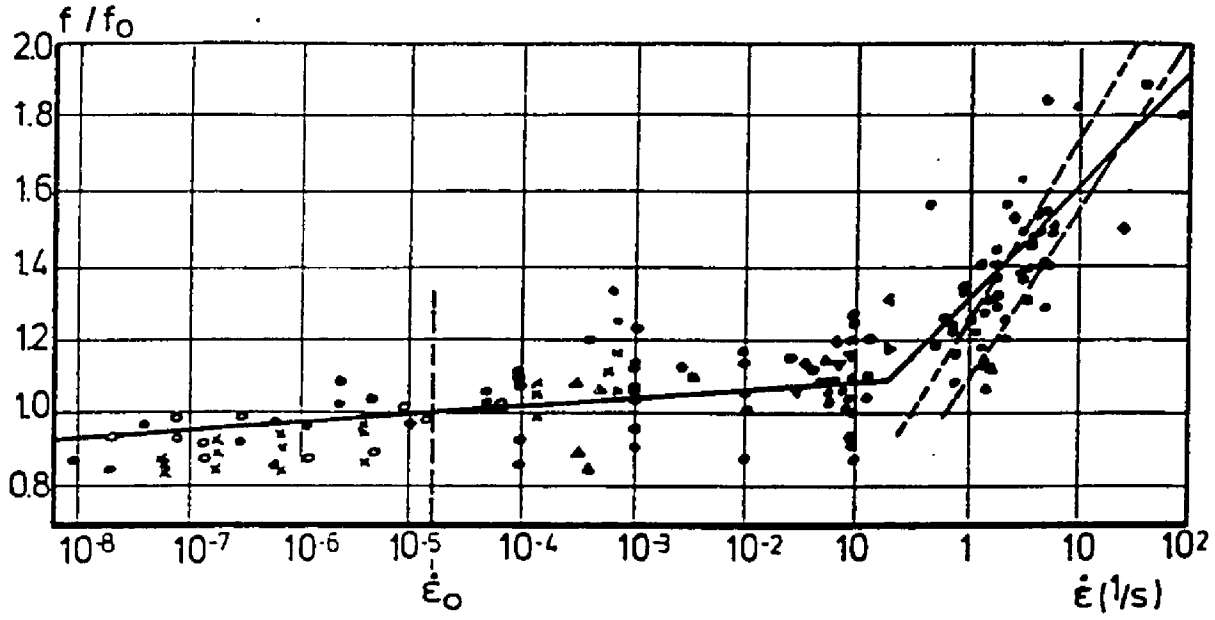

Figure 4.4: Influence of the loading rate upon uniaxial compressive strength of concrete (179).

The stress strain relationships for concrete under static and impact rates of loading manifest differences in strains corresponding to the maximum stresses, see figure 4.5.

Hjorth (182) showed that the stiffness of the concrete increases with the rate of loading. The increase in the E-modulus can be described by similar expressions as those for compressive strength, according to Dargel (179).

Stellenbosch University http://scholar.sun.ac.za

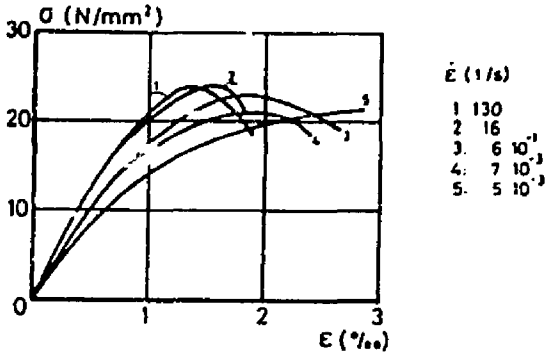

Figure 4.5: Stress-strain curves for concrete in compression at different strain rates (182).

$$E/E_o = 1{,}10 + 9{,}06 \cdot 10^{-3} \ln(\dot{\epsilon}) \qquad \text{for } \dot{\epsilon} \leq 0{,}191\ s^{-1}$$

$$E/E_o = 1{,}30 + 13 \ln(\dot{\epsilon}) \qquad \text{fo } \dot{\epsilon} > 0{,}191\ s^{-1} \qquad (4.3)$$

Where: E - Impact elasticity modulus

E_o = Static elasticity modulus

Figure 4.6 shows the proposed relationships together with the experimental results.

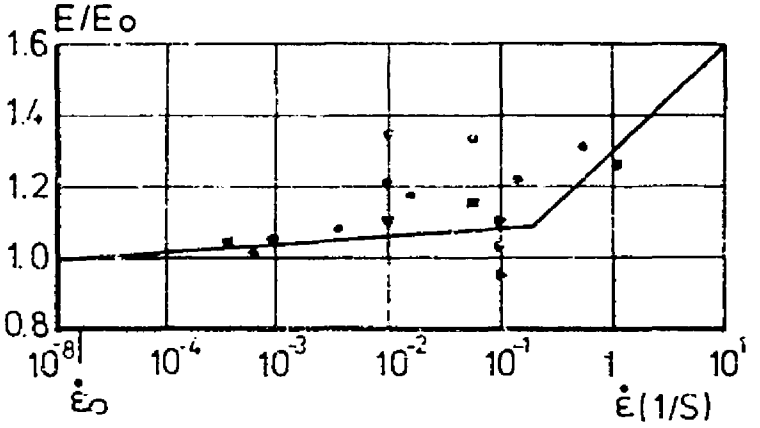

Figure 4 6: Influence of the loading rate upon the E-modulus (179)

Stellenbosch University http://scholar.sun.ac.za

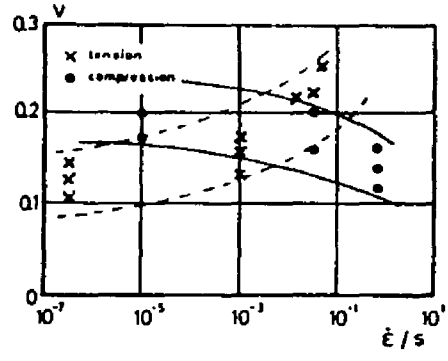

Figure 4.7: The effect of strain rate upon Poisson's ratio for σ/σ_{max} = 40% (173).

The influence of the stress rate upon Poisson's ratio is shown in figure 4.7. The value of poisson's ratio increases with increasing rate of tensile loading and decreases with increasing rate of compressive loading.

4.3.3 Calculation of tensile strength from cube (compressive) strength

If no additional tensile strength tests on concrete are available, the tensile strength can be calculated from the concrete cube strength. Reinhardt (134) proposed the two sets of formulae based on the Netherlands code of practice for concrete, VB 1974, and the CEB-FIP Model Code presented in table 4.3.

Table 4.3: Tensile strength formulae for concrete

Stress rate $\dot{\sigma}$	VB 1974	CEB-FIP
$(\dot{\sigma}/\dot{\sigma}_o) = 1$ (static)	$f_{tm} = 0,87[1+(1/20)f_{cu}]$	$f_{tm} = 0,225\ f_{cu}^{(2/3)}$
$(\dot{\sigma}/\dot{\sigma}_o) = 10^{5}$	$f_{tm} = 0,87[3,15+(1/40)f_{cu}]$	$f_{tm} = 1,10\ f_{cu}^{(1/3)}$
$(\dot{\sigma}/\dot{\sigma}_o) = 10^{6}$	$f_{tm} = 0,87[4,60+(1/80)f_{cu}]$	$f_{tm} = 3,10\ f_{cu}^{(1/10)}$

Stellenbosch University http://scholar.sun.ac.za

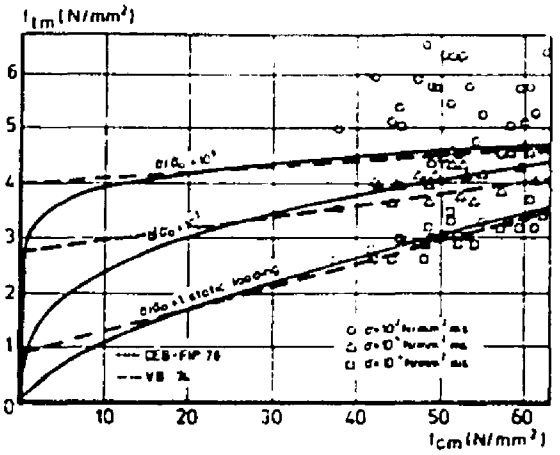

Figure 4.8: Relationship between concrete tensile strength and cube strength according to VB formulae and the modified CEM-FIP formulae (Zielinski 1982).

Where: f_{tm} = Tensile strength of concrete in N/mm²

f_{cu} = Compressive cube strength of concrete in N/mm²

Figure 4.8 shows the two sets of formulae plotted with test data.

4.3.4 Biaxial loading

Zielinski (174) investigated the influence of biaxial loading of concrete under impact and static conditions. He found that the increase in strength due to high rates of tensile loading was similar for concrete under uniaxial loading and for concrete subjected to biaxial compression-tension loading.

Zielinski also found that the stress-loading rate relationships determined in uniaxial tests can be used for extending failure envelopes of concrete under static compression-tension to higher rates of loading. Thus it seems as if the same procedures can be applied to constructing rate dependent failure envelopes of concrete under other combinations of multi axial loading.

The impact stress strain curves are in general steeper than the static ones and the strains at the ultimate stress, ε_u, are larger under impact loading than under static loading.

Stellenbosch University http://scholar.sun.ac.za

Zielinski concluded that further investigations on concrete under various combinations of multi-axial loading are required for verifying the rate-sensitiveness of concrete subjected to different loading conditions.

4.3.5 Shear

Investigations of the impact shear strength of concrete are very limited. A number of different factors might have influenced the limited results available as well. Thus it might be dangerous at this stage to predict the trend of the shear behaviour of concrete under impact loading.

Some static tests were compared (10) with strengths for dynamic load pulses with rise times of between 25 and 70 ms. For plain concrete the average increases in the ratio of shear strength to static strength were 15%.

4.4 Reinforcing steel

The behaviour of reinforcing steel at high rates of loading is of considerable importance, since it influences the deformations of concrete structures and their ability to absorb energy at impact loading. Despite extensive research activities in steel testing, little has been done with respect to the behaviour of reinforcing bars under impact loading.

Figure 4.9 shows stress-strain relationships (173) for a ribbed cold worked reinforcing steel (BST 420/500 RK), a ribbed self-hardening reinforcing steel (BST 420/500 RU) and a ribbed high-tensile steel (BST 1080/1320). Note that the effects of high rates of loading are not the same for the different reinforcing bars.

Stellenbosch University http://scholar.sun.ac.za

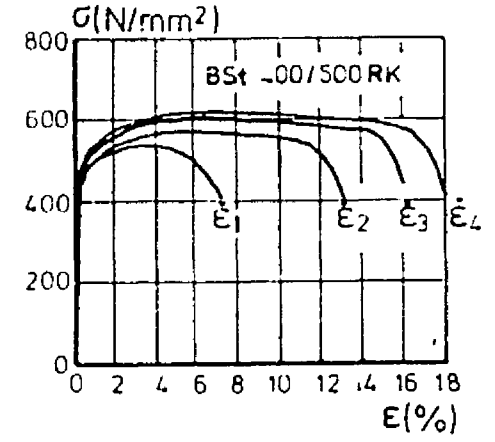

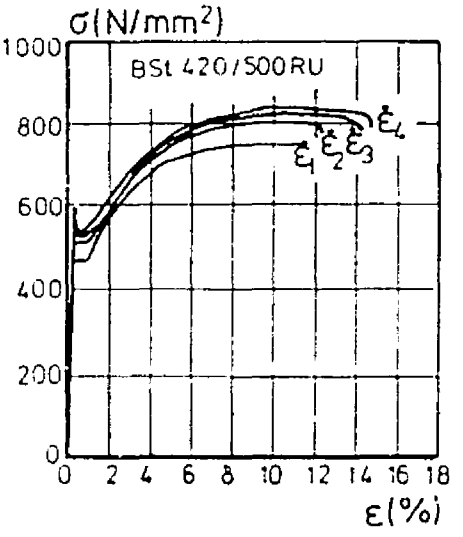

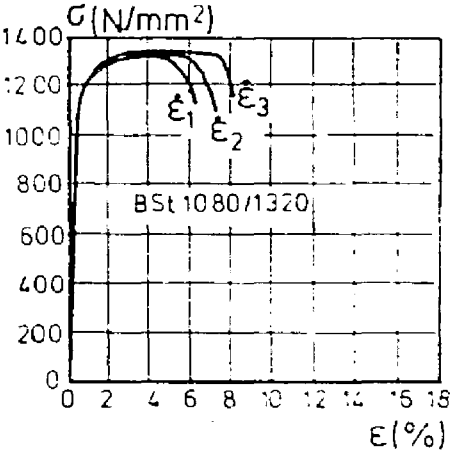

Figure 4.[illegible] Stress-strain curves for steel at several strain rates $\dot{\varepsilon}_1$ [illegible] $\dot{\varepsilon}_2$ [illegible] $\dot{\varepsilon}_3$ [illegible] $\dot{\varepsilon}_4$ - [illegible]

Stellenbosch University http://scholar.sun.ac.za

In the case of BST 420/500 RK steel, the tensile strength and elongation characteristics increased almost linearly with the logarithm of the rate of strain.

The tensile strength of BST 420/500 RU steel increased linearly with the rate of stressing, whereas the ductility was little affected by the rate of loading.

The behaviour of BST 1080/1320 steel was hardly affected by the rate of strain.

The influence of the rate of strain upon the tensile strength, σ, and the uniform elongation, ϵ, (at onset of necking) can be expressed by the formulae (173):

$$\sigma = A + B \ln(\dot{\epsilon}) \qquad (4.4)$$

$$\epsilon = C + D \ln(\dot{\epsilon})$$

Where: σ = Tensile stress of reinforcement
$\dot{\epsilon}$ = Strain rate
ϵ = Strain of reinforcement

The approximate values of the coefficients A, B, C and D are summarized in Table 4.4.

Table 4.4: Coefficients for rate effects on steel properties.

Coefficients / Steel	A	B	C	D
BST 420/500 RK	580	6,03	11,5	0,78
BST 420/500 RU	820	6,27	12,2	0,19
BST 1080/1320	-	-	5,5	0,19

As can be seen in figure 4.9, the E-modulus seems not to be influenced by the strain rate at all. Ammann (10) mentions that the influence of the strain rate on the E-modulus is very small indeed.

Stellenbosch University http://scholar.sun.ac.za

4.5 Bond between steel and concrete

4.5.1 Deformed or ribbed reinforcing bars

Vos (168) investigated the loading rate effect on the bond between concrete and ribbed steel. Figures 4.10 and 4.11 show the effects of four different loading rates for a low strength and a high strength concrete. The effect of loading rate is clear; there is a pronounced increase in the pull out resistance with a higher loading rate. Something that should be noted is that the increase of bond resistance due to a high loading rate is more pronounced for low strength concrete than that for high strength concrete.

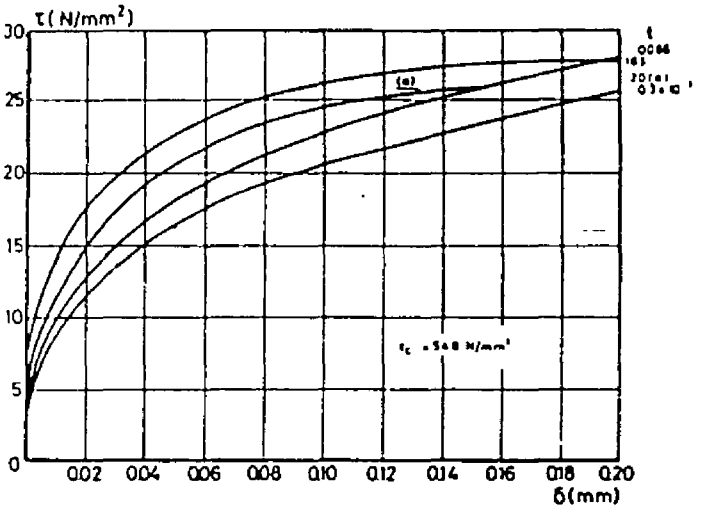

Figure 4.10: Bond stress slip curves of deformed bars at various loading rates for low strength concrete (22,7MPa). (173)

Stellenbosch University http://scholar.sun.ac.za

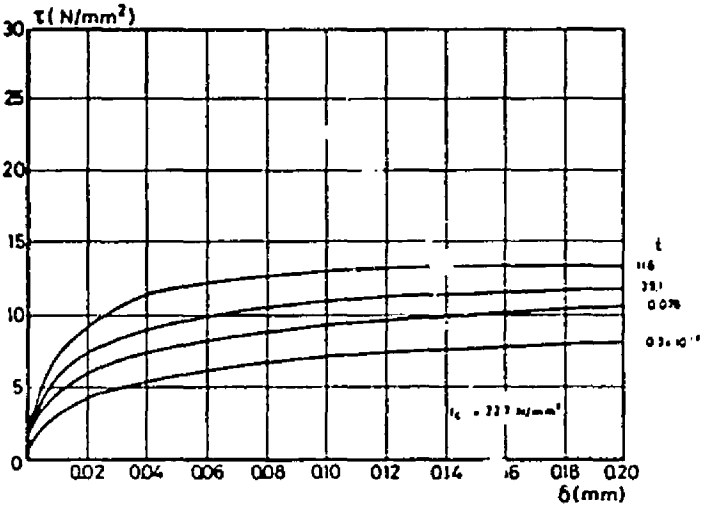

Figure 4.11: Bond stress-slip curves of deformed bars at various loading rates for high strength concrete (54.8MPa). (173)

The ribs of deformed bars oppose the bar displacements in the concrete. Due to very high intensity of stresses under the ribs, crushing and cracking of the concrete takes place. Since both the compressive strength and the tensile strength of the concrete are stress rate dependent, the bond of the deformed bars is also influenced by the rate of loading.

The following formula (168) is suggested for the bond strength and the rate of loading $\dot{\tau}$:

$$(\tau/\tau_o) = (\dot{\tau}/\dot{\tau}_o)^{\mu} \qquad (4.5)$$

Where: τ = bond strength

τ_o = bond strength corresponding to the static rate of loading of $0.3.10^{-3}$ N/mm²ms.

The exponent μ is a function of the compressive strength of the concrete f_c and the displacement δ between the bar and the concrete:

Stellenbosch University http://scholar.sun.ac.za

$$\mu = \{0,7(1-2,5\delta)\}/\{f_{cu}^{0,8}\} \qquad (4.6)$$

Where: δ = displacement in mm for: $0<\delta<0,2$mm

f_{cu} = concrete cube compressive strength in N/mm²

The relative rib surface area f_r should be between 0,065 and 0,1 for this formula.

4.5.2 Plain reinforcing bars

Figure 4.12 (168) indicates that the loading rate has no significant influence on the bond strength and bond stiffness. From these results and from that of other experimental investigations, it emerged that no further investigations on the bond resistance of plain reinforcing bars were necessary. It can thus be concluded that plain reinforcing bars are not sensitive to the rate of loading.

Similar results were obtained for prestressing strand tendons. Figure 4.13 shows the results for prestressing strand tendons at two loading rates.

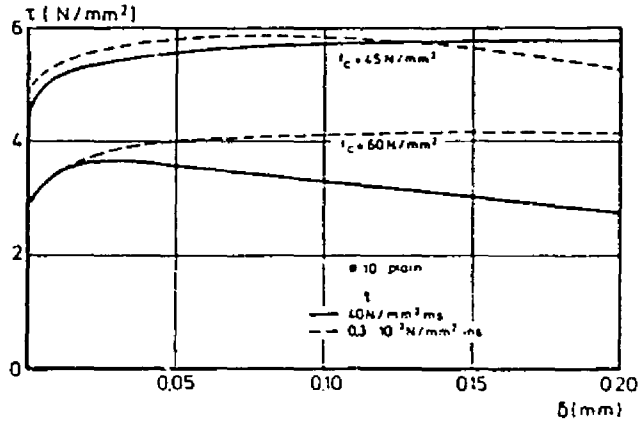

Figure 4.12: Bond stress slip curves of plain bars for a low and a high loading rate. (168)

Stellenbosch University http://scholar.sun.ac.za

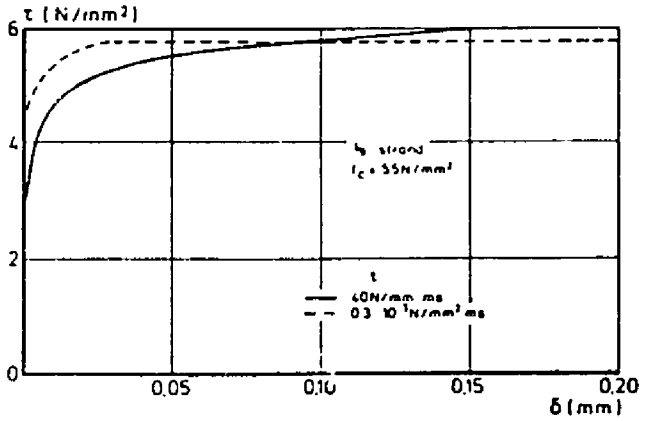

Figure 4.13: Bond stress slip curves of prestressing strand tendons for low and high loading rates. (168)

4.6 Conclusions

From the review in this chapter it is clear that the rate of loading has a significant influence on the relevant mechanical properties of steel and concrete. The majority of the studies also indicate that impact loads cause an increase in the magnitude of the failure load. Due to the complexity of this problem, most investigators did not introduce these results into recommended formulae. There seems to be general consensus that more investigations are necessary before such a step would be possible.

Stellenbosch University http://scholar.sun.ac.za

5. ANALYTICAL MODEL FOR THE DYNAMIC RESPONSE OF A CANTILEVER COLUMN

5.1 The set-up of the cantilever column

A horizontal impact load is introduced to a reinforced concrete cantilever column. An axial load is applied to the free end of the cantilever column. At the top of the column a concentrated mass of 200 kg is situated. The column is 1,6m in length and is 350mm deep and 150mm wide. The horizontal impact load is applied at a height of 0,74m. The set-up is shown in figure 5.1.

This set-up is similar to the set-up used in the experimental investigation described in Chapter 7 and Appendix B. For a more detailed description of the column and the measuring stations, etc. refer to Appendix B.

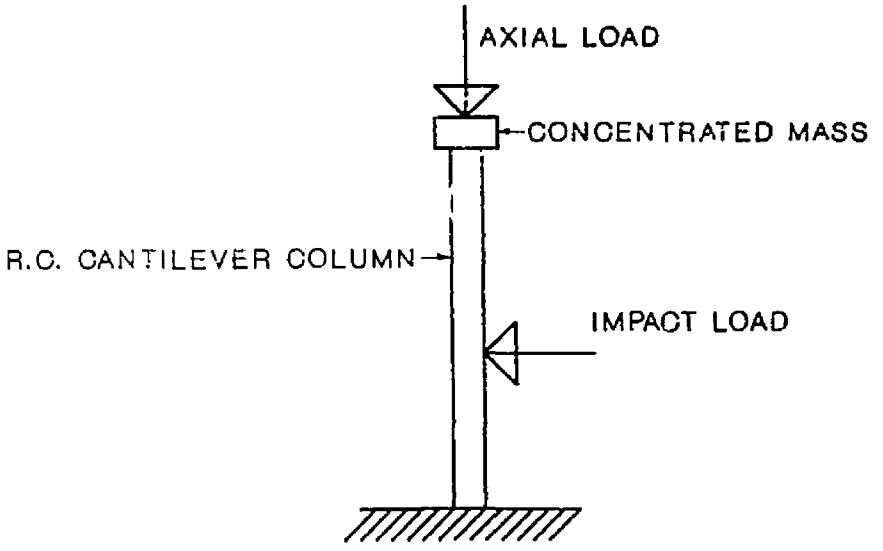

Figure 5.1: The set up of the cantilever column.

Stellenbosch University http://scholar.sun.ac.za

5.2 Introduction to the analytical model

In two recent studies of the beam impact problem, that of Hughes and Speirs (77) and Ammann (10), the Bernoulli-Euler beam theory and the Timoshenko beam theory were used. Hughes and Speirs actually used the simpler Bernoulli-Euler theory of free and forced vibrations of the beam. They indicated that in their specific case it was not necessary to use the mathematically more complicated Timoshenko theory which provide additionally for the shear deformation and the rotatory inertia of the beam. Their beam vibration equations were also mathematically quite simple and this simplified all their calculations. Their results obtained by this theory were very good and they showed that this type of approach is still one of the best methods to explain this problem.

Unfortunately the simple Bernoully-Euler theory cannot explain the behaviour of the column under investigation satisfactorily, because the shear deformation and stiffness as well as the inertia played a significant role. Moreover the column carried an axial load as well as a concentrated mass at the top of the column. All these factors complicated the mathematical modelling.

Most of the available literature (29, 79, 100, 121) on the subject of free vibrations of beams do not include all of the above mentioned additional parameters. Although they indicate that it is possible to add these parameters, they do not follow through with the calculations. This happened because as soon as one provide for these additional factors, the equations differ from beam to beam and the mathematics tend to explode. Whensome literature does investigate thess additional factors they normally investigate only the influence on a simply supported beam and also only for specific vibration modes. An excellent book on the subject of vibrations of such members is that of Magrab (100).

Stellenbosch University http://scholar.sun.ac.za

The rest of this chapter will be used to derive the analytical model and formulae used to predict the behaviour of the column under investigation. First the simplest case of only a cantilever column without provision for shear deformation, the rotatory inertia, an axial load and a concentrated mass at the top of the column will be investigated. This chapter is concluded with a theory which does provide for all the additional factors, but this will only be applicable for this specific case under consideration, although it can be modified to provide for similar cases.

The theories from the simplest to the complicated theory eventually used are given because the one follows from the other and thus the results of the simpler models are used to derive the more complicated models. The discussion of the simpler models or theories will also show why they could not be used for the investigations described in this dissertation.

5.3 Free vibrations of a cantilever column (without shear deformation and rotatory inertia)

In the formulation of continuum equations of motion for the straight non-uniform column shown in Fig. 5.2, the significant physical properties are assumed to be the flexural stiffness EI(x) and the mass per unit length m(x), both of which may vary arbitrarily with position x along the span L. In this case it will be considered that they are constant along the span L. The transverse displacement response y(x,t) is assumed to vary arbitrarily with position and time. The end support conditions, or boundary conditions, are also arbitrarily.

Stellenbosch University http://scholar.sun.ac.za

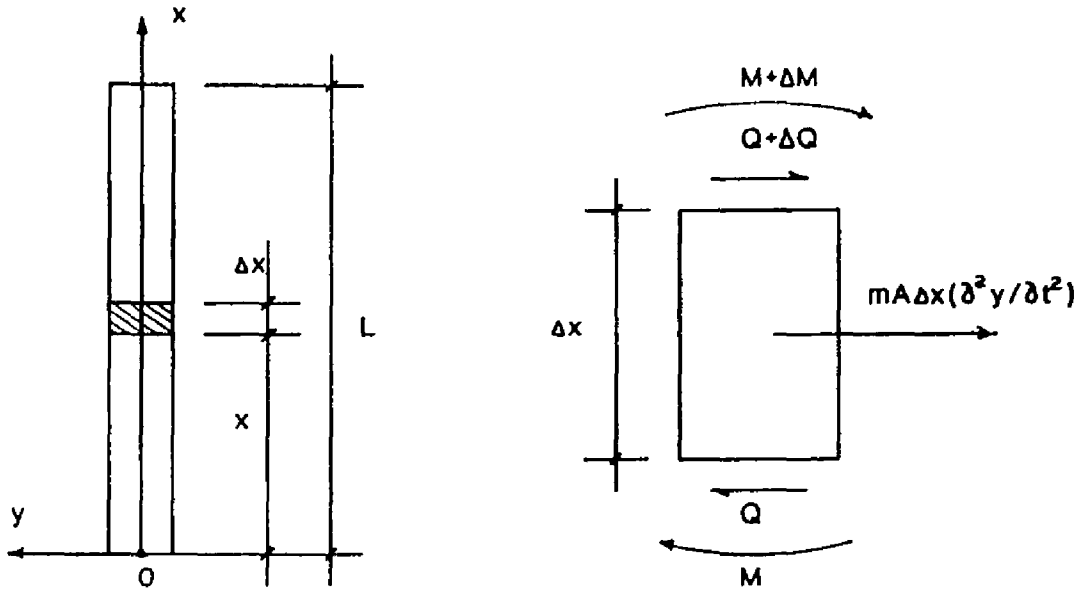

Figure 5.2: Forces on column element during free vibrations.

Inertia force on column element of length Δx is:

$$F_{\Delta m} = mA\Delta x(\partial^2 y/\partial t^2) \qquad (5.1)$$

Moment equilibrium: $(2Q+\Delta Q)\Delta x/2 = \Delta M$

but $Q = \partial M/\partial x = -EI(\partial^3 y/\partial x^3)$

thus $(\partial Q/\partial x) = -EI(\partial^4 y/\partial x^4) \qquad (5.2)$

For force equilibrium: $\Delta Q = m\Delta x(\partial^2 y/\partial t^2)$

but $\partial Q/\partial x = m(\partial^2 y/\partial t^2) \qquad (5.3)$

From (5.2) and (5.3): $EI(\partial^4 y/\partial x^4) + m(\partial^2 y/\partial t^2) = 0 \qquad (5.4)$

Where: A = Area
m = Mass per unit length
Q = Shear force
M = moment
E = Modulus of elasticity
I = Inertia moment

Stellenbosch University http://scholar.sun.ac.za

This equation, known as the simple beam equation, is only an approximation as said previously, because amongst other effects it neglects shear and rotatory inertia.

Assume that the beam displacement y(x,t) can be presented by:

$$y(x,t) = \sum_{i=0}^{\infty} y_i = \sum_{i=0}^{\infty} \emptyset_i(x)\, Y_i(t) \qquad (5.5)$$

In other words, it is assumed that the free vibration motions consist of a constant shape $\emptyset(x)$ and the amplitude which is varying with time according to Y(t). Substitution of Eq.(5.5) into Eq.(5.4) leads to:

$$\emptyset_i^{IV}(x)\, Y_i(t) + (m/EI)\, \emptyset_i(x)\, \ddot{Y}_i(t) = 0 \qquad (5.6)$$

Dividing by $\emptyset_i(x)Y_i(t)$ gives the desired separation:

$$\frac{\emptyset i^{IV}(x)}{\emptyset_i(x)} = a_i^4 = -\frac{m\, \ddot{Y}_i(t)}{EI\, Y_i(t)} \qquad (5.7)$$

Equation (5.7) can be written as:

$$\emptyset_i^{IV}(x) - a_i^4\, \emptyset_i(x) = 0 \qquad (5.8)$$

$$\ddot{Y}_i(t) + \Omega_i^2\, Y_i(t) = 0 \qquad (5.9)$$

where $\Omega_i^2 = (a_i^4 EI)/m$ or $a_i^4 = (m\Omega_i^2)/(EI)$ (5.10)

Equation (5.9) is the familiar free vibration for an undamped SDOF system and has the solution:

$$Y_i(t) = A_i \sin(\Omega_i t) + B_i \cos(\Omega_i t) \qquad (5.11)$$

in which the constants A and B depend on the initial velocity and displacement conditions.

Equation (5.8) can be solved in the usual way by assuming a solution of the form:

$$\emptyset(x) = Ce^{rx} \qquad (5.12)$$

Stellenbosch University http://scholar.sun.ac.za

Substituting (5.12) in (5.6) gives:

$$(s^4 - a^4)Ce^{sx} = 0$$

and thus: $s = \pm a, \pm ia$

Introducing this into (5.12) gives,

$$\emptyset(x) = C_1 e^{ax} + C_2 e^{-iax} + C_3 e^{ax} + C_4 e^{-ax} \qquad (5.13)$$

Expressing these exponential functions in terms of their trigonometric and hyperbolic equivalents, gives:

$$\emptyset(x) = A_1 \sin(ax) + A_2 \cos(ax) + A_3 \sinh(ax) + A_4 \cosh(ax) \qquad (5.14)$$

The four constants A_n in Equation (5.14) define the shape and amplitude of the beam vibration, and they can be evaluated by considering the boundary conditions at the ends of the column segments. The four end conditions may be used to express three of the four constants in terms of the fourth and will also provide an expression (called the frequency equation) from which the frequency parameter a can be evaluated. The fourth constant cannot be evaluated directly in a free vibration analysis, because it defines the amplitude of motion, which depends on the initial condition.

Thus

$$y_i = \{A_{1i}\sin(a_i x) + A_{2i}\cos(a_i x) + A_{3i}\sinh(a_i x) + A_{4i}\cosh(a_i x)\} \{A_i \sin(\Omega_i t) + B_i \cos(\Omega_i t)\} \qquad (5.15)$$

For $\Omega_i = 0$ the displacement is given from (5.7) by,

$$y_o = \{A_{1o}x^3 + A_{2o}x^2 + A_{3o}x + A_{4o}\}\{A_o t + B_o\} \qquad (5.16)$$

This displacement mode may be considered a vibration with zero frequency. The zero mode will be designated $\emptyset_o (i=0)$ and the higher vibration modes by $\emptyset_i (i=1;2;3;4;....)$. All the modes $i=1;2;3;....$ are solutions of the simple beam equation, thus any combination of these modes is also a solution.

Stellenbosch University http://scholar.sun.ac.za

The four boundary conditions for the cantilever column are as follows:

At x = 0: y = 0 and y^I = 0 and thus:

$$\emptyset(0) = 0 \qquad (5.17a)$$

$$\emptyset^I(0) = 0 \qquad (5.17b)$$

At x = L: M = 0 and Q = 0 and thus:

$$M = -EI\emptyset^{II}(L) = 0 \qquad (5.17c)$$

$$Q = -EI\emptyset^{III}(L) = 0 \qquad (5.17d)$$

First consider the zero frequency of the column:

with x = 0 : y_o = 0 and y_o^I = 0

with x = L : y_o^{II} = 0 and y_o^{III} = 0 (5.18)

From equation (5.16):

$$\emptyset_o = A_{1o}x^3 + A_{2o}x^2 + A_{3o}x + A_{4o} \qquad (5.19)$$

Substituting (5.16) into (5.18) gives the following values for the A-constants:

$$A_{1o} = A_{2o} = A_{3o} = A_{4o} = 0 \qquad (5.20)$$

And thus from (5.19) and (5.20) follows that the zero mode solution does not apply in this case because the zero mode equals zero:

$$\emptyset_o = 0$$

Now consider the higher modes, i ≠ 0.

Substitute the four boundary conditions from equations (5.17a-d) into the shape function of equation (5.14):

Stellenbosch University http://scholar.sun.ac.za

$$\emptyset(0) = 0 = A_1\sin(0) + A_2\cos(0) + A_3\sinh(0) + A_4\cosh(0)$$

thus $A_2 = -A_4$

$$\emptyset^{I}(0) = 0 = a\{A_1\cos(0) - A_2\sin(0) + A_3\cosh(0) + A_4\sinh(0)\}$$

thus $A_1 = -A_3$

$$\emptyset^{II}(L) = 0 = a^2\{-A_1\sin(aL) - A_2\cos(aL) + A_3\sinh(aL) + A_4\cosh(aL)\}$$

$$\emptyset^{III}(L) = 0 = a^3\{-A_1\cos(aL) + A_2\sin(aL) + A_3\cosh(aL) + A_4\sinh(aL)\}$$

Thus from the last four equations follows:

$$\begin{bmatrix} \sin(aL) + \mathrm{Sinh}(aL) & \cos(aL) + \cosh(aL) \\ \cos(aL) + \cosh(aL) & \sinh(aL) - \sin(aL) \end{bmatrix} \begin{bmatrix} A_1 \\ A_2 \end{bmatrix} = \begin{bmatrix} 0 \\ 0 \end{bmatrix}$$

For the coefficients to be non-zero, this equation requires that the determinant of the square matrix vanish. Setting this determinant to zero provides the equation known as the frequency equation. Thus the frequency equation for this specific case is given by:

$$1 + \cos(aL)\cosh(aL) = 0 \qquad (5.21)$$

The solution of this trancedential equation then provides the values of aL which represent the frequency of vibration of the cantilever column.

Let $aL = \theta$; then $\Omega_i = \theta_i^2\,[(EI)/(mL^4)]^{0.5}$ (5.22)

The values for θ_i are given in table 5.1.

Table 5.1: Values of θ_i for a simple cantilever column

	i=1	i=2	i=3	i=4	i=5
θ_i	1,875	4,694	7,855	10,996	14,137
For $i \geq 4$: $\theta_i \approx (i-\frac{1}{2})\pi$					

Stellenbosch University http://scholar.sun.ac.za

The coefficient A_2 can be expressed in terms of A_1 and thus equation (5.14) can be expressed in terms of only the first coefficient.

$$\phi_i(x) = A_1[\sin(a_i x) - \sinh(a_i x) + \beta\{\cosh(a_i x) - \cos(a_i x)\}] \tag{5.23}$$

with : $$\beta = \{\sin(a_i L) + \sinh(a_i L)\}/\{\cos(a_i L) + \cosh(a_i L)\} \tag{5.24}$$

By reshuffling the terms and adding the constants to the second part of equation (5.15) one arrives at the following well known shape function of a cantilever beam or column.

$$\phi_i(x) = \frac{\cosh(a_i x) - \cos(a_i x)}{\cos(a_i L) + \cosh(a_i L)} - \frac{\sinh(a_i x) - \sin(a_i x)}{\sin(a_i L) + \sinh(a_i L)} \tag{5.25}$$

5.4 Forced vibrations of a cantilever column (without shear deformation and rotatory inertia)

When the column impact problem is analyzed on the basis of column vibrations, a solution must be found for the equation of the forced vibration of the column:

$$EI(\partial^4 y/\partial x^4) + m(\partial^2 y/\partial t^2) = p(x,t) \tag{5.26}$$

This equation is similar to that for free vibrations but allows additionally for the external force per unit length, p(x,t), on the column. From equation (5.5) follows that y(x,t) is given by (for the non zero modes of the column):

$$y(x,t) = \sum_{i=1}^{\infty} \phi_i(x)\, Y_i(t) \tag{5.27}$$

Substituting equation (5.27) into equation (5.26) gives:

$$\sum_{i=1}^{\infty} m\, \phi_i(x)\, \ddot{Y}_i(t) + \sum_{i=1}^{\infty} \frac{d^2}{dx^2}\left[EI \frac{d^2\phi_i(x)}{dx^2} \right] Y_i(t) = p(x,t) \tag{5.28}$$

Multiply equation (5.28) by $\phi_n(x)$ and then integrate over the length of the beam:

Stellenbosch University http://scholar.sun.ac.za

$$\sum_{i=1}^{\infty} \ddot{Y}_i(t) \int_0^{\ell} m\, \phi_i(x)\, \phi_n(x)\, dx + \sum_{i=1}^{\infty} Y_i(t) \int_0^{\ell} \phi_n(x) \frac{d^2}{dx^2}\left[EI \frac{d^2\phi_i(x)}{dx^2}\right] dx = \int_0^{\ell} \phi_n(x)\, p(x,t)\, dx \qquad (5.29)$$

When the orthogonality relationships existing in the theory of the free vibrations are applied to the first two terms in equation (5.29), all the terms of the series expansions vanish except the n-th terms; thus:

$$\ddot{Y}_n(t) \int_0^{\ell} m\, \phi_n^2(x)\, dx + Y_n(t) \int_0^{\ell} \phi_n(x) \frac{d^2}{dx^2}\left[EI \frac{d^2\phi_n(x)}{dx^2}\right] dx = \int_0^{\ell} \phi_n(x)\, p(x,t)\, dx \qquad (5.30)$$

The motion of the n-th mode can be written as:

$$y_n(x,t) = \phi_n(x)\, Y_n \sin(\Omega_n t) \qquad (5.31)$$

Introducing this equation into the free vibration equation for the n-th mode and then dividing by $Y_n \sin(\Omega_n t)$, results in:

$$EI\, \phi_n^{IV}(x) - m\, \Omega_n^2\, \phi_n(x) = 0$$

Multiply this equation with $\phi_n(x)$ and integrate over column length to give the following:

$$\int_0^{\ell} \phi_n(x) \frac{d^2}{dx^2}\left(EI \frac{d^2\phi_n(x)}{dx^2}\right) dx = \Omega_n^2 \int_0^{\ell} \phi_n^2(x)\, m\, dx \qquad (5.32)$$

The right hand integral of equation (5.32) is the generalized mass of the column associated with the mode shape $\phi_n(x)$. When this mass is denoted by M_n, that is:

$$M_n = \int_0^{\ell} \phi_n^2(x)\, m\, dx \qquad (5.33)$$

The equation of motion can then be expressed in the abbreviated form:

$$M_n \ddot{Y}_n(t) + \Omega_n^2 M_n Y_n(t) = P_n(t) \qquad (5.34)$$

where: $$P_n(t) = \int_0^{\ell} \phi_n(x)\, p(x,t)\, dx \qquad (5.35)$$

Stellenbosch University http://scholar.sun.ac.za

$P_n(t)$ is the generalized load associated with the mode shape $\emptyset_n(x)$. Then the Duhamel integral expression gives:

$$Y_n(t) = \frac{1}{M_n \Omega_n} \int_0^t P_n(\tau) \sin\{\Omega_n(t-\tau)\}\, d\tau \qquad (5.36)$$

For a horizontal point load on the column which is varying with time:

$$\int_0^t P_n(\tau)\, d\tau = \emptyset_n(x_o) \int_0^t p(\tau)\, d\tau \qquad (5.37)$$

where: x_o = the position of the point load
= 0,4635L = 0,74m (for this particular case)

Substituting equations (5.37), (5.36) and (5.33) into equation (5.27), the complete displacement function for the column is given by:

$$y(x,t) = \sum_{n=1}^{\infty} \frac{\emptyset_n(x)\, \emptyset_n(x_o)}{m\, \Omega_n \int_0^L \emptyset_n^2(x)\, dx} \int_0^t p(\tau) \sin\{\Omega_n(t-\tau)\}\, d\tau \qquad (5.38)$$

When the displacement function, $y(x,t)$, is known, the moment at any position on the column, the shear at any position, the mode kinetic energy of the column, the mode potential energy of the column and the total mode energy of the column is known. Thus:

Moment: $M(x,t) = -EI\ (\partial^2 y/\partial x^2)$ (5.39)

Shear: $Q(x,t) = -EI\ (\partial^3 y/\partial x^3)$ (5.40)

Mode kinetic energy: $U_n(t) = \int_0^L \tfrac{1}{2}\, m\, (\partial y_n/\partial x)^2\, dx$ (5.41)

Mode potential energy: $V_n(t) = \int_0^L \tfrac{1}{2}\, EI\, (\partial^2 y_n/\partial x^2)^2\, dx$ (5.42)

Mode total energy: $W_n(t) = U_n(t) + V_n(t)$ (5.43)

The evaluation of equation (5.38) might give some problems and some mathematical manipulations is normally necessary. The value of $\emptyset_n(x)$ is given by eq. (5.25). According to Goldsmith (56):

Stellenbosch University http://scholar.sun.ac.za

$$\int_0^L \phi_n^2(x)\,dx = L\left[\frac{\cos^2(\theta_n)}{\sin^4(\theta_n)}\right] \qquad (5.44)$$

Equation (5.38) can be simplified to:

$$y(x,t) = \frac{1}{m\,L}\sum_{n=1}^{\infty}\left[\frac{z_n}{\Omega_n}\int_0^t p(\tau)\,\sin\{\Omega_n(t-\tau)\}\,d\tau\right] \qquad (5.45)$$

$$z_n = \left\{\frac{\sin^4(\theta_n)}{\cos^2(\theta_n)}\right\}\left[\frac{b}{c}-\frac{d}{e}\right]\left[\frac{f}{c}-\frac{g}{e}\right] \qquad (5.46)$$

with: $b = \cosh(a_n x) - \cos(a_n x)$

$c = \cosh(a_n L) + \cos(a_n L)$

$d = \sinh(a_n x) - \sin(a_n x)$

$e = \sinh(a_n L) + \sin(a_n L)$

$f = \cosh(a_n x_o) - \cos(a_n x_o)$

$g = \sinh(a_n x_o) - \sin(a_n x_o)$

The calculation of z_n involves numerical difficulties. It is inadvisable to use equation (5.46) as given, because it is numerical unstable. If the frequency equation, (5.21) is rewritten as:

$$\cos(\theta) = 1/\cosh(\theta)$$

it can be seen that for large θ, the right hand side is close to zero, so that the solutions are close to odd multiples of $\pi/2$, i.e.: $\theta_n = (n-\frac{1}{2})\pi$

Hence the solutions of θ_n occurs at values such that $\cos(\theta) \approx 0$, and $\cos(\theta_n)$ appears as a divisor in eq. (5.46) and thus also in eq. (5.45). However this equation, eq. (5.45), can be simplified at the solutions of θ_n, thus:

Stellenbosch University http://scholar.sun.ac.za

$$\cos(\theta)\{\cosh(\theta)+\cos(\theta)\} = \cos(\theta)\cosh(\theta) + \cos^2(\theta)$$

$$= -1 + \cos^2(\theta)$$

$$= -\sin^2(\theta)$$

Thus: $\{\sin^4(\theta)/\cos^2(\theta)\}/c^2 = [\sin^2(\theta)]/[\cos(\theta)\{\cosh(\theta)+\cos(\theta)\}]^2$

$$= \{\sin^4(\theta)\}/\{\sin^4(\theta)\} = 1$$

Therefore: $z_n = \{bfe^2 - ce(bg + fd) + c^2dg\}/e^2$ (5.47)

This expression for z_n avoids division by zero and should rather be used. The final expression for the displacement of the column is given by the following expression with z_n given by eq. (5.47)

$$y(x,t) = \frac{1}{m\,L}\sum_{n=1}^{\infty}\left[\frac{z_n}{\Omega_n}\int_0^t p(\tau)\,\sin\{\Omega_n(t-\tau)\}\,d\tau\right]$$

$$y(x,t) = \frac{1}{m\,L}\sum_{n=1}^{\infty}\frac{z_n}{\Omega_n}\left[\sin(\Omega_n t)\int_0^t p(\tau)\,\cos(\Omega_n\tau)d\tau - \cos(\Omega_n t)\int_0^t p(\tau)\,\sin(\Omega_n\tau)\,d\tau\right] \quad (5.48)$$

With a known load function equation (5.48) can easily be evaluated by numerical integration and summation of all the applicable modes. This means that the deflection function of the column is known and thus all the functions previously mentioned are also known.

Unfortunately this relative simple theory could not be used for the column under investigation. The first factor that had a significant influence on the behaviour of the column was the concentrated mass present at the top of the column. This mass influenced the frequency of the column remarkably. This means that this theory could not predict the behaviour of the column under investigation at all.

If a column without a concentrated mass at the top is to be investigated, this theory might be appropriate if the column is a slender column. If the column is not very slender, the shear

Stellenbosch University http://scholar.sun.ac.za

deformation and inertia as well as the rotatory inertia will influence the frequency of the column and thus this theory might not be appropriate. If only the first mode for such a case is necessary this theory can be used, because the first mode for a column (without provision for shear and rotationary inertia) is very close to a similar column with provision for shear and rotationary inertia. The higher the mode the bigger the percentage change between the frequencies for the above mentioned columns. Note that these two columns do not have a concentrated mass at the top. The change in frequencies for the above mentioned theories is clearly visible in table 5.2.

From the above it is clear that this particular theory was not applicable for the column under investigation although it might be used for other cantilever columns with different circumstances.

It was however necessary to derive this theory to understand the next theories and to indicate why this theory could not be used for the column under investigation, and because this theory might be applicable for other types of cantilever columns.

5.5 Free vibrations of a cantilever column with a concentrated mass at the top of the column (without provision for shear deformation and rotatory inertia)

The model is exactly the same as before except for a concentrated mass present at the top of the column. The influence of this concentrated mass on the column is that it changes the boundary conditions at the free end of the column. The moment and shear at the free end no longer vanish because of the inertia of the mass. The rotational and transverse forces acting on the end mass, shown in fig. 5.3 lead to the boundary condition equations:

$$EI\ \emptyset''(L) - \Omega^2\ \emptyset'(L)\ J = 0 \qquad (5.49)$$

$$EI\ \emptyset'''(L) + \Omega^2\ \emptyset(L)\ M_b = 0 \qquad (5.50)$$

Stellenbosch University http://scholar.sun.ac.za

Where: M_o = Mass of the concentrated mass at top of column.

For this theory all the equations up to and including equation (5.16) are exactly the same and that section will not be repeated here. The zero mode in this case is also zero and does not apply.

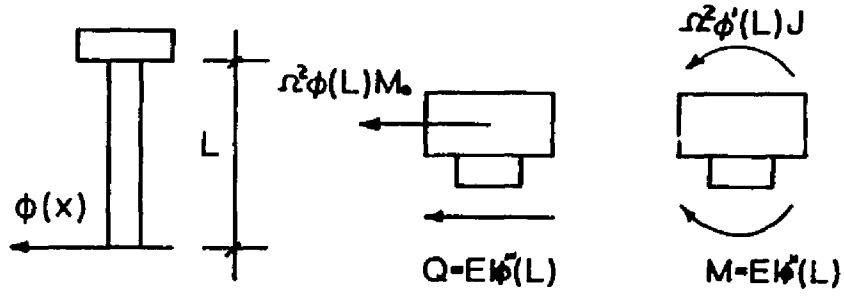

Figure 5.3: Column with concentrated mass at free end

In the specific case under investigation there was no inertia moment at the free end of the column due to the concentrated mass, because there was a hinge coupling between the mass and the column. In other words no moment could be transferred from the mass to the column but a shear force could be transferred.

The boundary conditions for a cantilever column with a concentrated mass at the free end with a hinge coupling between the column and the mass are:

At x = 0: $y = 0$ and $y^{I} = 0$ and thus:

$$\emptyset(0) = 0 \qquad (5.51a)$$

$$\emptyset^{I}(0) = 0 \qquad (5.51b)$$

At x = L: $M = 0$ and $Q = -\Omega^2 \emptyset(L) M_o$

$$\emptyset^{II}(L) = 0 \qquad (5.51c)$$

$$\emptyset^{III}(L) = -(\Omega^2/EI)\,\emptyset(L)\,M_o$$

$$\therefore \; -\mu a^4 L \emptyset(L) \qquad (5.51d)$$

Stellenbosch University http://scholar.sun.ac.za

With: $\mu = M_o/mL$ (5.52)

and a^4 as given by equation (5.10)

Substitute the four boundary conditions from equations (5.51a-d) into the shape function of equation (5.14):

$$\emptyset(0) = 0 = A_1\sin(0) + A_2\cos(0) + A_3\sinh(0) + A_4\cosh(0)$$

thus $A_2 = -A_4$

$$\emptyset^I(0) = 0 = a\{A_1\cos(0) - A_2\sin(0) + A_3\cosh(0) + A_4\sinh(0)\}$$

thus $A_1 = -A_3$

$$\emptyset^{II}(L) = 0 = a^2\{-A_1\sin(aL) - A_2\cos(aL) + A_3\sinh(aL) + A_4\cosh(aL)\}$$

$$\begin{aligned}\emptyset^{III}(L) &= -\mu a^4 L\{A_1\sin(aL) + A_2\cos(aL) + A_3\sinh(aL) + A_4\cosh(aL)\} \\ &= a^3\{-A_1\cos(aL) + A_2\sin(aL) + A_3\cosh(aL) + A_4\sinh(aL)\}\end{aligned}$$

$$\begin{aligned}&\{\mu aL\sin(aL) - \cos(aL) - \mu aL\sinh(aL) - \cosh(aL)\}A_1 \\ &+ \{\mu aL\cos(aL) + \sin(aL) - \mu aL\cosh(aL) - \sinh(aL)\}A_2 = 0\end{aligned}$$

Let: $h = \sin(aL) + \sinh(aL)$

$j = \cos(aL) + \cosh(aL)$

$k = \mu aL\sin(aL) - \cos(aL) - \mu aL\sinh(aL) - \cosh(aL)$

$l = \mu aL\cos(aL) + \sin(aL) - \mu aL\cosh(aL) - \sinh(aL)$

Then from the four boundary conditions and the four previous equations follows:

$$\begin{bmatrix} h & j \\ k & l \end{bmatrix} \begin{bmatrix} A_1 \\ A_2 \end{bmatrix} = \begin{bmatrix} 0 \\ 0 \end{bmatrix}$$

For the coefficients to be non-zero, this equation requires that the determinant of the square matrix vanish. Setting this determinant to zero provides the frequency equation for the cantilever column with a concentrated mass at the free end. The frequency equation for this specific case is then given by:

$$hl - kj = 0 \quad (5.53)$$

Stellenbosch University http://scholar.sun.ac.za

According to Magrab (100) this frequency equation can be simplified to:

$$\mu aL\,\{\tanh(aL) - \tan(aL)\} + 1 + \sec(aL)\,\mathrm{sech}(aL) = 0 \qquad (5.54)$$

From equations (5.54), (5.53) and (5.52) it is obvious that the frequency of this column is directly dependent on μ, or the ratio between the total mass of the column and the mass of the concentrated mass at the free end of the column. For the column under investigation the value of $\mu \approx 1$. When $M_o = 0$ equation (5.54) reduces to equation (5.21). When $M_o \rightarrow \infty$ equation (5.54) becomes:

$$\tanh(aL) - \tan(aL) = 0 \qquad (5.55)$$

which yields the natural frequency coefficient for a column clamp at the one end and simply supported at the other end.

With $aL = \theta$, the values of θ_i are given in table 5.2 for different values of μ.

Table 5.2: Values of θ_i for a cantilever column with a concentrated mass at the free end.

mode i \ μ	0	.1	1	10	∞
1	1,87509	1,72276	1,24790	0,73579	0,00000
2	4,69416	4,39949	4,03129	3,93861	3,92668
3	7,85461	7,45091	7,13424	7,07549	7,69690
4	10,99557	10,52182	10,25699	10,21520	10,21018
5	14.13717	13,61409	13,38790	13,35554	13,35177
6	17,27876	16,71956	16,52258	16,49650	16,49336
7	20,42035	19,83350	19,65977	19,63747	19,63495
8	23,56194	22,95342	22,79791	22,77875	22,77655

Again the coefficient A_2 can be expressed in terms of A_1 and by adding the constant A_1 to the second part of equation (5.15) the shape function of the cantilever column can be derived.

$$\emptyset_i(x) = \sin(a_i x) \quad \sinh(a_i x) + \beta\{\cosh(a_i x) - \cos(a_i x)\} \qquad (5.56)$$

with :

$$\beta = \{\sin(a_i L) + \sinh(a_i L)\}/\{\cos(a_i L) + \cosh(a_i L)\} \qquad (5.57)$$

Stellenbosch University http://scholar.sun.ac.za

5.6 Forced vibration of a cantilever column with a concentrated mass at the free end (without shear deformation and rotatory inertia taken into account)

This theory is very similar to the first theory. Again a solution must be found for the forced vibration equation of this column:

$$EI(\partial^4 y/\partial x^4) + m(\partial^2 y/\partial t^2) = p(x,t) - \mu mL(\partial^2 y/\partial t^2) \quad (5.58)$$

Again the deflection is given by:

$$y(x,t) = \sum_{i=1}^{\infty} \emptyset_i(x)\, Y_i(t) \quad (5.59)$$

Substituting equation (5.59) into (5.58) gives:

$$\sum_{i=1}^{\infty} m\, \emptyset_i(x)\, \ddot{Y}_i(t) + \sum_{i=1}^{\infty} \frac{d^2}{dx^2}\left[EI\frac{d^2\emptyset_i(x)}{dx^2}\right] Y_i(t) = p(x,t) - \sum_{i=1}^{\infty} \mu mL\emptyset_i(x)\ddot{Y}_i(t) \quad (5.60)$$

Multiply equation (5.60) by $\emptyset_n(x)$ and then integrate over the length of the column and then apply the orthogonality relationships. This will result that all the terms of the series expansions will vanish except the n-th terms, resulting in:

$$\ddot{Y}_n(t)\int_0^L m\,\emptyset_n^2(x)\,dx + Y_n(t)\int_0^L \emptyset_n(x)\,\frac{d^2}{dx^2}\left[EI\,\frac{d^2\emptyset_n(x)}{dx^2}\right] dx = \int_0^L \emptyset_n(x)\, p(x,t)\, dx - \mu mL\,\emptyset_n(L)\,\ddot{Y}_n(t) \quad (5.61)$$

The motion of the n-th mode can be written as:

$$y_n(x,t) = \emptyset_n(x)\, Y_n \sin(\Omega_n t) \quad (5.62)$$

Introducing this equation into the free vibration equation for the n-th mode and then dividing by $Y_n\sin(\Omega_n t)$, results in:

$$EI\,\emptyset^{IV}(x) - m\Omega_n^2\,\emptyset_n(x) - m\mu L\Omega_n^2\,\emptyset_n(x) = 0$$

Multiplying this equation by $\emptyset_n(x)$ and integrate over the column length to give:

Stellenbosch University http://scholar.sun.ac.za

$$\int_0^L \phi_n(x) \frac{d^2}{dx^2}\left(EI \frac{d^2\phi_n(x)}{dx^2}\right) dx = \Omega_n^2 \left[m\int_0^L \phi_n^2(x)\, dx + \mu mL\phi_n^2(L) \right] \qquad (5.64)$$

The term in the square brackets on the right hand side of equation (5.64) is the generalized mass of the column and the concentrated mass associated with the mode shape $\phi_n(x)$. When this mass is denoted by M_n, that is:

$$M_n = m \left\{ \int_0^L \phi_n^2(x)dx + \mu L\, \phi_n^2(L) \right\} \qquad (5.65)$$

The equation of motion can then be expressed in the abbreviated form:

$$M_n \ddot{Y}_n(t) + \Omega_n^2 M_n Y_n(t) = P_n(t) \qquad (5.66)$$

where: $$P_n(t) = \int_0^t \phi_n(x)\, p(x,t)\, dx \qquad (5.67)$$

$P_n(t)$ is the generalized load associated with the mode shape $\phi_n(x)$. Then the Duhamel integral expression gives:

$$Y_n(t) = \frac{1}{M_n \Omega_n} \int_0^t P_n(\tau) \sin\{\Omega_n(t-\tau)\}\, d\tau \qquad (5.68)$$

For a horizontal point load on the column which is varying with time:

$$\int_0^t P_n(\tau)\, d\tau = \phi_n(x_o) \int_0^t p(\tau)\, d\tau \qquad (5.69)$$

where: x_o = the position of the point load
= 0,4635L = 0,74m (for this particular case)

Substituting equations (5.69), (5.68) and (5.65) into equation (5.59), the complete displacement function for a cantilever column with a concentrated mass at the free end is known:

$$y(x,t) = \sum_{n=1}^{\infty} \frac{\phi_n(x)\, \phi_n(x_o)}{\{m\, \Omega_n [\mu L\phi_n^2(L) + \int_0^L \phi_n^2(x)dx\ ]\}} \int_0^t p(\tau) \sin\{\Omega_n(t-\tau)\}\, d\tau \qquad (5.70)$$

When the displacement function is known, the moment, the shear, the mode kinetic energy, the mode potential energy and the total

Stellenbosch University http://scholar.sun.ac.za

mode energy of the column can be calculated from equations (5.39) to (5.43).

Each parameter of equation (5.70) is quite easy to calculate, except one of the terms of the denominator which is given by:

$$\int_0^L \emptyset_n^2(x)\,dx = (L/4\theta_n)\,\{\theta_n + \tfrac{1}{4}(1-\beta_n^2)\sin(2\theta_n) + \tfrac{1}{4}(1+\beta_n^2)\sinh(2\theta_n) - \tfrac{1}{2}\beta_n\cos(2\theta_n) + \tfrac{1}{2}\beta_n\cosh(2\theta_n) + (\beta^2-1)\cos(\theta_n)\sinh(\theta_n) - (\beta^2+1)\sin(\theta_n)\cosh(\theta_n) - 2\beta_n\sin(\theta_n)\sinh(\theta_n)\} \qquad (5.71)$$

with: $$\beta = \{\sin(\theta_n) + \sinh(\theta_n)\} / \{\cos(\theta_n) + \cosh(\theta_n)\} \qquad (5.57)$$

and: $$\emptyset_n(x) = \sin(a_n x) - \sinh(a_n x) + \beta\{\cosh(a_n x) - \cos(a_n x)\} \qquad (5.56)$$

Thus the final expression for the displacement of a cantilever column with a concentrated mass at the top of the column is given by the following expression:

$$y(x,t) = \sum_{n=1}^{\infty} \frac{\emptyset_n(x)\,\emptyset_n(x_o)}{\{m\,\Omega_n[\mu L\emptyset_n^2(L) + \int_0^L \emptyset_n^2(x)dx\,]\}} \int_0^t p(\tau)\sin\{\Omega_n(t-\tau)\}\,d\tau \qquad (5.70)$$

with:

$$\int_0^t p(\tau)\sin\{\Omega_n(t-\tau)\}\,d\tau = \sin(\Omega_n t)\int_0^t p(\tau)\cos(\Omega_n\tau)d\tau - \cos(\Omega_n t)\int_0^t p(\tau)\sin(\Omega_n\tau)\,d\tau\,] \qquad (5.72)$$

With a known load function, equations (5.70) to (5.72) can easily be evaluated by numerical integration and summation for all the applicable modes of the column.

Stellenbosch University http://scholar.sun.ac.za

Once again this theory was not used for the columns under investigation because it did not allow for the shear deformation and the rotatory inertia of the column and as previously mentioned these two factors play quite an important role in the behaviour of this column, due to its very low slenderness. The shear deformation and rotatory inertia tend to change the frequency of the column, especially the frequency of the higher modes of vibration. This means that if one is only interested in say the first mode of vibration for what ever reason, this theory will be more than adequate and the more complicated theory that does provide for the additional factors will not be necessary.

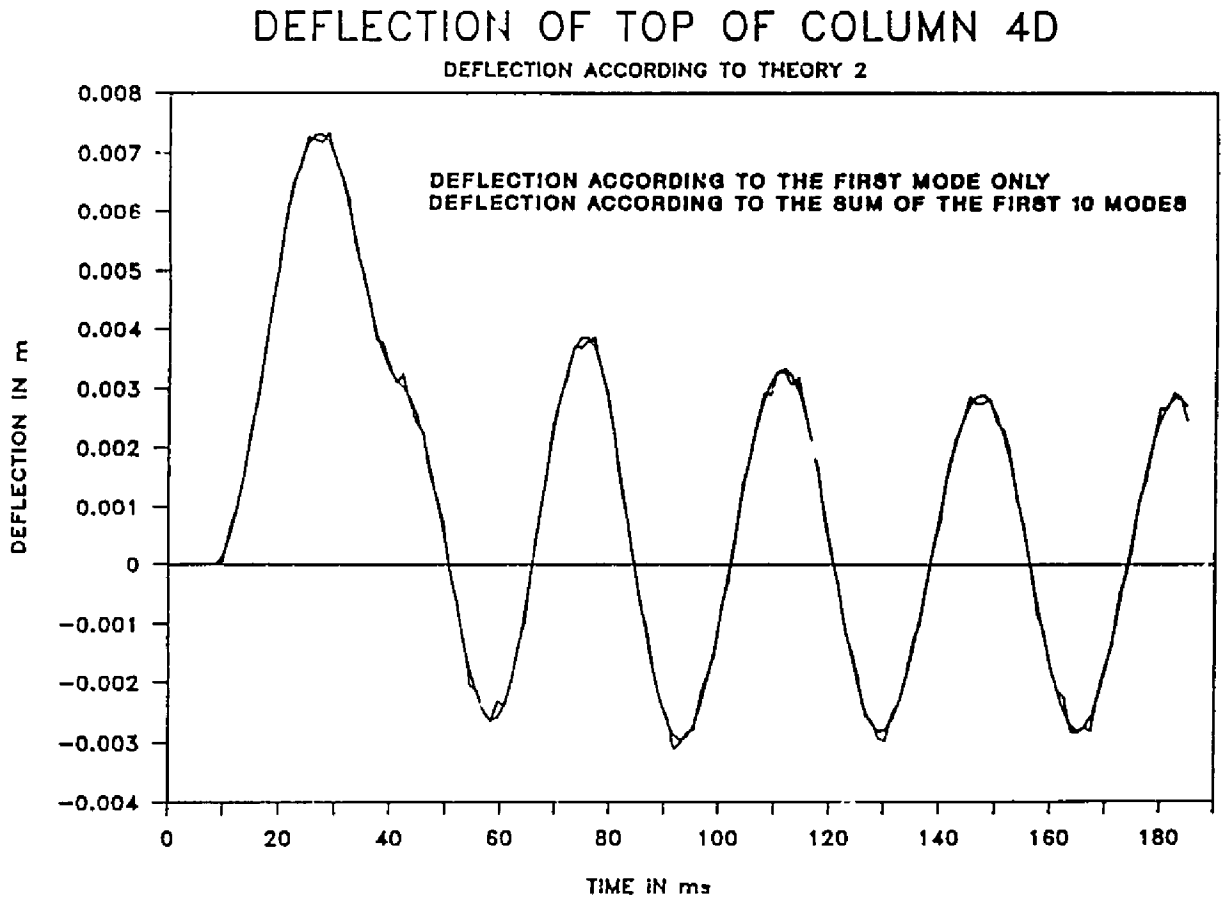

Figure 5.4: Deflection of the top of a typical column according to the second theory.

Note that according to this theory the moments and shears in the column are much more dependent on the vibration frequency coefficient **a**, because the factor, **a**, appears in the numerator of

Stellenbosch University http://scholar.sun.ac.za

the moment function as a second power and in the shear function as a third power but in the displacement function it does not appear in the numerator. This also means that the moment and shear functions will converge more slowly than the displacement function. This is clearly visible in fig. 5.4, where the first mode of the deflection of a typical column is plotted with the sum of the first ten modes of the same column. (This plot is according to this second theory and not the final theory.) This frequency influence on the deflection, moment and shear of the column also explains why this theory's deflection of the top of the column is very similar to that of the next theory. Unfortunately their moment and shear differ so much that this theory does not give an accurate account of the shear and moment behaviour of the columa under investigation.

In other words if one is only interested in the deflection of the column, this theory will give a very good simulation of the behaviour of the column, but if one is interested in the moment and shear behaviour this theory will not be adequate to predict the response of the column.

5.7 Free vibrations of a cantilever column with a concentrated mass at the top of the column, with a constant axial load on the column and with provision for shear deformation and rotatory inertia.

With this theory provision is made for the axial load on the column that is present as well as for shear deformation and rotatory inertia of the column. The boundary conditions for this column is exactly the same as that for the second theory, but the shape function for this theory is different.

The effects of the axial load, shear deformation and rotatory inertia on the free vibrations of a column can be evaluated from the equation of motion, which reads as follows:

Stellenbosch University http://scholar.sun.ac.za

$$EI\frac{\partial^4 y}{\partial x^4} + N\frac{\partial^2 y}{\partial x^2} + m\frac{\partial^2 y}{\partial t^2} - \underbrace{mr^2\frac{\partial^4 y}{\partial x^2 \partial t^2}}_{\text{Rotationary}} + \underbrace{\frac{m}{\alpha AG}\left(mr^2\frac{\partial^4 y}{\partial t^4}\right)}_{\text{Shear and rotationary}} - \underbrace{EI\frac{\partial^4 y}{\partial x^2 \partial t^2}}_{\text{Shear deformation}} = 0 \qquad (5.72)$$

With: N = Axial load on column

m = Mass of column per unit length

r^2 = I/A = Radius of gyration of the cross section

αA = Effective shear area of the section

α = Area reduction factor

= 5/6 for a rectangular section

G = Modulus of shear

E = Strain modulus

I = Second moment of area

Assume that the column displacement y(x,t) can be presented by:

$$y(x,t) = \sum_{i=0}^{\infty} y_i = \sum_{i=0}^{\infty} \emptyset_i(x)\, Y_i(t) \qquad (5.5)$$

Or in short: $y(x,t) = \emptyset(x)\, Y(t)$ (5.73)

Substituting equation (5.73) into (5.72):

$$EI\, \emptyset^{IV}(x)\, Y(t) + N\, \emptyset^{II}(x)\, Y(t) + m\, \emptyset(x)\, \ddot{Y}(t) - mr^2\, \emptyset^{II}(x)\, \ddot{Y}(t) + \{m/\alpha AG\}\{mr^2\, \emptyset(x)\, \ddot{\ddot{Y}}(t) - EI\, \emptyset^{II}(x)\, \ddot{Y}(t)\} = 0 \qquad (5.74)$$

It can be shown that the contribution of the term $\{(m/\alpha AG)mr^2\, \emptyset(x)\, \ddot{\ddot{Y}}(t)\}$ is very small and thus to simplify the rest of the theory this term will be omitted.

Assume that $y(x,t) = \emptyset(x)Y\sin(\Omega t)$ and then divide by $Y\sin(\Omega t)$:

Stellenbosch University http://scholar.sun.ac.za

$$EI\emptyset^{IV}(x) + N\emptyset^{II}(x) - m\Omega^2\emptyset(x) + m\Omega^2r^2\emptyset^{II}(x) + (m\Omega^2/\alpha AG)EI\emptyset^{II}(x) = 0 \qquad (5.75)$$

Let $a^4 = (m\Omega^2/EI)$ (5.10)

Divide by EI:

$$\emptyset^{IV}(x) + \{N/EI + a^4r^2(1 + E/\alpha G)\}\emptyset^{II}(x) - a^4\emptyset(x) = 0 \qquad (5.76)$$

Let: $g^2 = N/EI + a^4r^2(1 + E/\alpha G)$ (5.77)

Substituting Equation (5.77) into equation (5.76):

$$\emptyset^{IV}(x) + g^2\,\emptyset^{II}(x) - a^4\,\emptyset(x) = 0 \qquad (5.78)$$

The solution for eq. (5.78) can be obtained in the standard way by assuming a solution of:

$$\emptyset(x) = Ce^{sx} \qquad (5.79)$$

Thus $(s^4 + g^2s^2 - a^4)Ce^{sx} = 0$ (5.80)

With the solution for s: $s = \pm i\delta \pm \epsilon$ (5.81)

With: $\delta = [(a^4 + g^4/4)^{0.5} + g^2/2]^{0.5}$ (5.82)

and $\epsilon = [(a^4 + g^4/4)^{0.5} - g^2/2]^{0.5}$ (5.83)

This leads to the shape function:

$$\emptyset(x) = D_1 \sin(\delta x) + D_2 \cos(\delta x) + D_3 \sinh(\epsilon x) + D_4 \cosh(\epsilon x) \qquad (5.84)$$

The four constants D_n define the shape and amplitude of the column vibration and they can be evaluated by considering the boundary conditions at the ends of the column segments. The four end conditions may be used to express three of the four constants in terms of the fourth and will also provide an expression (the frequency equation) from which the frequency parameter, a, can be evaluated. The fourth constant cannot be evaluated directly in a

Stellenbosch University http://scholar.sun.ac.za

free vibration analysis, because it defines the amplitude of motion, which depends on the initial condition.

The four boundary conditions for the cantilever column under investigation are:

At x = 0: $y = 0$ and $y^I = 0$ and thus:

$$\emptyset(0) = 0 \qquad (5.85a)$$

$$\emptyset^I(0) = 0 \qquad (5.85b)$$

At x = L: $M = 0$ and $Q = -\Omega^2\, \emptyset(L)\, M_o$

$$\emptyset^{II}(L) = 0 \qquad (5.85c)$$

$$\emptyset^{III}(L) = -(\Omega^2/EI)\, \emptyset(L)\, M_o$$

$$= -\mu\, a^4\, L\, \emptyset(L) \qquad (5.85d)$$

With: $$\mu = M_o/mL \qquad (5.52)$$

M_o = Mass of the concentrated mass at free end

mL = Mass of the column

and a^4 as given by equation (5.10)

Substitute the four boundary conditions of equations (5.85a-d) into the shape function of equation (5.84):

$$\emptyset(0) = 0 = D_1\sin(0) + D_2\cos(0) + D_3\sinh(0) + D_4\cosh(0)$$

thus: $$D_2 = -D_4$$

$$\emptyset^I(0) = 0 = \delta D_1\cos(0) - \delta D_2\sin(0) + \epsilon D_3\cosh(0) + \epsilon D_4\sinh(0)$$

thus: $$D_3 = -(\delta/\epsilon)D_1$$

$$\emptyset^{II}(L) = 0$$

$$= -\delta^2 D_1\sin(\delta L) - \delta^2 D_2\cos(\delta L) + \epsilon^2 D_3\sinh(\epsilon L) + \epsilon^2 D_4\cosh(\epsilon L)$$

Stellenbosch University http://scholar.sun.ac.za

thus: $\{\delta^2\sin(\delta L) + \delta\epsilon\sinh(\epsilon L)\}D_1 + \{\delta^2\cos(\delta L) + \epsilon^2\cosh(\epsilon L)\}D_2 = 0$

$$\phi'''(L) = -\mu a^4 L \{D_1\sin(\delta L) + D_2\cos(\delta L) + D_3\sinh(\epsilon L) + D_4\cosh(\epsilon L)\}$$

$$= -\delta^3 D_1\cos(\delta L) + \delta^3 D_2\sin(\delta L) + \epsilon^3 D_3\cosh(\epsilon L) + \epsilon^3 D_4\sinh(\epsilon L)$$

thus:

$$\{\mu a^4 L\sin(\delta L) - (\mu\delta a^4 L/\epsilon)\sinh(\epsilon L) - \delta^3\cos(\delta L) - \delta\epsilon^2\cosh(\epsilon L)\}\ D_1$$

$$+ \{\mu a^4 L\cos(\delta L) - \mu a^4 L\cosh(\epsilon L) + \delta^3\sin(\delta L) - \epsilon^3\sinh(\epsilon L)\}\ D_2 = 0$$

Let:

$$h = \delta^2\sin(\delta L) + \delta\epsilon\sinh(\epsilon L) \qquad (5.86a)$$

$$j = \delta^2\cos(\delta L) + \epsilon^2\cosh(\epsilon L) \qquad (5.86b)$$

$$k = \mu a^4 L\sin(\delta L) - (\mu\delta a^4 L/\epsilon)\sinh(\epsilon L) - \delta^3\cos(\delta L) - \delta\epsilon^2\cosh(\epsilon L) \qquad (5.86c)$$

$$l = \mu a^4 L\cos(\delta L) - \mu a^4 L\cosh(\epsilon L) + \delta^3\sin(\delta L) - \epsilon^3\sinh(\epsilon L) \qquad (5.86d)$$

Then from the four boundary conditions and the four previous equations follows:

$$\begin{bmatrix} h & j \\ k & l \end{bmatrix} \begin{bmatrix} D_1 \\ D_2 \end{bmatrix} = \begin{bmatrix} 0 \\ 0 \end{bmatrix} \qquad (5.87)$$

For the coefficients to be non-zero, equation (5.87) requires that the determinant of the square matrix vanish. Setting this determinant to zero provides the frequency equation for the cantilever column under investigation. The frequency equation is then given by:

$$hl - kj = 0 \qquad (5.88)$$

From equations (5.52), (5.76), (5.77), (5.82) and (5.83) it is quite evident that the frequency parameter, **a**, is dependent on nearly all the parameters of a specific column. For example it is dependent on N, E, I, α, G, r and μ (or in other words of the

Stellenbosch University http://scholar.sun.ac.za

ratio between the concentrated mass and the mass of the column). This dependency make it nearly impossible to derive a universal formula or theory for the frequency of this type of columns. The influence of E is relative small if one is working with the normal type of concrete. The influence of the axial load, N, is also quite small. Their influence will be discussed later in the thesis.

The influence of the I value is significant in calculating the frequency factor. The Army Corps of Engineers (145) recommended that, to account for the cracking of the concrete, an average moment of inertia should be used which is based on the following expression:

$$I_a = \frac{1}{2} (I + I_{cr}) \qquad (5.89)$$

where: I_a = average inertia moment of the concrete section

I = moment of the gross concrete section (neglecting the steel area)

I_{cr} = moment of inertia of the cracked section

Others like Hughes and Speirs (77) used only the inertia moment of the cracked section because they assume that the concrete section cracked very soon after the impact load is applied to the column.

A typical column under investigation had the following parameters:

$N = 100$ kN

$E = 26$ GPa

$I = (1/12)bh^3 = 5.359 \times 10^{-4}$ m^4

$I_{cr} = 0,045\ bh^3 = 2.894 \times 10^{-4}$ m^4

$I_a = \frac{1}{2} (I + I_{cr}) = 4.127 \times 10^{-4}$ m^4

Stellenbosch University http://scholar.sun.ac.za

$\alpha = 5/6$

$G = \{E/2(1+\nu)\}$ and $E/\alpha G = 2(1+\nu)/\alpha = 2.88$

$r^2 = I/A$

$M_b = mL$ and thus $\mu = 1$

The values for a_n and θ_n for the given parameters is given in table 5.3.

Table 5.3: Values of a_n and θ_n for a cantilever column with the above mention parameters

I	I_a	I_{cr}	I_a	I_{cr}
mode n	a_n	a_n	θ_n	θ_n
1	0,780927	0,780955	1,249483	1,2495280
2	2,43791924	2,46054196	3,9006708	3.9368670
3	4,02109979	4,12943832	6,4337597	6,607:013
4	5,31247798	5,54508441	8,4999668	8,8721351
5	6,37887359	6,73915856	10,2061978	10,7826537
6	7,28663266	7,76356561	11,6586123	12,4217050
7	8,08291145	8,66268369	12,9326583	13,8602939
8	8,79797841	9,46828977	14,0767655	15,1492636
9	9,45172842	10,20243200	15,1227655	16,3238912
10	10,05743169	10,88043849	16,0918907	17,4087016

The coefficient D_2 can be expressed in terms of D_1 and by adding the constant D_1 to the second part of equation (5.15), the shape function for this cantilever column can be derived:

$$\emptyset_1(x) = \sin(\delta_1 x) - (\delta_1/\epsilon_1)\sinh(\epsilon_1 x) + \beta_1 \{\cosh(\epsilon_1 x) - \cos(\delta_1 x)\} \quad (5.90)$$

with:

$$\beta_1 = \{\delta_1^2 \sin(\delta_1 L) + \delta_1 \epsilon_1 \sinh(\epsilon_1 L)\} / \{\delta_1^2 \cos(\delta_1 L) + \epsilon_1^2 \cosh(\epsilon_1 L)\} \quad (5.91)$$

Stellenbosch University http://scholar.sun.ac.za

5.8 Forced vibration of a cantilever column with a concentrated mass at the top of the column, with an axial load on the column and with provision for shear deformation and rotatory inertia.

A solution must be found for the forced vibration equation for this column:

$$EI\frac{\partial^4 y}{\partial x^4} + N\frac{\partial^2 y}{\partial x^2} + m\frac{\partial^2 y}{\partial t^2} - mr^2\frac{\partial^4 y}{\partial x^2 \partial t^2} - \frac{m}{\alpha AG}\left(EI\frac{\partial^4 y}{\partial x^2 \partial t^2}\right) = p(x,t) - \mu mL(\partial^2 y/\partial t^2) \qquad (5.92)$$

Assume that the displacement function can be presented by:

$$y(x,t) = \sum_{i=1}^{\infty} \emptyset_i(x)\, Y_i(t) \qquad (5.93)$$

Substitute equation (5.93) into equation (5.92):

$$\sum_{i=1}^{\infty} m\, \emptyset_i(x)\, \ddot{Y}_i(t) + \sum_{i=1}^{\infty} \frac{d^2}{dx^2}\left[EI\frac{d^2\emptyset_i(x)}{dx^2}\right]Y_i(t) + \sum_{i=1}^{\infty} N\, Y_i(t)\, \frac{d^2\emptyset_i(x)}{dx^2}$$

$$- \sum_{i=1}^{\infty} mr^2\, \ddot{Y}(t)\,(1 + E/\alpha G)\, \frac{d^2\emptyset_i(x)}{dx^2} = p(x,t) - \sum_{i=1}^{\infty} \mu mL\, \emptyset_i(x)\ddot{Y}_i(t) \qquad (5.94)$$

Multiply equation (5.94) by $\emptyset_n(x)$ and then integrate over the length of the column and then apply the orthogonality relationships. This will result that all the terms of the series expansions will vanish except the n-th terms, resulting in:

$$\ddot{Y}_n(t)\int_0^L m\, \emptyset_n^2(x)\, dx + Y_n(t)\int_0^L \emptyset_n(x)\, \frac{d^2}{dx^2}\left[EI\, \frac{d^2\emptyset_n(x)}{dx^2}\right] dx$$

$$+Y_n(t)\int_0^L N\, \emptyset_n(x)\, \left[\frac{d^2\emptyset_n(x)}{dx^2}\right]dx - \ddot{Y}_n(t)\int_0^L (1+E/\alpha G)mr^2\, \emptyset_n(x)\left[\frac{d^2\emptyset_n(x)}{dx^2}\right]dx$$

$$= \int_0^L \emptyset_n(x)\, p(x,t)\, dx - \mu mL\, \emptyset_n^2(L)\, \ddot{Y}_n(t) \qquad (5.95)$$

Stellenbosch University http://scholar.sun.ac.za

The motion of the n-th mode can be written as:

$$y_n(x,t) = \emptyset_n(x)\, Y_n \sin(\Omega_n t) \qquad (5.96)$$

Introducing this equation into the free vibration equation for the n-th mode and then dividing by $Y_n \sin(\Omega_n t)$, results in:

$$EI\, \emptyset^{IV}(x) + N\, \emptyset^{II}(x) - m\Omega_n^2\, \emptyset_n(x) + mr^2\Omega_n^2(1+E/\alpha G)\, \emptyset_n^{II}(x) - m\mu L\Omega_n^2\, \emptyset_n(x) = 0$$

Multiply this equation by $\emptyset_n(x)$ and integrate over the length of the column:

$$\int_0^L \emptyset_n(x)\, \frac{d^2}{dx^2}\left(EI\, \frac{d^2\emptyset_n(x)}{dx^2}\right) dx + \int_0^L \emptyset_n(x)\, N\, \frac{d^2\emptyset_n(x)}{dx^2}\, dx$$

$$= \Omega_n^2 \left[m\left\{\int_0^L \emptyset_n^2(x)dx - r^2(1+E/\alpha G)\int_0^L \emptyset_n(x)\emptyset_n^{II}(x)dx + \mu L\emptyset_n^2(L)\right\}\right] \qquad (5.97)$$

The term in square brackets on the right hand side of equation (5.97) can be regarded as the generalized mass of the column associated with the mode shape $\emptyset_n(x)$. When this mass is denoted by M_n, i.e.:

$$M_n = m\left\{\int_0^L \emptyset_n^2(x)dx - r^2(1+E/\alpha G)\int_0^L \emptyset_n(x)\emptyset_n^{II}(x)dx + \mu L\emptyset_n^2(L)\right\} \qquad (5.98)$$

The equation of motion can then be expressed in the abbreviated form:

$$M_n\, Y_n(t) + \Omega_n^2\, M_n\, Y_n(t) = P_n(t) \qquad (5.99)$$

where:

$$P_n(t) = \int_0^L \emptyset_n(x)\, p(x,t)\, dx \qquad (5.100)$$

$P_n(t)$ is the generalized load associated with the mode shape $\emptyset_n(x)$. Then the Duhamel integral expression gives:

Stellenbosch University http://scholar.sun.ac.za

$$Y_n(t) = \frac{1}{M_n \Omega_n} \int_0^t P_n(\tau) \sin\{\Omega_n(t-\tau)\}\, d\tau \qquad (5.101)$$

For a horizontal point load on the column which is varying with time:

$$\int_0^t P_n(\tau)\, d\tau = \emptyset_n(x_o) \int_0^t p(\tau)\, d\tau \qquad (5.102)$$

where: x_o = the position of the point load
= 0,4635L = 0,74m (for this particular case)

Substituting equations (5.102), (5.101) and (5.98) into equation (5.93), gives the complete displacement function of the column for this theory.

$$y(x,t) = \sum_{n=1}^{\infty} \frac{\emptyset_n(x)\ \emptyset_n(x_o)}{M_n\ \Omega_n} \int_0^t p(\tau) \sin\{\Omega_n(t-\tau)\}\, d\tau \qquad (5.103)$$

with:

$$\int_0^t p(\tau) \sin\{\Omega_n(t-\tau)\}\, d\tau = \sin(\Omega_n t) \int_0^t p(\tau) \cos(\Omega_n \tau) d\tau - \cos(\Omega_n t) \int_0^t p(\tau) \sin(\Omega_n \tau)\, d\tau \ ] \qquad (5.104)$$

With:

$$\emptyset_n(x) = \sin(\delta_n x) - (\delta_n/\epsilon_n)\sinh(\epsilon_n x) + \beta_n \{\cosh(\epsilon_n x) - \cos(\delta_n x)\} \qquad (5.90)$$

$$\beta_n = \{\delta_n^2 \sin(\delta_n L) + \delta_n \epsilon_n \sinh(\epsilon_n L)\} / \{\delta_n^2 \cos(\delta_n L) + \epsilon_n^2 \cosh(\epsilon_n L)\} \qquad (5.91)$$

$$\int_0^L \emptyset_n(x)\ \emptyset_n{}^{II}(x)\, dx = -\delta^2 L - (\beta^2 L/2)(\delta^2-\epsilon^2) + \beta\delta/2 + (\delta/4)(1-\beta^2)\sin(2\delta L) + (\beta^2+1)[\delta(\delta^2-\epsilon^2)/(\delta^2+\epsilon^2)]\sin(\delta L)\cosh(\epsilon L) + (\beta^2\epsilon - \delta^2/\epsilon)[(\delta^2-\epsilon^2)/(\delta^2+\epsilon^2)]\cos(\delta L)\sinh(\epsilon L) - (\beta/\epsilon)(\delta^2-\epsilon^2)\sin(\delta L)\sinh(\epsilon L) + \beta\delta\sin^2(\delta L) + \tfrac{1}{4}[(\delta^2/\epsilon)+\beta^2\epsilon]\sinh(2\epsilon L) - (\beta\delta/2)\cosh(2\epsilon L) \qquad (5.105)$$

Stellenbosch University http://scholar.sun.ac.za

$$\int_0^L \emptyset_n^2(x)\,dx = (L/2)[1+2\beta^2-(\beta^2/\epsilon^2)] + (\beta\delta/2\epsilon^2) + (1/4\delta)(\beta^2-1)\sin(2\delta L) - [2\delta(\beta^2+1)/(\delta^2+\epsilon^2)]\sin(\delta L)\cosh)\epsilon L) + [2\{(\delta^2/\epsilon)-\beta^2\epsilon\}/\{\delta^2+\epsilon^2\}]\cos(\delta L)\sinh(\epsilon L) + [2\beta\{(\delta^2/\epsilon)+\epsilon\}/\{\delta^2+\epsilon^2\}]\sin(\delta L)\sinh(\epsilon L) - (\beta/\delta)\sin^2(\delta L) + (1/4\epsilon)\{(\delta^2/\epsilon^2)+\beta^2\}\sinh(2\epsilon L) - (\beta\delta/2\epsilon^2)\cosh(2\epsilon L) \qquad (5.106)$$

Note that in equations (5.105) and (5.106) the subscripts, n, has been omitted to save space.

With the displacement function of the column known, the moment and shear of the column is also known:

$$M(x,t) = -EI\,(\partial^2 y/\partial x^2) = -EI \sum_{n=1}^{\infty} \emptyset_n''(x)\,Y_n(t) \qquad (5.107)$$

and

$$Q(x,t) = -EI\,(\partial^3 y/\partial x^3) = -EI \sum_{n=1}^{\infty} \emptyset_n'''(x)\,Y_n(t) \qquad (5.108)$$

with:

$$\emptyset_n''(x) = -\delta^2\sin(\delta x) - \delta\epsilon\sinh(\epsilon x) + \beta\{\epsilon^2\cosh(\epsilon x) + \delta^2\cos(\delta x)\} \qquad (5.109)$$

$$\emptyset_n'''(x) = -\delta^3\cos(\delta x) - \delta\epsilon^2\cosh(\epsilon x) + \beta\{\epsilon^3\sinh(\epsilon x) - \delta^3\sin(\delta x)\} \qquad (5.110)$$

With a known load function, equations (5.103), (5.107) and (5.108) can be evaluated by numerical integration and summation of the contributions of all the selected vibration modes of the column.

Stellenbosch University http://scholar.sun.ac.za

This theory was used to describe the behaviour of the test columns analytically and it was found to be quite accurate. The measured load function was used with this theory. The correlation between the theory and the tests will be discussed in a later chapter 6.

5.9 Impact load on column (77)

One of the problems that might be encountered with the previous theory is that the load function is not known. In such a case the impact load function must first be determined in some or other way. In the rest of this chapter a method to find the impact load function will be reproduced. The method of finding the impact force is an iterative method and needs a computer program. This method was not followed in this report and thus will only be discussed briefly to indicate that it is possible to do it and for the sake of completeness.

Consider the impact of a striker, of mass m_s and initial velocity v_o, with a uniform cantilever column initially at rest. The impact occurs at a impact point $x = x_o$. Suppose the impact zone obeys a Hertz-type contact law with $p(t) = Kq^{3/2}(t)$. Where p is the impact load, K is a deformation constant for the impact zone and q is the deformation of the impact zone. The column behaviour can be described by the vibration model as discussed in the previous section.

The deformation of the impact zone is then given by:

$$q(t) = y_s(t) - y(x_o,t) \qquad (5.111)$$

where y_s and y are the displacement of the striker and column at $x = x_o$, respectively. Equation. (5.111), is the column impact equation.

Now: $$q = (p/K)^{2/3} \qquad (5.112)$$

Stellenbosch University http://scholar.sun.ac.za

$$y_s = v_o t - \frac{1}{m_s} \int_o^t dt \int_o^t p(\tau)\, d\tau \qquad (5.113)$$

and $y(x_o,t)$ as given by equation (5.103)

$$\left[\frac{p}{K}\right]^{2/3} = v_o t - \frac{1}{m_s} \int_o^t dt \int_o^t p(\tau)\, d\tau - \sum_{n=1}^{N} \frac{\phi_n(x)\ \phi_n(x_o)}{M_n\ \Omega_n} \int_o^t p(\tau)\, \sin\{\Omega_n(t-\tau)\}\, d\tau \qquad (5.114)$$

Unfortunately this equation cannot be solved in closed form, but it may be solved by the use of numerical techniques to give the impact force history. When the impact force history is known the third theory, as discussed in the previous section, can be used to find the displacement function, the column moment and shear.

To derive the solution for equation (5.114), two approximations are introduced: (1) The infinite summation over modes is replaced by a finite summation.

(2) The integrations with respect to time are replaced by summations over a finite number of time intervals.

For the j-th time interval, i.e. for

$$t_{j-1} \leq t \leq t_j$$

the linear approximation for the force history is given by:

$$p(t) = p_{j-1} + [(t-t_{j-1})/(t_j-t_{j-1})](p_j-p_{j-1})$$

$$= [t_j p_{j-1} - t_{j-1} p_j + (p_j-p_{j-1})t] \ / \ \Delta t \qquad (5.115)$$

In equation (5.114), the terms

$$v_o t - \frac{1}{m_s} \int_o^t dt \int_o^t p(\tau)\, d\tau$$

represent the displacement of the striker. At a time t_m during the course of the impact, we define:

Stellenbosch University http://scholar.sun.ac.za

$$D_m = \int_0^{t_m} dt \int_0^t p(\tau)\, d\tau \qquad (5.116)$$

It can be shown that the following recurrence relation for the displacement of the striker holds for D_m, for m = 0,1,2,...

$$D_{m+1} = D_m + (\Delta t)^2 [G_m + (p_{m+1} - p_m)/6] \qquad (5.117)$$

where:

$$G_m = \sum_{j=1}^{m} p_j \qquad \text{by definition}$$

In equation (5.114) the term

$$\sum_{n=1}^{N} \frac{\emptyset_n(x)\, \emptyset_n(x_o)}{M_n\, \Omega_n} \int_0^t p(\tau)\, \sin\{\Omega_n(t-\tau)\}\, d\tau$$

represents the beam displacement. At a time t_m during the course of impact, define

$$S_{n,m} = \int_0^{t_m} p(\tau)\, \sin\{\Omega_n(t_m-\tau)\}\, d\tau \qquad (5.118)$$

and

$$C_{n,m} = \int_0^{t_m} p(\tau)\, \cos\{\Omega_n(t_m-\tau)\}\, d\tau \qquad (5.119)$$

Note that the subscript n, which is required here to distinguish between vibration modes and which is only used for this purpose, does not enter into the derivation of the recurrence relations. It can be shown that the following recurrence relations holds for $S_{n,m}$ and $C_{n,m}$, for m = 0,1,2,...

$$S_{n,m+1} = \cos(\Omega_n \Delta t)\, S_{n,m} + \sin(\Omega_n \Delta t)\, C_{n,m}$$
$$+ [1 - \{\sin(\Omega_n \Delta t)/\Omega_n \Delta t\}]\{(p_{m+1} - p_m) / \Omega_n\}$$
$$+ \{1 - \cos(\Omega_n \Delta t)\} p_m / \Omega_n \qquad (5.120)$$

Stellenbosch University http://scholar.sun.ac.za

$$C_{n,m+1} = \cos(\Omega_n \Delta t)\, C_{n,m} - \sin(\Omega_n \Delta t)\, S_{n,m} + [1 - \{\cos(\Omega_n \Delta t)/\Omega_n \Delta t\}]\{(p_{m+1} - p_m) / \Omega_n\} + \{\sin(\Omega_n \Delta t) p_m\} / \Omega_n \qquad (5.121)$$

Note that $S_{n,o} = C_{n,o} = 0$ by definition. The term in equation (5.114) which represents the displacement of the column can be written, using equation (5.120):

$$\sum_{n=1}^{N} \frac{\phi_n(x)\, \phi_n(x_o)}{M_n\, \Omega_n}\, S_{n,m+1} \qquad (5.122)$$

at time t_{m+1}, in which, again, the force history enters only through terms which can be calculated using recurrence relations. Equations (5.120) and (5.121) are both required because the calculation of a sine term $S_{n,m+1}$ requires both the previous sine and cosine terms $S_{n,m}$ and $C_{n,m}$.

At a time t_{m+1} the approximation to equation (5.114) contains the unknown p_{m+1} in both sides of the equation and the known force history (p_1, p_2, ... , p_m) in terms which can be calculated using recurrence relations. Because the left hand side contains the fractional power, 2/3, the equation has to be solved by an iterative method. The approximation to equation (5.114) can be written at time t_{m+1}:

$$(p_{m+1})^{2/3} = A_m + BF_{m+1} \qquad (5.123)$$

where:

$$A_m = v_o(m+1)\Delta t - \frac{D_m + (\Delta t)^2 (G_m - p_m/6)}{m_s} - \sum_{n=1}^{N} \frac{\phi_n(x)\, \phi_n(x_o)}{M_n\, \Omega_n} [\cos(\Omega_n \Delta t)\, S_{n,m} + \sin(\Omega_n \Delta t)\, C_{n,m} + \frac{p_m \{(\sin(\Omega_n \Delta t)/(\Omega_n \Delta t)) - \cos(\Omega_n \Delta t)\}}{\Omega_n}] \qquad (5.124)$$

Stellenbosch University http://scholar.sun.ac.za

and

$$B = -\frac{(\Delta t)^2}{6m_s} - \sum_{n=1}^{\infty} \frac{\phi_n(x)\,\phi_n(x_0)}{M_n\,\Omega_n}\left\{1 - \frac{\sin(\Omega_n \Delta t)}{\Omega_n \Delta t}\right\} \qquad (5.125)$$

Note that B does not vary with time. Also, it can be seen that B is negative, because all the physical constants in it are positive and the term in braces can be shown to be positive; hence equation (5.123) has a positive solution, which is unique if A_m is positive, and it has no solution if A_m is negative. During calculations it will be found that A_m remains positive until the force becomes very small near the end of the impact. p_{m+1} can now be found by using equation (5.123) and using an iterative method up to the required degree of accuracy. Thus starting with the known value of p, where m = 0, and continues from there for the consecutive values of p, the load history can be obtained.

Stellenbosch University http://scholar.sun.ac.za

6. CORRELATION BETWEEN THEORY AND TEST RESULTS.

6.1 Introduction

The correlation between the theory and the test results depends on the accuracy of both. In this section the theory and test results will be compared and discrepancies will be discussed.

6.2 The theory

As discussed in chapter 5, "Theory 3" (paragraphs 5.7 and 5.8) will be used to predict the response of the axially loaded column, subjected to a horizontal impact load. The theory is based on the Timoshenko beam theory for the free and forced vibrations of a beam or column. This theory provides for shear and rotatory inertia.

The accuracy of the theory depends not only on the length of the time interval used for the integration but also on the number of modes assumed in the solution. Although very high modes might be excited the test results indicate that it is not necessary to use these high modes. Many authors (77) consider the probability of the excitation of these high modes to be very low. These high modes are sometimes associated with very large shear and rotatory energy. In such a case this theory would be inadequate.

Figure 6.1 shows the deflection history of the top of the column due to the measured load history. The deflection according to the first mode and the deflection according to the sum of the first ten modes are plotted on the same graph. From this graph it is clear that only the first mode is important to calculate the deflection of the column for this specific study. The reason for this independence of the number of modes used, is because the vibration frequency coefficients, δ and ϵ, do not appear in the numerator of the deflection function.

Stellenbosch University http://scholar.sun.ac.za

The moment and shear are more dependent on the number of modes used to calculate their values than the deflection of the column. Figure 6.2 shows the bending moment at the bottom of the column according to the first mode and the sum of the first ten modes on the same graph. From this graph it is clear that the number of modes used, play a very important role. The same can be seen for the shear at the bottom of the column in figure 6.3, which shows the shear according to the first mode and the sum of the first ten modes on the same graph. The reason for the sensitivity of the moment and shear to the number of modes considered, is that the frequency coefficients, δ and ϵ, appear in the numerator of the moment function as a second power and in the shear function as a third power. This is also the reason why the moment and shear are more influenced by the shear and rotatory inertia. The provision for shear and rotatory inertia influences the frequency coefficients of the higher modes and only marginally compared to that of the first mode.

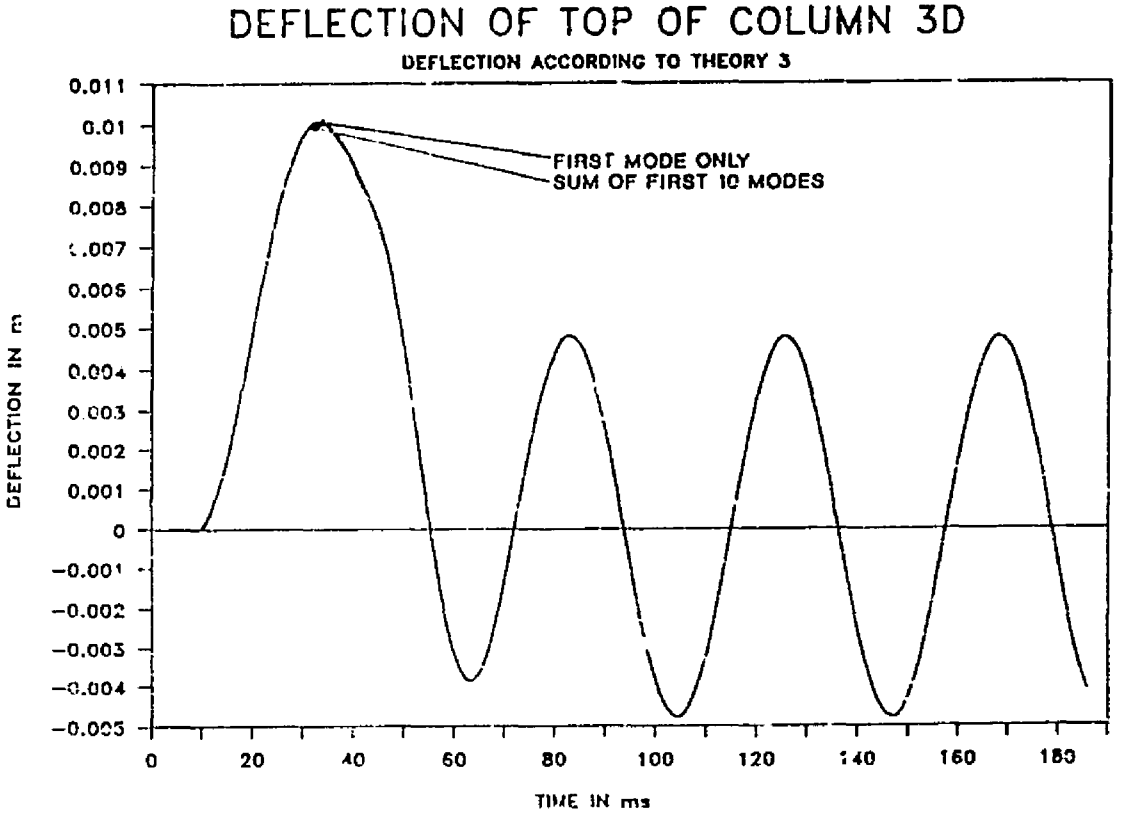

Figure 6.1: Deflection of top of column Theory 3.

Stellenbosch University http://scholar.sun.ac.za

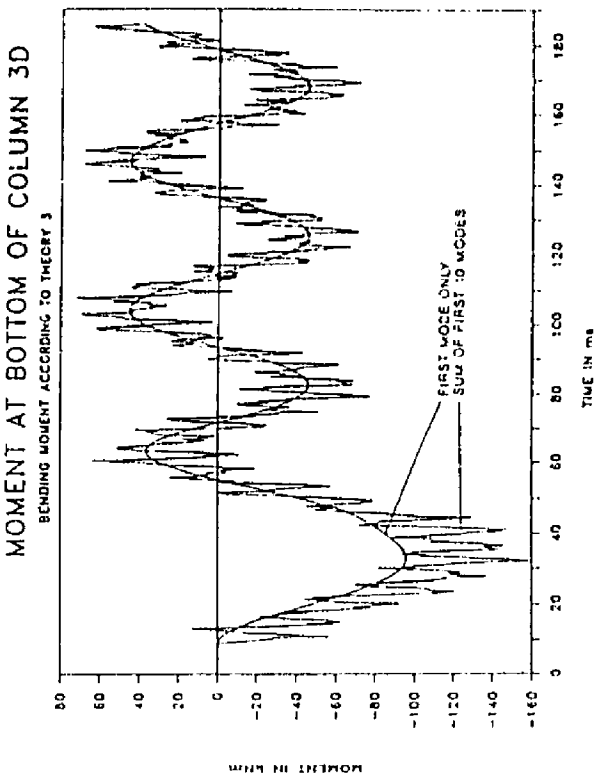

Fig. 6.2: Flexural moment.

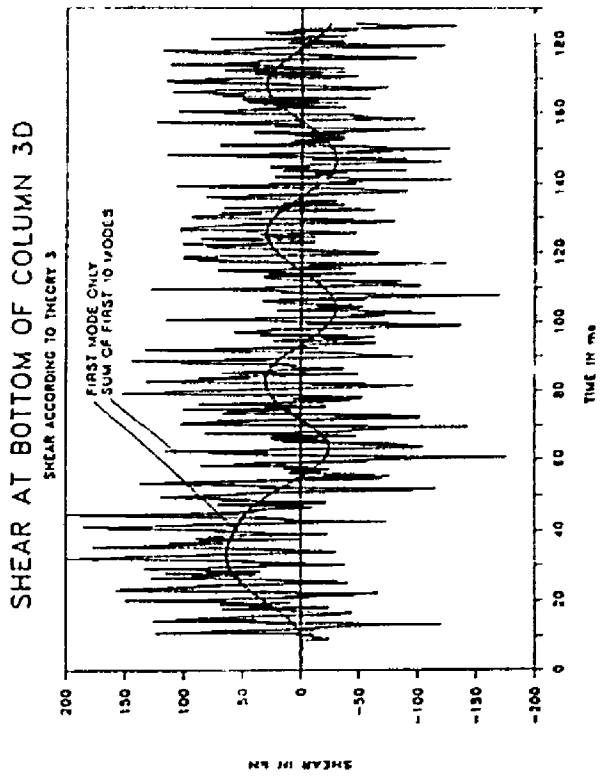

Fig. 6.3: Shear Force.

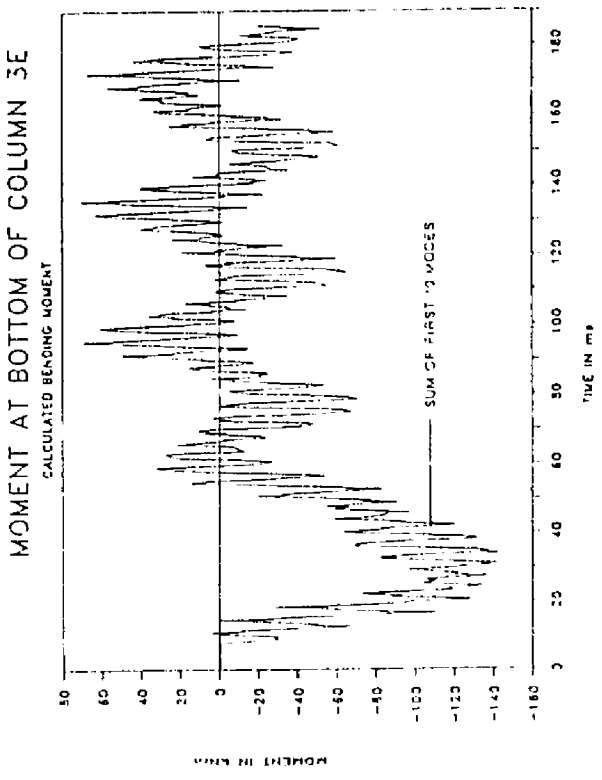

Fig. 6.4: Moment 10 modes.

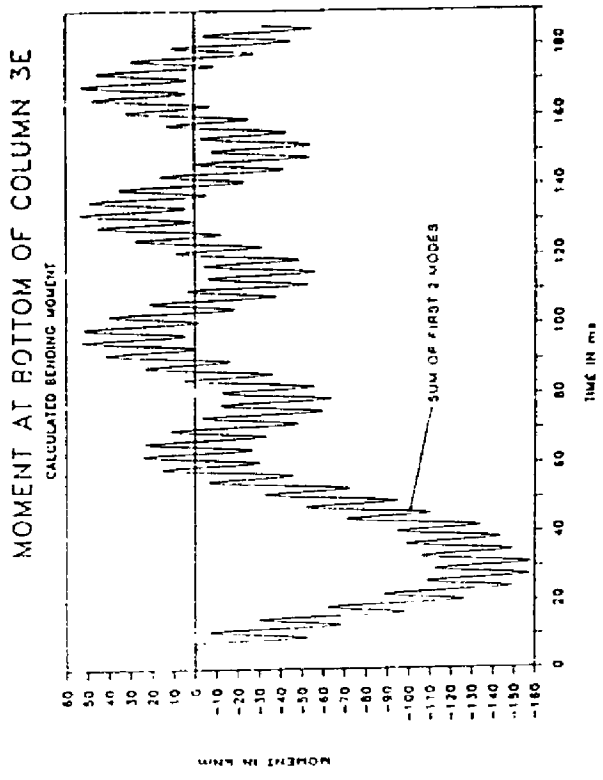

Fig. 6.5: Moment - 2 modes.

Stellenbosch University http://scholar.sun.ac.za

Figures 6.4 and 6.5 show the sum of the first two modes and the sum of the first ten modes for the bending moment at the bottom of Column 3E. From these two graphs it is clear that for this study the sum of the first two modes overestimates the bending moment at the bottom of the column, while the sum of the first ten modes gives a better estimate of the bending moment and the shear force.

In all the analysis the measured load function were used to compute the theoretical values used in this chapter.

6.2.1 Variables influencing the results of the theory.

As discussed in chapter 5, the choices of the following variables have a significant influence on the results of the theory, because all of them has a influence on the frequency parameter, a:

N = Axial load on the column.

E = The elasticity modulus of the concrete

I = Inertia moment of the section

M_o = Mass of concentrated mass at free end of column

mL = Mass of column

A = Area of concrete section

The axial load, N, in all the tests was 100 kN except for one group it was 20 kN. Unfortunately this theory does not provide for the increase in the axial load during the impact, as was measured during the tests. Because the axial load influence the frequency parameter it was not possible to built in such a provision. The comparisons of the theoretical results with the experimental values, as discussed in paragraph 6.4, indicate that excluding the variation in axial load in the theoretical prediction, results in a omissible error

Stellenbosch University http://scholar.sun.ac.za

From chapter 4 one can derive an increased elasticity modulus, E, to be used in the theory to increase the accuracy of the theory, for impact purposes. It was however found that the E-value does not have a large influence on the frequency parameter. The increase of the E-value, for the strain rates present in the tests, is also only in the region of 5%. Thus it is not necessary to use an increased E-value especially if one is not even 100% sure about the static E-value of the concrete.

The choice of the inertia moment of the section or the second moment of the area, I, is however very important. Some authors (146) suggested that an average value (see equation 5.89) should be used, while other authors (77) suggested that a cracked value for I should be used. In the comparisons of the theory with the test results in this study the average value was used. Although it is believed that the section cracks very soon after the impact started, it was found that the average value for the inertia moment of the section, I, gave better results when compared with the test results, than the cracked value for I.

All the columns were analysed using a cracked value for the section as well as an average value for the section. About 500 graphs of all the results were drawn and examined and compared with each other and the test results. Due to a lack of space these graphs will not be shown here, but it was concluded that the average value (equation 5.89) gave better comparisons with the test results (refer to paragraph 6.4).

The concentrated mass, M_x, was in the region of 200 kg. This was within a few kilograms exactly the same as that of the concrete column. For this specific test set-up it was however very difficult to establish the effective concentrated mass because it was connected to two sway frames (refer to Appendix B for the test set-up). For the purpose of the comparison of the theory with the test results a value of [illegible] was however assumed. This assumption might lead to [illegible] between the frequency of the test column and that of the theory

Stellenbosch University http://scholar.sun.ac.za

The area, A, of the section was in all the tests the same and the area reduction factor for shear, α, was taken as 5/6 as is common practice for rectangular sections.

6.3 The test results

All the test results are given in Appendix B. Unfortunately the deflection of the column could not be measured because the available instruments, to measure the deflection, could not respond quickly enough and thus their readings would not be reliable.

The theoretical accelerations and strains compared (figures 6.23 to 6.54) with the accelerations measured at the top of the column and with the strain measured at two positions on the back side of the column as well as with the compression forces transferred through the footing of the column to the floor. The comparison of the compression forces gave very reasonable results.

For details of the measuring stations and their exact positions can be found in Appendix B and will not be discussed here.

6.4 Comparisons

In the comparisons of the theoretical and the test results, the first 50 ms, or the impact phase, is the important part of the response, hence these parts of the graphs need to be compared. During the impact phase the largest moments, shear forces and strains occur. All the columns that failed also failed during the impact phase, as could be expected. Following the impact phase some section properties might have changed from the assumed properties and thus there might be slight differences with the theory. If the column failed during the impact phase the rest of the graph would be of no interest as the case the theory does not provide for failure of the column. To investigate the correlation between the theory and the test results only the

Stellenbosch University http://scholar.sun.ac.za

first 50 ms or the impact phase will be considered although the total measuring period is shown on the graphs.

Although the theory was applied to all the test columns only a limited number of graphs are presented in this chapter due to limited space. These graphs would however be adequate to indicate the degree of correlation between the theoretical and test results.

Ten modes were used for the theoretical analysis. Although all the different number of modes between one and ten had been tested, ten modes for the analysis showed the best comparative results.

6.4.1 Compression force transferred through footing

The bending moments and shear forces generated in the column during an impact could hardly be measured directly. Therefore the correlation between the experimental and theoretical bending moment and shear in the test column, need to be evaluated indirectly. To achieve this it was decided to calculate the compression force, C (fig 6.6), transferred by the footing to the floor. This is a good measure of both the shear, V, and moment, M, exerted by the column on the footing. This is then compared to the measured compression force, K.

From figure 6.6 the following calculations follow:

$$\text{Sum of moments around O} \quad 0,92A + M + 0,44Q - 1,84C = 0$$

$$\text{Thus:} \quad C = (0,92A + M + 0,44Q)/1,84 = K \qquad (6.1)$$

From equation (6.1) the calculated compression force is known and this can then be compared with the measured compression force, K. Only the compression force was used for the comparisons because the results of the tension load cells were unreliable.

Stellenbosch University http://scholar.sun.ac.za

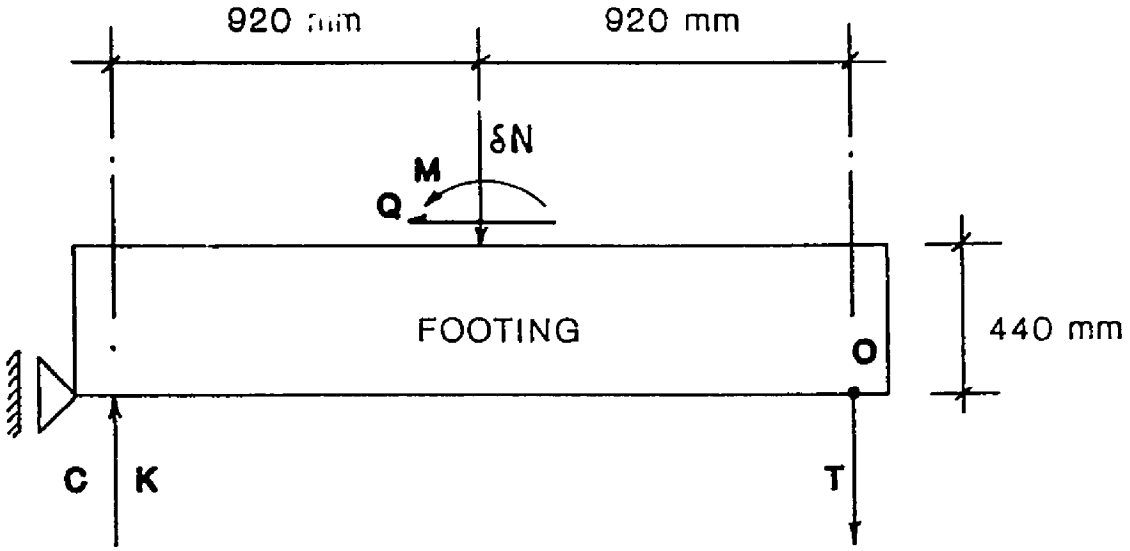

δN = MEASURED VARIATION IN AXIAL LOAD
M = CALCULATED FLEXURAL MOMENT
Q = CALCULATED SHEAR FORCE
C = CALCULATED VARIATION IN COMPRESSION FORCE
K = MEASURED VARIATION IN COMPRESSION FORCE
T = MEASURED VARIATION IN TENSION FORCE

Figure 6.6: Forces acting on footing of column

Figures 6.7 to 6.22 show the comparisons of a number of the test columns graphically. From the graphs it is clear that the correlation between the calculated peak values of the compression force is fair. The maximum values of some is as close as 1% from each other. The average differences between the maximum values of the theory and the test results were found to be only 7.3%. If the two highest differences are omitted, the average difference of the rest is only 5.8%.

For two of the columns there was a difference of above 15%. In these two cases the theory overestimated the experimental values. This only occurred with some of the last test columns. This can be contributed to the fact that some energy was absorbed by the footing system, because the bolts fastening the footing to the floor lost a small amount of tension during the preceding tests. This loss of tension might have influenced the accuracy of the load cells under the footing as well. Although these factors

Stellenbosch University http://scholar.sun.ac.za

might have influenced the accuracy of the last few columns it meant only an error of 7% - 8%, which is still acceptable.

The correlation between the calculated values of the variation in the compression force and the test results show that the theory predicts the shear and the bending moment in the column fairly accurately. The small differences, as discussed in the previous paragraphs, are very small and thus this theory can be considered to be acceptable for predicting the maximum shear forces and bending moments in the column under a horizontal impact loading.

6.4.2 Acceleration of top of column

Figures 6.23 to 6.32 show a number of graphs of the predicted acceleration and the measured acceleration at the top of the column. To clarify the graphs for easier interpretation, the smoothed curve (data was smoothed with a computer program) of the measured acceleration is used and the theoretical results are based on the first two modes only. The theoretical acceleration curve is the second derivative with respect to time of the deflection at the top of the column.

The simplifications, described in the previous paragraph, are one of the reasons why the maximum values of the theoretical and measured accelerations differ as much as shown in figures 6.23 to 6.32. What the graphs do show is that the theoretical curve and the measured curve follows exactly the same trend during the impact phase although their maximum values differ. Figure 6.27 shows some excellent results for column 2C. Although the first peak of this graph differed with something like 100 m/s^2, the rest of the graph corresponds favourably. In all the graphs the theoretical and experimental peaks occur at the same moment.

Bearing in mind the simplifications used in the graphs of the accelerations it is clear that the theory is able to give an acceptable prediction of the acceleration response of the column.

Stellenbosch University http://scholar.sun.ac.za

The theory can also predict the expected time of the peaks of the acceleration curve quite accurately, as discussed in the previous paragraph. Therefore it can be concluded that the proposed theoretical model is quite acceptable despite the fact that no provision is made for the variation in axial load during impact.

6.4.3 Concrete strain of the column

Figures 6.33 to 6.46 show the concrete strain measured 160 mm from the bottom of the column, on the back side (compression side) of a number of columns, with the predicted concrete strain. Figures 6.47 to 6.54 show the concrete strain measured 750 mm from the bottom of the column, on the back side of a number of columns, with the calculated concrete strain.

The concrete strain can be calculated if the bending moment is known. The bending moment follows from the theory, as described in chapter 5. The stress in the concrete is then given by:

$$\sigma = (My)/I \qquad (6.2)$$

Where: σ = Stress in concrete
M = Bending moment at the desired section
y = Distance from centroid of section to desired position
I = Moment of inertia of section

The strain is then given by:

$$\epsilon = \sigma/E \qquad (6.3)$$

Where: ϵ = Strain in concrete
E = Elasticity modulus of concrete

The average moment of inertia of the section, I_a, was used and the increased elasticity modulus, corresponding to the strain rate present, was used. The y value used, was the value corresponding with the average moment of inertia of the section.

Stellenbosch University http://scholar.sun.ac.za

Differences between the measured strain and the calculated strain can be attributed to the chosen values of I, E and especially y. These selected values as described in the previous paragraph were found to yield good results.

From figures 6.33 to 6.46 it is clear that the measured strain corresponds very well with the predicted values. The average difference between the maximum values of the measured and calculated strains are only in the region of 10%. Bearing in mind the assumptions, described in the previous paragraph, this figures show that the theory can predict the maximum strain in the column quite adequately and thus the prediction of the maximum bending moment is good. Figure 6.36 show a graph where the failure of the strain gauge occurred. The strain gauge normally failed with the failure of the column and thus this strain gauge gives an indication of the exact time of failure of the column during the impact. Even up to failure the measured value followed the theoretical value closely. The strain gauges measuring range were between -0,002mm/mm up to +0,002mm/mm. When this ultimate values were reached a constant value was indicated, although the strain might be higher. This cut-off can be seen in figures 6.43 and 6.46.

Figures 6.47 to 6.54 show the concrete strain directly behind the impact zone. Both the curves of the calculated and measured values show an immediate tension strain. This tension strain peak of the two curves is within 10% of each other. During the impact phase (the part of the graph that is of interest for this study) both of the curves for the calculated and measured strain show the same trend, although they differ in magnitude after the first peak. These differences can be due to a number of factors. The important part of this specific set of graphs is however the first tension peak and the magnitude of that peak. This peak is closely predicted by the theory used and even the frequency of the higher mode peaks present on the first peak corresponds very well with the measured curve

Stellenbosch University http://scholar.sun.ac.za

6.5 Conclusion

The simplest method to prove the reasonable correlation between the theory derived in chapter 5 and the test results is to compare the theoretical and test results graphically. Figures 6.7 to 6.54 show such comparisons.

From these comparisons one can conclude that the theory derived in chapter 5, predicts the bending moments and shear forces with reasonable accuracy (as is clear from the comparisons of the compression forces and the concrete strain) at least during the impact phase, that is, critical stage of the response.

The correlation between the theory and the test results was not proved by statistical analysis due to insufficient data.

Stellenbosch University http://scholar.sun.ac.za

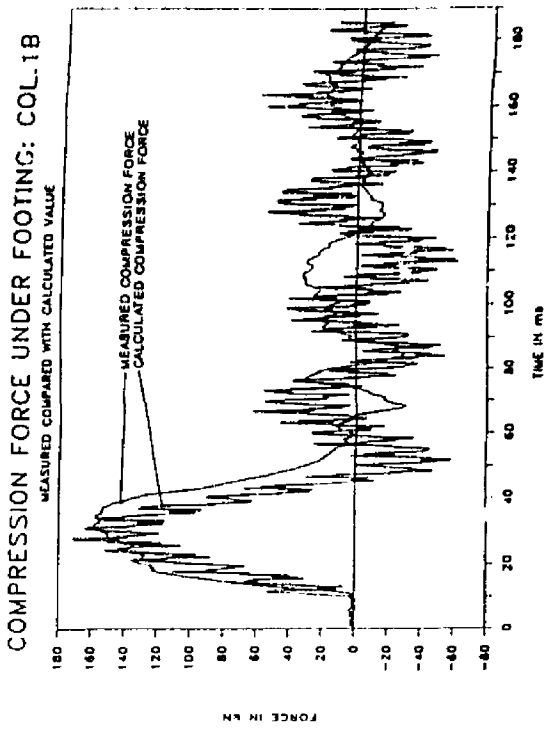

Fig.6.7: Compression - Col.1B

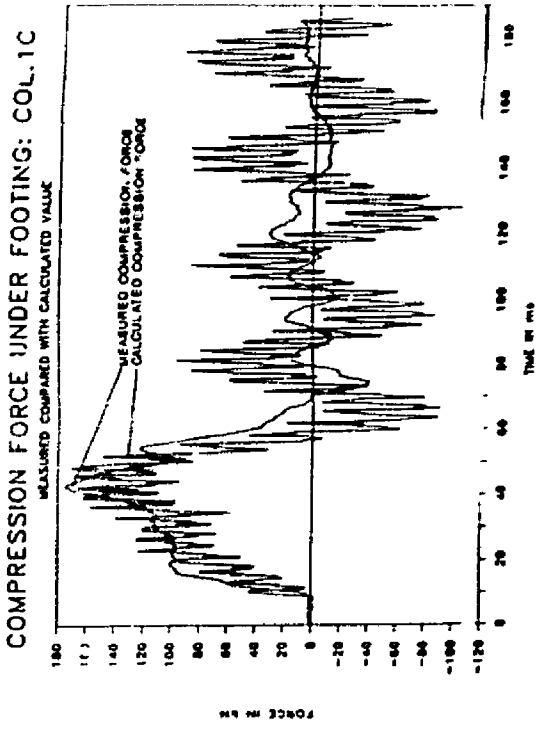

Fig.6.8: Compression - Col.1C

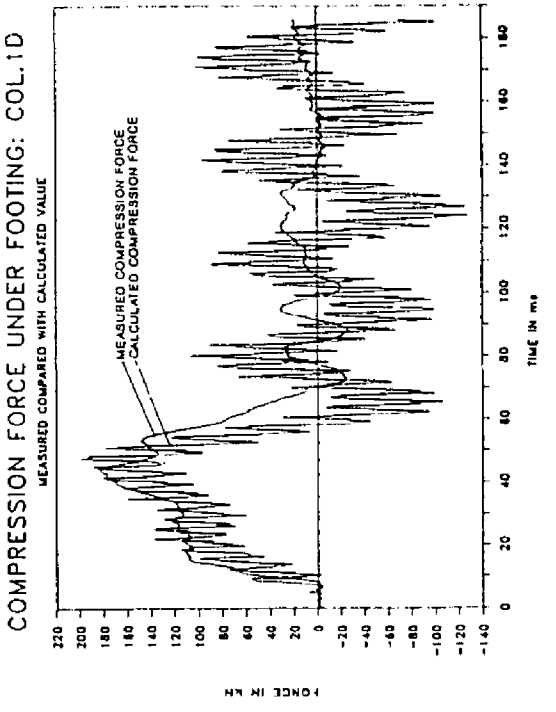

Fig.6.9: Compression - Col.1D

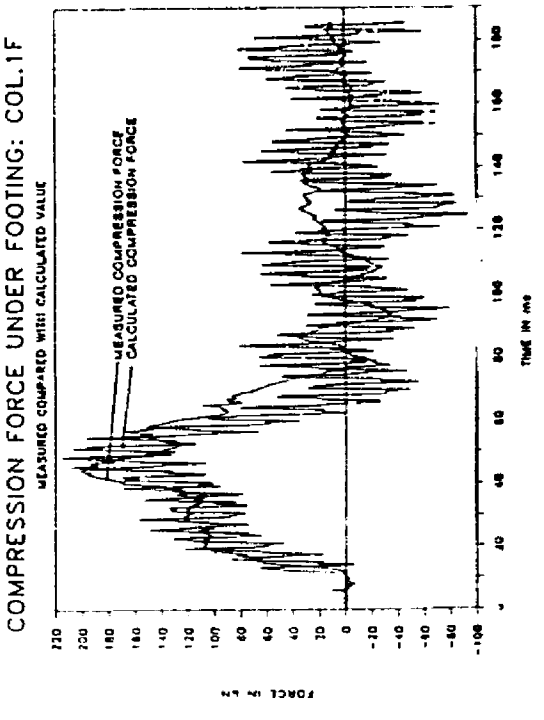

Fig.6.10: Compression - Col.1F

Stellenbosch University http://scholar.sun.ac.za

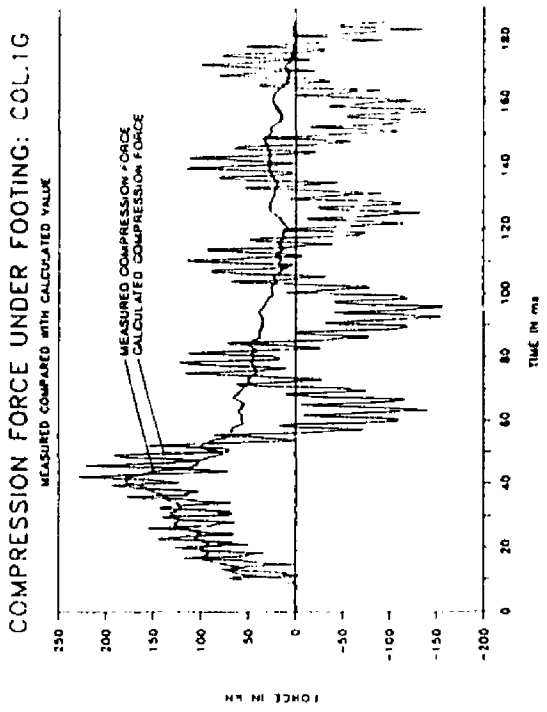

Fig.6.11: Compression Col.1G

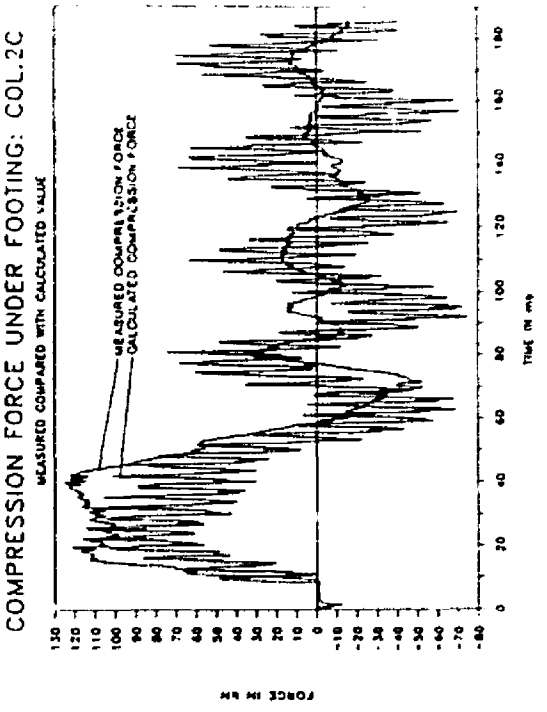

Fig.6.12: Compression - Col.2C

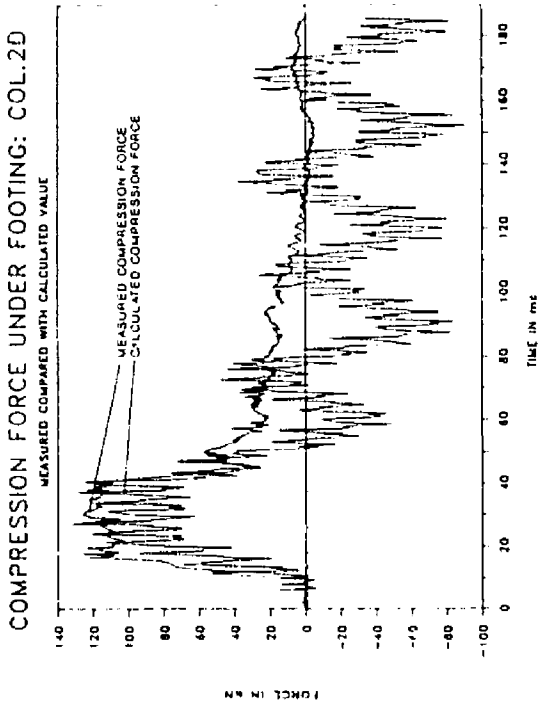

Fig.6.13: Compression Col.2D

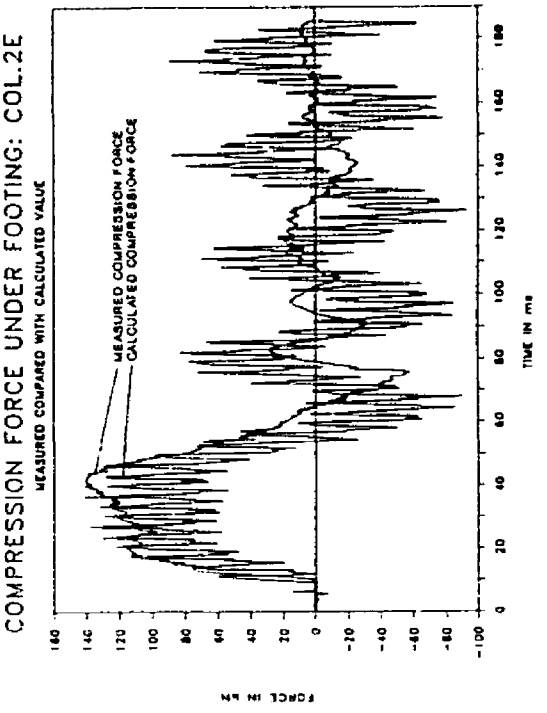

Fig.6.14: Compression Col.2E

Stellenbosch University http://scholar.sun.ac.za

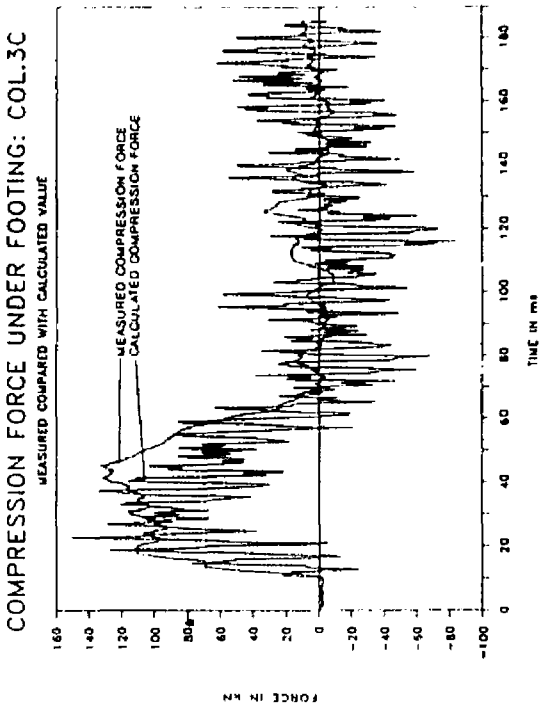

Fig.6.15: Compression - Col.3C

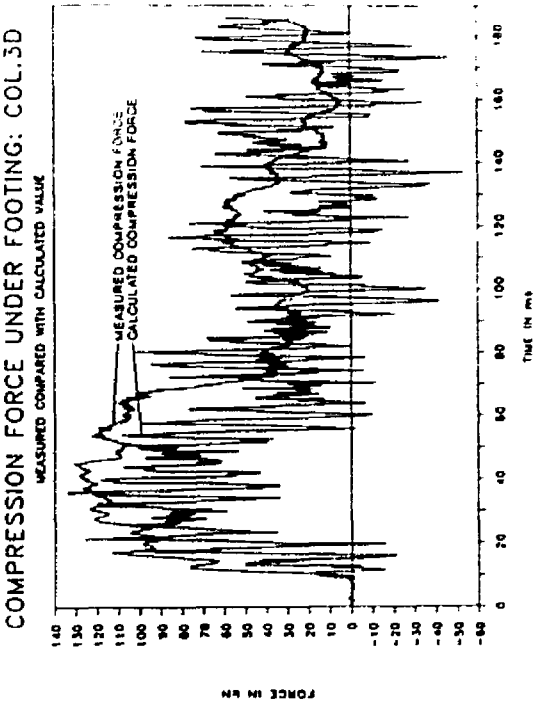

Fig.6.16: Compression - Col.3D

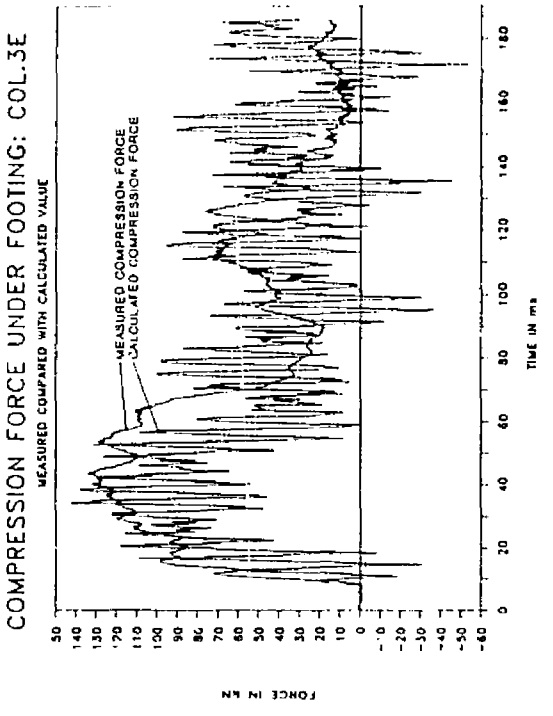

Fig.6.17: Compression Col.3E

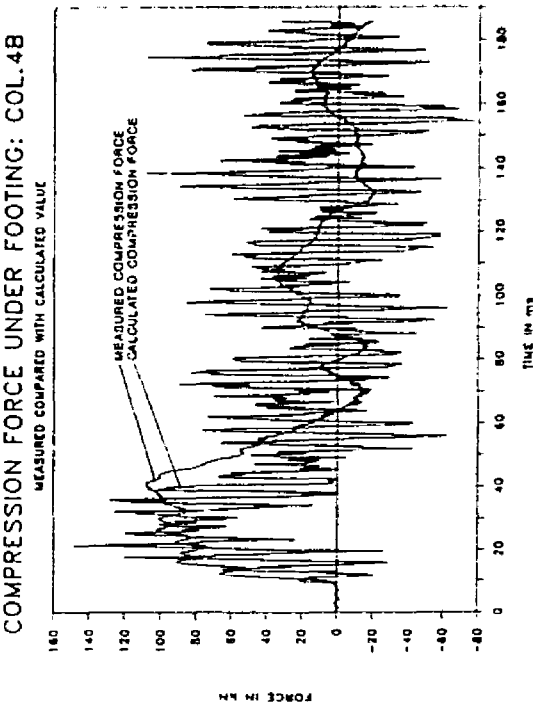

Fig.6.18: Compression Col.4B

Stellenbosch University http://scholar.sun.ac.za

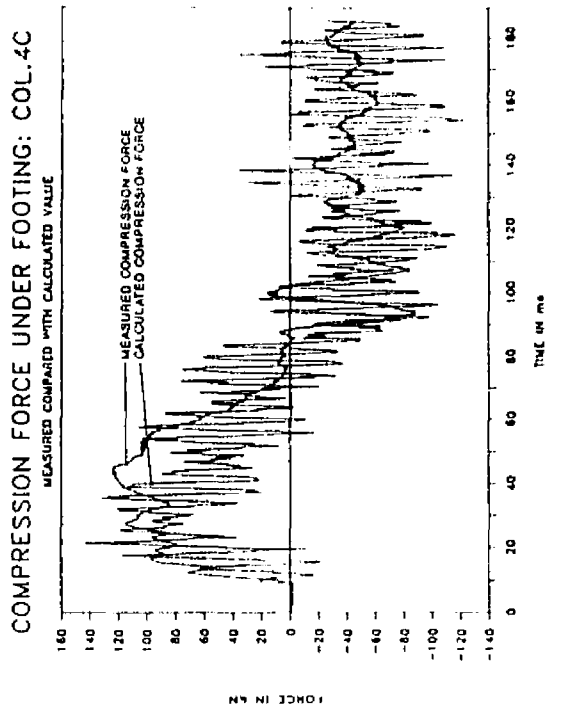

Fig.6.19: Compression Col.4C

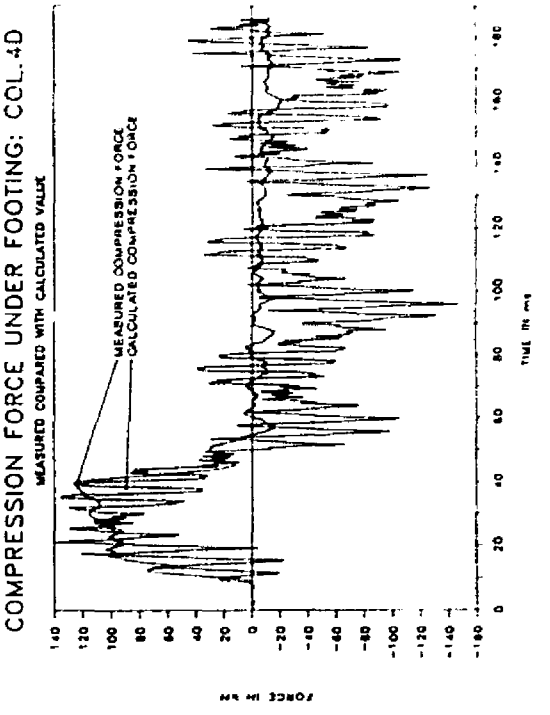

Fig.6.20: Compression - Col.4D

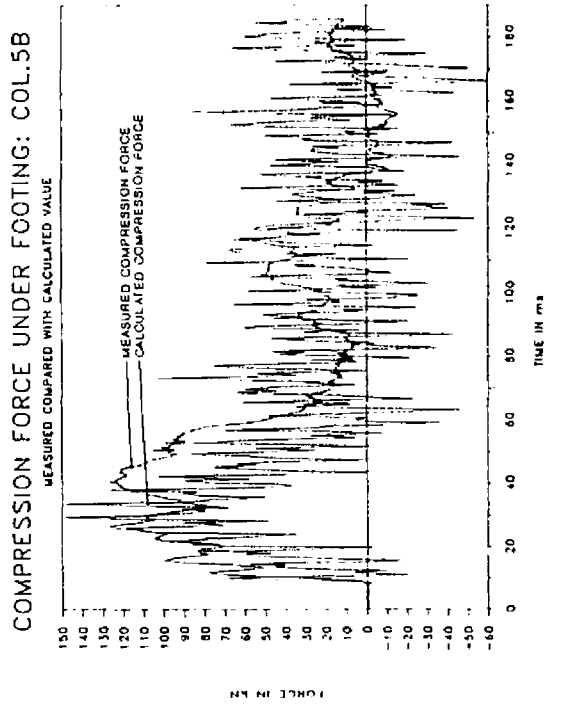

Fig.6.21: Compression Col.5B

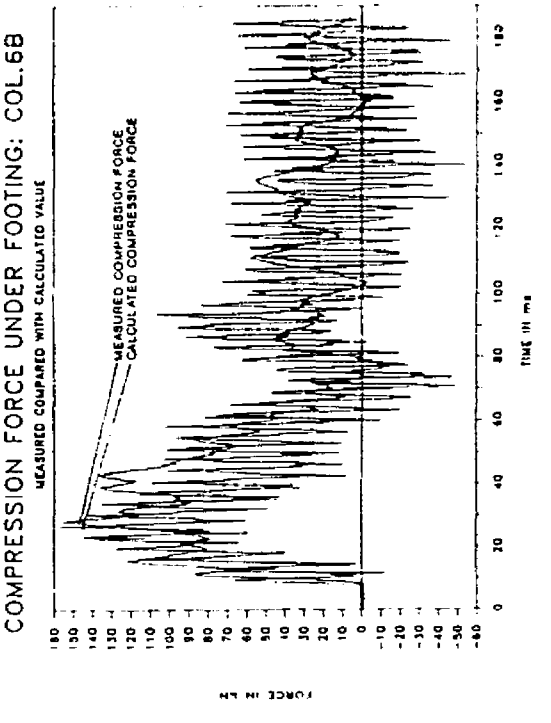

Fig.6.22: Compression - Col.6B

Stellenbosch University http://scholar.sun.ac.za

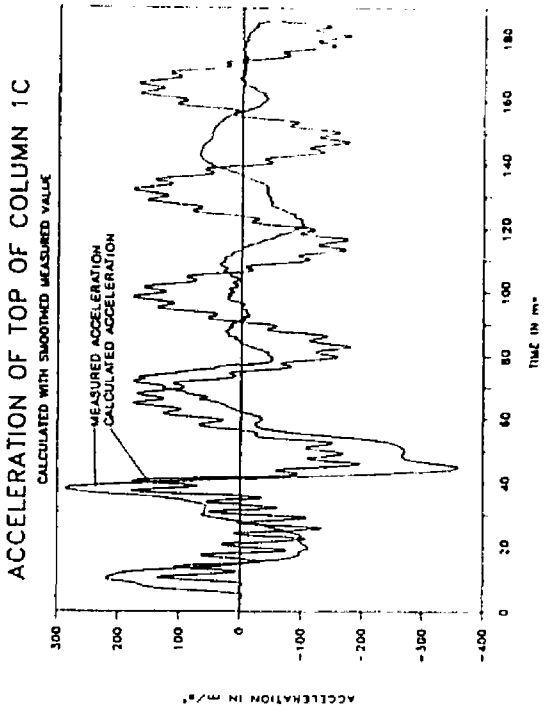

Fig.6.23: Acceleration Col.1C

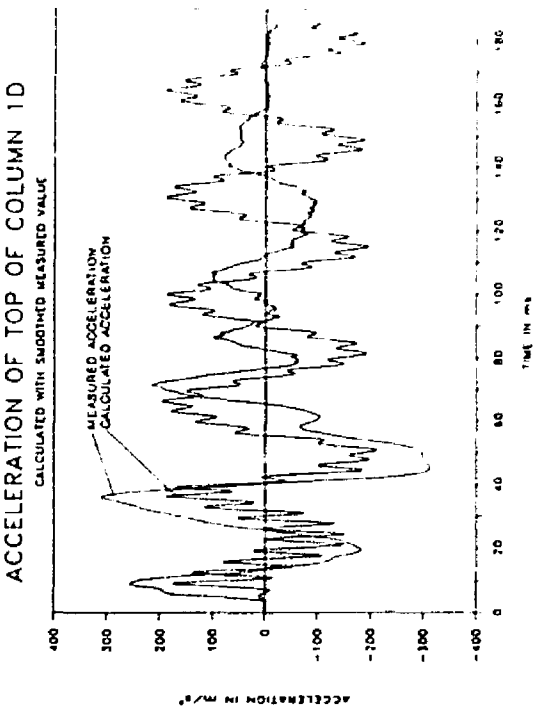

Fig.6.24: Acceleration Col.1D

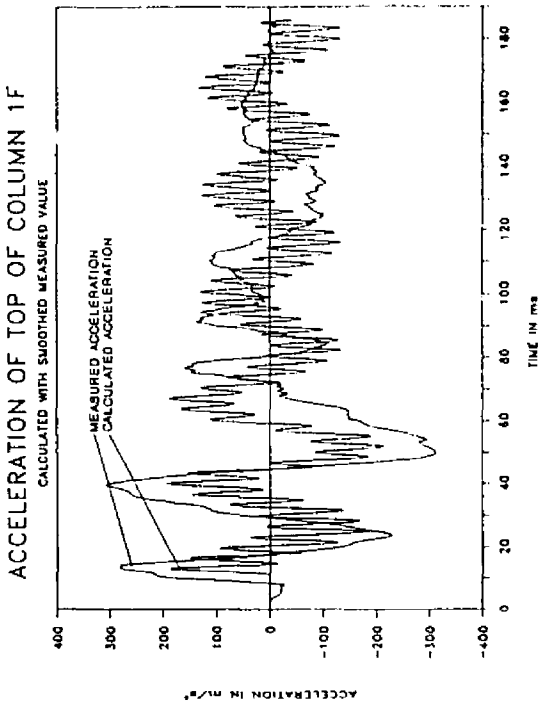

Fig.6.25: Acceleration Col.1F

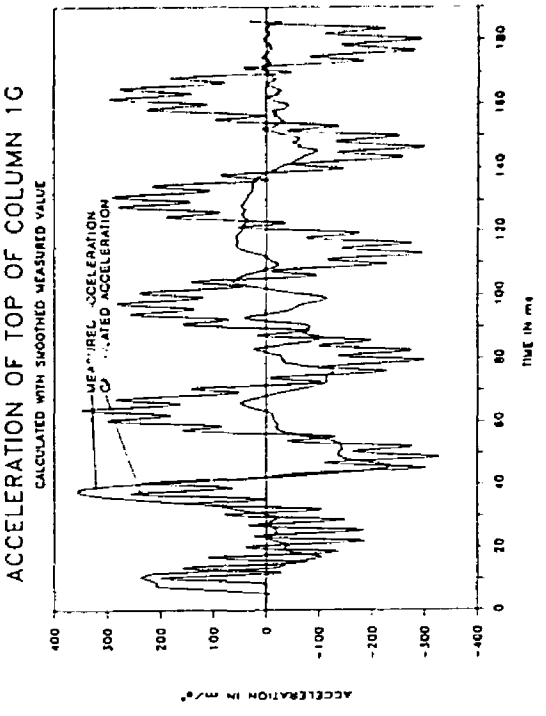

Fig.6.26: Acceleration Col.1G

Stellenbosch University http://scholar.sun.ac.za

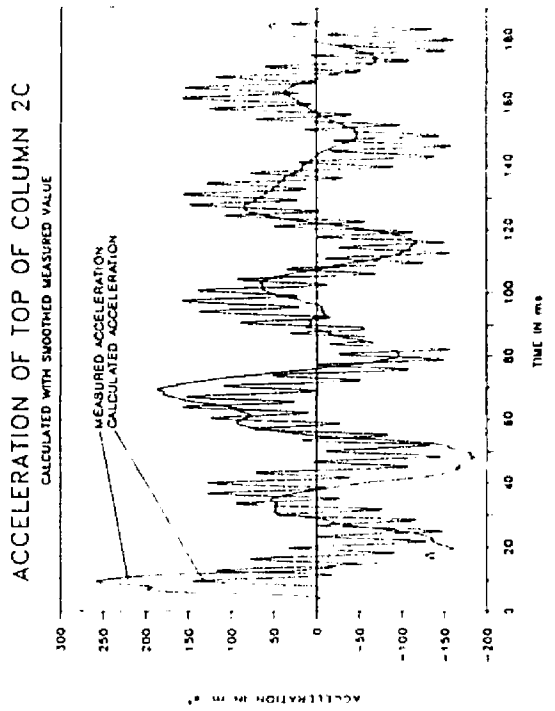

Fig.6.17 Acceleration Col 2C

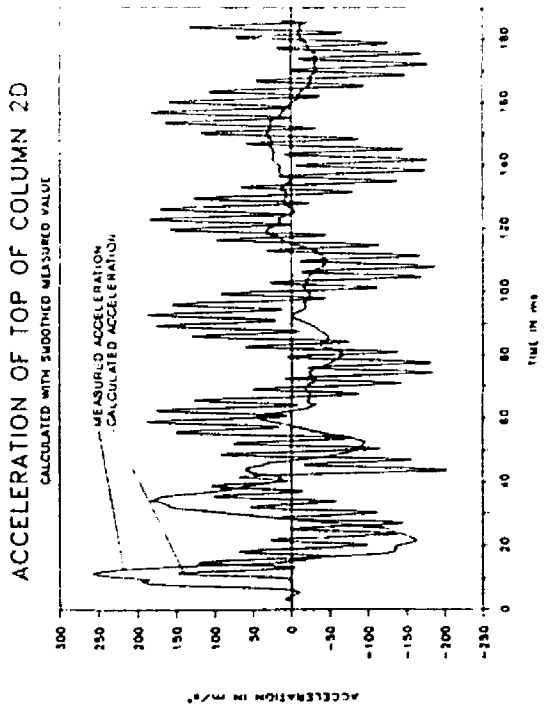

Fig.6.18 Acceleration Col 2D

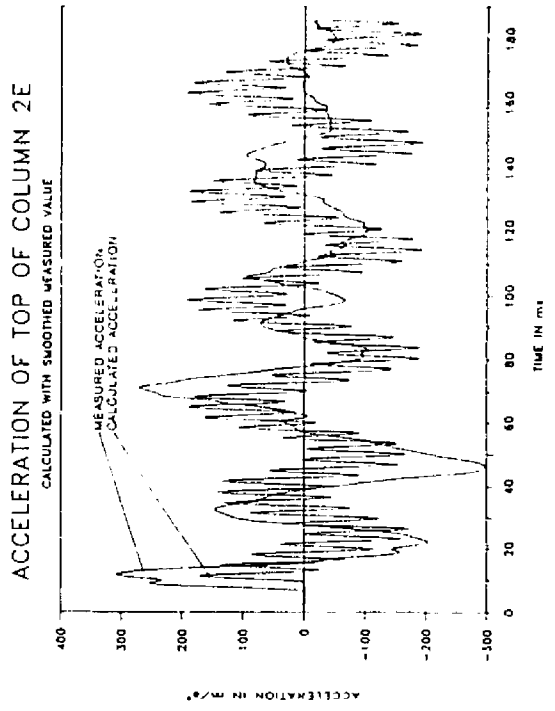

Fig.6.19 Acceleration

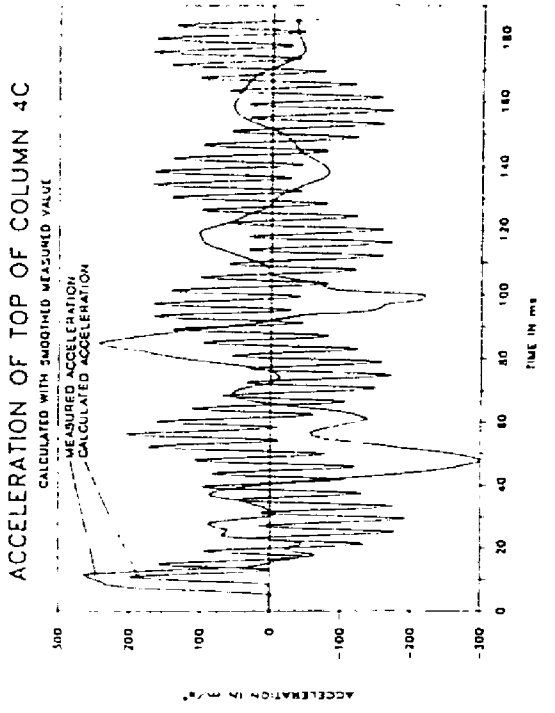

Acceleration Col 4C

Stellenbosch University http://scholar.sun.ac.za

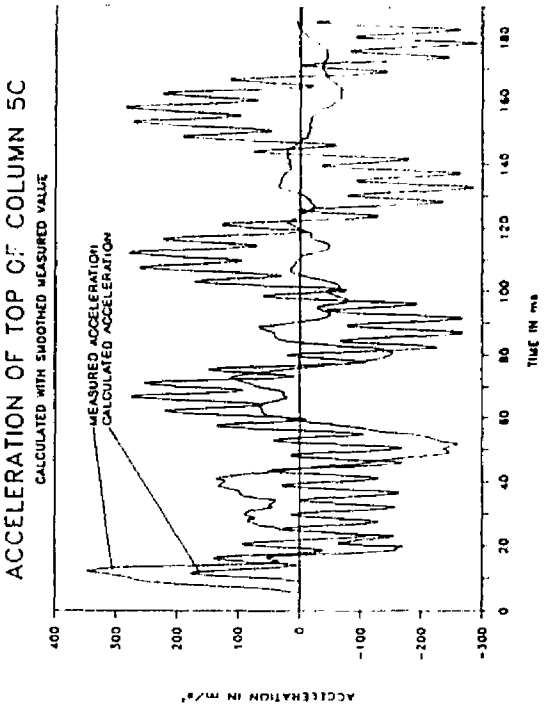

Fig.6.31: Acceleration - Col.5C

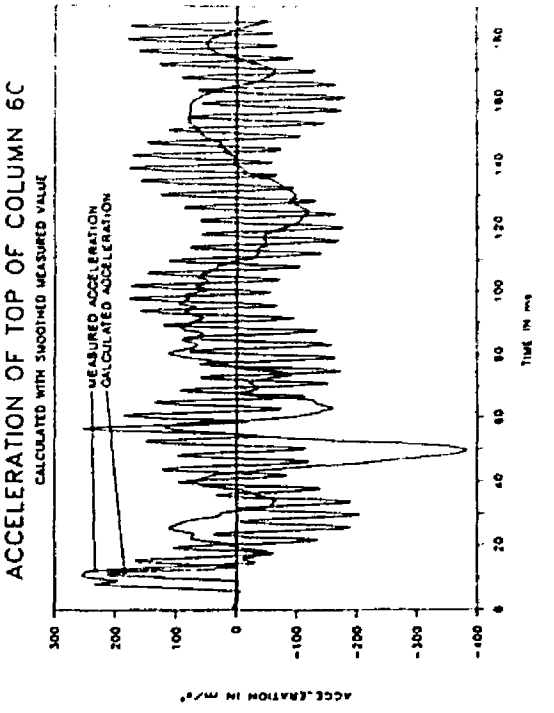

Fig.6.32: Acceleration - Col.6C

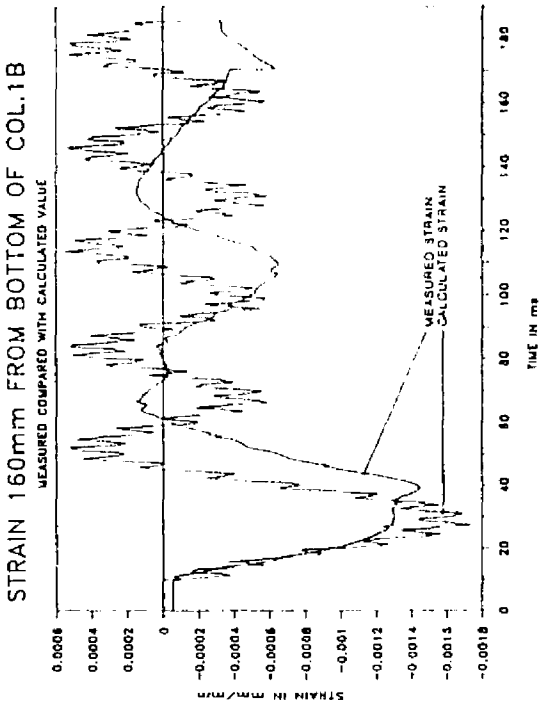

Fig.6.33: Strain - Col.1B

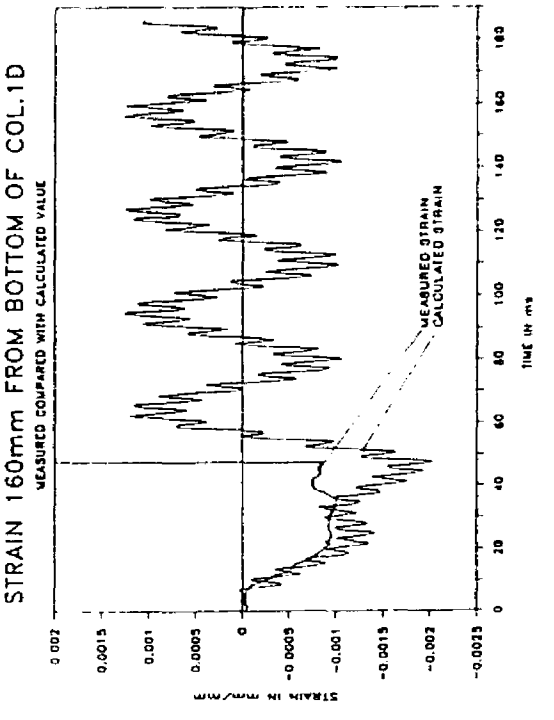

Fig.6.34: Strain - Col.1D

Stellenbosch University http://scholar.sun.ac.za

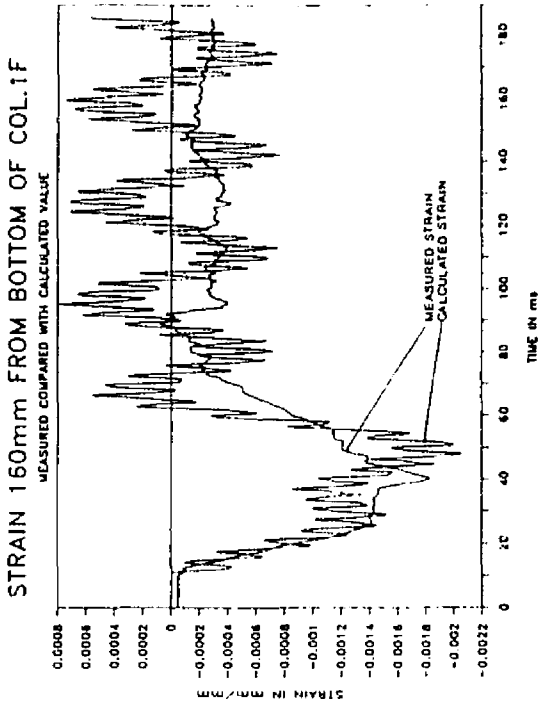

Fig.6.35: Strain - Col.1F

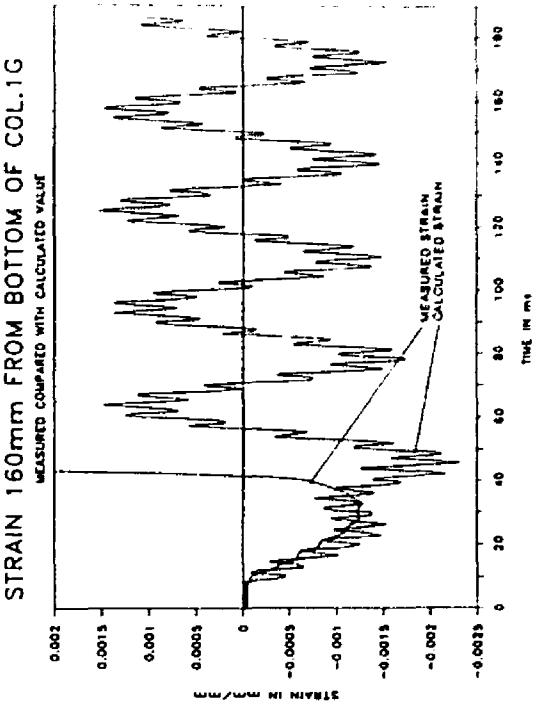

Fig.6.36: Strain - Col.1G

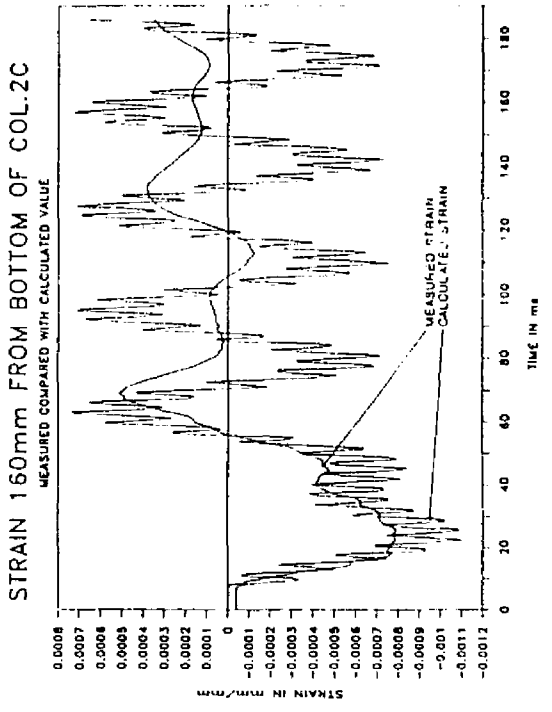

Fig.6.37: Strain - Col.2C

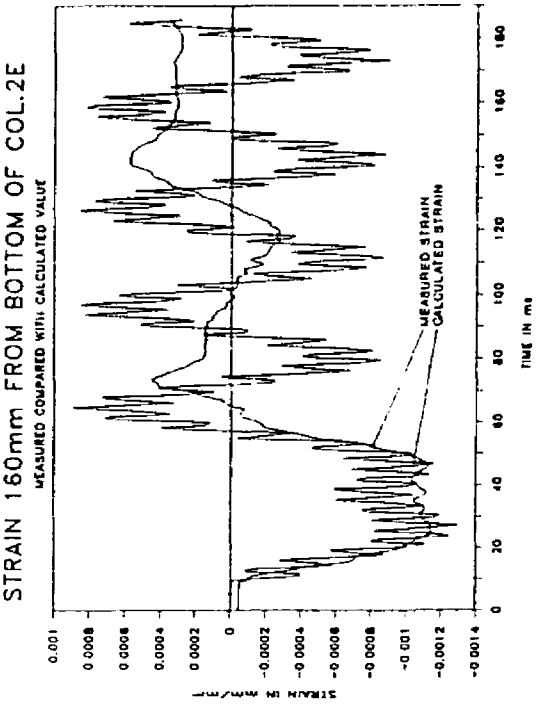

Fig.6.38: Strain - Col.2E

Stellenbosch University http://scholar.sun.ac.za

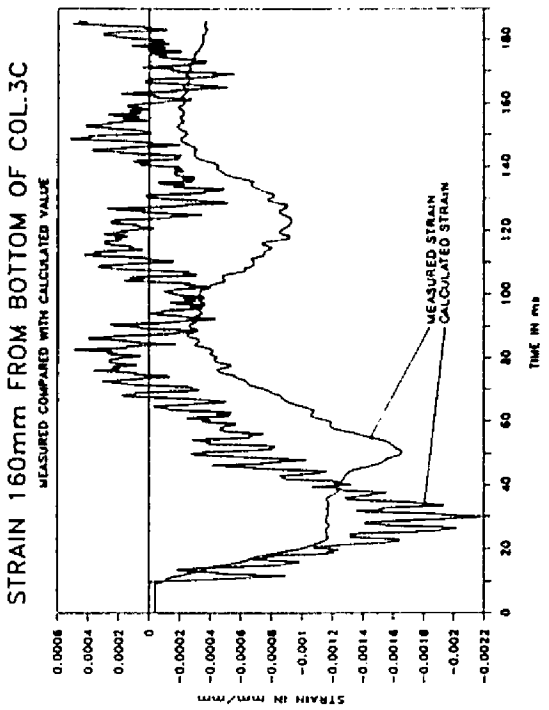

Fig.6.39: Strain - Col.3C

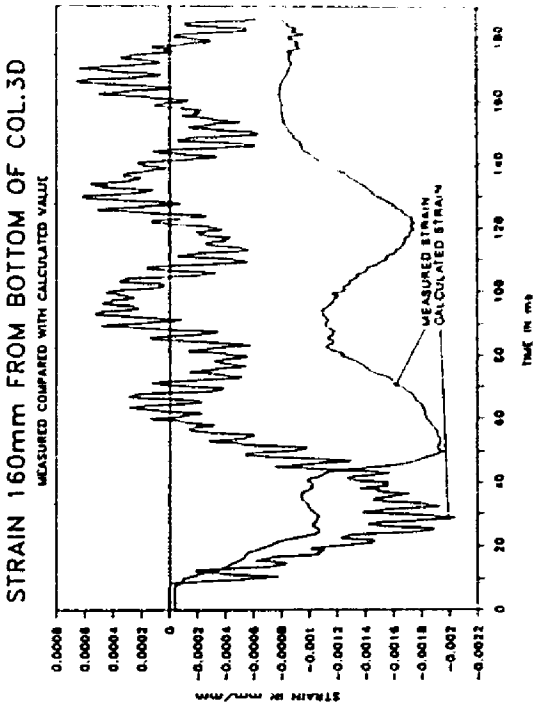

Fig.6.40: Strain - Col.3D

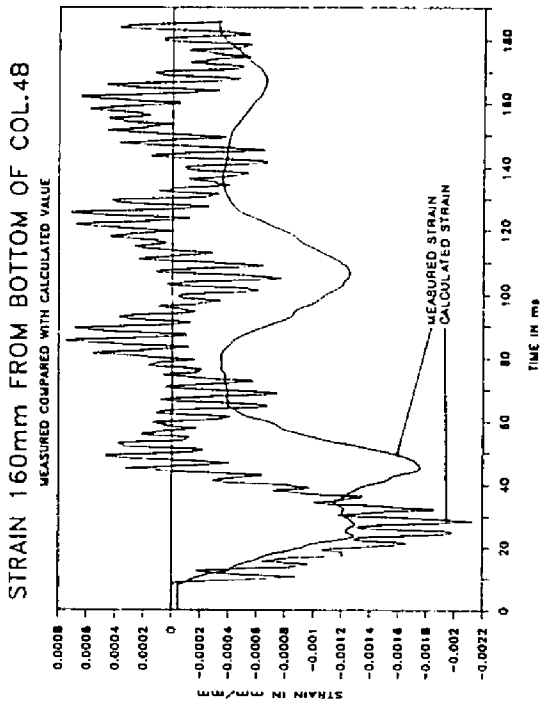

Fig.6.41: Strain - Col.4B

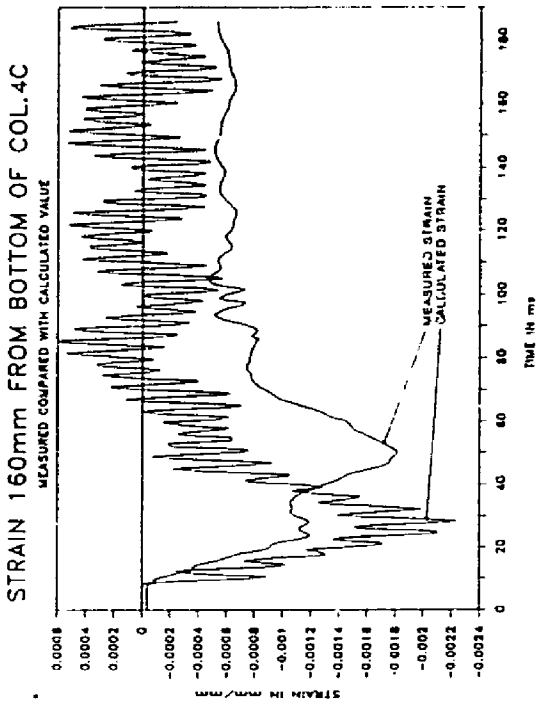

Fig.6.42: Strain - Col.4C

Stellenbosch University http://scholar.sun.ac.za

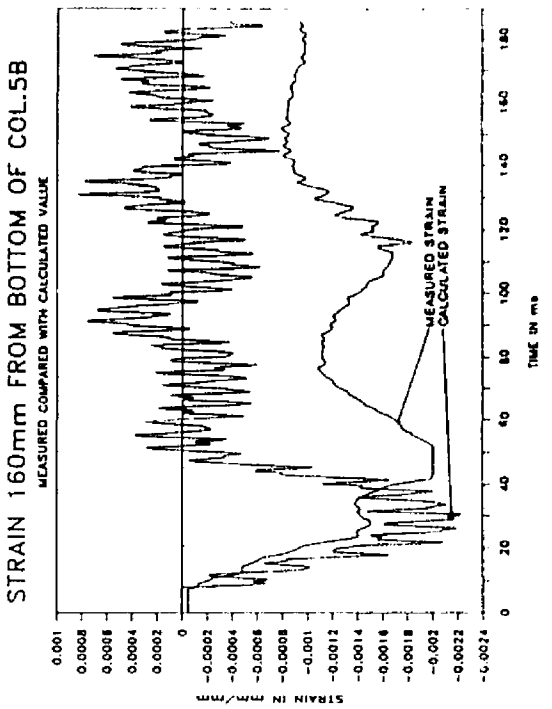

Fig.6.43: Strain - Col.5B

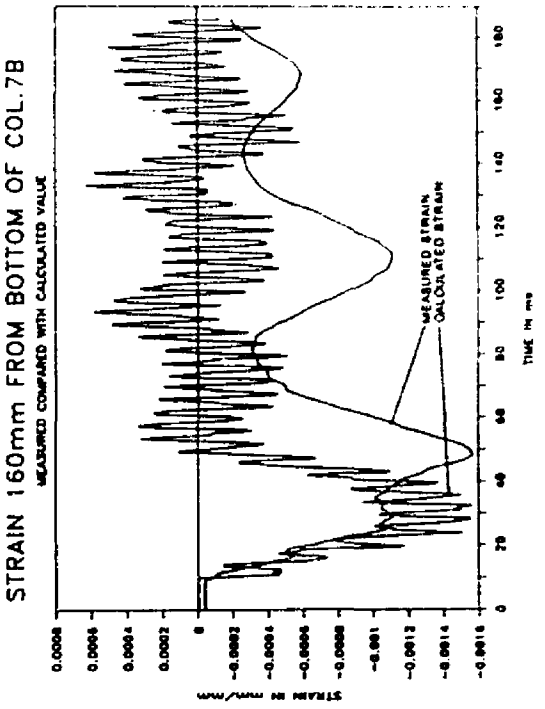

Fig.6.44: Strain - Col.7B

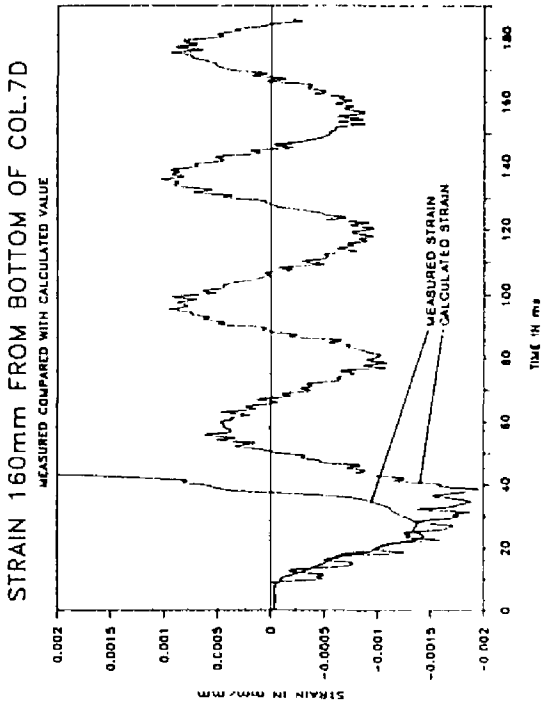

Fig.6.45: Strain - Col.7D

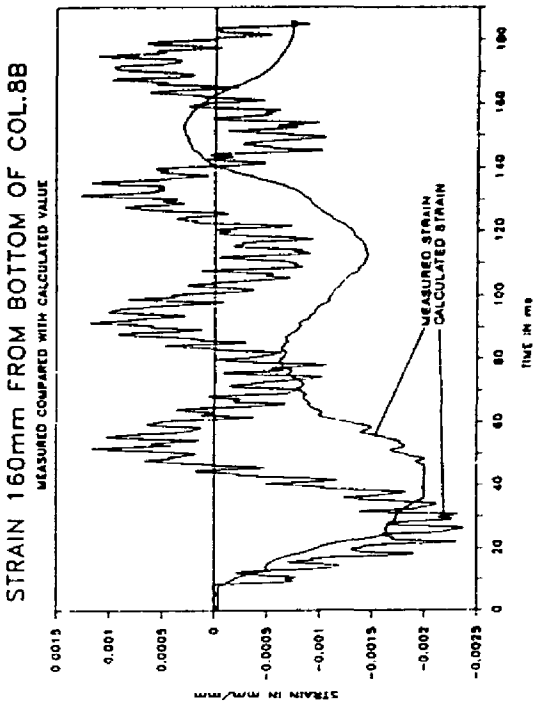

Fig.6.46: Strain - Col.8B

Stellenbosch University http://scholar.sun.ac.za

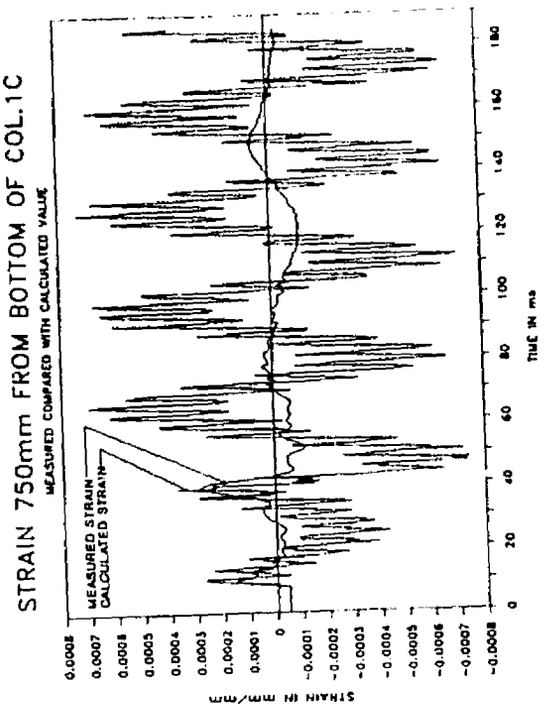

Fig.6.47: Strain - Col.1C

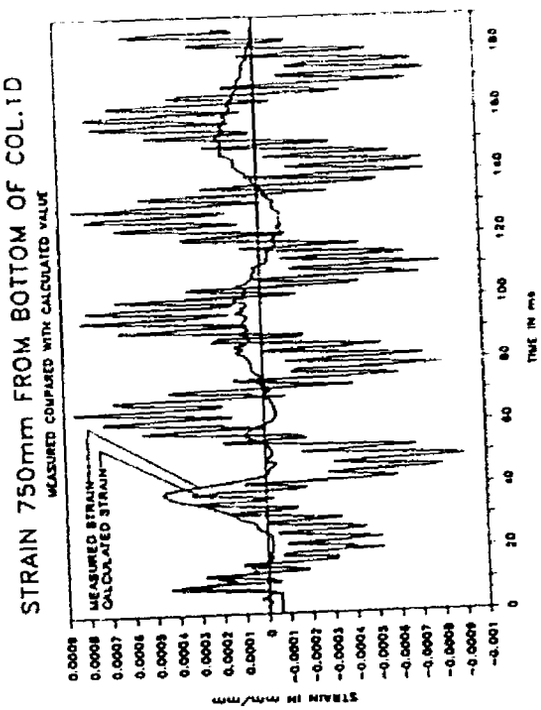

Fig.6.48: Strain - Col.1D

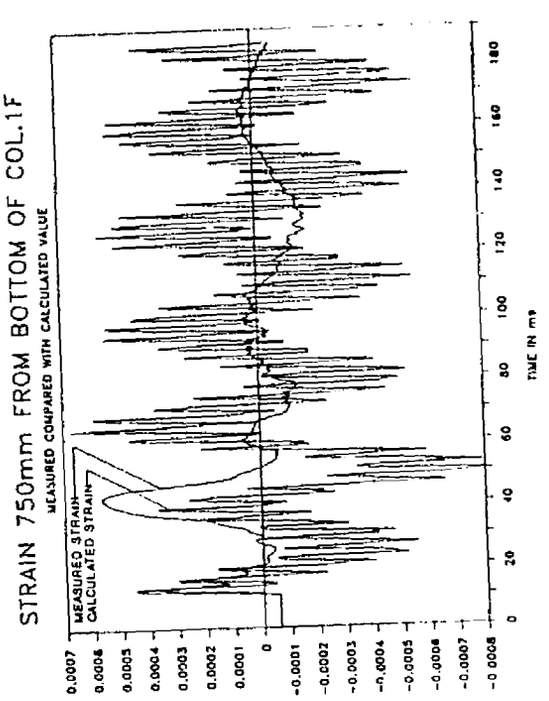

Fig.6.49: Strain - Col.1F

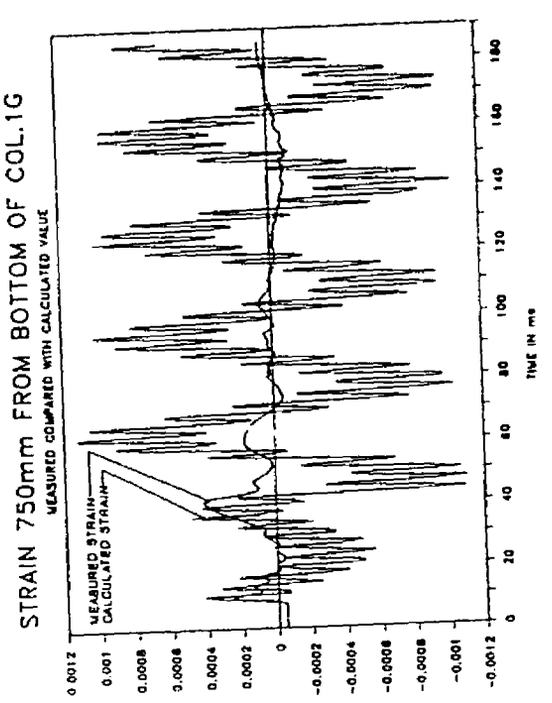

Fig.6.50: Strain - Col.1G

Stellenbosch University http://scholar.sun.ac.za

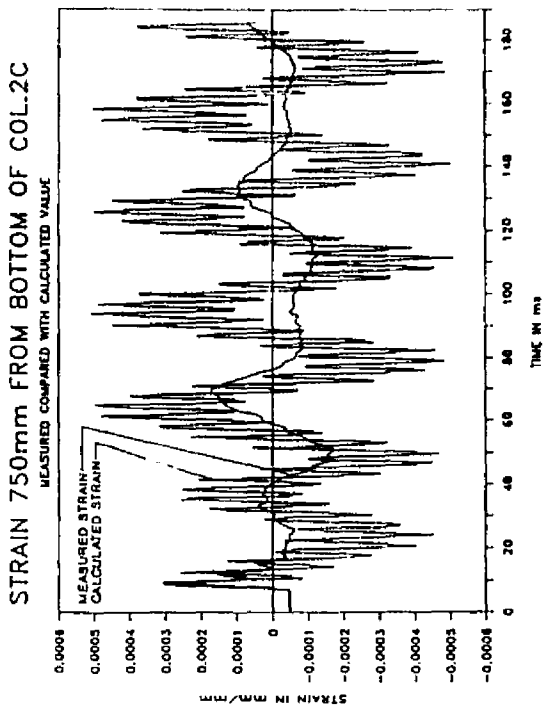

Fig.6.51: Strain - Col.2C

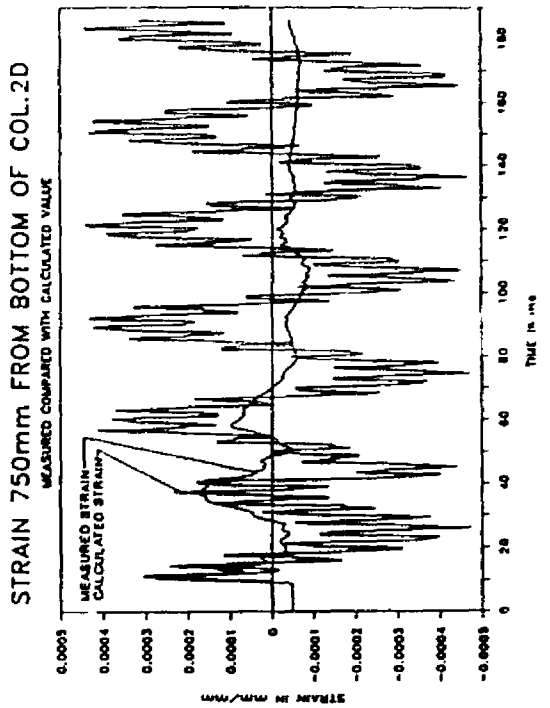

Fig.6.52: Strain - Col.2D

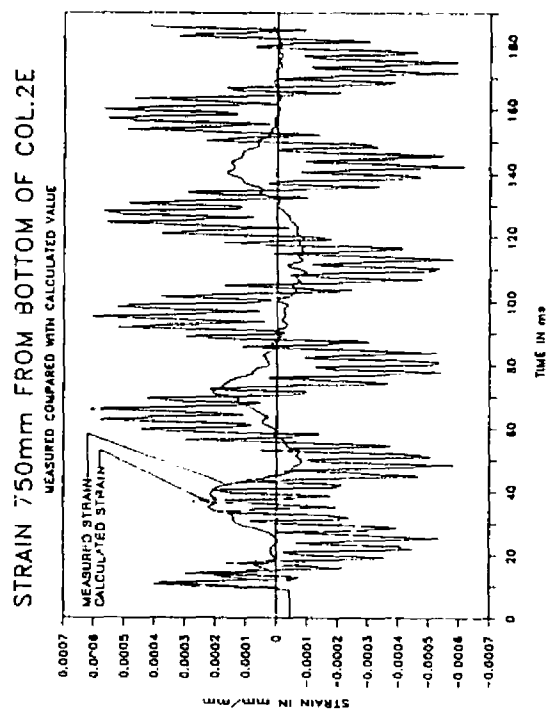

Fig.6.53: Strain - Col.2E

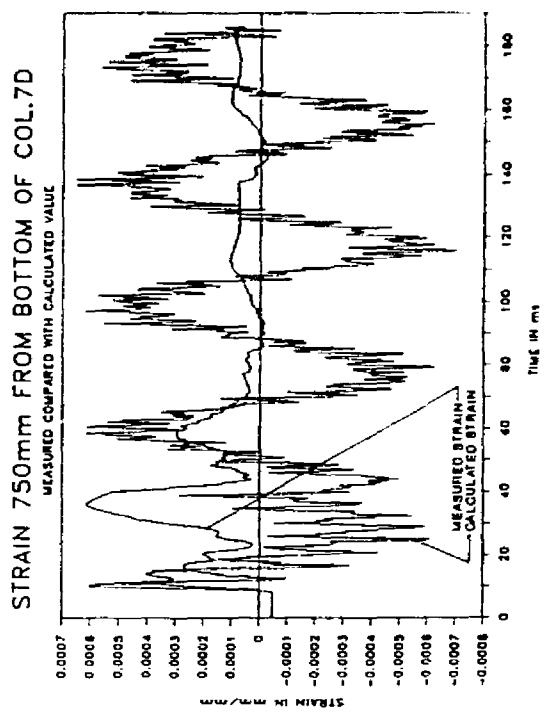

Fig.6.54: Strain - Col.7D

Stellenbosch University http://scholar.sun.ac.za

7. EXPERIMENTAL INVESTIGATION AND RESULTS.

7.1 Introduction

In this chapter the experimental investigation and results will be discussed. As indicated in chapter 1, the experimental investigation is the most important part of this dissertation. Therefore a very comprehensive report on the experimental work is given in Appendix B. All the results of all the tests are given in the Appendix in graphical form. The results presented in the Appendix contain an almost inexhaustible source of information and thus should be very valuable for further investigations of different aspects of this problem. The difficulties experienced with some of the tests and instrumentation are also discussed in the Appendix. It is the wish of the author that the detailed results and the short discussions of each test should help to facilitate further investigations.

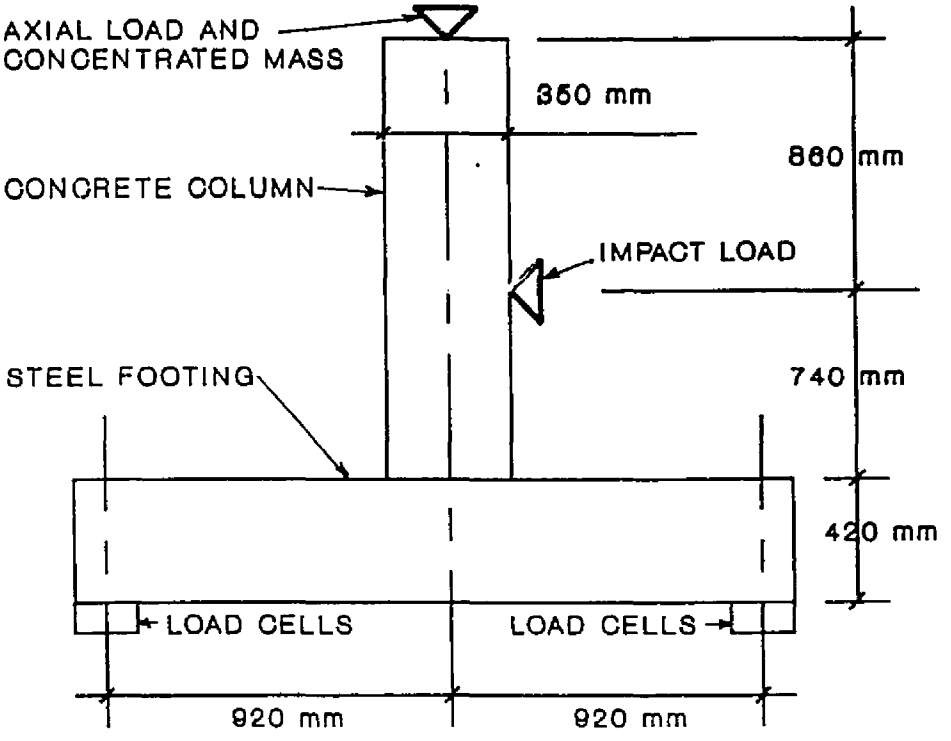

Figure 7.1:Experimental set-up.

Stellenbosch University http://scholar.sun.ac.za

In this chapter the most important results will be discussed and only a selection of typical results will be given to illustrate various aspects. For more results the reader is referred to Appendix B.

The instrumentation used, is also described in detail in Appendix B and thus will not be dealt with in this chapter. Details of the test columns as well as the test arrangement are also shown and discussed in the Appendix.

7.2 Experimental investigation

A total of 39 cantilever columns were tested under impact and or static loadings. The test columns were subjected to a horizontal impact load and or a horizontal static load while it was also subjected to an axial load. Of the 39 tests, the first three tests were used to evaluate and verify the test system as well as the instrumentation used. These results indicated where the test system and instrumentation had to be modified or improved. None of these preliminary results were used in any analysis.

The remaining 36 columns were divided into eight groups of columns. With each group the influence of a specific aspect or parameter on the behaviour of the column was investigated. The first column of each group was tested statically (with a horizontally applied load), up to failure of the column, to determine the static strength of the column. The remaining columns in that group were then tested dynamically under an impact load. The second column in the group (the first to be subjected to an impact load) was subjected to an impact load which peaked at a value close to the static failure load of the first column. With the third column in each group it was tried to introduce an impact load to the column that was just below or

Stellenbosch University http://scholar.sun.ac.za

in the region of the impact failure load of that group of columns. With the last column of each group it was tried to induce failure under the impact load. In some groups more than four columns were tested. If a column did not fail under the impact load, an increasing horizontal static load was immediately applied to the column to determine the reserve strength of the column.

With the first group the influence of an increase in the percentage of longitudinal reinforcement was investigated. With the second group the influence of less stirrups, with the same longitudinal reinforcement as that of group one, was investigated. The third group was used as a reference for all the other groups. Group three also had less longitudinal reinforcement and fewer stirrups than that of group one. Group four was exactly the same as group three but with a larger stirrup spacing. Group five was exactly the same as group three but with varying concrete strengths. This group was used to investigate the repeatability of the tests. Group six was the same as group three, but with only 1/5 of the axial load of group three. Thus the sixth group was used to investigate the influence of the axial load on the columns. Groups seven and eight were used together with group three to investigate the influence of the concrete strength on the columns. The concrete compressive cube strength of group seven was about 10 MPa lower than that of group three, while the concrete compressive cube strength of group eight was about 10 MPa higher than that of group three.

Normally all the parameters were kept constant except for the parameter under investigation. Table 7.1 summarizes and compares some of the test parameters and results.

TABLE 7.1 : Test results

Column No	Reinforcing			Concrete 7-day (MPa) Strength		Striker Mass (kg)	Impact Vel. (m/s)	Perm. Buffer defl. (mm)	Max. horizontal impact (kN)	Max. hor. static load (kN)	Axial load excl. 2 kN of load beam						Angles of major cracks with long. axis degrees	Type of failure
	Longitudinal	%	Stirrups	Compr.	Tens.						Static			Impact				
											Initial	Max.	% up	Initial	Max.	% up		
1A	8Y16	3,0	R8 @ 100	30,78	3,27	-	-	-	-	169,7●	97,9	105,2	7,7	-	-	-	29°; 39°; 57°	3
1B				32,16	4,02	750	6,398	75	182,2	180,2	96,4	101,5	5,3	98	140	42,9	30°; 40°; 61°	3
1C				29,91	3,37	950	6,611	120	283,9	177,8	98,0	104,0	6,1	99	138	39,4	32°; 40°; 57°	3
1D				31,89	3,77	1150	6,644	132	268,5	184,6	99,9	105,0	5,1	98	160	63,3	31°; 37°; 55°	3
1E				28,76	3,03	-	-	-	-	185,1	98,3	104,0	5,8	-	-	-	31°; 36°; 56°	3
1F				28,99	2,87	1250	6,940	132	259,2	170,9	97,7	100,0	2,4	98	158	61,2	27°; 36°; 63°	3
1G				28,01	2,97	1450	6,683	144	328,0	-	-	-	-	96	128	33,3	36°; 50°●	2
2A	8Y16	3,0	R8 @ 250	30,78	3,31	-	-	-	-	158,3	97,6	102,6	5,1	-	-	-	29°; 38°●	4
2B				29,08	2,63	750	7,123	108	-	147,6	97,6	101,0	3,5	-	-	-	40°●; 54°	4
2C				30,84	3,32	750	6,462	105	125,0	139,0	98,3	102,5	4,3	97	125	28,9	34°●; 54°	4
2D				30,63	3,38	950	6,407	127	165,6	-	-	-	-	98	130	32,7	33°●; 41°	2
2E				29,10	3,07	850	6,522	111	160,9	157,5	98,3	103,1	4,9	97	128	32,0	37°●	4
3A	4Y16	1,5	R8 @ 150	27,53	2,59	-	-	-	-	117,0	98,0	104,0	6,1	-	-	-	41°; 54°	3
3B				26,50	2,64	650	6,766	91	-	116,0	99,6	105,8	6,2	98	155	58,2	41°; 54°	3
3C				26,35	3,00	850	7,222	111	147,1	115,4	98,9	101,7	2,8	97	176	81,4	37°; 54°	3
3D				25,35	2,83	1050	6,517	118	178,4	118,3	102,9	121,0	17,6	98	188	91,8	39°; 57°	3
3E				31,69	3,64	1150	6,751	122	206,4	119,6	98,6	116,5	18,2	99	200	202,0	47°; 62°	3
4A	4Y16	1,5	R8 @ 200	30,80	3,33	-	-	-	-	116,2	96,7	102,5	6,0	-	-	-	45°; 60°	3
4B				28,10	3,03	650	6,652	92	121,6	116,9	98,0	116,0	18,4	97	148	52,6	41°; 60°	3
4C				28,90	2,81	850	7,137	107	151,4	117,0	98,9	110,0	11,2	98	170	73,5	44°; 63°	3
4D				30,10	3,27	1050	6,439	118	197,5	-	-	-	-	97	160	65,0	35°●; 60°	2
5A	4Y16	1,5	R8 @ 150	26,40	2,85	-	-	-	-	117,5	98,6	105,0	6,5	-	-	-	41°; 53°; 67°	3
5B				23,00	2,79	850	7,195	111	146,4	111,6	98,7	114,0	15,5	97	160	65,0	36°●; 51°; 71°	3
5C				19,70	2,37	1150	6,749	122	175,6	-	-	-	-	98	155	58,2	41°●; 66°	2
6A	4Y16	1,5	R8 @ 150	29,30	3,30	-	-	-	-	110,2	18,8	27,4	45,7	-	-	-	26°; 47°; 60°	3
6B				28,20	2,80	650	6,931	86	147,7	114,0	20,4	36,4	78,4	0	100	100,0	37°; 45°; 63°	3
6C				30,00	3,43	850	7,163	105	157,1	116,0	20,2	36,2	79,2	20	130	650,0	33°; 50°; 57°	3
6D				30,00	3,36	1150	6,660	126	224,6	-	-	-	-	20	88	440,0	45°●	2
7A	4Y16	1,5	R8 @ 150	41,50	4,06	-	-	-	-	126,2	98,8	112,5	13,9	-	-	-	38°; 51°; 71°	3
7B				37,90	3,62	750	7,123	105	149,8	125,0	98,5	119,6	21,4	100	165	165,0	37°; 53°; 68°	3
7C				37,40	3,67	950	6,716	111	167,0	123,4	98,9	118,1	19,4	97	180	185,6	39°; 57°	3
7D				36,70	3,19	1250	7,046	124	229,8	-	-	-	-	99	154	155,6	41°●; 56°	2
8A	4Y16	1,5	R8 @ 150	16,40	1,73	-	-	-	-	107,4	98,4	103,1	4,8	-	-	-	32°; 45°; 65°	3
8B				16,60	1,83	650	6,820	84	131,3	106,4	98,3	114,0	16,0	98	152	155,1	29°; 41°; 59°	3
8C				18,20	2,18	950	7,051	107	181,9	-	-	-	-	98	153	155,1	30°●; 50°	2
8D				19,80	2,29	850	7,091	100	164,6	-	-	-	-	98	156	159,2	34°●; 48°; 67°	2

● Unreliable result due to rotational slip at footing

Stellenbosch University http://scholar.sun.ac.za

Stellenbosch University http://scholar.sun.ac.za

* The crack along which the shear failure of the column occurred. (Normally all the cracks fanned out from the rear bottom corner of the column.)

** Four failure types of the columns were possible:

Type 1: Flexural failure of the column under the impact test conditions.

Type 2: Shear failure of the column under the impact test conditions.

Type 3: Flexural failure of the column under the static test conditions.

Type 4: Shear failure of the column under the static test conditions.

7.2 Failure criterion.

Two failure criteria were used for the columns. The first criterion is for flexural failure of the column and the second for shear failure.

When a column's deflection increased without any increase in the horizontally applied load, it was considered as a flexural failure of the column. Obviously this criterion would be very difficult to be applied to an impact test. Therefore after the impact, the column was inspected visually and if there was little recovery of the deflection of the column, it was considered to have failed in flexure. The remaining bearing capacity, for a horizontally applied load, of the column was also determined by executing subsequently a static test, as mentioned earlier, on the column.

Stellenbosch University http://scholar.sun.ac.za

The shear failure criterion was primarily based on the visual inspection of the column. If a diagonal crack widened to the extend that no more shear forces could be transferred, the column was considered to have failed in shear. Only a slight increase (figures B.294 and B.346) and then a dramatic drop (figure B.280) in the measured axial reaction, during the static test, also indicated a shear failure. During the impact tests, a dramatic drop in the measured axial reaction also indicated a shear failure of the column. This is contrary to what happened in case of a flexural failure. In the latter instance the measured axial resistance gradually approached a sustained maximum during both the static and impact tests.

7.4 Static test results.

The static test columns were analyzed according to the modified compression field theory of Collins and Vecchio (30, 31, 164, 165, 166 and 167). This theory predicts the response of a reinforced or prestressed concrete section under shear, moment and axial load. The theory is described very extensively in the mentioned papers and books and thus will not be repeated here.

A spreadsheet computer program, UMNV, by Maritz (184) was used for the analysis of the static test columns. The program UMNV (Ultimate Moment, Normal force and shear (V)) is based on the modified compression field theory and uses with some modifications an algorithm given by Collins and Mitchell (31).

The results of the program for the static tests of each group of columns are presented graphically in figures 7.2 to 7.8 and the comparisons between the measured values and the predicted values are given in Table 7.2. Figures 7.2 to 7.8 show the M/V diagrams (moment/shear diagrams) for the different groups of columns. The details of the groups of columns are given in Appendix B.

Stellenbosch University http://scholar.sun.ac.za

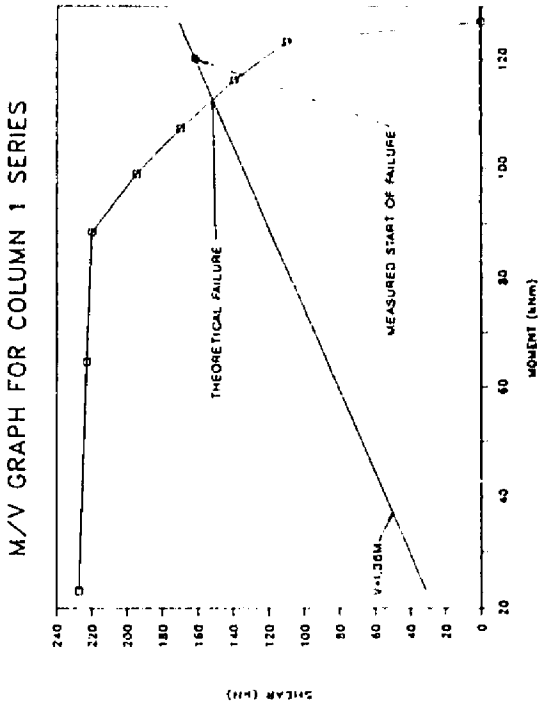

Figure 7.2: M/V - Group 1

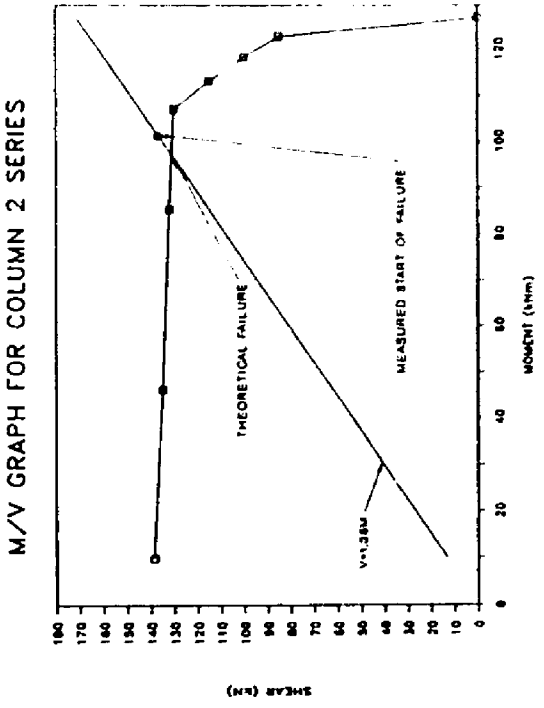

Figure 7.3: M/V - Group 2

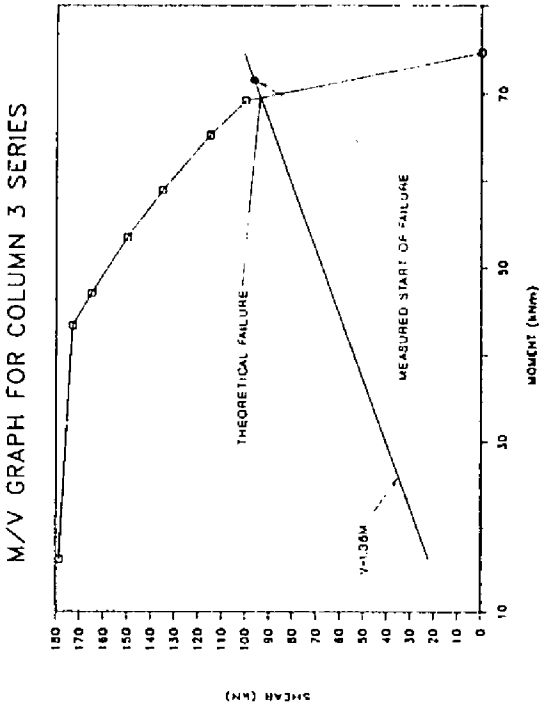

Figure 7.4: M/V - Group 3

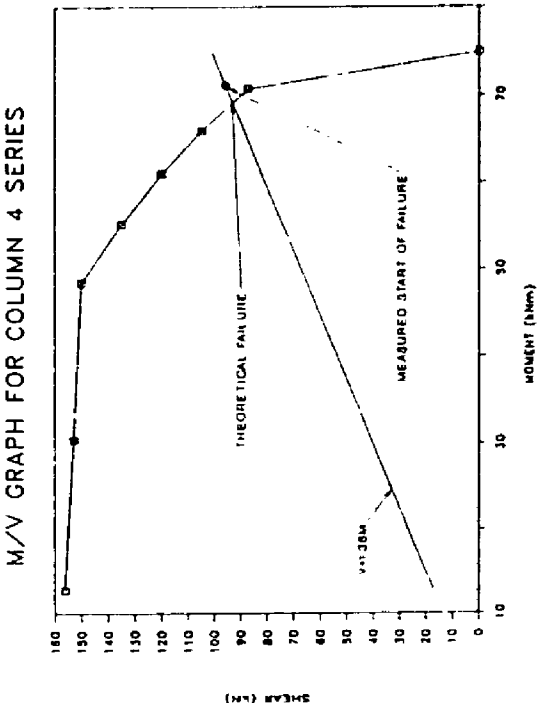

Figure 7.5: M/V - Group 4

Stellenbosch University http://scholar.sun.ac.za

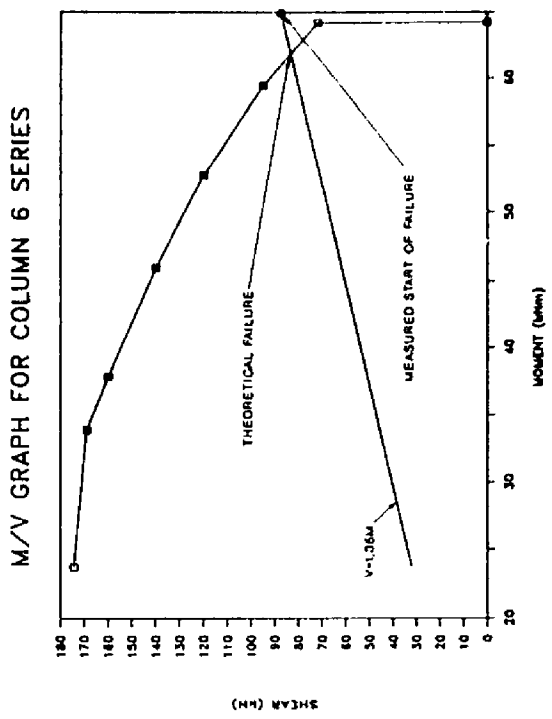

Figure 7.6: M/V - Group 6

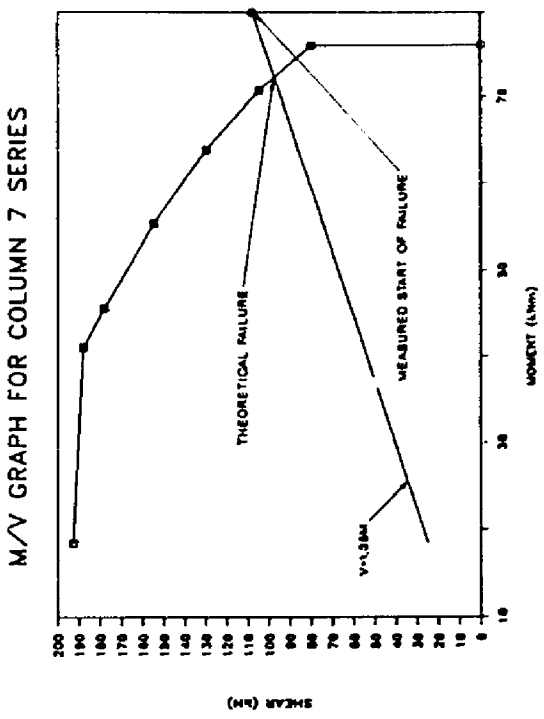

Figure 7.7: M/V - Group 7

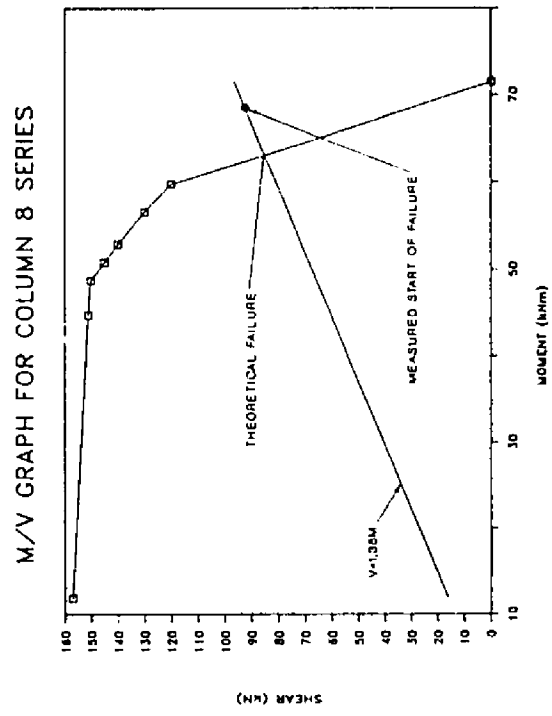

Figure 7.8: M/V - Group 8

Stellenbosch University http://scholar.sun.ac.za

The predicted failure loads are compared with the measured values at the start of failure of the columns. Although the ultimate failure was a little higher, the start of failure of the column was considered as the acceptable criterion. The "measured" moment and shear were derived directly from the measured, horizontally applied, static load. For the theoretical value a constant axial load similar the the original axial load applied to the test column was accepted.

Table 7.2: Summary of static test results

Col	Program UMNV Results (Predicted failure values)			Measured Results (Measured start of failure)		
Group	Shear (kN)	Moment (kNm)	Dominating type of failure	Shear (kN)	Moment (kNm)	Dominating type of failure
1	152	113	Flexure	162	120	Flexure
2	131	97	Shear	137	102	Shear
3	94	70	Flexure	97	72	Flexure
4	93	69	Flexure	96	71	Flexure
6	83	62	Flexure	95	70	Flexure
7	98	73	Flexure	108	80	Flexure
8	86	64	Flexure	91	67	Flexure

Table 7.2 shows that this theory predicts the start of the failure of the columns quite accurately. It under estimates this failure value with an average of as little as 6%.

7.5 Results of impact tests.

7.5.1 Reserve strength of columns.

If a test column did not fail under the impact load, a subsequent increasing static load was immediately applied to the column to determine its reserve strength. In Table 7.3 the static failure

Stellenbosch University http://scholar.sun.ac.za

load of an undamaged column is listed along with the static failure load of a damaged equivalent column, that is, a column which was subjected to an impact load but did not fail.

Table 7.3: Results of reserve strength tests of the columns

Column	Impact Load (kN)	Failure load of similar col. tested statically (kN)	Reserve Failure Load (kN)	Difference (kN)	Difference %	Type of Failure
1B	182,2	185,1	180,2	4,9	2,6	Flexure
1C	283,9	185,1	177,8	7,3	3,9	Flexure
1D	268,5	185,1	184,6	0,5	0,3	Flexure
1F	259,2	185,1	170,9	14,2	7,7	Flexure
2C	125,0	158,3	139,0	19,3	12,2	Shear
2E	160,9	158,3	157,5	0,8	0,5	Shear
3C	147,1	117,0	115,4	1,6	1,4	Flexure
3D	178,4	117,0	118,3	-1,3	1,1	Flexure
3E	206,4	117,0	119,6	-2,6	2,2	Flexure
4B	121,6	116,2	116,9	-0,7	0,6	Flexure
4C	151,4	116,2	117,0	-0,8	0,7	Flexure
5B	146,4	113,5	111,6	1,9	1,7	Flexure
6B	147,7	110,2	114,0	-3,8	3,4	Flexure
6C	157,1	110,2	116,0	-5,8	5,3	Flexure
7B	149,8	126,2	125,0	1,2	1,0	Flexure
7C	167,0	126,2	123,4	2,8	2,2	Flexure
8B	131,3	107,4	106,4	1,0	0,9	Flexure

The results in Table 7.3 show that although cracks developed during the impact phase, the ultimate resistance of the columns were not significantly affected. The average of the percentage difference between the undamaged and damaged columns is only 2,8% If the two highest differences are omitted, the average percentage difference is only 1,85%. Some of the column's reserve strength was even slightly higher than that of the undamaged column. This means that if a column was subjected to an impact load and it did not fail, then the reserve strength of the column would be within 2% of the original value of an undamaged column.

Another interesting aspect is that if the undamaged column, tested statically, failed in flexure then the damaged column, tested statically, also failed in flexure. If the undamaged

Stellenbosch University http://scholar.sun.ac.za

column failed in shear then the damaged column tested statically also failed in shear. To confirm this type of behaviour for a wide spectrum of parameters, further tests will have to be undertaken.

These substantial reserve strengths of the columns indicate that if a column was damaged under impact conditions it need not be replaced unless the column failed completely. If the cracks could be repaired, with say an epoxy, the column would retain its ultimate static resistance and should be safe.

7.5.2 Influence of concrete strength

Figure 7.9 shows the maximum impact and static loads plotted against the concrete strength of the columns. All these columns were exactly the same except for the concrete strength. From this graph one can see clearly the influence of the higher strength concrete.

Three lines are shown on the graph. The bottom line presents the static flexural failure loads of all the test columns. As can be seen, this line runs through the failure values of the undamaged columns as well as through the values of the damaged columns (the reserve strength of the impact test columns). The second line represents the shear capacity of the statically tested columns as computed with the UMNV-program. The top line is drawn as a best fitted line through the ultimate impact shear failure loads of the columns as calculated with the free vibration theory derived in Chapter 5.

From figure 7.9 the influence the concrete strength can be seen clearly. Unfortunately all the impact failures were shear failures while similar columns tested under static conditions failed in flexure. This means that it is not possible to evaluate the exact percentage flexural strength increase of the columns due to an increase in the concrete strength. On the

Stellenbosch University http://scholar.sun.ac.za

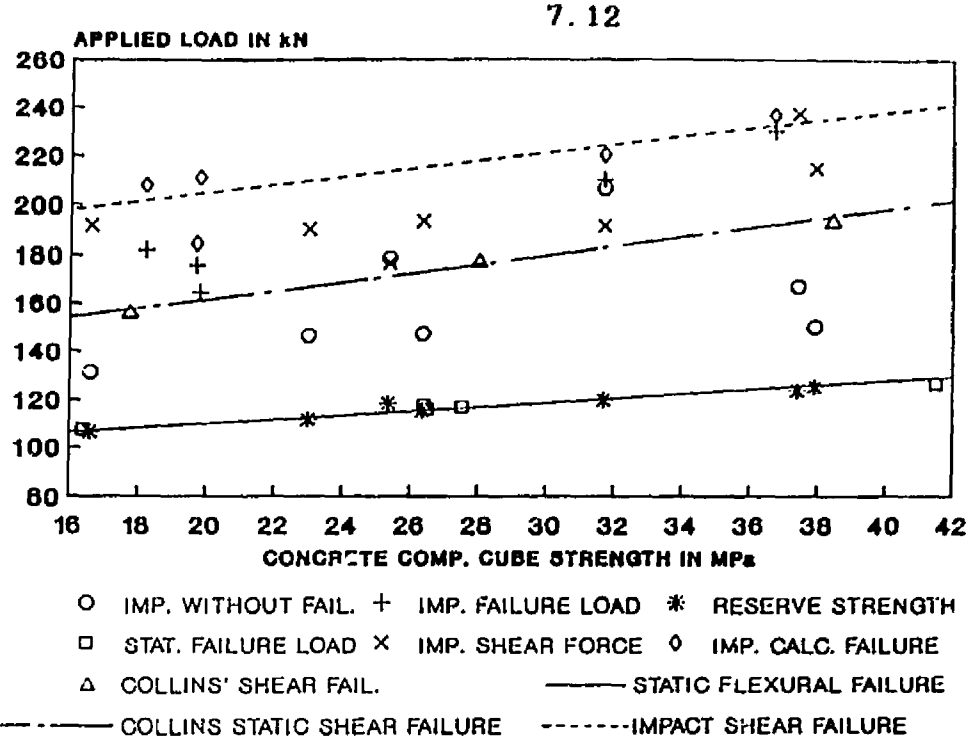

Figure 7.9: Influence of concrete strength on strength of dynamic and statically tested columns.

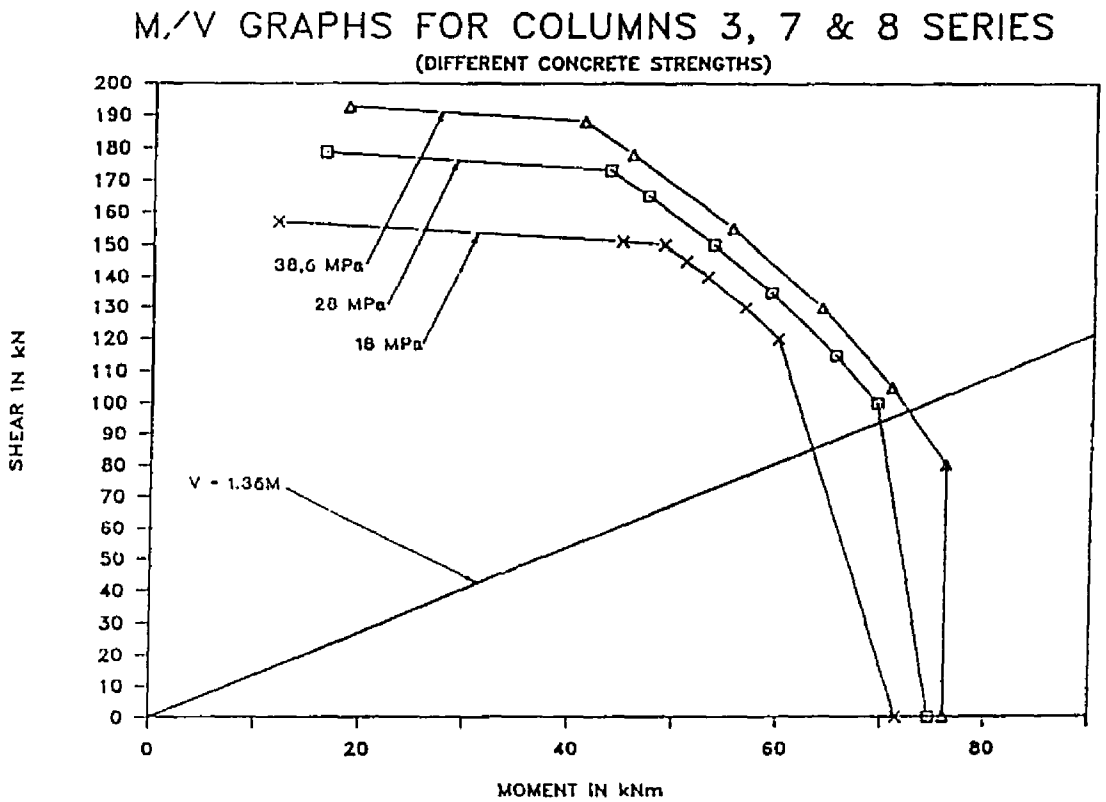

Figure 7.10: Increase in strength of statically tested columns due to increase in concrete strength (from UMNV-program).

Stellenbosch University http://scholar.sun.ac.za

other hand, the increase from the static shear strength of the column to the dynamic shear failure of the columns can be evaluated and from the above graph it is in the region of about 28%.

From the figure follows that the impact flexural strength of a column is 90% above the static value. Although the column did not fail in flexure after that increase, this increase is constant with the increase of the concrete strength.

Thus the same strength increase of the dynamic tested columns can be expected as that of the statically tested columns, due to an increase in concrete strength. In other words, the percentage increase in strength from the static strength to the impact strength of a column would be constant for a concrete of different compressive strengths. Figure 7.10 shows the strength increase of the statically tested columns as computed with UMNV for a static load.

7.5.3 Influence of shear reinforcement.

Figure 7.11 shows the influence of shear reinforcement on the static strengths of the columns by means of two M/V graphs for column groups 1 and 2. The columns of the two groups are exactly the same except for the shear reinforcement. Group 1 columns had R8 stirrups with a spacing of 100 mm, while group 2 columns had R8 stirrups with a spacing of 250 mm. Under static loading, group one columns failed in flexure while group two columns failed in shear.

Figure 7.12 shows the static M/V graphs for groups 3 and 4 columns. The columns of groups three and four were exactly the same except for the shear reinforcement of the columns. Group three had R8 stirrups with a 150 mm spacing, while group four had a spacing of 200 mm for its stirrups. From these two graphs the influence of the shear reinforcement is clearly visible.

Stellenbosch University http://scholar.sun.ac.za

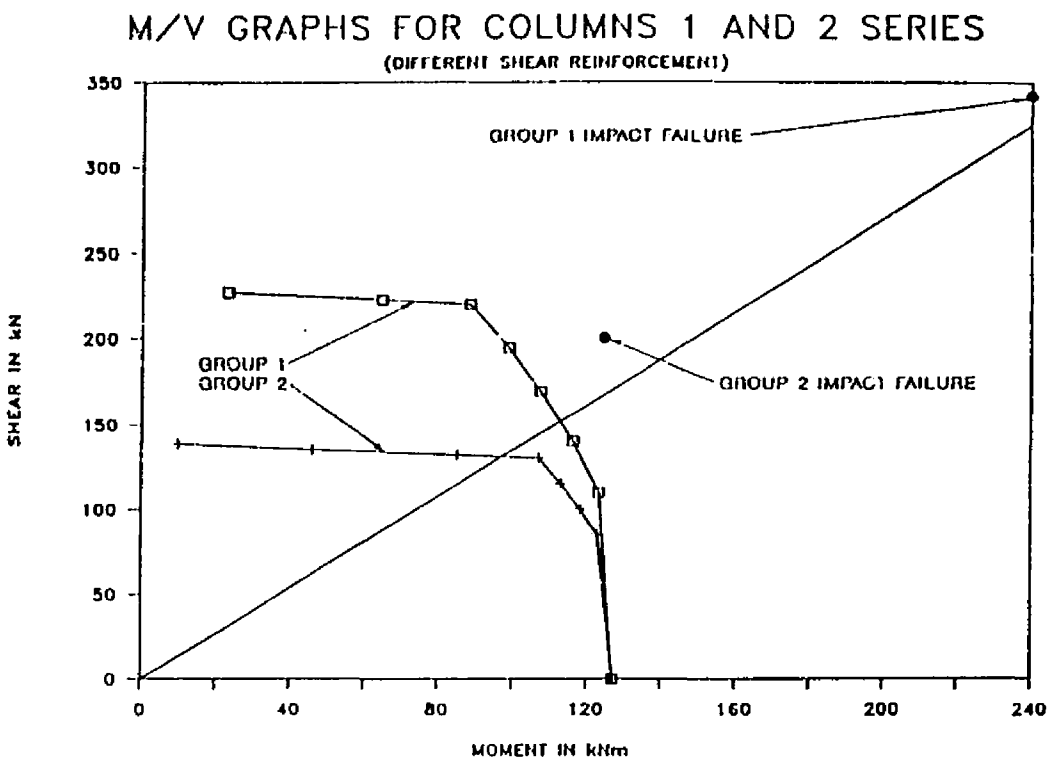

Figure 7.11: Static M/V graphs for column groups 1 and 2.

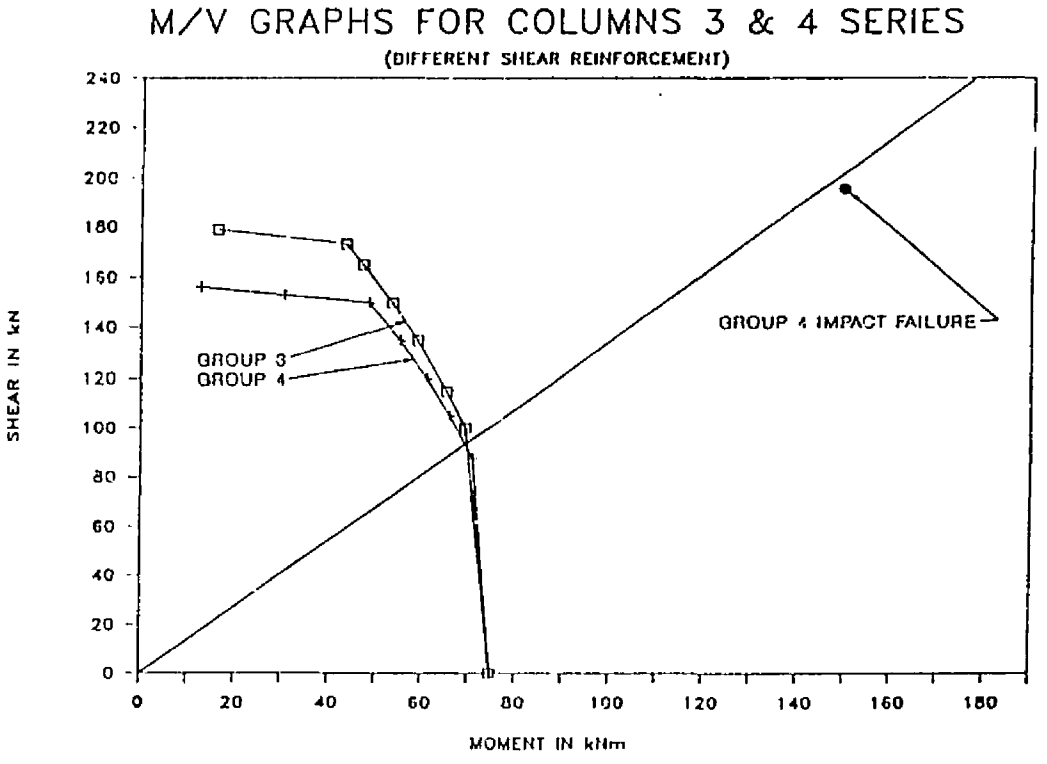

Figure 7.12: Static M/V graphs for column groups 3 and 4.

Stellenbosch University http://scholar.sun.ac.za

Figures 7.11 and 7.12 show two different aspects of shear reinforcement for the columns. With the two groups of columns of figure 7.12, both groups will fail in flexure under static conditions, while with the two groups of columns of figure 7.11, the one group will fail in flexure and the other in shear under static conditions.

Both figures 7.11 and 7.12 also show the impact failure points of these groups of columns. Obviously the data are very limited, but from the data available it is clear that if a column fails in shear under the static conditions, the strength increase under impact conditions is very limited compared to the strength increase of a column that fails in flexure under static conditions. The failure points shown on these two graphs are the points calculated with the theory derived in Chapter 5. If only the maximum impact load is considered and all the dynamic forces etc. are excluded, the strength increase from static to impact of group two is nearly zero. This can be seen in fogures 7.17 and 7.18. If the impact shear failure (calculated with the theory derived in Chapter 5 with the measured impact load) of these groups 1 and 2 are compared with their ultimate static shear (predicted by the modified compression theory), both these groups show an increase of somewhere between 40 and 50%.

Figure 7.12 shows something very interesting. Although columns of group 4 had less shear reinforcement than that of group 3, their flexural strength increase from static to impact conditions (according to the theory derived in Chapter 5) are in the same order (about 100%). On the other hand, the shear strength increase of group 3 was higher than that of group 4. The shear increase of group 3 was about 120% and that of group 4 about 100%. The increase of the shear of group 3 above the ultimate static shear capacity according to the modified compression theory was about 24% and that of group 4 was 25%. These two values compare quite good.

Stellenbosch University http://scholar.sun.ac.za

This means that a column will fail in shear under impact conditions if an ultimate shear force is reached, which is some percentage higher than the ultimate static shear capacity predicted by the M/V graphs. For groups 1 and 2 this value was somewhere between 40 and 50% and for groups 3 and 4 it was somewhere between 20 and 30%. More tests are necessary to clarify these results.

Thus to ensure a significant increase in the strength of the column from static to dynamic, one should ensure that adequate shear reinforcement is provided to ensure a flexural failure under static conditions.

7.5.4 Influence of longitudinal reinforcement.

The influence of the longitudinal or main reinforcement on the static strengths of the columns is illustrated by the M/V graphs (moment-shear graphs) for column groups 1 and 3 in figure 7.13. Group 1 had 3,06% longitudinal reinforcement, while group 3 had only 1,53%. Obviously the flexural strength of the columns is more sensitive to the percentage of longitudinal reinforcement than the shear strength.

Under impact loading the flexural strength increase above the static case was for both groups in the region of 100% above the predicted value according to the static M/V graph. Columns of both groups failed in shear under impact loading. Hence the flexural strength increase might even be relatively higher than the increase in shear strength though the latter is also for both groups in the region of a100% plus above the original expected shear.

If the impact failure loads (shear and moment) are compared with the ultimate static loads for maximum shear and maximum flexure, from the M/V graphs, it becomes very interesting. For both groups the increase of the flexure moment above the ultimate static value for pure flexure is in the region of 90 to 100%.

Stellenbosch University http://scholar.sun.ac.za

For the shear the increases differ. For group 1 the increase of the shear from the ultimate static value to the failure value is 44%. For group 3 the value is in the region of 25 to 30%. This value 25 to 30% is also visible on figure 7.9 where columns with the same longitudinal and shear reinforcement (including group 3) is plotted against concrete strength. The difference between the top two lines on the graph is about 28%. From this it appears as if an increase in longitudinal reinforcement tends to increase the shear capacity.

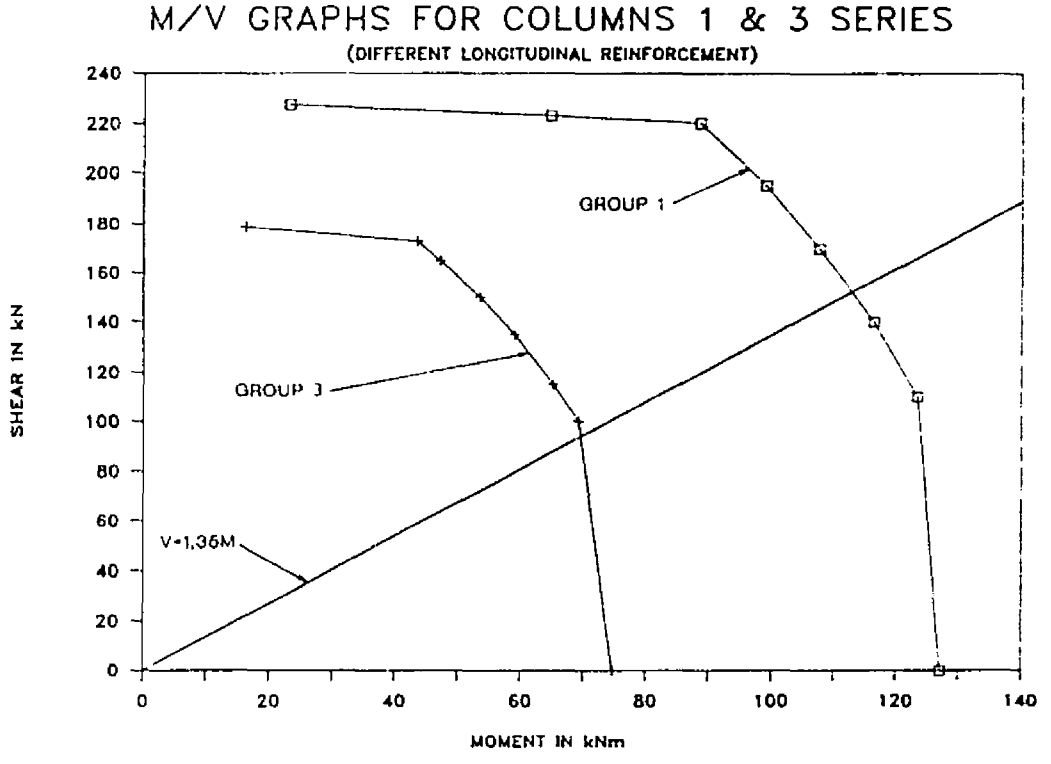

Figure 7.13: M/V graphs for column groups 1 and 3.

Thus the longitudinal reinforcement influences the increase of both the flexural and shear capacity above the ultimate static flexure and shear values of the M/V graphs. An increase in the longitudinal steel tends to increase the percentage increase of the shear above the ultimate static shear capacity of the column

Stellenbosch University http://scholar.sun.ac.za

while for the flexural increase, the percentage increase seems to stay a constant.

7.5.5 Influence of the axial load.

Figure 7.13 shows the static M/V graphs (moment-shear graphs) of column groups 3 and 6. These columns were exactly the same except for the difference in axial load of the two groups. Group 3 had the standard axial load of 100 kN and group 6 had an axial load of 20 kN. The impact failure points of group 6, as calculated by the proposed theory, is also shown in figure 7.14.

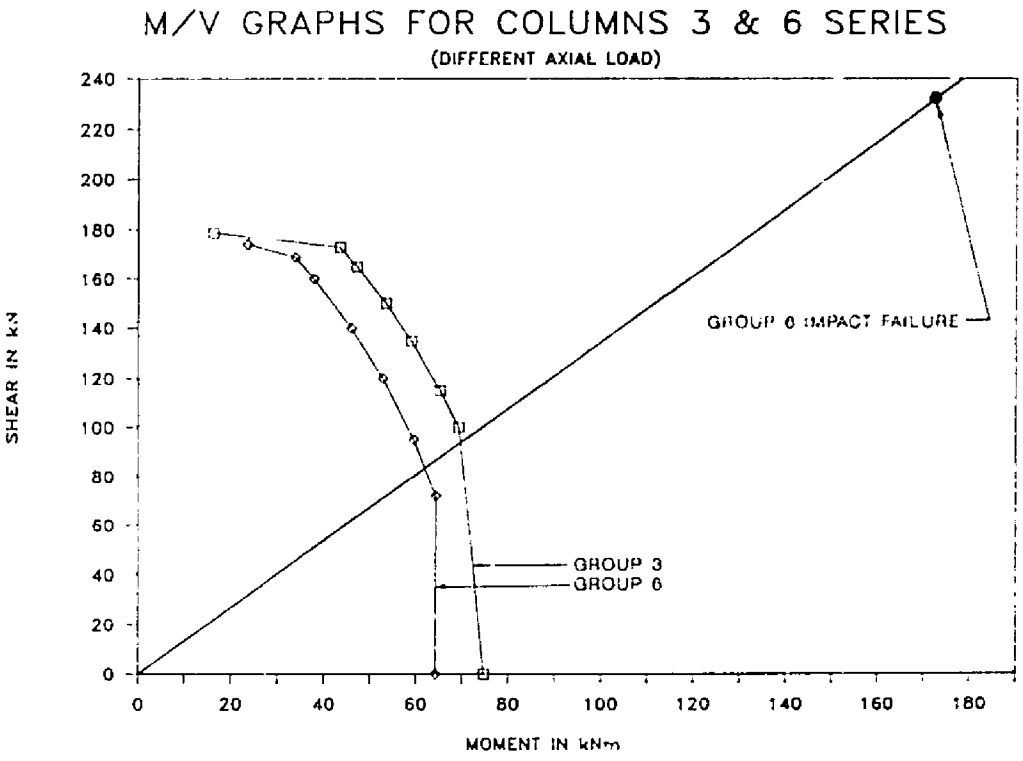

Figure 7.14: Static M/V graphs (moment shear) for column groups 3 and 6.

During the static test, both types of columns failed in flexure. Columns with the lower axial load failed at a little lower value than the columns with the higher axial load. This was predicted

Stellenbosch University http://scholar.sun.ac.za

by the M/V graphs. The ultimate shear failure value of the two groups as predicted by the M/V graphs are very close to each other as well.

7.5.6 Repeatability of results.

The columns of group five were used to verify the repeatability of the tests. Column 5A was identical to column 3A, hence, these columns were used to verify the repeatability of the static test. The measured deflection was nearly exactly the same for the two columns, as were the decrease and increase in the axial loads during the tests. The loads transferred through the footing to the floor of the laboratory were also exactly the same. The horizontal failure load for column 3A was 97 kN and that of column 5A, 97.5 .

Columns 5C and 8D were identical and again these two columns were used to prove the repeatability of the impact tests. The impact load history of column 5C peaked at a value of 175.6 kN, the maximum calculated bending moment was 164 kNm and the maximum calculated shear force was 188 kN. The impact load history of column 8D peaked at a value of 164.6 kN, the maximum calculated bending moment was 178 kNm and the maximum calculated shear force was 206 kN. In other words, these values were within 9% of each other. The maximum measured strain of the two columns were within 4% of each other. The forces transferred through the footing of the columns were also within 7% of each other. The maximum axial loads measured were within 2% of each other. The graphs registered by all the measuring instruments followed the same trend.

All the graphs mentioned in the previous two paragraphs are shown in Appendix B. All these results indicate that the repeatability of both the static and impact tests were very good and both type of tests gave consistent results.

Stellenbosch University http://scholar.sun.ac.za

7.6 Effects of the impact on the columns.

7.6.1 Moment and Shear.

From the previous discussions it is clear that the strength of a column is much higher under impact conditions than under static conditions. This increased strength is dependent on the reinforcement provided (longitudinal and shear reinforcement) as well as the concrete strength.

All the impact failures of the columns were shear failures. Only one column failed in flexure. This was one of the preliminary columns used to test and evaluate the equipment.

Figures 7.16 to 71.29 show the maximum calculated flexural moments and shear forces (calculated with the theory derived in Chapter 5), due to impact loading on a column, plotted against the deflection at the top of the column derived from the measured accelerations at the top of the column. These values are plotted together with the measured static test results of each group of columns. The impact deflections were derived from the measured accelerations by integrating the measured acclerations twice with respect to time. The dotted line in these figures is a suggested force-deflection relationship for the impact situation.

By comparing the suggested impact force-deflection curve with the measured static curve (Figures 7.16 to 7.29), it is quite evident that the column displays a significantly higher strength (capacity or resistance) under impact loading than under static loading.

The increase in the moment capacity of the column under impact loading could not be evaluated because all the columns, as already mentioned, failed in shear. No column failure under impact loading could be classified as a flexural failure, because the moment kept increasing as the column deflected. This was

Stellenbosch University http://scholar.sun.ac.za

confirmed by the measured loads transferred through the footing to the laboratory floor as shown in Figures 6.7 to 6.22.

To induce a flexural failure of the column under impact conditions it seems necessary to generate a flexural moment more than 100% bigger than the ultimate static moment (for maximum moment) given by the M/V graph for that column. It seems more likely that the column will fail in shear before such a value can be reached, except for a totally under reinforced member.

From the previous paragraph follows that many more tests have to be done to investigate the flexural failure of cantilever columns under impact loading, before any conclusions can be drawn.

The increase in the shear capacity of a column subjected to an impact load differed remarkably from the moment's increased capacity. The impact shear failure loads were compared with the ultimate static shear capacity (for max. shear) as given by the M/V graphs, rather than with the shear force where the columns are predicted to fail in flexure under static conditions. This showed, as discussed earlier, that the shear capacity increase is related to the shear as well as to the longitudinal reinforcement provided. All the columns with 1,53% longitudinal reinforcement (groups 3 to 8, including group 4 with less shear reinforcement) showed an increase of 20 to 30% in the shear capacity (Figures 7.54 to 7.58). The columns with 3,06% longitudinal reinforcement (group 1, and group 2 with less shear reinforcement) showed an increase of 40 - 50% (Figures 7.52 to 7.53).

7.6.2 Axial load on a column.

With the static tests the axial loads dropped slightly as soon as the first load step of the horizontal load was applied. This drop in the axial load continued with further load steps, until the first crack in the column became visible. As soon as the first crack became visible, the axial load began to rise with a further increase of the horizontal load. This shows that the

Stellenbosch University http://scholar.sun.ac.za

Table 7.4: Axial load's increases (loading beam weight of 2 kN not included)

Column	Static tests			Impact tests		
	Initial (kN)	Maximum (kN)	Increase (kN)	Initial (kN)	Maximum (kN)	Increase (kN)
1A	97,9	105,2	7,3	-	-	-
1B	96,4	101,5	5,1	98	140	42
1C	98,0	104,0	6,0	99	138	39
1D	99,9	105,0	5,1	98	160	62
1E	98,3	104,0	5,7	-	-	-
1F	97,7	100,0	2,3	98	158	60
1G	-	-	-	96	128	32
2A	97,6	102,6	5,0	-	-	-
2B	97,6	101,0	3,4	-	-	-
2C	98,3	102,5	4,2	97	125	28
2D	-	-	-	98	130	32
2E	98,3	103,1	4,8	97	128	31
3A	98,0	104,0	6,0	-	-	-
3B	99,6	105,8	6,2	98	155	57
3C	98,9	101,7	2,8	97	176	79
3D	102,9	121,0	18,1	98	188	90
3E	98,6	116,5	17,9	99	200	101
4A	96,7	102,5	5,8	-	-	-
4B	98,0	116,0	18,0	97	148	51
4C	98,9	110,0	11,1	98	170	72
4D	-	-	-	97	160	63
5A	98,6	105,0	6,4	-	-	-
5B	98,7	114,0	15,3	97	160	63
5C	-	-	-	98	155	57
6A	18,8	27,4	8,6	-	-	-
6B	20,4	36,4	16,0	0	100	100
6C	20,2	36,2	16,0	20	130	110
6D	-	-	-	20	88	68
7A	98,8	112,5	13,7	-	-	-
7B	98,5	119,6	21,1	100	165	65
7C	98,9	118,1	19,2	97	180	83
7D	-	-	-	99	154	55
8A	98,4	103,1	4,7	-	-	-
8B	98,3	114,0	15,7	98	152	54
8C	-	-	-	98	153	55
8D	-	-	-	98	156	58

Stellenbosch University http://scholar.sun.ac.za

development of cracks tends to lengthen the column and if the axial load application system cannot deflect upwards without an increase in the original axial load, the axial load will begin to increase. The rise in the axial load will be directly proportional to the stiffness of the axial load application system. During the investigation the axial load beam was stiffened (from column 3D to the last column) and as can be seen in Table 7.4 the axial load for the static tests increased from that stage on. For the columns that were subjected to an impact load before the static test was done, the axial load immediately started to increase as soon as the static horizontal load was applied. This was due to the fact that the concrete already had cracked during the impact. These cracks then simply began to widen as soon as the static load was applied.

The axial loads increased substantially during the impact phases of the tests. The increases ranged from as little as 32kN up to 110kN, that is, increases from 32% to 110%. As indicated in the previous paragraph, these increases were directly proportional to the stiffness of the axial load beam. The amount with which the axial load increased during the impact is also an indication of the crack width with the maximum loads.

Table 7.4 shows the increases in the axial load for the static as well as for the dynamic impact tests. An interesting aspect of these load increases during the dynamic tests is that the increase for the columns with lower shear reinforcement was lower than similar columns with higher shear reinforcement. This is understandable because these columns failed at a lower shear force and thus at a lower flexural moment. This resulted in somewhat smaller flexural cracks and thus a smaller lengthening tendency of the column and thus a lower axial load. Some of the other columns that failed under the impact conditions also showed a smaller increase in the axial load than their counterparts in the same group. This indicated that the shear failure load was reached before the maximum moment could cause the bigger cracks and the corresponding increase in the axial load.

Stellenbosch University http://scholar.sun.ac.za

7.7 Comparison of experimental results with the modified compression field theory.

7.7.1 Measured extreme combinations of moment (M) and shear (V)

In order to determine the maximum effective shear and moment generated at the bottom of a column during an experiment under impact loading, the inertia forces and moments acting on the column had to be estimated from the recorded accelerations at 0,6 m and 1,55 m from the bottom of the column. These inertia actions could not be determined exactly from only two measuring points. However the extreme combinations of moment (M) and shear (V) can be derived as follows:

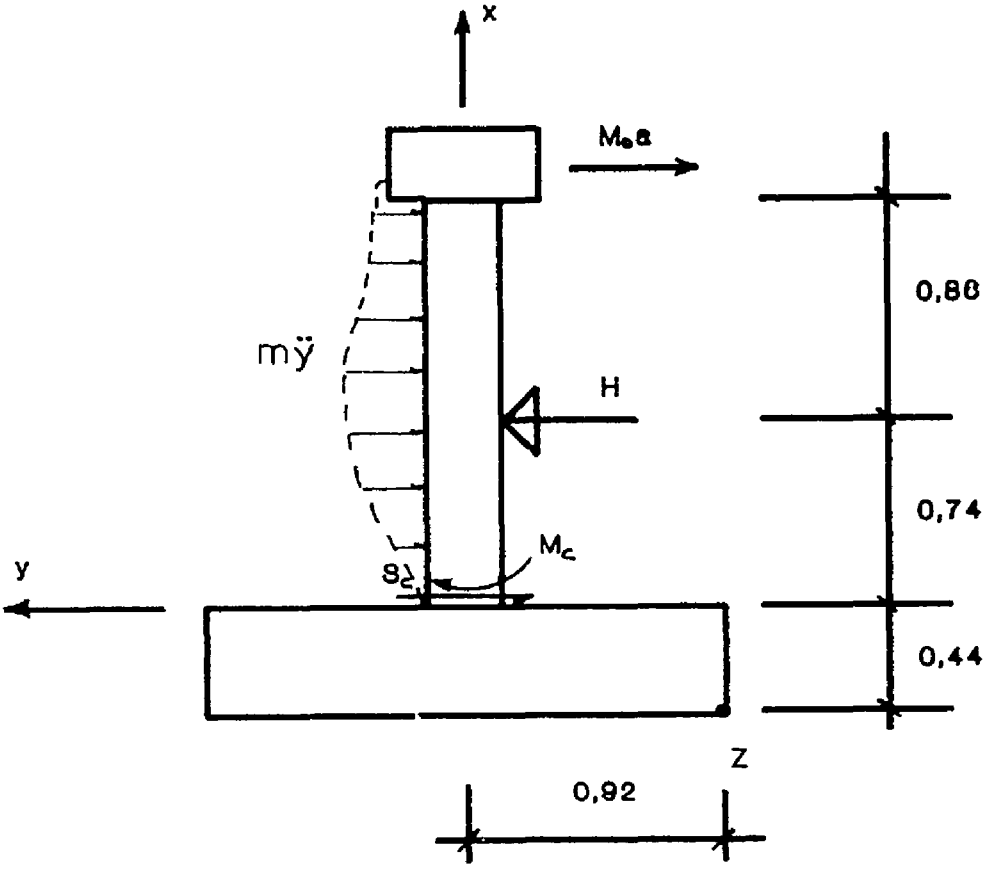

Figure 7.15: Forces acting on column.

Stellenbosch University http://scholar.sun.ac.za

Assume $y = ax^3 + bx^2 + cx + d$ (7.1)

where: y = Acceleration of column at any position
a, b, c, d = Constants
x = Position on column measured from the bottom

For x = 0: y = 0 and dy/dx = 0

Thus $y = ax^3 + bx^2 = \partial^2 y/\partial t^2$

y was measured at x = 0,6 and 1,55 and can therefore be calculated from the measured accelerations at any given time.

From Figure 7.15:

$$S' = H - M_o\, a - \int_o^{1,6} m\ddot{y}\, dx = H - I \quad (7.2)$$

and $S = S' - \Delta S = H - (I + \Delta I)$ (7.3)

Where: S' = Shear at bottom of footing without provision for error in inertia force of column
S = Shear at bottom of footing with provision for error in inertia force
H = Measured impact load
M_o = Concentrated mass at top of column
a = Acceleration of mass at top of column
m = Mass of column per unit length
I = Total inertia force of column
ΔS = Error in calculated shear force
ΔI = Error in inertia forces

$$M_z' = 1,18H + 0,92N - M_o a\, 2,04 - \int_o^{1,6} m\ddot{y}(x + 0,44)\, dx \quad (7.4)$$

$$= 1,18H + 0,92N - I\bar{x}$$

Where: M_z' = Moment around z without provision for error
N = Measured change in axial load on column
$\bar{x}$ = Height of resultant lateral inertia force of column.

Let Δx = error in x and ΔM = error in the calculated moment,

then: $M_{z\ meas} = M_z' - \Delta M = 1,18H + 0,92N - (I + \Delta I)(\bar{x} + \Delta\bar{x})$ (7.5)

Stellenbosch University http://scholar.sun.ac.za

and $\Delta M = [\Delta I\bar{x} + I\Delta\bar{x} + \Delta\bar{x}\Delta I]$ (7.6)

The <u>first limit</u> for the extreme values is: $\Delta\bar{x} = 0$

$$\Delta I = \Delta M/\bar{x}$$

$$S_{bc} = S = S' - \Delta S = H - I - \Delta M/\bar{x} \quad (7.7)$$

$$M_{x\ \text{meas}} = M_x' - \Delta M$$

Thus: $M_{bc} = M_{x\ \text{meas}} - 0,92N - 0,44S$ (7.8)

Where: S_{bc} = Shear at bottom of column

M_{bc} = Moment at bottom of column

For the first limit, plot M_{bc} against S_{bc} from equations (7.7) and (7.8).

The <u>second limit</u> for the extreme values is: $\Delta = 0$

$$\Delta M = I\Delta\bar{x}$$

$$S_{bc} = S = S' = H - I \quad (7.9)$$

$$M_{bc} = M_{x\ \text{meas}} - 0,92N - 0,44S \quad (7.10)$$

For the second limit, plot M_{bc} against S_{bc} from equations (7.9) and (7.10).

The moment was taken around the tension load cells (point z in figure 7.15) to eliminate the values of the tension load cells, because the readings of the tension load cells were a little suspect.

The extreme measured moment and shear in the column can now be plotted for each time interval as shown in Figures 7.30 to 7.51. Only the results of the first three groups of columns are shown due to a lack of space. The higher values curve in each figure is the shear force curve and the other curve is the moment curve.

7.7.2 <u>Comparison of the first and second limits with the M/V values as well as with the theoretical values.</u>

In Figures 7.52 to 7.58 the results obtained from the calculations of paragraph 7.7.1 are compared with the M/V graphs

Stellenbosch University http://scholar.sun.ac.za

as well as with the theoretical values obtained from the theory derived in Chapter 5. Only the maximum values for the first and second limits were plotted.

The M/V graphs in Figures 7.52 to 7.58 show a curve for static loading as well as a curve for impact loading. The impact loading curve is explained in Chapter 8.

From these graphs it is clear that the impact loading M/V curves under estimate the impact strength of the columns. The values obtained from the first and second limits can also be reasonably compared with the values from the theoretical model derived in Chapter 5. This once again indicates that the theoretical model derived in Chapter 5 gives reasonable values for the shear and moment generated in the column.

7.8 Local Damage

From the photographs shown in Appendix B (for example Figure B.40) it is clear that the local damage was only superficial and only a little spalling occurred. This was expected with this "soft" type of impact used in the experiments (refer to Chapter 3 for more details on the local damage with impact).

Stellenbosch University http://scholar.sun.ac.za

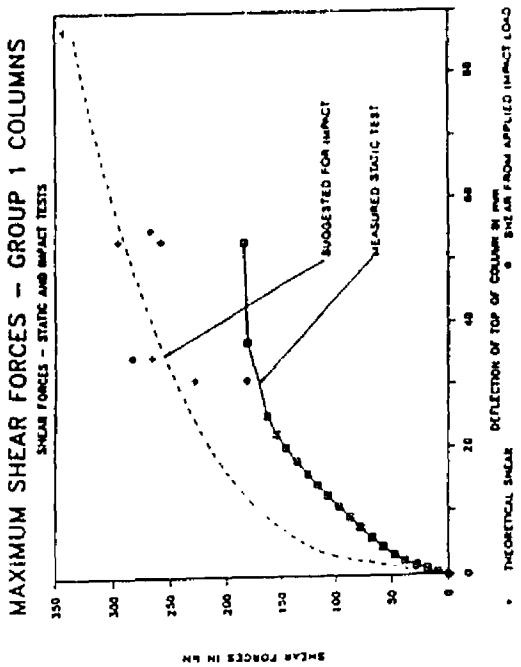

Fig. 7.16: Shear - Group 1

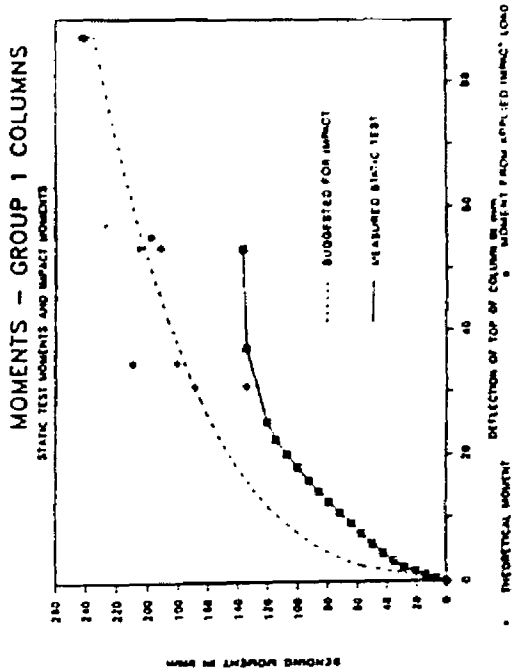

Fig. 7.17: Moment - Group 1

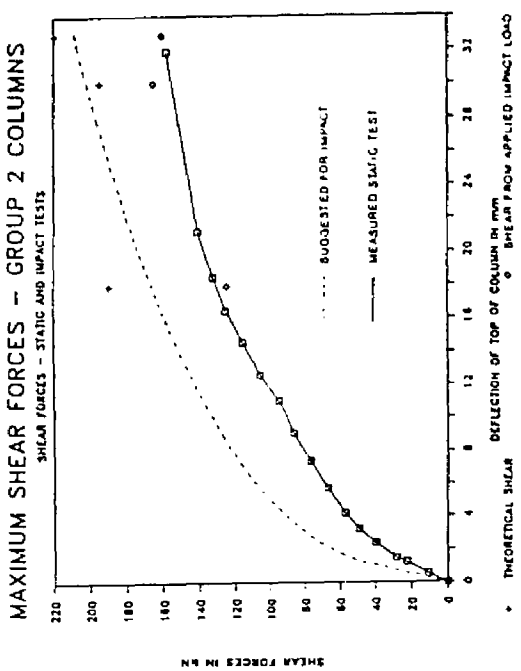

Fig. 7.18: Shear - Group 2

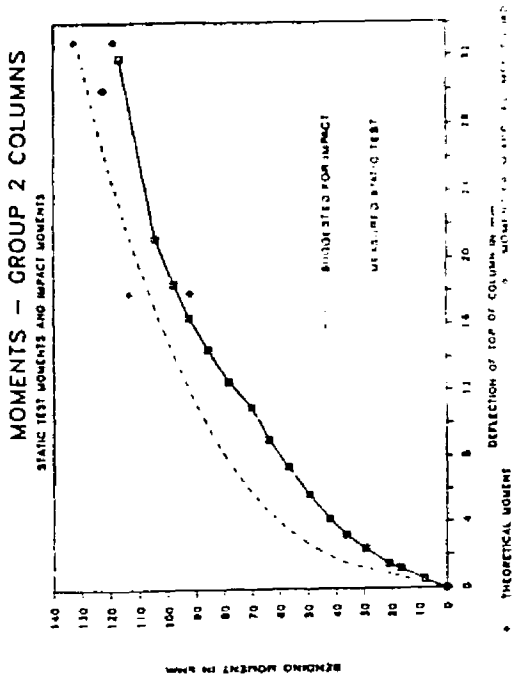

Fig. 7.19: Moment - Group 2

Stellenbosch University http://scholar.sun.ac.za

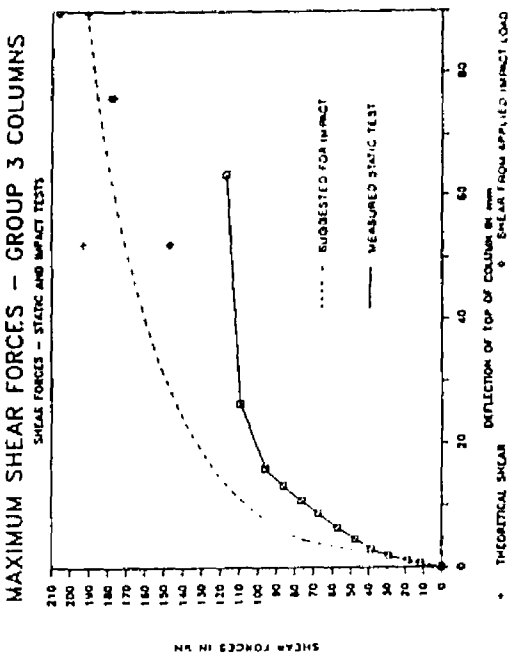

Fig. 7.[illegible] Shear – Group 3

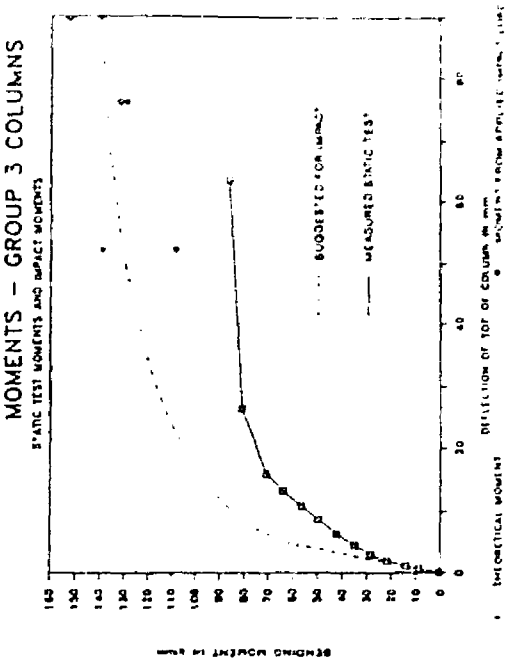

Fig. 7.[illegible] Moments – Group 3

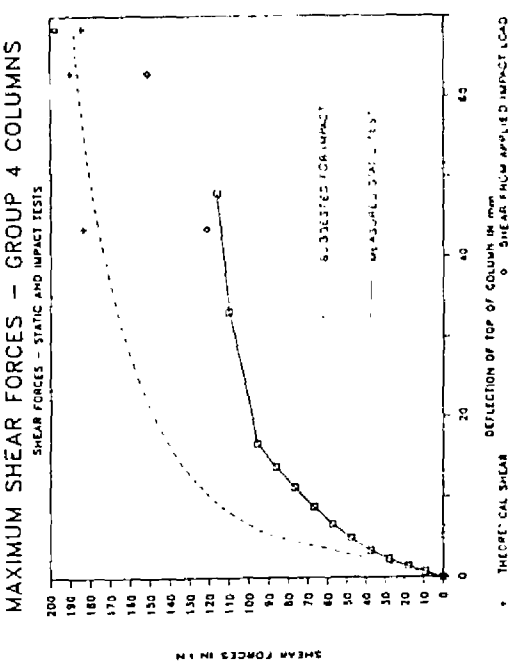

Fig. 7.[illegible] Shear – Group 4

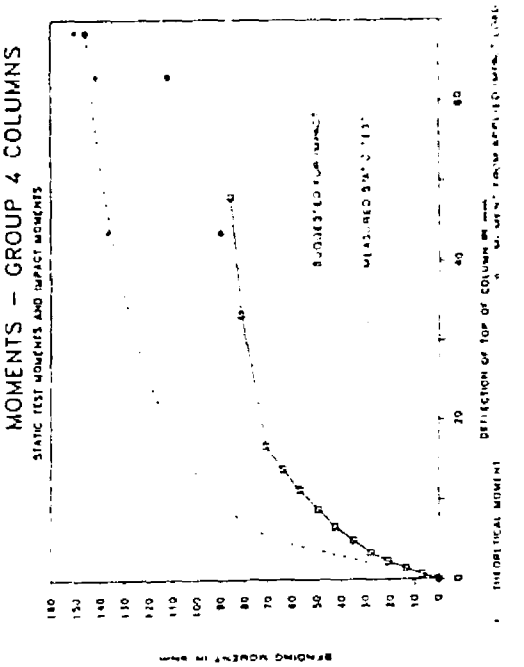

Fig. 7.[illegible] Moments – Group 4

Stellenbosch University http://scholar.sun.ac.za

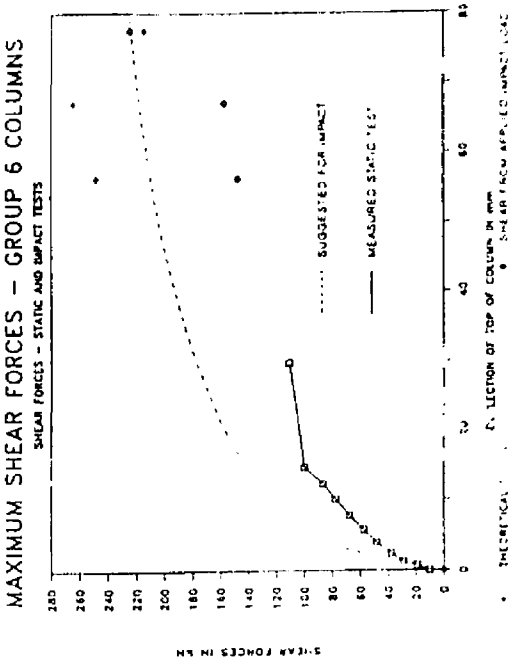

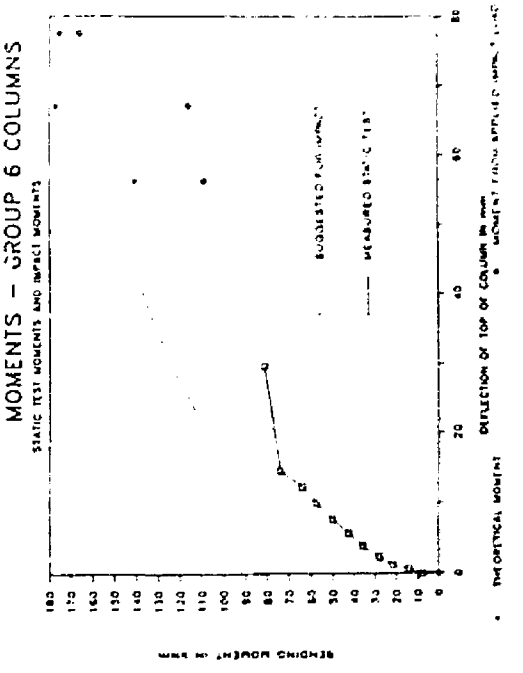

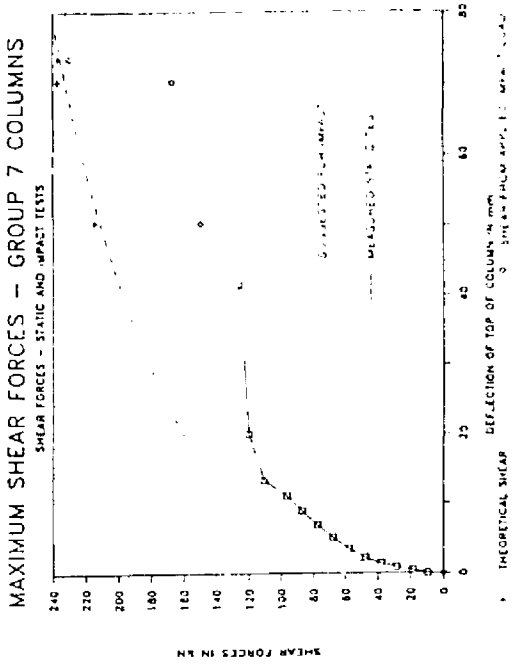

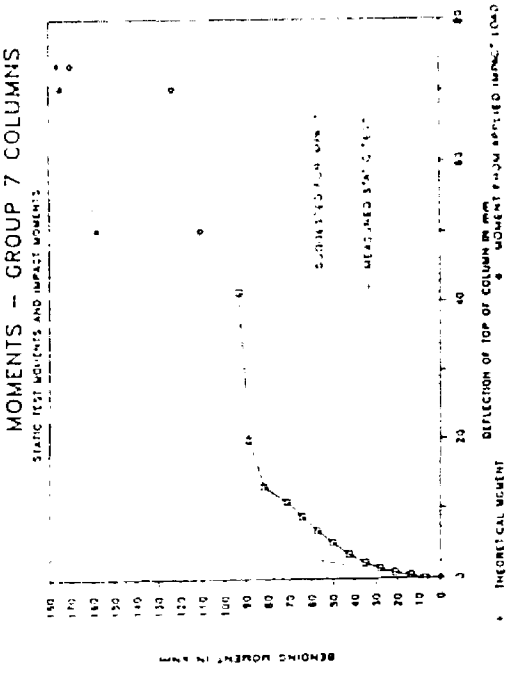

Stellenbosch University http://scholar.sun.ac.za

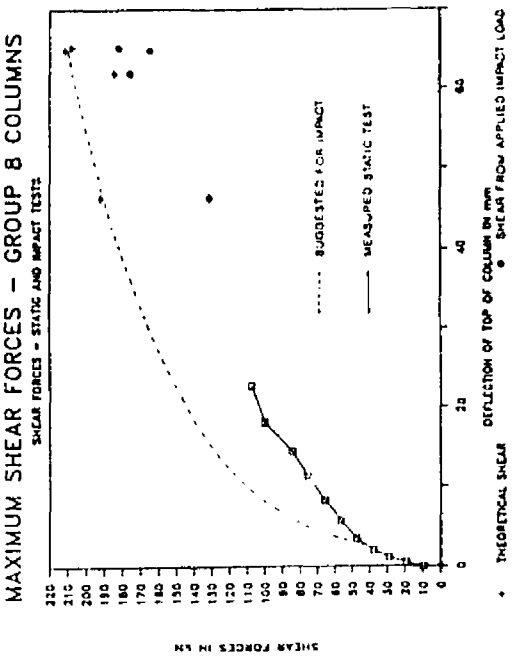

Fig. 7.28: Shear – Group 8

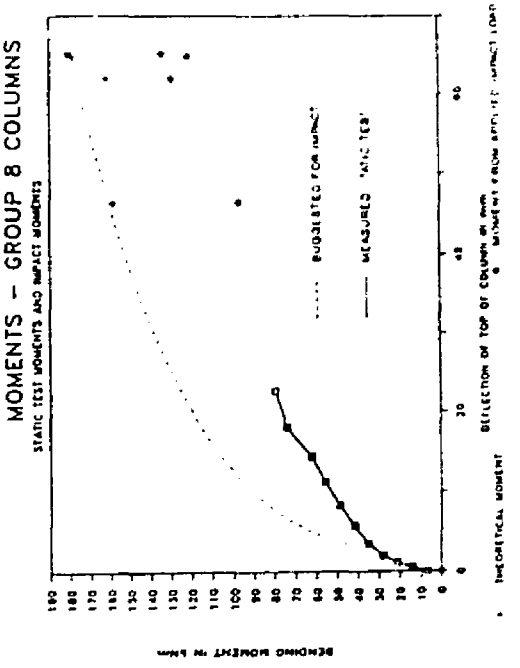

Fig. 7.29: Moment – Group 8

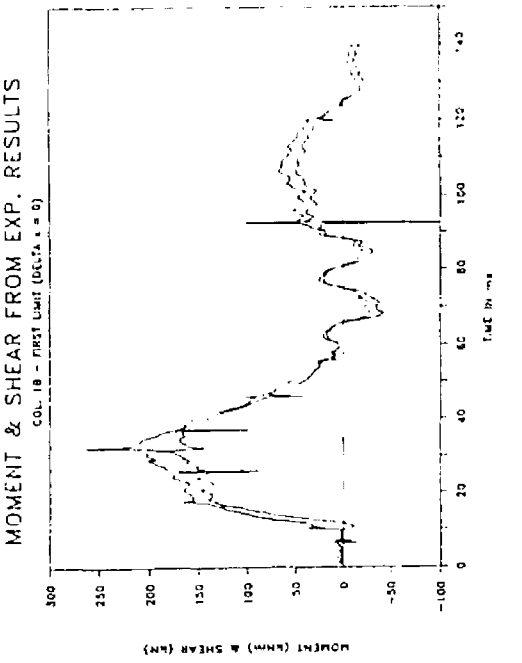

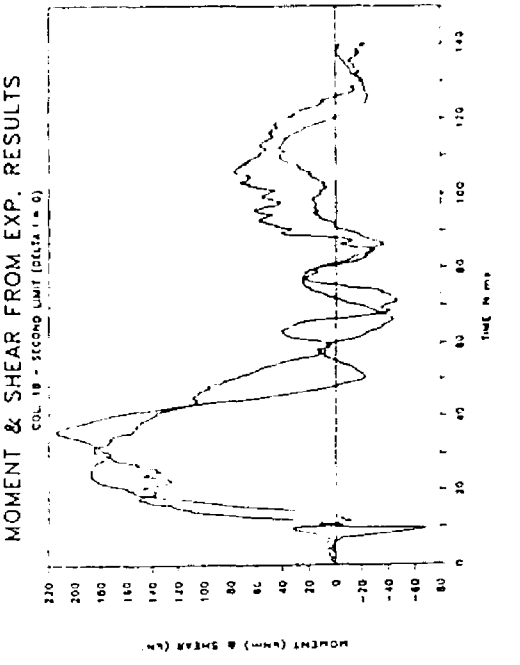

Stellenbosch University http://scholar.sun.ac.za

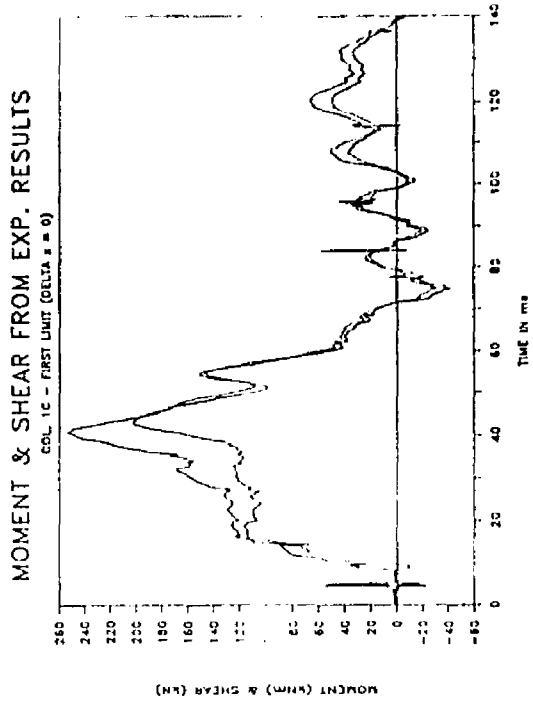

Fig. 7.32: 1st Limit Col.1C

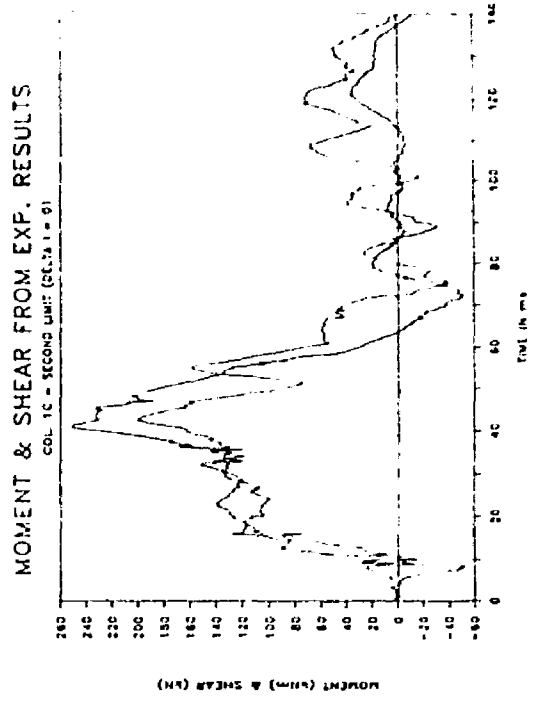

Fig. 7.33: 2nd Limit - Col.1C

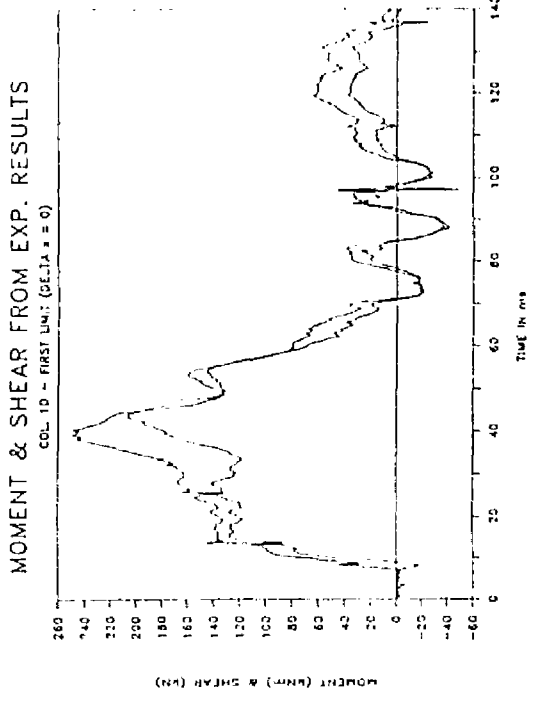

Fig. 7.34 1st Limit Col.1

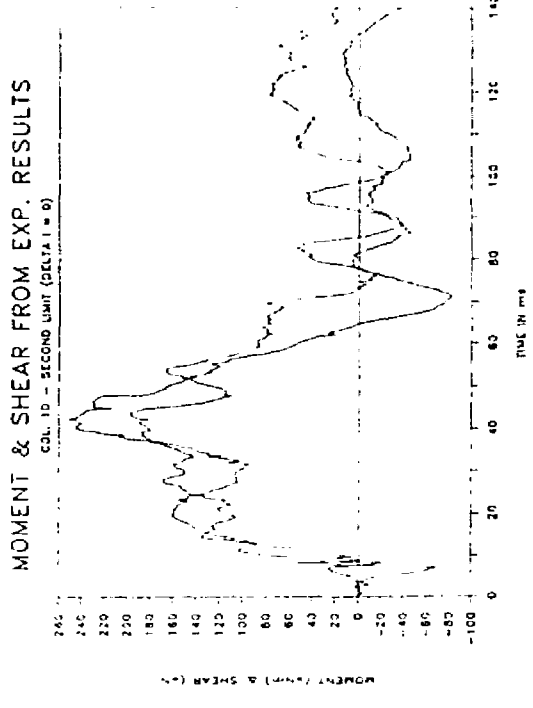

2nd Limit Col.1D

Stellenbosch University http://scholar.sun.ac.za

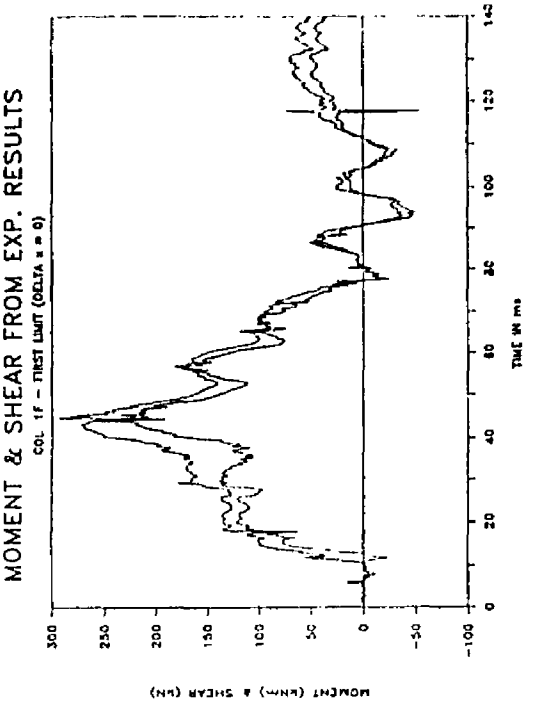

Fig. 7.36: 1st Limit - Col.1F

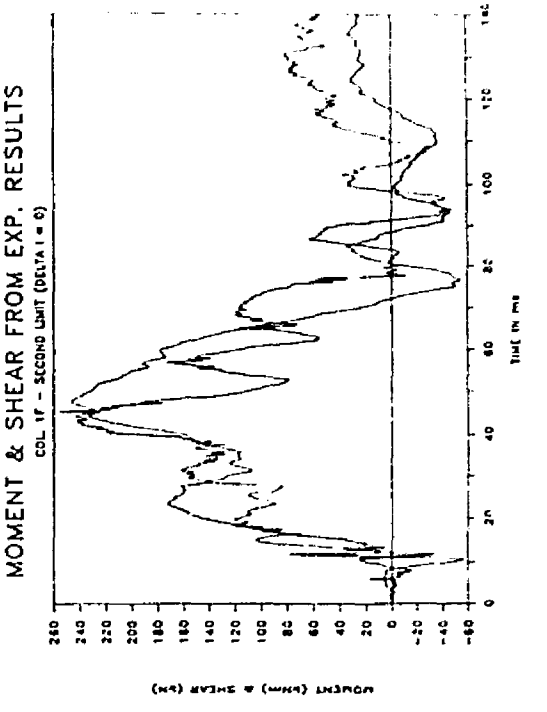

Fig. 7.37: 2nd Limit - Col.1

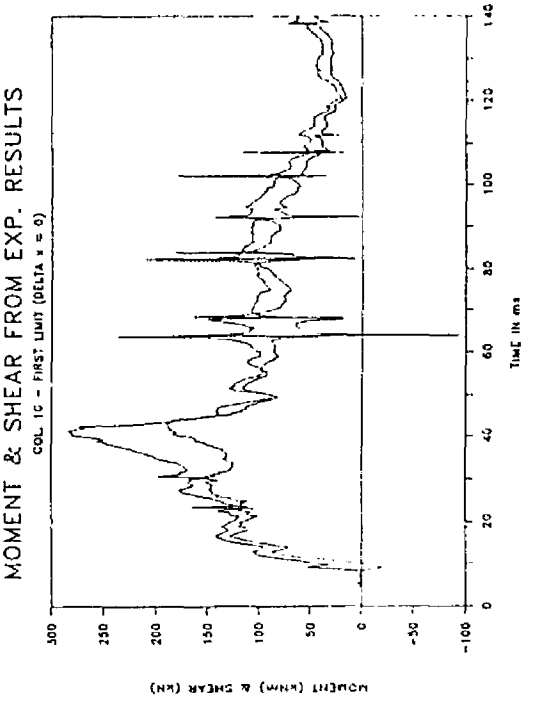

Fig. 7.38: 1st Limit - Col 1G

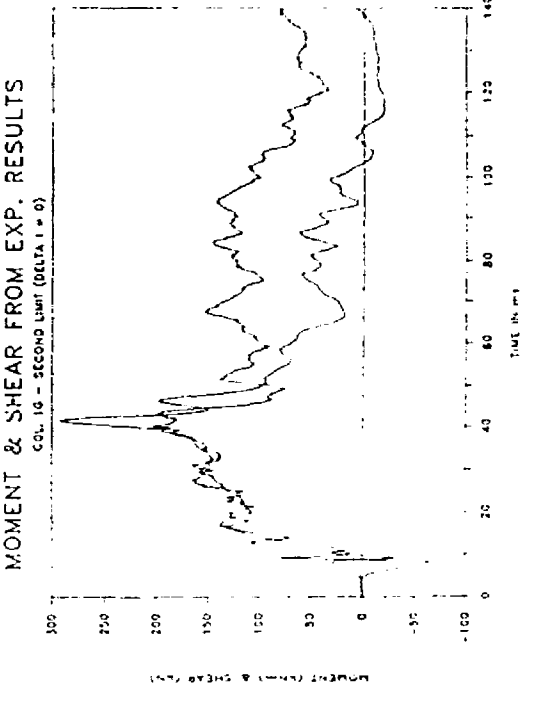

Fig. 7.39: 2nd Limit - Col.1G

Stellenbosch University http://scholar.sun.ac.za

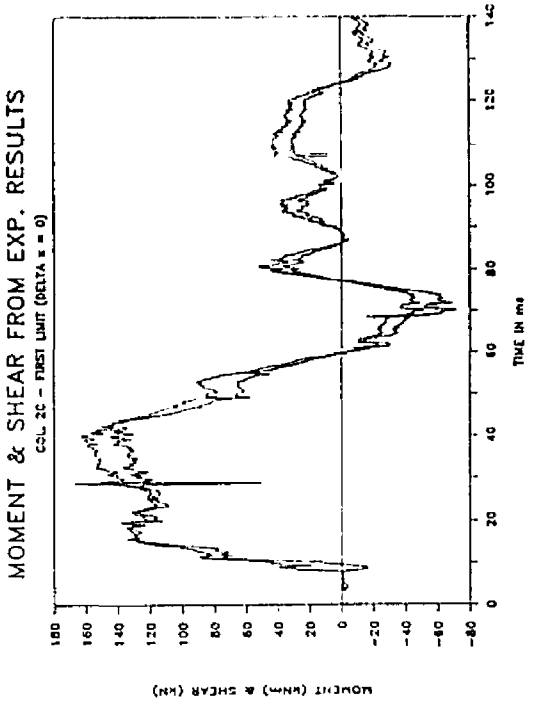

Fig. 7.40: 1st Limit - Col.2C

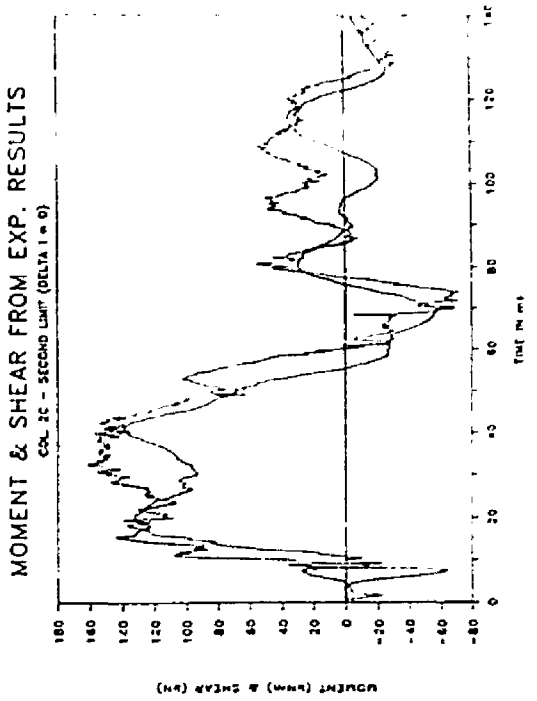

Fig. 7.41: 2nd Limit - Col.2C

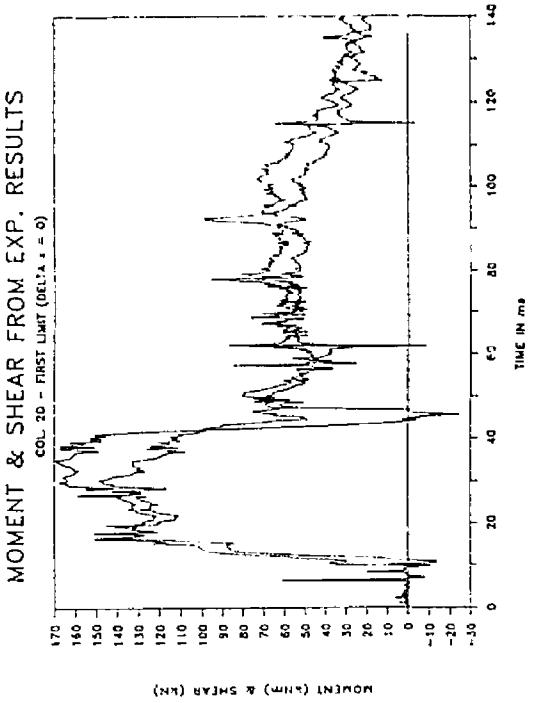

Fig. 7.42: 1st Limit Col.2D

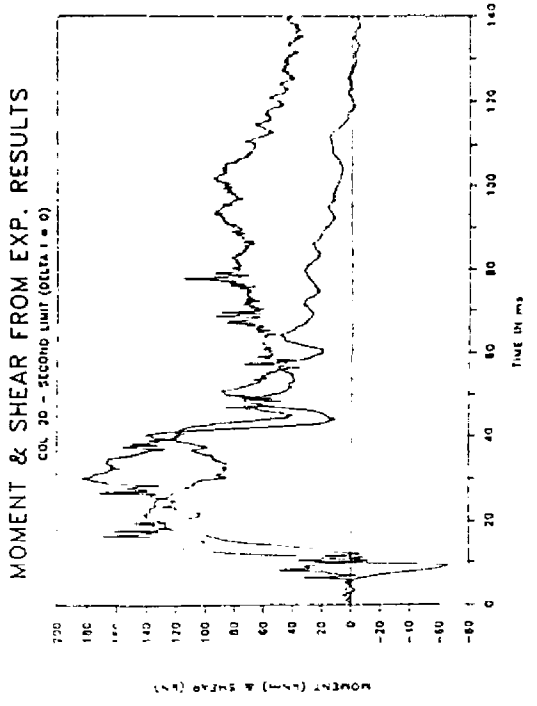

Fig. 7.43: 2nd Limit Col.2D

Stellenbosch University http://scholar.sun.ac.za

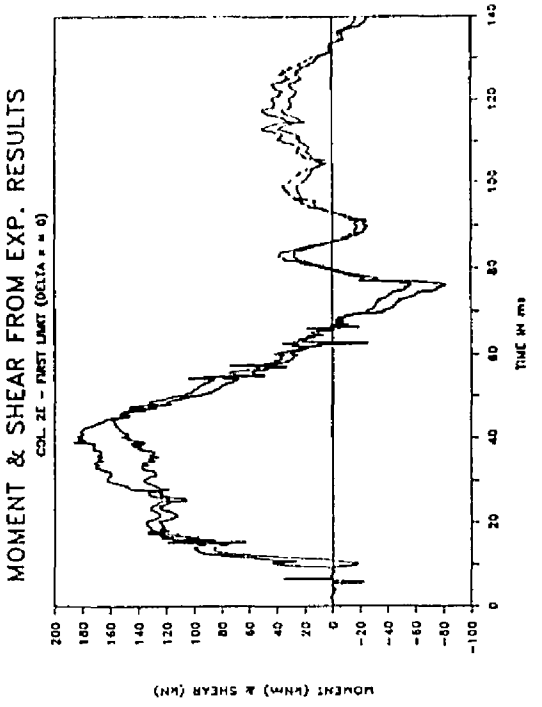

Fig. 7.44: 1st Limit - Col.2E

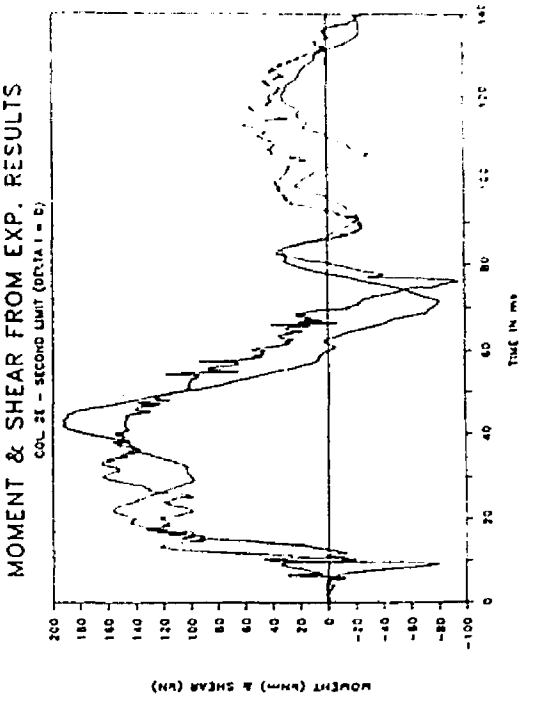

Fig 7.45: 2nd Limit - Col.2E

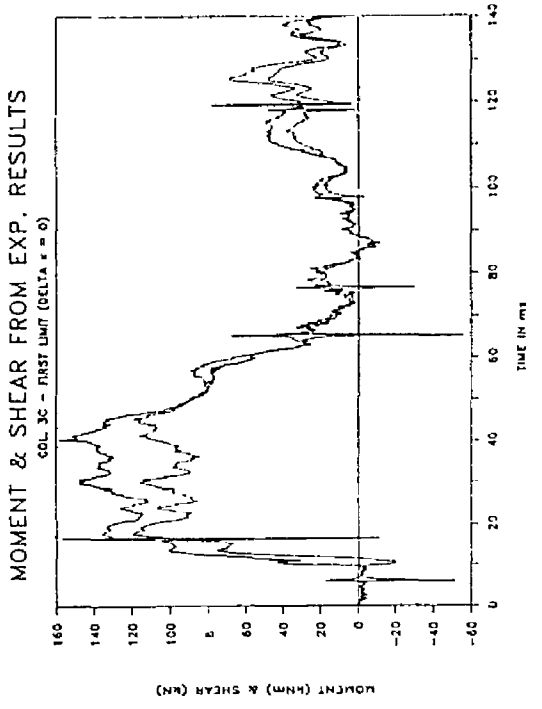

Fig 7.46: 1st Limit [illegible] Col.3C

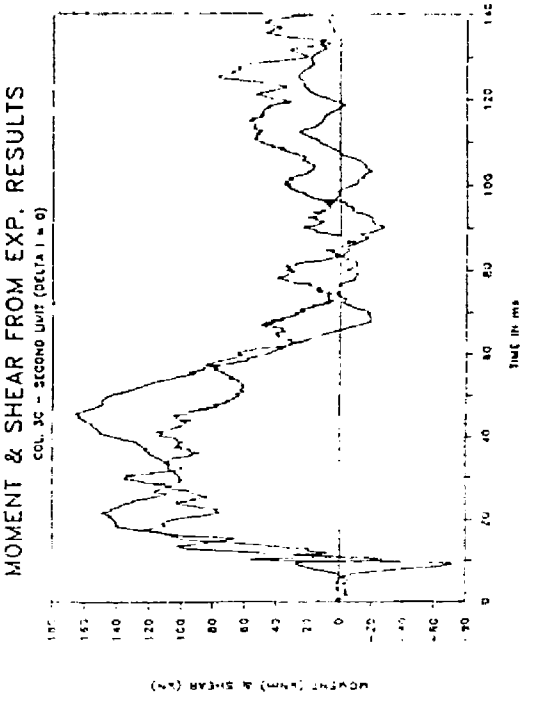

Stellenbosch University http://scholar.sun.ac.za

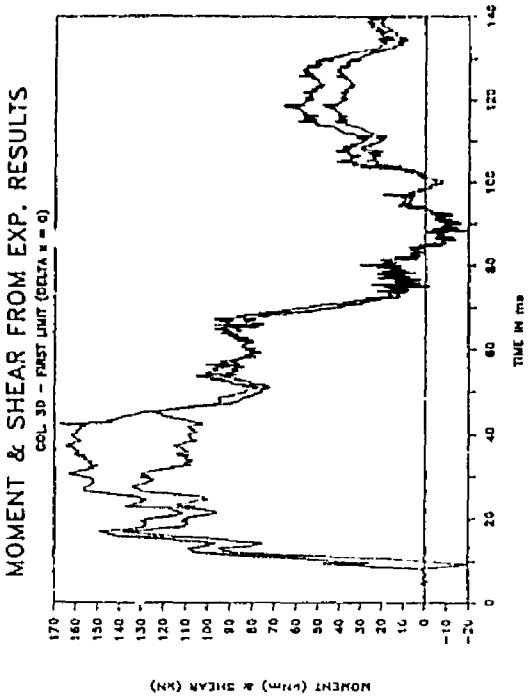

Fig. 7.48: 1st Limit - Col.3D

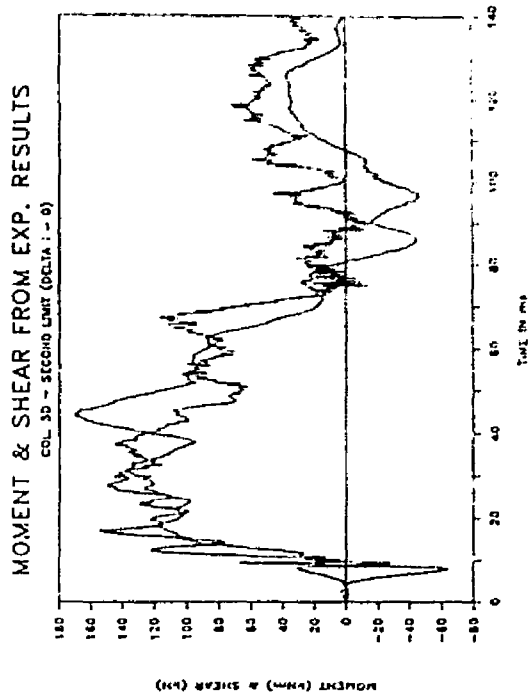

Fig. 7.49: 2nd Limit - Col.3D

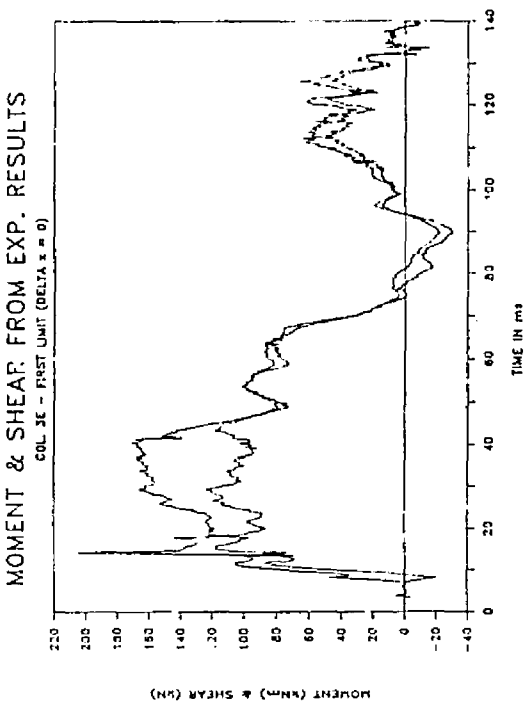

Fig. 7.50: 1st Limit - Col. 3E

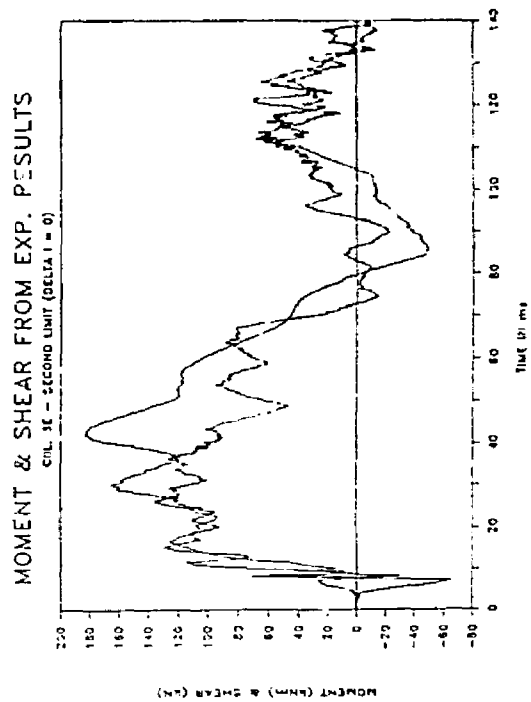

Fig. 7.51: 2nd Limit - Col. 3E

Stellenbosch University http://scholar.sun.ac.za

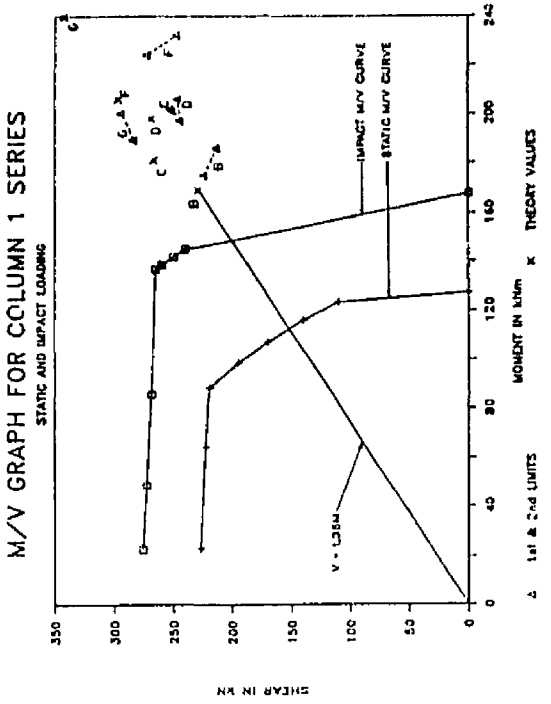

Fig. 7.52: M/V Graph - Group 1

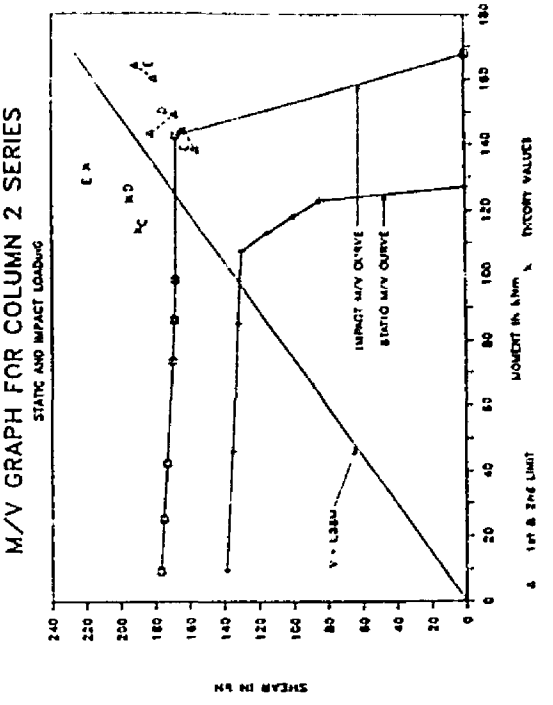

Fig. 7.53: M/V Graph - Group 2

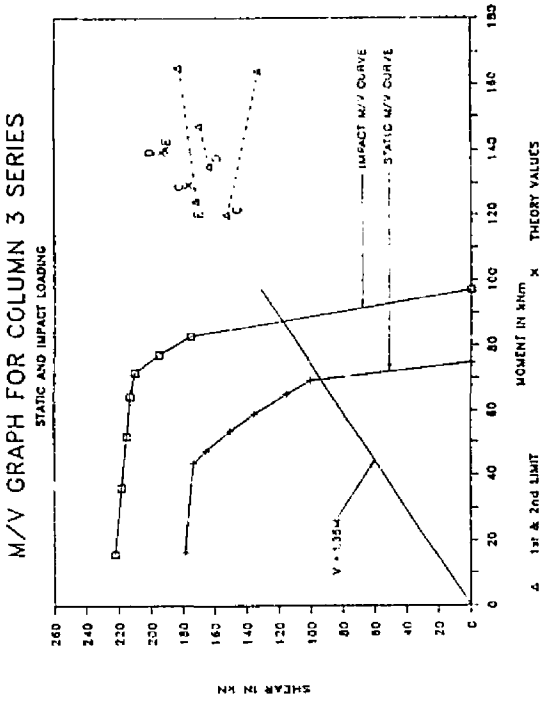

Fig. 7.54: M/V Graph - Group 3

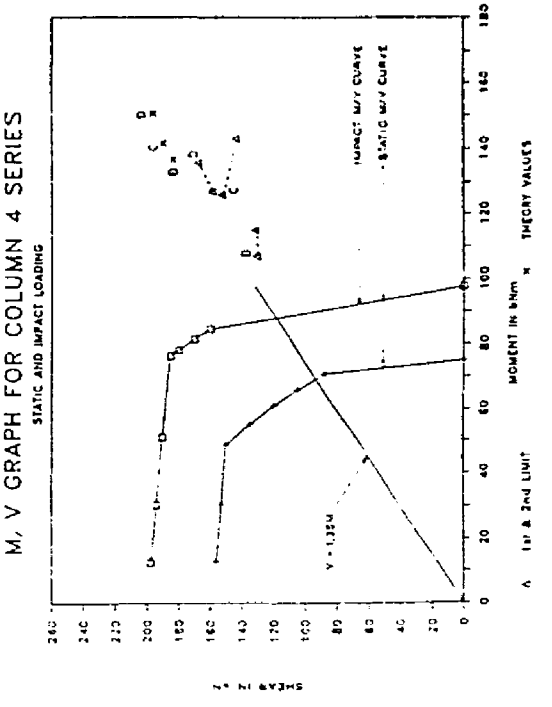

Fig. 7.55: M/V Graph - Group 4

Stellenbosch University http://scholar.sun.ac.za

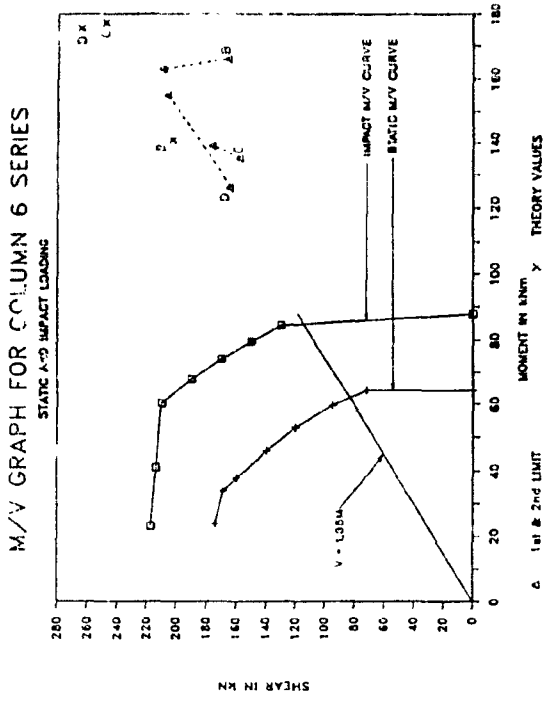

Fig. 7.56: M/V Graph - Group 6

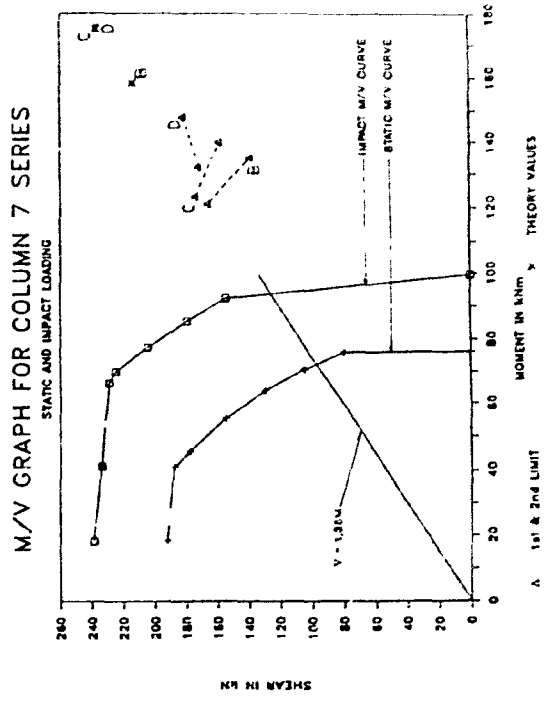

Fig. 7.57: M/V Graph - Group 7

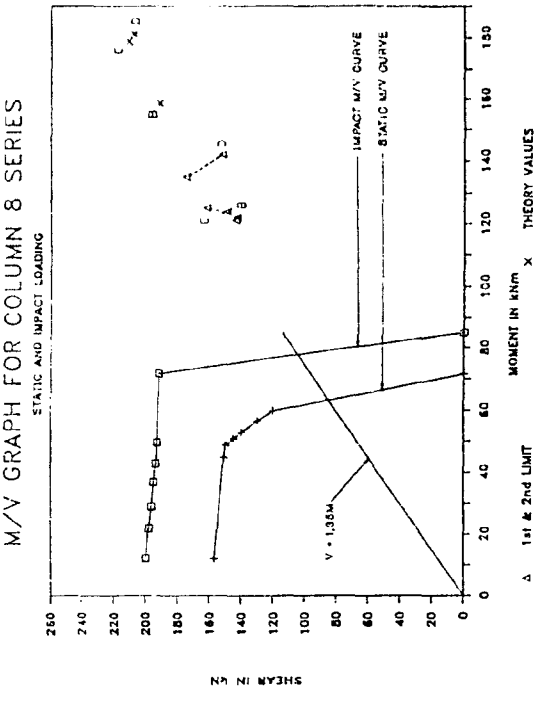

Fig. 7.58: M/V graph - Group 8

Stellenbosch University http://scholar.sun.ac.za

8. DESIGN AND RECOMMENDATIONS

8.1 Introduction.

In this section a lower bound solution will be given for design purposes. The safest solution would be to design the column to resist the maximum impact load as a quasi-static load. In other words, the increases in the strengths of the materials under impact conditions are ignored. This however would be not a an economical solution. A better lower bound solution would be to use the increased strengths of the reinforced concrete under impact loading.

8.2 Design solution for a column subjected to an impact load.

A good lower bound solution can be found by modifying the material properties as suggested in the literature discussed in chapter 4. An upper bound solution is also given after considering the test results.

8.2.1 Modification of material properties.

The tensile strength of concrete under impact loading is given by equation (4.1):

$$f_{tm}/f_{tmo} = (\dot{\sigma}/\dot{\sigma}_o)^{(1/(1+B))}$$

$$= (100)^{0.042} = 1,21$$

Where: f_{tmo} = Static tensile strength of concrete
f_{tm} = Impact tensile strength of concrete
$\dot{\sigma}$ = Impact stress rate
$\dot{\sigma}_o$ = Static stress rate

Stellenbosch University http://scholar.sun.ac.za

Or from Table 4.3 the tensile strength is given by:

$$f_{tm} = 1,1\ f_{cm}^{(1/3)}$$

Where: f_{cm} = compressive cube strength of concrete.

The latter equation was used in the following equations.

The increased concrete compressive strength under the impact conditions is given by equation (4.2):

$$f/f_o = 1,10 + 9,06.10^{-3} \ln(\dot{\epsilon})$$

Where: f = Impact compressive strength of concrete
f_o = Static compressive strength of concrete
$\dot{\epsilon}$ = Strain rate

The increase in the elasticity modulus, E, is given by equation (4.3):

$$E/E_o = 1,10 + 9,06.10^{-3} \ln(\dot{\epsilon})$$

Where: E = Impact elasticity modulus of concrete
E_o = Static elasticity modulus of concrete.

The increased strength of the reinforcing steel is given by equation (4.4) (refer also to the tensile strength tests on the reinforcement as discussed in Appendix B paragraph B.10):

$\sigma = 499 + 6,27 \ln(0,01) = 470$ MPa (For stirrups)
$\sigma = 756 + 6,03 \ln(0,01) = 728$ MPa (For main reinforcement)

According to the literature (Chapter 4) the E-modulus for the reinforcement stays more or less constant under high strain and stress rates and thus it is not necessary to modify their values.

Stellenbosch University http://scholar.sun.ac.za

8.2.2 Application of the modified compression field theory

The modified compression field theory of Collins and Vecchio (30, 31, 164, 165, 166 and 167) was used to predict the response of the columns under the impact conditions. The modified material properties, as discussed in the previous section of this chapter, was used instead of the static material properties. The same spreadsheet computer program, UMNV, by Marits (165), as discussed in Chapter 7, was used for the analysis of the impact tested columns.

Figures 8.1 to 8.7 shows the results for each series of columns. The dynamic or impact M/V (moment/shear) graphs are shown together with the static graphs. The calculated shear forces and moments for the impact tests, of the columns which did not fail under impact, are also shown on the graphs as well as the shear forces and moments of the columns which did fail under impact conditions. These theoretical values were obtained by using the theory derived in Chapter 5 and by using the measured impact load function.

These figures show that the M/V graphs predicted in all the cases a lower failure value than the actual failure of the columns. As mentioned in Chapter 7, all the columns which failed under impact loading, failed in shear. The graphs show that the shear forces of all the columns that did not fail under impact loading were lower or just in the region of the ultimate shear forces of the M/V graphs. The shear forces of the columns that did fail under impact loading were above the ultimate shear force of the M/V graphs.

Unfortunately the M/V graphs predict dominant flexural failures for six of the seven groups of columns under static and under impact loading. For static loading, as shown in Chapter 7, the predictions of flexural failure were very accurate. Failure under impact loading occurred shear although six of the seven M/V graphs predicted a dominant flexural failure. From figures 8.1 to 8.7 it seems as if the impact moment the cantilever column can

Stellenbosch University http://scholar.sun.ac.za

withstand, will continue to increase until the impact shear force reaches the maximum shear capacity of the column, as predicted by the M/V graphs. At this stage a shear failure will occur under impact conditions. This means that moments of 50 to 100% higher than the ultimate moment, as predicted by the M/V graphs, were reached before the ultimate shear failure loads were reached and thus the columns failed in shear. This increase in the moment could have been higher if the ultimate shear was not reached. Unfortunately there is a lack of experimental data in this region and thus no definite conclusion can be made.

The most important aspect is however that the modified compression field theory provides a lower bound solution. The solution for the impact shear failure is acceptable, but for this specific case the prediction for moment failure is very conservative.

For design purposes, the M/V graph for a specific column can be calculated with the modified compression field theory. Then for a lower bound solution one should ensure that the impact design loads are lower than the values predicted by the M/V graph for impact loading. For an upper bound solution a column can be designed so that the design loads are above the predicted values from the M/V graph but the shear should not be higher than the ultimate shear load of the columns, as predicted by the M/V graph. In other words, the moment of an upper bound solution might be significantly higher than the ultimate predicted moment for that section, but the shear should be lower than the ultimate predicted shear for that column. Due to a lack of data on impact bending failures for cantilever columns, the upper bound for bending failure should be not higher than say 80% than the ultimate predicted bending moment. Figure 8.8 shows the suggested lower and upper bounds for the design of this specific type of cantilever columns. In all the impact designs, the modified parameters should be used.

Stellenbosch University http://scholar.sun.ac.za

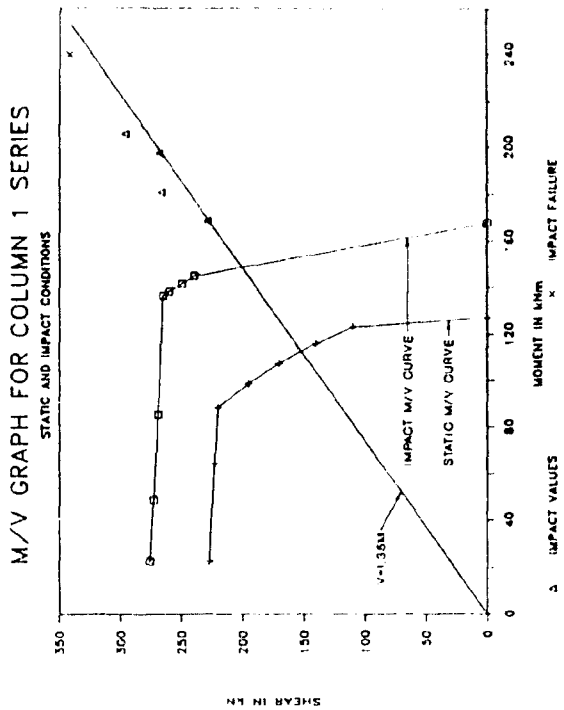

Fig. 8.1: M/V Graphs - Group 1

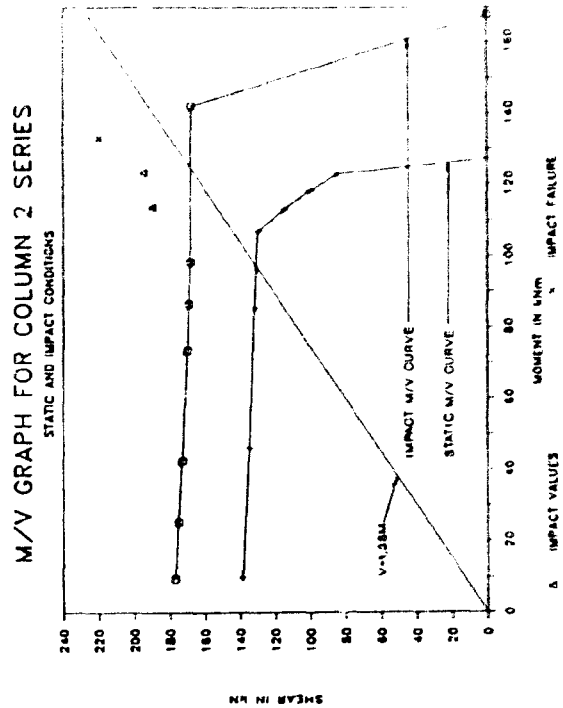

Fig. 8.2: M/V Graphs - Group 2

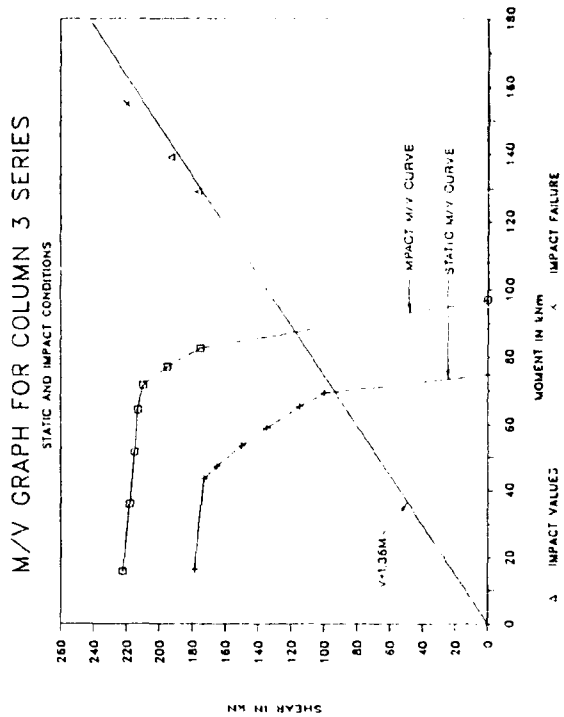

Fig. 8.3: M/V Graphs - Group 3

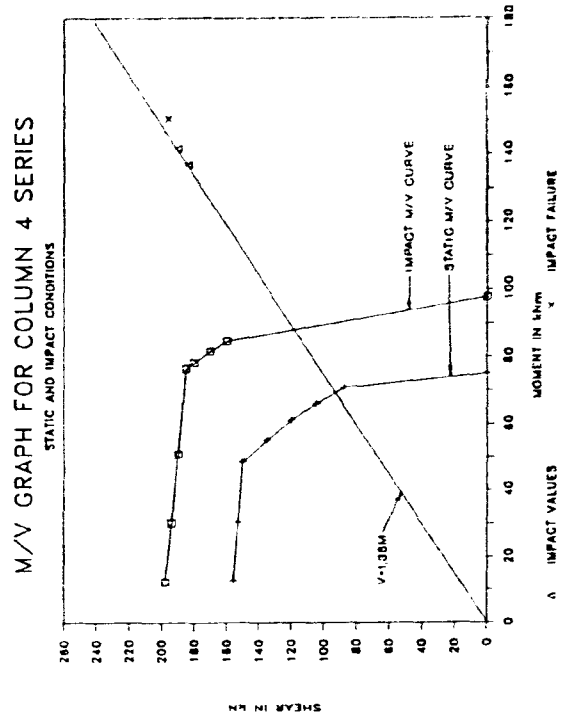

Fig. 8.4: M/V Graphs - Group 4

Stellenbosch University http://scholar.sun.ac.za

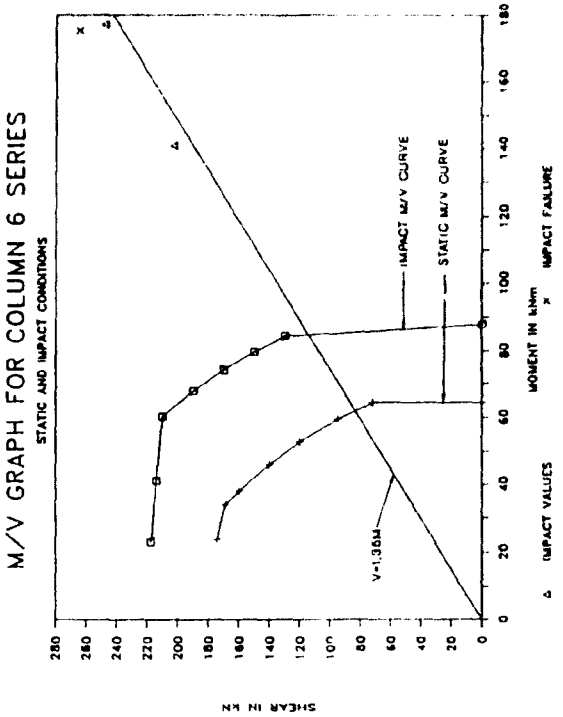

Fig. 8.5: M/V Graphs - Group 6

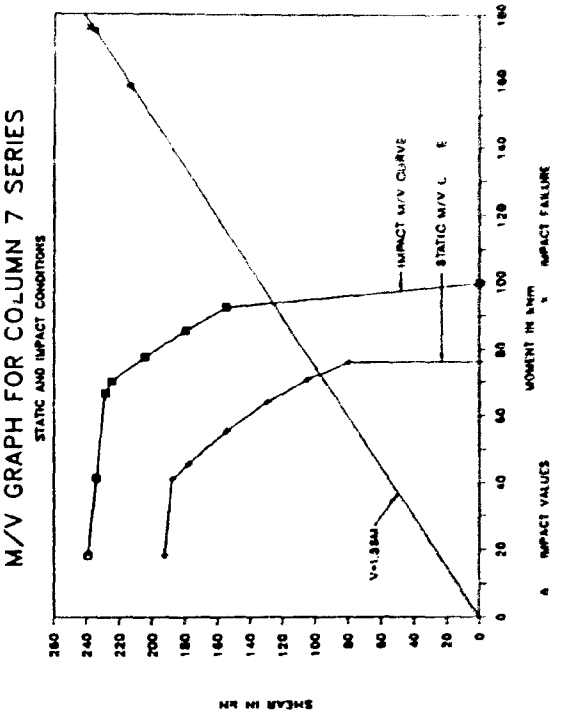

Fig. 8.6: M/V Graphs - Group 7

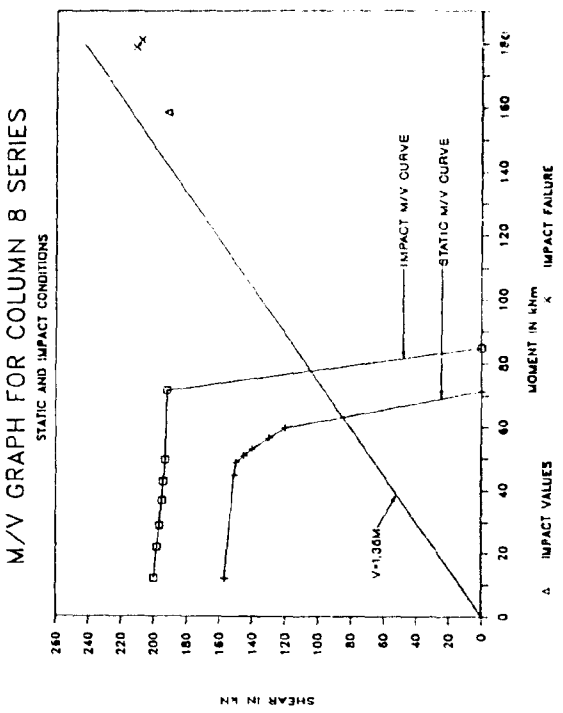

Fig. 8.7: M/V Graphs - Group 8

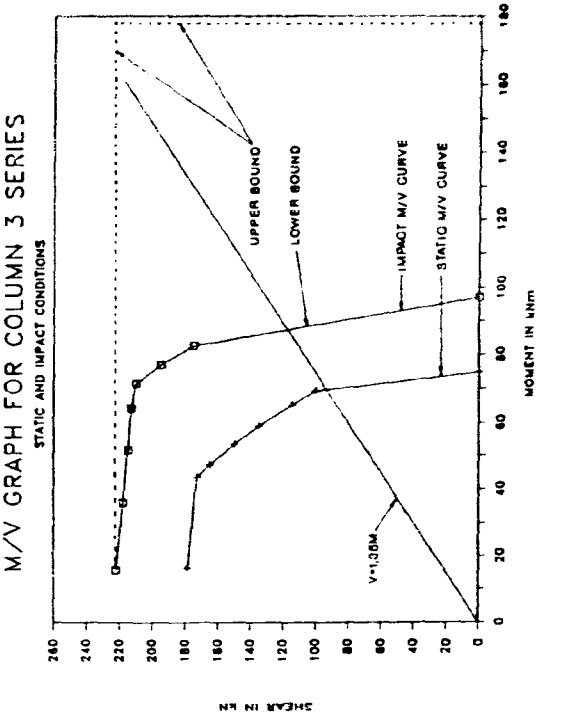

Fig. 8.8: Lower & Upper Bounds

Stellenbosch University http://scholar.sun.ac.za

8.2.3 Reserve strength of columns.

As indicated and discussed in Chapter 7, the columns that were subjected to an impact load, and did not fail, showed a static reserve strength more or less equal to the static strength of the undamaged columns. This means that if a column was subjected to an impact load, it might not be necessary to replace the column if the column did not fail under the impact load.

8.2.4 Axial load increase.

During the horizontal impact of a column, the axial load increases dramatically. This increase, as discussed in Chapter 7, is due to the lengthening of the column and the stiffness of the axial loading system. The stiffness of the axial loading system plays a very important part in the increase of the axial load. The stiffer the loading system, the higher the increase in the axial load. For some of the test specimens an increase of 100% in the axial load was registered (Table 7.4).

This increase in the axial load should be kept in mind, not only with the design of the column but also with the design of the loading system. In other words if the axial load is supplied by say a bridge deck, the increase in the axial load will introduce an additional reaction load on the bridge deck itself. Thus provisions in the design of the bridge deck should be made for this increase in the axial load. The stiffer the bridge deck, the higher the additional reaction force on the bridge deck.

Stellenbosch University http://scholar.sun.ac.za

8.3 Design steps for a cantilever column subjected to a horizontally applied impact load.

8.3.1 Impact design.

The following steps is recommended for the design of a cantilever column subjected to a horizontally applied impact load:

1. Establish the impact load history. Use the method as described in Chapter 5 or use functions as described in some of the literature for example (146). A report by Struck and Voggenreiter (155) discusses in detail the range of possible loadings and gives examples, taken from the literature, of possible magnitudes and durations. A measured impact load function can also be used (as in this study) if available.

2. Choose a column and reinforcement.

3. Find the maximum shear force and bending moment by using the theory derived and discussed in Chapter 5.

4. Modify the material properties as discussed in Chapter 4 and Chapter 7.

5. Use the modified compression field theory of Collins and Vecchio (30, 31, 164, 165, 166 and 167) to find the M/V graph for the specific column. Use the modified material properties. This M/V graph is a lower bound solution for the problem. A "upper bound" solution can be found as shown in Figure 8.8.

6. If the M/V graph indicate that the column will fail under impact conditions, choose another column section or change the reinforcement of the column. Then repeat the whole procedure from step 3.

Stellenbosch University http://scholar.sun.ac.za

7. After finding the desired column, ensure that the bridge deck or loading system can withstand the anticipated increase in the axial load.

This is a very lengthy procedure but it will provide a relative economical solution.

8.3.2 Static solution.

An uneconomical but a safe solution would be to find the maximum impact load anticipated and then to continue and design the column as if this load is a quasi-static load. In such a situation the material properties are not modified at all and the quasi-static material properties are used. The M/V graphs are then calculated as usual and they then represents a lower bound solution for this problem.

Figures 8.9 to 8.15 shows the quasi-static M/V curves with the impact M/V curves for all the columns. On these graphs the applied maximum shears and moments for the different tests are also shown. These values were calculated at the bottom of the column, directly from the maximum measured impact load applied to the column and they were not calculated with the dynamic analysis of the column as described in Chapter 5. In other words the maximum impact load was measured and then it was used as if it was a quasi-static load acting on the column.

From these graphs it is clear that the impact strength of the columns are under estimated by this type of static solution. The solution is however safe and very simple.

Stellenbosch University http://scholar.sun.ac.za

8.3.3 Precautions.

The most important precaution one should take with the design of a column subjected to a horizontally applied impact load is to ensure that the column is safe under shear. The shear strength increase of such a column is very much lower than that of the flexural strength. Thus if a column will fail in shear statically, the impact strength increase of such a column will be very low. If the column will fail in flexure under static conditions, the strength increase of the column will be much higher. In such a case the strength increase of the column might even be as high as 100%, depending on the ultimate shear strength of the column. This phenomena is clearly illustrated in figure 8.8 by the suggested upper bound solution.

Thus to ensure safety of a cantilever column under impact loading, shear failure of the column should be prevented.

Stellenbosch University http://scholar.sun.ac.za

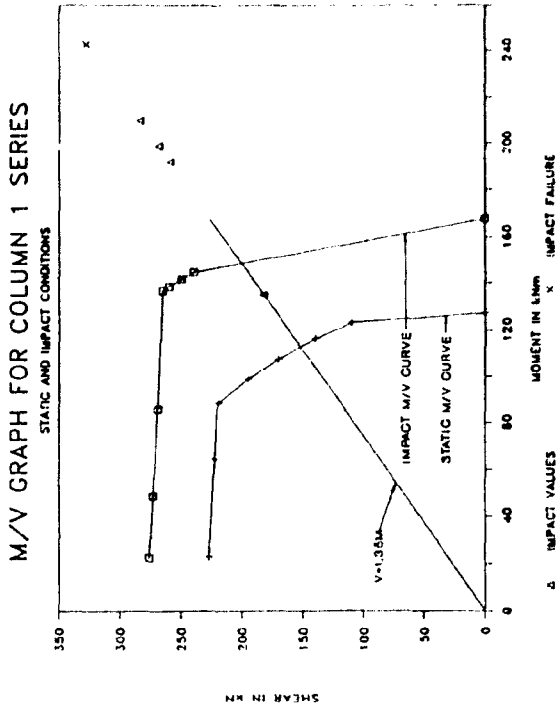

Fig.8.9: M/V Graphs - Group 1

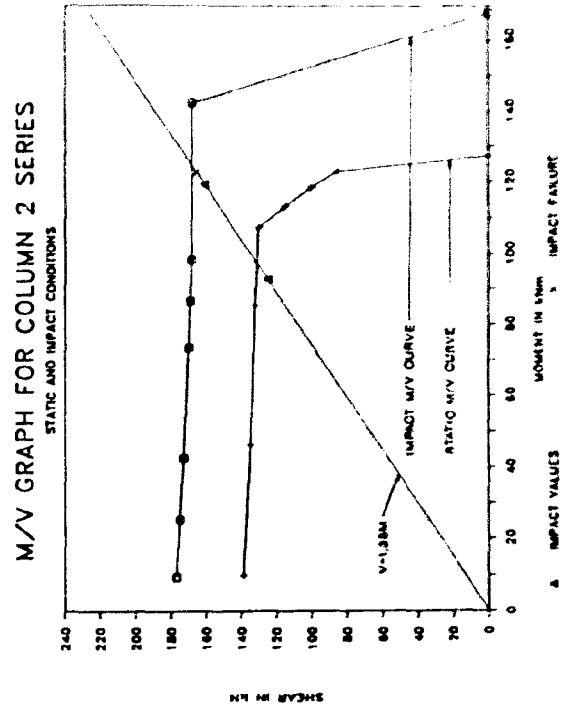

Fig.8.10: M/V Graphs - Group 2

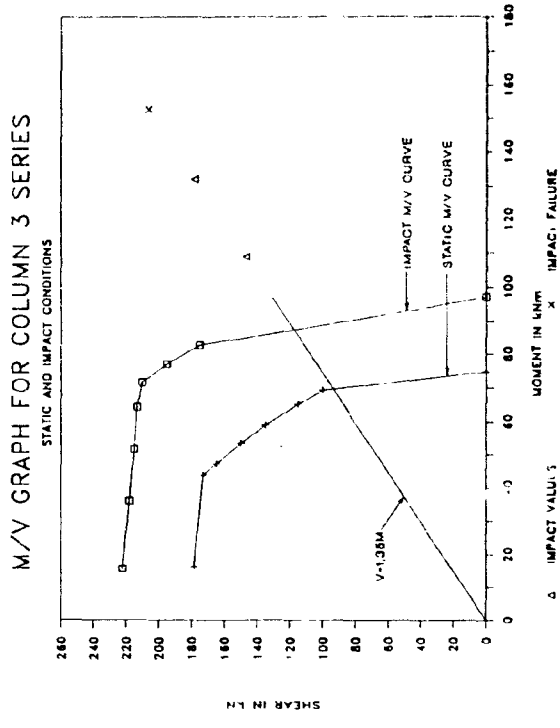

Fig.8.11: M/V Graphs - Group 3

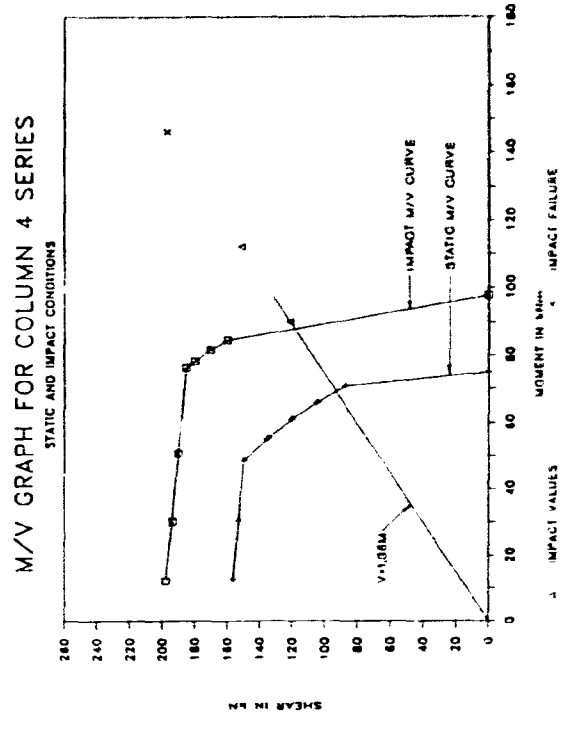

Fig.8.12: M/V Graphs - Group 4

Stellenbosch University http://scholar.sun.ac.za

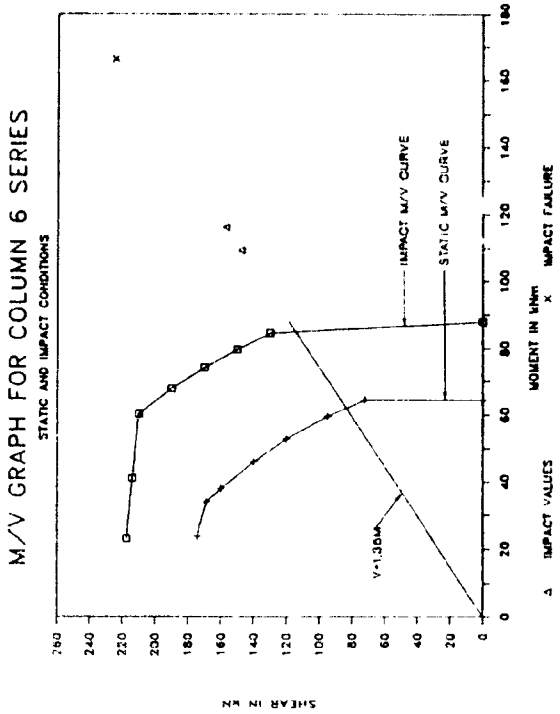

Fig.8.13: M/V Graphs - Group 6

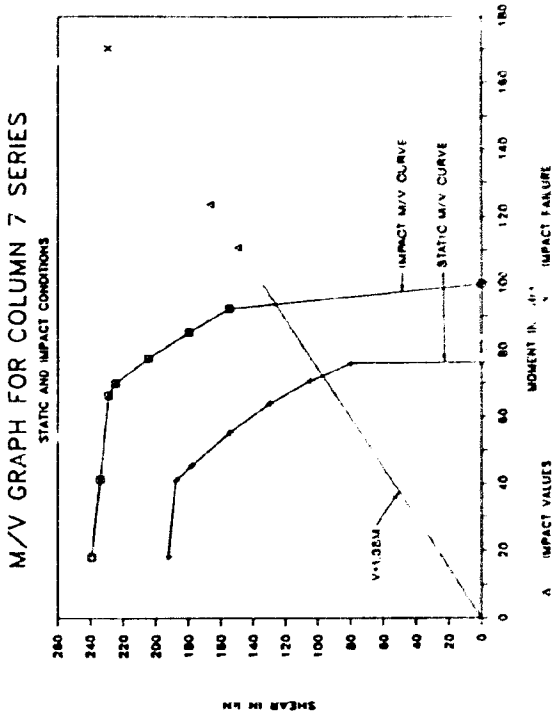

Fig.8.14: M/V Graphs - Group 7

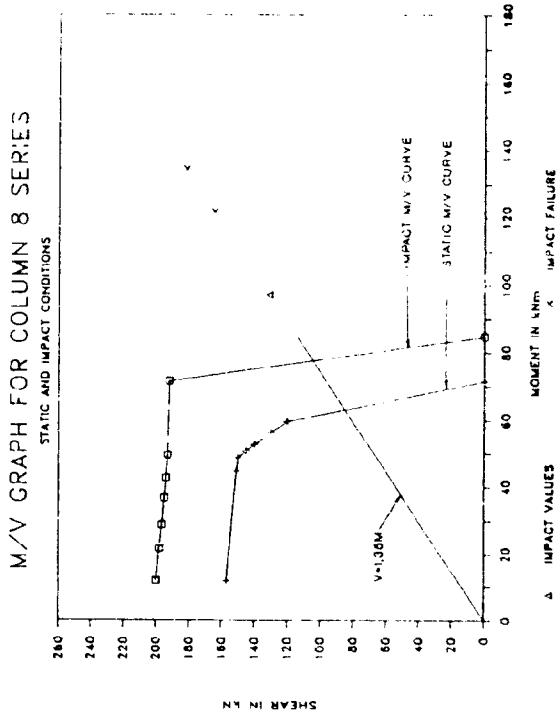

Fig.8.15: M/V Graphs - Group 8

Stellenbosch University http://scholar.sun.ac.za

9. RECOMMENDATIONS FOR FUTURE RESEARCH AND CONCLUSIONS.

This research project can be used as a foundation for further research of a reinforced concrete cantilever column subjected to a lateral impact load. From the experimental investigations and the theoretical studies, a number of recommendations for future research and studies can be made.

It is recommended that the following aspects of the problem of a column subjected to a lateral impact load should be researched in the future:

1. Material properties of the reinforced concrete column. Very little research has been done on the response of concrete to multi-axial impact loading.

2. A more extensive research program should be undertaken. The impact flexural failure, especially, should be investigated. An accurate deflection measuring system, for the column under impact conditions, will facilitate this investigation. An extensive series of tests to investigate the influence of each variable will also help to understand the column impact problem better.

3. A more simple design method for a column under lateral impact loadings should also be investigated. Even if this means a design method based on empirical values from an extensive research program. This will make the whole problem more accessible to the practising engineer. Special attention should be given to predict the failure load and mechanism accurately.

4. A good finite elements computer program to predict the response of such a column more accurately should also be investigated. Special attention should be given to the material model for the concrete under impact conditions.

Stellenbosch University http://scholar.sun.ac.za

5. A more refined analytical model might be investigated. The modified compression field theory might be incorporated in the analytical model derived in Chapter 5. By incorporating this theory a time step analysis can be done, where in each time step the crack widths can be calculated with the modified compression field theory. With a known crack width, the increase in the axial load can be calculated as well as a new inertia moment for the section. Then a new mode frequency can be calculated. These new parameters can ther be used for the next time step. This should to be done for each mode and for a number of cross sections. By using this method the increase in the axial load during impact can also be predicted. As can be seen, this will be a very lengthy process and the results might not be that much better than the relative simple method derived in Chapter 5.

6. The inertia forces acting on the column should be determined more accurately during the experimental investigation. This will facilitate the determination of the actual moments and shears generated in the column.

7. If the same experimental arrangements are used for future research, the axial loading system should be changed to a system where the axial load is not attached to the column but more like the situation in a real bridge.

8. The influence of a higher axial load should also be investigated.

9. A column with an axial load but without the concentrated mass at the top of the column, should also be investigated. In such a case the axial load can be applied to the column by means of an unbonded prestressed tendon. In such a case the axial load can easily be measured with a load cell. This will also simplify the theoretical analysis of the column as discussed in Chapter 5.

10. The influence of successive impact loads on a column should also be investigated.

Stellenbosch University http://scholar.sun.ac.za

11. Columns hinged at the top and fixed at the bottom should also be investigated.

12. The experimental results given in Appendix B are very extensive and thus can be used for further investigations of the different aspects.

As stated earlier one of the most important parts of this dissertation is Appendix B. This Appendix gives a complete and detailed report of the experimental work done in the laboratory and should facilitate future research.

Unfortunately too little test data are available to draw any final conclusions on most of the aspects investigated. A relative simple, economical and safe design procedure was however presented. This design procedure can be used by the general practising engineer without any knowledge of large computer programs. The procedure would, however, still be more refined pending further research results.

Stellenbosch University http://scholar.sun.ac.za

APPENDIX A. BIBLIOGRAPHY

1. Abdel-Rohman, M., Sawan, J., "Impact Effect on R/C Slabs: Analytical Approach," Journal of Structural Engineering, ASCE, Vol. 111, No. 7, July, 1985, pp 1590-1601.

2. ACI Committee 349, "ACI Standard Code Requirements for Nuclear Safety Related Concrete Structures," (ACI 349-80).

3. ACI Committee 349, "Proposed addition to: Commentary on Code Requirements for Nuclear Safety Related Concrete Structures (ACI 349-76)," Journal of the American Concrete Institute, Title no. 75-4, Vol. 75 No. 2, Feb., 1978, pp 41-48.

4. ACI Committee 349, "Proposed addition to: Commentary on Code Requirements for Nuclear Safety Related Concrete Structures (ACI 349-76)," Journal of the American Concrete Institute, Title no. 74-4, Vol. 74 No. 2, Feb., 1977, pp 53-58.

5. ACI Publication SP-24, "Models for Concrete Structures." Detroit, 1970.

6. ACI Publication SP-73, Harris, H. G., (Ed.), "Dynamic Modelling of Concrete Structures." Detroit, 1982.

7. Addis, B. J., (Ed), "Fulton's Concrete Technology," Portland Cement Institute, Midrand, South Africa, 1986.

8. Adeli, H., Amin, A. M., "Local Effects of Impactors on Concrete Structures," Nuclear Engineering and Design, Vol. 88, No. 3, 1985, pp. 301-317.

9. Albritton, G. E., "Deep Slabs Subjected to Static and Blast Loading," Journal of the Structural Division, ASCE, Vol. 95, No. 11, Nov., 1969, pp. 2449-2462.

Stellenbosch University http://scholar.sun.ac.za

10. Ammann, W., "Stahlbeton- und Spannbetontragwerke unter Stossartiger Belastung," Bericht Nr.142, Institut fÜr Baustatik und Konstruktion ETH ZÜrich, Juni, 1983.

11. Armstrong, B. M., James, D. B., Latham, D. J., Taylor, V., Wilson, C., Heighington, K., "Toughness of Reinforcing Bars and Its Influence on the Impact Resistance of Reinforced Concrete," The First International Conference on Concrete For Hazard Protection, The Concrete Society, Edinburgh, 27-30 September 1987, pp.241 254.

12. Attalla, I., Nowotny, B., "Missile Impact on Reinforced Concrete Structure," Nuclear Engineering and Design, Vol. 37, 1976, pp. 321-332.

13. Bazant, Z. P., Kim, S. S., "Plastic-Fracturing Theory for Concrete," Journal of the Engineering Mechanics Division, ASCE, Vol. 105, No. 3, June, 1979, pp. 407-428.

14. Bazant, Z. P., Oh, B. H., "Strain-Rate Effect in Rapid Tiaxial Loading of Concrete," Journal of the Engineering Mechanics, ASCE, Vol. 108, No. 5, Oct., 1982, pp 764-782.

15. Bodner, S. R., Symonds, P. S., "Experiments on Dynamic Plastic Loading of Frames," International Journal of Solids and Structures, Vol.15, pp.1-13, 1979.

16. Brandes, K., Limberger, E., Herter, J., "Experimental Verification of Punching Shear Failure of Slabs Subjected to Aircraft Impact Loads," Transactions of the 8 th International Conference on Structural Mechanics in Reactor Technology (SMIRT)," Aug. 19-23. 1985, Brussels, Belgium, Paper J5/6, pp 197-201.

Stellenbosch University http://scholar.sun.ac.za

17. Buchhardt, F., Magiera, G., Matthees, W., Damping, M., "Interactions Between Material Nonlinearity and Damping for Aircraft Impact Analysis," Transactions of the 8 th International Conference on Structural Mechanics in Reactor Technology (SMIRT)," Aug. 19-23, 1985, Brussels, Belgium, Paper J5/5, pp 191-196.

18. Buyukozturk, O., "Nonlinear Analysis of Reinforced Concrete Structures," Computers and Structures, Vol. 7, 1977, pp 149-156.

19. Buyukozturk, O., Connor, J. J., "Nonlinear Dynamic Response of Reinforced Concrete under Impulsive Loading: Research Status and Needs," Nuclear Engineering and Design, Vol. 50, 1978, pp 83-92.

20. Carney, J. F., Austin, C. D., Reid, S. R., "Modeling of Steel Tube Vehicular Crash Cushion," Journal of Transportation Engineering, ASCE, Vol. 109, No. 3, May, 1983, pp 331-346.

21. Carney, J. F., Sazinski, R. J., "Portable Energy Absorbing System for Highway Service Vehicles," Transportation Engineering Journal, ASCE, Vol. 104, No. 4, July, 1978, pp 407-421.

22. Carpinteri, A., "Mechanical Damage and Crack Growth in Concrete," Marthinus Nijhoff Publishers, Dordrecht, 1986.

23. CEB Design Manuel on Cracking and Deformations. Prepared by Comitè Euro-International du Bèton (CEB), 1985.

24. Cernica, J. N., Charignon, M. J., "Ultimate Static and Impulsive Loading of Reinforced Concrete Beams," Journal of the American Concrete Institute, Title no. 60-57, Vol. 60, No. 57, Sept., 1963, pp 1219-1227.

Stellenbosch University http://scholar.sun.ac.za

25. Chandra, J., Flaherty, J. E., (Ed.), "Computational Aspects of Penetration Mechanics," Proceedings of the Army Research Office Workshop on Computational Aspects of Penetration Mechanics held at the Ballistic Research Laboratory at Aberdeen Proving Ground, Maryland, 27-29 April, 1982, Springer-Verlag Berlin Heidelberg 1983.

26. Chandra, V., Szecsei, G., "Sunshine Skyway Bridge Ship Impact Design of Low Level Approaches," PCI Journal, pp.96-123, July-August 1988.

27. Chang, W. S., "Impact of Solid Missiles on Concrete Barriers," Journal of the Structural Division, ASCE, Vol. 107, No. 2, Feb., 1981, pp 257-271.

28. Clifton, J. R , Knab, L. I., "Impact Testing of Concrete," Cement and Concrete Research, Vol. 14, 1983, pp 541-548.

29. Clough, R. W., Penzien, J., "Dynamics of Structures," McGraw-Hill, Inc., 1975.

30. Collins, M. P., "Prestressed Concrete Structures - A Post-Graduate Course at the University of Canterbury," May-August 1983.

31. Collins, M. P., Mitchell D., "Prestressed Concrete Basics," Canadian Prestressed Concrete Institute, Canada, 1987.

32. Coon, M. D., Evans, R. J., "Incremental Constitutive Laws and Their Associated Failure Criteria with Application to Plain Concrete," International Journal of Solids and Structures, Vol. 8, 1972, pp. 1169-1183.

33. Cracknell, C. J., Jarman, D. A., "Effect of Heavy Impact Loads on Structural Members," Concrete, Vol. 7, No. 9, Sept., 1973. pp 49-50.

Stellenbosch University http://scholar.sun.ac.za

34. Crutzen, Y. R., Hibbitt, H. H., "Automatic Nonlinear Solutions in Structural Analysis Using Abaqus," Transactions of the 8 th International Conference on Structural Mechanics in Reactor Technology (SMIRT)," Aug. 19-23, 1985, Brussels, Belgium, Paper B8/1, pp 281-286.

35. Degen, P. P., "Perforation of Reinforced Concrete Slabs by Rigid Missiles," Journal of the Structural Division, ASCE, Vol. 106, No. 7, July, 1980, pp 1623-1642.

36. Degen, P., Furrer, H., Jemielewski, J., "Structural Analysis and Design of a Nuclear Power Plant Building for Airsraft Crash Effects," Nuclear Engineering and Design, Vol. 37, 1976, pp. 249-268.

37. Dilger, W. H., Ghali, A., "Response of Spun Cast Concrete Poles to Vehicle Impact," Prestressed Concrete Institute Journal, Vol. 31, No. 1, Jan.-Febr., 1986, pp 62-82.

38. Donea, J., Giuliani, G., Halleux, J. P., "Prediction of the Nonlinear Dynamic Response of Structural Components Using Finite Element Analysis," Nuclear Engineering and Design, Vol. 37, 1976.

39. Drittler, K., Gruner, P,. "The Force Resulting from Impact of Fast-flying Military Aircraft upon a Rigid Wall," Nuclear Engineering and Design, Vol. 37, 1976, pp. 245-248.

40. Drittler, K., Gruner, P., "Calculation of the Total Force Acting upon a Rigid Wall by Projectiles," Nuclear Engineering and Design, Vol. 37, 1976, pp. 231-244.

41. Eibl, J., "Soft and Hard Impact," The First International Conference on Concrete For Hazard Protection, The Concrete Society, Edinburgh, 27-30 September 1987, pp.175-186.

Stellenbosch University http://scholar.sun.ac.za

42. Eibl, J., "The Design of Impact Endangered Concrete Structures," Transactions of the 8 th International Conference on Structural Mechanics in Reactor Technology (SMIRT)," Aug. 19-23, 1985, Brussels, Belgium, Paper H6/3, pp 265-270.

43. Eibl, J., Block, K., "Zweischalige Wandkonstruktionen aus Stahlbeton unter "Weicher" Stobbeanspruchung - Flugzeugabsturz-," Beton und Stahlbetonbau, Vol. 77, No. 2, Feb., 1982, pp 44-48.

44. Eibl, J., Feyerabend, M., "Stoßbelastung von Normalkraftbeanspruchten Stabförmigen Tragwerksteilen aus Stahl, Holz und Stahlbeton," University of Karlsruhe, December, 1984.

45. Fardis, M. N., Buyukozturk, O., "Shear Stiffness of Concrete by Finite Elements," Journal of the Structural Division, ASCE, Vol. 106, No. 6, June, 1980, pp. 1311-1327.

46. Fardis, M. N., Nacar, A., Delitchatsios, M. A., "R/C Containment Safety Under Hydrogen Detonation," Journal of Structural Engineering, ASCE, Vol. 109, No. 11, Nov., 1983, pp 2511 2527.

47. Fiquet, G., Dacquet, S., "Study of the Perforation of Reinforced Concrete Slabs by Rigid Missiles." Experimental Study Part II," Nuclear Engineering and Design. Vol. 41, 1977, pp. 103-120.

48. Flade, D., Steinhilber, H., Malcher, L., "Impulse Excitation of the Outer HDR-Containment with a Pendular Falling Weight," Transactions of the 8 th International Conference on Structural Mechanics in Reactor Technology (SMIRT)," Aug. 19-23, 1985, Brussels, Belgium, Paper J5/4, pp 185-190.

Stellenbosch University http://scholar.sun.ac.za

49. Freiman, S. W., Fuller, E. R., (Ed.), "Fracture Mechanics for Ceramics, Rocks, and Concrete," ASTM Special Technical Publication 745, (Proceedings of Symposium held in Chicago, June, 23-24, 1980.), American Society for Testing and Materials, 1981.

50. Frènay, J. W., "Behaviour of a Single Crack in Plain and Reinforced Concrete Subjected to Sustained Shear Loading," Delft University of Technology, Faculty of Civil Engineering, Report 5-86-11, November 1986.

51. Frènay, J. W., Liqui Lung, G., Pruijssers, A. F., "Shear Transfer Across a Single Crack in Reinforced Concrete," Delft University of Technology, Faculty of Civil Engineering, Report 5-86-5, November 1986.

52. Furnes, O., Amdahl, J., "Computer Simulation Study of Offshore Collisions and Analysis of Ship-platform Impacts," Dynamic Analysis of Offshore Structures: Recent Developments, Ed. Colin L Kirk, 1982, pp 43-51.

53. Gardner, J. W., "Calculation of the Forces Acting upon a Rigid Structure from an Aircraft Impact," International Journal of Impact Engineering, Vol. 2, No. 4, 1984, pp 345-356.

54. Ghaboussi, J. G. Millavec, W., Isenberg, J., "R/C Structures Under Impact Loading," Journal of Structural Engineering, ASCE, Vol. 110, no. 3, March, 1984, pp 505-522.

55. Godinas, A., Charlier, R., Cescotto, S., "On the Modelling of Contact Problems with Friction by the Finite Element Method," Transactions of the 8 th International Conference on Structural Mechanics in Reactor Technology (SMIRT)," Aug. 19-23, 1985, Brussels, Belgium, Paper B4/2, pp 149-154.

56. Goldsmith, W., "Impact: The Theory and Physical Behaviour of Colliding Solids," Edward Arnold Publishers, London, 1960.

Stellenbosch University http://scholar.sun.ac.za

57. Goldstein, S., Berriaud, C., Labrot, R., "Study of the Perforation of Reinforced Concrete Slabs by Rigid Missiles, Experimental Study Part III, Nuclear Engineering and Design, Vol. 41, 1977, pp. 121-128.

58. Gopalakrishna, H.S., Wolde-Tinsae, A. M., "Damage Probability of Turbine Missile Impact," Journal of Structural Engineering, ASCE, Vol. 110, No. 12, Dec., 1984, pp 2909-2923.

59. Gueraud, R., Sokolovsky, A., Kavyrchine, M., Astruc,M., "Study of the Perforation of Reinforced Concrete Slabs by Rigid Missiles," Experimental Study Part I, Nuclear Engineering and Design, Vol. 41, 1977, pp. 91-102.

60. Gupta, Y. M., Seaman, L., "Local Response of Reinforced Concrete to Missile Impacts," Nuclear Engineering and Design, Vol. 45, 1978, pp. 507-514.

61. Haldar, A., "Energy-Balanced Approach to Evaluate Local Effects of Impact of Non Deformable Missiles on Concrete Structures," Transactions of the 8 th International Conference on Structural Mechanics in Reactor Technology (SMIRT)," Aug. 19-23, 1985, Brussels, Belgium, Paper J6/3, pp 209-214.

62. Haldar, A., "Impact of Solid Missiles on Concrete Barriers - Discussion," Journal of Structural Engineering, ASCE, Vol. 107, No. 11, Nov., 1981, pp 2307-2309.

63. Haldar, A., Hamieh, H. A., "Local Effect of Solid Missiles on Concrete Structures," Journal of Structural Engineering, ASCE, Vol. 110, No. 5, May, 1984, pp 948-960.

64. Haldar, A., Hatami, M., Miller, F. J., "Concrete Structures: Penetration Depth Estimation," Journal of Structural Engineering, ASCE, Vol. 109, No. 1, Jan., 1983, pp 245-250.

Stellenbosch University http://scholar.sun.ac.za

65. Hamilton, W. A., "Dynamic Response of Pretensioned Prestressed Concrete Beams." Journal of the American Concrete Institute, Title no. 65-63, Vol. 65, No. 63, Oct., 1968, pp 851-855.

66. Hibbitt, H. D., "Abaqus/Epgen - A General Purpose Finite Element Code with Emphasis on Nonlinear Applications," Nuclear Engineering and Design, Vol. 77, 1984, pp. 271-297.

67. Hibbitt, H. D , Marcal, P. V., Rice, J. R., "An Incremental Finite Element Formulation for Problem of Large Strain, and Large Displacement," International Journal of Solids and Structures, Vol. 6, No. 6, 1970, pp. 1069-1086.

68. Hoffmann, A., Jamet, P., Lepareux, M., Millard, A., Barbe, B., Maurel, P., "Ultimate Flexural Behaviour of Reinforced Concrete Shells Under Static and Dynamic Loading," Transactions of the 8 th International Conference on Structural Mechanics in Reactor Technology (SMIRT)," Aug. 19-23, 1985, Brussels, Belgium, Paper J1/8, pp 31-38.

69. Hughes, B. P., "Design of Prestressed Fibre Reinforced Concrete Beams for Impact," Journal of the American Concrete Institute, Title no. 78-25, Vol. 78, No. 4, Jul./Aug., 1981, pp. 276-281.

70. Hughes, B. P., "Limit States of Impact and CP110," Concrete, Vol. 7, No. 8, Aug., 1973, pp 37-40.

71. Hughes, B. P., Gregory, R., "Concrete Subjected to High Rates of Loading in Compression," Magazine of Concrete Research, Vol. 24, No. 78, March, 1972, pp. 25-36.

72. Hughes, B. P., Mahmood, A. T., "Impact Behaviour of Concrete Beams in Flexure," Magazine of Concrete Research, Vol. 36: No. 128, Sept., 1984, pp 157-164.

Stellenbosch University http://scholar.sun.ac.za

73. Hughes, B. P., Nourbakhsh, F., "Influence of Contact Zone Behaviour on the Impact Resistance of Concrete Beams," The First International Conference on Concrete For Hazard Protection, The Concrete Society, Edinburgh, 27-30 September 1987, pp.227-239.

74. Hughes, B. P., Watson, A. J., "Compressive Strength and Ultimate Strain of Concrete under Impact Loading," Magazine of Concrete Research, Vol. 30, No. 105, Dec., 1978, pp 189-199.

75. Hughes, G., "Hard Missile Impact on Reinforced Concrete," Nuclear Engineering and Design, Vol. 77, No. 1, 1984, pp. 23-35.

76. Hughes, G., Beeby, A. W., "Investigation of the Effect of Impact Loading on Concrete Beams," The Structural Engineer, Vol. 60B, No. 3, Sept., 1982, pp 45-52.

77. Hughes, G., Speirs, D. M., "An Investigation of the Beam Impact Problem," Cement and Concrete Association Technical Report 546, April, 1982.

78. IABSE, Reports of the Working Commissions, Vol.33, "Advanced Mechanics of Reinforced Concrete," Delft, 1981.

79. Jacobsen, L. S., Ayre, R. S., "Engineering Vibrations," McGraw-Hill Book Company, New York, 1958.

80. Jenq, Y. S., Shah, S. P., "A Fracture Toughness Criterion For Concrete," Engineering Fracture Mechanics, Vol.21, No.5, pp.1055-1069, 1985.

81. Johnson, G. R., "Analysis of Elastic Plastic Impact Involving Severe Distortions," Journal of Applied Mechanics, ASME, Sept., 1976, pp. 439-444.

82. Johnson, G. R., "High Velocity Impact Calculations in Three Dimensions," Journal of Applied Mechanics, ASME, Mar., 1977, pp. 95-100.

Stellenbosch University http://scholar.sun.ac.za

83. Johnson, W., "Impact Strength of Materials," Edward Arnold Publishers, 1972.

84. Jones, N., Wierzbicki, T., (Ed), "Structural Crashworthiness," Butterworths, London.85. Jones, R. C., Hribar, J. A., "Grain Size and LOading Rate Effects on Steel," Journal of the Engineering Mechanics Division, ASCE, Vol.5, pp.43-69, October 1964.

86. Kaplin, S. A., "Factors Affecting the Relationship of Loading and Measured Compressive Strength of Concrete," Magazine of Concrete Research, Vol. 32, No. 111, June, 1980. pp. 79-88.

87. Kar, A. K., "Impactive Effects of Tornado Missiles and Aircraft," Journal of the Structural Division, ASCE, Vol. 105, No. 11, Nov., 1979, pp 2243-2260.

88. Kar, A. K., "Local Effects of Tornado-Generated Missiles," Journal of the Structural Division, ASCE, Vol. 104, No. 5, May, 1978, pp 809-816.

89. Kavyrchine, M., Struck, W., "The Effect of Impact Loading on Buildings (State of the Art Report) Part 6: Practical Application to Testing, Design and Research," Materiaux et Constructions, Vol. 8, No. 44, Mar./April. 1975, pp. 125-129.

90. Kennedy, R. P., "A Review of Procedures for the Analysis and Design of Concrete Structures to Resist Missile Impact Effects," Nuclear Engineering and Design, Vol. 37, No. 2, May, 1976, pp. 183-203.

91. Kinslow, R., (Ed.), "High-Velocity Impact Phenomena," Academic Press, New York and London, 1970.

92. Kong, F. K., Evans, R. H., "Reinforced and Prestressed Concrete," 3rd edition, Van Nostrand Reinhold (UK) Co. Ltd., 1987.

Stellenbosch University http://scholar.sun.ac.za

93. Krajcinovic, D., Fanella, D., "A Micromechanical Damage Model for Concrete," Engineering Fracture Mechanics, Vol 25, Nos 5/6, pp.585-596, 1986.

94. Krajcinovic, D., Silva, M. A. "Analysis of Tests on Impact Strength of Concrete Arror Blocks," International Journal of Impact Engineering, Vol. 2, No. 4, 1984, pp 331 343.

95. Krauthammer, T., "Structural Concrete for Protection Against Terrorism," The First International Conference on Concrete For Hazard Protection, The Concrete Society, Edinburgh, 27-30 September 1987, pp.89-100.

96. Krauthammer, T., Bazeos, N., Holmquist, T. J., "Modified SDOF Analysis of R/C Box type Structures," Journal of Structural Engineering, ASCE, Vol. 112, No. 4, April, 1986, pp 726-744.

97. Labra, J. J., "Protective Structure Response to Vehicle Impact," Journal of the Structural Division, ASCE, Vol. 105, No. 6, June, 1979, pp 991-1005.

98. Langhaar, H. L., "Dimensional Analysis and Theory of Models," John Wiley and Sons, New York, 1951.

99. Loo, Y., Santos, A. F., "Impact Deflection Analysis of Concrete Beams," Journal of Structural Engineering, ASCE, Vol. 112, No. 6,Jun., 1986, pp 1297 1312.

100. Magrab, E. B., "Vibrations of Elastic Structural Members," Sijthoff & Noordhoff Publishers, The Netherlands, 1979.

101. Mainstone, R. J., "The Effect of Impact Loading on Buildings (State of the Art Report) Part 4: Properties of Materials at High Rates of Straining or Loading," Materiaux et Constructions, Vol. 8, No. 44, May - Apr., 1975, pp. 107 116.

Stellenbosch University http://scholar.sun.ac.za

102. Mainstone, R. J., Kavyrchine, M., "The Effect of Impact Loading on Buildings (State of the Art Report) Part 1: Introduction," Materiaux et Constructions, Vol. 8, No. 44, Mar./April, 1975, pp. 79-80.

103. Martin, J. B., Symonds, P. S., "Mode Approximations for Impulsively-loaded Rigid-Plastic Structures," Journal of the Engineering Mechanics Division, ASCE, Vol.5, pp.43-66, October 1966.

104. Maurel, P., Lacoste, J. M., Hoffmann, A., Jamet, P., "Three Dimensional Dynamic Analysis of a Thick Reinforced Concrete Slab Subjected to the Impact of a Projectile," Transactions of the 8 th International Conference on Structural Mechanics in Reactor Technology (SMIRT)," Aug. 19-23, 1985, Brussels, Belgium, Paper J6/1, pp 203-207.

105. Mavis, F. T., Greaves, M. J., "Destructive Impulse Loading of Reinforced Concrete Beams," Journal of the American Concrete Institute, Title no. 54 14, Vol. 54, No 14, Sept., 1957, pp 233-252.

106. Mavis, F. T., Richards, F. A., "Impulse Testing of Concrete Beams," Journal of the American Concrete Institute, Title no. 52 8, Vol. 52, No. 8, Sept., 1955, pp 93-102.

107. Mavis, F. T., Stewart, J. J., "Further Tests of Dynamically Loaded Beams," Journal of the American Concrete Institute, Title no. 55 74, Vol. 55, No. 74, May, 1959, pp 1215-1223.

108. McMahon, P., Meyers, B. L., Buchert, K. P., "Impact of Deformable Missiles on Concrete Walls," Journal of the Power Division, ASCE, Vol. 104, No. 1, Apr., 1978, pp 187-197.

109. McMahon, P. M., Sen, S. K., Meyers, B. L., Buchert, K. P., "Structural Response of R.C. Slabs to Tornado Missiles," Journal of the Structural [illegible], ASCE, Vol. 105, No. 3, Mar., 1979, pp 547-561

Stellenbosch University http://scholar.sun.ac.za

110. Mescall, J., Weiss, V., (Ed.), "Material Behavior under High Stress and Ultrahigh Loading Rates," (Proceedings of the 29th Sagamoore Army Materials Conference, held July 19-23, 1982, at Lake Placid, New York,) Plenum Press, New York and London, 1983.

111. Miles, J. C., Tufton, E. P. S., "Affordable Damage in Impact," The First International Conference on Concrete For Hazard Protection, Th Concrete Society, Edinburgh, 27-30 September 1987, pp.255-265.

112. Mills, C. A., Atkins, W. S., "The Design of Concrete Structures to Resist Explosions and Weapon Effects," The First International Conference on Concrete For Hazard Protection, The Concrete Society, Edinburgh, 27-30 September 1987, pp.61-73.

113. Mlakar, P. F., Vitaya Udom, K. P., Cole, R. A., "Dynamic Tensile Compressive Behavior of Concrete," Journal of the American Concrete Institute, Vol. 82, No. 4, Jul. Aug., 1985, pp 484 491.

114. Morales, W. J., "Displacement Bounds for Blast Loaded Structures," Journal of the Engineering Mechanics Division, ASCE, Vol.4, pp.965-974, August, 1972.

115. Nilson, A. H., "Nonlinear Analysis of Reinforced Concrete by the Finite Element Method," Journal of the American Concrete Institute, Vol. 65, 1968, pp. 757-766.

116. Nilsson, L., "Impact Loading on Concrete Structures," Chalmers University of Technology, Department of Structural Mechanics, Publication 79:1, Göteborg, 1979.

117. Norris, C. H., Hansen, P. J., Holley, M. J., Biggs, J. M., Namyet, S., "Structural Design for Dynamic Loads," McGraw-Hill Book Co., 1959, pp 12" 131

Stellenbosch University http://scholar.sun.ac.za

118. Ohnuma, H., Nomachi, S. G., "Dynamic Response and Local Rupture of Reinforced Concrete Beam and Slab under Impact Loading," Transactions of the 8 th International Conference on Structural Mechanics in Reactor Technology (SMIRT)," Aug. 19-23, 1985, Brussels, Belgium, Paper J5/3, pp 179-184.

119. Ottosen, N. S., "A Failure Criterion for Concrete," Journal of the Engineering Mechanics Division, ASCE, Vol. 103, No. 4, Aug., 1977, pp. 527-535.

120. Ottosen, N. S., "Constitutive Model for Short Time Loading of Concrete," Journal of the Engineering Mechanics, ASCE, Vol. 105, No. 1, Febr., 1979, pp 127-141.

121. Paz, M., "Structural Dynamics: Theory and Computation," Van Nostrand Reinhold Company, New York, 1980.

122. Penzien, J., Hansen, R.J., "Static and Dynamic Elastic Behavior of Reinforced Concrete Beams," Journal of the American Concrete Institute, Title no. 50-32, Vol. 50, No. 32, March, 1954, pp 545-567.

123. Perrone, N., "Impulsively Loaded Strain Hardened Rate Sensitive Rings and Tubes," International Journal of Solids and Structures, Vol. 6, No. 8, Aug., 1970, pp. 1119-1132.

124. Perrone, N., "Thick-Walled Rings for Energy Absorbing Bridge Rail Systems," Report No. FHWA-RD-73-71, Federal Highway Administration, Washington, D.C., Dec., 1972.

125. Perry, E. S., Burns, N. H., Thompson, J. N., "Behavior of Concrete Beams Reinforced with Steel Plates Subjected to Dynamic Loads," Journal of the American Concrete Institute, Title no. 64-57, Vol. 64, No. 57, Oct., 1967, pp 662-668.

126. Perry, S. H., Dinic, G., Brown, I. C., "Design of Structural Concrete Slabs Against Extreme Hard Impact at Intermediate Velocities (Up to 25m/s)," The First International Conference on Concrete For Hazard Protection, The Concrete Society, Edinburgh, 27-30 September 1987, pp 215-218.

Stellenbosch University http://scholar.sun.ac.za

127. Poepsel, P. H., Dowd, W. M., "Design of Deep Foundations for Ship Impact Loading, Apalachicola River Bridge, Florida," The First International Conference on Concrete For Hazard Protection, The Concrete Society, Edinburgh, 27-30 September 1987, pp.37-48.

128. Popp, C., "Schlag-Biegeversuche mit Unterschiedlich Bewehrten Stahlbetonbalken," Deutscher Ausschuss für Stahlbeton, No. 249, 1975, 52p.

129. Popp, C., "Untersuchungen über das Verhalten von Beton bei Schlagartiger Beanspruchung," Deutscher Asschuss für Stahlbeton, No. 281, 1977, 66p.

130. Preece, B. W., Davies, J. D., "Models for Structural Concrete," CR Books Ltd, London, 1964.

131. Pruijssers, A. F., "Description of the Stiffness Relation for Mixed-mode Fracture Problems in Concrete Using the Rough-crack Model of Walraven," Delft University of Technology, Faculty of Civil Engineering, Report 5-85-2.

132. Rebora, B., Zimmermann, Th., Wolf, J. P., "Dynamic Rupture Analysis of Reinforced Concrete Shells," Nuclear Engineering and Design, Vol. 37, 1976, pp. 269-297.

133. Reddy, T. Y., Reid, S. R., "Phenomena Associated with the Crushing of Metal Tubes Between Rigid Plates," International Journal of Solids and Structures, Vol. 16, 1980, pp. 545-562.

134. Reinhardt, H. W., "Concrete under Impact Loading. Tensile Strength and Bond," Heron, Vol.27, No.3, 1982.

135. Reinhardt, H. W., "Fracture Mechanics of an Elastic Softening Material like Concrete," Heron, Vol.29, No.2, 1984.

Stellenbosch University http://scholar.sun.ac.za

136. Reinschmidt, K. F., Hansen, R. J., Yang, C. Y., "Dynamic Tests of Reinforced Concrete Columns," Journal of the American Concrete Institute, Title no. 61-20, Vol. 61, No. 20, March, 1964, pp 317-333.

137. Ross, H. E., Smith, D. G., "Impact Behaviour of Barriers on Nonlevel Terrain," Transportation Engineering Journal, ASCE, Vol. 107, No. 1, Jan., 1981, pp 69-79.

138. Ross, T. J., "Dynamic Rate Effects on Timoshenko Beam Response," Journal of Applied Mechanics, ASME, Vol. 52, No. 2, June, 1985, pp 439-445.

139. Ross, T. J., Krawinkel, H., "Impulsive Direct Shear Failure in R/C Slabs," Journal of Structural Engineering, ASCE, Vol. 111, No. 8, Aug., 1985, pp 1661-1677.

140. Ross, T. J., Wong, F. S., "Timoshenko Beams with Rotational End Constraints," Journal of Engineering Mechanics, ASCE, Vol. 111, No. 3, March, 1985, pp 416-430.

141. Sahlin, S., Nilsson, L., "The Effect of Impact Loading on Buildings (State of the Art Report) Part 3: Theoretical Analysis of Stress and Strain Propagation During Impact," Materiaux et Constructions, Vol. 8, No. 44, Mar./April, 1975, pp. 88-101.

142. Sasse, H. R., Müller, F., Thormählen, U., "Stützenstöbe im Stahlbeton-Fertigteilbau mit Unbewehrten Elastomerlagern," Beton und Stahlbetonbau, Vol. 77, No. 11, Nov., 1982, pp 282-285.

143. Schrader, E. K., "Impact Resistance and Test Procedure for Concrete," Journal of the American Concrete Institute, Vol. 78, No. 2, Mar.-Apr., 1981, pp 141-146.

Stellenbosch University http://scholar.sun.ac.za

144. Schwarzkopp, D., Zinn, R., "Simplified Nonlinear Analysis of Reinforced Concrete Plates Under Projectile Impact Including Penetration and Projectile Deformation Effects," The First International Conference on Concrete For Hazard Protection, The Concrete Society, Edinburgh. 27-30 September 1987, pp.49-60.

145. Second ASCE Conference on Civil Engineering and Nuclear Power, "Vol. IV: Impactive and Impulsive Loads," Sept. 15-17, 1980, Knoxville, Tennessee.

146. Second ASCE Conference on Civil Engineering and Nuclear Power, "Vol. V: Report of the ASCE Committee on Impactive and Impulsive Loads," Sept. 15-17, 1980, Knoxville, Tennessee.

147. Shah, S. P., (Ed.), "Application of Fracture Mechanics to Cementitious Composites," Martinus Nijhoff Publishers, 1985.

148. Shaw, W. A., Allgood, J. R., "Blast Resistance of Reinforced Concrete Beams Influenced by Grade of Steel." Journal of the American Concrete Institute, Title no. 55-60, Vol. 55, No. 60, March, 1959, pp 935-945.

149. Sheridan, A. J., "Response of Concrete to High Explosive Detonation," The First International Conference on Concrete For Hazard Protection, The Concrete Society, Edinburgh. 27-30 September 1987, pp.75-87.

150. Skov, K., Olesen, S., "Impact Resistance of Reinforced and Prestressed Concrete Members." Materials and Structures, Vol. 8, No. 44, 1975, pp 116-125.

151. Skov, S., Olsen, S., "The Effect of Impact Loading on Buildings (State of the Art Report) Part 5: Impact Resistance of Reinforced and Prestressed Concrete Members." Materiaux et Constructions, Vol. 8, No. 44, Mar./April. 1975, pp. 116-125.

Stellenbosch University http://scholar.sun.ac.za

152. Sliter, G. E. "Assessment of Empirical Concrete Impact Formulas," Journal of the Structural Division, ASCE, Vol. 106, No. 5, May, 1980, pp 1023-1045.

153. Smith, P. D., Mays, G. C., "Novel Mesh-Reinforced Concrete for Protection Against Blast and Impact Loading," The First International Conference on Concrete For Hazard Protection, The Concrete Society, Edinburgh, 27-30 September 1987, pp.201-213.

154. Stangenberg, F., "Zum Verhalten von Stahlbetotragwerken unter Stobbelastungen," Beton und Stahlbeton, Vol. 78, No. 8, Aug., 1983, pp 225-230.

155. Struck, W., Voggenreiter, W., "The Effect of Impact Loading on Buildings (State of the Art Report) Part 2: Examples of Impact and Impulsive Loading in the Field of Civil Engineering," Materiaux et Constructions, Vol. 8, No. 44, Mar./April, 1975, pp. 81 87.

156. Suaris, W., Shah, S. P., "Constitutive Model for Dynamic Loading of Concrete," Journal of Structural Engineering, ASCE, Vol. 111, No. 3, March, 1985, pp 563 576.

157. Suaris, W., Shah, S. P., "Mechanical Properties of Materials Subjected to Impact," RILEM-CEB-IABSE-IASS-Interassociation Symposium on Concrete Structures under Impact and Impulsive Loading, BAM, Berlin, 1982, pp. 33-62.

158. Suaris, W., Shah, S. P., "Properties of Concrete Subjected to Impact," Journal of Structural Engineering, ASCE, Vol. 109, No. 7, July, 1983, pp 1727-1741.

159. Suaris,W., Shah, S. P., "Rate-Sensitive Damage Theory for Brittle Solids," Journal of the Engineering Mechanics Division, ASCE, Vol. 110, No. 6, June, 1984, pp. 985-997.

Stellenbosch University http://scholar.sun.ac.za

160. Trott, J. J., Fox, E. N., "Comparison of the Behaviour of Concrete Beams under Static and Dynamic Loading," Magazine of Concrete Research, Vol. 11, No. 31, March, 1959,, pp 15-24.

161. Uchida, T., Tsubota, H., Yamada, T., "Experimental Investigations on Reinforced Concrete Slabs Subjected to Impact Loading," Transactions of the 8 th International Conference on Structural Mechanics in Reactor Technology (SMIRT)," Aug. 19-23. 1985, Brussels, Belgium, Paper J5/1, pp 173-178.

162. Van Breugel, K., "Concrete and the Economy of Hazard Protection," The First International Conference on Concrete For Hazard Protection, The Concrete Society, Edinburgh, 27-30 September 1987, pp.3-14.

163. Van Mier, J. G. M., "Fracture of Concrete under Complex Stress," Heron, Vol.31, No.3, 1986.

164. Vecchio, F. J., "Nonlinear Analysis of Reinforced Concrete Frames Subjected to Thermal and Mechanical Loads," ACI Structural Journal, Title no.84-s51, pp.492-501, Nov.-Dec. 1987.

165. Vecchio, F. J., Collins, M. P., "Predicting the Response of Reinforced Concrete Beams Subjected to Shear Using Modified Compression Field Theory," ACI Structural Journal, Title no.85-S27, pp.258-268, May-June 1988.

166. Vecchio, F. J., Collins, M. P., "The Modified Compression-Field Theory for Reinforced Concrete Elements subjected to Shear," ACI Structural Journal, Title no.83-22, pp.219-231, March-April 1986.

167. Vecchio, F., Collins, M. P., "The Response of Reinforced Concrete to In-Plane Shear and Normal Stresses," University of Toronto, Department of Civil Engineering, Publication N 82 03, March 1982.

Stellenbosch University http://scholar.sun.ac.za

THE BEHAVIOUR OF REINFORCED CONCRETE CANTILEVER COLUMNS UNDER LATERAL IMPACT LOAD

by

Matthys Johannes Loedolff

VOLUME 2

University of Stellenbosch

September 1989

Stellenbosch University http://scholar.sun.ac.za

CONTENTS

Stellenbosch University http://scholar.sun.ac.za

Stellenbosch University http://scholar.sun.ac.za

Stellenbosch University http://scholar.sun.ac.za

APPENDIX B: EXPERIMENTAL INVESTIGATION

Forty cantilever columns were tested. Of these forty tests, ten columns were loaded statically to failure by increasing the horizontal load, while the other thirty columns were subjected to an impact load. If failure did not occur during the impact an increasing static load was applied until failure occurred.

B.1 Test arrangement

The arrangement used for the impact tests on the columns is shown in figures (B.1), (B.2), (B.3) and (B.4). The impactor or striker was a pendulum type of striker suspended from a frame which was cantilevered from two upper floors of the laboratory. The impactor or striker was hoisted into the required position by a cable which ran through a system of pulleys and then pulled by a ten ton overhead crane. The striker was released by a specially designed release mechanism to ensure that the striker swung as smoothly as possible. The striker was fitted with a specially designed load plate to measured the impact load history (See figures B.10 and B.13). A buffer consisting of a configuration of pipes was provided to simulate the typical crumpling action of a vehicle have when it would crash head on into a relatively rigid barrier.

The cantilever column was clamped into a steel frame acting as a footing, which was designed to be very rigid to minimize deformation of the footing during the impact and thus to ensure measurements as accurate as possible. The column was also prevented to rotate inside the steel footing and prevented to be forced through the steel footing by the axial load on top of the column. The steel footing was fixed to the floor in such a way that the tension and compression forces under the footing could be measured by four specially designed load cells.

Stellenbosch University http://scholar.sun.ac.za

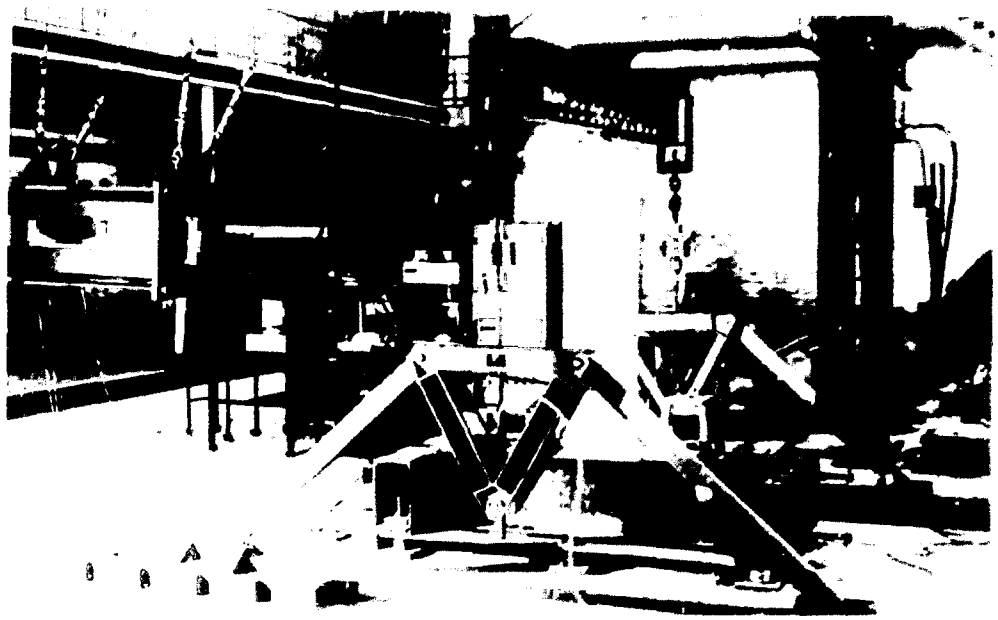

Figure B.1: Arrangement for the impact test on the cantilever column. Note the striker, axial load beam, sway frames, steel footing and the instrumentation in the back ground.

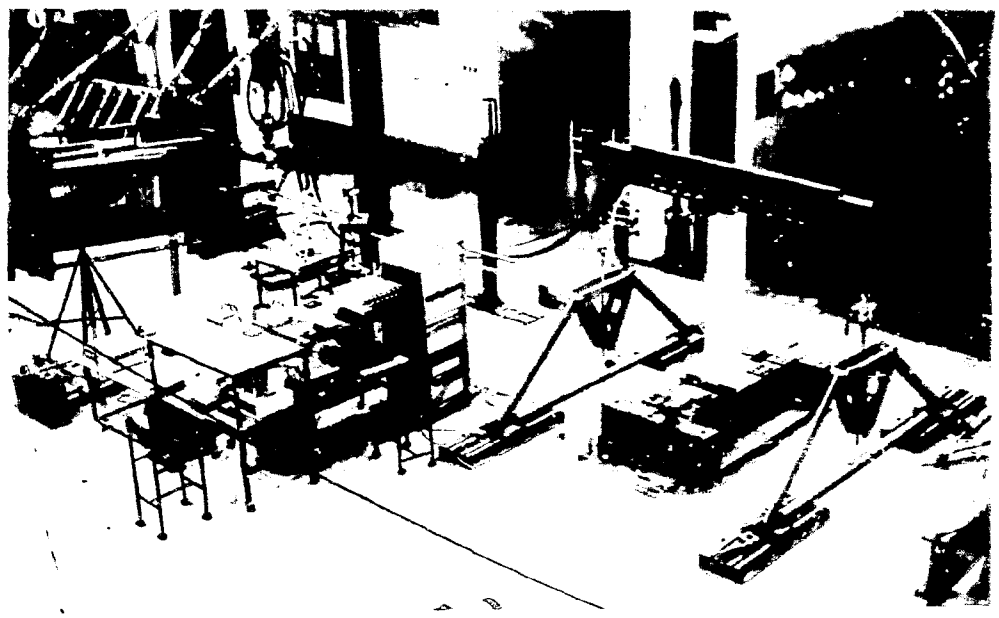

Figure B.2: The arrangement seen from above

Stellenbosch University http://scholar.sun.ac.za

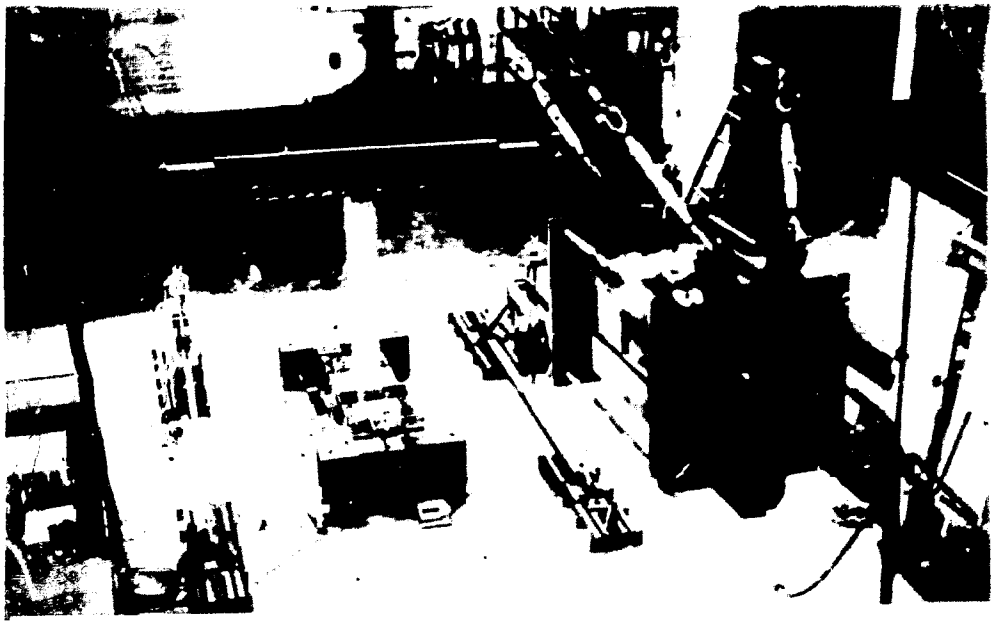

Figure B.3: The arrangement seen from the striker's side.

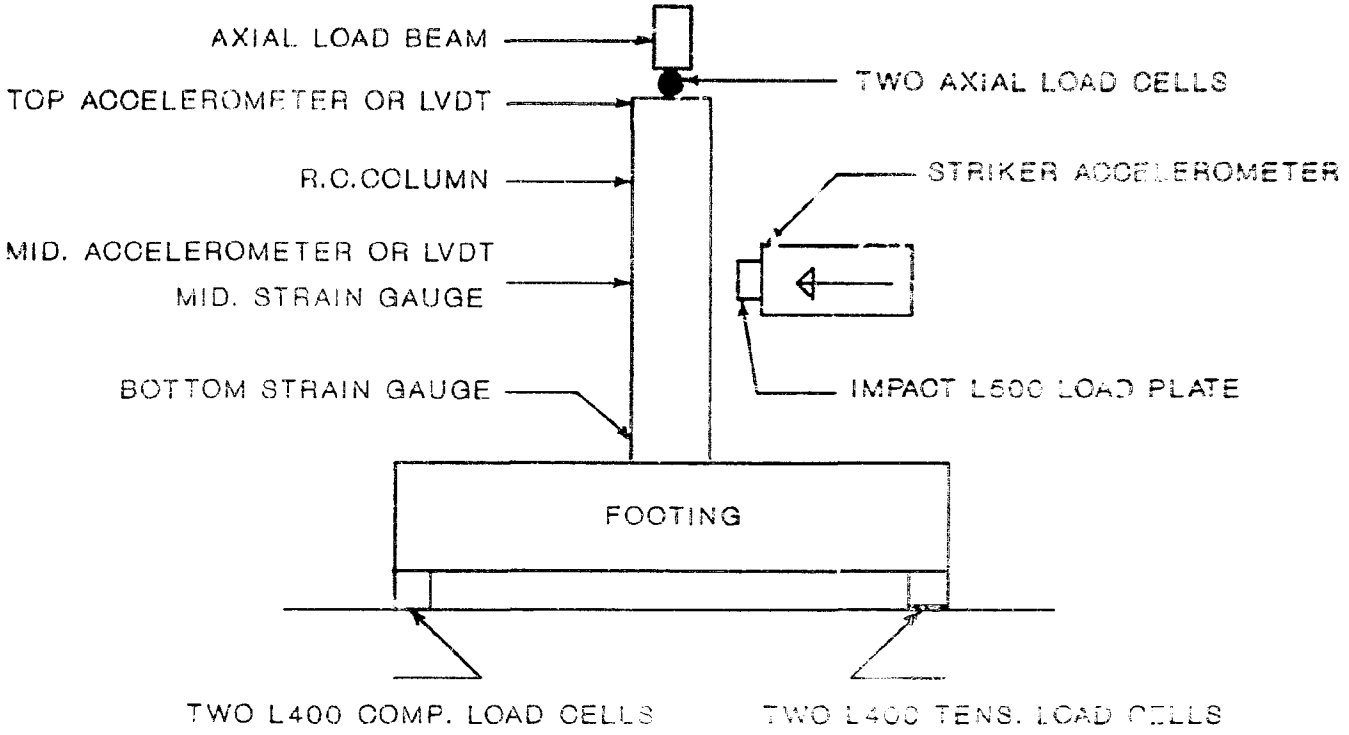

Figure B.4: Test arrangement with the measuring stations.

Stellenbosch University http://scholar.sun.ac.za

An axial load was applied to the column through a load beam fixed to two sway frames (see figure B.6). A hinge between the load beam and the column was provided to prevent any transfer of moment from the load beam to the column. The purpose of the sway frames was to apply the axial load on the column and to allow this axial load to move laterally with the column without changing in magnitude. In other words, if the axial load did increase or decrease it was not due to the movement of the sway frames but due to axial strains in the column.

For the static test a horizontal load was applied by a jack to the column at the point of impact loading. The arrangement for the static test is shown in figure (B.5).

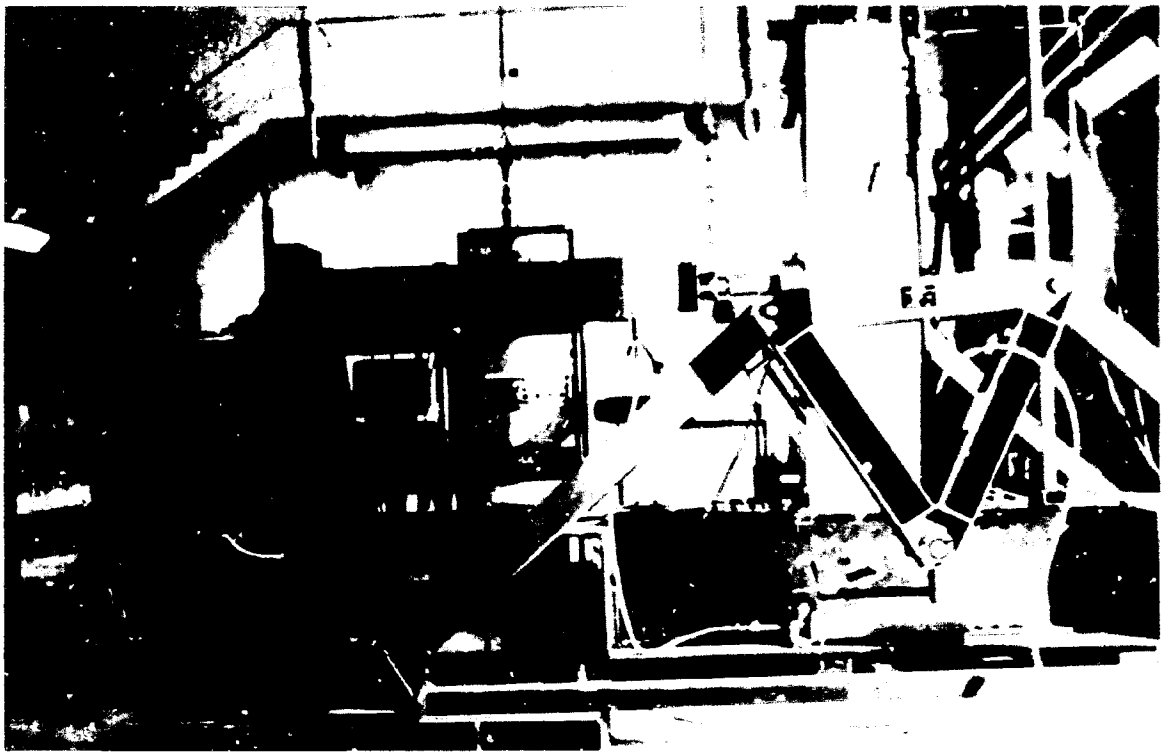

Figure B.5: Arrangement for the static test on the columns

Stellenbosch University http://scholar.sun.ac.za

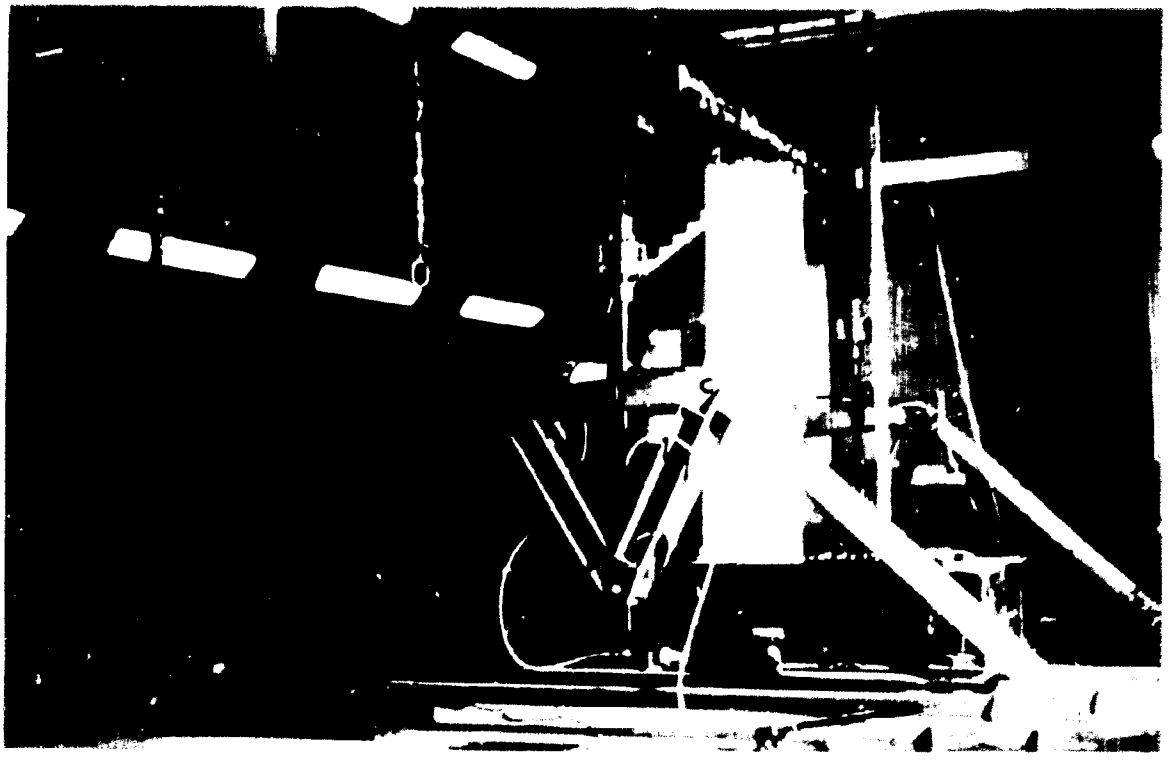

Figure B.6: Arrangement for the static test – showing the axial load beam and the LVDT's.

B.2 Apparatus and their design

B.2.1 Cantilevered frame

The four cables from which the striker was hanging were fixed through four rod end bearings to a three dimensional frame cantilevered from two upper balconies of the laboratory. Figure B.7 is a diagrammatic presentation of the cantilevered frame. The structure was designed to withstand a maximum of 20 kN per cable, in other words an 80 kN downwards load on the structure with an acceptable safety factor.

Stellenbosch University http://scholar.sun.ac.za

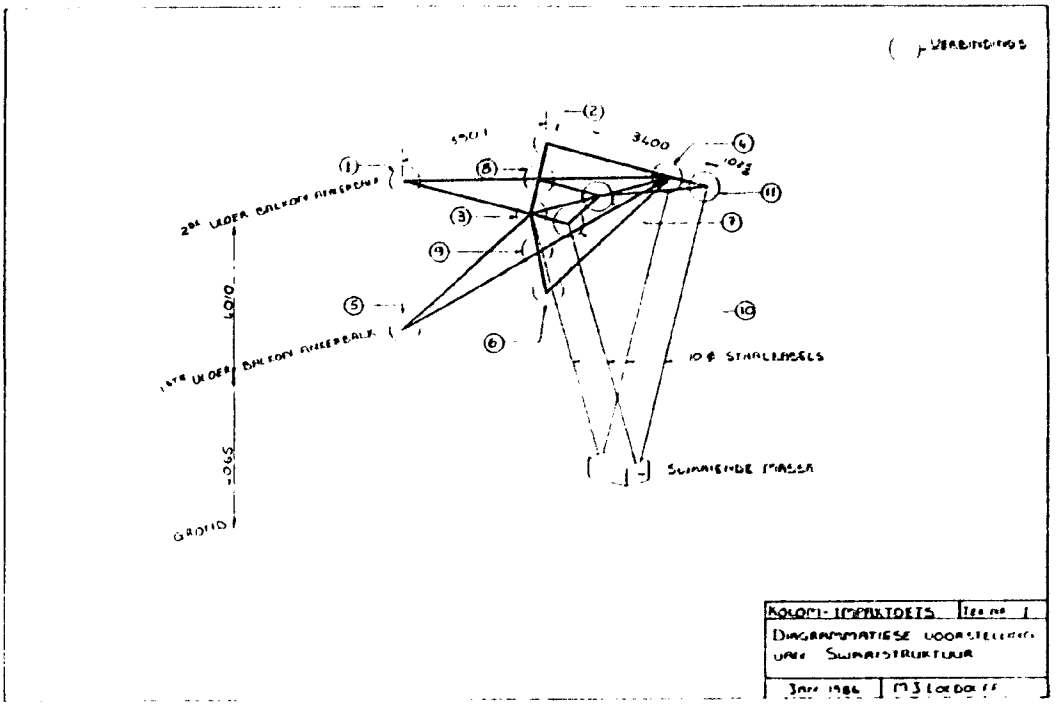

Figure B.7: Diagrammatic representation of the three dimensional cantilevered frame.

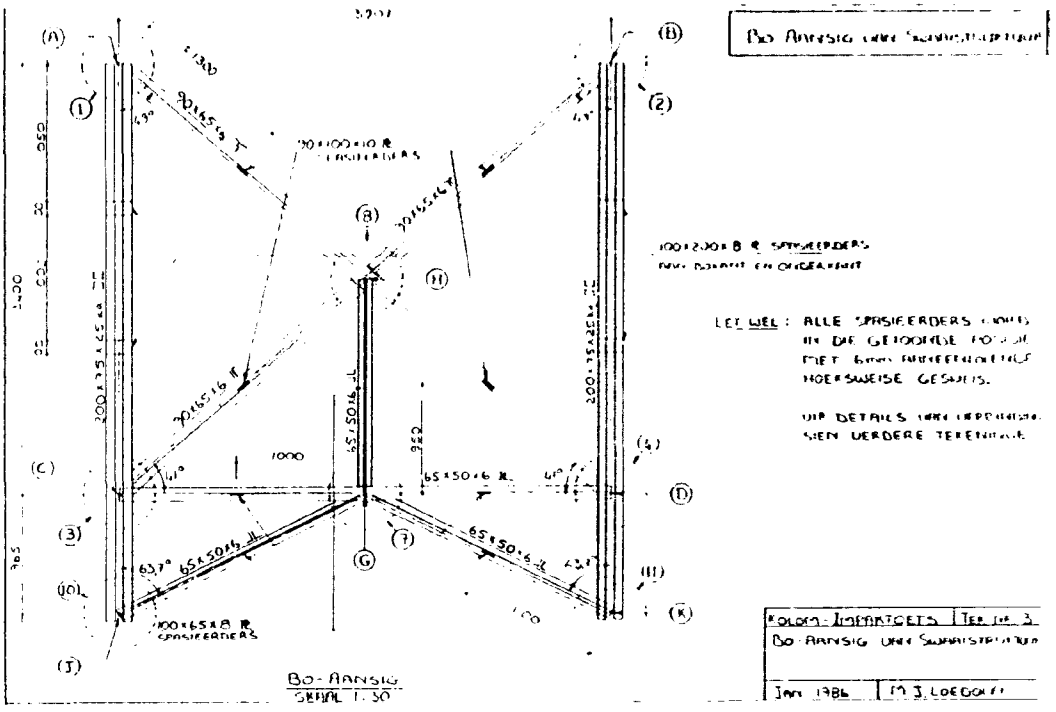

Figure B.8: Top elevation of the cantilevered frame.

Stellenbosch University http://scholar.sun.ac.za

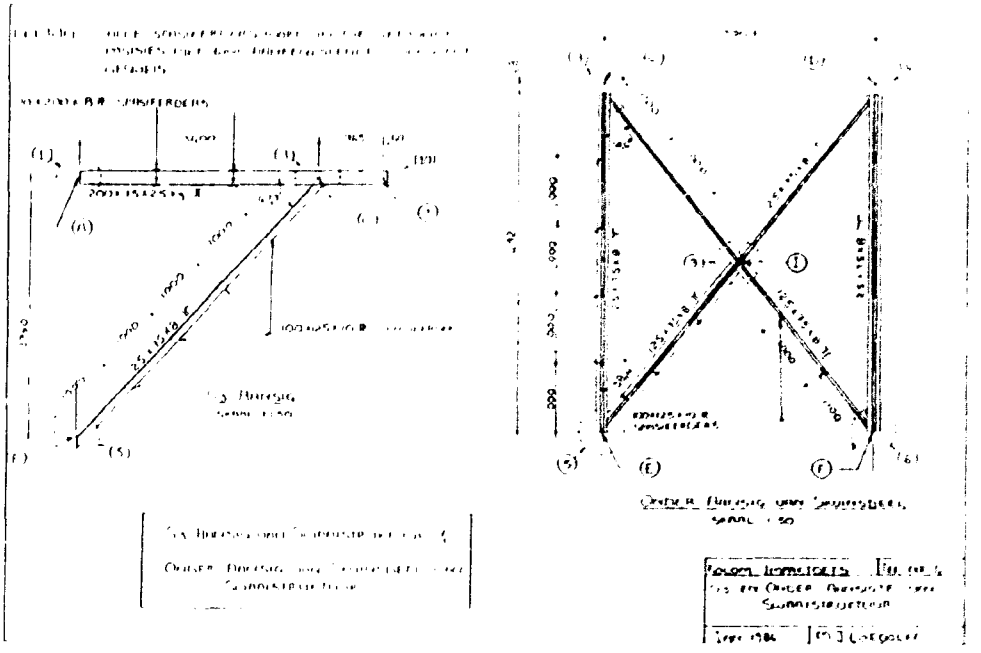

Figure B.9: Side and bottom elevation of cantilevered frame.

With this maximum load the deflection of the furthest cantilever point had to be a minimum and the structure had to be stable enough to ensure a smooth run by the impactor or striker. In other words, the structure was designed to withstand vibrations and excessive deflections when the striker was released. This three dimensional structure was fixed to the top balcony by 8 M20 bolts and to the first floor by 8 M16 bolts.

Although the construction and installation of this structure was difficult, it was very stable during the tests and thus ensured smooth runs by the striker.

Stellenbosch University http://scholar.sun.ac.za

B.2.2 Striker or Impactor

The striker (figure B.10) consisted of a cradle like structure fitted with a buffer system, a load plate and a release mechanism. The cradle was designed to carry the striker mass in the form of lead slabs. The mass of the striker could be changed by changing the number of lead slabs in the cradle. The mass of each lead slabs was exactly 100 kg. The mass of the cradle only, plus the load plate and buffer system was 450 kg. The total mass was varied from 650 kg to 1450 kg during the experiments.

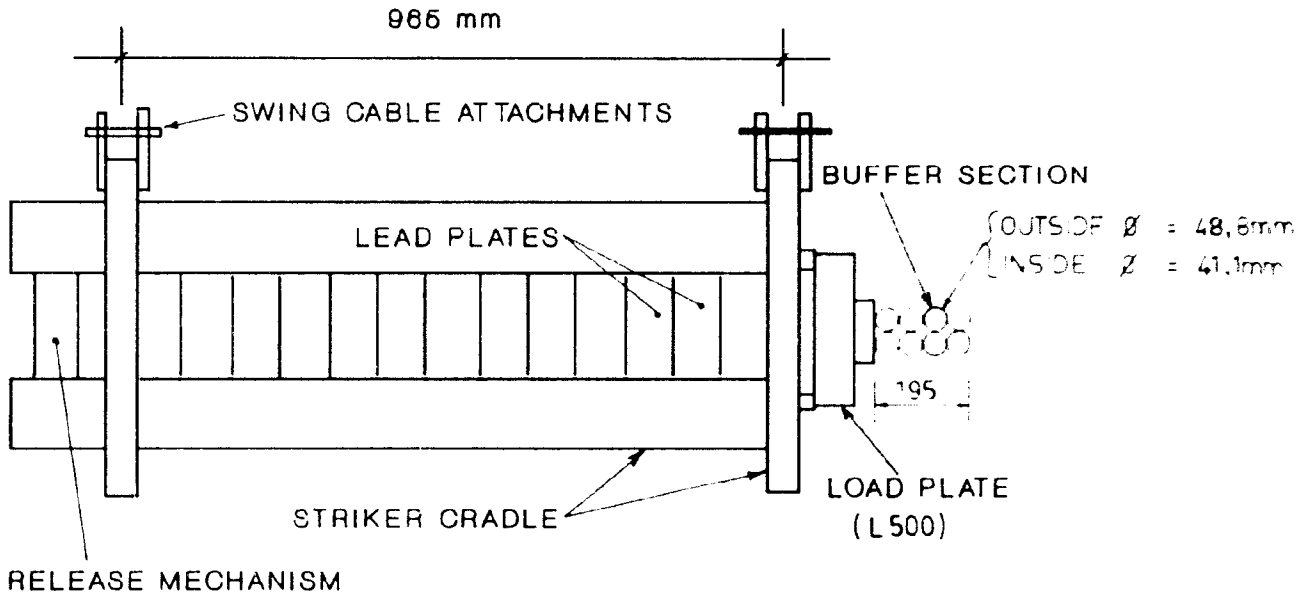

Figure B.10: The striker system. (schematic representation)

The design of the load plate, measuring the load history during the impact, will be discussed under instrumentation.

B.2.2.1 The buffer system.

An eight pipe buffer system was used for all the tests except for the first three tests when a seven pipe system was used. This buffer system was used to create the desired impact load history.

Stellenbosch University http://scholar.sun.ac.za

This buffer also simulates the energy absorption capabilities of the vehicle.

Reference (146) discusses this impact load history for vehicles. As can be expected, the crushing strength of the vehicle has a significant influence on the resulting impact force on the column. Reference (146) indicates a duration time for the impact of somewhere between 40ms to 100ms. This values correspond very well with the test results of this investigation where the duration time was 50 to 60ms. Reference (146) also mentions that the automobile impact problem is very similar to that of an aircraft and that the same theoretical formulation (Riera formula) can be used for both.

The design of the buffer section is discussed in detail in Appendix C. In figure B.11 the permanent deformation or deflection of the buffer system is plotted against the maximum measured impact load. This graph can be used to find the K-factor of the Hertz contact law as referred to in Chapter 5.

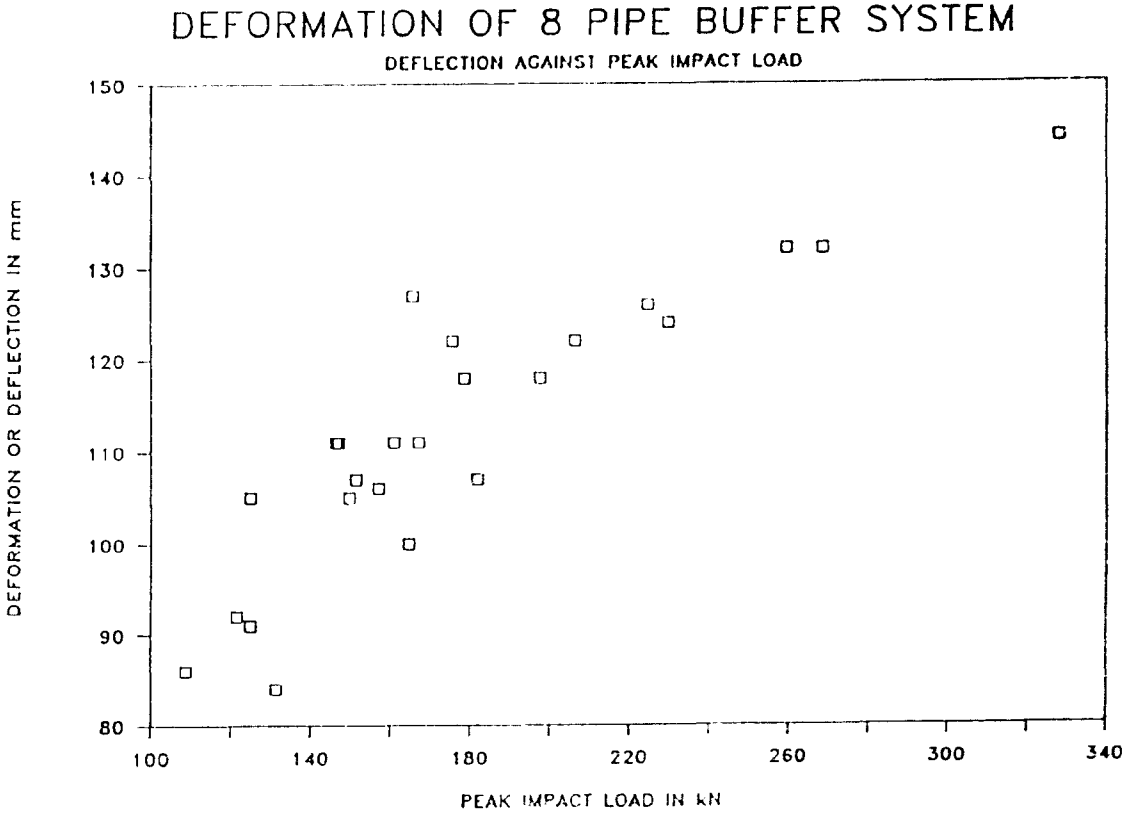

Figure B.11: Permanent deformation of buffer system.

Stellenbosch University http://scholar.sun.ac.za

B.2.2.2 The release mechanism

The release mechanism was designed to release the striker without disturbing its motion and thus improving the control of its movement. A number of mechanisms were considered. Even a nylon rope to be cut through were considered. The main characteristic of this release mechanism was to ensure a sudden release without disturbing the flow of the striker movement. The mechanism used was a lever system with a sliding release which was pulled out to release the striker.

B.2.2.3 Hoisting system of striker

The striker was hoisted into position by a cable running over two pulleys and then fixed to an overhead crane. The falling height of the striker could be changed by changing the height of one of the pulleys. With this series of tests the falling height was kept constant at a height of 2,7m and thus the impact velocity was more or less constant as well.

B.2.3 Axial load system

An axial load was introduced to the column through a loading beam (shown in figures B.1 - B.3) connected to two sway frames. Between the loading beam and each sway frame was a chain and a HBM U2 20 ton load cell. The chain was to ensure that no moment could be transferred from the sway frames to the load beam and vice versa. The load cells was used to monitor the axial load on the column before, during and after the impact. By means of a Enerpac RCH-202T jack fixed to each sway frame, an axial load could be introduced to the column through the connection between the sway frame and the loading beam.

Stellenbosch University http://scholar.sun.ac.za

Between the loading beam and the column a hinge was provided to prevent a moment transfer from the loading beam to the column. A shear force could be transferred from the beam to the column, otherwise the loading beam would have fallen from the column during the impact due to its inertia.

B.2.4 Steel footing.

The steel footing is shown in figure B.12 as well as in figures B.1 - B.3. The footing was designed to be very rigid to prevent distortion and thus increasing the accuracy of the forces measured under the footing. In other words, very little energy was dissipated by distortion of the footing and most of the energy was transferred to the laboratory floor. This energy transfer was then registered by means of the load cells under the footing.

The steel footing was stressed to the floor by four Dywidag bolts. which passed through the four load cells under the footing. On the compression side, the two load cells were above the laboratory floor (between the floor and the footing). On the tension side the two load cells were under the floor and the tension transferred to the floor was measured as a compression load by those two load cells. Additionally, provision was made to prevent sliding of the footing on the floor. Unfortunately this sliding force, or shear force, transferred to the floor could not be measured in this set-up.

The column was prevented to rotate inside the footing itself by four horizontal reinforcing bars casted into the column and extending from the column into the steel footing on both sides of the column. An additional steel channel profile was positioned over the footing of the reinforced concrete column and bolted to the steel footing. After the column was positioned inside the footing, the remaining openings between the reinforced concrete column footing and the steel footing was filled up by pumping a cement pump grout into these cavities.

Stellenbosch University http://scholar.sun.ac.za

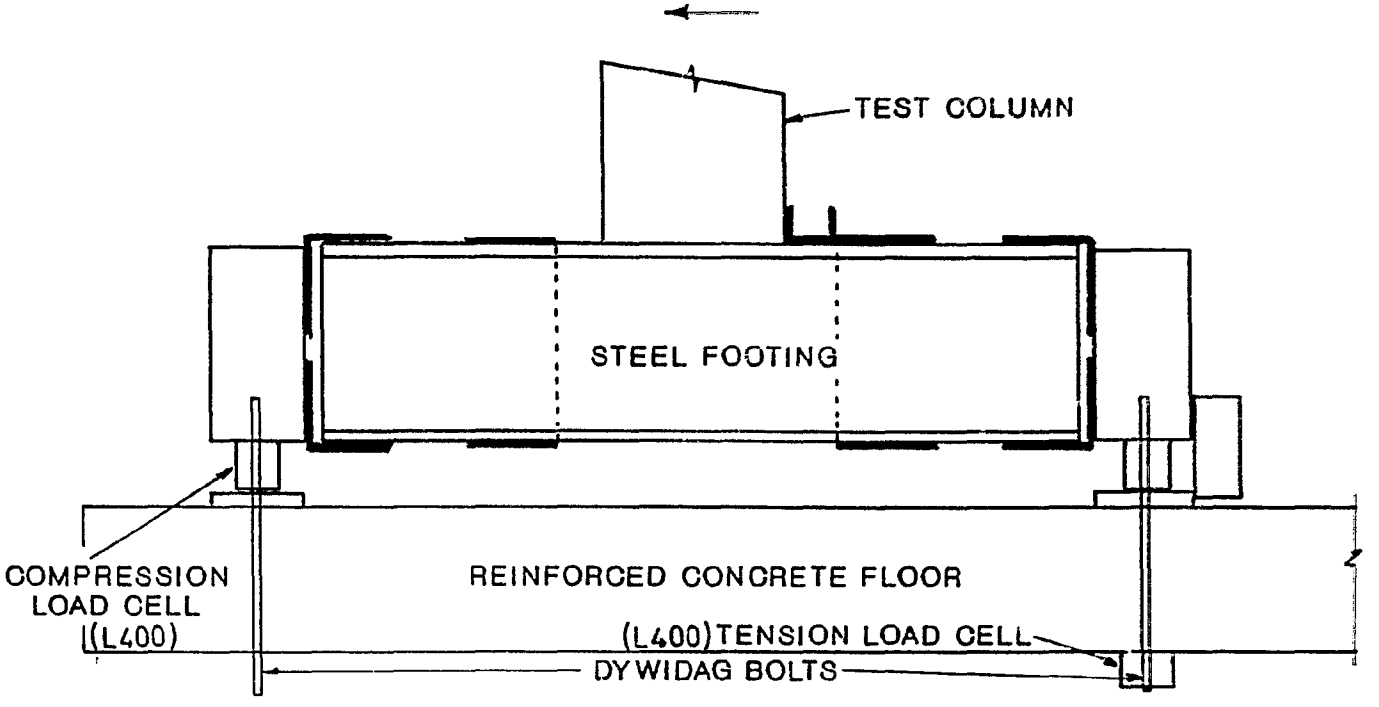

Figure B.12: Steel footing of reinforced concrete column.

B.2.5 Strutframe for static test.

This strutframe was designed to apply a static horizontal load to the column for the static test phase of the column. The strutframe was designed to develop minimum rotations and deflections during the test in order to keep a constant horizontal load on the column for each applied load step. For the design, the prop system was analyzed by the computer program STRUDL.

A Enerpac RCH-606 jack was fixed to the strutframe through which the horizontal load was applied to the column. Between the jack and the column a HBM C2 load cell was inserted to monitor the horizontal load applied to the column.

The strutframe was fixed to the laboratory floor with four Dywidag bolts. The strutframe is shown in figure B.5.

Stellenbosch University http://scholar.sun.ac.za

B.3 Instrumentation

The following phenomena and variables were monitored during the dynamic impact phase of a test on a column:

1. The impact load history was monitored with a L500 Load Plate (figure B.13) fixed to the striker behind the buffer of the striker.

2. The deceleration of the striker was monitored with a HBM B12/500 accelerometer.

3. The impact velocity of the striker was measured with a specially designed instrument and a Hewlett-Packard Model 5315A universal counter (refer to paragraph B.3.3).

4. The axial load on the column was regidtered by two HBM U2 20 ton load cells fixed between the load beam and the two sway frames.

5. The acceleration of the column at two separate positions. Position 1 was 600 mm and position 2, 1550 mm from the bottom of the column. Both accelerometers were HBM B12/2000 accelerometers although for the first few columns one of the accelerometers was a Kyowa product.

6. The strain on the back side of the column was measured at two positions as well. Two Kyowa (type KC-120-A1-11) concrete strain gauges of length 120mm were used. Position 1 was 690 - 810 mm and position 2, 100 - 220 mm from the bottom of the column. In other words, position 1 was directly behind the impact zone of the striker and position 2 was as close to the bottom of the column as possible but still high enough to ensure that this strain gauge was not damaged during the early stages of the impact.

Stellenbosch University http://scholar.sun.ac.za

7. The compression and tension loads transferred from the footing to the floor wer measured with four L400 Load cells. Two of the load cells monitored the compression load transferred to the footing, while the other two load cells monitored the tension loads transferred to the floor. The load cells were situated 920mm from the center of the column in the direction of impact.

During the static test of a column the axial load, the foot load cells and the strain gauges were monitored as during the impact test. Additionally the following variables were monitored as well:

1. The deflection of the column at two positions with two HBM W100 LVDT's. Position 1 was 600 mm and position 2, 1550 mm from the bottom of the column.

2. The horizontal static load was measured with a HBM C2 50 ton load cell. This load was applied horizontally to the column 740mm from the bottom of the column.

B.3.1 The L500 load plate

The L500 load plate was specially designed and then calibrated to measure and monitor the impact load history. The load plate is shown in figure B.13. On the back of the steel plate four 120 ohm 5mm strain gauges were fixed to the steel plate in a full bridge setting. The bolts fastening the load plate to the striker were torqued to a specified 5fp (Imperial units) torque. This was to ensure that the rigidity of the two supports was the same as that during the calibration of the load plate. The load plate was 65mm thick to keep the maximum stress well below the yield stress of the steel to ensure continuous accurate recordings of the impact load histories.

Stellenbosch University http://scholar.sun.ac.za

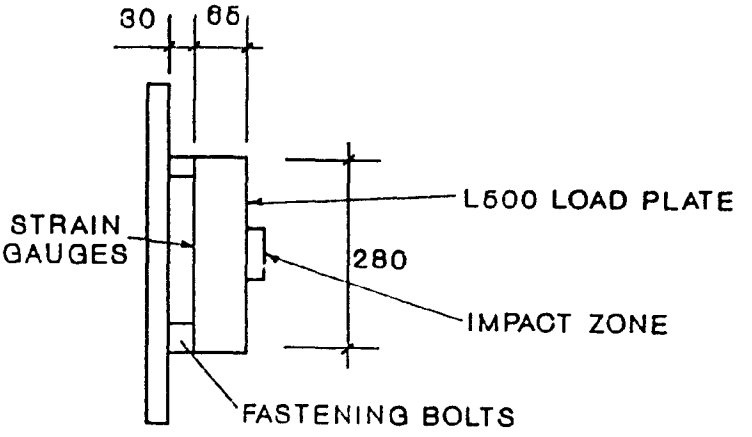

Figure B.13: The L500 load plate

The strain gauges on the back of the load plate measured the strain in the steel in two directions and these readings were converted to the actual applied load by means of a formula built into the computer program which monitored all the readings during the impact test. The load plate was calibrated through a HBM C2 50 ton load cell to a maximum of 500kN. A fourth order equation (equation B.1) was used to describe the curve. Figure B.14 shows the curve fitted to the measured data points.

$$y = 0,35134x + 7,6547.10^{-4}x^2 - 5,3508.10^{-7}x^3 + 1,25782.10^{-10}x^4 \qquad (B.1)$$

After the calibration was done, a dynamic test was performed on the load plate to establish the accuracy of the load plate readings compared to the readings of a HBM C2 load cell. The results of this dynamic test is given in figure B.15. As can be seen the results are acceptable. The graph shows that the C2 load cell reached a maximum of 500 kN and then it stayed constant because higher readings for this load cell were ignored by the computer.

Stellenbosch University http://scholar.sun.ac.za

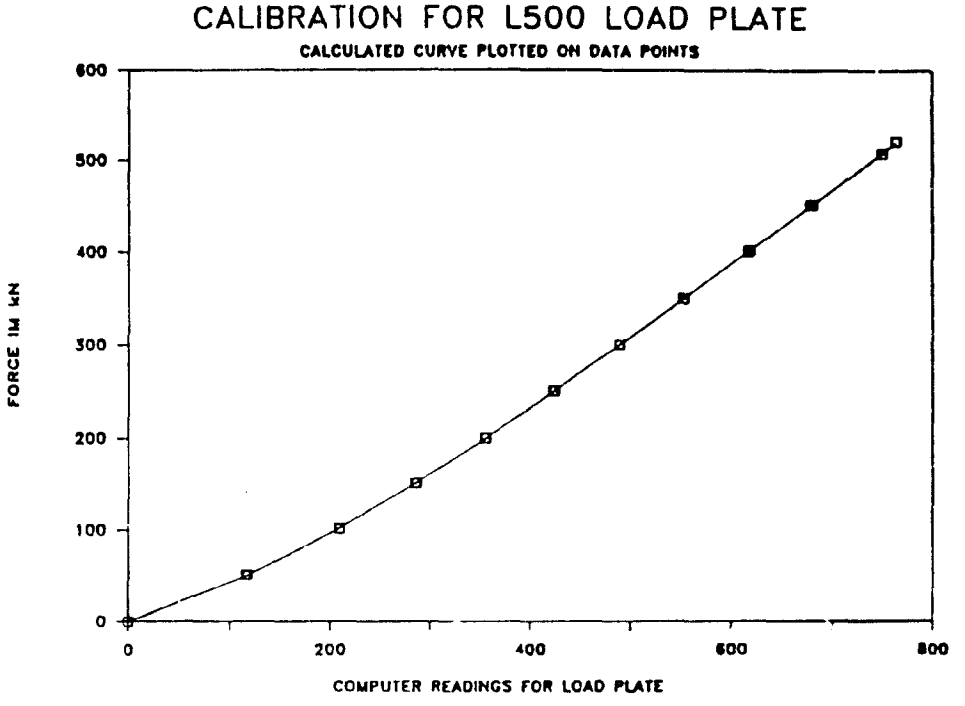

Figure B.14: Calibration curve fitted to the data points.

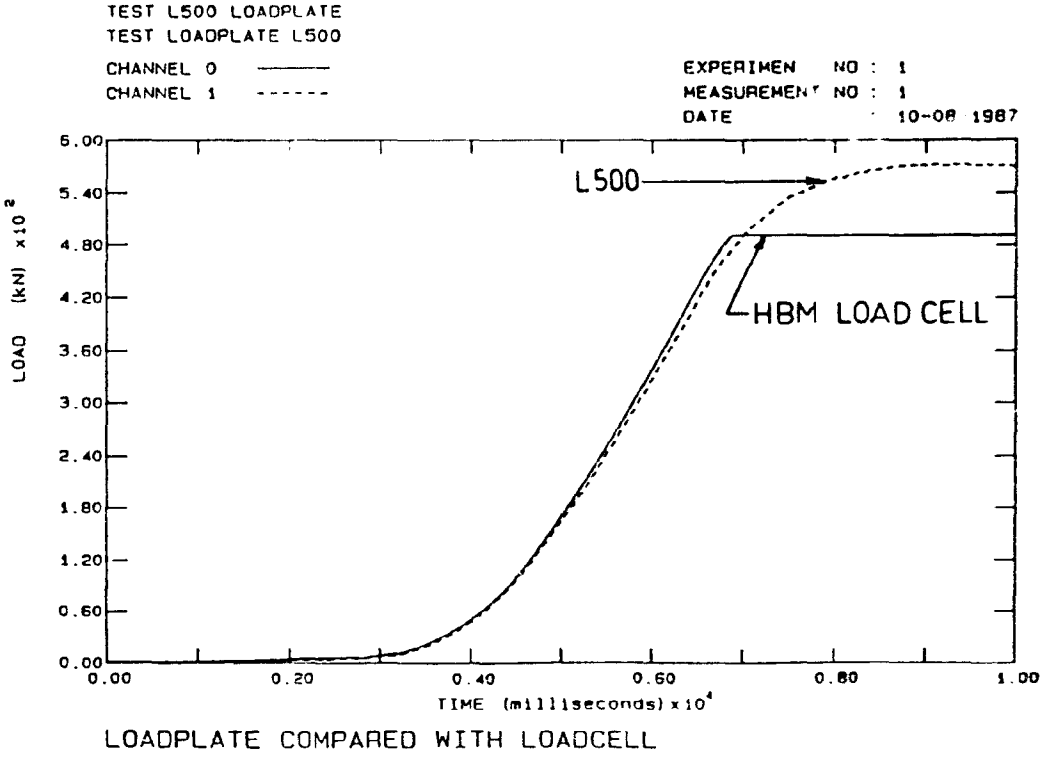

Figure B.15: Dynamic test of L500 load plate compared with a HBM C2 Load cell.

Stellenbosch University http://scholar.sun.ac.za

B.3.2 L400 footing load cells

The L400 compression load cell was specially designed to measure the forces transferred from the footing to the laboratory floor. On the compression side of the footing, the load cells were placed between the footing and the floor, while on the tension side the load cells were placed below the floor (see figure B.12). The maximum design load for these load cells was 400 kN to prevent excessive distortion and flow of the steel and thus to ensure constant accurate readings during the tests. To allow for possible tension forces to be measured by the load cells (which might occur during the vibration of the column during the dynamic tests), each load cell was pre-compressed, by means of the Dywidag bolts, to 50 kN. By the pre-compression a tension load will be measured by a release in the pre-compression and will be registered by the computer as a negative or tension load.

The L400 load cell consisted of a solid steel cylinder with a hole in the middle to allow for the Dywidag bolts passing through them. On the outside of this steel cylinder four 120 ohm 5mm strain gauges were fixed in a full bridge setting. These strain gauges measured the strains exerted on the cylinder and were then converted to the actual load by formulae in the computer program used to measure and monitor the loads.

Once again the L400 load cells (numbered as numbers 2, 3, 5 and 6) were calibrated against a HBM C2 load cell. Again a forth order equation was fitted to the data points to be programmed into the computer. Although each of the four load cells had a different equation, it was decided to use only one of them for all four L400 load cells. After the calibration and the programming of the computer with the curve fitting formula, the load cells were tested dynamically. The test results of the four L400 load cells is shown in figures B.16 to B.19. From these four graphs it is clear that the results were acceptable up to 400 kN which was the ultimate design value for these load cells.

Stellenbosch University http://scholar.sun.ac.za

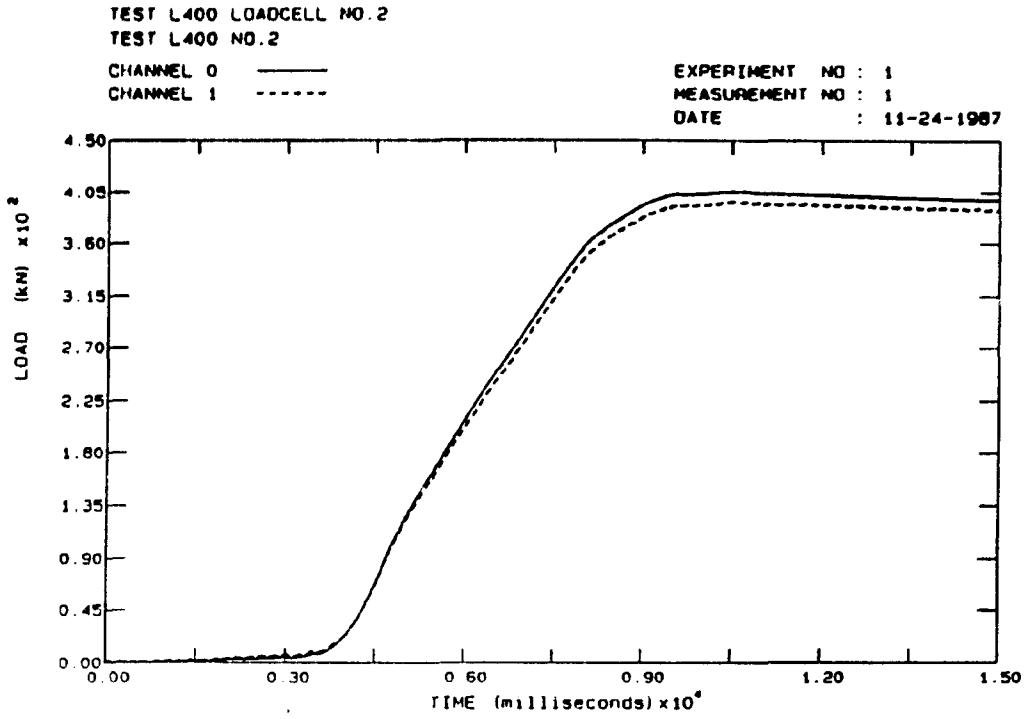

Figure B.16: Test results of load cell L400 No.2.

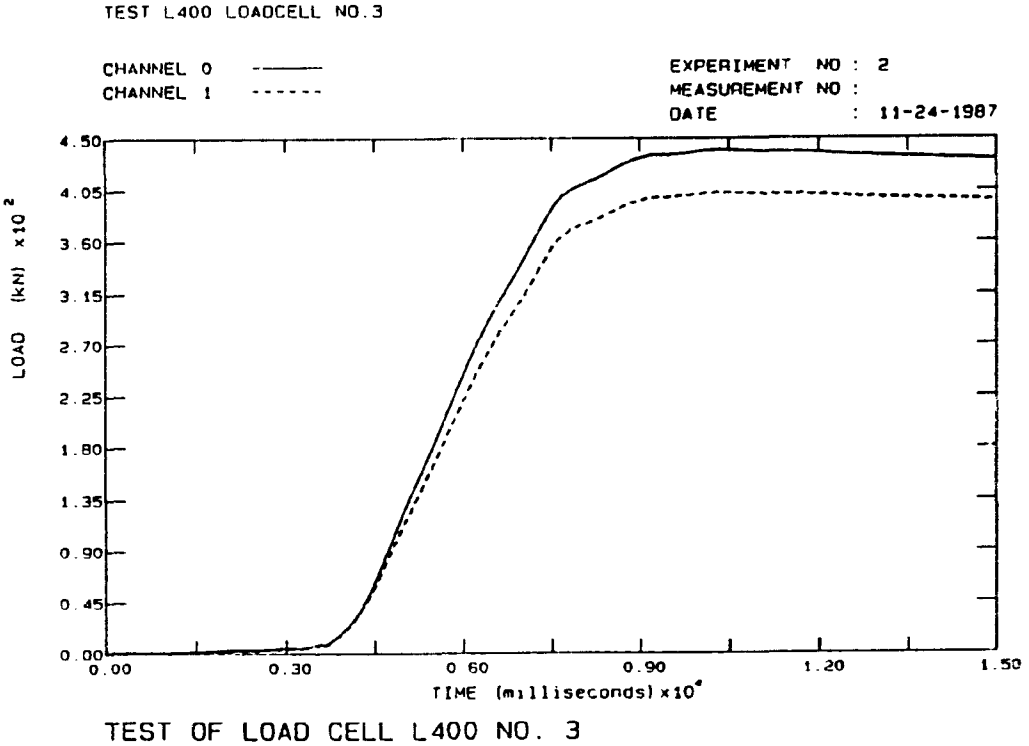

Figure B.17: Test results of load cell L400 No.3.

Stellenbosch University http://scholar.sun.ac.za

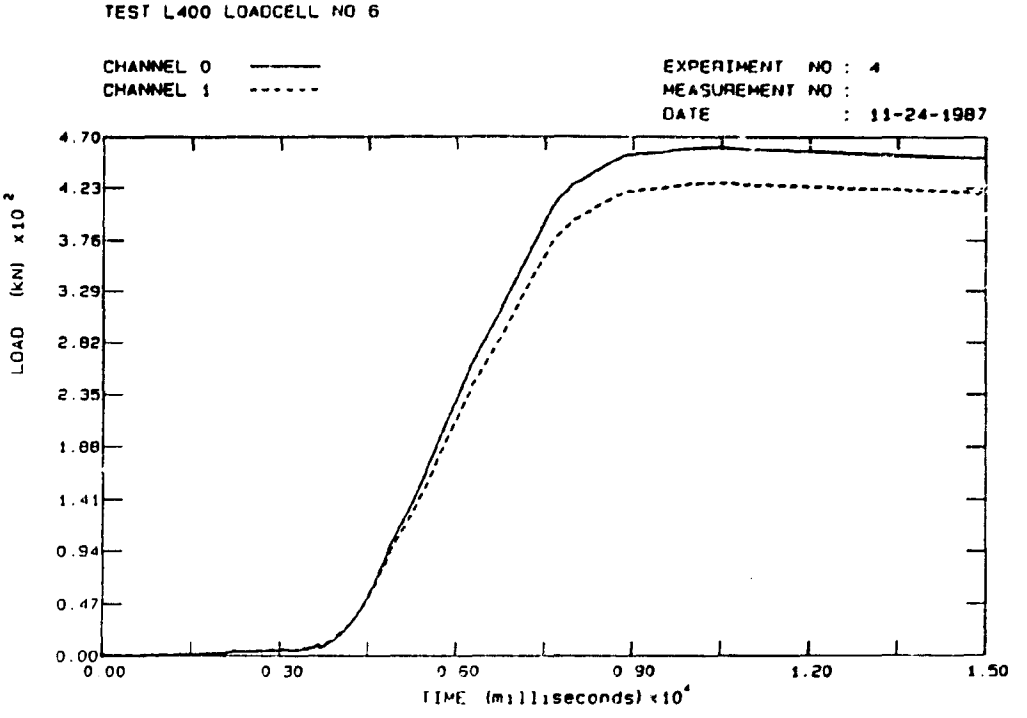

TEST OF LOAD CELL L400 NO. 6

Figure B.18: Test results of load cell L400 No.6.

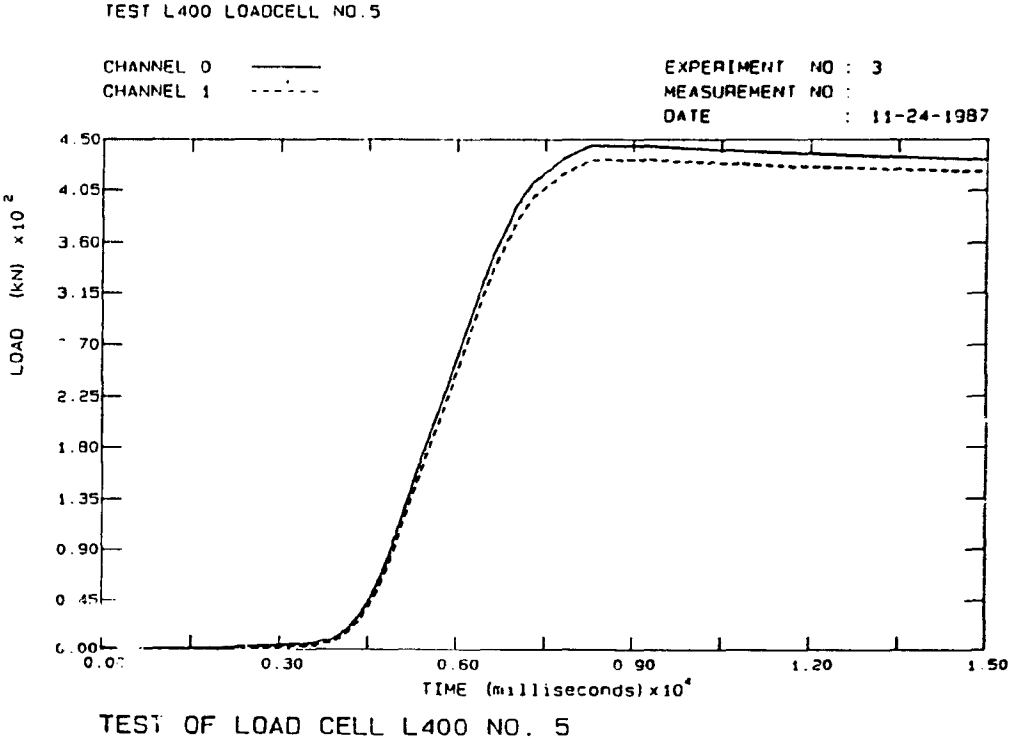

TEST OF LOAD CELL L400 NO. 5

Figure B.19: Test results of load cell L400 No.5.

Stellenbosch University http://scholar.sun.ac.za

B.3.3 Velocity measuring instrument

This velocity measuring instrument was also specially designed and built to measure the velocity of the striker just before impact, that is, the impact velocity. This instrument consisted of two sets of small photocells at a fixed distance from each other and a Hewlett-Packard universal counter. The two sets of photocells were exactly 100 mm from each other. When the striker passed the first set of photocells, the universal counter was triggered and when the striker passed the second set of photocells the counter was stopped. The universal counter then gave the time elapsed from the trigger of the system until it stopped. Dividing the distance (100 mm) by the elapsed time gave the velocity of the striker.

B.3.4 The concrete strain gauges

Two concrete strain gauges, Kyowa type no. KC-120-A1-11, of 120 mm length were used on each column. Both strain gauges were fixed to the back of the column to measure mainly the anticipated compression strains of the concrete. Concrete strain gauges are not effective in zones where tension strain is observed because the concrete cracks which normally results in the destruction of the strain gauge. For this reason, all the strain gauges were used on the back of the column. The first strain gauge was positioned directly behind the impact zone on the column in other words 690 - 810 mm from the bottom of the column. The second strain gauge was position as close to the bottom as possible but still high enough not to be damaged by the local cracking that was anticipated at the connection between the footing of the column and the column itself. This strain gauge was positioned 100 - 220 mm from the bottom of the column.

Stellenbosch University http://scholar.sun.ac.za

B.3.5 The axial load cells

Two HBM U2 20 ton load cells were used to measure and monitor the axial load on the column. These load cells did not only register the initially applied load but also registered the variation of the axial load during the impact test. The summation of the registered values of the two load cells gave the total axial load on the column.

B.3.6 The accelerometers

Three accelerometers were used during the impact test. One accelerometer, a HBM B12/500 accelerometer, was situated on the striker and registered the deceleration of the striker. The natural frequency of this accelerometer is 500 Hz and its nominal acceleration is 100 m/s^2.

The other two accelerometers were two HBM B12/2000 accelerometers and they were positioned on the column itself. The one was 600 mm and the other one 1550 mm from the bottom of the column. For the first few tests a Kyowa accelerometer was used, instead of one of the HBM accelerometers, in the position 600 mm from the bottom. This Kyowa's positive direction was the opposite of the HBM's and this can be seen in the results of the first few tests. The natural frequency of the B12/2000 accelerometer is 2000 Hz and its nominal acceleration is 2500 m/s^2.

B.3.7 The deflection meters.

During the static tests the accelerometers were changed for two HBM W100 LVDT's. Their positions on the column were exactly the same as that of the accelerometers, in other words, 600 mm and 1550 mm from the bottom of the column. The LVDT's were used to measure the deflection of the column. Unfortunately the LVDT's could not be used during the impact test because they could not

Stellenbosch University http://scholar.sun.ac.za

register the actual values fast enough. Howevere, under the static conditions these LVDT's performed excellent.

B.4 The amplifier and computer system (data acquisition system).

All the instruments were connected to two six channel HBM amplifiers. These amplifiers were connected to two Olivetti M24 micro computers. All the readings were then taken by these two Olivetti's and stored in their RAM memory during the impact test and transferred to floppy disks after the test. A trigger mechanism was used to trigger the two computers to begin their readings.

B.4.1 The trigger mechanism.

A trigger mechanism was necessary to start the readings by the Olivetti's as only a limited number of readings could be taken during a specific run. The total run for all the readings took only 0,186 seconds.

The trigger mechanism produced a steady 5 volt current monitored by the computer when it was in the ready state. When the striker passed a certain point, a micro switch was closed and this allowed a drop in the constant 5 volt produced by the trigger mechanism. This drop in the voltage of the trigger mechanism was registered by the computers and this then allowed the computers to start taking readings. In other words, the computers were brought into a ready state, waiting for the fall in the voltage from the trigger mechanism, before they began their readings.

Stellenbosch University http://scholar.sun.ac.za

B.4.2 The Amplifiers.

Two six channel HBM KWS 673.D8 amplifiers were used. The front panel of the amplifier is shown in figure B.20. All twelve measuring instruments were connected to the KWS 3073 amplifiers in the KWS 673 amplifier. The amplifiers were then connected to two micro computers. The amplifiers and computers set-up is shown in figures B.21 and B.22.

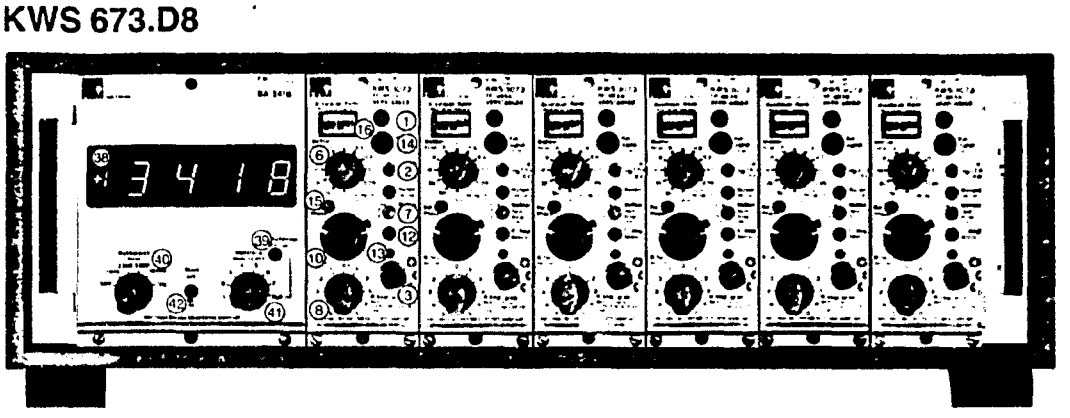

Figure B.20: Front panel of the HBM KWS 673.D8 Amplifier.

B.4.3 The micro computers.

During the impact test two Olivetti M24 micro computers were used to register all the readings during the impact and the static tests. The computers needed 50 microseconds for each reading. This meant that if six channels have to be read, a minimum of 300 microseconds were needed for each cycle. Twelve channels had to be read during an impact test. If only one computer was used it meant that at least 600 microseconds were needed for each cycle to read each channel only once. To minimize the cycle time, two microcomputers were used and each had six channels connected to it.

Stellenbosch University http://scholar.sun.ac.za

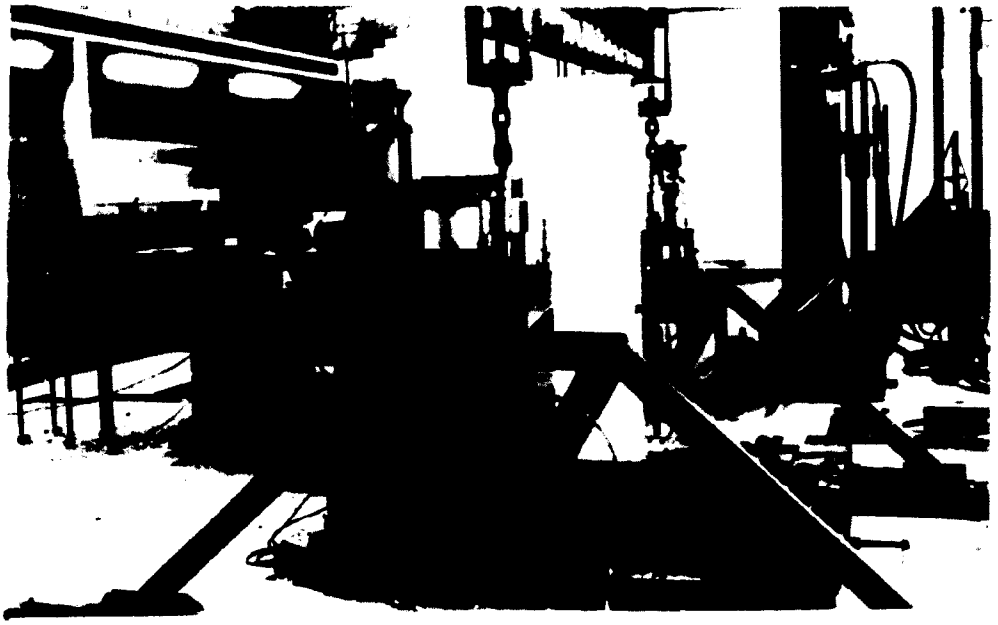

Figure B.21: The test column with the instrumentation in the back ground.

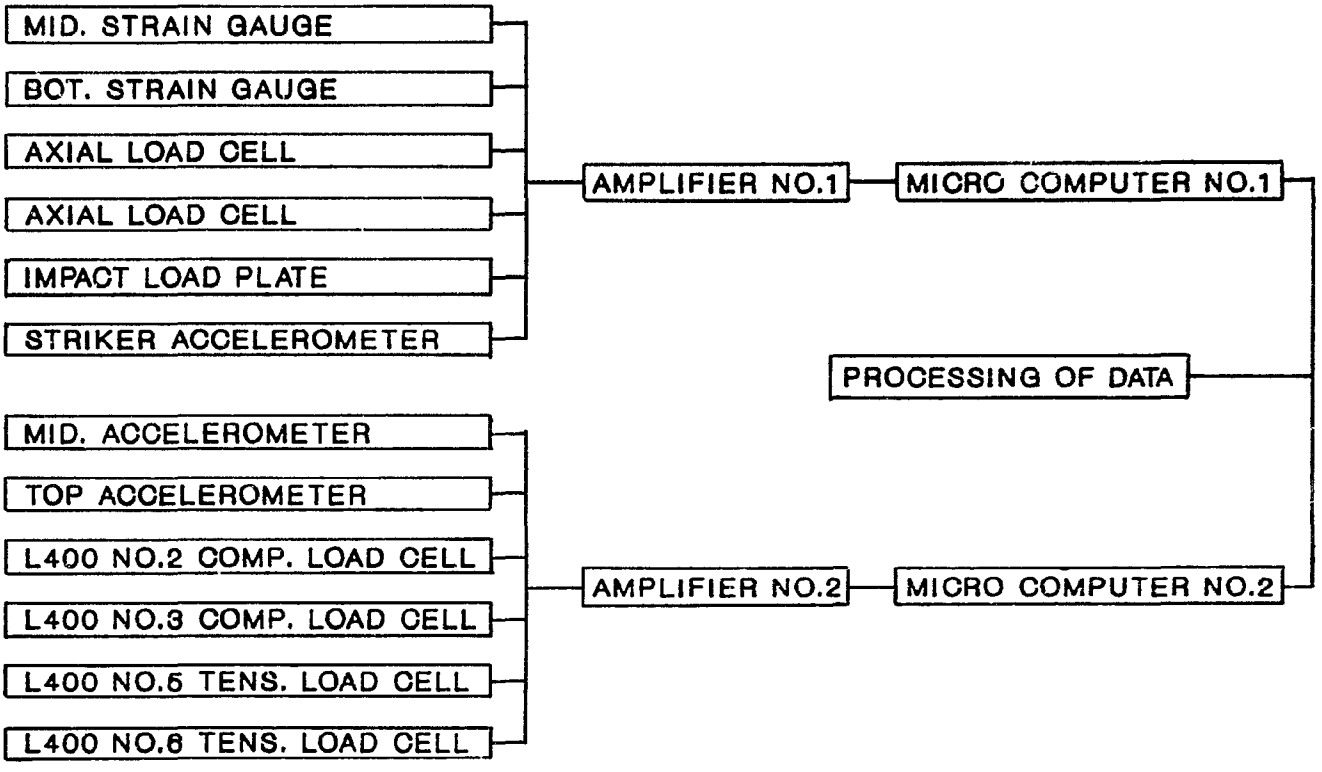

Figure B.22: A diagramatic presentation of the data acquisition system.

Stellenbosch University http://scholar.sun.ac.za

Each channel was read 600 times with a cycle time of 310 microseconds. In other words each computer took and registered 3600 readings within 186 milliseconds. This meant that a total of 7200 readings were taken and registered by the two computers in 0,186 seconds (in less than a fifth of a second).

The computers stored all the readings in its RAM memory during the test and afterwards it was transferred to floppy discs. The static tests set-up was exactly the same but with the static tests time was not a factor and by using a different computer program every reading was immediately stored on floppy discs.

B.4.4 Computer programs.

Existing computer programs (180) for data acquisition were used in these experiments. Minor modifications were introduced by the author. The computer program IMPACT was used for the dynamic impact tests on the columns. This program allows the user to specify the instruments to be used and there connection positions to the computer; for the noting of zero readings and for the specification of the cycle period and the number of cycles to be registered. Then it brings the computer into a ready state waiting for the trigger mechanism. As soon as the computer is triggered it will read the specified channels in succession every 50 microseconds. Having completed the specified cycle period it will return to the first channel and start a new cycle of readings. This will continue until the specified number of cycles are reached. During this process all the accumulated data is stored in the RAM memory of the computer to save time. After all the readings have been taken the data is transferred to floppy discs from where it can be processed further.

A second computer program, IMPLOT, was used to read the data files from the IMPACT-program and then plot the data on graphs.

Stellenbosch University http://scholar.sun.ac.za

For the static tests a program called COSTPAM was used. It differs from IMPACT in that time is not a factor and thus readings can be taken at any convenient time. In other words, during a static test the user can wait until the system has stabilized under a new load step for example, before the readings of the channels are recorded. The readings are then immediately stored on floppy discs before the next set of readings are taken.

B.5 Photography.

A photographic record of each column test (impact and static) was produced. These records consisted of video recordings as well as photos taken with a 35mm camera.

A special video camera with a very high shutter speed was used to record the impact part of the test. The high shutter speed was necessary to improve the quality of the pictures dramatically when the video was watched frame by frame. The high shutter speed eliminated any blurring of the pictures. By watching the impact, frame by frame and in slow motion, very valuable information about the motion of the column and the striker was gathered, such as the rebound of the impactor. This explained certain rebound peaks on the measured impact load history. The video camera was also used to follow the crack growth of the cracks during the static tests.

Each column was photographed from both sides to record the crack patterns as well as the type of failure of the columns.

Stellenbosch University http://scholar.sun.ac.za

B.6 Test Procedures

B.6.1 Preliminary tests.

Before the series of tests were started, four columns were used to test the apparatus and instrumentation. These preliminary tests were very valuable and the following modifications flowed forth fro these:

1. A column cross section could finally be selected which would ensure failure under impact and static conditions which were in reach of the capacity of the designed equipment and apparatus. This also ensured that a good shear pattern could develop. The original column cross section was based on a quarter scale of a typical bridge column.

2. The concrete column was supplied with a deeper cross section inside the steel footing. During the preliminary tests it was found that if the same column cross section extends into the steel, cracks developed in the concrete within the footing. This was undesirable. The increased section within the footing solved the problem. During the following tests, cracks only developed in the column above the footing.

3. All the instrumentation was tested and minor adjustments were made.

4. The whole pendulum mechanism of the striker and its release mechanism were tested and a smooth predictable run for the striker was ensured.

5. A little anti-rotation beam, as discussed earlier (paragraph B.2.4), was also supplied during this test phase because it was found that the column could rotate a little bit inside the steel footing. This modification prevented any rotation of the column inside the steel footing.

Stellenbosch University http://scholar.sun.ac.za

6. A standard buffer system for all further tests was established.

B.6.2 Series of tests.

The series of tests were divided into eight groups. Each group of tests covered the influence of a specific parameter on the behaviour of the column. All the columns in each group were identical and were tested at the same concrete age.

Within each group of columns, at least one of the columns was tested statically until failure. This column was never subjected to an impact test. The rest of the columns were then tested under impact loading. Columns did not fail under the impact loading, were then further statically tested up to failure. This following static test on an impact damaged column was to establish the reserve strength of the column after subjection to an impact load. It was tried to apply a large enough impact force to at least one of the columns of each group such as to cause failure under impact conditions.

The groups of columns were as follows:

1. With group one the influence of heavier longitudinal reinforcement than in the reference group was investigated.

2. With group two the influence of less shear reinforcement (stirrups), compared to that of group one, was investigated.

3. Group three was used as a reference for the other groups to be compared with.

4. Group four had less shear reinforcement than that of group three but more than that of group two.

Stellenbosch University http://scholar.sun.ac.za

5. With this group the influence of a lower strength concrete was tried to be established, but the change in concrete strength, compared to that of group three, was too small. Hence this group was used to verify the repeatability of this type of tests.

6. This group investigated the influence of the axial load on the column. Only one fifth of the axial load applied to the other groups, was applied to these group of columns.

7. Group seven invest.gated the influence of a higher concrete strength as that of the reference group three.

8. Group eight investigated the influence of a lower concrete strength as that of the reference group three.

B.6.3 Dimensions and reinforcement of columns.

All the columns had exactly the same dimensions. The section above the footing or from the bottom of the column to the top of the column was a uniform section of 1,6m with a cross section of 350mm x 150mm. The footing section of the column (the section inside the steel footing) had a length of 400mm and a cross section of 630mm x 150mm. The dimensions of a typical column is shown in figure B.23.

The reinforcement of the columns can be divided into four types of reinforcement. Type one consisted of 3% longitudinal reinforcement with R8@100 as stirrups. Type two had 3% longitudinal reinforcement with R8@250 as stirrups. Type three (the standard) had 1,5% longitudinal reinforcement with R8@150 as stirrups. Group four had 1,5% longitudinal reinforcement with R8@200 as stirrups. The different types of reinforcement is summurized in figure B.23.

Stellenbosch University http://scholar.sun.ac.za

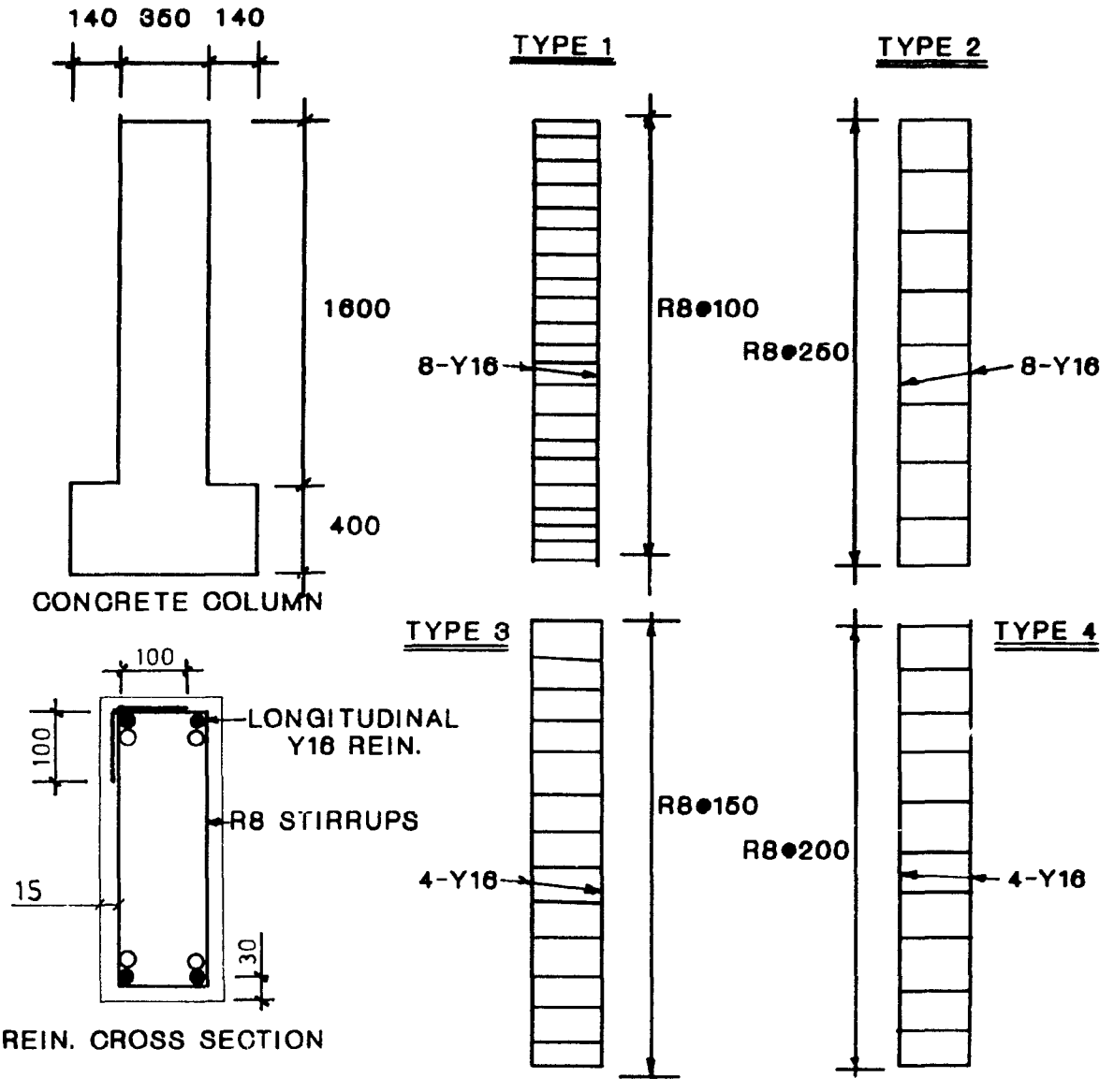

Figure B.23: Concrete column dimensions and types of reinforcing for the different columns.

B.7 Summary of all the tests on the different columns.

Some of the results of the series of tests are summarized in Table B.1 and Table B.2. The first four preliminary tests are not shown in this summary because, as previously indicated, these four tests were only used to identify problems with the apparatus and instrumentation.

Stellenbosch University http://scholar.sun.ac.za

TABLE B.1: Test data

Column No.	Rein. Type	Concrete strength		Striker Mass (kg)	Impact Velocity (m/s)	Permanent Buffer Deflection (mm)
		Compr. 7 day (MPa)	Tens. (MPa)			
1A	1	30,78	3,27	–	–	–
1B	1	32,16	4,02	750	6,398	75
1C	1	29,91	3,37	950	6,611	120
1D	1	31,89	3,77	1150	6,644	132
1E	1	28,76	3,03	–	–	–
1F	1	28,99	2,87	1250	6,940	132
1G	1	28,01	2,97	1450	6,683	144
2A	2	30,78	3,31	–	–	–
2B	2	29,08	2,63	750	7,123	108
2C	2	30,84	3,32	750	6,462	105
2D	2	30,63	3,38	950	6,407	127
2E	2	29,10	3,07	850	6,522	111
3A	3	27,53	2,59	–	–	–
3B	3	26,50	2,64	650	6,766	91
3C	3	26,35	3,00	850	7,222	111
3D	3	25,35	2,83	1050	6,517	118
3E	3	31,69	3,64	1150	6,751	122
4A	4	30,80	3,33	–	–	–
4B	4	28,10	3,03	650	6,652	92
4C	4	28,90	2,81	850	7,137	107
4D	4	30,10	3,27	1050	6,439	118
5A	3	26,40	2,85	–	–	–
5B	3	23,00	2,79	850	7,196	111
5C	3	19,70	2,37	1150	6,749	122
6A	3	29,30	3,30	–	–	–
6B	3	28,20	2,80	650	6,931	86
6C	3	30,00	3,43	850	7,163	106
6D	3	30,00	3,36	1150	6,660	126
7A	3	41,50	4,06	–	–	–
7B	3	37,90	3,62	750	7,123	105
7C	3	37,40	3,67	950	6,716	111
7D	3	36,70	3,19	1250	7,046	124
8A	3	16,40	1,73	–	–	–
8B	3	16,60	1,83	650	6,820	84
8C	3	18,20	2,18	950	7,051	107
8D	3	19,80	2,29	850	7,091	100

Stellenbosch University http://scholar.sun.ac.za

TABLE B.2: Test results

Column No.	Max. Hor. Impact Load (kN)	Max. Hor. Static Load (kN)	Range of diagonal Cracks (Angles With Vertical Axis)	Type** of Failure
1A	-	169,7***	29°; 39°; 57°	Type 3
1B	182,2	180,2	30°; 40°; 61°	Type 3
1C	283,9	177,8	32°; 40°; 57°	Type 3
1D	268,5	184,6	31°; 37°; 55°	Type 3
1E	-	185,1	31°; 36°; 56°	Type 3
1F	259,2	170,9	27°; 36°; 63°	Type 3
1G	328,0	-	36°; 50°*	Type 2
2A	-	158,3	29°; 38°*	Type 4
2B	-	147,6	40°*; 54°	Type 4
2C	125,0	139,0	34°*; 54°	Type 4
2D	165,6	-	33°*; 41°;	Type 2
2E	160,9	157,5	37°*	Type 4
3A	-	117,0	41°; 54°	Type 3
3B	-	116,0	41°; 54°	Type 3
3C	147,1	115,4	37°; 54°	Type 3
3D	178,4	118,3	39°; 57°	Type 3
3E	206,4	119,6	47°; 62°	Type 3
4A	-	116,2	45°; 60°	Type 3
4B	121,6	116,9	41°; 60°	Type 3
4C	151,4	117,0	44°; 63°	Type 3
4D	197,5	-	35°*; 60°	Type 2
5A	-	117,5	41°; 53°; 67°	Type 3
5B	146,4	111,6	36°; 51°; 71°	Type 3
5C	175,6	-	41°*; 66°	Type 2
6A	-	110,2	26°; 47°; 60°	Type 3
6B	147,7	114,0	37°; 46°; 63°	Type 3
6C	157,1	116,0	33°; 50°; 57°	Type 3
6D	224,6	-	45°*	Type 2
7A	-	126,2	38°; 51°; 71°	Type 3
7B	149,8	125,0	37°; 53°; 68°	Type 3
7C	167,0	123,4	39°; 67°	Type 3
7D	229,8	-	41°*; 53°	Type 2
8A	-	107,4	32°; 48°; 65°	Type 3
8B	131,3	106,4	29°; 41°; 59°	Type 3
8C	181,9	-	30°*; 50°	Type 2
8D	164,6	-	34°*; 48°; 67°	Type 2

Stellenbosch University http://scholar.sun.ac.za

* The major crack along which the failure of the column occurred. (Normally all the cracks fanned out from the rear bottom corner of the column.) See figures B.25 to B.129.

** Four failure types of the columns were possible:

Type 1: Flexural failure of the column under the impact test conditions.

Type 2: Shear failure of the column under the impact test conditions.

Type 3: Flexural failure of the column under the static test conditions.

Type 4: Shear failure of the column under the static test conditions.

*** Unreliable value.

B.8 Detail reports of each test column.

This section contains a detail report of every column tested. The behaviour of each column during each test is described and more details of the columns are also given.

B.8.1 Column 1A. (figures B.24 and B.25)

Reinforcement: Main: 4-Y16 + 4-Y16 (3,07 %)
Stirrups: 20-R8@100
Concrete cover: 23 mm

Concrete mix:			
	Water	-	27 kg
	Cement	-	54 kg
	Sand	-	114,68 kg
	Stone	-	169,54 kg

Stellenbosch University http://scholar.sun.ac.za

TABLE B.3. Details of concrete cubes from column 1A

NUMBER	CASTING DATE	DATE TESTED	AGE DAYS	MASS (kg)	SPLIT (kN)	FORCE (kN)	STRENGTH (MPa)
ML-1A1	28/03/88	04/04/88	7	8,42	119,7	695,23	30,90
ML-1A2	28/03/88	04/04/88	7	8,44	-	699,62	31,10
ML-1A3	28/03/88	04/04/88	7	8,36	111,7	642,02	28,53
ML-1A4	28/03/88	04/04/88	7	8,42	-	731,51	32,51
ML-1A5	28/03/88	25/04/88	28	8,44	-	918,40	40,82
ML-1A6	28/03/88	25/04/88	28	8,43	-	943,31	41,92

This column failed in flexure. The tension steel started to yield and at failure the column's deflection increased without any increase in the horizontal load. The ultimate horizontal force the column could withstand was 169,7 kN which represents an ultimate flexural moment at the base of the column of 123,9 kNm.

The first crack to developed was a "flexural" crack right at the bottom of the column as could be expected. This crack started to develop at a horizontal load of 60 kN. Most of the cracks started as "flexural" cracks before it changed to "shear" cracks, developing in the direction of the rear corner of the column. There were three significant "shear" cracks. The one crack developed at an angle of about 39,3° and the second one at an angle of about 57° and the third one at an angle of 29,4° with the vertical axis of the column.

The axial load dropped as soon as the first horizontal load step was applied to the column and then suddenly the axial force started to increase as the horizontal force increased further. The latter can be attributed to the fact that the column started to crack and thus lengthened due to the shift of the neutral axis to a position further away from the column center line. This results in an increase in the axial force since the top of the column was restraint by the loading beam. In figure B.28 it can be seen that the axial load started to rise at a horizontal load of 50 to 60 kN and as mentioned earlier the first crack was visible at a load of 60 kN. Unfortunately this column started to rotate inside the footing and thus this test was repeated later.

Stellenbosch University http://scholar.sun.ac.za

Figure B.24: Crack pattern of Column 1A seen from one side. The numbers next to the lines indicate the horizontal load in kN.

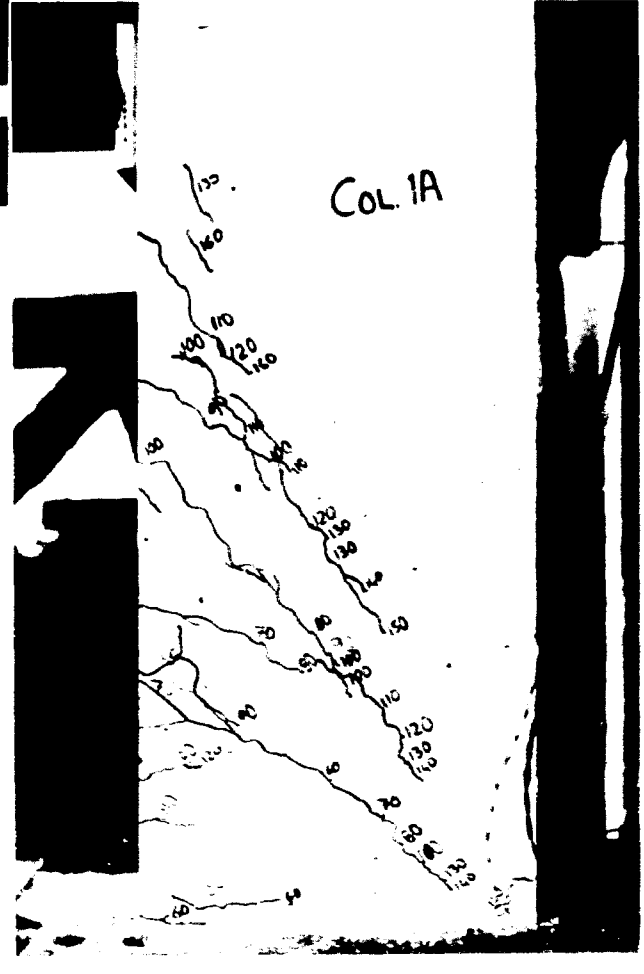

Figure B.25: Crack pattern of Column 1A seen from the other side of the column.

Stellenbosch University http://scholar.sun.ac.za

Figures B.24 and B.25 show the crack pattern visible on the two sides of the column. Figures B.130 to B.133 show graphically the recorded test data.

B.8.2 Column 1B. (figures B.26 - B.29)

Reinforcement: Main: 4-Y16 + 4-Y16 (3,07 %)
Stirrups: 20-R8@100
Concrete cover: 23 mm

Concrete mix: Water - 27 kg
Cement - 54 kg
Sand - 114,68 kg
Stone - 169,54 kg

TABLE B.4: Details of concrete cubes from column 1B

NUMBER	CASTING DATE	DATE TESTED	AGE DAYS	MASS (kg)	SPLIT (kN)	FORCE (kN)	STRENGTH (MPa)
ML-1B1	31/03/88	07/04/88	7	8,60	124,6	687,80	30,57
ML-1B2	31/03/88	07/04/88	7	8,50	-	751,35	33,39
ML-1B3	31/03/88	07/04/88	7	8,48	159,9	710,76	31,59
ML-1B4	31/03/88	07/04/88	7	8,52	-	745,00	33,11
ML-1B5	31/03/88	28/04/88	28	8,46	-	926,22	41,17
ML-1B6	31/03/88	28/04/88	28	8,52	-	968,87	43,06

Impact phase of test on Column 1B

During the impact test it was tried to introduce an impact force to the column which was the same in magnitude as the failure load of the static test (Column 1A) in this series of tests. The impact load was 182,2 kN, compared to the static failure load of Column 1A of 169,7 kN. Unfortunately the static test of Column 1A was not satisfactorily, as previously mentioned and that test was repeated as Column 1E. With the static test of Column 1E the ultimate static load was 185,087 kN. This value compares very good with the impact load of Column 1B.

Stellenbosch University http://scholar.sun.ac.za

During the impact test only a few major cracks developed. A horizontal crack right at the bottom of the column was visible. Three diagonal cracks were also visible, but they did not developed significantly. The diagonal cracks were only faint cracks and they formed angles of 61°, 40° and 30° with the vertical axis of the column. This corresponds very good with the cracks of Columns 1A and 1E, that is, the static tests.

The axial load increased immediately with the impact and this indicated that the concrete cracked very early during the impact test. This early cracking was also assumed in the theory discussed in chapter 5.

The impact load history was the typical type of function one can expect of an impact of a "soft" type of impactor or striker such as a car, a truck or a train.

Static phase of test on Column 1B

After the impact test, the column was subjected to an immediate static test to determine the reserve strength of the column. The column was step loaded with a static horizontal force in steps of 10 kN. The maximum static load the column could withstand was 180,2 kN. This corresponded very well with the static failure load of Column 1E of 185kN. This indicated that the column's strength was not seriously diminished by the impact although the impact load had been a little higher than the static failure load.

Although the diagonal cracks developed further during the static test it never looked as if the column would fail in shear. The "flexural" crack soon started to enlarge. In the end the column failed in flexure as the longitudinal steel yielded. At failure the horizontal force stayed nearly constant while the deflection increased all the time as a plastic hinge was formed.

Stellenbosch University http://scholar.sun.ac.za

Figure B.26: Crack pattern of Column 1B seen from one side after the impact phase.

Figure B.27: Crack pattern of Column 1B seen from the other side of the column.

Stellenbosch University http://scholar.sun.ac.za

Figure B.28: Crack pattern of Column 1B seen from one side after the static test.

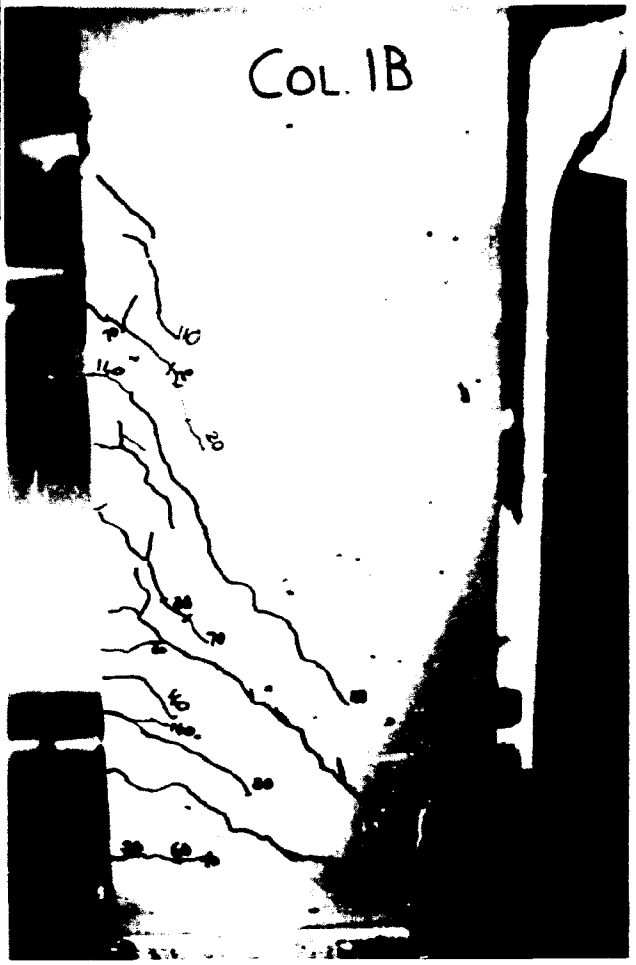

Figure B.29: Crack pattern of Column 1B seen from the other side of the column.

Stellenbosch University http://scholar.sun.ac.za

In this case the axial load started to increase as soon as the static load was applied. This indicated that the cracks immediately started to enlarge and by doing this increased the length of the column, resulting in the higher axial load.

The damaged column 1B started to fail at a top deflection of around 28mm while the undamaged column 1E started to fail at a top deflection of 25mm. Exactly the same relation was exhibited by the deflection at midheightof the column. The deflection of Column 1A was ignored because the column started to rotate inside the footing and this influenced the deflection of the column dramatically.

Figures B.26 and B.27 show the crack pattern visible on the two sides of the column after the impact test. Figures B.28 and B.29 show the crack pattern of the column after the static test. Figures B.134 to B.161 show graphically the recorded test data.

B.8.3 Column 1C. (figures B.30 -B.31)

Reinforcement: Main: 4-Y16 + 4-Y16 (3,07 %)
Stirrups: 20-R8@100
Concrete cover: 23 mm

Concrete mix: Water - 27 kg
Cement - 54 kg
Sand - 114,68 kg
Stone - 169,54 kg

TABLE B.5: Details of concrete cubes from column 1C

NUMBER	CASTING DATE	DATE TESTED	AGE DAYS	MASS (kg)	SPLIT (kN)	FORCE (kN)	STRENGTH (MPa)
ML-1C1	04/04/88	11/04/38	7	8,42	111,0	654,00	29,07
ML-1C2	04/04/88	11/04/88	7	8,36	-	692,00	30,76
ML-1C3	04/04/88	11/04/88	7	8,36	127,0	675 00	30,00
ML-1C4	04/04/88	11/04/88	7	8,39	-	671,00	29,82
ML-1C5	04/04/88	02/05/88	28	8,34	-	957,77	42,57
ML-1C6	04/04/88	02/05/88	28	8.44	-	947,54	42,11

Stellenbosch University http://scholar.sun.ac.za

Figure B.30: Crack pattern of Column 1C seen from one side after the impact phase.

Figure B.31: Crack pattern of Column 1C seen from the other side of the column.

Stellenbosch University http://scholar.sun.ac.za

Impact phase of test on Column 1C

It was tried to introduce an impact force to this column which was greater than the static failure load of Column 1A as well as the impact load of Column 1B. The impact force was 283,9 kN. With the static test of Column 1E the ultimate static load was 185,087 kN. Although the impact load was nearly a 100 kN higher than the static failure load, the column did not fail under the impact loading.

During the impact test a few cracks developed. A horizontal crack right at the bottom of the column was visible. Three diagonal cracks that started as "flexural" cracks were also present. The diagonal cracks formed angles of 57°, 39,5° and 32° with the vertical axis of the column. This corresponded closely with the cracks of Columns 1A and 1E, the static tests, and the cracks of Column 1B, the impact test.

The axial load increased immediately with the impact and just after impact it started to decrease and increase innearly the same frequency as the strain gauges. The increase in the axial load also indicated that the column cracked. The column lengthened due to the cracking and this increased the axial load.

The impact load history was again typical of what one could expect of an impact of a "soft" type of impactor such as a car, a truck or a train. This impact load history differed from that of Column 1B in that it had a very high second peak compared to that for the previous column. This very high second peak was the result of a completely compressed buffer system.

Static phase of test on Column 1C

After the impact test, a static test was done on the column to determine what static load the column could withstand after such an impact. The column was step loaded with a static horizontal load in steps of 10 kN. The maximum static load the column could withstand was 177,8 kN. This corresponded very well with the static failure load of Column 1E (185kN) and that of Column 1B

Stellenbosch University http://scholar.sun.ac.za

(180,2 kN). This indicated that the column was not seriously damaged during the impact, although the impact load was considerably higher than that of the static failure load of Column 1E.

Although the diagonal cracks developed further during the static test it never looked as if the column will fail in shear. The "flexural" crack soon started to enlarge. In the end the column failed in flexure. While the horizontal force stayed nearly constant the deflection increased all the time, indicating a flexural failure.

In this case the axial load started to increase as soon as the static load was applied. This indicate that the cracks immediately started to enlarge and by doing this increased the length of the column resulting in the higher axial load.

During the impact test the bottom strain gauge was damaged and thus during the static test this strain gauge gave a zero reading. The damaged column 1B started to fail at a top deflection of around 31mm while the undamaged column 1E started to fail at a top deflection of 25mm and the previous column Column 1B started to fail at a deflection of around 28 mm.

Figures B.30 and B.31 show the crack pattern visible on the both sides of the column after the impact test. Figures B.162 to B.189 show graphically the recorded test data.

B.8.4 Column 1D.

Reinforcement: Main: 4-Y16 + 4-Y16 (3,07 %)
Stirrups: 20-R8@100
Concrete cover: 23 mm

Stellenbosch University http://scholar.sun.ac.za

Concrete mix: Water - 27 kg
Cement - 54 kg
Sand - 114,68 kg
Stone - 169,54 kg

TABLE B.6: Details of concrete cubes from column 1D

NUMBER	CASTING DATE	DATE TESTED	AGE DAYS	MASS (kg)	SPLIT (kN)	FORCE (kN)	STRENGTH (MPa)
ML-1D1	07/04/88	14/04/88	7	8,42	142,5	724,65	32,21
ML-1D2	07/04/88	14/04/88	7	8,44	-	748,45	33,26
ML-1D3	07/04/88	14/04/88	7	8,42	124,'	671,85	29,86
ML-1D4	07/04/88	14/04/88	7	8,38	-	725,60	32,25
ML-1D5	07/04/88	05/05/88	28	8,46	-	971,99	43,20
ML-1D6	07/04/88	05/05/88	28	8,39	-	967,68	43,01

Impact phase of test on Column 1D

With this impact test it was tried to introduce an impact load to the column which was greater than the impact load of the impact test on Column 1C. The impact force was 268,5 kN compared to the static failure force of Column 1E of 185,1kN. Although the impact load was nearly 184 kN higher than the static failure load of Column 1E, the column did not fail under the impact loading. Due to the use of a different buffer system in this test, the impact load was lower than that of Column 1C. Thus this test can be used to prove the repeatability of the impact tests. This test showed that the repeatability is acceptable.

During the impact test a few cracks developed. A horizontal crack right at the bottom of the column was visible. Three diagonal cracks that started as "flexural" cracks were also present. The major diagonal cracks formed angles of 54,8°, 36,6° and 31° with the vertical axis of the column. This corresponded with the cracks of Columns 1A and 1E, the static tests, and the cracks of Columns 1B and 1C, the impact tests.

Stellenbosch University http://scholar.sun.ac.za

Figure B.32: Crack pattern of Column 1D seen from one side after the impact test.

Figure B.33: Crack pattern of Column 1D seen from the other side of the column.

Stellenbosch University http://scholar.sun.ac.za

The impact peak is very much higher than that of Column 1B and can be contributed to the buffer system which was nearly completely compressed. Unfortunately the lower strain gauge was damaged during the impact phase of the test.

The axial load increased immediately with the impact. The increase in the axial load indicated that the column cracked with the impact. By cracking, the column lengthened, which resulted in the increase in the axial load.

The impact load history was again typical of what one could expect of an impact of a "soft" type of impactor such as a car, a truck or a train. After the second peak smaller third and fourth peaks were present. These two peaks were the result of the column's movement. Due to this vibration of the column, the column is actually impacting the mass as indicated by the further peaks in the load history. This "impact" was responsible for the rebound of the striker.

Static phase of test on Column 1D

After the impact test, a static test was done on the column to determine what force the column could withstand after such an impact. The column was step loaded with a static horizontal load in steps of 10 kN. The maximum static load the column could withstand was 184,61 kN. This corresponds very well with the static failure load of Column 1E (185 kN) and that of Column 1B (180,2 kN) and that of Column 1C (177,8 kN). This indicated that the column was not damaged seriously during the impact although the impact load was considerably higher than that of the static failure load of Column 1E.

Although the major diagonal cracks developed further during the static test it never looked as if the column will fail in shear. The "flexural" crack soon started to enlarge. In the end the column failed in flexure. While the horizontal load stayed nearly constant the deflection kept increasing, indicating a flexural failure of the column.

Stellenbosch University http://scholar.sun.ac.za

In this case the axial load started to increase as soon as the static load was applied. This indicate that the existing cracks immediately started to enlarge, increased the length of the column, resulting in the increase in the axial load.

As indicated with the impact test the bottom strain gauge was damaged and only a zero reading from this strain gauge was recorded. The damaged column 1B started to fail at a top deflection of around 29mm while the undamaged column 1E started to fail at a top deflection of 25mm and the previous columns Column 1B and Column 1C started to fail at deflections of 28mm and 31mm respectively.

When all the results of this test is compared with the other columns in this group it is clear that the repeatability of this kind of tests is acceptable.

Figures B.32 and B.33 show the crack pattern visible on both sides of the column after the impact test. Figures B.190 to B.217 show graphically the recorded test data.

B.8.5 Column 1E. (figures B.34 to B.35)

Reinforcement: Main: 4-Y16 + 4-Y16 (3,07 %)
Stirrups: 20-R8@100
Concrete cover: 23 mm

Concrete mix:	Water	-	27 kg
	Cement	-	54 kg
	Sand	-	114,68 kg
	Stone	-	169,54 kg

Stellenbosch University http://scholar.sun.ac.za

Figure B.34: Crack pattern of Column 1E seen from one side. The figures indicate the horizontal applied load in kN.

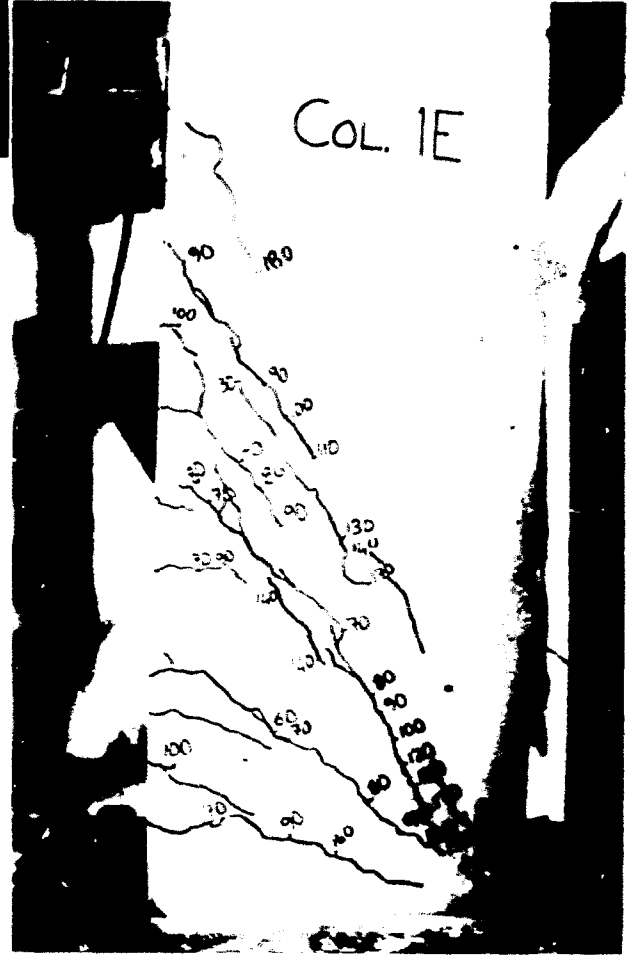

Figure B.35: Crack pattern of Column 1E seen from the other side of the column.

Stellenbosch University http://scholar.sun.ac.za

TABLE B.7: Details of concrete cubes from column 1E

NUMBER	CASTING DATE	DATE TESTED	AGE DAYS	MASS (kg)	SLPIT (kN)	FORCE (kN)	STRENGTH (MPa)
ML-1E1	25/04/88	02/05/88	7	8,36	113,48	601,93	26,75
ML-1E2	25/04/88	02/05/88	7	8,40	-	612,64	27,23
ML-1E3	25/04/88	02/05/88	7	8,42	100,4	638,45	28,38
ML-1E4	25/04/88	02/05/88	7	8,40	-	656,36	29,17
ML-1E5	25/04/88	23/05/88	28	8,45	-	925,87	41,15
ML-1E6	25/04/88	23/05/88	28	8,43	-	932,47	41,44

Static phase of test on Column 1E

This column was the repeat test of Column 1A. The column was step loaded with a static horizontal load in steps of 10 kN. This column failed in flexure. The tension steel started to yield and at failure the column's deflection increased without any increase in the horizontal load. The ultimate horizontal load the column could withstand was 185,087 kN which represents a ultimate bending moment at the base of the column of 136,96 kNm.

The diagonal crack pattern developed quite well. The first crack to develop was a horizontal crack right at the bottom of the column. This crack started to develop with a horizontal load of 60 kN. Most of the major cracks started as a flexural crack before it changed to a diagonal crack, developing in the direction of the rear corner of the column. There were three major diagonal cracks. The one crack developed at an angle of 30,7° and the second one at an angle of 35,5° and the third one at an angle of 55,6° with the vertical axis of the column.

The axial load started to decrease as soon as a horizontal load was applied to the column and then suddenly the axial load started to increase as the horizontal load increased further. This was due to the fact that the column started to crack and thus lengthened and by lengthening the axial load increased. With a 60 kN horizontal load the first bending crack was visible and at that point the axial load started to rise, thus this

Stellenbosch University http://scholar.sun.ac.za

confirms that the development of cracks was responsible for the rise in the axial load, as described earlier.

With a top deflection of 25 mm, the column started to fail, but the ultimate deflection of the column was about 53mm. This indicated that the reinforcement yielded while the column deflected further.

Figures B.34 and B.35 show the crack pattern visible on both sides of the column after the static test. Figures B.218 to B.221 show graphically the recorded test data.

B.8.6 Column 1F. (figures B.36 to B.39)

Reinforcement: Main: 4-Y16 + 4-Y16 (3,07 %)
Stirrups: 20-R8@100
Concrete cover: 23 mm

Concrete mix: Water - 27 kg
Cement - 54 kg
Sand - 114,68 kg
Stone - 169,54 kg

TABLE B.8: Details of concrete cubes from column 1F

NUMBER	CASTING DATE	DATE TESTED	AGE DAYS	MASS (kg)	SPLIT (kN)	FORCE (kN)	STRENGTH (MPa)
ML-1F1	28/04/88	05/05/88	7	8,43	109,7	608,79	27,06
ML-1F2	28/04/88	05/05/88	7	8,50	-	601,05	26,71
ML-1F3	28/04/88	05/05/88	7	8,48	93,2	630,88	28,04
ML-1F4	28/04/88	05/05/88	7	8,42	-	673,53	29,93
ML-1F5	28/04/88	26/05/88	28	8,48	-	791,98	35,20
ML-1F6	28/04/88	26/05/88	28	8,50	-	902,18	40,10

Impact phase of test on Column 1F

With this impact test it was tried to introduce an impact force to the column which was large enough to let the column fail under the impact load. The impact force was 259,245 kN compared to the

Stellenbosch University http://scholar.sun.ac.za

static failure force of Column 1E of 185,1kN. Although the impact load was 74 kN higher than the static load the column did not fail under the impact load. Although a heavier mass was used with this impact test, the maximum impact load was lower than that of Column's 1C and 1D.

After the impact loading a horizontal crack right at the bottom of the column was visible. Three major diagonal cracks were also present. The major diagonal cracks formed angles of 62,7°, 36,1° and 25,6° with the vertical axis of the column. This corresponded very good with the cracks of Columns 1A and 1E, the static tests, and the cracks of Columns 1B, 1C and 1D, the impact tests.

The axial load increased immediately with the impact. The increase in the axial load indicated that the column cracked and thus lengthened, resulting in the higher axial load.

The second peak of the impact load history was quite high compared to some of the other columns, but it compared very well with that of Columns 1C and 1D. After the second peak a smaller third peak was present. This third peak was an indication of the column impacting the mass. This "impact" was confirmed by the video recordings.

Static phase of test on Column 1F

After the impact test, a static test was done on the column to determine what force the column could withstand after such an impact. The column was step loaded with a static horizontal load in steps of 10 kN. The maximum static load the column could withstand was 170,91 kN. This corresponded with the static failure load of Column 1E (185 kN), that of Column 1B (180,2 kN) and that of Column 1C (177,8 kN). This indicated that the column was not damaged seriously during the impact, although the impact load was considerably higher than that of the static failure load of Column 1E.

Stellenbosch University http://scholar.sun.ac.za

Figure B.36: Crack pattern of Column 1F seen from one side after the impact phase

Figure B.37: Crack pattern of Column 1F seen from the other side of the column.

Stellenbosch University http://scholar.sun.ac.za

Figure B.38: Crack pattern of Column 1F seen from one side after the static test.

Figure B.39: Crack pattern of Column 1F seen from the other side of the column.

Stellenbosch University http://scholar.sun.ac.za

Although the major diagonal cracks developed further during the static test it never looked as if the column might fail in shear. The "flexural" crack soon started to enlarge. In the end the column failed in flexure. While the horizontal force stayed nearly constant the deflection kept increasing, which indicated a flexural failure.

With this static test the axial load started to increase as soon as the static load was applied. This indicated that the cracks immediately started to enlarge and thus increased the length of the column, resulting the increase in the axial load.

The impact damaged Column 1F started to fail at a top deflection of around 32mm while the undamaged Column 1E started to fail at a top deflection of 25mm, while the previous columns Column 1B, 1C and 1D started to fail at deflections of around 28mm, 31mm and 30mm respectively.

Figures B.36 and B.37 show the crack pattern visible on both sides of the column after the impact test. Figures B.38 and B.39 show the crack pattern visible after the static test. Figures B.222 to B.249 show graphically the recorded test data.

B.8.7 Column 1G. (figures B.40 to B.41)

Reinforcement: Main: 4-Y16 + 4-Y16 (3,07 %)
Stirrups: 20-R8@100
Concrete cover: 23 mm

Concrete mix:	Water	-	27 kg
	Cement	-	54 kg
	Sand	-	114,68 kg
	Stone	-	169,54 kg

Stellenbosch University http://scholar.sun.ac.za

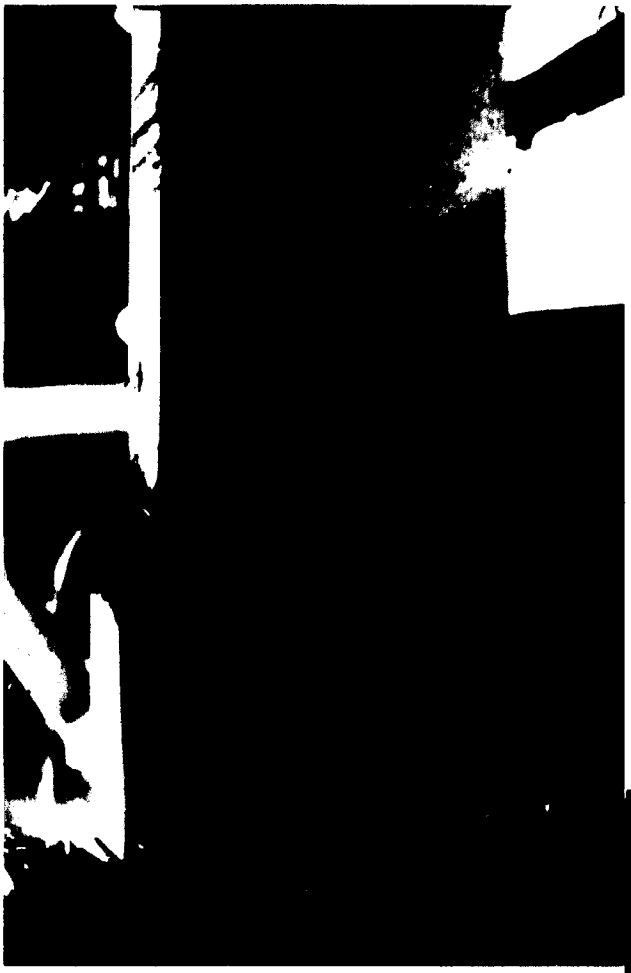

Figure B.40: Crack pattern and failure of Column 1G seen from one side.

Figure B.41: Crack pattern and failure of Column 1G seen from the other side.

Stellenbosch University http://scholar.sun.ac.za

TABLE B.9: Details of concrete cubes from column 1G							
NUMBER	CASTING DATE	DATE TESTED	AGE DAYS	MASS (kg)	SPLIT (kN)	FORCE (kN)	STRENGTH (MPa)
ML-1G1	19/05/88	26/05/88	7	8,39	107,7	619,42	27,53
ML-1G2	19/05/88	26/05/88	7	8,45	-	629,51	27,98
ML-1G3	19/05/88	26/05/88	7	8,42	102,5	612,03	27,20
ML-1G4	19/05/88	26/05/88	7	8,45	-	630,92	28,04
ML-1G5	19/05/88	16/06/88	28	8,62	-	871.36	38,73
ML-1G6	19/05/88	16/06/88	28	8,38	-	893,30	39,70

Impact phase of test on Column 1G

With this impact test it was tried to introduce an impact load to the column which was great enough to let the column fail under the impact loading. The impact force was 327,997 kN compared to the static failure force of Column 1E of 185,1kN. The impact failure load was 77,2% higher than the static failure load of Column 1E. The column failed in shear. Interestingly, all the other columns in this series of tests failed in flexure with the static test.

During the impact test two major diagonal cracks developed, forming angles of 50,4° and 36,1° with the vertical axis of the column. The column failed along the 50,4° diagonal crack. Only a small horizontal crack right at the bottom of the column was visible after the impact failure and it looked as if this crack had not a chance to develop. The 36,1° crack corresponded with the diagonal cracks of the rest of the columns in this group.

Unfortunately the bottom strain gauge was damaged during the impact loading. The damage of this strain gauge gave an indication of the time the failure crack reached the rear face of the column. This showed that the crack reached the rear face of the column even before the maximum impact load was registered.

After the first and second peak of the impact load history, a series of further peaks were also present. This further peaks were due to the failure of the column and the striker which "caught" up with the column at those specific points.

Stellenbosch University http://scholar.sun.ac.za

Figures B.40 and B.41 show the visible crack pattern and the failure cracks of the column, from both sides. Figures B.250 to B.273 show graphically the recorded test data.

B.8.8 Column 2A. (figure B.42 to B.43)

Reinforcement: Main: 4-Y16 + 4-Y16 (3,07 %)
Stirrups: 8-R8@250
Concrete cover: 23 mm

Concrete mix: Water - 27 kg
Cement - 54 kg
Sand - 114,68 kg
Stone - 169,54 kg

TABLE B.10: Details of concrete cubes from column 2A

NUMBER	CASTING DATE	DATE TESTED	AGE DAYS	MASS (kg)	SLPIT (kN)	FORCE (kN)	STRENGTH (MPa)
ML-2A1	11/04/88	18/04/88	7	8,40	112,0	654,87	29,11
ML-2A2	11/04/88	18/04/88	7	8,50	-	726,78	32,30
ML-2A3	11/04/88	18/04/88	7	8,42	122,1	-	-
ML-2A4	11/04/88	18/04/88	7	8,47	-	695,69	30,92
ML-2A5	11/04/88	09/05/88	28	3,40	-	960.63	42,69
ML-2A6	11/04/88	09/05/88	28	8,48	-	939.95	41,78

Static test of column 2A

This column failed in shear. Two major diagonal cracks developed quite early. The cracks formed shear angles of 38° and 29° with the vertical axis of the column. The shear cracks started in the middle of the column and then grew towards the front and rear faces of the column. This is typical of shear failure. These two cracks widened to more than 2mm. The horizontal failure load was 158,31 kN, or in other words, the shear failure force was 158,31 kN. This horizontal load corresponds with a bending moment of 117,15 kNm.

Stellenbosch University http://scholar.sun.ac.za

Figure B.42: Crack pattern of Column 2A seen from one side after the static test.

Figure B.43: Crack pattern of Column 2A seen from the other side of the column.

Stellenbosch University http://scholar.sun.ac.za

At failure there were only a few horizontal cracks visible. When the horizontal load was released, the shear cracks did not close as in the case of the flexural failure of Column 1E.

The axial load started to decrease as soon as a horizontal load was applied to the column, before the axial load sunddenly started to increase as the horizontal load increased further. Once again this is due to the fact that the column started to crack and thus lengthened and by lengthening the axial load increased because the axial load beam retarded the lengthening.

At a horizontal force of about 125 kN the strain at the rear bottom of the column suddenly started to decrease again. This can be explained by the fact that the shear cracks reached the faces of the column and thus shear became dominant over flexure and thus the strain was slightly relaxed, as indicated by the strain gauge at the rear bottom of the column.

Figures B.42 and B.43 show the visible crack pattern on the column after the static test. Figures B.274 to B.277 show graphically the recorded test data.

B.8.9 Column 2B. (figures B.44 to B.47)

Reinforcement: Main: 4-Y16 + 4-Y16 (3,07 %)
Stirrups: 8-R8@250
Concrete cover: 23 mm

Concrete mix:	Water	-	27 kg
	Cement	-	54 kg
	Sand	-	114,68 kg
	Stone	-	169,54 kg

Stellenbosch University http://scholar.sun.ac.za

Figure B.44: Crack pattern of Column 2B seen from one side after the impact phase.

Figure B.45: Crack pattern of Column 2B seen from the other side of the column.

Stellenbosch University http://scholar.sun.ac.za

Figure B.46: Crack pattern of Column 2B seen from one side after the static test.

Figure B.47: Crack pattern of Column 2B seen from the other side of the column.

Stellenbosch University http://scholar.sun.ac.za

TABLE B.11: Details of concrete cubes from column 2B

NUMBER	CASTING DATE	DATE TESTED	AGE DAYS	MASS (kg)	SPLIT (kN)	FORCE (kN)	STRENGTH (MPa)
ML-2B1	14/04/88	21/04/88	7	8,37	97,2	623,59	27,72
ML-2B2	14/04/88	21/04/88	7	8,40	-	654,30	29,08
ML-2B3	14/04/88	21/04/88	7	8,32	88,8	524,03	23,29
ML-2B4	14/04/88	21/04/88	7	8,36	-	654,26	29,08
ML-2B5	14/04/88	12/05/88	28	8,38	-	974,59	43,32
ML-2B6	14/04/88	12/05/88	28	8,39	-	929,15	41,30

Impact phase of test on Column 2B

It was tried to introduce an impact load to the column which had the same magnitude as the failure load of the static test (Column 2A) in this series of tests. Unfortunately the computers were triggered too early. Thus no data were recorded for the impact tests. In spite of this problem, a static test was done on the column immediately after the impact test.

During the impact test one major "shear" crack developed, starting in the middle of the column and spreading towards the edges (but it did not reach the edges). This "shear" crack formed an angle of 39,6° with the vertical axis of the column. Apparently there were no significant horizontal cracks visible after the impact loading.

Static phase of test on Column 2B

After the impact test, a static test was done on the column to determine the reserve strength of the column. The column was step loaded with a static horizontal load in steps of 10 kN. During the static test the "shear" crack which developed during the impact test phase started to increase in width at quite a low horizontal force. With a horizontal force of 20 kN another "shear" crack developed forming an angle of 54°. This "shear" crack did not develop further. Exactly the same behaviour was found in the static test of Col. 2A.

Stellenbosch University http://scholar.sun.ac.za

The first "shear" crack developed and it was soon clear that this crack would be the failure mechanism of this column. At a maximum horizontal load of 147,6 kN the column failed in shear. This horizontal load corresponds with a flexural moment of 109,22 kNm. This column could not reach the static failure load of Column 2A (158,31 kN). At failure only a few "flexural" cracks were visible, but these cracks did not develop. Once again when the horizontal force was released there was no sign of rehabilitation of the column or that the cracks closed as in the case of the flexural failures of the column 1 series.

Again the axial load dropped as soon as a horizontal force was applied to the column before it suddenly started to increase as the horizontal load increased further. This could be attributed to the cracking and thus the lengthening of the column which was retraint to a certain degree by the axial loading beam.

At a horizontal force of about 116 kN the strain at the rear bottom of the column suddenly started to decrease again. Exactly the same happened to the static test of Col. 2A, but in the case of 2A the strain only started to drop at a Horizontal force of 125 kN. This can be explained by the fact that the "shear" cracks reached the faces of the column and thus shear became dominant over flexure with the result of relaxing the compression strain slightly, as indicated by the strain gauge at the rear bottom of the column.

The damaged Column 2B started to fail at a top deflection of just over 20 mm while the undamaged Column 2A started to fail at a top deflection of just under 20 mm.

Figures B.44 and B.45 show the visible crack pattern on both sides of the column after the impact test. Figures B.46 and B.47 show the crack pattern after the static test. Figures B.278 to B.281 show graphically the recorded test data.

Stellenbosch University http://scholar.sun.ac.za

B.8.10 Column 2C. (figures B.48 to B.51)

Reinforcement: Main: 4-Y16 + 4-Y16 (3,07 %)
Stirrups: 8-R8@250
Concrete cover: 23 mm

Concrete mix: Water - 27 kg
Cement - 54 kg
Sand - 114,68 kg
Stone - 169,54 kg

TABLE B.12: Details of concrete cubes from column 2C

NUMBER	CASTING DATE	DATE TESTED	AGE DAYS	MASS (kg)	SPLIT (kN)	FORCE (kN)	STRENGTH (MPa)
ML-2C1	18/04/88	25/04/88	7	8,42	113,5	622,64	27,67
ML-2C2	18/04/88	25/04/88	7	8,43	-	701,49	31,18
ML-2C3	18/04/88	25/04/88	7	8,37	121,0	618,26	27,48
ML-2C4	18/04/88	25/04/88	7	8,34	-	686,57	30,51
ML-2C5	18/04/88	16/05/88	28	8,57	-	894,67	39,76
ML-2C6	18/04/88	16/05/88	28	8,50	-	901,46	40,06

Impact phase of test on Column 2C

With this impact test it was tried to introduce an impact load to the column which was the same in magnitude as the failure load of the static test (Column 2A) in this series of tests. Unfortunately the impact load was lower. The impact load was 125 kN compared to the static failure load of Column 2A of 158,31 kN.

During the impact loading a clear "shear" crack developed, starting in the middle of the column and spreading towards the edges (but it did not reach the edges). This shear crack formed an angle of 34° with the vertical axis of the column. There was only one faint horizontal crack visible at the bottom of the column after the impact loading.

The axial load increased immediately with the impact, indicating the cracking of the concrete at a very early stage.

Stellenbosch University http://scholar.sun.ac.za

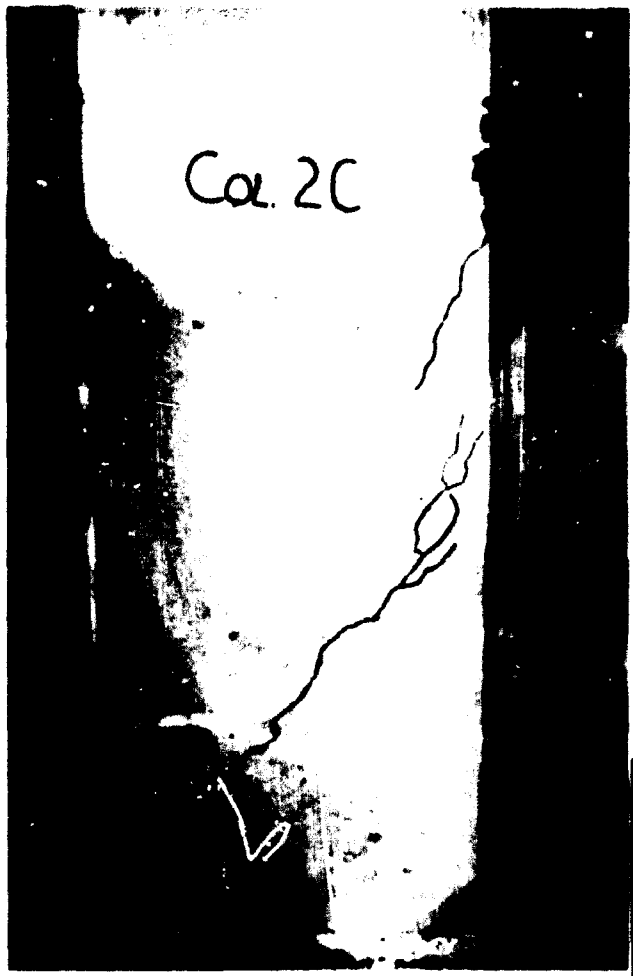

Figure B.48: Crack pattern of Column 2C seen from one side after the impact phase.

Figure B.49: Crack pattern of Column 2C seen from the other side of the column.

Stellenbosch University http://scholar.sun.ac.za

Figure B.50: Crack pattern of Column 2C seen from one side after the static test.

Figure B.51: Crack pattern of Column 2C seen from the other side of the column.

Stellenbosch University http://scholar.sun.ac.za

Static phase of test on Column 2C

After the impact test, a static test was done on the column to determine what the reserve strength of the column was after such an impact. The column was step loaded with a static horizontal load in steps of 10 kN. During the static test the "shear" crack which developed during the impact test phase started to increase in width at quite a low horizontal load. With a horizontal load of 20 kN another diagonal crack developed, forming an angle of 54°. This diagonal crack did not develop further. Exactly the same behaviour was found in the static tests of Columns 2A and 2B.

The first "shear" crack developed and it had been clear that this crack would be the failure mechanism of this column. At a maximum horizontal load of 139 kN the column failed in shear. This horizontal load corresponds with a flexural moment of 102,1 kNm at the bottom of the column. This column could not reach the static failure load of column 2A (158,31 kN). Once again when the horizontal force was released there was no sign of rehabilitation of the column or that the cracks closed as in the case of the flexural failures of the column 1 series. After this test the same conclusion as with column 2B can be reached, that is, that if a column that will fail in shear under static loading conditions was subjected to an impact load (without failure of the column under the impact loading) that column could not reach the original static failure load of an undamaged column, when tested with a static load. This seems not to be the case with a flexural failure type of column.

Again the axial load dropped as soon as a horizontal load was applied to the column before it suddenly started to increase as the horizontal load increased further. Again this was due to the cracking of the concrete.

At a horizontal l . of about 108 kN the strain at rear bottom of the column suddenly started to decrease again. Exactly the same happened to the static test of Col. 2A, but in the case of 2A the

Stellenbosch University http://scholar.sun.ac.za

strain only started to drop at a horizontal load of 125 kN. Once again this was due to the "shear" cracks that reached the faces of the column indicating the dominance of the shear and the slight relaxation of the compression strain, as indicated by the strain gauge at the rear bottom of the column.

The damaged Column 2C started to fail at a top deflection of around 20 mm while the undamaged Column 2A started to fail at a top deflection of just under 20 mm.

Figures B.48 and B.49 show the visible crack pattern on both sides of the column after the impact test. Figures B.50 and B.51 show the crack pattern after the static test. Figures B.282 to B.309 show graphically the recorded test data.

B.8.11 Column 2D. (figures B.52 to B.53)

Reinforcement: Main: 4-Y16 + 4-Y16 (3,07 %)
Stirrups: 8-R8@250
Concrete cover: 21 mm

Concrete mix:

Water	-	27 kg
Cement	-	54 kg
Sand	-	114,68 kg
Stone	-	169,54 kg

TABLE B.13: Details of concrete cubes from column 2D

NUMBER	CASTING DATE	DATE TESTED	AGE DAYS	MASS (kg)	SPLIT (kN)	FORCE (kN)	STRENGTH (MPa)
ML-2D1	21/04/88	28/04/88	7	8,40	127,4	672,61	29,89
ML-2D2	21/04/88	28/04/88	7	8,36	-	682,72	30,34
ML-2D3	21/04/88	28/04/88	7	8,34	111,0	651,59	28,96
ML-2D4	21/04/88	28/04/88	7	8,42	-	712,13	31,65
ML-2D5	21/04/88	19/05/88	28	8,43	-	914,89	40,66
ML-2D6	21/04/88	19/05/88	28	8,36	-	935,87	41,59

Stellenbosch University http://scholar.sun.ac.za

Figure B.52: Failure and crack pattern of Column 2D seen from one side after the impact phase.

Figure B.53: Failure and crack pattern of Column 2D seen from theother side of the column.

Stellenbosch University http://scholar.sun.ac.za

Impact phase of test on Column 2D

With this impact test it was tried to let the column just fail under the impact load. The column failed completely in shear. The maximum impact load was 165,6 kN. This failure load was just higher than the static failure load of 158,31 kN of Column 2A.

Two diagonal cracks developed during the impact. The two cracks formed angles of 33° and 40,5° with the vertical axis of the column. The failure crack was the 33° crack. This 33° corresponded with the 34° failure shear crack of Column 2C. No horizontal cracks were visible after the impact loading.

Once again it was very interesting that the impact failure load was quite close to the static failure load. In the case of a typical flexural failure of the series 1 columns, the impact load the column could withstand was considerably higher than the static load the column could withstand. In other words, a column that would fail in shear during a static test is very suspect under impact loading.

The bottom strain gauge was damage during the impact. This damage occurred at about the time the "shear" crack reached the rear face of the column.

The axial load increased immediately with the impact and just after impact it started to decrease and kept decreasing, while the recorded axial load of Column 2C started to oscillate after the initial impact.

No static test was possible due to a complete shear failure of this column during the impact phase of the test.

Figures B.52 and B.53 show the visible crack pattern on both sides of the column after the impact test. Figures B.310 to B.333 show graphically the recorded test data.

Stellenbosch University http://scholar.sun.ac.za

B.8.12 Column 2E. (figures B.54 to B.57)

Reinforcement: Main: 4-Y16 + 4-Y16 (3,07 %)
Stirrups: 8-R8@250
Concrete cover: 21 mm

Concrete mix: Water - 27 kg
Cement - 54 kg
Sand - 114,68 kg
Stone - 169,54 kg

TABLE B.14: Details of concrete cubes from column 2E

NUMBER	CASTING DATE	DATE TESTED	AGE DAYS	MASS (kg)	SPLIT (kN)	FORCE (kN)	STRENGTH (MPa)
ML-2E1	02/05/88	09/05/88	7	8,42	114,7	589,79	26,21
ML-2E2	02/05/88	09/05/88	7	8,39	-	632,31	28,10
ML-2E3	02/05/88	09/05/88	7	8,35	102,3	594,22	26,41
ML-2E4	02/05/88	09/05/88	7	8,44	-	677,23	30,10
ML-2E5	02/05/88	30/05/88	28	8,38	-	842,79	37,46
ML-2E6	02/05/88	30/05/88	28	8,38	-	883,03	39,25

Impact phase of test on Column 2E

With this impact test it was tried to introduce an impact load to the column just below the previous impact shear failure load of Column 2D (165,6 kN). The maximum impact load on this column was 160,89 kN. This load was just lower than the failure impact load and thus, as expected, the column did not fail completely under this impact loading. This impact load was just higher than the static failure load of Column 2A of 158,21 kN.

Only one clear "shear" crack developed during the impact phase of this test. This crack formed an angle of 36,6° with the vertical axis of the column. This corresponded with the "shear" cracks of the other columns in this series of tests. (Column 2A - 38°; Column 2B - 39,6°; Column 2C - 34°; Column 2D - 33° & 40,5°.) Once again there was no visible horizontal cracks at the bottom of the column after the impact loading. The axial load increased immediately with the impact.

Stellenbosch University http://scholar.sun.ac.za

Figure B.54: Crack pattern of Column 2E seen from one side after the impact phase.

Figure B.55: Crack pattern of Column 2E seen from the other side of the column.

Stellenbosch University http://scholar.sun.ac.za

Figure B.56: Crack pattern of Column 2E seen from one side after the static test.

Figure B.57: Crack pattern of Column 2E seen from the other side of the column.

Stellenbosch University http://scholar.sun.ac.za

Static phase of test on Column 2E

After the impact test, a static test was done on the column to determine the reserve strength of the column. The column was step loaded with a static horizontal load in steps of 10 kN. During the static test the "shear" crack which developed during the impact loading phase, started to increase in width at quite a low horizontal load. No other diagonal cracks did develop during the static phase of this test. The original "shear" crack developed to form the shear failure mechanism.

At a maximum horizontal force of 157,5 kN the column failed in shear. This horizontal load corresponds with a flexural moment at the bottom of the column of 116,5 kNm. This column could just not reach the static failure load of column 2A of 158,31kN. Once again when the horizontal force was released there was no sign of rehabilitation of the column or that the cracks closed as in the case of the flexural failures of the column 1 series. Although this column performed much better under the static loading than the previous columns 2B, 2C and 2D the same conclusion, as with the other columns of series two, can be made. That is, that after an impact load was introduced to a shear failure type of column, the column could not reach the original static failure load of an undamaged column. This seems not to be the case with a column failing in flexure under static loading.

Again the axial load dropped as soon as a horizontal load was applied to the column before it suddenly started to increase as the horizontal load increased further. Once again this was due to the cracking of the column.

Unfortunately the strain gauge at the rear bottom of the column was damaged and thus the values of this strain gauge was unreliable. The damaged column 2E started to fail at a top deflection of just above 20 mm (the same as columns 2B and 2C) while the undamaged column 2A started to fail at a top deflection of just under 20 mm.

Stellenbosch University http://scholar.sun.ac.za

Figures B.54 and B.55 show the visible crack pattern on both sides of the column after the impact test. Figures B.56 and B.57 show the crack pattern after the static test. Figures B.334 to B.361 show graphically the recorded test data.

B.8.13 Column 3A. (figures B.58 to B.59)

Reinforcement: Main: 2-Y16 + 2-Y16 (1,53 %)
Stirrups: 14-R3@150
Concrete cover: 23 mm

Concrete mix: Water - 27 kg
Cement - 54 kg
Sand - 114,68 kg
Stone - 169,54 kg

TABLE B.15: Details of concrete cubes from column 3A

NUMBER	CASTING DATE	DATE TESTED	AGE DAYS	MASS (kg)	SLPIT (kN)	FORCE (kN)	STRENGTH (MPa)
ML-3A1	05/05/88	12/05/88	7	8,34	99,6	621,84	27,61
ML-3A2	05/05/88	12/05/88	7	8,38	-	613,29	27,26
ML-3A3	05/05/88	12/05/88	7	8,40	83,5	608,64	27,05
ML-3A4	05/05/88	12/05/88	7	8,36	-	623,33	27,71
ML-3A5	05/05/88	02/06/88	28	8,45	-	886,54	39,40
ML-3A6	05/05/88	02/06/88	28	8,38	-	904,93	40,22

Static test on Column 3A

The column was step loaded with a static horizontal load, in steps of 10 kN. With a 40 kN horizontal load (moment of 29,6 kNm at bottom of column) the first horizontal crack started to develop at the bottom of the column. With a 50 kN horizontal load two further horizontal cracks started to develop just above the first one. With a 60 kN horizontal load yet another horizontal crack developed higher up. The 50 kN and 60 kN horizontal cracks developed into diagonal cracks with angles of 40,5° and 54° with the vertical axis of the column, respectively.

Stellenbosch University http://scholar.sun.ac.za

Figure B.58: Crack pattern of Column 3A seen from one side after the static test.

Figure B.59: Crack pattern of Column 3A seen from the other side of the column.

Stellenbosch University http://scholar.sun.ac.za

Although the diagonal cracks did develop, the column failed in flexure with a static horizontal load of 116,97 kN. This horizontal load corresponds with a bending moment of 86,6 kNm at the bottom of the column. This maximum load was only reached after a considerable increase in the deflection of the column. From a horizontal load of about 105 kN the deflection increased considerably without an excessive increase in the applied load, indicating yielding of the reinforcement.

Again the axial load started to decrease as soon as a horizontal load was applied to the column before it suddenly started to increase as the horizontal load increased further. This was once again due to the cracking of the concrete. As previously mentioned, the first "flexural" crack was visible with a 40 kN horizontal load. On the graph of the axial loads (figure B.364) it can be seen that the axial load started to increase with the 40 kN horizontal load.

The strain at the rear bottom of the column continued to increase up to failure of the column. This meant that no crack reached the rear face of the column to release the compression strain on the rear side of the column.

At a top deflection of about 16 mm the column started to fail. At a deflection of 63 mm an ultimate load of 116,97kN was reached.

Figures B.58 and B.59 show the crack pattern after the static test. Figures B.362 to B.365 show graphically the recorded test data.

B.8.14 Column 3B. (figures B.60 to B.63)

Reinforcement: Main: 2-Y16 + 2-Y16 (1,53 %)
Stirrups: 14-R8@150
Concrete cover: 23 mm

Stellenbosch University http://scholar.sun.ac.za

Concrete mix: Water - 27 kg
Cement - 54 kg
Sand - 114,68 kg
Stone - 169,54 kg

TABLE B.16: Details of concrete cubes from column 3B

NUMBER	CASTING DATE	DATE TESTED	AGE DAYS	MASS (kg)	SPLIT (kN)	FORCE (kN)	STRENGTH (MPa)
ML-3B1	09/05/88	16/05/88	7	8,40	97,4	597,04	26,54
ML-3B2	09/05/88	16/05/88	7	8,37	-	603,34	26,82
ML-3B3	09/05/88	16/05/88	7	8,34	89,4	573,96	25,51
ML-3B4	09/05/88	16/05/88	7	8,37	-	587,43	26,12
ML-3B5	09/05/88	06/06/88	28	8,46	-	843,02	37,47
ML-3B6	09/05/88	06/06/88	28	8,38	-	833,63	37,05

Impact phase of test on Column 3B

With this impact test it was tried to introduce an impact load to the column which was the same in magnitude as the static failure load of Column 3A. Unfortunately the cable connecting the load plate (which measured the impact force) with the instruments broke just before impact and thus the impact load history could not be recorded. The impact load was estimated to be about 125 kN. This was just above the static failure load of 116,97kN of Column 3A.

During the impact two horizontal and two diagonal cracks developed. One of the horizontal cracks was right at the bottom of the column while the other one started about 140 mm from the bottom. The two diagonal cracks which formed angles of 40,5° and 54° with the vertical axis of the column. As was the case with the series one tests where flexural failure occurred the cracks closed after the impact and the damage did not look very serious.

The axial load increased immediately with the impact. Once again this indicated that the concrete cracked just after impact and thus the assumption of the theory of chapter 5 that the concrete cracks with impact is good.

Stellenbosch University http://scholar.sun.ac.za

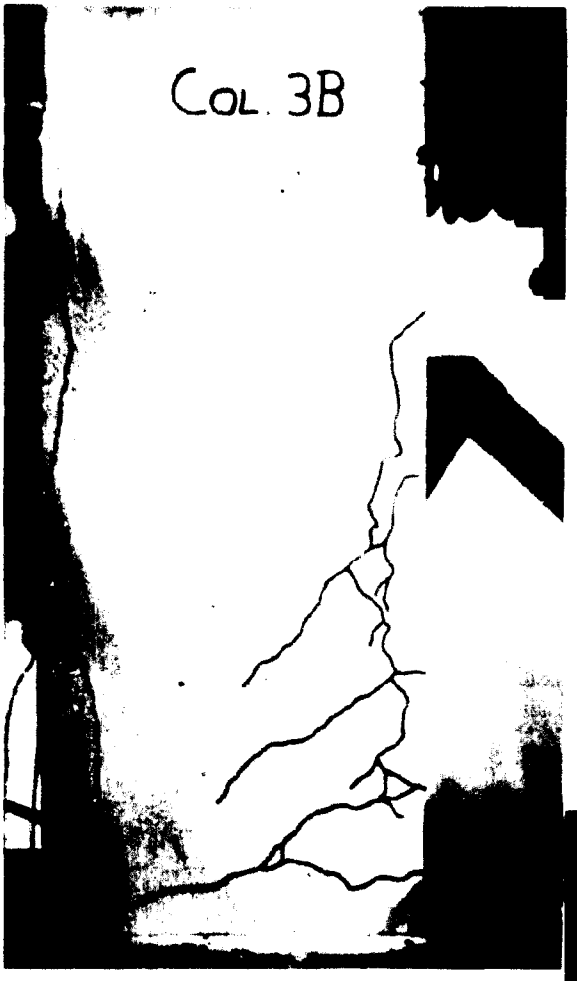

Figure B.60: Crack pattern of Column 3B seen from one side after the impact phase.

Figure B.61: Crack pattern of Column 3B seen from the other side of the column.

Stellenbosch University http://scholar.sun.ac.za

Figure B.62: Crack pattern of Column 3B seen from one side after the static test.

Figure B.63: Crack pattern of Column 3B seen from the other side of the column.

Stellenbosch University http://scholar.sun.ac.za

Static phase of test on Column 3B

After the impact test, a static test was done on the column to determine what load the column could withstand after such an impact. The column was step loaded with a static horizontal load in steps of 10 kN. During the static test the horizontal cracks soon started to enlarge, although they were slow to increase in length. The two diagonal cracks developed slowly but it never looked as if the column might fail in shear. The diagonal cracks angles of 40,5° and 54° corresponded very well with that of the static test of Column 3A.

The column failed at static horizontal load of 116,01 kN. This corresponds with a bending moment of 85,85 kNm at the bottom of the column. This static failure load was nearly exactly the same as that of Column 3A and Column 3C. This confirms the results of the series one tests that after an impact load was introduced to a flexural failure type of column, the reserve strength (under static loading) of the column is the same if not higher than the strength of an undamaged column like Column 3A.

The axial load immediately started to increase as soon as the horizontal load was applied. This happened because the column already had cracked under the impact loading and these cracks immediately enlarged as soon as the horizontal load was applied. This lengthened the column, resulting in the increased axial load.

As was found with the strain of Column 3A, the strain measured at the rear bottom of the column increased all the time during the test. This indicated that no cracks reached the rear face of the column, like in the shear failures of the number two series columns.

The damaged column 3B started to fail at a top deflection of around 27 mm while the undamaged column 3A started to fail at a top deflection of about 16 mm. This column failed completely at a deflection of 42 mm while Column 3A failed completely at a deflection of 63 mm.

Stellenbosch University http://scholar.sun.ac.za

Figures B.60 and B.61 show the visible crack pattern on both sides of the column after the impact test. Figures B.62 and B.63 show the crack pattern after the static test. Figures B.366 to B.392 show graphically the recorded test data.

B.8.15 Column 3C. (figures B.64 to B.67)

Reinforcement: Main: 2-Y16 + 2-Y16 (1,53 %)
Stirrups: 14-R8@150
Concrete cover: 23 mm

Concrete mix: Water - 27 kg
Cement - 54 kg
Sand - 114,68 kg
Stone - 169,54 kg

TABLE B.17: Details of concrete cubes from column 3C

NUMBER	CASTING DATE	DATE TESTED	AGE DAYS	MASS (kg)	SPLIT (kN)	FORCE (kN)	STRENGTH (MPa)
ML-3C1	12/05/88	19/05/88	7	8,42	100,7	592,43	26,33
ML-3C2	12/05/88	19/05/88	7	8,45	-	598,45	26,60
ML-3C3	12/05/88	19/05/88	7	8,37	111,2	590,06	26,22
ML-3C4	12/05/88	19/05/88	7	8,44	-	590,21	26,23
ML-3C5	12/05/88	09/06/88	28	8,36	-	891,69	39,63
ML-3C6	12/05/88	09/06/88	28	8,33	-	855,72	38,03

Impact phase of test on Column 3C

With this impact test it was tried to introduce an impact lod to the column which was greater than the static failure load of Column 3A. The impact load introduced to the column peaked at a load of 147,063 kN This was considerably higher (25,7% higher) than the static failure load of 116,97 kN of Column 3A.

Stellenbosch University http://scholar.sun.ac.za

Figure B.64: Crack pattern of Column 3C seen from one side after the impact phase.

Figure B.65: Crack pattern of Column 3C seen from the other side of the column.

Stellenbosch University http://scholar.sun.ac.za

Figure B.66: Crack pattern of Column 3C seen from one side after the static test.

Figure B.67: Crack pattern of Column 3C seen from the other side of the column.

Stellenbosch University http://scholar.sun.ac.za

During the impact two horizontal cracks and two diagonal cracks developed. One of the horizontal cracks was right at the bottom of the column while the other one started at about 75mm from the bottom. The two diagonal cracks formed angles of 37,3° and 53,4° with the vertical axis of the column. This crack pattern was nearly exactly the same as that of Columns 3A and 3B. As was the case with the series one tests where flexural failure (static loading) occurred, most of the cracks closed after the impact and the damage did not look very serious, although the cracks were a little bigger than that of the previous impact test of Column 3B.

The axial load increased immediately with the impact.

Static phase of test on Column 3C

After the impact test, a static test was done on the column to determine the reserve strength of the column. The column was step loaded with a static horizontal load in steps of 10 kN. During the static test the horizontal cracks soon started to enlarge although they were slow to increase in length. The two diagonal cracks developed slowly but it never looked as if the column can fail in shear. The diagonal cracks angles of 37,3° and 53,4° corresponded with that of the static tests of Columns 3A and 3B.

The column failed at static horizontal load of 115,39 kN. This corresponds with a bending moment of 85,4 kNm at the bottom of the column. This static failure load was nearly exactly the same as that of Column 3A and Column 3B. This confirmed the results of the series one tests that after an impact load was introduced to a flexural failure type of column (static loading) the reserve strength of the column would be the same if not higher than the static strength of an undamaged column, like Column 3A.

The axial load again dropped a little but then it stayed nearly constant for most of the test except that at the end of the test in started to increase. Unfortunately the load beam started to for a plastic hinge resulting in the constant axial load on the column.

Stellenbosch University http://scholar.sun.ac.za

The damaged Column 3C started to fail at a top deflection of around 25 mm while the undamaged Column 3A started to fail at a top deflection of about 16 mm. This column and Column 3B failed completely at deflections of 44 mm and 42 mm respectively, while Column 3A failed completely at a deflection of 63 mm. This indicated that the longitudinal steel of column 3A had to be work hardened before it could reach that ultimate failure load, while Column's 3B and 3C have already been work hardened by the impact loading.

Figures B.64 and B.65 show visible the crack pattern on both sides of the column after the impact test. Figures B.66 and B.67 show the crack pattern after the static test. Figures B.393 to B.420 show graphically the recorded test data.

B.8.16 Column 3D. (figures B.68 to B.71)

Reinforcement: Main: 2-Y16 + 2-Y16 (1,53 %)
Stirrups: 14-R8@150
Concrete cover: 23 mm

Concrete mix:

Water	-	27 kg
Cement	-	54 kg
Sand	-	114,68 kg
Stone	-	169,54 kg

TABLE B.18: Details of concrete cubes from column 3D

NUMBER	CASTING DATE	DATE TESTED	AGE DAYS	MASS (kg)	SPLIT (kN)	FORCE (kN)	STRENGTH (MPa)
ML-3D1	16/05/88	23/05/88	7	8,42	109,4	569,43	25,31
ML-3D2	16/05/88	23/05/88	7	8,39	-	569,08	25,29
ML-3D3	16/05/88	23/05/88	7	8,43	90,9	552,68	24,56
ML-3D4	16/05/88	23/05/88	7	8,37	-	572,44	25,44
ML-3D5	16/05/88	13/06/88	28	8,36	-	823,14	36,58
ML-3D6	16/05/88	13/06/88	28	8,40	-	820,85	36,48

Stellenbosch University http://scholar.sun.ac.za

Figure B.68: Crack pattern of Column 3D seen from one side after the impact phase.

Figure B.69: Crack pattern of Column 3D seen from the other side of the column.

Stellenbosch University http://scholar.sun.ac.za

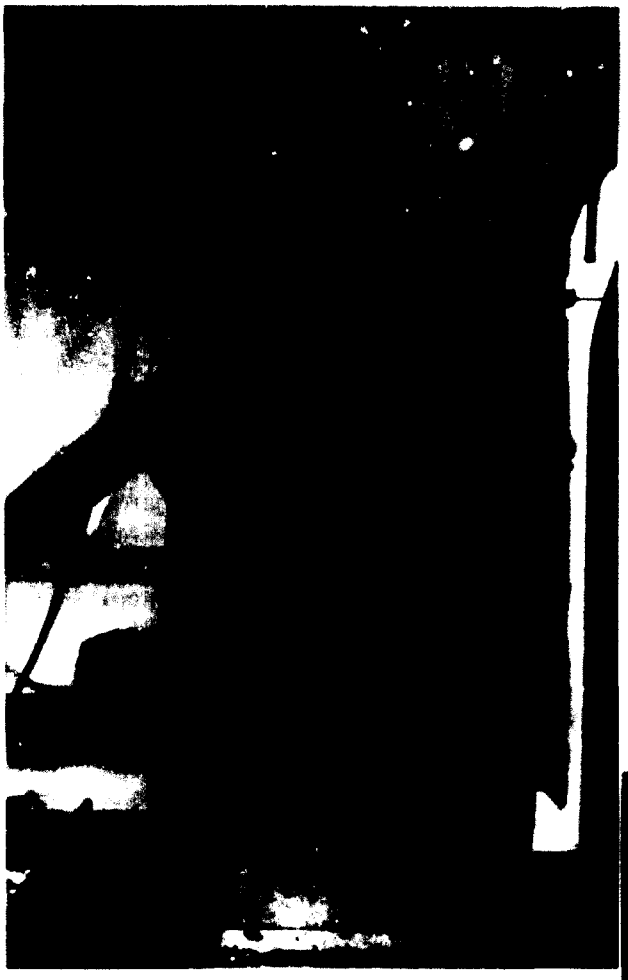

Figure B.70: Crack pattern of Column 3D seen from one side after the static test.

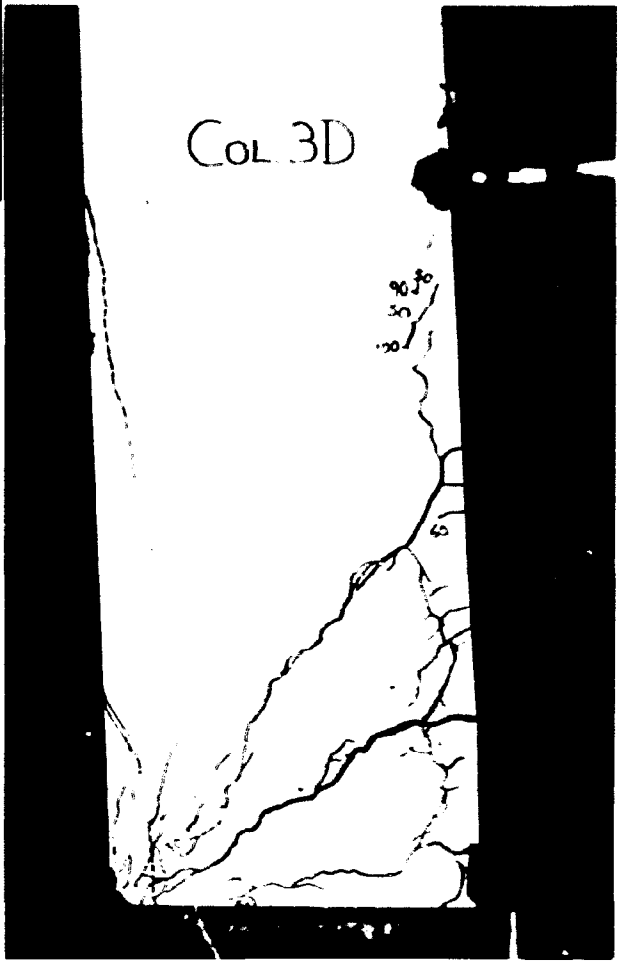

Figure B.71: Crack pattern of Column 3D seen from the other side of the column.

Stellenbosch University http://scholar.sun.ac.za

Impact phase of test on Column 3D

With this impact test it was tried to introduce an impact load to the column which was greater than the impact load on Column 3C. The impact loading introduced to the column peaked at a load of 178,42kN compared to the load of 147.063 kN of Column 3C. These was considerably higher (53,5% higher) than the static failure load of 116,97 kN of Column 3A and 21,3% higher than the impact load on Column 3C.

During the impact two major horizontal and two major diagonal cracks developed. One of the horizontal cracks was right at the bottom of the column while the other one started 70mm above the bottom. The two diagonal cracks which formed angles of 38.5° and 56,6° with the vertical axis of the column. This crack pattern was nearly exactly the same as that of Columns 3A, 3B and 3C. As was the case with the series one tests where flexural failure occurred, the cracks closed after the impact.

The graphs (figures B.422 and B.424) of the axial loads indicate a very small decrease with impact and then it immediately increased to nearly double the original axial load on the column. The axial load oscillated around a higher median than the original load. This indicated that the column had permanent damage as was indicated by the diagonal crack of 56,6°.

Static phase of test on Column 3D

After the impact test, a static test was done on the column to determine the reserve strength of the column. The column was step loaded with a static horizontal load in steps of 10 kN. During the static test, the horizontal cracks soon started to enlarge although they were slow to increase in length. The two diagonal cracks developed slowly. The one crack of 56,6° was a few millimeters wide at the start of the static test and it looked as if the column might fail in shear. The diagonal cracks angles of 38,5° and 56,6° corresponded with the static tests of Columns 3A, 3B and 3C.

Stellenbosch University http://scholar.sun.ac.za

The column failed at static horizontal load of 118,31 kN. This corresponds with a flexural moment of 87,5 kNm at the bottom of the column. This static failure load was nearly exactly the same as that of Columns 3A, 3B and 3C. This once again confirmed the results of the series one tests, that is, that after an impact load was introduced to a flexural failure type of column (under static loading) the static reserve strength of the column would be the same if not higher than the static strength of an undamaged column, like Column 3A.

Similar to Column 3B, the axial load immediately started to increase as soon as the static horizontal load was applied. This indicated that the column was damaged during the impact loading and that the cracks immediately started to enlarge as soon as the horizontal load was applied.

The strain measured at the rear bottom of the column increased all the time during the static test, similar to the behaviour of the strains of Columns 3A, 3B and 3C. This indicated that no cracks reached the rear face of the column, like in the shear failures of the number two series columns, to slightly release the strain.

The damaged column 3D started to fail at a top deflection of about 25 mm while the undamaged column 3A started to fail at a top deflection of about 16 mm. This column and Columns 3B and 3C failed completely at deflections of 48 mm, 44 mm and 42 mm respectively, while Column 3A failed completely at a deflection of 63 mm.

Figures B.68 and B.69 show the visible crack pattern on both sides of the column after the impact test. Figures B 70 and B.71 show the crack pattern after the static test. Figures B.421 to B.448 show graphically the recorded test data.

Stellenbosch University http://scholar.sun.ac.za

B.8.17 Column 3E, (figures B.72 to B.75)

Reinforcement: Main: 2 Y16 + 2 Y16 (1,53 %)
Stirrups: 14 R8@150
Concrete cover: 23 mm

Concrete mix:

Water		27,5 kg
Cement		55,0 kg
Sand	-	114,68 kg
Stone	-	169,54 kg

TABLE B.19: Details of concrete cubes from column 3E

NUMBER	CASTING DATE	DATE TESTED	AGE DAYS	MASS (kg)	SPLIT (kN)	FORCE (kN)	STRENGTH (MPa)
ML-3E1	16/06/88	23/06/88	7	8,46	138,7	684,90	30,44
ML-3E2	16/06/88	23/06/88	7	8,40	-	725,68	32,25
ML-3E3	16/06/88	23/06/88	7	8,41	118,3	684,86	30,44
ML-3E4	16/06/88	23/06/88	7	8,37	-	756,58	33,63
ML-3E5	16/06/88	14/07/88	28	8,48	-	1005,53	44,69
ML-3E6	16/06/88	14/07/88	28	8,46	-	1038,71	46,16

Impact phase of test on Column 3E

With this impact test it was tried to introduce an impact load to the column which was greater than the impact load on Column 3D. The impact loading introduced to the column peaked at a load of 206,4316 kN compared to the load of 178,42 kN of Column 3D. This was considerably higher (76,5% higher) than the static failure load of 116,97 kN of Column 3A and 15,7% higher than the impact load on Column 3D.

During the impact two major horizontal and two major diagonal cracks developed. One of the horizontal cracks was right at the bottom of the column while the other one started about 50 mm above the bottom of the column. The two major diagonal cracks formed angles of 46,7° and 61,5° with the vertical axis of the column. This crack pattern differed from that of Columns 3A, 3B, 3C and 3D. This difference was probably due to the considerable difference in the concrete strength of this column and the other

Stellenbosch University http://scholar.sun.ac.za

columns in this series. As was the case with the series one tests where flexural failure occurred the cracks closed after the impact. This column was supposed to fail during the impact test but it did not, because of the higher concrete strength. Although it did not fail, it was clear from the cracks etc. that this column was on the verge of failure during the impact loading phase.

At this stage it looked as if a column will not fail in flexure, but that it would rather fail in shear.

The graphs (figures B.450 and B.452) of the axial loads indicated a small decrease with impact and then it immediately increased to nearly double the original axial load on the column. The axial load oscillated around a higher median than the value of the original load. This indicated permanent damage of the column.

Similar impact load histories were present with all the other impact tests. A third peak on the load function indicated the column "impacting" the striker again due to the oscillation of the column.

Static phase of test on Column 3E

After the impact test, a static test was done on the column to determine the reserve strength of the column. The column was step loaded with a static horizontal load in steps of 10 kN. During the static test the major horizontal cracks soon started to enlarge. The two major diagonal cracks developed slowly and in the end it looked as if the column might fail in shear.

The column failed at static horizontal load of 119,5594 kN. This corresponds with a bending moment of 88,5 kNm at the bottom of the column. This static failure load was similar to that of Columns 3A, 3B, 3C and 3D. This confirmed the results of the series one tests, that is, that after an impact load was introduced to a flexural failure type of column (static test) the reserve strength of the column would be the same region as the static failure strength of an undamaged column like. Column 3A.

Stellenbosch University http://scholar.sun.ac.za

Figure B.92: Crack patterns of Column 3F seen from one side after the first load cycle

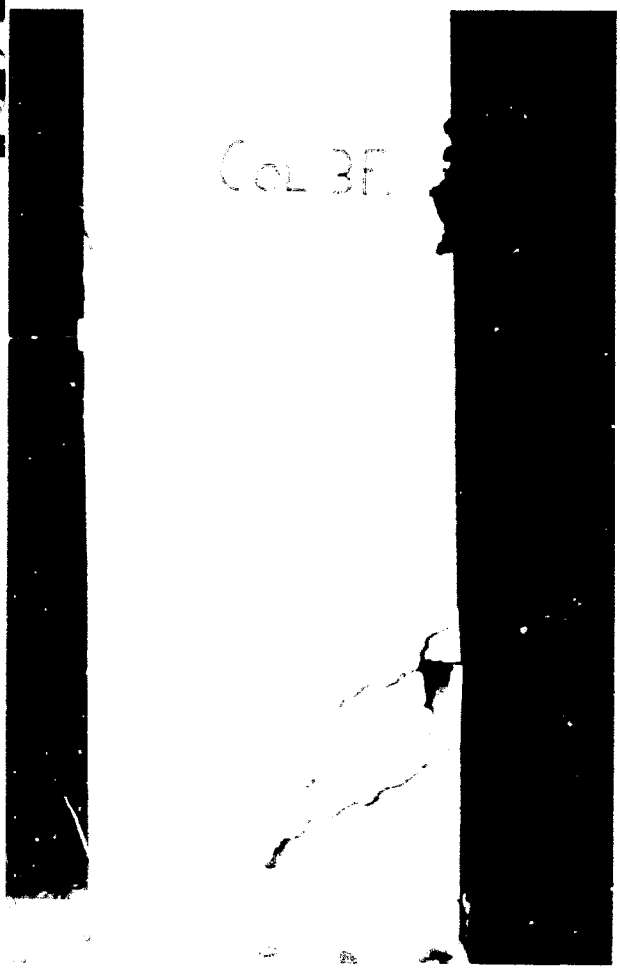

Figure B.93: Crack patterns of Column 3F seen from the other side of the beam

Stellenbosch University http://scholar.sun.ac.za

Figure B.74: Crack pattern of Column 3E seen from one side after the static test.

Figure B.75: Crack pattern of Column 3E seen from the other side of the column.

Stellenbosch University http://scholar.sun.ac.za

Similar to the static tests of Column 3B and 3D, the axial load immediately started to increase as soon as the static horizontal load was applied. This indicated that the column was damaged during impact and that the cracks immediately started to enlarge and thus increased the length of the column and the axial load on the column.

Once again the bottom strain gauge indicated that no cracks reached the rear face of the column, unlike the case with the shear failures of the number two series of columns.

The damaged Column 3E started to fail at a top deflection of around 38 mm while the undamaged column 3A started to fail at a top deflection of about 16 mm. This indicated that considerable damage was done to this column with the impact loading. This column and Columns 3B, 3C and 3D failed completely at deflections of 56 mm, 44 mm, 42 mm and 48 mm respectively, while Column 3A failed completely at a deflection of 63 mm.

Figures B.72 and B.73 show the visible crack pattern on both sides of the column after the impact test. Figures B.74 and B.75 show the crack pattern after the static test. Figures B.449 to B.476 show graphically the recorded test data.

B.8.18 Column 4A. (figures B.76 to B.77)

Reinforcement: Main: 2-Y16 + 2-Y16 (1,53 %)
Stirrups: 10-R8@200
Concrete cover: 23 mm

Concrete mix:		
	Water	27,5 kg
	Cement	55 kg
	Sand	114,68 kg
	Stone	169,54 kg

Stellenbosch University http://scholar.sun.ac.za

TABLE B.20: Details of concrete cubes of column 4A

NUMBER	CASTING DATE	DATE TESTED	AGE DAYS	MASS (kg)	SLPIT (kN)	FORCE (kN)	STRENGTH (MPa)
ML-4A1	23/05/88	30/05/88	7	8,36	113,7	665,10	29,56
ML-4A2	23/05/88	30/05/88	7	8,40	-	704,31	31,30
ML-4A3	23/05/88	30/05/88	7	8,42	121,5	670,84	29,82
ML-4A4	23/05/88	30/05/88	7	8,44	-	733,04	32,58
ML-4A5	23/05/88	20/06/88	28	8,44	-	931,14	41,38
ML-4A6	23/05/88	20/06/88	28	8,41	-	947,69	42,12

Static test on Column 4A

The column was step loaded with a static horizontal load in steps of 10 kN. At a 50 kN horizontal load (moment of 37,0 kNm) the first horizontal crack started to develop at the bottom of the column. This horizontal crack was quite a long crack which suggested that the crack started to develop just after the load was increased from 40 kN to 50 kN. At 50 kN horizontal load two more diagonal cracks formed. The diagonal cracks formed angles of 40,5° and 65,4° respectively with the vertical axis of the column.

Initially it looked as if the column would fail in flexure because the horizontal cracks kept widening, while the diagonal cracks stayed dormant. With a horizontal load of just under 70 kN the one diagonal crack forming an angle of about 45° with the vertical axis of the column suddenly increased in width. With a 80 kN horizontal load it looked as if the column might fail in shear along this 45° diagonal crack. With a 90 kN load this diagonal crack reached the back face of the column. At a 100 kN load the development of the diagonal crack stopped and the column started to fail in flexure. The deflection started to increase dramatically while the horizontal force increased only slightly. The horizontal force reached an ultimate load of 116,16 kN (corresponding with a bending moment of 86 kNm at the bottom of the column). Typical to a flexural failure the cracks closed as soon as the horizontal force subsided to zero although their was a permanent deflection present.

Stellenbosch University http://scholar.sun.ac.za

Again the axial load started to drop as soon as the horizontal load was applied to the column, before it suddenly started to increase as the horizontal load increased further. As previously mentioned, the first horizontal crack was visible between a 40 and 50 kN horizontal load. The graphs of the axial loads (figure B.479) show that the axial load started to increase between the 40 kN and 50kN horizontal loads. Thus the graph corresponded very well with the crack development of the column. With a 100 kN horizontal load, the column started to fail in flexure. This is also clearly visible on the graphs (figure B.479) of the axial loads, because the axial loads rose considerably at that stage. This considerable rise can be explained by the increasing crack widths resulting in a lengthening of the column and thus a higher axial load.

The graph of the strain (figure B.478) at the rear bottom of the column is a very good indication of the failing mechanism of the column. Up to about a 70 kN horizontal load the flexural mechanism was the dominant mechanism and thus the strain increased considerably. From just under 70 kN up to about 90 kN the shear mechanism was the dominant factor and this is clearly visible on the strain graph because in that area the increase in strain was quite small compared to the previous part of the test. At 90 kN the shear crack reached the back face of the column and on the graph it can be seen that the strain was slightly released. At this stage the flexural mechanism took over, resulting in only a slight decrease in the strain.

At a top deflection of about 17 mm the column started to fail. At a deflection of 48 mm the column reach an ultimate load of 116,16 kN.

Figures B.76 and B.77 show the crack pattern after the static test. Figures B.477 to B.480 show graphically the recorded test data.

Stellenbosch University http://scholar.sun.ac.za

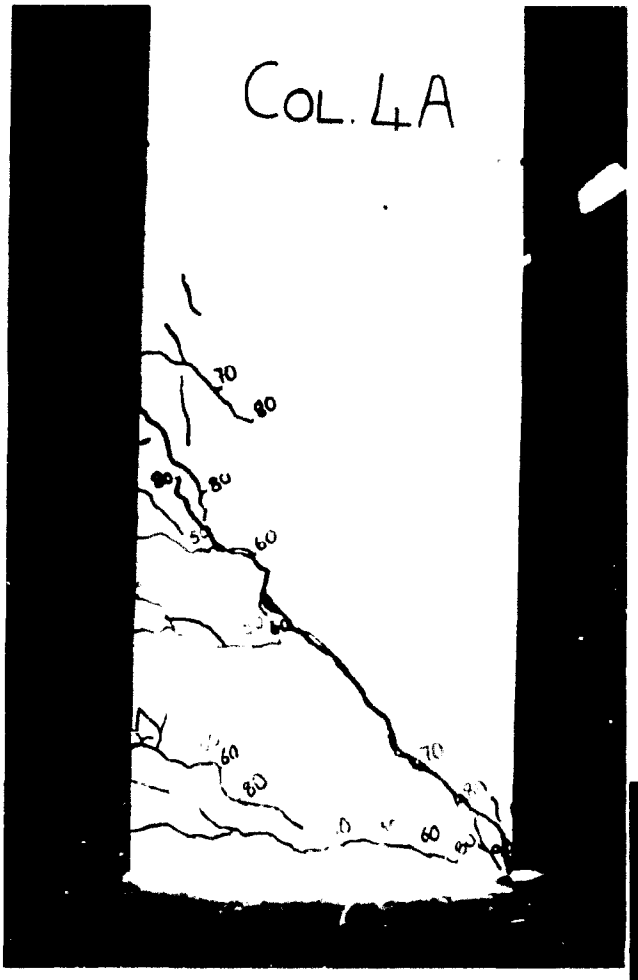

Figure B.76: Crack pattern of Column 4A seen from one side after the static test.

Figure B.77: Crack pattern of Column 4A seen from the other side of the column.

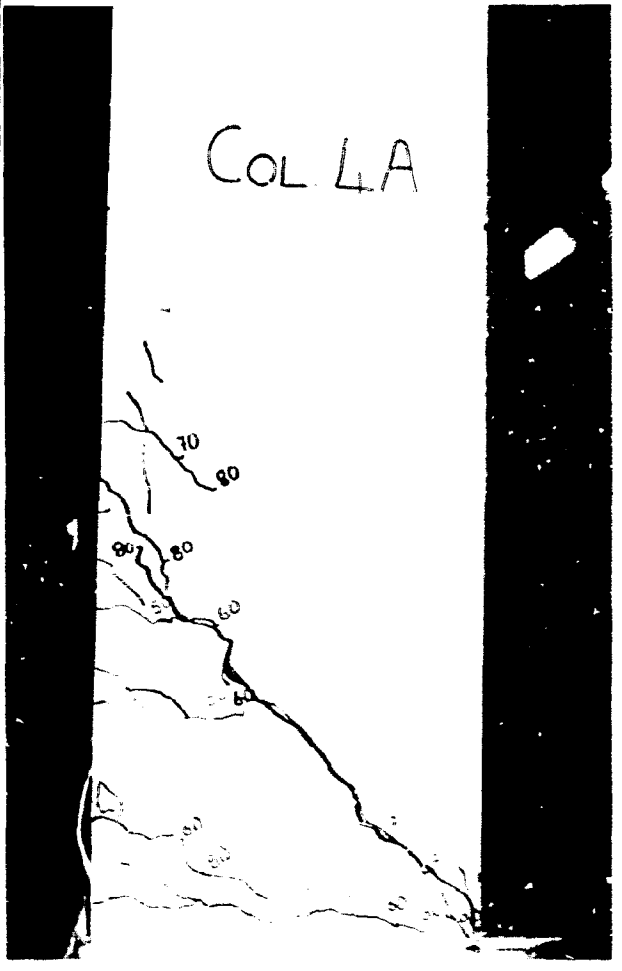

Stellenbosch University http://scholar.sun.ac.za

B.8.19 Column 4B. (figures B.78 to B.81)

Reinforcement: Main: 2-Y16 + 2-Y16 (1,53 %)
Stirrups: 10-R8@200
Concrete cover: 23 mm

Concrete mix: Water - 27,5 kg
Cement - 55 kg
Sand - 114,68 kg
Stone - 169,54 kg

TABLE B.21: Details of concrete cubes from column 4B

NUMBER	CASTING DATE	DATE TESTED	AGE DAYS	MASS (kg)	SPLIT (kN)	FORCE (kN)	STRENGTH (MPa)
ML-4B1	26/05/88	02/06/88	7	8,34	112,4	632,71	28,12
ML-4B2	26/05/88	02/06/88	7	8,42	-	624,55	27,76
ML-4B3	26/05/88	02/06/88	7	8,43	101,7	630,18	28,01
ML-4B4	26/05/88	02/06/88	7	8,42	-	622,69	27,68
ML-4B5	26/05/88	23/06/88	28	8,38	-	862,21	38.32
ML-4B6	26/05/88	23/06/88	28	8,60	-	857,90	38,13

Impact phase of test on Column 4B

With this impact test it was tried to introduce an impact load to the column which was the same in magnitude as the failure load of the static test of Column 4A. The impact loading introduced to the column peak at a maximum load of 154,425 kN. This peak was the first peak of the load function and of very short duration (only about 0,3ms). The second peak was lower than the first peak and peaked at 121,6 kN. This longer duration peak was the important one and it compared favourably with the static failure load of 116,16 kN of Column 4A.

During the impact two major horizontal cracks and two major diagonal cracks developed. One of the horizontal cracks was right at the bottom of the column while the other one started about 75mm above the bottom of the column. The two major diagonal cracks formed angles of 41,2° and 50° with the vertical axis of the column.

Stellenbosch University http://scholar.sun.ac.za

Just after the impact loading started, the axial load dropped slightly but immediately after the slight drop it increased.

Static phase of test on Column 4B

After the impact test, a static test was done on the column to determine the static reserve strength of the column. The column was step loaded with a static horizontal load in steps of 10 kN. During the static test the horizontal cracks soon started to increase in width although they were slow to increase in length. The two major diagonal cracks developed slowly and it never looked as if the column would fail in shear. The diagonal cracks angles of 41,2° and 60° corresponded very well with the diagonal cracks of the static test of Column 4A (45° and 60°).

The column failed in flexure at a static horizontal load of 116,88 kN. This corresponds with a flexural moment of 85,65 kNm at the bottom of the column. This static failure load was nearly exactly the same as that of Column 4A (116,16 kN). This once again confirmed the results of the series one tests, that is, that after an impact load was introduced to a flexural failure type of column (static test) the reserve static strength of the column would be similar to that of an undamaged column like Column 4A.

In this case the axial load did not drop but it immediately started to increase as soon as the horizontal load was applied. This happened because existing cracks immediately started to enlarge as soon as the horizontal force was applied and this lead to the lengthening the column and an increased axial load.

The damaged column 4B started to fail at a top deflection of about 30 mm while the undamaged column 4A started to fail at a top deflection of 16 - 17 mm. This column failed completely at a top deflection of 48 mm while Column 4A also failed completely at a top deflection of 48 mm.

Stellenbosch University http://scholar.sun.ac.za

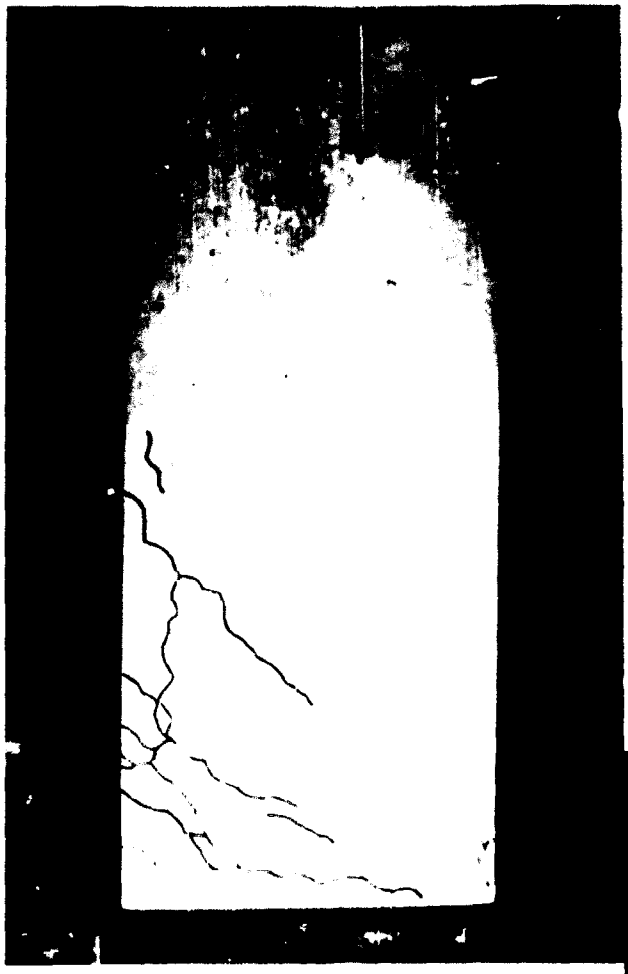

Figure B.78: Crack pattern of Column 4B seen from one side after the impact phase.

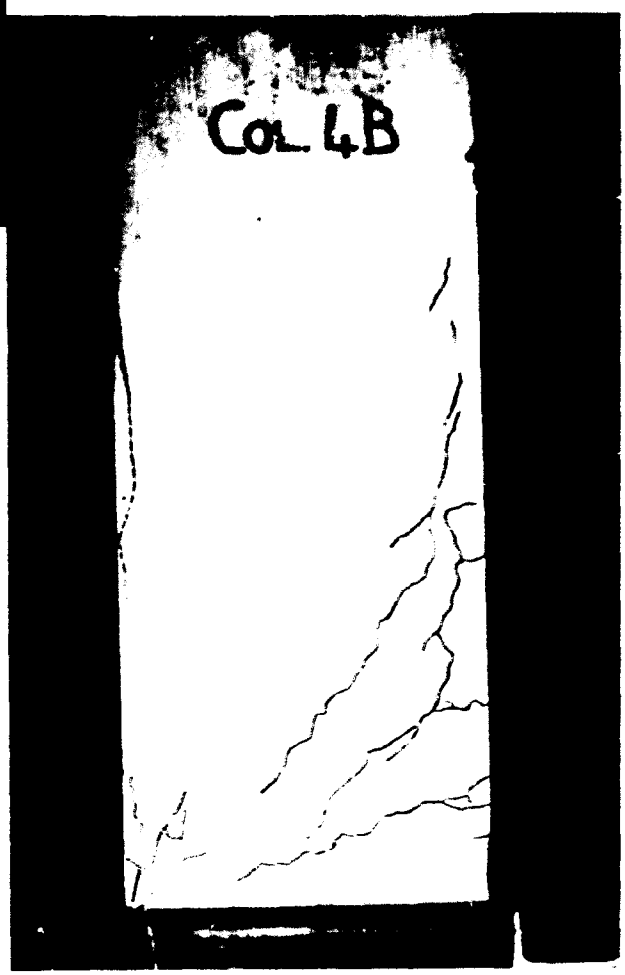

Figure B.79: Crack pattern of Column 4B seen from the other side of the column.

Stellenbosch University http://scholar.sun.ac.za

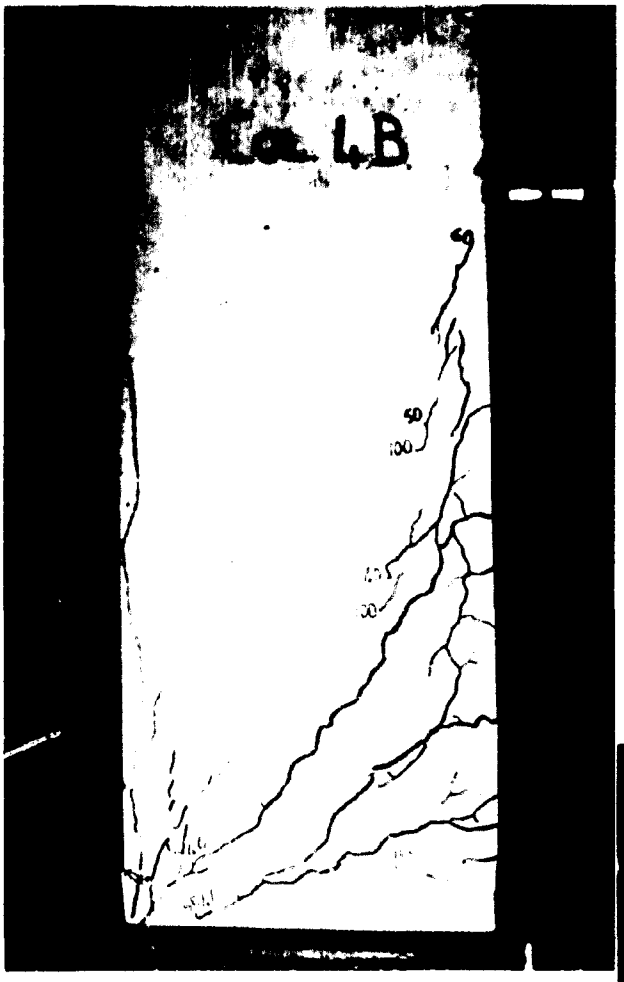

Figure B.80: Crack pattern of Column 4B seen from one side after the static test.

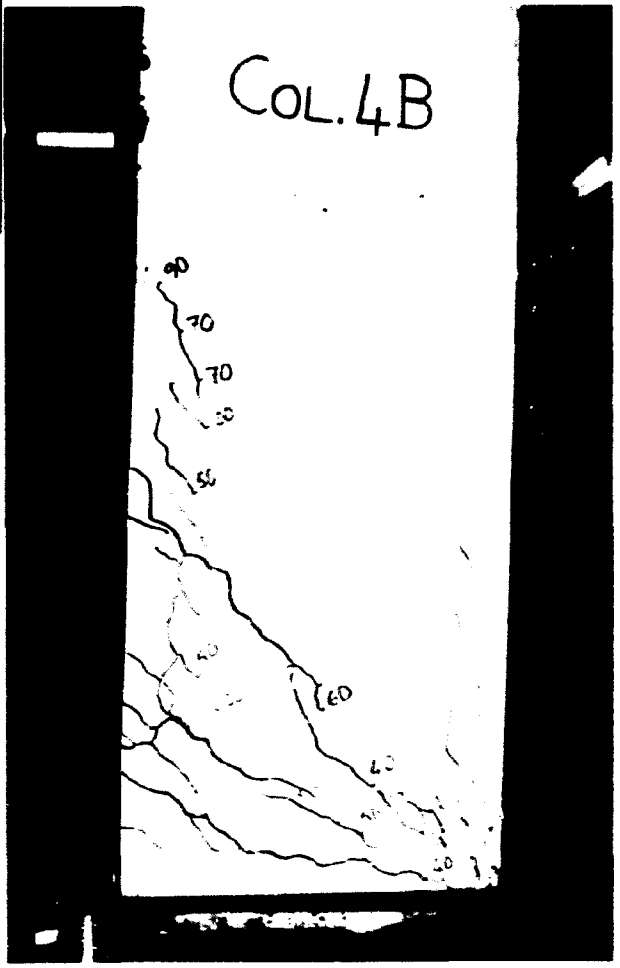

Figure B.81: Crack pattern of Column 4B seen from the other side of the column.

Stellenbosch University http://scholar.sun.ac.za

Figures B.78 and B.79 show the visible crack pattern on both sides of the column after the impact test. Figures B.80 and B.81 show the crack pattern after the static test. Figures B.481 to B.508 show graphically the recorded test data.

B.8.20 Column 4C. (figures B.82 to B.85)

Reinforcement: Main: 2-Y16 + 2-Y16 (1,53 %)
Stirrups: 10-R8@200
Concrete cover: 23 mm

Concrete mix: Water - 27,5 kg
Cement - 55 kg
Sand - 114,68 kg
Stone - 169,54 kg

TABLE B.22: Details of concrete cubes from column 4C

NUMBER	CASTING DATE	DATE TESTED	AGE DAYS	MASS (kg)	SPLIT (kN)	FORCE (kN)	STRENGTH (MPa)
ML-4C1	30/05/88	06/06/88	7	8,42	107,6	621,19	27,61
ML-4C2	30/05/88	06/06/88	7	8,39	-	653,08	29,03
ML-4C3	30/05/88	06/06/88	7	8,48	90,8	626,42	27,84
ML-4C4	30/05/88	06/06/88	7	8,46	-	649,19	28,85
ML-4C5	30/05/88	27/06/88	28	8,38	-	866,06	38,49
ML-4C6	30/05/88	27/06/88	28	8,50	-	866,51	38,51

Impact phase of test on Column 4C

With this impact test it was tried to introduce an impact load to the column which was much greater in magnitude as the failure load of the static test of Column 4A. The impact loading applied to the column peak at a value of 151,42 kN. This peak was the longer duration peak, in other words the second peak, and thus the important one. This peak was 30,3% higher than that of the static failure load of Column 4A (116,16 kN). Although this load was considerably higher than the static failure load of Column 4A, the column did not fail with the impact loading.

Stellenbosch University http://scholar.sun.ac.za

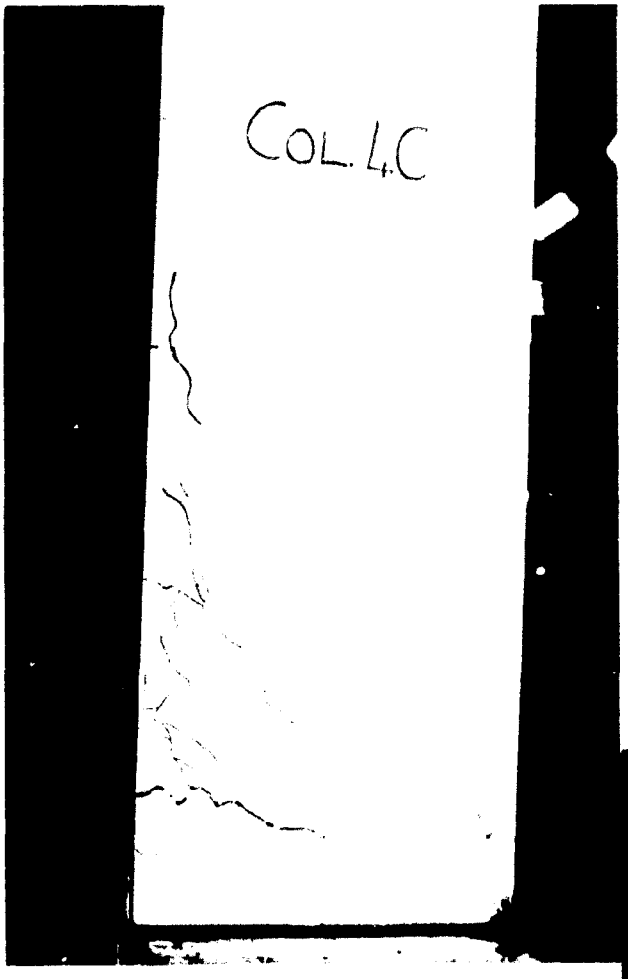

Figure B.82: Crack pattern of Column 4C seen from one side after the impact phase.

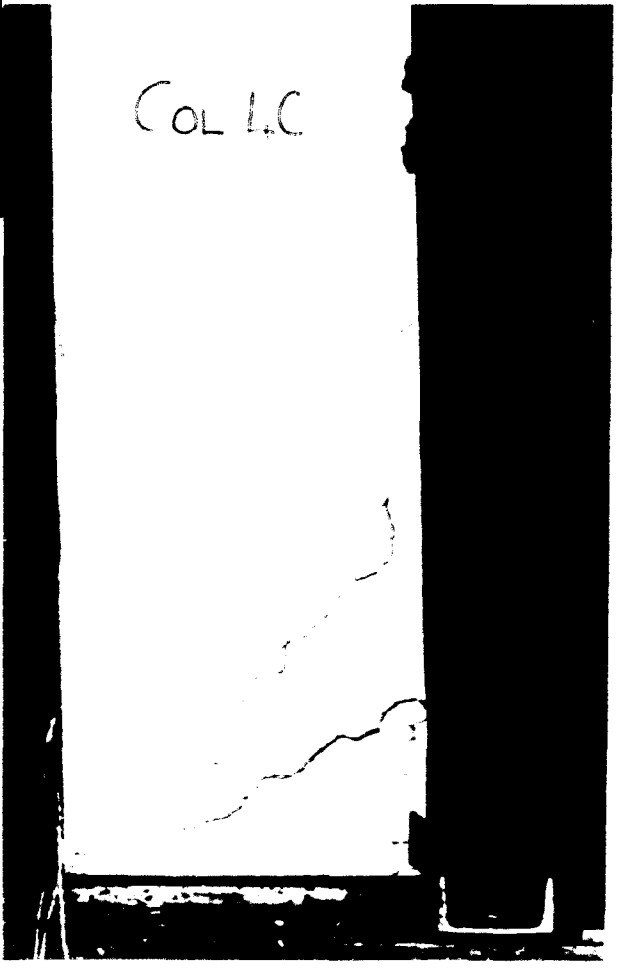

Figure B.83: Crack pattern of Column 4C seen from the other side of the column.

Stellenbosch University http://scholar.sun.ac.za

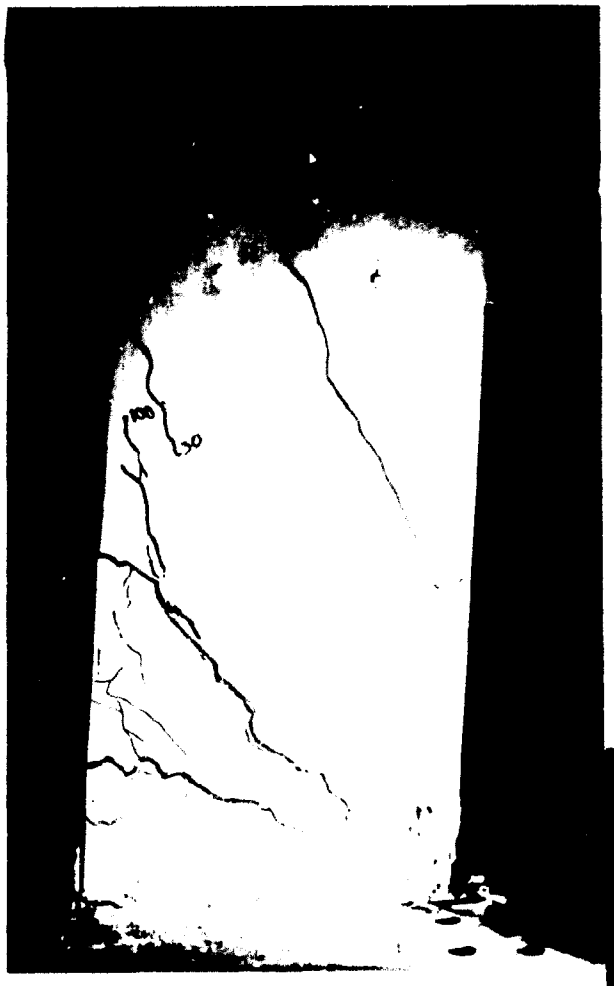

Figure B.84: Crack pattern of Column 4C seen from one side of the column.

Figure B.85: Crack pattern of Column 4C seen from the other side of the column.

Stellenbosch University http://scholar.sun.ac.za

During the impact phase of this test one of the bars connecting the sway frames with the axial load beam snapped (due to metal fatigue) and released all the axial load on the column. This happened just after the start of the impact loading. Up to that stage of the test the results were reliable, but after that point the results should be seen in the context of no axial load on the column.

During the impact two major horizontal cracks and two major diagonal cracks developed. One of the horizontal cracks was right at the bottom of the column while the other one started at about 75mm above the bottom. The two diagonal cracks formed angles of 44,2° and 62,7° with the vertical axis of the column.

Just after the impact loading started, the axial load dropped slightly before it immediately started to increase. During this increase phase, axial load beam snapped and the axial load dropped to zero. The increase in the axial load was once again due to the cracking of the concrete resulting in an increased length of the column and thus an icreased axial load.

Static phase of test on Column 4C

After the impact test, a static test was done on the column to determine the static reserve strength of the column. The column was step loaded with a static horizontal load in steps of 10 kN. During the static test the horizontal cracks soon started to increase in width, although they were slow to increase in length. The two major diagonal cracks developed slowly and it never looked as if the column would fail in shear. The diagonal cracks angles of 44,2° and 62,7° corresponded with the diagonal cracks of the static test of Column 4A of 45° and 60°.

The column failed at a static horizontal load of 116,97 kN. This corresponds with a bending moment of 86,6 kNm at the bottom of the column. This static failure load was nearly exactly the same as that of Columns 4A and 4B (116,16 and 116,88 kN respectively). This confirmed the results of the series one tests, that is, that after an impact load was introduced to a flexural failure type of

Stellenbosch University http://scholar.sun.ac.za

column (static test) the static reserve strength of the column would be similar to the static strength of an undamaged column, like Column 4A.

The axial load immediately started to increase as soon as the horizontal load was applied. Existing cracks immediately increased in width as soon as the static horizontal load was applied. This lengthened the column, resulting in the increase in the axial load.

The damaged column 4C started to fail at a top deflection of around 32 mm while the undamaged column 4A started to fail at a top deflection of about 16 - 17 mm. This column failed completely at a deflection of 52 mm, while Column 4A failed completely at a deflection of 48 mm as well.

Figures B.82 and B.83 show the visible crack pattern on both sides of the column after the impact test. Figures B.84 and B.85 show the crack pattern after the static test. Figures B.509 to B.536 show graphically the recorded test data.

B.8 21 Column 4D. (figures B.86 to B.87)

Reinforcement: Main: 2-Y16 + 2-Y16 (1,53 %)
Stirrups: 10-R8@200
Concrete cover: 23 mm

Concrete mix:	Water	-	27,5 kg
	Cement	-	55 kg
	Sand	-	114,68 kg
	Stone	-	169,54 kg

Stellenbosch University http://scholar.sun.ac.za

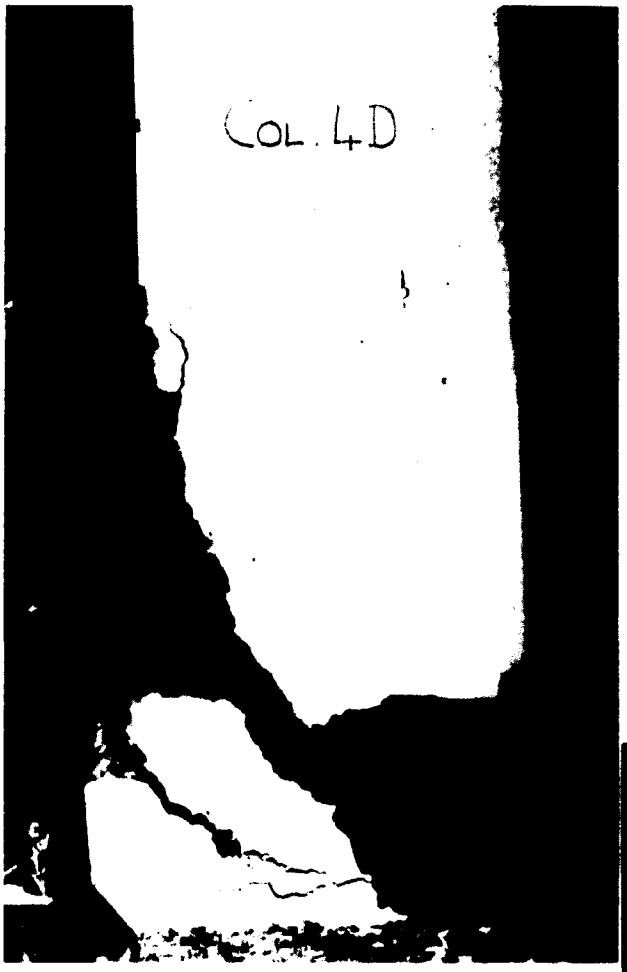

Figure B.86: Failure and crack pattern of Column 4D seen from one side after the impact phase.

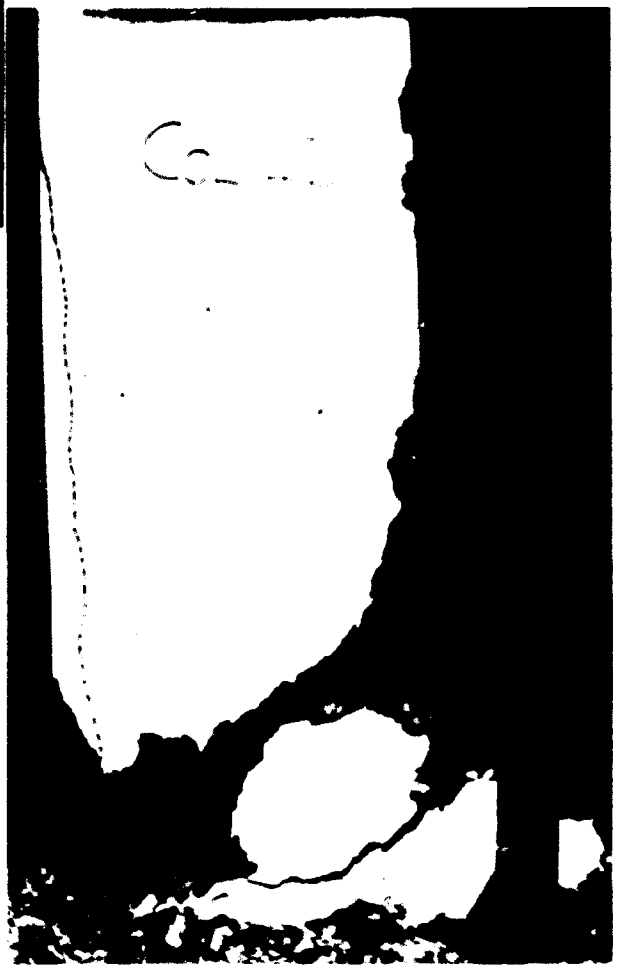

Figure B.87: Failure and crack pattern of Column 4D seen from the other side of the column.

Stellenbosch University http://scholar.sun.ac.za

TABLE B.23: Details of concrete cubes from column 4D

NUMBER	CASTING DATE	DATE TESTED	AGE DAYS	MASS (kg)	SPLIT (kN)	FORCE (kN)	STRENGTH (MPa)
ML-4D1	02/06/88	09/06/88	7	8,44	122,1	658,04	29,25
ML-4D2	02/06/88	09/06/88	7	8,48	-	681,81	30,30
ML-4D3	02/06/88	09/06/88	7	8,52	110,2	629,81	28,00
ML-4D4	02/06/88	09/06/88	7	8,48	-	676,62	30,07
ML-4D5	02/06/88	30/06/88	28	8,45	-	861,44	38,29
ML-4D6	02/06/88	30/06/88	28	8,46	-	845,54	37,58

Impact phase of test on Column 4D

With this impact test it was tried to introduce an impact force to the column which was greater than the impact force on Column 4C and one that should force impact failure of the column. The impact loading applied to the column peaked at a load of 197,46kN compared to the peak load of 151.42 kN of Column 4C. This was considerably higher (70,0% higher) than the static failure load of 116,16 kN of Column 4A and 30,4% higher than the impact load on Column 4C. The column failed in shear under the impact loading.

During the impact two major horizontal cracks and two major diagonal cracks developed. One of the horizontal cracks was right at the bottom of the column while the other one started about 50 mm above the bottom of the column. The two major diagonal cracks formed angles of 34,7° and 60,2° with the vertical axis of the column. This crack pattern was ver similar to that of Columns 4A and 4B. The column failed along the 34,7° diagonal crack in shear.

Unfortunately the rear bottom strain gauge was damaged during the impact test and the readings after about 45 ms was unreliable. The damage to this strain gauge gave an indication of the time when the diagonal crack reached the rear face of the column. This showed that the crack reached the rear face of the column just after the peak of the impact loading was registered.

Stellenbosch University http://scholar.sun.ac.za

The axial load first decreased slightly before it started to increased. After the impact the axial load dropped to zero which indicated that a complete column failure occurred. With a shear failure the axial load should drop to zero because the column lost its load bearing capacity.

After the impact test, no static test could be done because the column failed completely in shear.

Figures B.86 and B.87 show the visible crack pattern on both sides of the column after the impact test. Figures B.537 to B 560 show graphically the recorded test data.

B.8.22 Column 5A. (figures B.88 to B.89)

Reinforcement: Main: 2-Y16 + 2-Y16 (1,53 %)
Stirrups: 14-R8@150
Concrete cover: 23 mm

Concrete mix:

Water	-	26,7 kg
Cement	-	44 kg
Sand	-	125,0 kg
Stone	-	178,0 kg

TABLE B.24: Details of concrete cubes from column 5A

NUMBER	CASTING DATE	DATE TESTED	AGE DAYS	MASS (kg)	SLPIT (kN)	FORCE (kN)	STRENGTH (MPa)
ML-5A1	06/06/88	13/06/88	7	8,44	101,8	529,44	23,53
ML-5A2	06/06/88	13/06/88	7	8,40	-	594,41	26,42
ML-5A3	06/06/88	13/06/88	7	8,38	99,8	583,12	25,92
ML-5A4	06/06/88	13/06/88	7	8,36	-	592,27	26,32
ML-5A5	06/06/88	04/07/88	28	8,38	-	764,05	33,96
ML-5A6	06/06/88	04/07/88	28	8,40	-	764,66	33,98

Stellenbosch University http://scholar.sun.ac.za

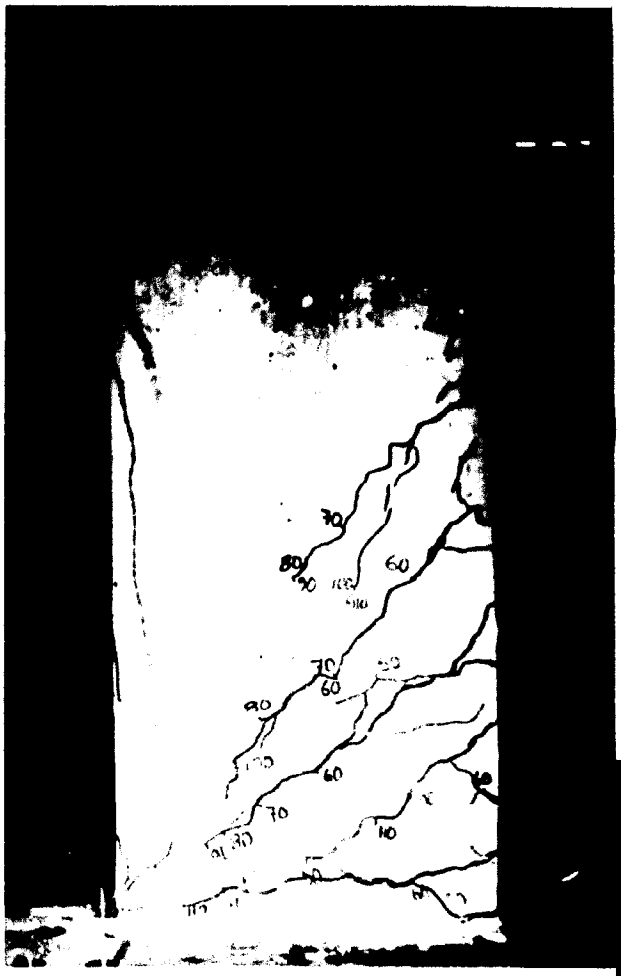

Figure B.88: Crack pattern of Column 5A seen from one side after the static test.

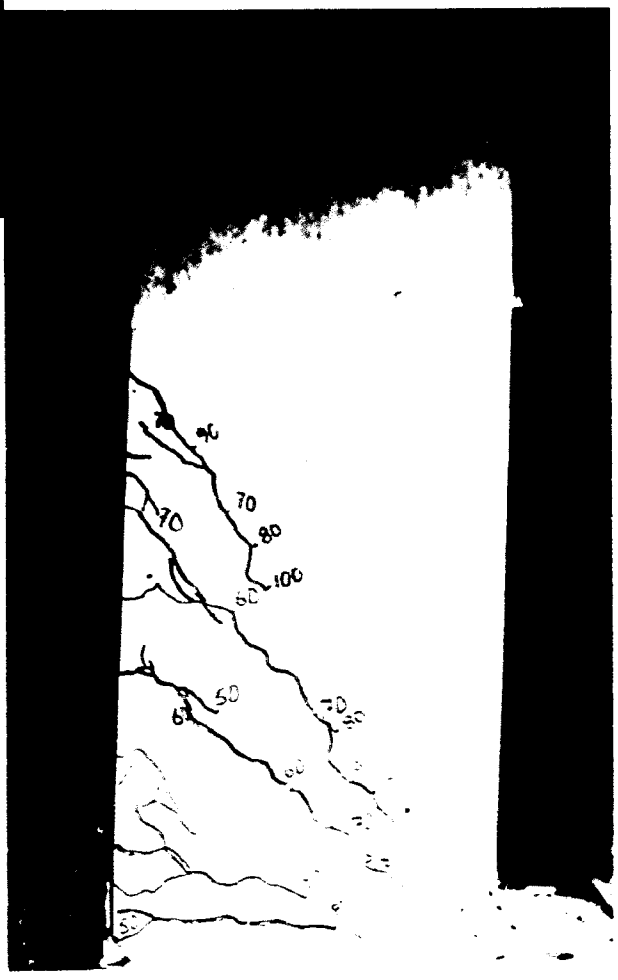

Figure B.89. Crack pattern of Column 5A seen from the other side of the column.

Stellenbosch University http://scholar.sun.ac.za

Static test on Column 5A

With this test it was tried to test a column with a concrete compressive strength about 8 - 10 MPa lower than that of the series three columns. Although the cement/water ratio was lowered from 2 to 1,65, the concrete compressive strength was in the same region as that of the series 3 tests. This meant that this tests could only be used to prove the repeatability of this kind of tests.

The column was step loaded with a static horizontal load in steps of 10 kN. At a 50 kN horizontal load (moment of 37,0 kNm) the first horizontal crack started to develop at the bottom of the column. At about 60 kN horizontal load two further cracks developed a little bit higher up on the column. With a 70 kN horizontal load another crack developed even higher up. The 50 kN, 60 kN and 70kN cracks developed into diagonal cracks with angles of 41,2°, 53,4° and 66,8° with the vertical axis of the column. This could be compared with the results of Column 3A.

Although the diagonal cracks did develop the column failed in flexure with a static horizontal load of 117,50 kN. This horizontal load corresponds with a bending moment of 86,95 kNm at the bottom of the column. This ultimate load was only reached after a considerable increase in the deflection of the column starting with a horizontal load of about 100kN.

Again the axial load started to drop as soon as a horizontal load was applied to the column, before it suddenly started to increase as the horizontal force increased further. Again this was due to the cracking of the concrete. As previously mentioned, the first horizontal crack was visible with a 50 kN horizontal load. The graphs of the axial loads (figure B.563) shows that the axial load started to increase with a 50 kN horizontal load.

The strain at the rear bottom of the column continued to increase up to failure of the column. This meant that no crack reached the rear face of the column to release the compression strain on the rear side of the column.

Stellenbosch University http://scholar.sun.ac.za

At a top deflection of about 17,5 mm the column started to fail. At a deflection of 53 mm the column reached an ultimate load of 117,5 kN.

All the results compared acceptably with that of Column 3A. This proved the repeatability of this type of tests.

Figures B.88 and B.89 show the crack pattern after the static test. Figures B.561 to B.564 show graphically the recorded test data.

B.8.23 Column 5B (figures B.90 to B.93)

Reinforcement: Main: 2-Y16 + 2-Y16 (1,53 %)
Stirrups: 14-R8@150
Concrete cover: 23 mm

Concrete mix:

Water	-	26,7 kg
Cement	-	44 kg
Sand	-	125,00 kg
Stone	-	178,00 kg

TABLE B.25: Details of concrete cubes from column 5B

NUMBER	CASTING DATE	DATE TESTED	AGE DAYS	MASS (kg)	SPLIT (kN)	FORCE (kN)	STRENGTH (MPa)
ML-5B1	10/06/88	17/06/88	7	8,33	100,3	484,20	21,52
ML-5B2	10/06/88	17/06/88	7	8,58	-	532,65	23,67
ML-5B3	10/06/88	17/06/88	7	8,38	96,6	501,06	22,27
ML-5B4	10/06/88	17/06/88	7	8,48	-	501,94	22.31
ML-5B5	10/06/88	08/07/88	28	8,45	-	695,42	30,91
ML-5B6	10/06/88	08/07/88	28	8,45	-	735,71	32,70

Impact phase of test on Column 5B

With this impact test it was tried to introduce an impact load to the column which was greater than the static failure load of the static test of Column 5A. The impact loading applied to the

Stellenbosch University http://scholar.sun.ac.za

column peaked at a load of 146,398 kN This was considerably higher (24,6% higher) than the static failure load of 117,50 kN of Column 5A.

During the impact a horizontal crack and three major diagonal cracks developed. The horizontal crack was right at the bottom of the column. The three major diagonal cracks formed angles of 36,1° and 51,3° and 71,1° with the vertical axis of the column. This crack pattern was very similar to that of Column 5A. Similar to the series one tests where flexural failure occurred, with the static tests, the cracks closed after the impact and the damage did not look very serious

Static phase of test on Column 5B

After the impact test, a static test was done on the column to determine the reserve strength of the column. The column was step loaded with a static horizontal load in steps of 10 kN. During the static test the horizontal cracks soon started to increase in width, although they were slow to increase in length. The diagonal cracks developed slowly and it never looked as if the column would fail in shear. The diagonal cracks angles of 36,1°; 51,3° and 71,1° corresponded with that of the static test of Column 5A.

The column failed at static horizontal load of 111,61 kN. This corresponds with a bending moment of 82,6 kNm at the bottom of the column. This static failure load was a little lower than that of Column 5A. This lower value was due to a lower concrete compression strength, than that of Column 5A.

Stellenbosch University http://scholar.sun.ac.za

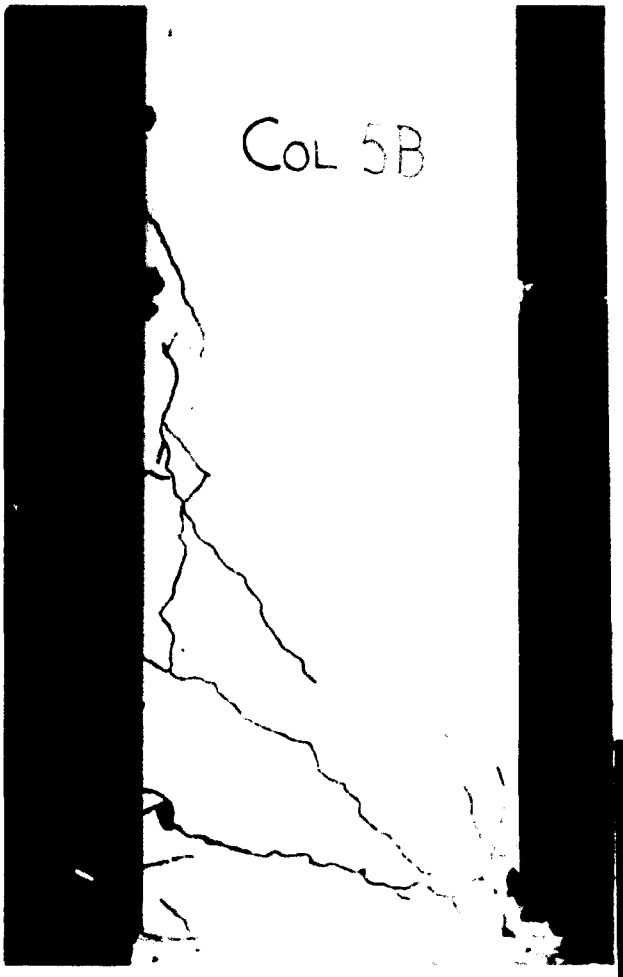

Figure B.90: Crack pattern of Column 5B seen from one side after the impact phase.

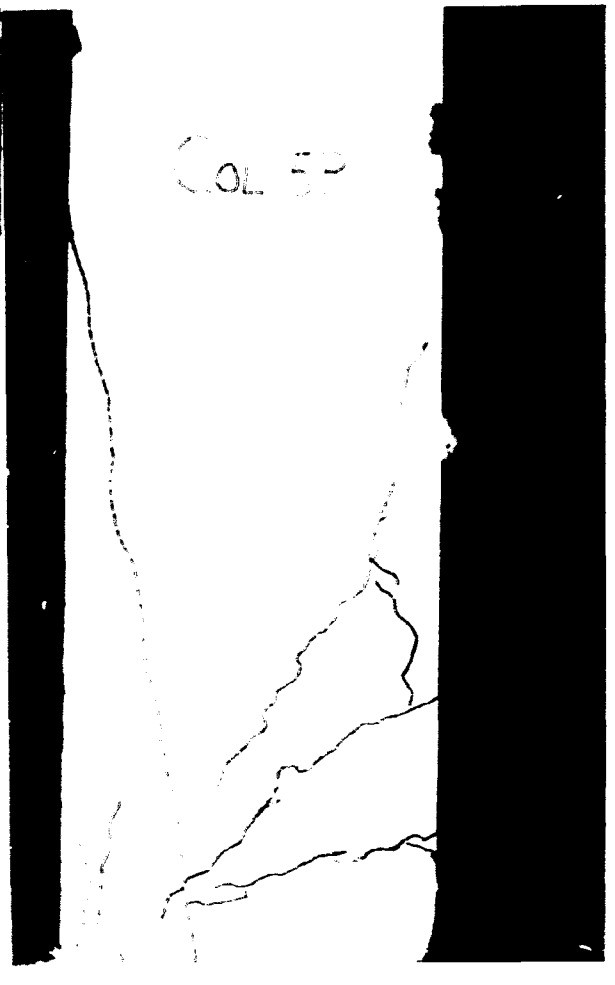

Figure B.91: Crack pattern of Column 5B seen from the other side of the column.

Stellenbosch University http://scholar.sun.ac.za

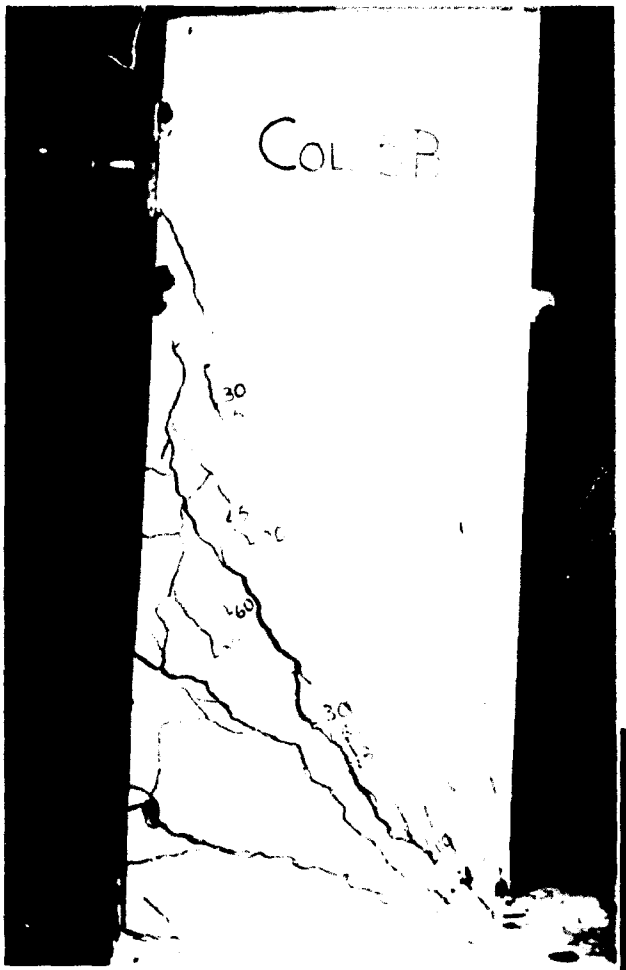

Figure B.92: Crack pattern of Column 5B seen from one side after the static test

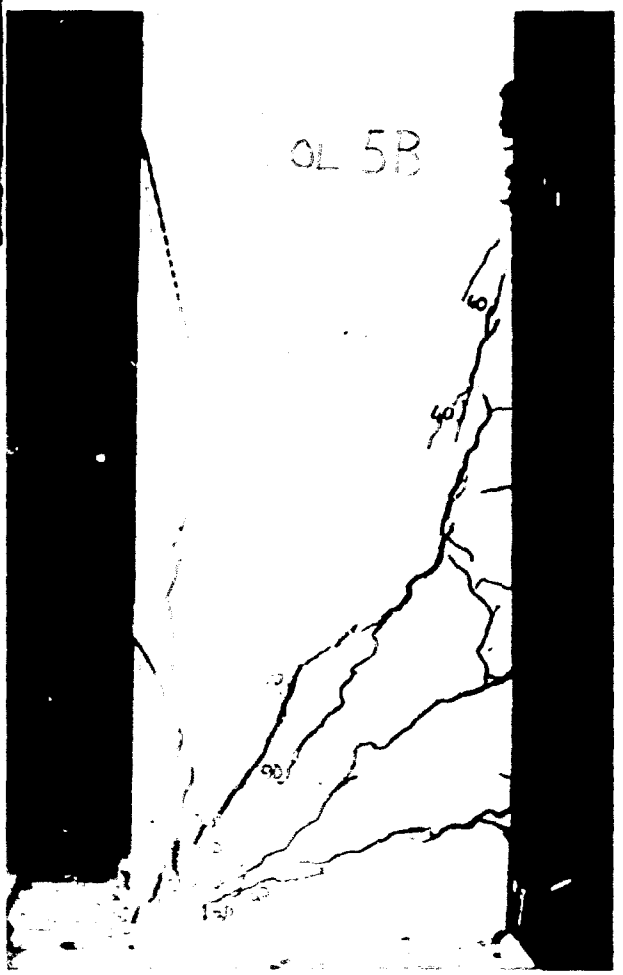

Figure B.93: Crack pattern of Column 5B seen from the other side of the column.

Stellenbosch University http://scholar.sun.ac.za

The axial load immediately increased as soon as the horizontal load was applied to the column. This was due to the fact that the concrete of the column was already cracked by the impact test and thus the cracks started to increase in width as soon as the horizontal load was applied. The widening of the cracks lengthened the column, resulting in the increased axial load.

Similar to Column 5A, the strain measured at the rear bottom of the column increased all the time during the test. This indicated that no cracks reached the rear face of the column (like in the shear failures of the number two series columns) and thus releasing the strain in that region of the column. Just before failure the strain dropped which indicated that a crack reached the back face of the column to release the strain in that region.

The damaged column 5B started to fail at a top deflection of around 35 mm while the undamaged Column 5A started to fail at a top deflection of about 17,5 mm. This column failed completely at a deflection of 44 mm, while Column 5A failed completely at a deflection of 53 mm.

Figures B.90 and B.91 show the visible crack pattern on both sides of the column after the impact test. Figures B.92 and B.93 show the crack pattern after the static test. Figures B.565 to B.592 show graphically the recorded test data.

B.8.24 Column 5C. (figures B.94 to B.95)

Reinforcement: Main: 2-Y16 + 2-Y16 (1,53 %)
Stirrups: 14-R8@150
Concrete cover: 23 mm

Stellenbosch University http://scholar.sun.ac.za

Figure B.94: Crack pattern of Column 5C seen from one side after the impact phase.

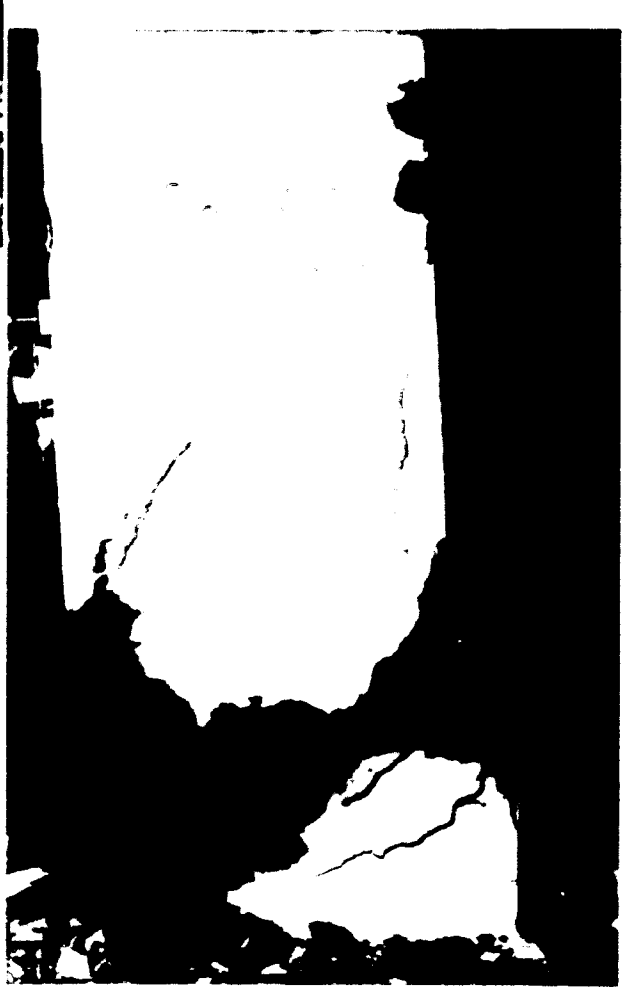

Figure B.95: Crack pattern of Column 5C seen from the other side of the column.

Stellenbosch University http://scholar.sun.ac.za

Concrete mix:

Water	-	26,7 kg
Cement	-	44 kg
Sand	-	125,00 kg
Stone	-	178,00 kg

TABLE B.26: Details of concrete cubes from column 5C

NUMBER	CASTING DATE	DATE TESTED	AGE DAYS	MASS (kg)	SPLIT (kN)	FORCE (kN)	STRENGTH (MPa)
ML-5C1	30/05/88	06/06/88	7	8,48	95,5	440,71	19,59
ML-5C2	30/05/88	06/06/88	7	8,43	-	446,36	19,84
ML-5C3	30/05/88	06/06/88	7	8,44	71,8	416,45	18,51
ML-5C4	30/05/88	06/06/88	7	8,38	-	439,99	19,56
ML-5C5	30/05/88	27/06/88	28	8,51	-	632,37	28,11
ML-5C6	30/05/88	27/06/88	28	8,53	-	647,51	28,78

Impact phase of test on Column 5C

With this impact test it was tried to introduce an impact load to the column which would force a column impact failure. The impact loading peaked at a value of 175,64kN and the column failed in shear. The diagonal cracks present formed angles of 66° and 40,6° with the vertical axis of the column. The column failed along the 40,6° diagonal crack. The undamaged column tested statically (Column 5A) failed in flexure with a maximum horizontal load of 117,5kN, but the concrete of that column had a higher compressive strength than this one did. Although this column was of a lower strength, its impact resistance was nearly 50% (49,5%) higher than the static resistance of Column 5A and, additionally, this column failed in shear compared to the static flexural failures of Columns 5A and 5B.

Only a small horizontal crack right at the bottom of the column was visible after the impact failure of the column.

Unfortunately the bottom strain gauge was damaged during the impact test as can be seen by a sudden rise to a tension strain of 0,002mm/mm in figure B.599. This damage to the strain gauge

Stellenbosch University http://scholar.sun.ac.za

gave an indication of the time when the shear crack had reached the rear face of the column. This showed that the crack reached the rear face of the column just after the peak of the impact loading was registered. Looking at the graph of the middle strain gauge (figure B.597) one can see that the tension peaks corresponded closely with the peaks of the impact load. This shows that after the failure of the column the column was unable to let the striker rebound and thus the striker caught up with the column at these points and gave the column further smaller impact loads. This further smaller impact loads resulted in the tension peaks on the rear side of the column.

The axial load first dropped slightly before it started to increase. After the impact loading, the axial load dropped to zero which indicated that the column failed completely.

After the impact test, no static test could be done because the column failed completely in shear during the impact phase of the column.

Figures B.94 and B.95 show the visible crack pattern on both sides of the column after the impact test. Figures B.593 to B.616 show graphically the recorded test data.

B.8.25 Column 6A. (figures B.96 to B.97)

Reinforcement: Main: 2-Y16 + 2-Y16 (1,53 %)
Stirrups: 14-R8@150
Concrete cover: 23 mm

Concrete mix:			
	Water	-	27,5 kg
	Cement	-	55 kg
	Sand	-	114,68 kg
	Stone	-	169,54 kg

Stellenbosch University http://scholar.sun.ac.za

TABLE B.27: Details of concrete cubes from column 6A

NUMBER	CASTING DATE	DATE TESTED	AGE DAYS	MASS (kg)	SLPIT (kN)	FORCE (kN)	STRENGTH (MPa)
ML-6A1	15/06/88	22/06/88	7	8,42	121,3	651,44	28,95
ML-6A2	15/06/88	22/06/88	7	8,43	-	654,76	29,10
ML-6A3	15/06/88	22/06/88	7	8,46	111,5	639,04	28,40
ML-6A4	15/06/88	22/06/88	7	8,38	-	665,25	29,57
ML-6A5	15/06/88	13/07/88	28	8,46	-	836,38	37,17
ML-6A6	15/06/88	13/07/88	28	8,46	-	878,19	39,03

Static test on Column 6A

With this series of columns the influence of the axial load was investigated. With this series, the initial axial load on the column was 20kN (in other words 10 kN / sway frame) compared to the 100kN of the other tests.

The column was step loaded with a static horizontal load in steps of 10 kN. With a 30 kN horizontal load (moment of 22,2 kNm) the first horizontal cracks developed at the bottom of the column as well as 60 mm above the bottom of the column. With a 40kN horizontal load a further crack started 170 mm above the bottom. With a 70 kN horizontal load two more cracks started 220 mm and 480 mm above the bottom of the column. The last three cracks developed into diagonal cracks. The diagonal cracks formed angles of 26°, 46,6° and 59,7°, respectively, with the vertical axis of the column.

With a 90 kN horizontal load the first diagonal crack reached the rear face of the column. Above this horizontal load the top deflection of the column started to increase dramatically while the horizontal load showed only a slight increase. An ultimate load of 110,219 kN (corresponding with a bending moment of 81,6 kNm) was finally reached. Typical to a flexural failure the cracks closed as soon as the horizontal load subsided to zero although there was a permanent deflection present. With the static tests where the axial load was a 100 kN, the maximum

Stellenbosch University http://scholar.sun.ac.za

static horizontal load was in the region of 116 kN compared to the slightly lower static load of 110 kN of this test where the axial load was only 20 kN. In other words the higher axial load increased the ultimate static load with about 5 to 6%.

Again the axial load started to drop as soon as a horizontal force was applied to the column, before it suddenly started to increase as the horizontal force increased further. As previously mentioned, the first horizontal crack was visible with a 30 kN horizontal load. On the graph of the axial loads (figure B.619) it can be seen that the axial load started to increase just before the 30 kN horizontal load. Thus the graph corresponded with the crack development of the column. With a 90 kN horizontal load, the column started to fail in flexure. This is also clearly visible on the graph of the axial loads, because the axial loads increased considerably at that stage. This considerable increase can be explained by the increasing crack widths resulting in a lengthening of the column and thus a higher axial load. The ultimate axial load was nearly 18 kN per load cell higher than the original load, this is an increase of 180%. The 18 kN increase corresponded with the increase of about 15 kN per load cell of that of Column 5A.

With this test only the bottom strain gauge was measured as the middle strain gauge did not show any significant changes in the previous static tests. The graph of the strain at the rear bottom of the column was a very good indication of the failure mechanism of the column. Unlike the case of Column 5A it can be seen that the flexural mechanism was always the dominant failure mechanism in this static test of Column 6A and thus the strain increased all the time until the flexural failure.

At a top deflection of about 15 mm the column started to fail. At a top deflection of 48 mm the column reach an ultimate static horizontal load of 110,219 kN. These deflections compared favourably with the deflections of Column 5A.

Stellenbosch University http://scholar.sun.ac.za

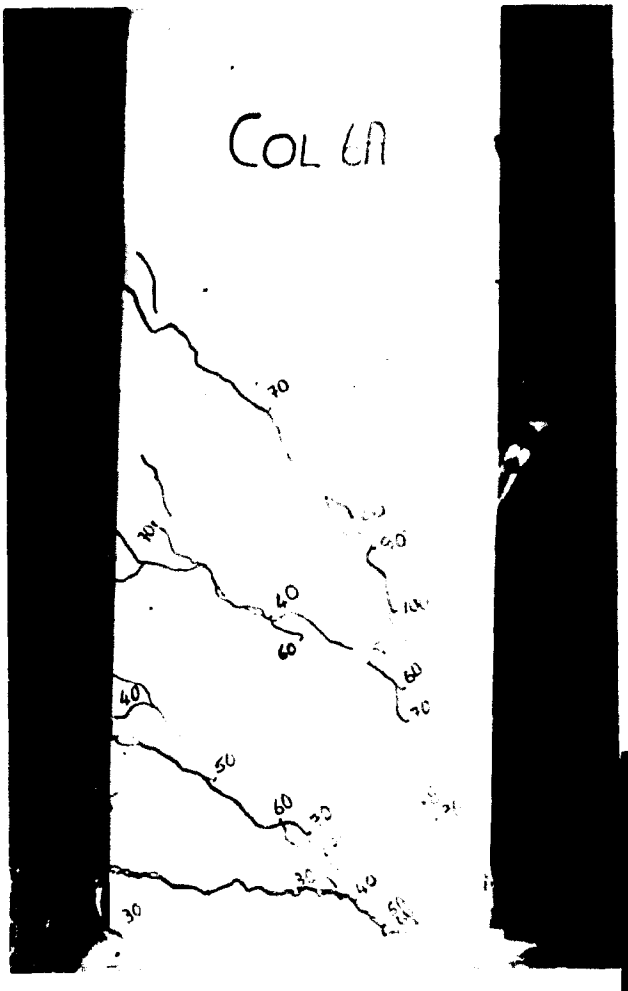

Figure B.96: Crack pattern of Column 6A seen from one side after the static test.

Figure B.97: Crack pattern of Column 6A seen from the other side of the column.

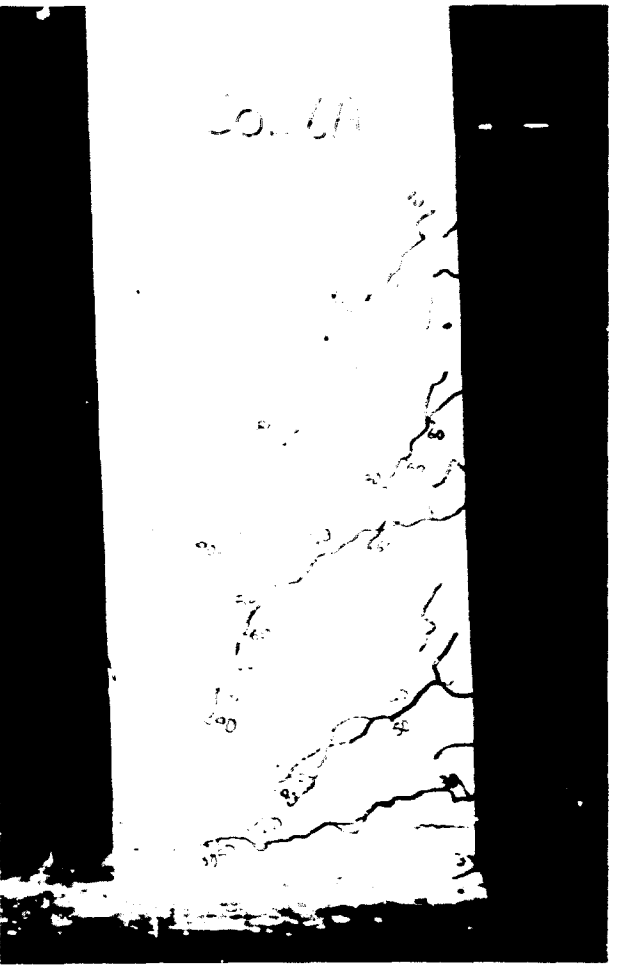

Stellenbosch University http://scholar.sun.ac.za

Figures B.96 and B.97 show the crack pattern after the static test. Figures B.617 to B.620 show graphically the recorded test data.

B.8 26 Column 6B. (figures B.98 to B.101)

Reinforcement: Main: 2-Y16 + 2-Y16 (1,53 %)
Stirrups: 14-R8@150
Concrete cover: 23 mm

Concrete mix: Water - 27,5 kg
Cement - 55 kg
Sand - 114,68 kg
Stone - 169,54 kg

TABLE B.28: Details of concrete cubes from column 6B

NUMBER	CASTING DATE	DATE TESTED	AGE DAYS	MASS (kg)	SPLIT (kN)	FORCE (kN)	STRENGTH (MPa)
ML-6B1	20/06/88	27/06/88	7	8,46	97,3	632,90	28,13
ML-6B2	20/06/88	27/06/88	7	8,44	-	622,22	27,65
ML-6B3	20/06/88	27/06/88	7	8,38	100,6	627,07	27,87
ML-6B4	20/06/88	27/06/88	7	8,38	-	636,14	28,28
ML-6B5	20/06/88	18/07/88	28	8,43	-	869,00	38,62
ML-6B6	20/06/88	18/07/88	28	8,45	-	864,19	38,41

Impact phase of test on Column 6B

With this impact test there were no axial loads present due to a small problem during the test. With this impact test it was tried to introduce an impact load to the column which was more or less in the same region as the static failure load of the undamaged Column 6A. The impact loading applied to the column peaked at a load of 147,7286 kN. This was the very short first peak of the impact load function and can thus be ignored. The second longer duration peak, peaked at a value of 108,77 kN. This was very close to the static failure load of Column 6A (110,219 kN).

Stellenbosch University http://scholar.sun.ac.za

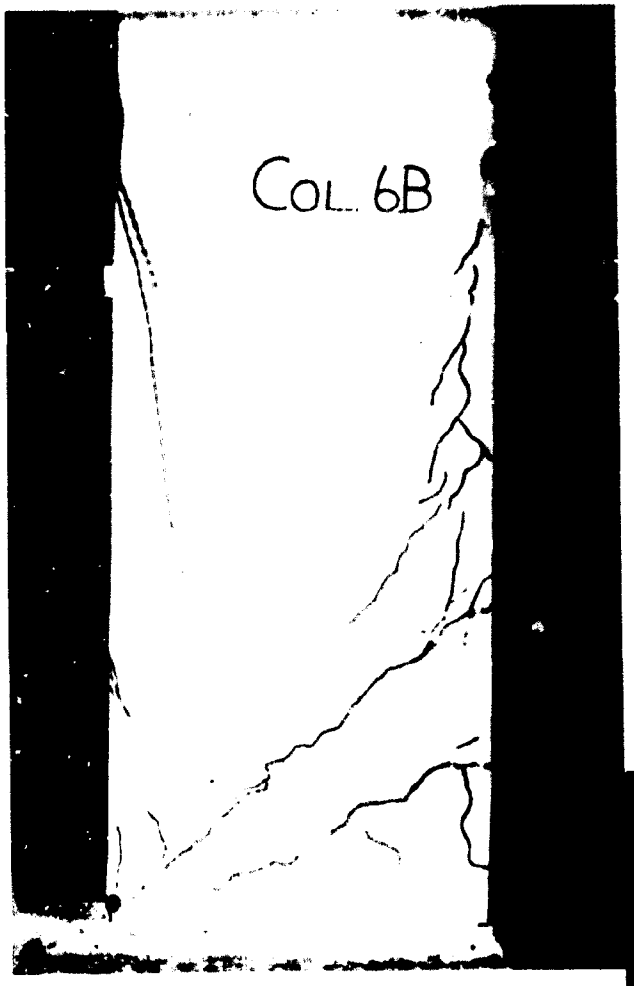

Figure B.98: Crack pattern of Column 6B seen from one side after the impact phase.

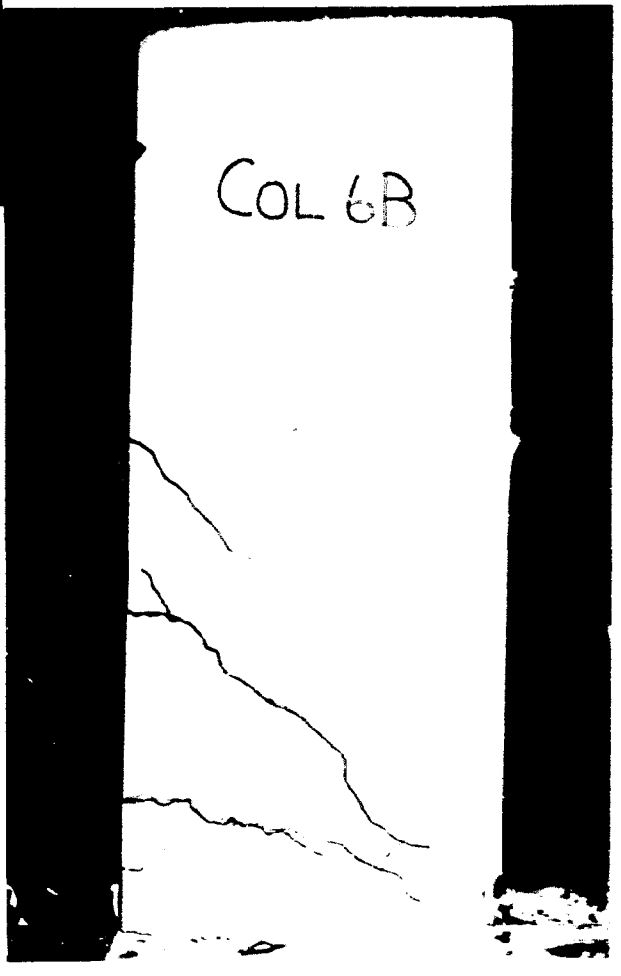

Figure B.99: Crack pattern of Column 6B seen from the other side of the column.

Stellenbosch University http://scholar.sun.ac.za

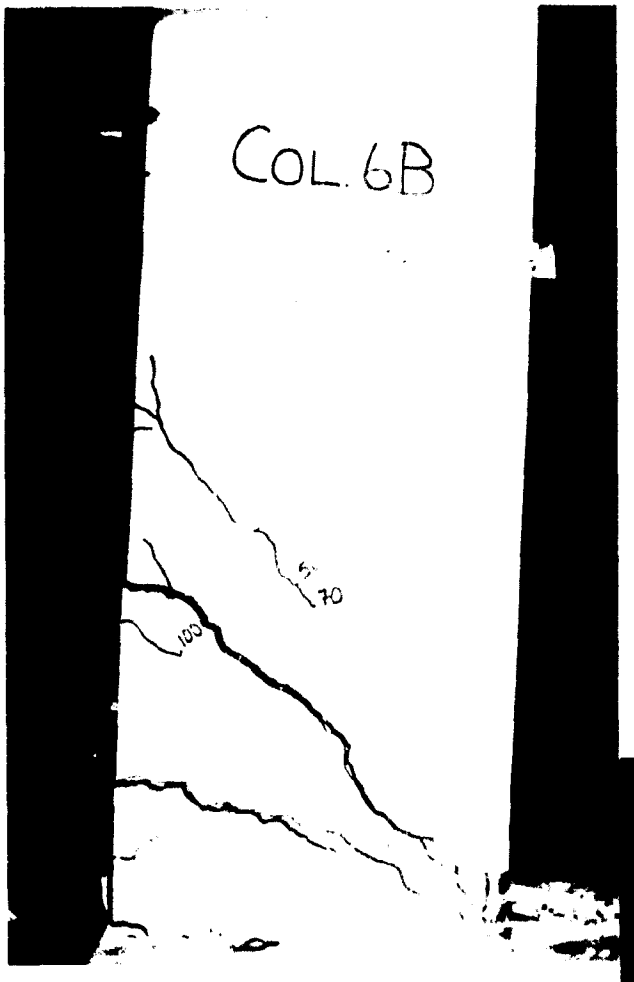

Figure B.100: Crack pattern of Column 6B seen from one side after the static test.

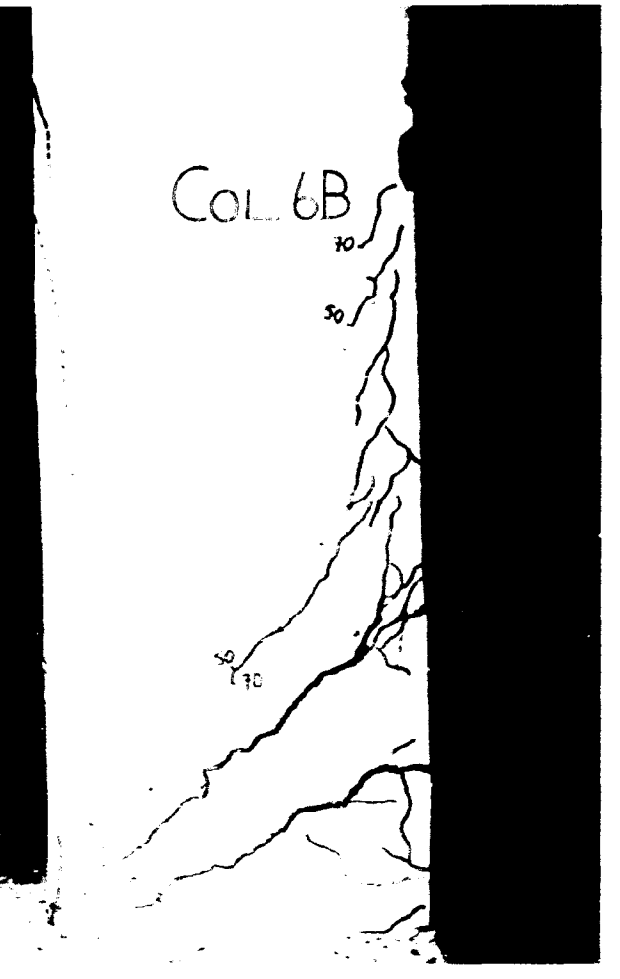

Figure B 101: Crack pattern of Column 6B seen from the other side of the column.

Stellenbosch University http://scholar.sun.ac.za

During the impact loading a horizontal crack and three major diagonal cracks developed. The horizontal crack was right at the bottom of the column. The three major diagonal cracks formed angles of 37,3° and 45,8° and 62,8° with the vertical axis of the column. This crack pattern was very similar to that of Column 6A. Once again, as with the series one tests where flexural failure occurred under static conditions the cracks closed after the impact loading and the damage did not look very serious.

The axial load increased immediately after the impact loading started. The axial load of each load cell peaked at a value of nearly 53 kN and reach a second peak of nearly the same magnitude as the first peak but the second peak occurred just after the impact load subsided.

The third small peak of the impact load history indicated the rebound point of the impacting mass. In other words, at that stage the column "impacted" with the striker to let it rebound.

Static phase of test on Column 6B

After the impact test, a static test was done on the column to determine the reserve strength of the column. The column was step loaded with a static horizontal load in steps of 10 kN. During the static test the horizontal cracks soon increased in width, although they were slow to increase in length. The major diagonal cracks developed slowly and it never looked as if the column would fail in shear. The diagonal cracks angles of 37,3°; 45,8° and 62,8° corresponded with the static test of Column 6A.

The column failed at a static horizontal load of 113,95 kN. This corresponds with a bending moment of 84,3 kNm at the bottom of the column. This static failure load was a little higher than that of Column 6A. This higher value was due to a higher concrete compression strength than that of Column 6A.

The axial load immediately started to increase as soon as the horizontal load was applied to the column. This was due to the existing cracks in the concrete which immediately increased in

Stellenbosch University http://scholar.sun.ac.za

width as the static horizontal load was applied to the column. The widening of the cracks lengthened the column, resulting in the increased the axial load.

The damaged Column 6B started to fail at a top deflection of around 35 mm while the undamaged Column 6A started to fail at a top deflection of about 15 mm. Column 6B failed completely at a top deflection of 52 mm, while Column 6A failed completely at a top deflection of 48mm.

Figures B.98 and B.99 show the visible crack pattern on both sides of the column after the impact test. Figures B.100 and B.101 show the crack pattern after the static test. Figures B.621 to B.648 show graphically the recorded test data.

B.8.27 Column 6C. (figures B.102 to B.105)

Reinforcement: Main: 2-Y16 + 2 Y16 (1,53 %)
Stirrups: 14-R8@150
Concrete cover: 23 mm

Concrete mix:	Water	-	27,5 kg
	Cement	-	55,0 kg
	Sand	-	114,68 kg
	Stone	-	169,54 kg

Stellenbosch University http://scholar.sun.ac.za

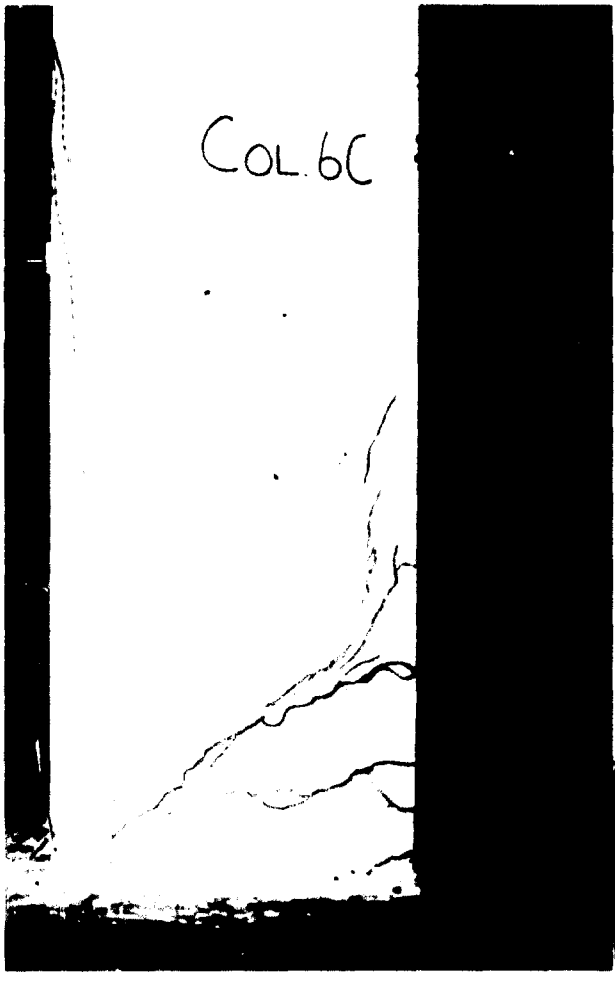

Figure B.102: Crack pattern of Column 6C seen from one side after the ingress of glycerin.

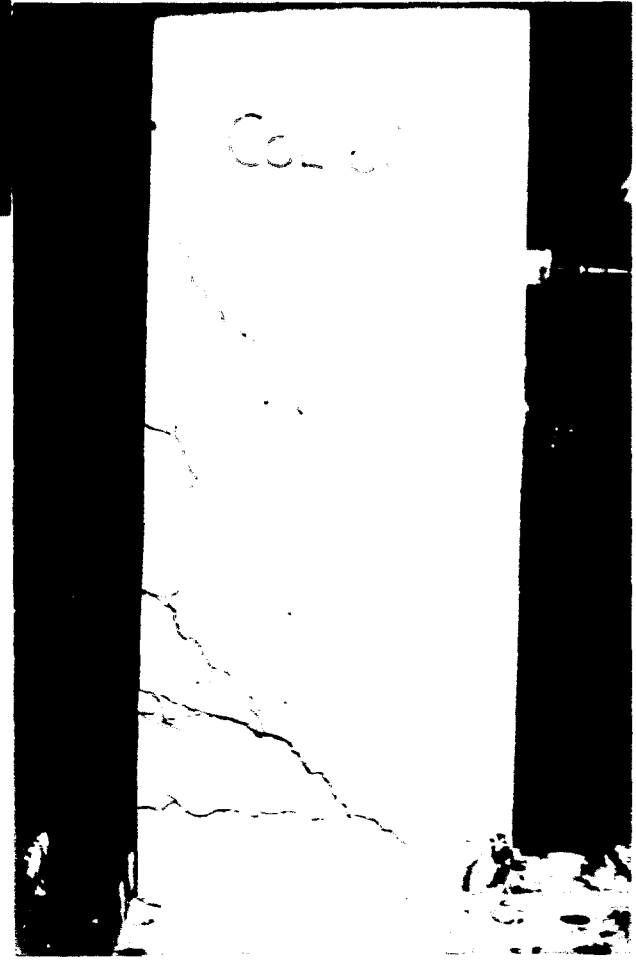

Figure B.103: Crack pattern of Column 6C seen from the other side of the column.

Stellenbosch University http://scholar.sun.ac.za

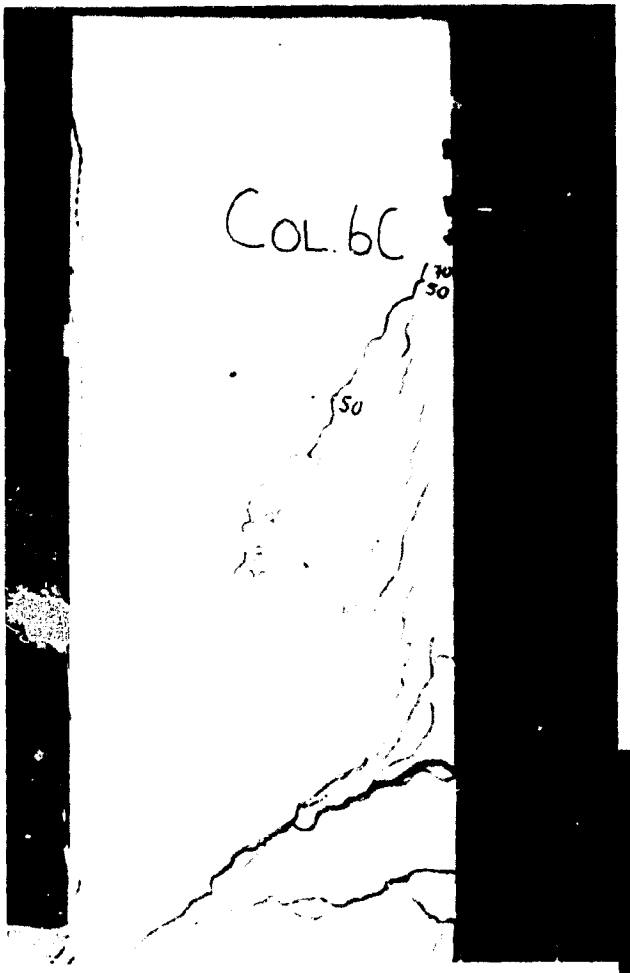

Figure B.104: Crack pattern of Column 6C seen from one side after the static test.

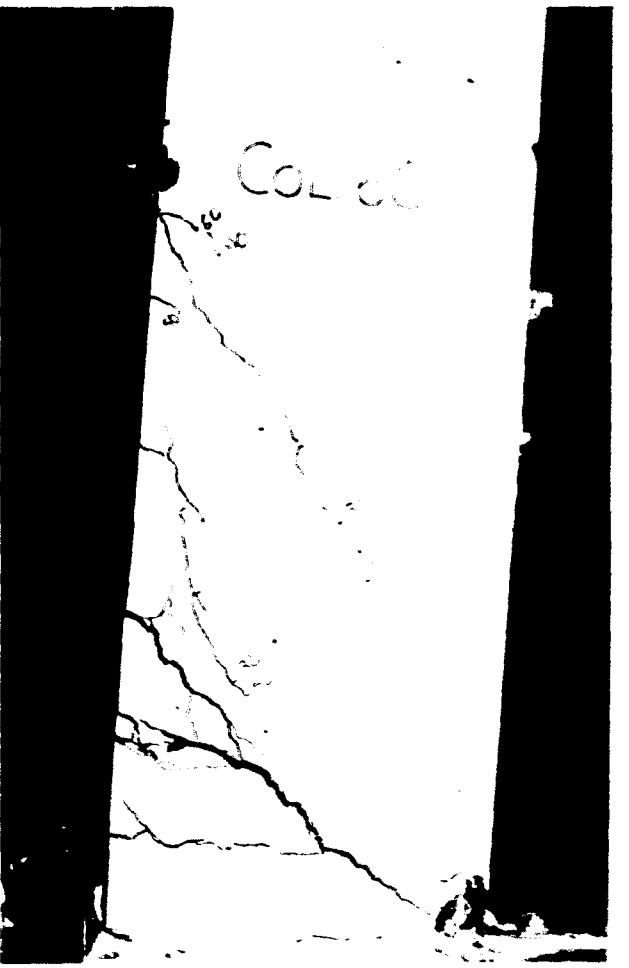

Figure B.105: Crack pattern of Column 6C seen from the other side of the column.

Stellenbosch University http://scholar.sun.ac.za

TABLE B.29: Details of concrete cubes from column 6C

NUMBER	CASTING DATE	DATE TESTED	AGE DAYS	MASS (kg)	SPLIT (kN)	FORCE (kN)	STRENGTH (MPa)
ML-6C1	22/06/88	29/06/88	7	8,34	124,4	695,35	30,90
ML-6C2	22/06/88	29/06/88	7	8,44	-	659,26	29,30
ML-6C3	22/06/88	29/06/88	7	8,42	118,4	629,09	27,96
ML-6C4	22/06/88	29/06/88	7	8,41	-	669,52	29,76
ML-6C5	22/06/88	20/07/88	28	8,38	-	933,69	41,50
ML-6C6	22/06/88	20/07/88	28	8,48	-	902,53	40,11

Impact phase of test on Column 6C

With this impact test it was tried to introduce an impact load to the column which was greater than the static failure load of the static test of Column 6A, but just lower than the expected impact failure load for this series of columns. Once again the axial load was only 20 kN. The impact loading applied to the column peaked at a load of 157,124 kN. This was considerably higher (42,6% higher) than the static failure load of 110,219 kN of Column 6A.

During the impact two horizontal cracks and two diagonal cracks developed. One of the horizontal cracks was right at the bottom of the column while the other one started 80 mm above the bottom. The two major diagonal cracks formed angles of 49,5° and 56,7° with the vertical axis of the column. The crack pattern of Column 6C was very similar to that of Columns 6A and 6B. Similar to the series one tests, the cracks closed after the impact and the damage did not look very serious.

The axial load increased immediately when the impact loading was applied. Once again, as with of Column 6B, there was a very high second peak present in the recorded axial load history. The first peak reached a value of 66 kN (per load cell), which was 56 kN (or 560%) higher than the original value. This 56 kN compared with the 53 kN of Column 6B which had no original axial load. This indicated that the magnitude of the original applied axial load had very little influenced on the increase in the axial load

Stellenbosch University http://scholar.sun.ac.za

on the column during the horizontal impact loading of the column. This suggested that the increase of the axial load was directly proportional to the length increase in the column and thus to the cracking of the column.

Static phase of test on Column 6C

After the impact test, a static test was done on the column to determine the reserve strength of the column. The column was step loaded with a static horizontal load in steps of 10 kN. The two major diagonal cracks developed slowly and it never looked as if the column would fail in shear. A third diagonal crack developed and formed an angle of 32,5° with the vertical axis of the column. The diagonal cracks angles of 32,5° and 49,5° and 56,7° corresponded with that of the static test of Column 6A and of Column 6B.

The column failed at a static horizontal load of 116,015 kN. This corresponds with a flexural moment of 85,85 kNm at the bottom of the column. This static failure load was a little higher than that of Columns 6A and 6B, but this could be contributed to the little higher compressive strength of the concrete. This confirmed the results of the previous tests, that is, that after an impact loading was applied to a flexural failure type of column (under static loading) the static reserve strength of the column would be the same if not higher than the static strength of an undamaged column like Column 6A.

The axial load started to increase as soon as the horizontal load was applied. This was once again due to the existing cracks which immediatley started to increase in width. The axial load increased from 10 kN to nearly 25 kN per load cell.

The damaged column 6C started to fail at a top deflection of around 35 mm while the undamaged column 3A started to fail at a top deflection of about 15 mm. This column and Column 6B failed completely at deflections of 53 mm and 52 mm, respectively, while Column 6A failed completely at a deflection of 48 mm.

Stellenbosch University http://scholar.sun.ac.za

Figures B.102 and B.103 show the visible crack pattern on both sides of the column after the impact test. Figures B.104 and B.105 show the crack pattern after the static test. Figures B.649 to B.676 show graphically the recorded test data.

B.8.28 Column 6D. (figures B.106 to B.107)

Reinforcement: Main: 2-Y16 + 2-Y16 (1,53 %)
Stirrups: 14-R8@150
Concrete cover: 23 mm

Concrete mix:

Water	-	27,5 kg
Cement	-	55 kg
Sand	-	114,68 kg
Stone	-	169,54 kg

TABLE B.30: Details of concrete cubes from column 6D

NUMBER	CASTING DATE	DATE TESTED	AGE DAYS	MASS (kg)	SPLIT (kN)	FORCE (kN)	STRENGTH (MPa)
ML-6D1	24/06/88	01/07/88	7	8,47	118,6	627,10	27,87
ML-6D2	24/06/88	01/07/88	7	8,47	-	675,21	30,01
ML-6D3	24/06/88	01/07/88	7	8,38	118,6	681,39	30,28
ML-6D4	24/06/88	01/07/88	7	8,50	-	670,39	29,80
ML-6D5	24/06/88	22/07/88	28	8,45	-	970,52	43,13
ML-6D6	24/06/88	22/07/88	28	8,46	-	959,14	42,63

Stellenbosch University http://scholar.sun.ac.za

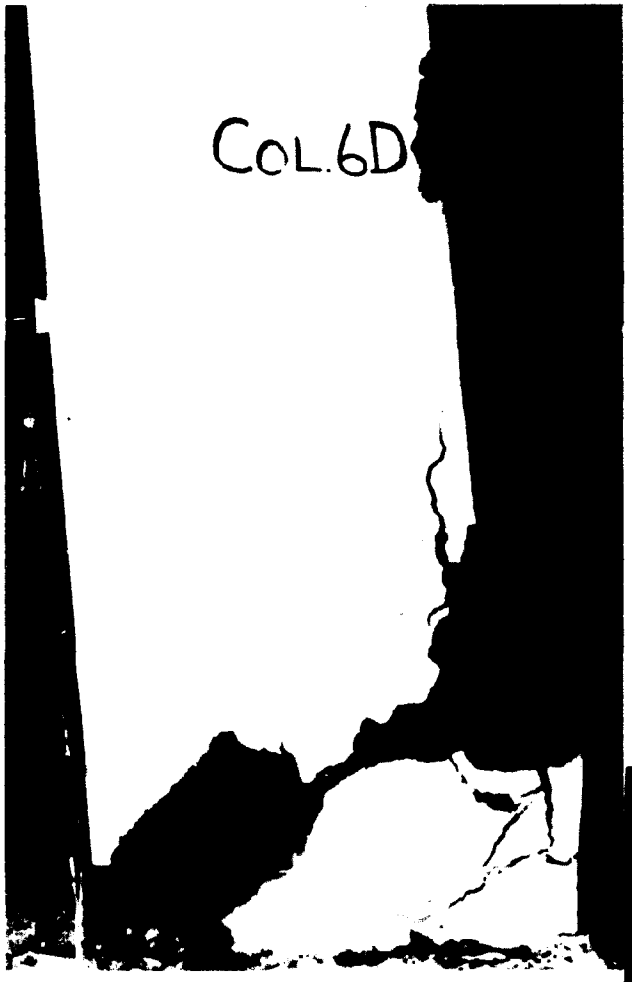

Figure B.106: Failure and crack pattern of Column 6D seen from one side after the impact phase.

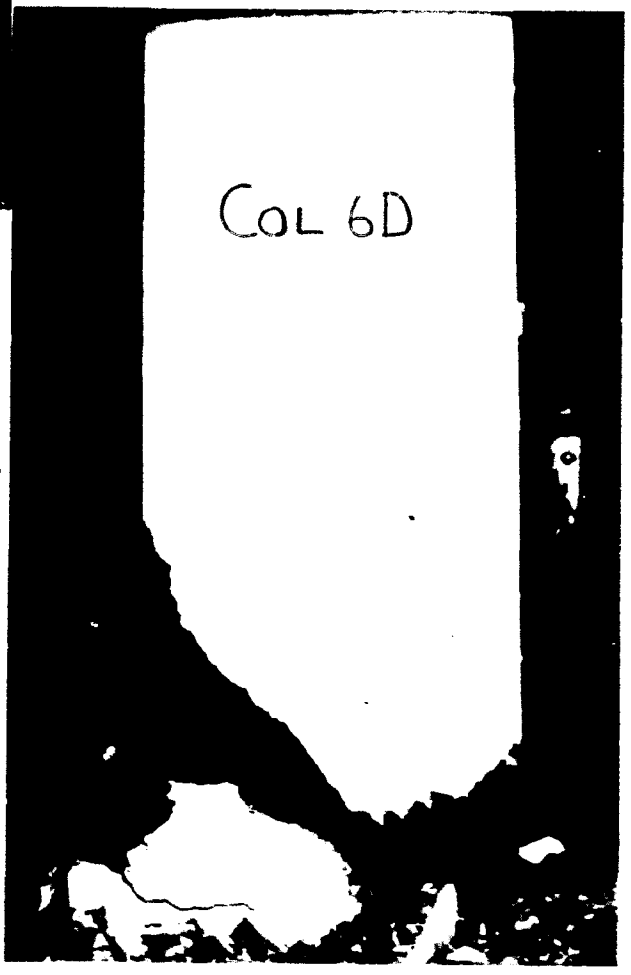

Figure B.107: Failure and crack pattern of Column 6D seen from the other side of the column.

Stellenbosch University http://scholar.sun.ac.za

Impact phase of test on Column 6D

With this impact test it was tried to introduce an impact load large enough to force an impact failure of the column. Once again the total axial load was only 20 kN compared to the 100 kN of the other tests. The impact load history peaked at a value of 224,6487 kN and the column failed in shear. There was only one major diagonal crack. The column failed in shear along this crack. This crack formed an angle of about 45 to 46° with the vertical axis of the column. The undamaged column tested statically (Column 6A) failed in flexure with a maximum static horizontal load of 110 kN. This column's impact resistance was nearly double that of the static resistance of Column 6A and, additionally, this column failed in shear compared to the flexural failure of the statically tested Column 6A.

Only a small horizontal crack right at the bottom of the column was visible after the impact failure of the column.

Unfortunately both the strain gauges broke before the maximum impact load was registered and thus no further readings were available form these strain gauges.

The axial load graphs showed no small initial drop. It looked as if this small initial drop only occurred when the initial axial load was high. This small fall in the axial indicated that the column actually "shortened" slightly before the first crack occured, that is if the initial axial load was high enough. After the impact, the axial load dropped to zero which indicated that the column failed completely. Again the axial load of each load cell peaked at a maximum value of 47 kN, or in other words, it was 37 kN higher than the initial load per load cell. This lower value compared to the previous two tests in this series was ascribed to the different failure mechanism of this column.

After the impact test, no static test could be done because the column failed completely in shear during the impact phase of the test.

Stellenbosch University http://scholar.sun.ac.za

Figures B.106 and B.107 show the visible crack pattern and failure mechanism from both sides of the column after the impact test. Figures B.677 to B.700 show graphically the recorded test data.

B.8.29 Column 7A. (figures B.108 to B.109)

Reinforcement: Main: 2 Y16 + 2-Y16 (1,53 %)
Stirrups: 14-R8@150
Concrete cover: 23 mm

Concrete mix: Water - 28,14 kg
Cement - 71,77 kg
Sand - 108,50 kg
Stone - 162,70 kg

TABLE B.31: Details of concrete cubes from column 7A

NUMBER	CASTING DATE	DATE TESTED	AGE DAYS	MASS (kg)	SLPIT (kN)	FORCE (kN)	STRENGTH (MPa)
ML-7A1	27/06/88	04/07/88	7	8,50	156,1	925,46	41,13
ML-7A2	27/06/88	04/07/88	7	8,39	-	935,64	41,58
ML-7A3	27/06/88	04/07/88	7	8,54	131,1	936,54	41,62
ML-7A4	27/06/88	04/07/88	7	8,54	-	938,50	41,71
ML-7A5	27/06/88	25/07/88	28	8,50	-	1295,87	57,59
ML-7A6	27/06/88	25/07/88	28	8,49	-	1277,18	56,76

Static test on Column 7A

With this series of columns the influence of a concrete with a higher compressive strength than the reference group 3 was investigated. In this series the initial axial load on the column was again 100kN (in other words 50 kN / sway frame) as in all the other series of tests except for the series 6 tests.

Stellenbosch University http://scholar.sun.ac.za

Figure B.108: Crack pattern of Column 7A seen from one side after the static test.

Figure B.109: Crack pattern of Column 7A seen from the other side of the column.

Stellenbosch University http://scholar.sun.ac.za

The column was step loaded with a static horizontal load in steps of 10 kN. With a 50 kN horizontal load (moment of 37 kNm) the first horizontal cracks started to develop at the bottom of the column. Two further cracks also started higher up on the column (120mm and 280mm from the bottom respectively). With a 70 kN horizontal load one more crack started 450 mm above the bottom of the column. The last three cracks soon developed into diagonal cracks. The diagonal cracks formed angles of 37,9°, 51,3° and 71,1° with the vertical axis of the column.

The ultimate static horizontal load reached by this column was 126,22 kN (a bending moment of 93,4 kNm at the bottom of the column). This was only reached after a considerable deflection which started at a horizontal load of 110 kN. The cracks closed as soon as the horizontal force subsided to zero although their was permanent deflection present. During previous tests with the lower strength concrete of the reference group 3, the maximum horizontal loads were in the region of 116 to 117 kN compared to the slightly higher load of 126 kN of Column 7A. In other words, the higher compressive strength concrete increased the ultimate load with about 8 to 9%.

Again the axial load started to decrease as soon as the horizontal load was applied to the column before it suddenly started to increase as the horizontal load increased further. As previously mentioned, the first horizontal crack was visible with a 50 kN horizontal load. The graphs of the axial loads (figure B.703) showed that the axial load started to increase just before the 50 kN horizontal load. Thus the graph corresponded very well with the crack development of the column. Wit a 110 kN horizontal load, the column started to fail in flexure. This was also clearly visible on the graph of the axial loads, because the axial loads increased considerably at that stage. This considerable increase could be explained by the increasing crack widths resulting in a lengthening of the column and thus a higher axial load. The ultimate axial load was nearly 22 kN higher than the original load, this was an increase of about 44%.

Stellenbosch University http://scholar.sun.ac.za

With this test only the bottom strain gauge was measured as the middle strain gauge did not show any significant changes in the previous static tests. The graph of the strain at the rear bottom of the column was a very good indication of the failing mechanism of the column. Unlike the case of Column 5A it can be seen that the flexural mechanism was always the dominant failing mechanism in this test (Column 7A) and thus the strain kept increasing until the flexural failure of the column. This was similar to the behaviour of Column 6A.

At a top deflection of about 20 mm the column started to fail. At a deflection of 63 mm the column reach an ultimate static load of 126,22 kN.

Figures B.108 and B.109 show the crack pattern after the static test. Figures B.701 to B.704 show graphically the recorded test data.

B.8.30 Column 7B. (figures B.110 to B.113)

Reinforcement: Main: 2-Y16 + 2-Y16 (1,53 %)
Stirrups: 14-R8@150
Concrete cover: 23 mm

Concrete mix:			
	Water	-	28,14 kg
	Cement	-	71,77 kg
	Sand	-	108,50 kg
	Stone	-	162,70 kg

Stellenbosch University http://scholar.sun.ac.za

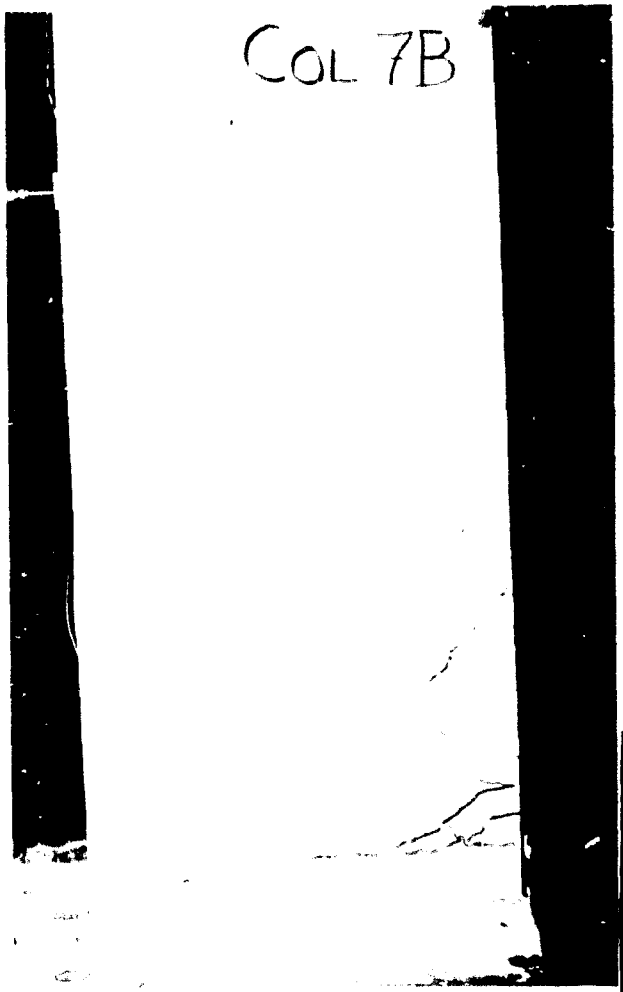

Figure B.111: Crack pattern of Column 7B seen from one side of the column.

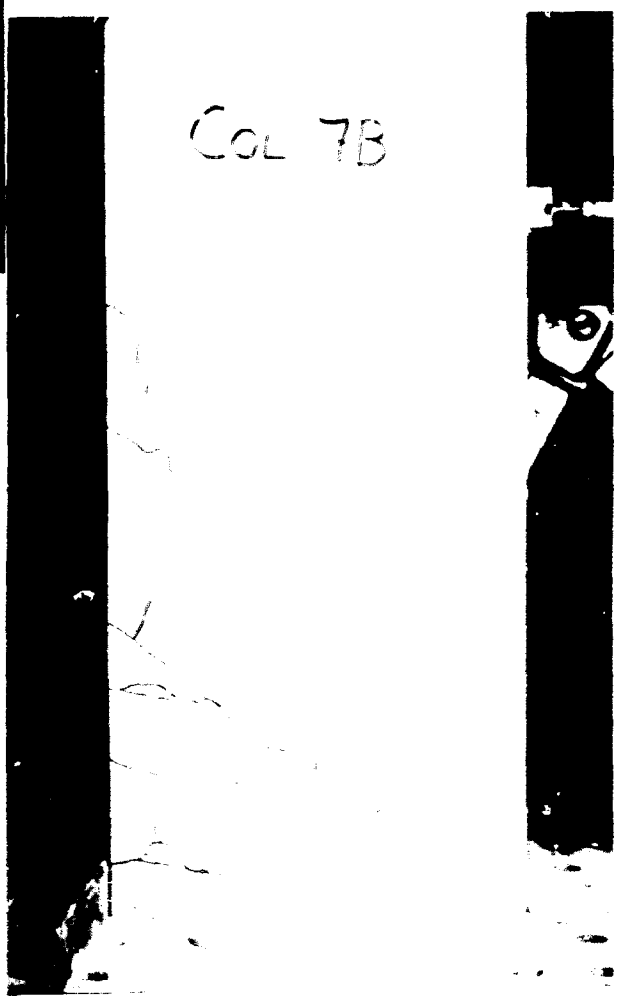

Figure B.112: Crack pattern of Column 7B seen from the other side of the column.

Stellenbosch University http://scholar.sun.ac.za

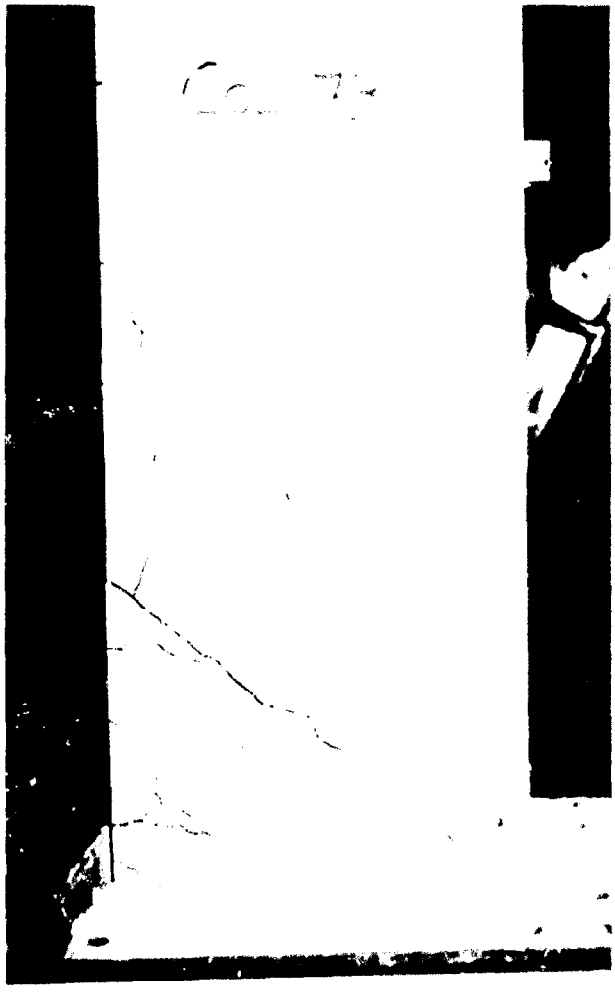

Figure B.113: Crack pattern of Column 7B seen from the other side of the column.

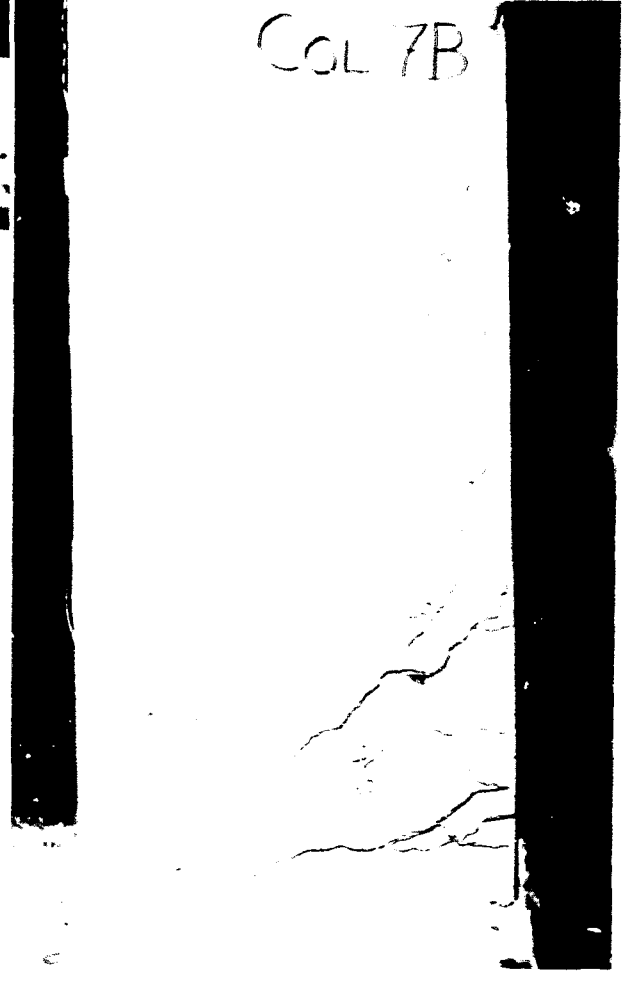

Stellenbosch University http://scholar.sun.ac.za

TABLE B.32: Details of concrete cubes from column 7B

NUMBER	CASTING DATE	DATE TESTED	AGE DAYS	MASS (kg)	SPLIT (kN)	FORCE (kN)	STRENGTH (MPa)
ML-7B1	29/06/88	06/07/88	7	8,51	129,4	853,33	37,93
ML-7B2	29/06/88	06/07/88	7	8,47	-	860,99	38,27
ML-7B3	29/06/88	06/07/88	7	8,46	126,3	850,31	37,79
ML 7B4	29/06/88	06/07/88	7	8,51		842,79	37,46
ML-7B5	29/06/88	27/07/88	28	8,50	-	1200,04	53,34
ML-7B6	29/06/88	27/07/88	28	8,55		1160,21	51,56

Impact phase of test on Column 7B

With this impact test the concrete compressive strength was once again higher than the reference test, to investigate the influence of the higher concrete strength on the test. With this impact test it was tried to introduce an impact load to the column which was more or less in the same region as the static failure load of the undamaged Column 7A. The impact loading applied to the column peaked at a load of 149,7646 kN. This was the very short first peak of the impact load function and can thus be ignored. The second longer duration peak, peaked at a value of 130,2 kN. This was very close to the static failure load of Column 7A of 132,332 kN.

During the impact a horisontal crack and three diagonal cracks developed. The horisontal crack was right at the bottom of the column. The three diagonal cracks formed angles of 36,7° and 53,4° and 66,7° with the vertical axis of the column. These crack pattern was very similar to that of Column 7A. After the impact loading the cracks closed and the damage did not look very serious.

The axial load showed a small decrease before it increased. This confirmed the theory that if the initial axial load was big enough, there will be a slight drop in the axial load immediately after the impact loading started and just before the cracks forced the axial load to increase. The axial load of each load

Stellenbosch University http://scholar.sun.ac.za

cell peaked at a value of nearly 83 kN. This peak was in the region of 33 kN higher (per load cell) than the initial loads.

Static phase of test on Column 7B

After the impact test, a static test was done on the column to determine the reserve strength of the column. The column was step loaded with a static horizontal load in steps of 10 kN. During the static test the horizontal cracks soon increased in width. The diagonal cracks developed slowly and it never looked as if the column might fail in shear. The diagonal cracks angles of 36,7°; 53,4° and 68,2° corresponded with that of the static test of Column 7A.

The column failed at a static horizontal load of 124,9721 kN. This corresponds with a bending moment of 92,5 kNm at the bottom of the column. This static failure load was a little lower than that of Column 7A. This lower value can be contributed to the little lower concrete compression strength of this column compared to that of Column 7A.

The axial load immediately started to increase as soon as the horizontal load was applied to the column. The existing cracks, from the impact test on the column, immediately increased in width as the static load was applied. These widening of the cracks lengthened the column, resulting in the increase in the axial load.

The damaged column 7B started to fail at a top deflection of around 26 mm while the undamaged column 7A started to fail at a top deflection of about 20 mm. This column failed completely at deflections of 57 mm, while Column 7A failed completely at a deflection of 63 mm.

Figures B.110 and B.111 show the visible crack pattern on both sides of the column after the impact test. Figures B.112 and B.113 show the crack pattern after the static test. Figures B.705 to B.732 show graphically the recorded test data.

Stellenbosch University http://scholar.sun.ac.za

B.8.31 Column 7C. (figures B.114 to B.117)

Reinforcement: Main: 2-Y16 + 2-Y16 (1,53 %)
Stirrups: 14-R8@150
Concrete cover: 23 mm

Concrete mix: Water - 28,14 kg
Cement - 71,77 kg
Sand - 108,50 kg
Stone - 162,70 kg

TABLE B.33: Details of concrete cubes from column 7C

NUMBER	CASTING DATE	DATE TESTED	AGE DAYS	MASS (kg)	SPLIT (kN)	FORCE (kN)	STRENGTH (MPa)
ML-7C1	01/07/88	08/07/88	7	8,52	117,0	835,31	37,12
ML-7C2	01/07/88	08/07/88	7	8,58	-	841,42	37,40
ML-7C3	01/07/88	08/07/88	7	8,51	143,6	845,56	37,58
ML-7C4	01/07/88	08/07/88	7	8,48	-	839,28	37,30
ML-7C5	01/07/88	29/07/88	28	8,48	-	1222,66	54,34
ML-7C6	01/07/88	29/07/88	28	8,51	-	1196,26	53,17

Impact phase of test on Column 7C

With this impact test the concrete compressive strength was again higher than the reference group, to investigate the influence of the higher concrete strength on the test. With this impact test it was tried to introduce an impact load to the column which was greater than the static failure load of the static test of Column 7A, but just lower than the expected impact failure load of this column. The axial load was also the standard 100 kN or 50 kN per load cell. The impact loading introduced to the column peaked at a load of 167,012 kN. This was considerably higher (32,3% higher) than the static failure load of 126,22 kN of Column 7A.

During the impact a horizontal crack and two diagonal cracks developed. The horizontal crack was right at the bottom of the column. The two diagonal cracks formed angles of 39,1° and 66,8° with the vertical axis of the column. This crack pattern was

Stellenbosch University http://scholar.sun.ac.za

very similar to that of Columns 7A and 7B, except for a third crack which did not develop with this column. As was the case with the series one tests, where flexural failure occurred with the static tests, the bending cracks closed after the impact.

The axial load showed a small decrease before it increased immediately with the impact loading of the column. This again confirmed the theory that if the initial axial load was large enough, there will be a slight drop in the axial load immediately after the impact, just before the development of cracks forced the axial load to increase. The first peak of the axial load history reached a value of about 90 kN (per load cell), which was 40 kN (or an 80% increase) higher than the original value. This 40 kN compared very good with the 33 kN of Column 7B. This indicated that the increase the axial load was directly proportional to the length increase of the column due to cracking of the column. The higher the horizontal impact load, the larger the cracks, and thus the higher the increase in the axial load.

Static phase of test on Column 7C

After the impact test, a static test was done on the column to determine the reserve strength of the column. The column was step loaded with a static horizontal load in steps of 10 kN. During the static test the horizontal cracks soon increased in width although they were slow to increase in length. The two major diagonal cracks developed slowly band it never looked as if the column might fail in shear. The diagonal cracks angles of 39,1° and 66,8° corresponded with that of the static tests of Columns 7A and 7B.

Stellenbosch University http://scholar.sun.ac.za

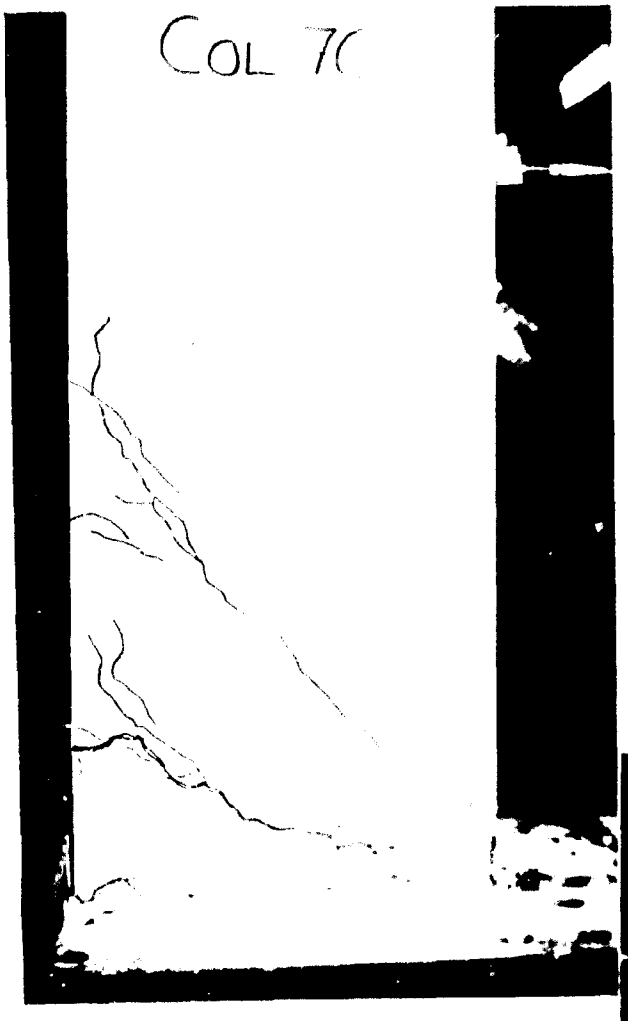

Figure B.114: Crack pattern of Column 7C seen from one side after the impact phase.

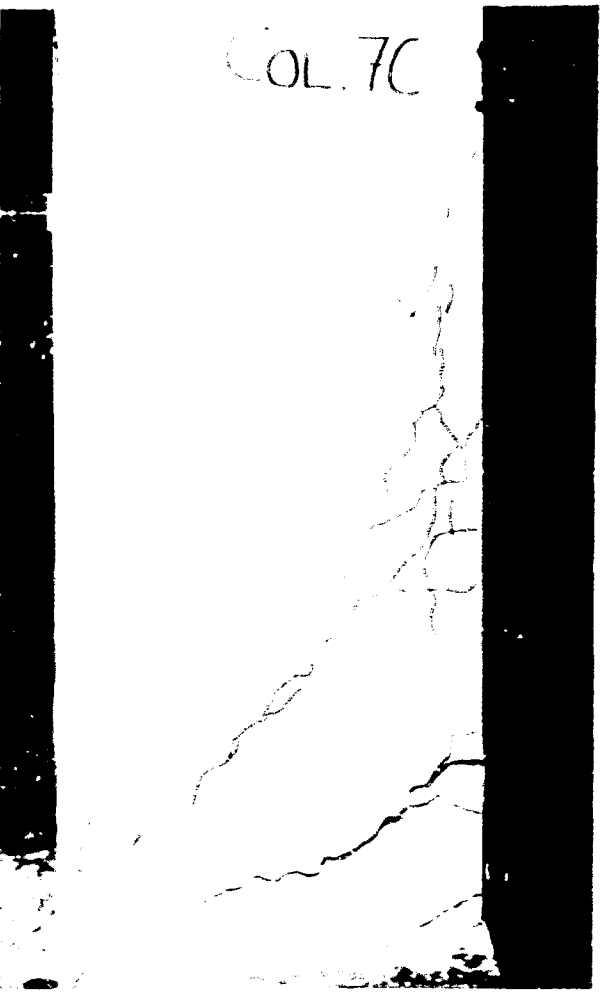

Figure B.115: Crack pattern of Column 7C seen from the other side of the column.

Stellenbosch University http://scholar.sun.ac.za

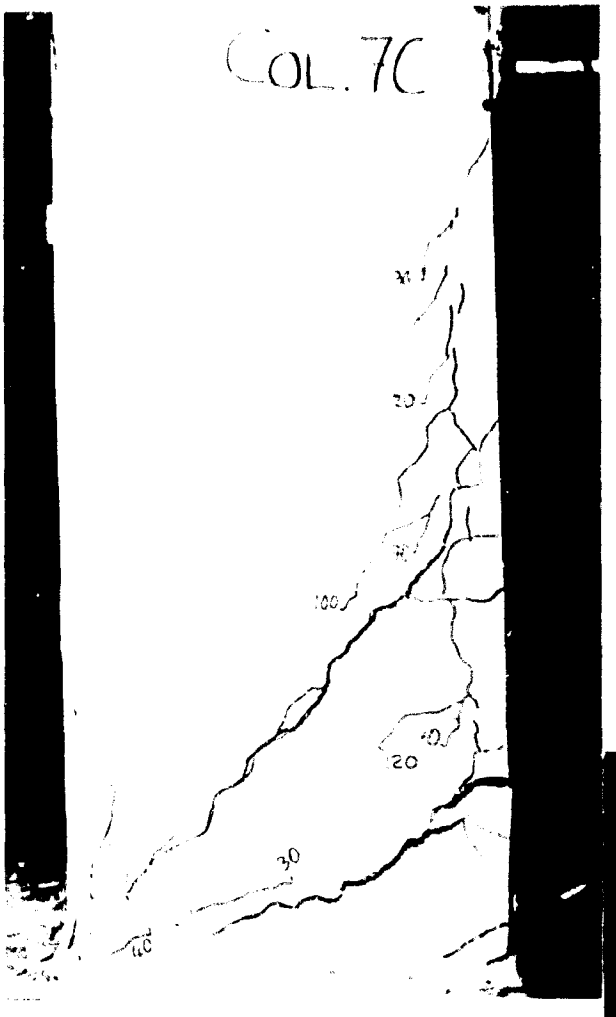

Figure B.116: Crack pattern of Column 7C seen from one side after the static test.

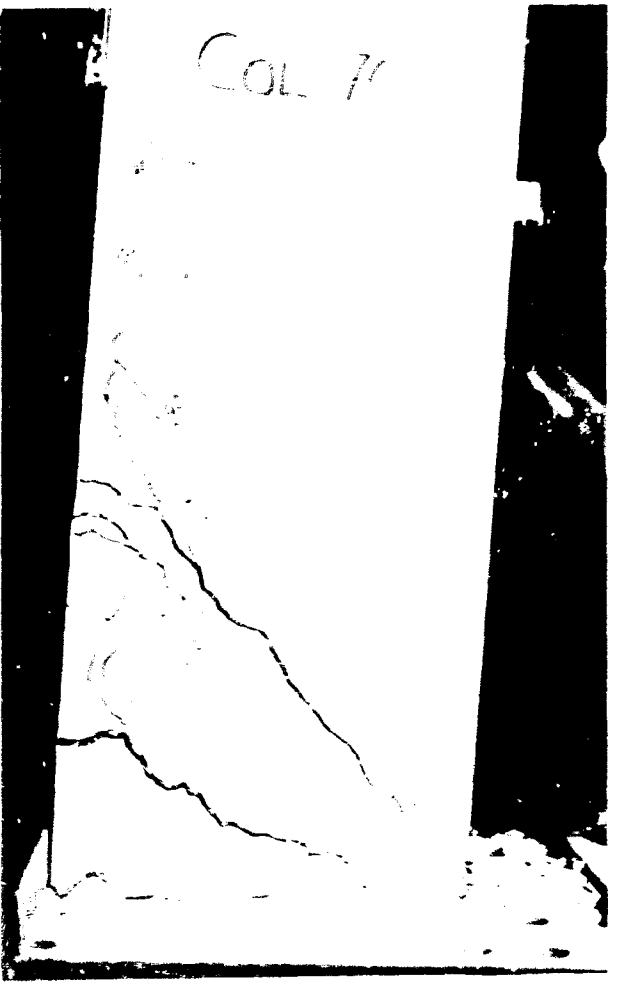

Figure B.117: Crack pattern of Colum 7C seen from the other side of the column.

Stellenbosch University http://scholar.sun.ac.za

The column failed at a static horizontal load of 123,3914 kN. This corresponds with a flexural moment of 91,31 kNm at the bottom of the column. This static failure load was a little lower than that of Columns 7A and 7B, but this could be contributed to a little lower compressive strength of the concrete.

The axial load started to increase as soon as the horizontal load was applied. This was once again due to the width increase of the existing cracks (cracks that developed during the impact test). The axial load increased from 50 kN to nearly 67 kN per load cell. This meant an increase of 17 kN per load cell.

As was found with the strain of Column 7A and Column 7B, the strain measured at the rear bottom of the column kept increasing during the static test. This indicated that no cracks reached the back of the column, like in the shear failures of the number two series columns.

The damaged Column 7C started to fail at a top deflection of around 30 mm, while the undamaged Column 7A started to fail at a top deflection of about 20 mm. This column and Column 7B failed completely at deflections of 58 mm and 57 mm, respectively, while Column 7A failed completely at a deflection of 63 mm.

Figures B.114 and B.115 show the visible crack pattern on both sides of the column after the impact test. Figures B.116 and B.117 show the crack pattern after the static test. Figures B.733 to B.760 show graphically the recorded test data.

Stellenbosch University http://scholar.sun.ac.za

B.8.32 Column 7D. (figures B.118 to B.119)

Reinforcement: Main: 2-Y16 + 2-Y16 (1,53 %)
Stirrups: 14-R8@150
Concrete cover: 23 mm

Concrete mix: Water - 28,14 kg
Cement - 71,77 kg
Sand - 108,50 kg
Stone - 162,70 kg

TABLE B.34: Details of concrete cubes from column 7D

NUMBER	CASTING DATE	DATE TESTED	AGE DAYS	MASS (kg)	SPLIT (kN)	FORCE (kN)	STRENGTH (MPa)
ML-7D1	04/07/88	11/07/88	7	8,46	121,3	825,94	36,71
ML-7D2	04/07/88	11/07/88	7	8,54	-	830,31	36,90
ML-7D3	04/07/88	11/07/88	7	8,47	104,2	820,17	36,45
ML-7D4	04/07/88	11/07/88	7	8,44	-	822,23	36,54
ML-7D5	04/07/88	01/08/88	28	8,49	-	1128,82	50,17
ML-7D6	04/07/88	01/08/88	28	8,58	-	1099,29	48,86

Impact phase of test on Column 7D

With this impact test the compressive strength of the concrete was again higher than the reference test (group 3), to investigate the influence of the higher concrete strength on the test. With this impact test it was tried to introduce an impact load to the column which would force column to fail under the impact loading. The axial load was the normal 100 kN. The impact load peaked at a value of 229,7711 kN and the column failed in shear. There were two diagonal cracks visible and they formed angles of 57,8° and 40,5° with the vertical axis of the column. There was also one small horizontal crack visible at the bottom of the column. The column failed in shear along the 40,5° diagonal crack. The undamaged column tested statically (Column 7A) failed in flexure with a maximum horizontal load of 126,22 kN. This column's impact resistance was 82% higher than that of the static resistance of Column 7A.

Stellenbosch University http://scholar.sun.ac.za

Figure B.118: Failure and crack pattern of Column 7D seen from one side after the impact phase.

Figure B.119: Failure and crack pattern of Column 7D seen from the other side of the column.

Stellenbosch University http://scholar.sun.ac.za

Again there was a slight drop in the axial load before it started to increase with the impact loading of the column. After the impact, the axial load dropped to zero which indicated that the column failed completely. Again the axial load of each load cell peaked at a maximum value of about 76 kN or in other words, it was 26 kN higher than the initial load per load cell. This was lower than the previous two tests in this series but it could be contributed to a the different failure mechanism of the column.

After the initial peaks of the impact load function, some further peaks were present. This peaks showed that after the failure of the column, the column was unable to let the striker rebound and thus the striker caught up with the column at these points and gave the column further small impact loads.

After the impact test, no static test could be done because the column failed completely in shear during the impact phase of the test.

Figures B.118 and B.119 show the visible crack pattern and failure from both sides of the column after the impact test. Figures B.761 to B.784 show graphically the recorded test data.

B.8.33 Column 8A. (figures B.120 to B.121)

Reinforcement: Main: 2-Y16 + 2-Y16 (1,53 %)
Stirrups: 14-R8@150
Concrete cover: 23 mm

Concrete mix:			
	Water	-	26,5 kg
	Cement	-	42,6 kg
	Sand	-	128,0 kg
	Stone	-	176,0 kg

Stellenbosch University http://scholar.sun.ac.za

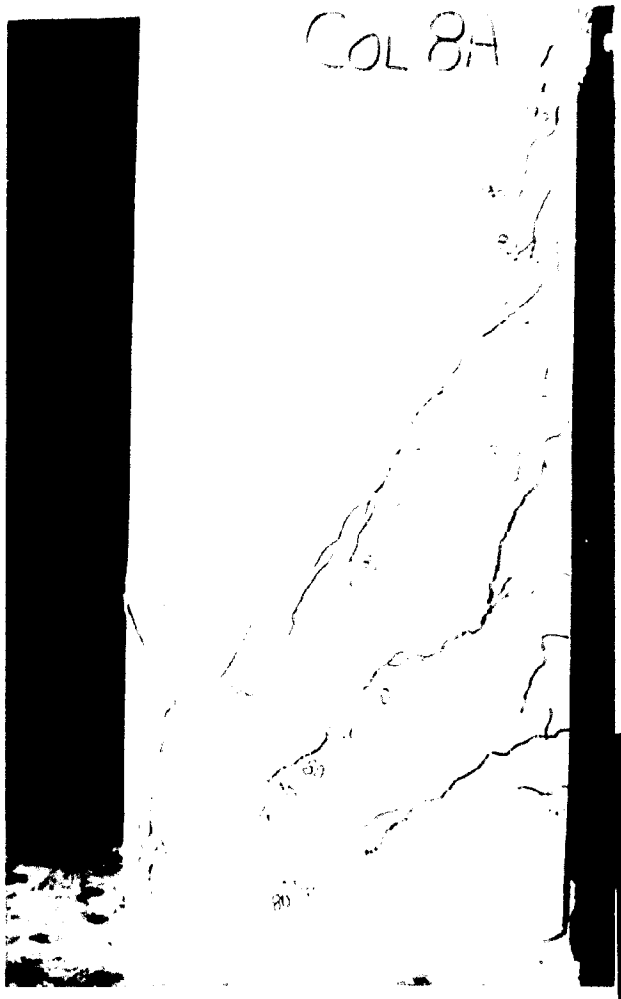

Figure B.120: Crack pattern of Column 8A seen from one side after the static test.

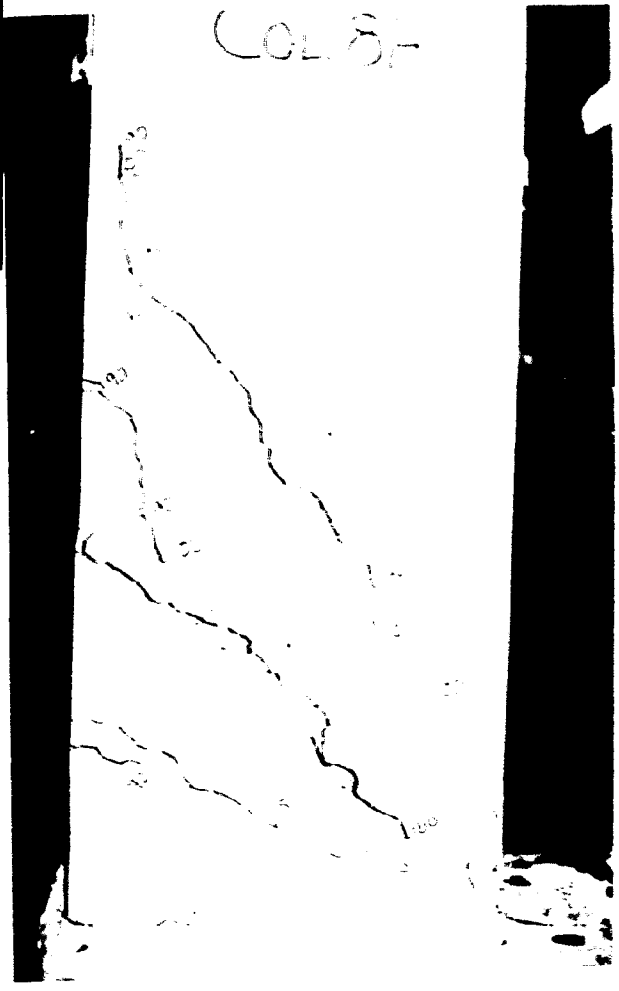

Figure B.121: Crack pattern of Column 8A seen from the other side of the column.

Stellenbosch University http://scholar.sun.ac.za

TABLE B.35: Details of concrete cubes from column 8A

NUMBER	CASTING DATE	DATE TESTED	AGE DAYS	MASS (kg)	SLPIT (kN)	FORCE (kN)	STRENGTH (MPa)
ML-8A1	06/07/88	13/07/88	7	[illegible]0	58,7	358,35	15,93
ML-8A2	06/07/88	13/07/88	7	[illegible]6		364,46	16,20
ML-8A3	06/07/88	13/07/88	7	8,48	63,6	370,98	16,49
ML-8A4	06/07/88	13/07/88	7	8,46	-	369,30	16,41
ML-8A5	06/07/88	03/08/88	28	8,50	-	544,70	24,21
ML-8A6	06/07/88	03/08/88	28	8,50	-	533,45	23,71

Static test on Column 8A

With this series of columns the influence of a lower concrete compression strength was investigated. In this series the initial axial load on the column was again 100kN (in other words 50 kN / sway frame) as in all the other series of tests except for the series 6 tests.

The column was step loaded with a static horizontal load in steps of 10 kN. With a 40 kN horizontal load (moment of 29,6 kNm) the first horizontal cracks started to develop at the bottom of the column. With a 50 kN two further cracks developed higher up on the column (160 mm and 320 mm above the bottom, respectively) and they developed into diagonal cracks. With a 70 kN horizontal load one more diagonal crack started higher up on the column. The three diagonal cracks formed angles of 32,5°, 47,6° and 65,4° with the vertical axis of the column.

The ultimate static horizontal load reached by this column was 107,393 kN (a bending moment of 79,5 kNm at the bottom of the column). This was only reached after a considerable deflection from a horizontal load of 90 kN. This indicated that after the 90 kN horizontal load, the reinforcement had to be strain hardened by the deflection of the column, before the ultimate load of 107,393 kN could be reached. The column failed in flexure. Once again the cracks closed as soon as the horizontal load was removed, although there was permanent deflection present. In the case of a shear failure no such rehabilitation

Stellenbosch University http://scholar.sun.ac.za

would have been present. The reference tests with the higher strength concrete failed at maximum horizontal load of 116 to 117 kN, compared to the slightly lower maximum load of 107,4 kN for this column (Column 8A). In other words, the lower concrete strength decreased the ultimate load with about 7 to 8%.

Again the axial load started to drop as soon as the horizontal load was applied to the column before it suddenly started to increase as the horizontal load increased further. As previously mentioned, the first horizontal crack was visible around a 40 kN horizontal load. The graphs of the axial loads (figure B.787) show that the axial load started to increase just before the 40 kN horizontal load. Thus the graph corresponded favourably with the crack development of the column. With a 100 kN horizontal load, the column started to fail in flexure. This was also clearly visible on the graph of the axial loads, because the axial loads increased considerably at that stage. This considerable increase can be explained by the increasing crack widths resulting in a lengthening of the column and thus a higher axial load. The ultimate axial load was nearly 20 kN higher than the initial axial load, this was an increase of about 39%.

With this test only the bottom strain gauge was measured as the middle strain gauge did not show any significant changes in the previous tests. The graph of the strain at the rear bottom of the column was a very good indication of the failing mechanism of the column. The flexural mechanism was always the dominant failing mechanism in this test (Column 8A) and thus the strain increased all the time until the flexural failure of the column.

At a top deflection of about 23 mm, the column started to fail. At a top deflection of 47 mm the column reach an ultimate load of 107,393 kN.

Figures B.120 and B.121 show the crack pattern after the static test. Figures B.785 to B.788 show graphically the recorded test data.

Stellenbosch University http://scholar.sun.ac.za

B.8.34 Column 8B. (figures B.122 to B.125)

Reinforcement: Main: 2-Y16 + 2-Y16 (1,53 %)
Stirrups: 14-R8@150
Concrete cover: 23 mm

Concrete mix:

Water	-	26,5 kg
Cement	-	42,6 kg
Sand	-	128,0 kg
Stone	-	176,0 kg

TABLE B.36: Details of concrete cubes from column 8B

NUMBER	CASTING DATE	DATE TESTED	AGE DAYS	MASS (kg)	SPLIT (kN)	FORCE (kN)	STRENGTH (MPa)
ML-8B1	07/07/88	14/07/88	7	8,40	69,8	373,31	16,59
ML-8B2	07/07/88	14/07/88	7	8,41	-	363,01	16,13
ML-8B3	07/07/88	14/07/88	7	8,41	59,4	379,94	16,87
ML-8B4	07/07/88	14/07/88	7	8,36	-	377,77	16,79
ML-8B5	07/07/88	04/08/88	28	8,44	-	534,67	23,76
ML-8B6	07/07/88	04/08/88	28	8,32	-	568,85	25,28

Impact phase of test on Column 8B

With this impact test the concrete compressive strength was lower than the reference tests (group 3), to investigate the influence of the lower concrete strength on the test. With this impact test it was tried to introduce an impact load to the column which was more or less in the same region as the static failure load of the undamaged Column 8A. The impact loading applied to the column peaked at a load of 173,5532 kN. This was the very short first peak of the impact load history and can thus be ignored. The second longer duration peak, peaked at a value of 131,3 kN. This was a little higher than the static failure load of Column 8A of 107,393 kN.

During the impact a horizontal crack and two major diagonal cracks developed. The horizontal crack was right at the bottom of the column. The two diagonal cracks formed angles of 40,5° and 59,0° with the vertical axis of the column. A third diagonal

Stellenbosch University http://scholar.sun.ac.za

crack only developed late during the static test that followed the impact test. This third diagonal crack formed an angle of 29,4° with the vertical axis of the column. Similar to the series one tests, the cracks closed after the impact and the damage did not look very serious.

The axial load showed a small decrease before it increased after the impact loading started. This small decrease was even smaller than in the previous cases, but this could be expected because this concrete's compression strength was very low and thus had a lower tensile strength and therefore would have cracked earlier. The axial load of each load cell peaked at a value of nearly 76 kN. This peak was nearly 27 kN higher (per load cell) than the initial axial load per load cell.

Static phase of test on Column 8B

After the impact test, a static test was done on the column to determine the reserve strength of the column. The column was step loaded with a static horizontal load in steps of 10 kN. During the static test the horizontal cracks soon increased in width. The major diagonal cracks developed slowly and it never looked as if the column might fail in shear. As mentioned earlier the third diagonal crack only developed late during the static test and formed an angle of 29,4° with the vertical axis of the column. The other two diagonal cracks formed angles of 40,5° and 59°. The diagonal cracks corresponded reasonably with that of the static test of Column 8A.

The column failed at a static horizontal load of 106,387 kN. This corresponds with a flexural moment of 78,7 kNm at the bottom of the column. This static failure load was a little lower than that of Column 8A (107,393).

Stellenbosch University http://scholar.sun.ac.za

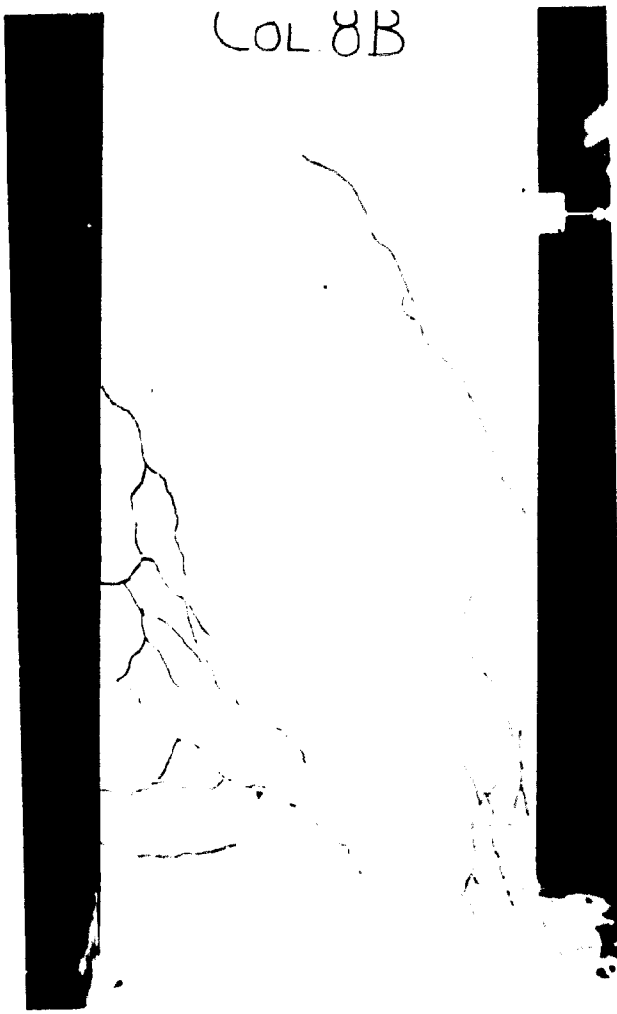

Figure B.122: Crack pattern of Column 8B seen from one side after the impact phase.

Figure B.123: Crack pattern of Column 8B seen from the other side of the column.

Stellenbosch University http://scholar.sun.ac.za

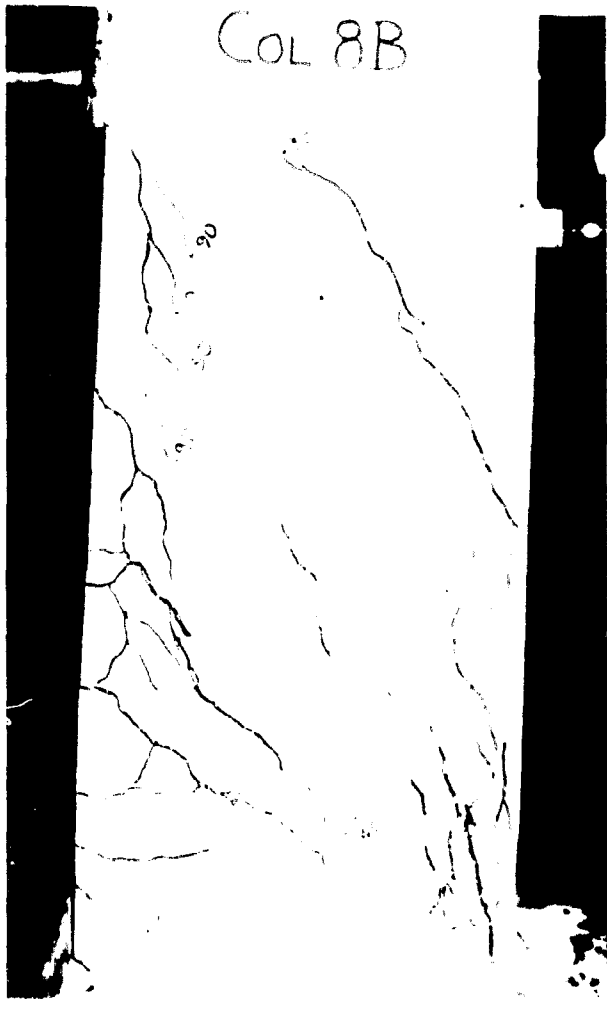

Figure B.124: Crack pattern of Column 8B seen from one side after the static test.

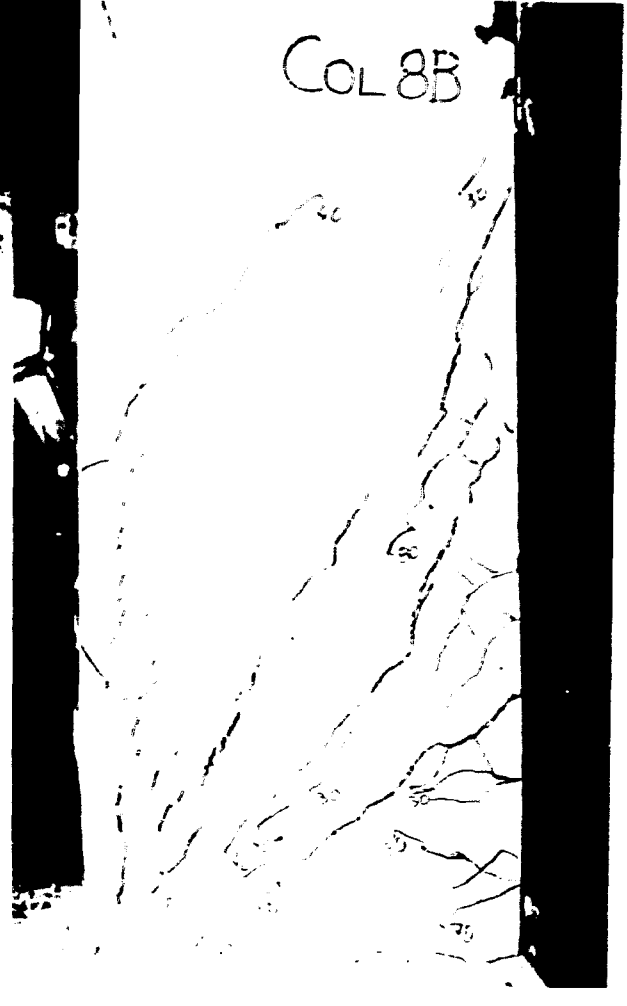

Figure B.125: Crack pattern of Column 8B seen from the other side of the column.

Stellenbosch University http://scholar.sun.ac.za

The axial load immediately started to increase as soon as the horizontal load was applied to the column. This was due to the widening of the existing cracks in the column (from the impact test) as soon as the static horizontal load was applied. The axial load per load cell increased from around 49 kN to around 60 kN. This 11 kN increase was lower than the 20 kN of Column 8A, but this can be contributed to the lower strength concrete.

The damaged column 8B started to fail at a top deflection of about 34 mm while the undamaged column 8A started to fail at a top deflection of about 23 mm. This column failed completely at a top deflection of 42 mm, while Column 8A failed completely at a top deflection of 47 mm.

Figures B.122 and B.123 show the visible crack pattern on both sides of the column after the impact test. Figures B.124 and B.125 show the crack pattern after the static test. Figures B.789 to B.816 show graphically the recorded test data.

B.8.35 Column 8C. (figures B.126 to B.127)

Reinforcement: Main: 2-Y16 + 2-Y16 (1,53 %)
Stirrups: 14-R8@150
Concrete cover: 23 mm

Concrete mix:	Water	-	26.5 kg
	Cement	-	42,6 kg
	Sand	-	128,0 kg
	Stone	-	176,0 kg

Stellenbosch University http://scholar.sun.ac.za

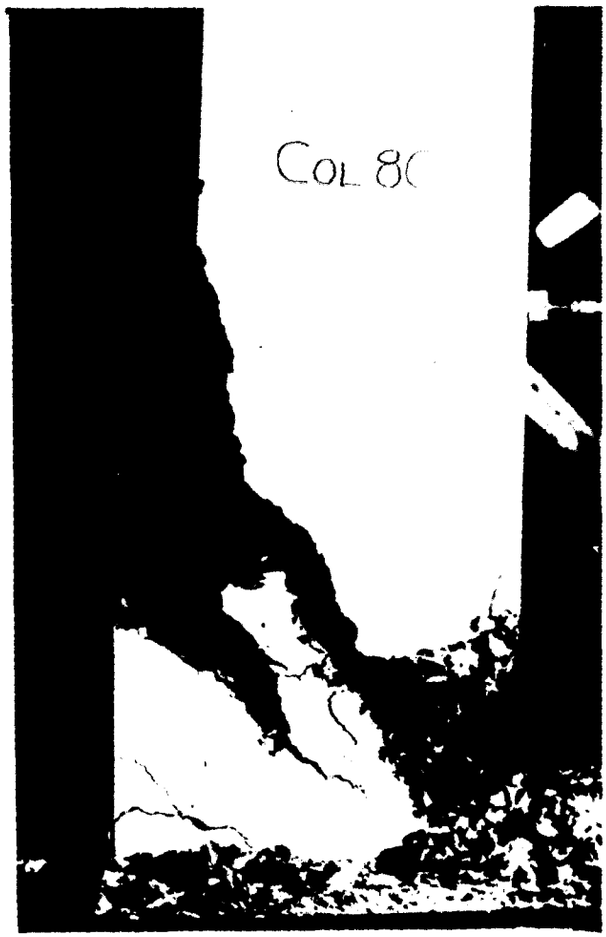

Figure B.126: Failure and crack pattern of Column 8C seen from one side after the impact phase.

Figure B.127: Failure and crack pattern of Column 8C seen from the other side of the column.

Stellenbosch University http://scholar.sun.ac.za

Table B.37: Details of concrete cubes from column 8C							
NUMBER	CASTING DATE	DATE TESTED	AGE DAYS	MASS (kg)	SPLIT (kN)	FORCE (kN)	STRENGTH (MPa)
ML-8C1	11/07/88	18/07/88	7	8,48	81,9	405,77	18,03
ML-8C2	11/07/88	18/07/88	7	8,46	-	404,63	17,98
ML-8C3	11/07/88	18/07/88	7	8,49	72,1	404,93	18,00
ML-8C4	11/07/88	18/07/88	7	8,44	-	420,53	18,69
ML-8C5	11/07/88	08/08/88	28	8,46	-	582,93	25,91
ML-8C6	11/07/88	08/08/88	28	8,54	-	540,35	24,02

Impact phase of test on Column 8C

With this impact test the compressive strength was again lower than the reference tests (group 3), to investigate the influence of the lower concrete strength on the test results. With this impact test it was tried to introduce an impact load to the column which was large enough to force the column to fail under the impact loading. The axial load was the normal 100 kN. The impact loading peaked at a load of 181,9124 kN and the column failed in shear. There were two diagonal cracks visible and they formed angles of 50,4° and 29,8° with the vertical axis of the column. There was also one small horizontal crack visible right at the bottom of the column. The column failed in shear along the 29,8° diagonal crack. The undamaged column tested statically, Column 8A, failed in flexure with a maximum horizontal load of 107,393 kN. This column's impact resistance was 69,4% higher than the static resistance of Column 8A and, additionally, this column failed in shear compared to the flexural failure of the statically tested Column 8A.

Unfortunately both the strain gauges were damaged just after the impact loading started and thus no further readings were available from these strain gauges.

Looking at the axial load graphs (figures B.818 and B.820) a small initial drop in the axial load can be seen. As with Column 8B this decrease was once again very small. This small fall in the axial load indicated that the column actually shortened

Stellenbosch University http://scholar.sun.ac.za

slightly before the first crack developed. Because this was a lower strength concrete than that of the reference group, the initial cracks developed earlier and thus the decrease in the axial load was smaller. After the impact the axial load dropped to zero which indicated that the column failed completely.

After the impact test, no static test could be done because the column failed completely in shear during the impact phase of the test.

Figures B.126 and B.127 show the visible crack pattern and the failure from both sides of the column after the impact test. Figures B.817 to B.840 show graphically the recorded test data.

B.8.36 Column 8D. (figures B.128 and B.129)

Reinforcement: Main: 2-Y16 + 2-Y16 (1,53 %)
Stirrups: 14-R8@150
Concrete cover: 23 mm

Concrete mix: Water - 26.5 kg
Cement - 42,6 kg
Sand - 128,0 kg
Stone - 176,0 kg

TABLE B.38: Details of concrete cubes from column 8D

NUMBER	CASTING DATE	DATE TESTED	AGE DAYS	MASS (kg)	SPLIT (kN)	FORCE (kN)	STRENGTH (MPa)
ML-8D1	12/07/88	19/07/88	7	8,42	87,2	432,63	19,23
ML-8D2	12/07/88	19/07/88	7	8,37	-	447,85	19,90
ML-8D3	12/07/88	19/07/88	7	8,42	74,4	446,70	19,85
ML-8D4	12/07/88	19/07/88	7	8,39	-	456,85	20,30
ML-8D5	12/07/88	09/08/88	28	8,39	-	640,76	28,48
ML-8D6	12/07/88	09/08/88	28	8,37	-	598,72	26,61

Stellenbosch University http://scholar.sun.ac.za

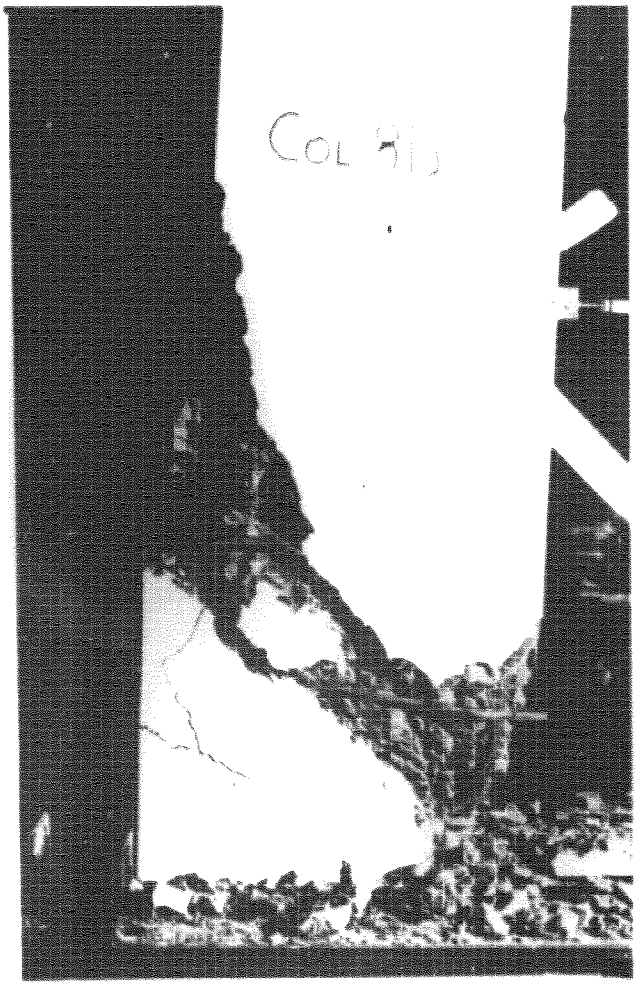

Figure B.128: Failure and crack pattern of Column 8D seen from one side after the impact phase.

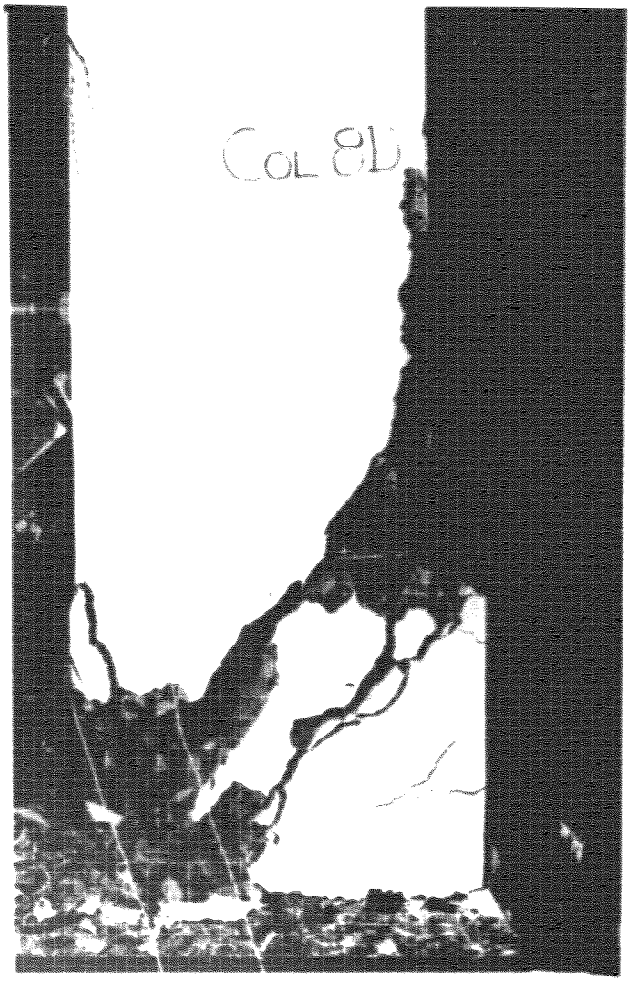

Figure B.129: Failure and crack pattern of Column 8D seen from the other side of the column.

Stellenbosch University http://scholar.sun.ac.za

Impact phase of test on Column 8D

With this impact test the concrete compression strength was again lower than that of the reference group 3, to investigate the influence of the lower concrete strength on the test. With this impact test it was tried to introduce an impact load to the column which would force the column to fail under the impact loading conditions. The axial load was the normal 100 kN. The impact loading peaked at a value of 164,6048 kN and the column failed in shear. There were three diagonal cracks visible and they formed angles of 66,8°, 47,6° and 33,9° with the vertical axis of the column. The 66,8° crack was a very faint crack compared to the other two cracks. There was also one small horizontal crack visible right at the bottom of the column. The column failed in shear along the 33,9° shear crack. The undamaged column, tested statically (Column 8A), failed in flexure with a maximum horizontal load of 107,393 kN. This column's impact resistance was 53,3% higher than the static resistance of Column 8A and additionally, this column failed in shear compared to the flexural failure of the statically tested column (Column 8A).

Unfortunately the bottom strain gauge was damaged just after the impact loading started and thus no further readings were available form that strain gauge.

Looking at the axial load graphs (figures B.842 and B.844) a small initial drop in the axial load can be seen. As with Column 8B this decrease was once again very small. The axial load of each load cell peaked at a value which was 28 kN higher than the initial load per load cell. This was very close to the 26 kN of the previous tests in this series (Column 8B, Column 8C).

Due to complete failure of the column no static test was done.

Figures B.128 and B.129 show the visible crack pattern and failure from both sides of the column after the impact test. Figures B.841 to B.863 show graphically the recorded test data.

Stellenbosch University http://scholar.sun.ac.za

B.9 Test results.

The best way to present all the results and the measurements of the tests is in the form of graphs. In this section all the graphs of the results and recorded data are given.

Some of the original graphs had lot of noise present on the graphs. These noise made it difficult to see the trend of each graph and to compare the different tests with each other. To eliminate these problems a certain degree of smoothing had been performed on these graphs. These smoothed graphs are thus also presented here to make this experimental report as comprehensive as possible. The smoothing was performed mathematically with the aid of a computer program. Smoothing was performed by the method simple moving averages considering 24 data points for each point plotted.

For each static test, four graphs are given:

1. The deflections of the column as measured 600mm and 1550mm from the bottom of the column were plotted against the applied horizontal load.

2. The strain of the concrete measured at two positions on the rear (100-220mm and 690-810mm from bottom) of the column were plotted against the horizontal applied load.

3. The axial loads on the column, as measured by the two load cells, were plotted against the horizontal applied load.

4. All the loads (compression and tension loads) transferred from the steel footing to the laboratory floor were plotted against the horizontal applied load.

For each dynamic test 24 graphs are given:

1. The first twelve graphs present the measurements as taken by the twelve measuring channels and recorded by the

Stellenbosch University http://scholar.sun.ac.za

computers during the impact test. These twelve channels are:

a. The impact load.

b. The deceleration of the impacting mass or striker.

c. The right hand axial load cell.

d. The left hand axial load cell.

e. The strain of the concrete measured 100-230mm from bottom of column.

f. The strain of the concrete measured 690-810mm from bottom of column.

g. The acceleration of the column 600mm from the bottom of the column.

h. The acceleration of the column 1550mm from the bottom of the column.

i. The compression force under the footing measured with the L400 no. 2 load cell.

j. The compression force under the footing measured with the L400 no. 3 load cell.

k. The tension force under the footing measured with the L400 no. 5 load cell.

l. The tension force under the footing measured with the L400 no. 6 load cell.

The output of these twelve channels are plotted against time.

2. The next four figures show the sum of the tension and compression loads as well as their smoothed values, plotted against time.

Stellenbosch University http://scholar.sun.ac.za

3. The next figure show the smoothed values of the deceleration of the striker plotted with the measured values, against time.

4. The next figure show all the external forces acting on the system combined in one figure.

5. The next two figures show the sum of the axial loads on the column as well as their smoothed values.

6. The next three figures show the smoothed values of the accelerations of the columns as originally measured as well as their smoothed values plotted on one graph.

7. The last figure show the combined strain as measured at the two mentioned positions, on one graph.

If a static test was done on a column after the dynamic test the same four graphs as that for a static test only are also given.

(The abbreviation, ISMI, used in figure B.131 means inductive strain measurement instrument. The ISMI was used to monitor the accuracy of the strain gauges and was only used with the static test on Column 1A.)

Stellenbosch University http://scholar.sun.ac.za

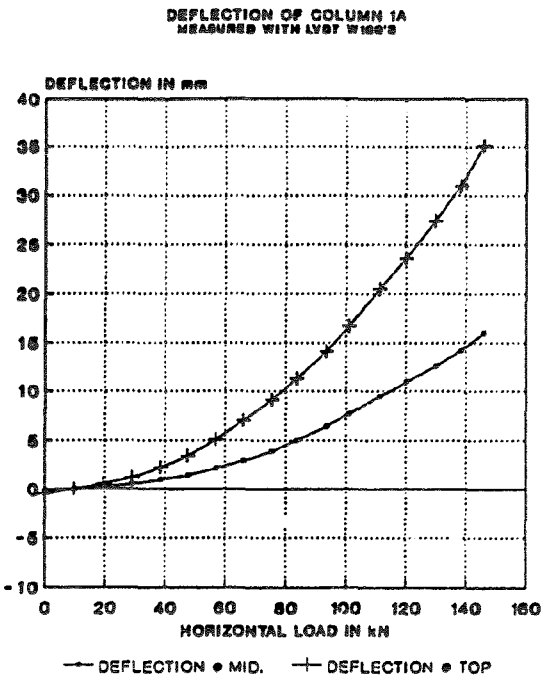

Fig. B.130: Deflection Col.1A

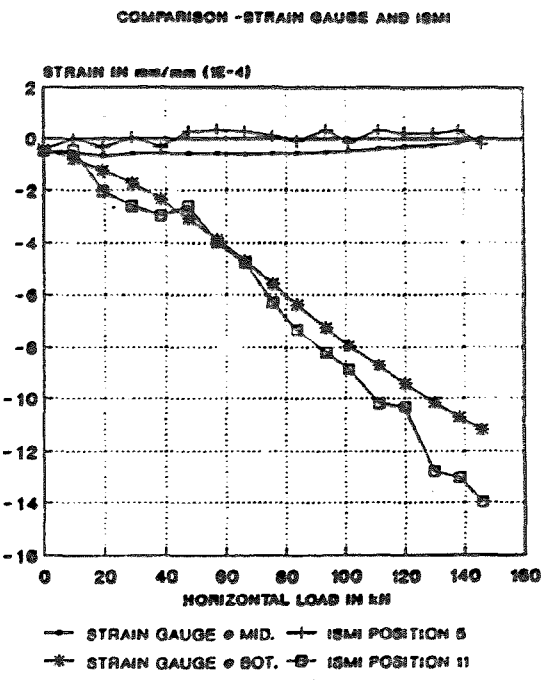

Fig. B.131: Strain Col.1A

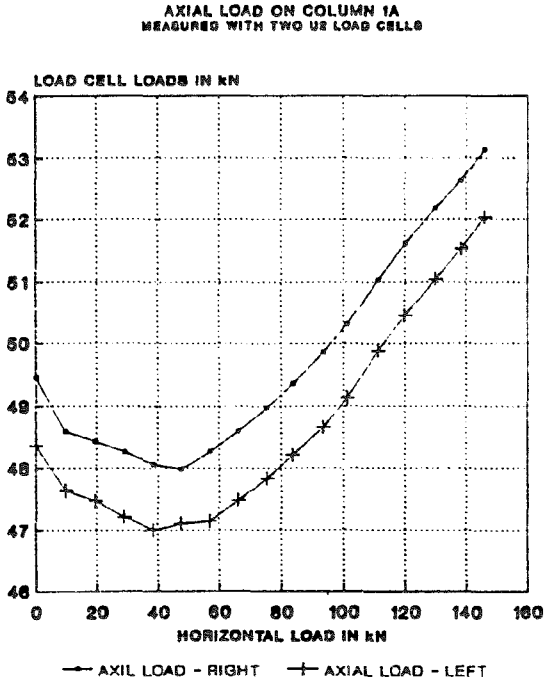

Fig. B.132: Axial load Col 1A

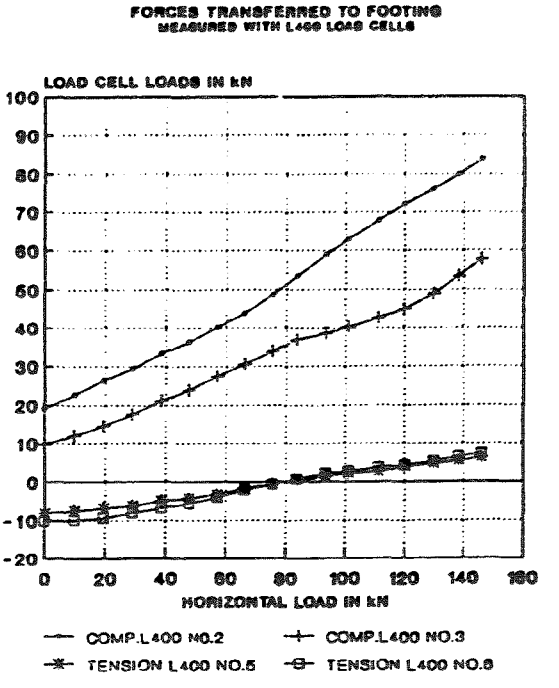

Fig B.133: Foot.loads Col.1A

Stellenbosch University http://scholar.sun.ac.za

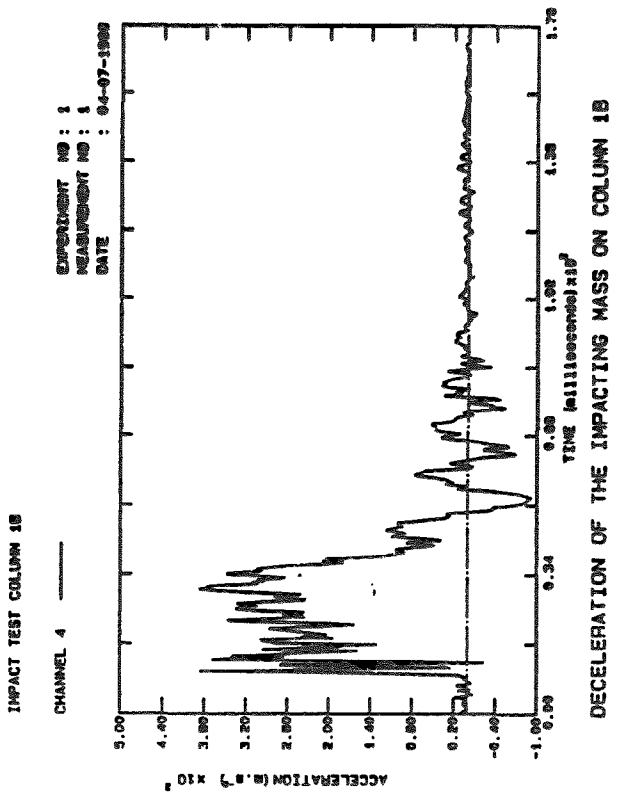

Fig. B.134: Decel. Col.1B

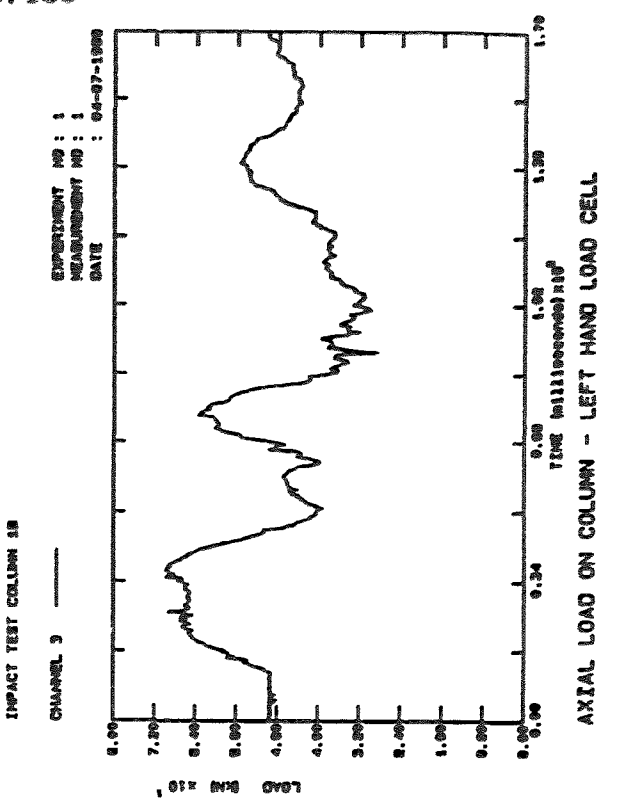

Fig. B.135: Axial load Col.1B

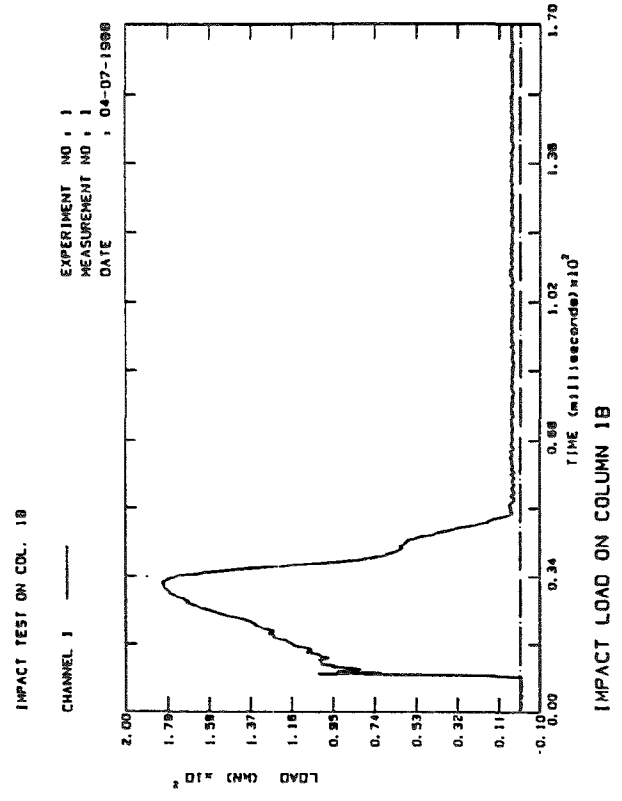

Fig. B.136: Impact Col 1B

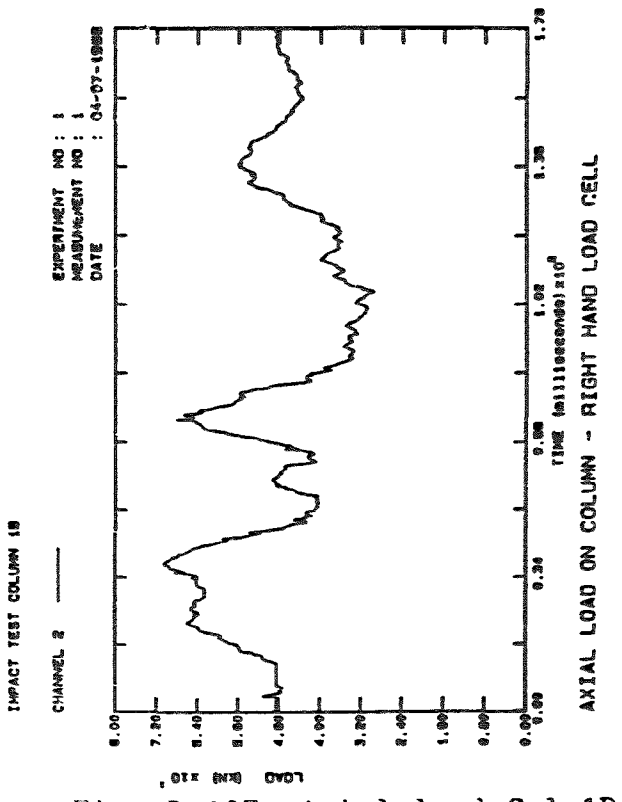

Fig. B.137: Axial load Col.1B

Stellenbosch University http://scholar.sun.ac.za

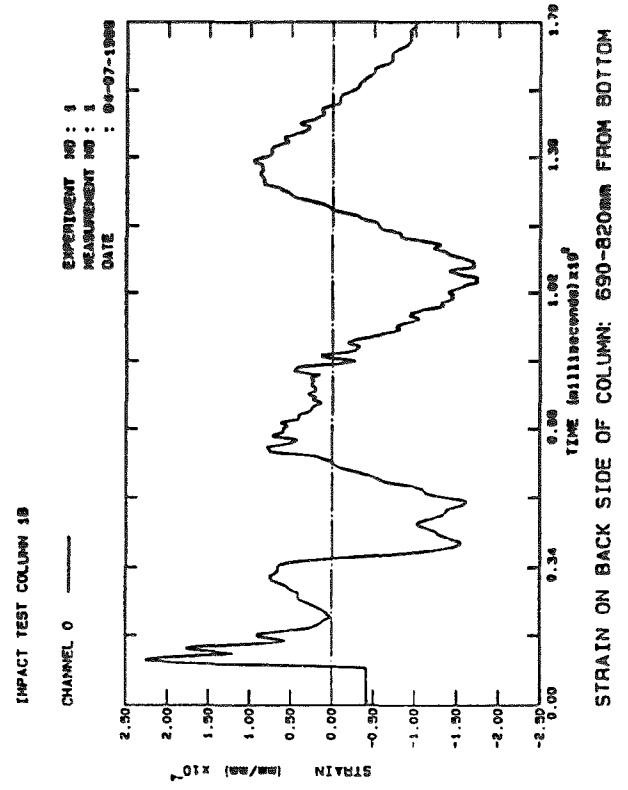

Fig. B.138: Strain Col.1B

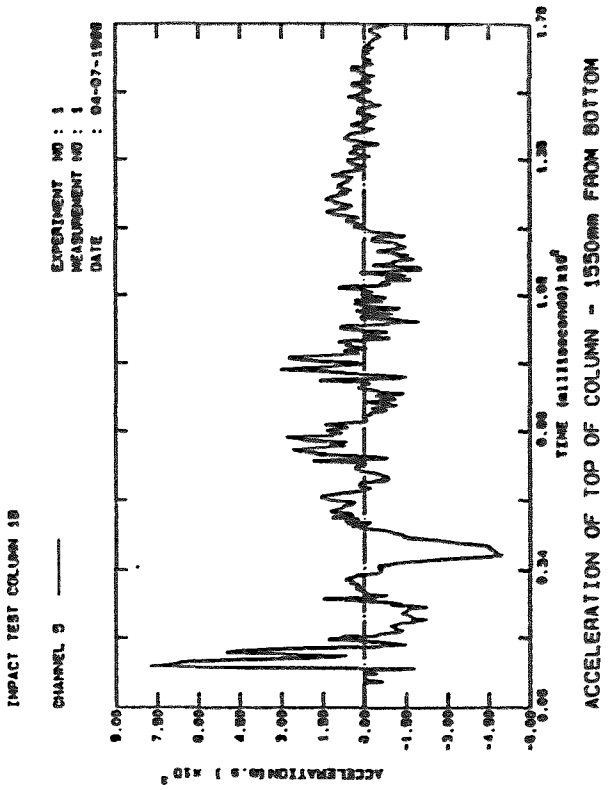

Fig. B.139: Accel. Col.1B

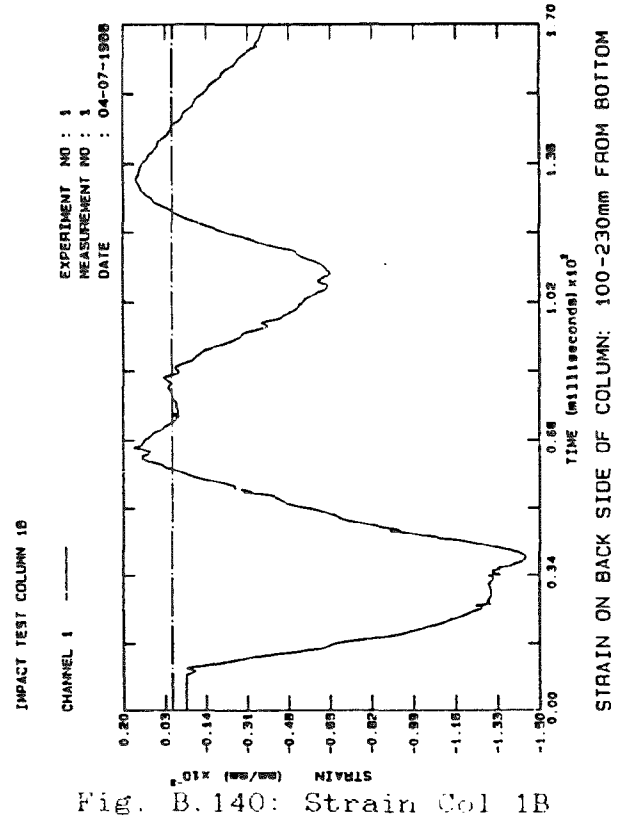

Fig. B.140: Strain Col 1B

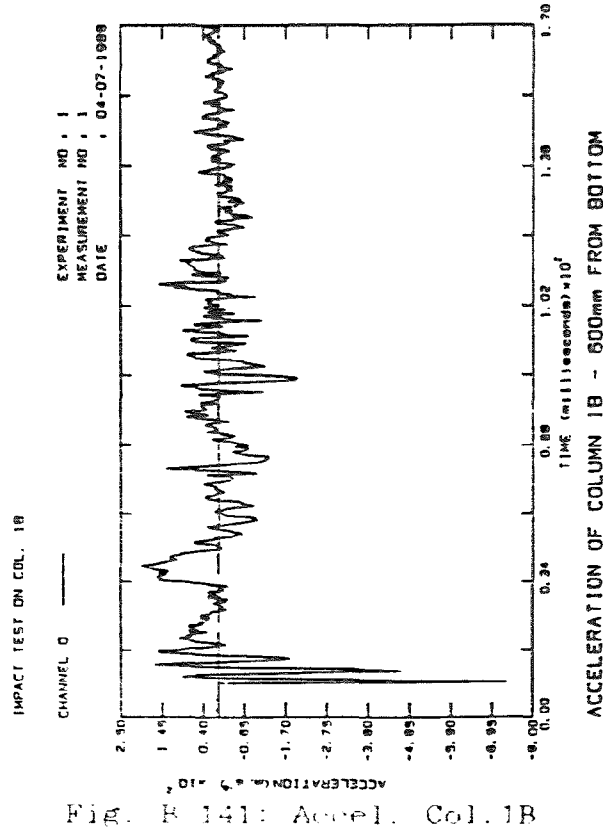

Fig. B.141: Accel. Col.1B

Stellenbosch University http://scholar.sun.ac.za

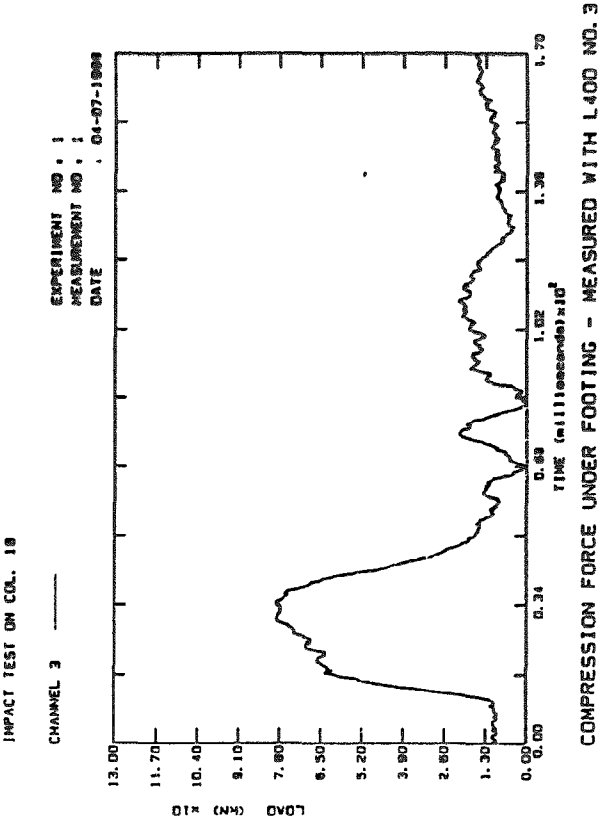

Fig. B.142: Comp. Col.1B

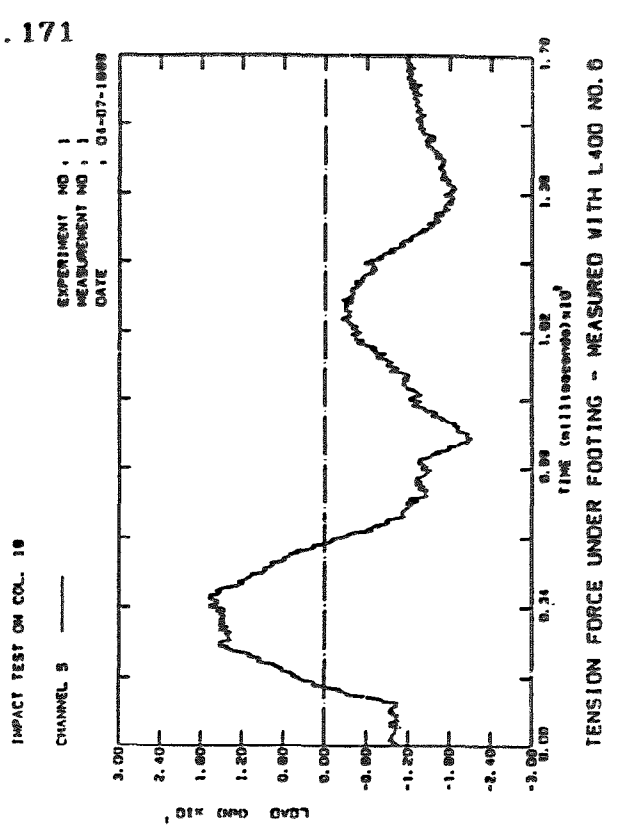

Fig. B.143: Tension Col.1B

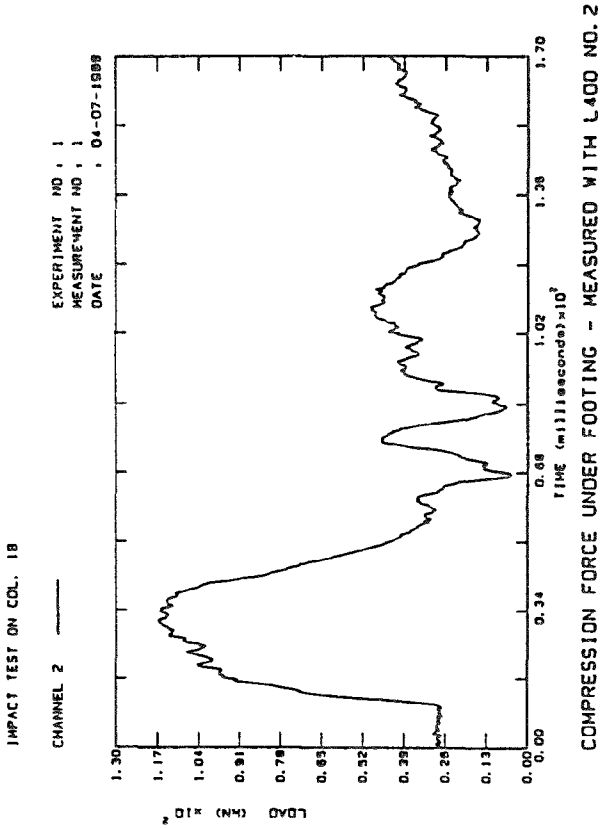

Fig. B.144: Comp. Col 1B

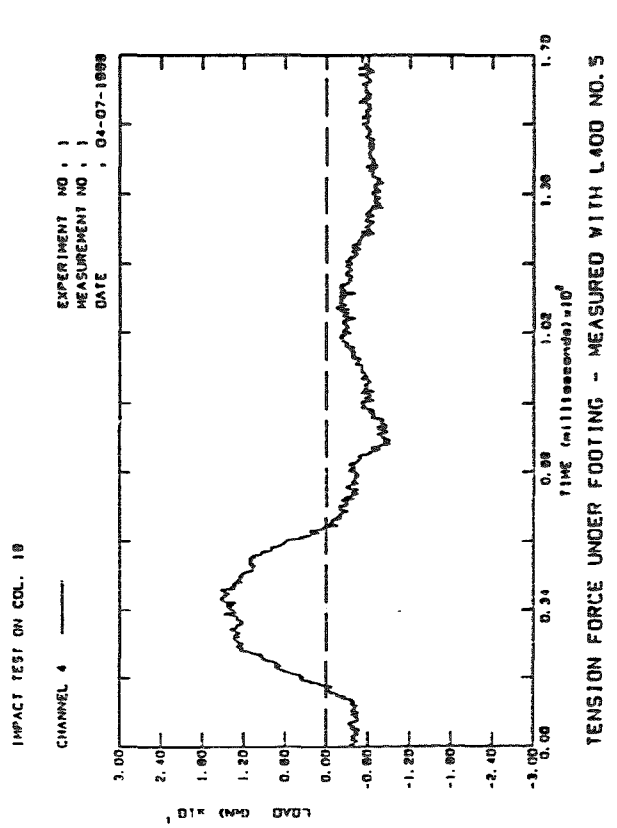

Fig. B.145: Tension Col.1B

Stellenbosch University http://scholar.sun.ac.za

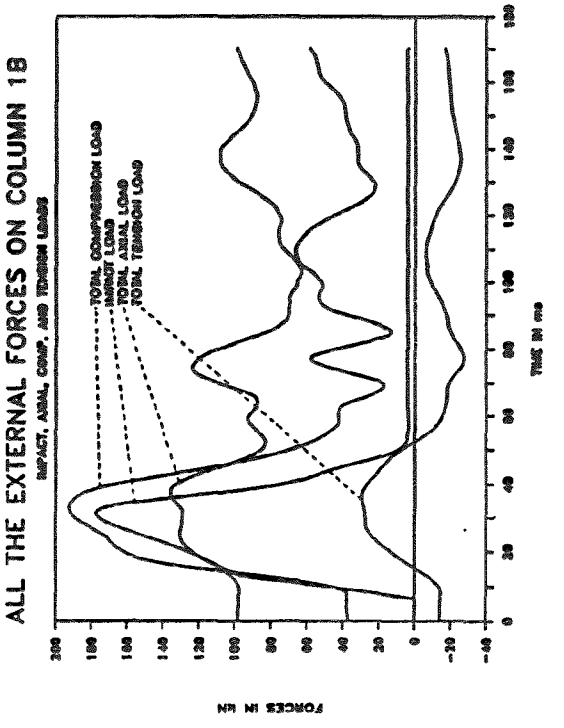

Fig. B.146: Ext. Loads Col.1B

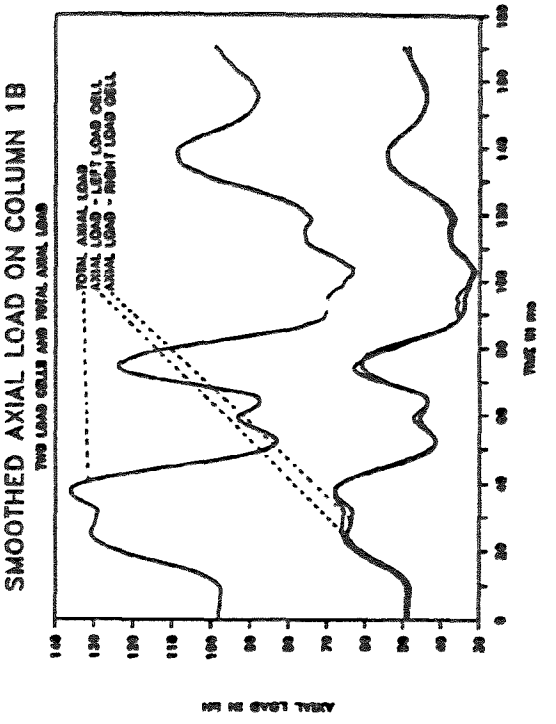

Fig. B.147: Smo. Axial Col.1B

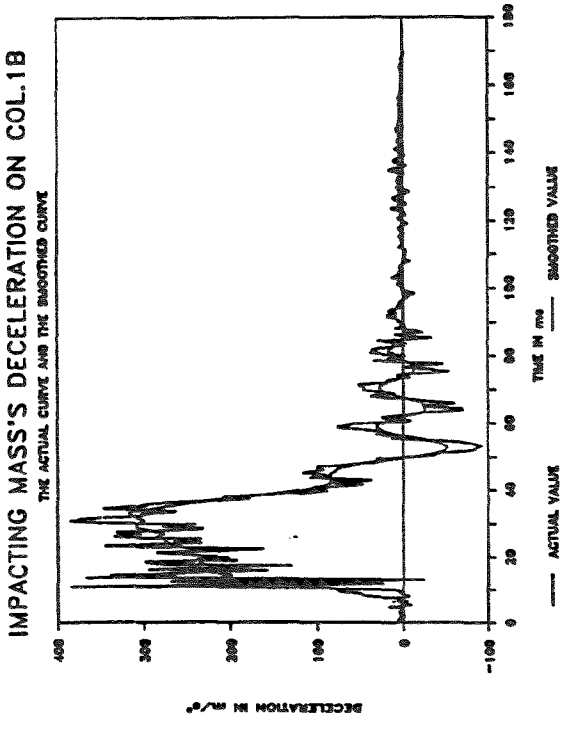

Fig. B.148: Smo.Decel. Col 1B

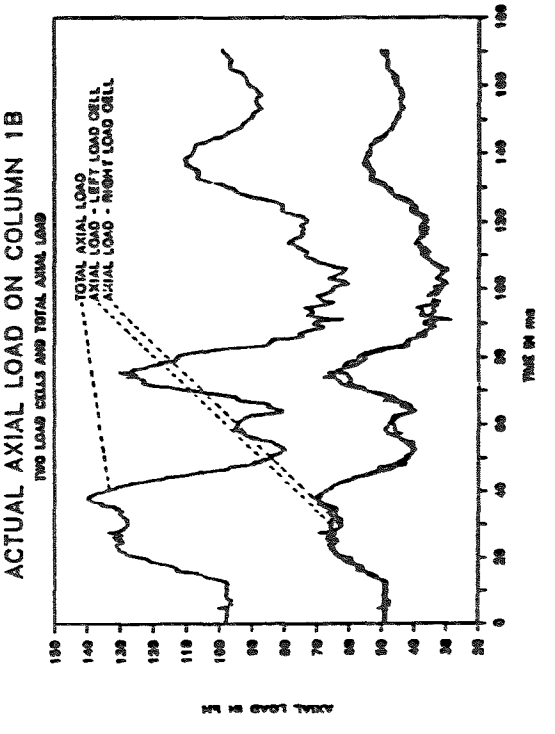

Fig. B.149: Axial loads Col.1B

Stellenbosch University http://scholar.sun.ac.za

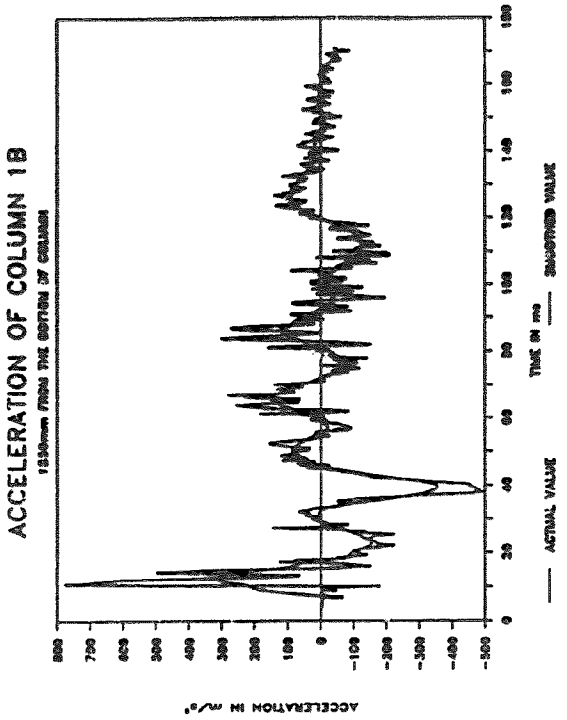

Fig. B.150: Smo.Accel. Col.1B

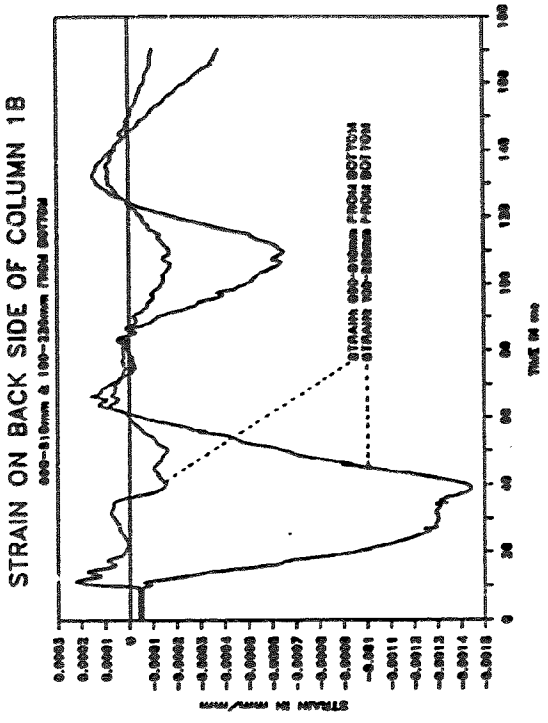

Fig. B.151: Strain Col.1B

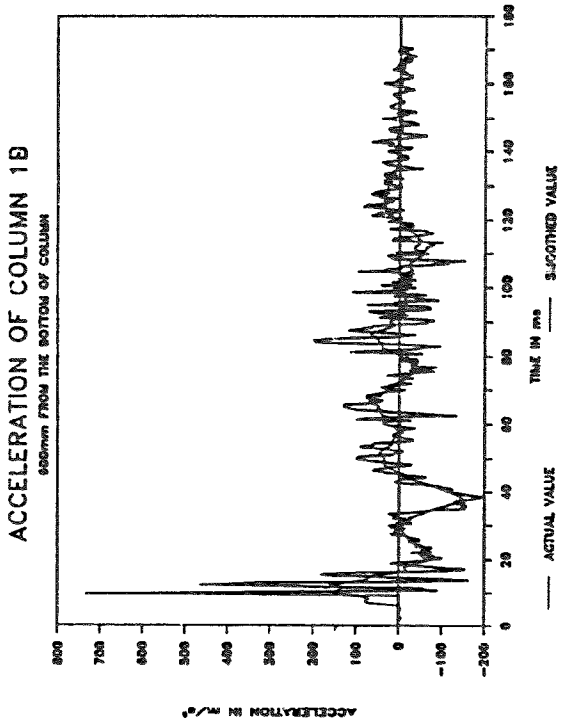

Fig. B.152: Smo.Accel. Col 1B

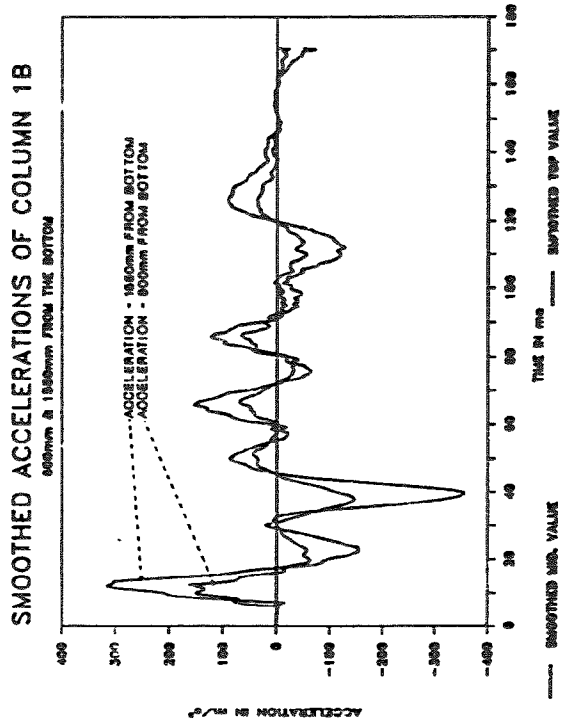

Fig. B.153: Smo. Accel. Col.1B

Stellenbosch University http://scholar.sun.ac.za

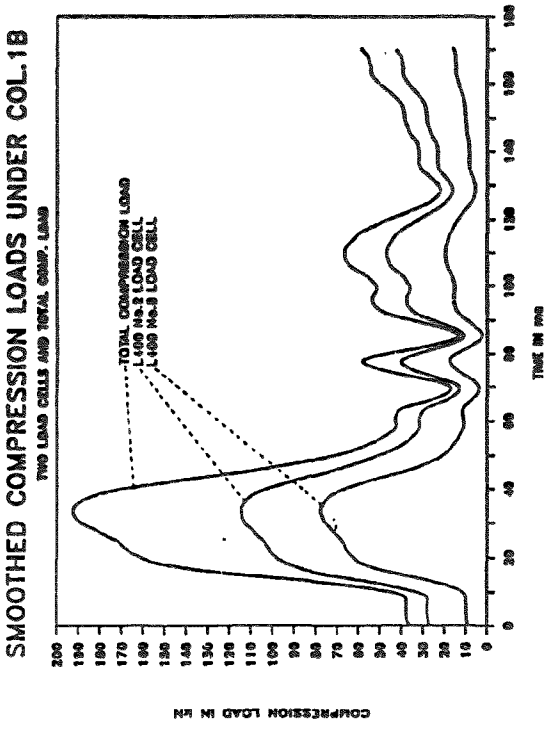

Fig. B.154: Smo. Comp. Col.1B

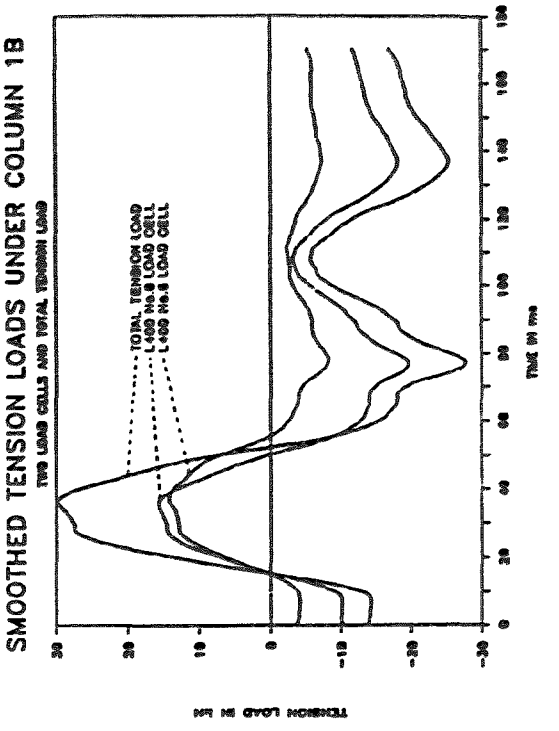

Fig. B.155: Smo. Tens. Col.1B

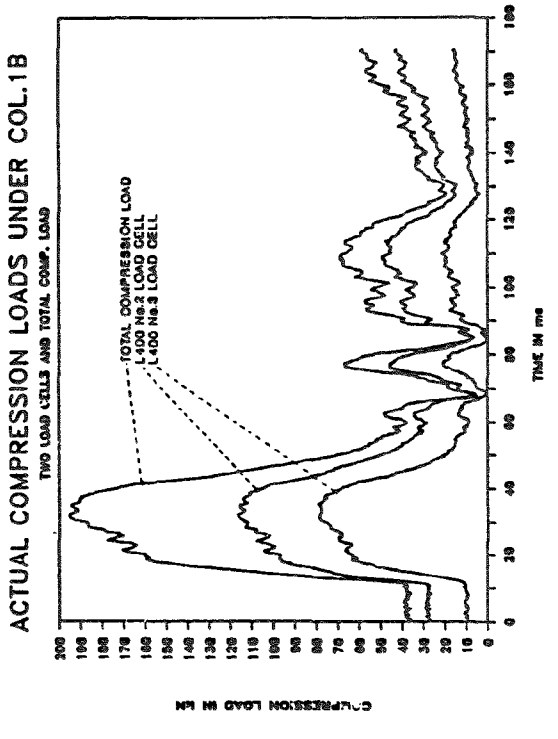

Fig. B.156: Comp. load Col 1B

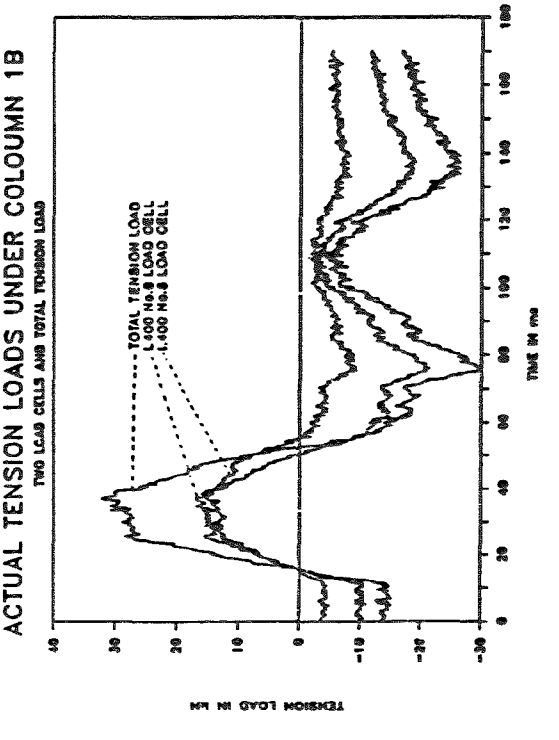

Fig. B.157: Tens. loads Col.1B

Stellenbosch University http://scholar.sun.ac.za

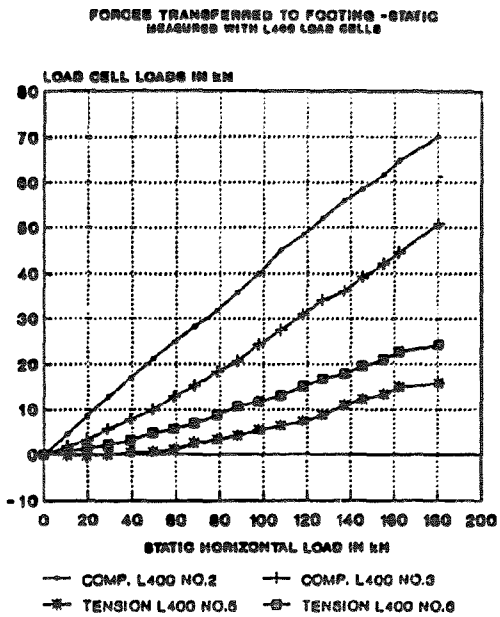

Fig. B.158: Foot. loads Col. 1B

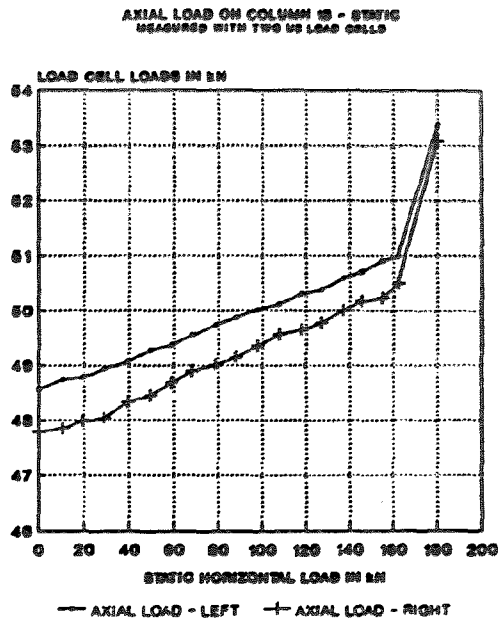

Fig. B.159: Axial loads Col. 1B

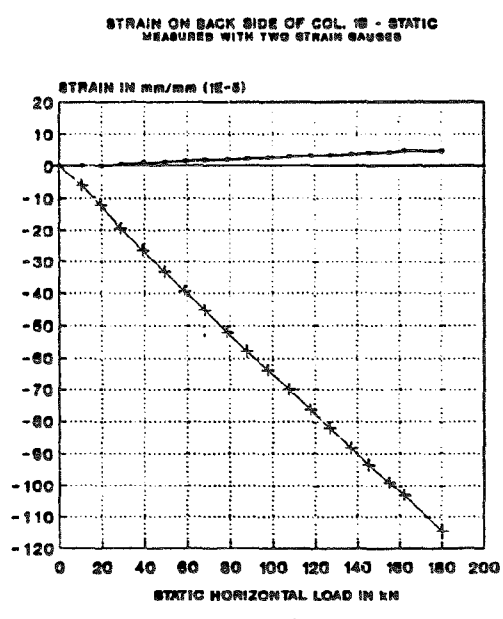

Fig. B.160: Strain Col. 1B

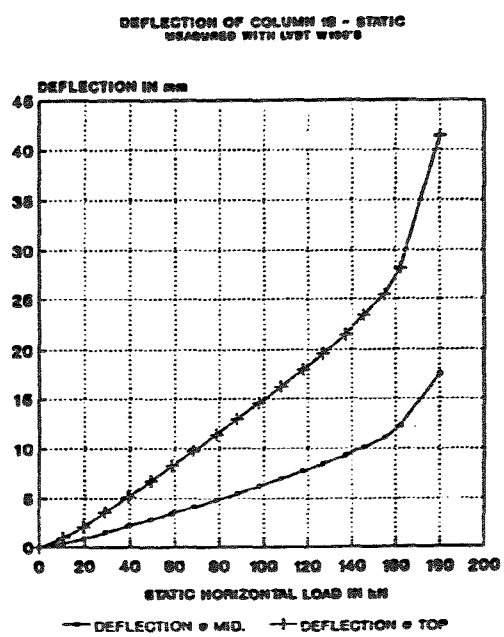

Fig. B.161: Deflection Col. 1B

Stellenbosch University http://scholar.sun.ac.za

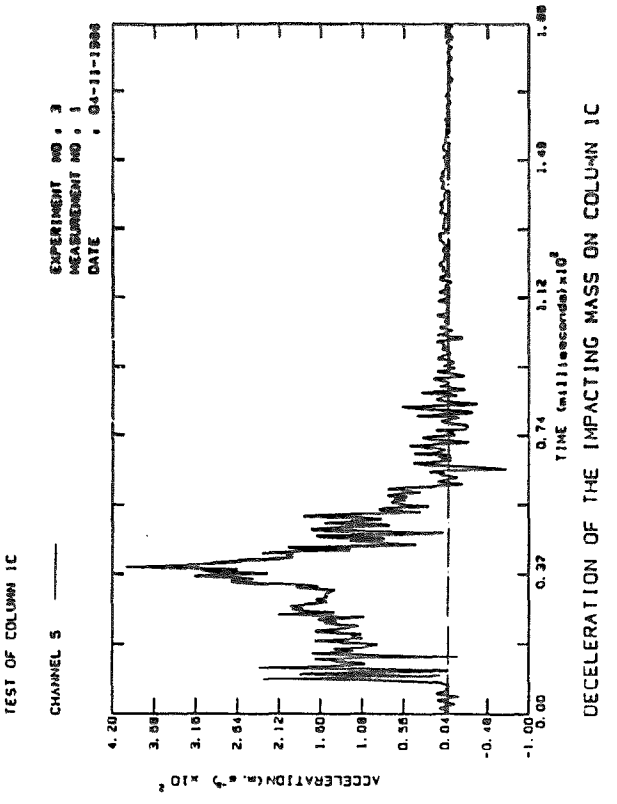

Fig. B.162: Decel. Col.1C

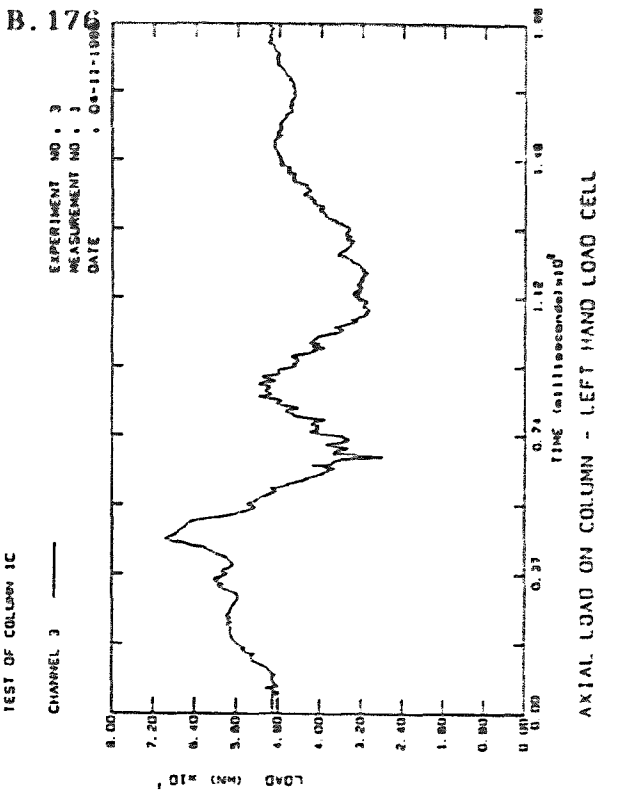

Fig. B.163: Axial load Col.1C

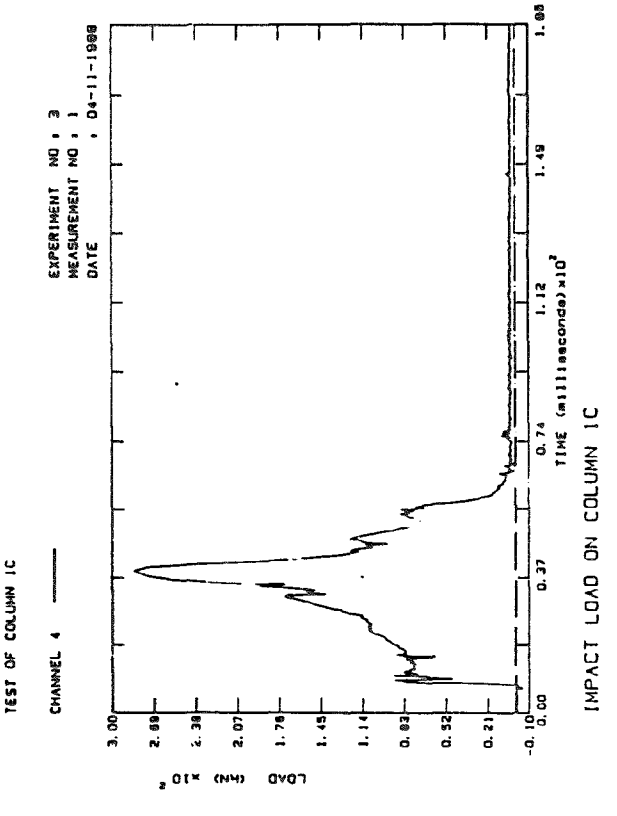

Fig. B.164: Impact Col.1C

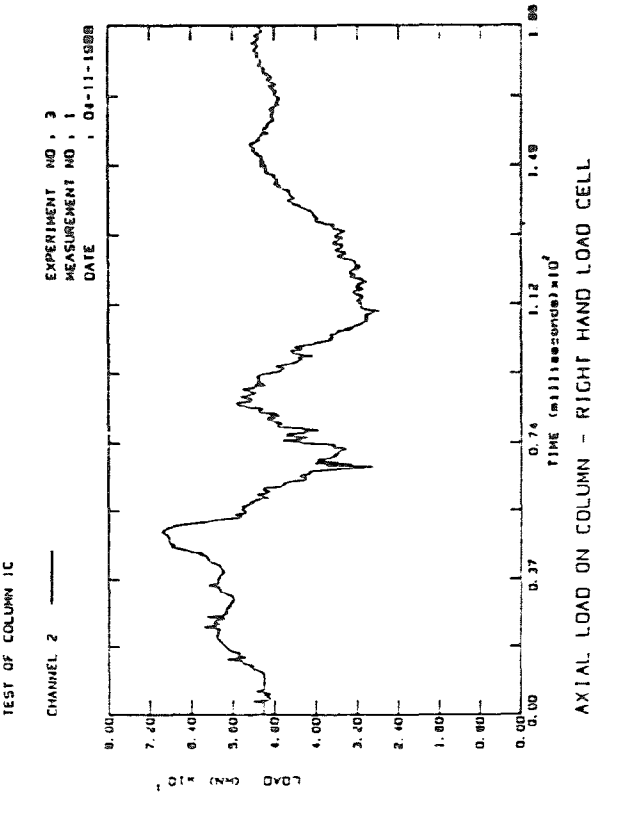

Fig. B.165: Axial load Col.1C

Stellenbosch University http://scholar.sun.ac.za

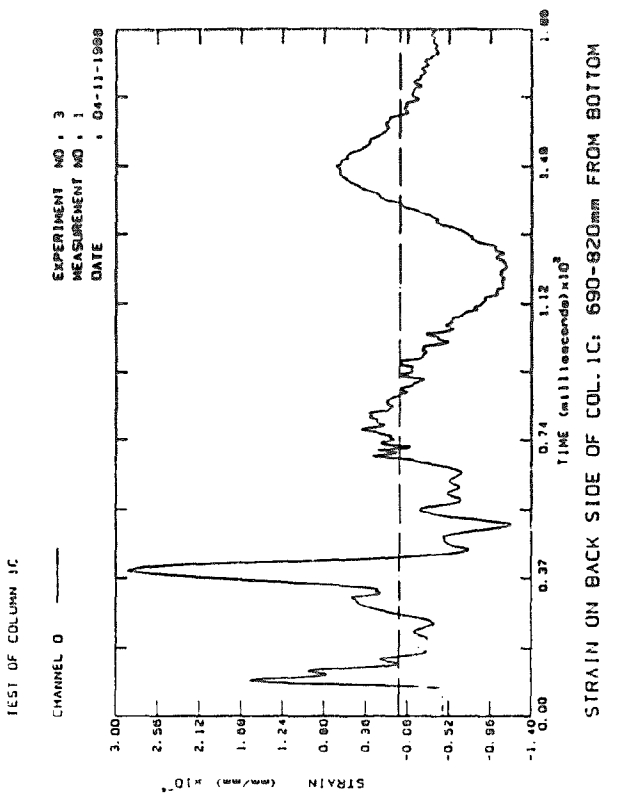

Fig. B.166: Strain Col. 1C

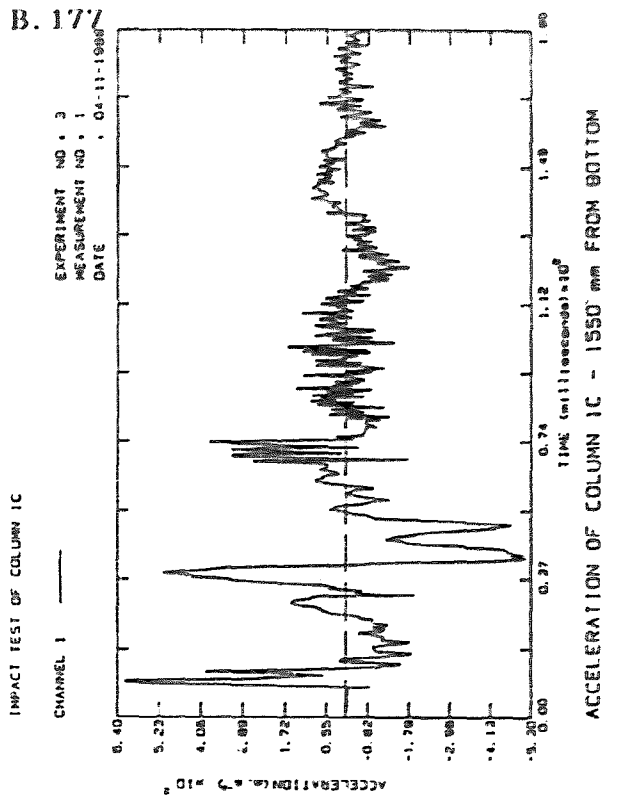

Fig. B.167 Accel. Col.1C

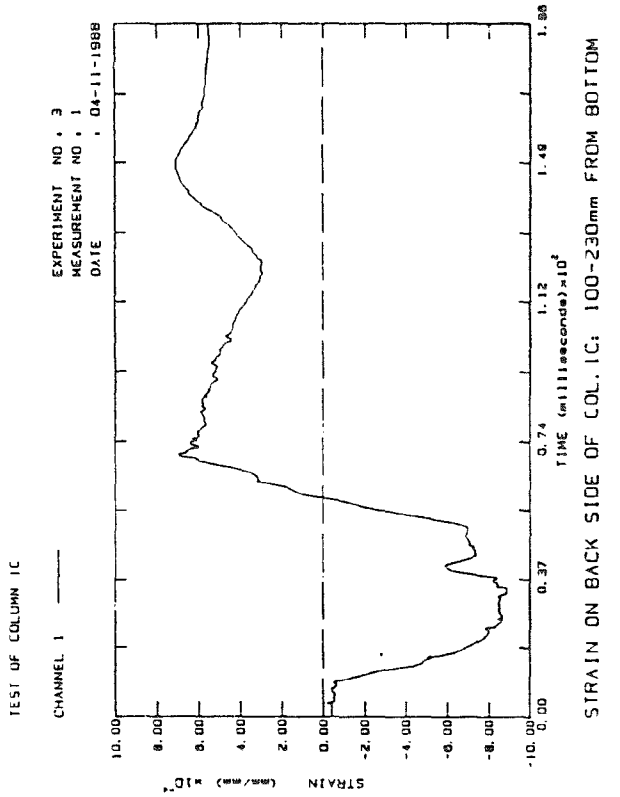

Fig. B.168: Strain Col. 1C

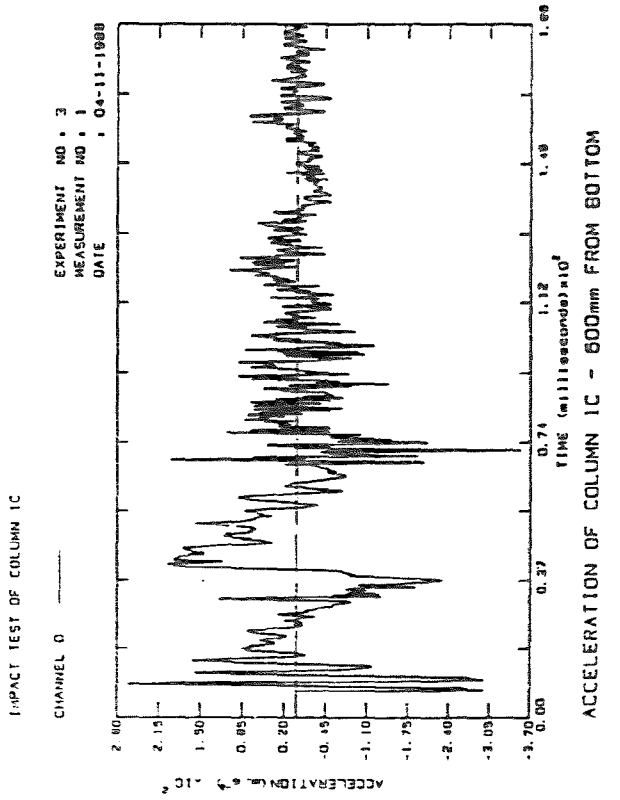

Fig. B.169: Accel. Col.1C

Stellenbosch University http://scholar.sun.ac.za

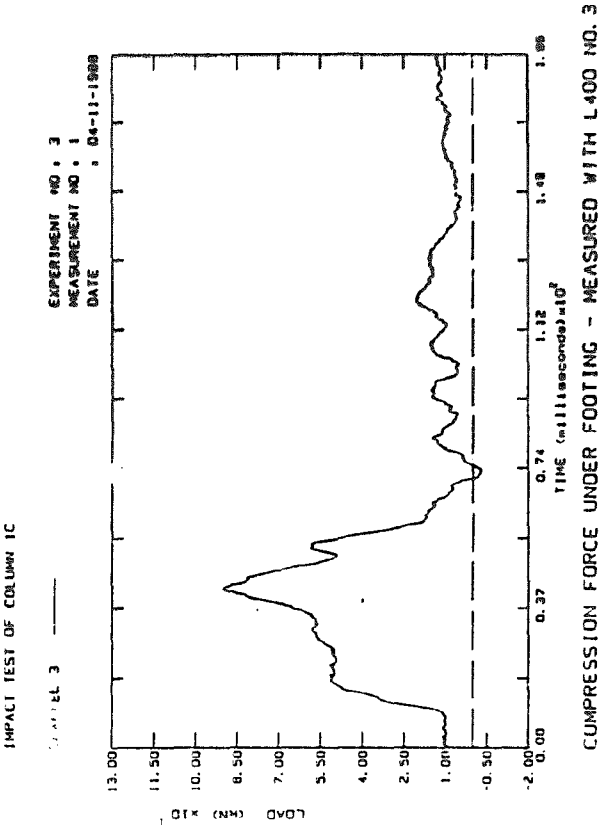

Fig. B.170: Comp. Col.1C

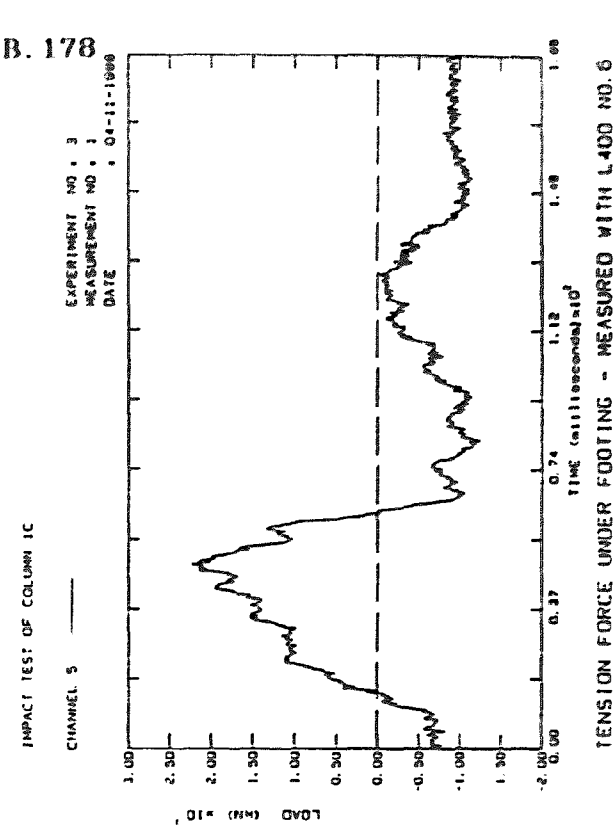

Fig. B.171: Tension Col.1C

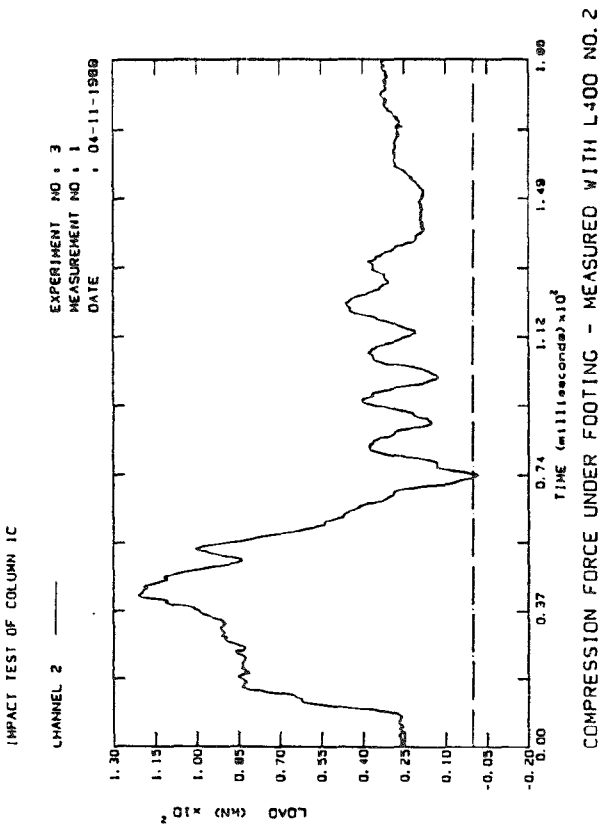

Fig. B.172: Comp. Col 1C

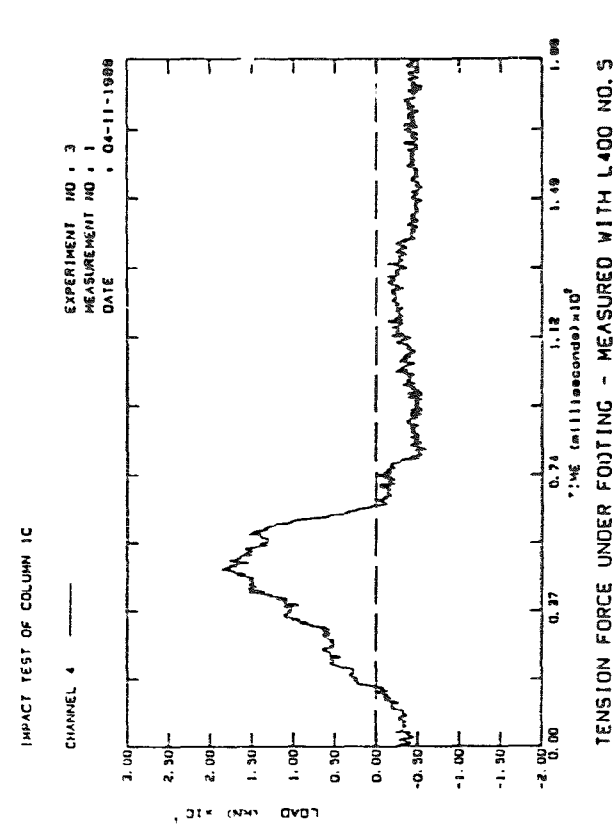

Fig. B.173: Tension Col.1C

Stellenbosch University http://scholar.sun.ac.za

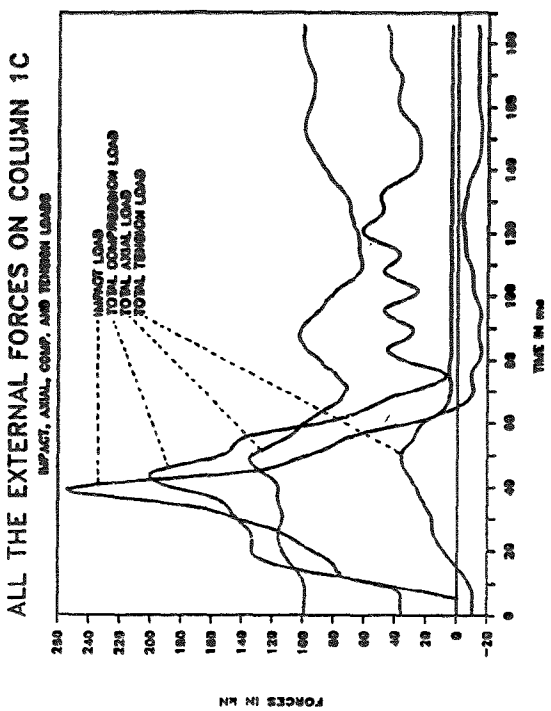

Fig. B.174: Ext. Loads Col.1C

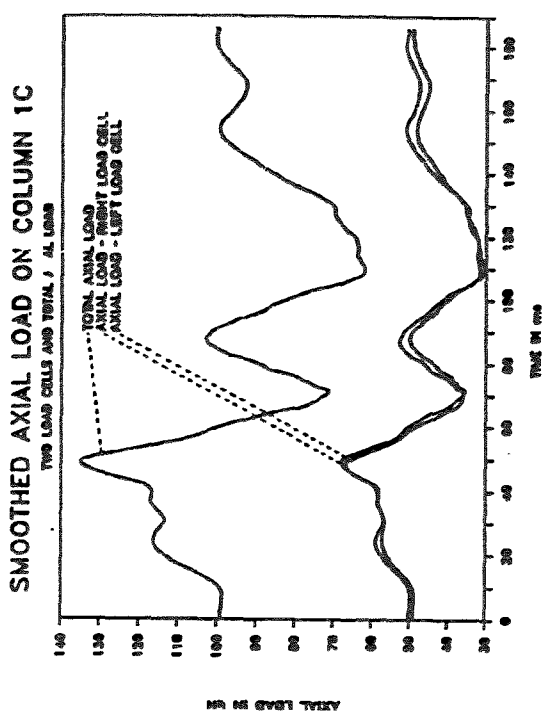

Fig. B.175: Smo. Axial Col.1C

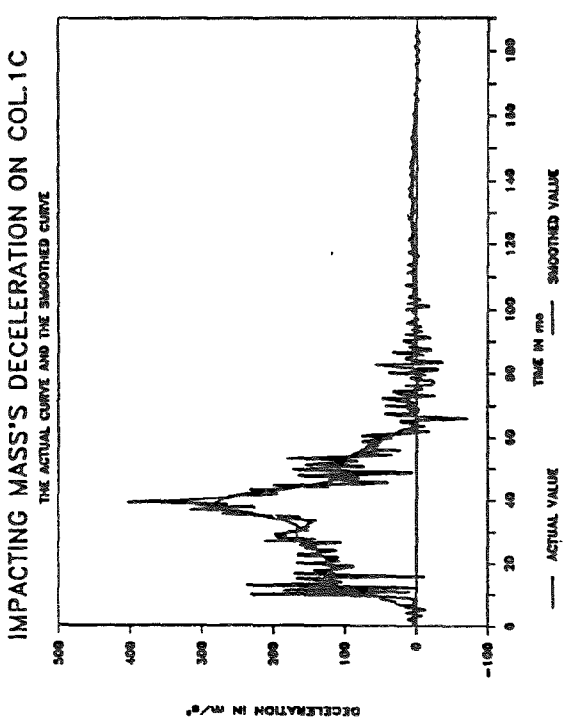

Fig. B.176: Smo.Decel. Col 1C

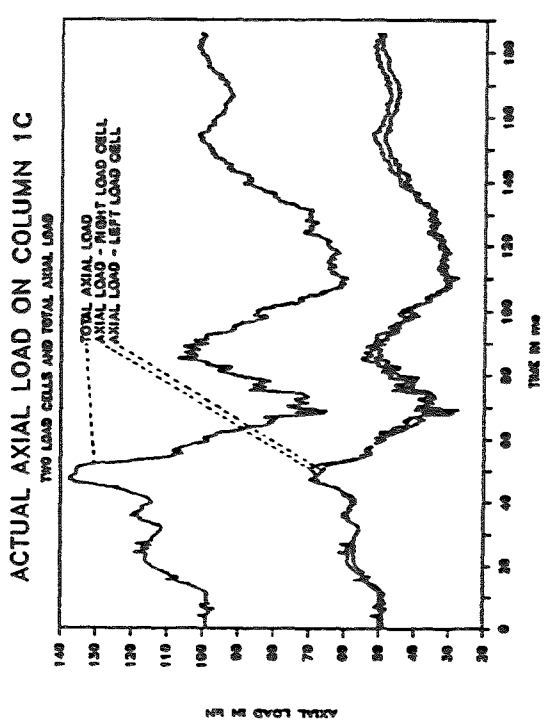

Fig. B.177: Axial loads Col.1C

Stellenbosch University http://scholar.sun.ac.za

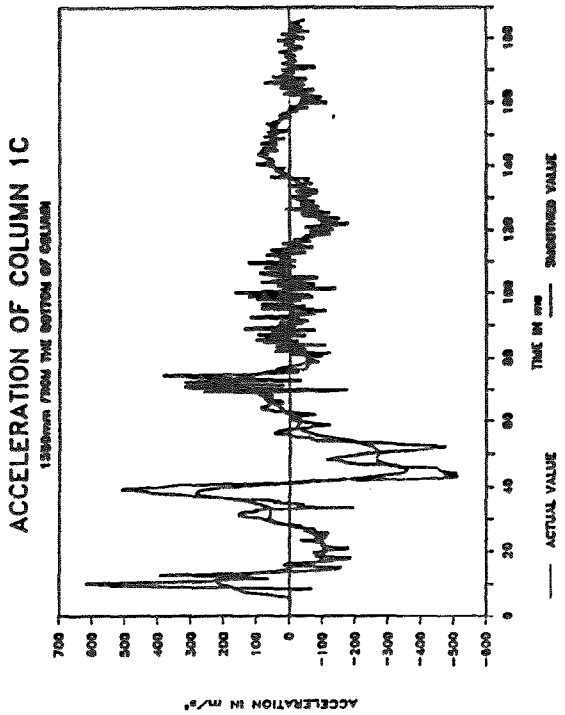

Fig. B.178 Smo.Accel. Col.1C

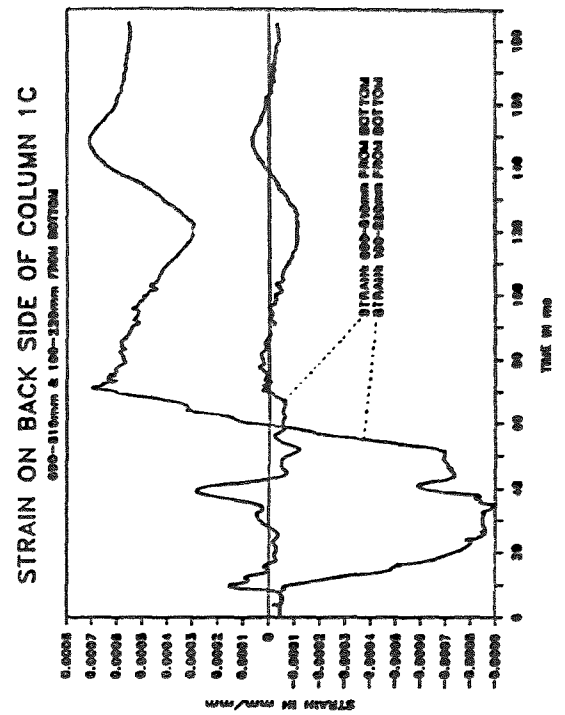

Fig. B.179: Strain Col.1C

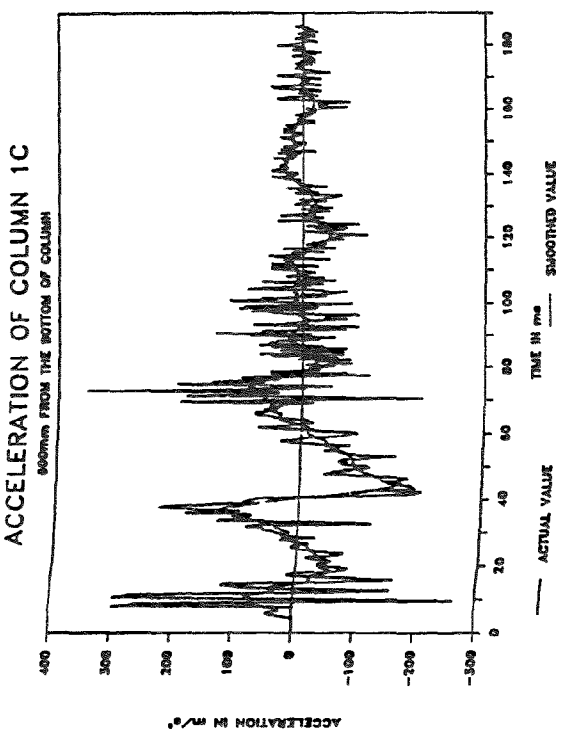

Fig. B.180: Smo.Accel. Col.1C

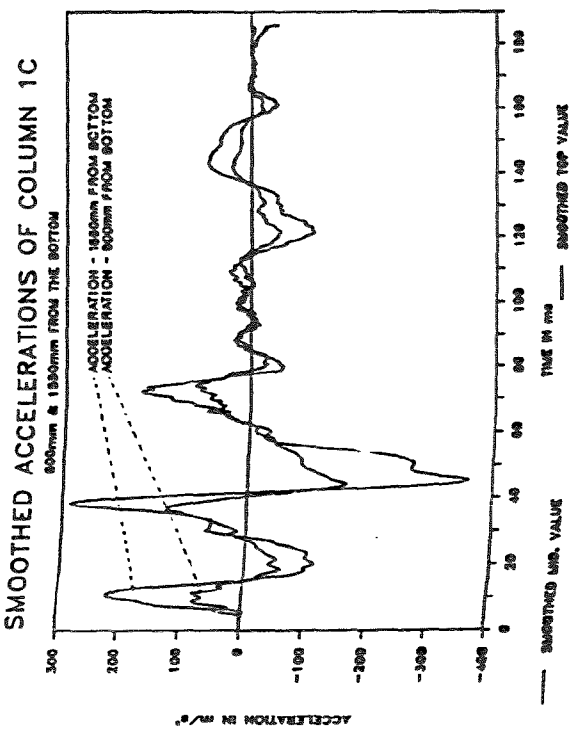

Fig. B.181: Smo. Accel. Col.1C

Stellenbosch University http://scholar.sun.ac.za

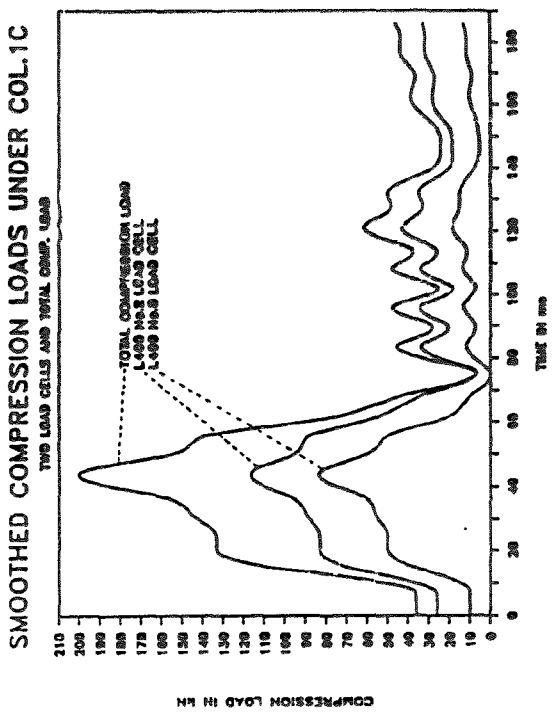

Fig. B.182: Smo. Comp. Col.1C

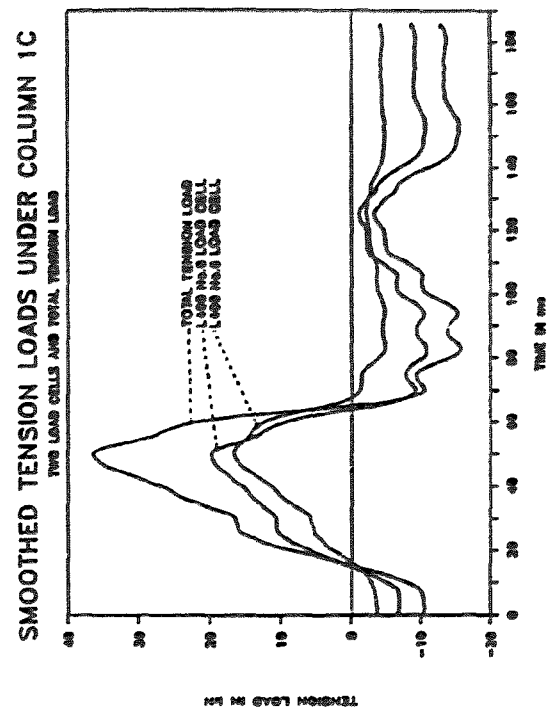

Fig. B.183: Smo. Tens. Col.1C

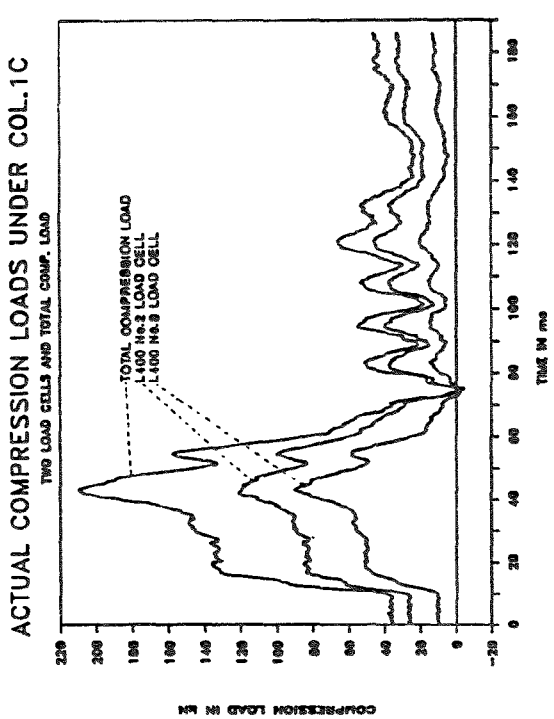

Fig. B.184: Comp. load Col 1C

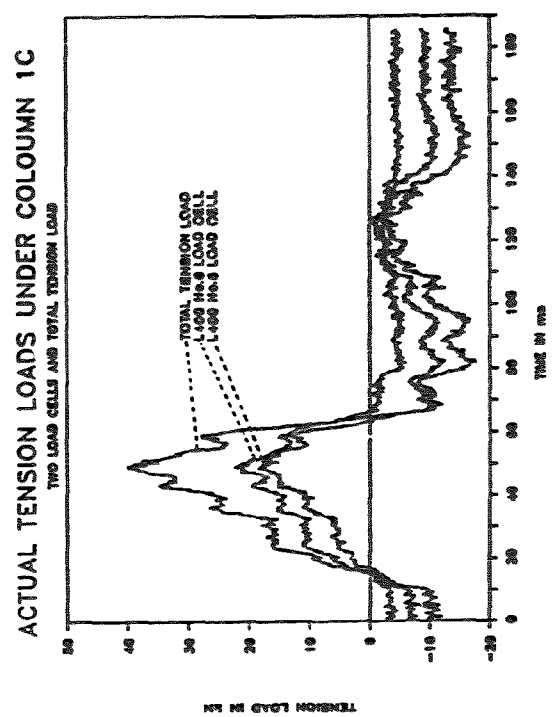

Fig. B.185: Tens. loads Col.1C

Stellenbosch University http://scholar.sun.ac.za

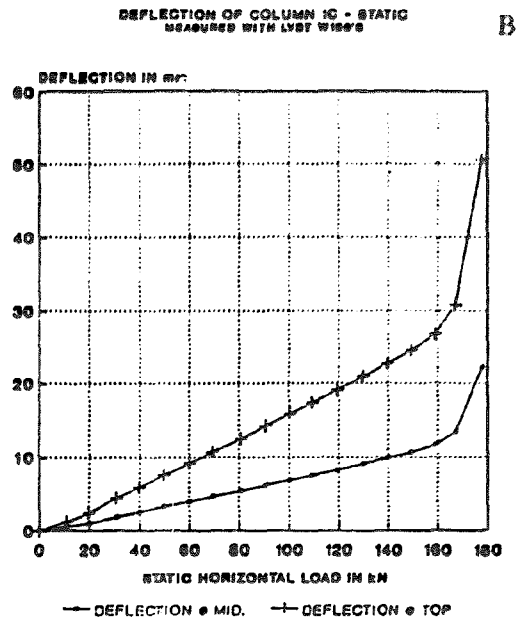

Fig. B.186: Deflection Col.1C

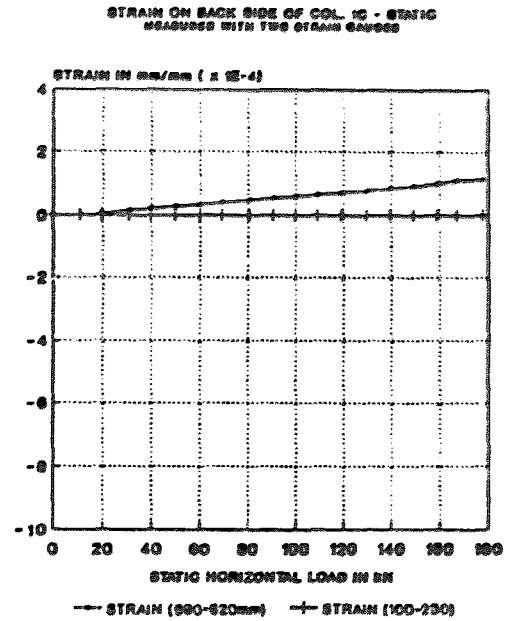

Fig. B.187: Strain Col.1C

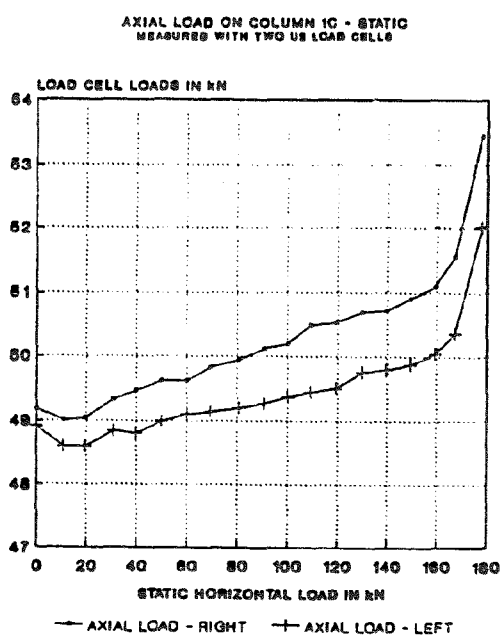

Fig. B.188: Axial load Col 1C

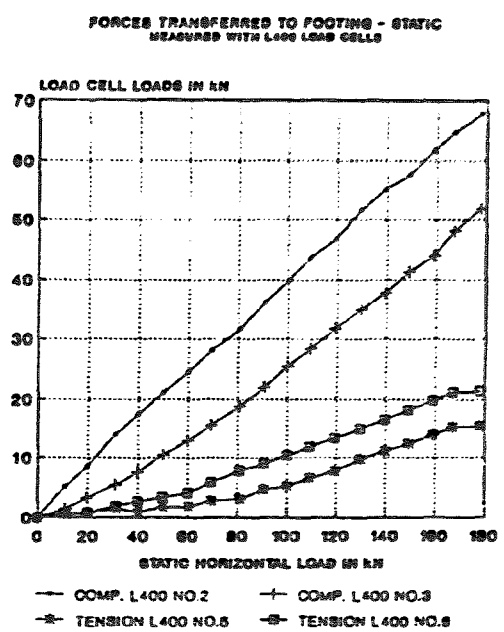

Fig. B.189: Foot.loads Col.1C

Stellenbosch University http://scholar.sun.ac.za

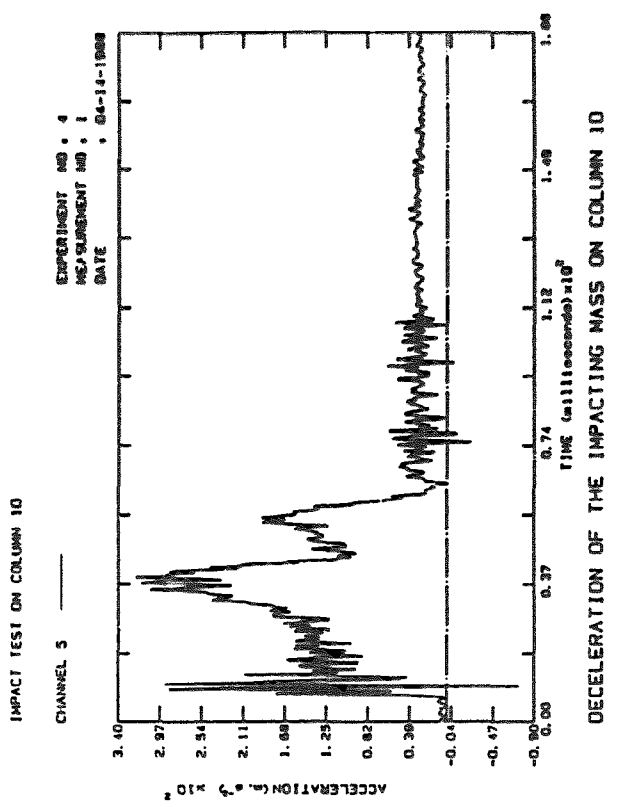

Fig. B.190: Decel. Col.1D

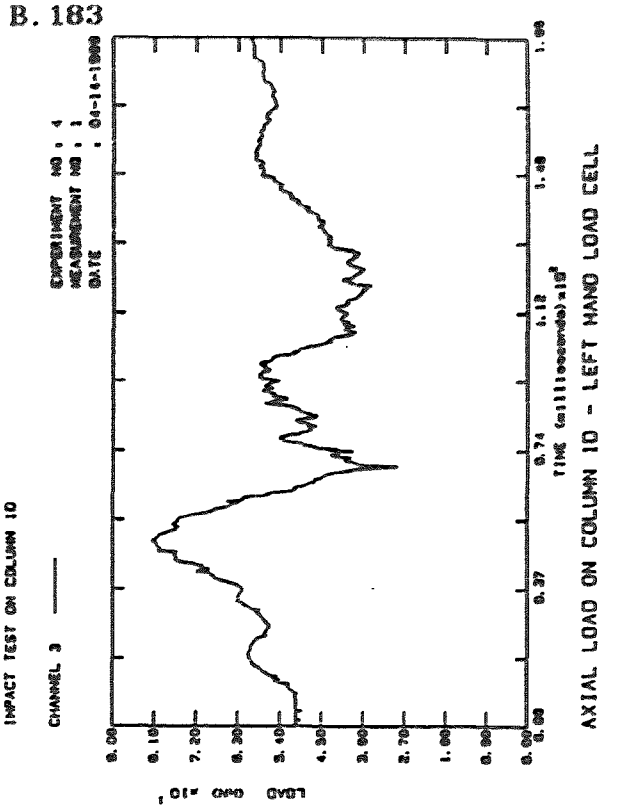

Fig. B.191: Axial load Col.1D

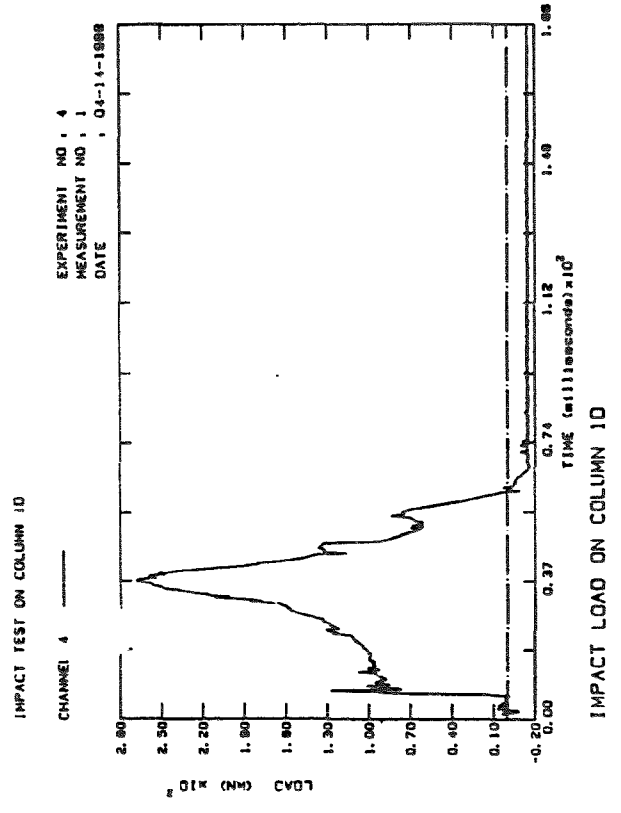

Fig. B.192: Impact Col 1D

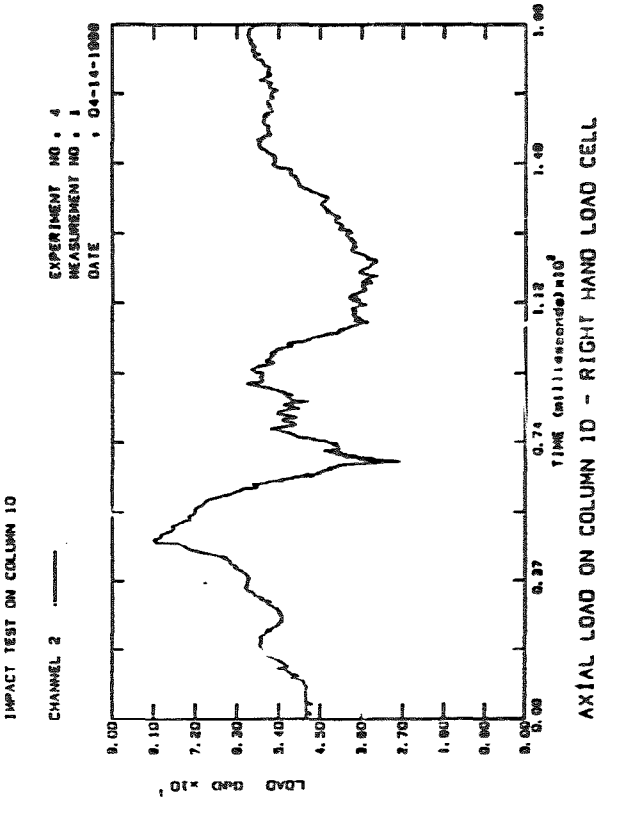

Fig. B.193: Axial load Col.1D

Stellenbosch University http://scholar.sun.ac.za

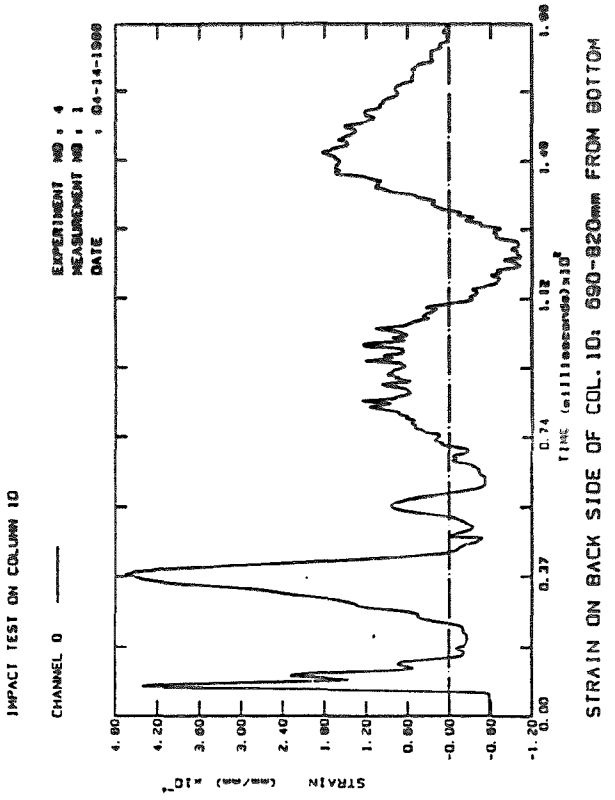

Fig. B.194: Strain Col.1D

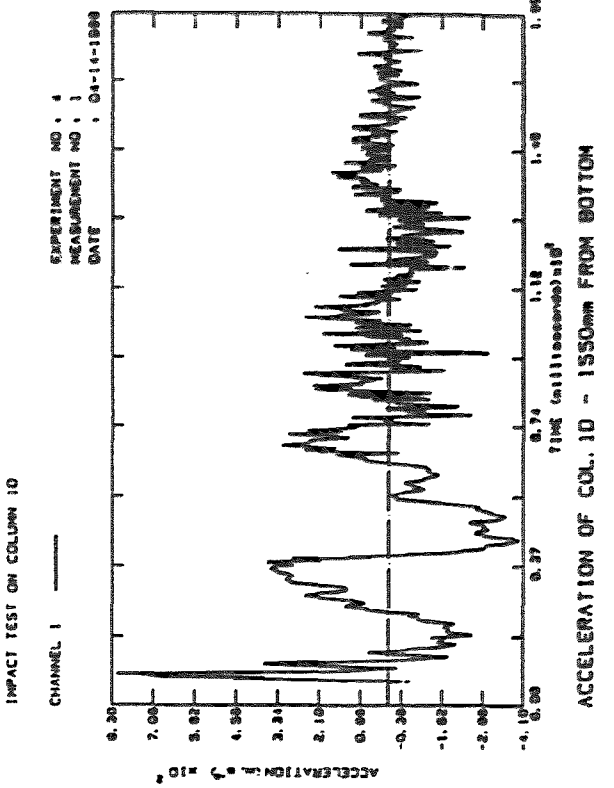

Fig. B.195: Accel. Col.1D

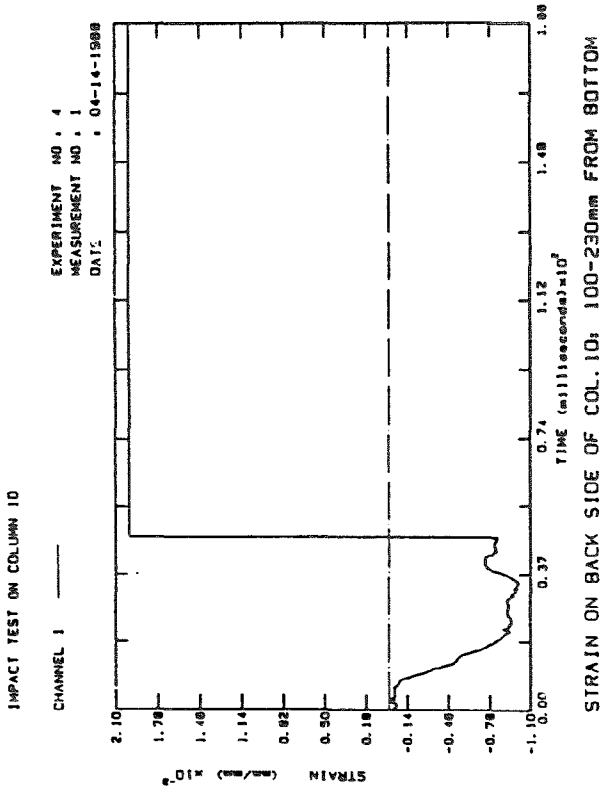

Fig. B.196: Strain Col 1D

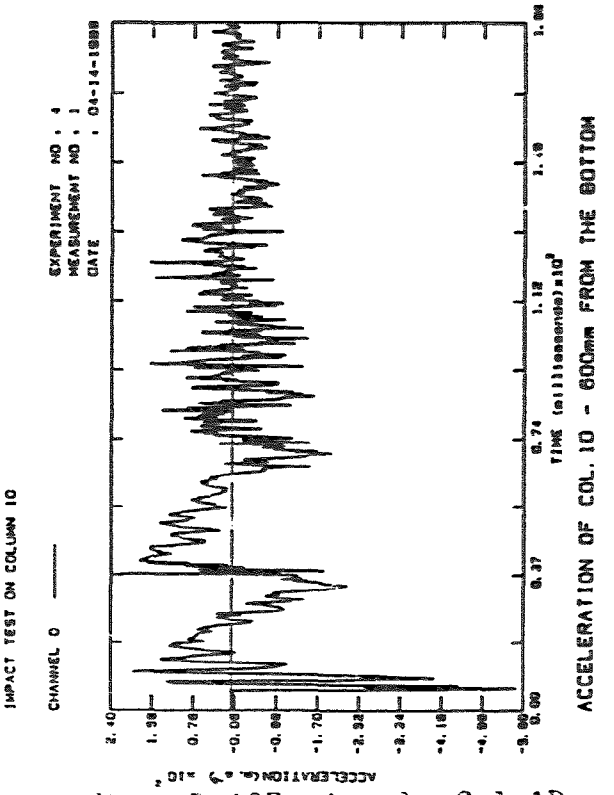

Fig. B.197: Accel. Col.1D

Stellenbosch University http://scholar.sun.ac.za

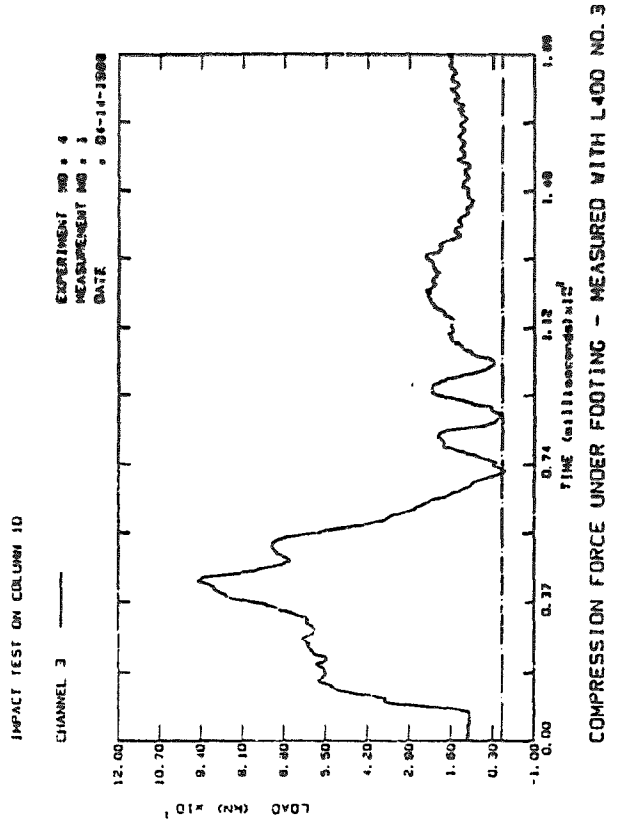

Fig. B.198: Comp. Col. 1D

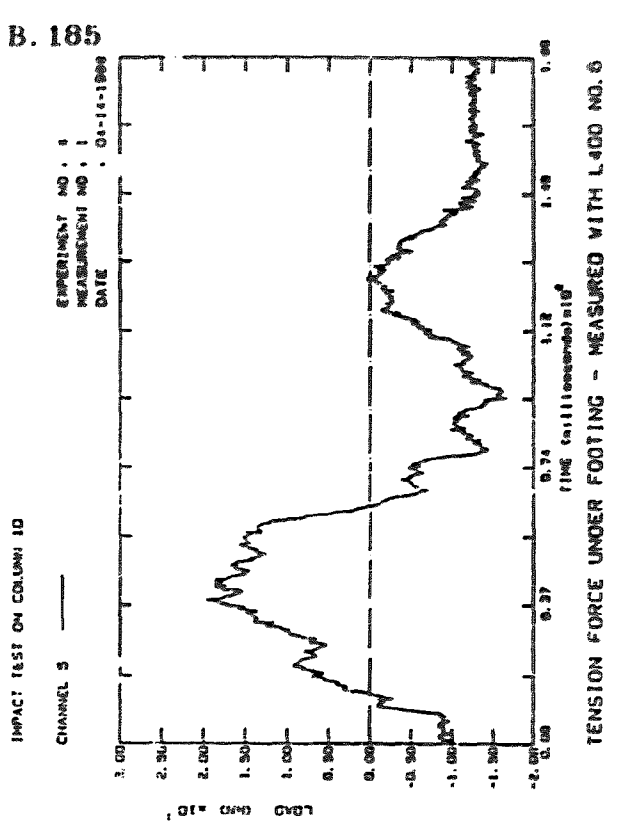

Fig. B.199: Tension Col. 1D

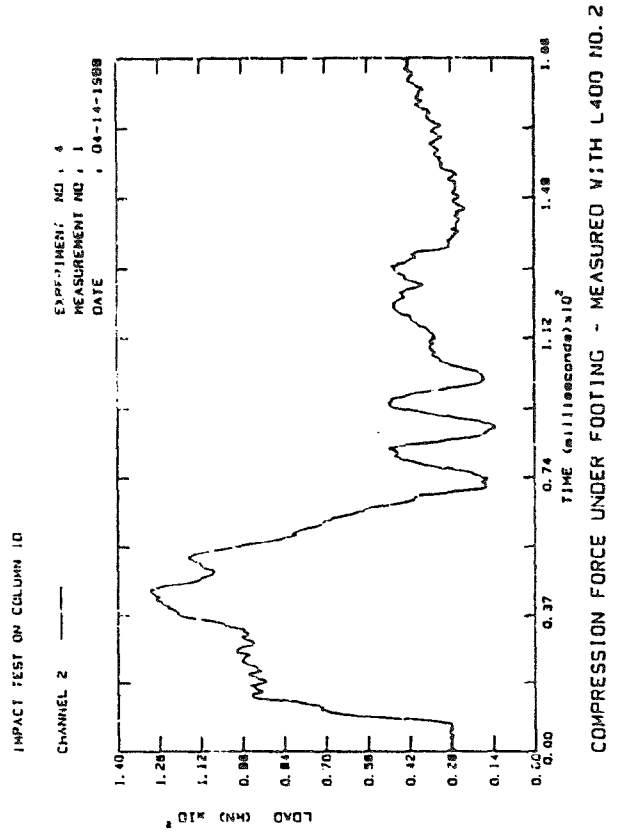

Fig. B.200: Comp. Col 1D

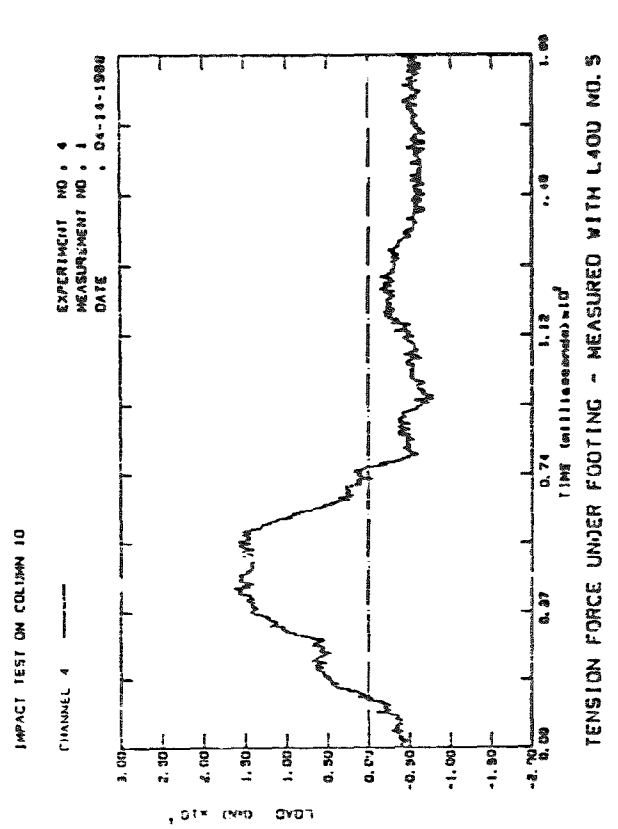

Fig. B.201: Tension Col.1D

Stellenbosch University http://scholar.sun.ac.za

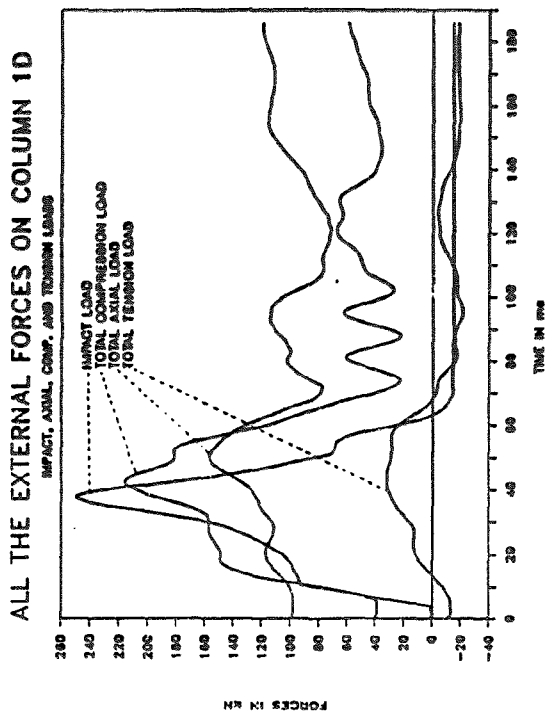

Fig. B.202: Ext. Loads Col.1D

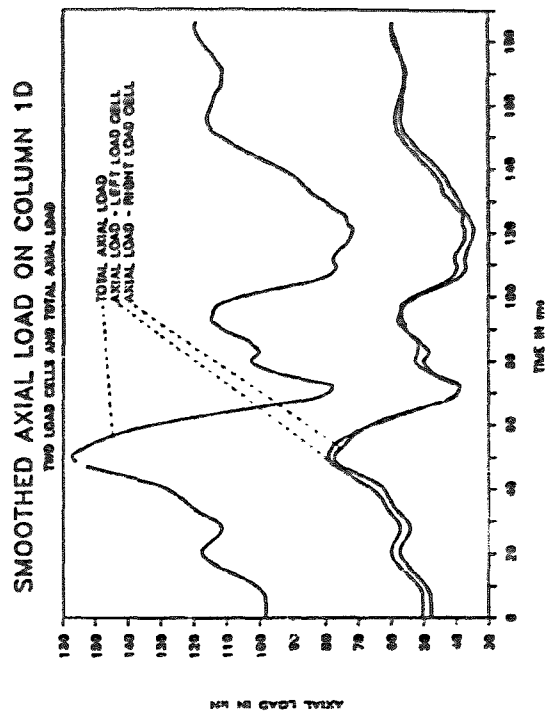

Fig. B.203: Smo. Axial Col.1D

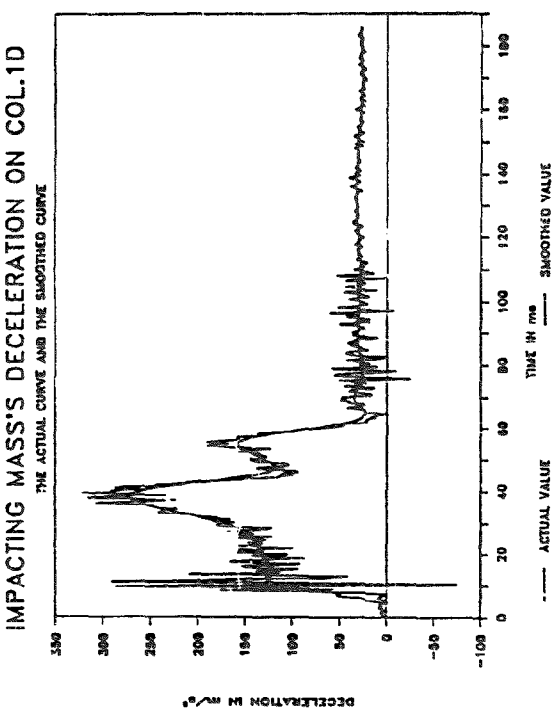

Fig. B.204: Smo Decel. Col 1D

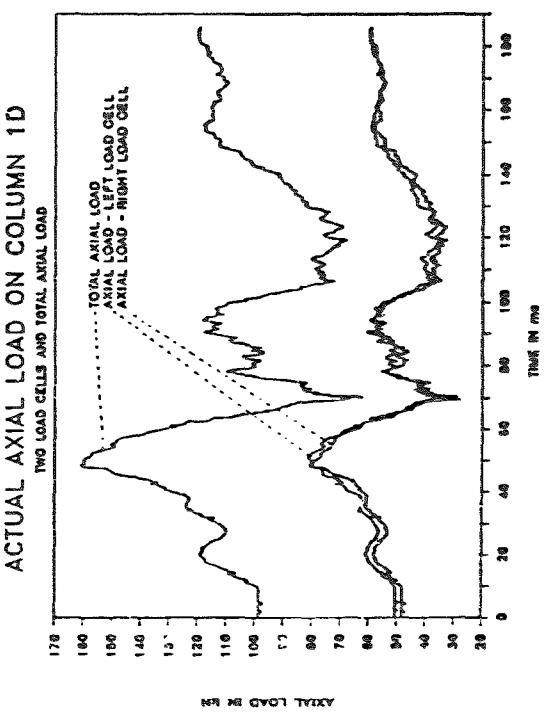

Fig. B.205: Axial Loads Col.1D

Stellenbosch University http://scholar.sun.ac.za

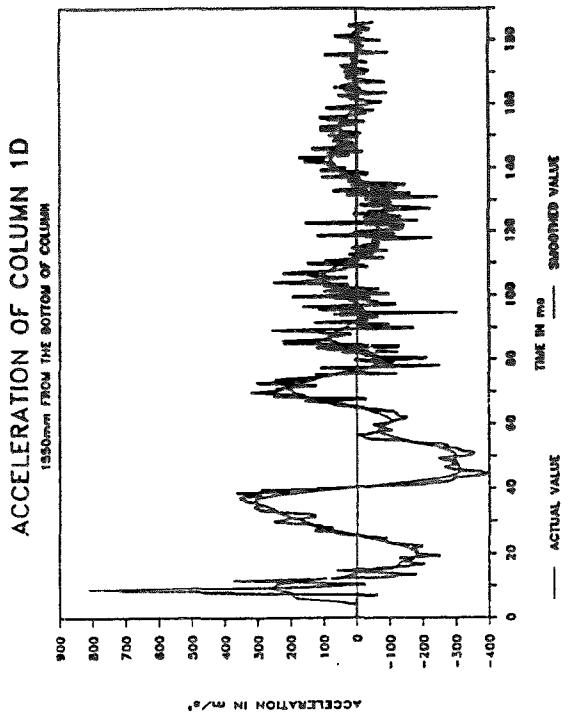

Fig. B.206: Smo.Accel. Col.1D

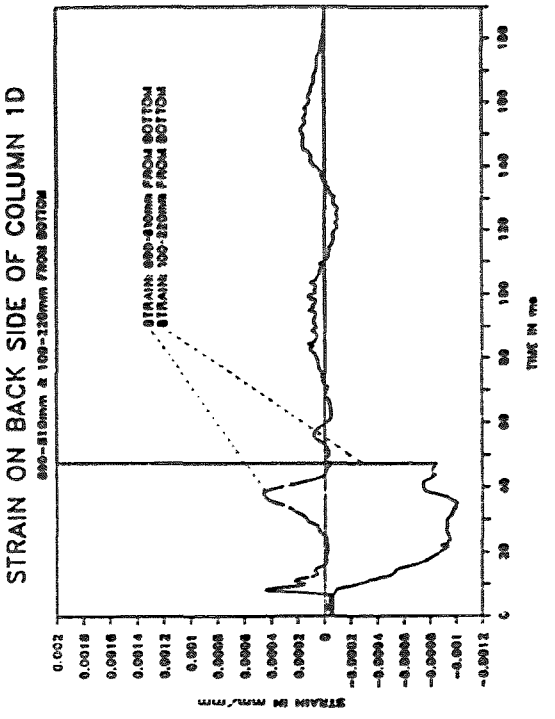

Fig. B.2[illegible] Strain Col.1D

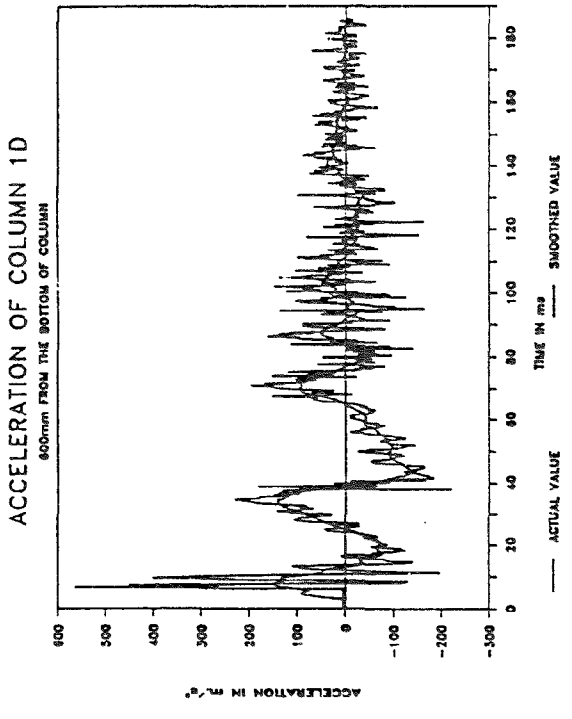

Fig. B.208: Smo.Accel. Col.1D

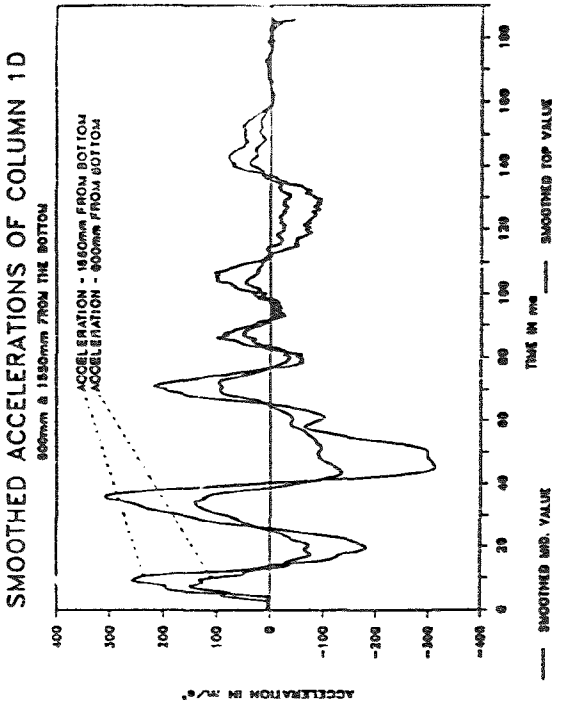

Fig. B.[illegible] Smo. Accel. Col.1D

Stellenbosch University http://scholar.sun.ac.za

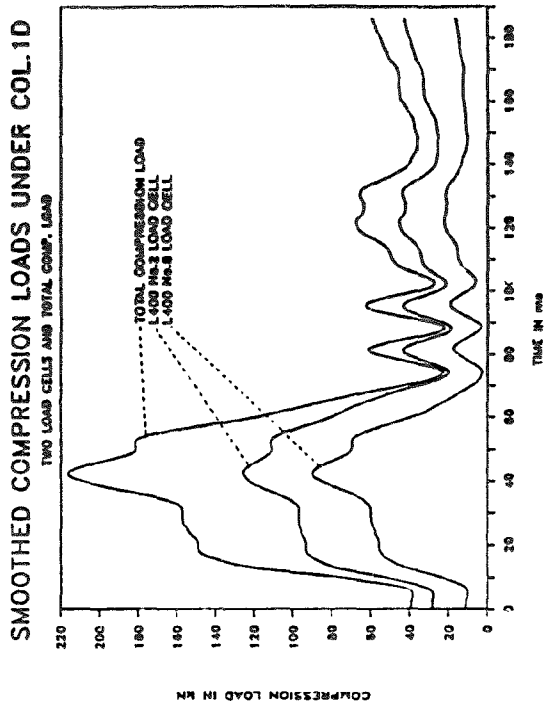

Fig. B.210: Smoothed Compression Loads Under Column 1D

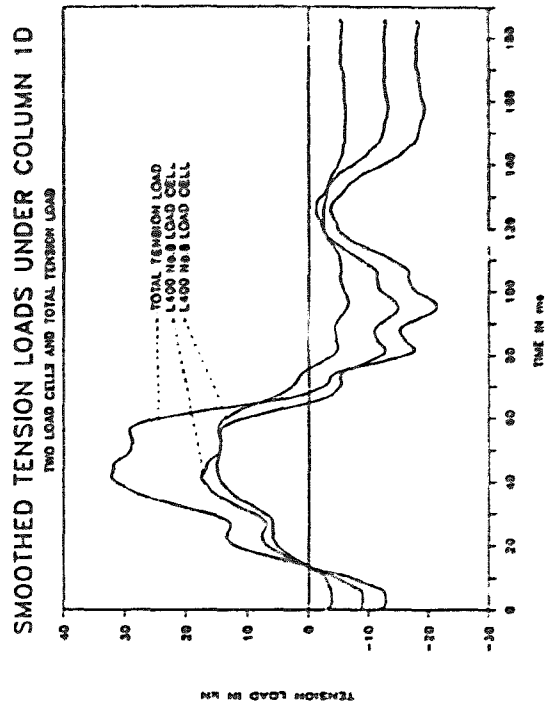

Fig. B.211: Smoothed Tension Loads Under Column 1D

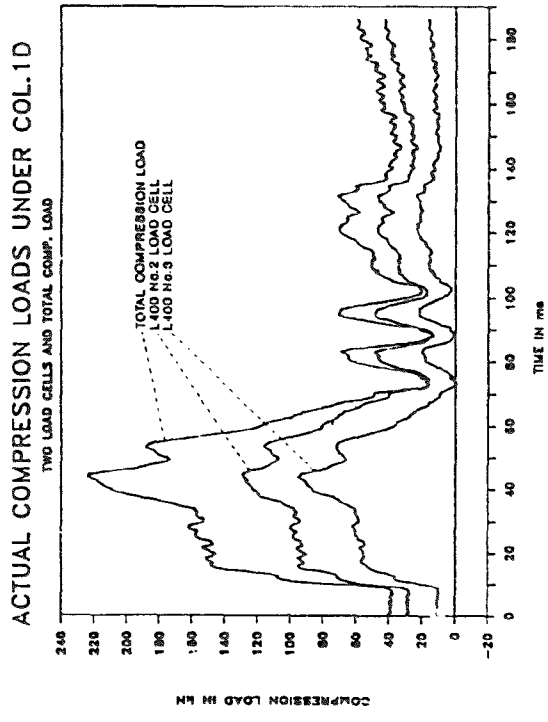

Fig. B.212: Actual Compression Loads Under Column 1D

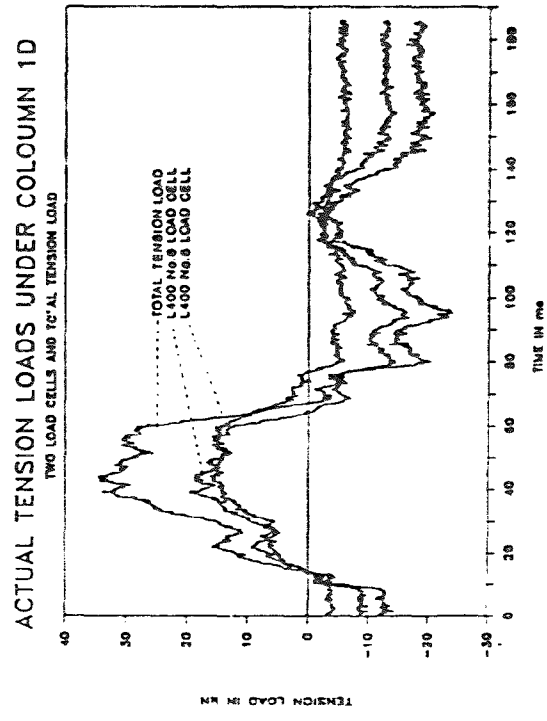

Fig. B.213: Actual Tension Loads Under Column 1D

Stellenbosch University http://scholar.sun.ac.za

DEFLECTION OF COLUMN 1D - STATIC
MEASURED WITH LVDT W10G

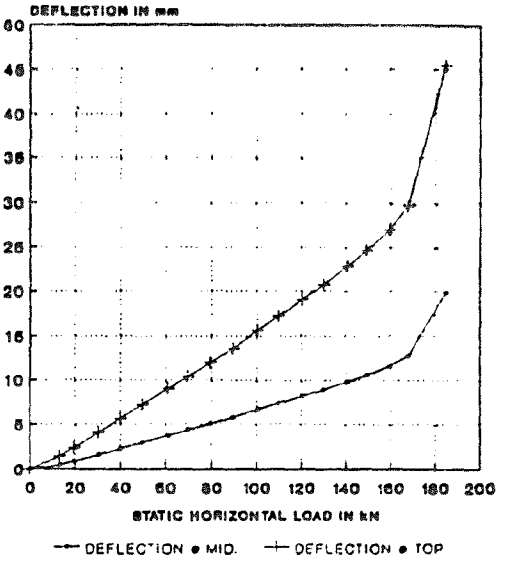

STRAIN ON BACK SIDE OF COL. 1D - STATIC
MEASURED WITH TWO STRAIN GAUGES

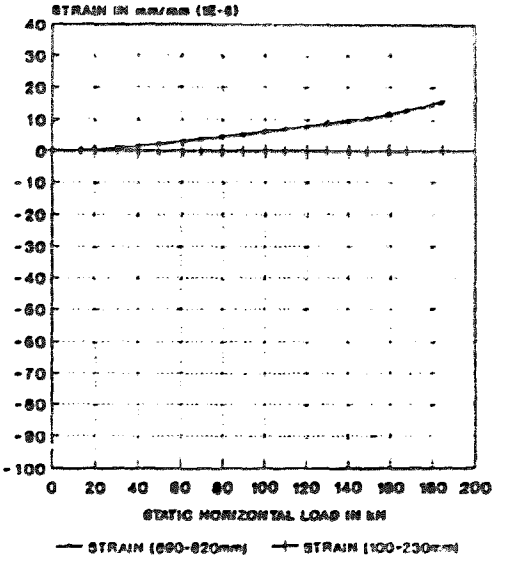

AXIAL LOAD ON COLUMN 1D - STATIC
MEASURED WITH TWO U8 LOAD CELLS

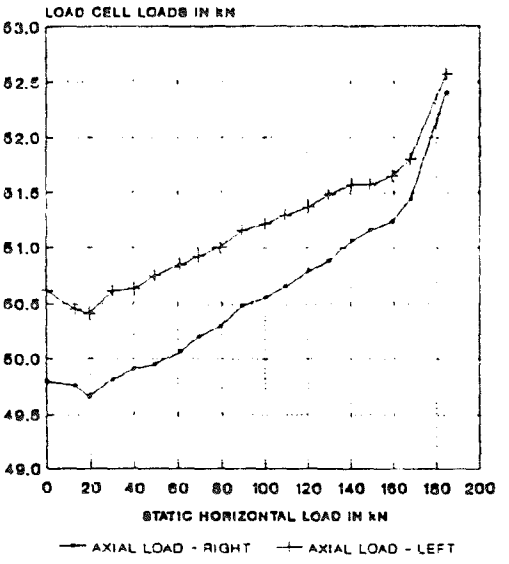

FORCES TRANSFERRED TO FOOTING - STATIC
MEASURED WITH L400 LOAD CELLS

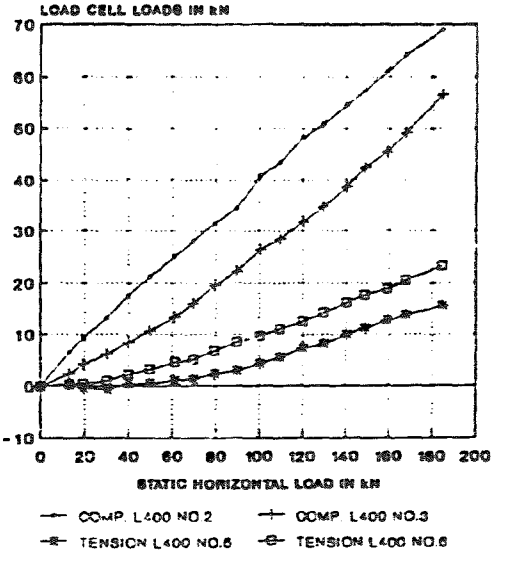

Stellenbosch University http://scholar.sun.ac.za

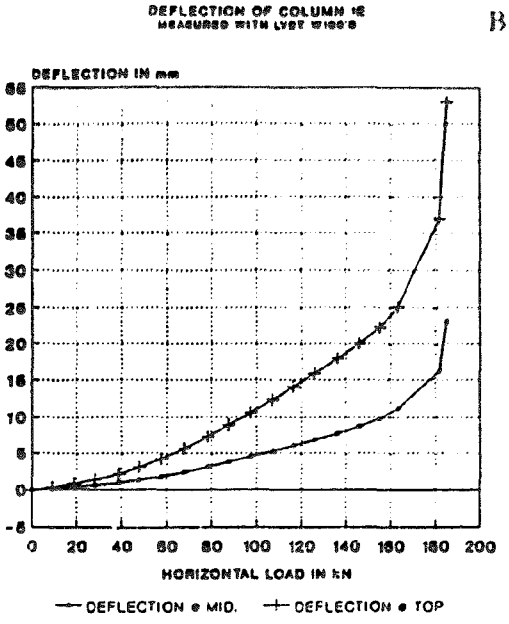

Fig. B.218: Deflection Col.1E

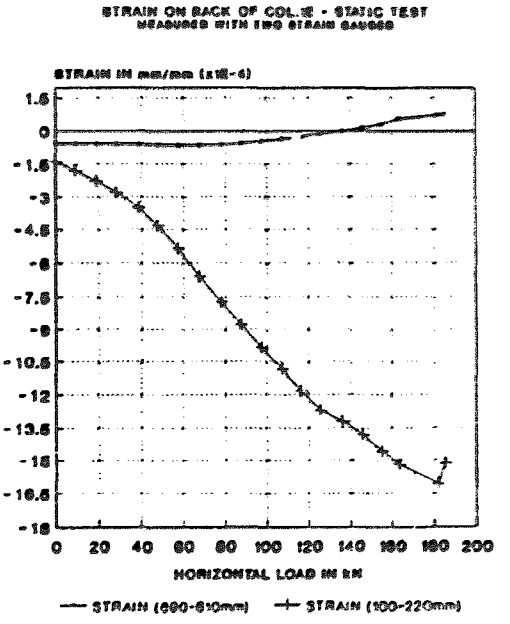

Fig. B.219: Strain Col.1E

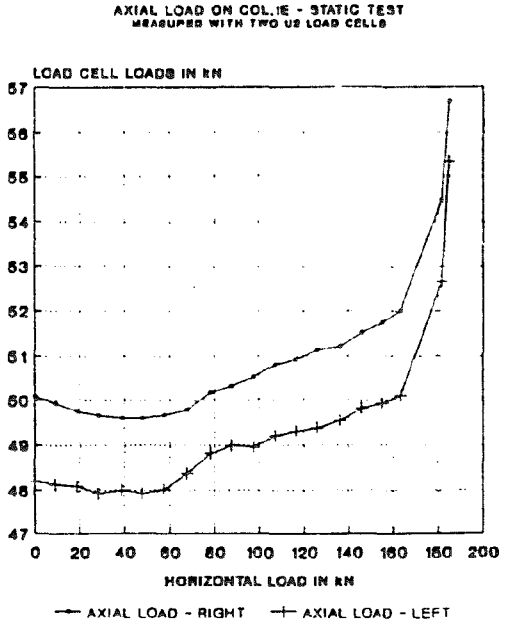

Fig. B.220: Axial Load Col.1E

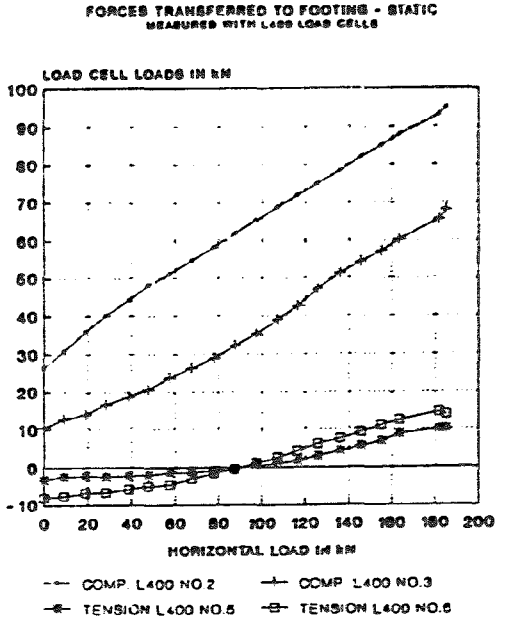

Fig. B.221: Forces Transferred to Footing Col.1E

Stellenbosch University http://scholar.sun.ac.za

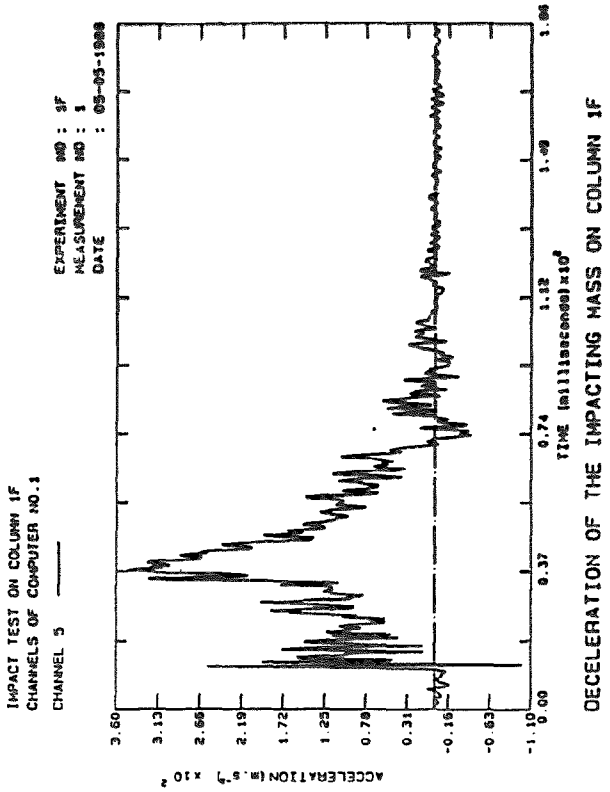

Fig. B.222: Decel. Col.1F

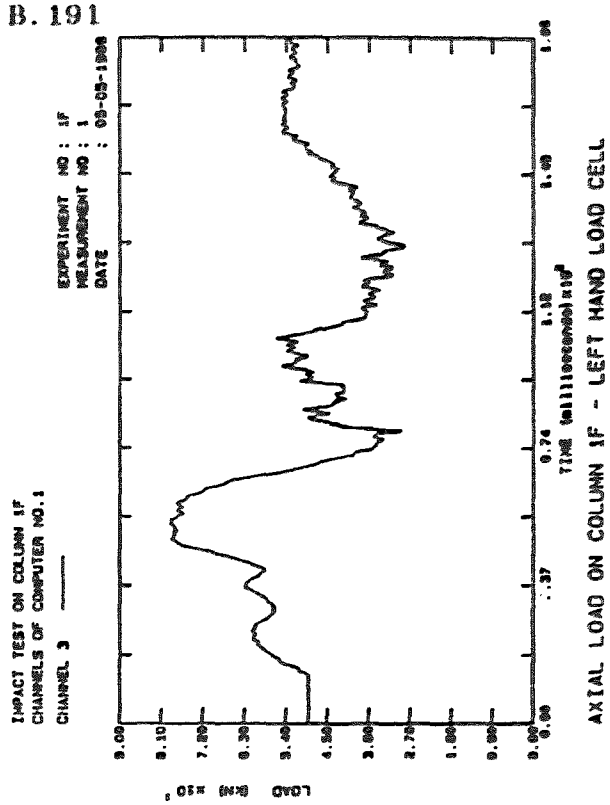

Fig. B.223: Axial load Col.1F

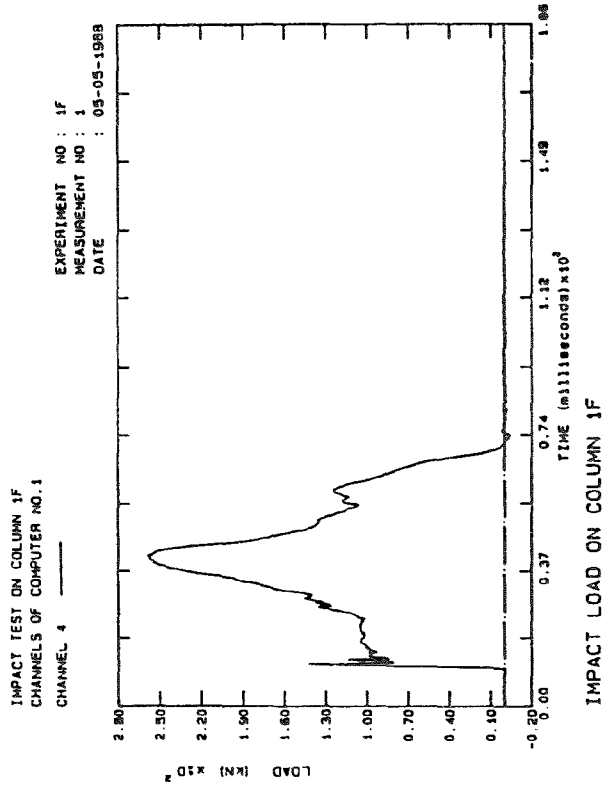

Fig. B.224: Impact Col 1F

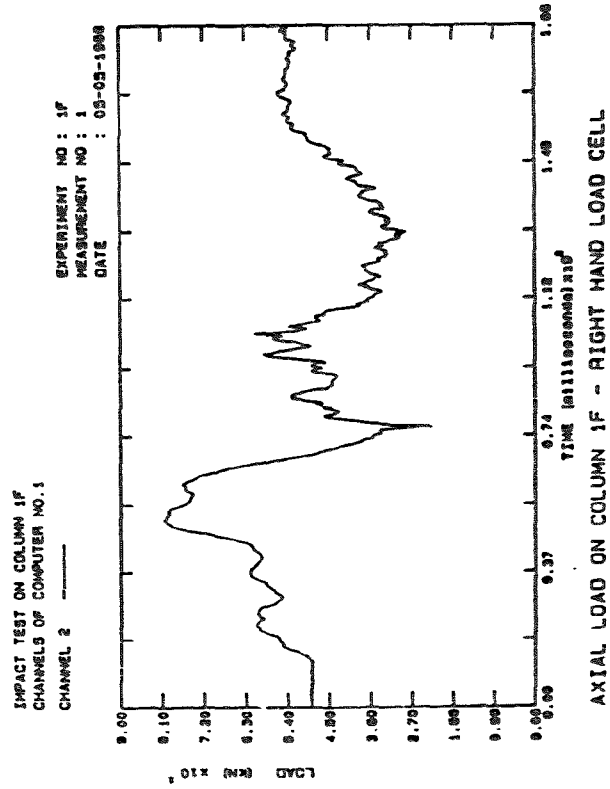

Fig. B.225: Axial load Col.1F

Stellenbosch University http://scholar.sun.ac.za

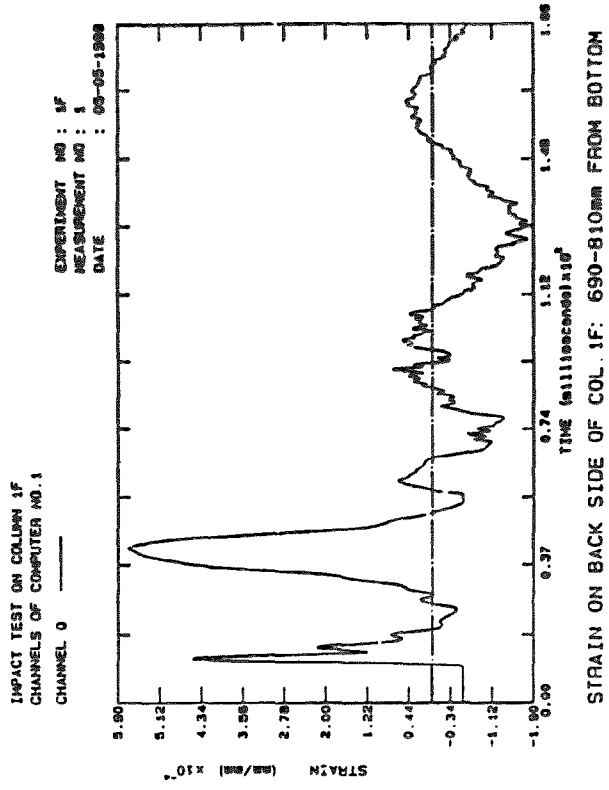

Fig. B.226: Strain Col.1F

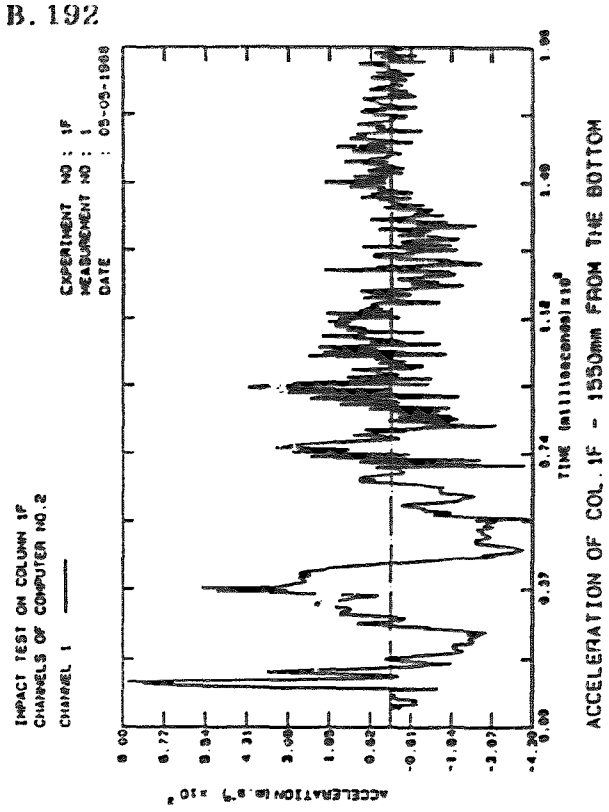

Fig. B.227: Accel Col.1F

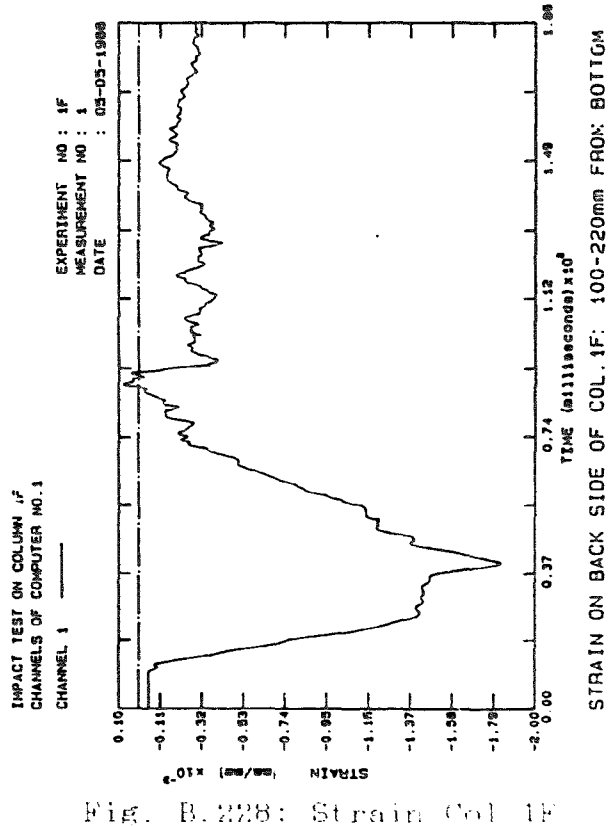

Fig. B.228: Strain Col 1F

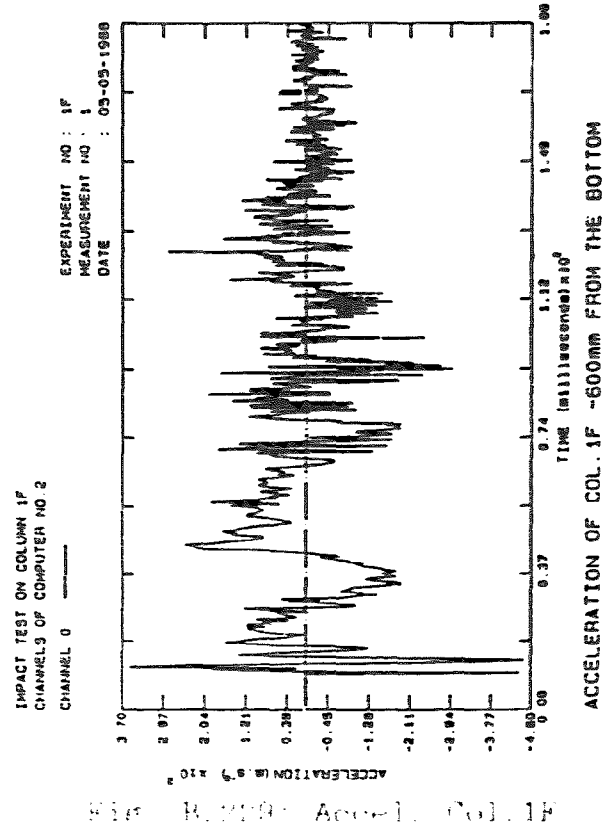

Fig. B.229: Accel. Col.1F

Stellenbosch University http://scholar.sun.ac.za

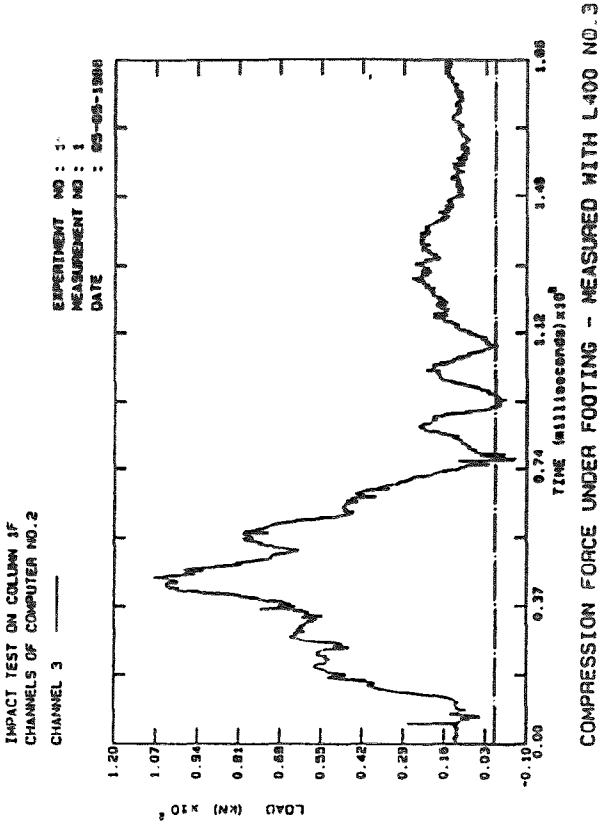

Fig. B.230: Comp. Col.1F

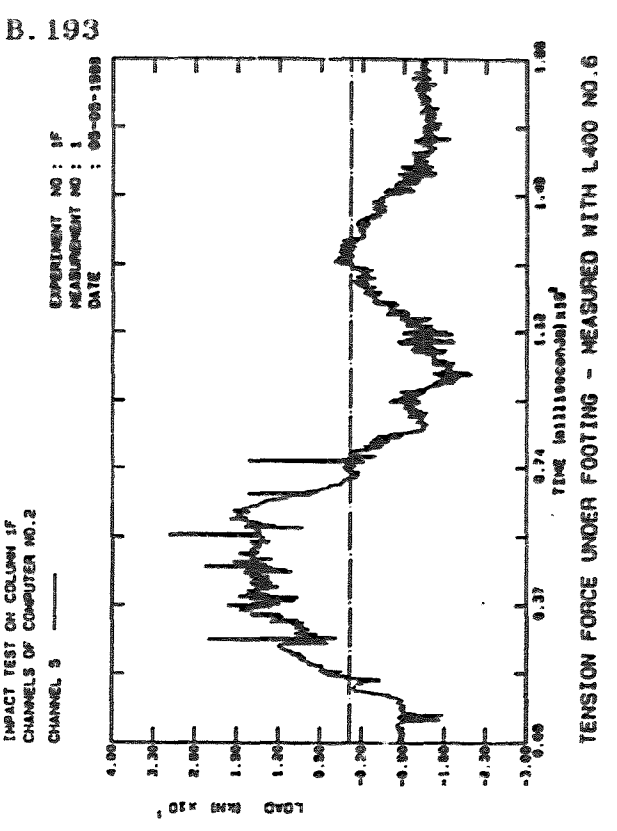

Fig. B.231: Tension Col.1F

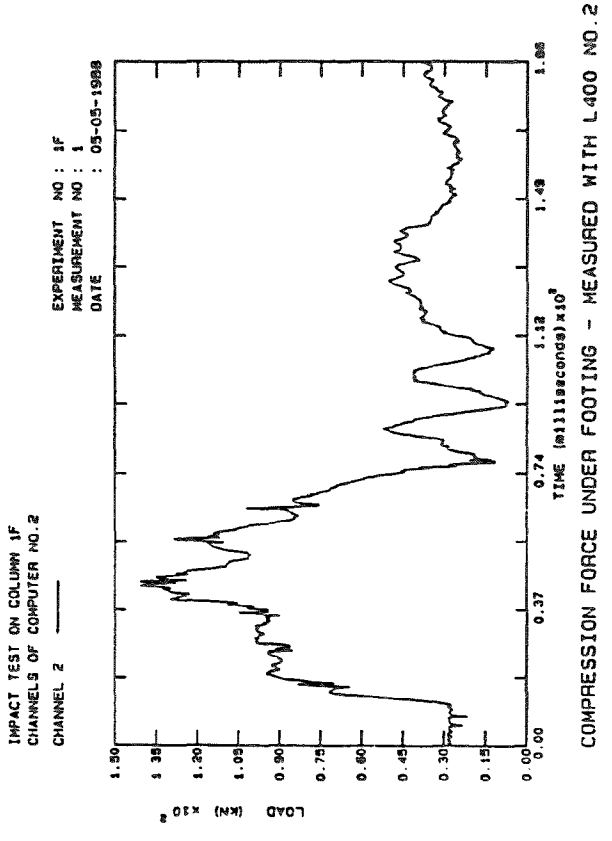

Fig. B.232: Comp. Col 1F

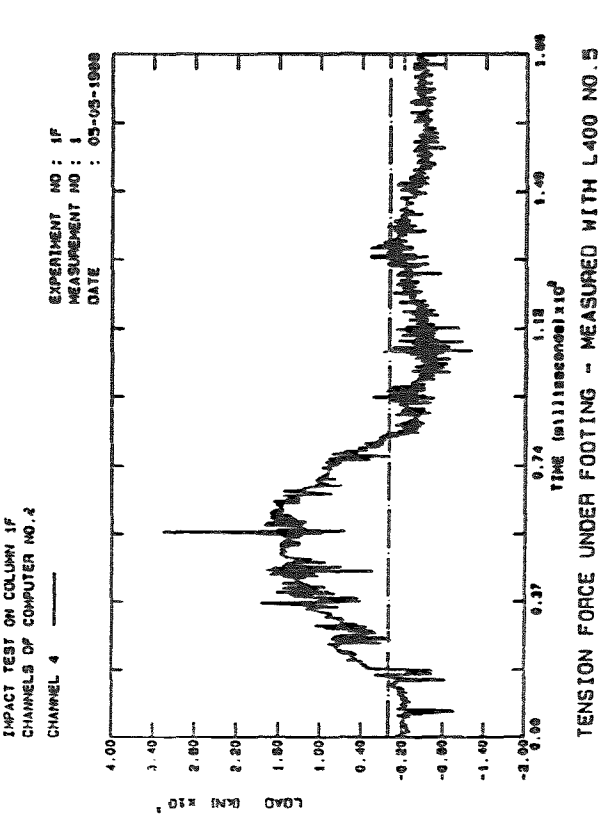

Fig. B.233: Tension Col.1F

Stellenbosch University http://scholar.sun.ac.za

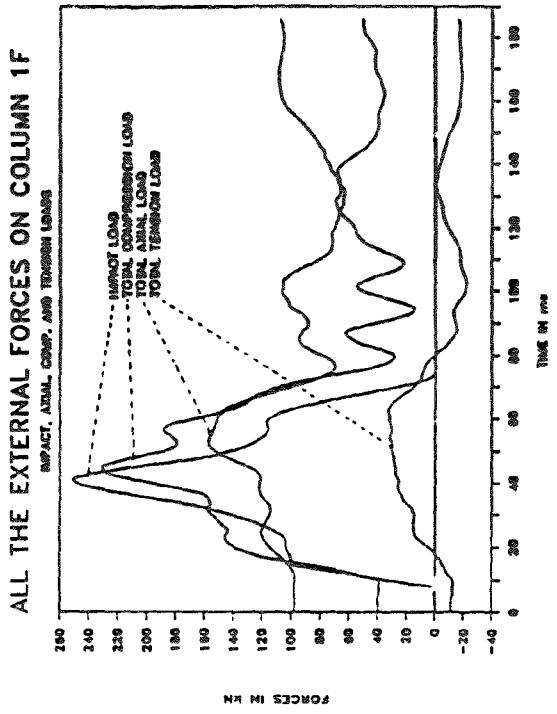

Fig. B.234: Ext. Loads Col.1F

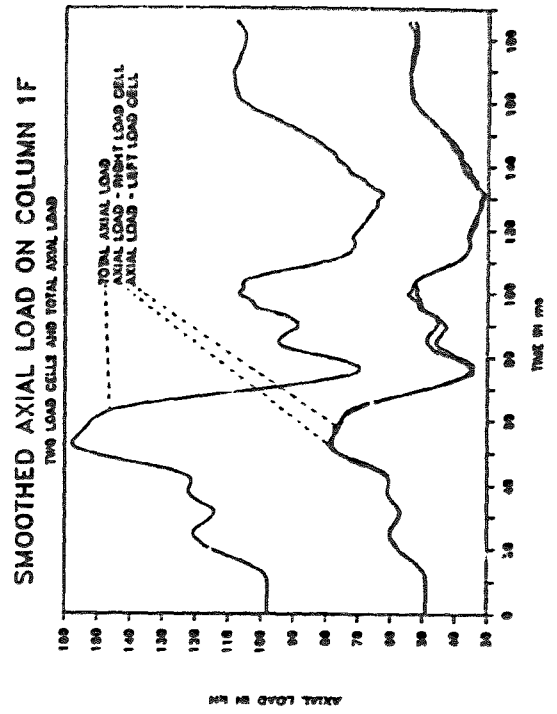

Fig. B.235: Smo. Axial Col.1F

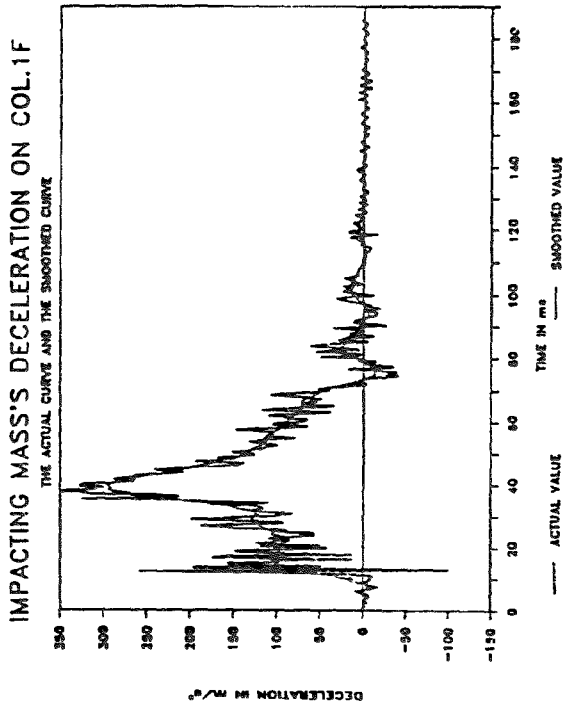

Fig. B.236: Smo. Decel. Col.1F

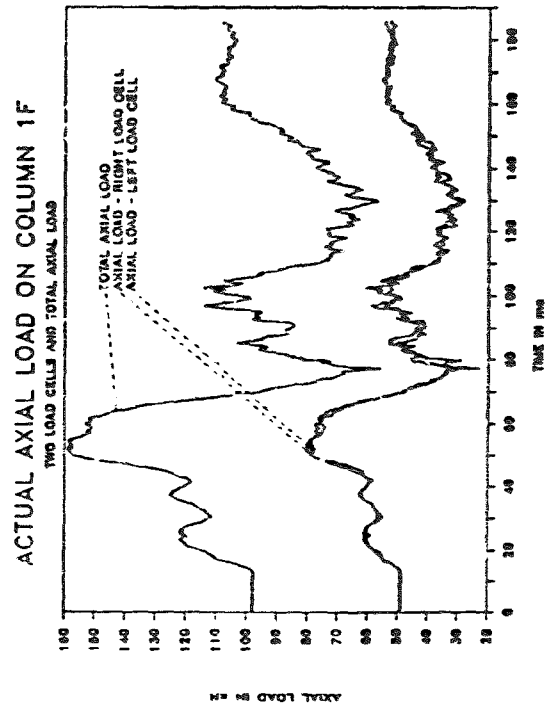

Fig. B.237: Axial loads Col.1F

Stellenbosch University http://scholar.sun.ac.za

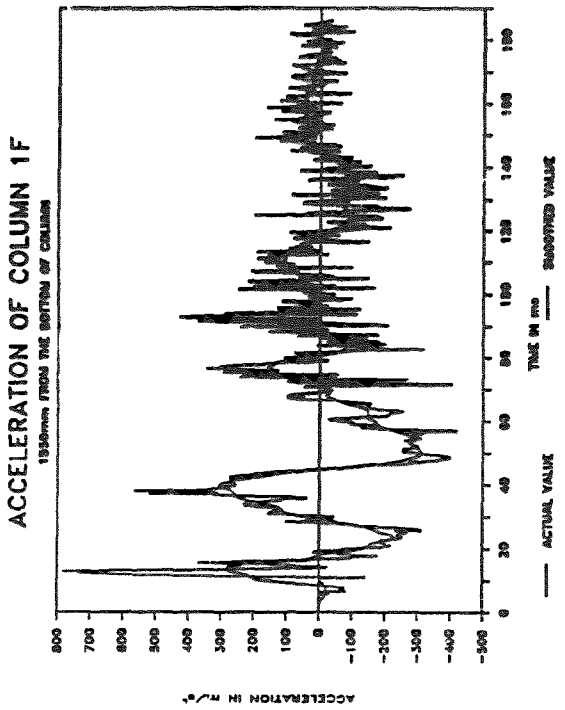

Fig. B.238: Smo.Accel. Col.1F

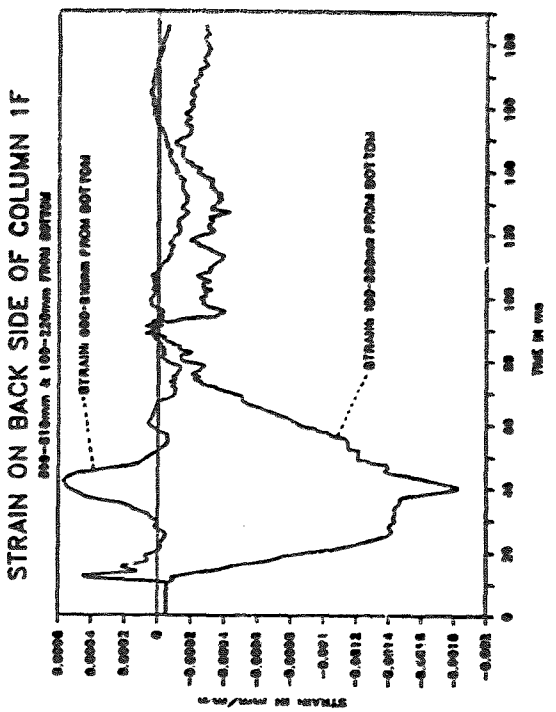

Fig. B.239: Strain Col.1F

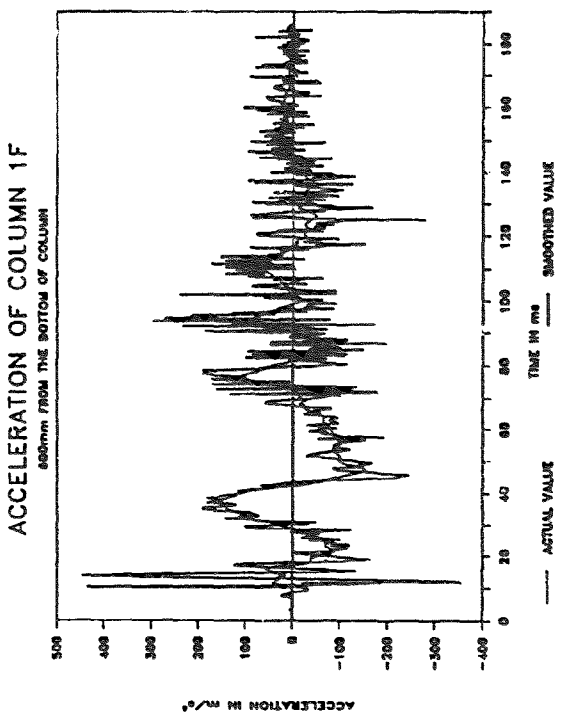

Fig. B.240: Smo.Accel. Col.1F

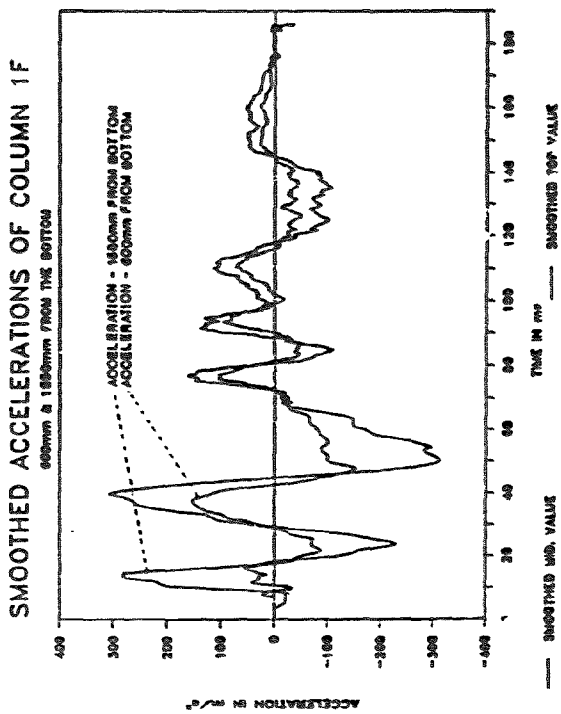

Fig. B.241: Smo. Accel. Col.1F

Stellenbosch University http://scholar.sun.ac.za

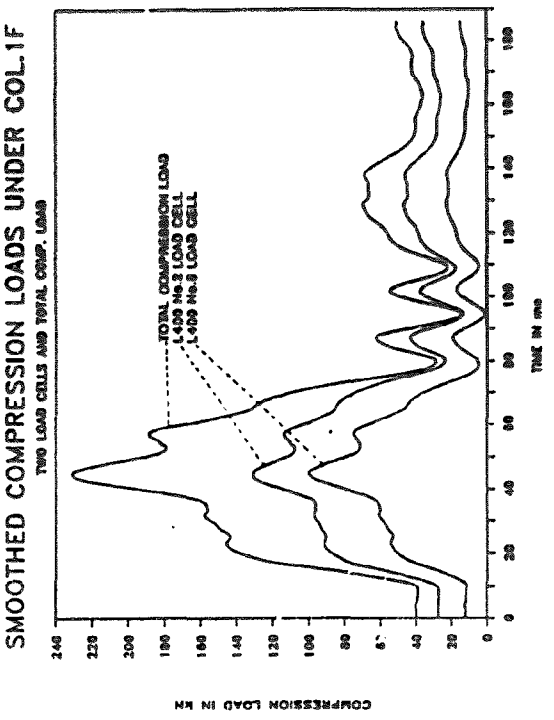

Fig. B.242: Smo. Comp. Col.1F

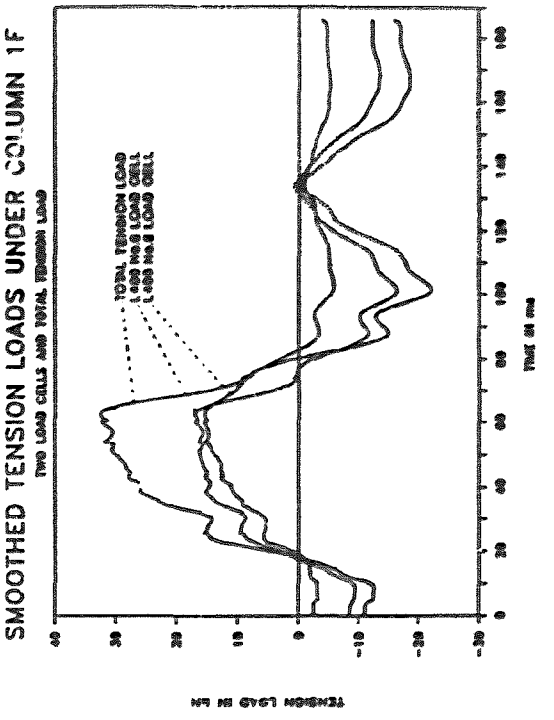

Fig. B.243: Smo. Tens. Col.1F

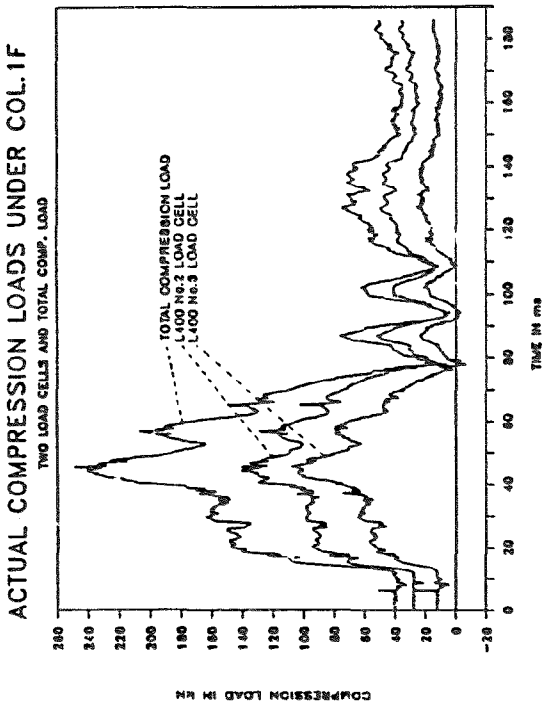

Fig. B.244: Comp. load Col 1F

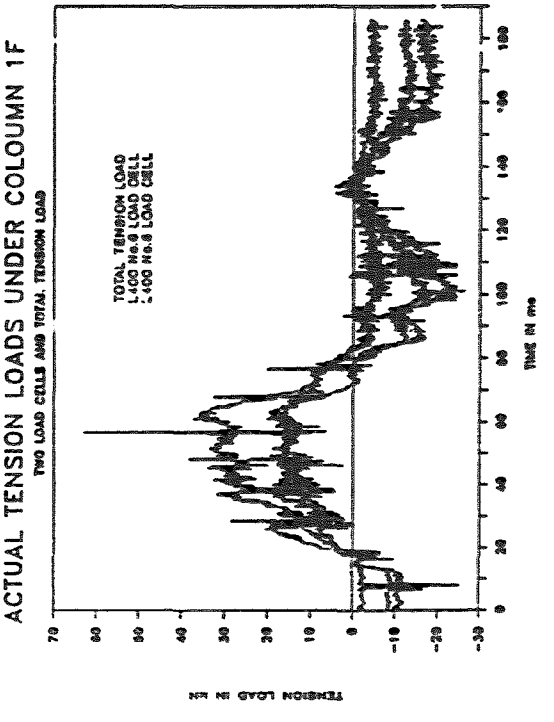

Fig. B.245: Tens. loads Col.1F

Stellenbosch University http://scholar.sun.ac.za

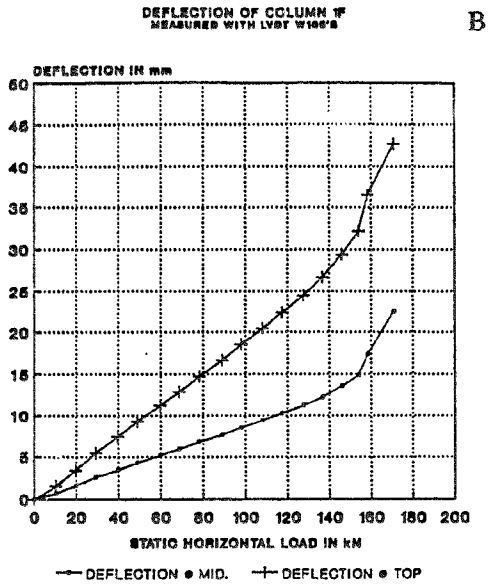

Fig. B.246: Deflection Col.1F

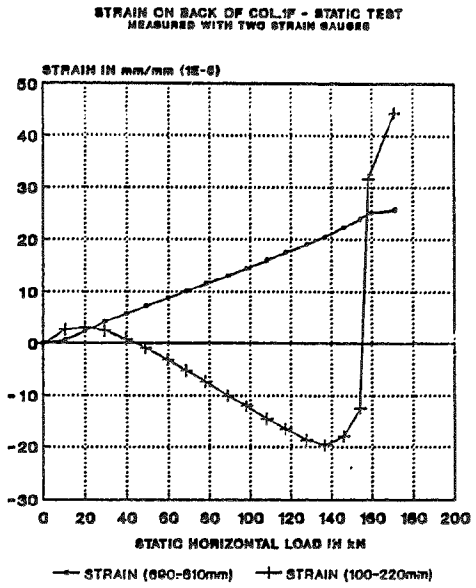

Fig. B.247: Strain Col.1F

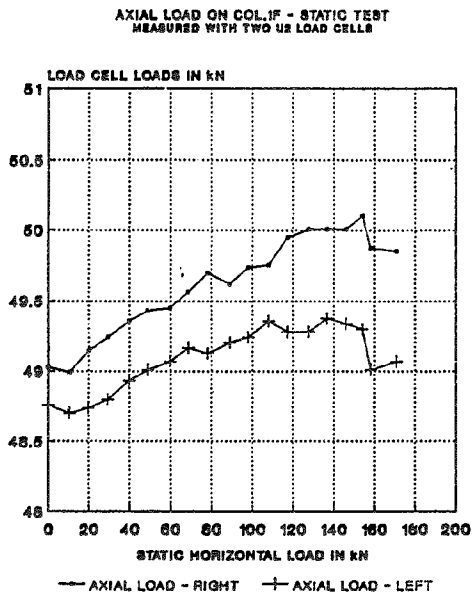

Fig. B.248: Axial load Col 1F

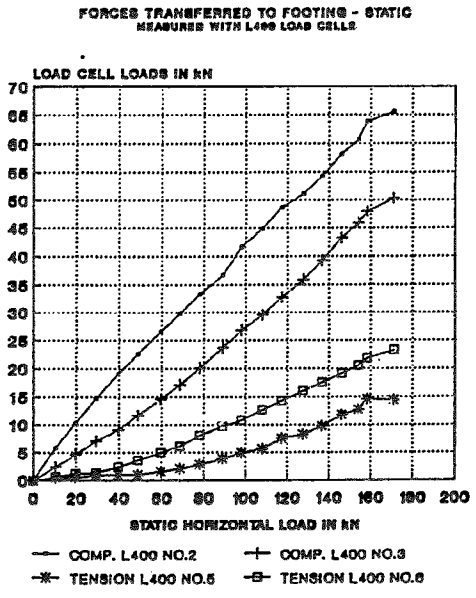

Fig. B.249: Foot.loads Col.1F

Stellenbosch University http://scholar.sun.ac.za

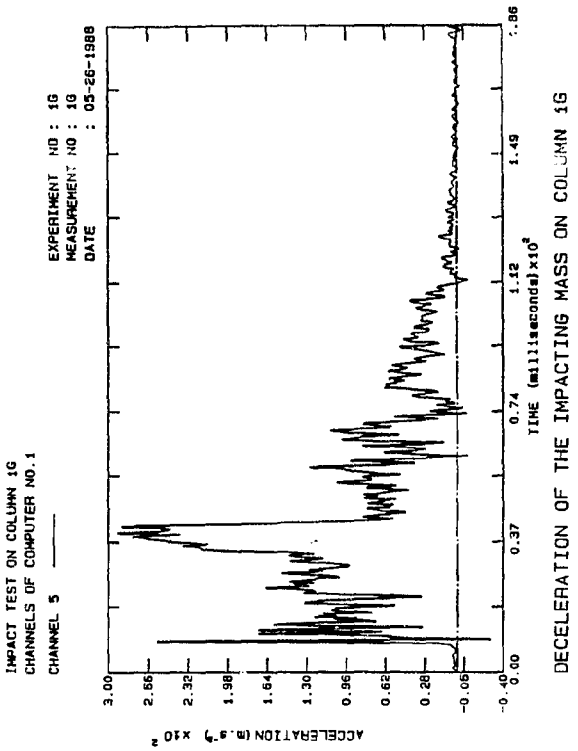

Fig. B.250: Decel. Col.1G

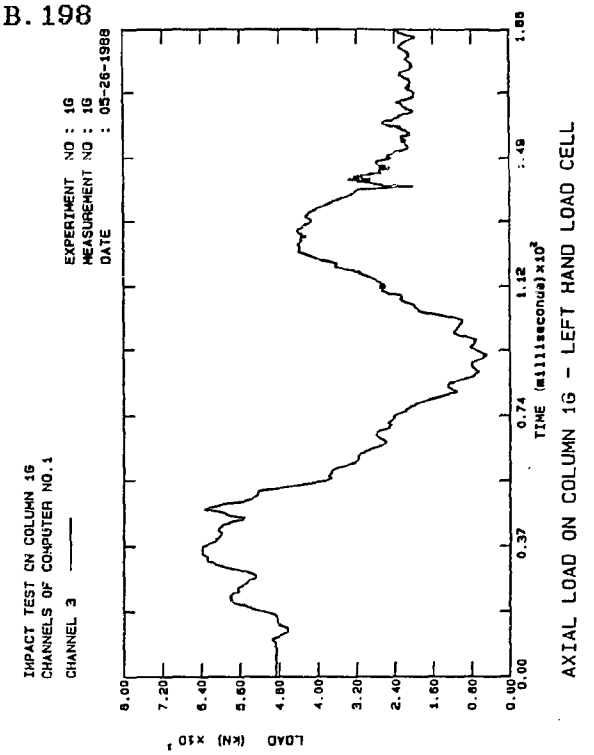

Fig. B.251: Axial load Col.1G

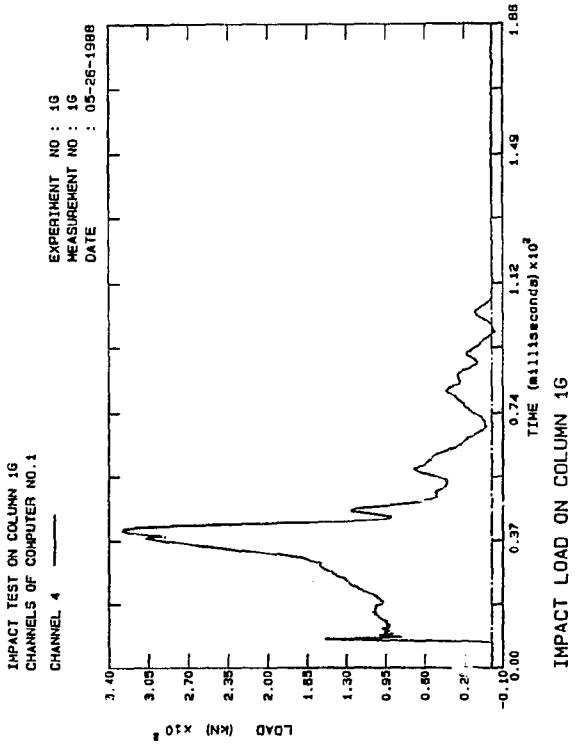

Fig. B.252: Impact Col 1G

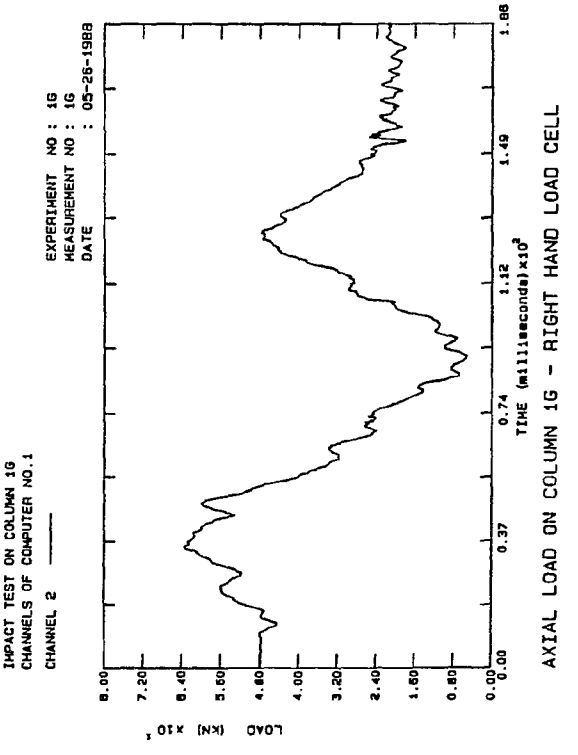

Fig. B.253: Axial load Col.1G

Stellenbosch University http://scholar.sun.ac.za

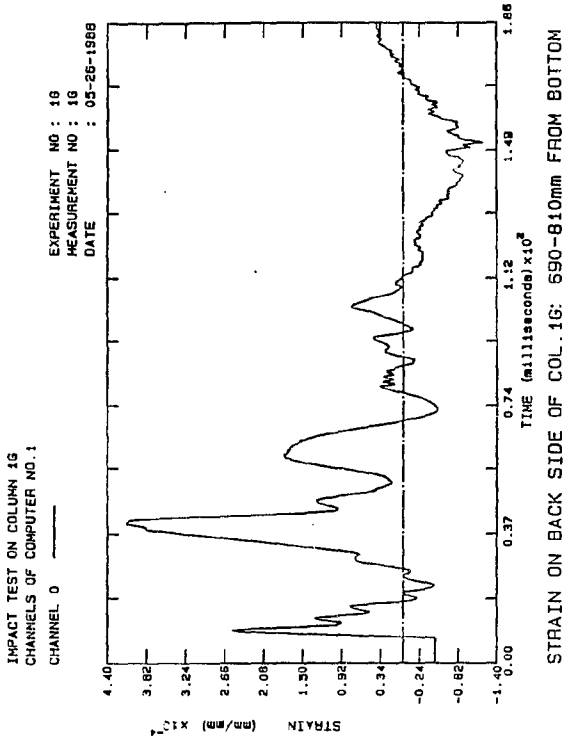

Fig. B.254: Strain Col.1G

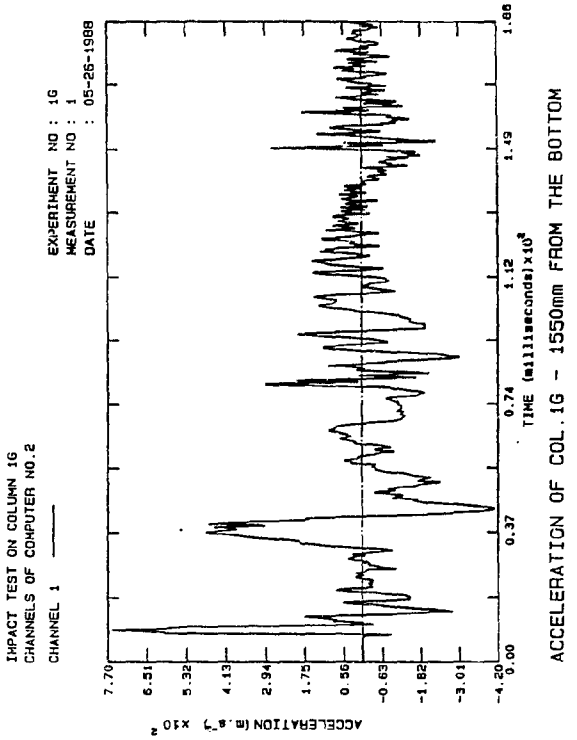

Fig. B.255: Accel. Col.1G

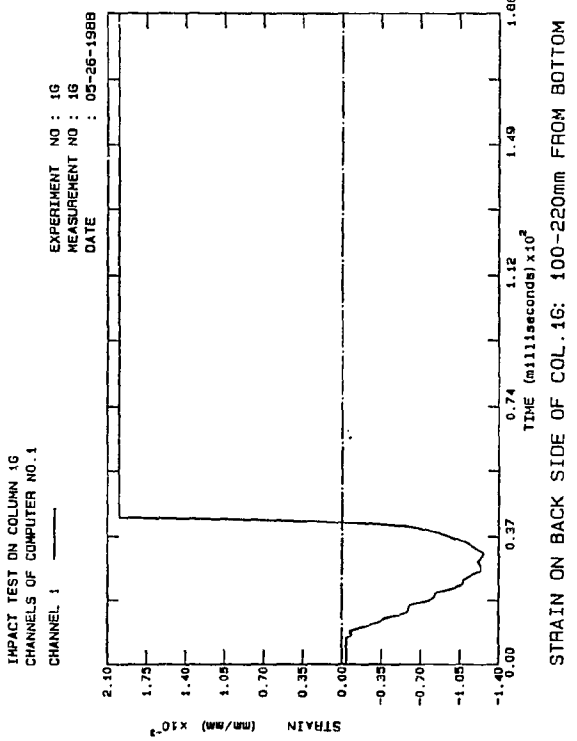

Fig. B.256: Strain Col 1G

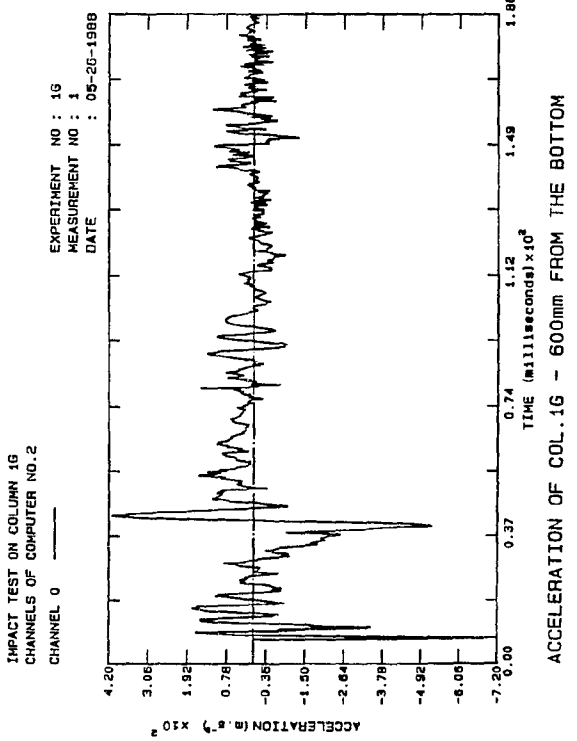

Fig. B.257: Accel. Col.1G

Stellenbosch University http://scholar.sun.ac.za

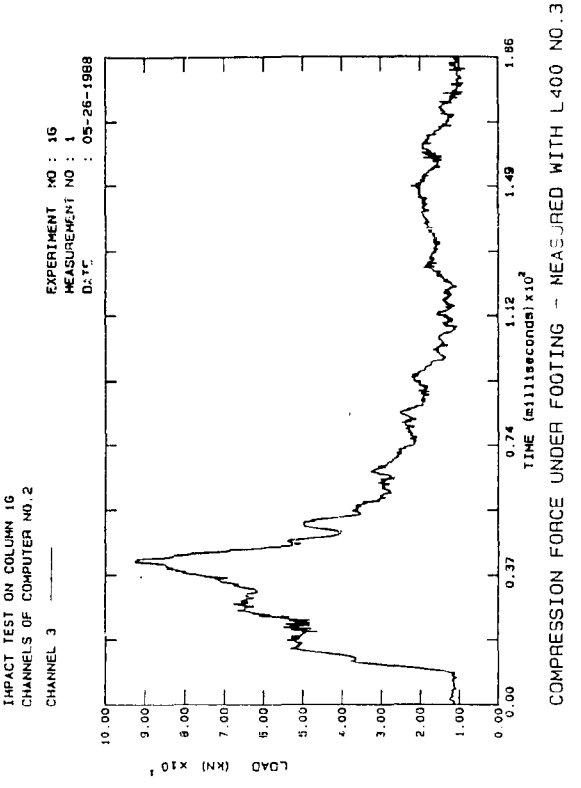

Fig. B.258: Comp. Col.1G

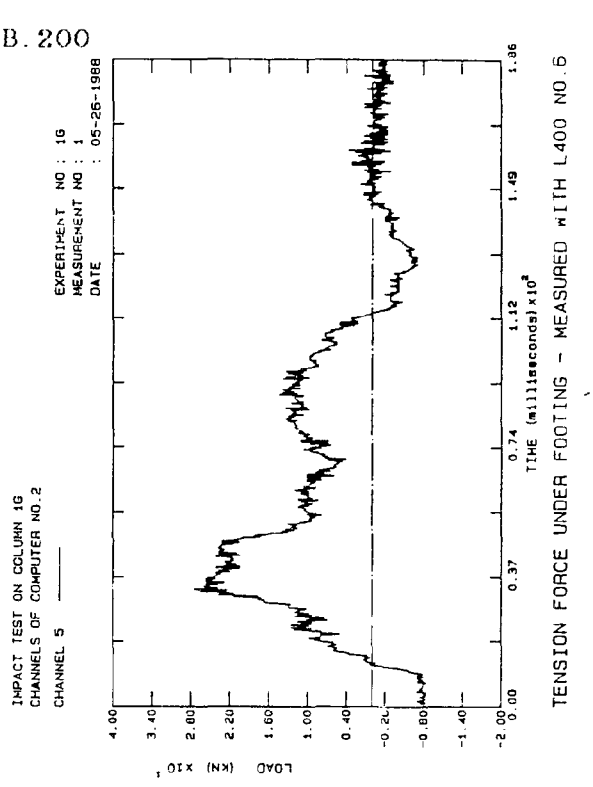

Fig. B.259: Tension Col.1G

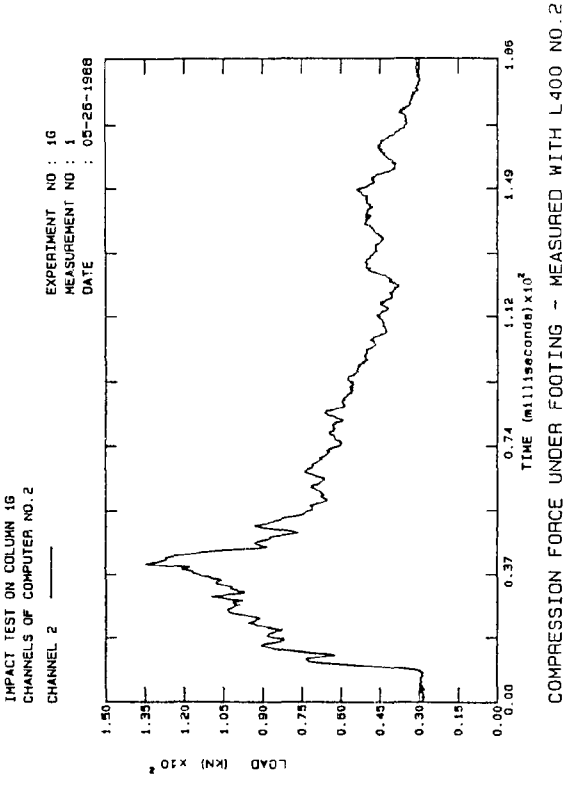

Fig. B.260: Comp. Col 1G

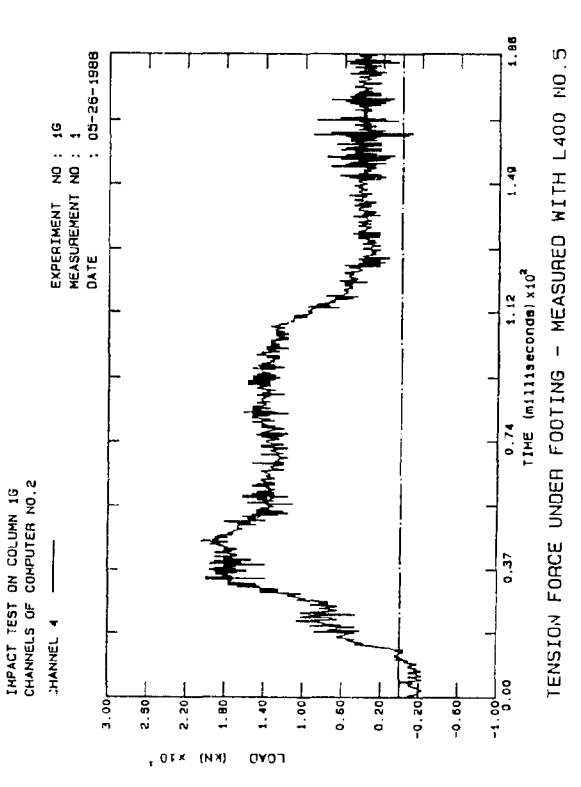

Fig. B.261: Tension Col.1G

Stellenbosch University http://scholar.sun.ac.za

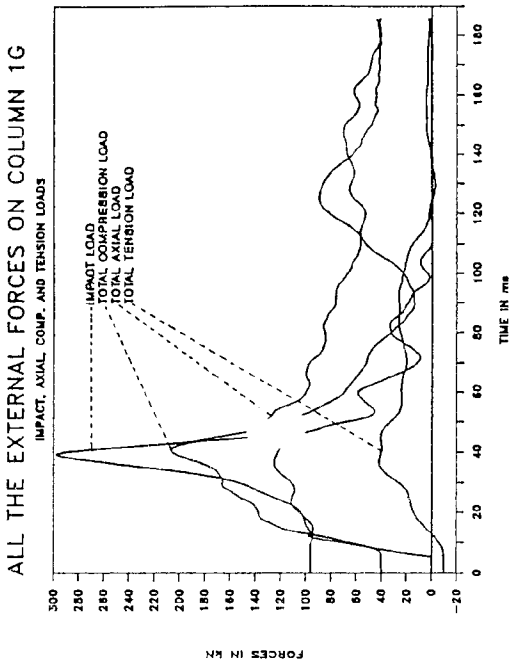

Fig. B.263: Ext. Loads Col.1G

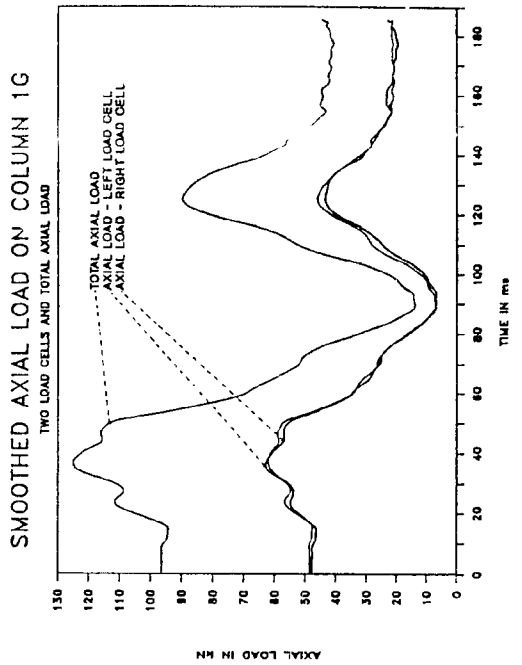

Fig. B.263: Smo. Axial Col.1G

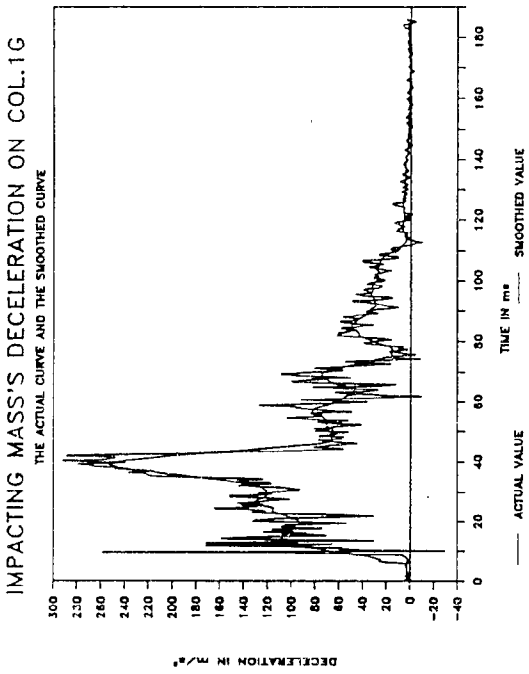

Fig. B.264: Smo.Decel. Col.1G

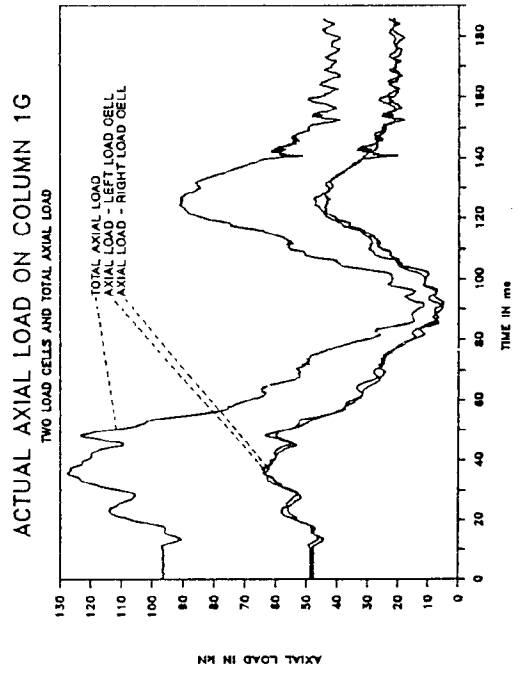

Fig. B.265: Axial loads Col.1G

Stellenbosch University http://scholar.sun.ac.za

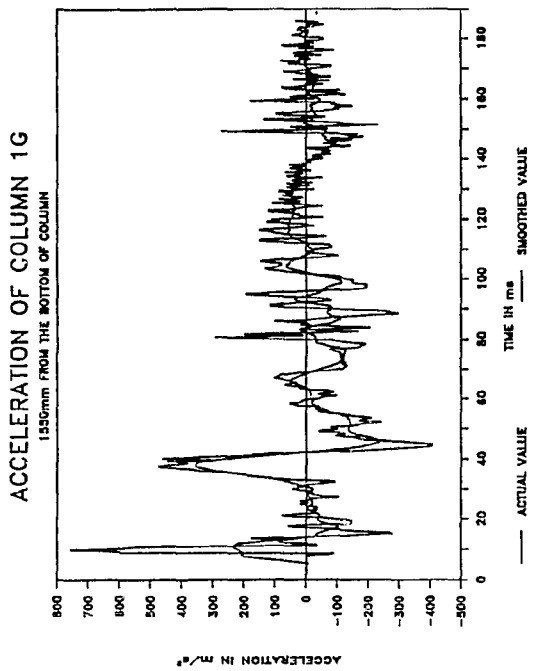

Fig. B.266: Smo.Accel. Col.1G

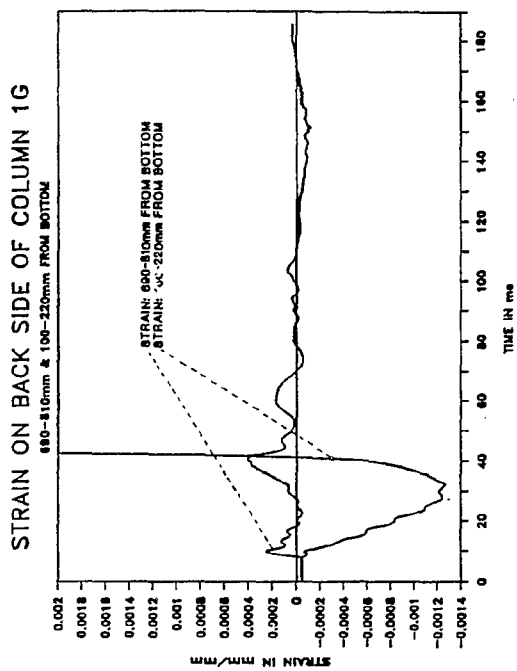

Fig. B.267: Strain Col.1G

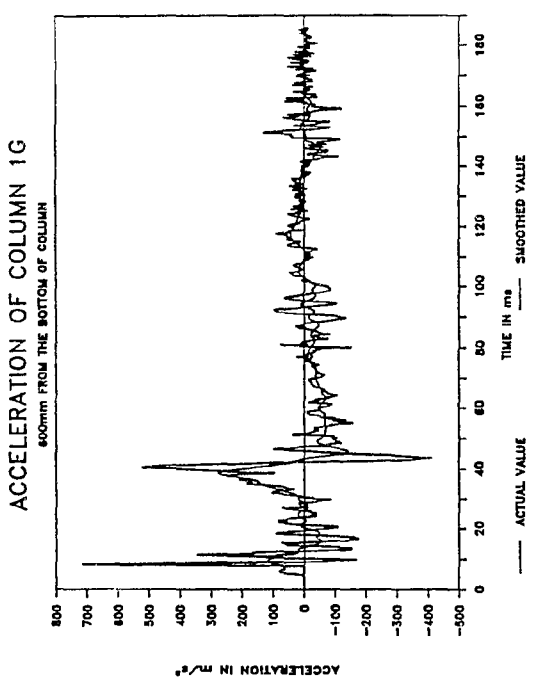

Fig. B.268: Smo.Accel. Col 1G

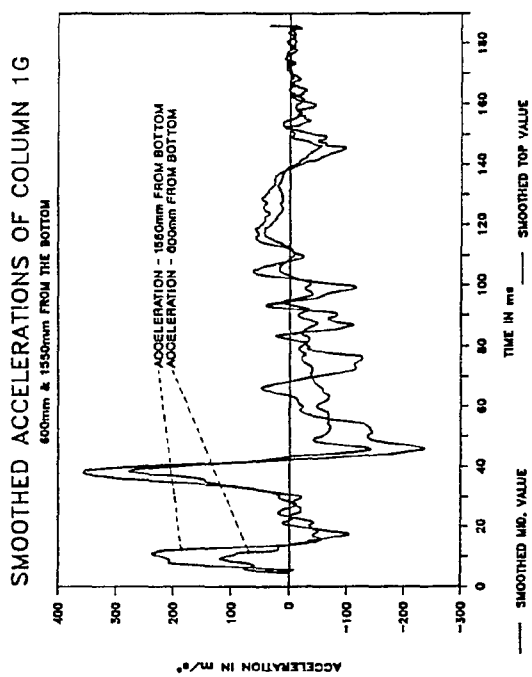

Fig. B.269: Smo. Accel. Col.1G

Stellenbosch University http://scholar.sun.ac.za

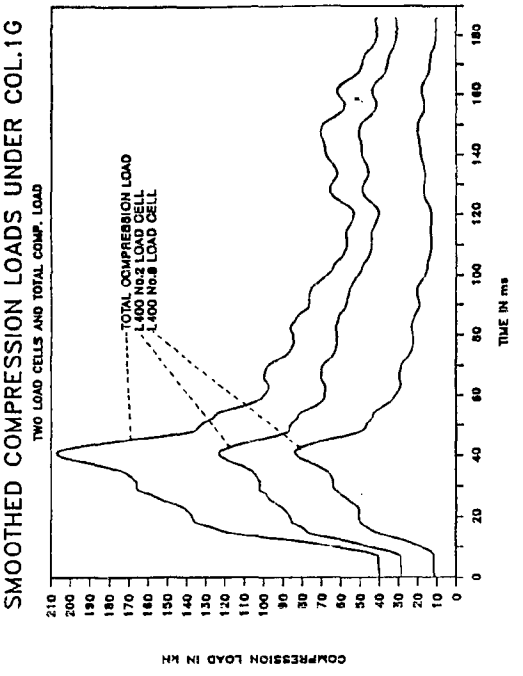

Fig. B.270: Smo. Comp. Col.1G

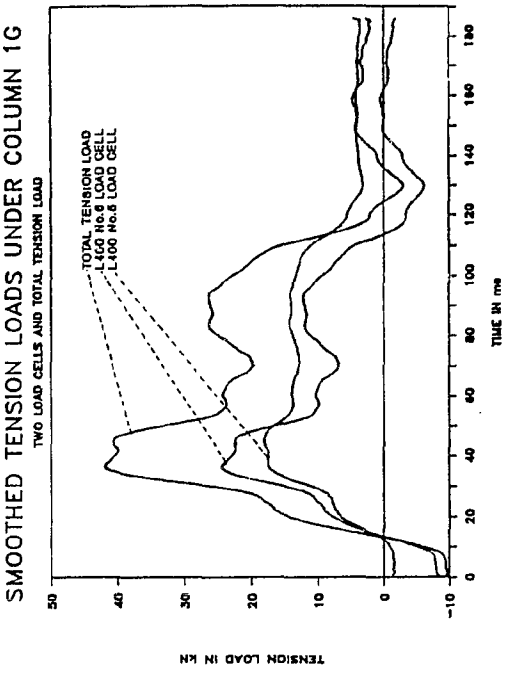

Fig. B.271: Smo. Tens. Col.1G

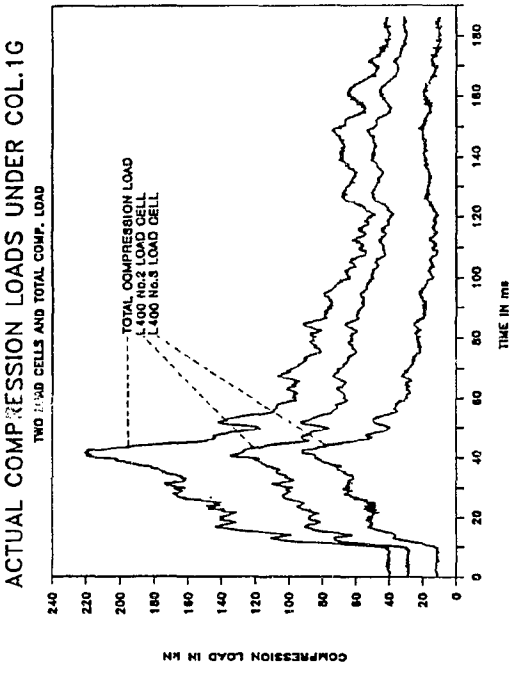

Fig. B.272: Comp. load Col 1G

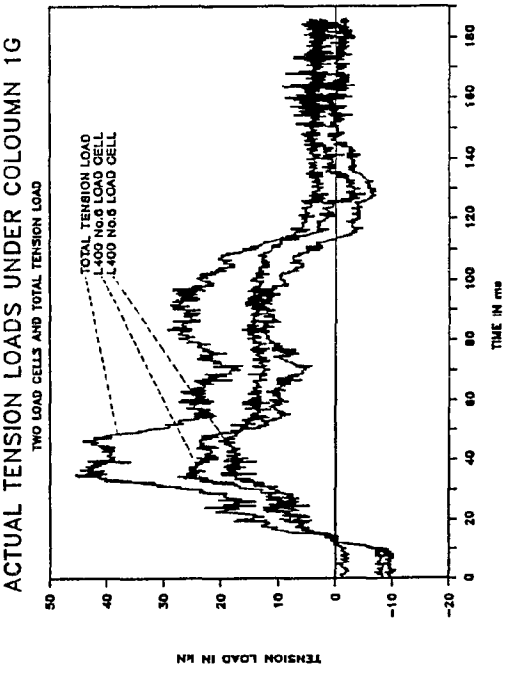

Fig. B.273: Tens. loads Col.1G

Stellenbosch University http://scholar.sun.ac.za

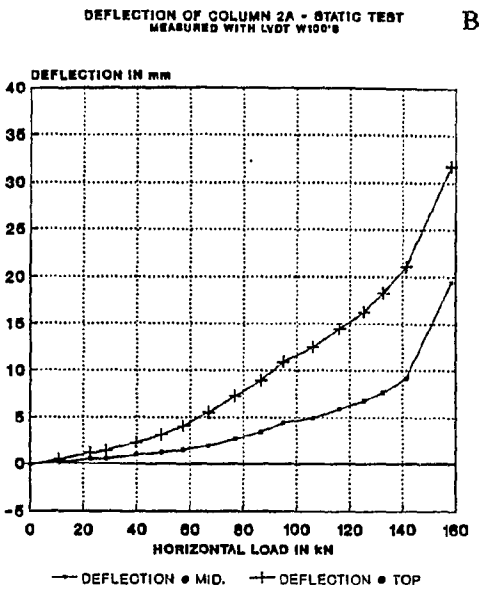

Fig. B.274: Deflection Col.2A

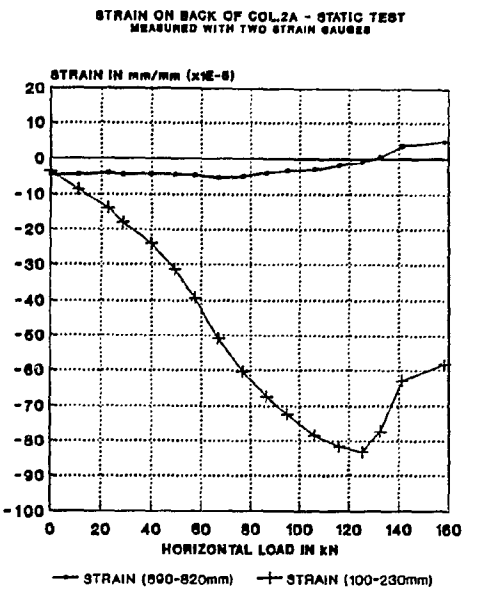

Fig. B.275: Strain Col.2A

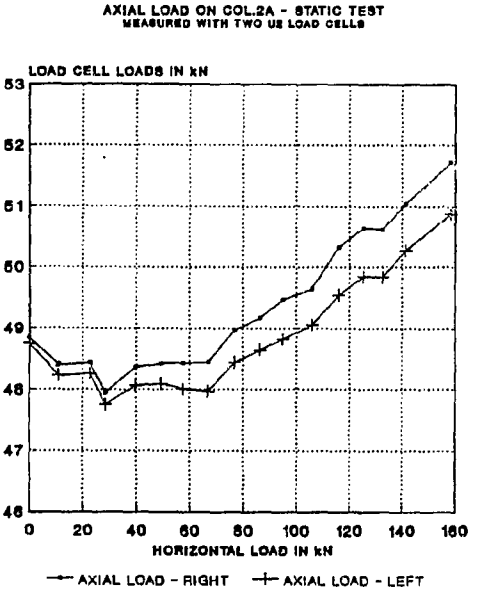

Fig. B.276: Axial load Col 2A

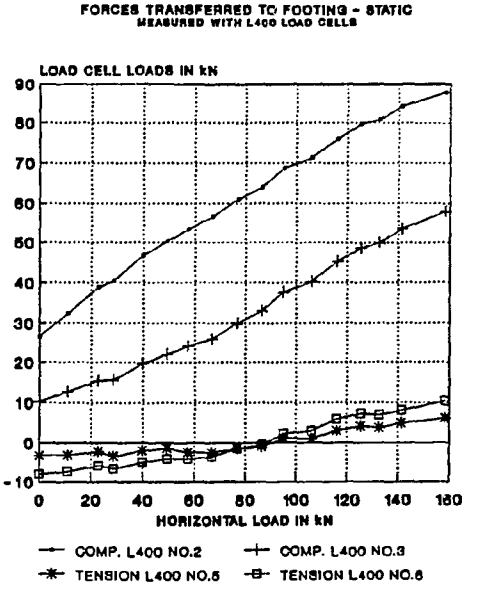

Fig. B.277: Foot. loads Col.2A

Stellenbosch University http://scholar.sun.ac.za

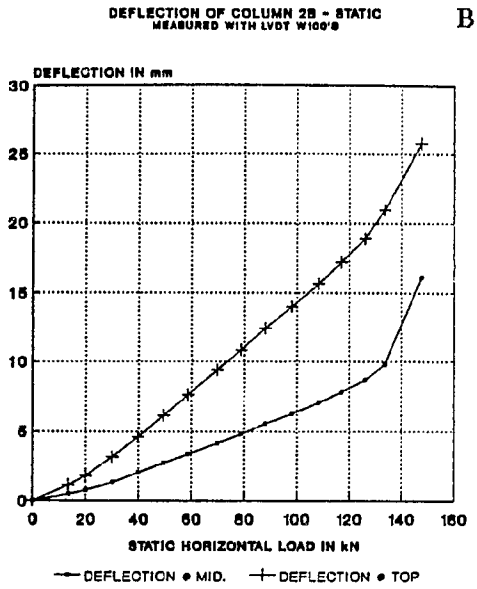

Fig. B.278: Deflection Col.2B

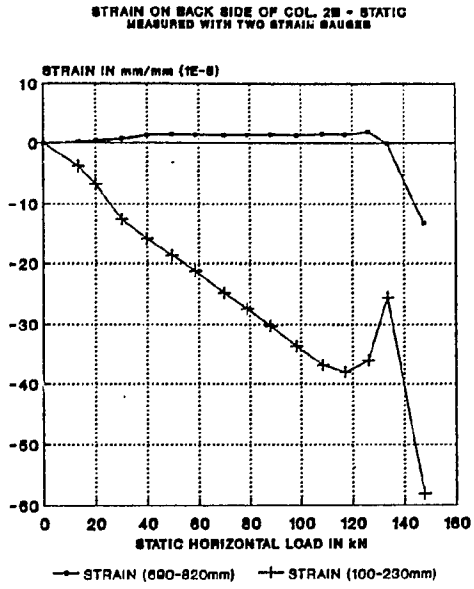

Fig. B.279: Strain Col.2B

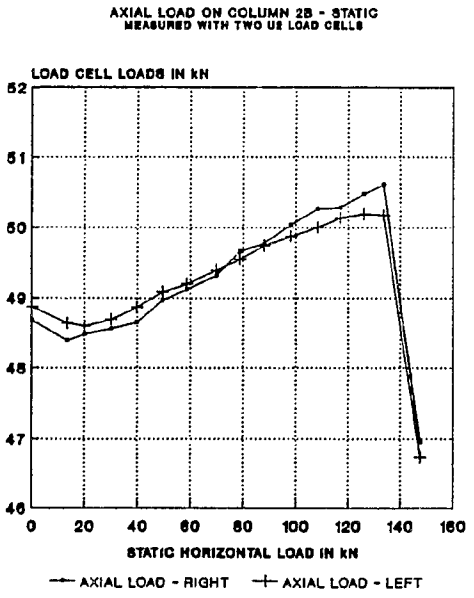

Fig. B.280: Axial load Col 2B

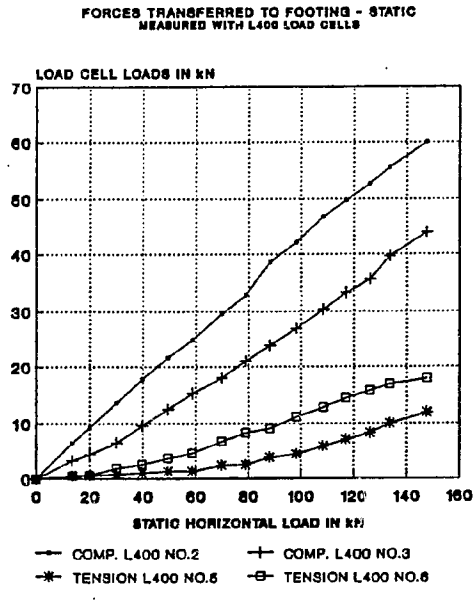

Fig. B.281: Foot.loads Col.2B

Stellenbosch University http://scholar.sun.ac.za

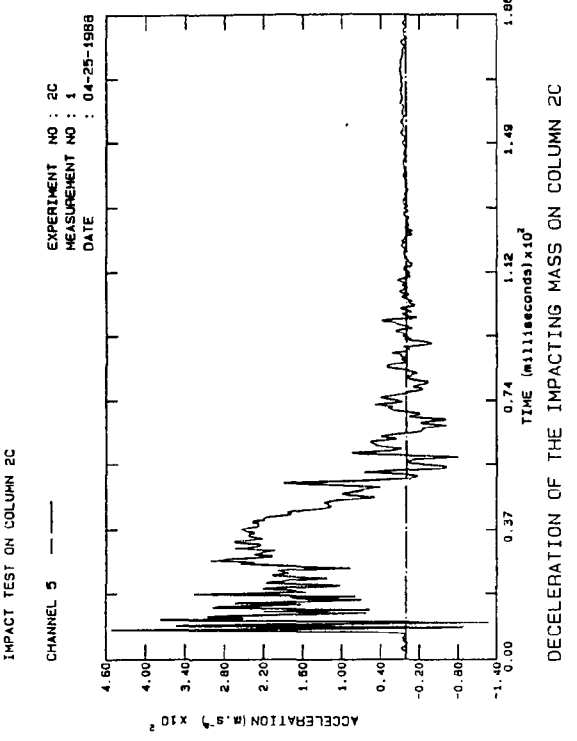

Fig. B.282: Decel. Col.2C

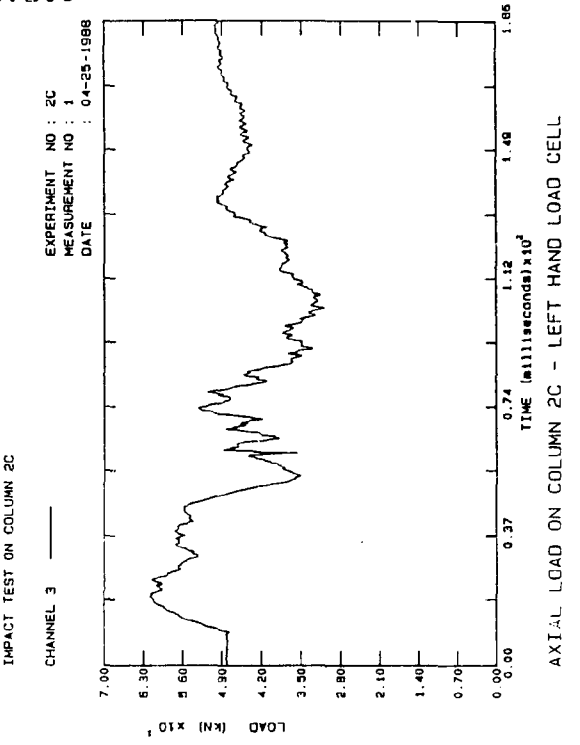

Fig. B.283: Axial load Col.2C

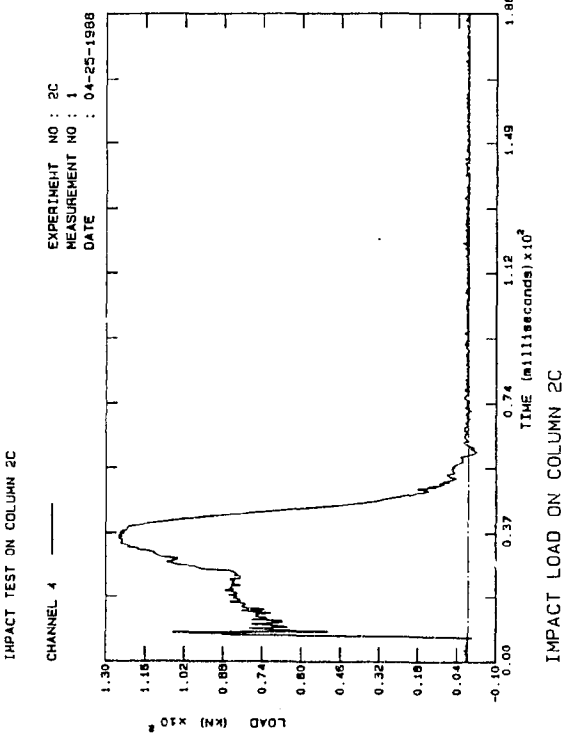

Fig. B.284: Impact. Col 2C

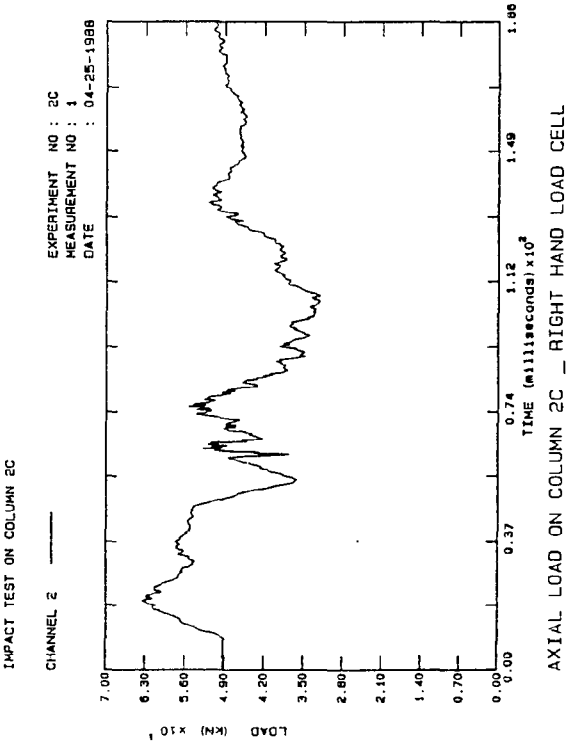

Fig. B.285: Axial load Col.2C

Stellenbosch University http://scholar.sun.ac.za

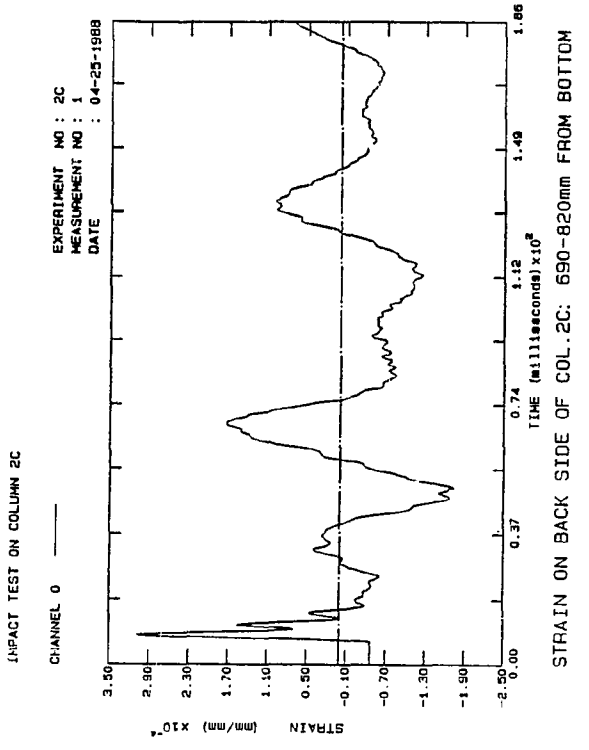

Fig. B.286: Strain Col.2C

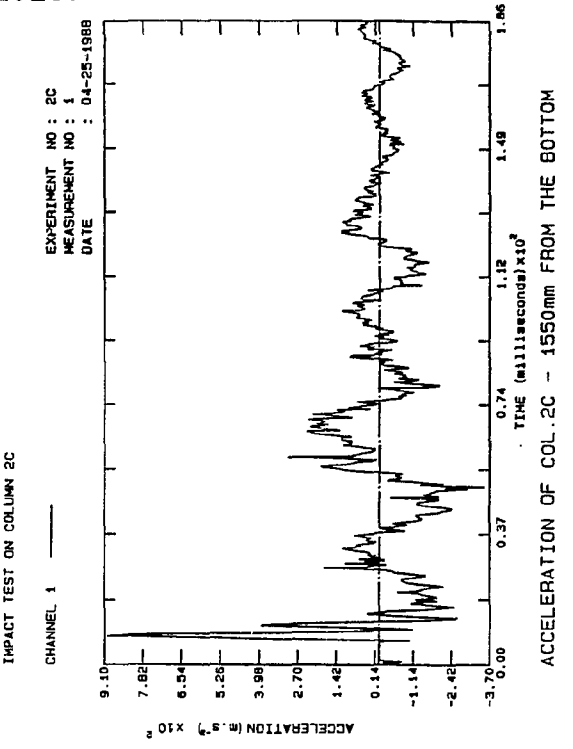

Fig. B.287: Accel. Col.2C

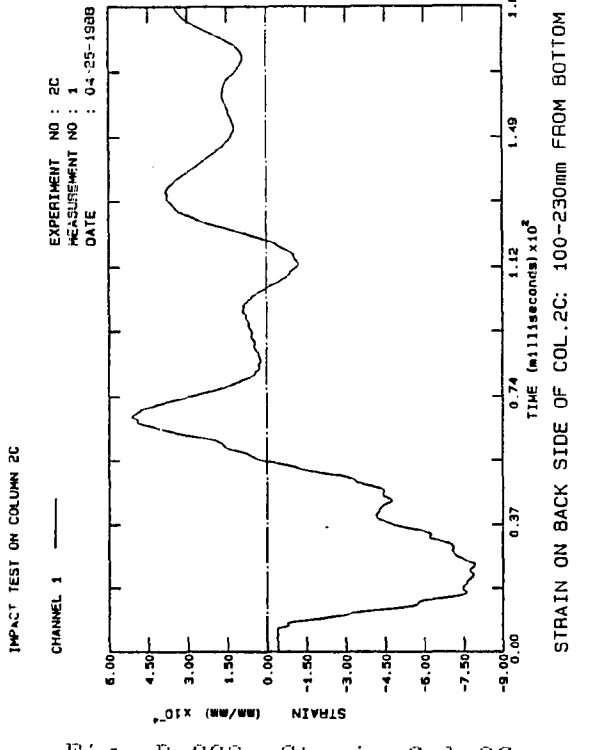

Fig. B.288: Strain Col 2C

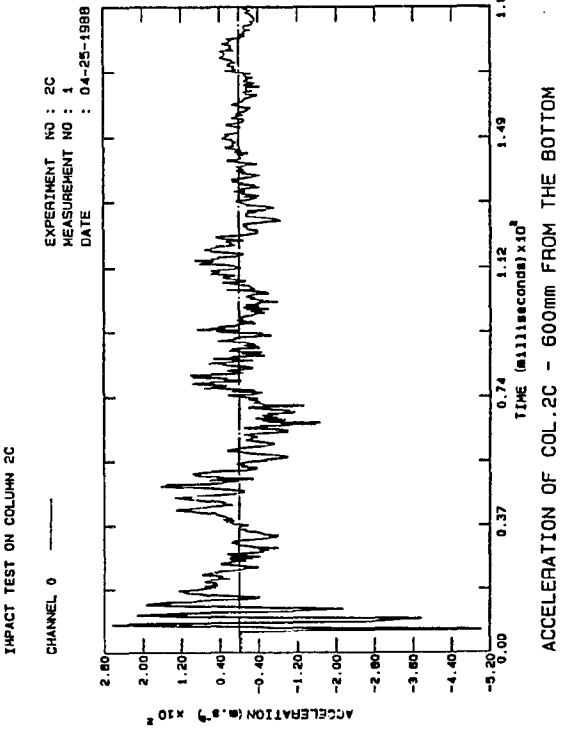

Fig. B.289: Accel. Col.2C

Stellenbosch University http://scholar.sun.ac.za

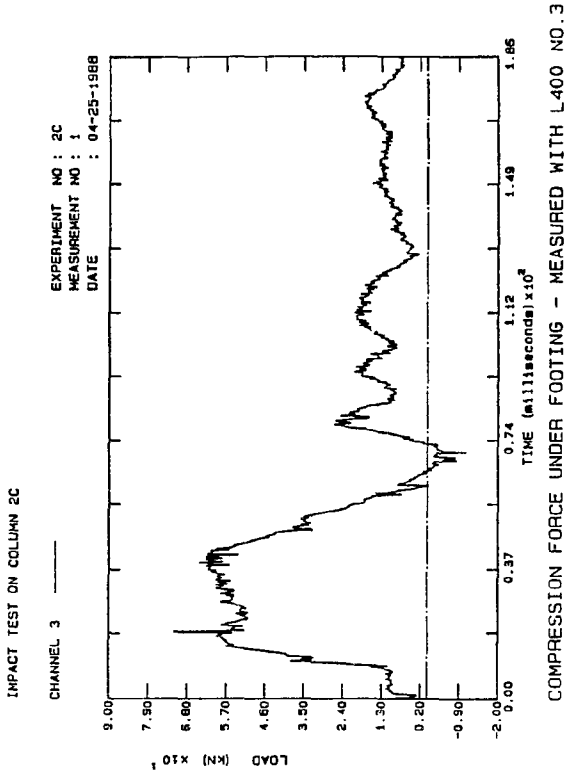

Fig. B.290: Comp. Col.2C

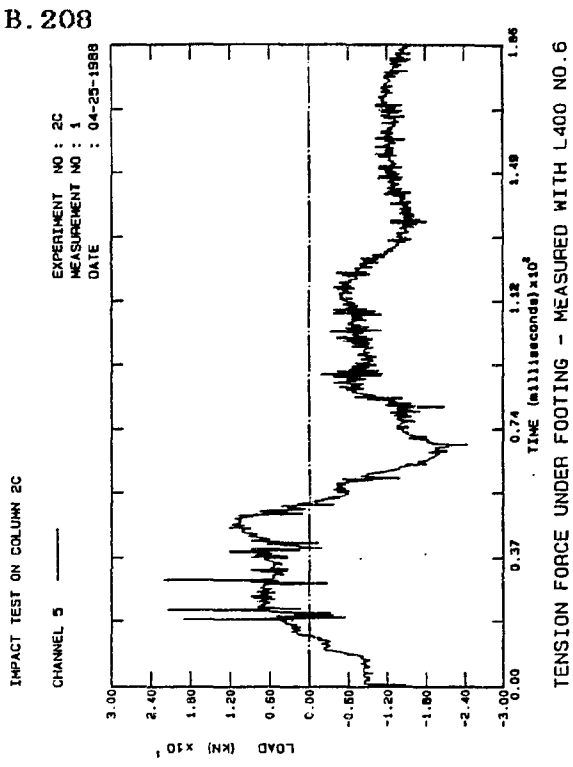

Fig. B.291: Tension Col.2C

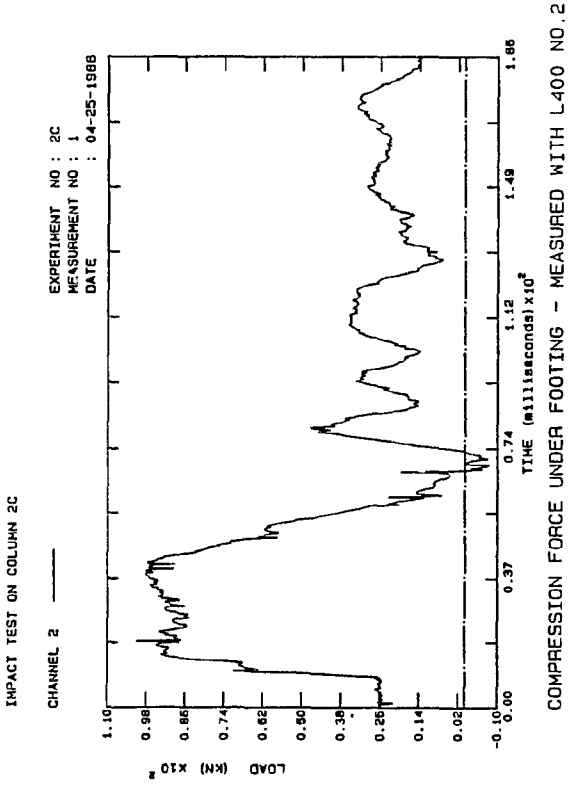

Fig. B.292: Comp. Col 2C

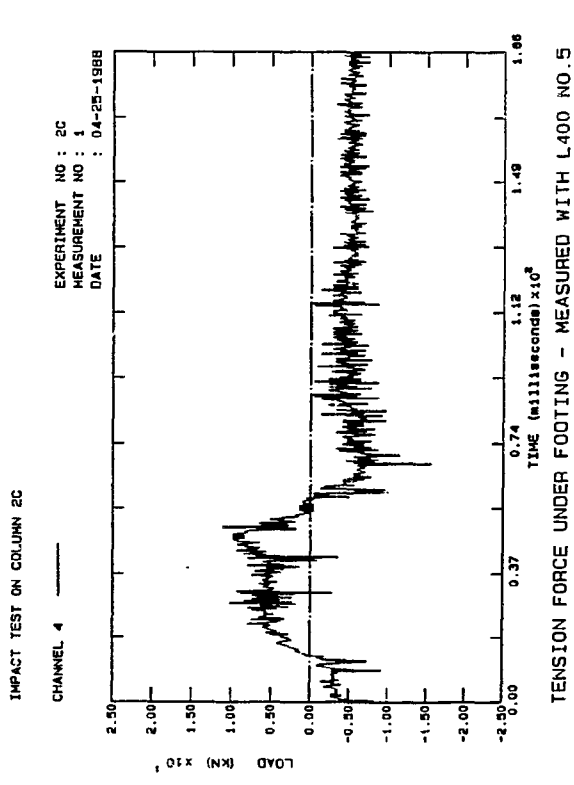

Fig. B.293: Tension Col.2C

Stellenbosch University http://scholar.sun.ac.za

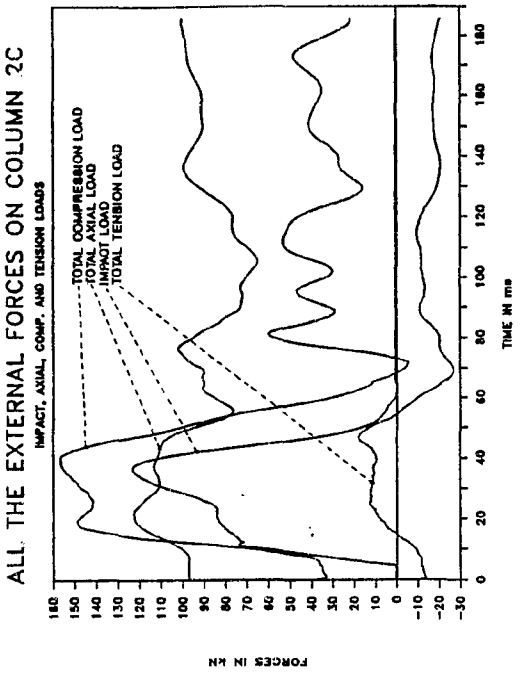

Fig. B.294: Ext. Loads Col.2C

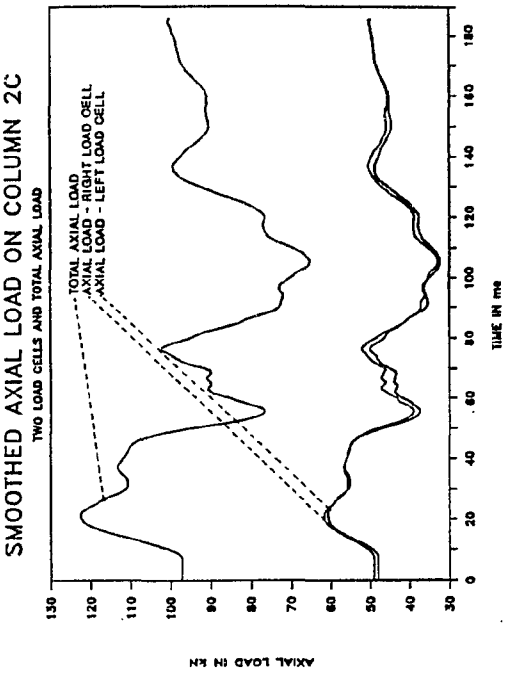

Fig. B.295: Smo. Axial Col.2C

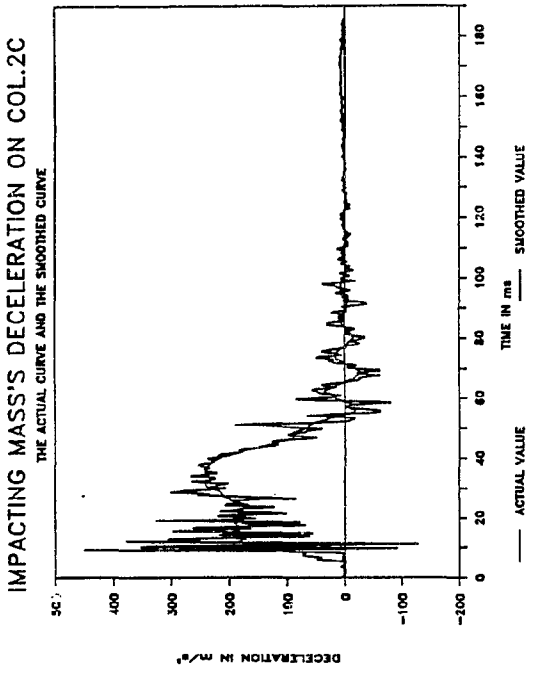

Fig. B.296: Smo.Decel. Col 2C

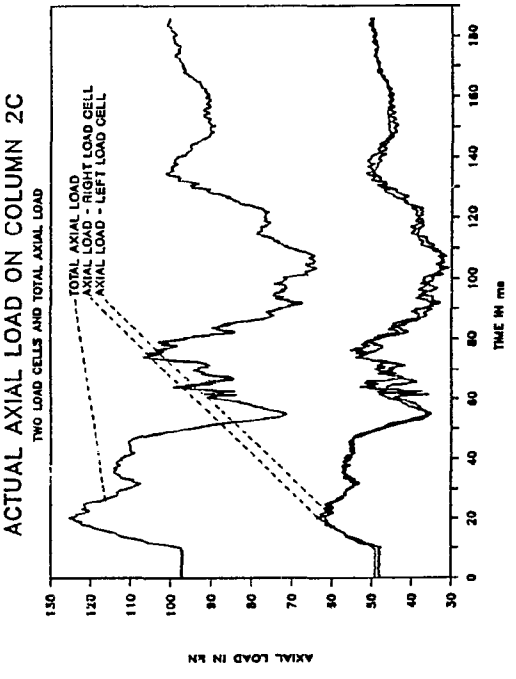

Fig. B.297: Axial loads Col.2C

Stellenbosch University http://scholar.sun.ac.za

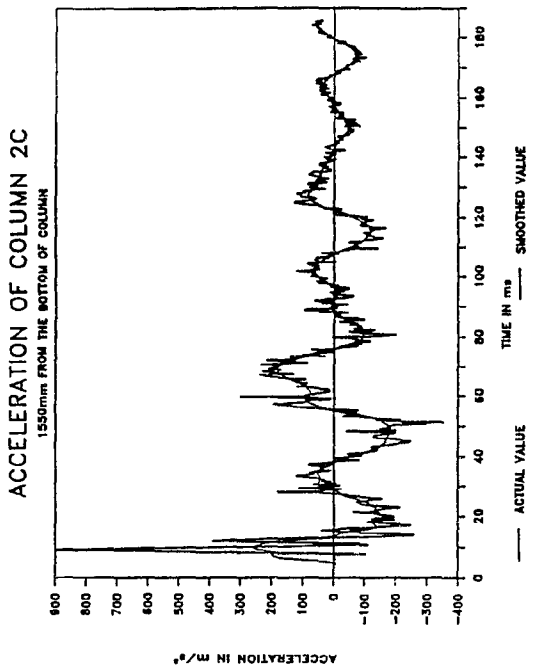

Fig. B.298: Smo.Accel. Col.2C

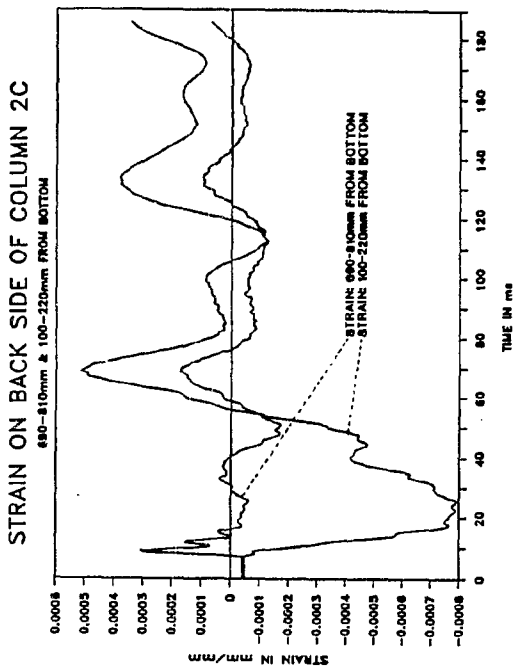

Fig. B.299: Strain Col.2C

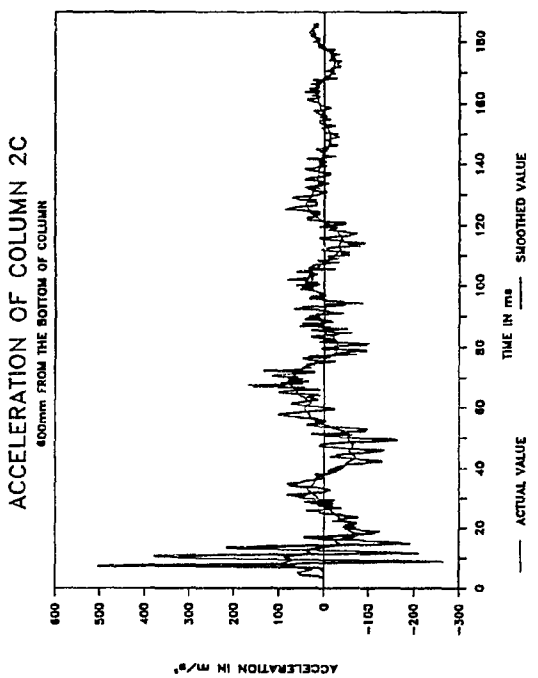

Fig. B.300: Smo.Accel. Col 2C

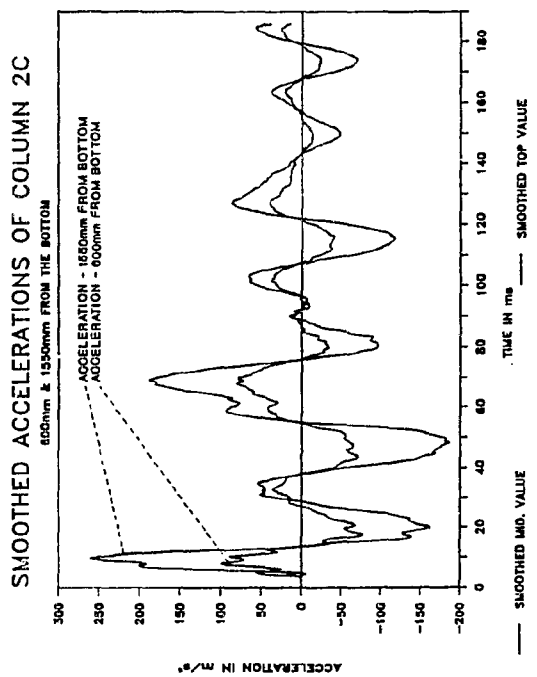

Fig. B.301: Smo. Accel. Col.2C

Stellenbosch University http://scholar.sun.ac.za

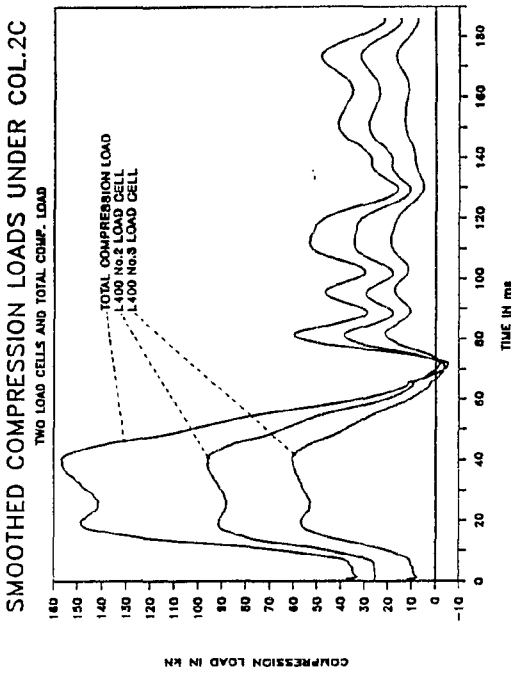

Fig. B.302: Smo. Comp. Col.2C

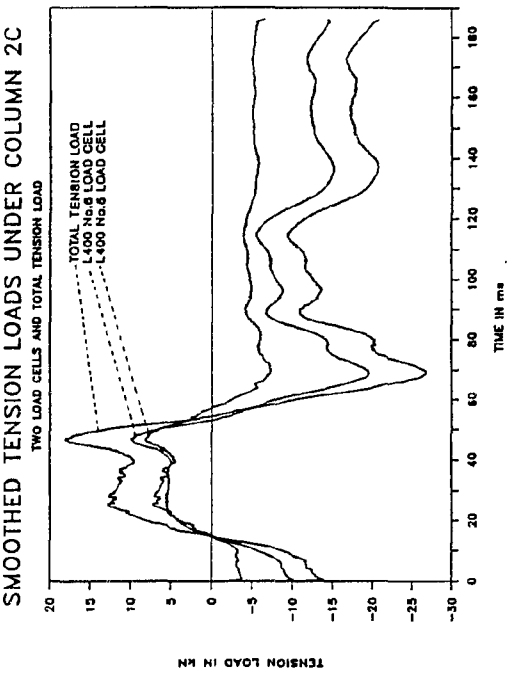

Fig. B.303: Smo. Tens. Col.2C

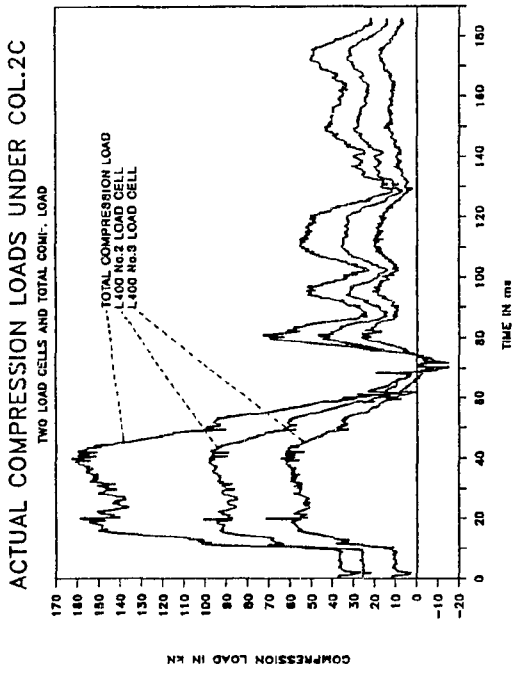

Fig. B.304: Comp. load Col 2C

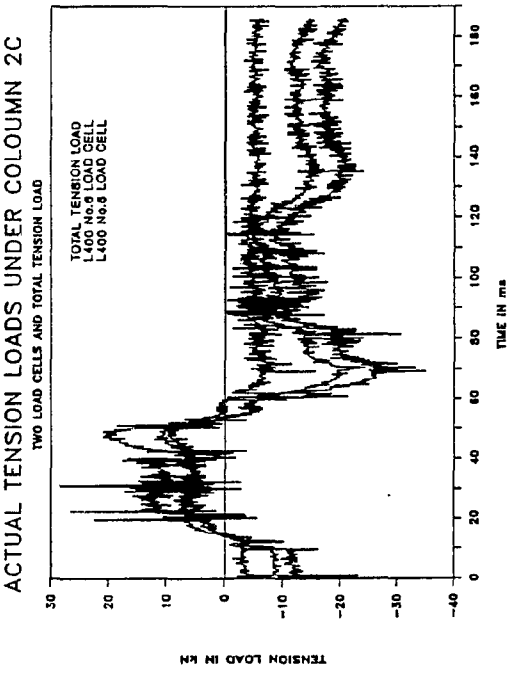

Fig. B.305: Tens. loads Col.2C

Stellenbosch University http://scholar.sun.ac.za

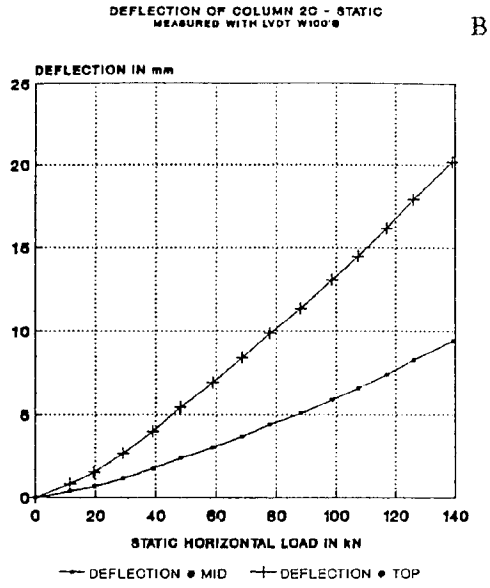

Fig. B.306: Deflection Col.2C

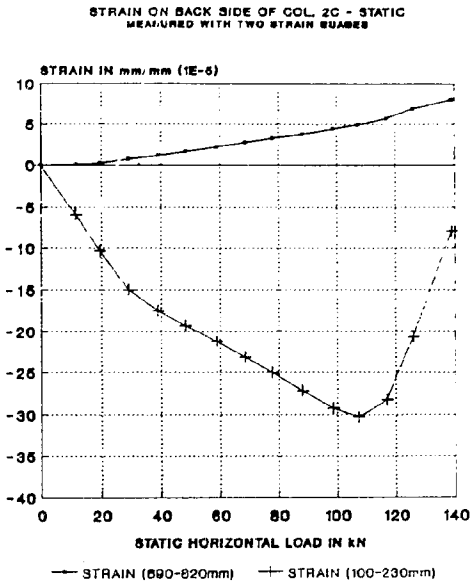

Fig. B.307: Strain Col.2C

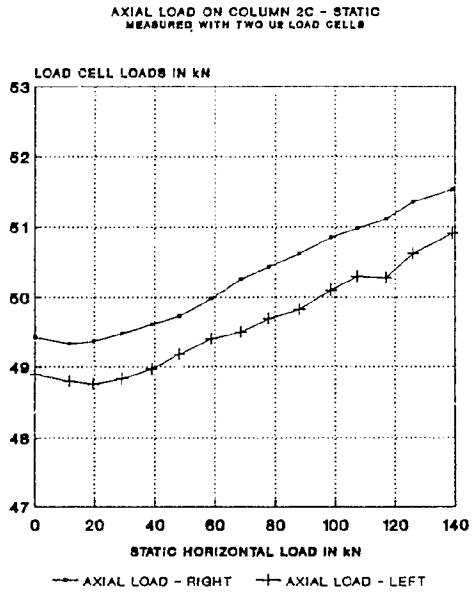

Fig. B.308: Axial load Col 2C

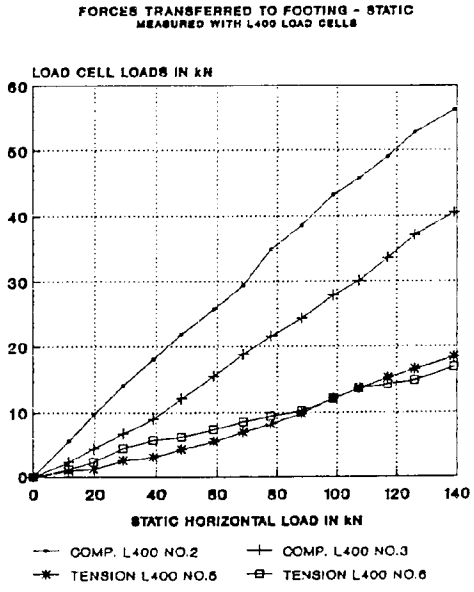

Fig. B.309: Foot. loads Col.2C

Stellenbosch University http://scholar.sun.ac.za

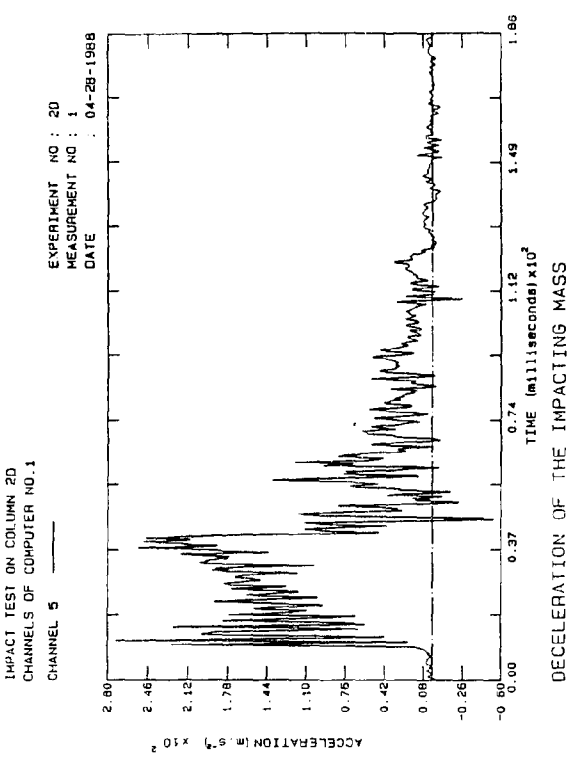

Fig. B.310: Decel. Col.2D

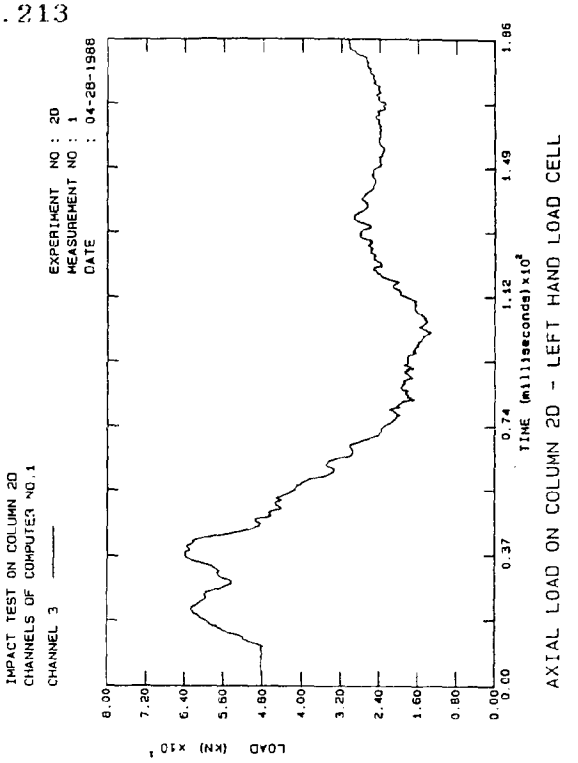

Fig. B.311: Axial load Col.2D

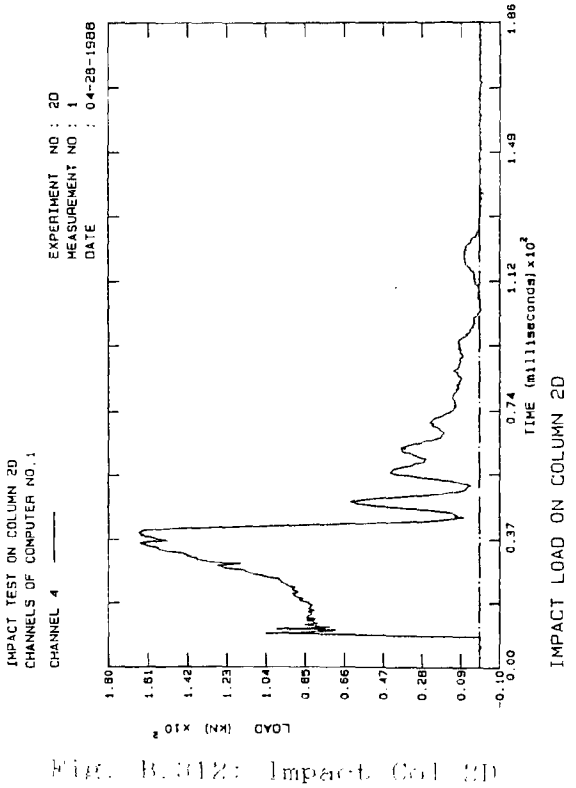

Fig. B.312: Impact Col.2D

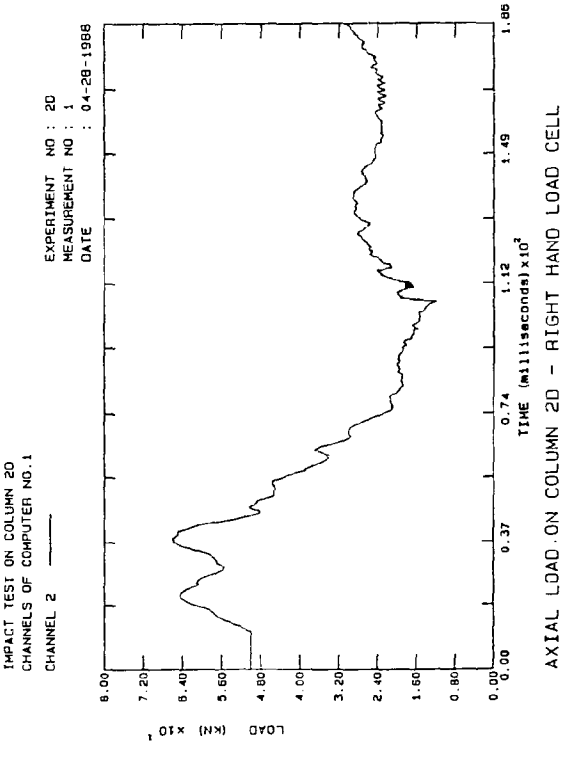

Fig. B.313: Axial load Col.2D

Stellenbosch University http://scholar.sun.ac.za

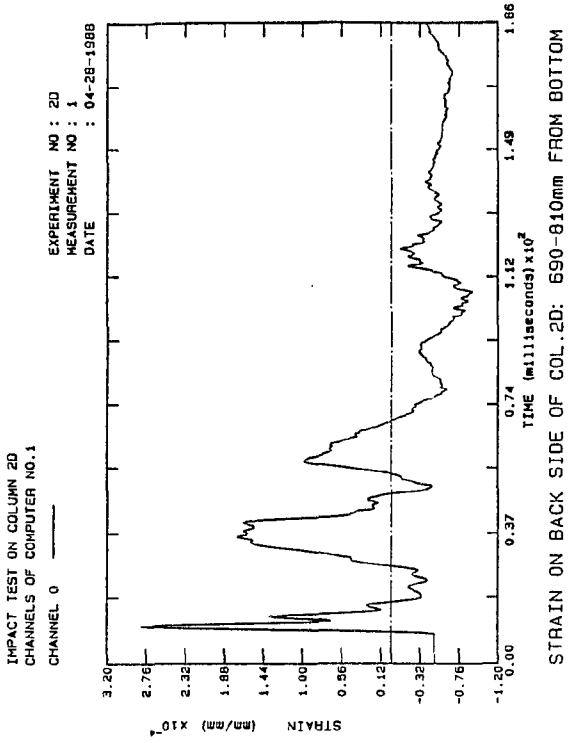

Fig. B.314: Strain Col.2D

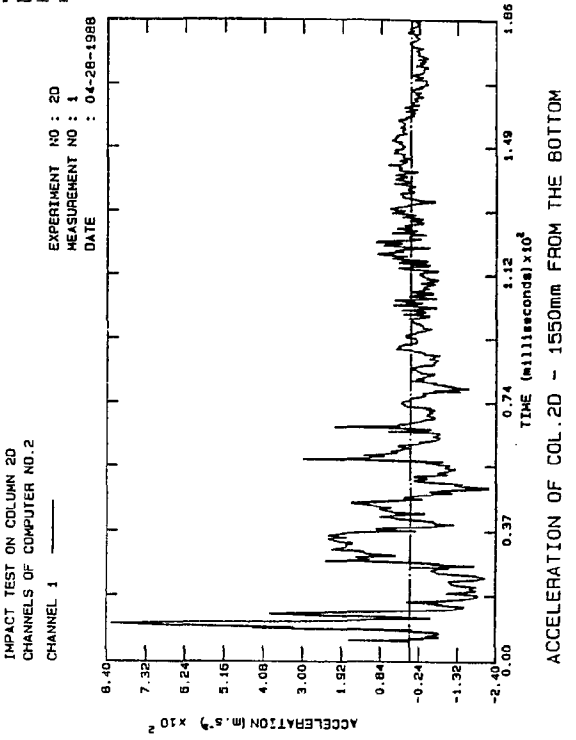

Fig. B.315: Accel. Col.2D

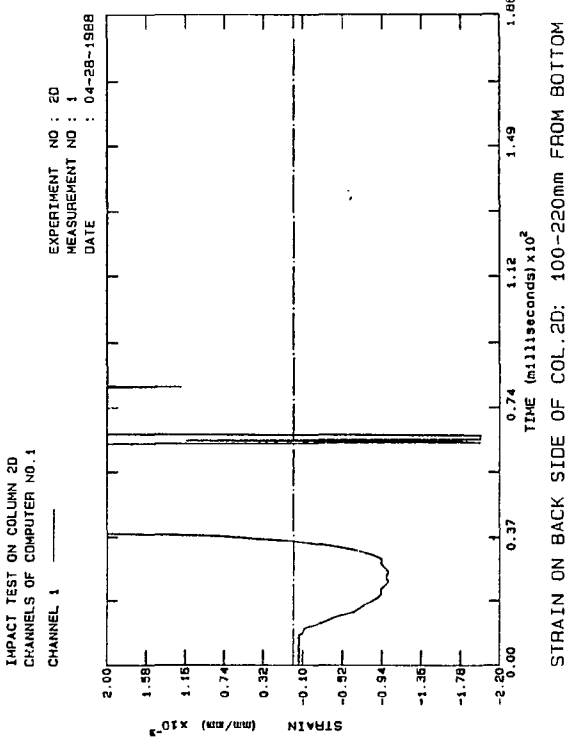

Fig. B.316: Strain Col 2D

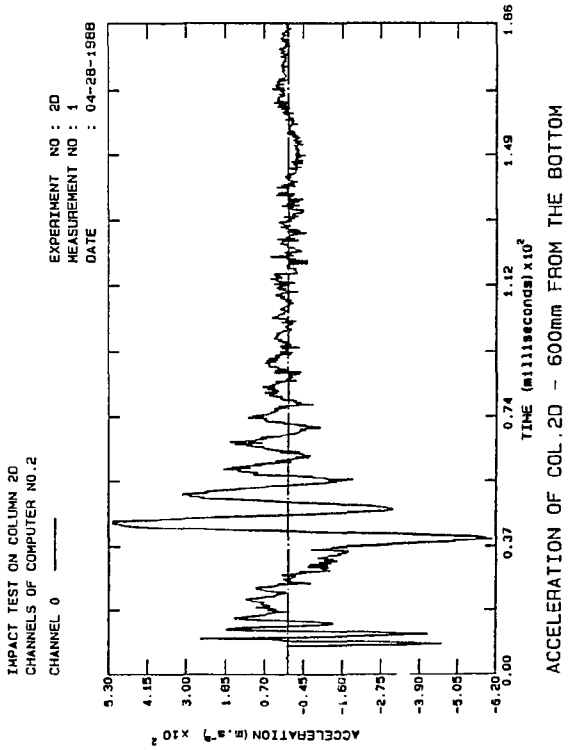

Fig. B.317: Accel. Col.2D

Stellenbosch University http://scholar.sun.ac.za

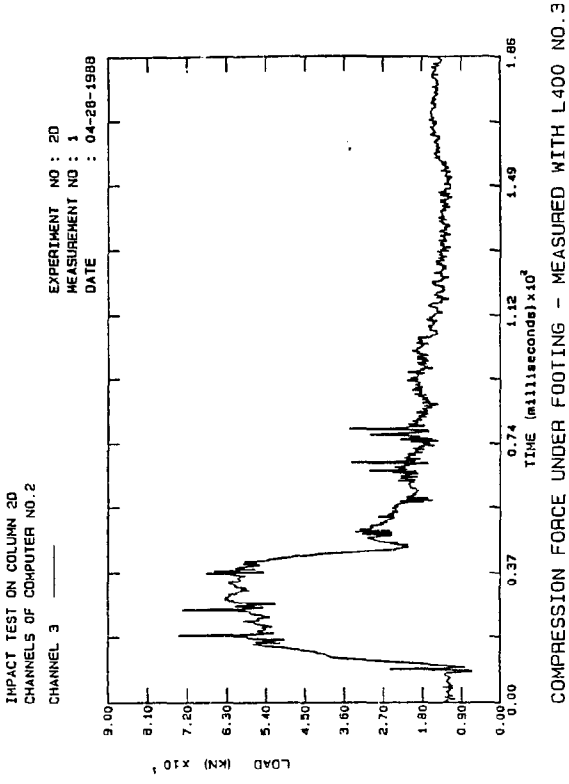

Fig. B.318: Comp. Col.2D

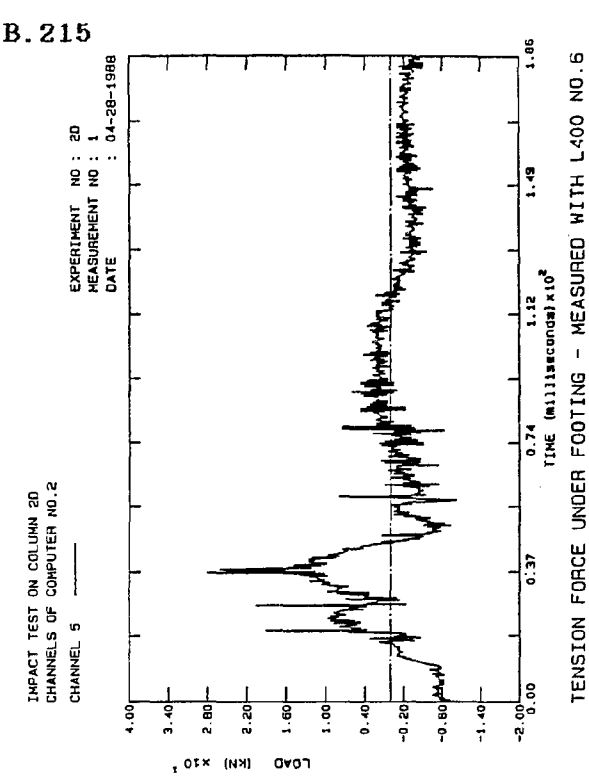

Fig. B.319: Tension Col.2D

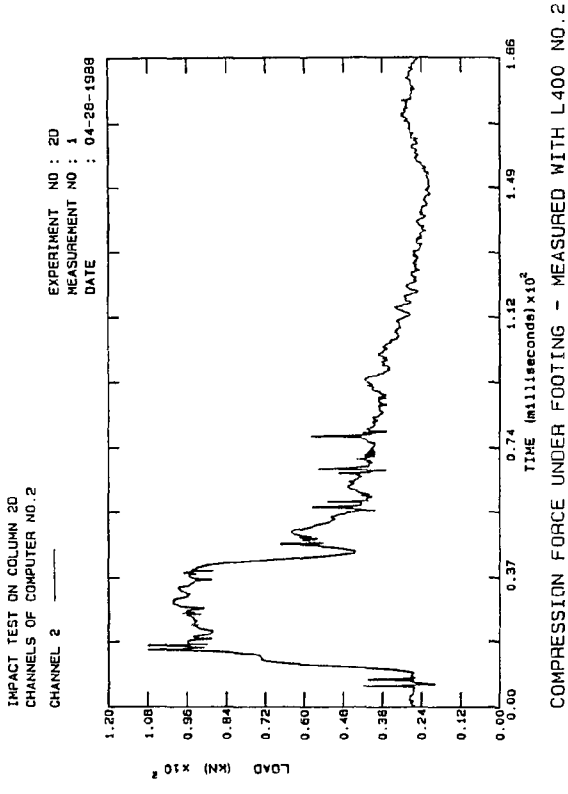

Fig. B.320: Comp. Col 2D

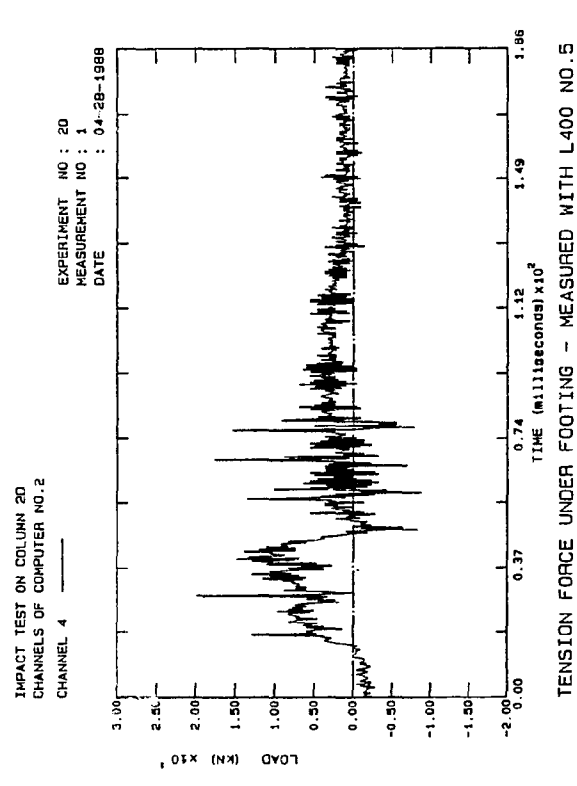

Fig. B.321: Tension Col.2D

Stellenbosch University http://scholar.sun.ac.za

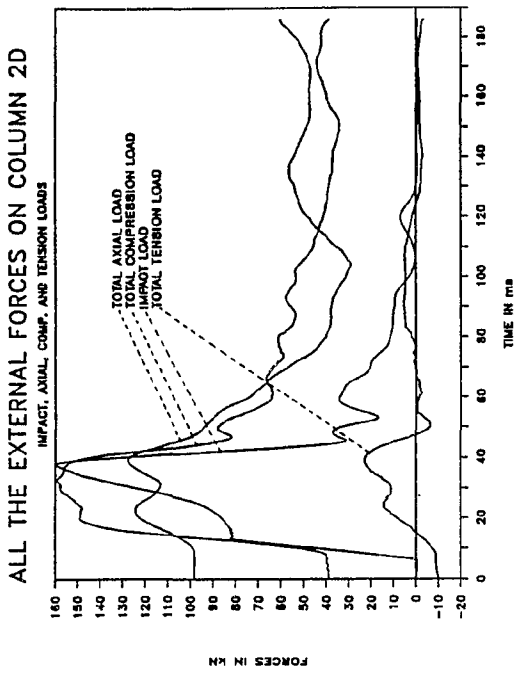

Fig. B.322: Ext. Loads Col.2D

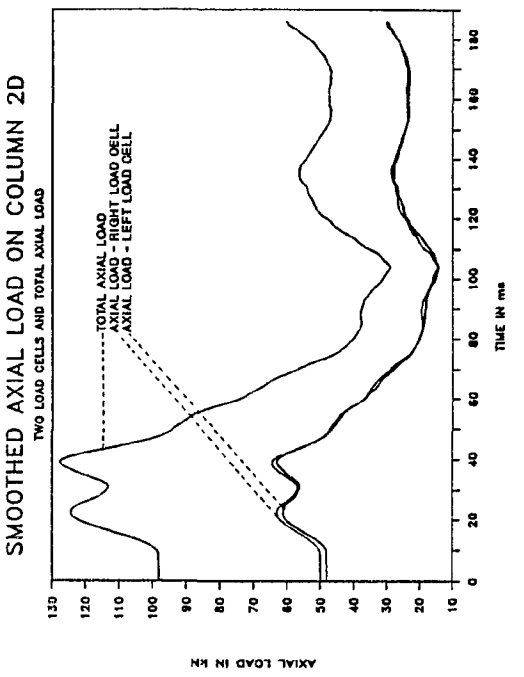

Fig. B.323: Smo. Axial Col.2D

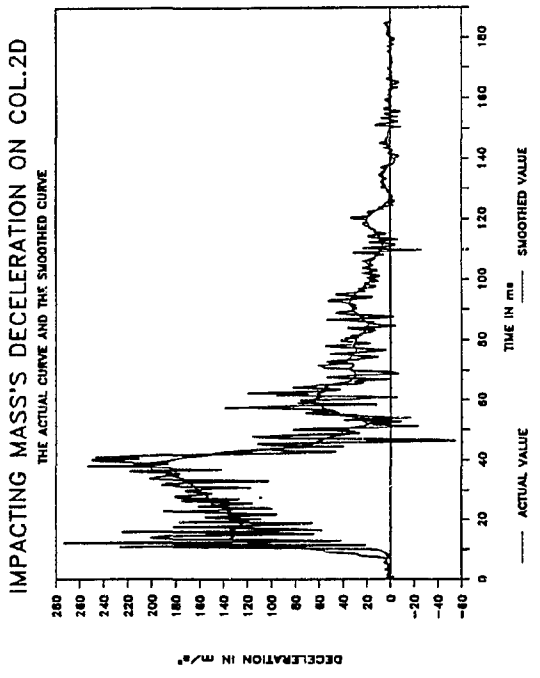

Fig. B.324: Smo.Decel. Col 2D

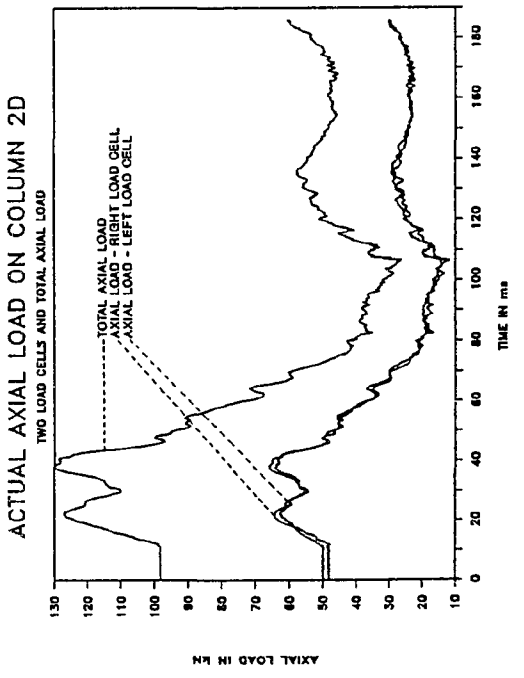

Fig. B.325: Axial loads Col.2D

Stellenbosch University http://scholar.sun.ac.za

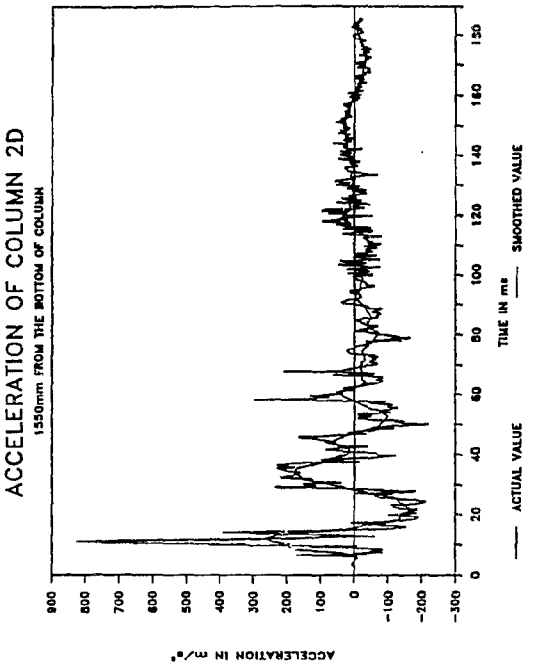

Fig. B.326: Smo.Accel. Col.2D

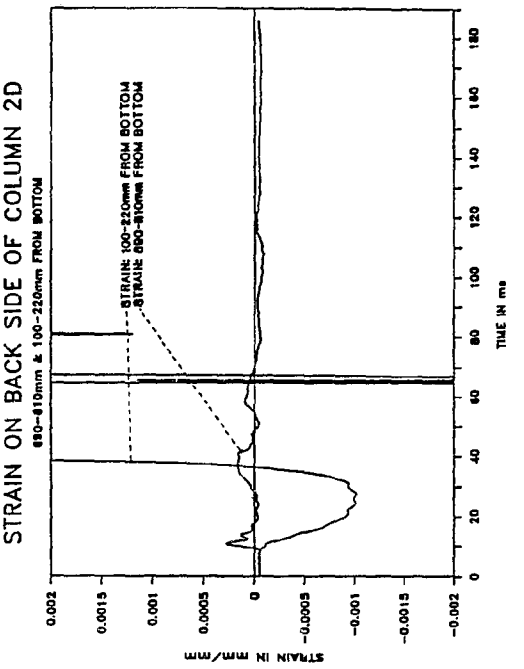

Fig. B.327: Strain Col.2D

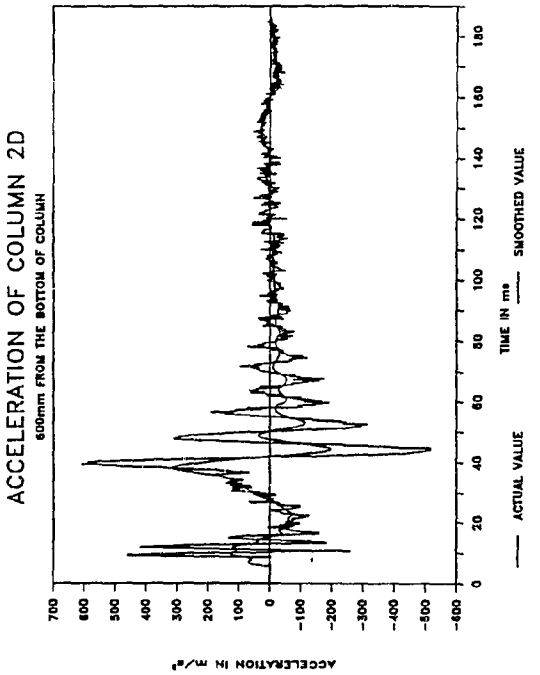

Fig. B.328: Smo.Accel. Col 2D

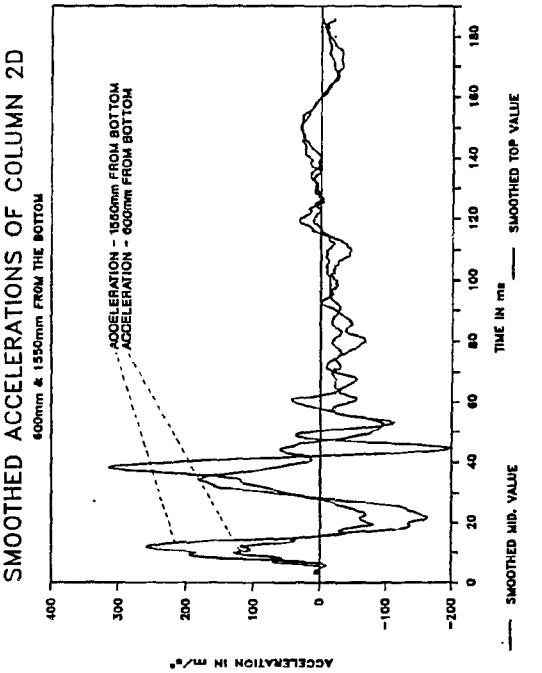

Fig. B.329: Smo. Accel. Col.2D

Stellenbosch University http://scholar.sun.ac.za

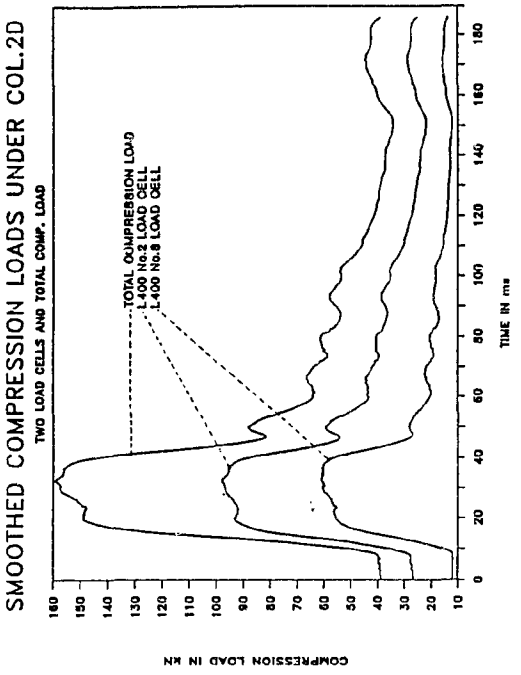

Fig. B.330: Smo. Comp. Col.2D

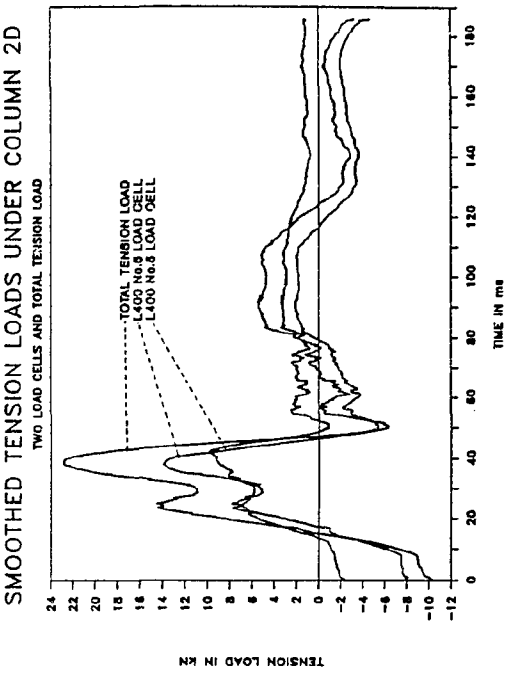

Fig. B.331: Smo. Tens. Col.2D

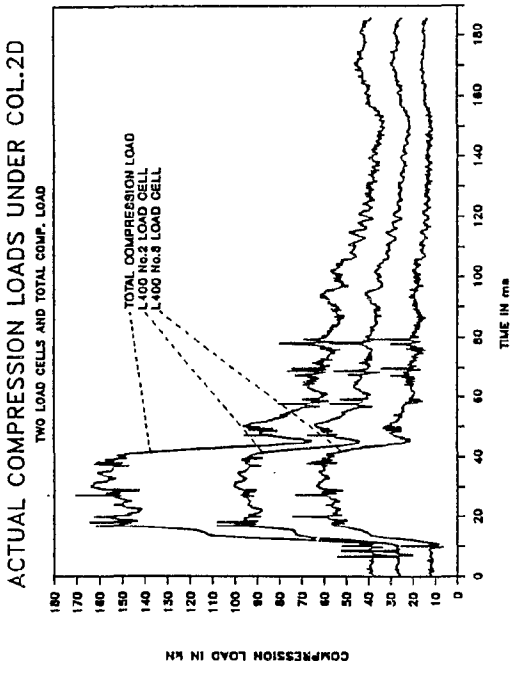

Fig. B.332: Comp. load Col 2D

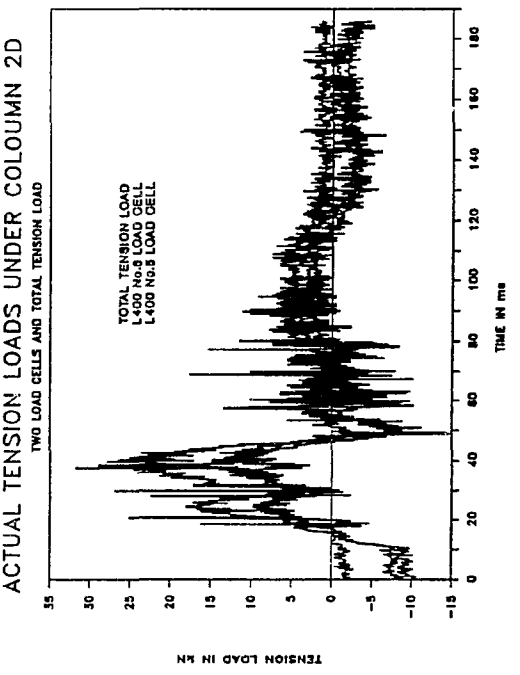

Fig. B.333: Tens. loads Col. 2D

Stellenbosch University http://scholar.sun.ac.za

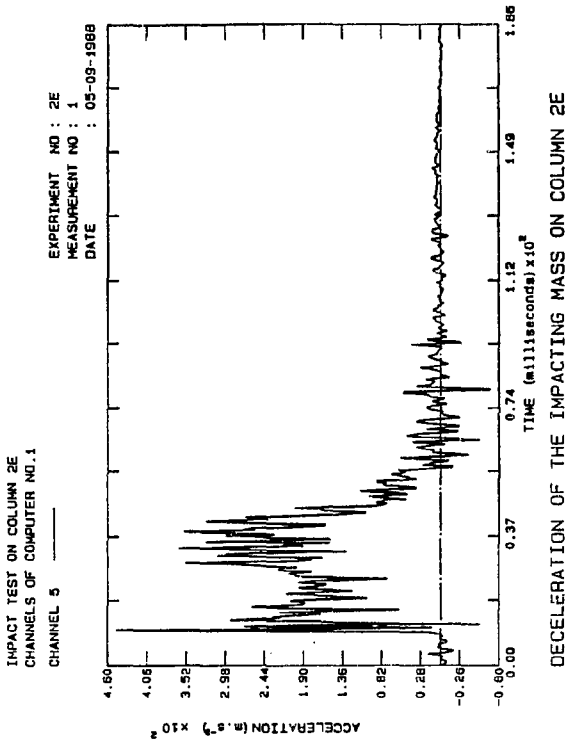

Fig. B.334: Decel. Col.2E

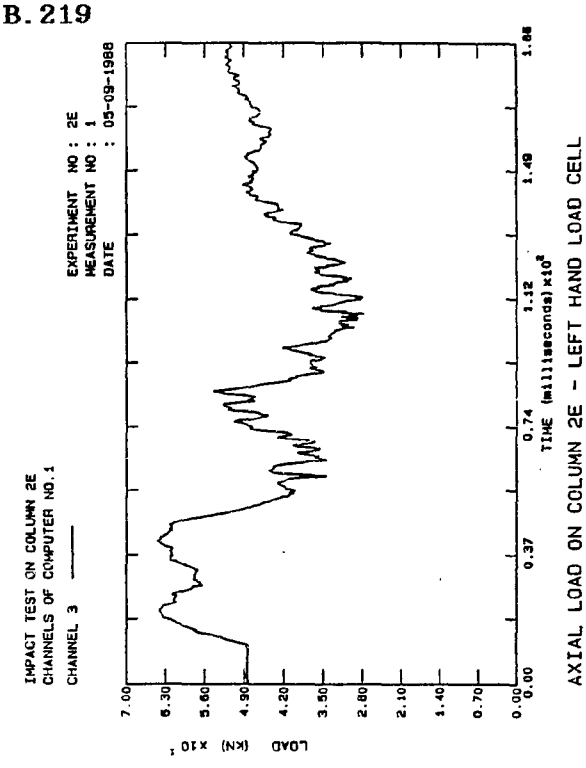

Fig. B.335: Axial load Col.2E

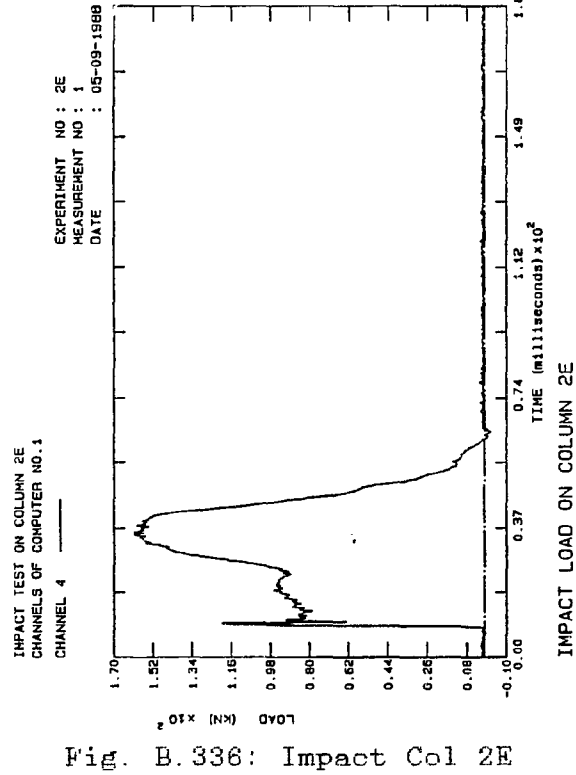

Fig. B.336: Impact Col 2E

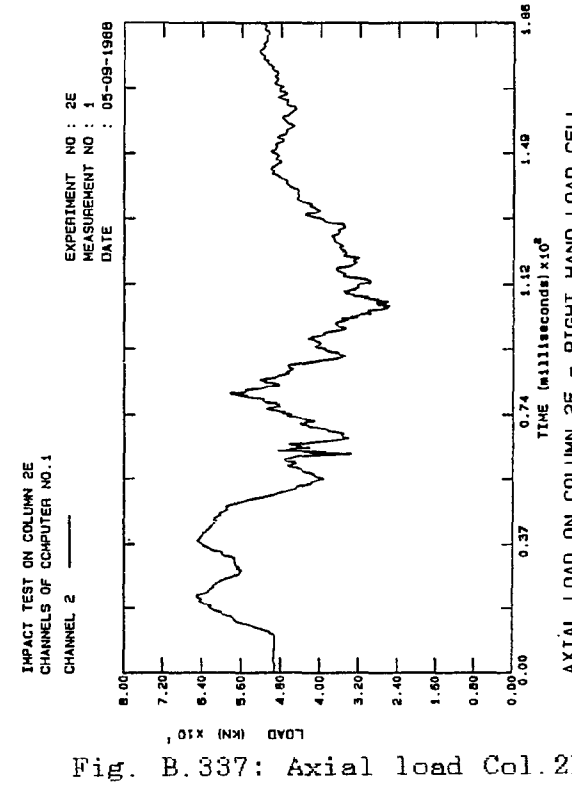

Fig. B.337: Axial load Col.2E

Stellenbosch University http://scholar.sun.ac.za

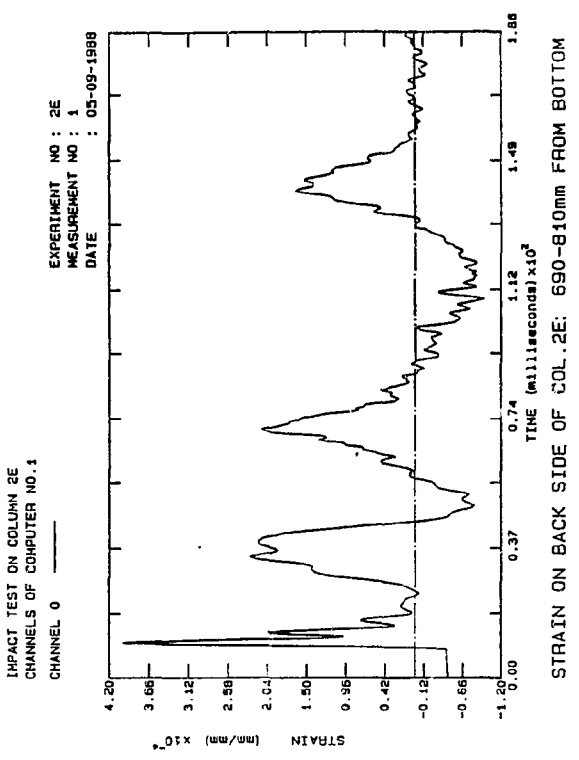

Fig. B.338: Strain Col.2E

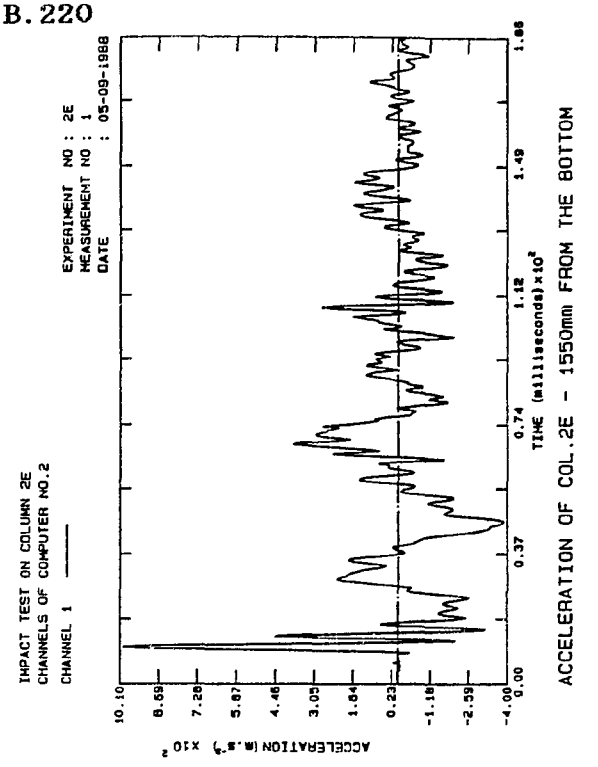

Fig. B.339: Accel. Col.2E

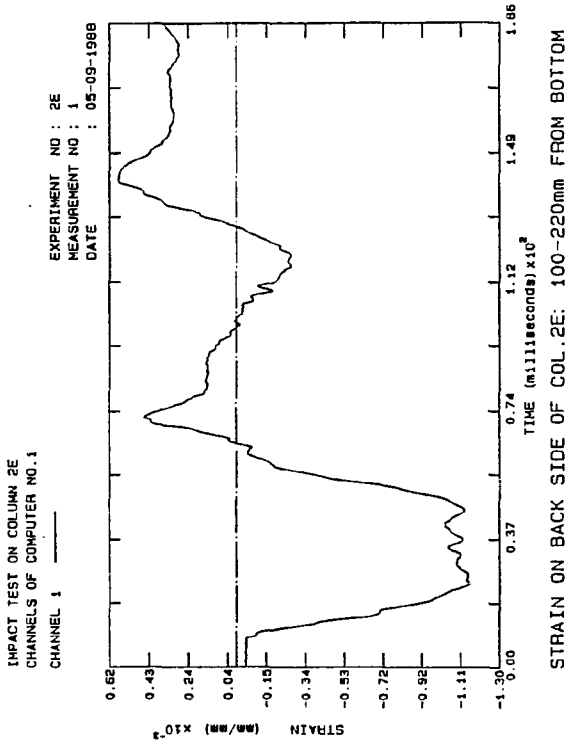

Fig. B.340: Strain Col 2E

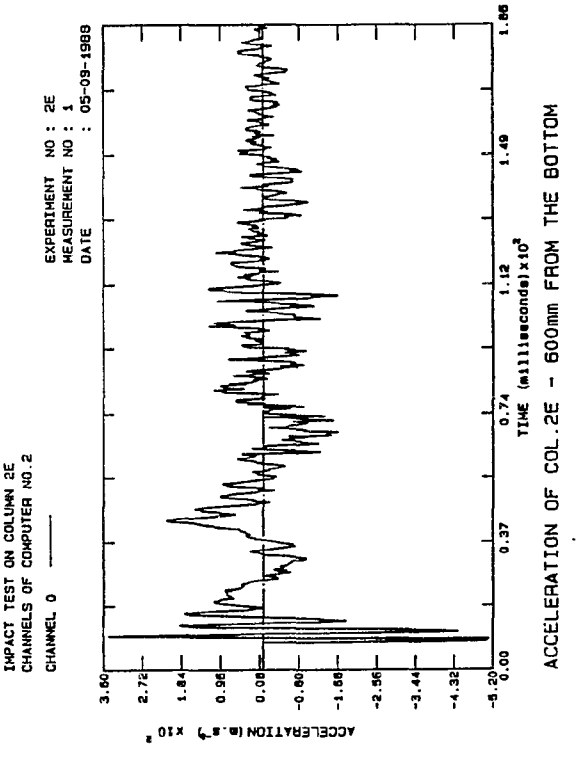

Fig. B.341: Accel. Col.2E

Stellenbosch University http://scholar.sun.ac.za

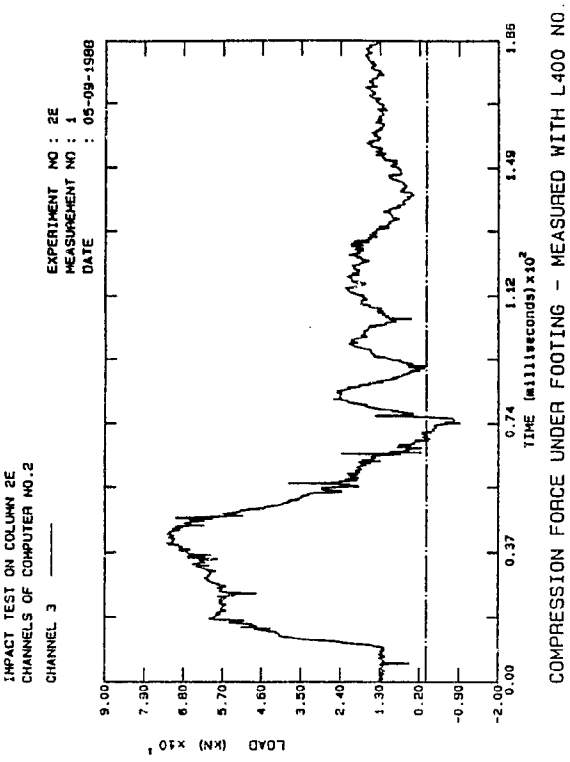

Fig. B.342: Comp. Col.2E

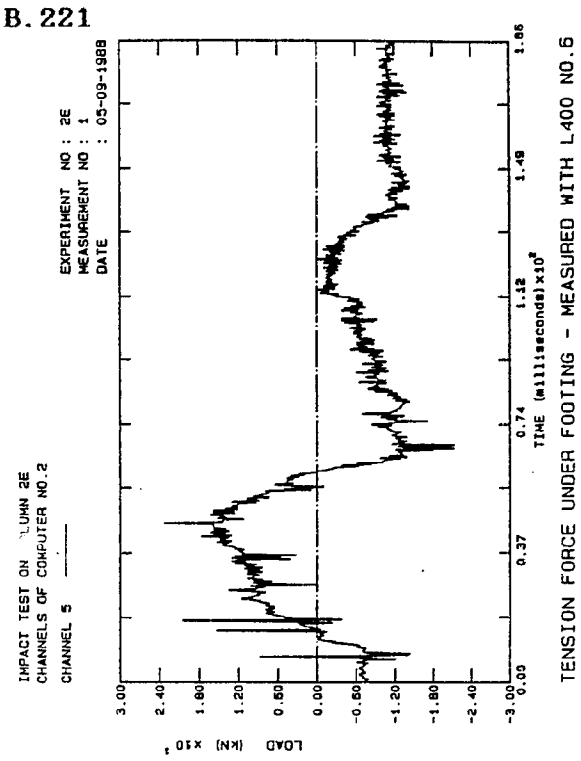

Fig. B.343: Tension Col.2E

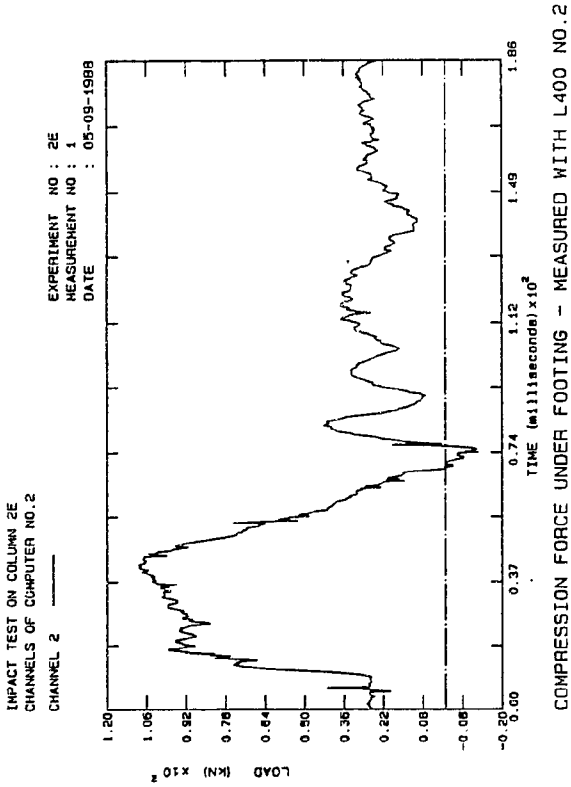

Fig. B.344: Comp. Col 2E

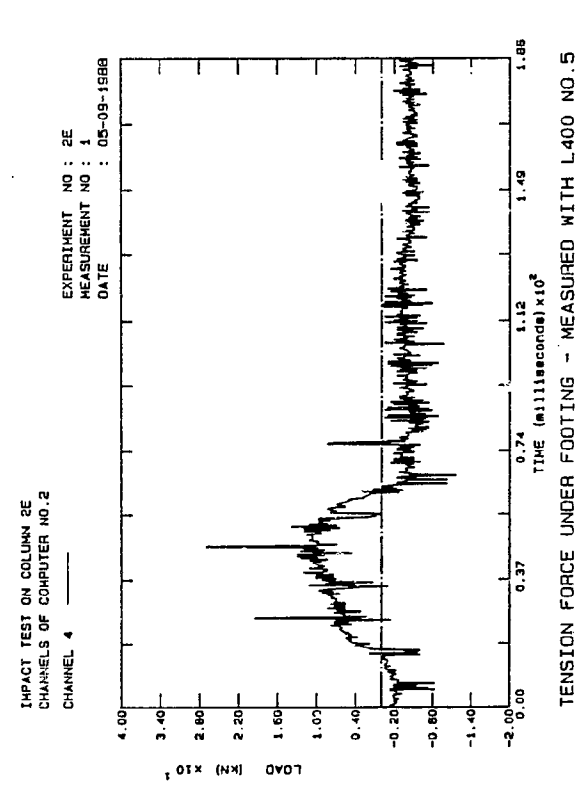

Fig. B.345: Tension Col.2E

Stellenbosch University http://scholar.sun.ac.za

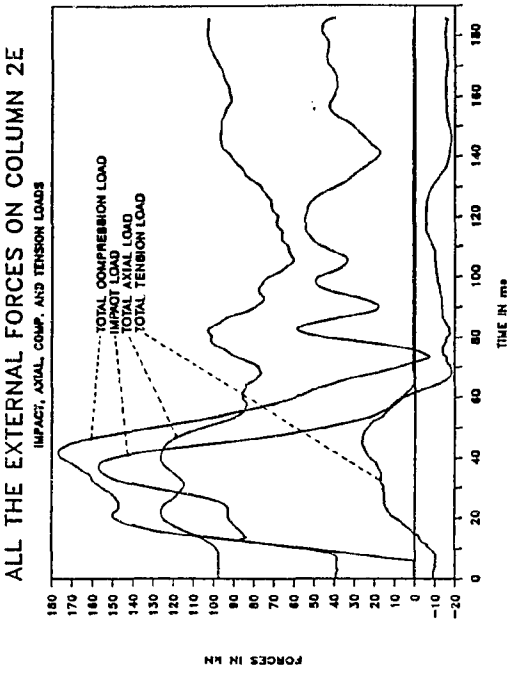

Fig. B.346: Ext. Loads Col.2E

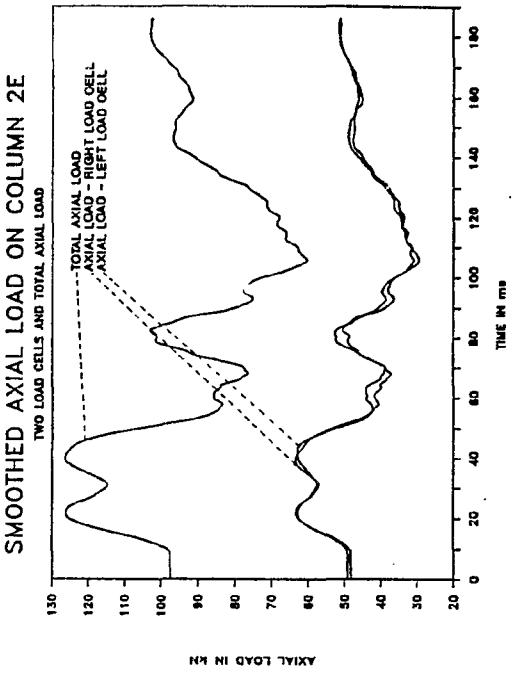

Fig. B.347: Smo. Axial Col.2E

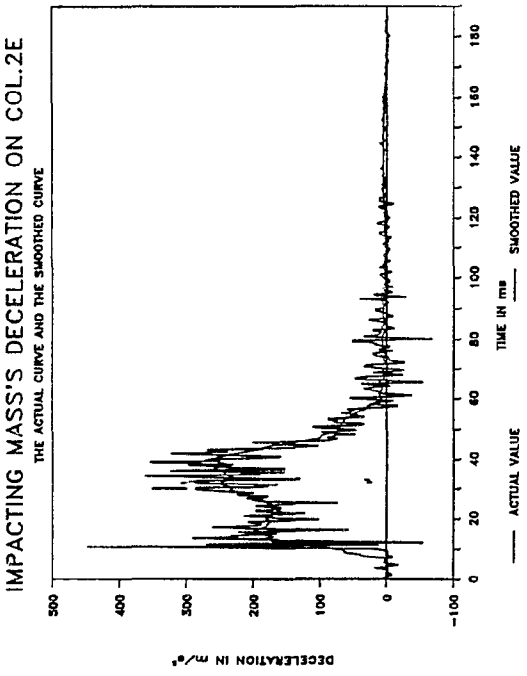

Fig. B.348: Smo.Decel. Col 2E

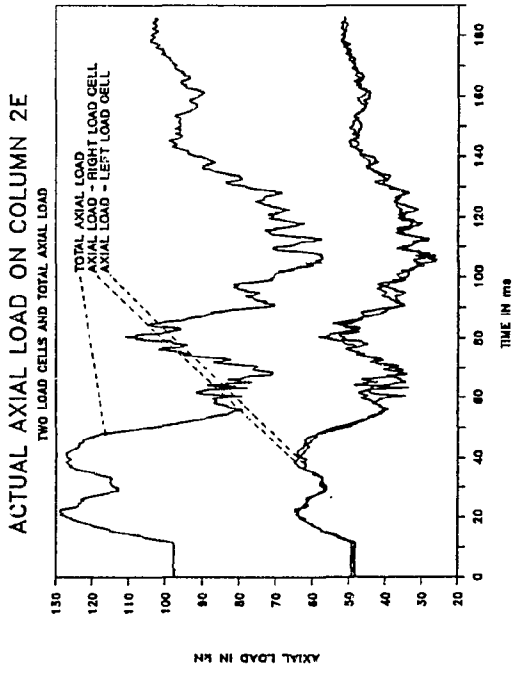

Fig. B.349: Axial loads Col.2E

Stellenbosch University http://scholar.sun.ac.za

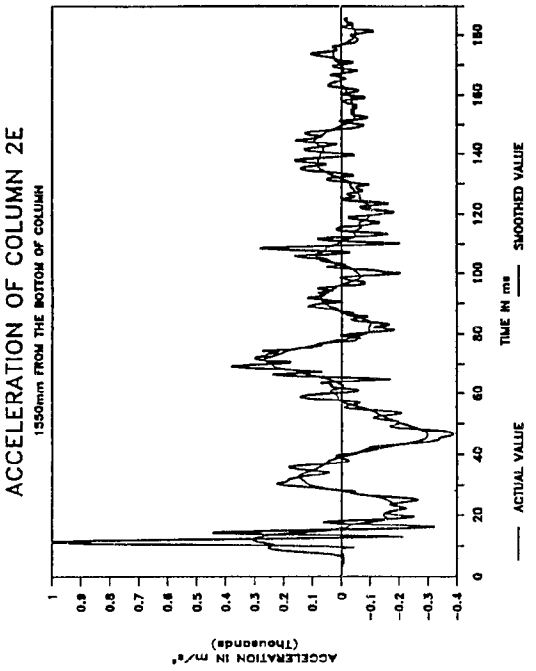

Fig. B.350: Smo.Accel. Col.2E

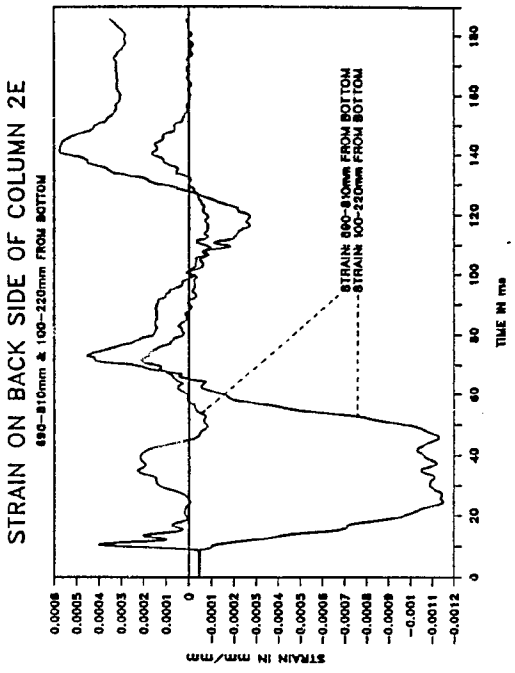

Fig. B.351: Strain Col.2E

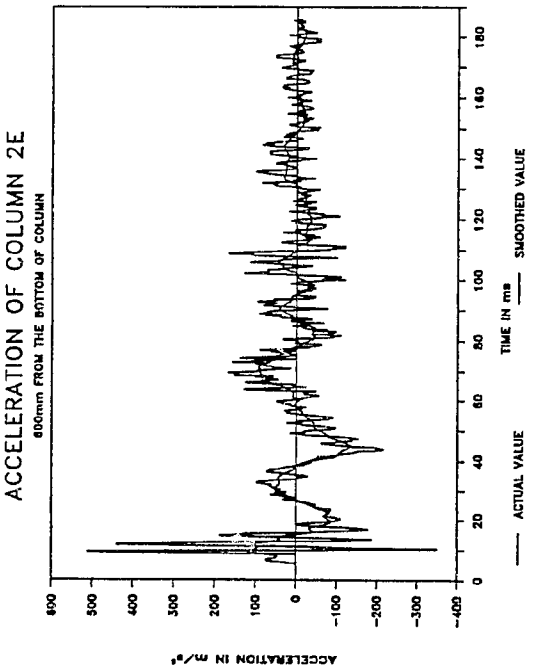

Fig. B.352: Smo.Accel. Col 2E

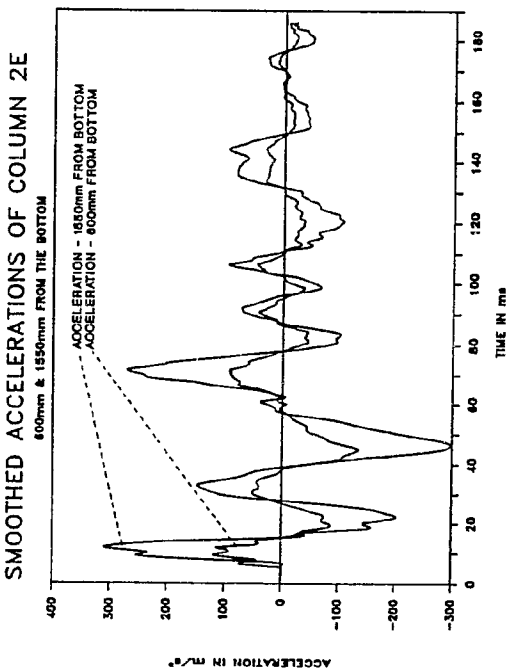

Fig. B.353: Smo. Accel. Col.2E

Stellenbosch University http://scholar.sun.ac.za

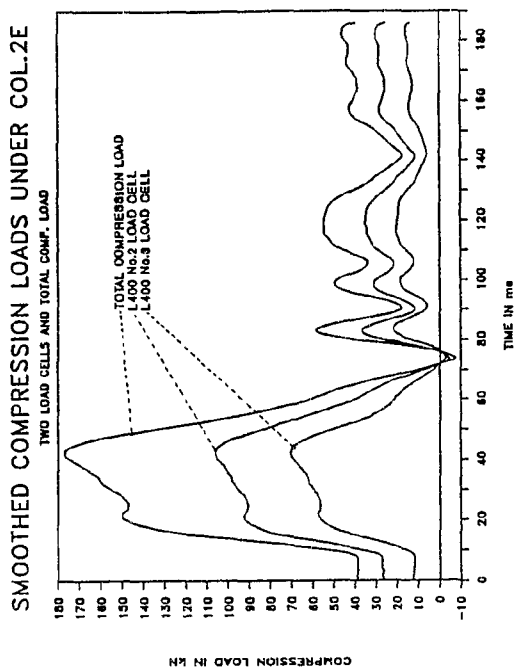

Fig. B.354: Smo. Comp. Col.2E

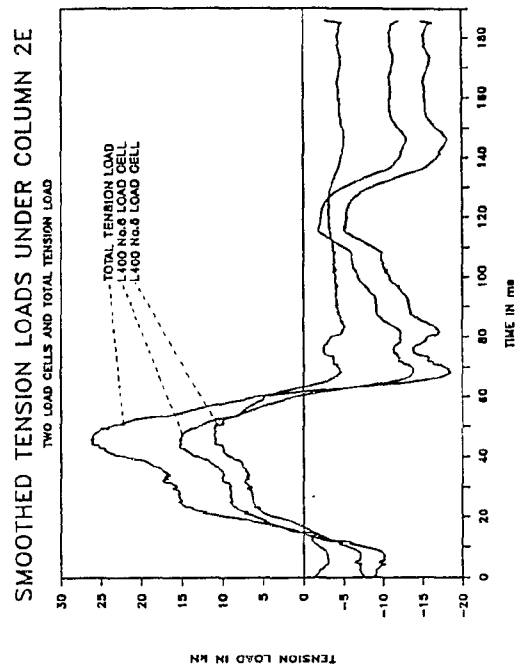

Fig. B.355: Smo. Tens. Col.2E

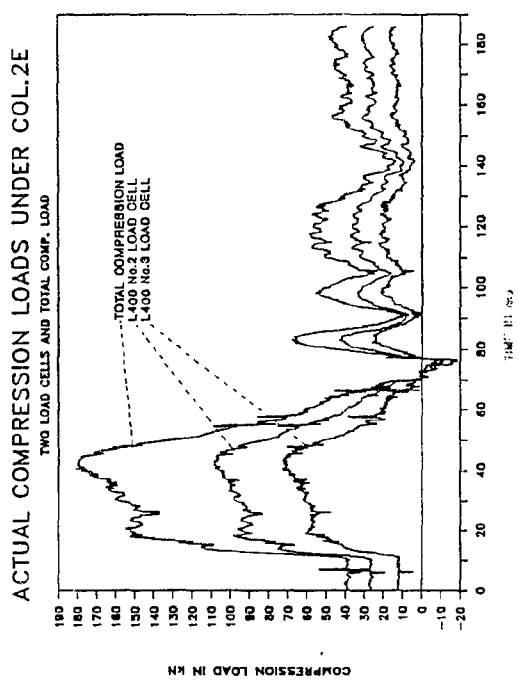

Fig. B.356: Comp. load Col 2E

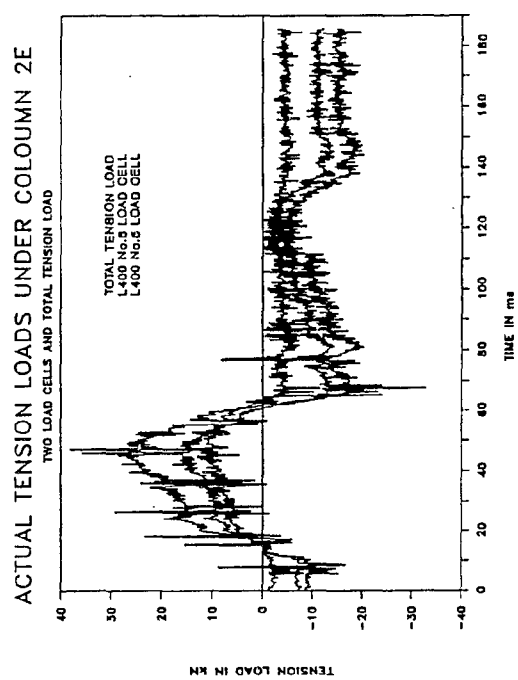

Fig. B.357: Tens. loads Col.2E

Stellenbosch University http://scholar.sun.ac.za

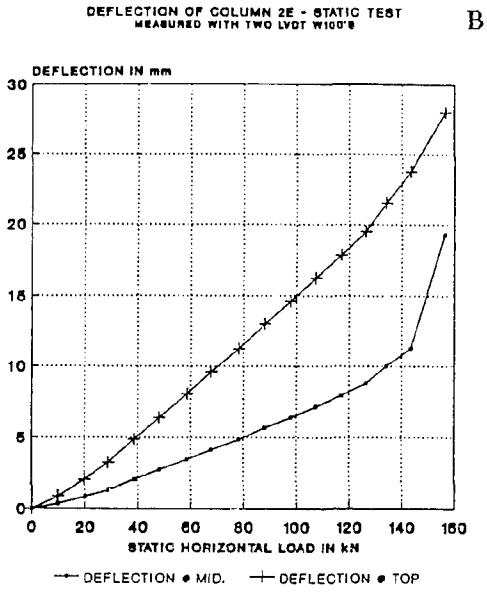

Fig. B.358: Deflection Col.2E

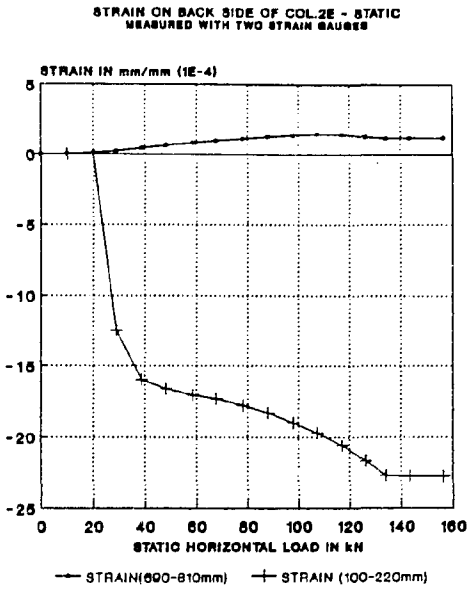

Fig. B.359: Strain Col.2E

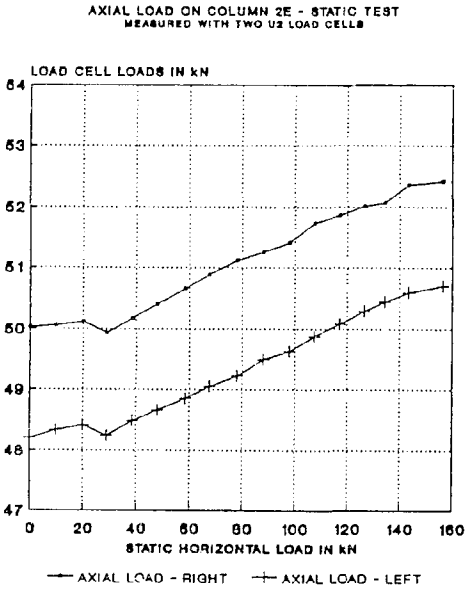

Fig. B.360: Axial load Col 2E

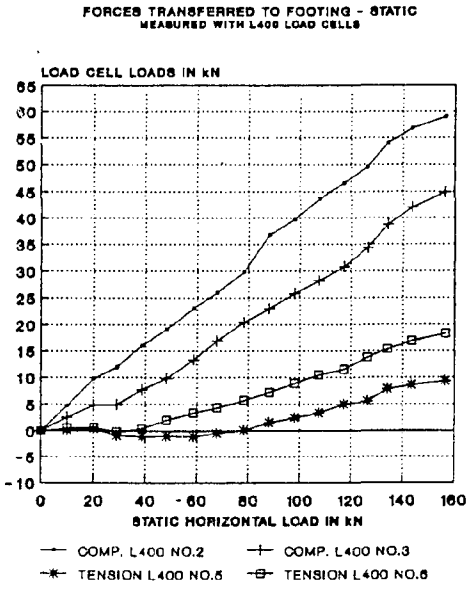

Fig. B.361: Foot. loads Col.2E

Stellenbosch University http://scholar.sun.ac.za

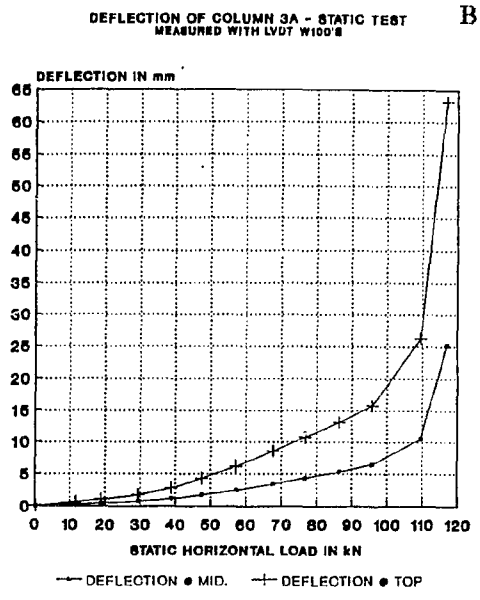

Fig. B.362: Deflection Col.3A

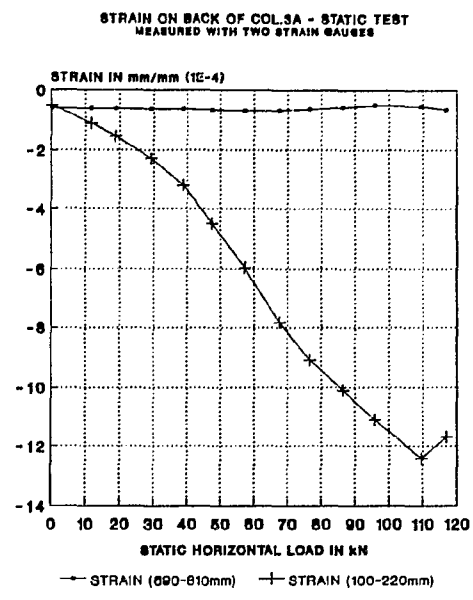

Fig. B.363: Strain Col.3A

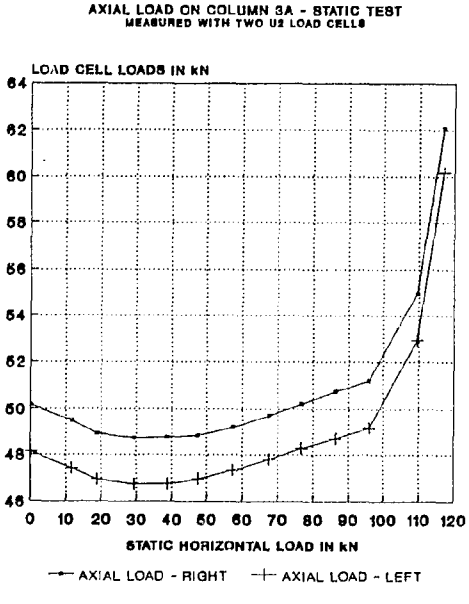

Fig. B.364: Axial load Col 3A

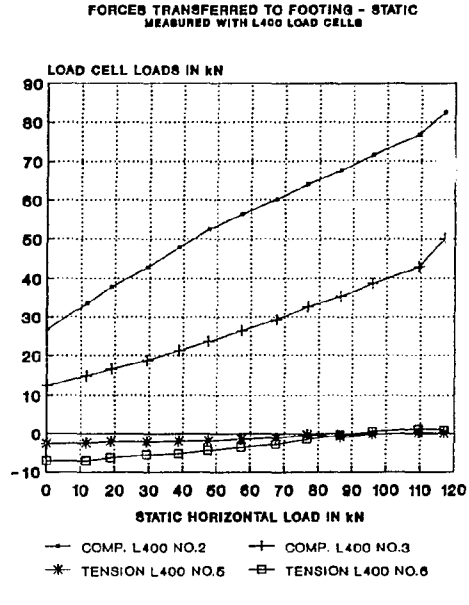

Fig. B.365: Foot. loads Col.3A

Stellenbosch University http://scholar.sun.ac.za

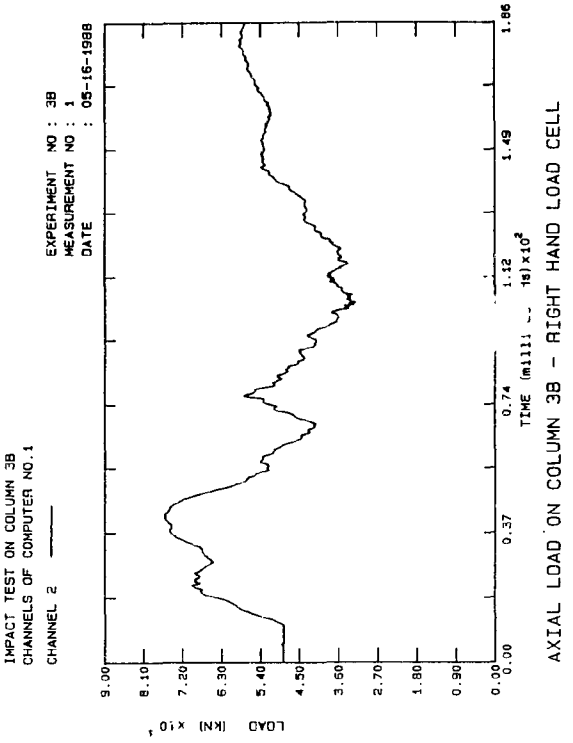

Fig. B.366: Axial load Col.3B

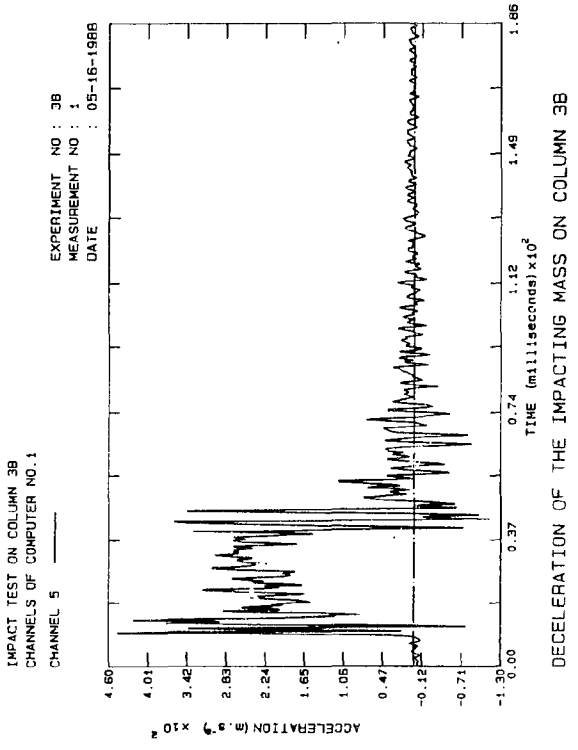

Fig. B.367: Decel. Col 3B

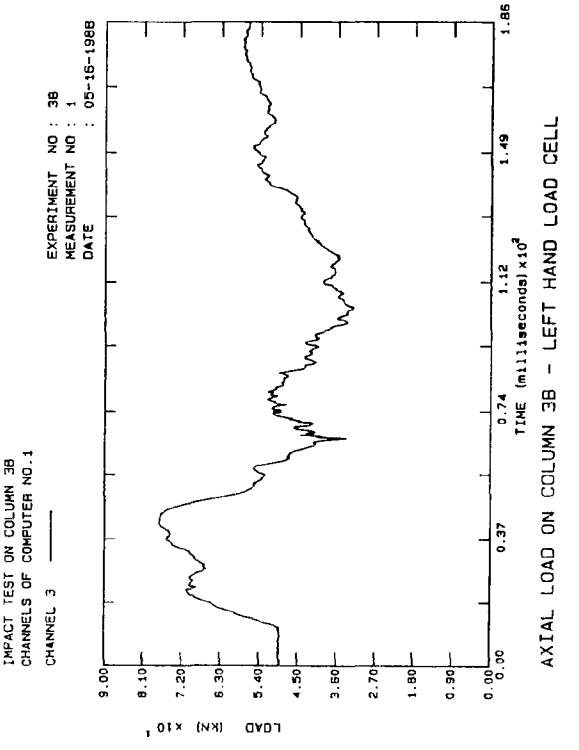

Fig. B.368: Axial load Col.3B

Stellenbosch University http://scholar.sun.ac.za

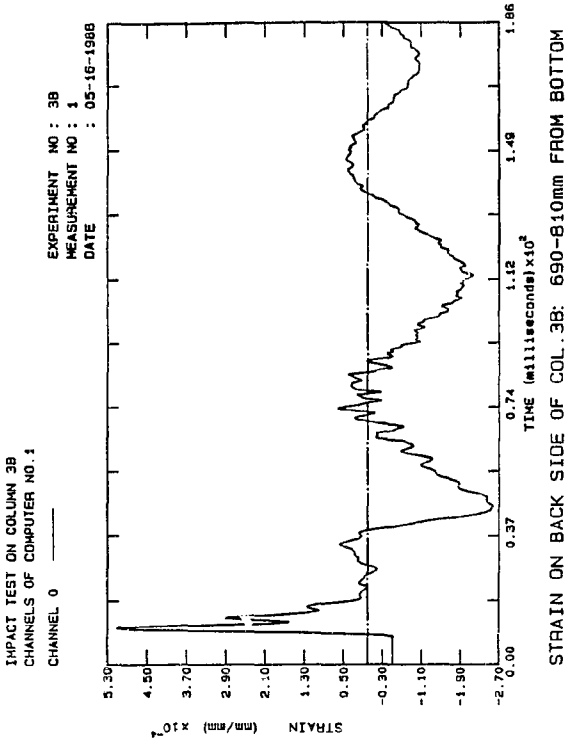

Fig. B.369: Strain Col.3B

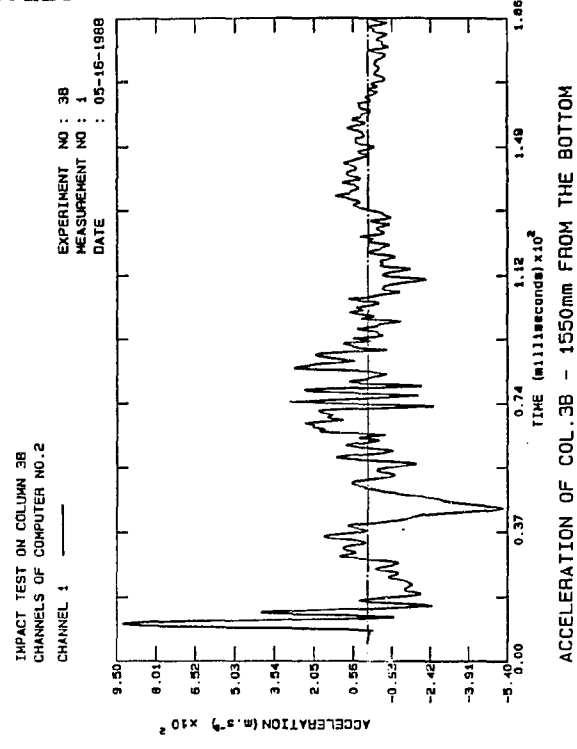

Fig. B.370: Accel. Col.3B

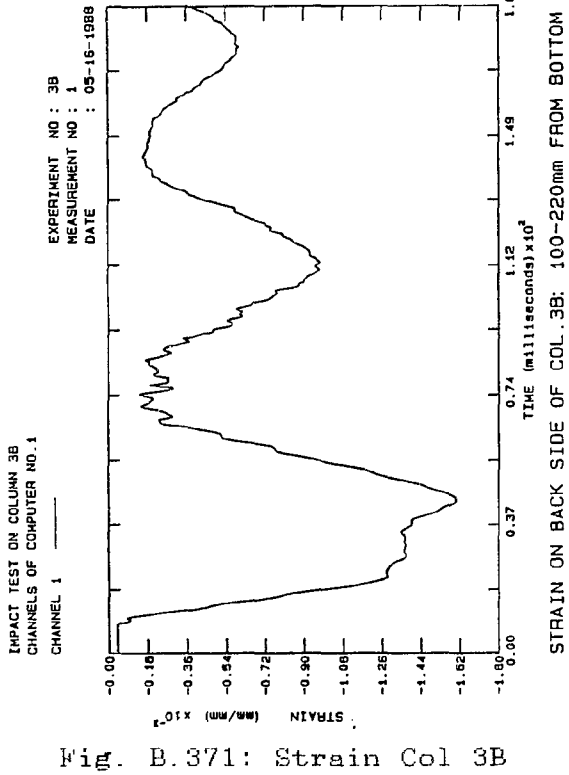

Fig. B.371: Strain Col 3B

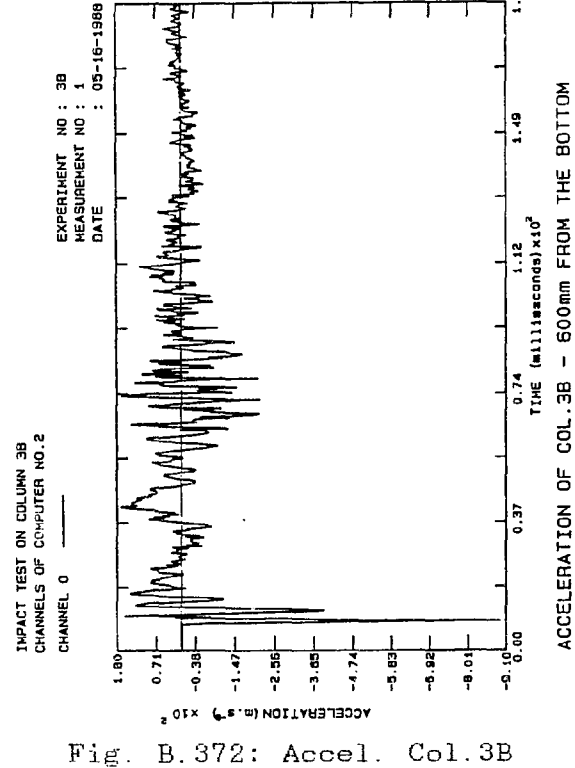

Fig. B.372: Accel. Col.3B

Stellenbosch University http://scholar.sun.ac.za

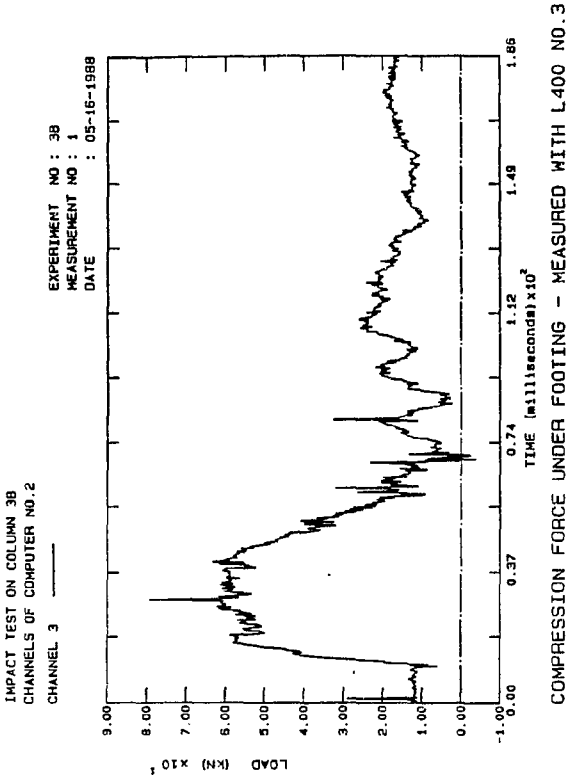

Fig. B.373: Comp. Col.3B

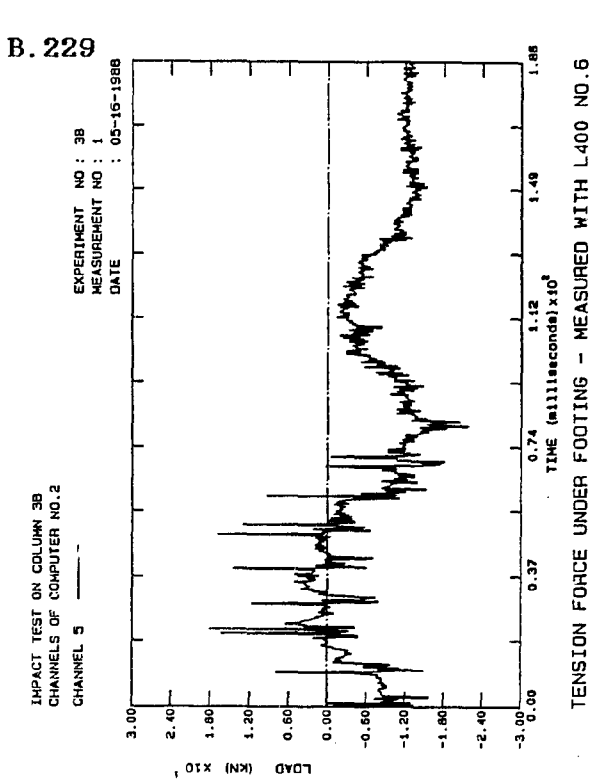

Fig. B.374: Tension Col.3B

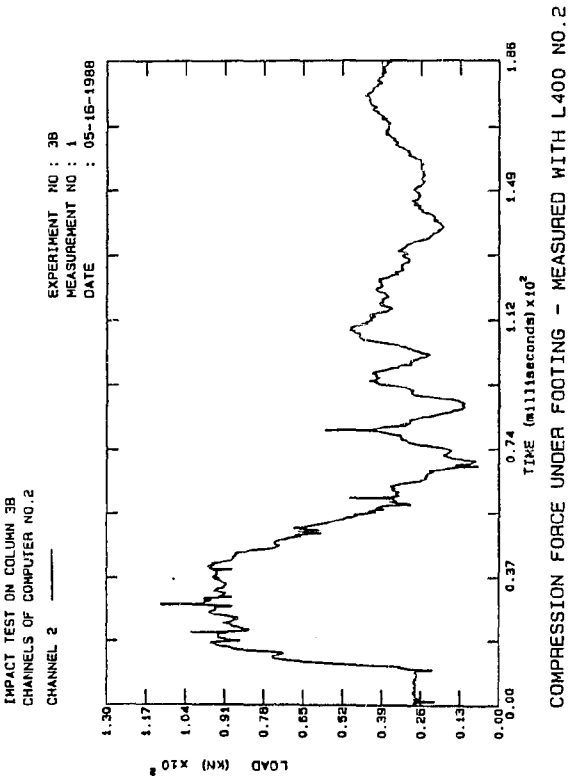

Fig. B.375: Comp. Col 3B

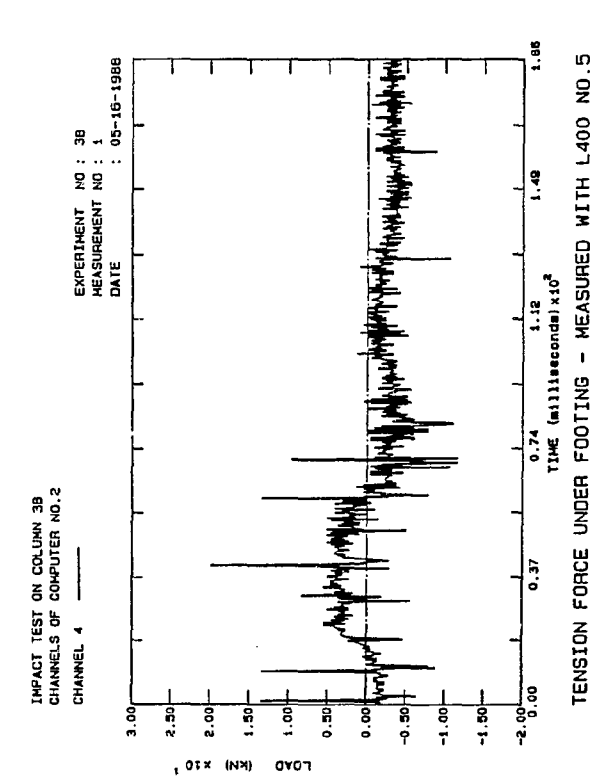

Fig. B.376: Tension Col.3B

Stellenbosch University http://scholar.sun.ac.za

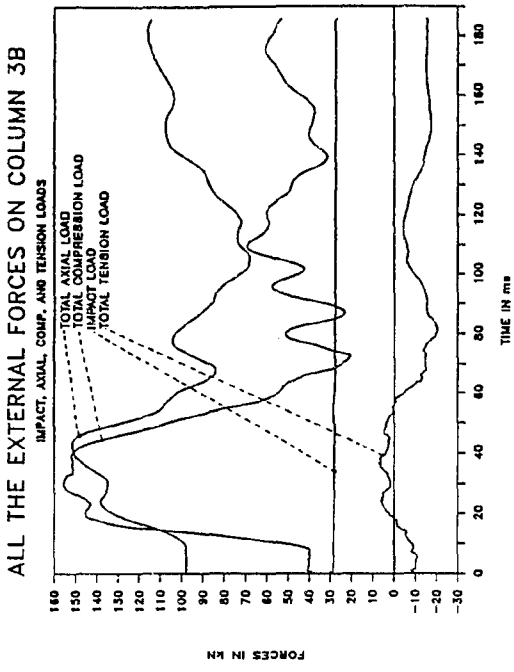

Fig. B.377: Ext. Loads Col.3B

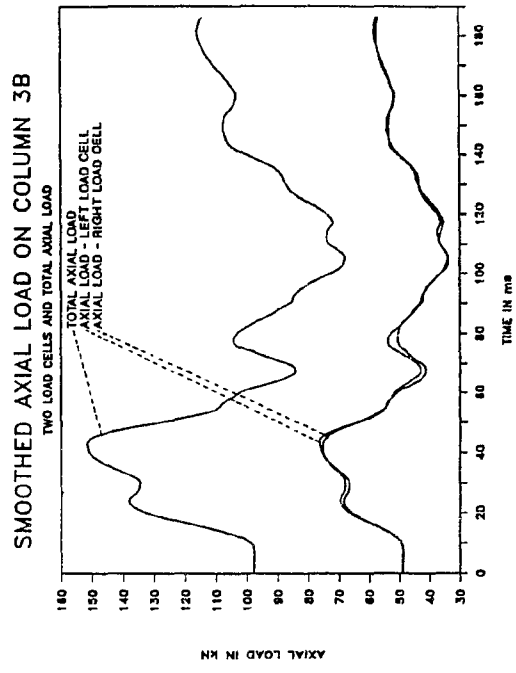

Fig. B.378: Smo. Axial Col.3B

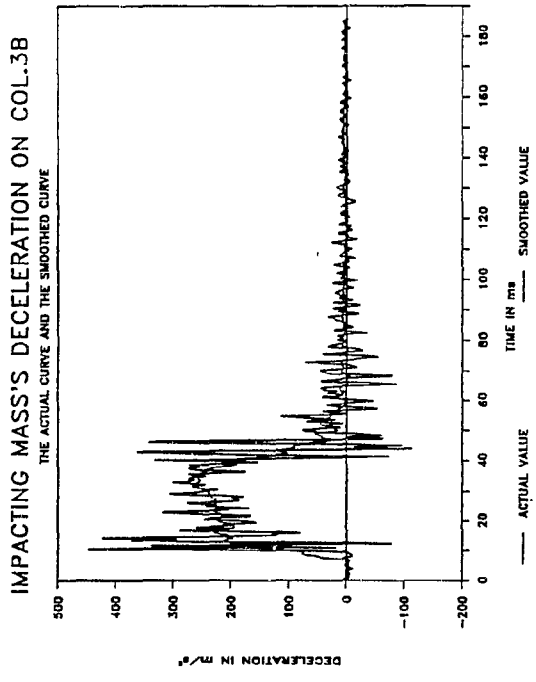

Fig. B.379: Smo.Decel. Col 3B

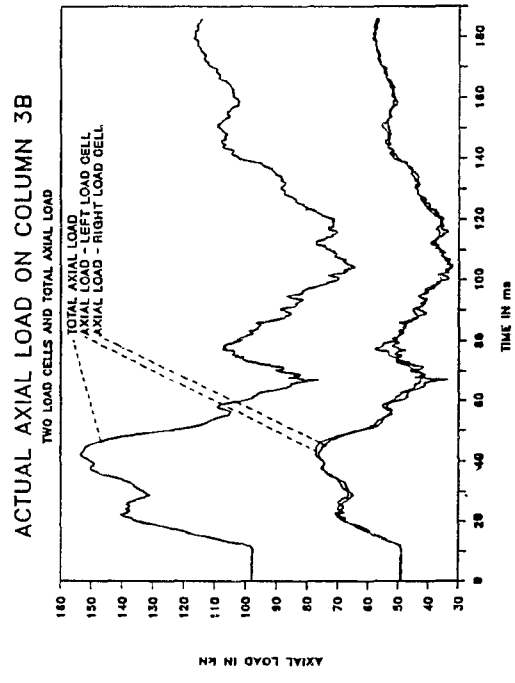

Fig. B.380: Axial loads Col.3B

Stellenbosch University http://scholar.sun.ac.za

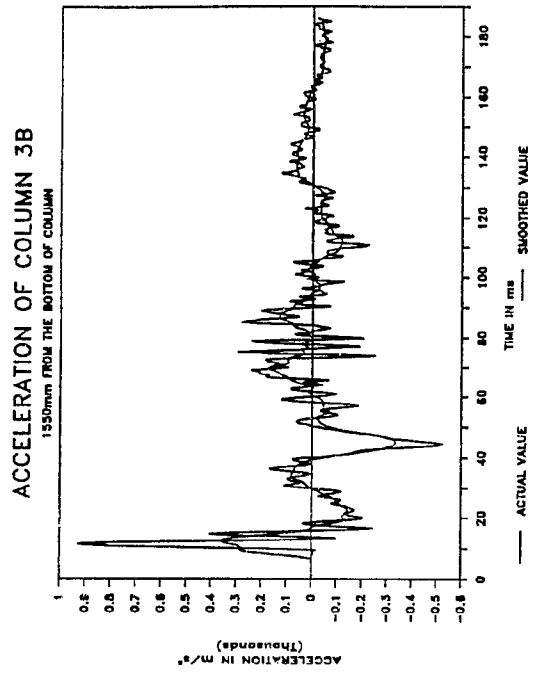

Fig. B.381: Smo.Accel. Col.3B

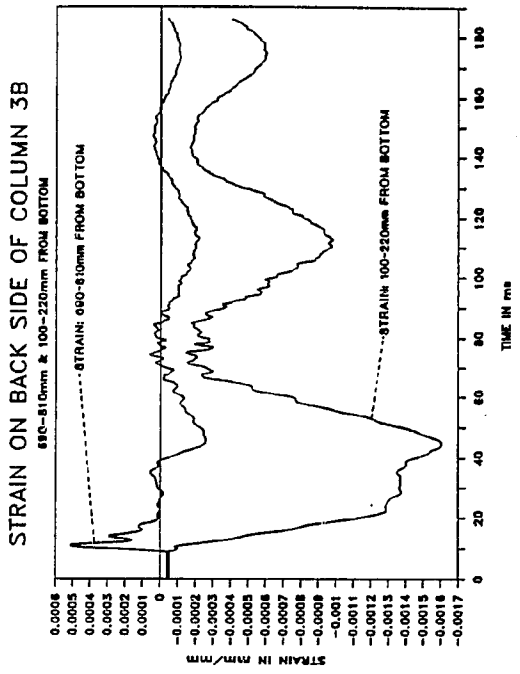

Fig. B.382: Strain Col.3B

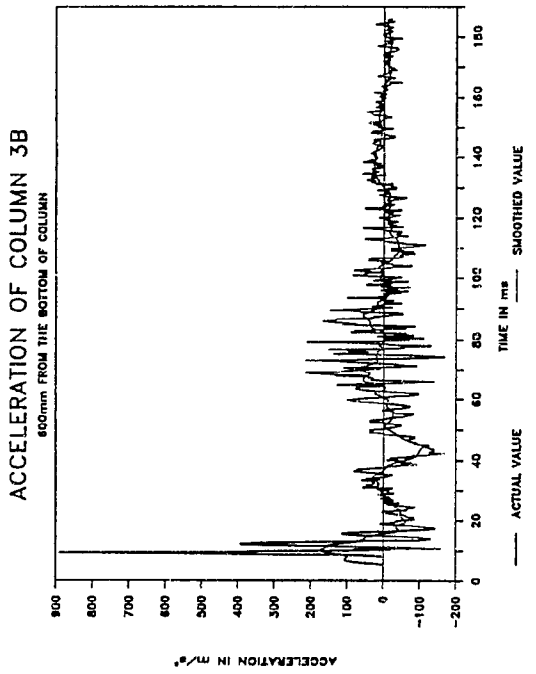

Fig. B.383: Smo.Accel. Col 3B

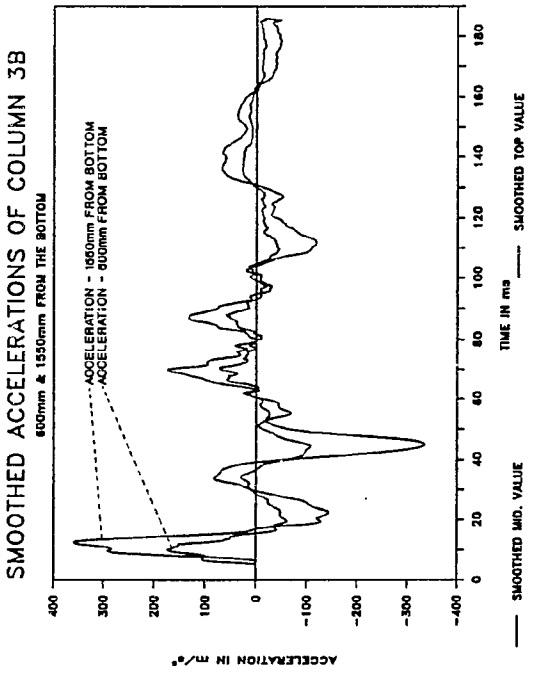

Fig. B.384: Smo. Accel. Col.3B

Stellenbosch University http://scholar.sun.ac.za

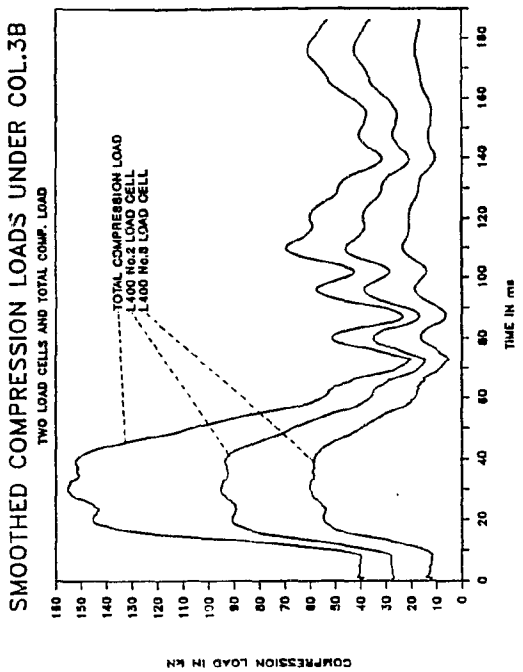

Fig. B.385: Smo. Comp. Col.3B

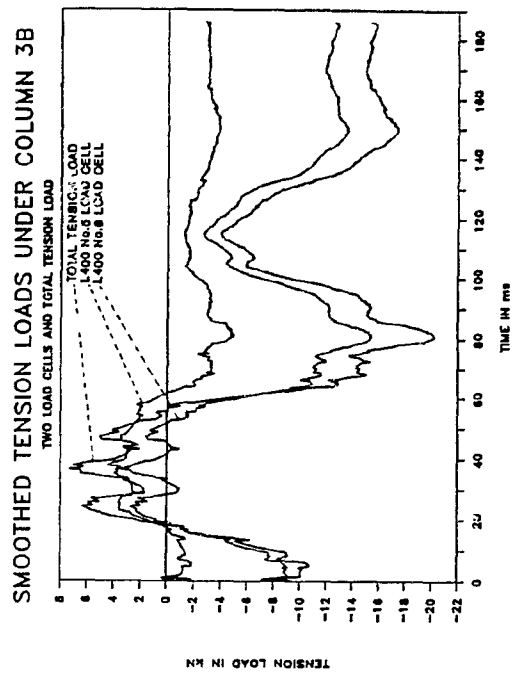

Fig. B.386: Smo. Tens. Col.3B

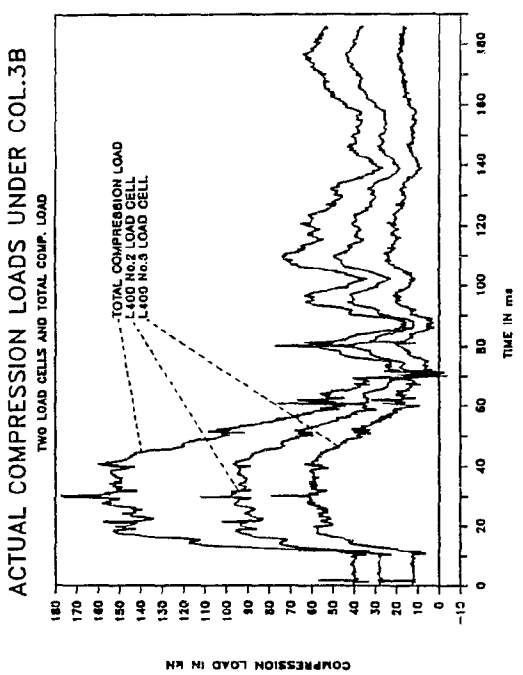

Fig. B.387: Comp. load Col 3B

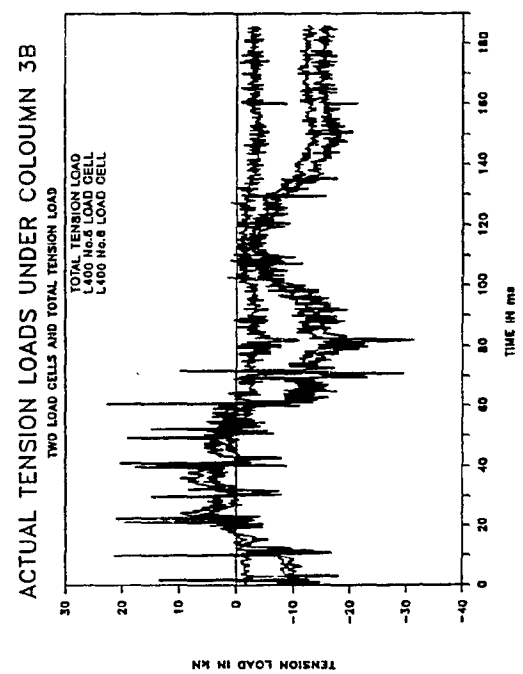

Fig. B.388: Tens. loads Col.3B

Stellenbosch University http://scholar.sun.ac.za

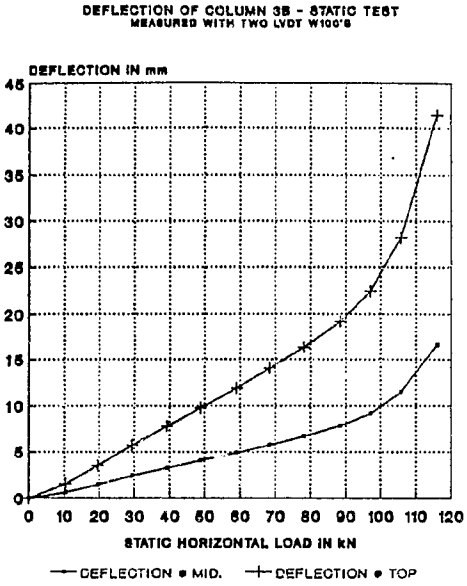

Fig. B.389: Deflection Col.3B

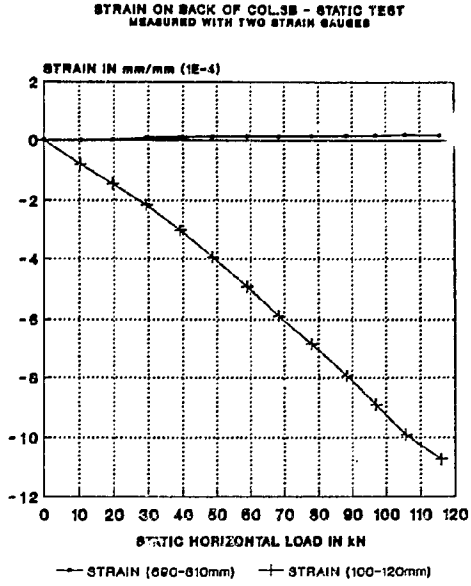

Fig. B.390: Strain Col.3B

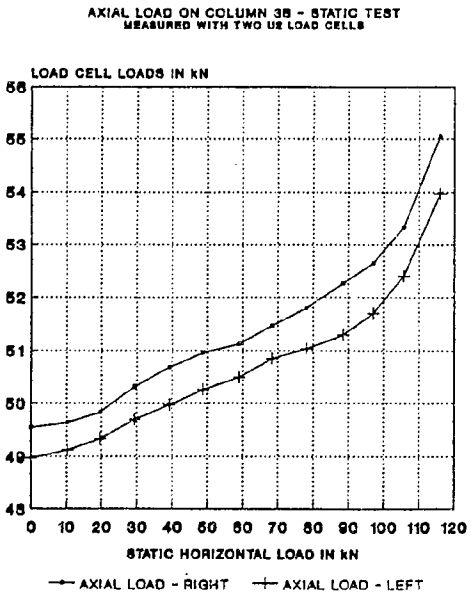

Fig. B.391: Axial load Col 3B

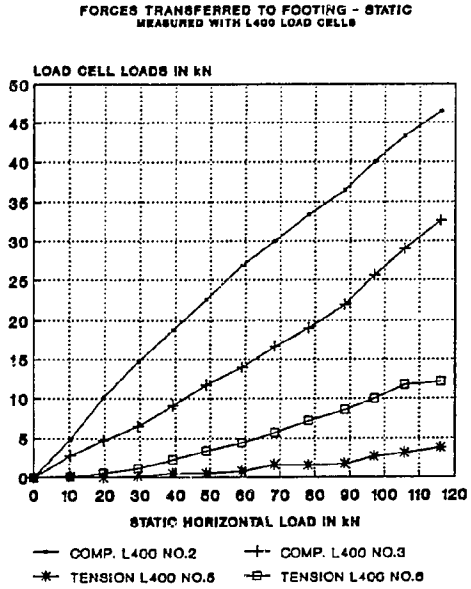

Fig. B.392: Foot.loads Col.3B

Stellenbosch University http://scholar.sun.ac.za

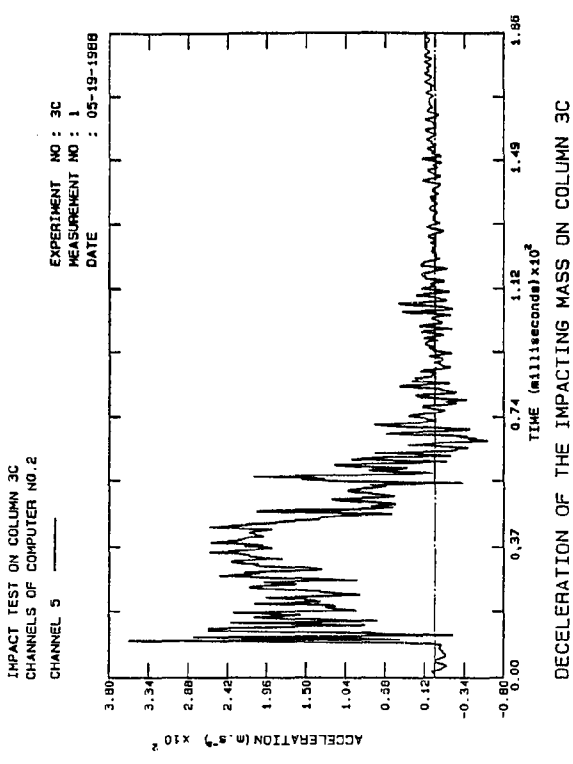

Fig. B.393: Decel. Col.3C

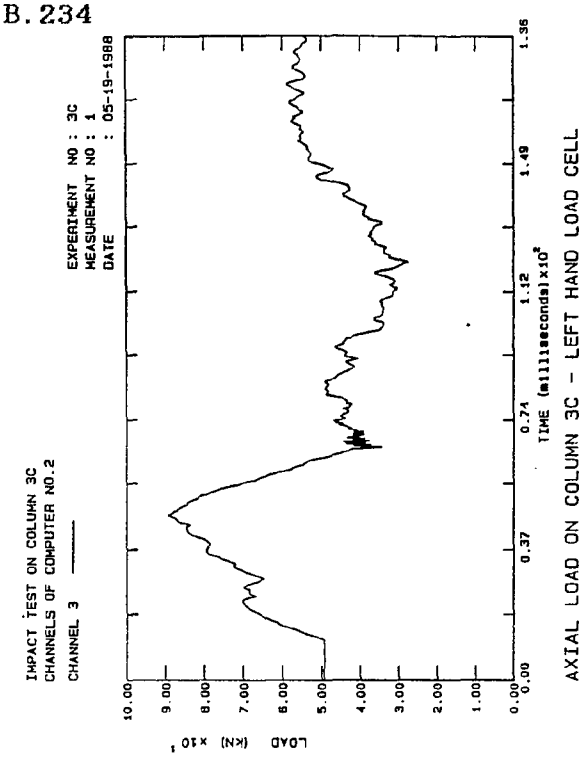

Fig. B.394: Axial load Col.3C

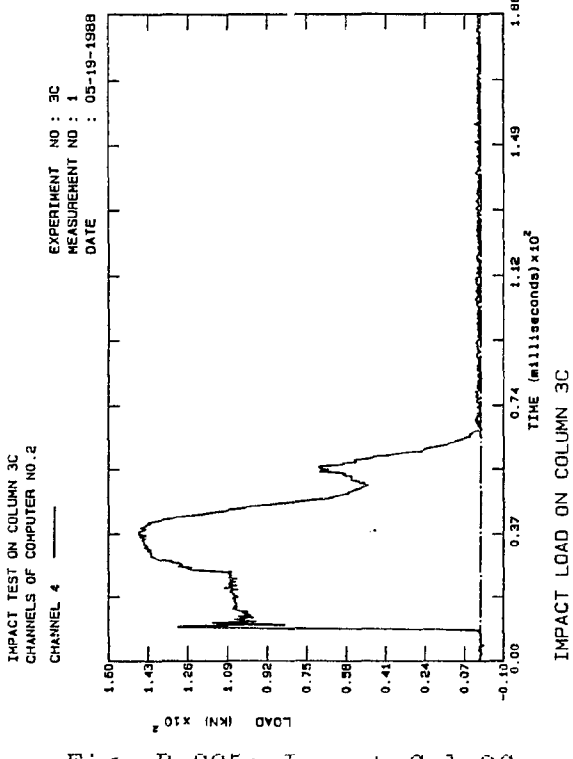

Fig. B.395: Impact Col 3C

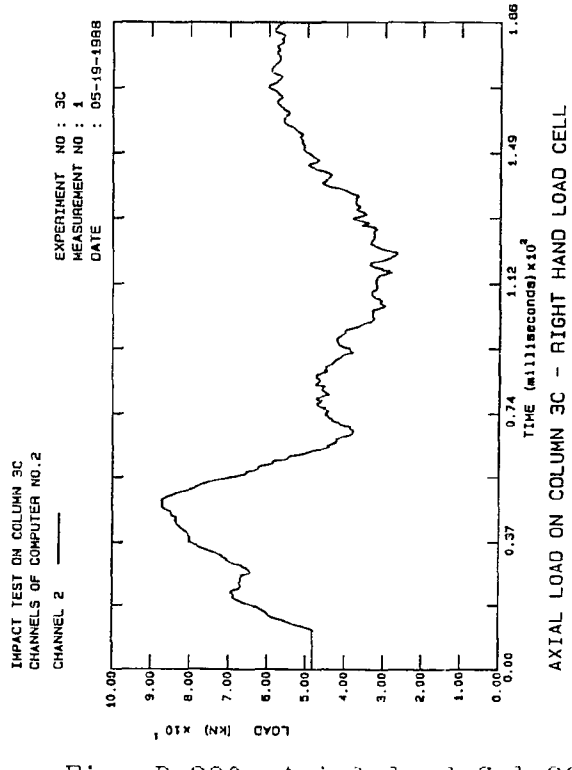

Fig. B.396: Axial load Col.3C

Stellenbosch University http://scholar.sun.ac.za

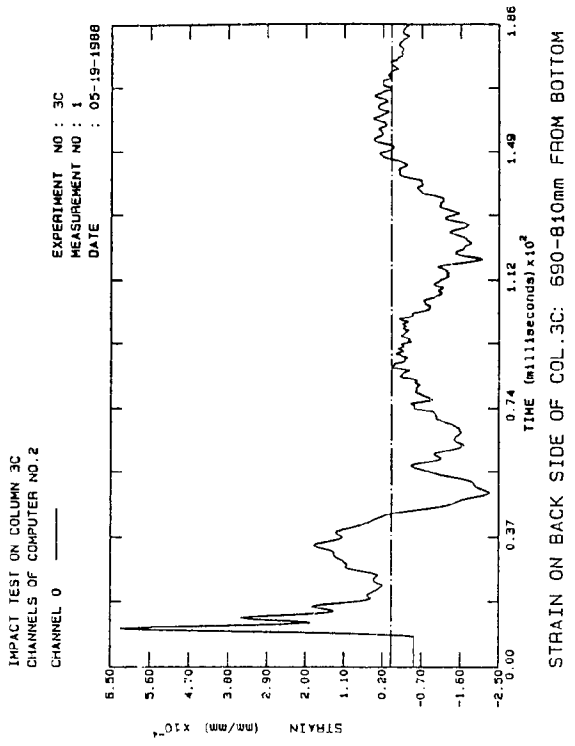

STRAIN ON BACK SIDE OF COL.3C: 690-810mm FROM BOTTOM

Fig. B.397: Strain Col.3C

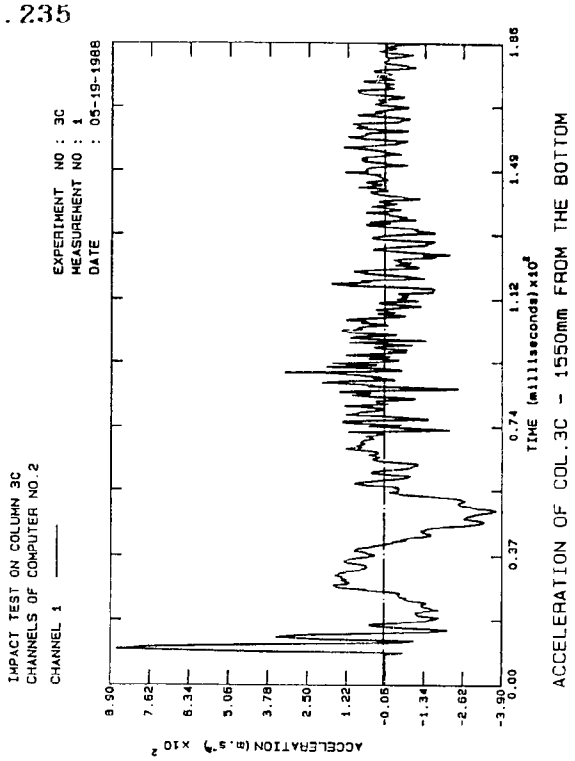

ACCELERATION OF COL.3C - 1550mm FROM THE BOTTOM

Fig. B.398: Accel. Col.3C

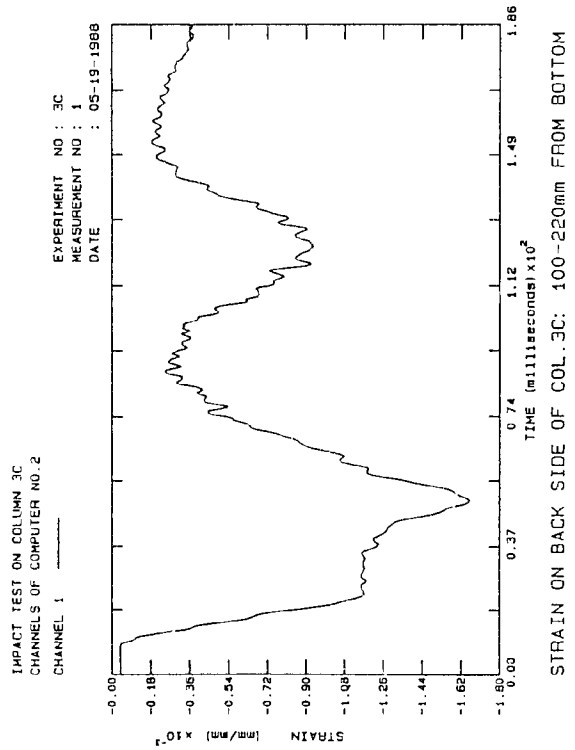

STRAIN ON BACK SIDE OF COL.3C: 100-220mm FROM BOTTOM

Fig. B.399: Strain Col.3C

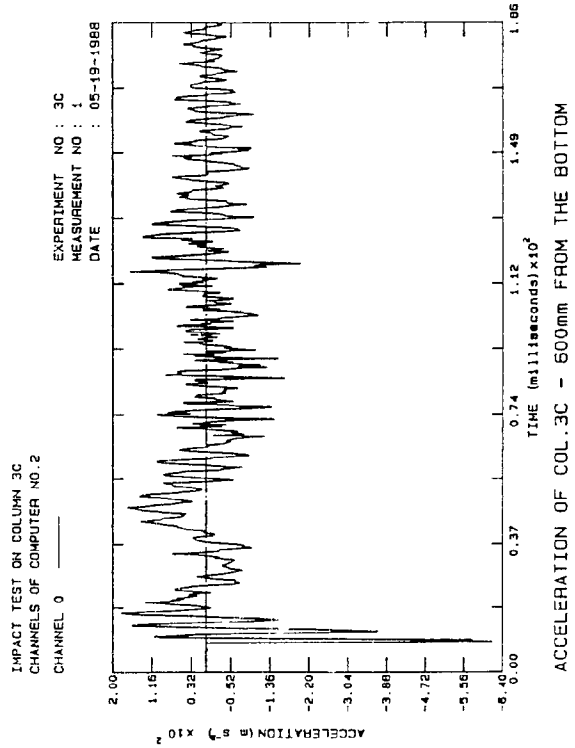

ACCELERATION OF COL.3C - 600mm FROM THE BOTTOM

Fig. B.400: Accel. Col.3C

Stellenbosch University http://scholar.sun.ac.za

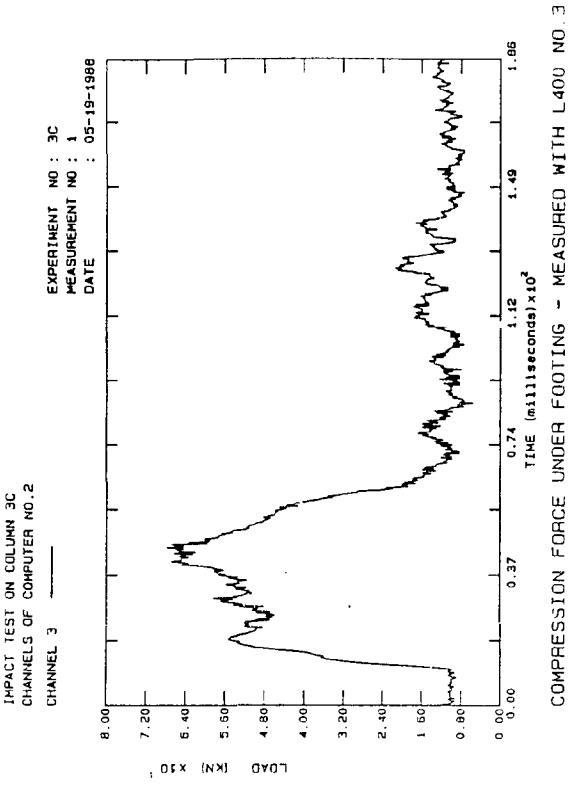

Fig. B.401: Comp. Col.3C

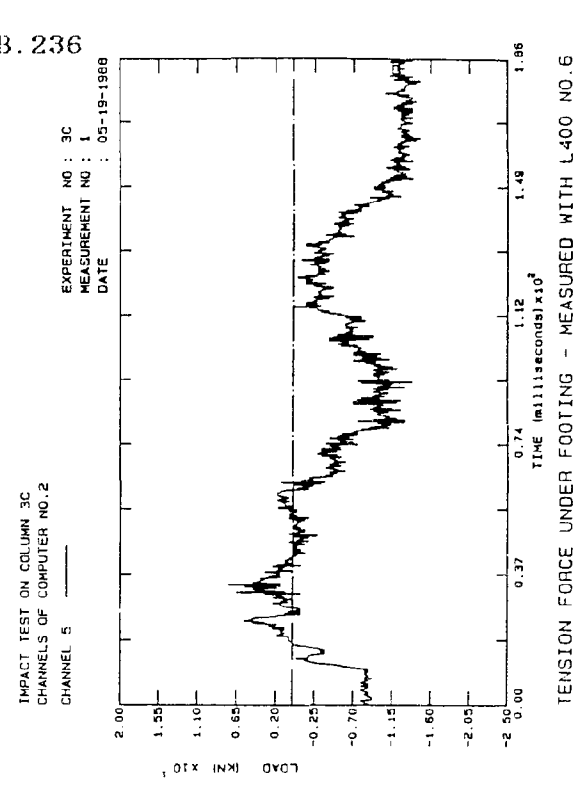

Fig. B.402: Tension Col.3C

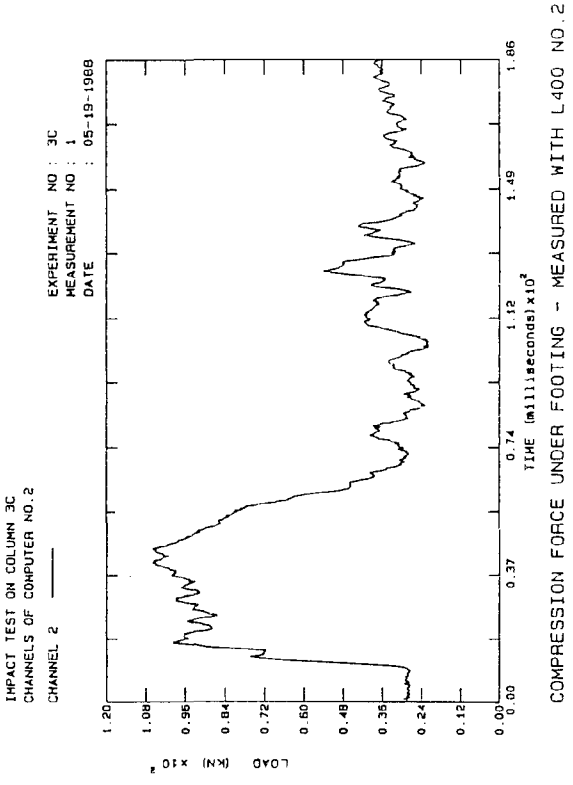

Fig. B.403: Comp. Col.3C

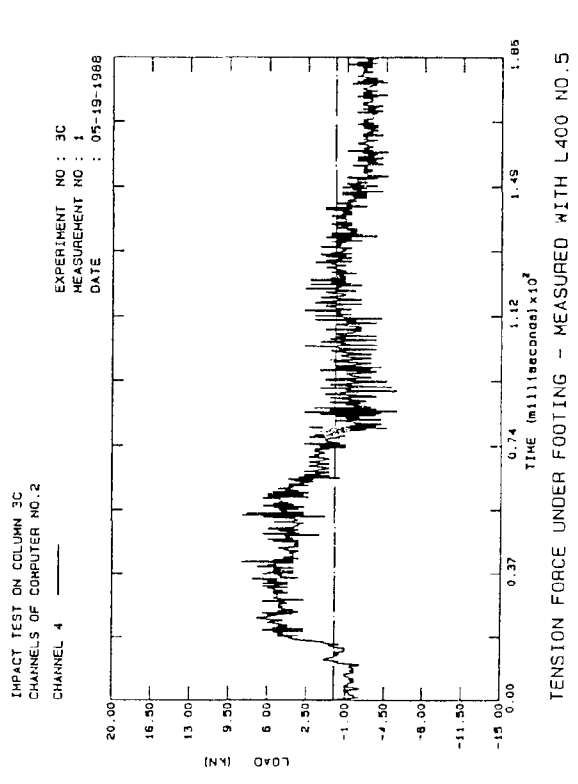

Fig. B.404: Tension Col.3C

Stellenbosch University http://scholar.sun.ac.za

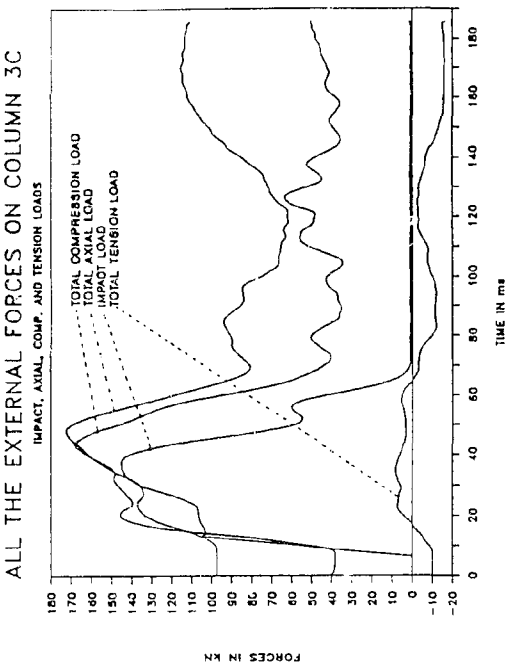

Fig. B.405: Ext Loads Col.3C

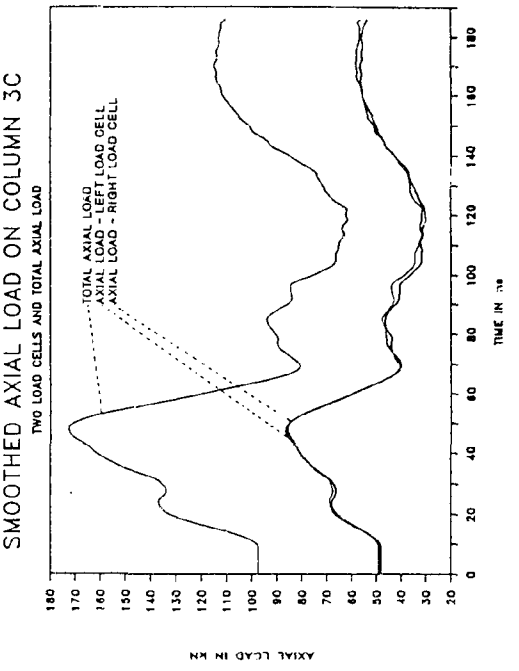

Fig. B.406: Smo. Axial Col.3C

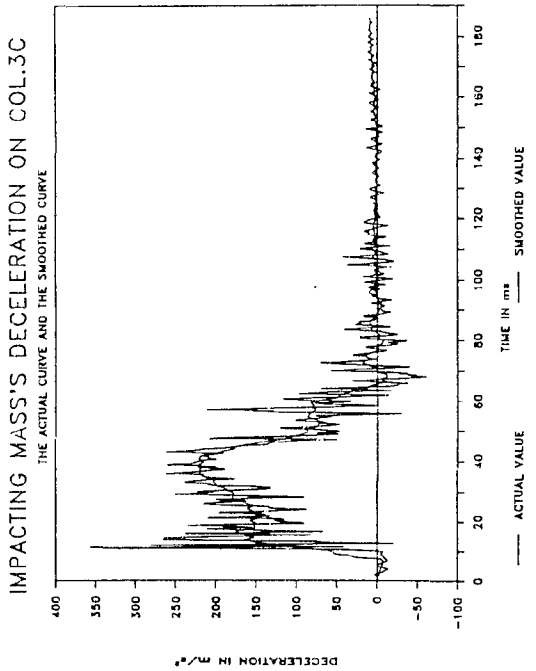

Fig. B.407: Smo. Decel Col.3C

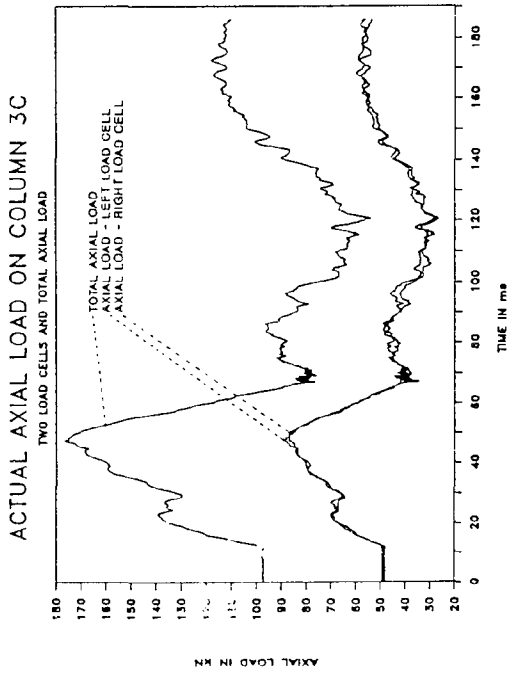

Fig. B.408: Axial Loads Col.3C

Stellenbosch University http://scholar.sun.ac.za

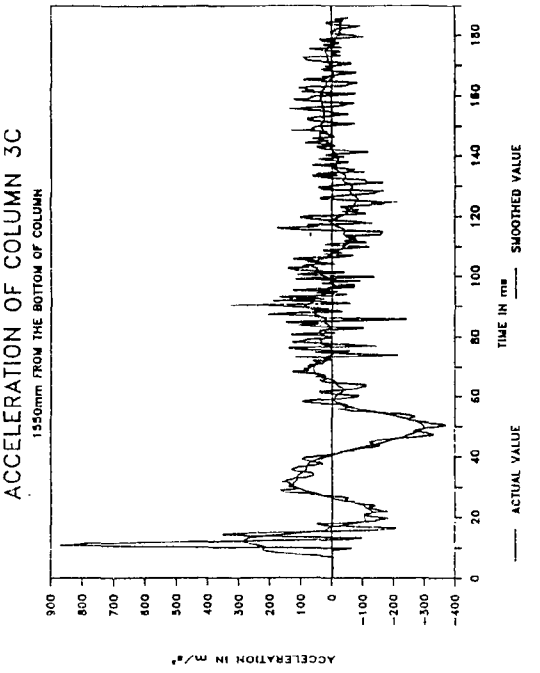

Fig. B.409: Smo.Accel. Col.3C

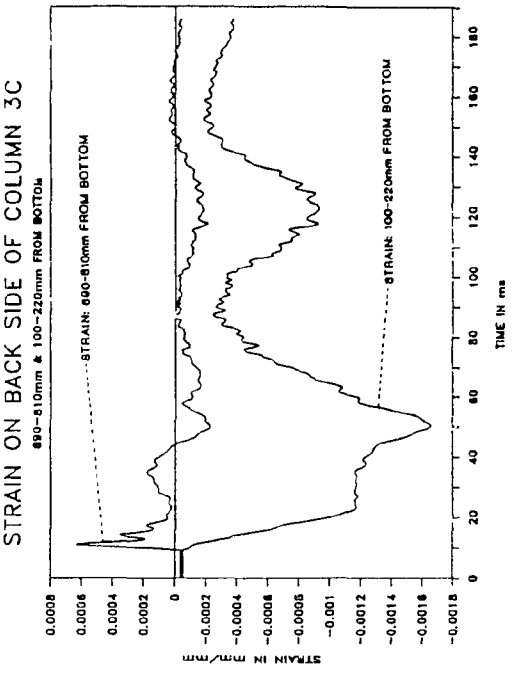

Fig. B.410: Strain Col.3C

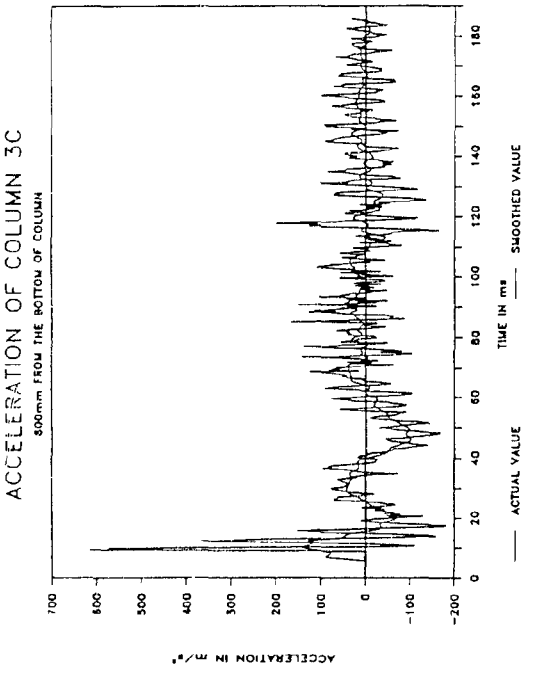

Fig. B.411: Smo.Accel. Col.3C

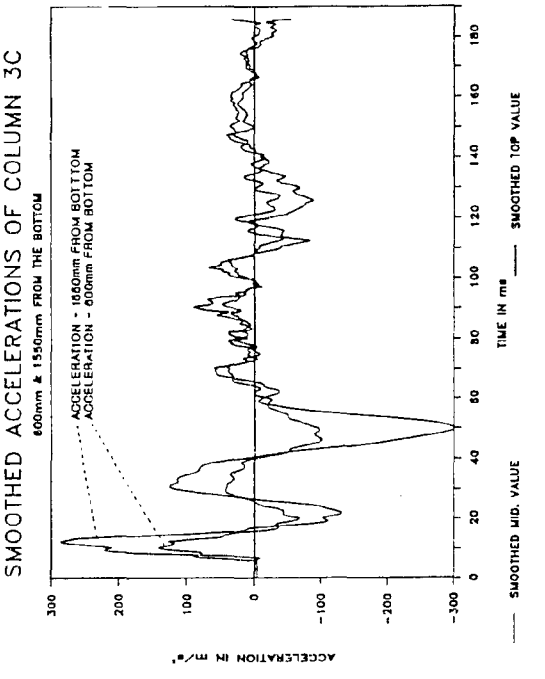

Fig. B.412: Smo. Accel Col.3C

Stellenbosch University http://scholar.sun.ac.za

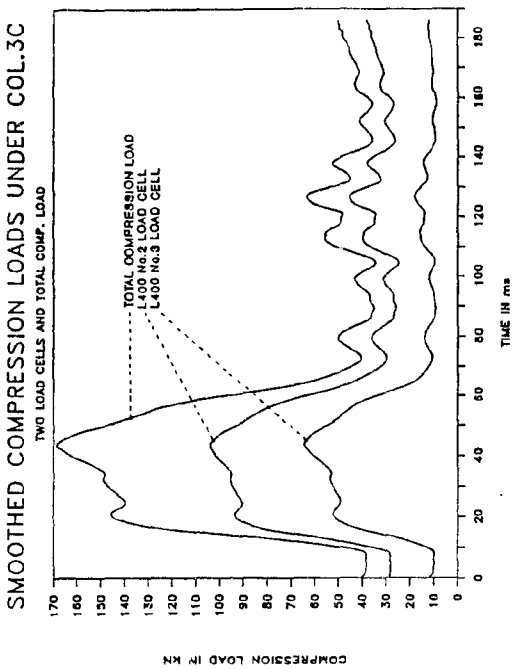

Fig. B.413: Smo. Comp. Col.3C

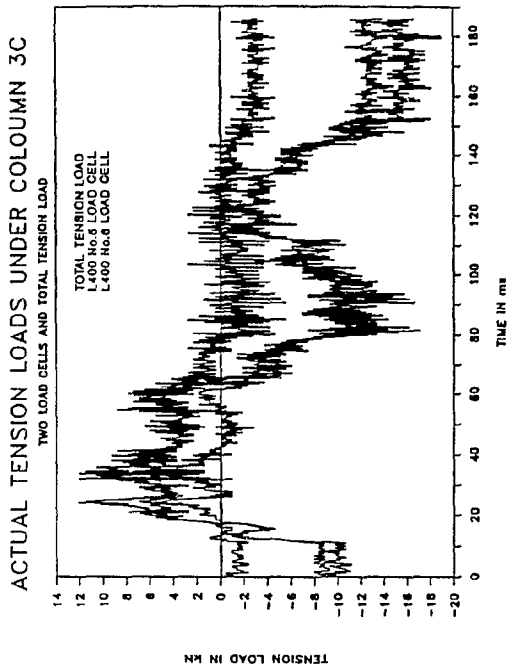

Fig. B.414: Smo. Tens. Col.3C

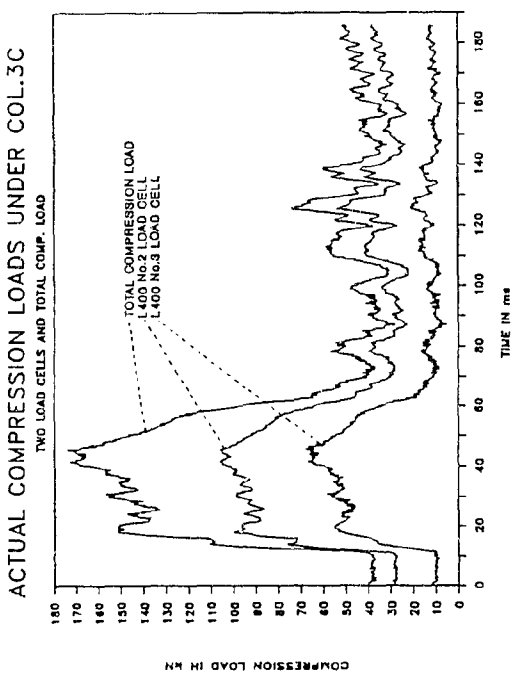

Fig. B.415: Comp. load Col 3C

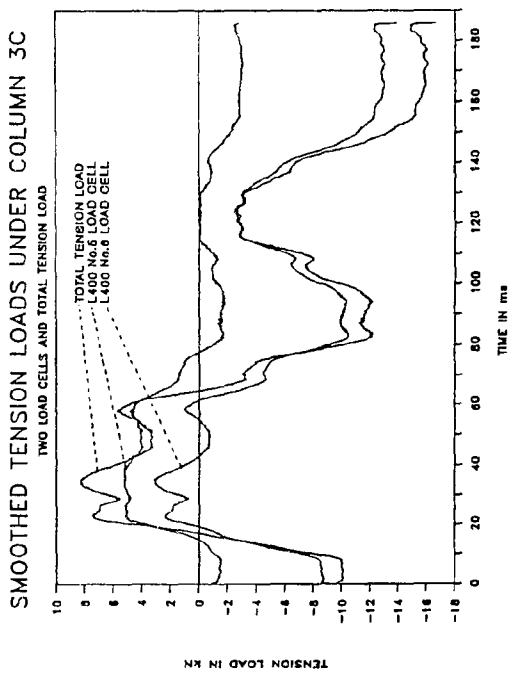

Fig. B.416: Tens. loads Col.3C

Stellenbosch University http://scholar.sun.ac.za

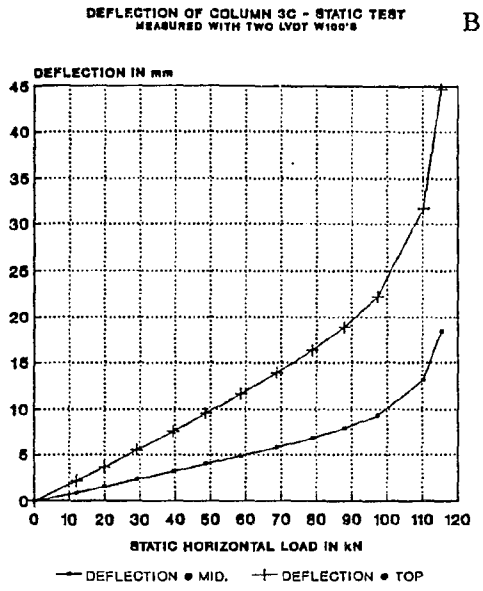

Fig. B.417: Deflection Col.3C

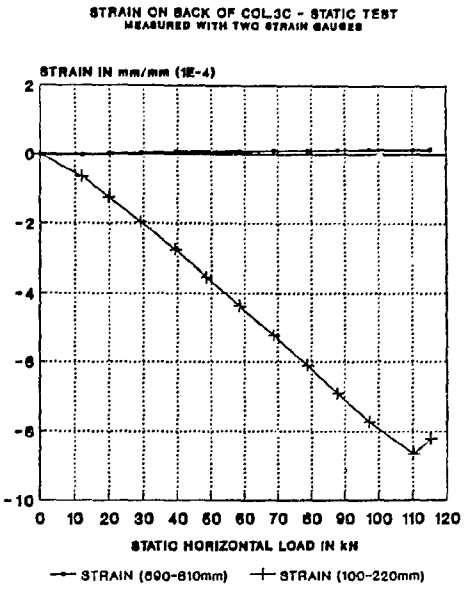

Fig. B.418: Strain Col.3C

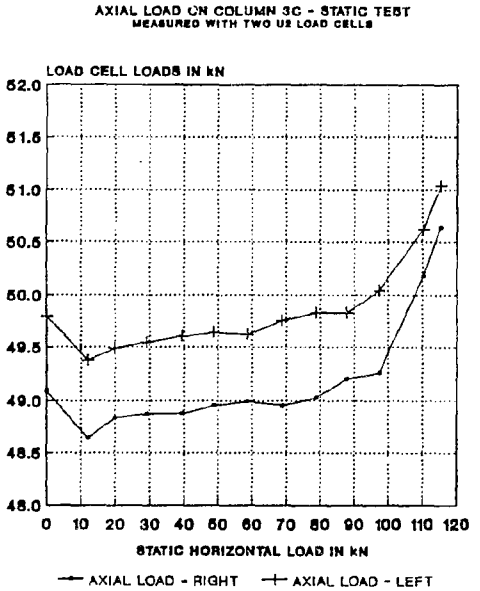

Fig. B.419: Axial load Col 3C

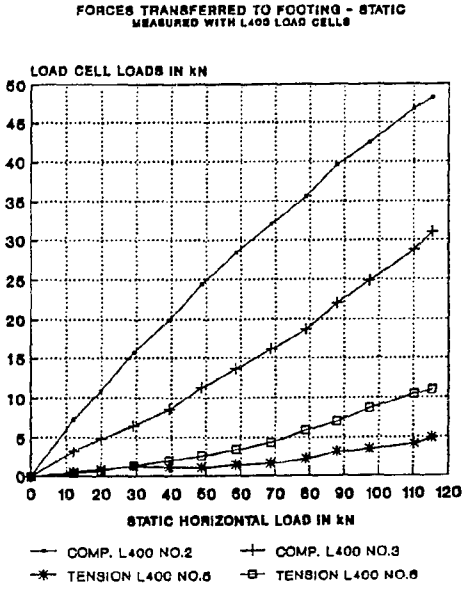

Fig. B.420: Foot.loads Col.3C

Stellenbosch University http://scholar.sun.ac.za

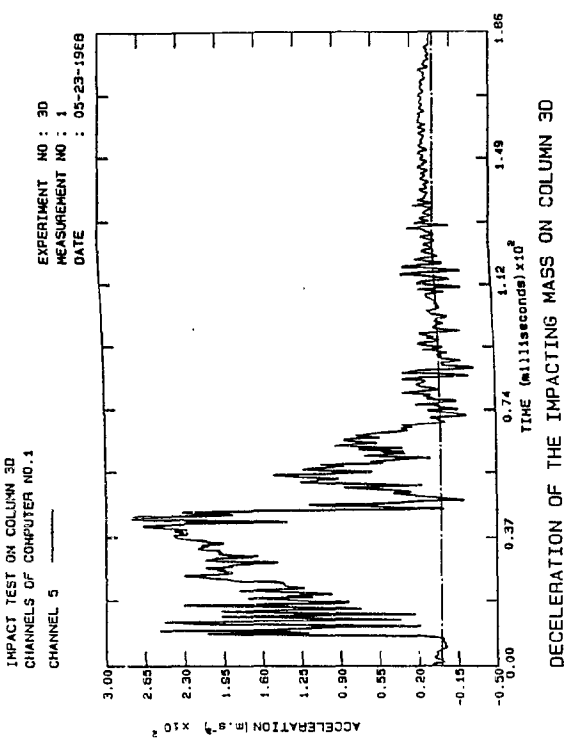

Fig. B.421: Decel. Col.3D

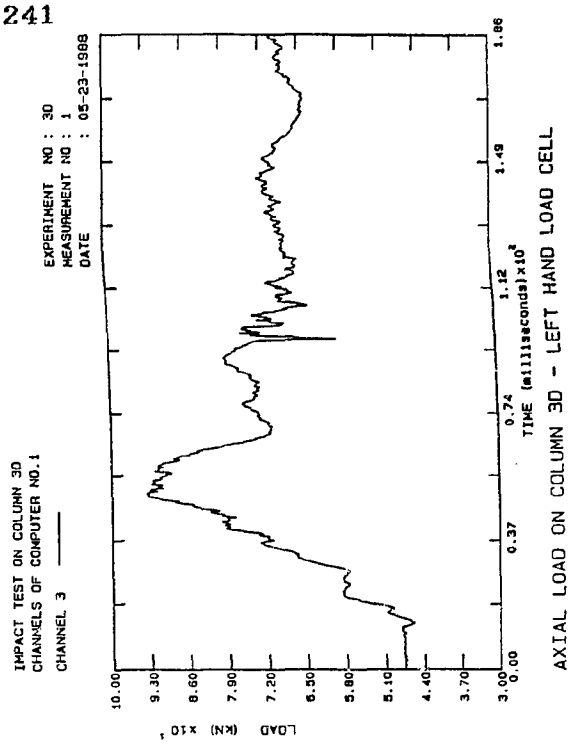

Fig. B.422: Axial load Col.3D

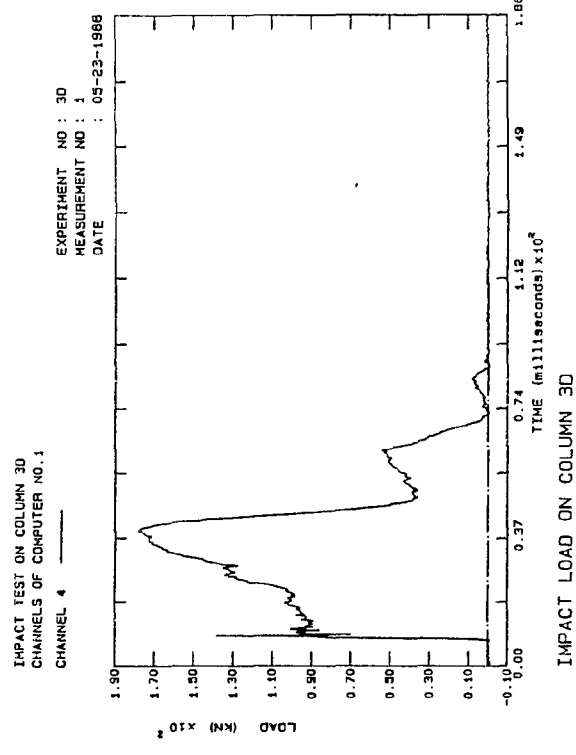

Fig. B.423: Impact Col 3D

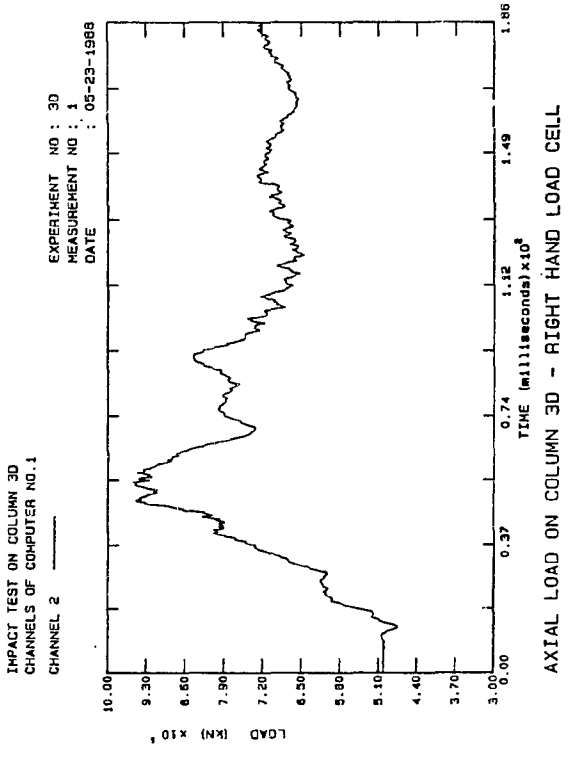

Fig. B.424: Axial load Col.3D

Stellenbosch University http://scholar.sun.ac.za

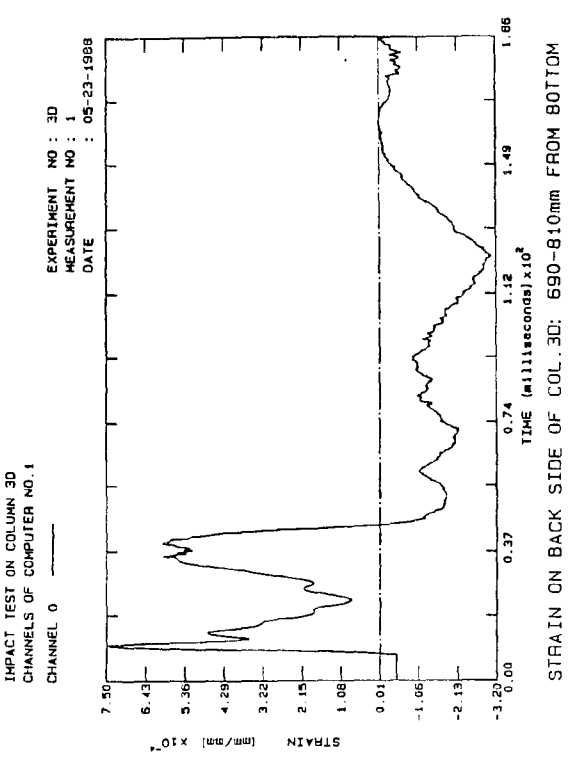

Fig. B.425: Strain Col.3D

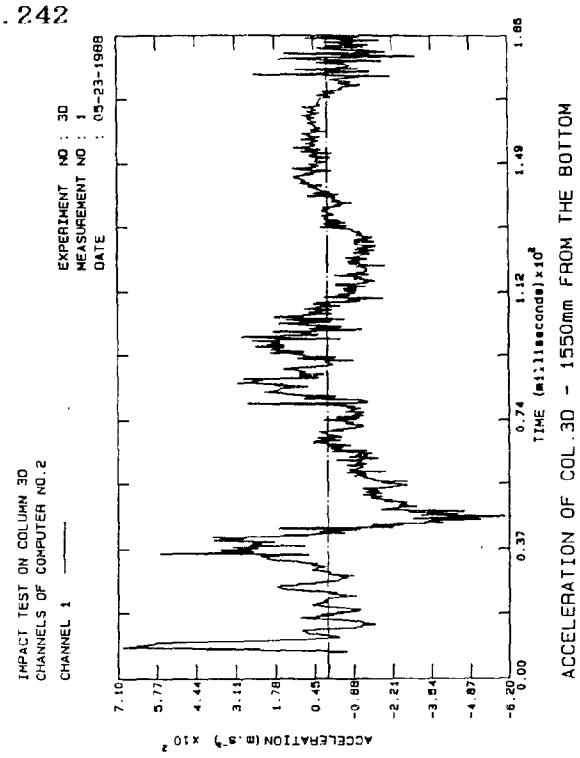

Fig. B.426: Accel. Col.3D

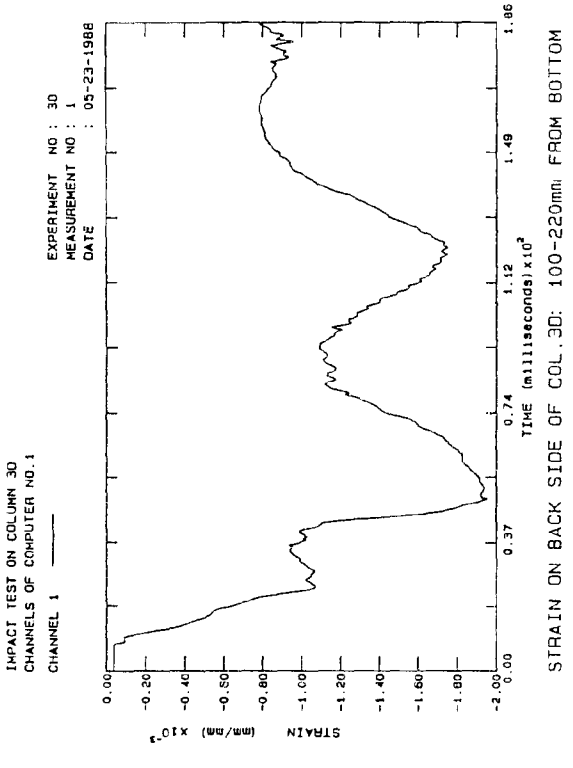

Fig. B.427: Strain Col 3D

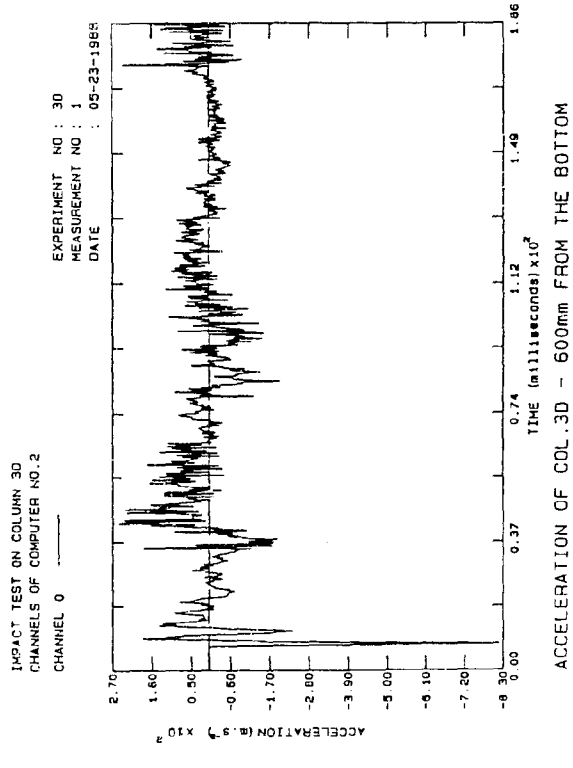

Fig. B.428: Accel Col.3D

Stellenbosch University http://scholar.sun.ac.za

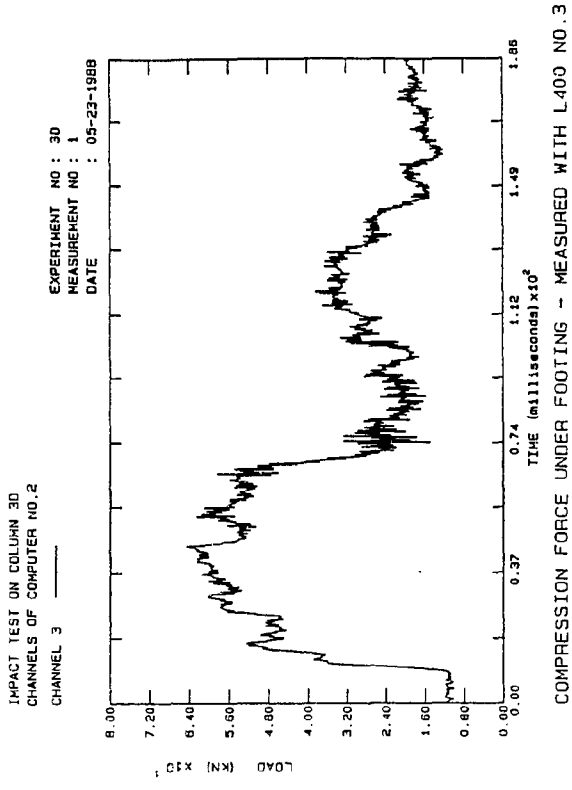

Fig. B.429: Comp. Col.3D

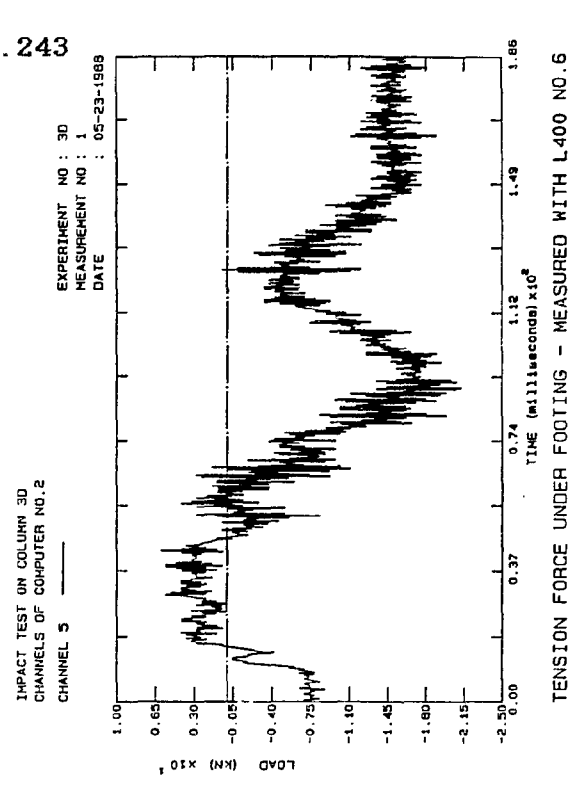

Fig. B.430: Tension Col.3D

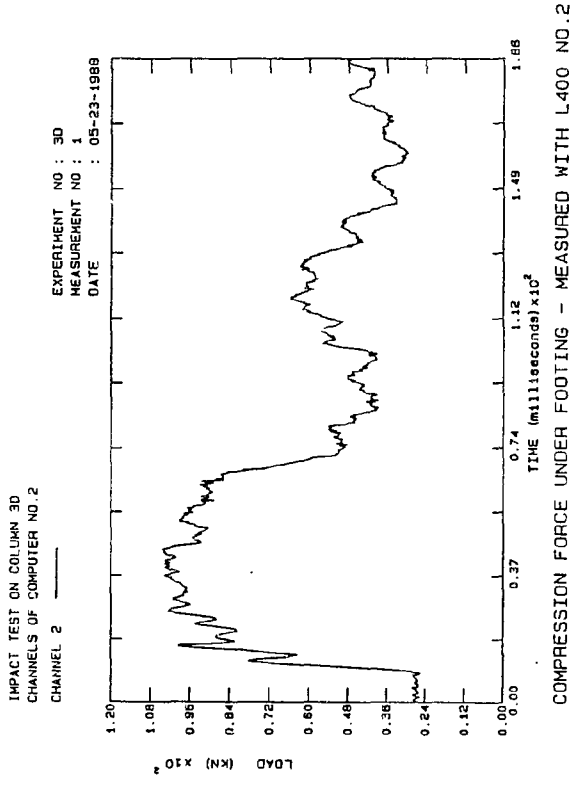

Fig. B.431: Comp. Col 3D

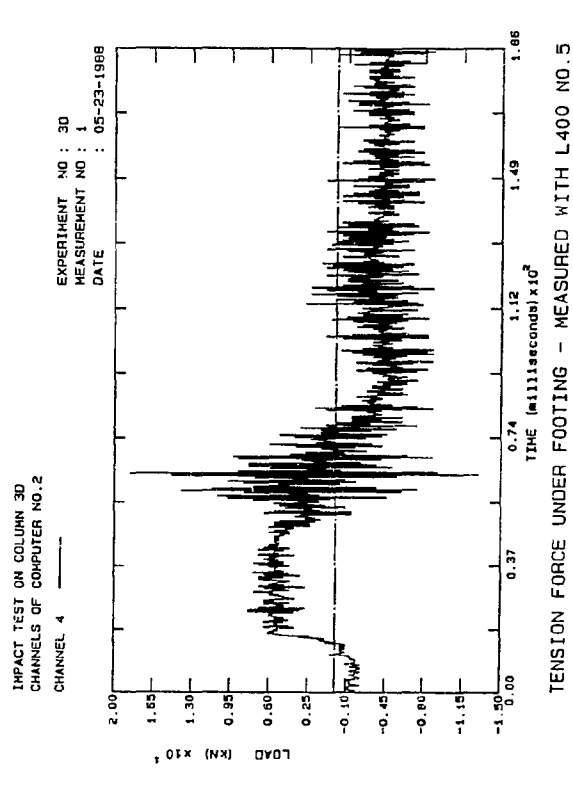

Fig. B.432: Tension Col.3D

Stellenbosch University http://scholar.sun.ac.za

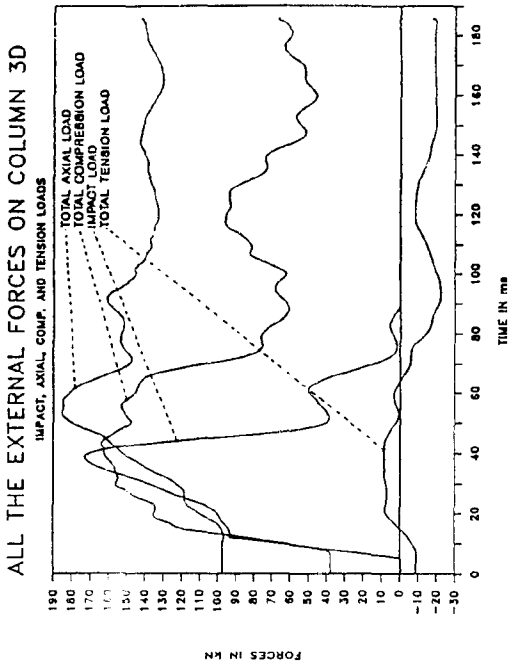

Fig. B.433: Ext. Loads Col.3D

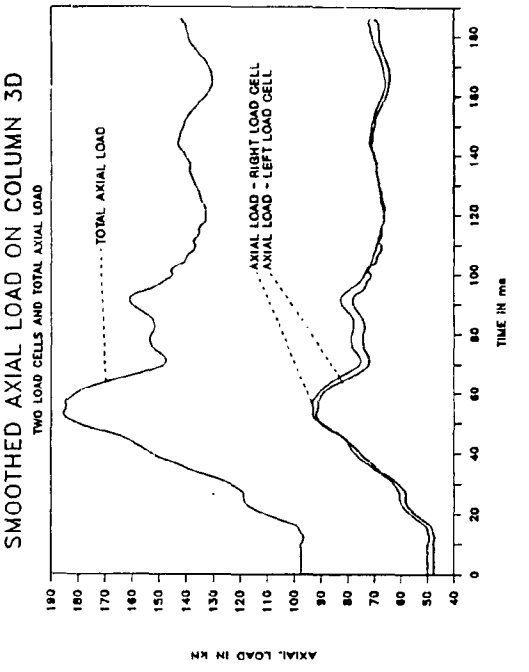

Fig. B.434: Smo. Axial Col.3D

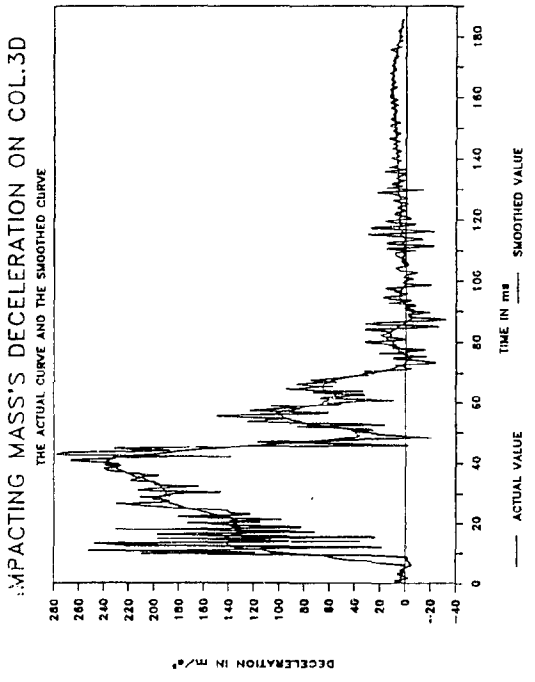

Fig. B.435: Smo.Decel. Col 3D

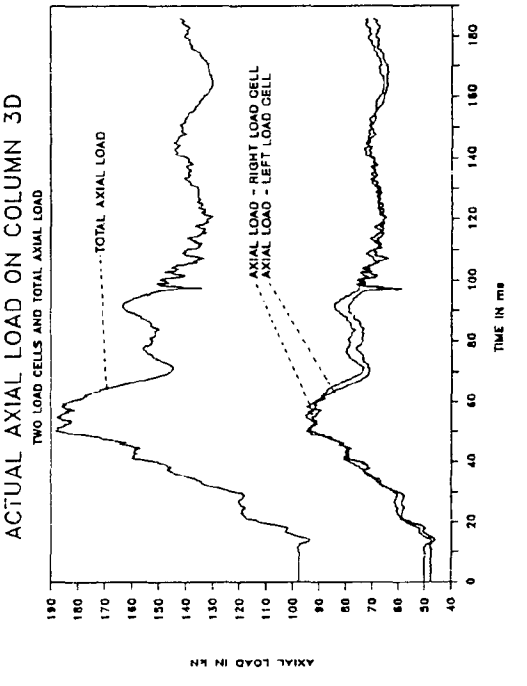

Fig. B.436: Axial loads Col.3D

Stellenbosch University http://scholar.sun.ac.za

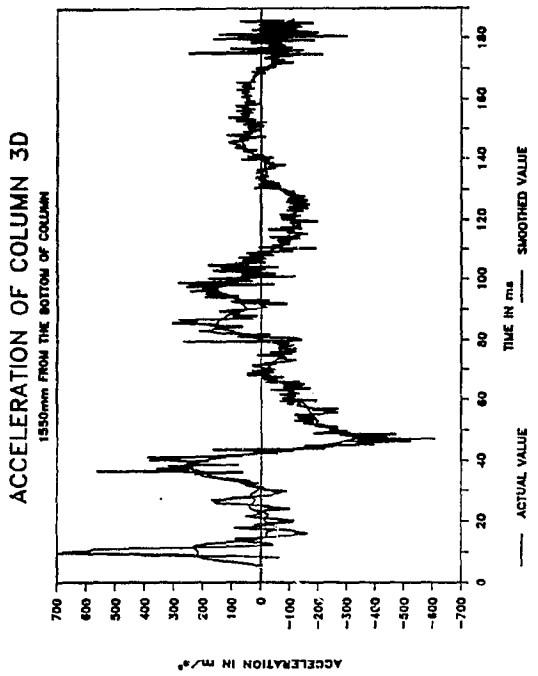

Fig. B.437: Smo.Accel. Col.3D

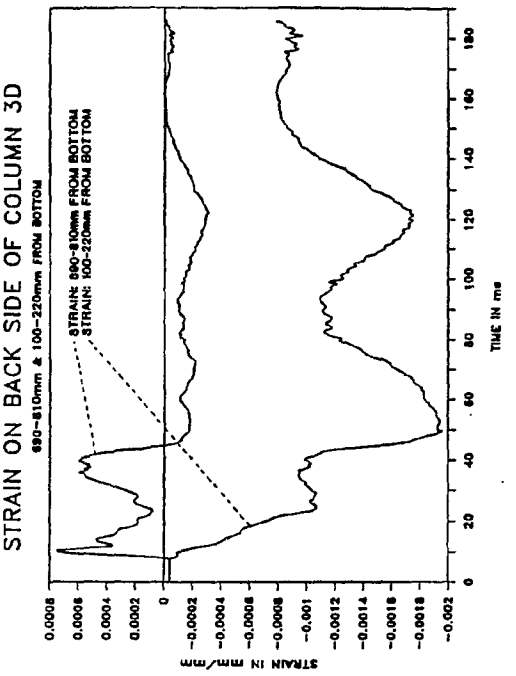

Fig. B.438: Strain Col.3D

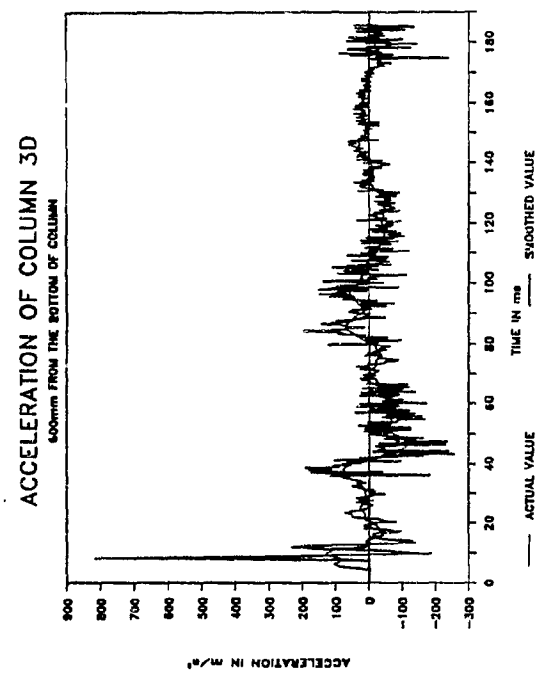

Fig. B.439: Smo.Accel. Col 3D

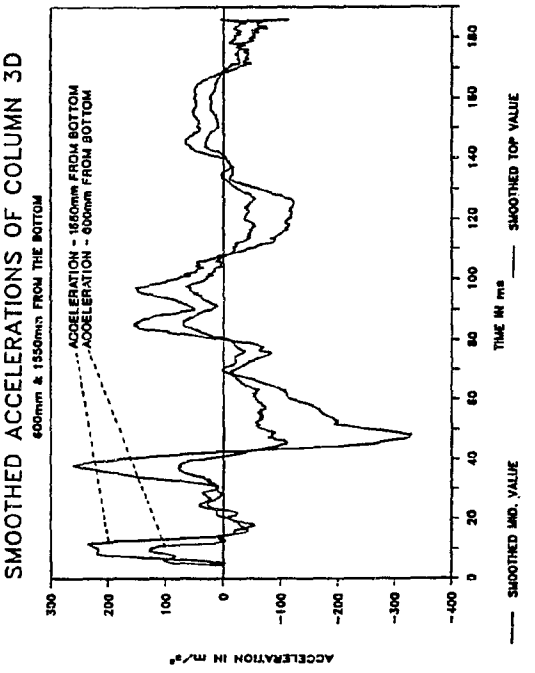

Fig. B.440: Smo. Accel. Col.3D

Stellenbosch University http://scholar.sun.ac.za

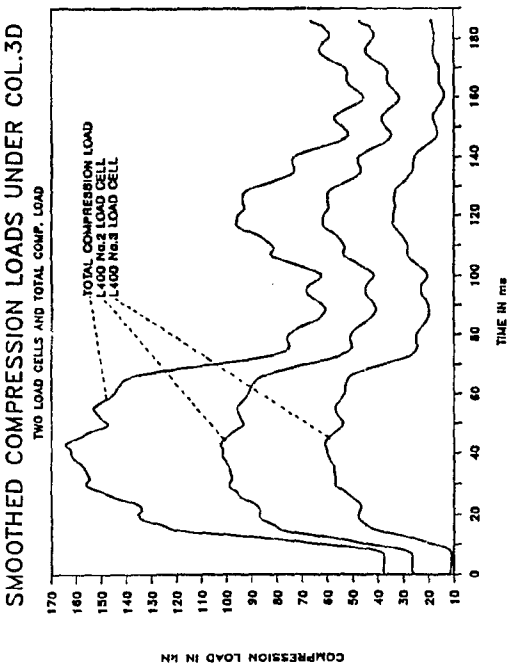

Fig. B.441: Smo. Comp. Col.3D

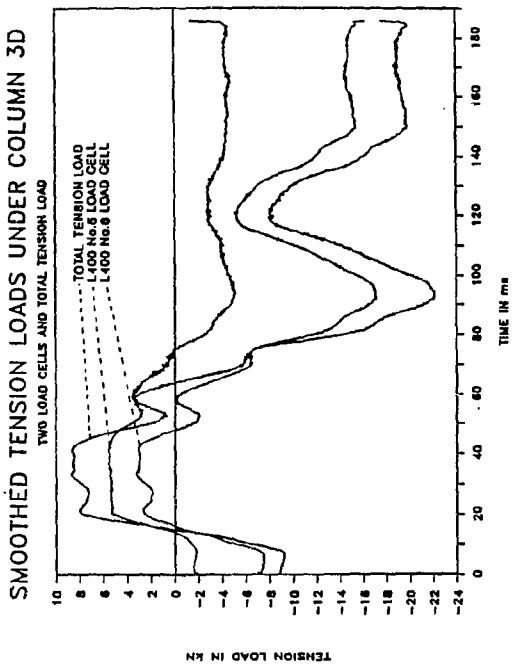

Fig. B.442: Smo. Tens. Col.3D

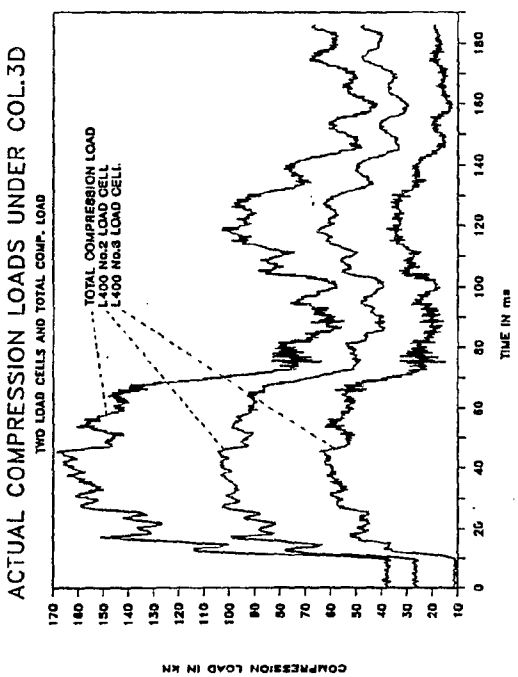

Fig. B.443: Comp. load Col 3D

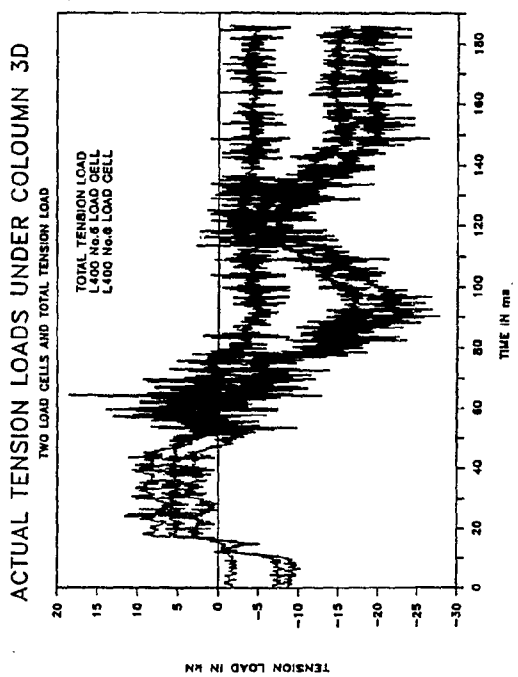

Fig. B.444: Tens. loads Col.3D

Stellenbosch University http://scholar.sun.ac.za

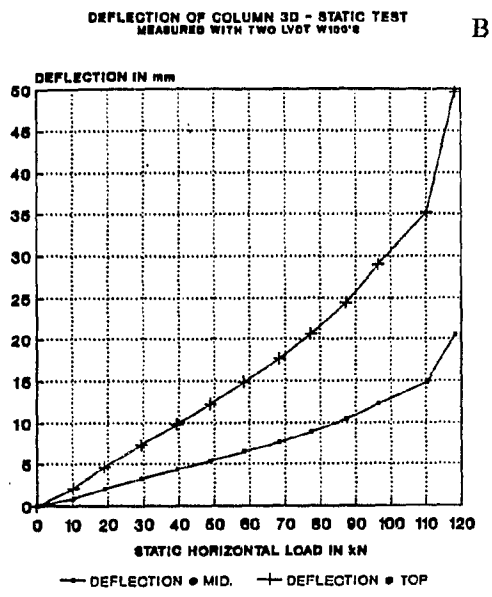

Fig. B.445: Deflection Col.3D

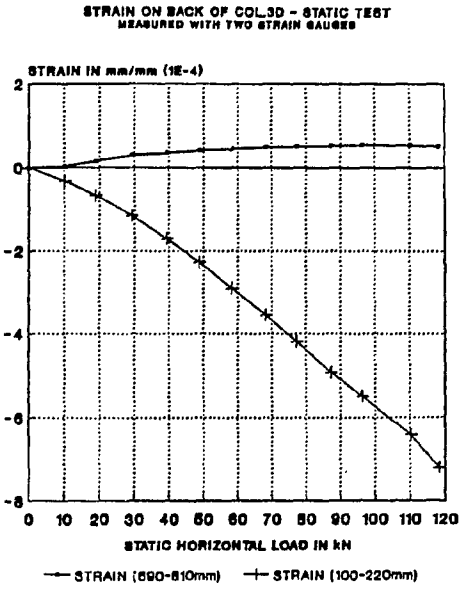

Fig. B.446: Strain Col.3D

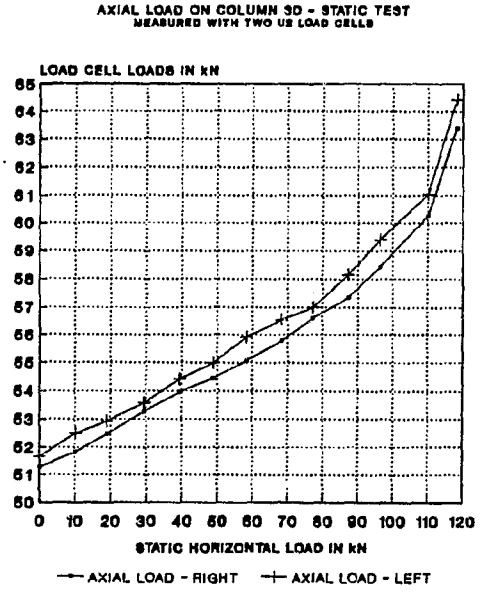

Fig. B.447: Axial load Col 3D

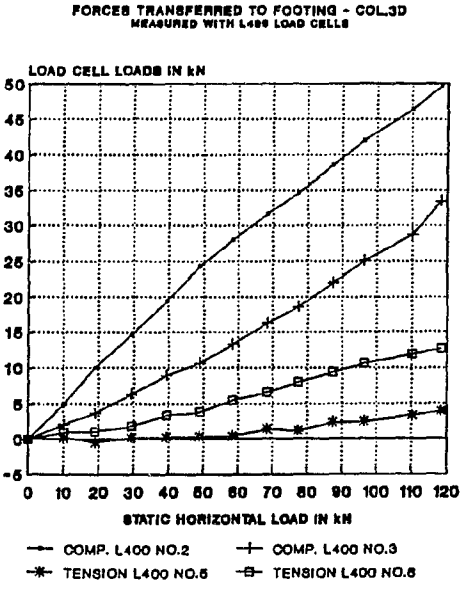

Fig. B.448: Foot.loads Col.3D

Stellenbosch University http://scholar.sun.ac.za

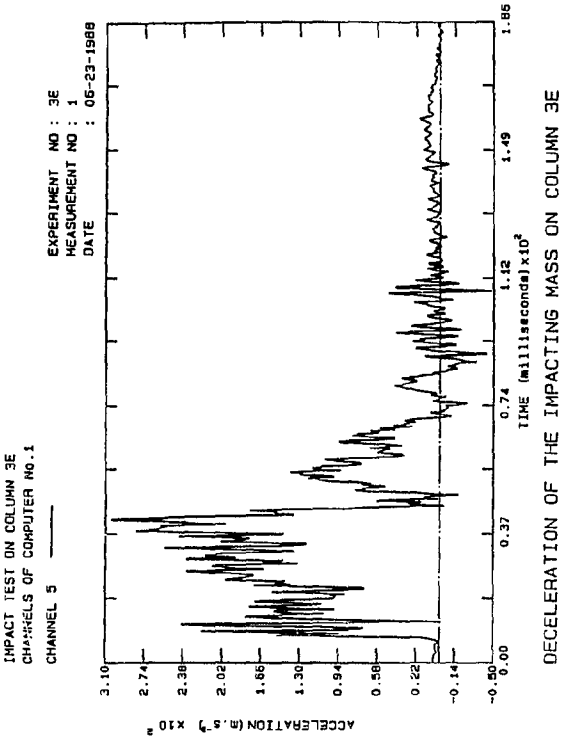

Fig. B.449: Decel. Col.3E

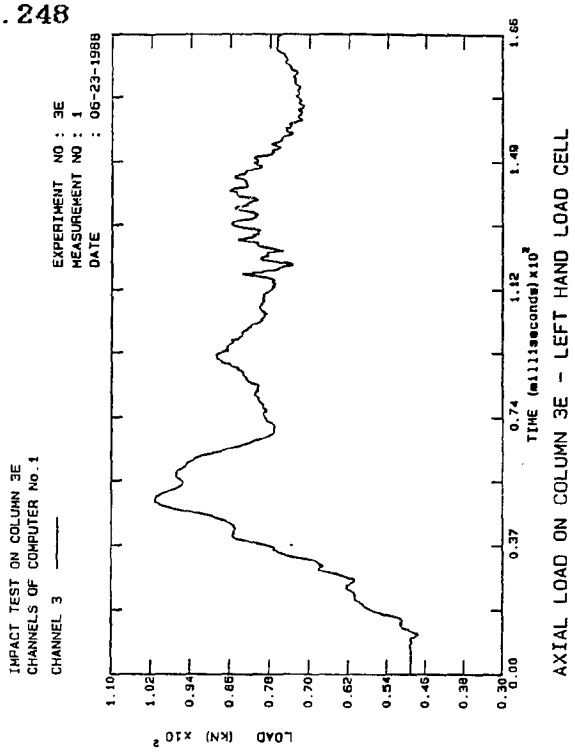

Fig. B.450: Axial load Col.3E

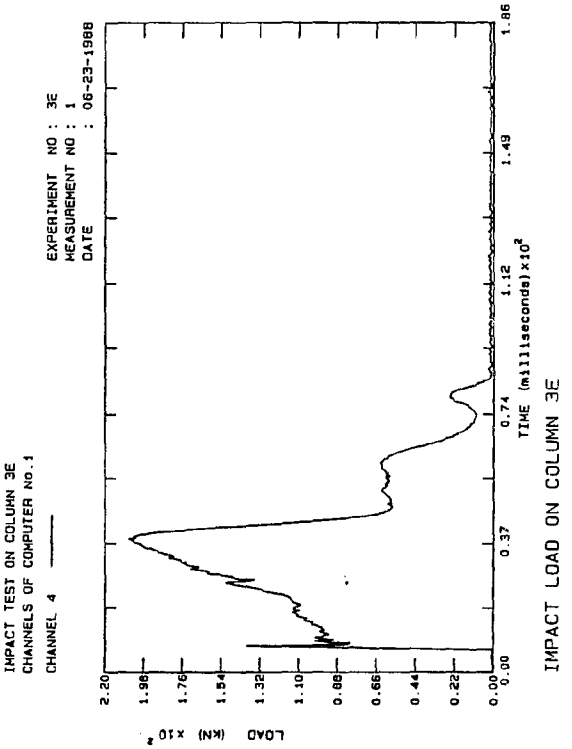

Fig. B.451: Impact Col 3E

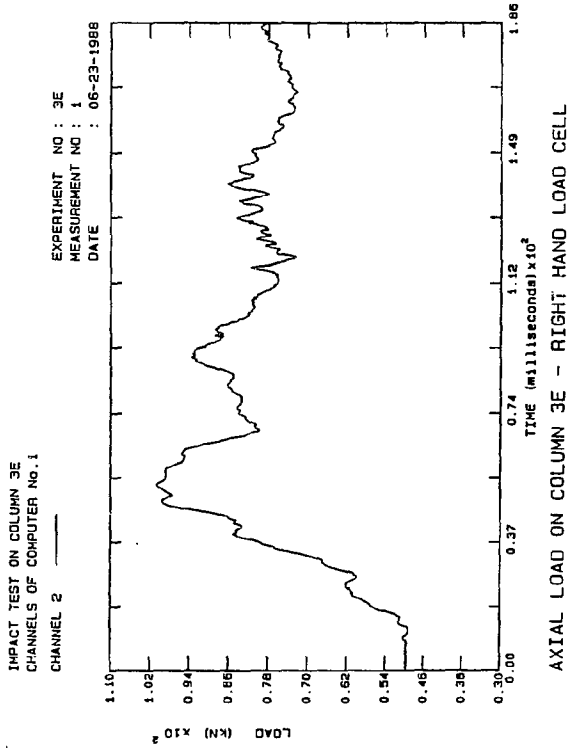

Fig. B.452: Axial load Col.3E

Stellenbosch University http://scholar.sun.ac.za

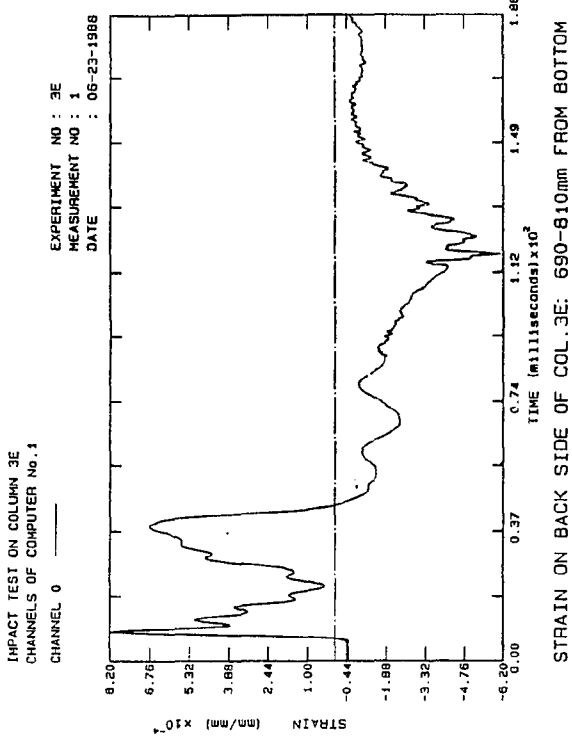

Fig. B.453: Strain Col.3E

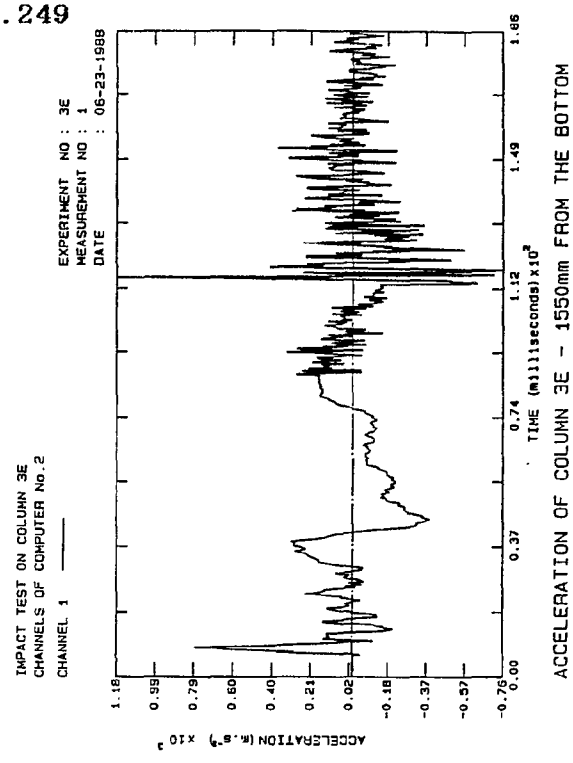

Fig. B.454: Accel. Col.3E

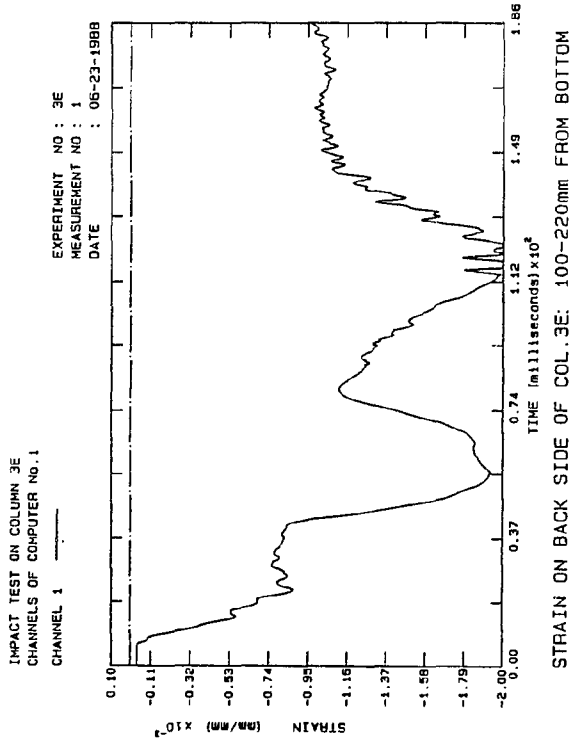

Fig. B.455: Strain Col 3E

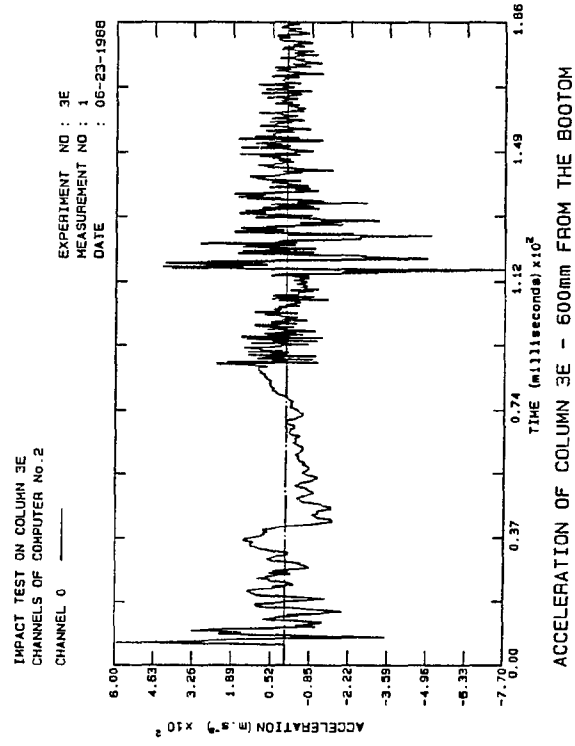

Fig. B.456: Accel. Col.3E

Stellenbosch University http://scholar.sun.ac.za

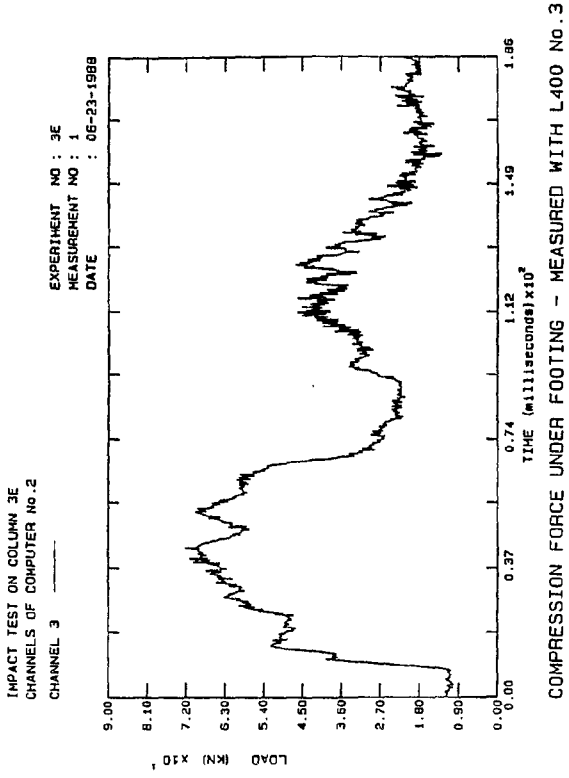

Fig. B.457: Comp. Col.3E

B.250

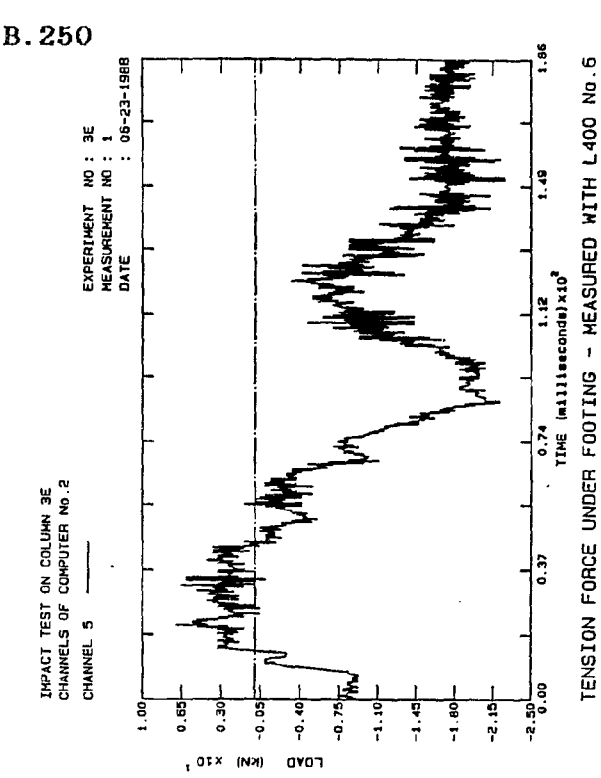

Fig. B.458: Tension Col.3E

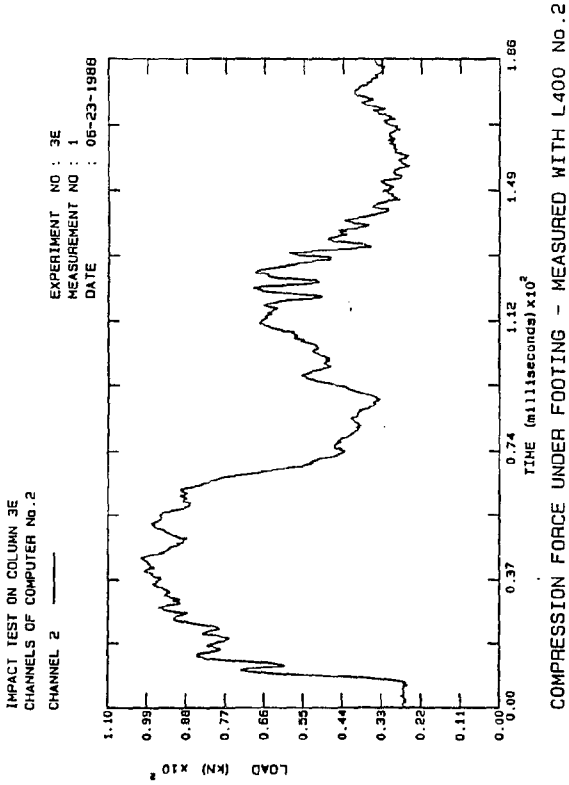

Fig. B.459: Comp. Col 3E

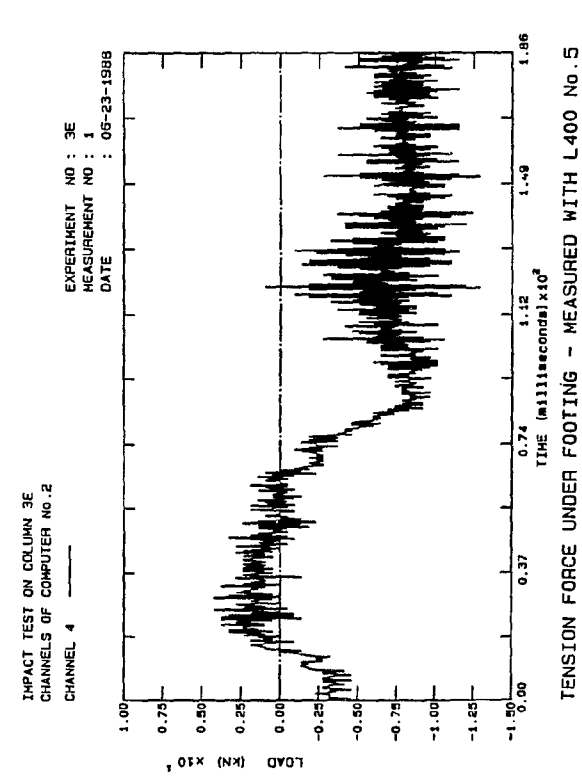

Fig. B.460: Tension Col.3E

Stellenbosch University http://scholar.sun.ac.za

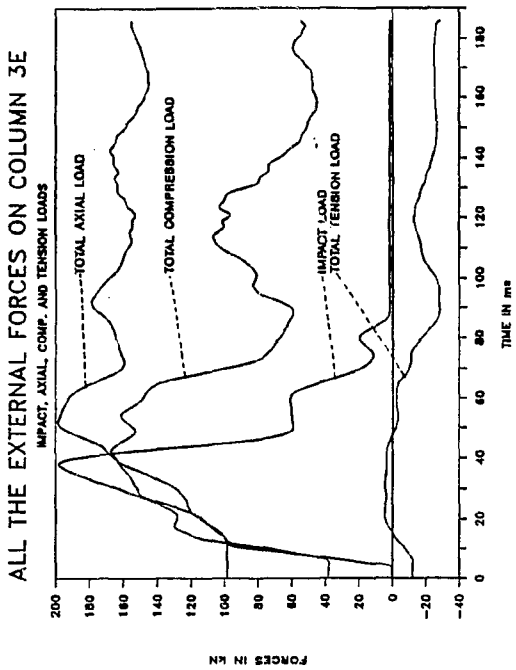

Fig. B.461: Ext. Loads Col.3E

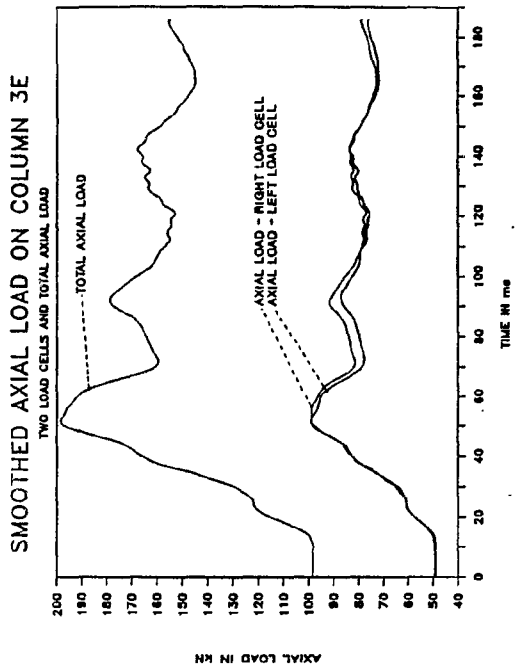

Fig. B.462: Smo. Axial Col.3E

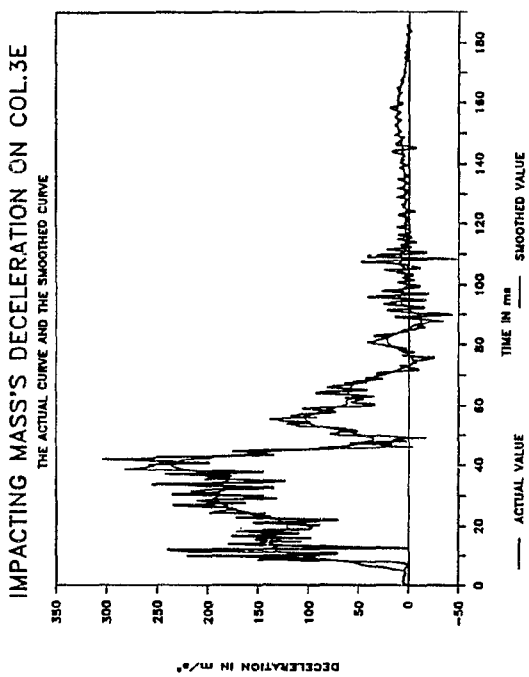

Fig. B.463: Smo.Decel. Col 3E

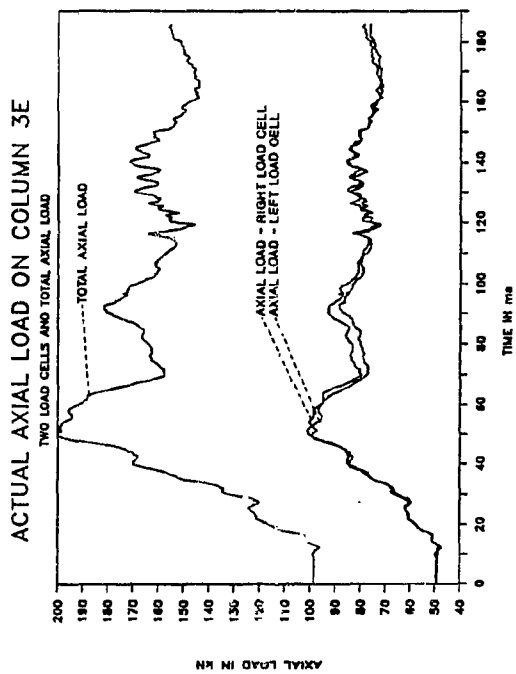

Fig. B.464: Axial loads Col.3E

Stellenbosch University http://scholar.sun.ac.za

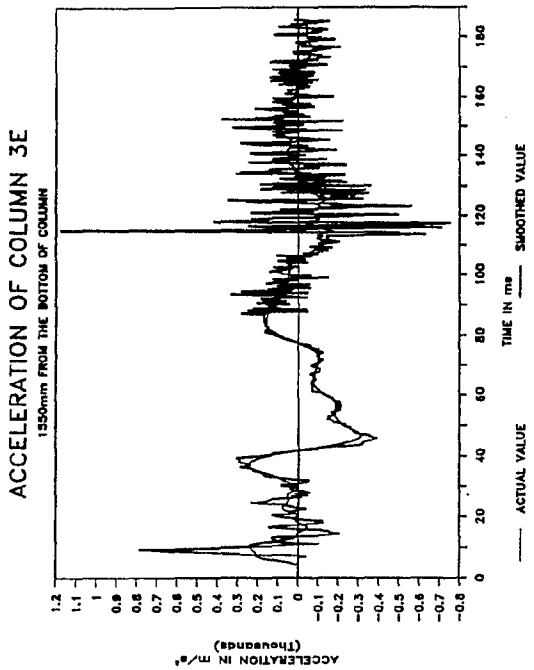

Fig. B.465: Smo.Accel. Col.3E

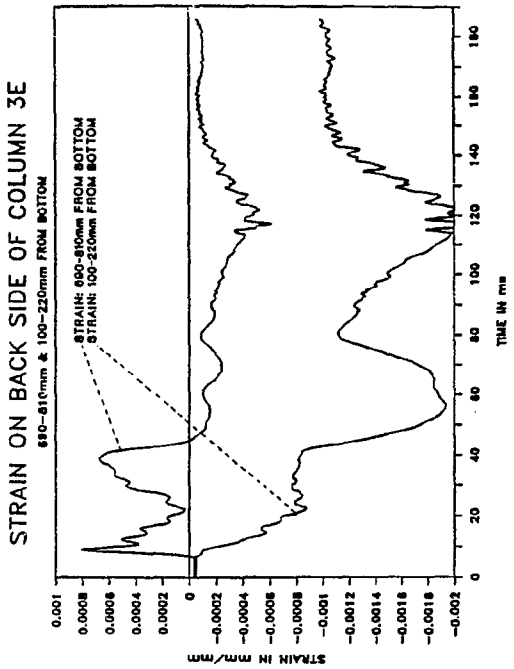

Fig. B.466: Strain Col.3E

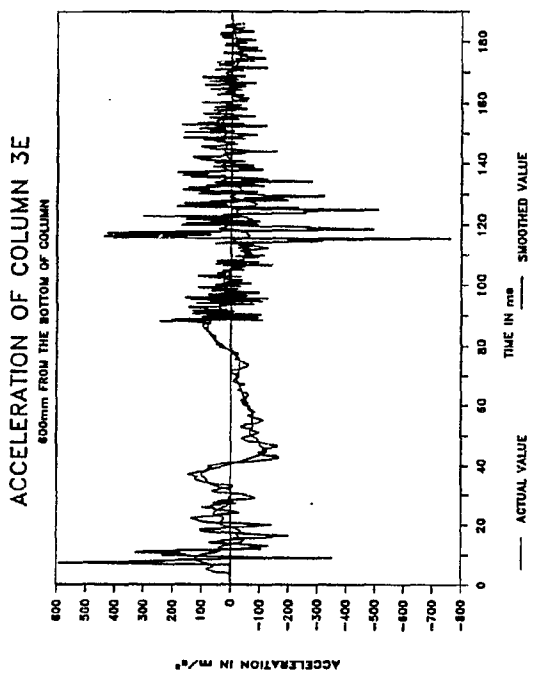

Fig. B.467: Smo.Accel. Col 3E

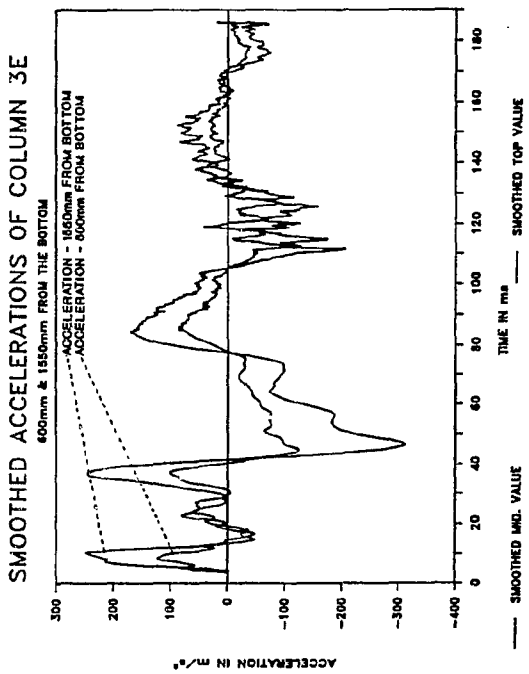

Fig. B.468: Smo. Accel. Col.3E

Stellenbosch University http://scholar.sun.ac.za

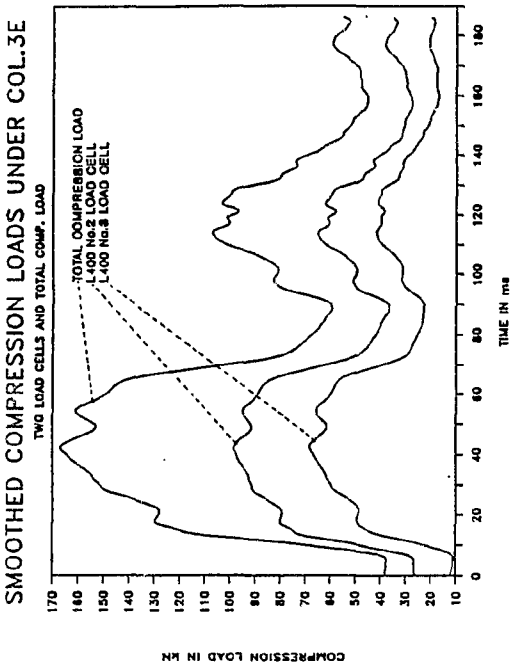

Fig. B.469: Smo. Comp. Col.3E

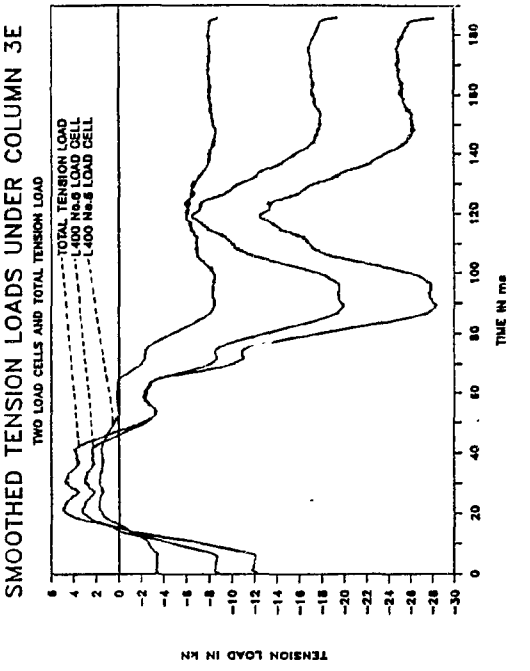

Fig. B.470: Smo. Tens. Col.3E

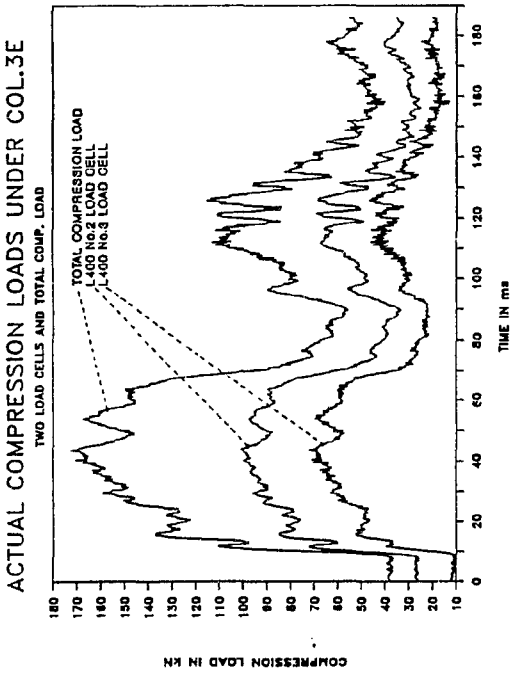

Fig. B.471: Comp. load Col 3E

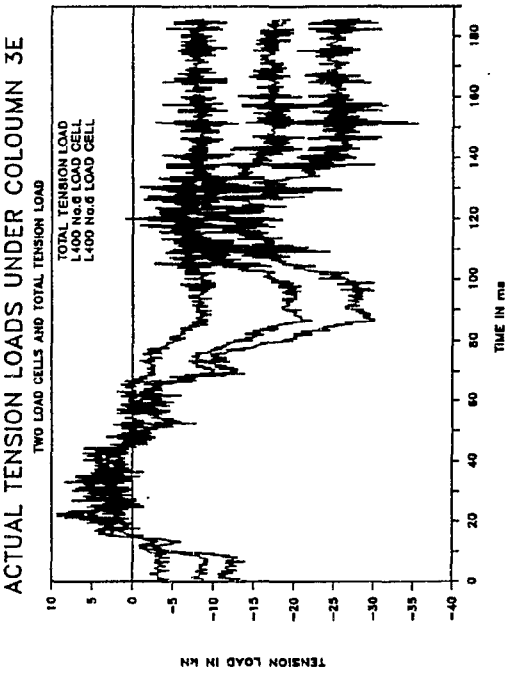

Fig. B.472: Tens. loads Col.3E

Stellenbosch University http://scholar.sun.ac.za

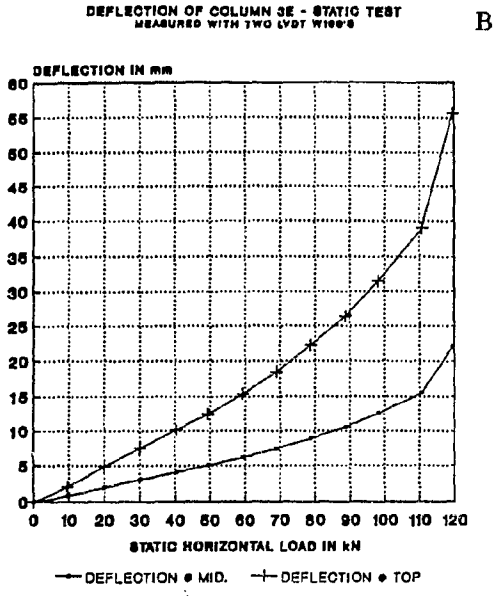

Fig. B.473: Deflection Col.3E

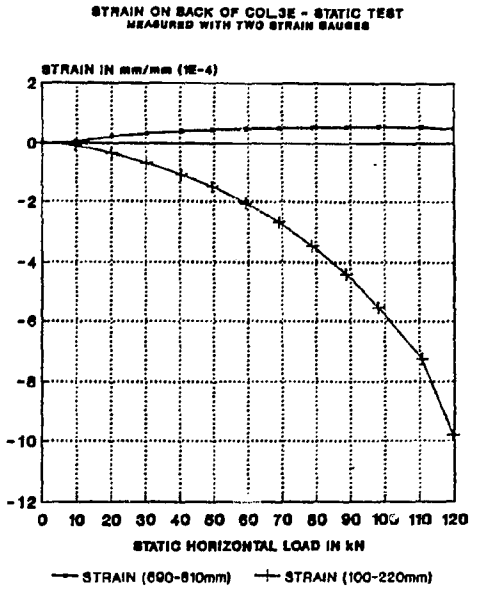

Fig. B.474: Strain Col.3E

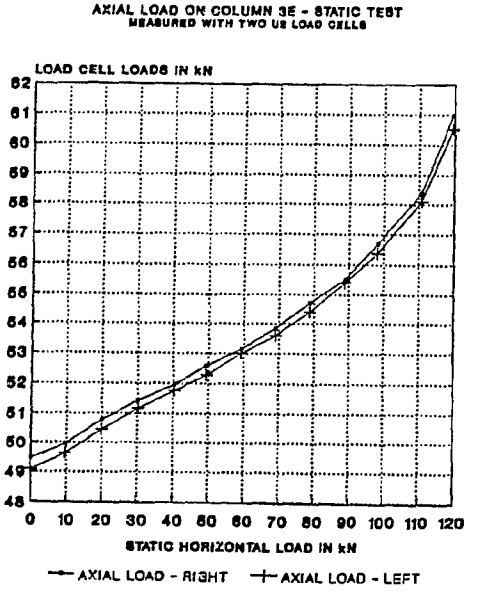

Fig. B.475: Axial load Col 3E

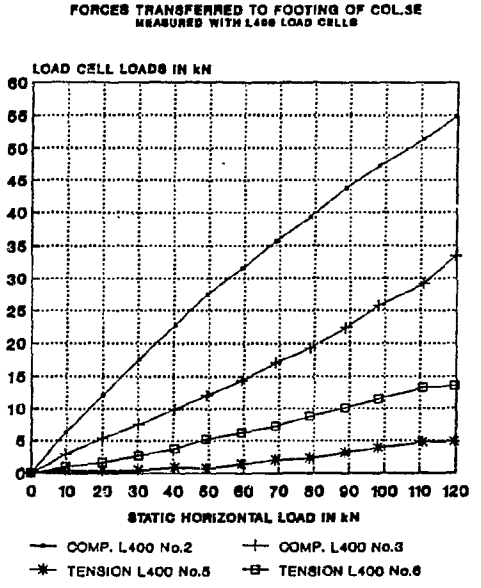

Fig. B.476: Foot.loads Col.3E

Stellenbosch University http://scholar.sun.ac.za

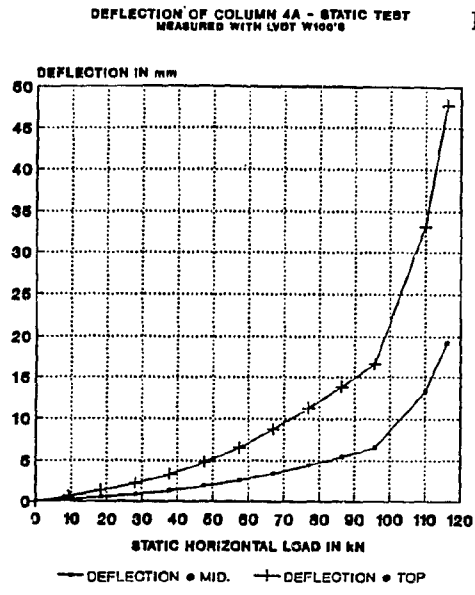

Fig. B.477: Deflection Col.4A

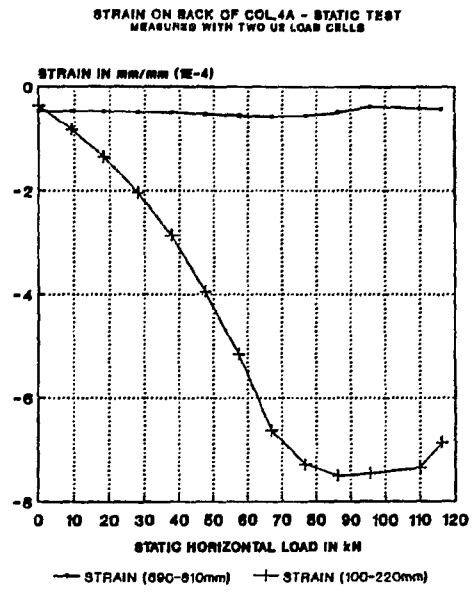

Fig. B.478: Strain Col.4A

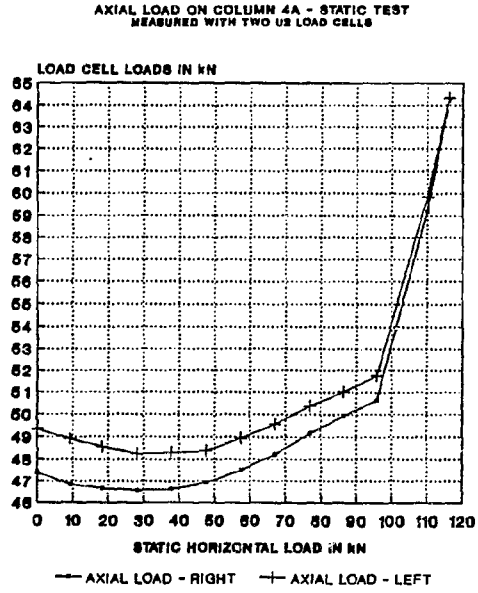

Fig. B.479: Axial load Col 4A

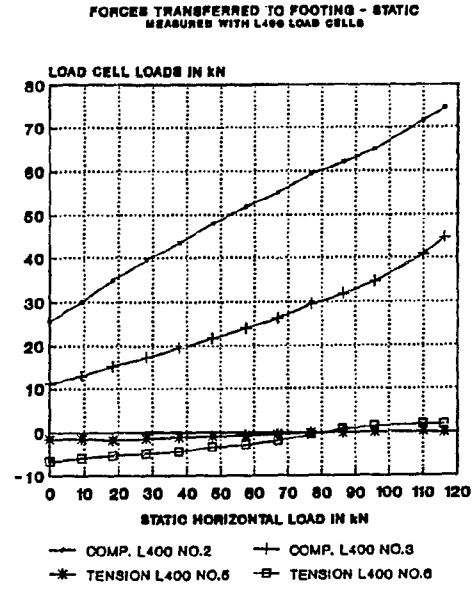

Fig. B.480: Foot.loads Col.4A

Stellenbosch University http://scholar.sun.ac.za

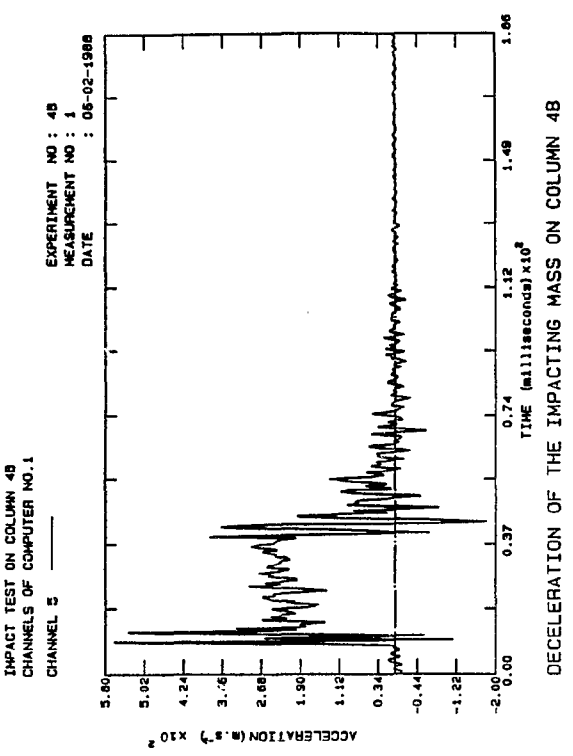

Fig. B.481: Decel. Col.4B

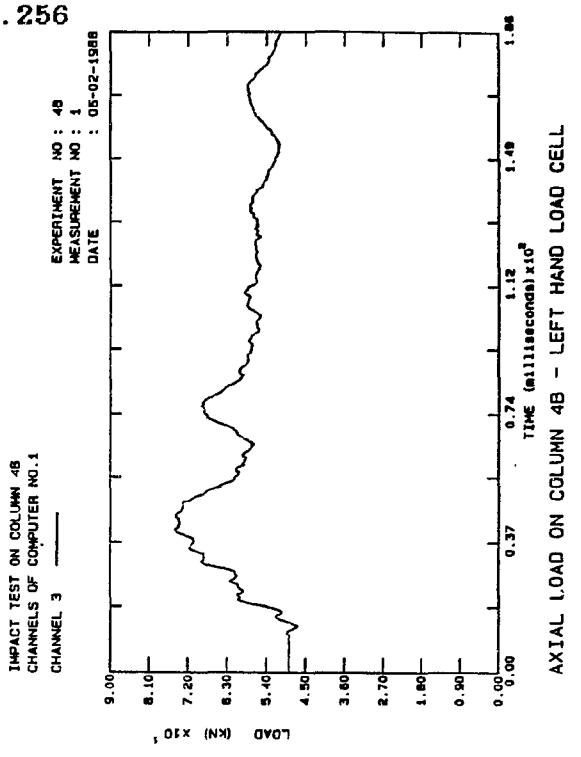

Fig. B.482: Axial load Col.4B

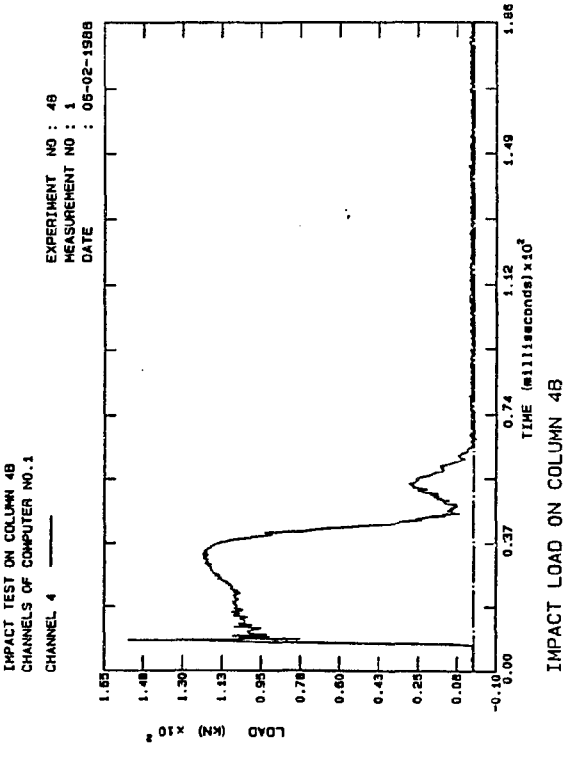

Fig. B.483: Impact Col 4B

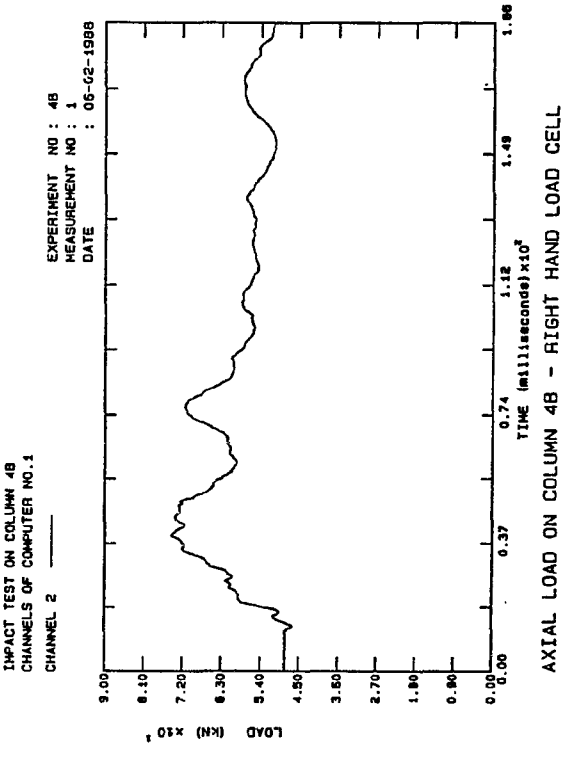

Fig. B.484: Axial load Col.4B

Stellenbosch University http://scholar.sun.ac.za

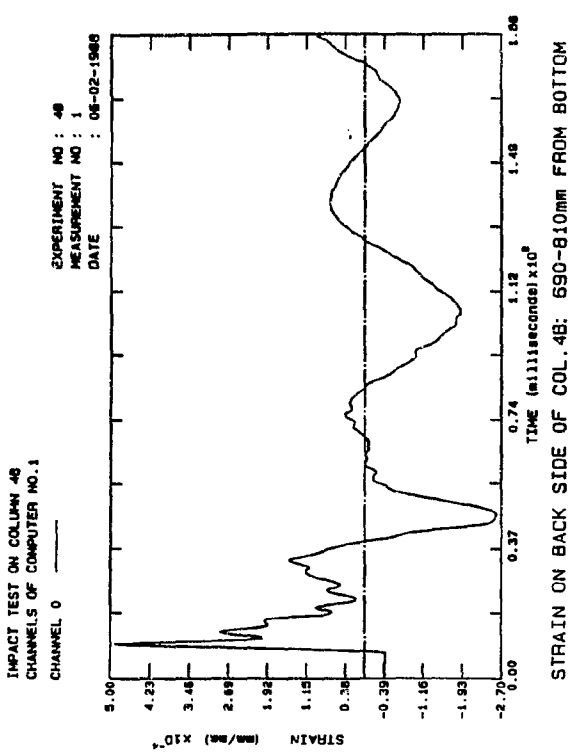

Fig. B.485: Strain Col.4B

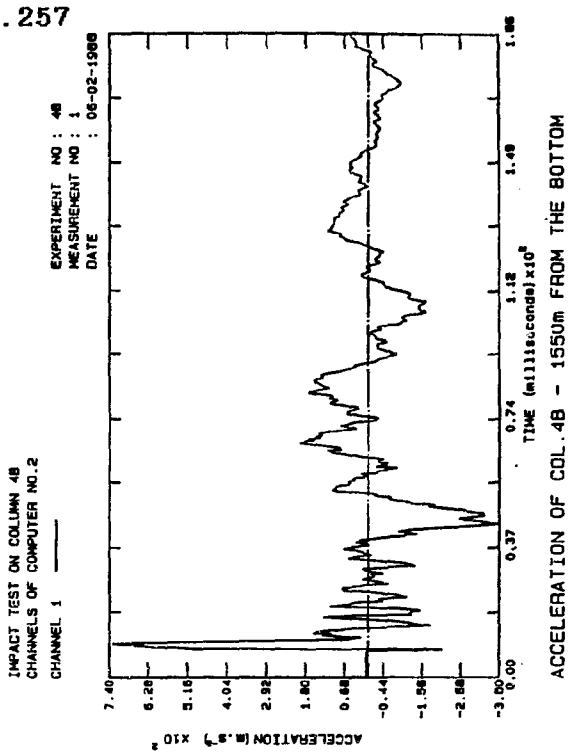

Fig. B.486: Accel. Col.4B

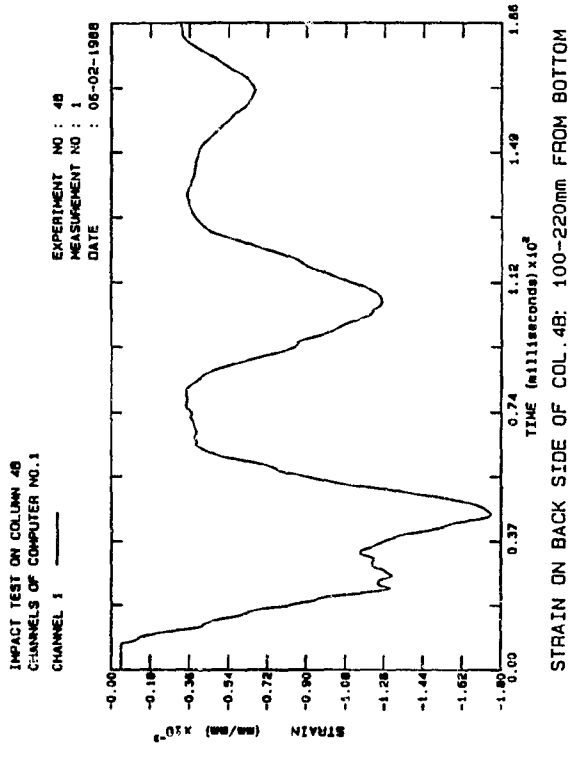

Fig. B.487: Strain Col 4B

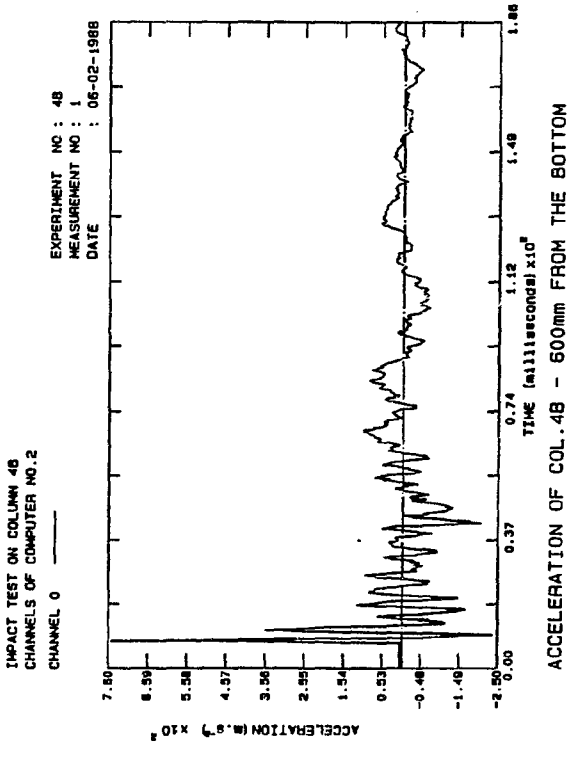

Fig. B.488: Accel. Col.4B

Stellenbosch University http://scholar.sun.ac.za

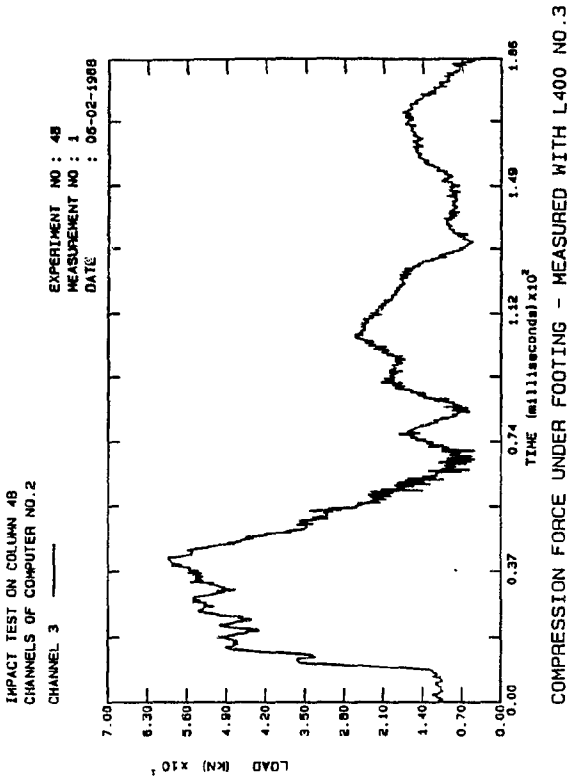

Fig. B.489: Comp. Col.4B

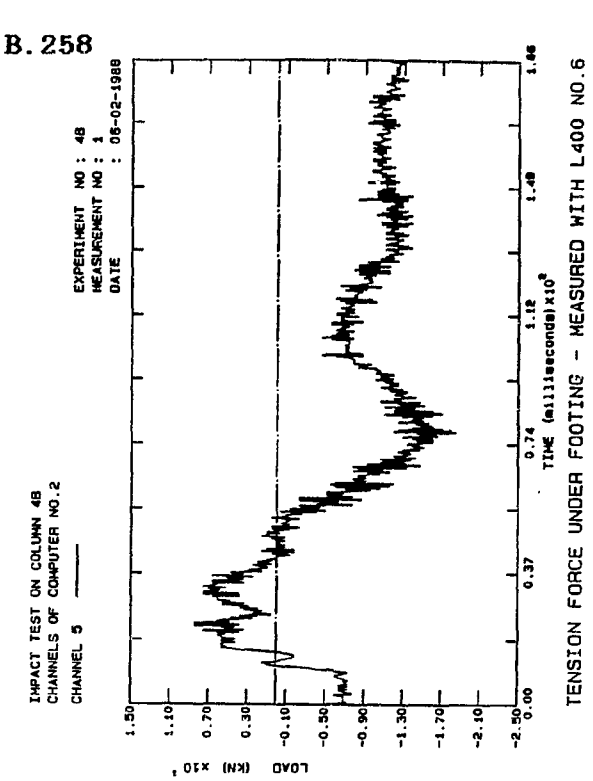

Fig. B.490: Tension Col.4B

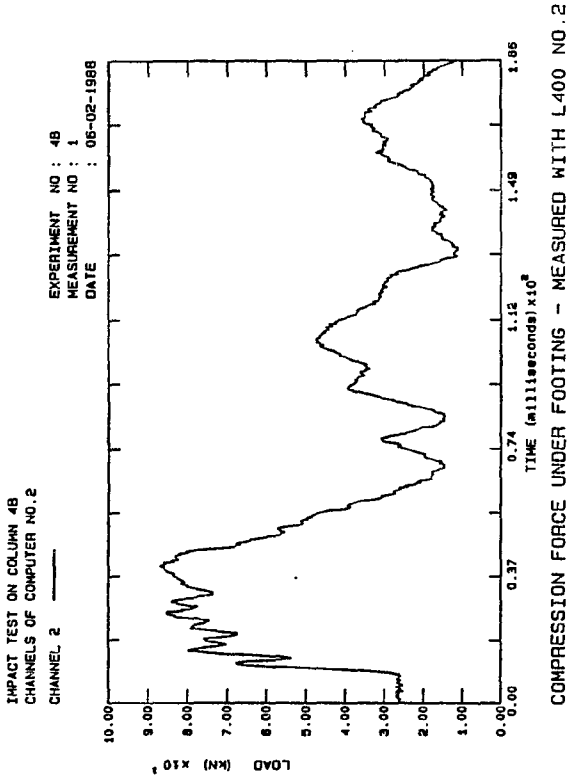

Fig. B.491: Comp. Col 4B

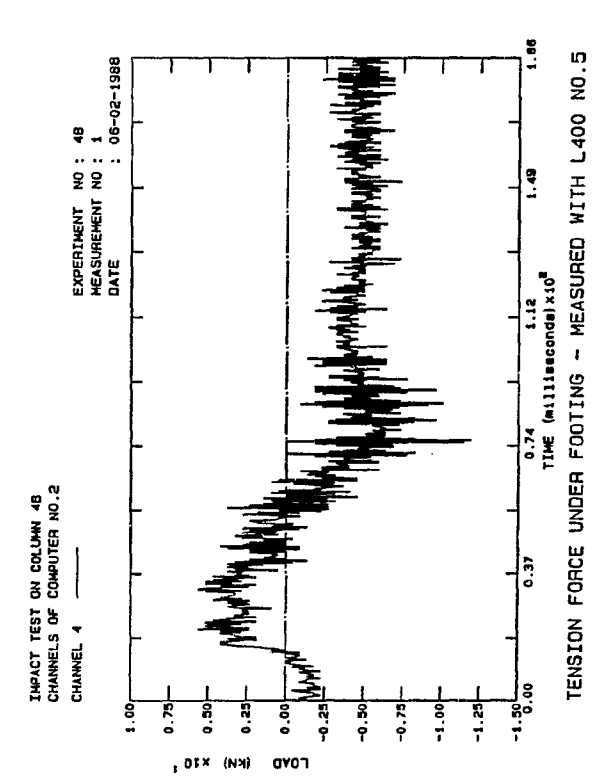

Fig. B.492: Tension Col.4B

Stellenbosch University http://scholar.sun.ac.za

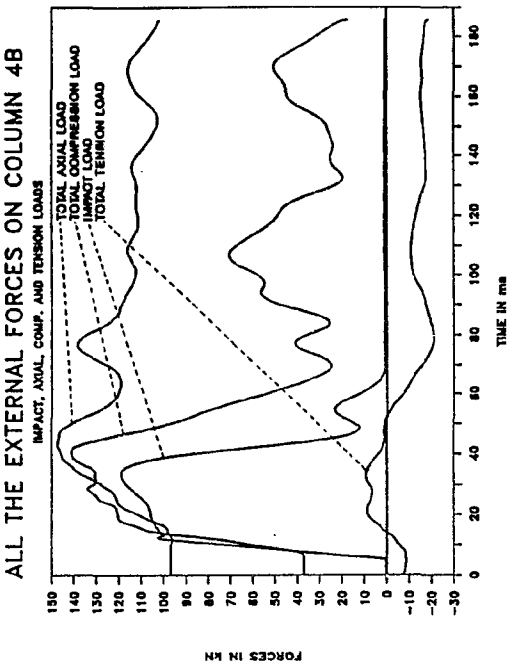

Fig. B.493: Ext. Loads Col.4B

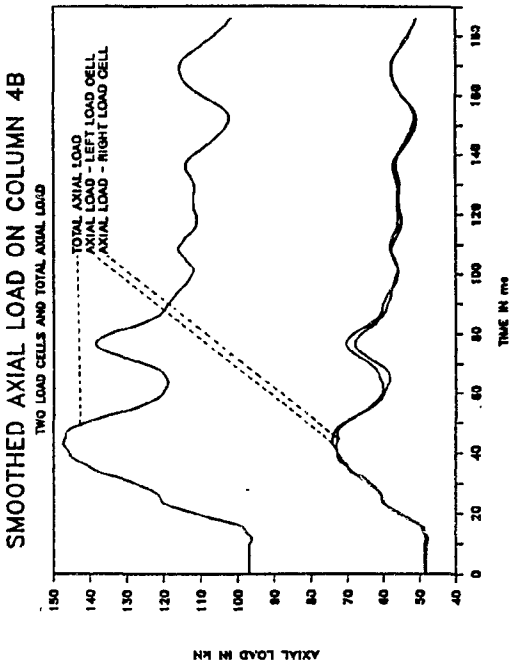

Fig. B.494: Smo. Axial Col.4B

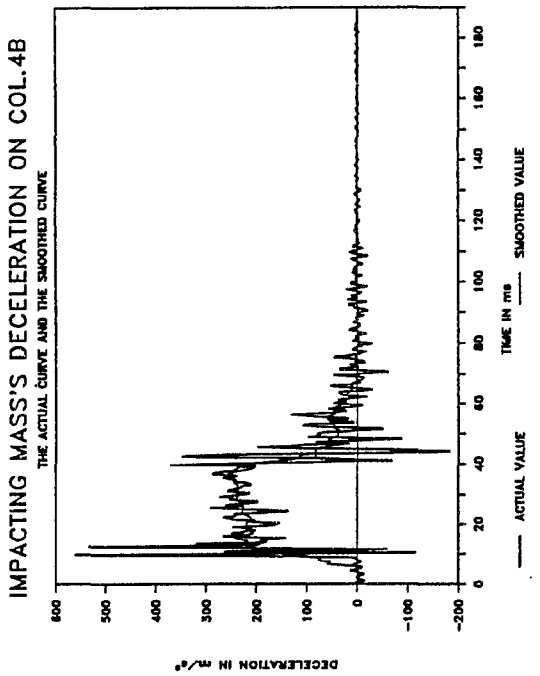

Fig. B.495: Smo.Decel. Col 4B

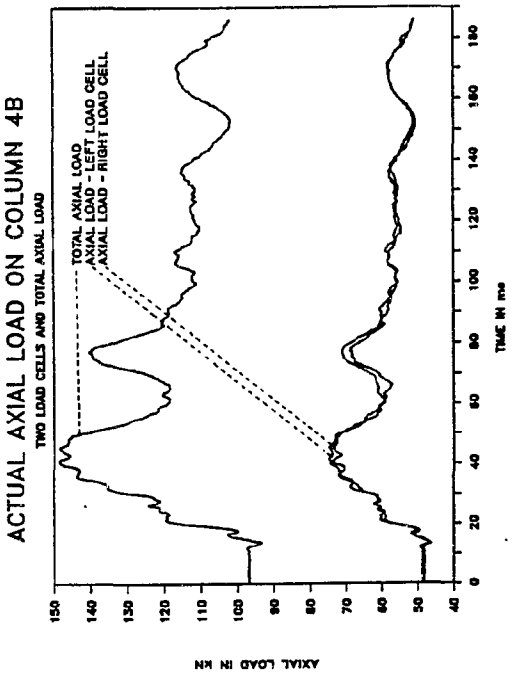

Fig. B.496: Axial loads Col.4B

Stellenbosch University http://scholar.sun.ac.za

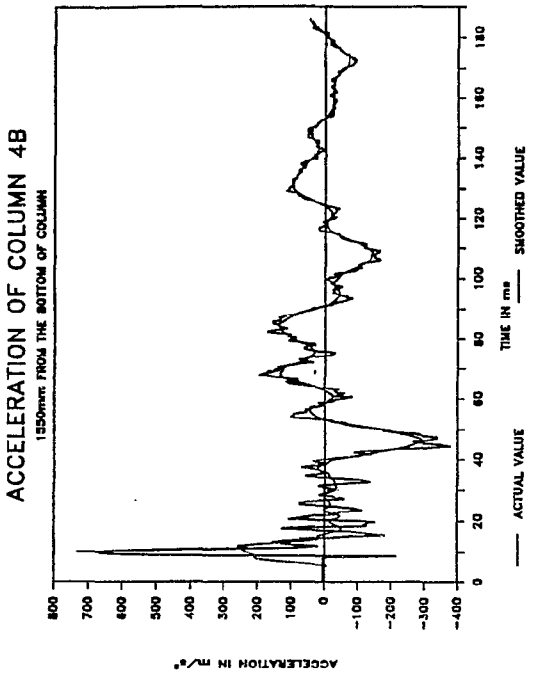

Fig. B.497: Smo.Accel. Col.4B

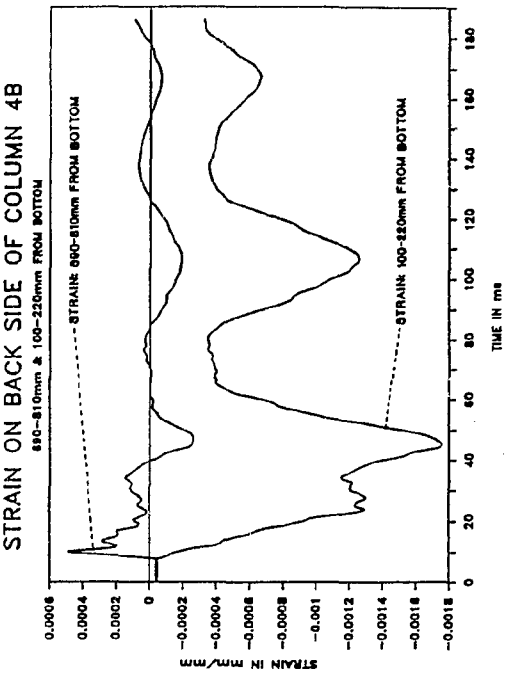

Fig. B.498: Strain Col.4B

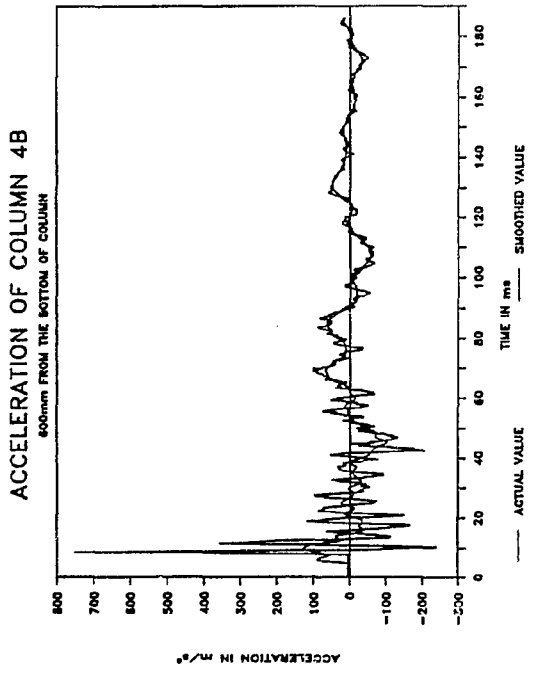

Fig. B.499: Smo.Accel. Col 4B

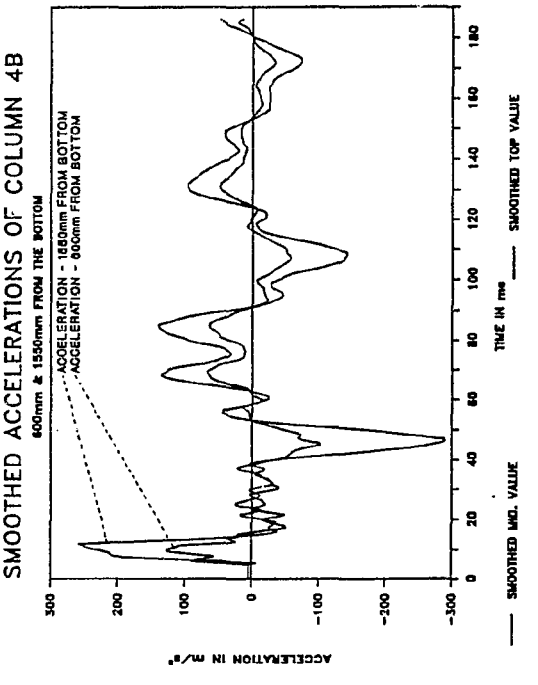

Fig. B.500: Smo. Accel. Col.4B

Stellenbosch University http://scholar.sun.ac.za

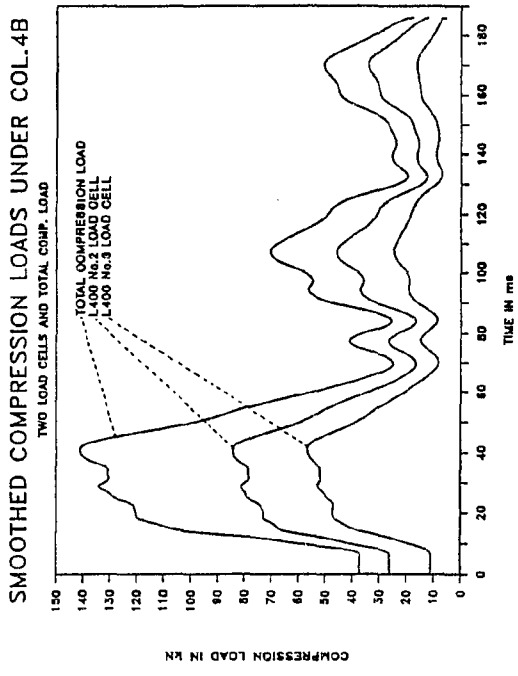

Fig. B.501: Smo. Comp. Col.4B

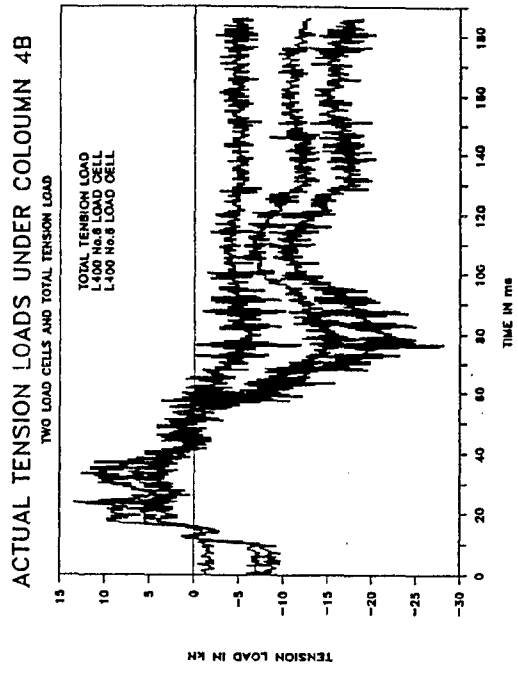

Fig. B.502: Smo. Tens. Col.4B

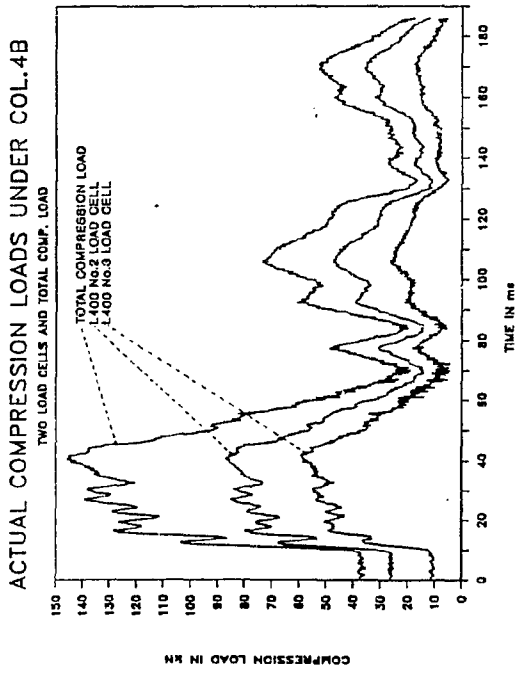

Fig. B.503: Comp. load Col 4B

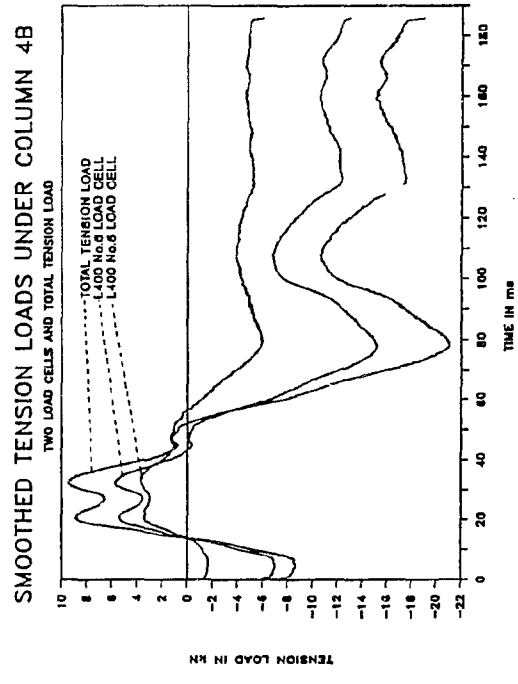

Fig. B.504: Tens. loads Col.4B

Stellenbosch University http://scholar.sun.ac.za

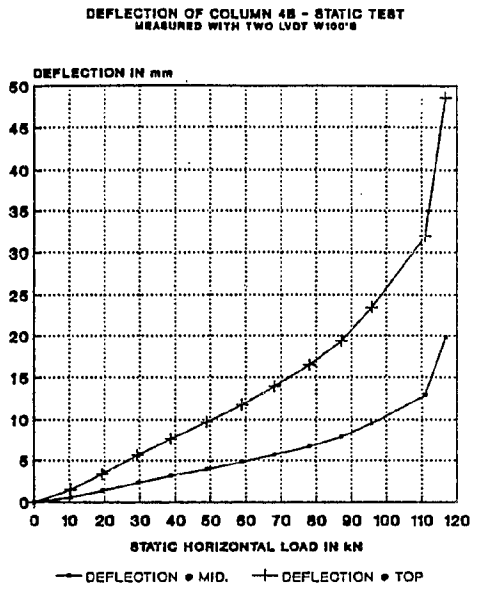

Fig. B.505: Deflection Col.4B

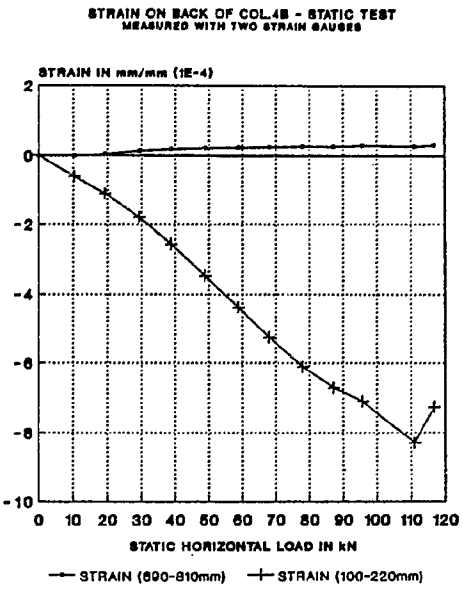

Fig. B.506: Strain Col.4B

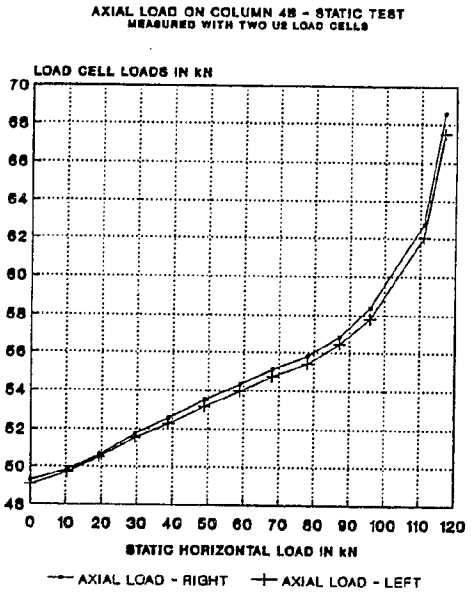

Fig. B.507: Axial load Col 4B

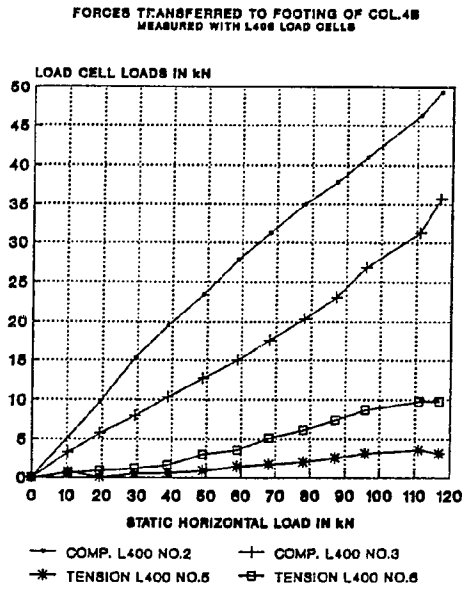

Fig. B.508: Foot.loads Col.4B

Stellenbosch University http://scholar.sun.ac.za

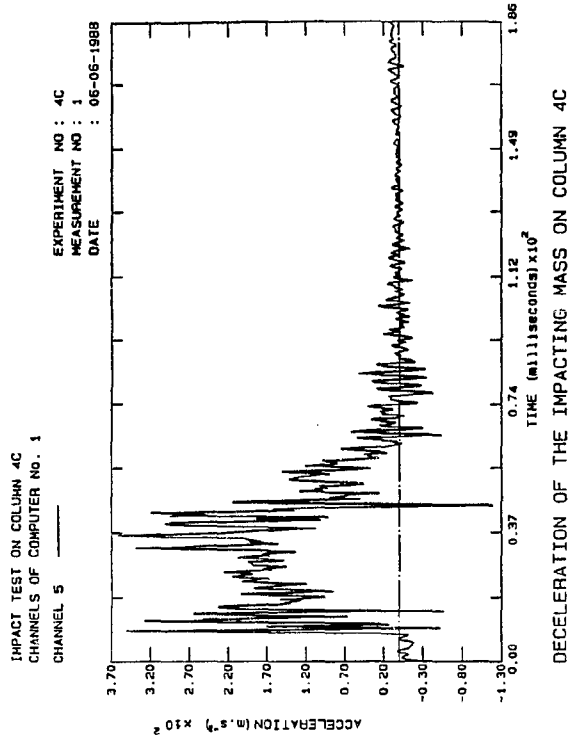

Fig. B.509: Decel. Col.4C

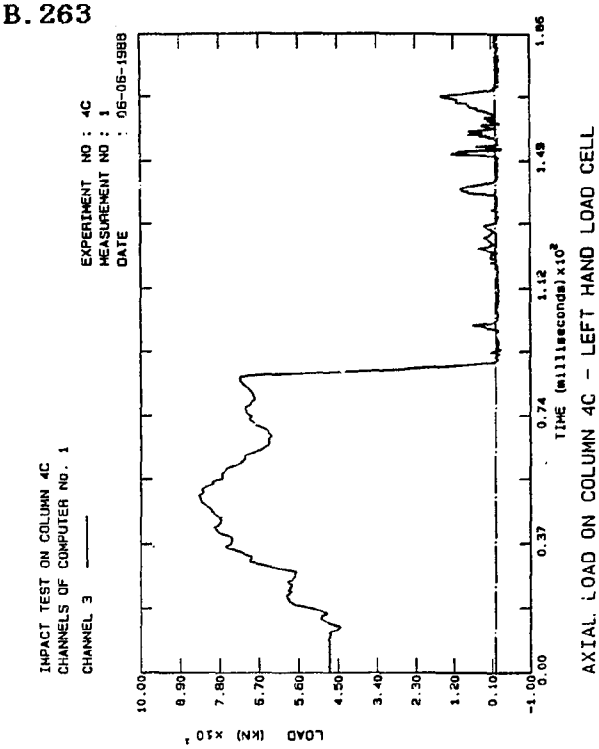

Fig. B.510: Axial load Col.4C

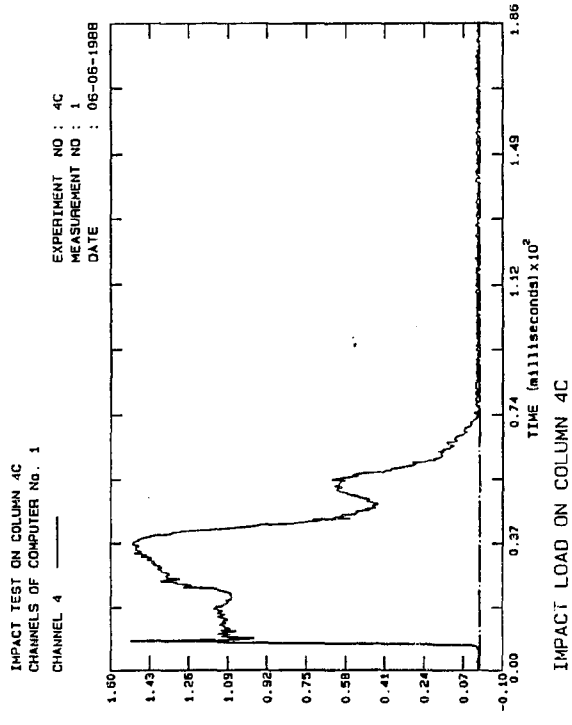

Fig. B.511: Impact Col 4C

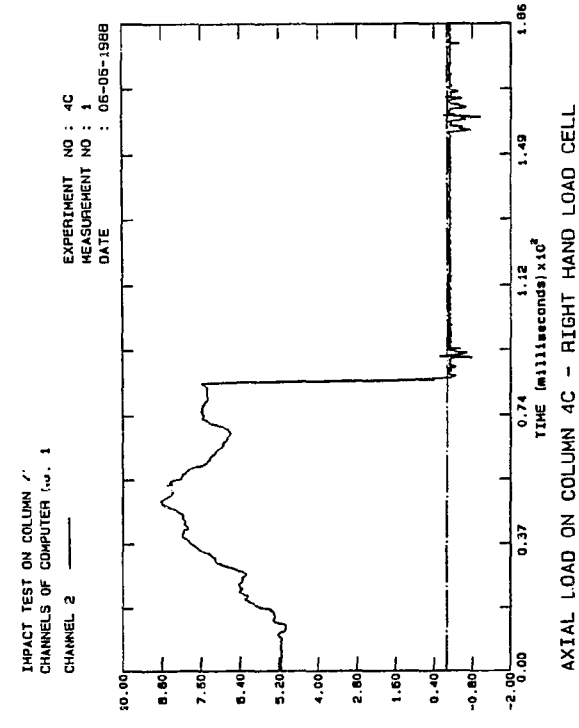

Fig. B.512: Axial load Col.4C

Stellenbosch University http://scholar.sun.ac.za

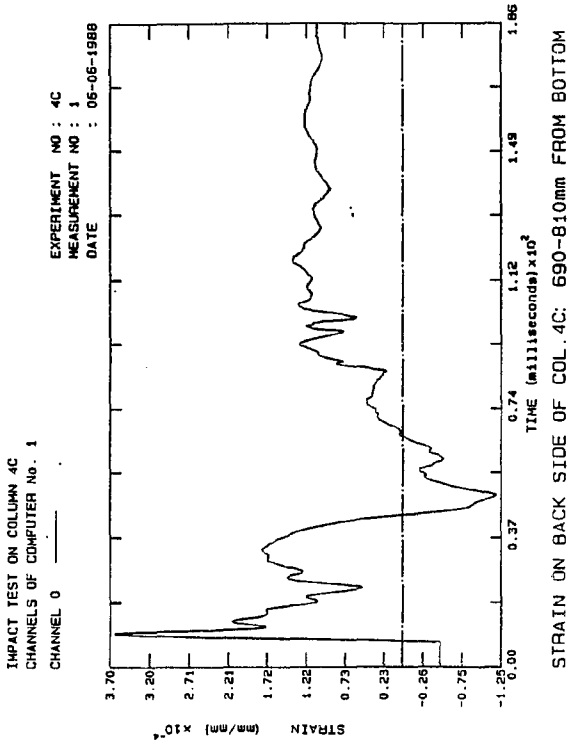

Fig. B.513: Strain Col.4C

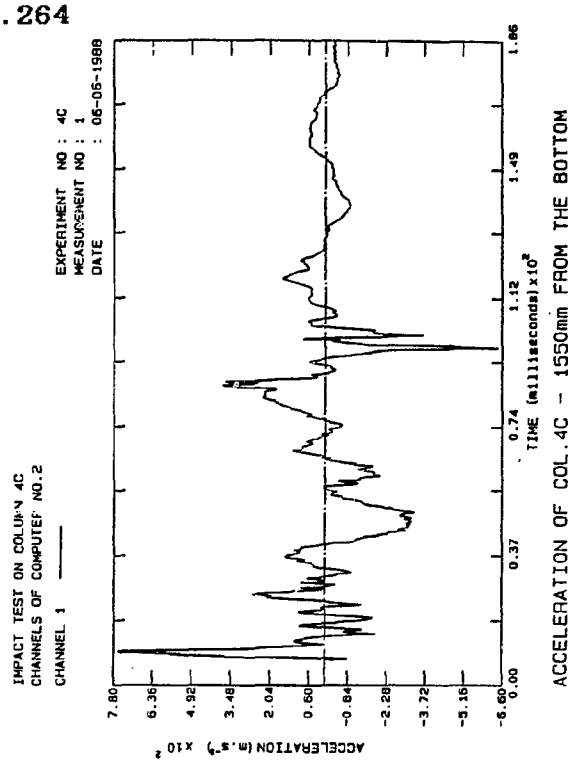

Fig. B.514: Accel. Col.4C

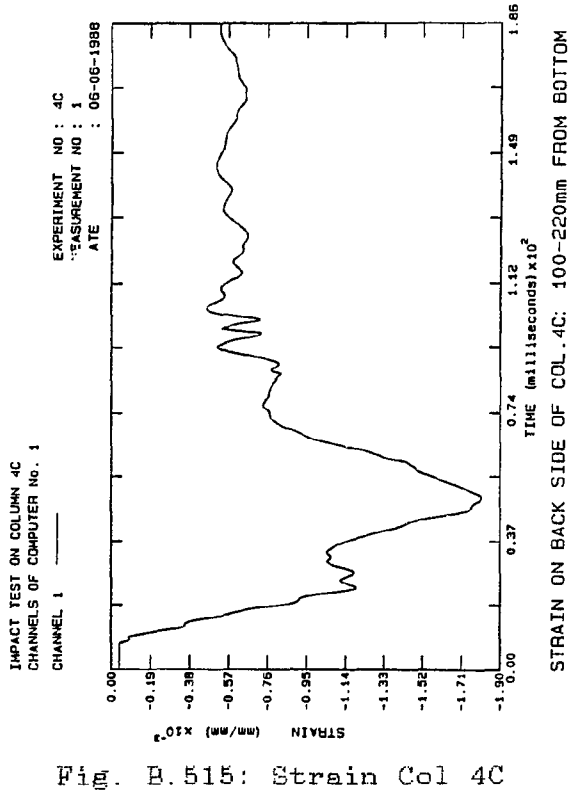

Fig. B.515: Strain Col 4C

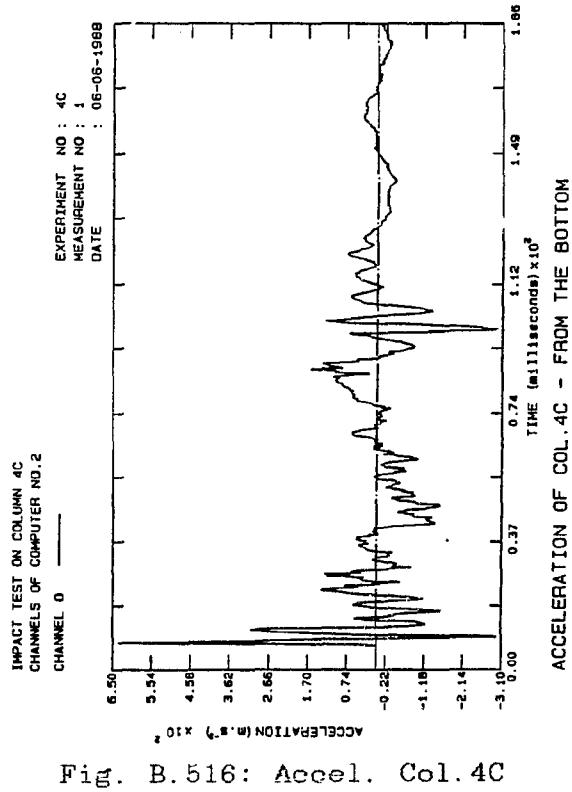

Fig. B.516: Accel. Col.4C

Stellenbosch University http://scholar.sun.ac.za

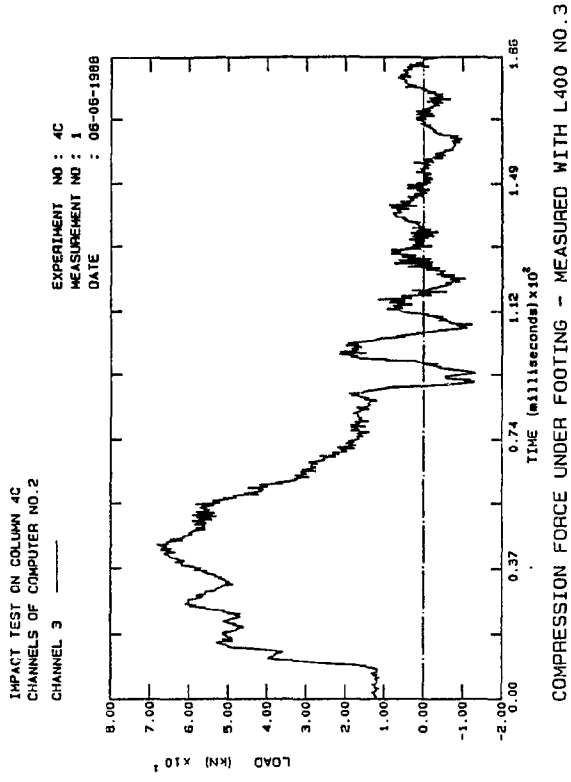

Fig. B.517: Comp. Col.4C

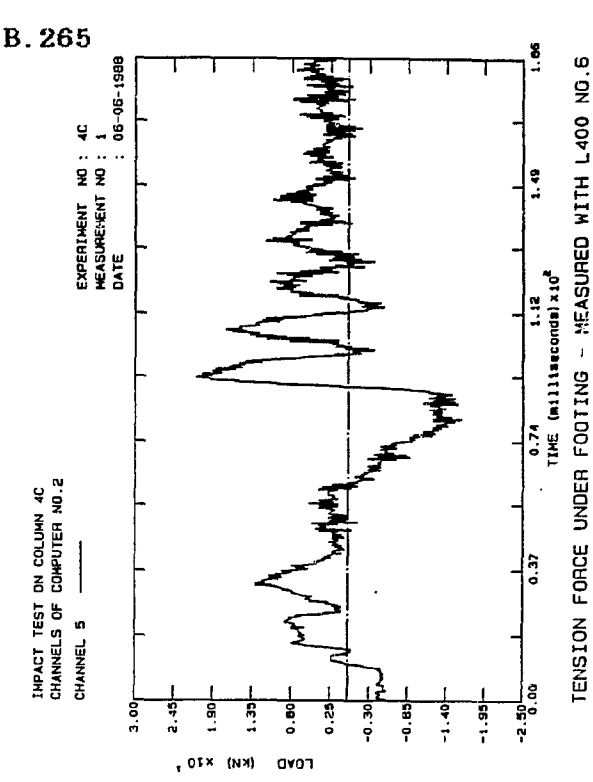

Fig. B.518: Tension Col.4C

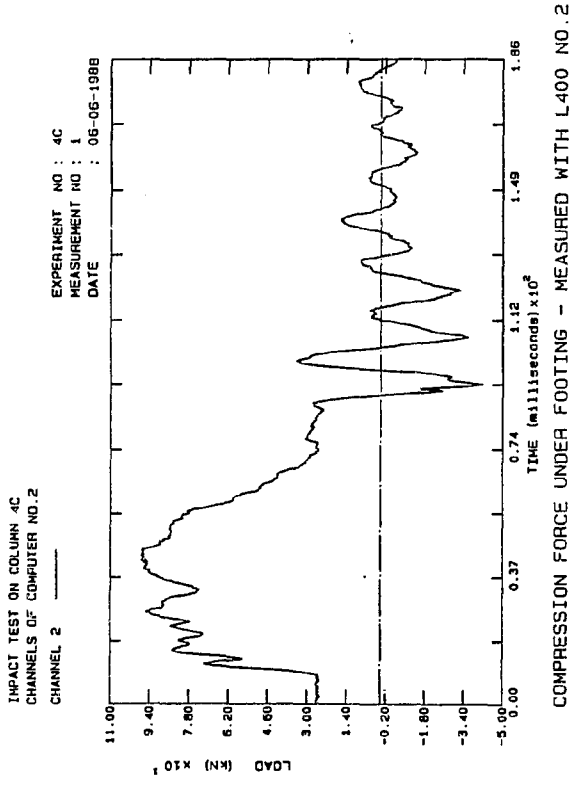

Fig. B.519: Comp. Col 4C

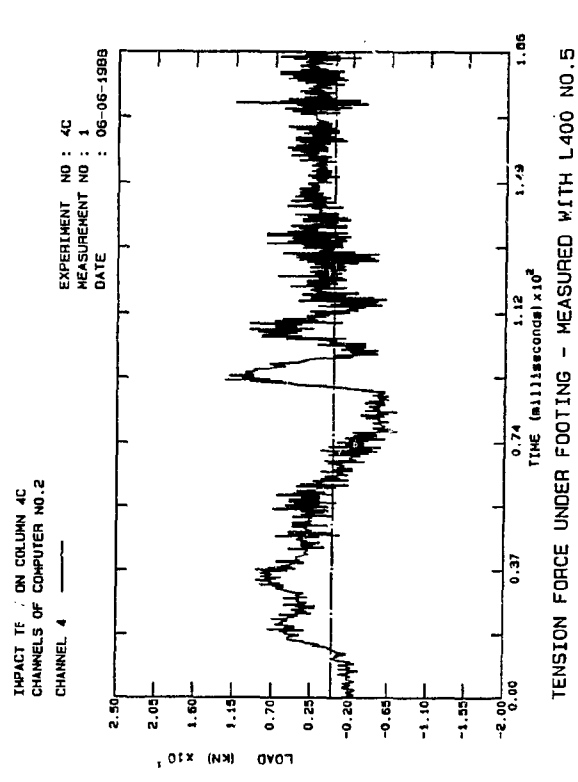

Fig. B.520: Tension Col.4C

Stellenbosch University http://scholar.sun.ac.za

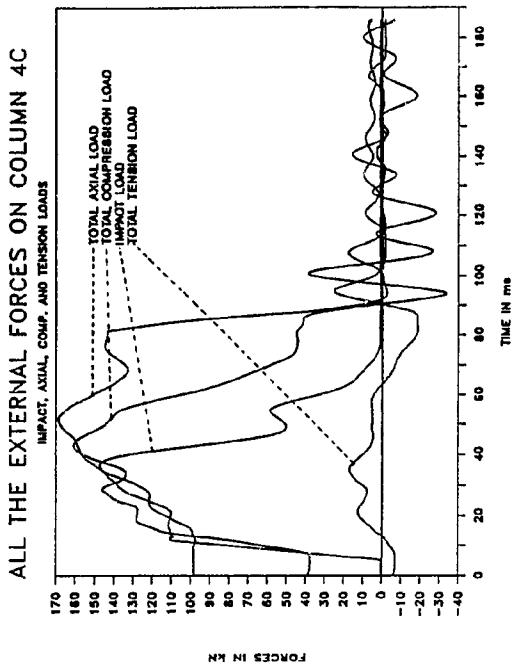

Fig. B.521: Ext. Loads Col.4C

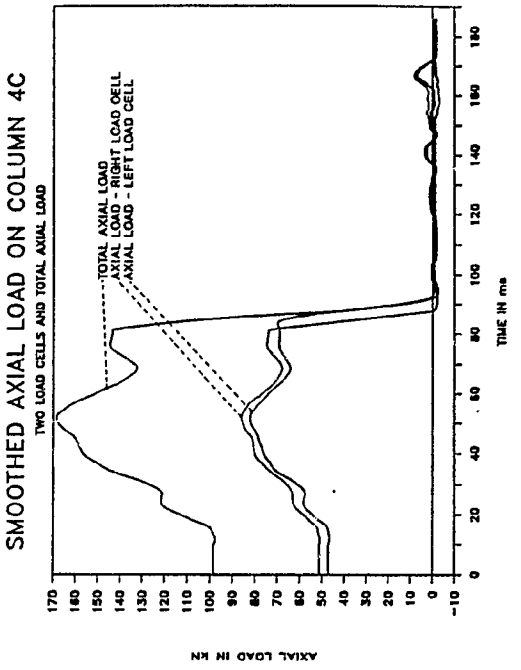

Fig. B.522: Smo. Axial Col.4C

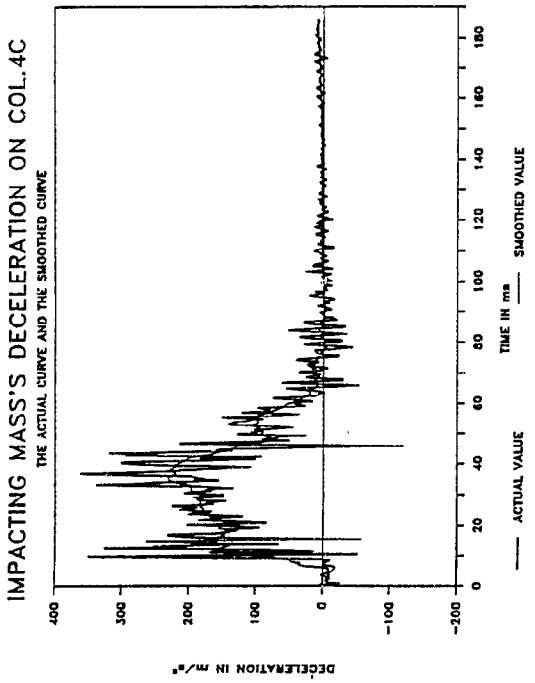

Fig. B.523: Smo.Decel. Col 4C

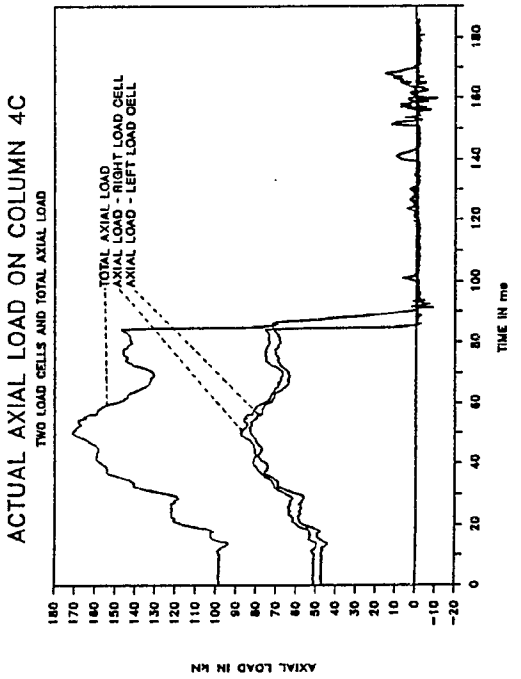

Fig. B.524: Axial loads Col.4C

Stellenbosch University http://scholar.sun.ac.za

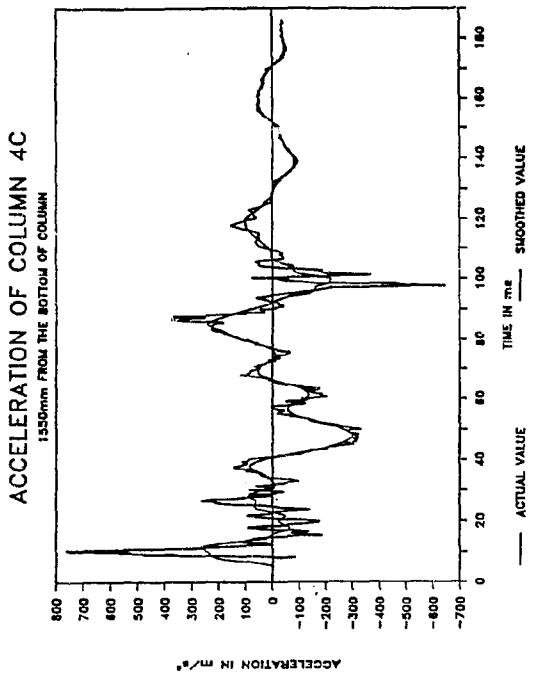

Fig. B.525: Smo.Accel. Col.4C

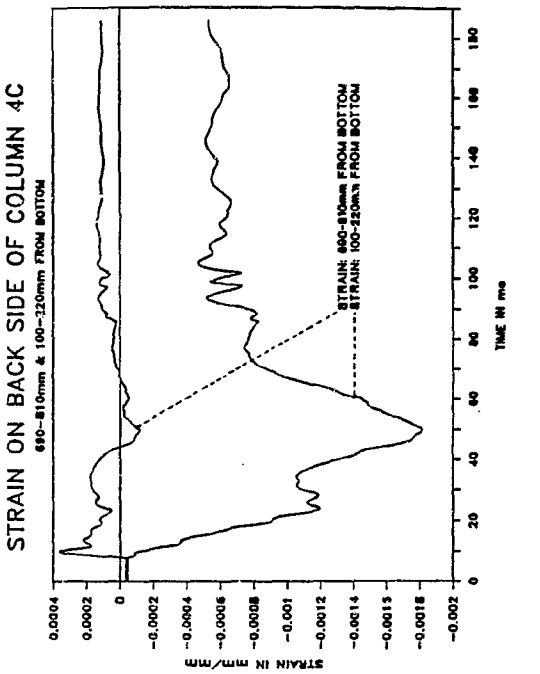

Fig. B.526: Strain Col.4C

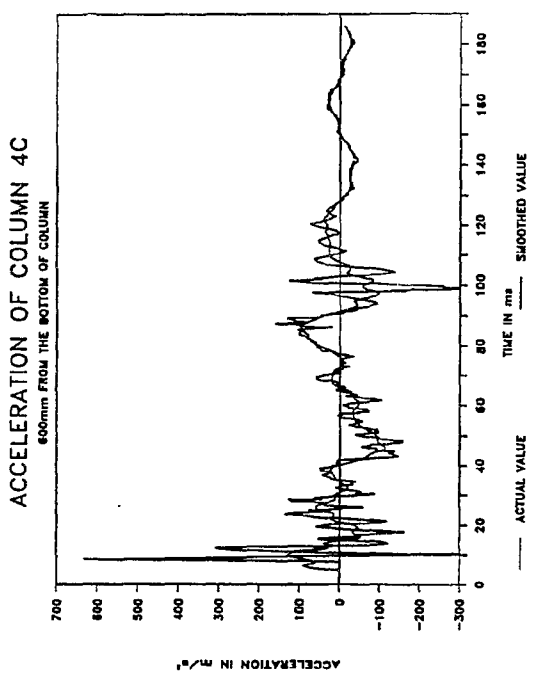

Fig. B.527: Smo.Accel. Col 4C

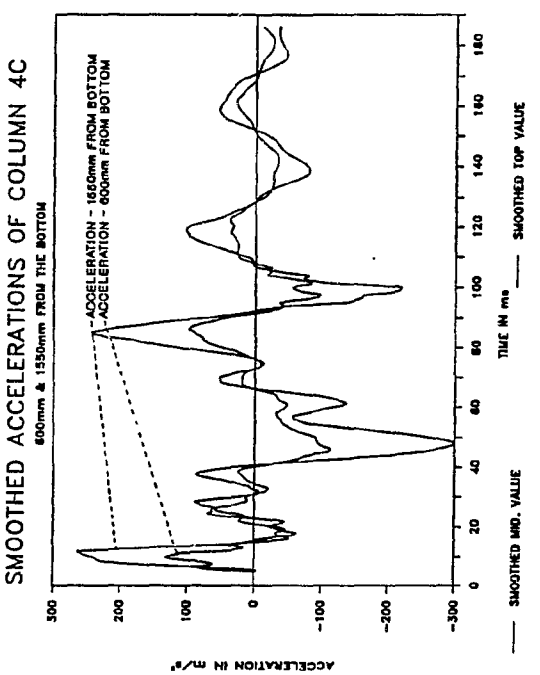

Fig. B.528: Smo. Accel. Col.4C

Stellenbosch University http://scholar.sun.ac.za

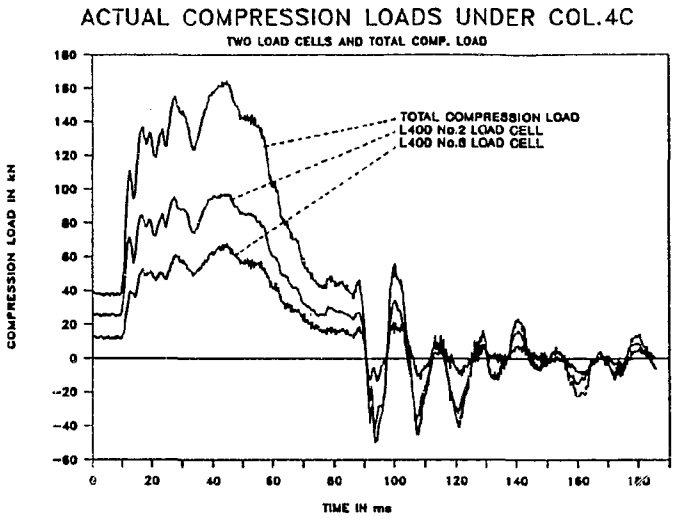

Fig. B.531: Comp. load Col 4C

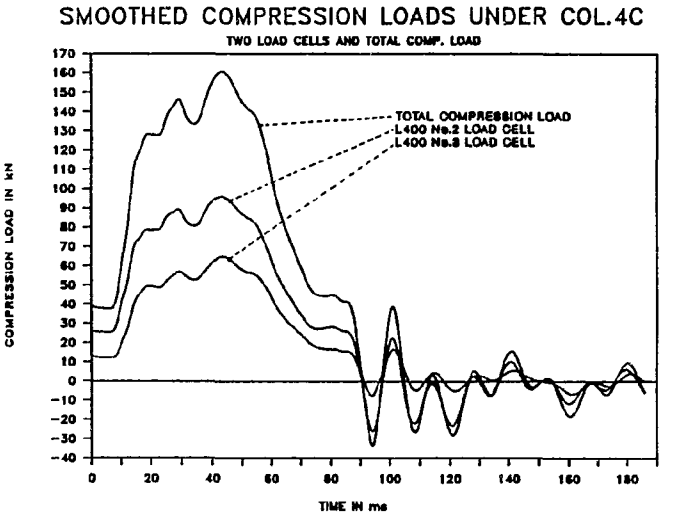

Fig. B.529: Smo. Comp. Col.4C

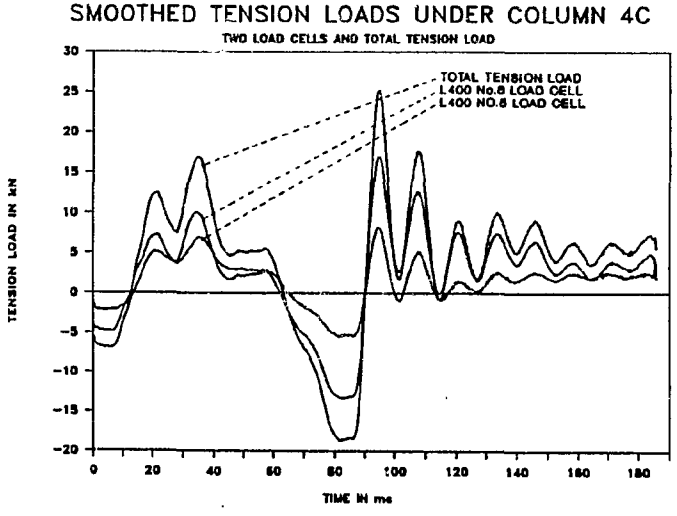

Fig. B.532: Tens. loads Col.4C

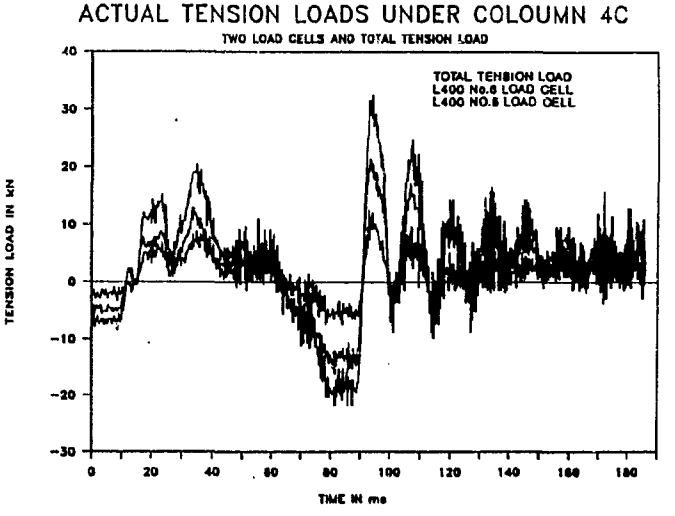

Fig. B.530: Smo. Tens. Col.4C

Stellenbosch University http://scholar.sun.ac.za

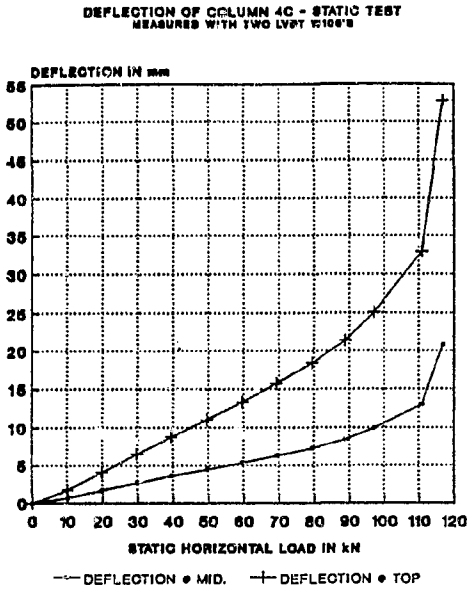

Fig. B.533: Deflection Col.4C

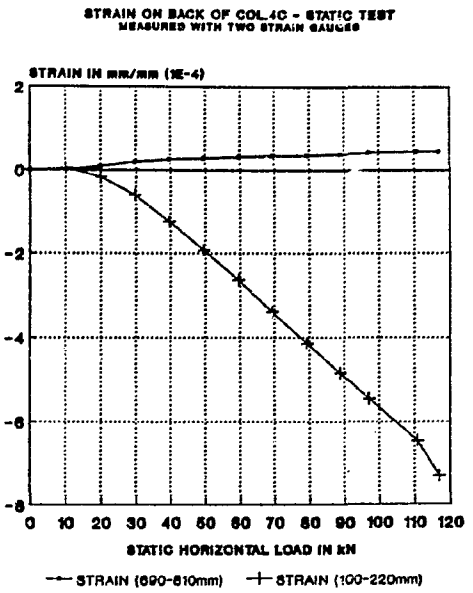

Fig. B.534: Strain Col.4C

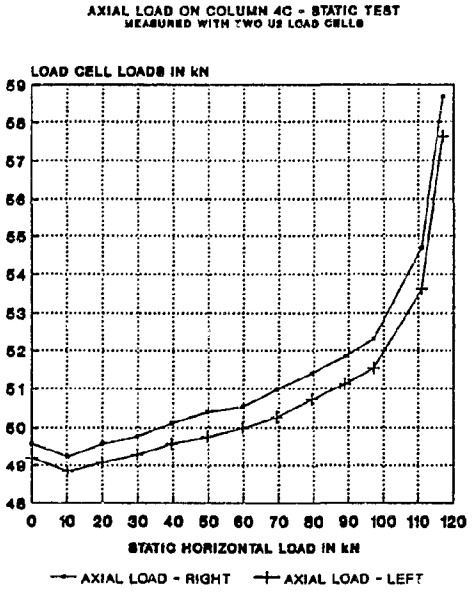

Fig. B.535: Axial load Col 4C

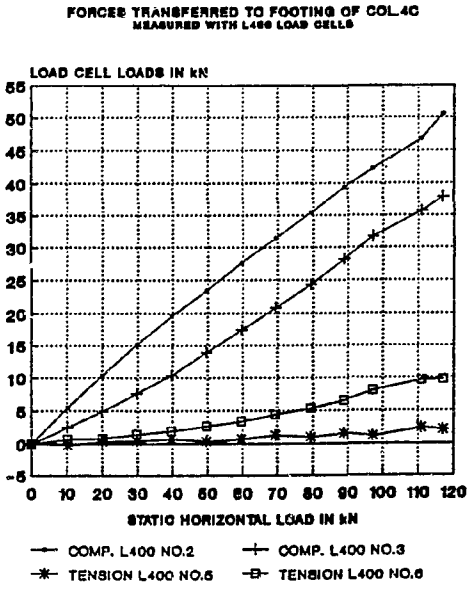

Fig. B.536: Foot.loads Col.4C

Stellenbosch University http://scholar.sun.ac.za

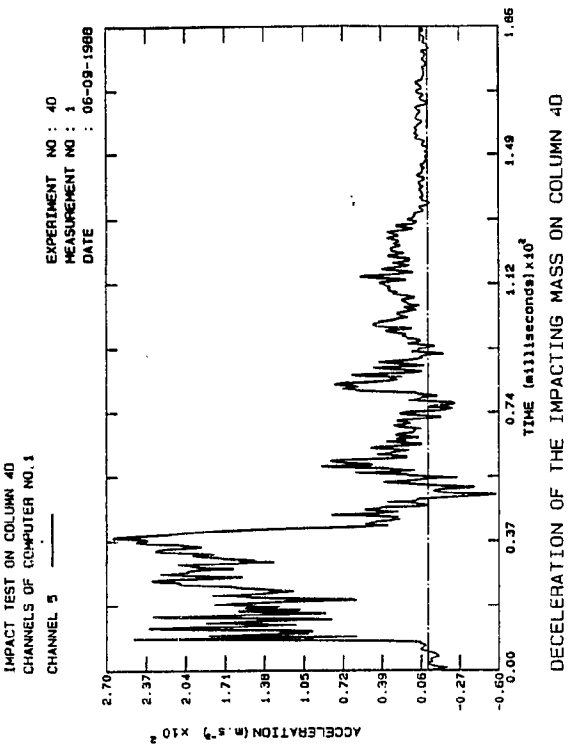

Fig. B.537: Decel. Col.4D

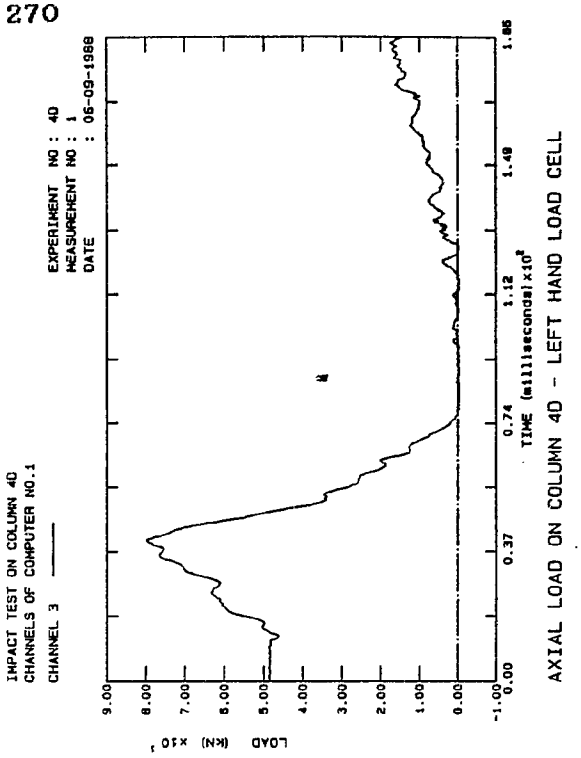

Fig. B.538: Axial load Col.4D

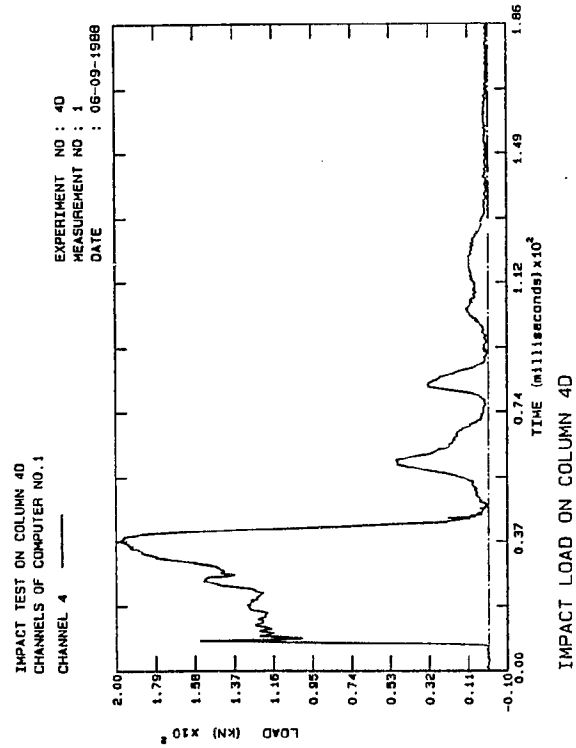

Fig. B.539: Impact Col 4D

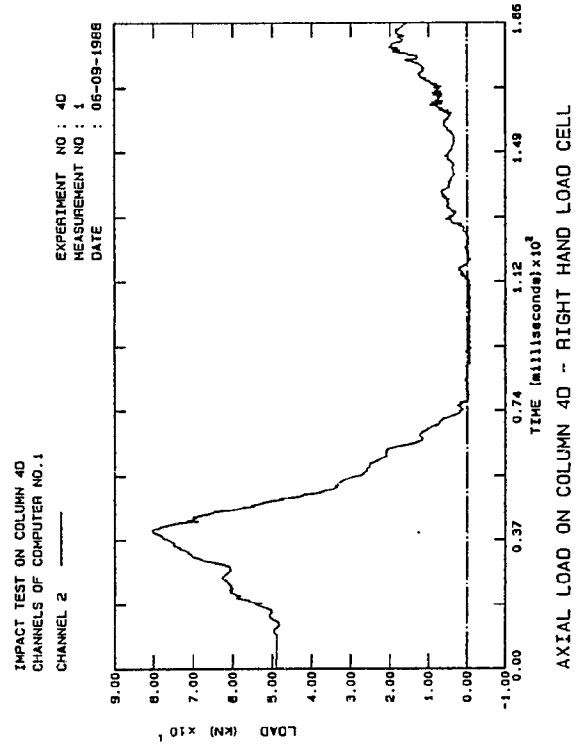

Fig. B.540: Axial load Col.4D

Stellenbosch University http://scholar.sun.ac.za

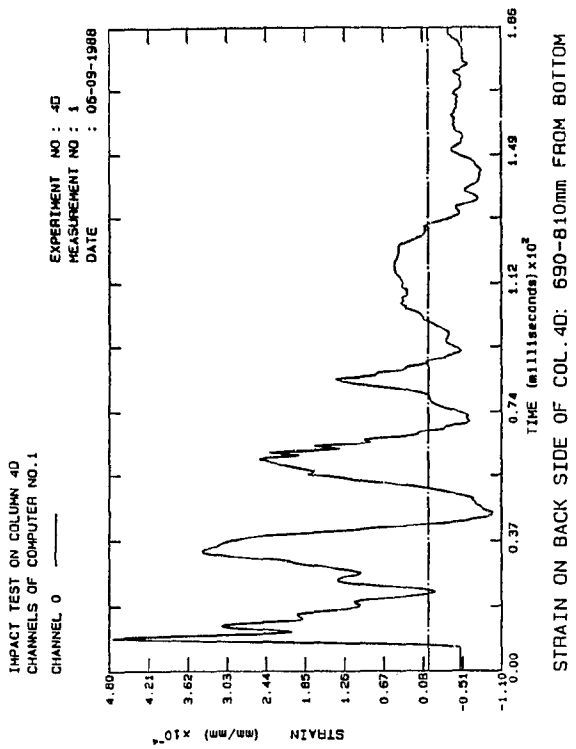

Fig. B.541: Strain Col.4D

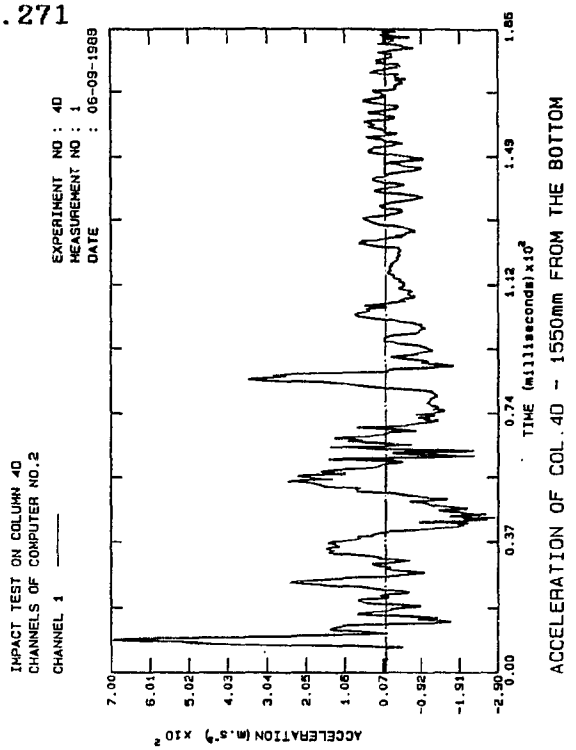

Fig. B.542: Accel. Col.4D

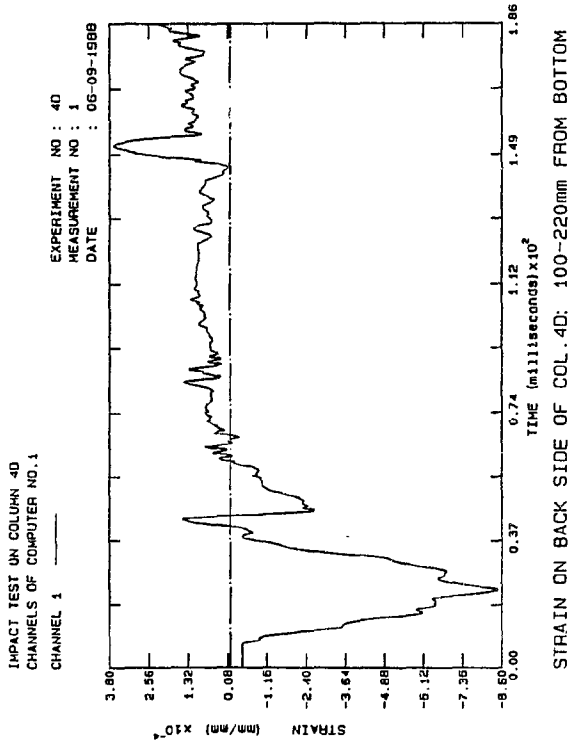

Fig. B.543: Strain Col 4D

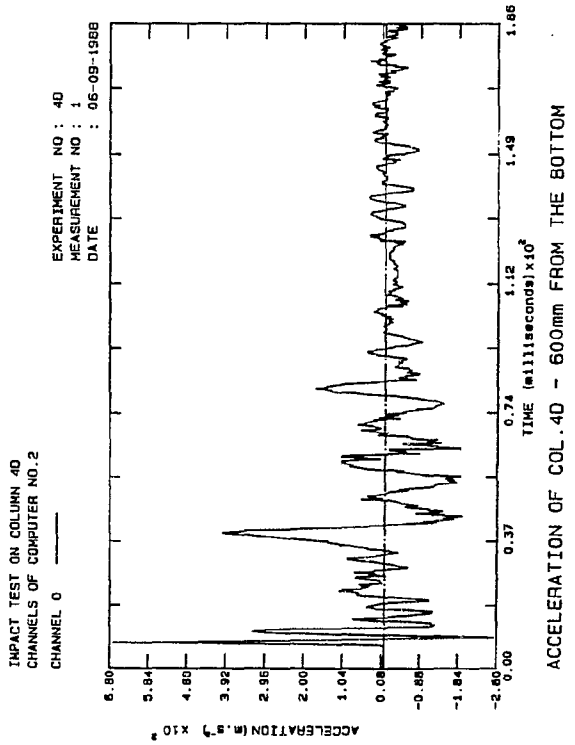

Fig. B.544: Accel. Col.4D

Stellenbosch University http://scholar.sun.ac.za

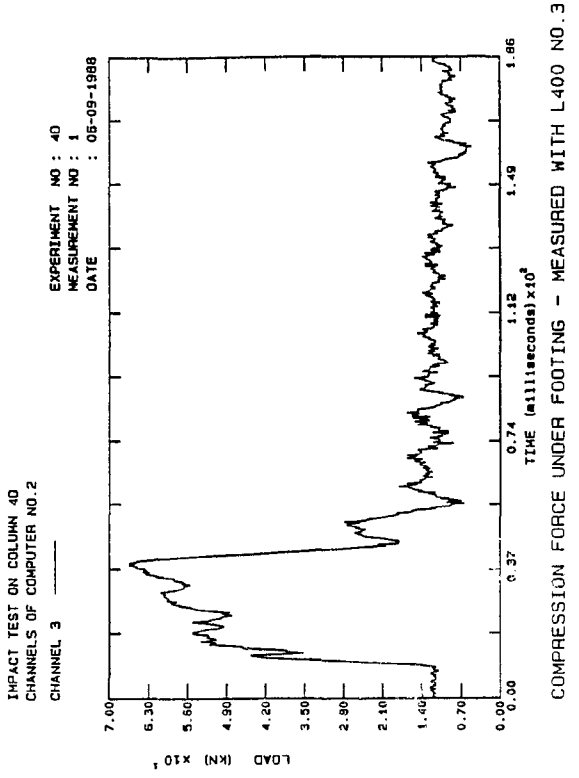

Fig. B.545: Comp. Col.4D

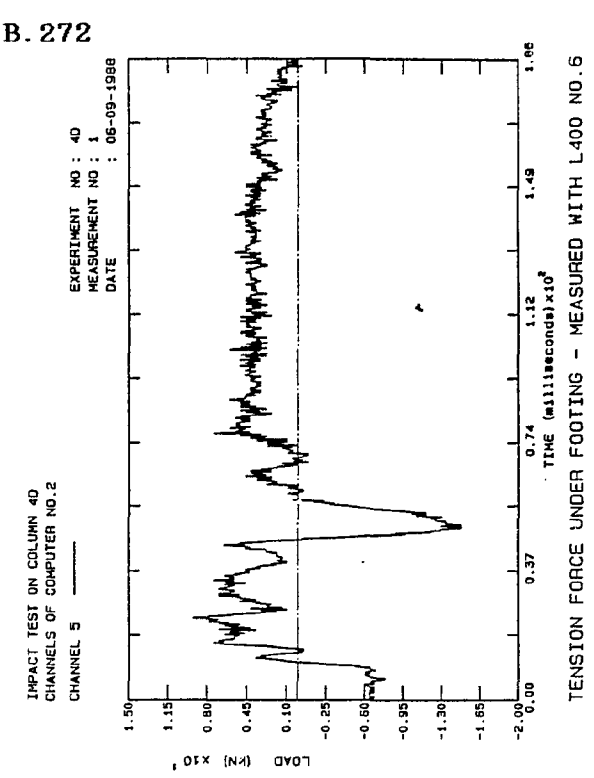

Fig. B.546: Tension Col.4D

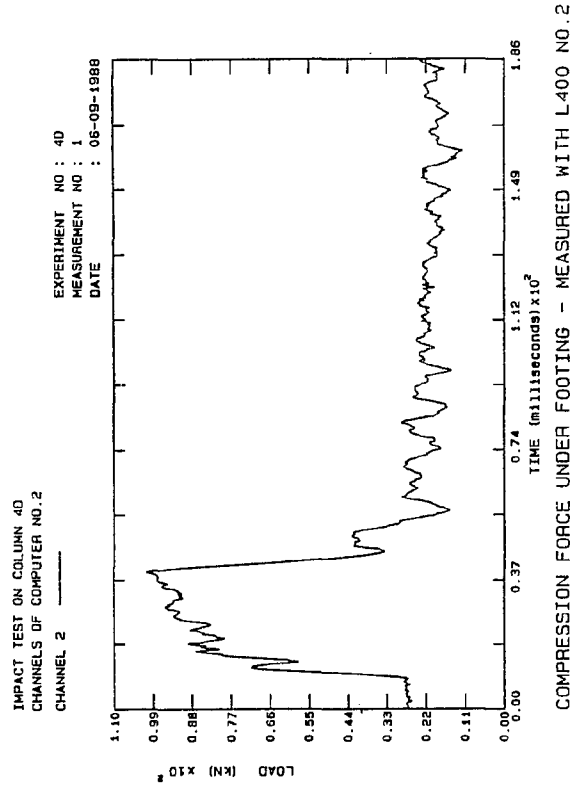

Fig. B.547: Comp. Col 4D

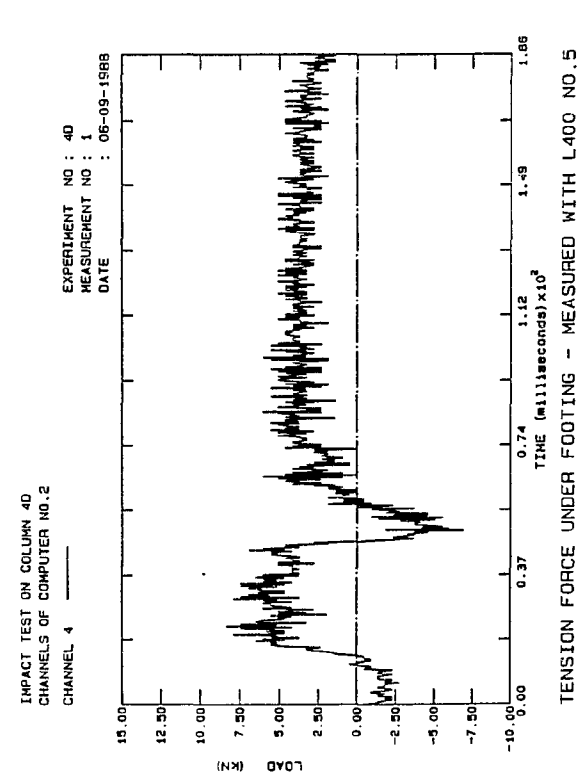

Fig. B.548: Tension Col.4D

Stellenbosch University http://scholar.sun.ac.za

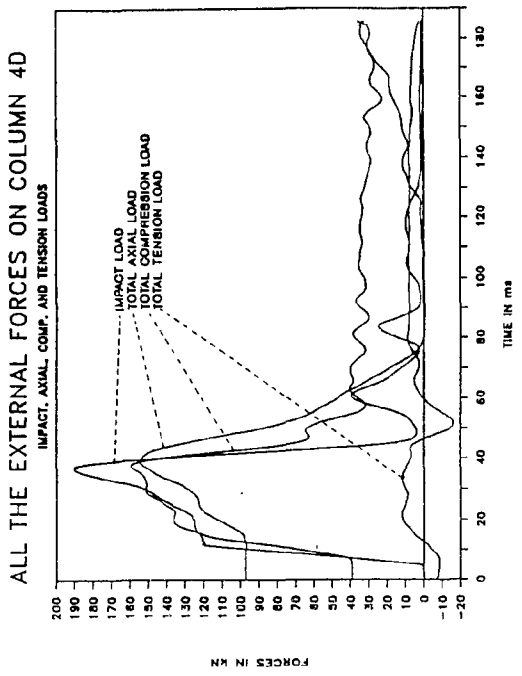

Fig. B.549: Ext. Loads Col.4D

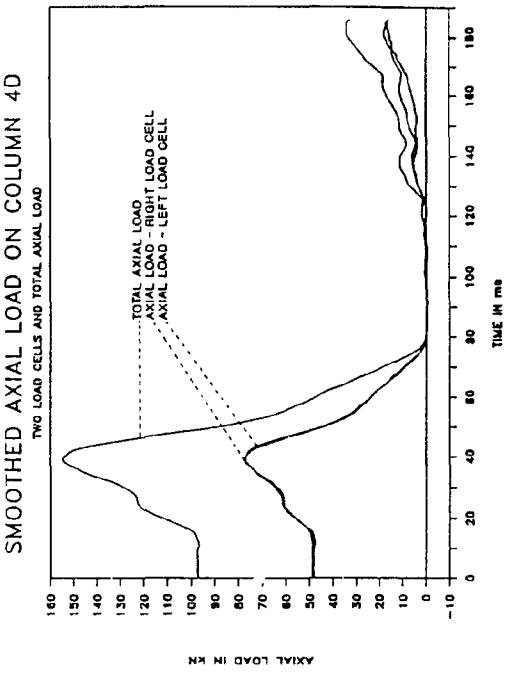

Fig. B.550: Smo. Axial Col.4D

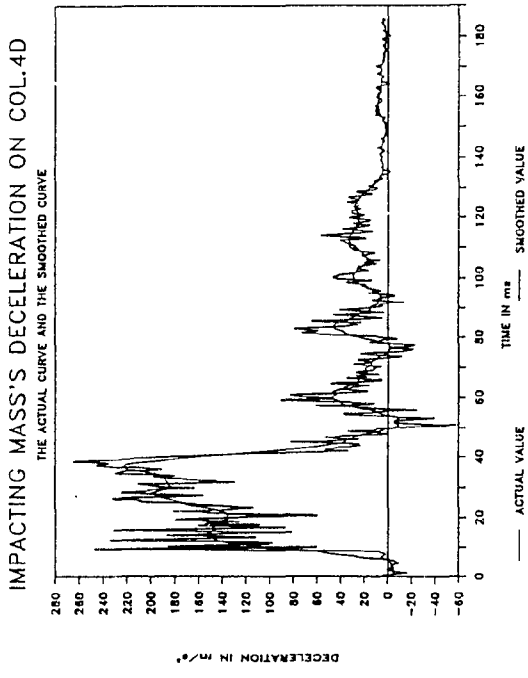

Fig. B.551: Smo.Decel. Col 4D

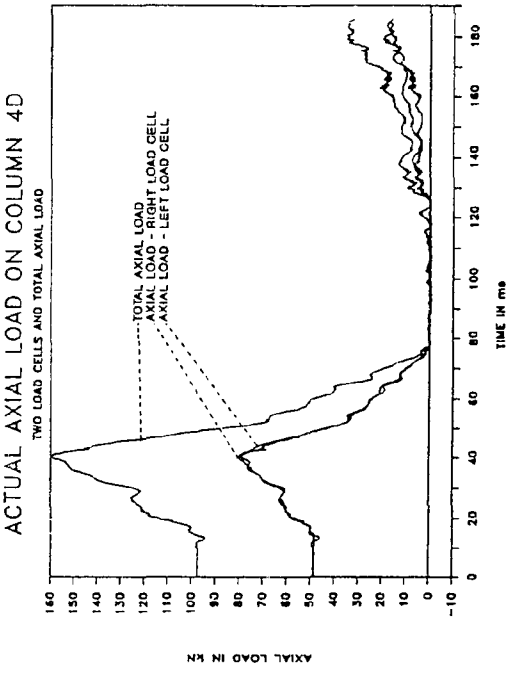

Fig. B.552: Axial loads Col.4D

Stellenbosch University http://scholar.sun.ac.za

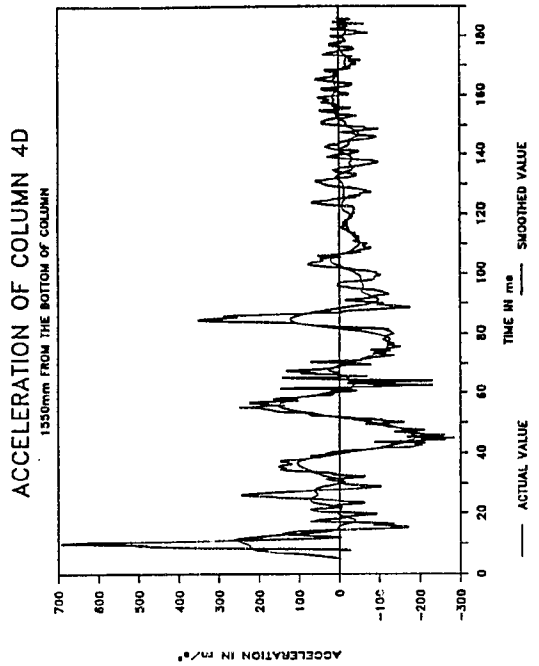

Fig. B.553: Smo.Accel. Col.4D

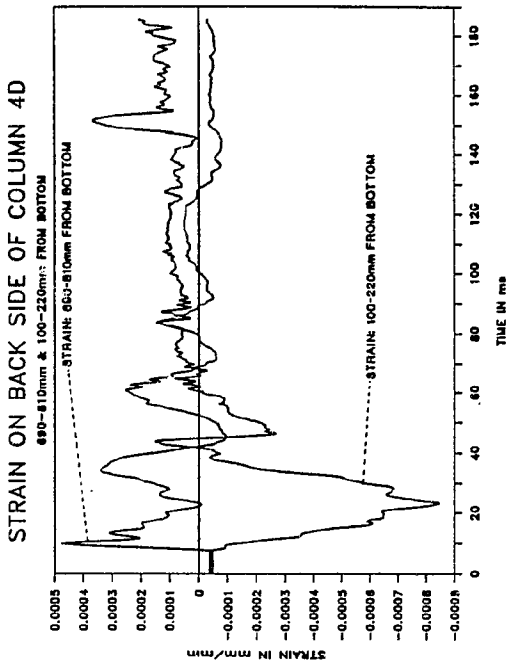

Fig. B.554: Strain Col.4D

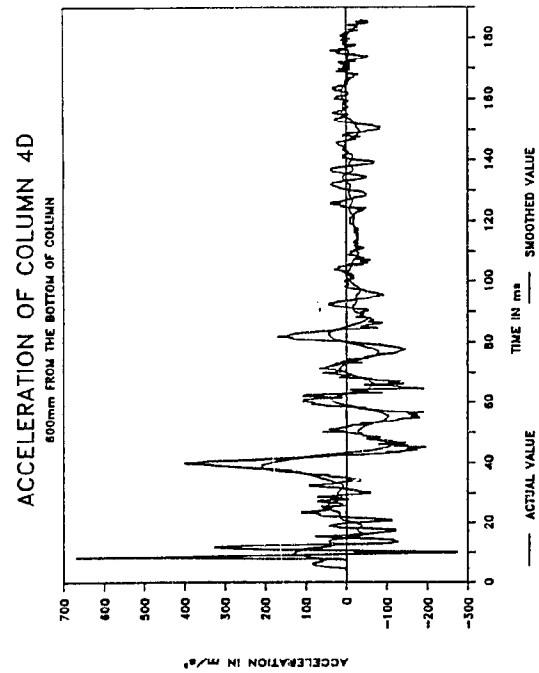

Fig. B.555: Smo.Accel. Col 4D

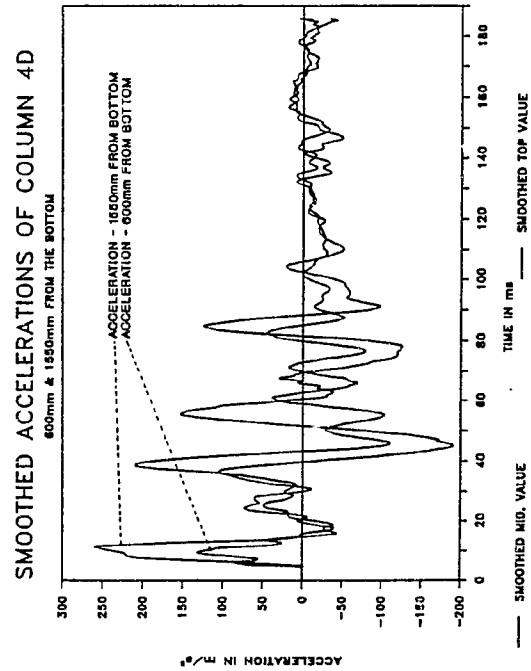

Fig. B.556: Smo. Accel. Col.4D

Stellenbosch University http://scholar.sun.ac.za

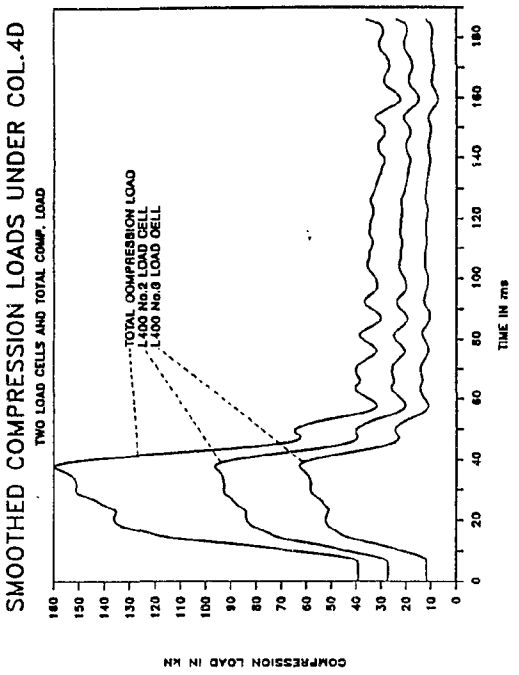

Fig. B.557: Smo. Comp. Col.4D

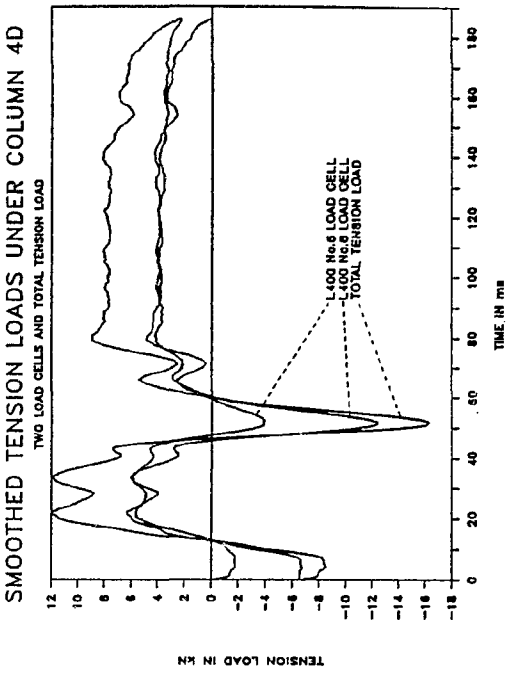

Fig. B.558: Smo. Tens. Col.4D

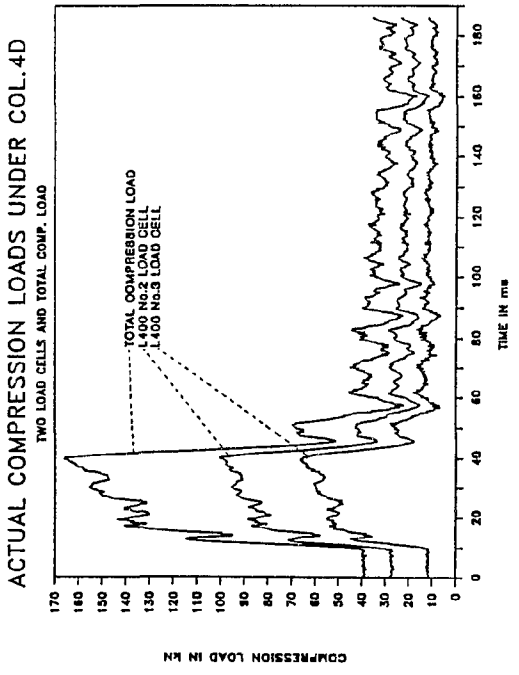

Fig. B.559: Comp. load Col 4D

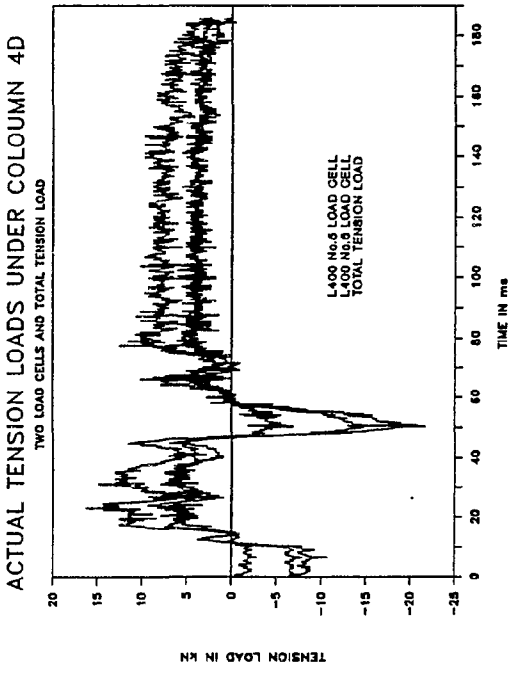

Fig. B.560: Tens. loads Col.4D

Stellenbosch University http://scholar.sun.ac.za

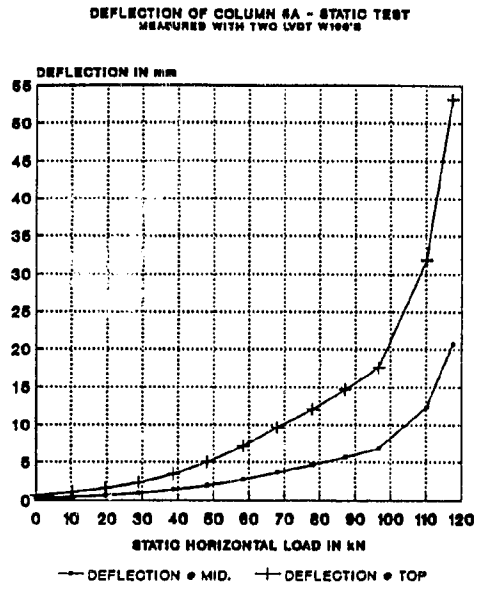

Fig. B.561: Deflection Col.5A

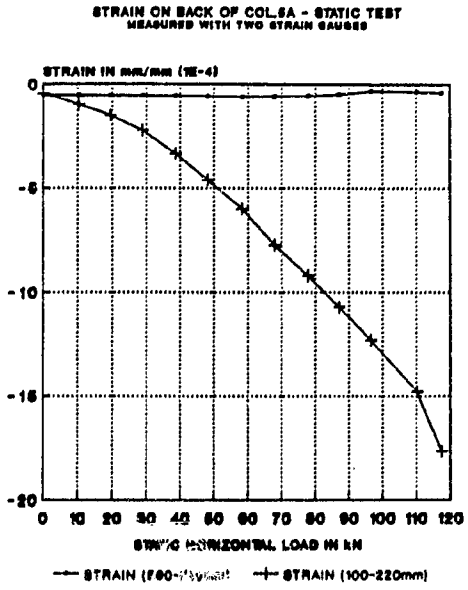

Fig. B.562: Strain Col.5A

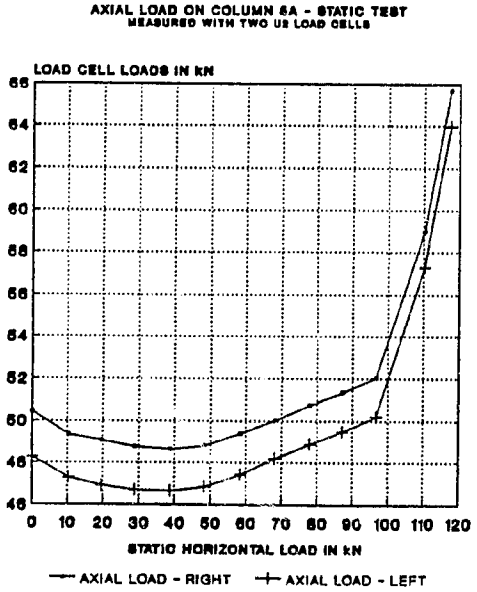

Fig. B.563: Axial load Col 5A

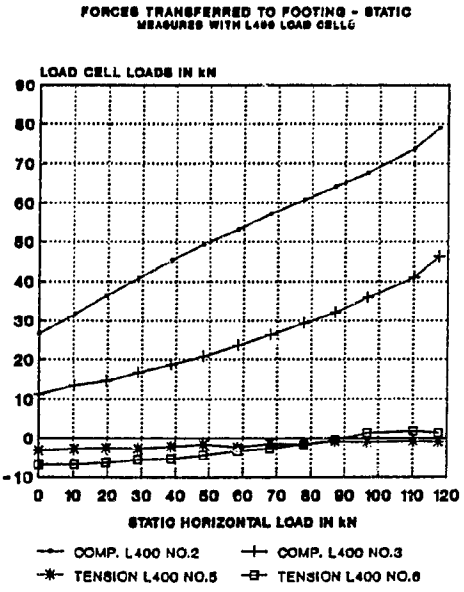

Fig. B.564: Foot.loads Col.5A

Stellenbosch University http://scholar.sun.ac.za

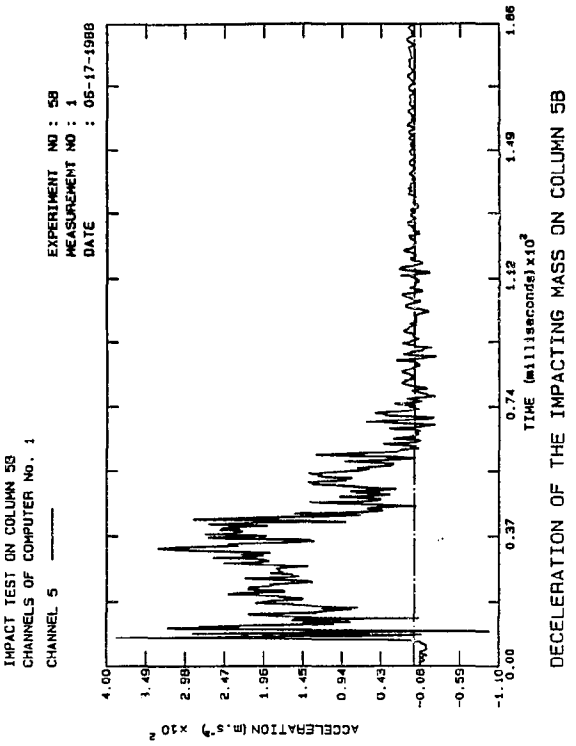

Fig. B.565: Decel. Col.5B

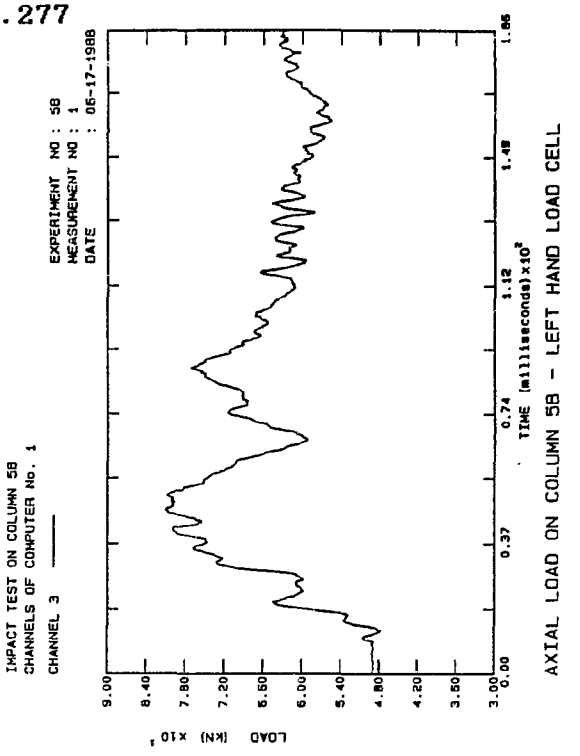

Fig. B.566: Axial load Col.5B

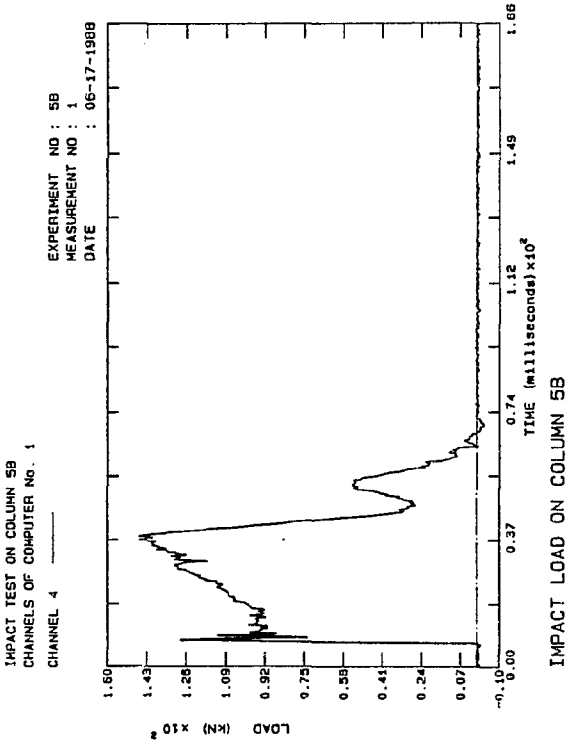

Fig. B.567: Impact Col 5B

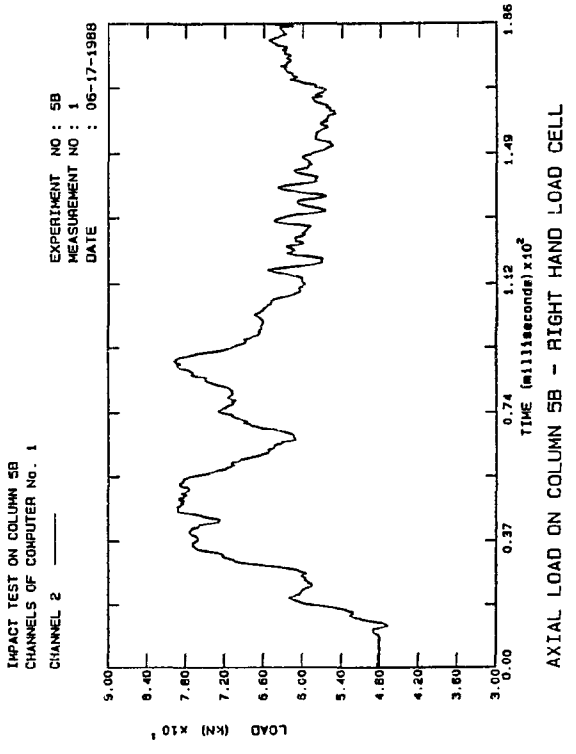

Fig. B.568: Axial load Col.5B

Stellenbosch University http://scholar.sun.ac.za

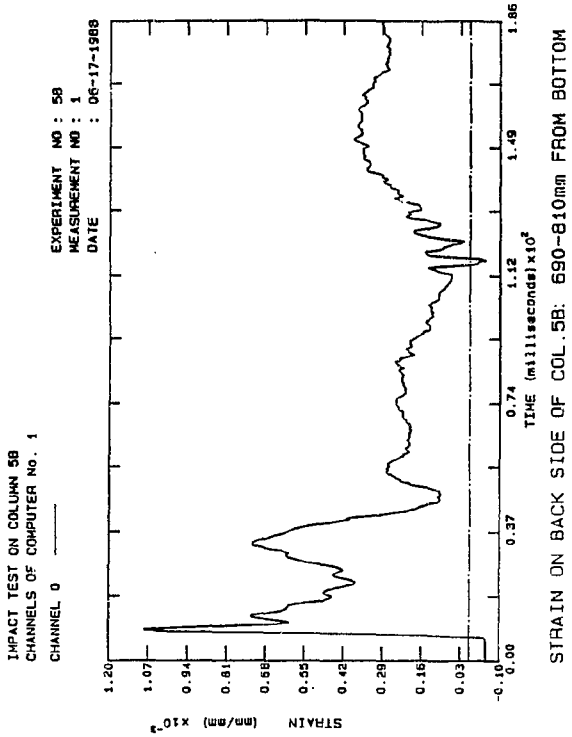

Fig. B.569: Strain Col.5B

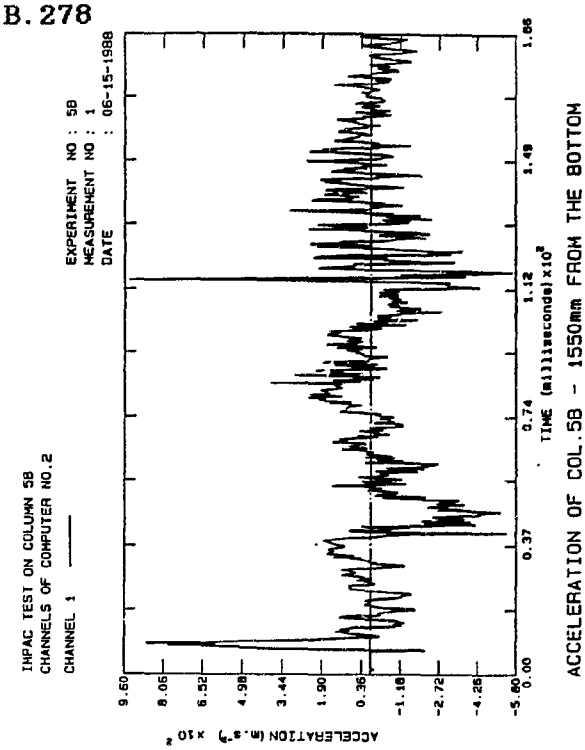

Fig. B.570: Accel. Col.5B

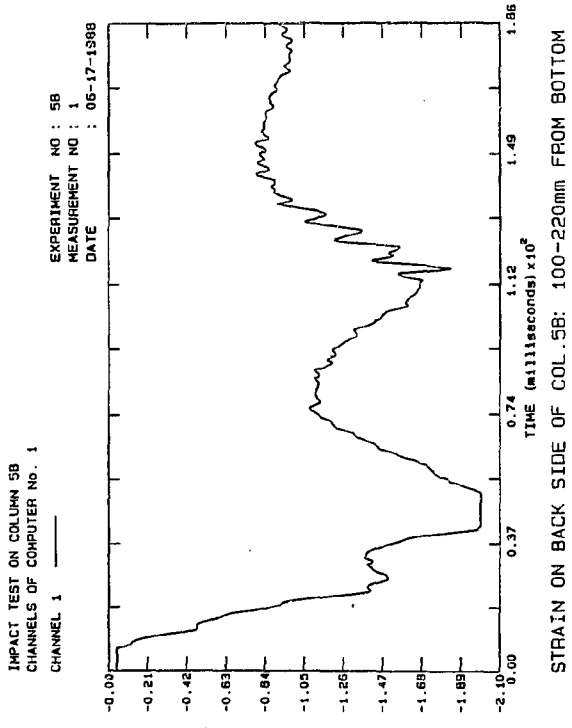

Fig. B.571: Strain Col 5B

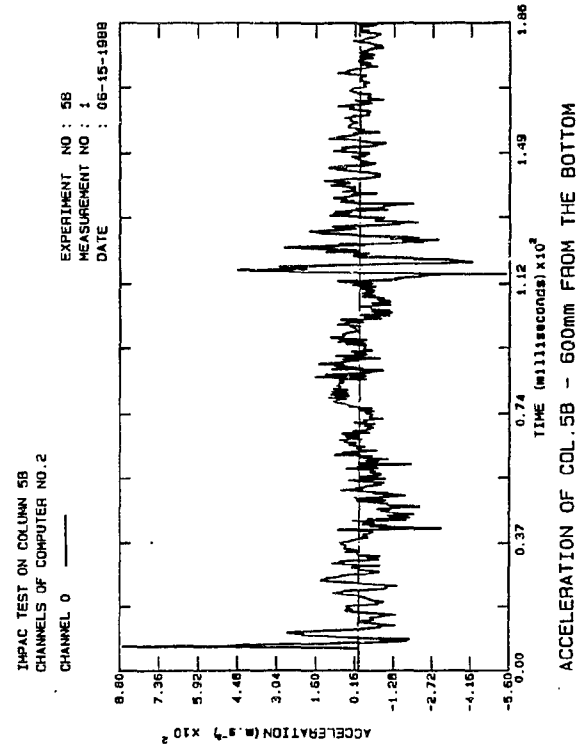

Fig. B.572: Accel. Col.5B

Stellenbosch University http://scholar.sun.ac.za

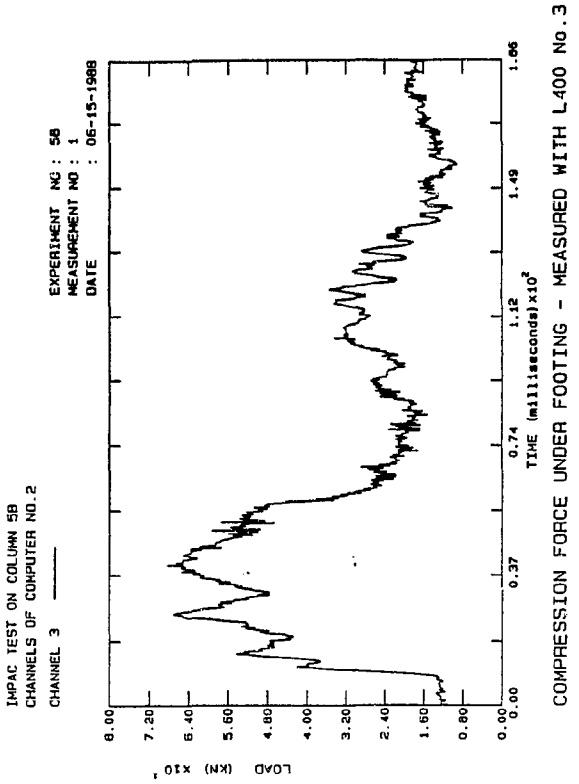

Fig. B.573: Comp. Col.5B

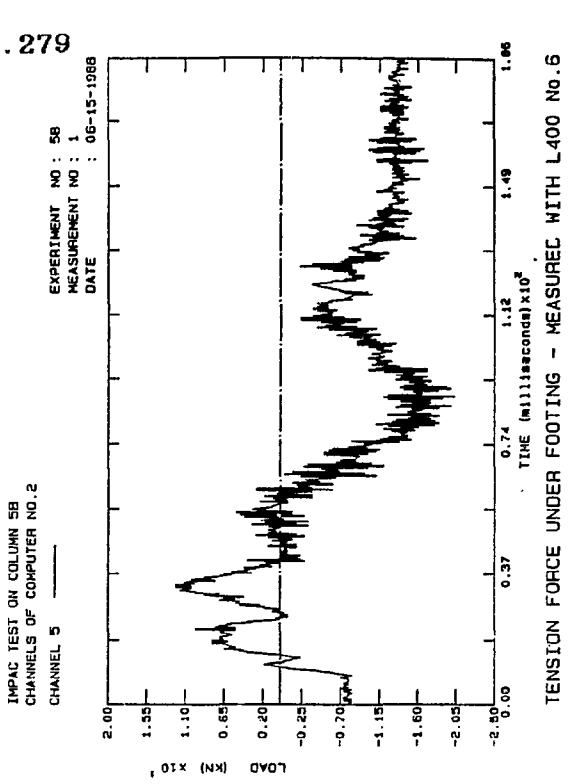

Fig. B.574: Tension Col.5B

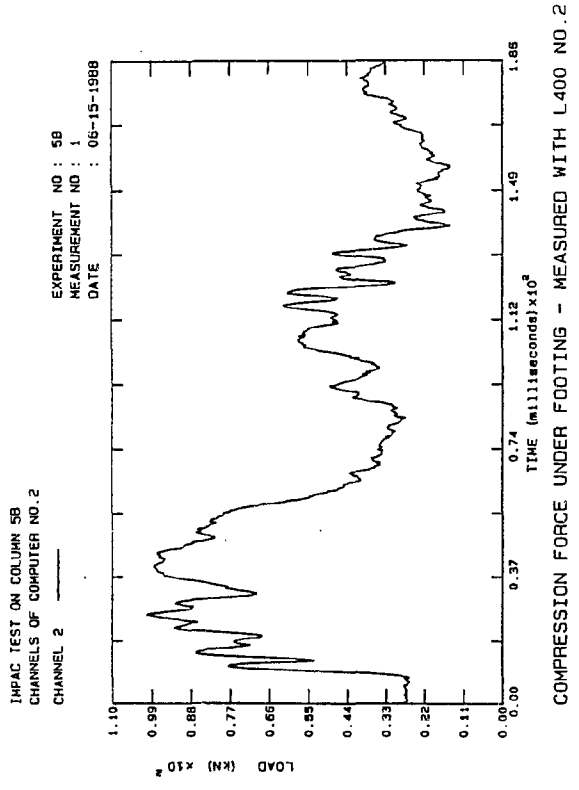

Fig. B.575: Comp. Col 5B

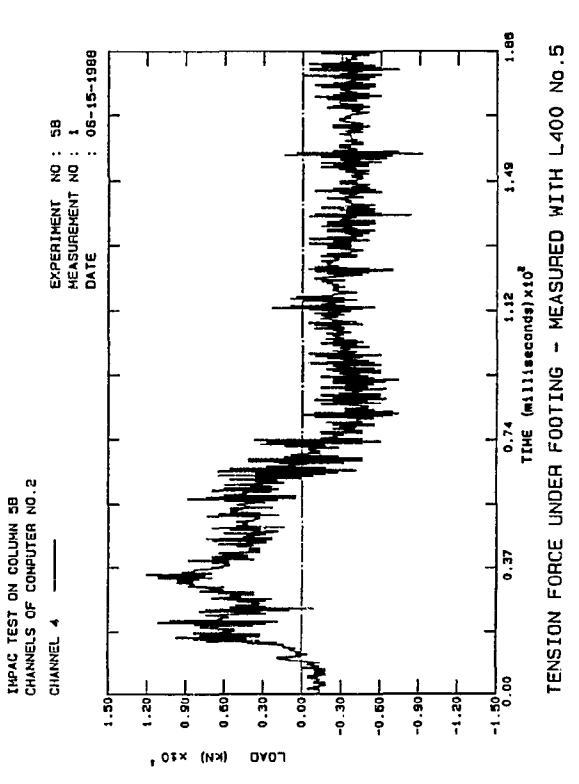

Fig. B.576: Tension Col.5B

Stellenbosch University http://scholar.sun.ac.za

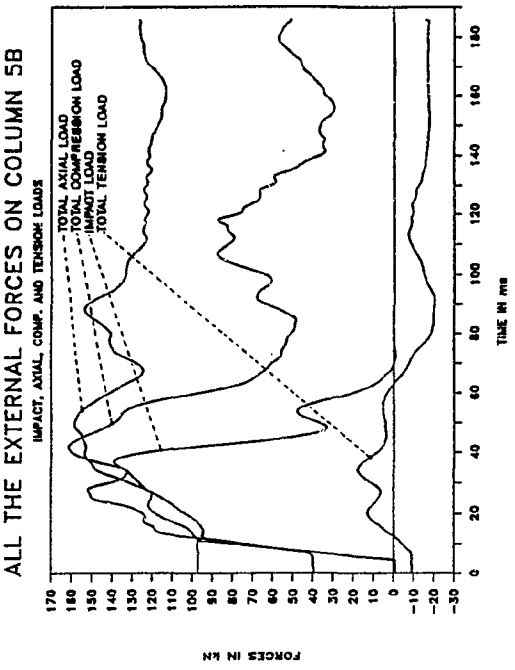

Fig. B.577: Ext. Loads Col.5B

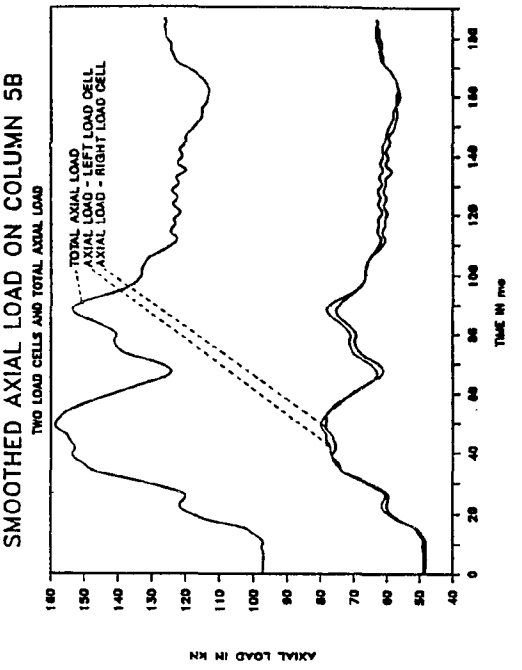

Fig. B.578: Smo. Axial Col.5B

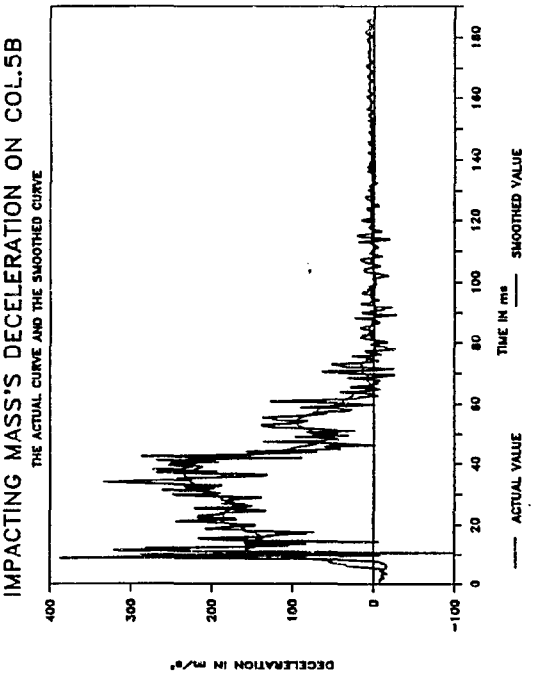

Fig. B.579: Smo.Decel. Col 5B

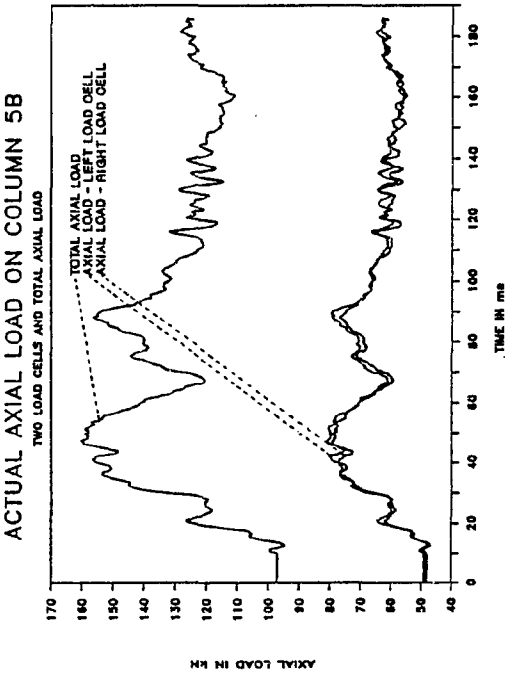

Fig. B.580: Axial loads Col.5B

Stellenbosch University http://scholar.sun.ac.za

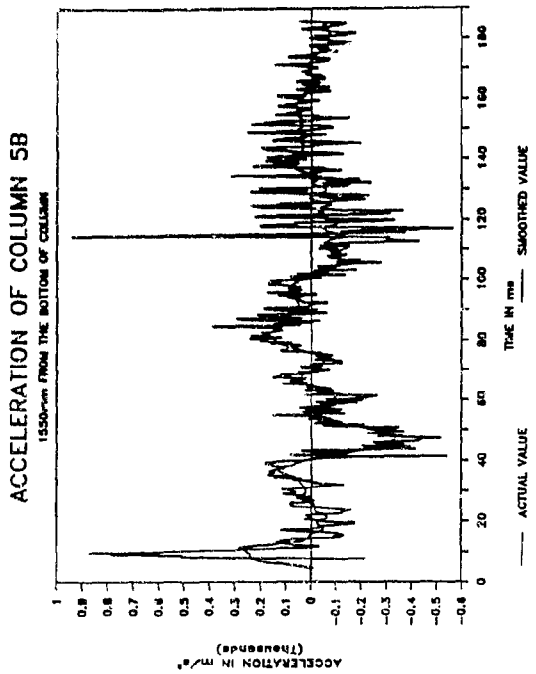

Fig. B.581: Smo.Accel. Col.5B

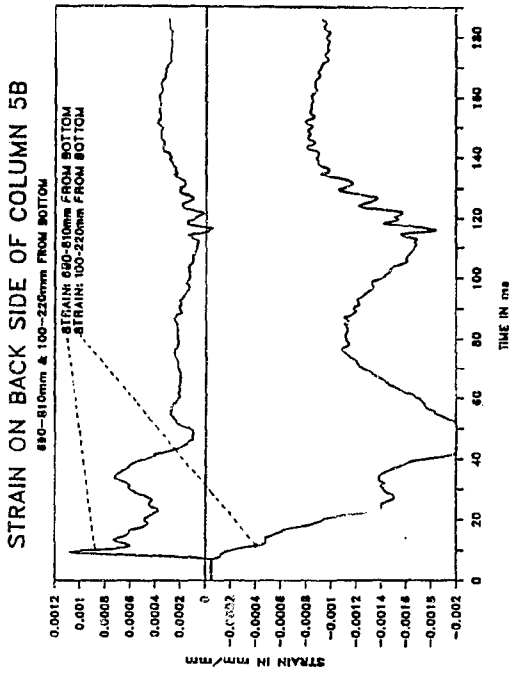

Fig. B.582: Strain Col.5B

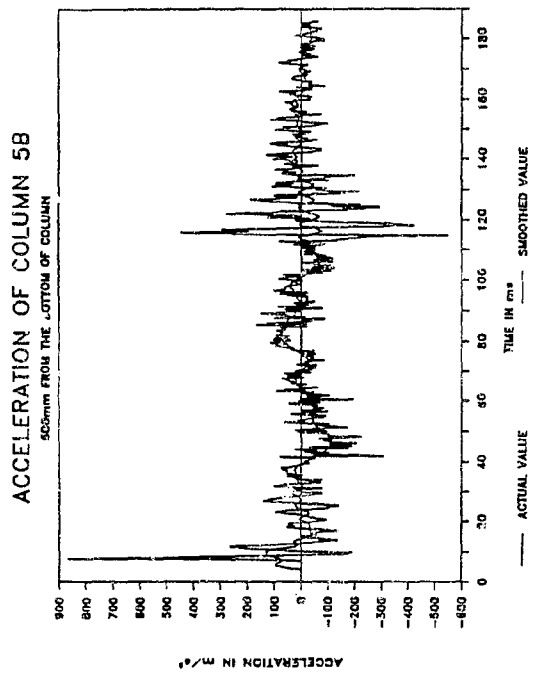

Fig. B.583: Smo.Accel. Col 5B

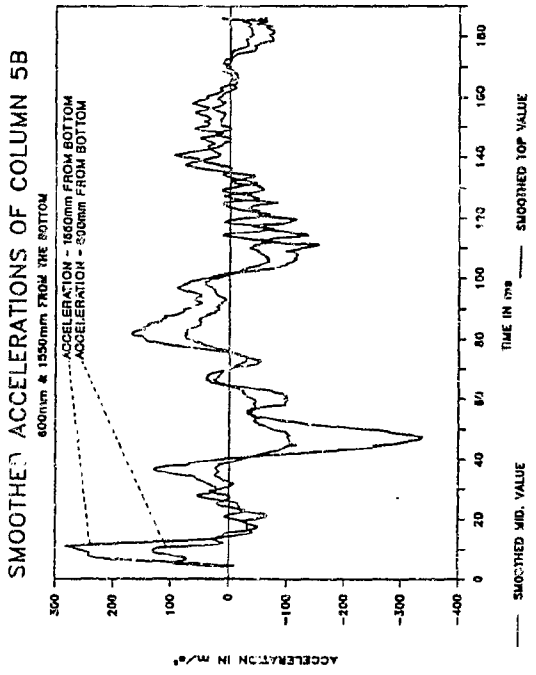

Fig. B.584: Smo. Accel. Col.5B

Stellenbosch University http://scholar.sun.ac.za

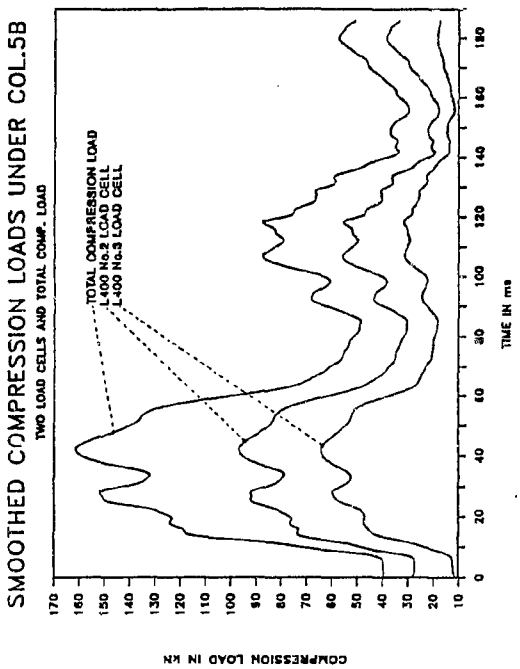

Fig. B.585: Smo. Comp. Col.5B

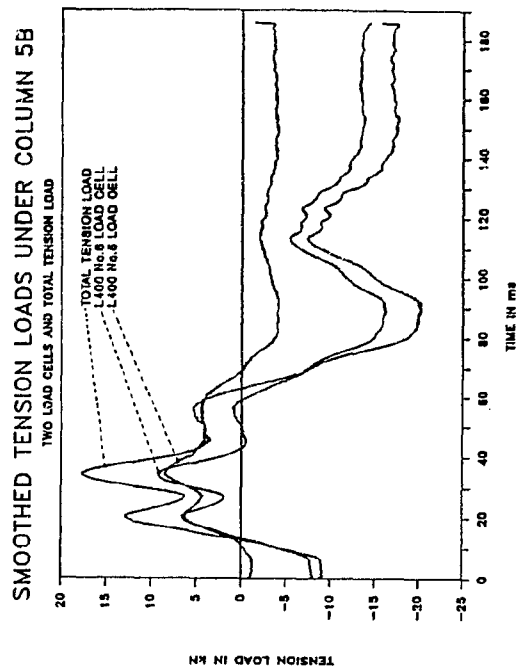

Fig. B.586: Smo. Tens. Col.5B

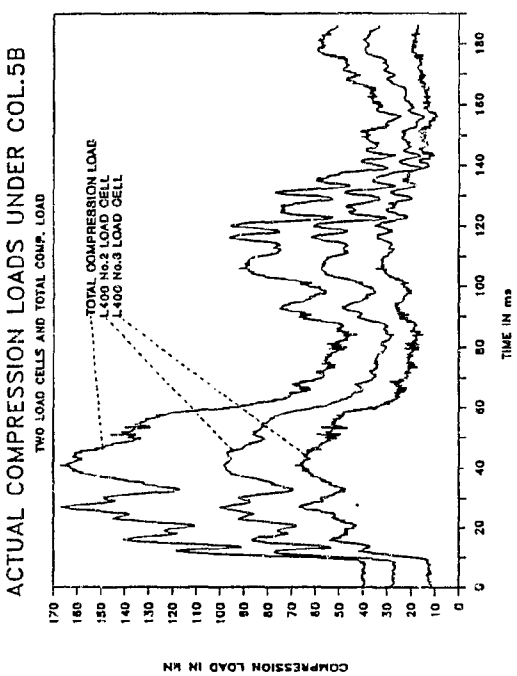

Fig. B.587: Comp. load Col 5B

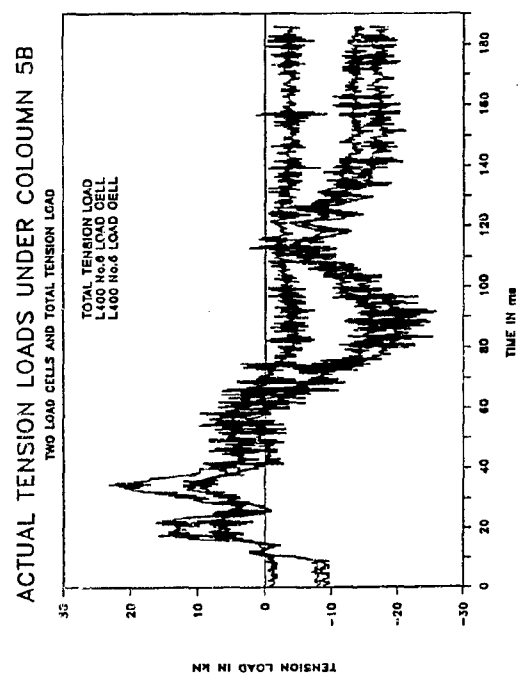

Fig. B.588: Tens. loads Col.5B

Stellenbosch University http://scholar.sun.ac.za

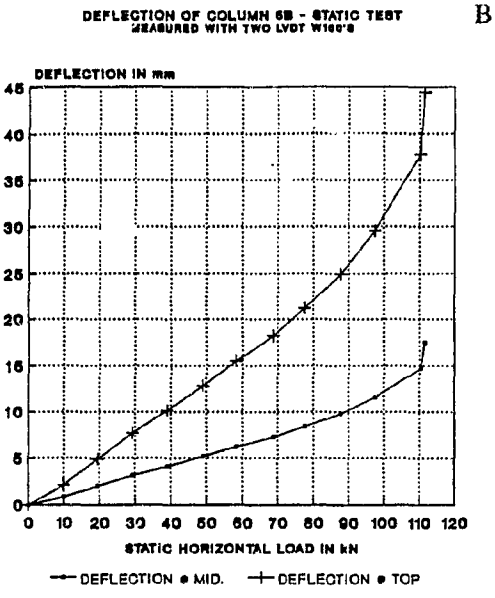

Fig. B.589: Deflection Col.5B

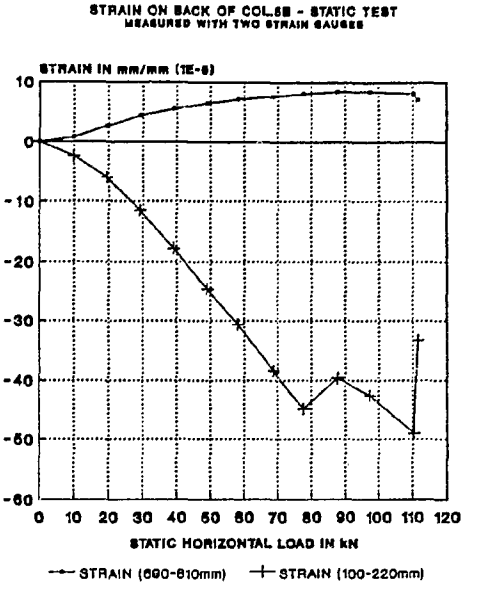

Fig. B.590: Strain Col.5B

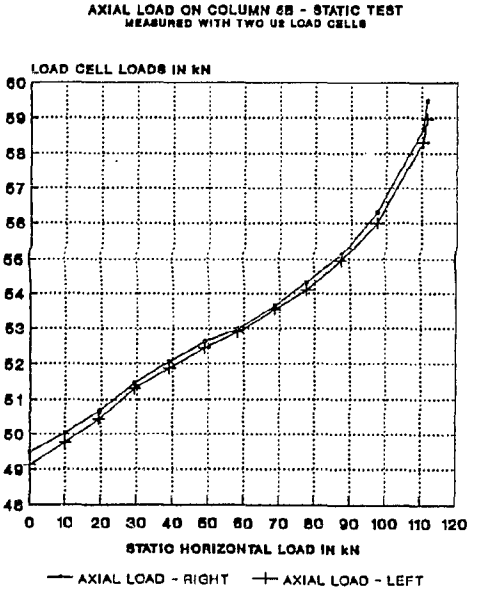

Fig. B.591: Axial load Col 5B

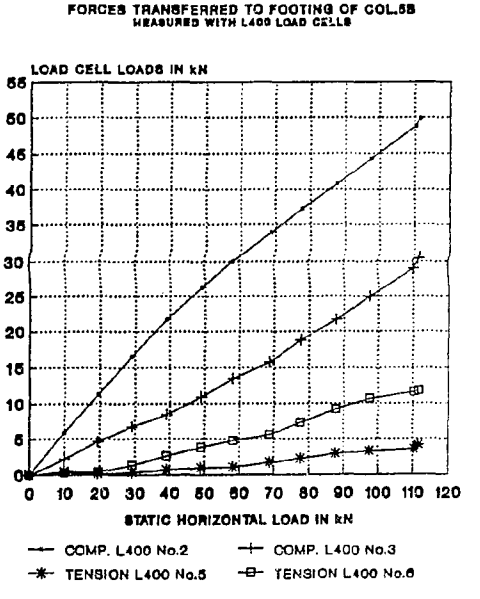

Fig. B.592: Foot.loads Col.5B

Stellenbosch University http://scholar.sun.ac.za

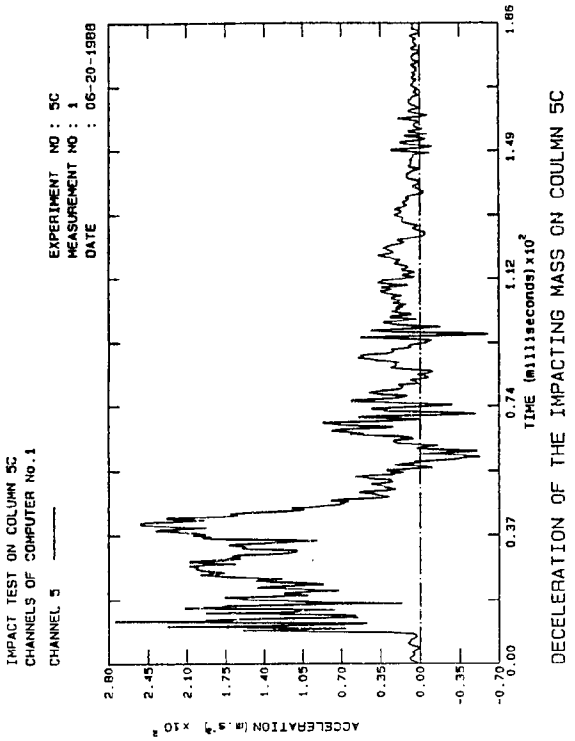

Fig. B.593: Decel. Col.5C

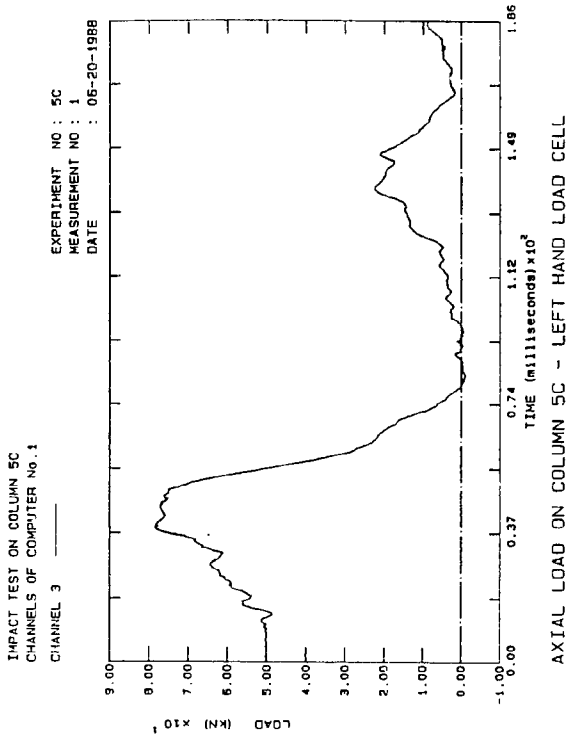

Fig. B.594: Axial load Col.5C

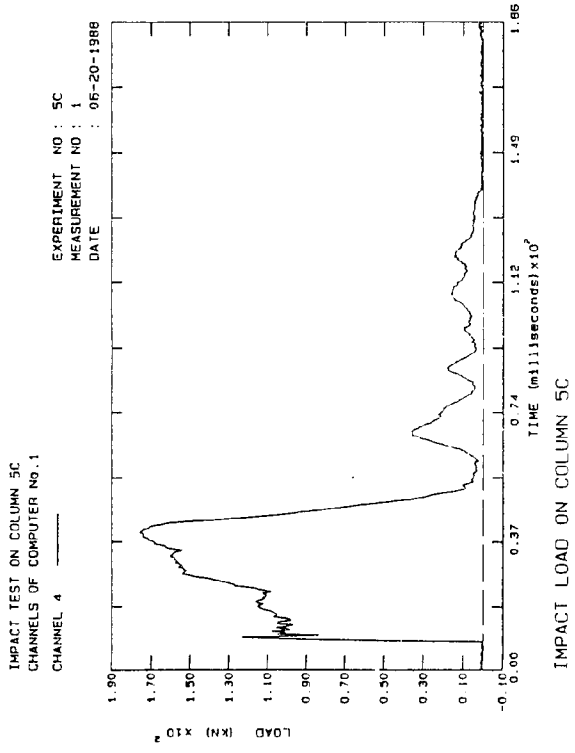

Fig. B.595: Impact Col 5C

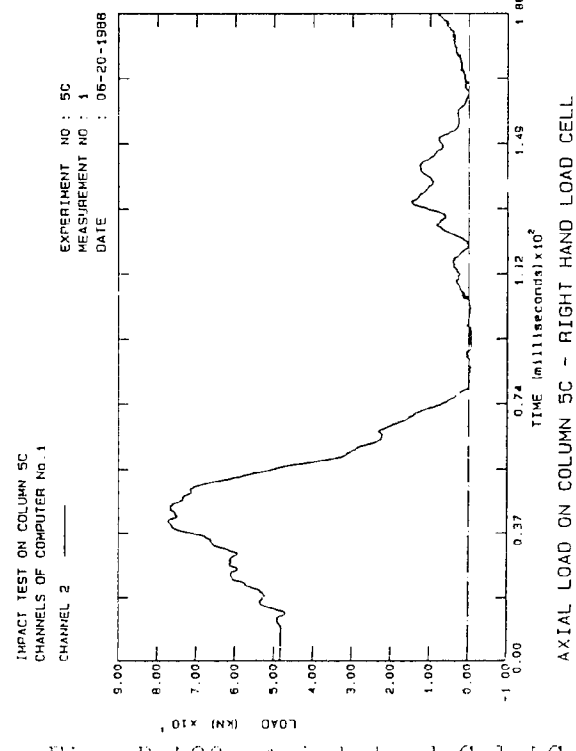

Fig. B.596: Axial load Col.5C

Stellenbosch University http://scholar.sun.ac.za

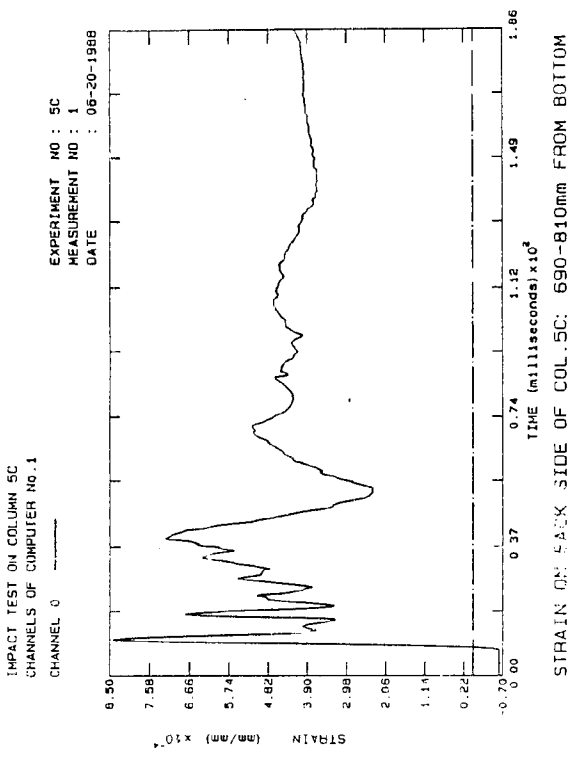

Fig. B.597: Strain Col.5C

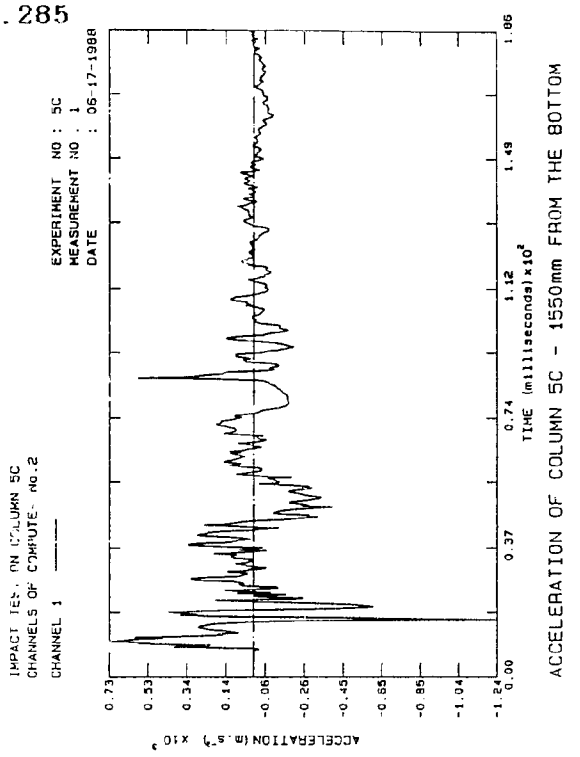

Fig. B.598: Accel. Col.5C

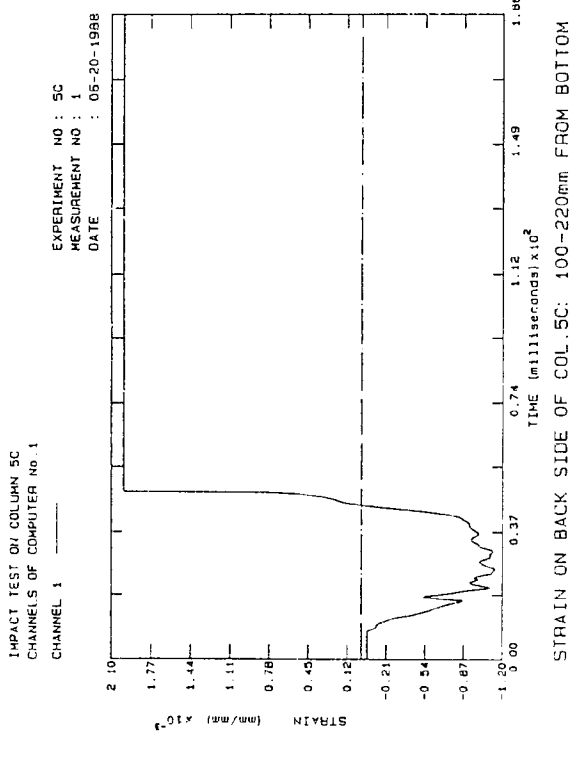

Fig. B.599: Strain Col.5C

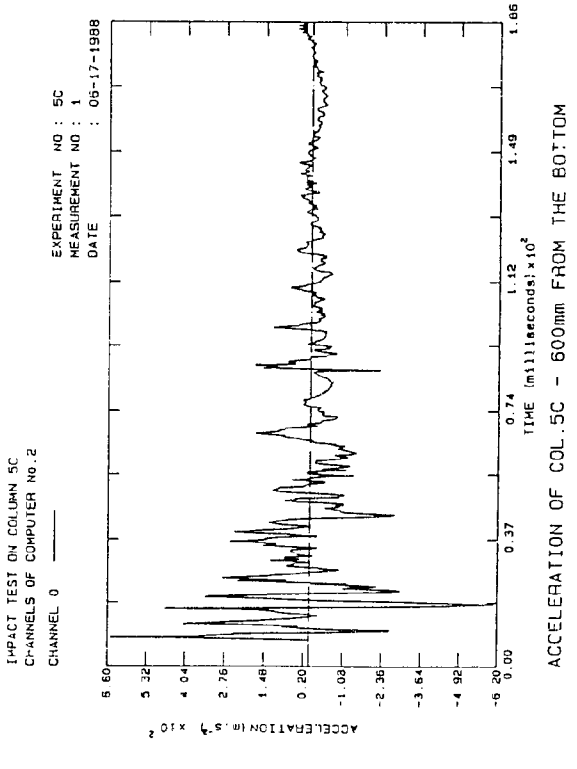

Fig. B.600: Accel. Col.5C

Stellenbosch University http://scholar.sun.ac.za

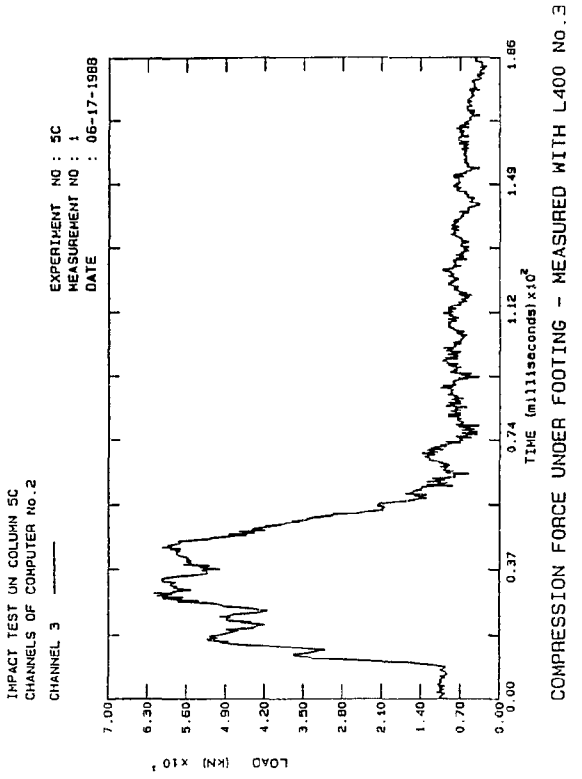

Fig. B.601: Comp. Col.5C

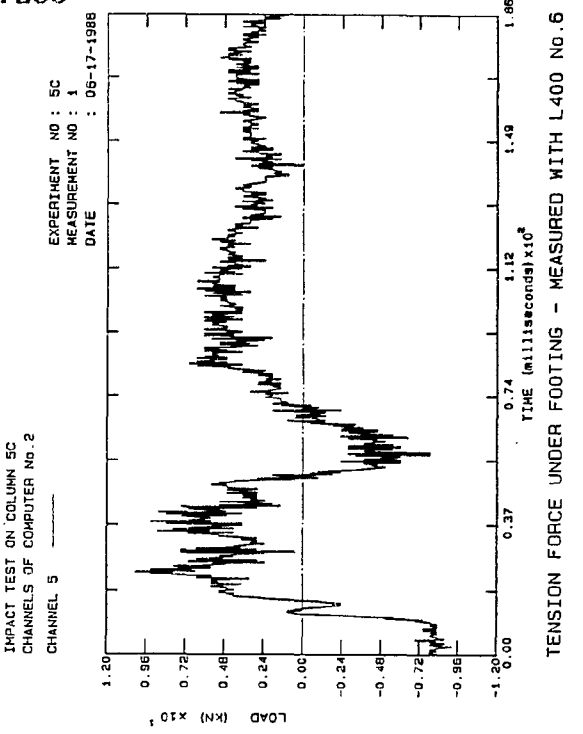

Fig. B.602: Tension Col.5C

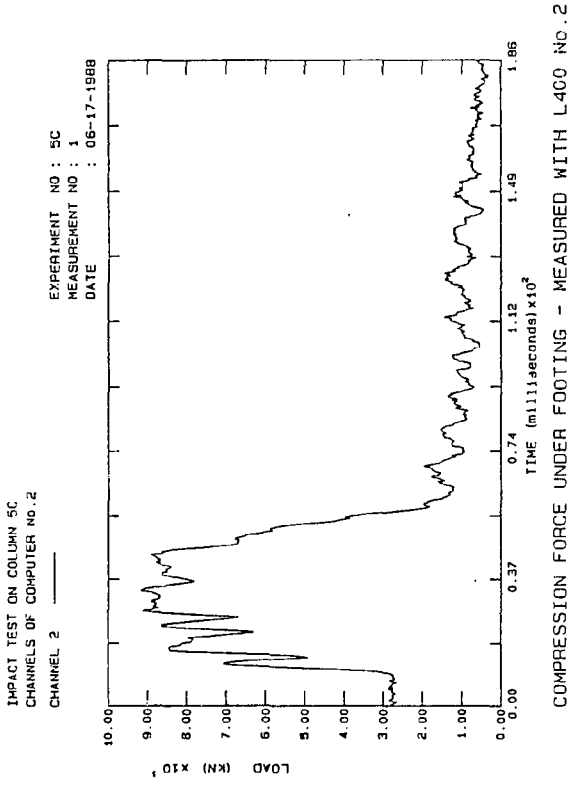

Fig. B.603: Comp. Col 5C

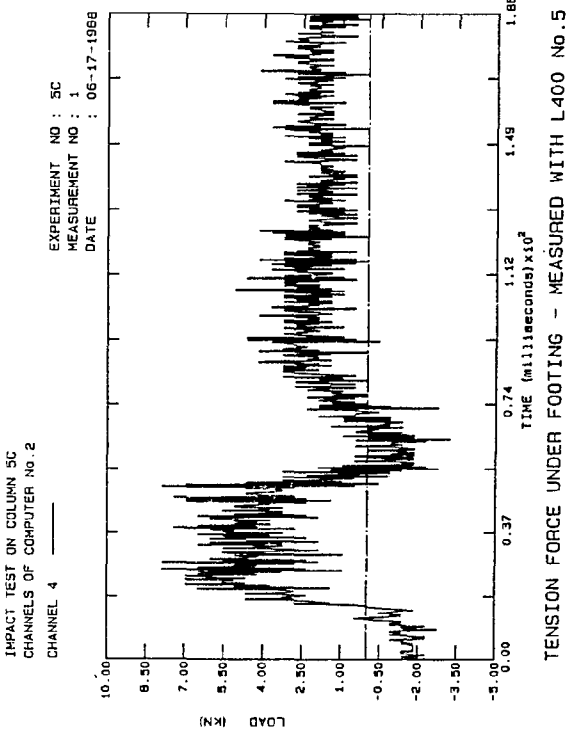

Fig. B.604: Tension Col.5C

Stellenbosch University http://scholar.sun.ac.za

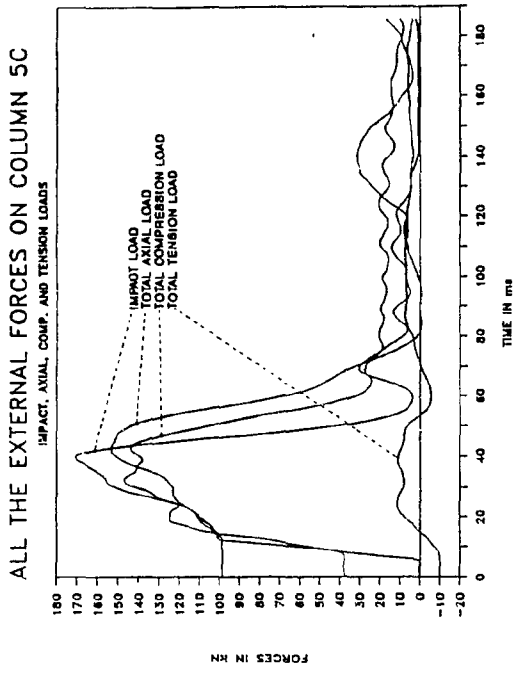

Fig. B.605: Ext. Loads Col.5C

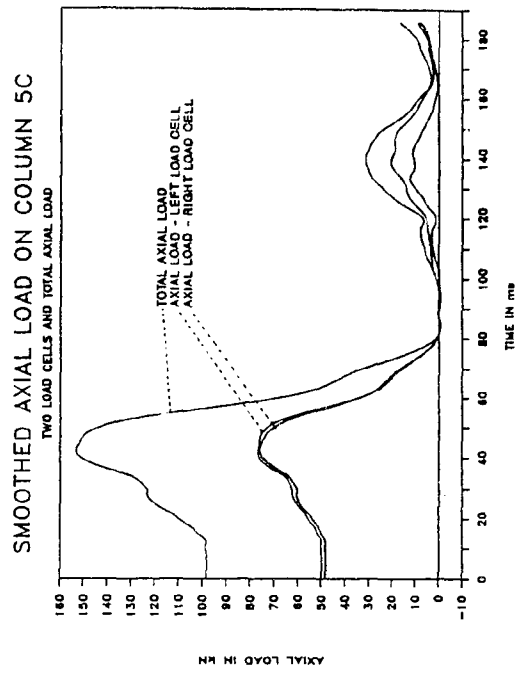

Fig. B.606: Smo. Axial Col.5C

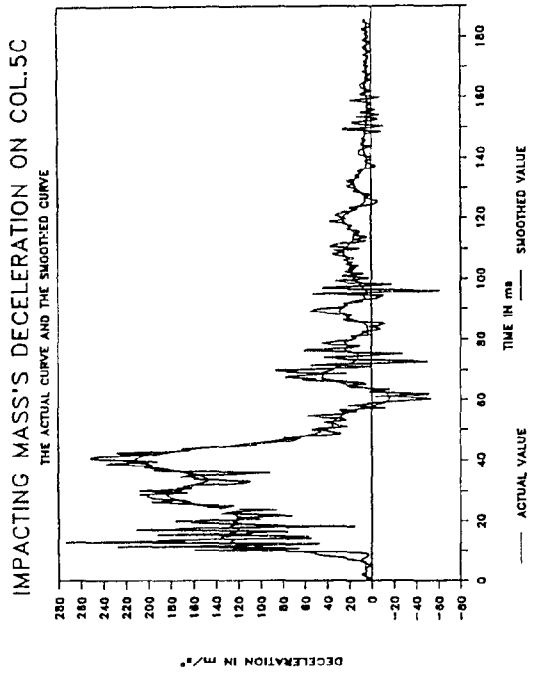

Fig. B.607: Smo.Decel. Col 5C

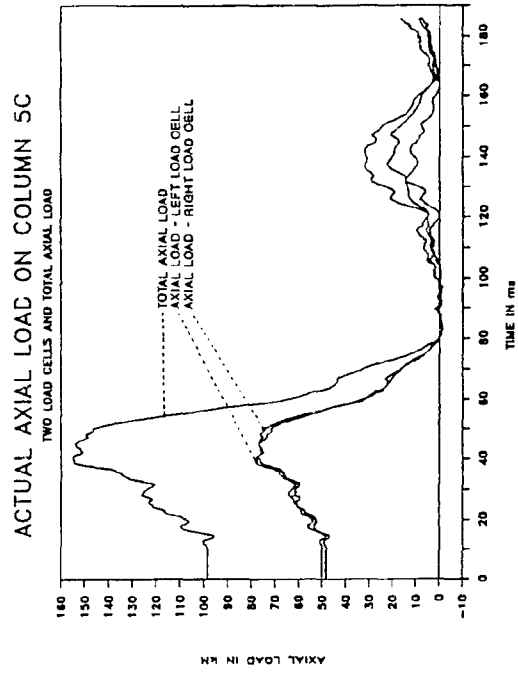

Fig. B.608: Axial Loads Col.5C

Stellenbosch University http://scholar.sun.ac.za

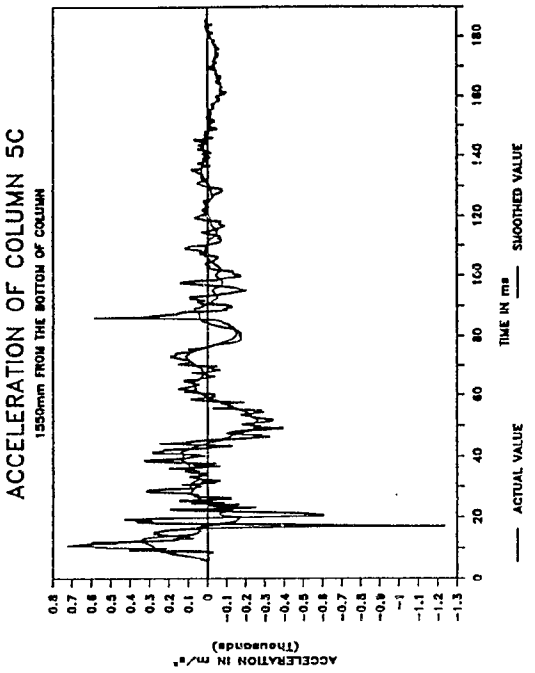

Fig. B.609: Smo.Accel. Col.5C

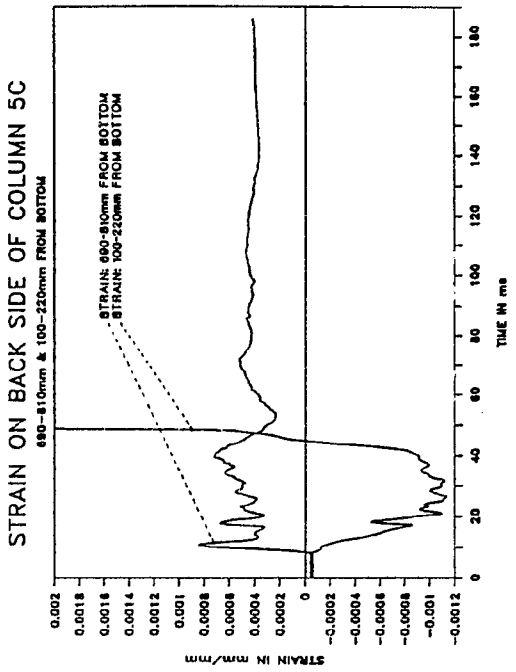

Fig. B.610: Strain Col.5C

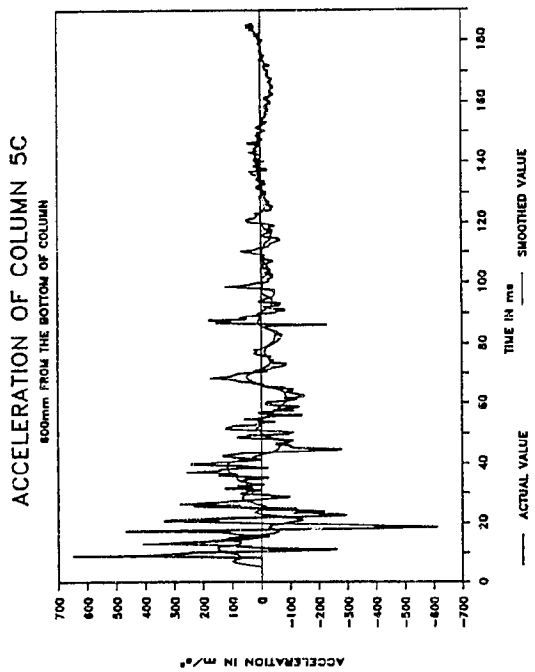

Fig. B.611: Smo.Accel. Col 5C

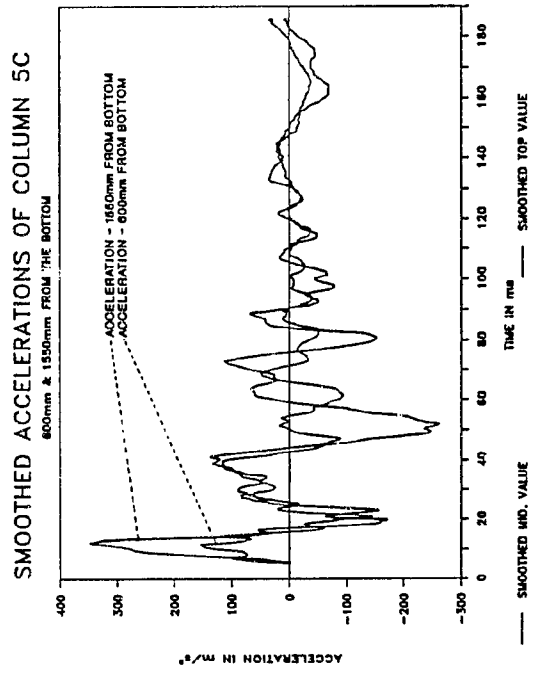

Fig. B.612: Smo. Accel. Col.5C

Stellenbosch University http://scholar.sun.ac.za

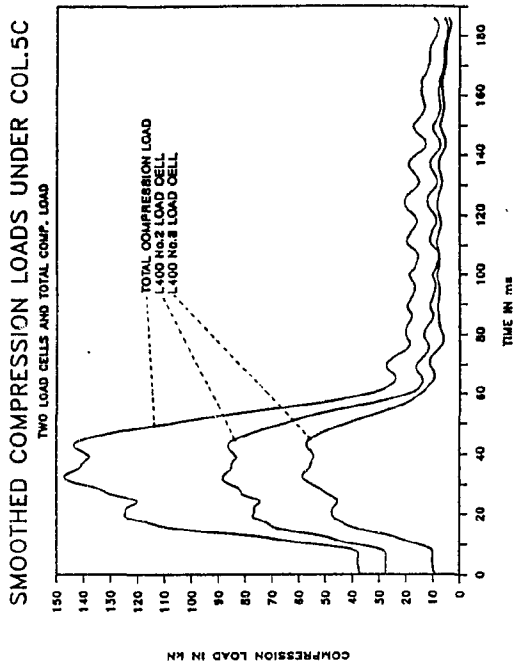

Fig. B.613: Smo. Comp. Col.5C

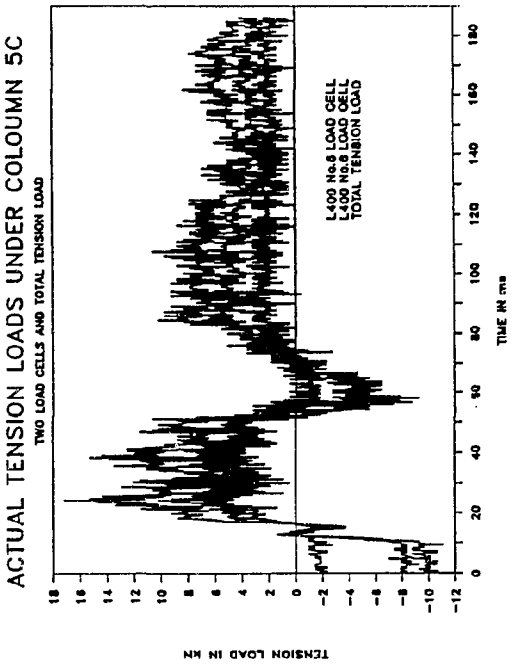

Fig. B.614: Smo. Tens. Col.5C

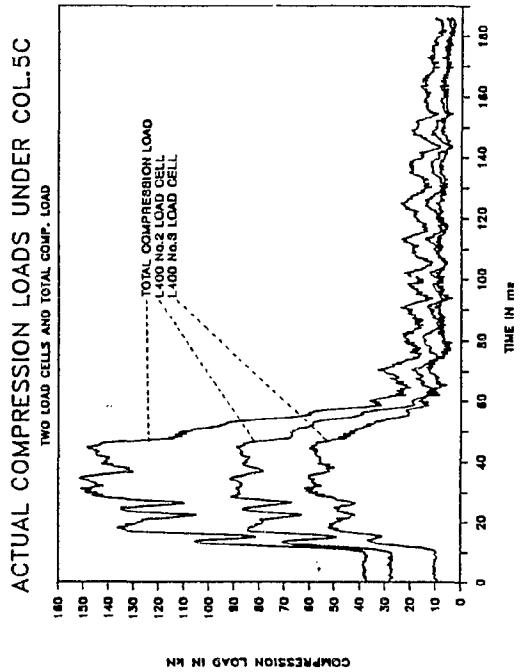

Fig. B.615: Comp. load Col 5C

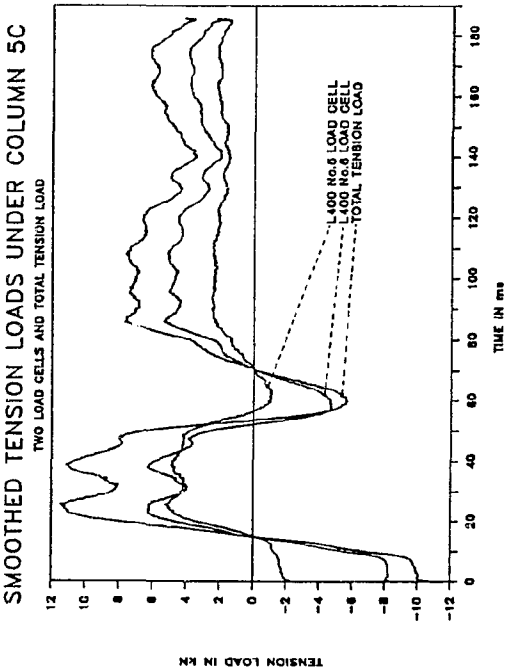

Fig. B.616: Tens. loads Col.5C

Stellenbosch University http://scholar.sun.ac.za

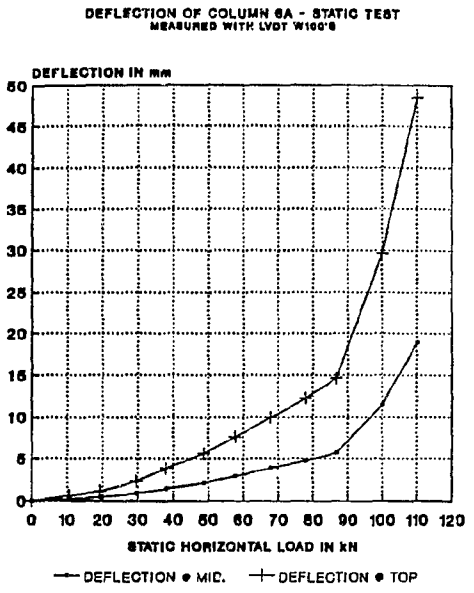

Fig. B.617: Deflection Col.6A

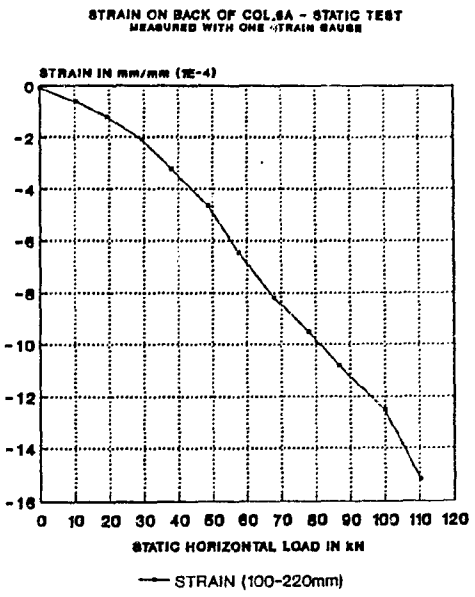

Fig. B.618: Strain Col.6A

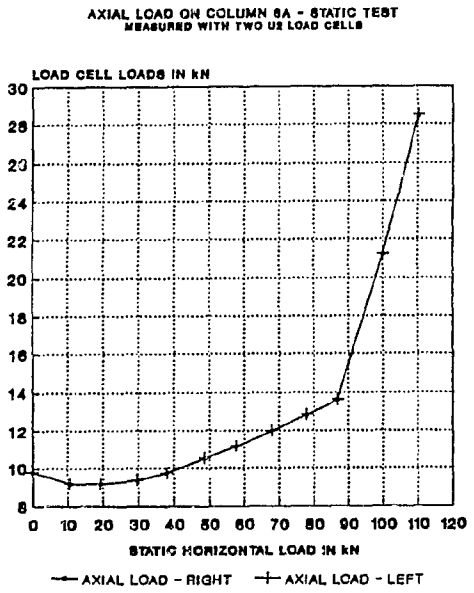

Fig. B.619: Axial load Col 6A

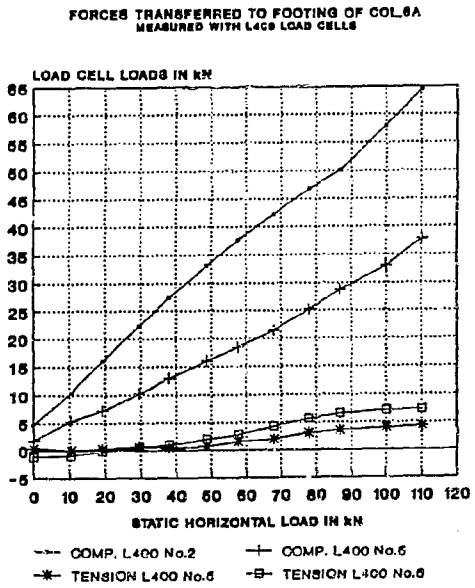

Fig. B.620: Foot.loads Col.6A

Stellenbosch University http://scholar.sun.ac.za

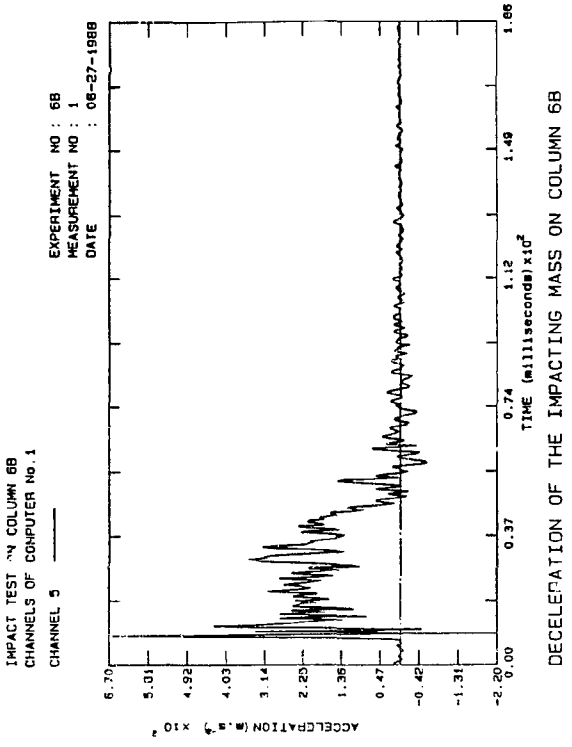

Fig. B.621: Decel. Col.6B

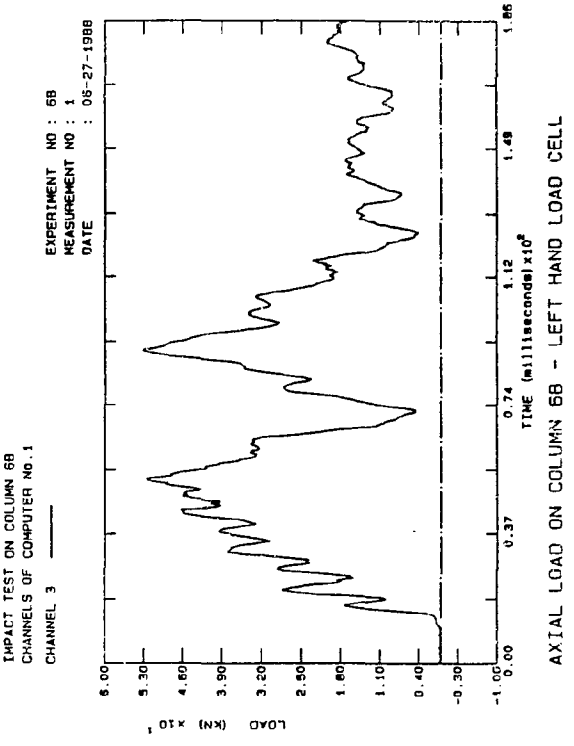

Fig. B.622: Axial load Col.6B

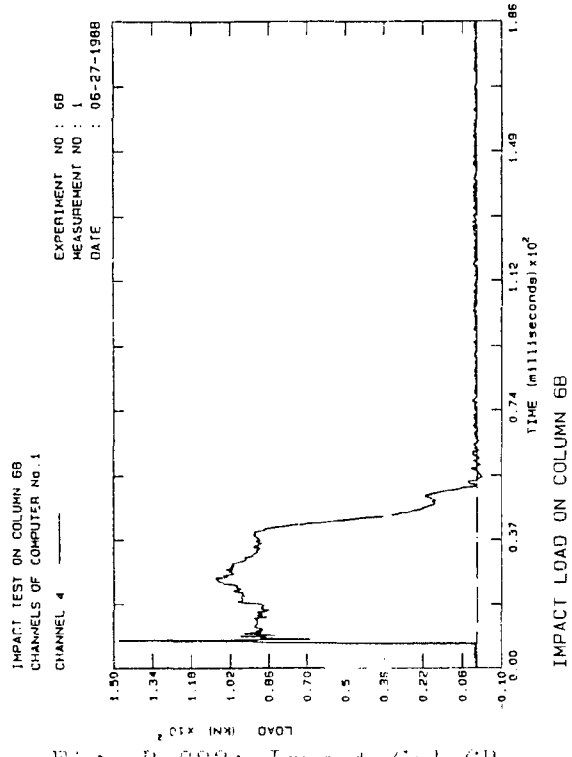

Fig. B.623: Impact Col 6B

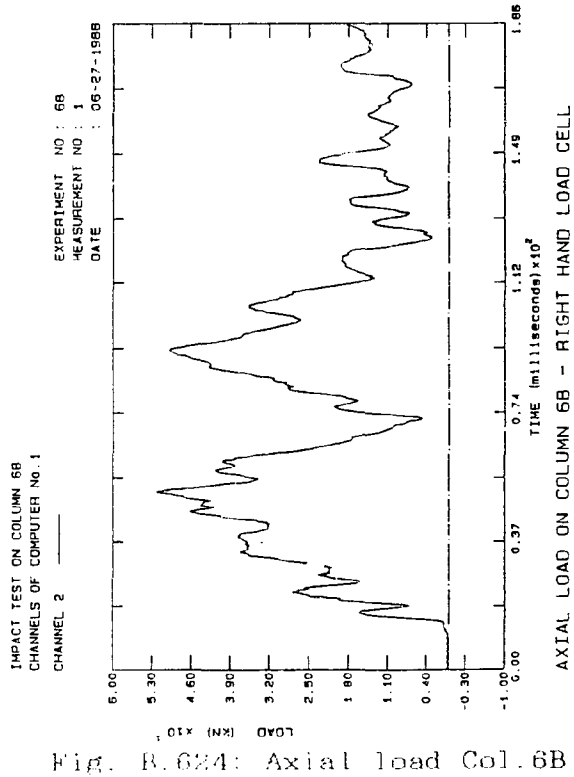

Fig. B.624: Axial load Col.6B

Stellenbosch University http://scholar.sun.ac.za

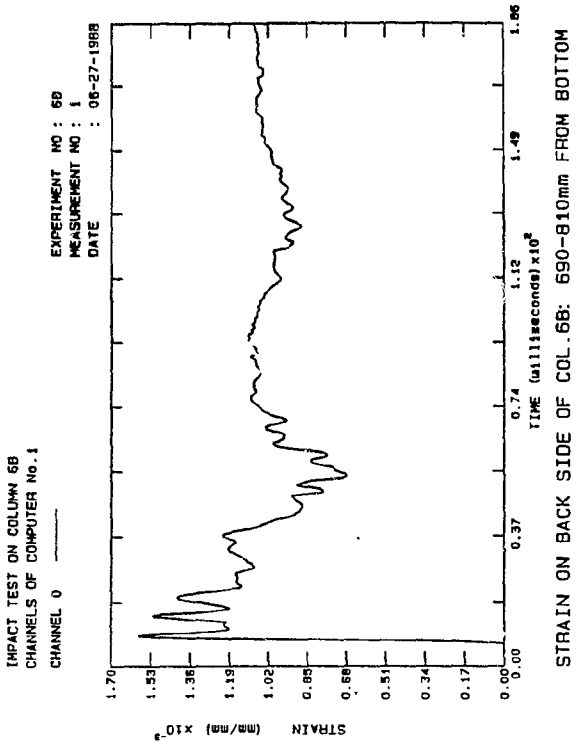

Fig. B.625: Strain Col.6B

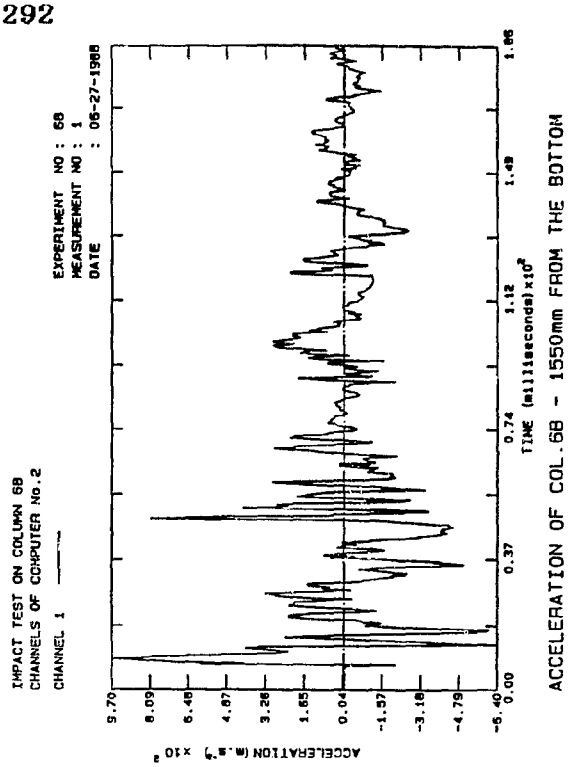

Fig. B.626: Accel. Col.6B

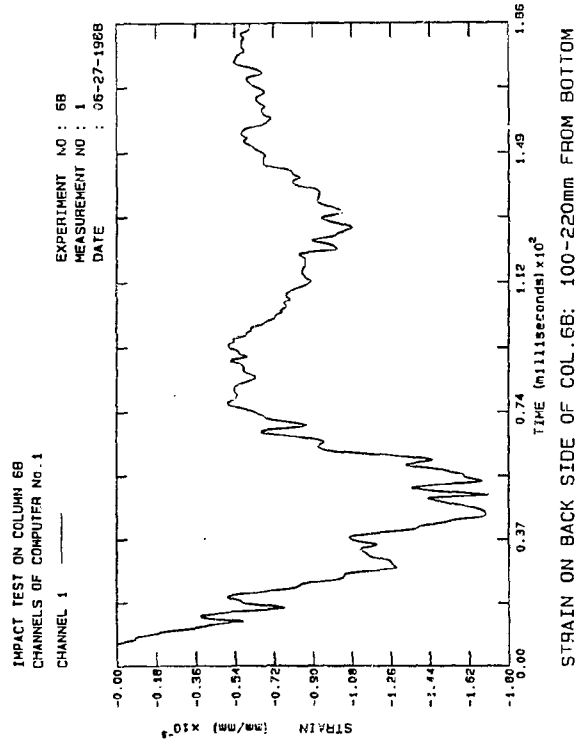

Fig. B.627: Strain Col 6B

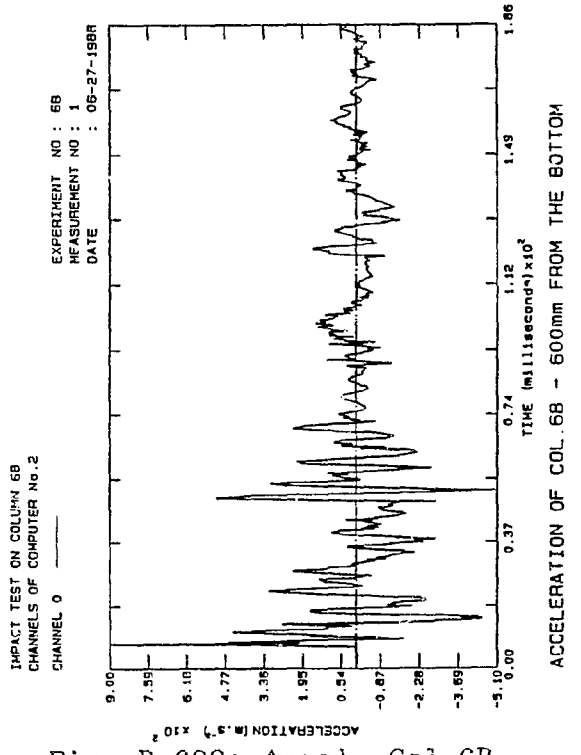

Fig. B.628: Accel. Col.6B

Stellenbosch University http://scholar.sun.ac.za

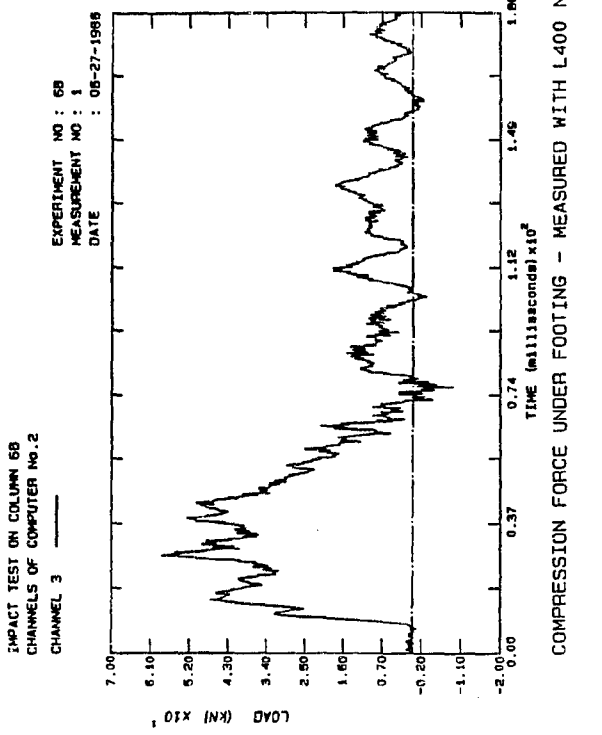

Fig. B.629: Comp. Col.6B

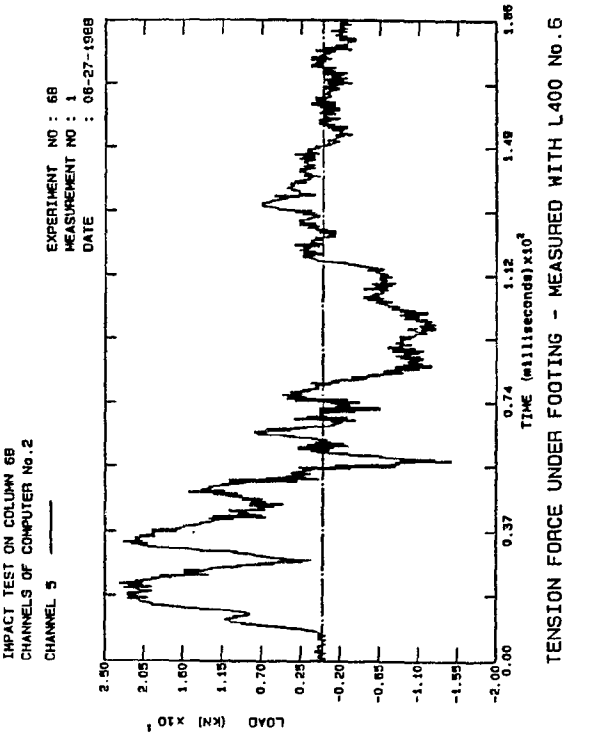

Fig. B.630: Tension Col.6B

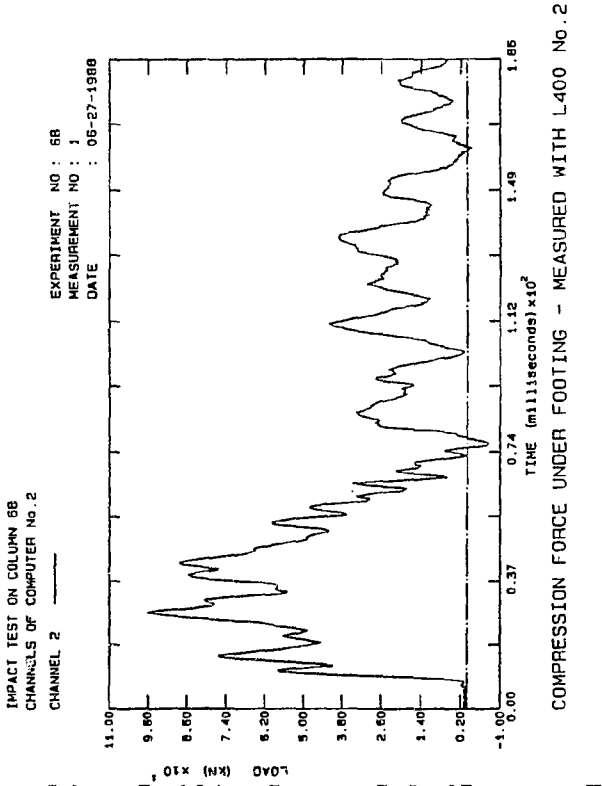

Fig. B.631: Comp. Col 6B

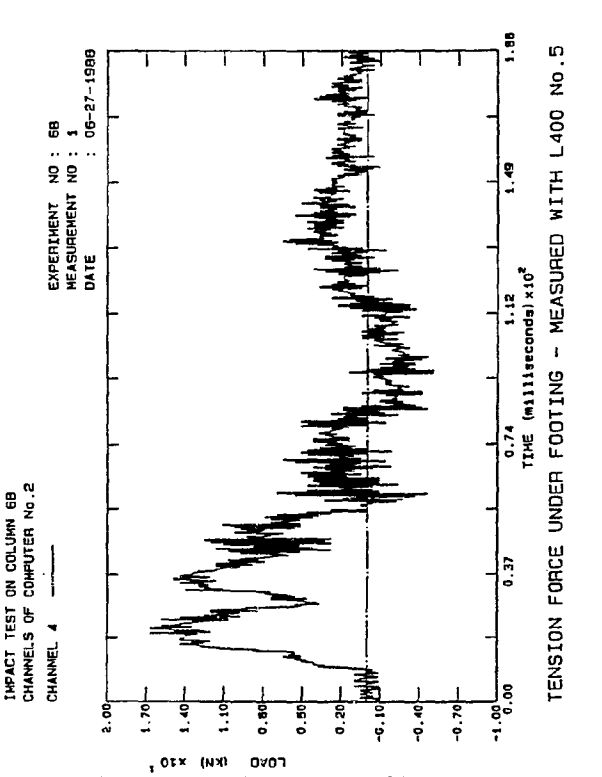

Fig. B.632: Tension Col.6B

Stellenbosch University http://scholar.sun.ac.za

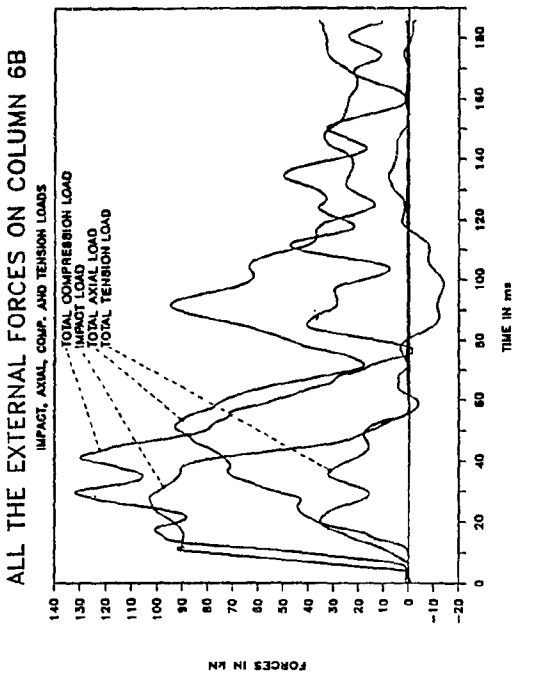

Fig. B.633: Ext. Loads Col.6B

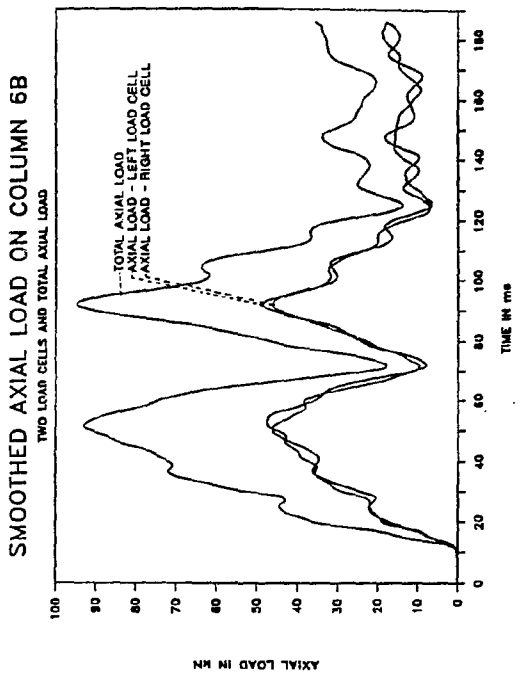

Fig. B.634: Smo. Axial Col.6B

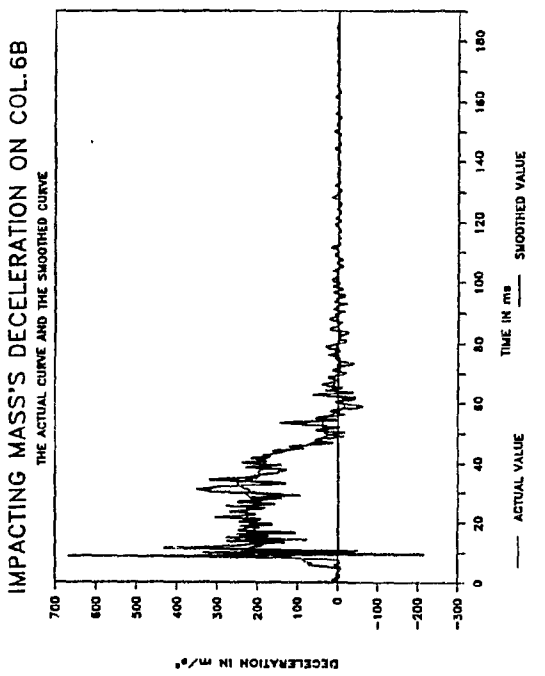

Fig. B.635: Smo.Decel. Col 6B

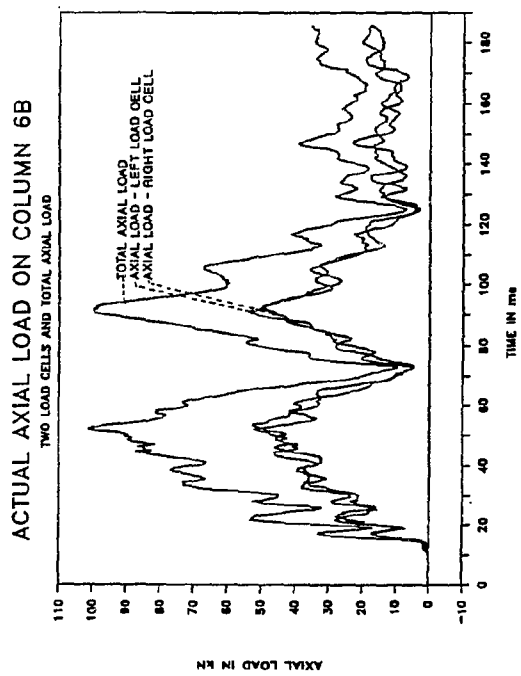

Fig. B.636: Axial loads Col.6B

Stellenbosch University http://scholar.sun.ac.za

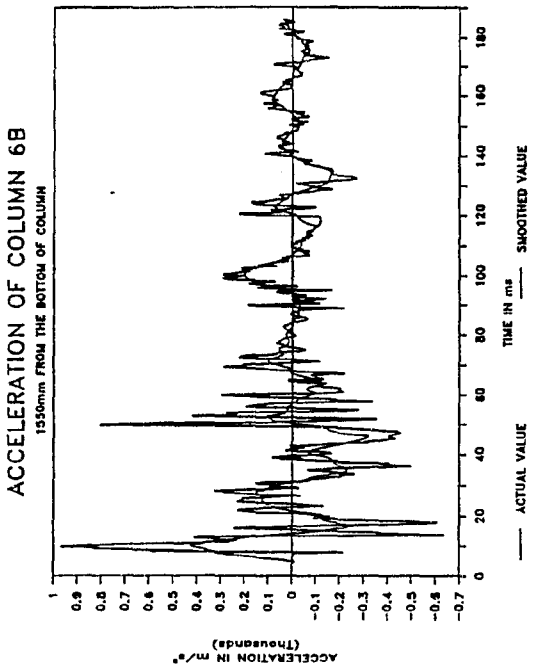

Fig. B.637: Smo.Accel. Col.6B

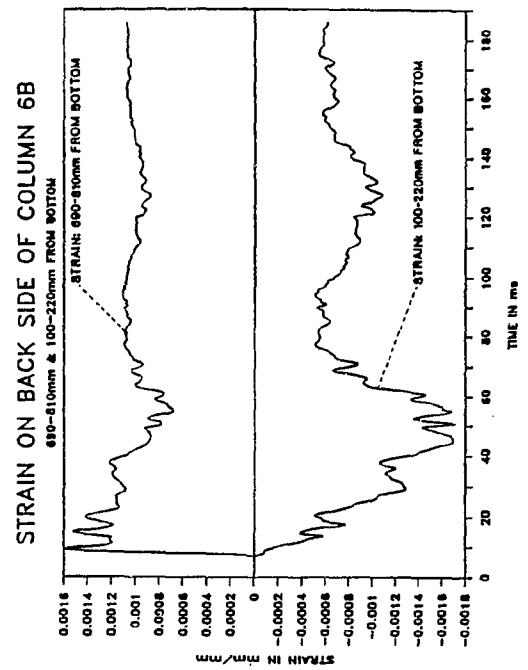

Fig. B.638: Strain Col.6B

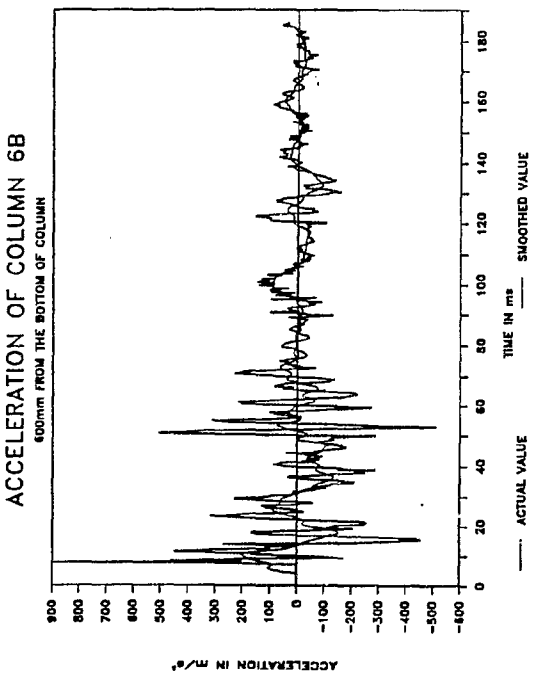

Fig. B.639: Smo.Accel. Col 6B

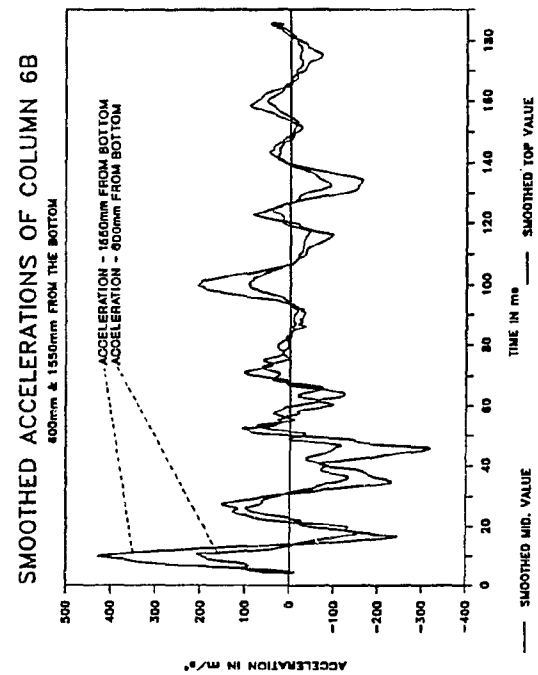

Fig. B.640: Smo. Accel. Col.6B

Stellenbosch University http://scholar.sun.ac.za

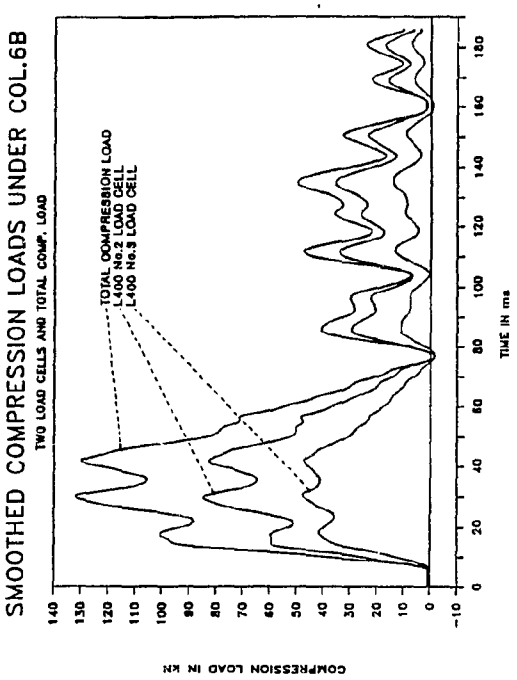

Fig. B.641: Smo. Comp. Col.6B

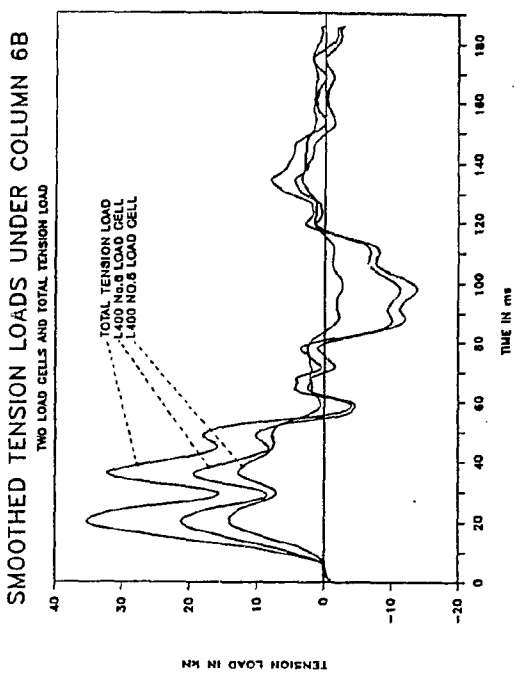

Fig. B.642: Smo. Tens. Col.6B

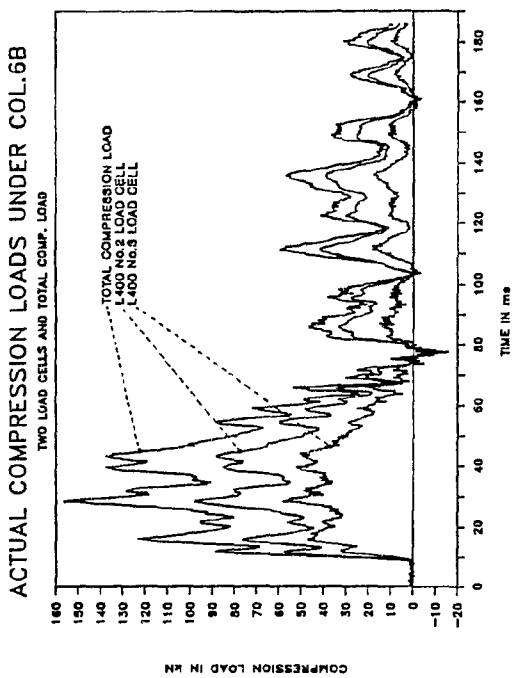

Fig. B.643: Comp. load Col 6B

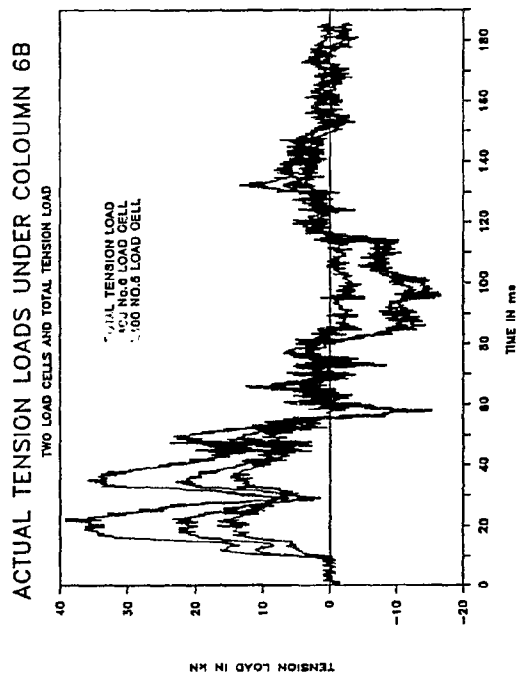

Fig. B.644: Tens. loads Col.6B

Stellenbosch University http://scholar.sun.ac.za

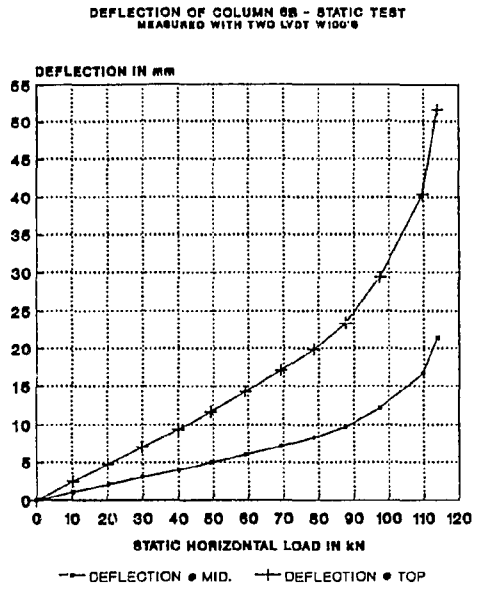

Fig. B.645: Deflection Col.6B

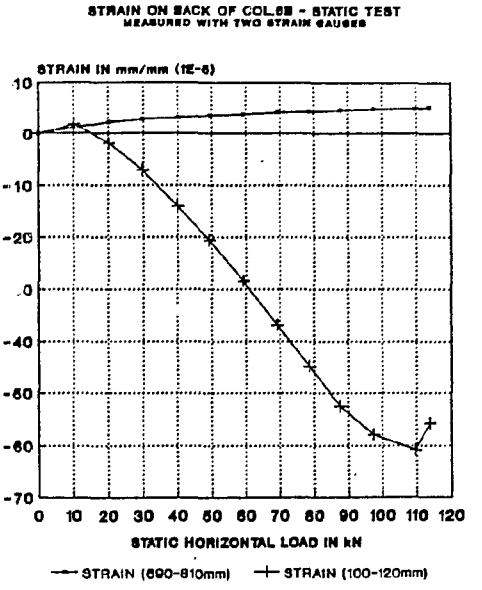

Fig. B.646: Strain Col.6B

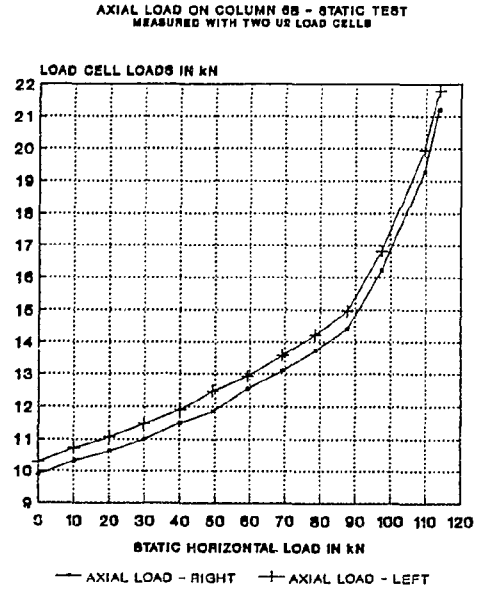

Fig. B.647: Axial load Col 6B

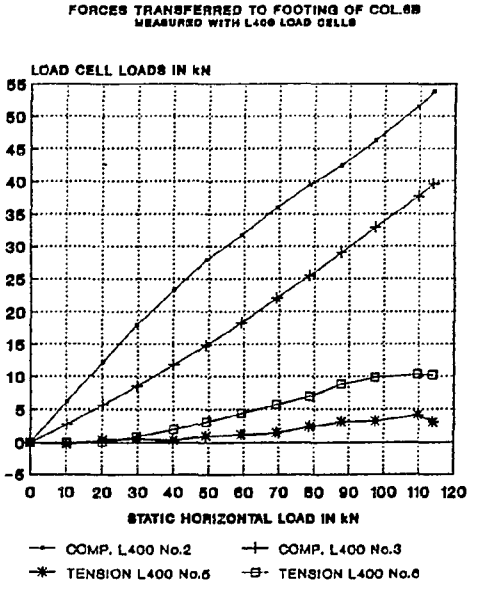

Fig. B.648: Foot.loads Col.6B

Stellenbosch University http://scholar.sun.ac.za

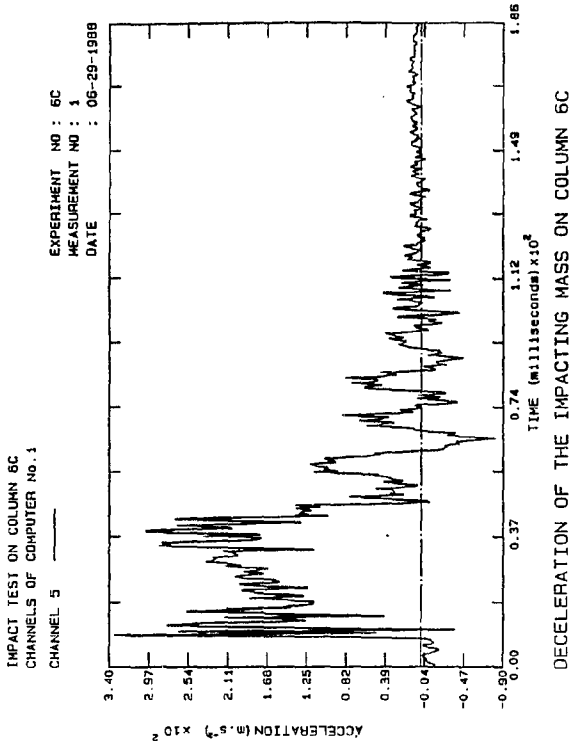

Fig. B.649: Decel. Col.6C

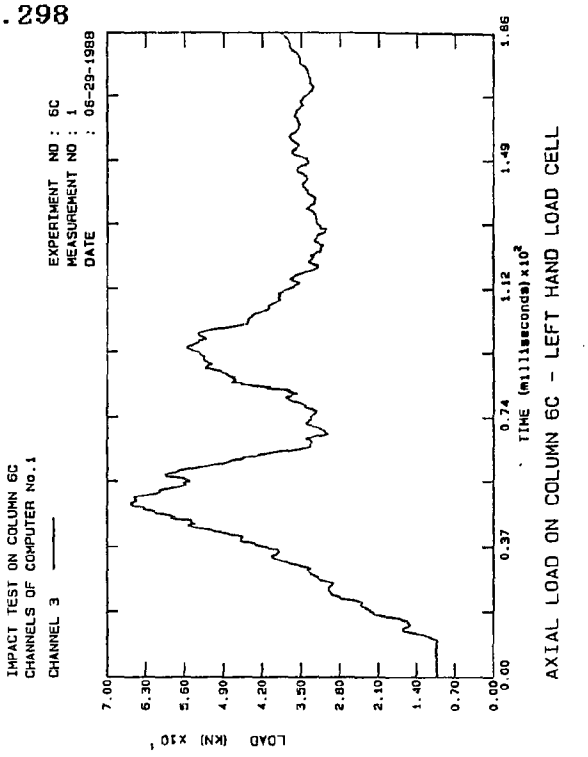

Fig. B.650: Axial load Col.6C

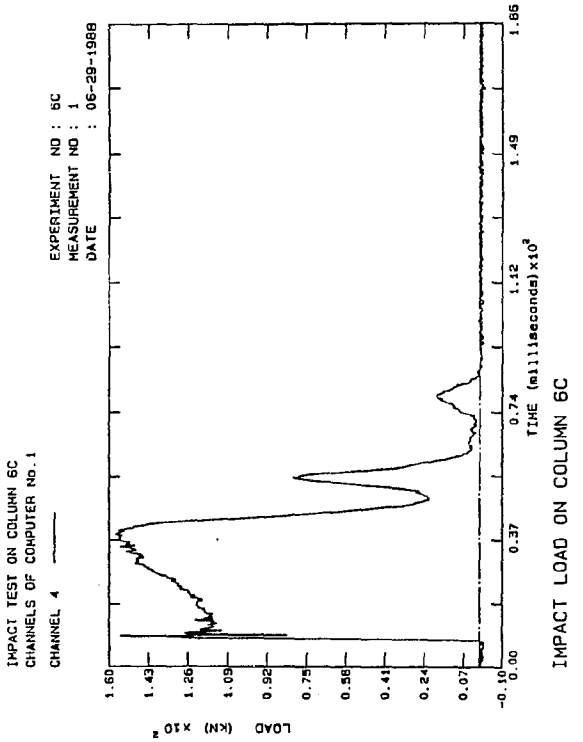

Fig. B.651: Impact Col 6C

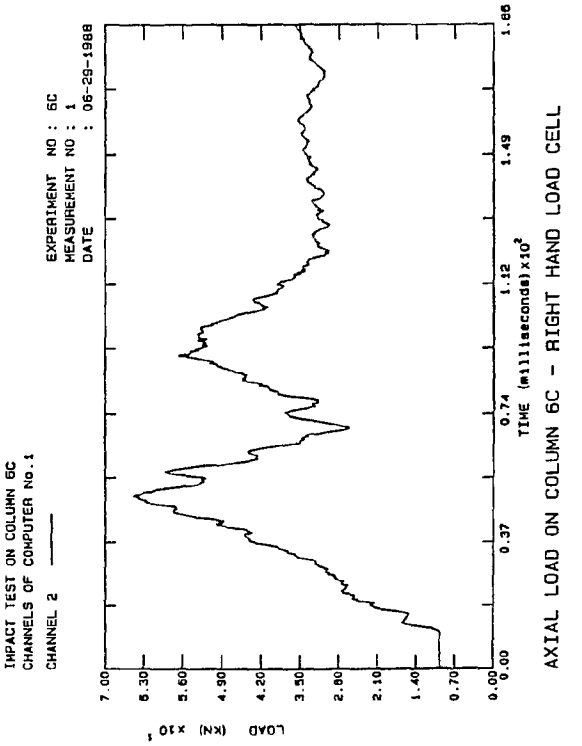

Fig. B.652: Axial load Col.6C

Stellenbosch University http://scholar.sun.ac.za

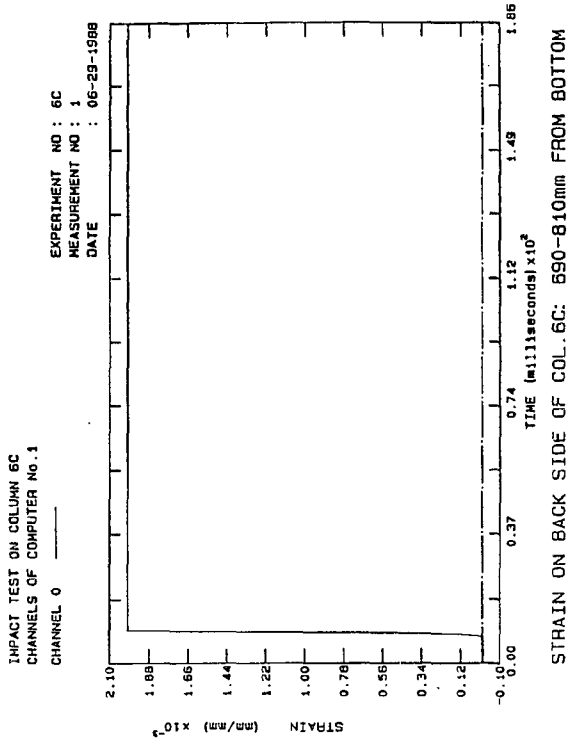

Fig. B.653: Strain Col.6C

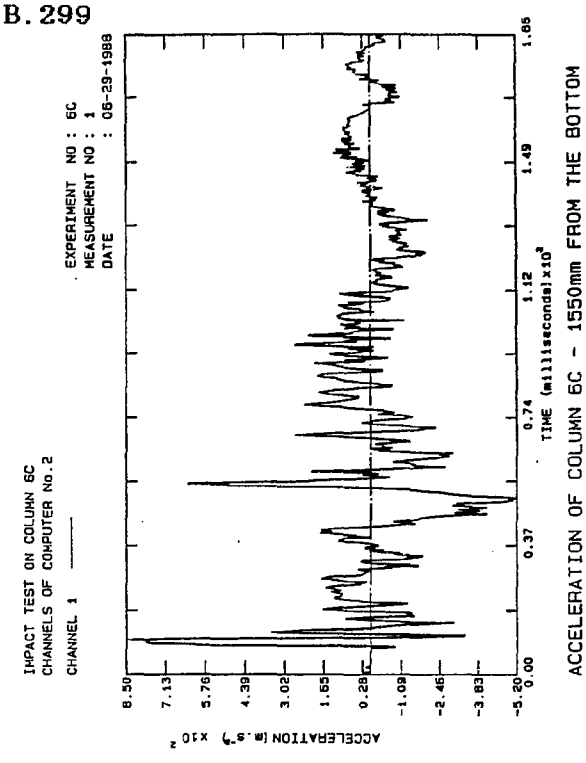

Fig. B.654: Accel. Col.6C

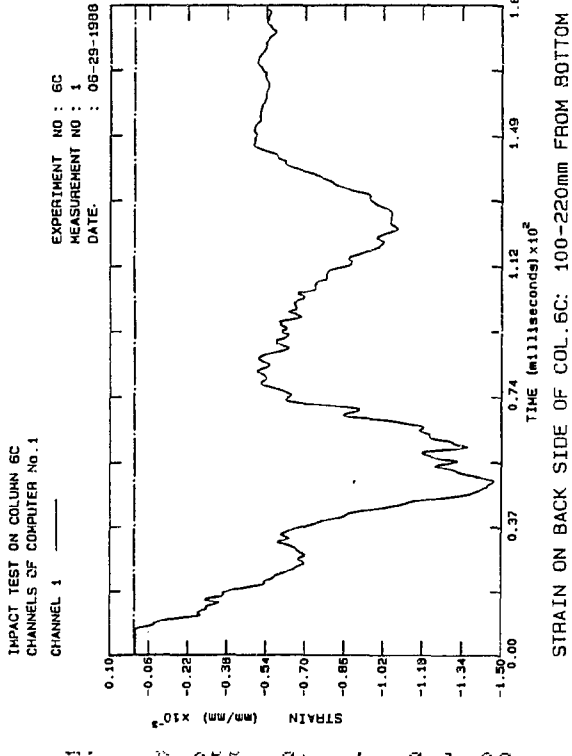

Fig. B.655: Strain Col 6C

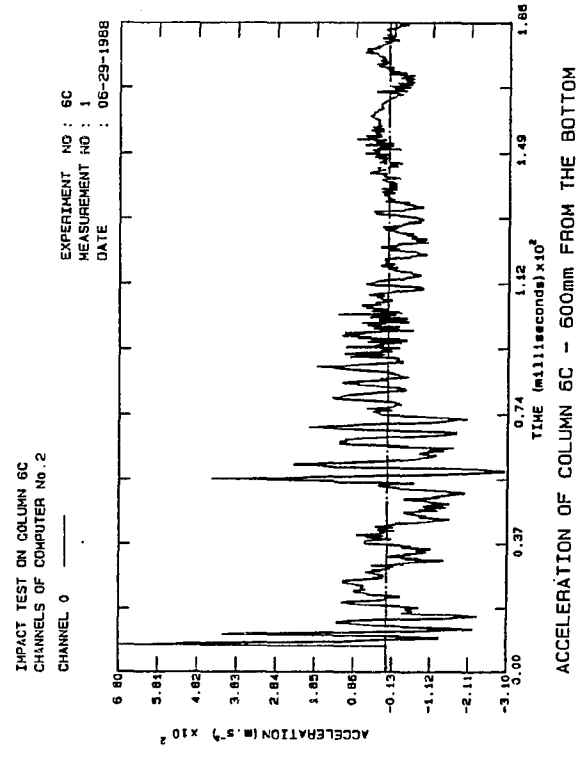

Fig. B.656: Accel. Col.6C

Stellenbosch University http://scholar.sun.ac.za

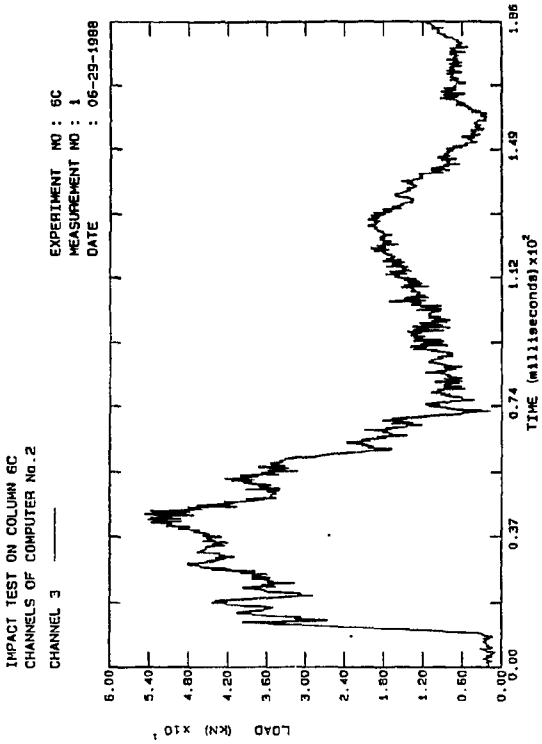

Fig. B.657: Comp. Col.6C

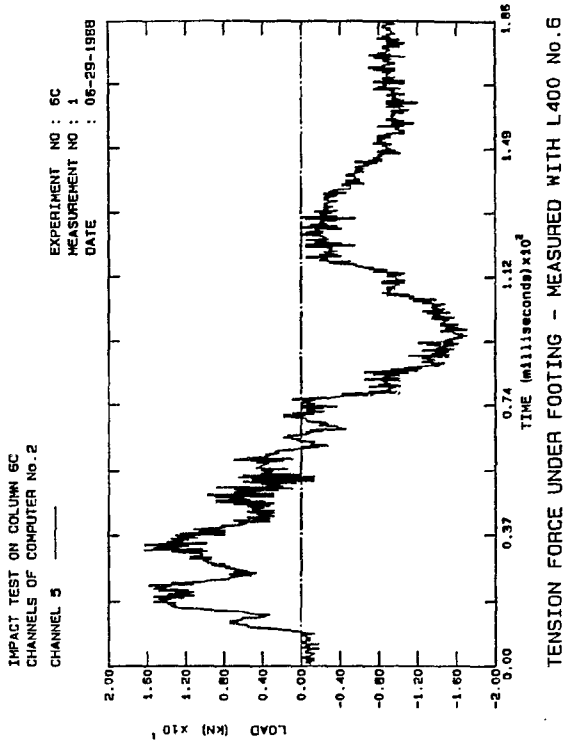

Fig. B.658: Tension Col.6C

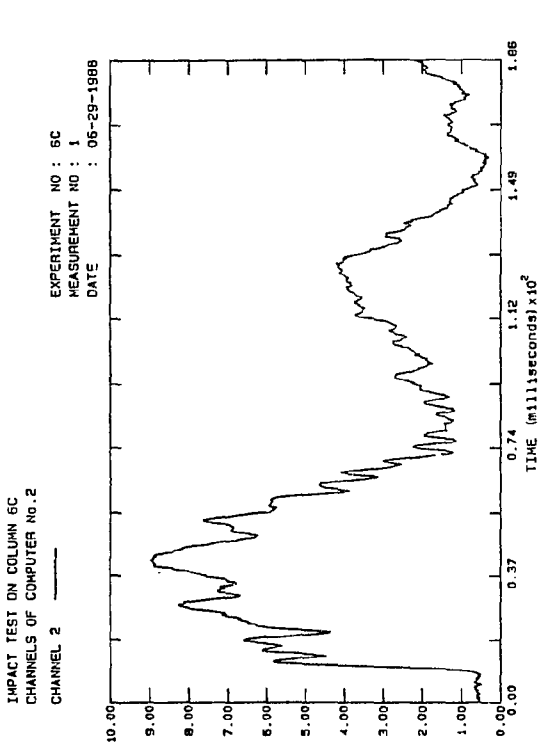

Fig. B.659: Comp. Col 6C

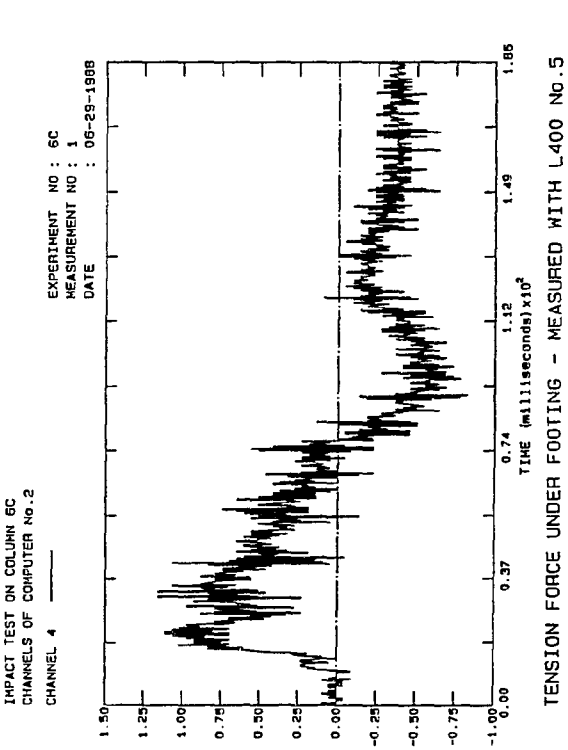

Fig. B.660: Tension Col.6C

Stellenbosch University http://scholar.sun.ac.za

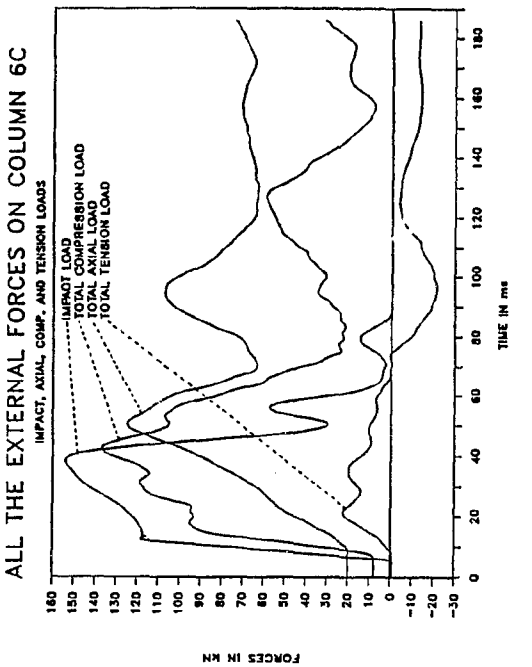

Fig. B.661: Ext. Loads Col.6C

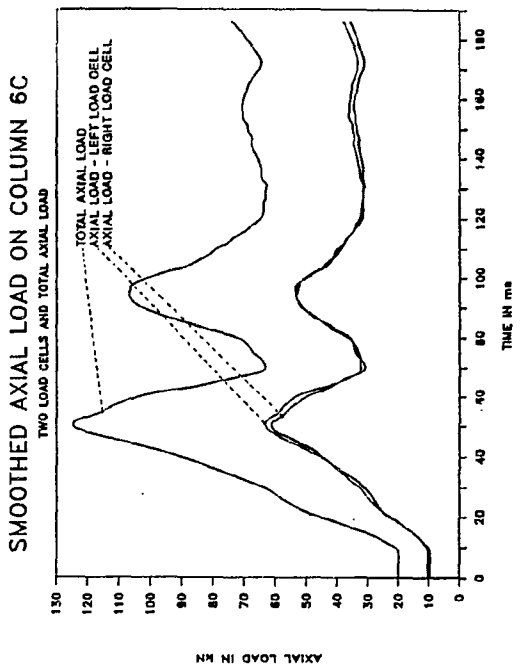

Fig. B.662: Smo. Axial Col.6C

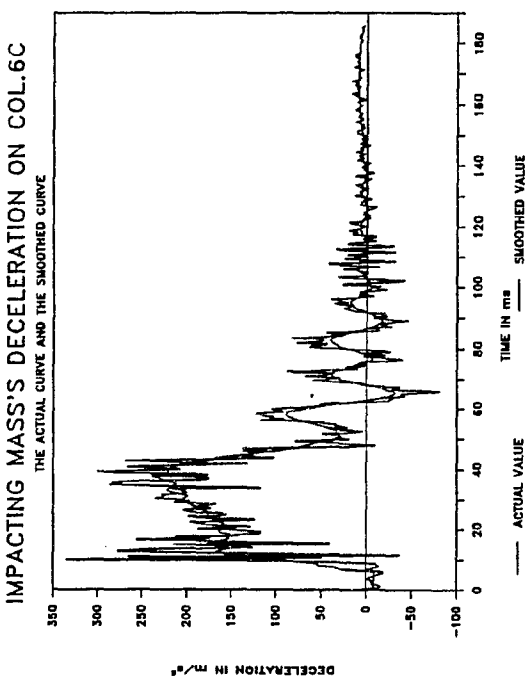

Fig. B.663: Smo.Decel. Col 6C

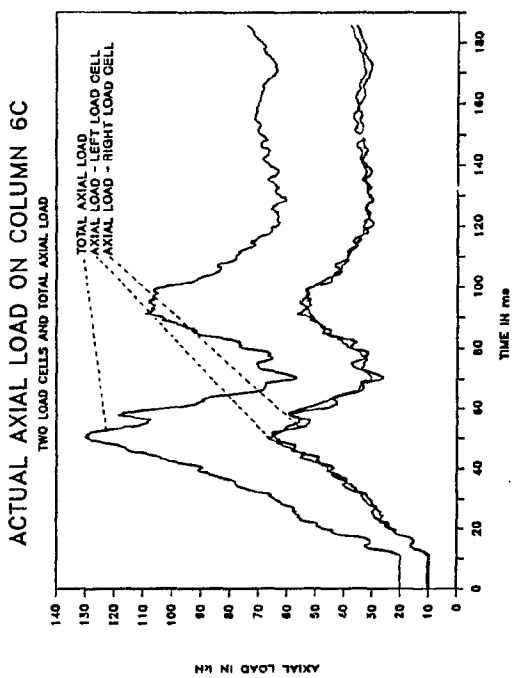

Fig. B.664: Axial loads Col.6C

Stellenbosch University http://scholar.sun.ac.za

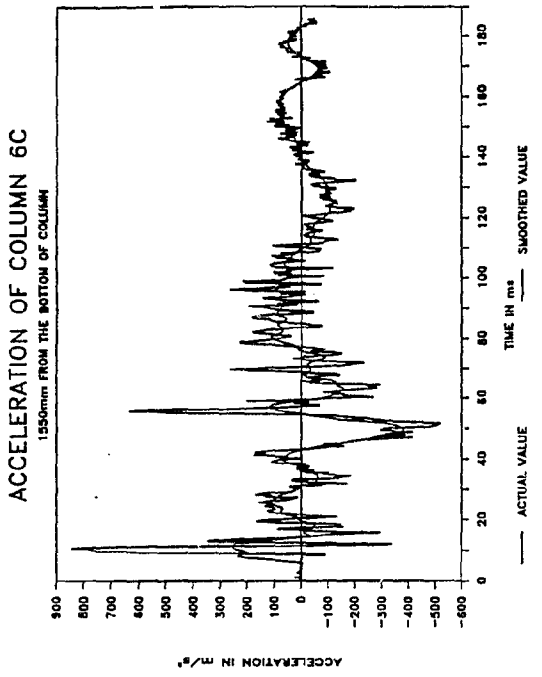

Fig. B.665: Smo.Accel. Col.6C

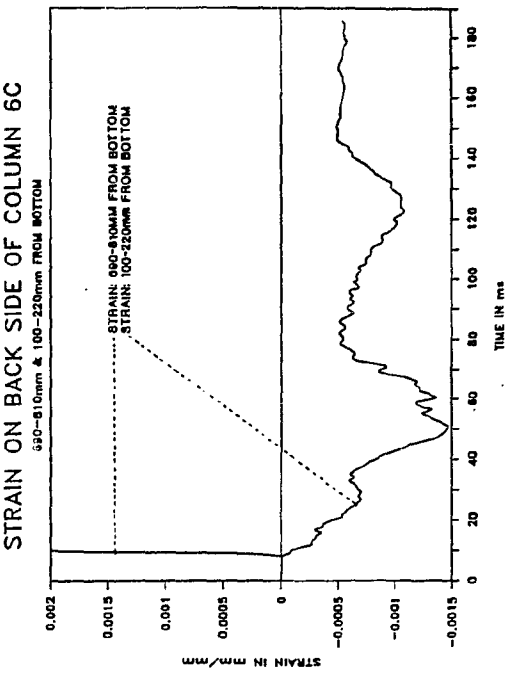

Fig. B.666: Strain Col.6C

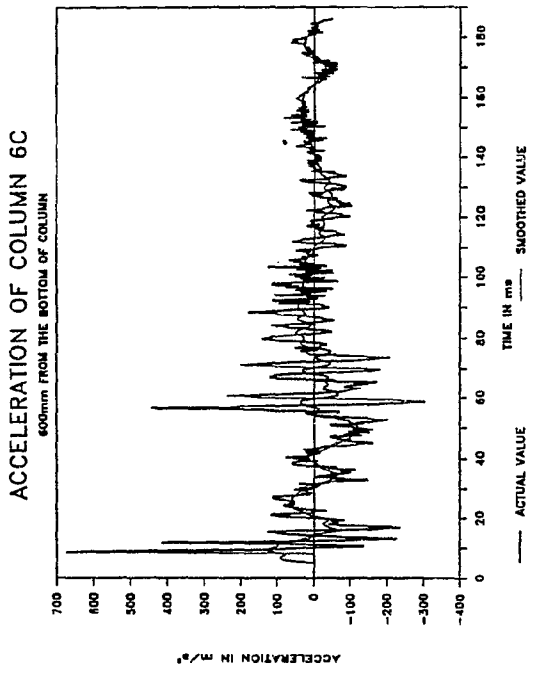

Fig. B.667: Smo.Accel. Col 6C

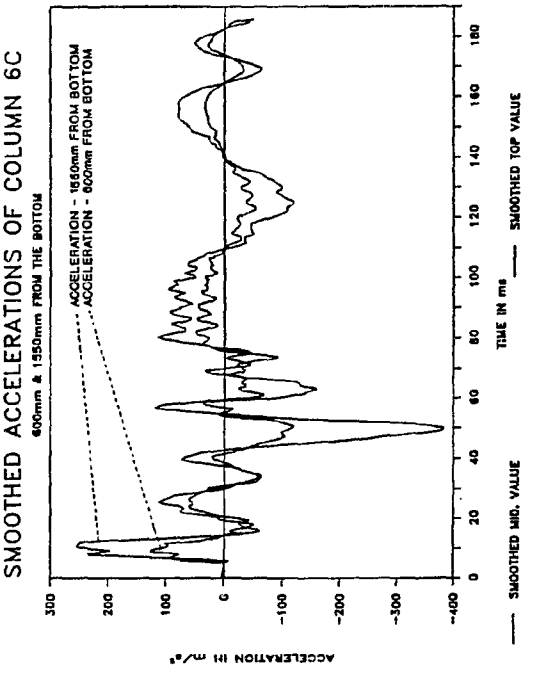

Fig. B.668: Smo. Accel. Col.6C

Stellenbosch University http://scholar.sun.ac.za

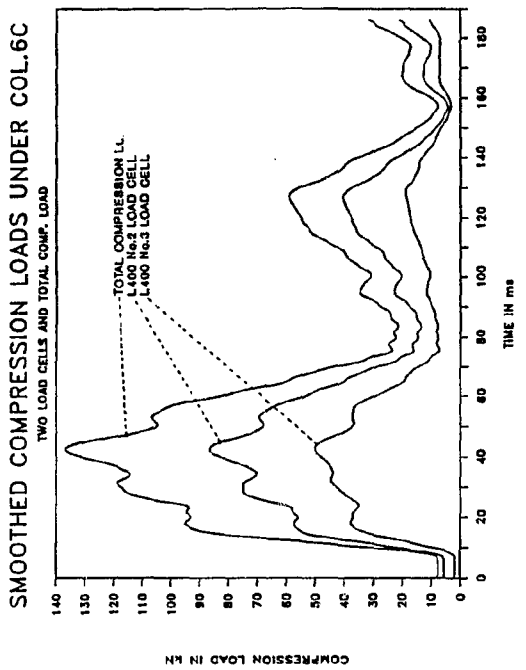

Fig. B.669: Smo. Comp. Col.6C

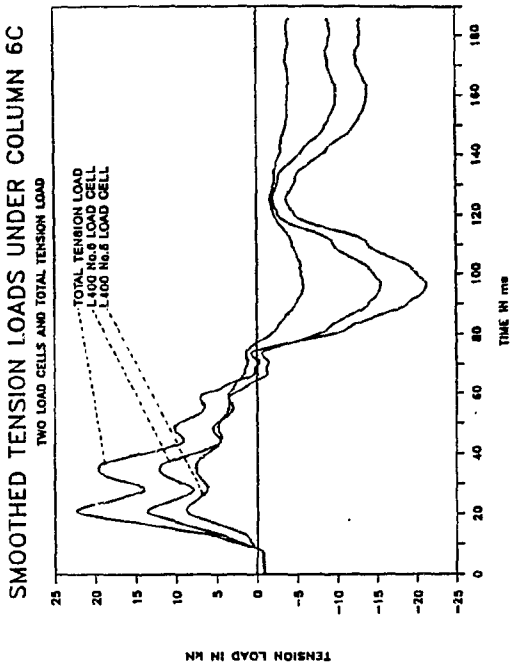

Fig. B.670: Smo. Tens. Col.6C

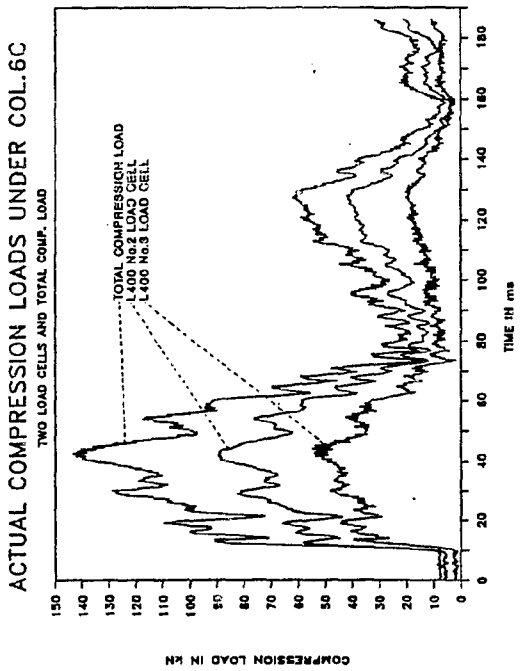

Fig. B.671: Comp. load Col 6C

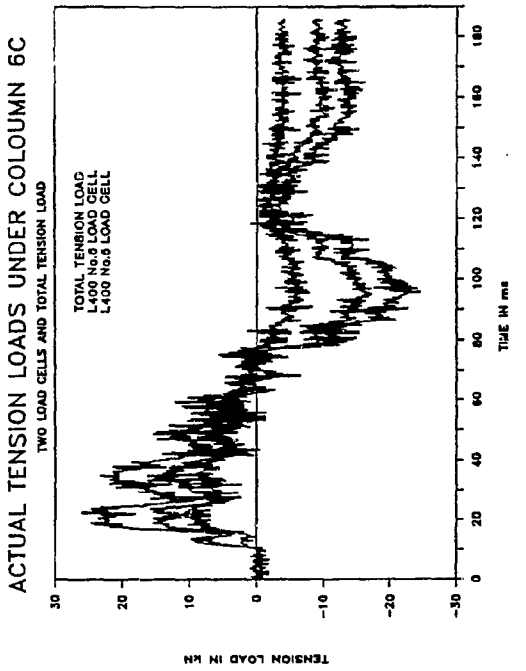

Fig. B.672: Tens. loads Col.6C

Stellenbosch University http://scholar.sun.ac.za

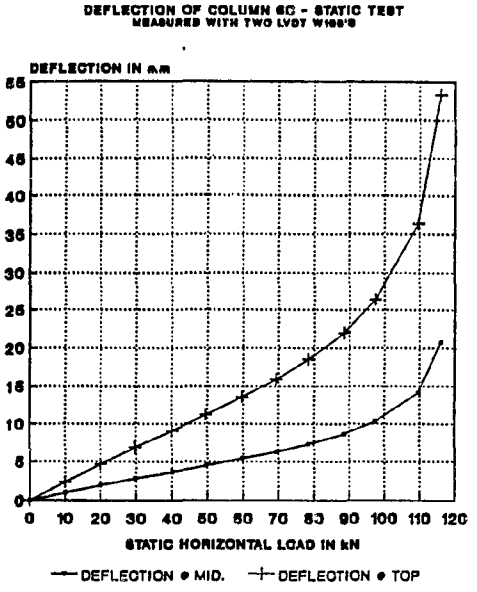

Fig. B.673: Deflection Col.6C

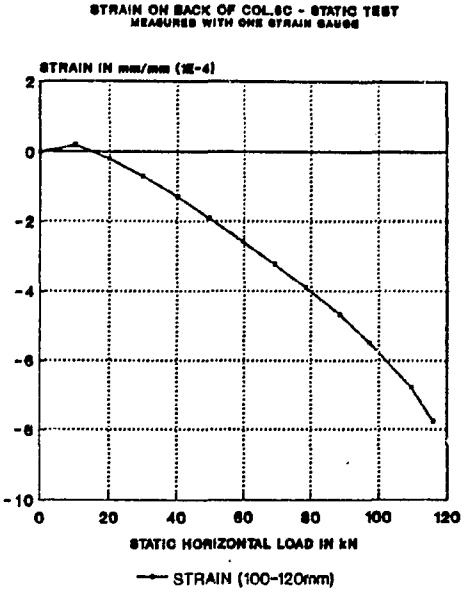

Fig. B.674: Strain Col.6C

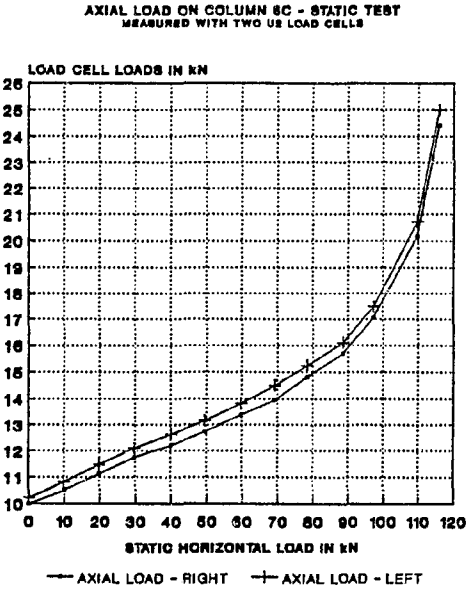

Fig. B.675: Axial load Col 6C

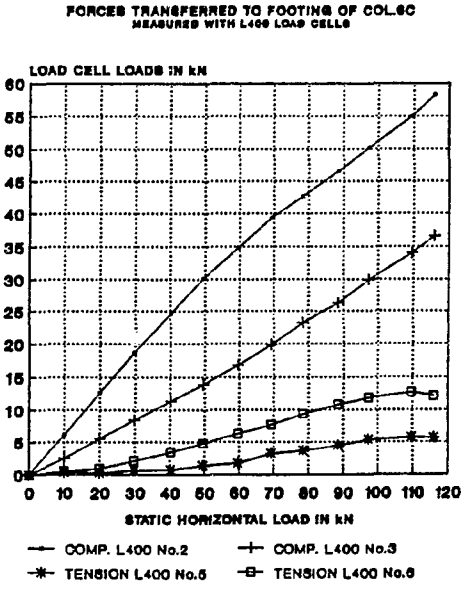

Fig. B.676: Foot.loads Col.6C

Stellenbosch University http://scholar.sun.ac.za

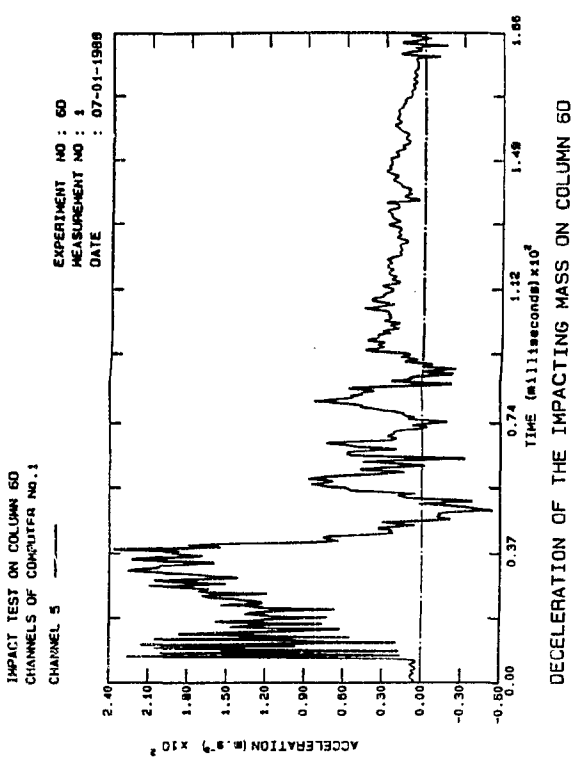

Fig. B.677: Decel. Col.6D

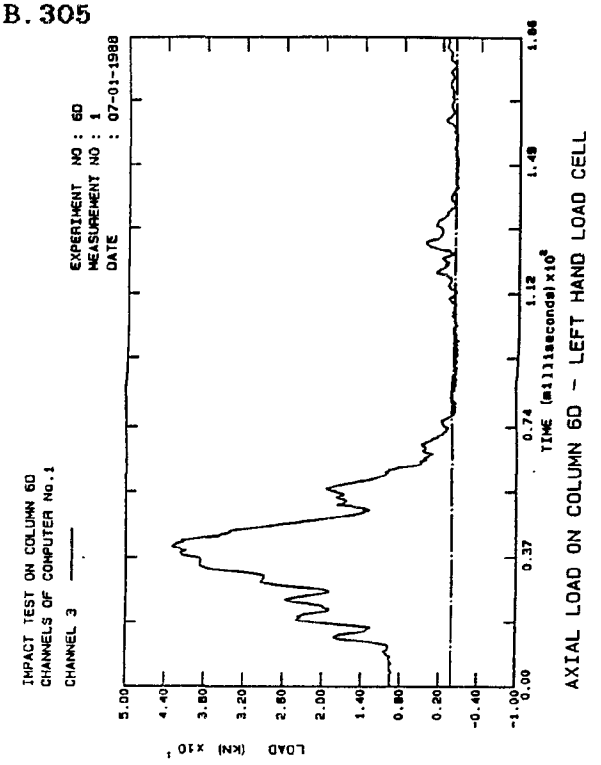

Fig. B.678: Axial load Col.6D

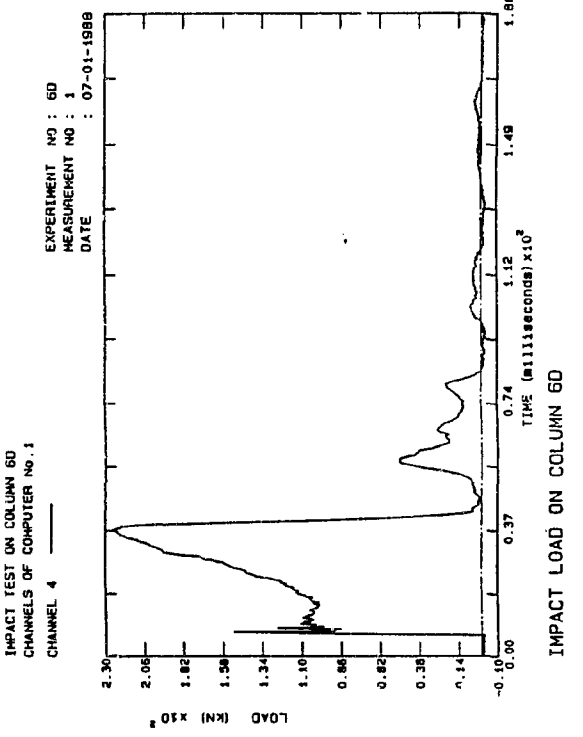

Fig. B.679: Impact Col 6D

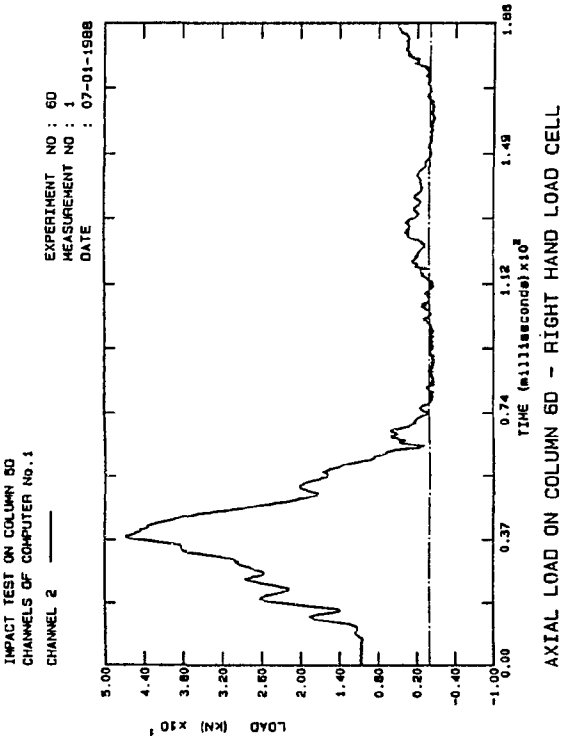

Fig. B.680: Axial load Col.6D

Stellenbosch University http://scholar.sun.ac.za

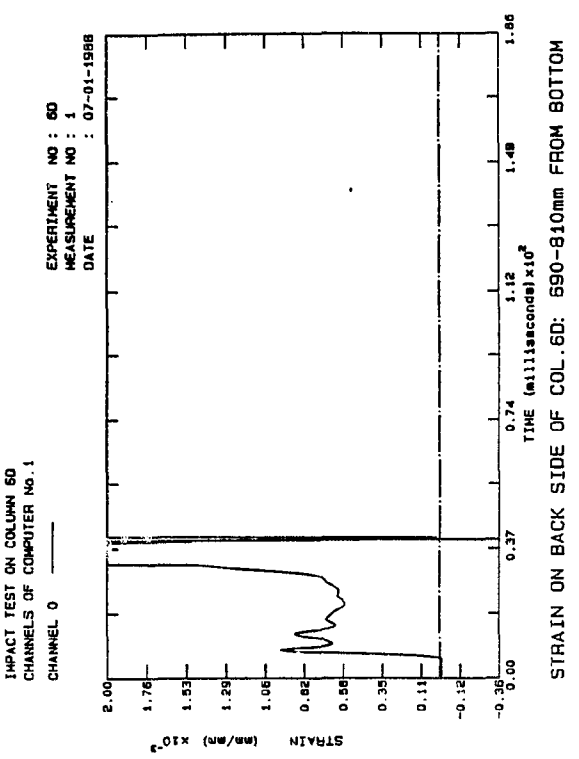

Fig. B.681: Strain Col.6D

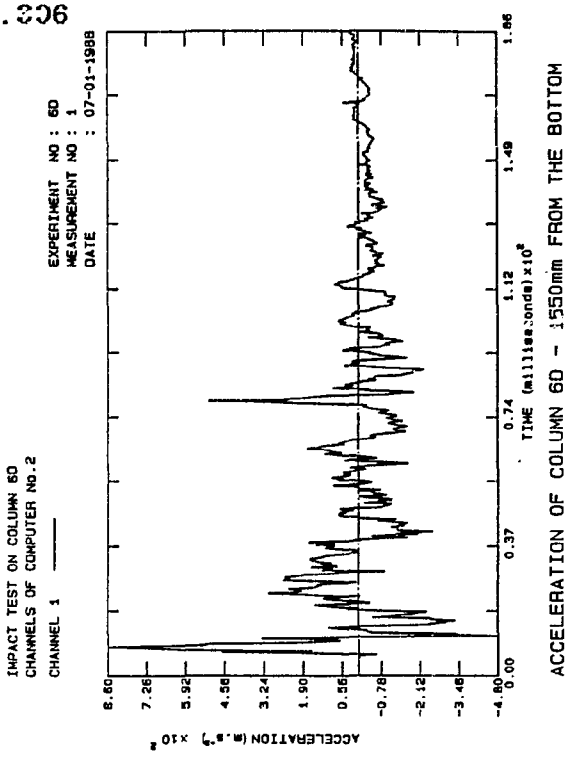

Fig. B.682: Accel. Col.6D

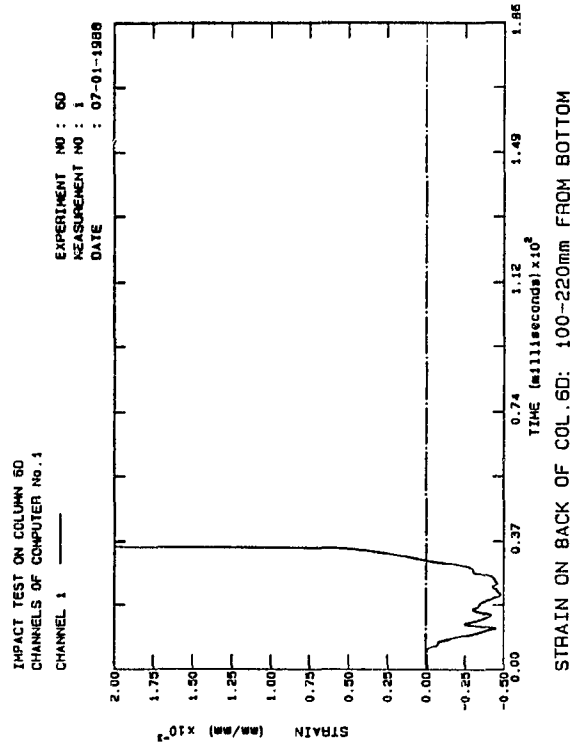

Fig. B.683: Strain Col 6D

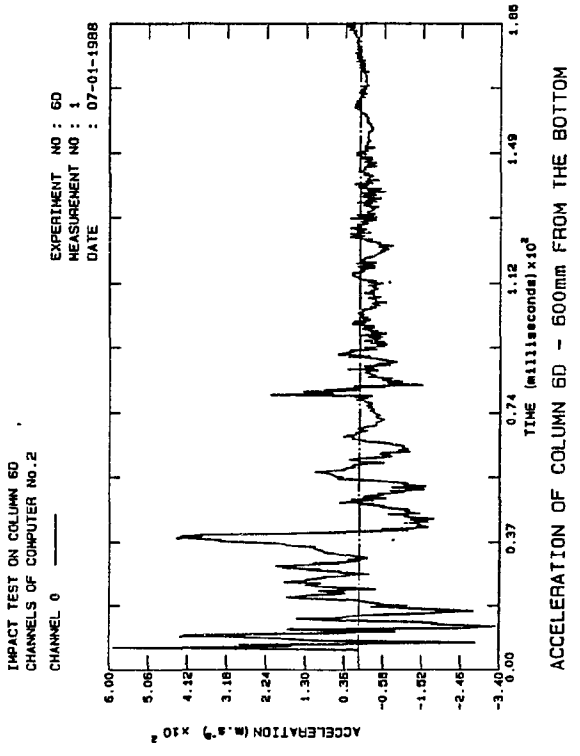

Fig. B.684: Accel. Col.6D

Stellenbosch University http://scholar.sun.ac.za

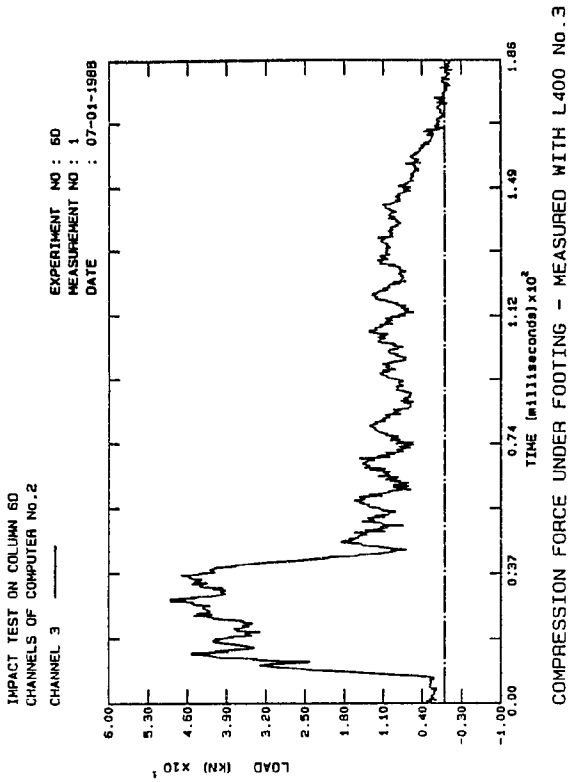

Fig. B.685: Comp. Col.6D

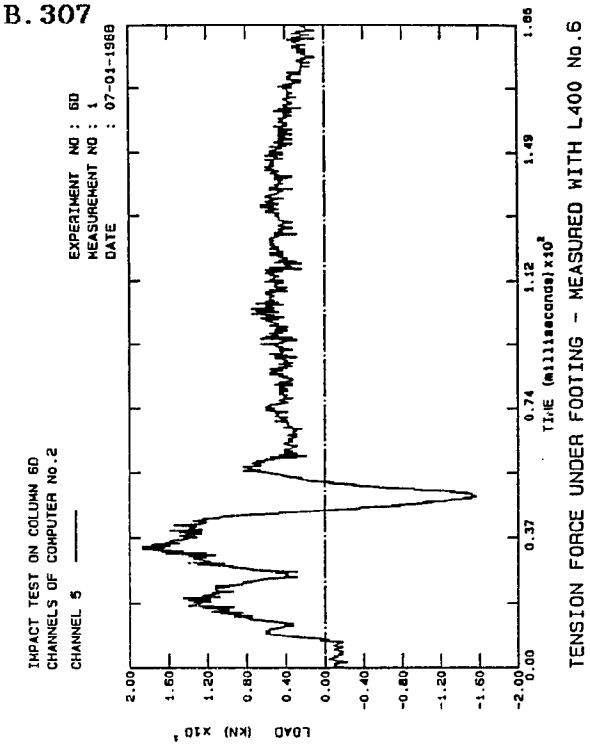

Fig. B.686: Tension Col.6D

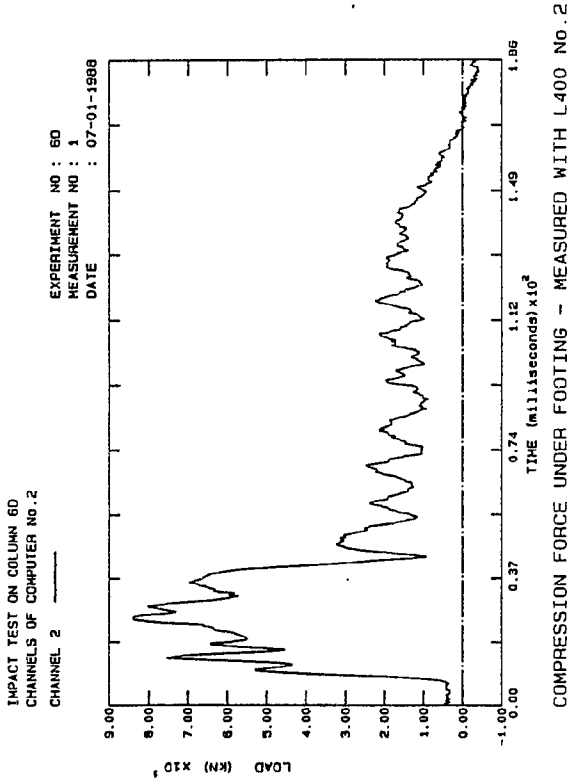

Fig. B.687: Comp. Col 6D

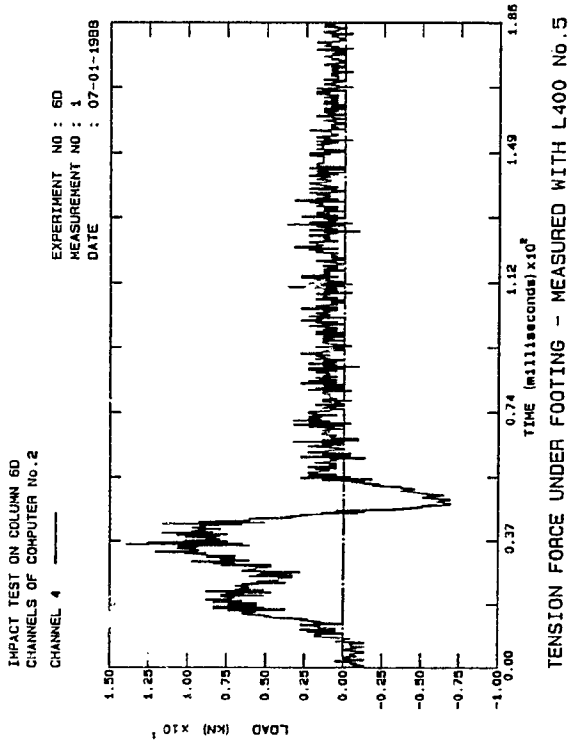

Fig. B.688: Tension Col.6D

Stellenbosch University http://scholar.sun.ac.za

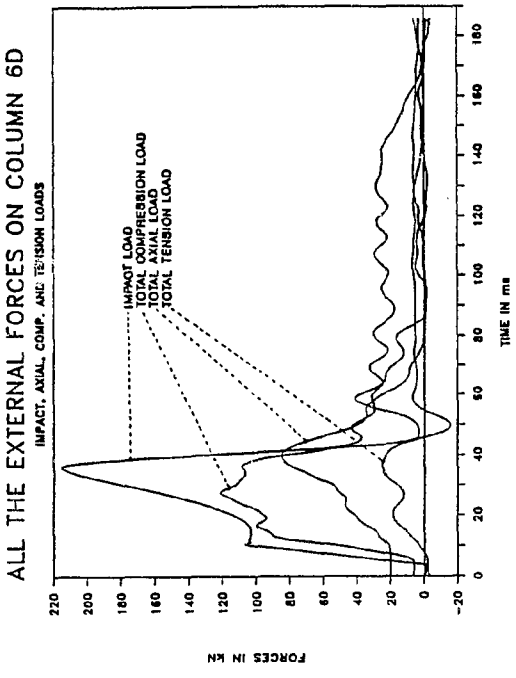

Fig. B.689: Ext. Loads Col.6D

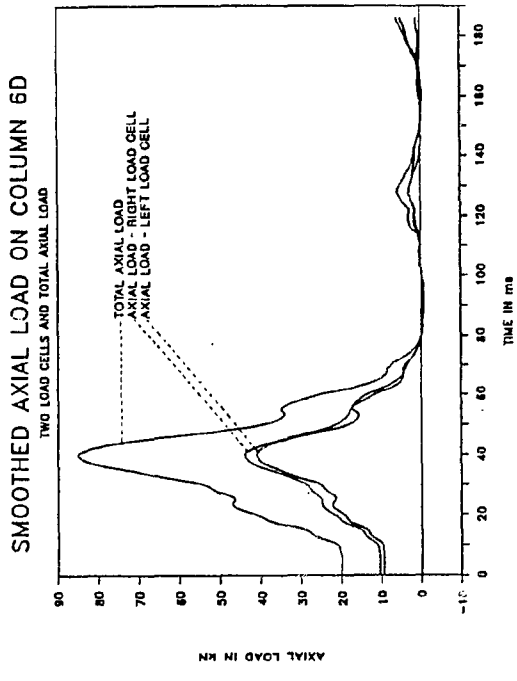

Fig. B.690: Smo. Axial Col.6D

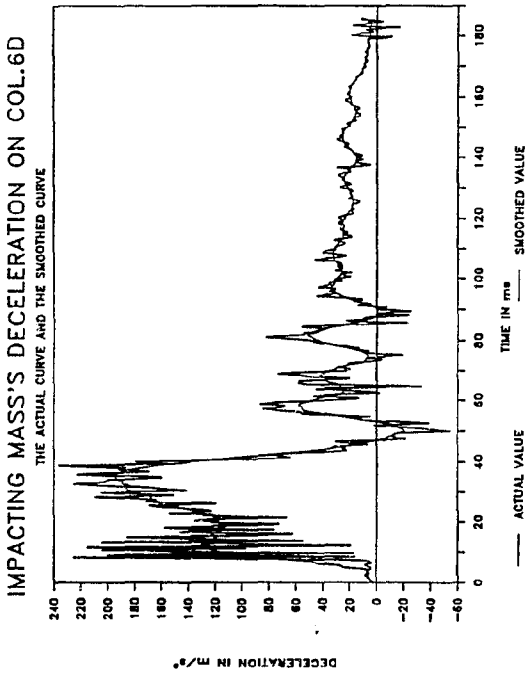

Fig. B.691: Smo.Decel. Col 6D

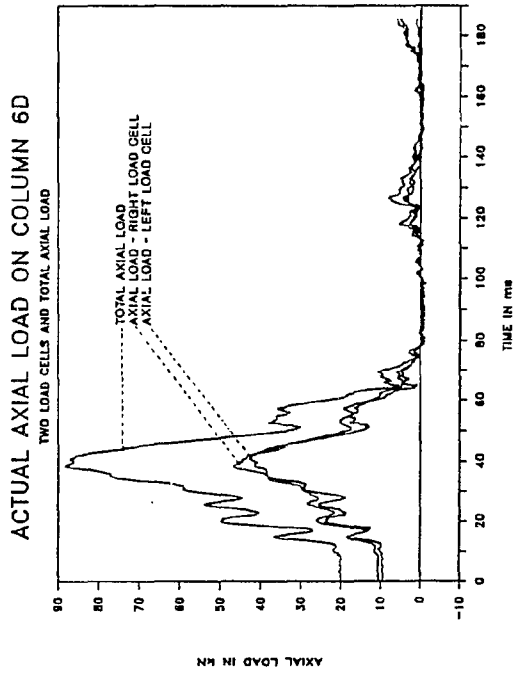

Fig. B.692: Axial loads Col.6D

Stellenbosch University http://scholar.sun.ac.za

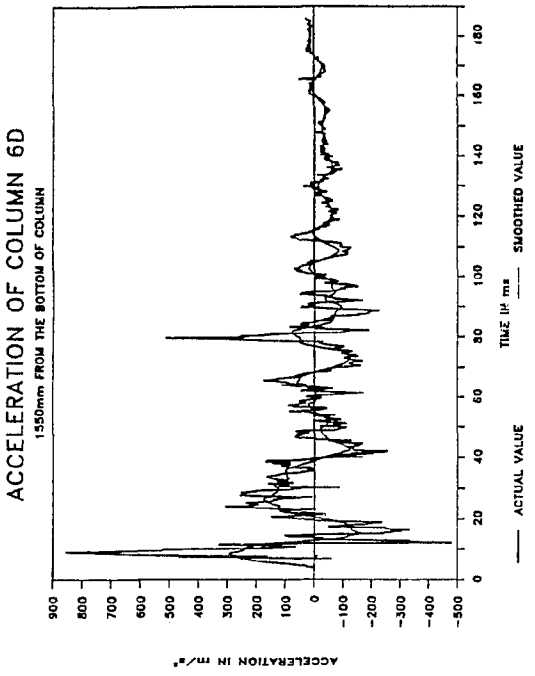

Fig. B.693: Smo.Accel. Col.6D

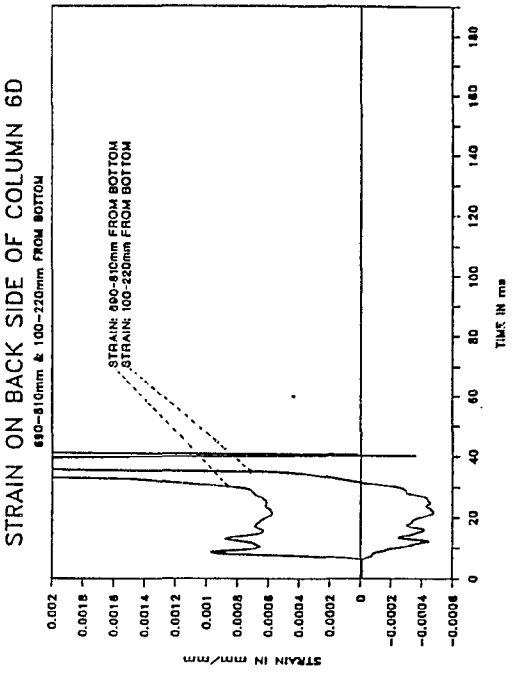

Fig. B.694: Strain Col.6D

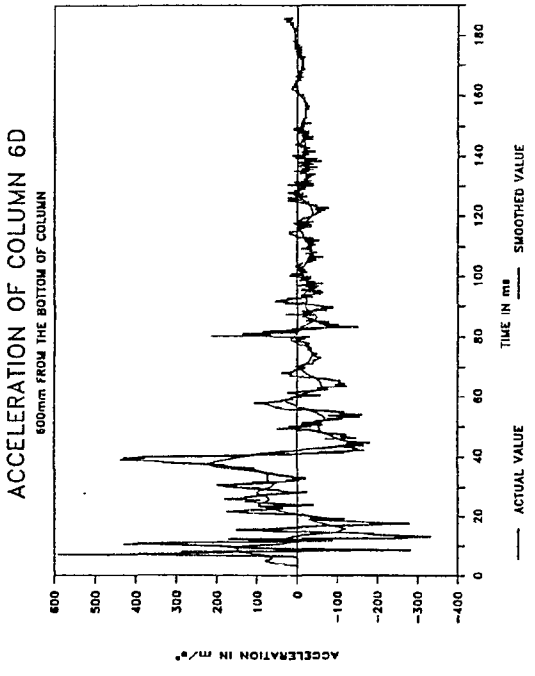

Fig. B.695: Smo.Accel. Col 6D

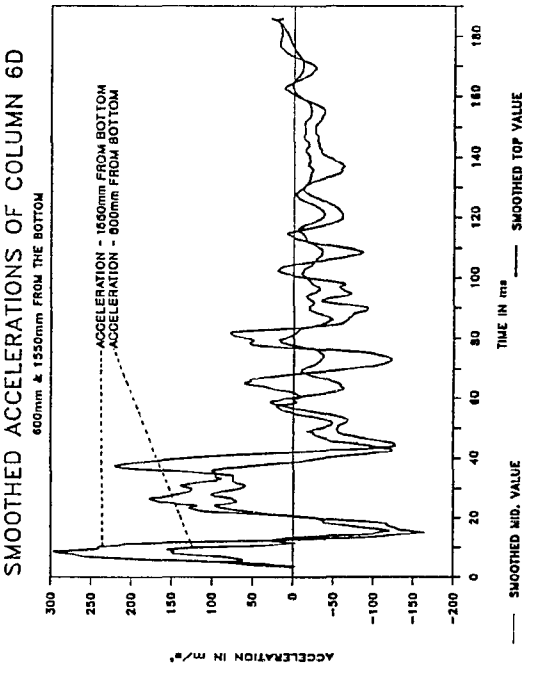

Fig. B.696: Smo. Accel. Col.6D

Stellenbosch University http://scholar.sun.ac.za

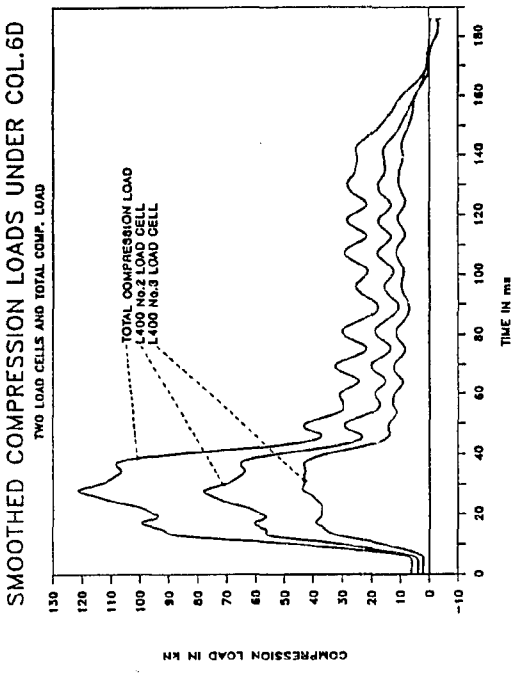

Fig. B.697: Smo. Comp. Col.6D

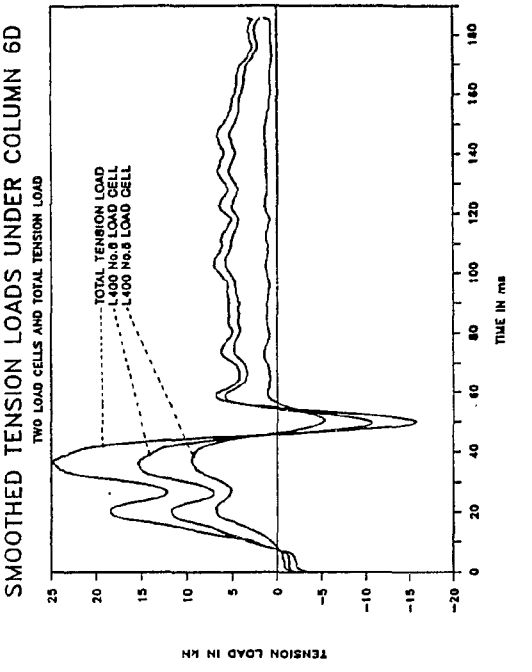

Fig. B.698: Smo. Tens. Col.6D

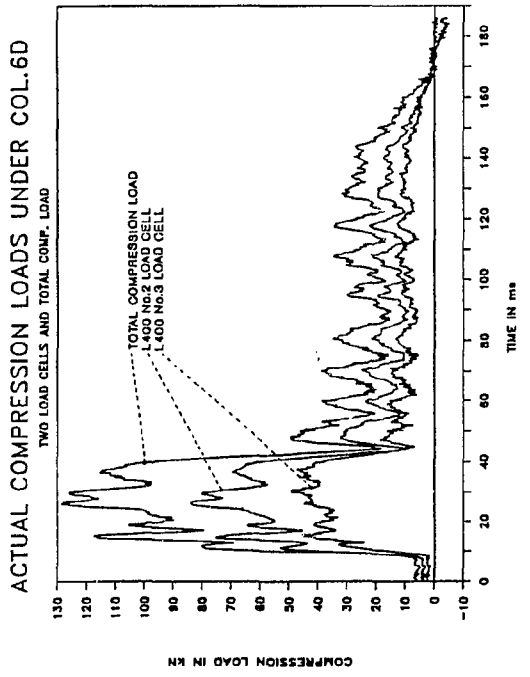

Fig. B.699: Comp. load Col 6D

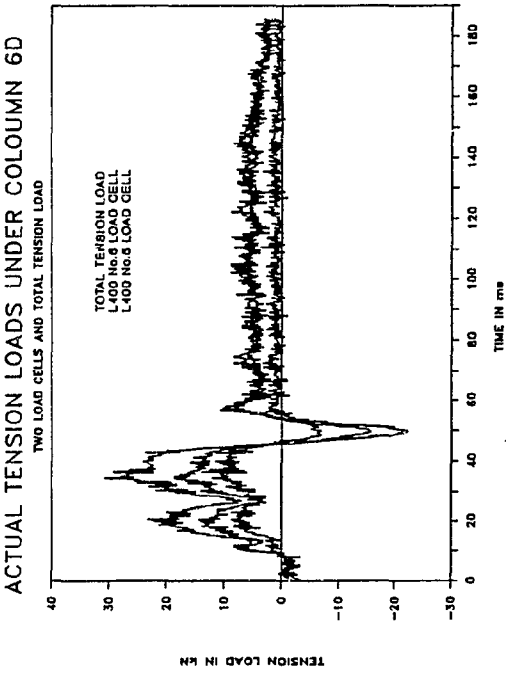

Fig. B.700: Tens. loads Col.6D

Stellenbosch University http://scholar.sun.ac.za

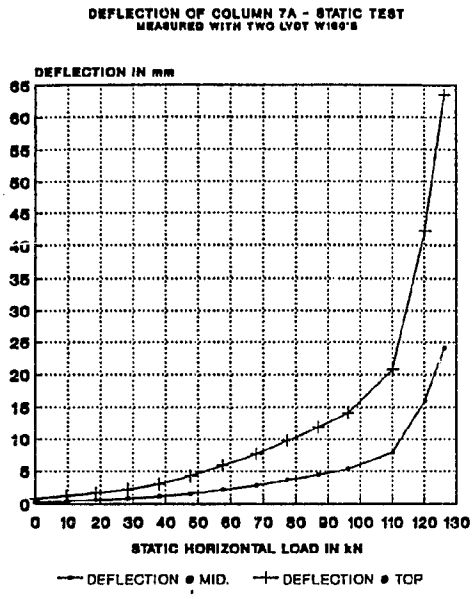

Fig. B.701: Deflection Col.7A

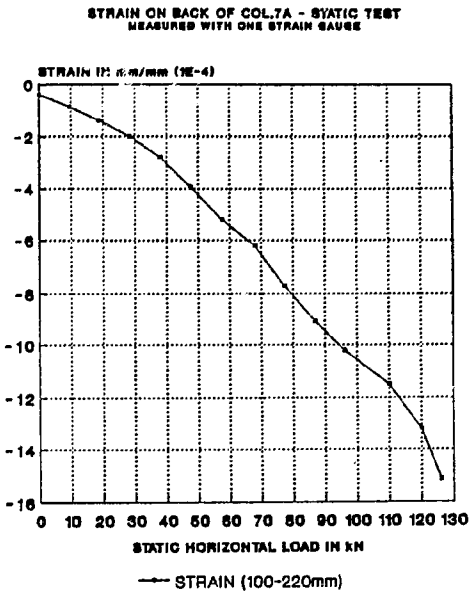

Fig. B.702: Strain Col.7A

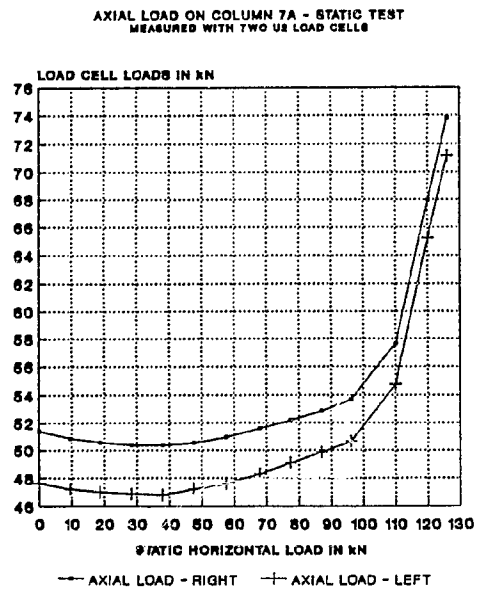

Fig. B.703: Axial load Col 7A

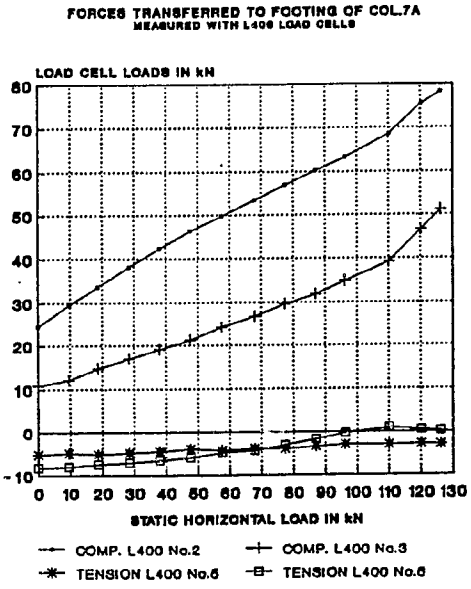

Fig. B.704: Foot.loads Col.7A

Stellenbosch University http://scholar.sun.ac.za

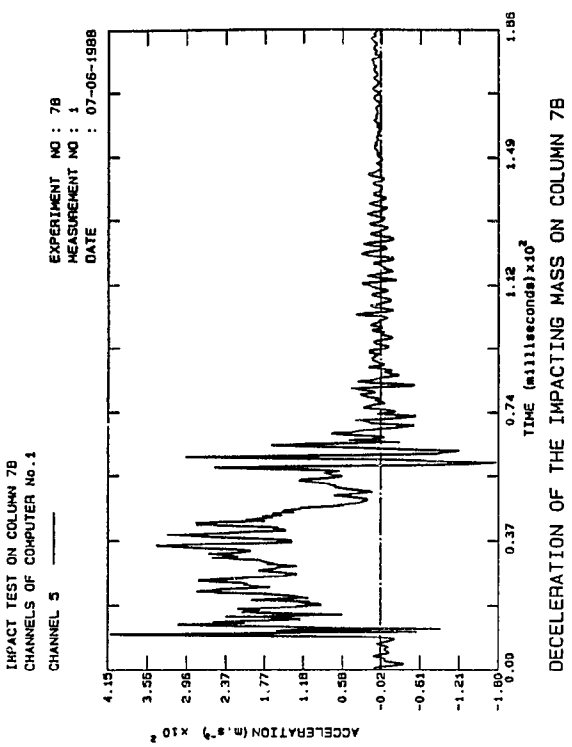

Fig. B.705: Decel. Col.7B

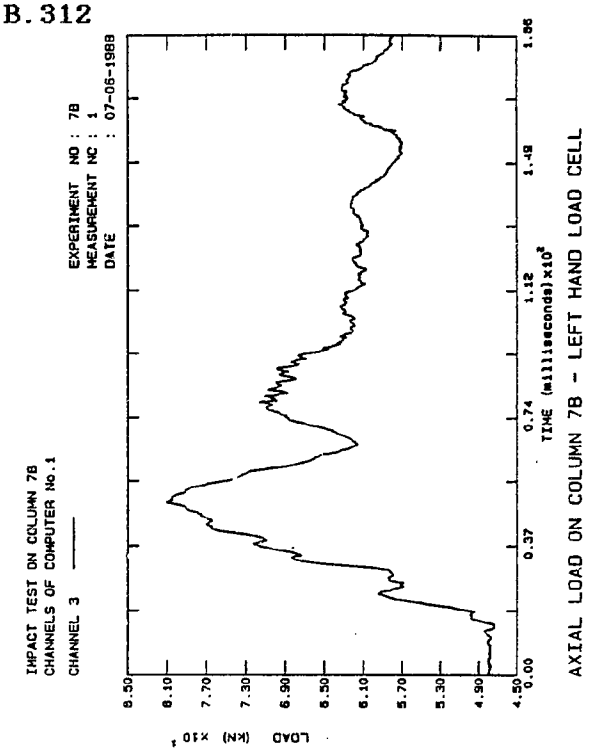

Fig. B.706: Axial load Col.7B

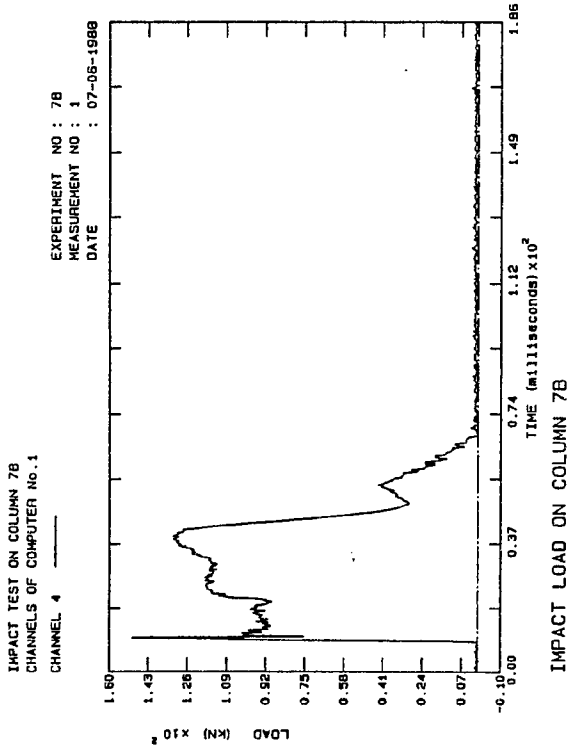

Fig. B.707: Impact Col 7B

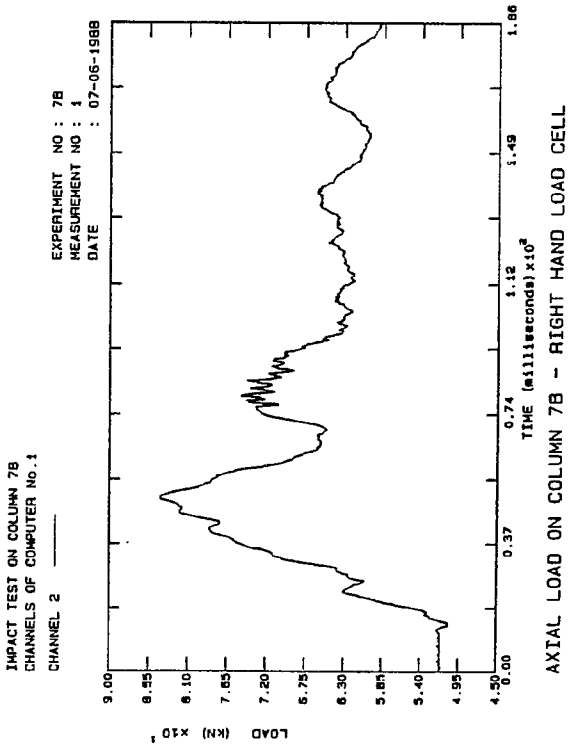

Fig. B.708: Axial load Col.7B

Stellenbosch University http://scholar.sun.ac.za

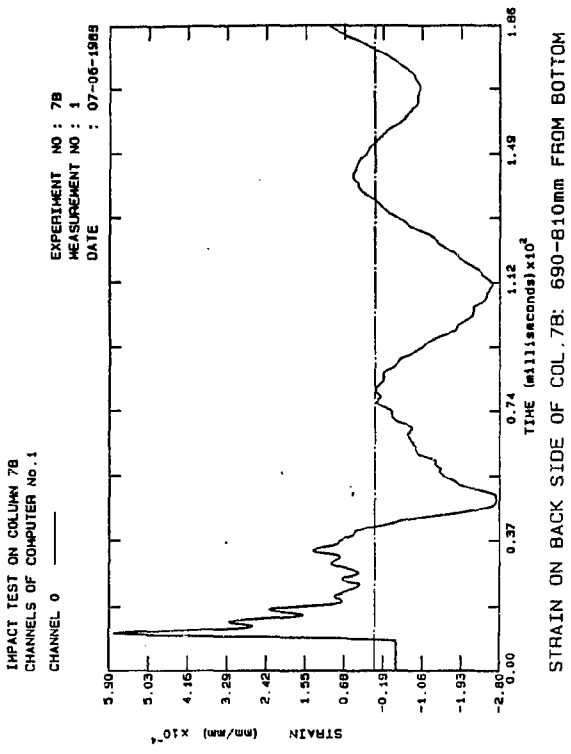

Fig. B.709: Strain Col.7B

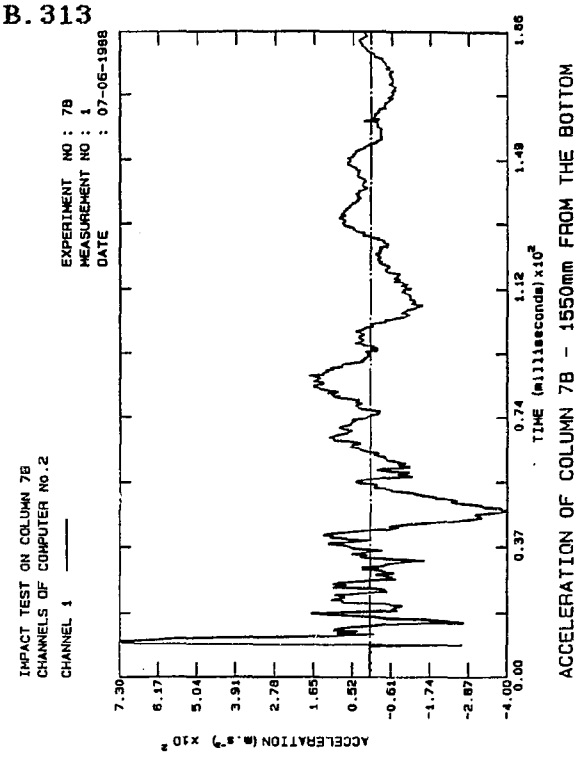

Fig. B.710: Accel. Col.7B

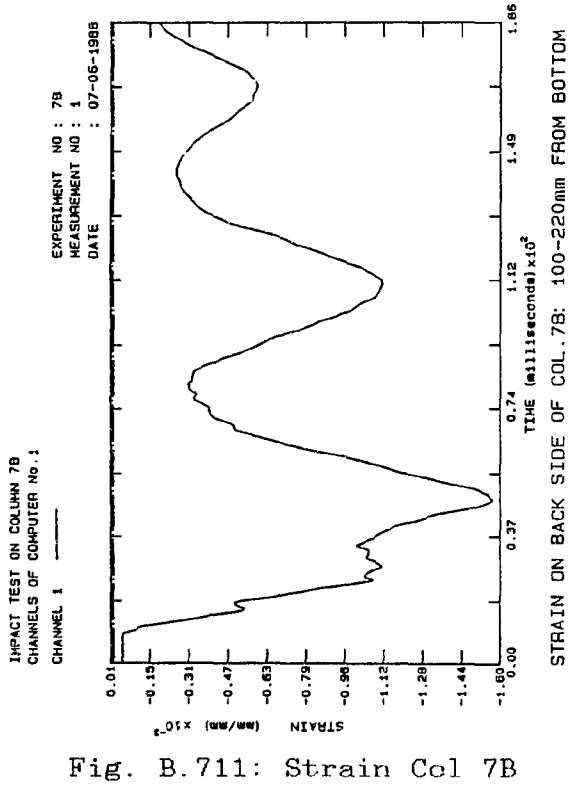

Fig. B.711: Strain Col 7B

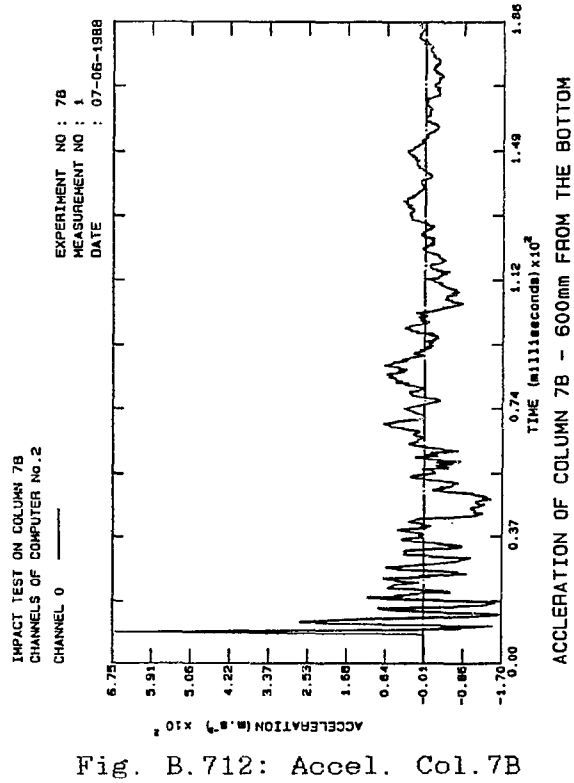

Fig. B.712: Accel. Col.7B

Stellenbosch University http://scholar.sun.ac.za

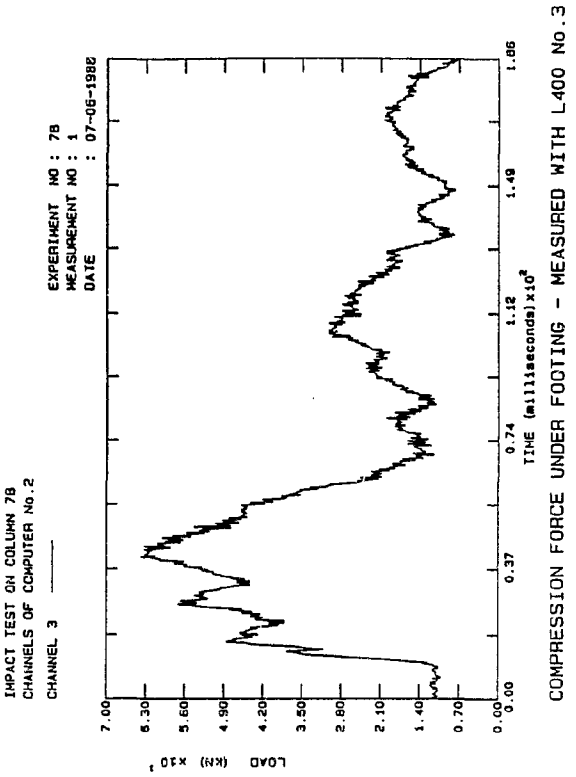

Fig. B.713: Comp. Col.7B

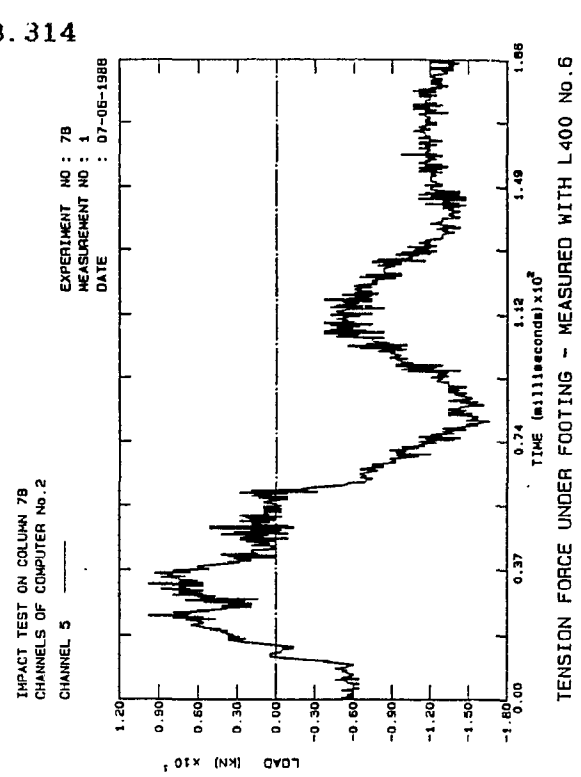

Fig. B.714: Tension Col.7B

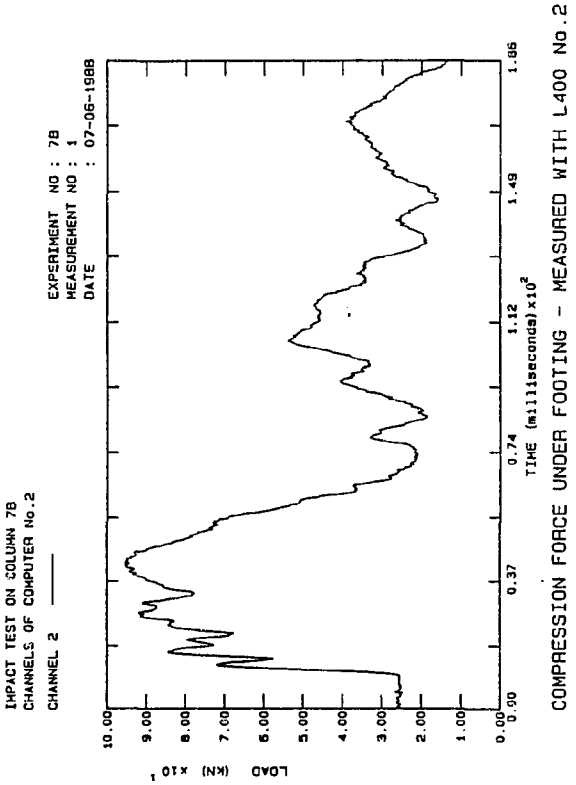

Fig. B.715: Comp. Col 7B

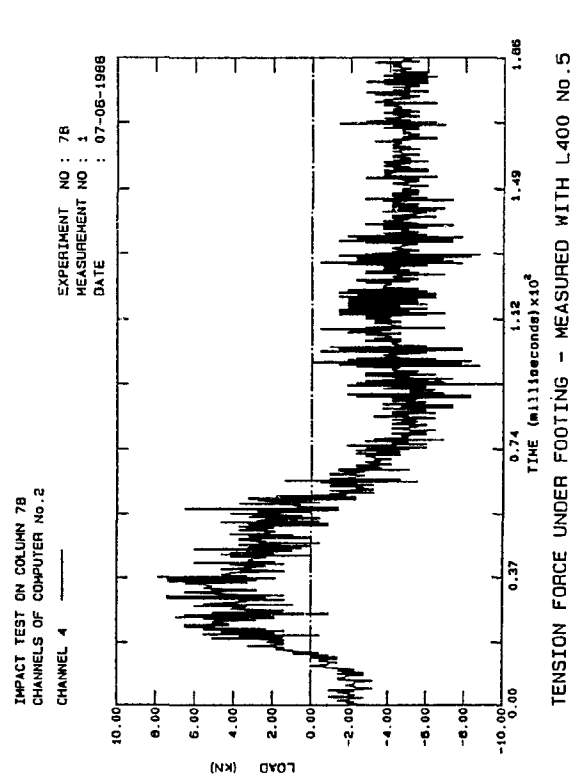

Fig. B.716: Tension Col.7B

Stellenbosch University http://scholar.sun.ac.za

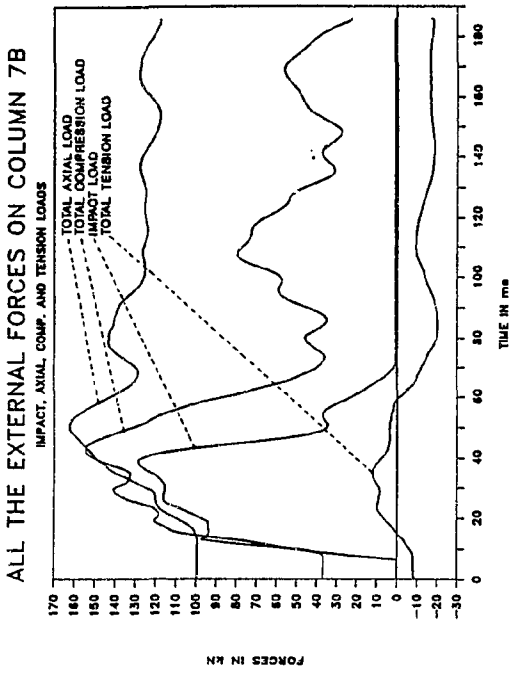

Fig. B.717: Ext. Loads Col.7B

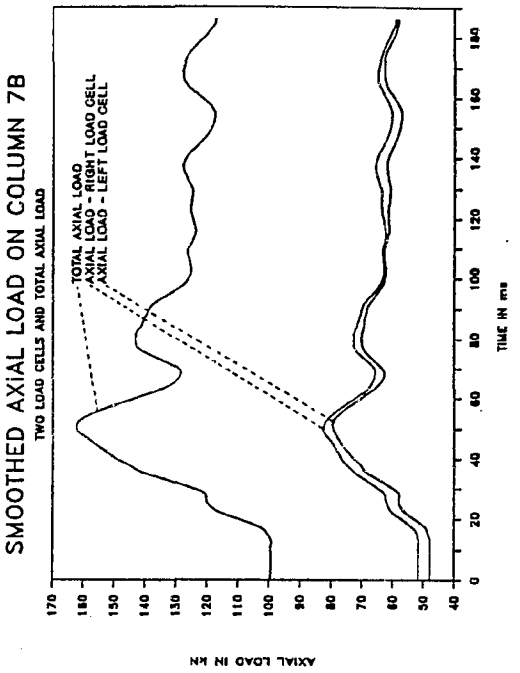

Fig. B.718: Smo. Axial Col.7B

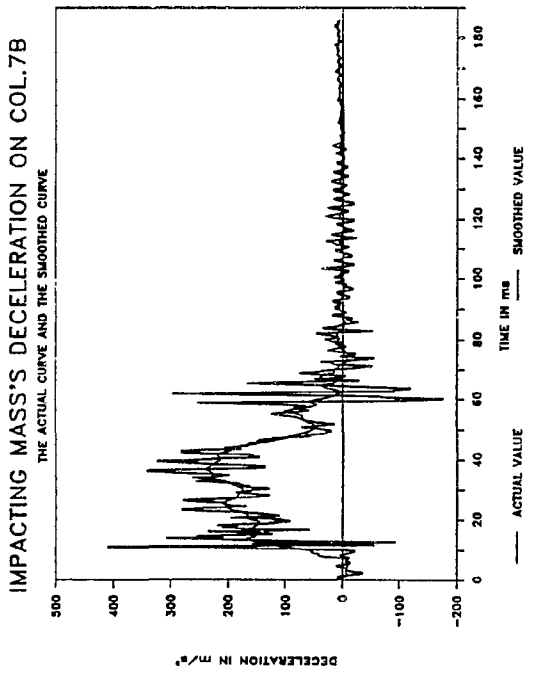

Fig. B.719: Smo.Decel. Col 7B

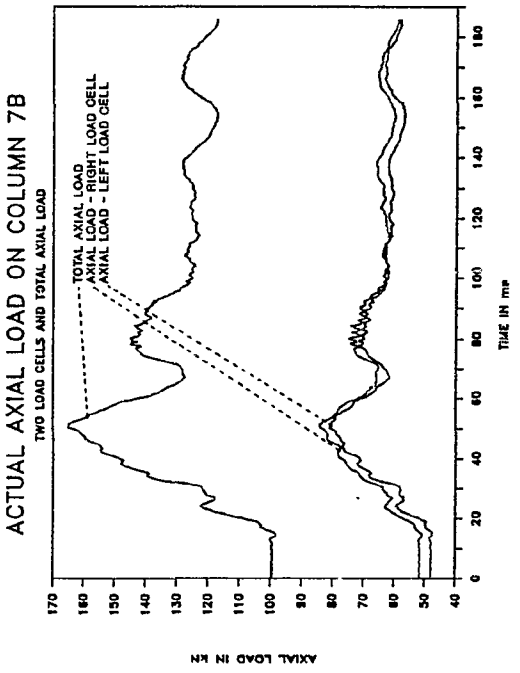

Fig. B.720: Axial loads Col.7B

Stellenbosch University http://scholar.sun.ac.za

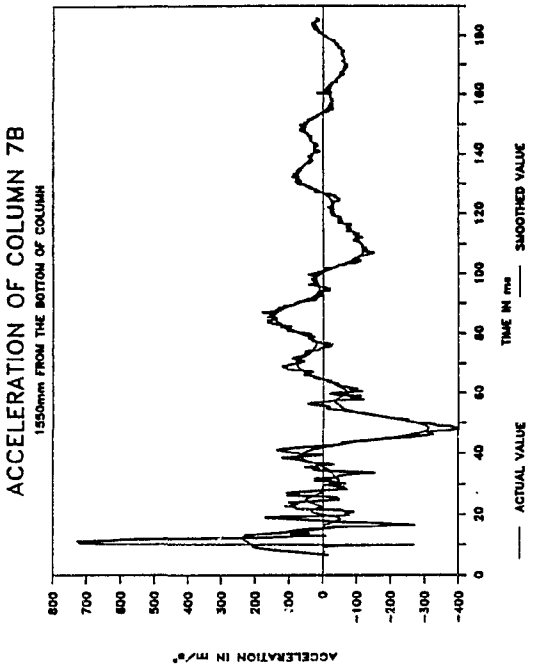

Fig. B.721: Smo.Accel. Col.7B

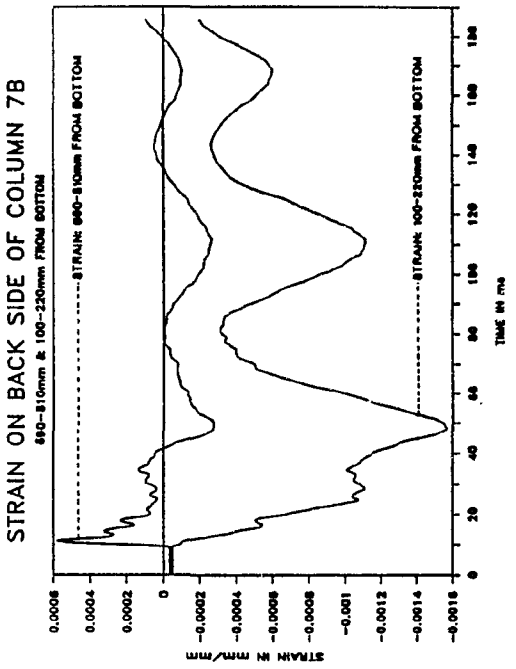

Fig. B.722: Strain Col.7B

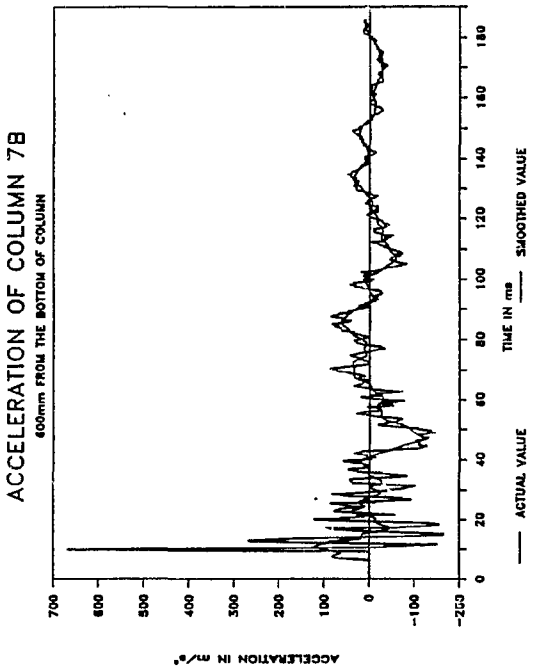

Fig. B.723: Smo.Accel. Col 7B

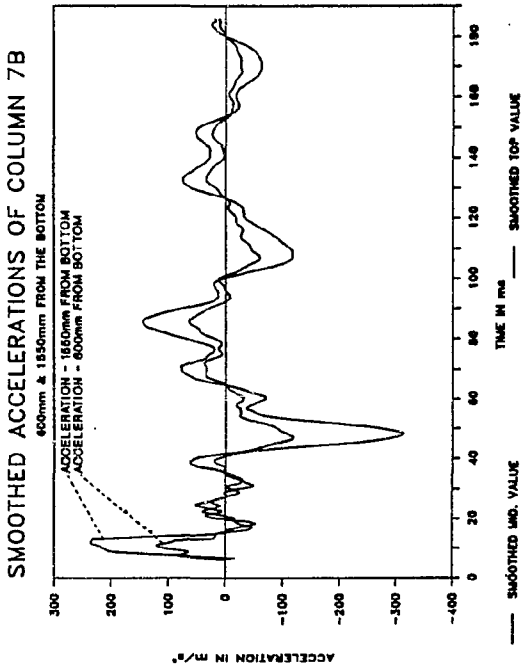

Fig. B.724: Smo. Accel. Col.7B

Stellenbosch University http://scholar.sun.ac.za

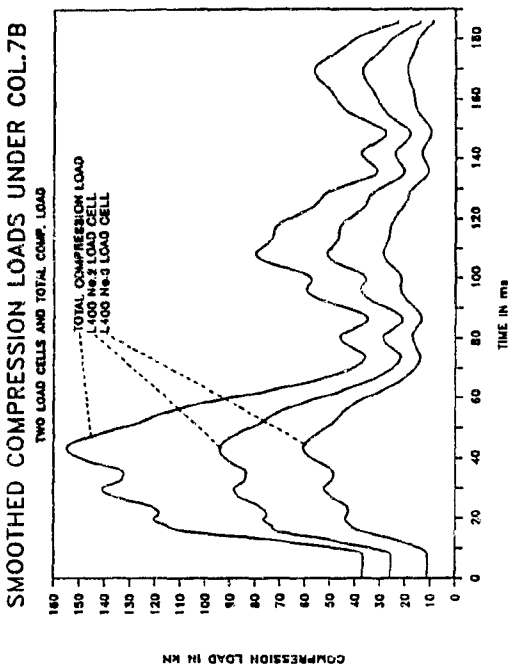

Fig. 3.725: Smo. Comp. Col.7B

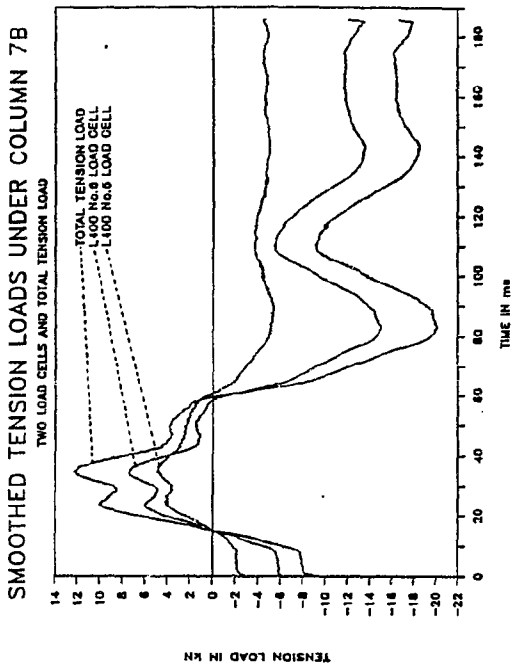

Fig. B.726: Smo. Tens. Col.7B

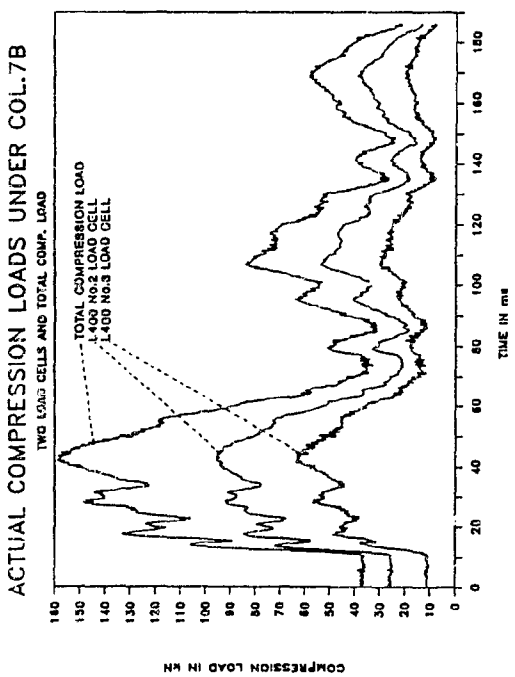

Fig. B.727: Comp. load Col 7B

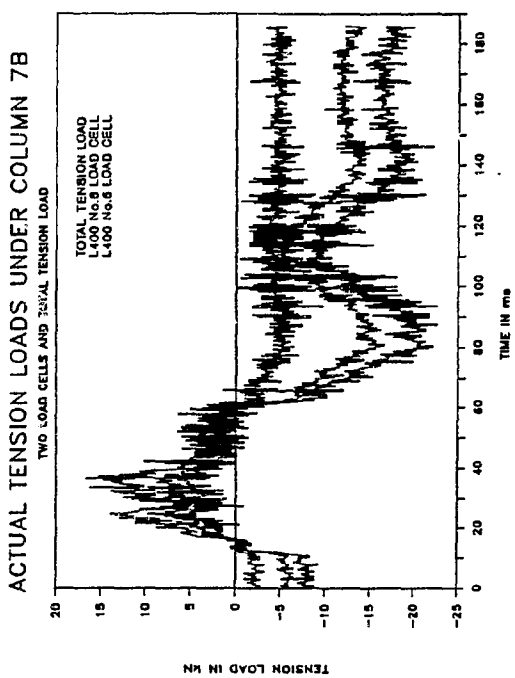

Fig. B.728: Tens. loads Col.7B

Stellenbosch University http://scholar.sun.ac.za

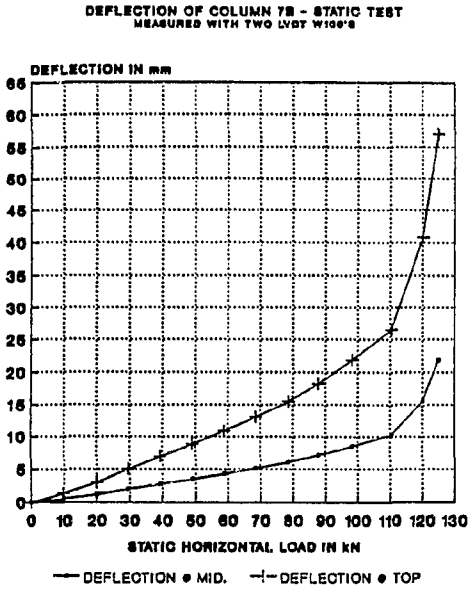

Fig. B.729: Deflection Col.7B

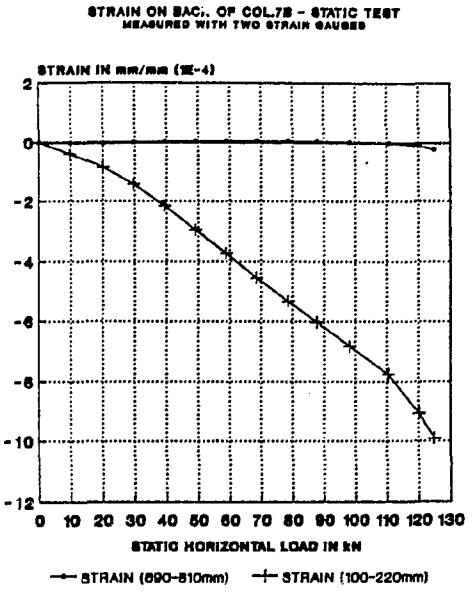

Fig. B.730: Strain Col.7B

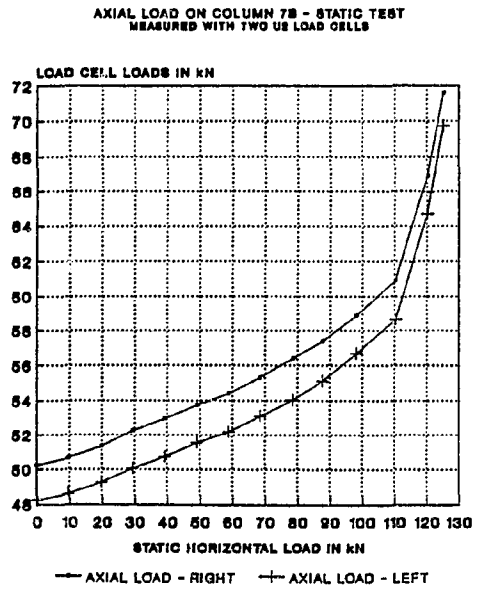

Fig. B.731: Axial load Col 7B

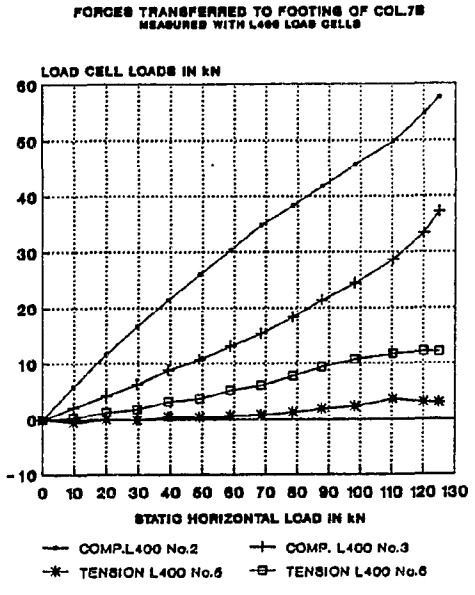

Fig. B.732: Foot.loads Col.7B

Stellenbosch University http://scholar.sun.ac.za

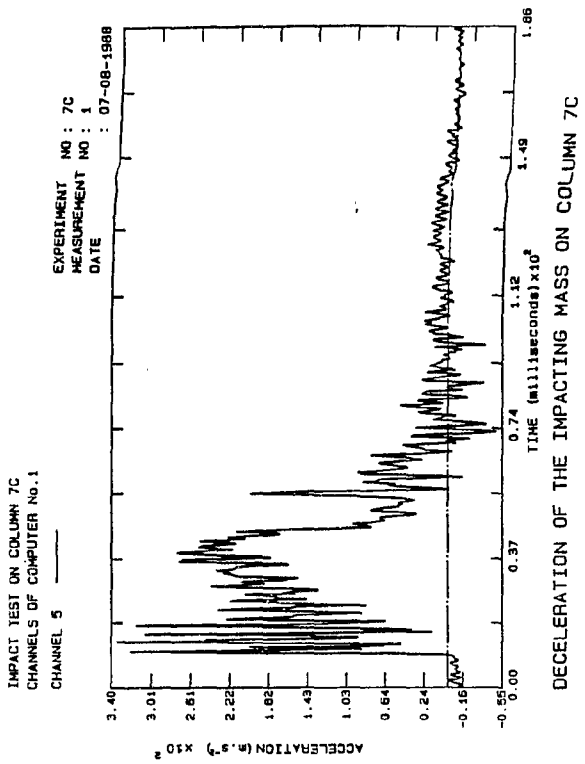

Fig. B.733: Decel. Col.7C

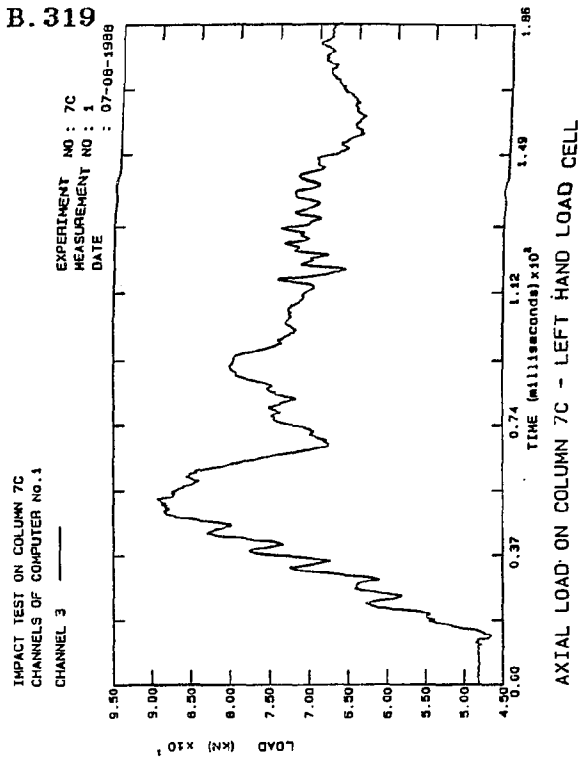

Fig. B.734: Axial load Col.7C

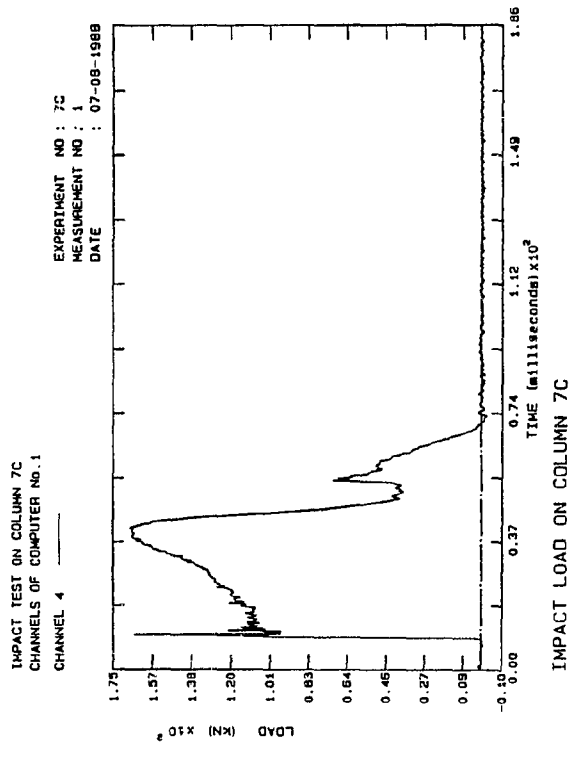

Fig. B.735: Impact Col 7C

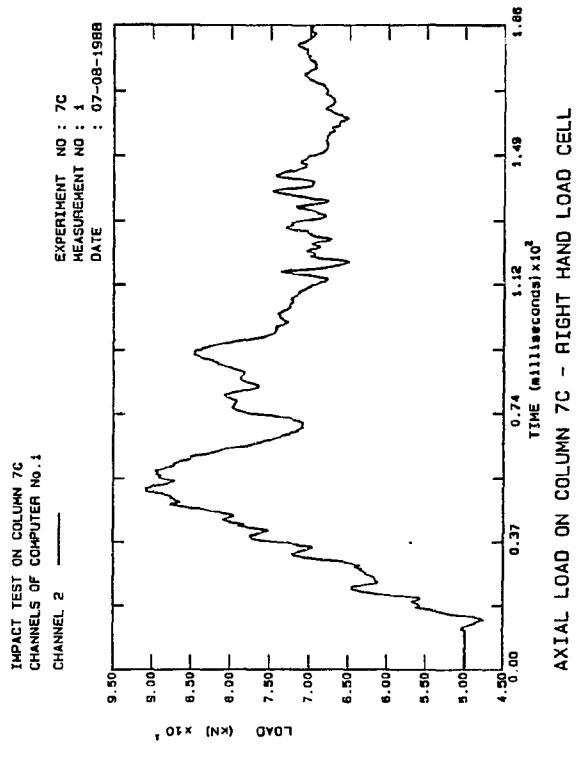

Fig. B.736: Axial load Col.7C

Stellenbosch University http://scholar.sun.ac.za

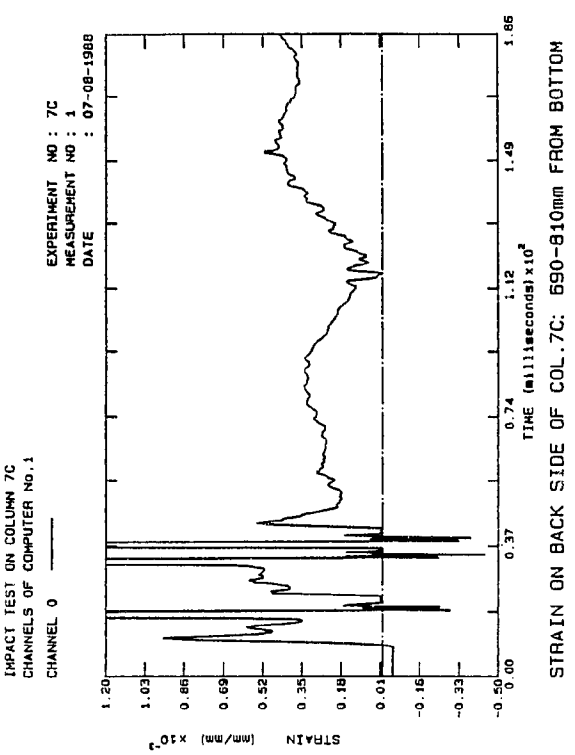

Fig. B.737: Strain Col.7C

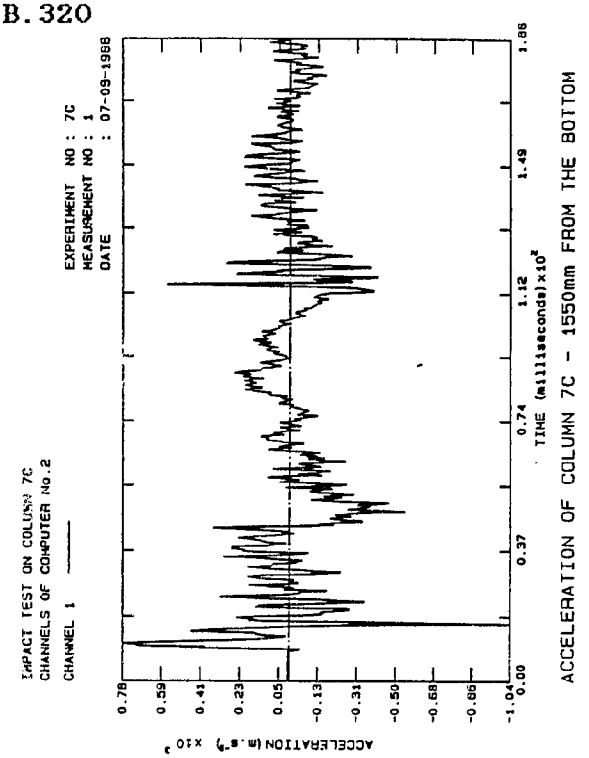

Fig. B.738: Accel. Col.7C

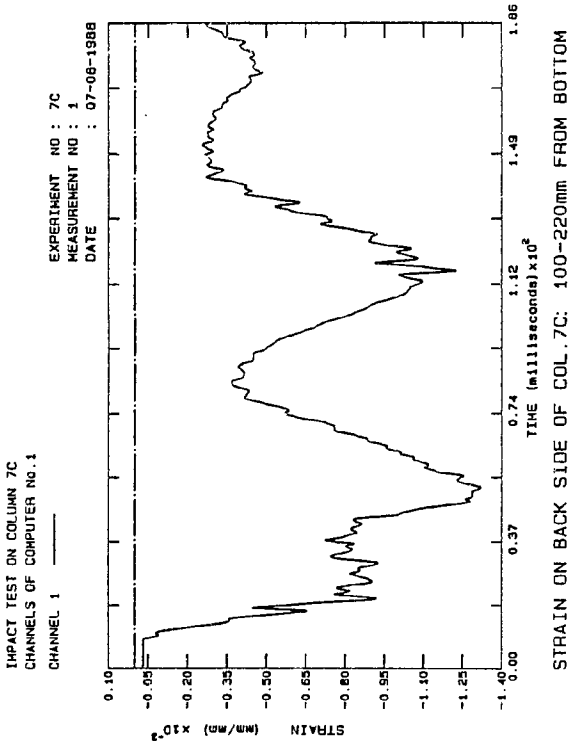

Fig. B.739: Strain Col 7C

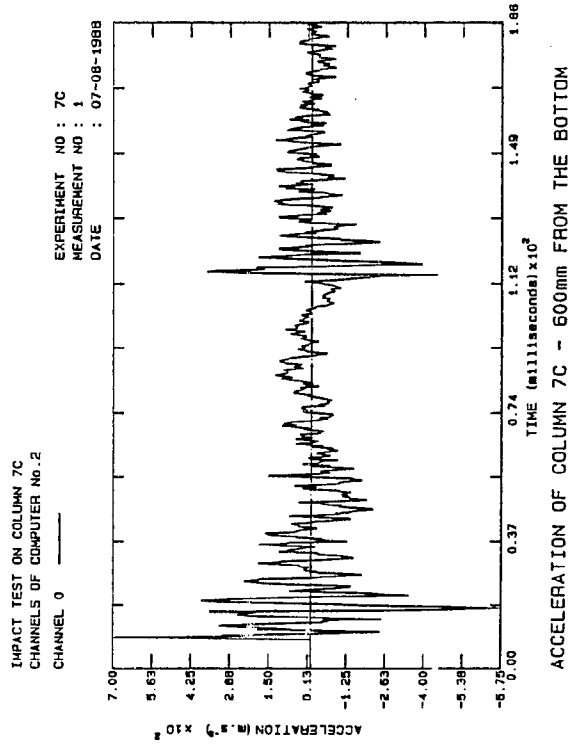

Fig. B.740: Accel. Col.7C

Stellenbosch University http://scholar.sun.ac.za

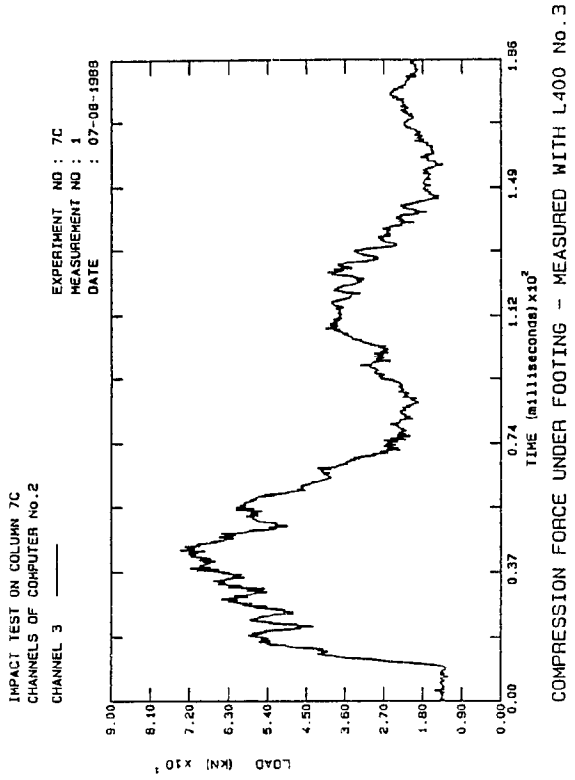

Fig. B.741: Comp. Col.7C

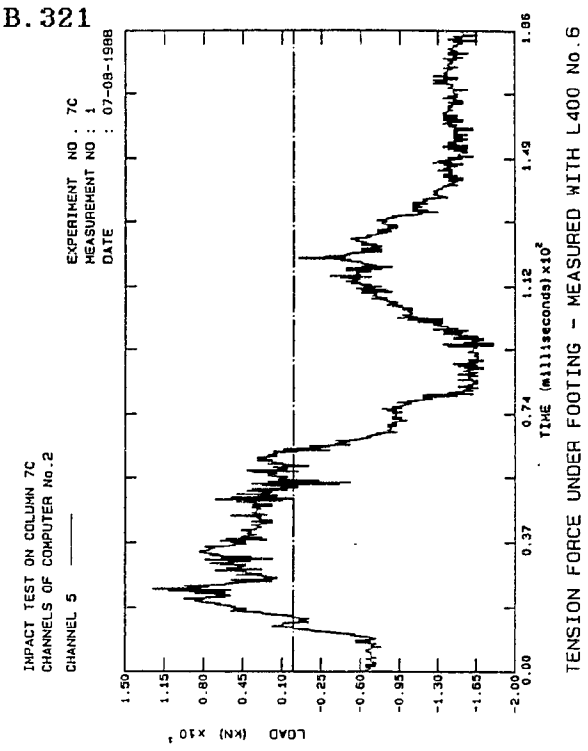

Fig. B.742: Tension Col.7C

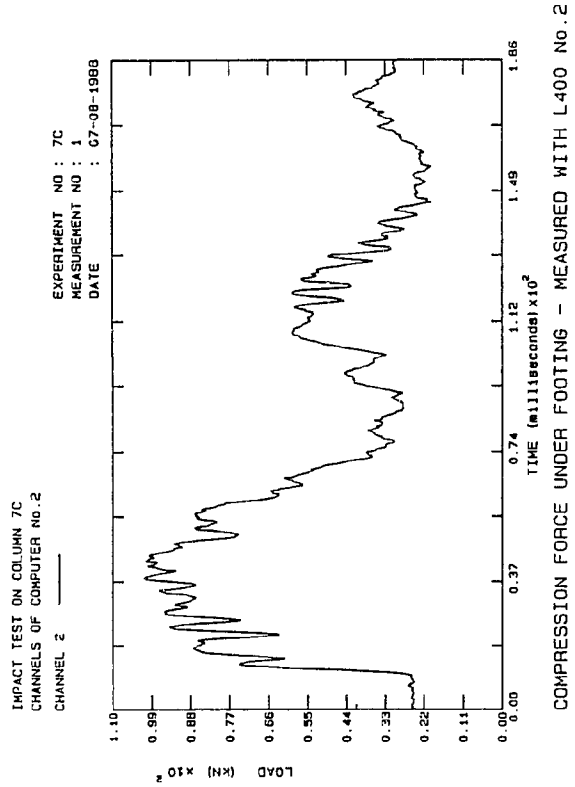

Fig. B.743: Comp. Col 7C

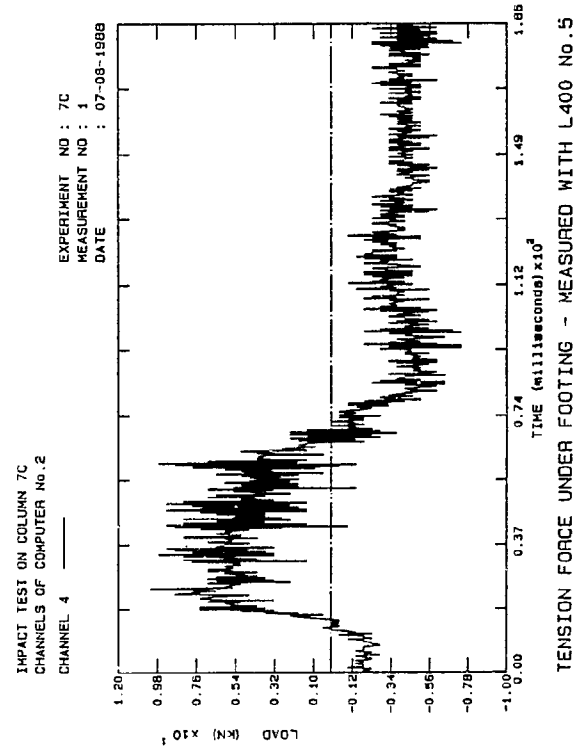

Fig. B.744: Tension Col.7C

Stellenbosch University http://scholar.sun.ac.za

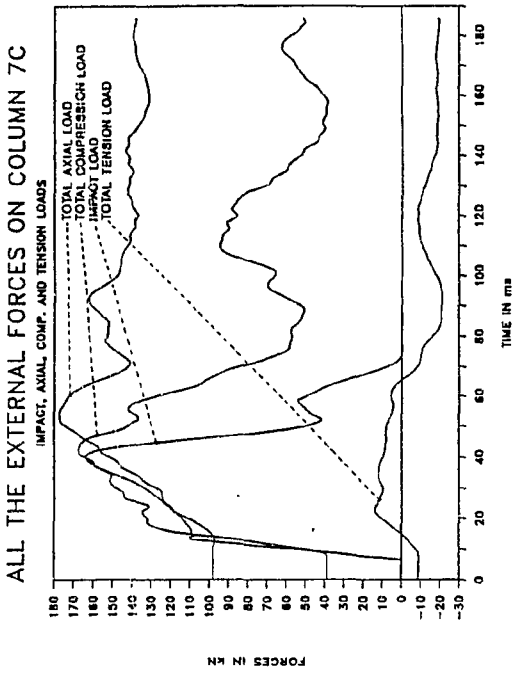

Fig. B.745: Ext. Loads Col.7C

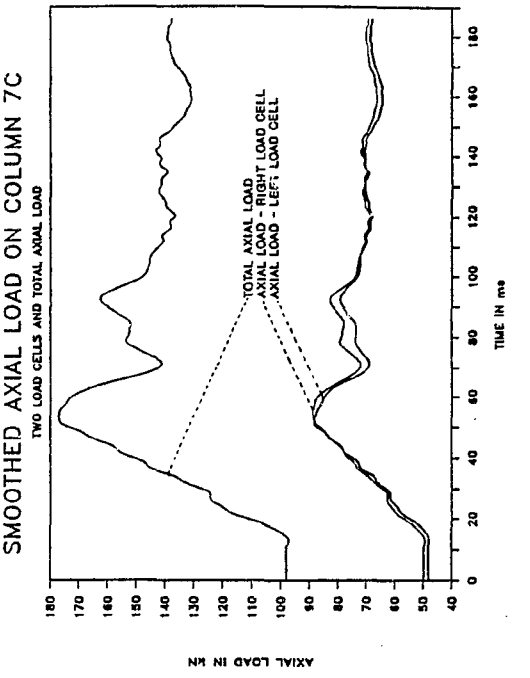

Fig. B.746: Smo. Axial Col.7C

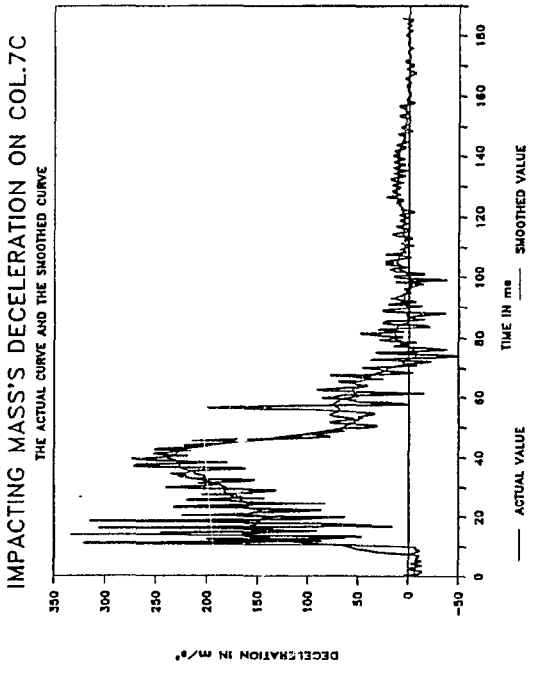

Fig. B.747: Smo.Decel. Col 7C

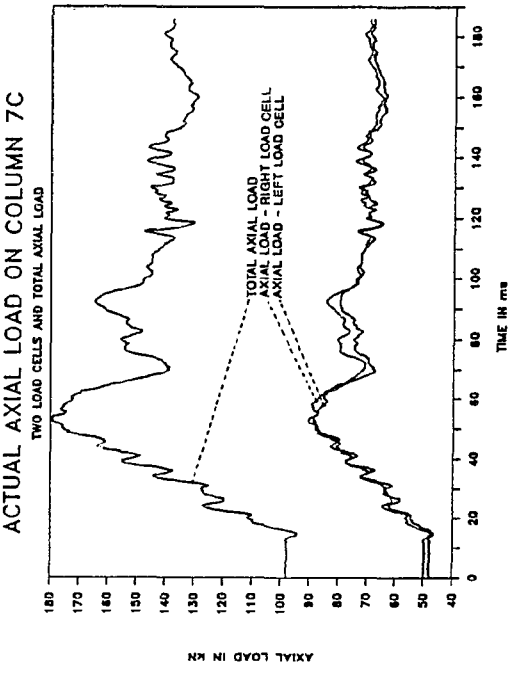

Fig. B.748: Axial loads Col.7C

Stellenbosch University http://scholar.sun.ac.za

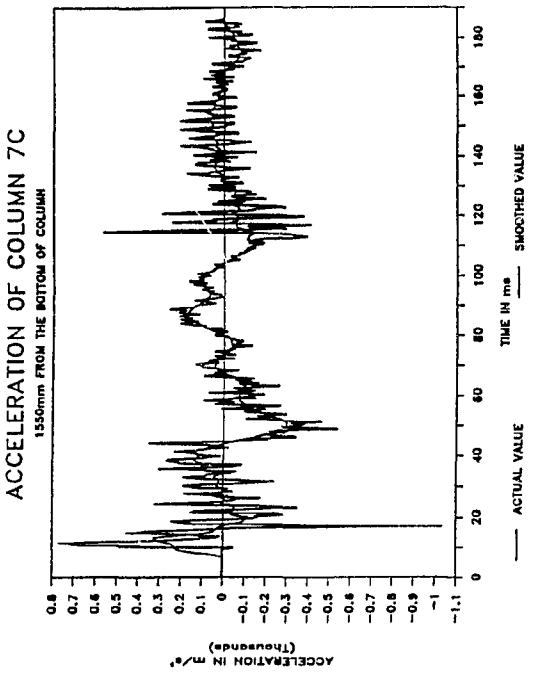

Fig. B.749: Smo.Accel. Col.7C

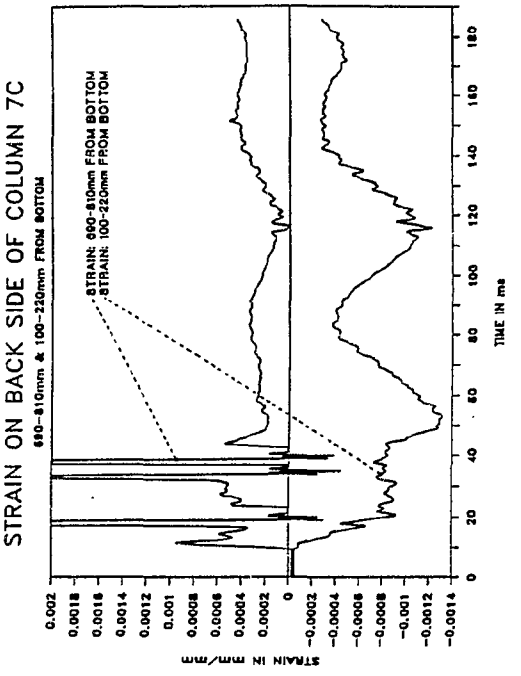

Fig. B.750: Strain Col.7C

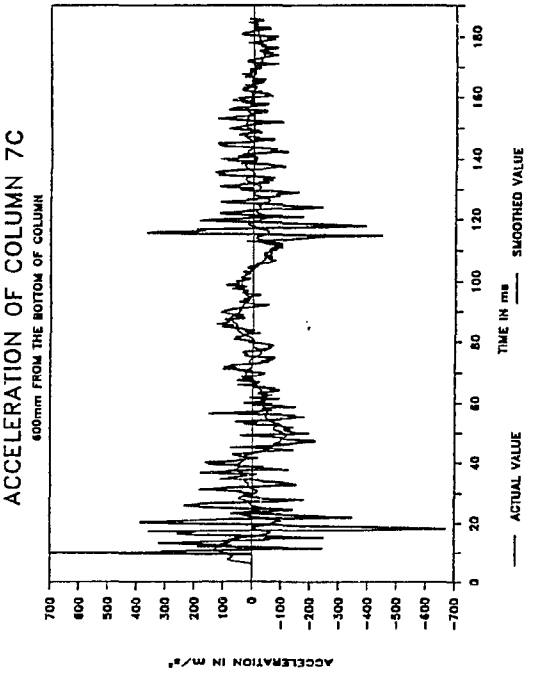

Fig. B.751: Smo.Accel. Col 7C

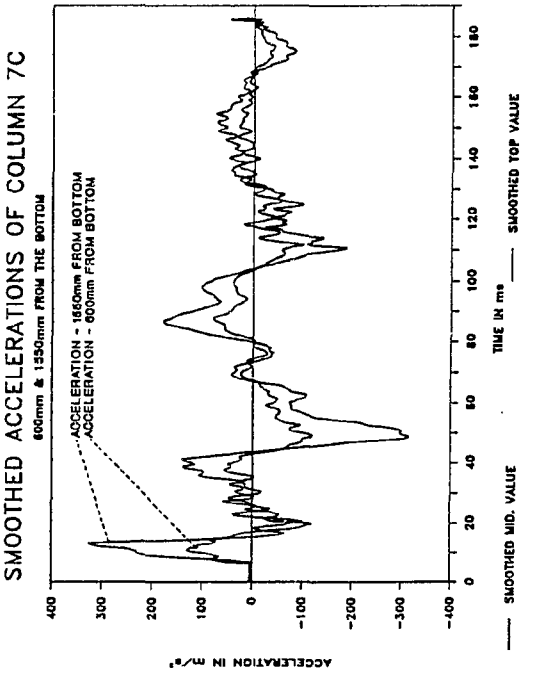

Fig. B.752: Smo. Accel. Col.7C

Stellenbosch University http://scholar.sun.ac.za

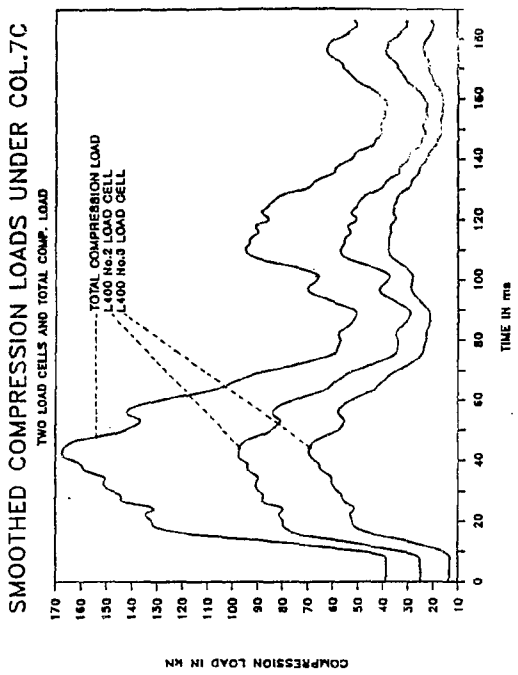

Fig. B.753: Smo. Comp. Col.7C

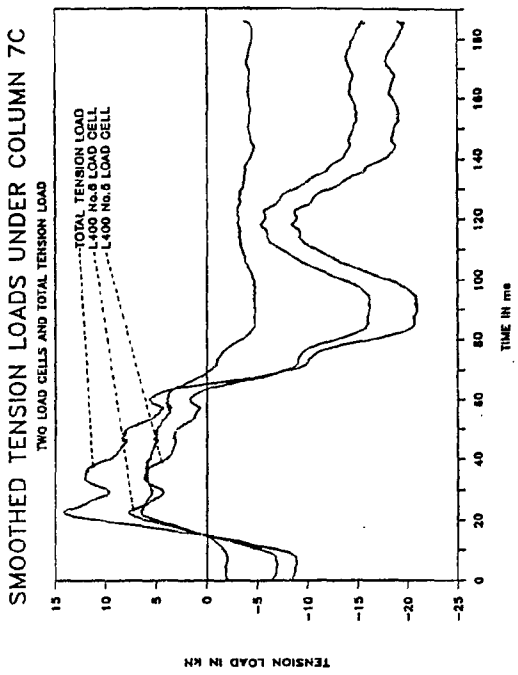

Fig. B.754: Smo. Tens. Col.7C

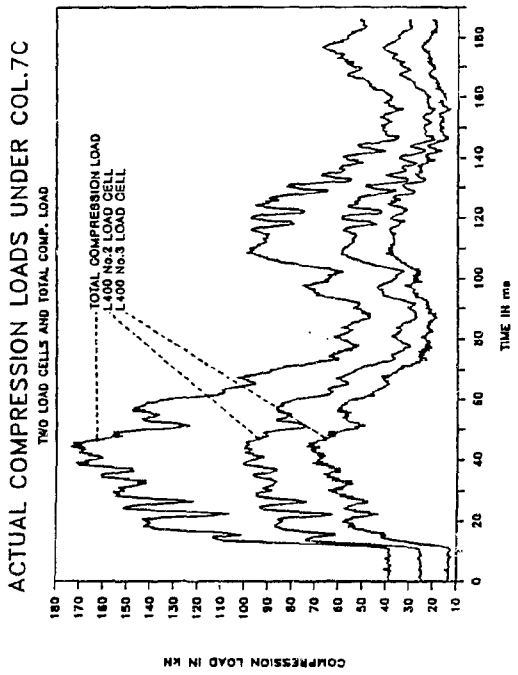

Fig. B.755: Comp. load Col 7C

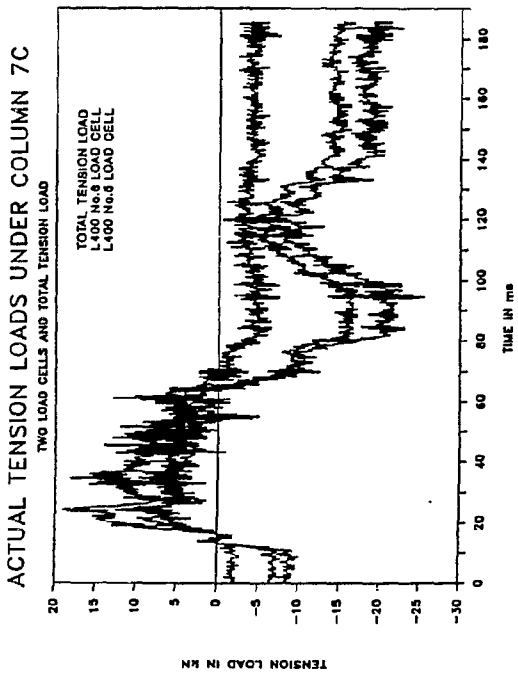

Fig. B.756: Tens. loads Col.7C

Stellenbosch University http://scholar.sun.ac.za

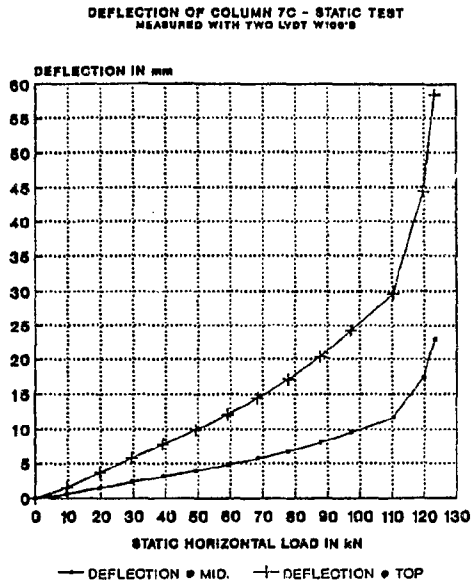

Fig. B.757: Deflection Col.7C

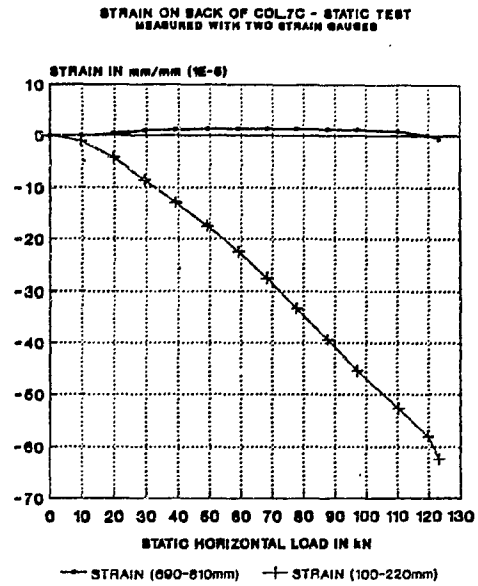

Fig. B.758: Strain Col.7C

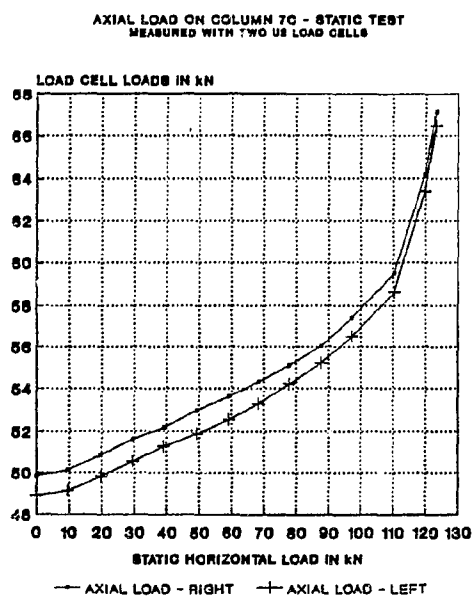

Fig. B.759: Axial load Col 7C

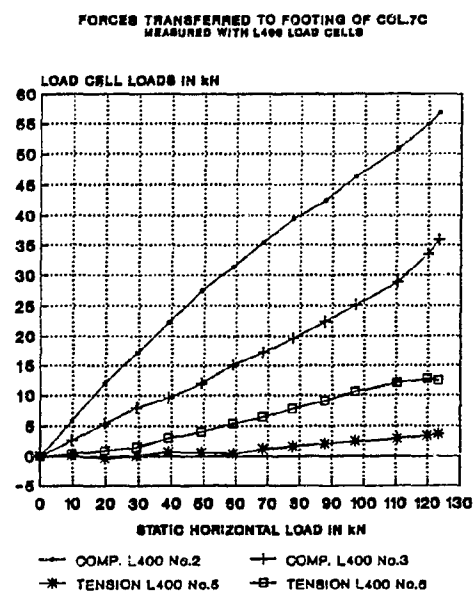

Fig. B.760: Foot.loads Col.7C

Stellenbosch University http://scholar.sun.ac.za

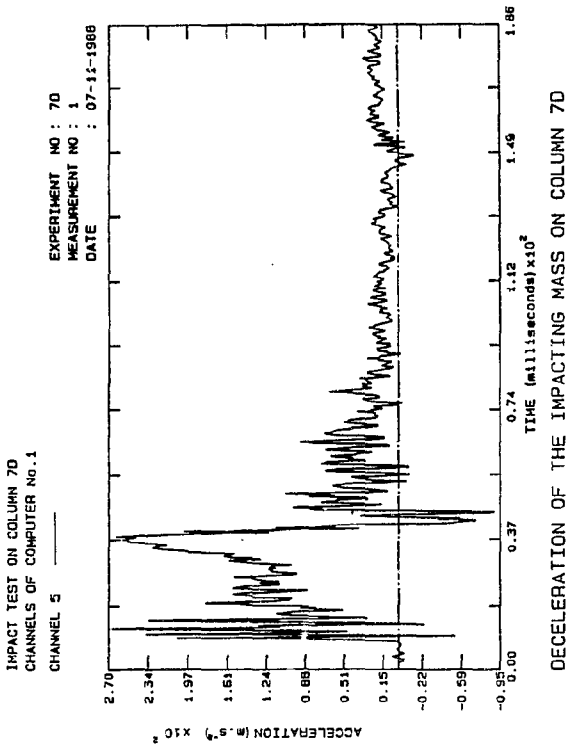

Fig. B.761: Decel. Col.7D

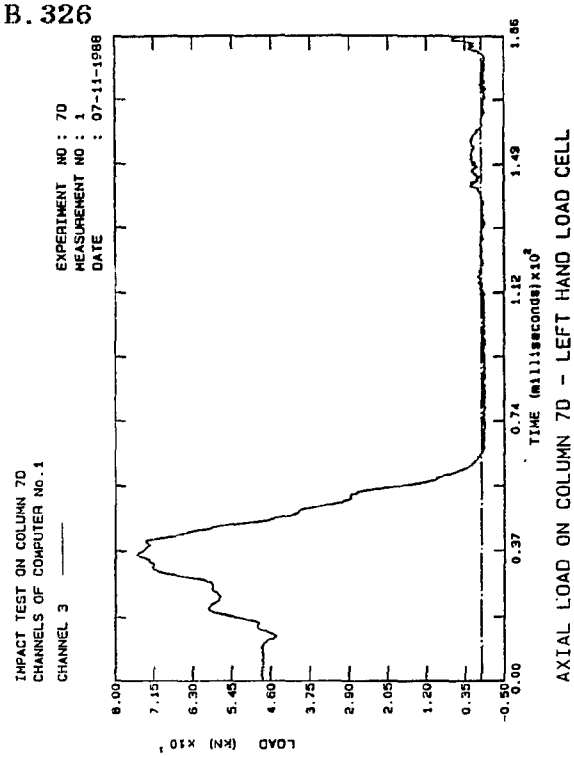

Fig. B.762: Axial load Col.7D

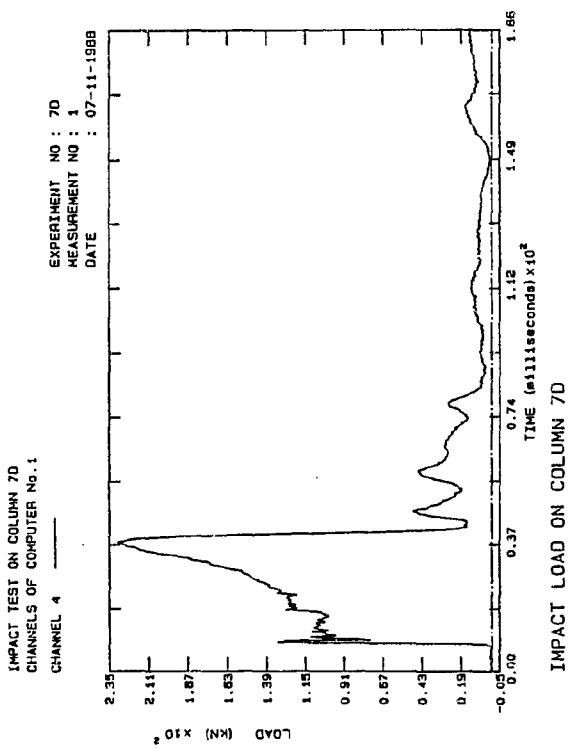

Fig. B.763: Impact Col 7D

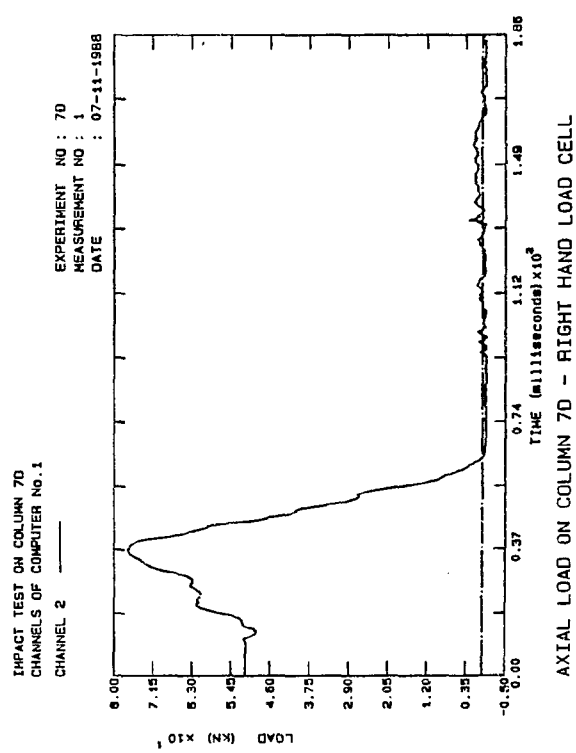

Fig. B.764: Axial load Col.7D

Stellenbosch University http://scholar.sun.ac.za

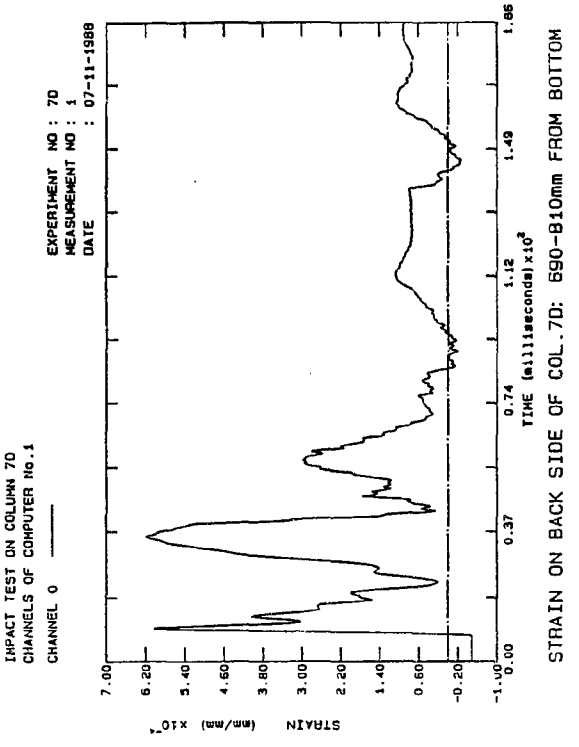

Fig. B.765: Strain Col.7D

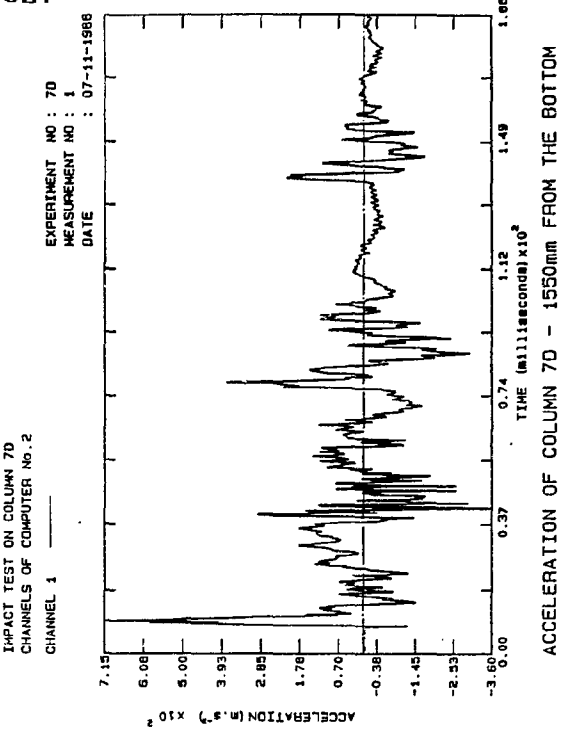

Fig. B.766: Accel. Col.7D

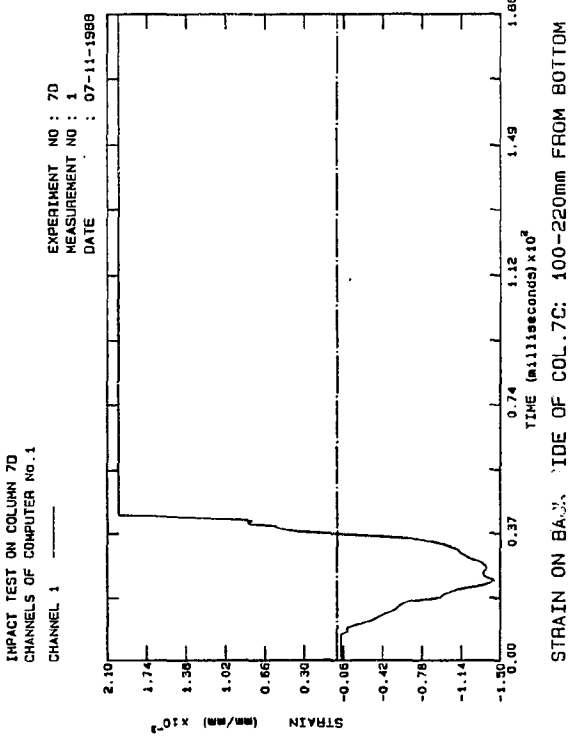

Fig. B.767: Strain Col 7D

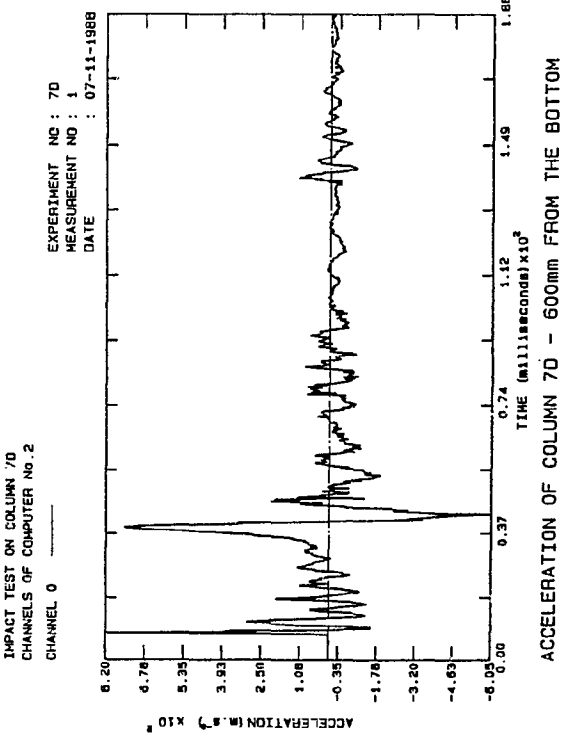

Fig. B.768: Accel. Col.7D

Stellenbosch University http://scholar.sun.ac.za

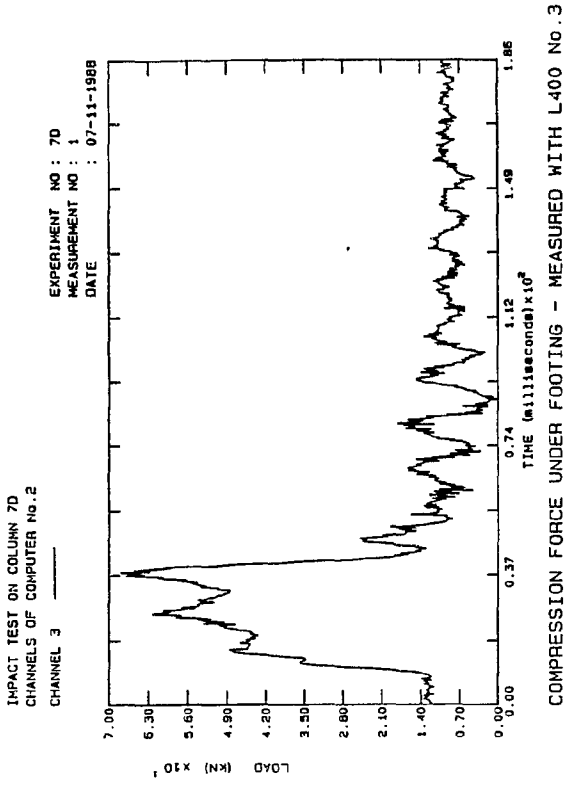

Fig. B.769: Comp. Col.7D

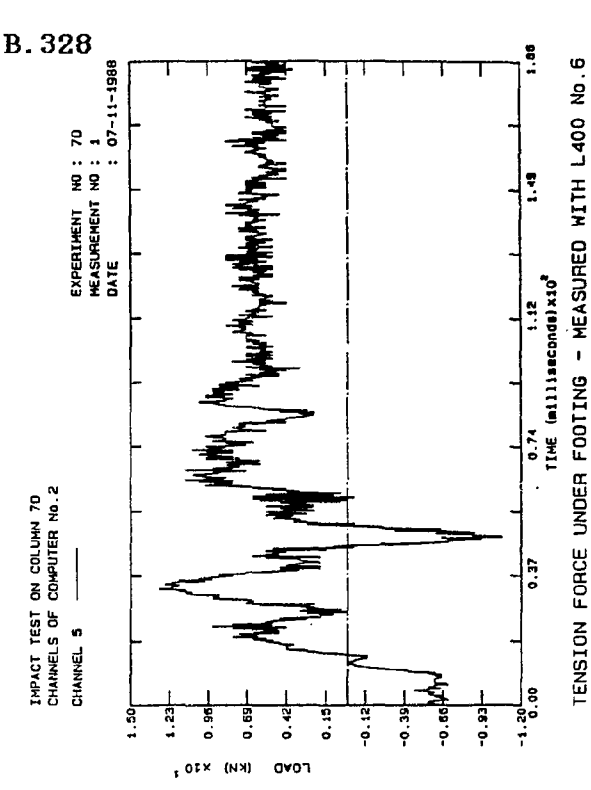

Fig. B.770: Tension Col.7D

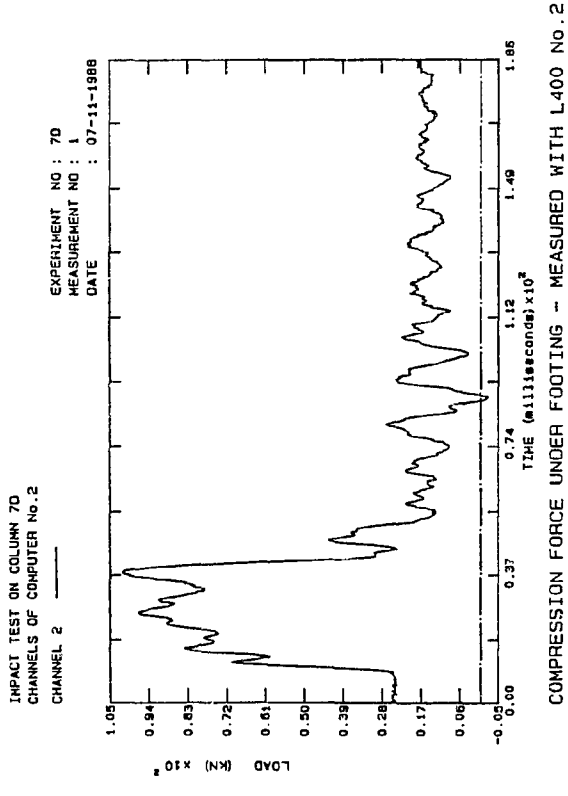

Fig. B.771: Comp. Col 7D

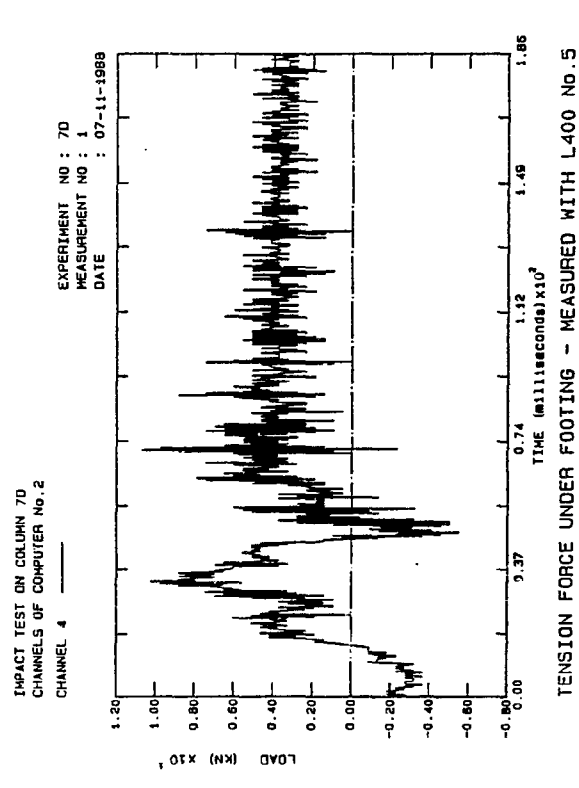

Fig. B.772: Tension Col.7D

Stellenbosch University http://scholar.sun.ac.za

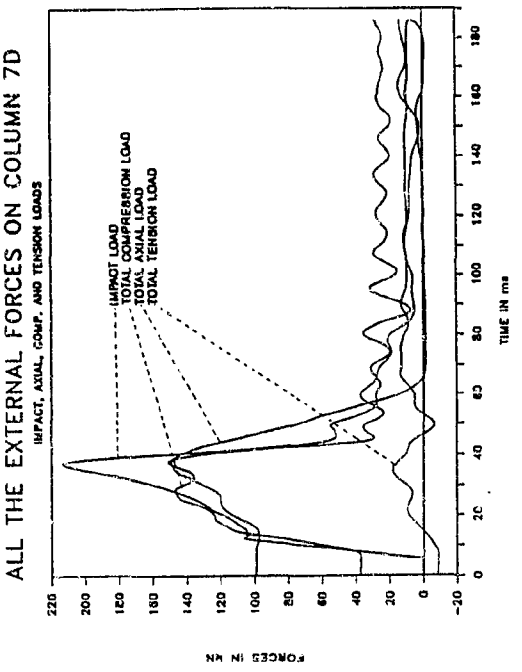

Fig. B.773: Ext. Loads Col.7D

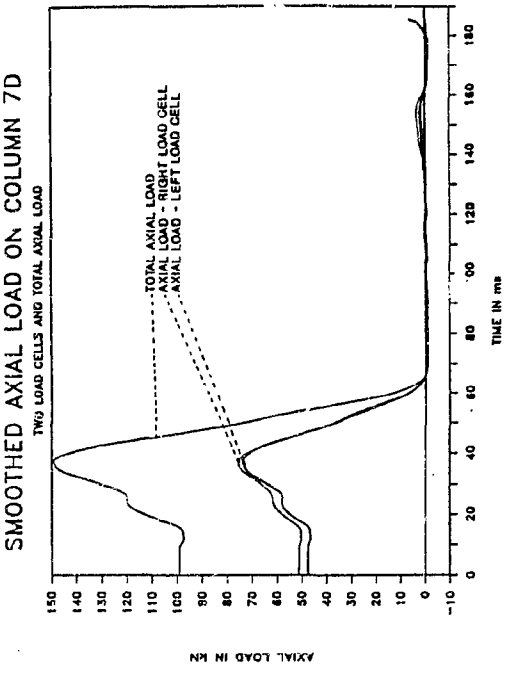

Fig. B.774: Smo. Axial Col.7D

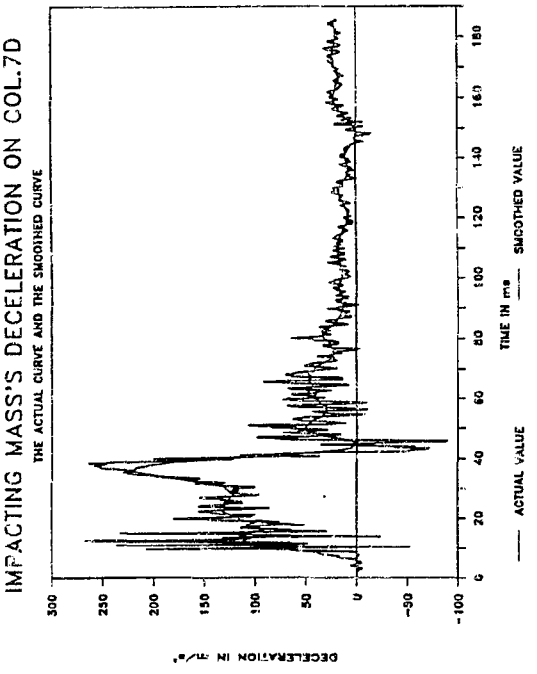

Fig. B.775: Smo Decel. Col 7D

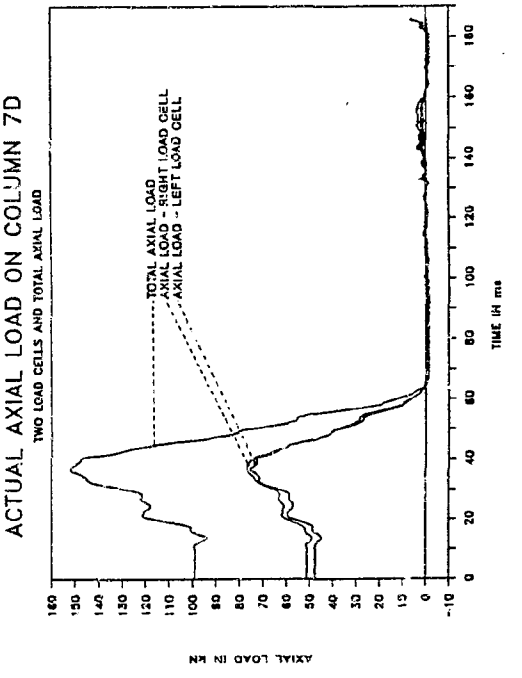

Fig. B.776: Axial loads Col.7D

Stellenbosch University http://scholar.sun.ac.za

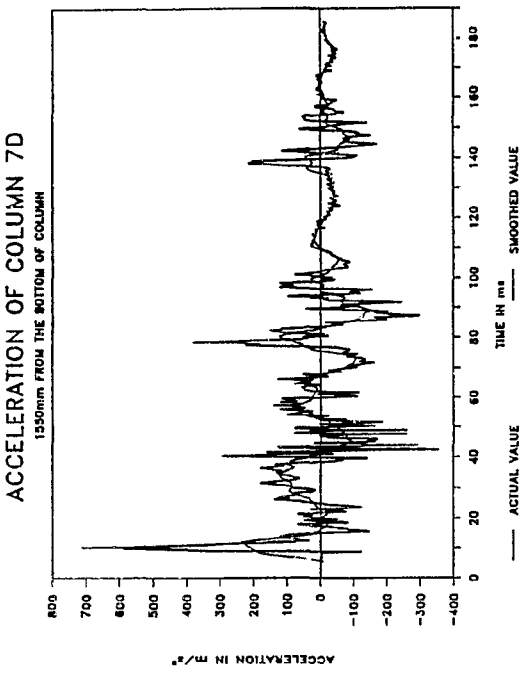

Fig. B.777: Smo.Accel. Col.7D

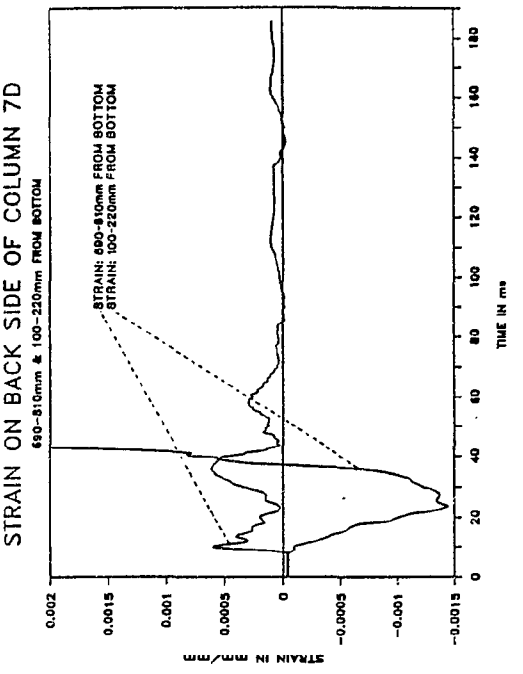

Fig. B.778: Strain Col.7D

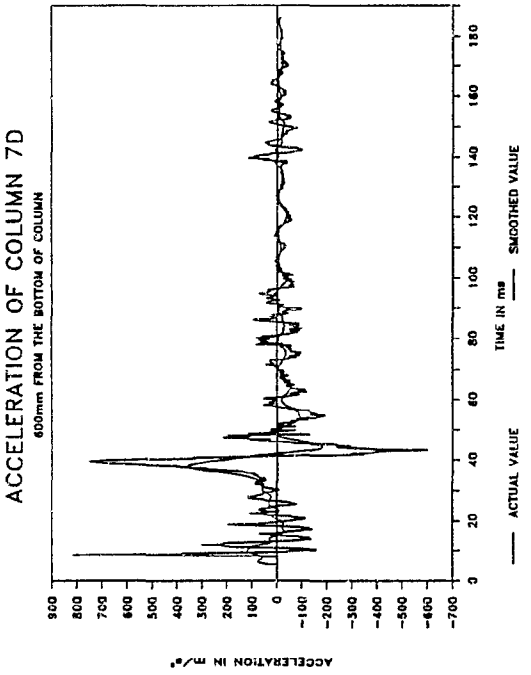

Fig. B.779: Smo.Accel. Col 7D

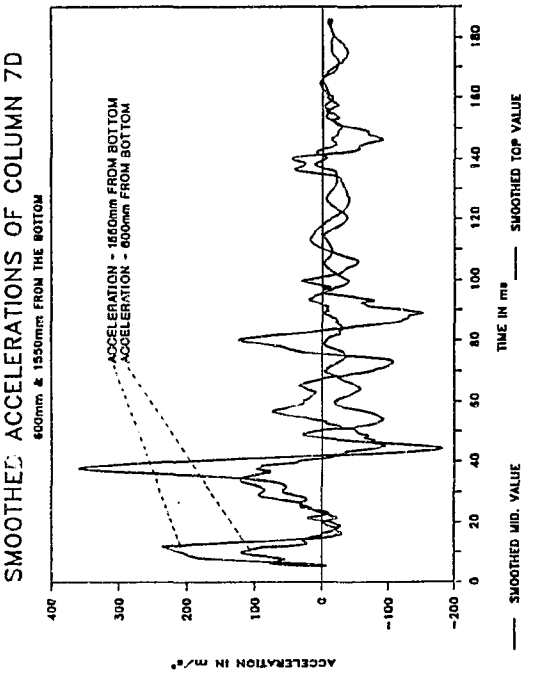

Fig. B.780: Smo. Accel. Col.7D

Stellenbosch University http://scholar.sun.ac.za

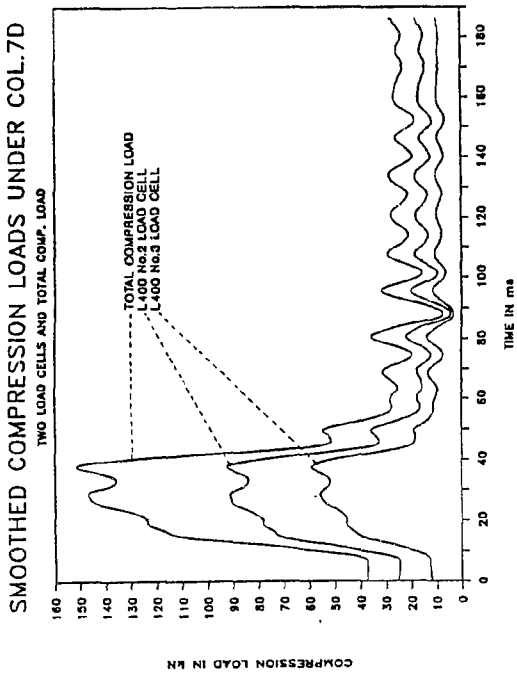

Fig. B.781: Smo. Comp. Col.7D

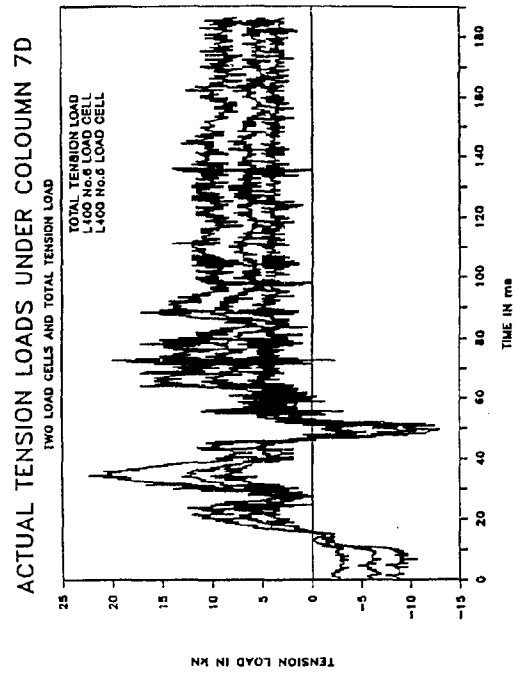

Fig. B.782: Smo. Tens. Col.7D

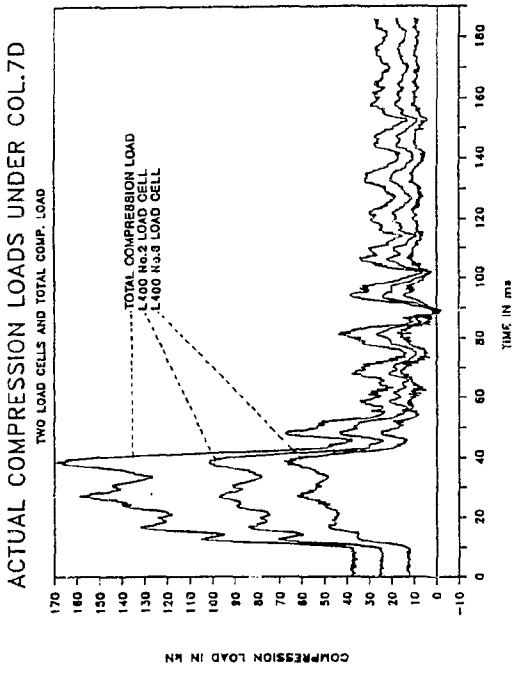

Fig. B.783: Comp. load Col 7D

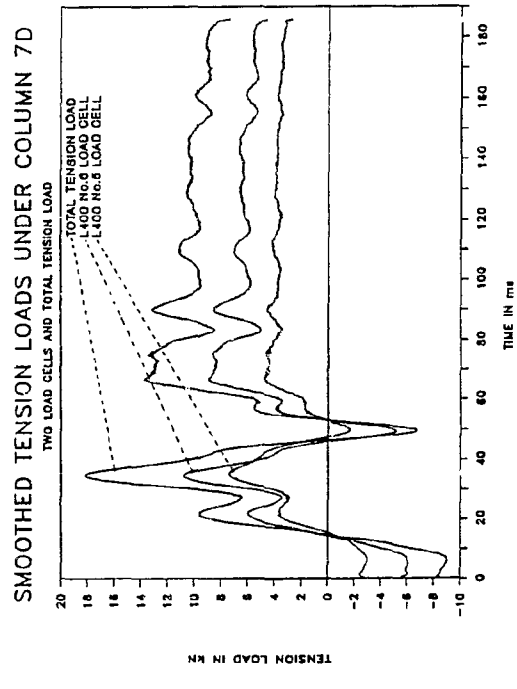

Fig. B.784: Tens. loads Col.7D

Stellenbosch University http://scholar.sun.ac.za

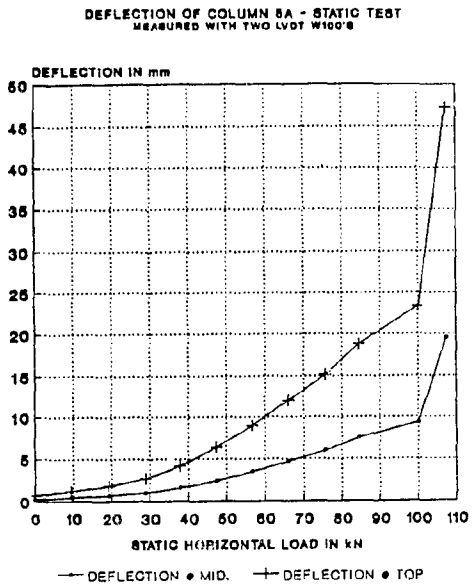

Fig. B.785: Deflection Col.8A

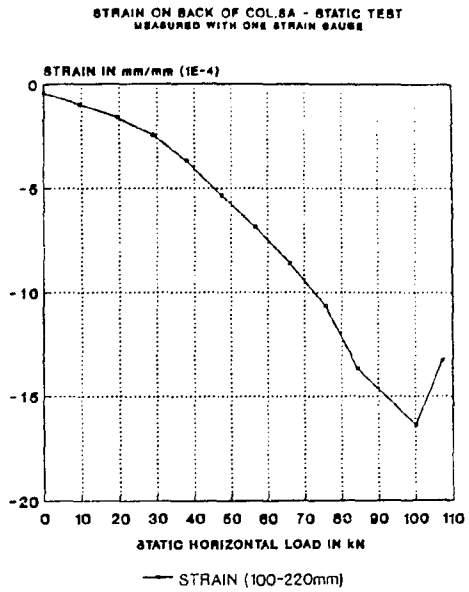

Fig. B.786: Strain Col.8A

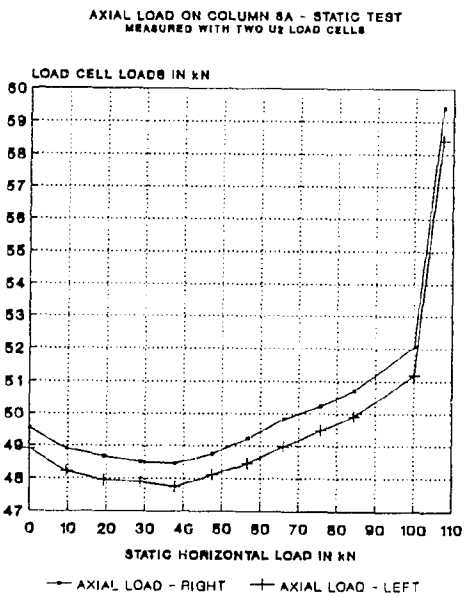

Fig. B.787: Axial load Col 8A

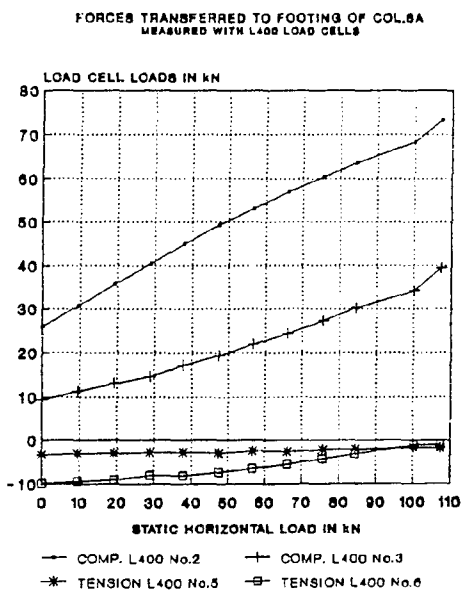

Fig. B.788: Foot. loads Col.8A

Stellenbosch University http://scholar.sun.ac.za

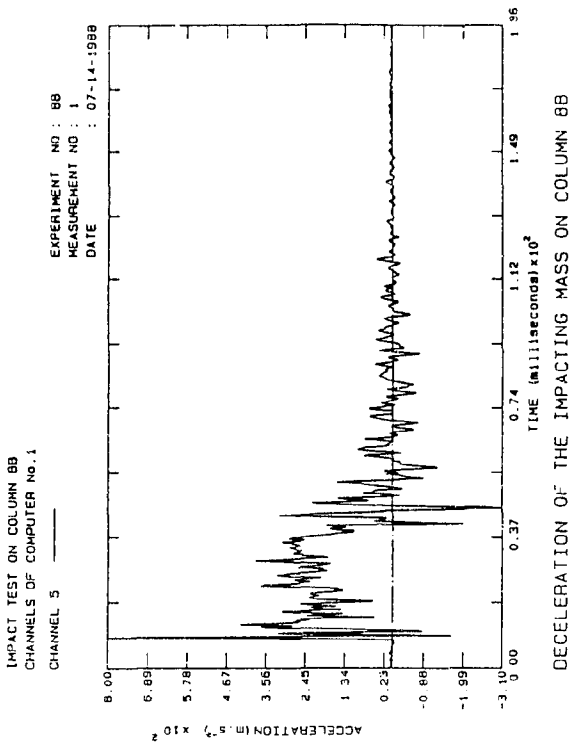

Fig. B.789: Decel. Col.8B

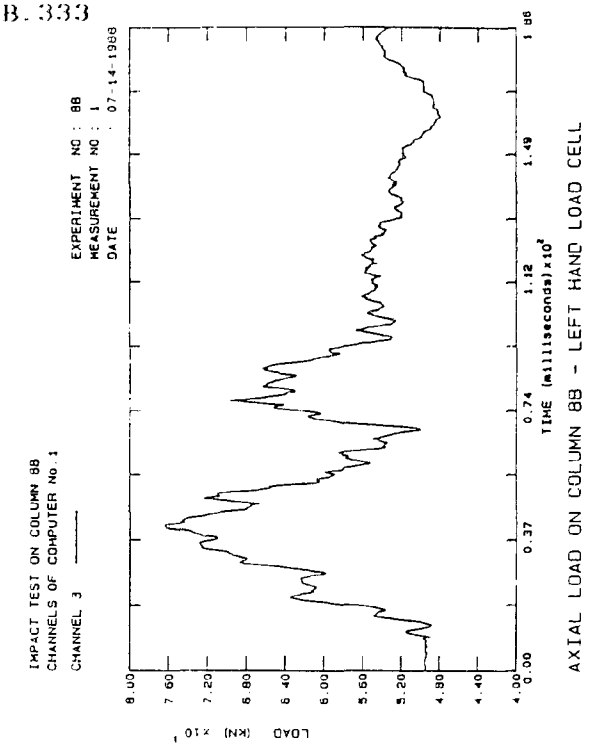

Fig. B.790: Axial load Col.8B

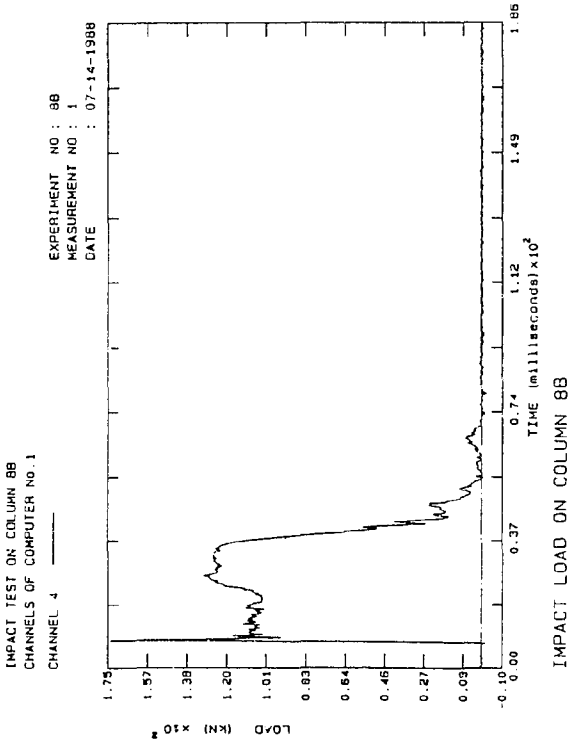

Fig. B.791: Impact Col 8B

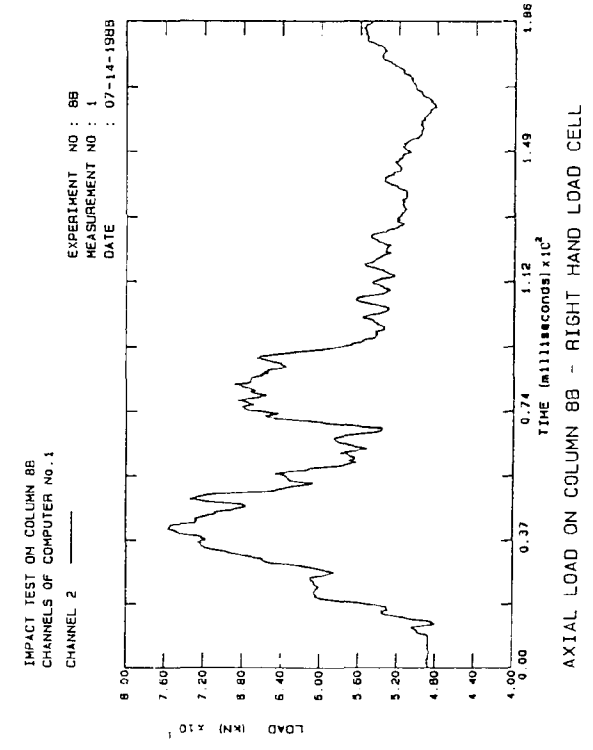

Fig. B.792: Axial load Col.8B

Stellenbosch University http://scholar.sun.ac.za

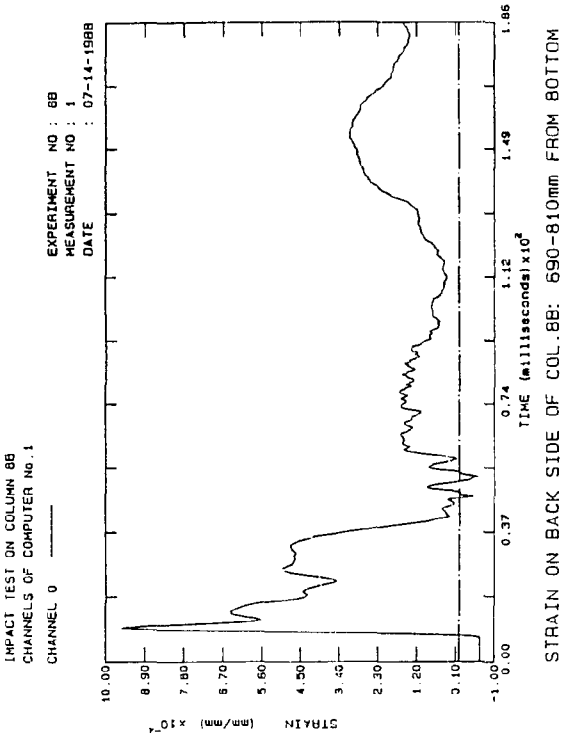

Fig. B.793: Strain Col.8B

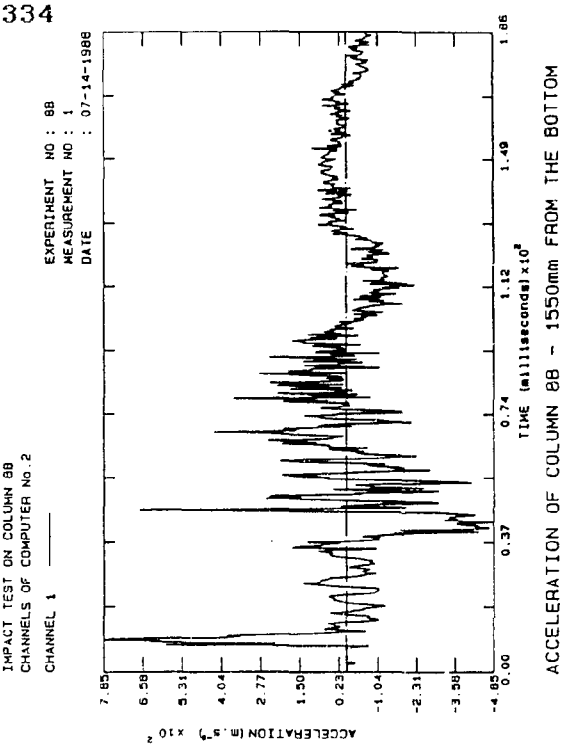

Fig. B.794: Accel. Col.8B

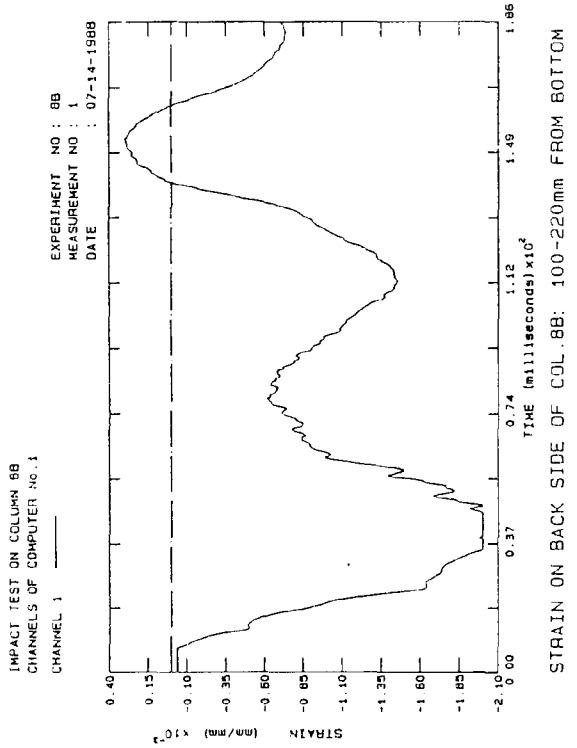

Fig. B.795: Strain Col.8B

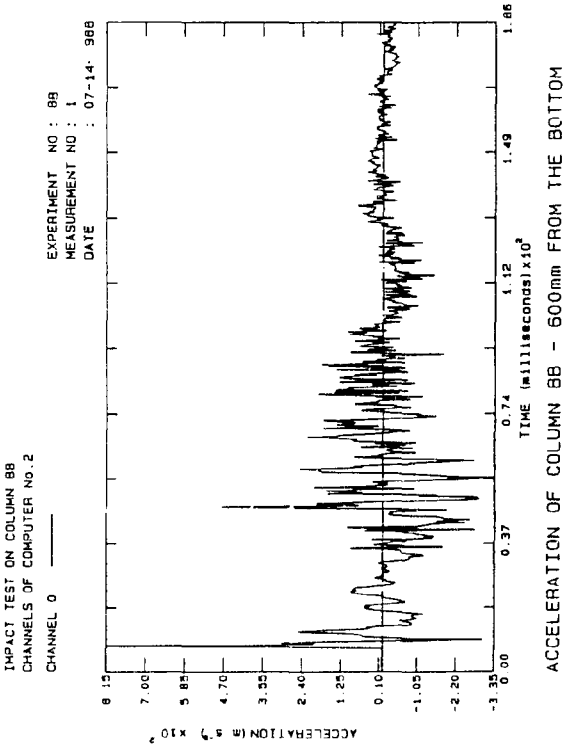

Fig. B.796: Accel. Col.8B

Stellenbosch University http://scholar.sun.ac.za

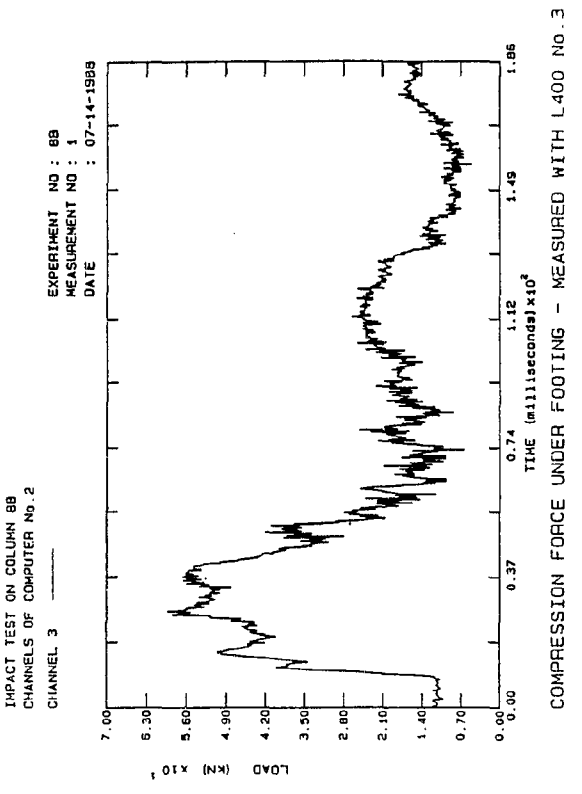

Fig. B.797: Comp. Col.8B

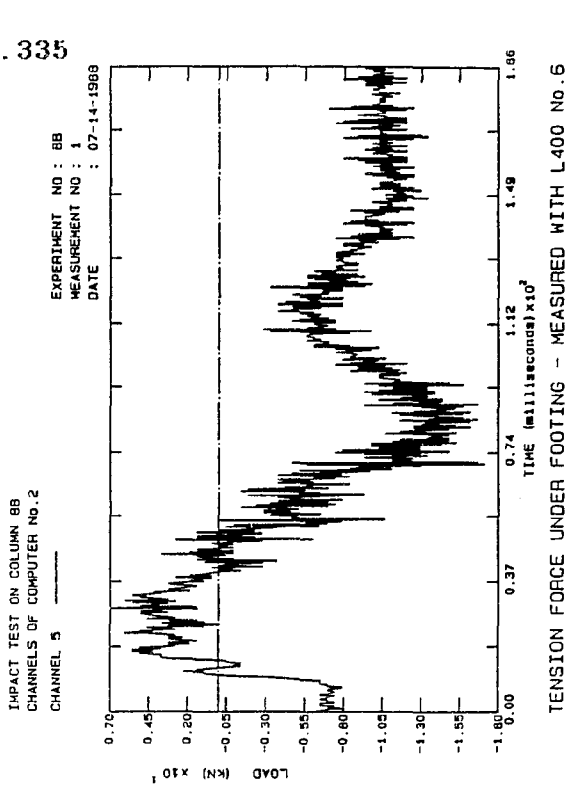

Fig. B.798: Tension Col.8B

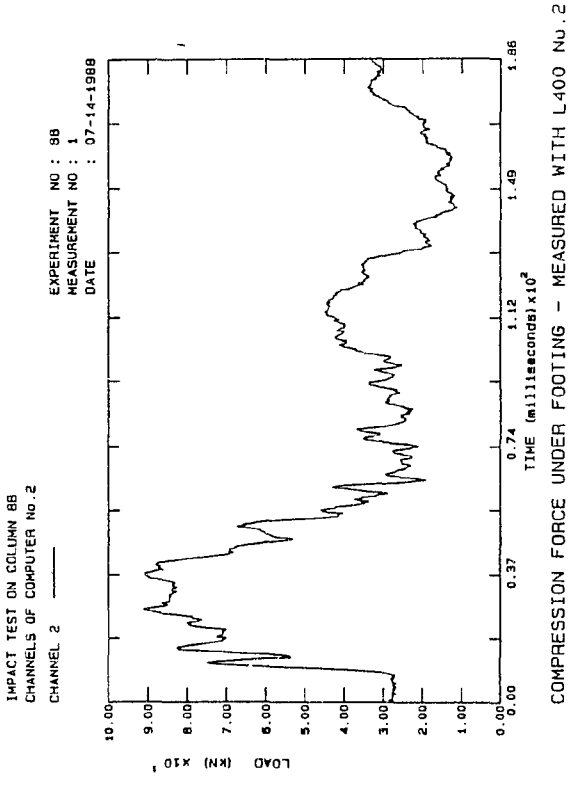

Fig. B.799: Comp. Col 8B

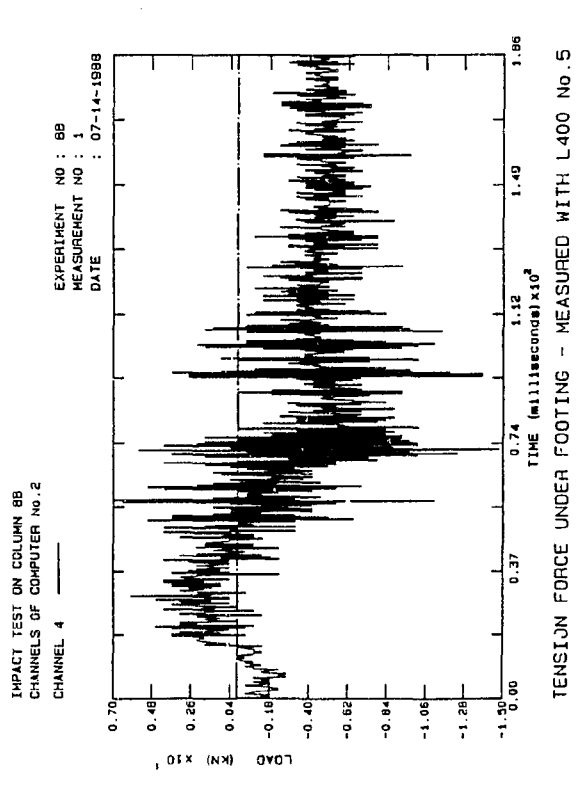

Fig. B.800: Tension Col. 8B

Stellenbosch University http://scholar.sun.ac.za

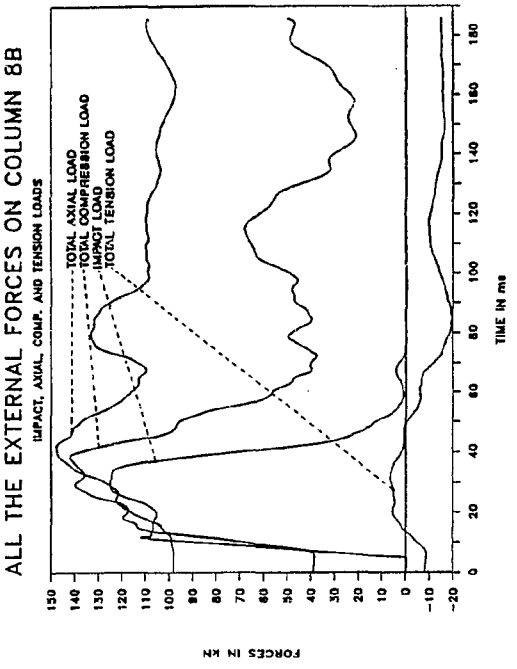

Fig. B.801: Ext. Loads Col.8B

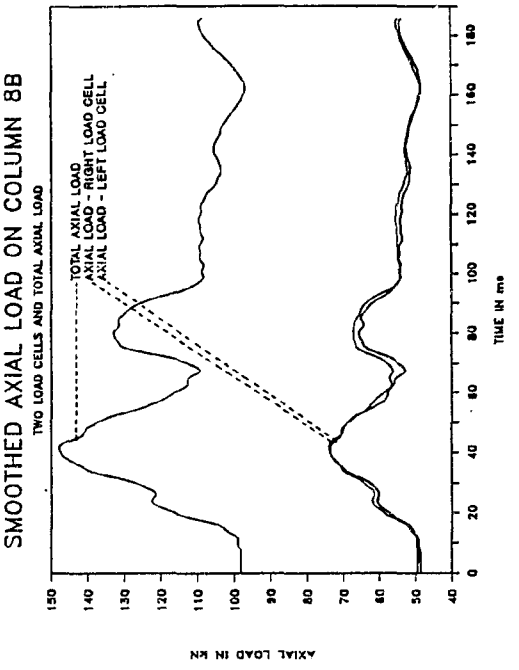

Fig. B.802: Smo. Axial Col.8B

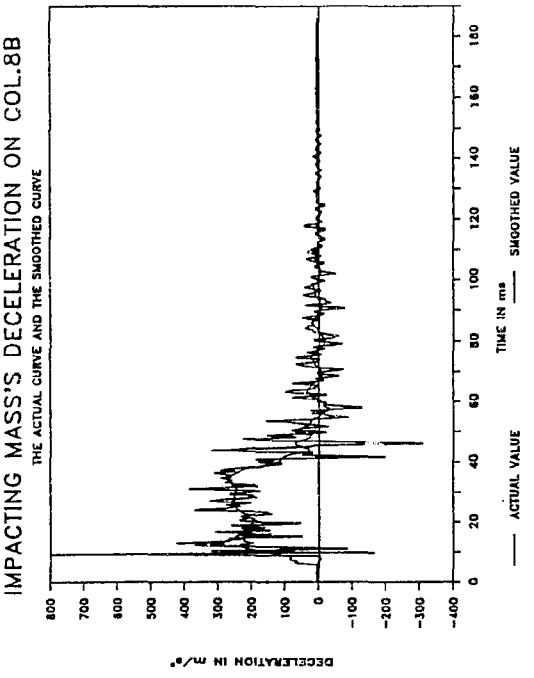

Fig. B.803: Smo.Decel. Col 8B

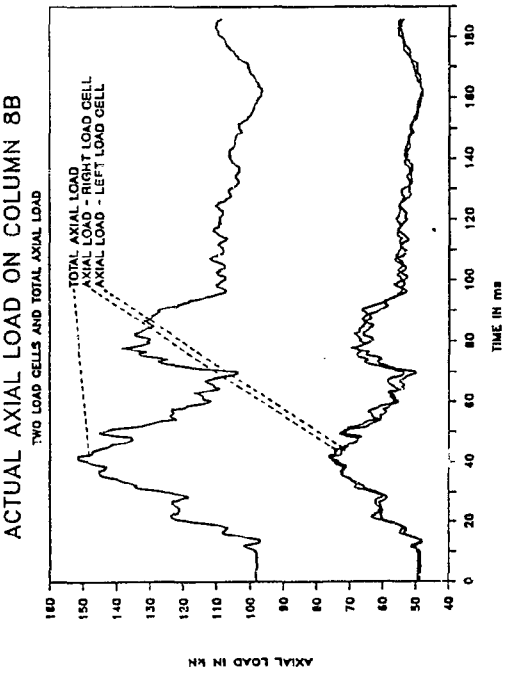

Fig. B.804: Axial loads Col.8B

Stellenbosch University http://scholar.sun.ac.za

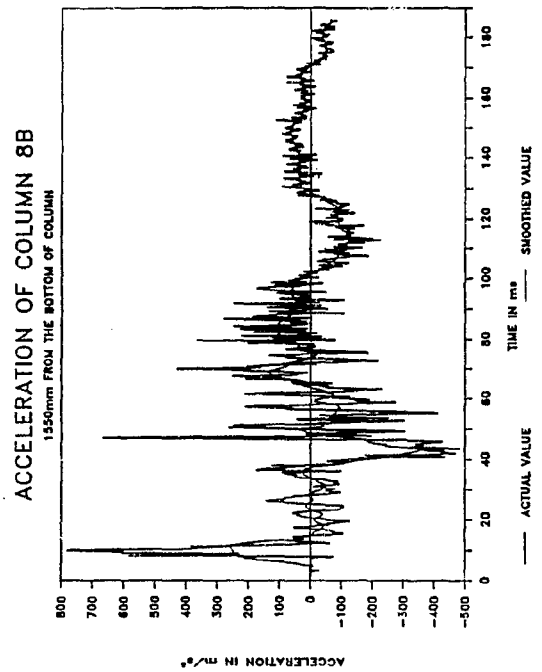

Fig. B.805: Smo.Accel. Col.8B

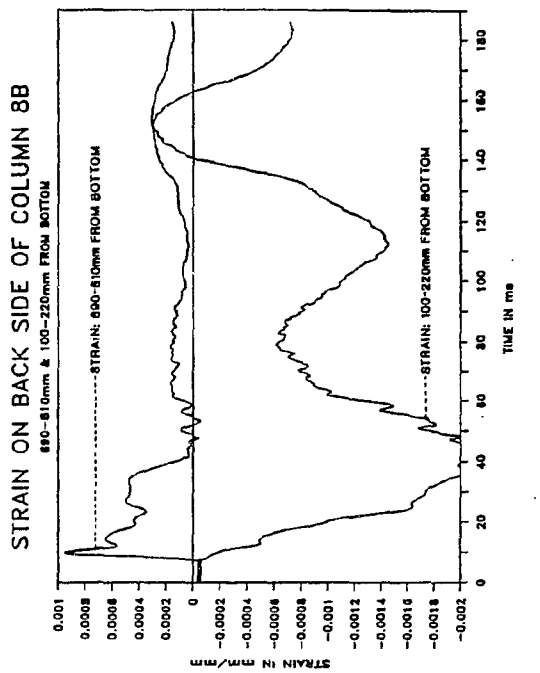

Fig. B.806: Strain Col.8B

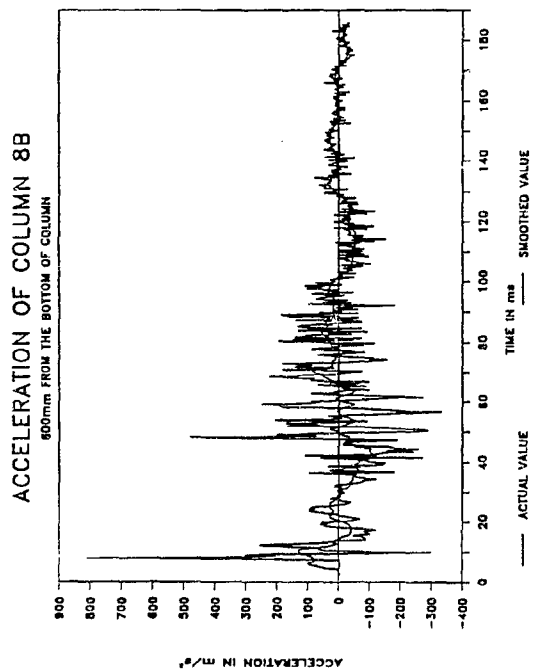

Fig. B.807: Smo.Accel. Col 8B

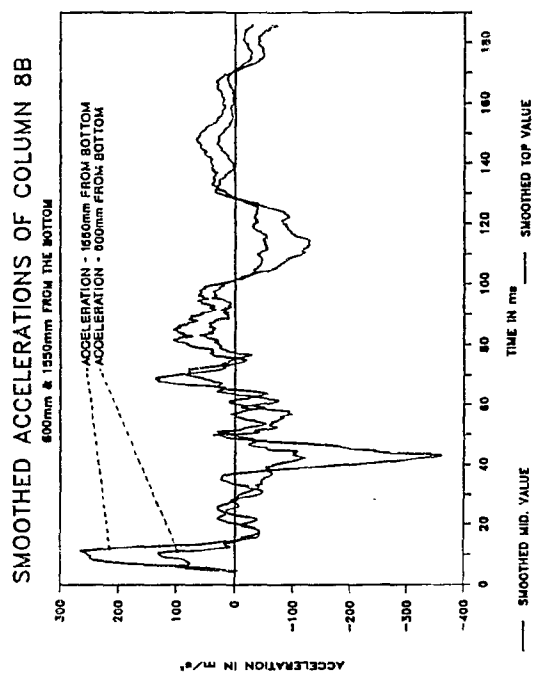

Fig. B.808: Smo. Accel. Col.8B

Stellenbosch University http://scholar.sun.ac.za

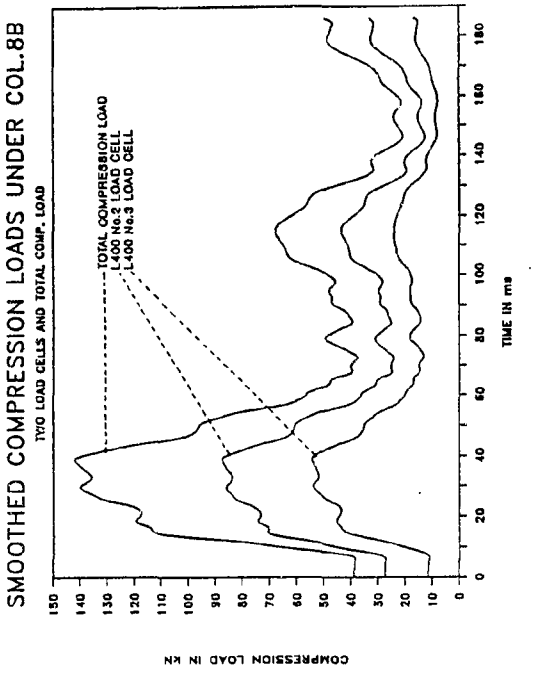

Fig. B.809: Smo. Comp. Col.8B

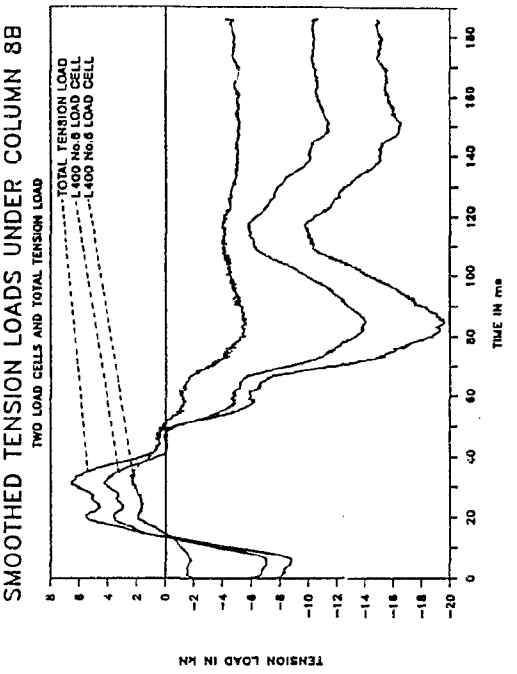

Fig. B.810: Smo. Tens. Col.8B

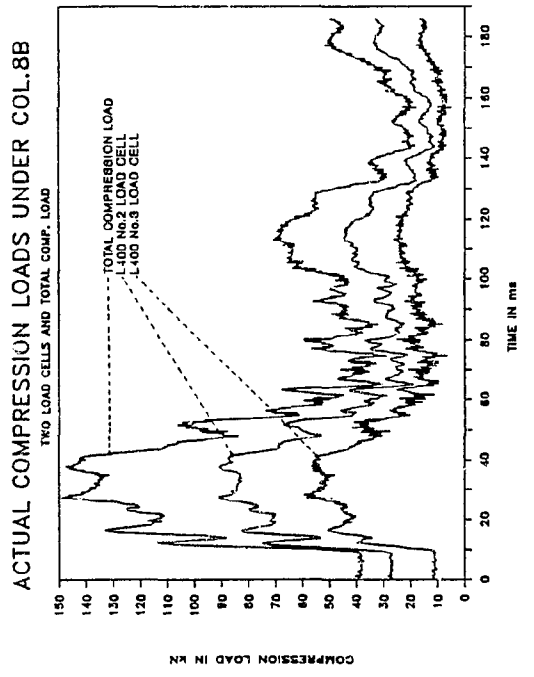

Fig. B.811: Comp. load Col 8B

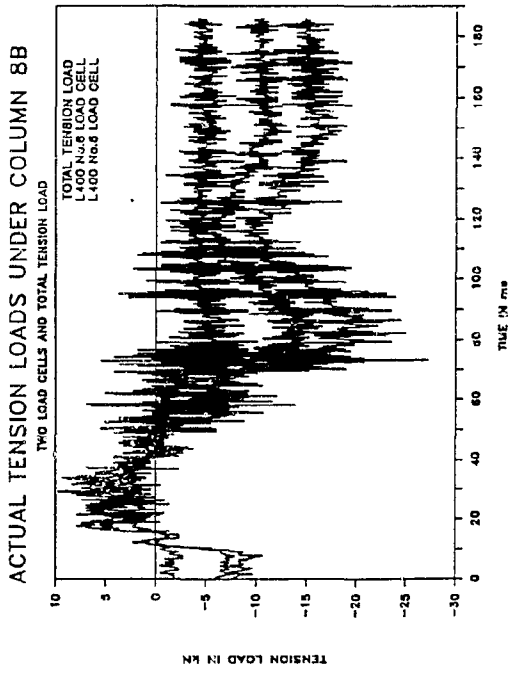

Fig. B.812: Tens. loads Col.8B

Stellenbosch University http://scholar.sun.ac.za

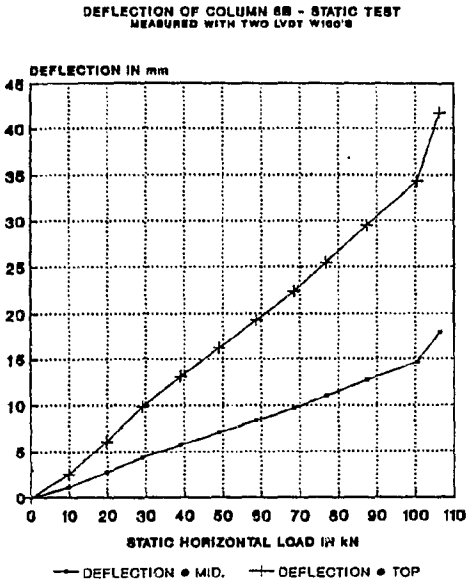

Fig. B.813: Deflection Col.8B

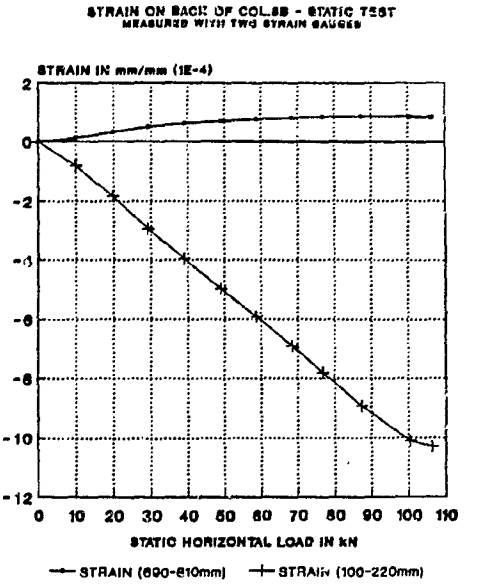

Fig. B.814: Strain Col.8B

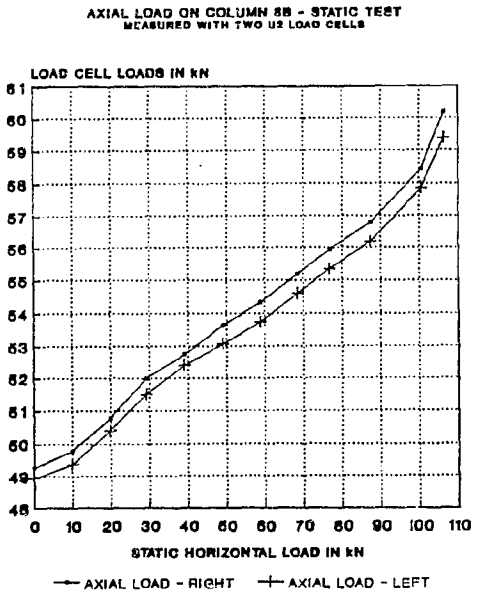

Fig. B.815: Axial load Col 8B

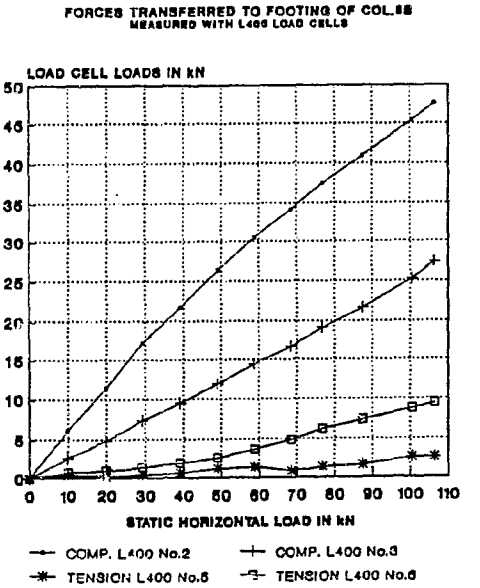

Fig. B.816: Foot.loads Col.8B

Stellenbosch University http://scholar.sun.ac.za

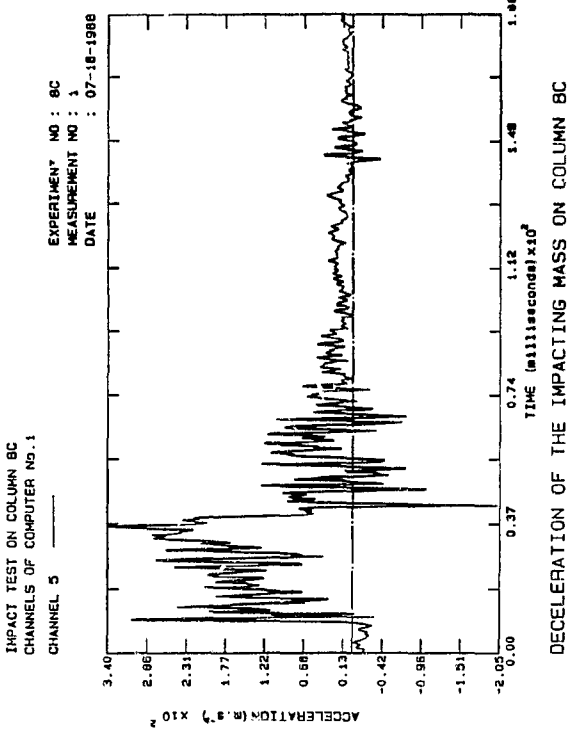

Fig. B.817: Decel. Col.8C

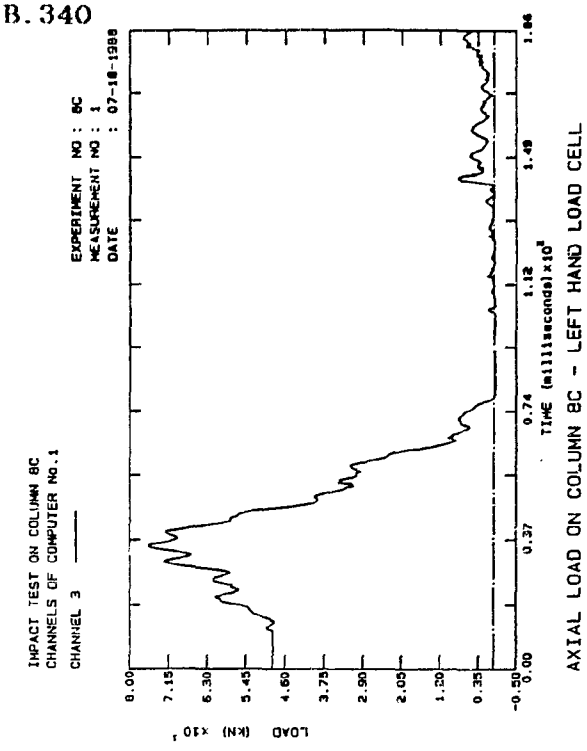

Fig. B.818: Axial load Col.8C

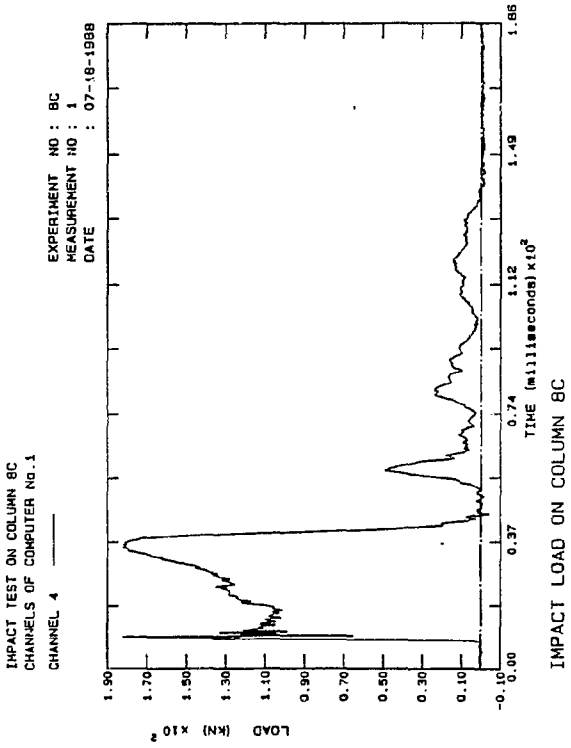

Fig. B.819: Impact Col 8C

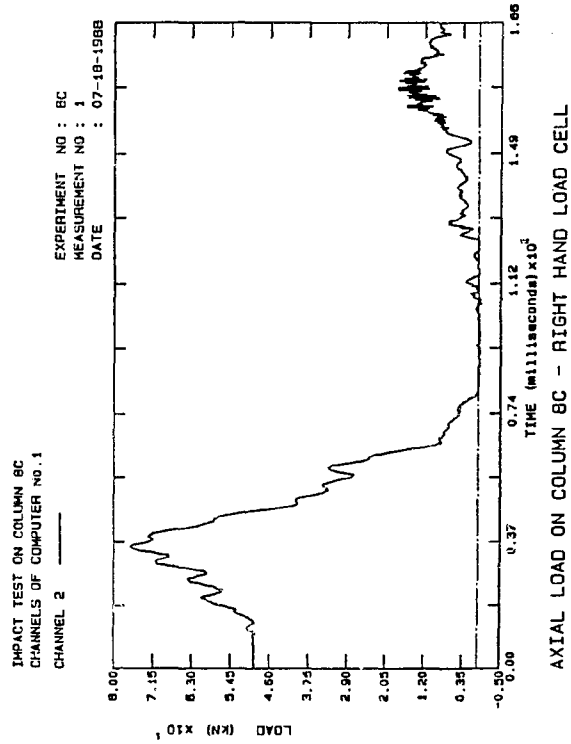

Fig. B.820: Axial load Col.8C

Stellenbosch University http://scholar.sun.ac.za

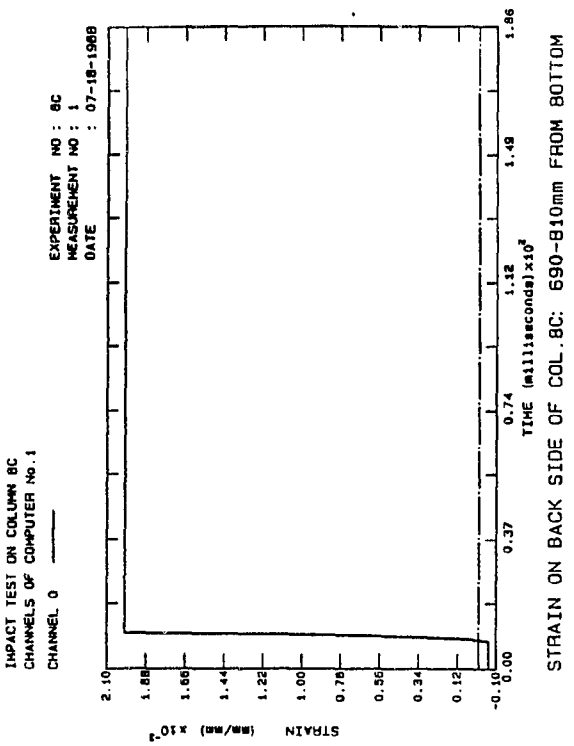

Fig. B.821: Strain Col.8C

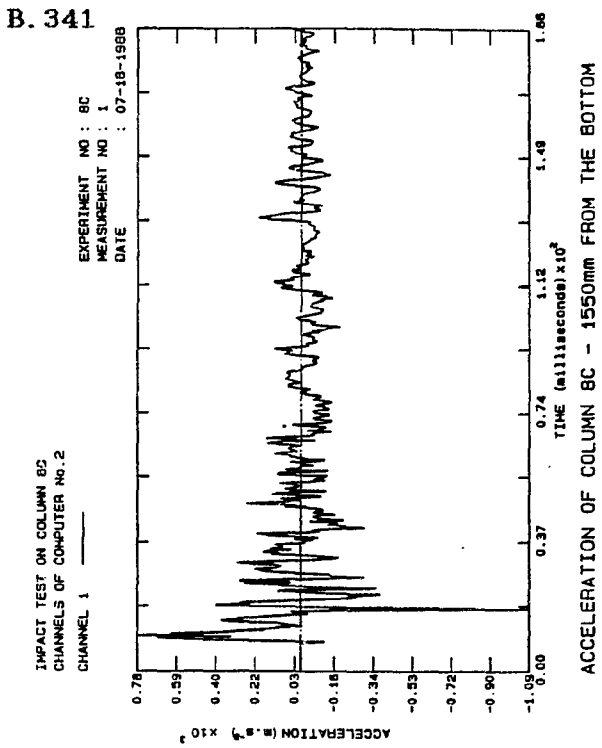

Fig. B.822: Accel. Col.8C

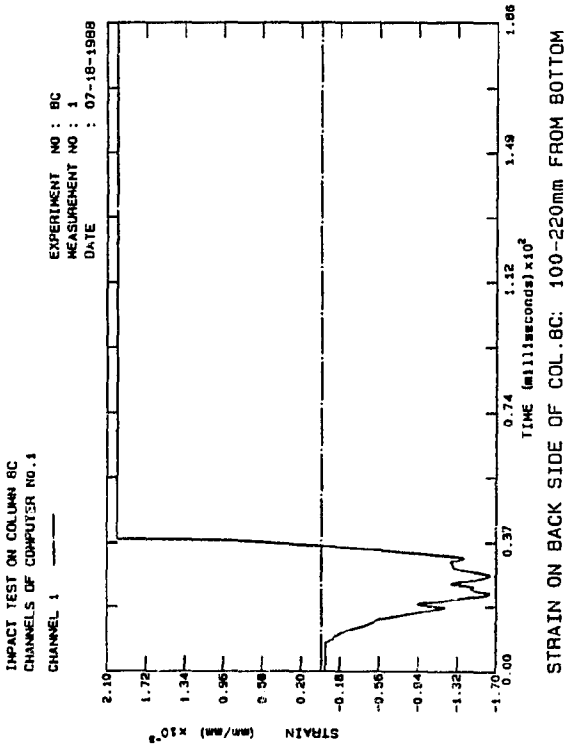

Fig. B.823: Strain Col 8C

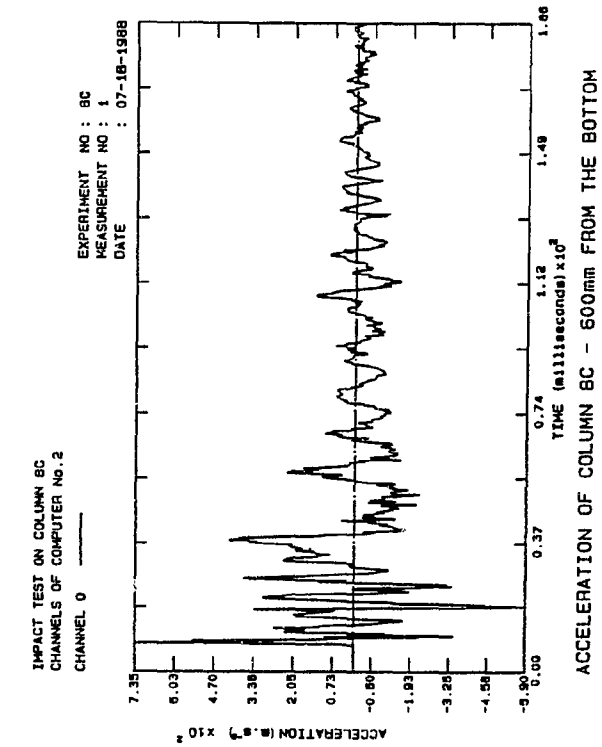

Fig. B.824: Accel. Col.8C

Stellenbosch University http://scholar.sun.ac.za

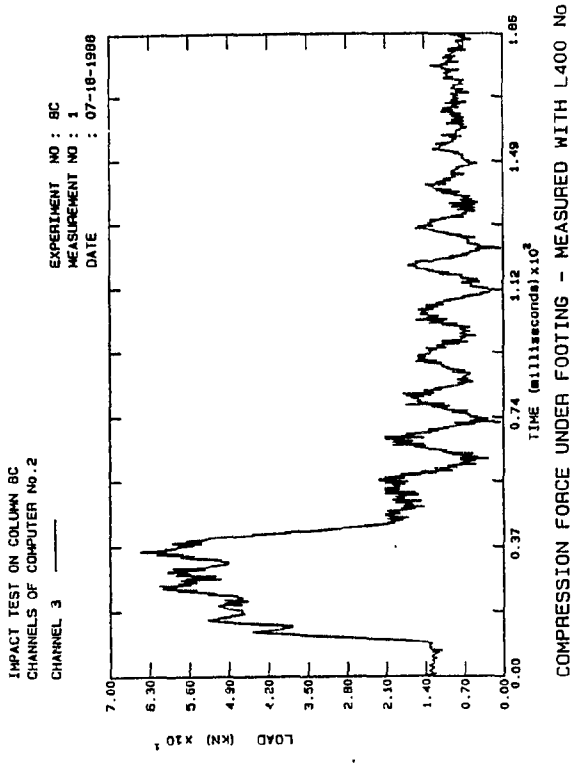

Fig. B.825: Comp. Col.8C

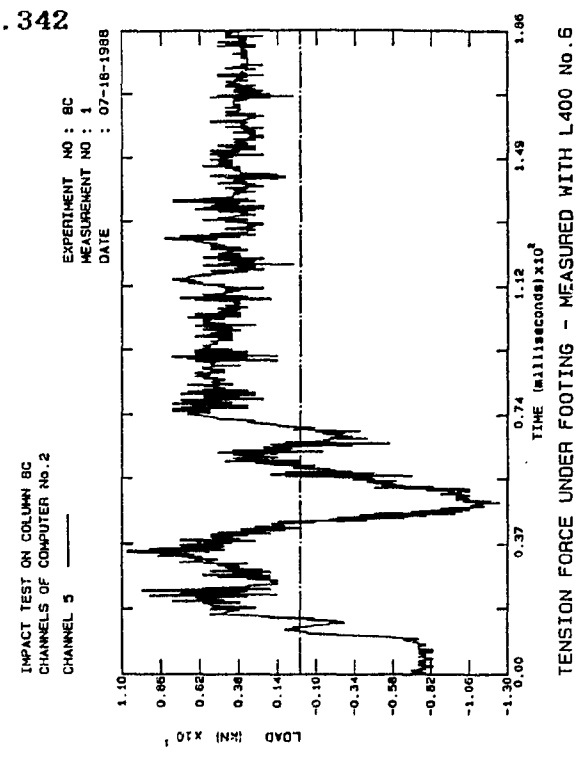

Fig. B.826: Tension Col.8C

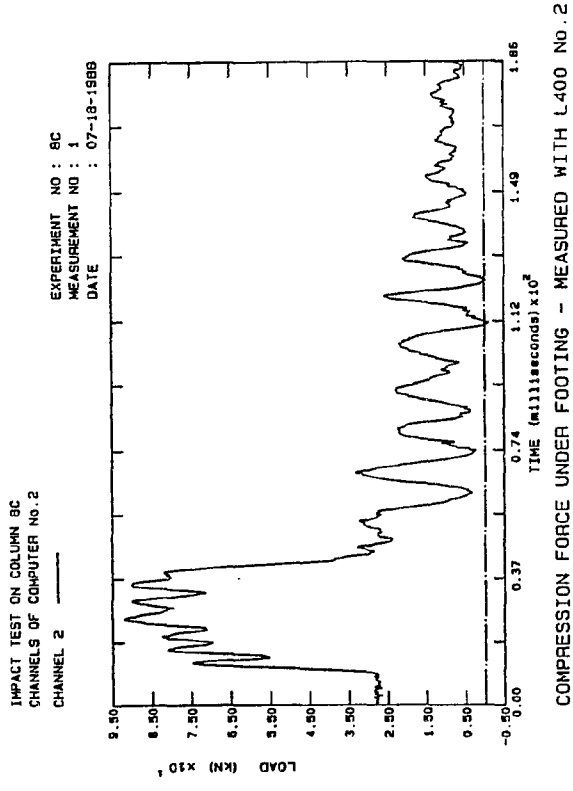

Fig. B.827: Comp. Col 8C

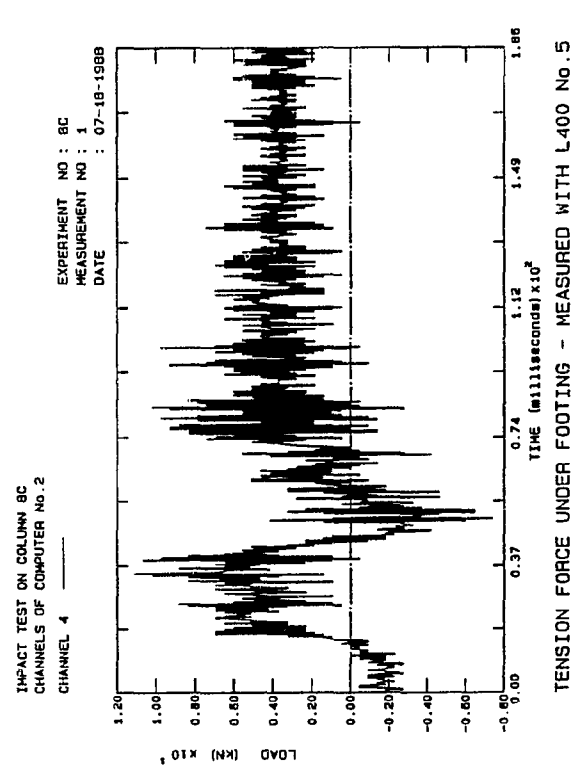

Fig. B.828: Tension Col.8C

Stellenbosch University http://scholar.sun.ac.za

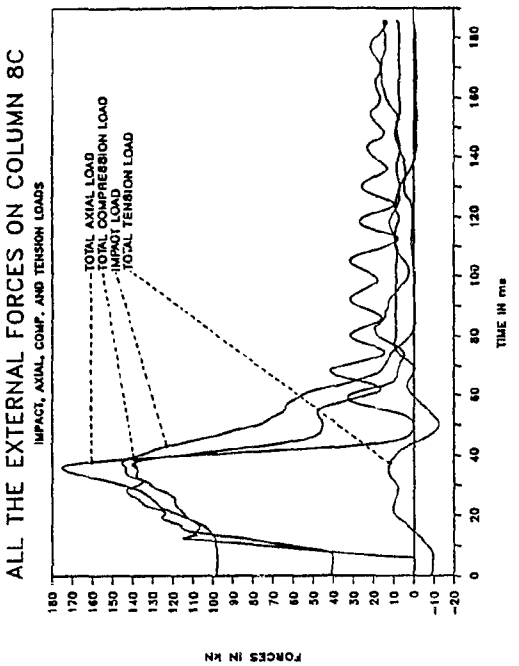

Fig. B.829: Ext. Loads Col.8C

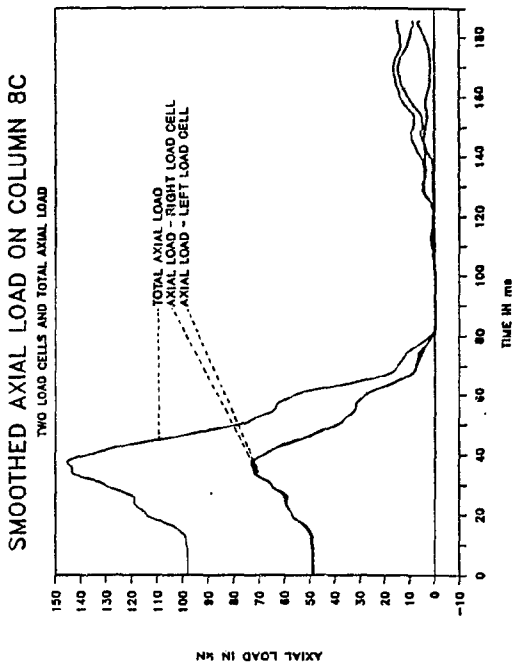

Fig. B.830: Smo. Axial Col.8C

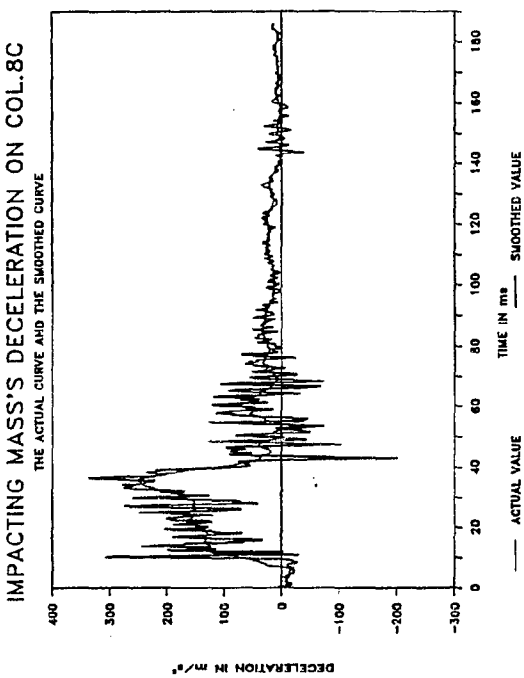

Fig. B.831: Smo.Decel. Col 8C

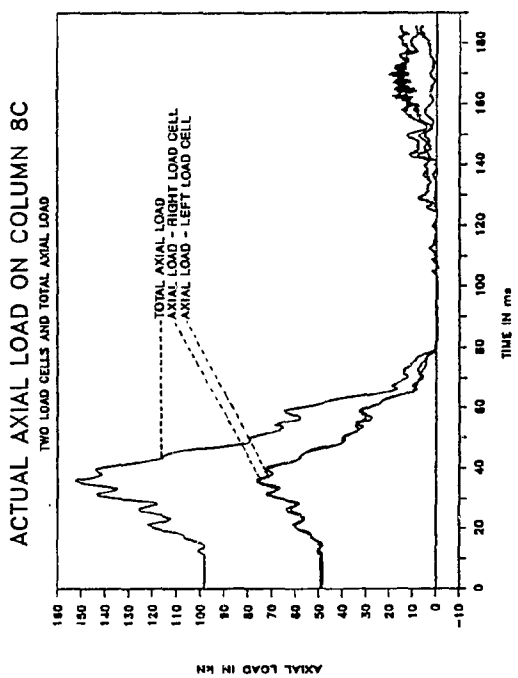

Fig. B.832: Axial loads Col.8C

Stellenbosch University http://scholar.sun.ac.za

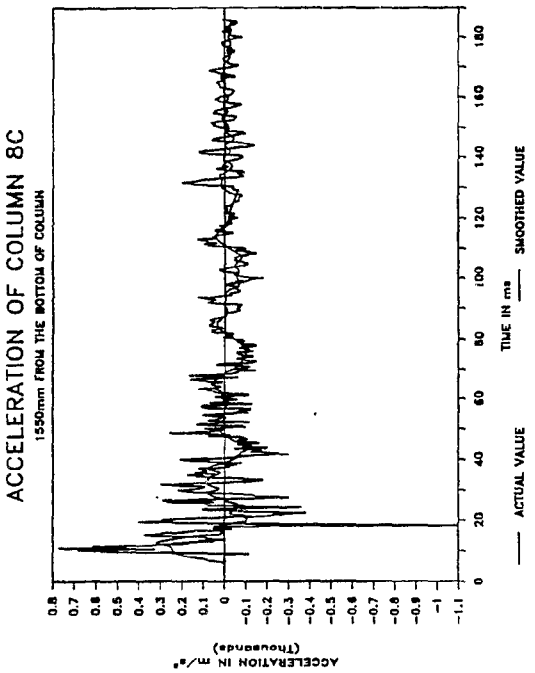

Fig. B.833: Smo.Accel. Col.8C

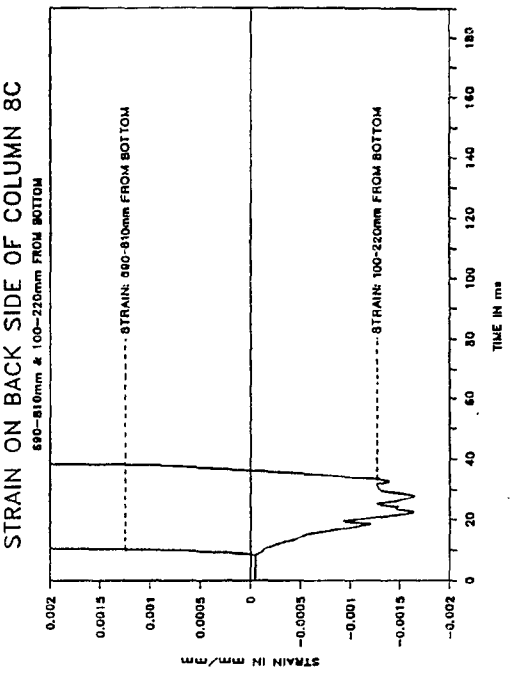

Fig. B.834: Strain Col.8C

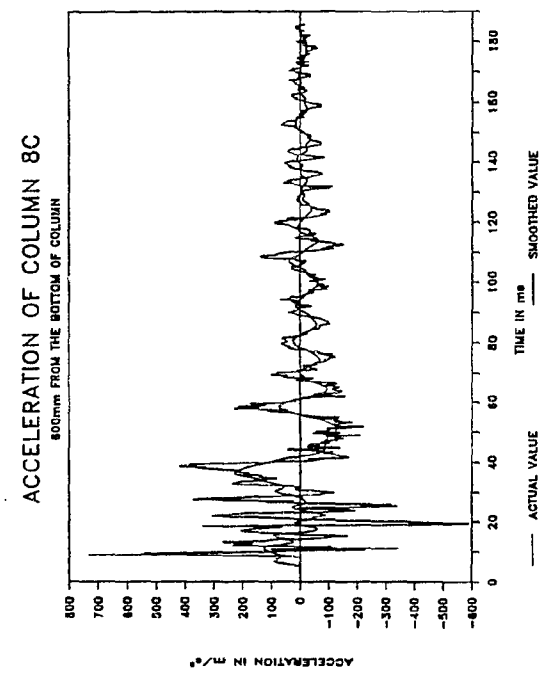

Fig. B.835: Smo.Accel. Col 8C

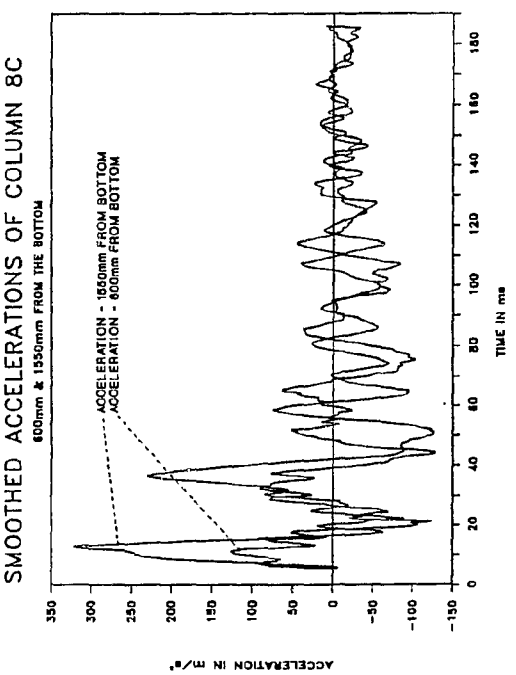

Fig. B.836: Smo. Accel. Col.8C

Stellenbosch University http://scholar.sun.ac.za

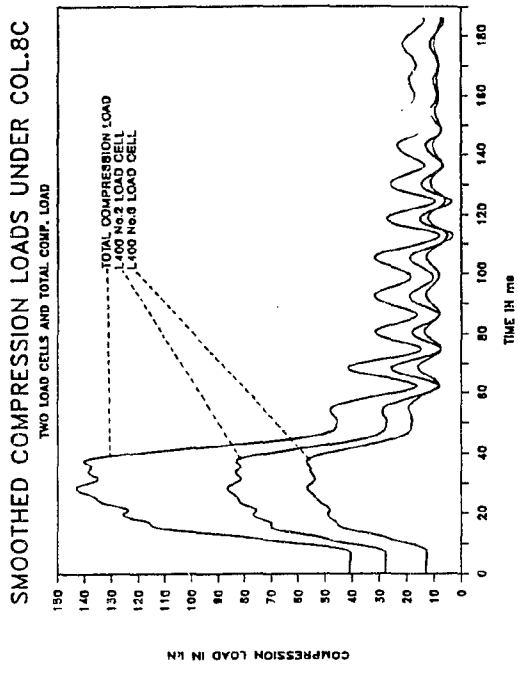

Fig. B.837: Smo. Comp. Col.8C

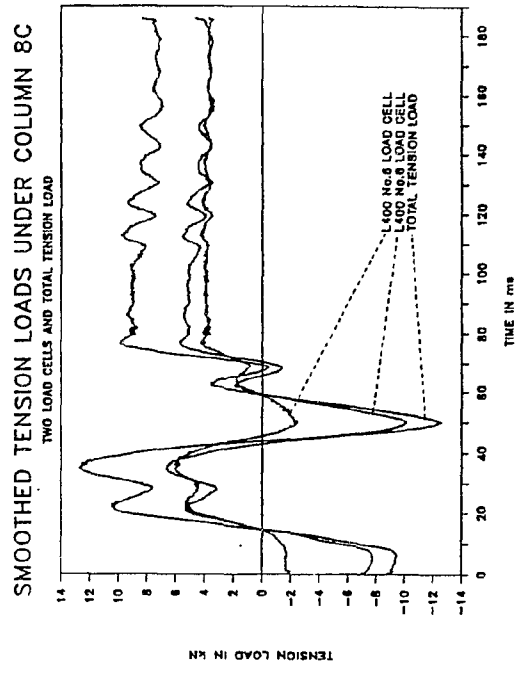

Fig. B.838: Smo. Tens. Col.8C

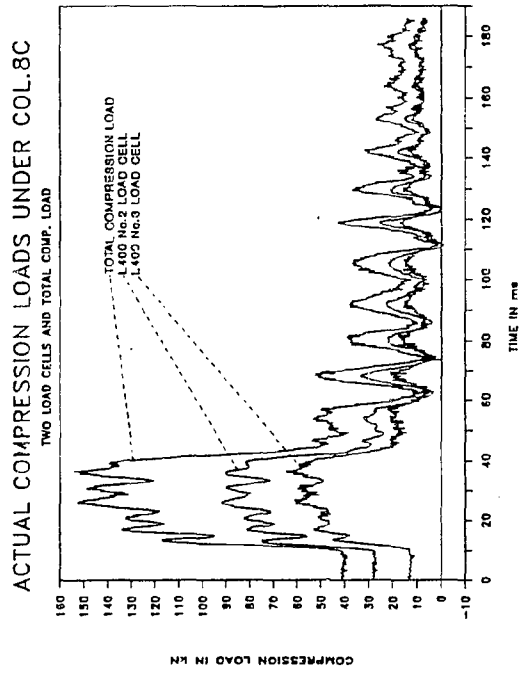

Fig. B.839: Comp. load Col 8C

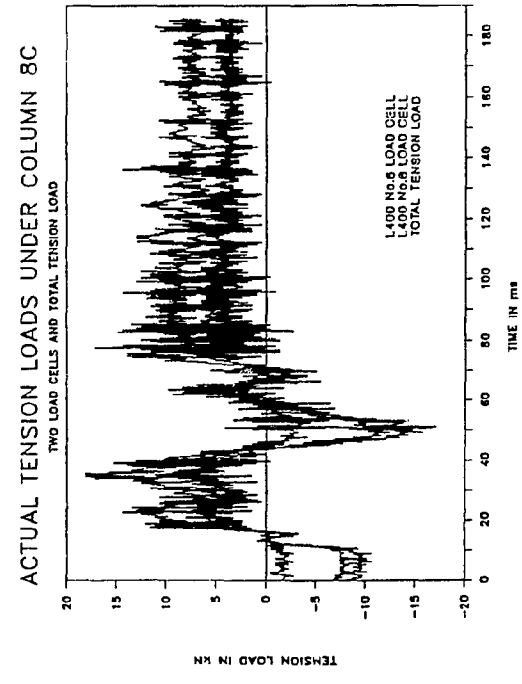

Fig. B.840: Tens. loads Col.8C

Stellenbosch University http://scholar.sun.ac.za

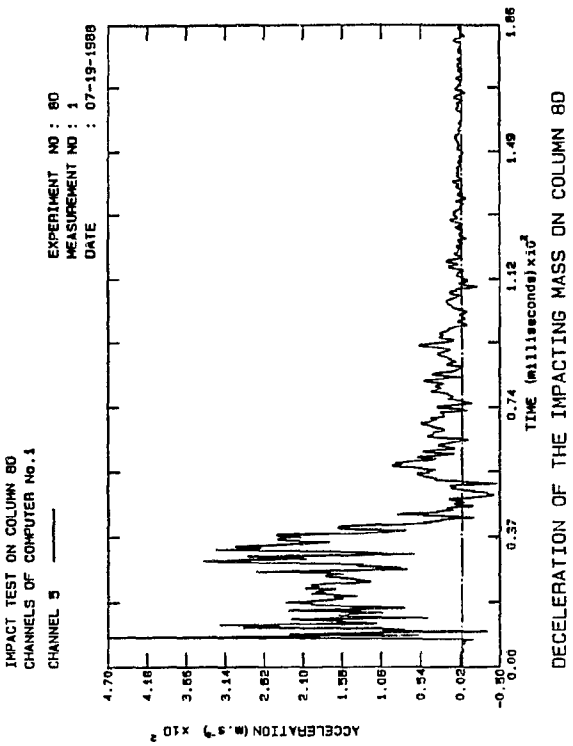

Fig. B.841: Decel. Col.8D

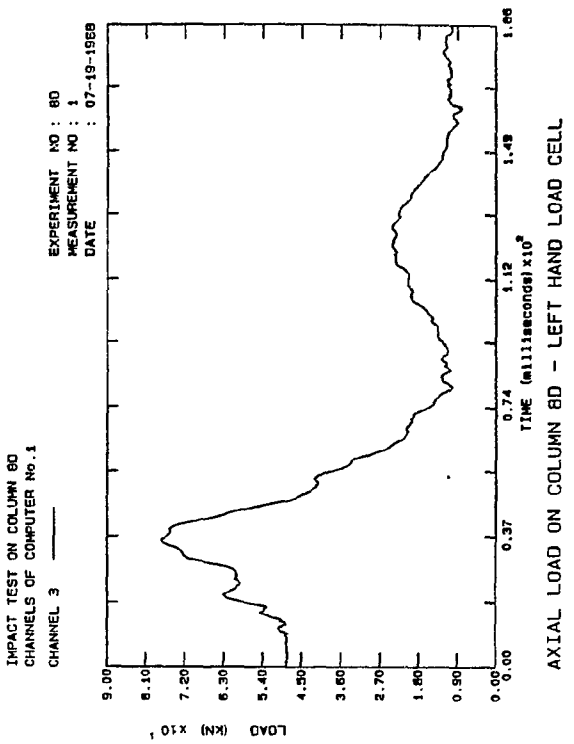

Fig. B.842: Axial load Col.8D

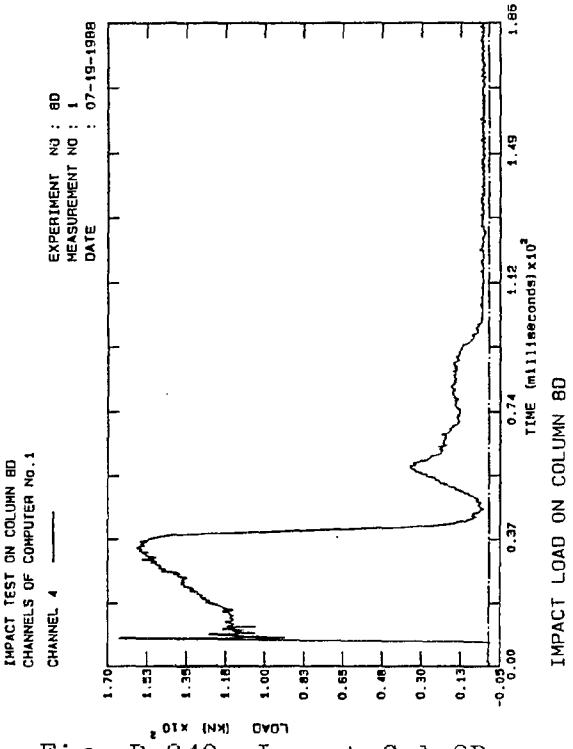

Fig. B.843: Impact Col 8D

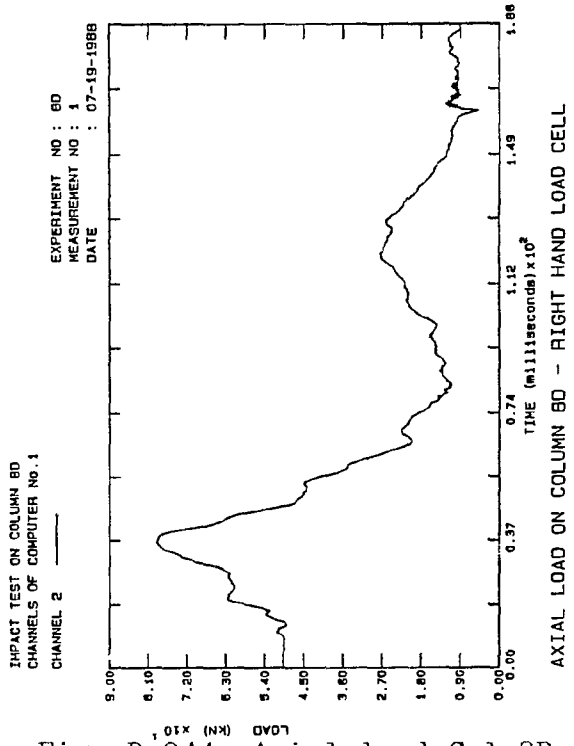

Fig. B.844: Axial load Col.8D

Stellenbosch University http://scholar.sun.ac.za

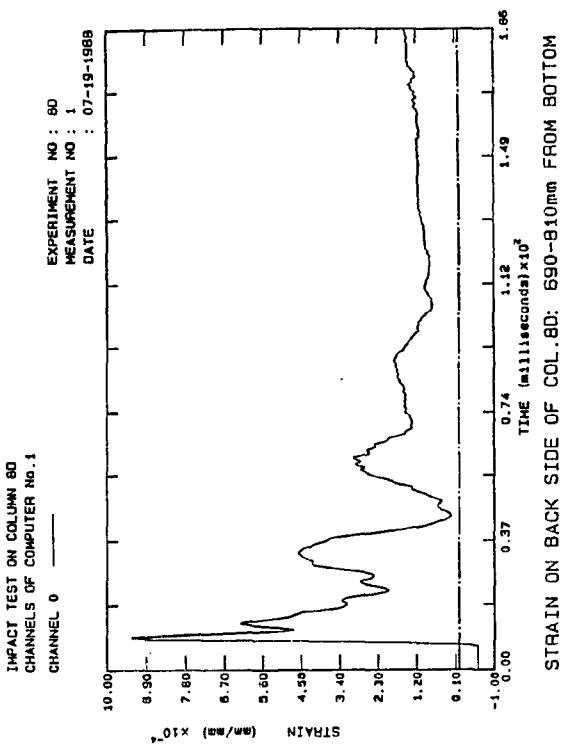

Fig. B.845: Strain Col.8D

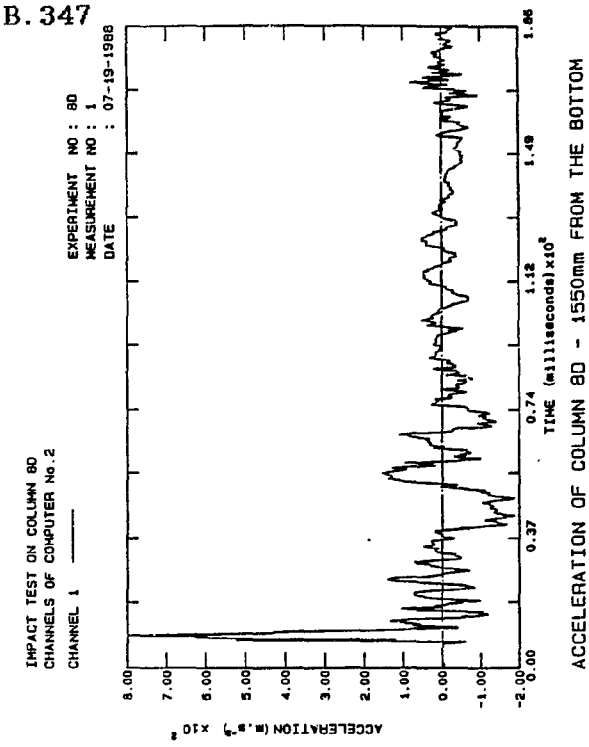

Fig. B.846: Accel. Col.8D

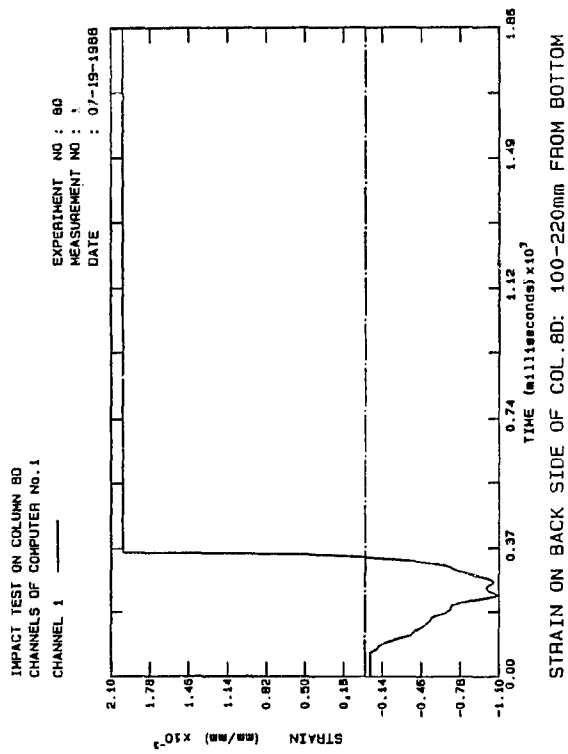

Fig. B.847: Strain Col 8D

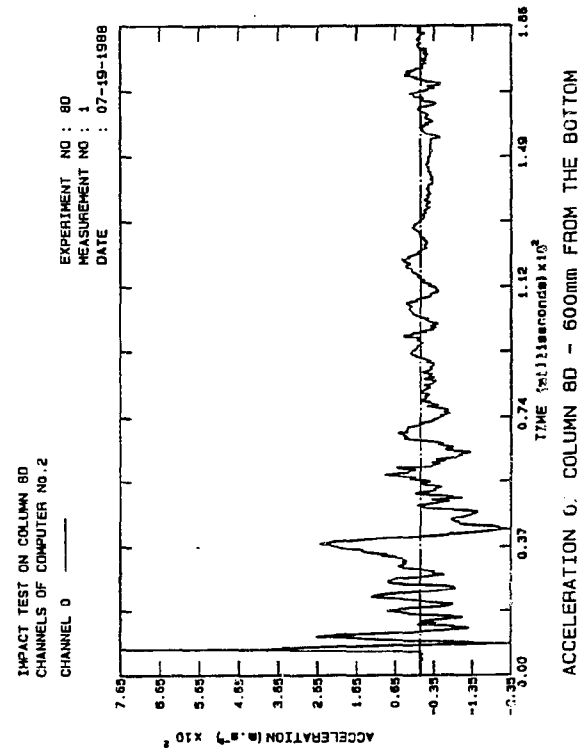

Fig. B.848: Accel. Col.8D

Stellenbosch University http://scholar.sun.ac.za

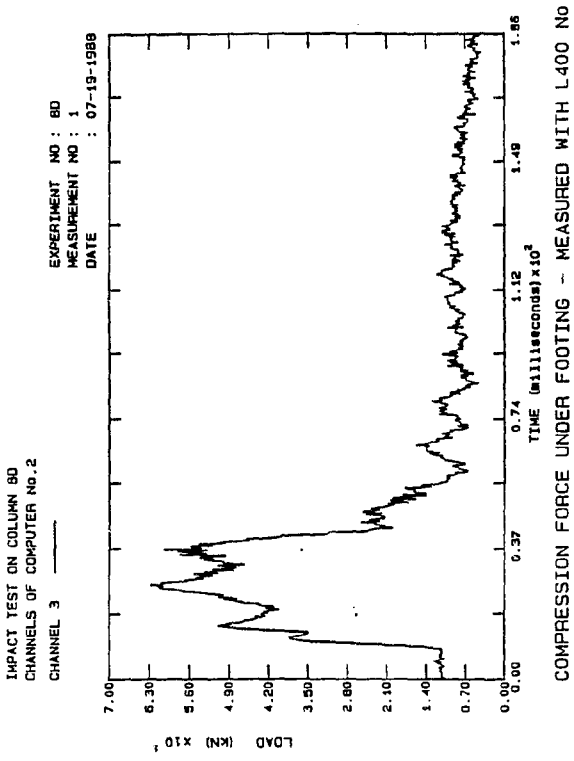

Fig. B.849: Comp. Col.8D

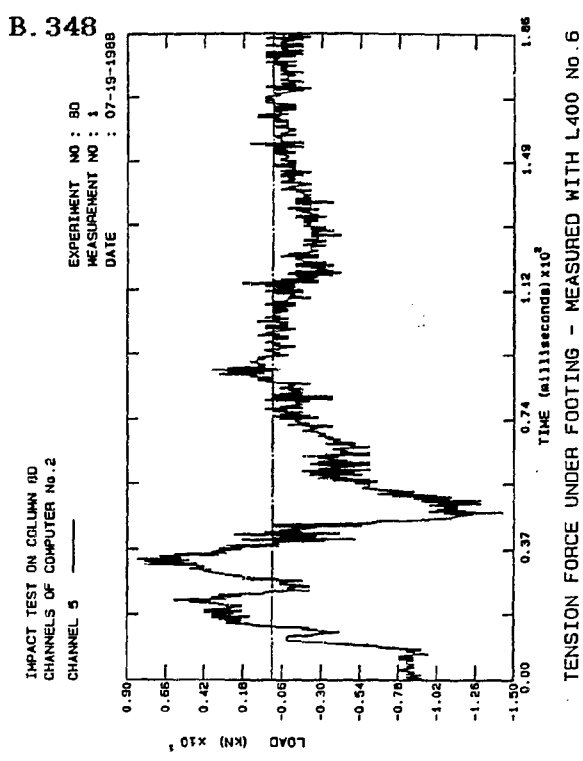

Fig. B.850: Tension Col.8D

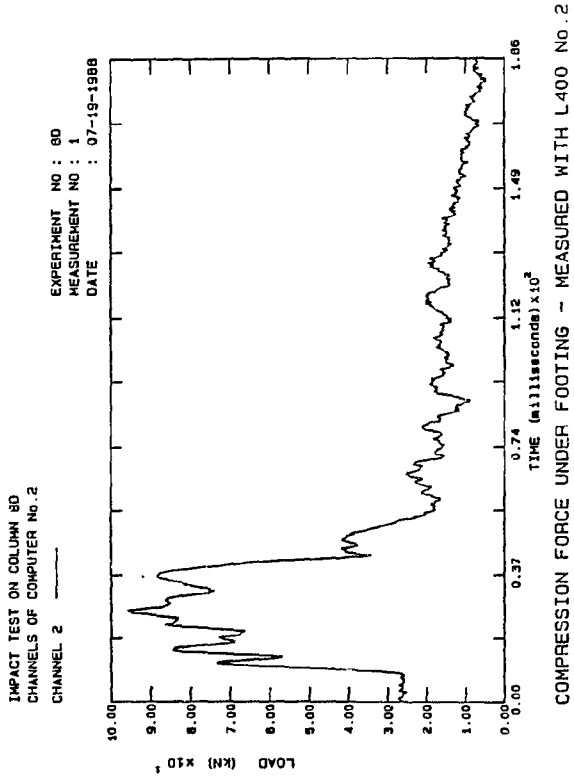

Fig. B.851: Comp. Col 8D

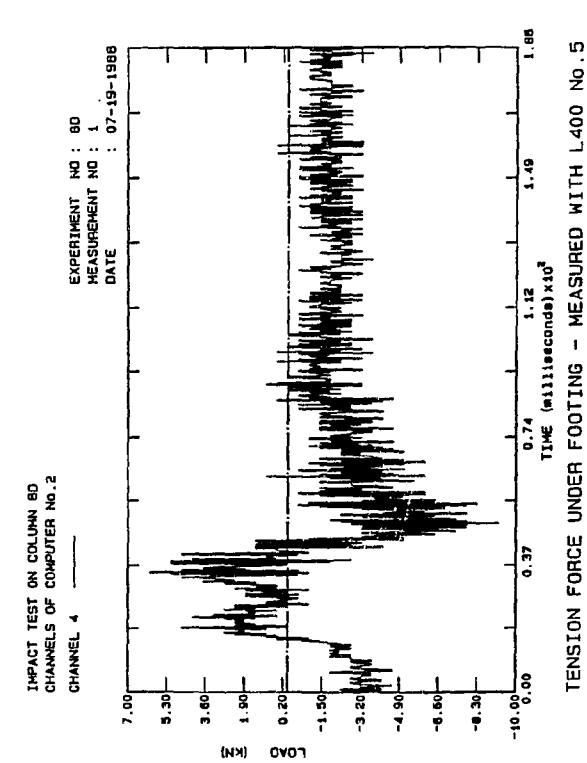

Fig. B.852: Tension Col.8D

Stellenbosch University http://scholar.sun.ac.za

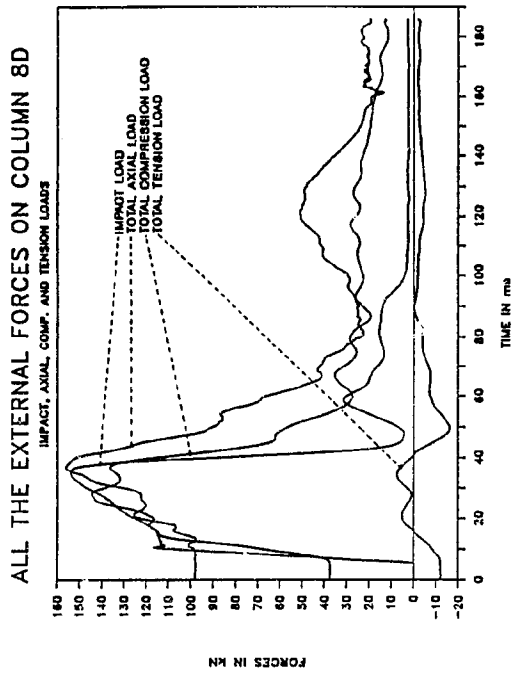

Fig. B.853: Ext., Loads Col.8D

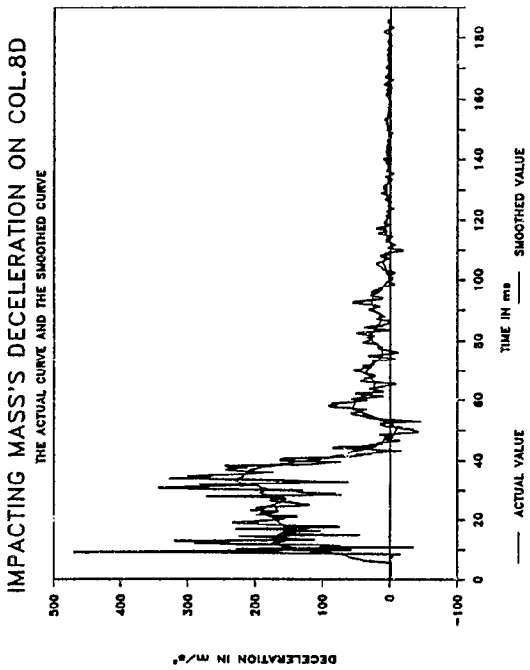

Fig. B.854: Smo.Decel. Col 8D

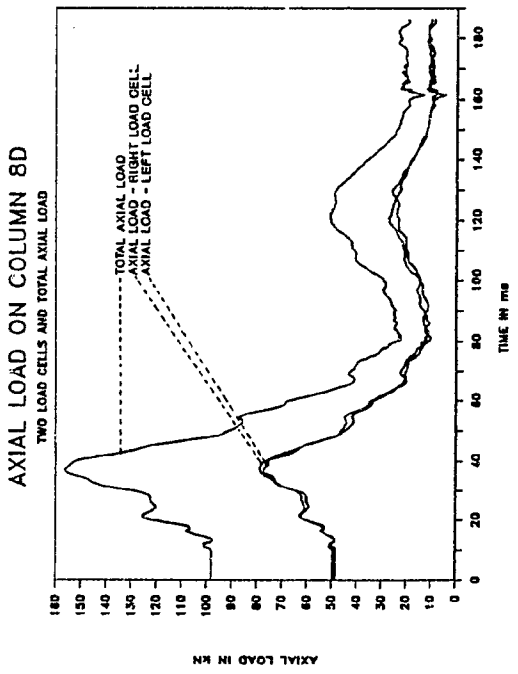

Fig. B.855: Axial loads Col.8D

Stellenbosch University http://scholar.sun.ac.za

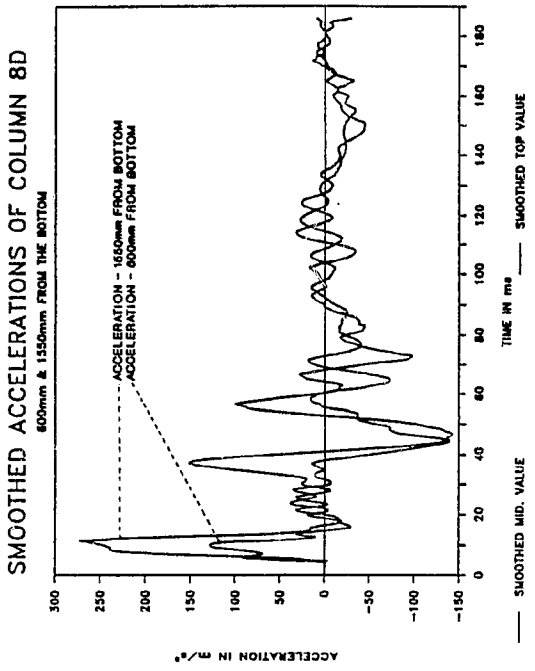

Fig. B.856: Smo.Accel. Col.8D

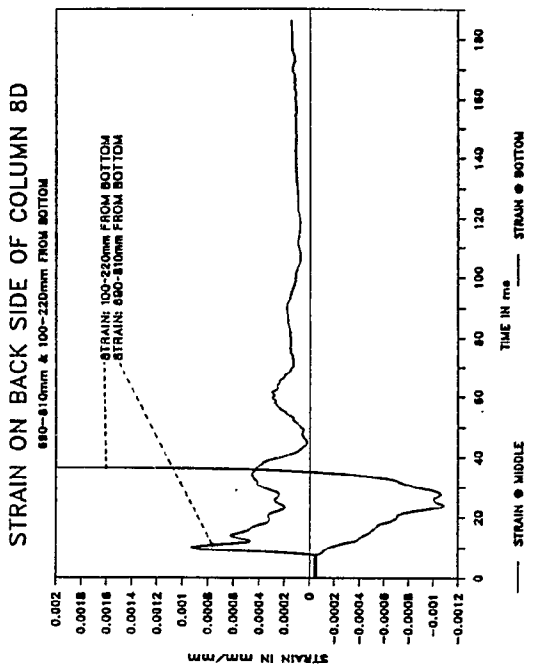

Fig. B.857: Strain Col.8D

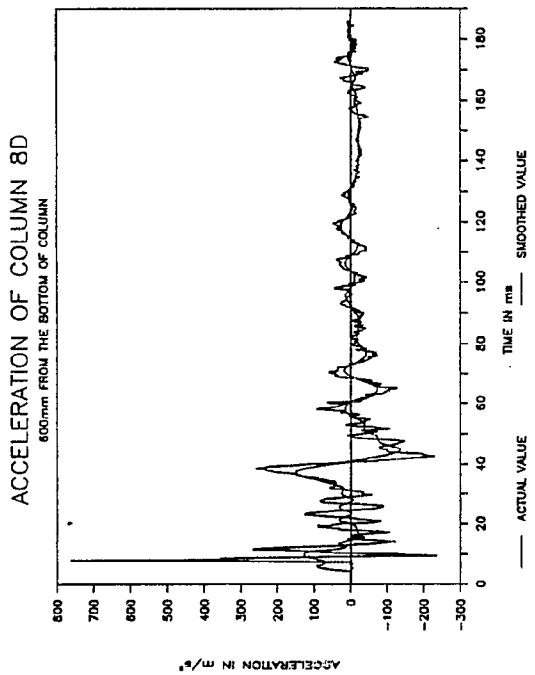

Fig. B.858: Smo.Accel. Col 8D

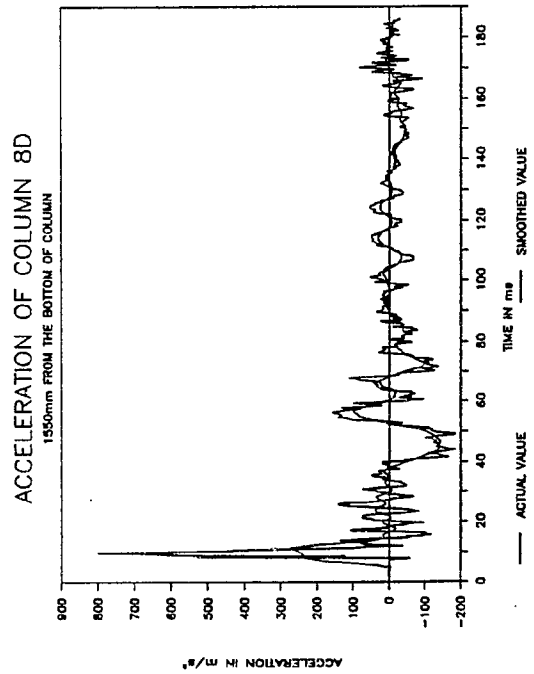

Fig. B.859: Smo. Accel. Col.8D

Stellenbosch University http://scholar.sun.ac.za

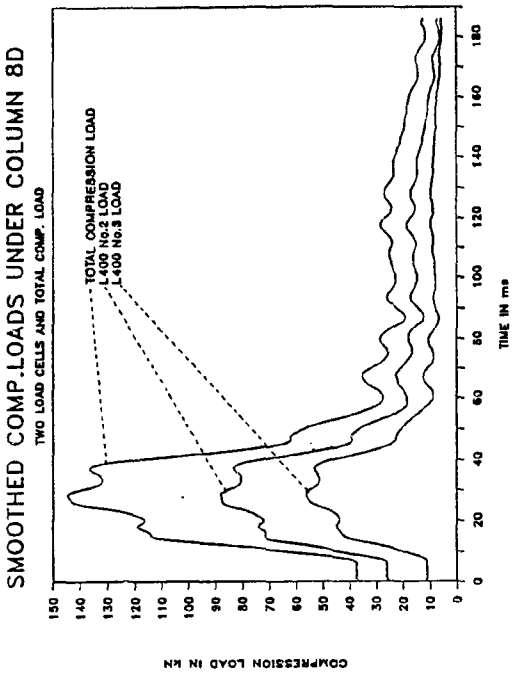

Fig. B.860: Smo. Comp. Col.8D

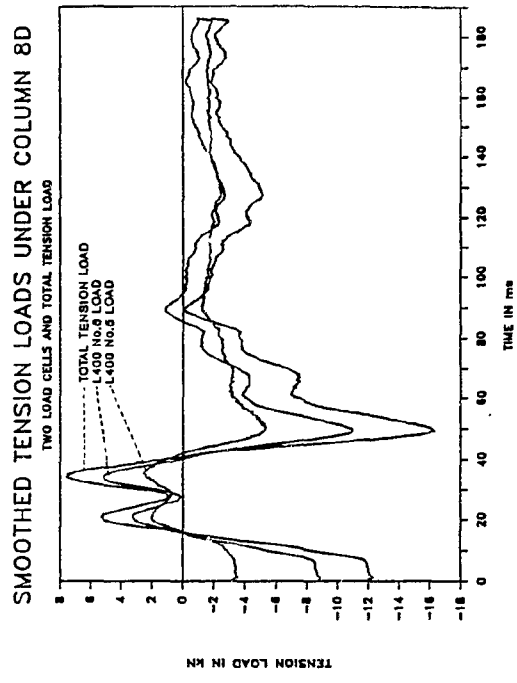

Fig. B.861: Smo. Tens. Col.8D

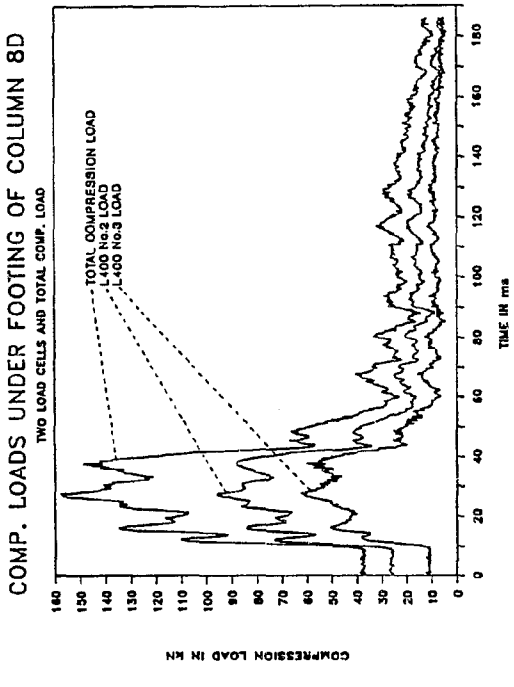

Fig. B.862: Comp. load Col 8D

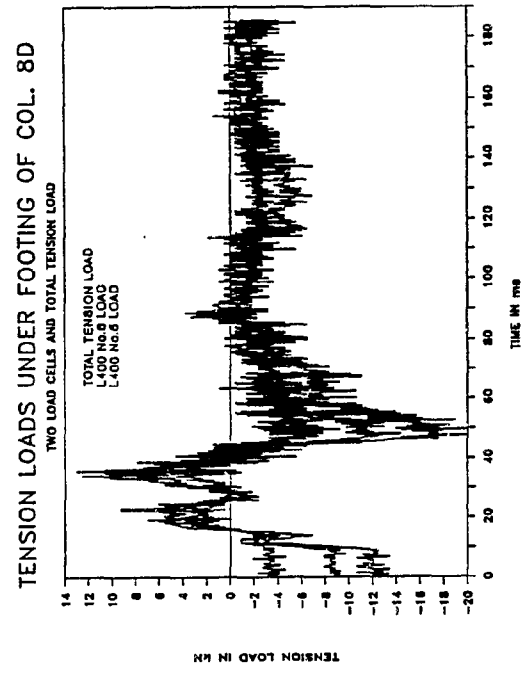

Fig. B.863: Tens. loads Col.8D

Stellenbosch University http://scholar.sun.ac.za

B.10 Reinforcement Data.

Samples of all the reinforcing steel were tested and all their test results are given in this section.

Two types of reinforcing bars were used. The main reinforcement was a high yield steel of 16 mm diameter deformed bars. The stirrups were a mild steel with a lower yield strength. The stirrups were 8 mm in diameter and was a smooth type of bar.

The following set of figures show the tensile strength test results of all the columns reinforcement graphically, as well as a summary of the test results (figures B.892 and B.904).

The average results of all the tests are:

Y16-Bars:	Elasticity Modulus:	207220,4 MPa
	Yield Stress:	518,6 MPa
	Ultimate Stress:	756,5 MPa
R8-Bars:	Elasticity Modulus:	202693,1 MPa
	Yield Stress:	376,3 MPa
	Ultimate Stress:	499,4 MPa.

Stellenbosch University http://scholar.sun.ac.za

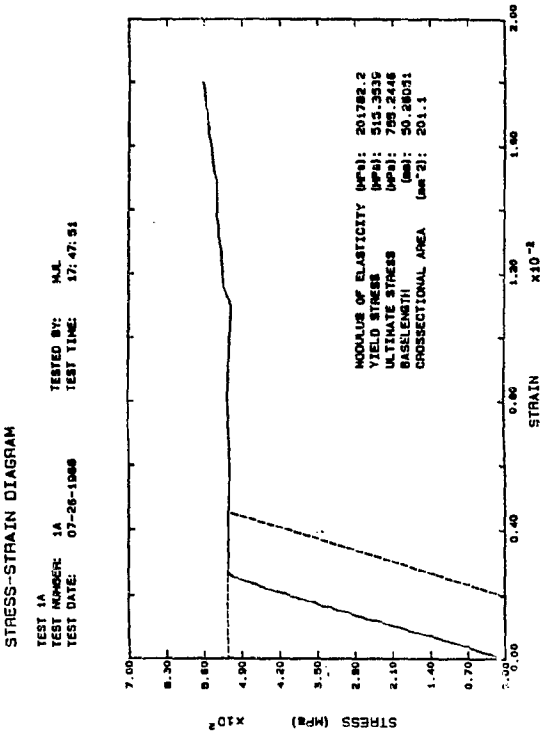

Fig.B.864: Column 1A

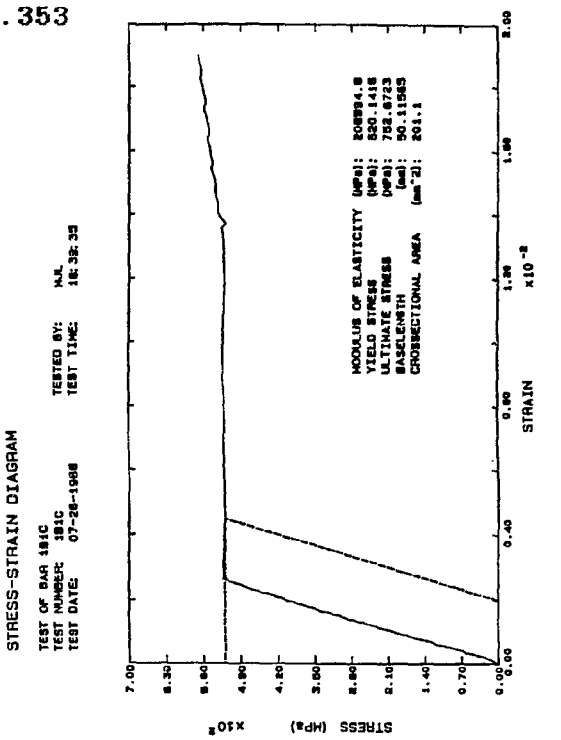

Fig.B.865: Column 1B

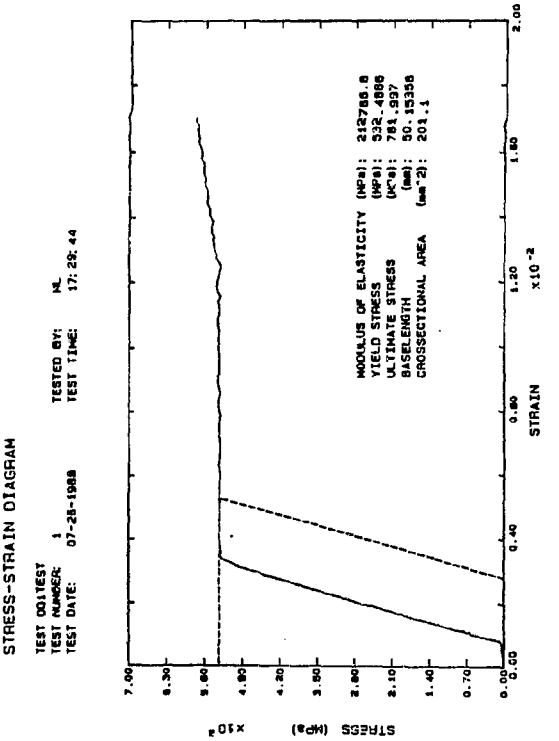

Fig.B.866: Column 1

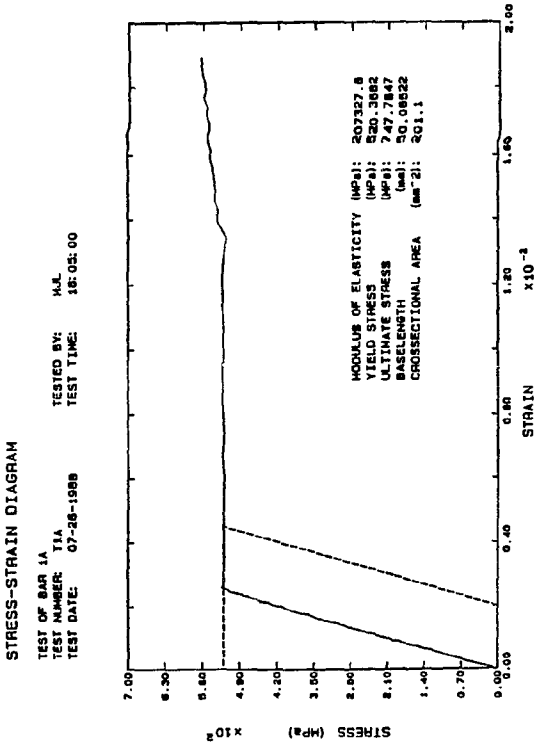

Fig. B.867: Column 1A

Stellenbosch University http://scholar.sun.ac.za

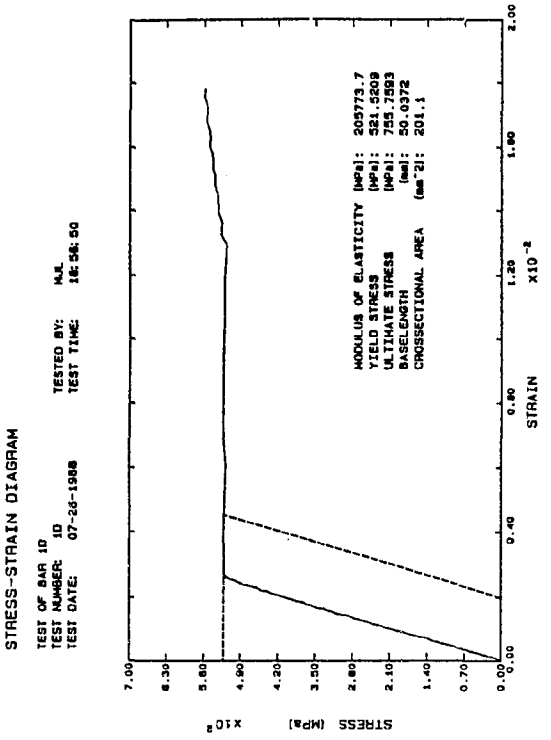

Fig.B.868: Column 1D

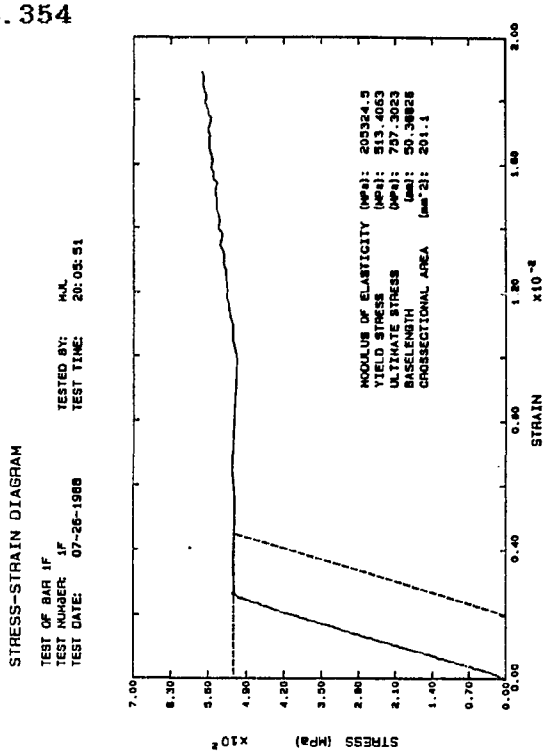

Fig.B.869: Column 1F

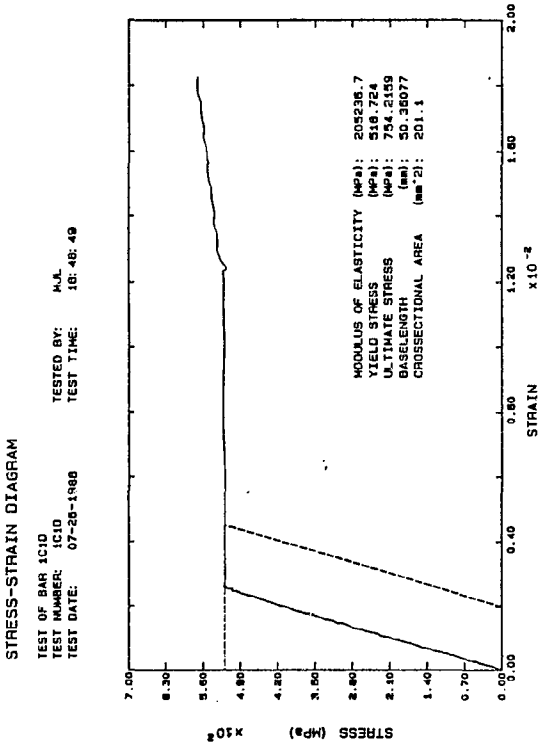

Fig.B.870: Column 1C

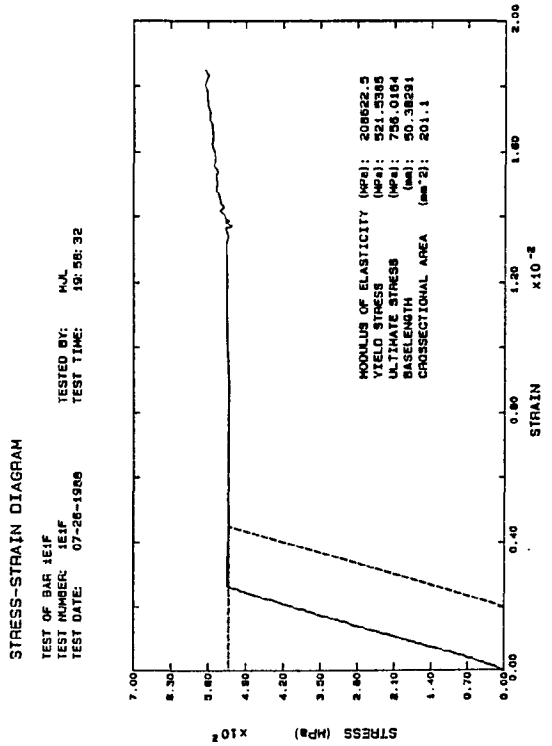

Fig. B.871: Column 1E

Stellenbosch University http://scholar.sun.ac.za

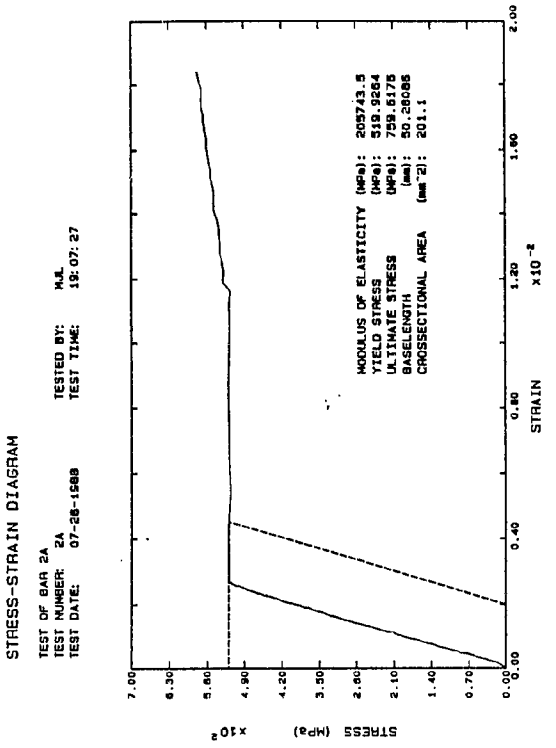

Fig.B.872: Column 2A

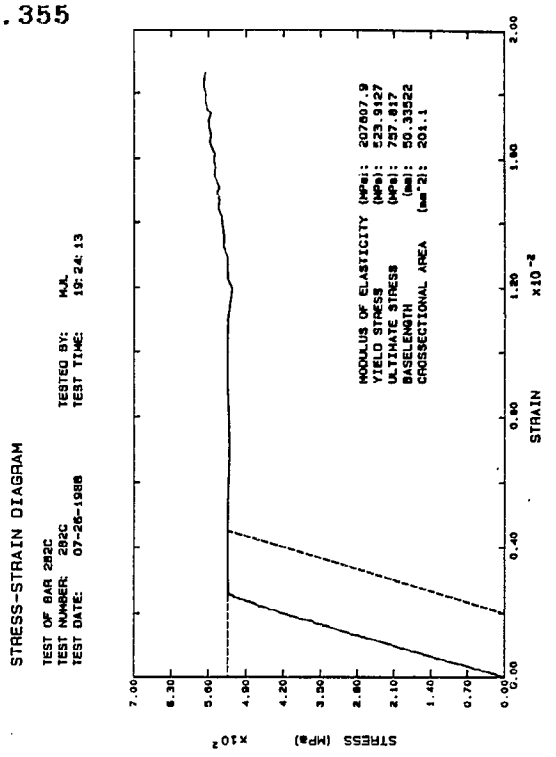

Fig.B.873: Column 2C

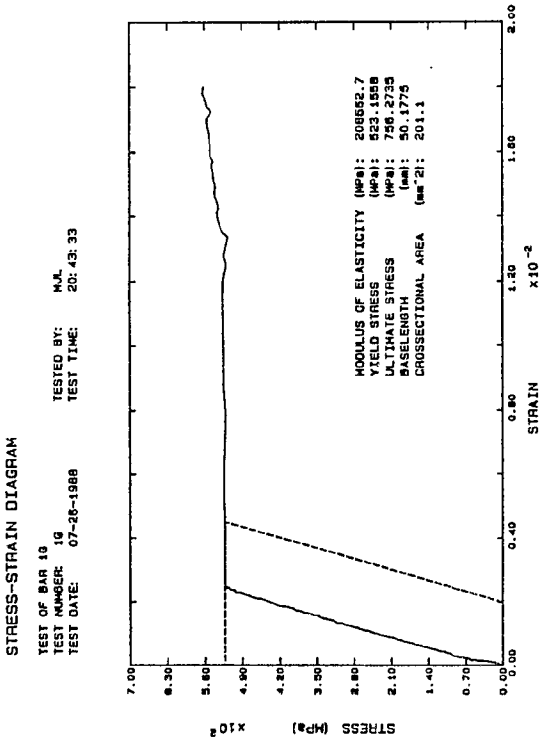

Fig.B.874: Column 1G

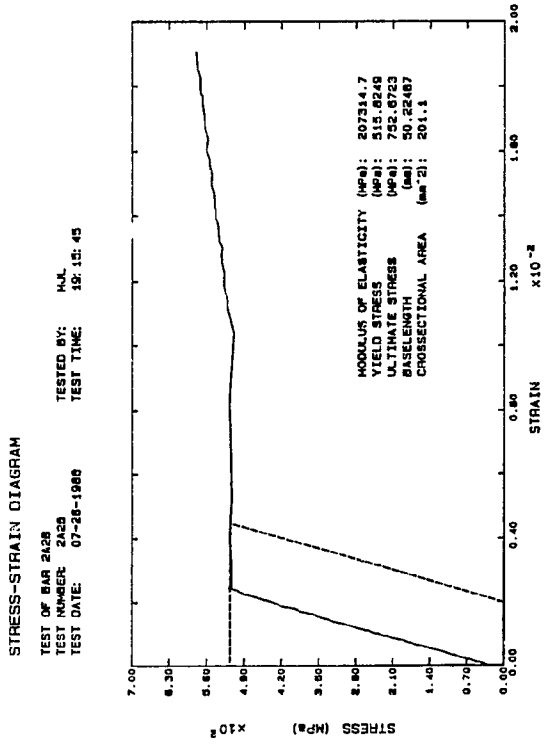

Fig. B.875: Column 2B

Stellenbosch University http://scholar.sun.ac.za

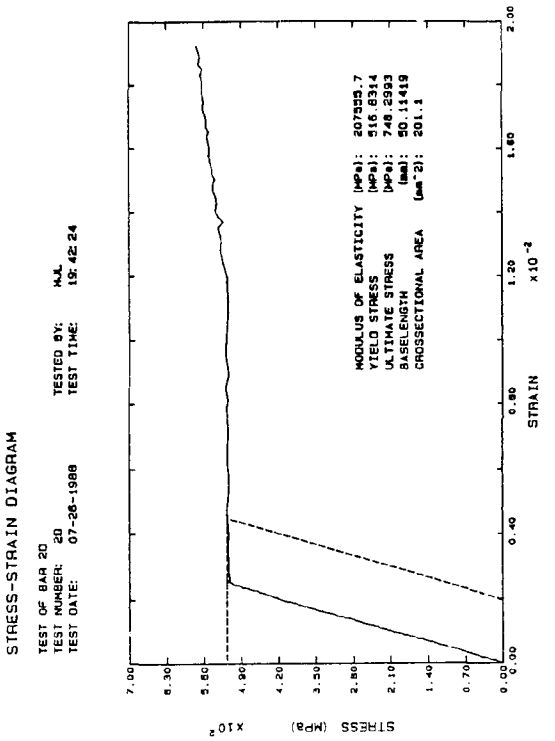

Fig.B.876: Column 2D

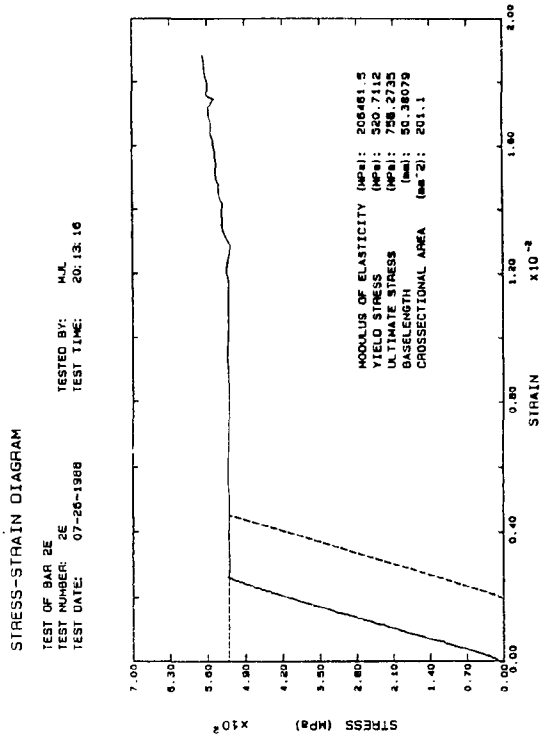

Fig.B.877: Column 2E

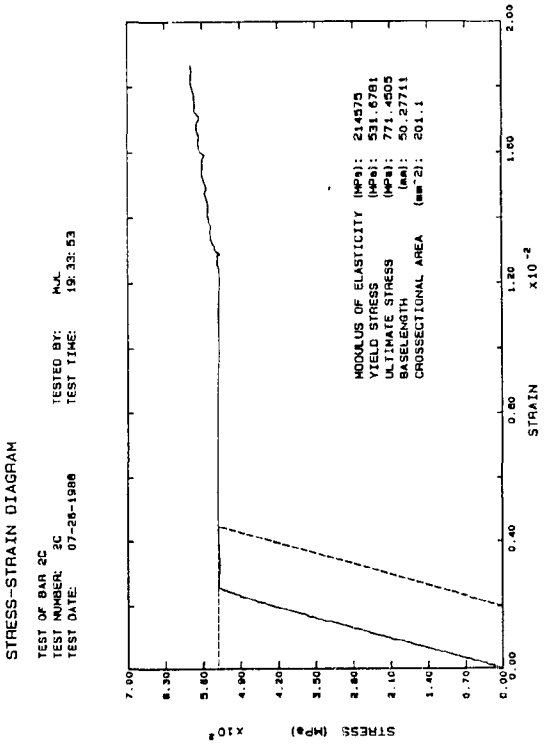

Fig.B.878: Column 2C

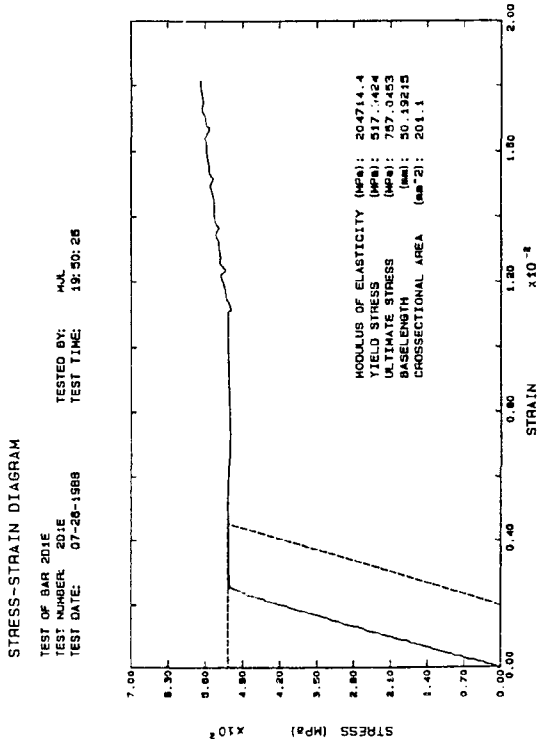

Fig. B.879: Column 2D

Stellenbosch University http://scholar.sun.ac.za

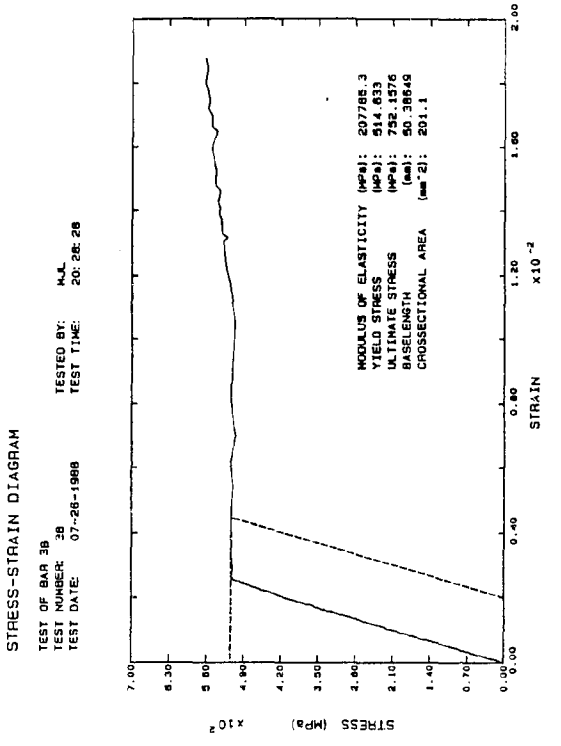

Fig.B.880: Column 3B

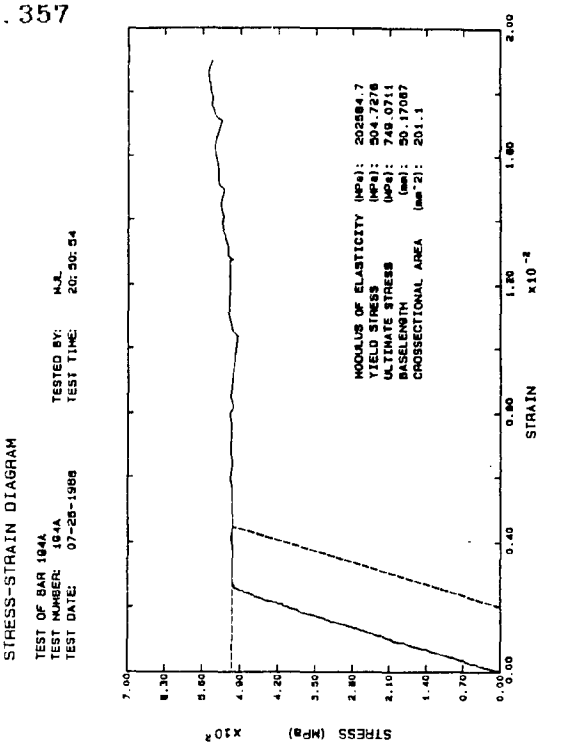

Fig.B.881: Column 4A

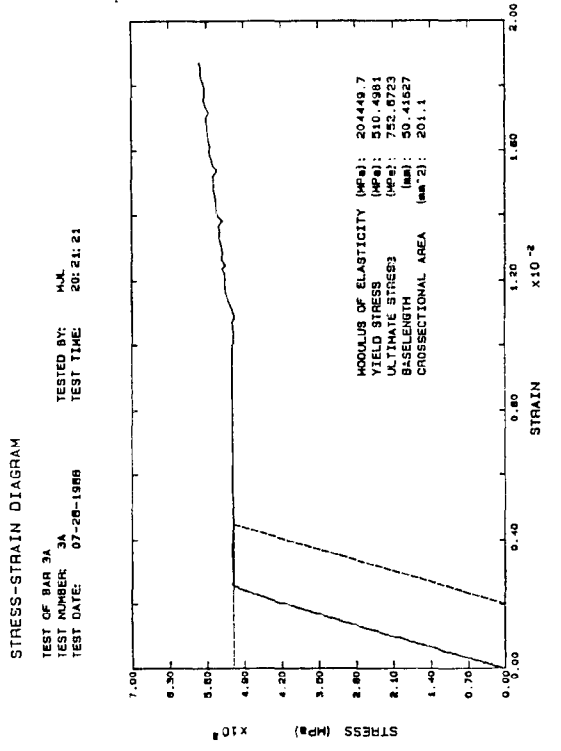

Fig.B.882: Column 3A

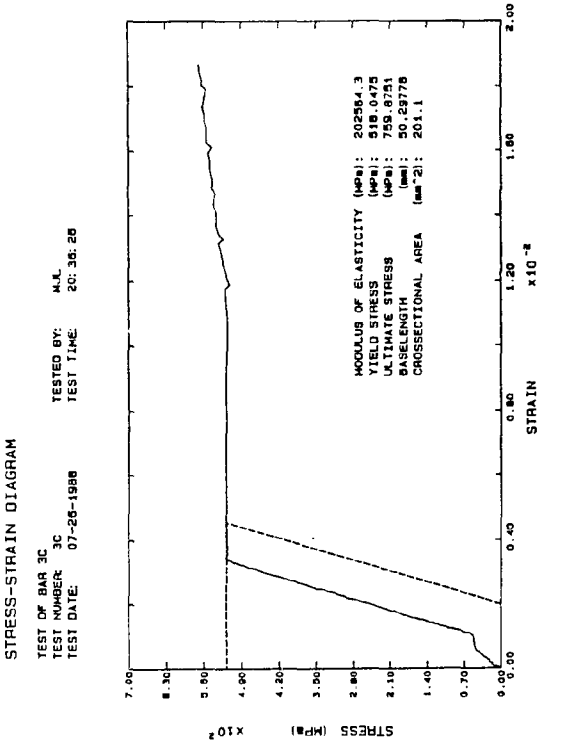

Fig. B.883: Column 3C

Stellenbosch University http://scholar.sun.ac.za

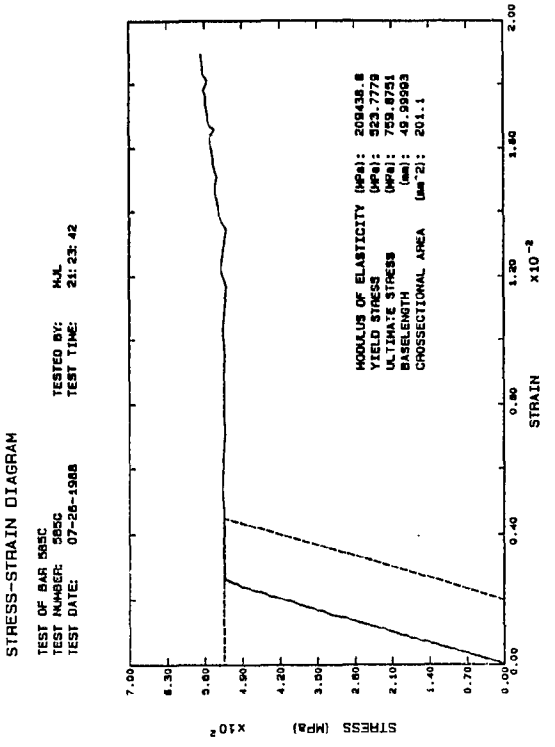

Fig.B.884: Column 5B & 5C

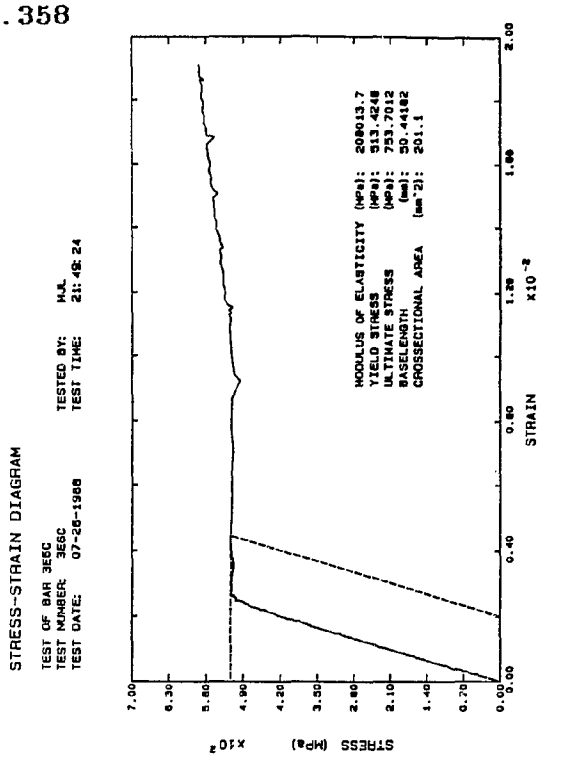

Fig.B.885: Column 3E & 6C

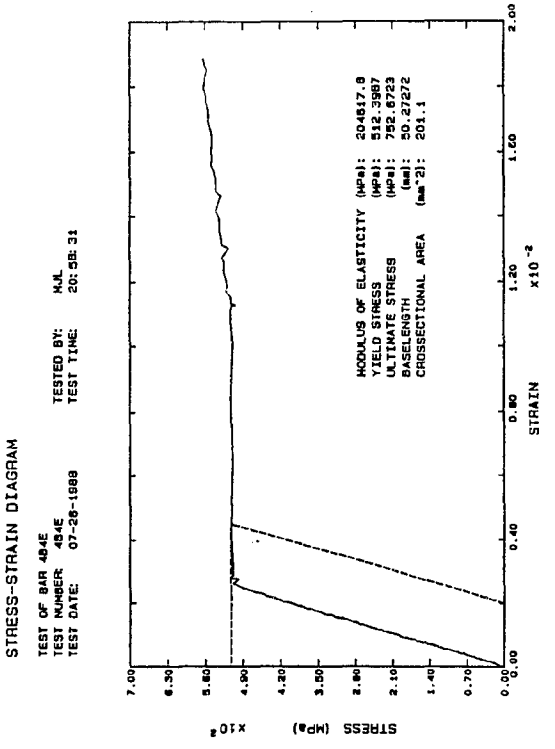

Fig.B.886: Column 4B & 4E

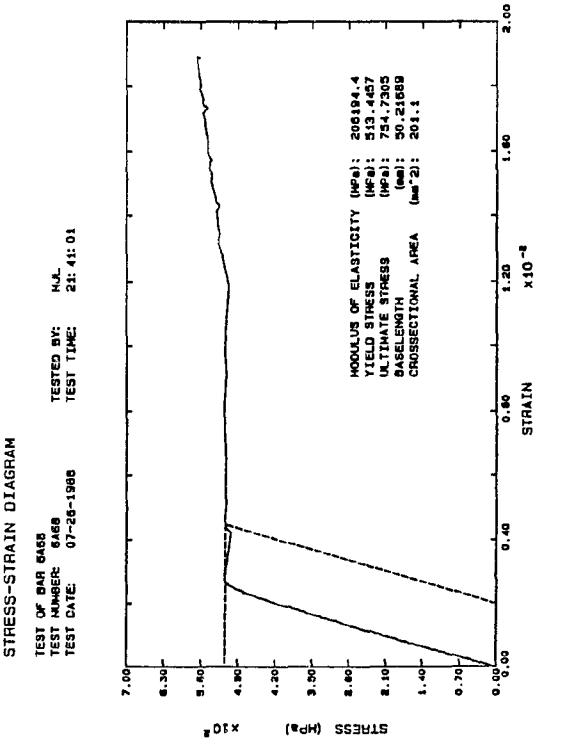

Fig. B.887: Column 6A & 6B

Stellenbosch University http://scholar.sun.ac.za

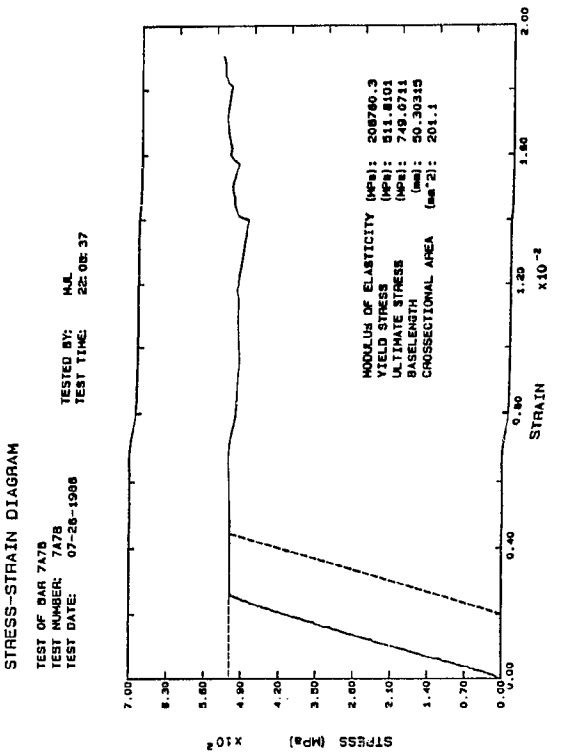

Fig.B.888: Column 7A & 7B

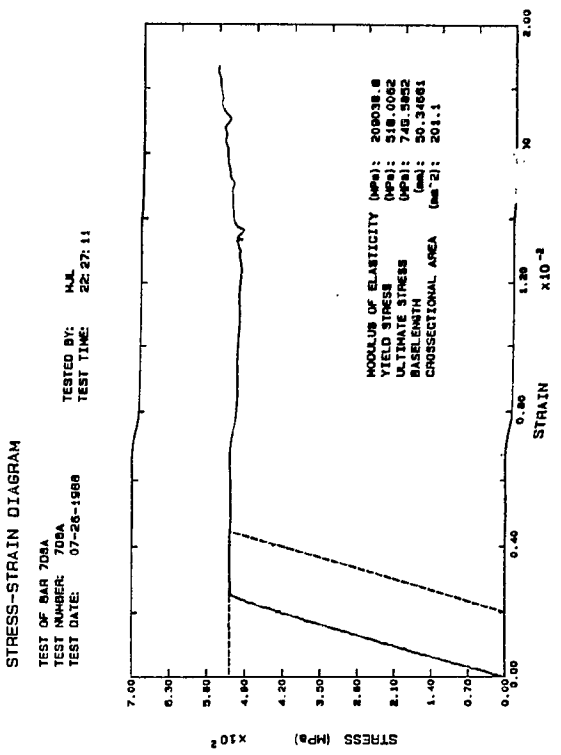

Fig.B.889: Column 7D & 8A

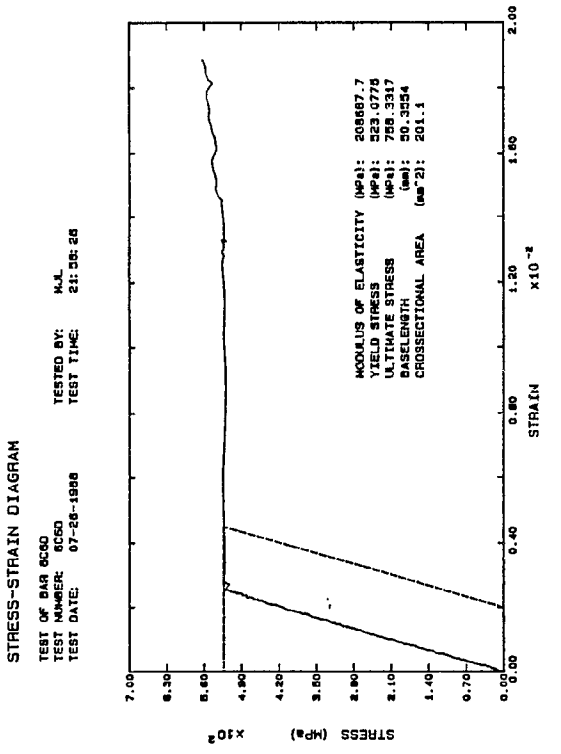

Fig.B.890: Column 6C & 6D

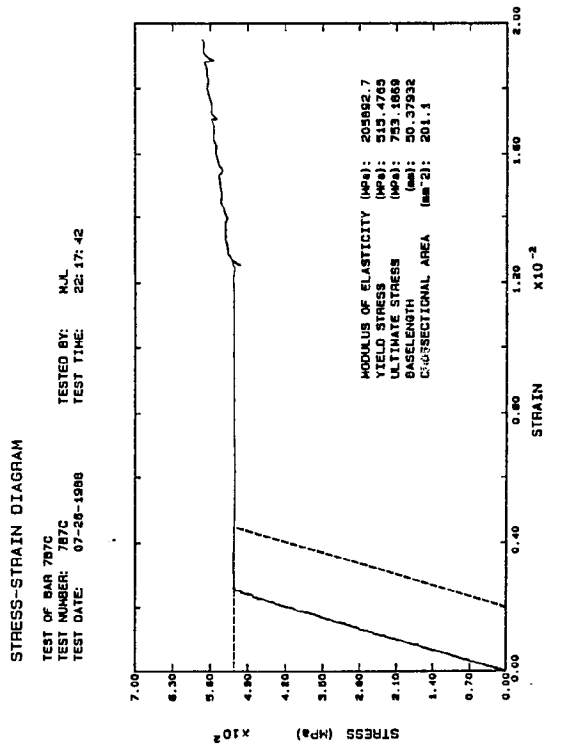

Fig. B.891: Column 7B & 7C

Stellenbosch University http://scholar.sun.ac.za

REBARS BAR No.	ELASTICITY MODULUS	YIELD	STRESS	ULTIMATE STRESS
8D	207663.4	0000	516.9304	759.3605
8C8D	207386.2	0000	518.5684	759.3605
8A8B	204465.5	0000	511.8476	754.2159
7D8A	209038.8	0000	518.0062	749.5852
7B7C	205892.7	0000	515.4765	753.1869
7A7B	208780.3	0000	511.8101	749.0711
6C6D	208687.7	0000	523.0775	758.3317
3E6C	208013.7	0640	513.4248	753.7012
6A6B	206194.4	0000	513.4457	754.7305
5C6A	208752.0	0000	521.2834	753.7012
5B5C	209438.8	0000	523.7778	758.8751
5A5B			523.4640	753.1868
4C4D			513.6448	752.6723
4B4E	204617.8	0000	512.3987	752.6723
1G4A	202584.7	0000	504.7276	749.0711
1G	208662.7	0000	523.1558	756.2735
3C	202564.3	0000	518.0475	759.8751
3B	207786.3	0000	514.6330	752.1576
3A	204449.7	0000	510.4981	752.6723
2E	206461.5	0000	520.7112	756.2735
1F	205324.5	0000	513.4063	757.3023
1E1F	208622.5	0000	521.5385	756.0164
2D1E	204714.4	0000	517.0424	757.0453
2D	207555.7	0000	516.8314	748.2993
2C	214575.0	0000	531.6781	771.4505
2B2C	207807.8	0000	523.9127	757.8170
2A2B	207314.7	0000	515.8249	752.6723
2A	205743.5	0000	519.9264	759.6176
1D	205773.7	0000	521.5209	755.7593
1C1D	205236.7	0000	518.7240	754.2159
1B1C	206994.8	0000	520.1418	752.6723
1A	207327.8	0000	520.3882	747.7847
1B	206565.8	0000	518.1350	758.8458
1AT	213926.2	0000	532.1828	777.1099
1AT1	201782.2	0000	515.3539	755.2446
1	212706.8	0000	532.4886	781.9870
AVERAGES	207220.3735		518.5562	756.4951

Fig.B.892: Summary of results for Y16-Bars.

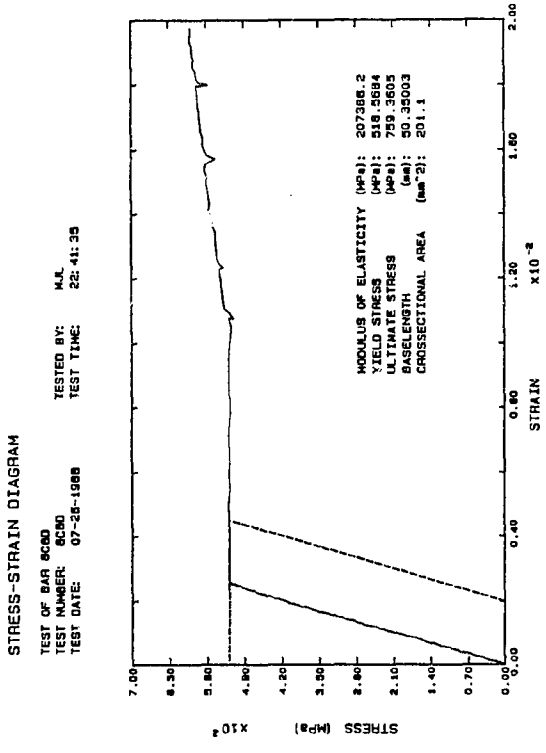

Fig.B.893: Column 8C & 8D

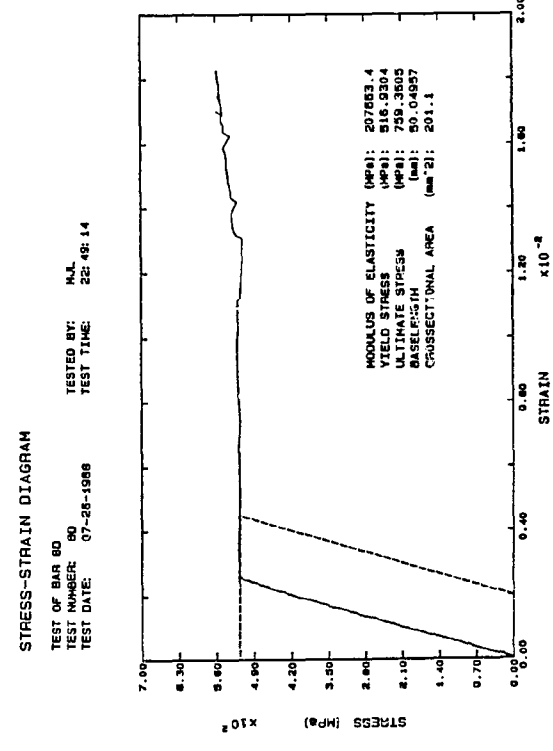

Fig. B.894: Column 8D

Stellenbosch University http://scholar.sun.ac.za

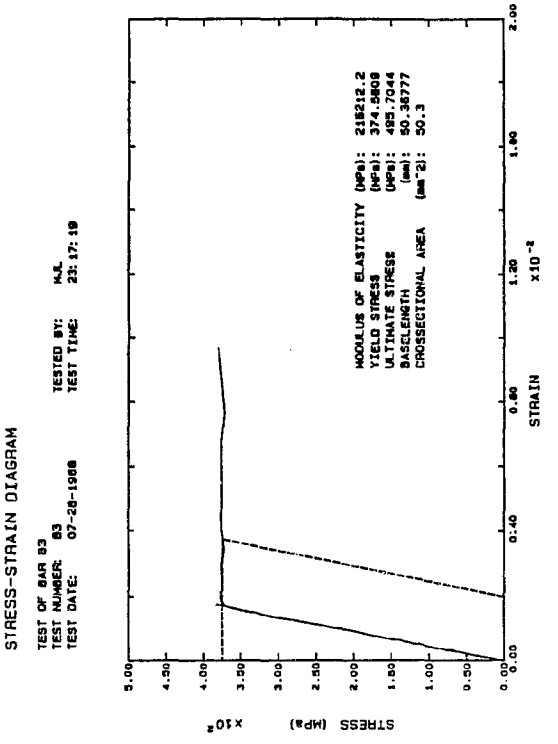

Fig.B.895: Sample B3

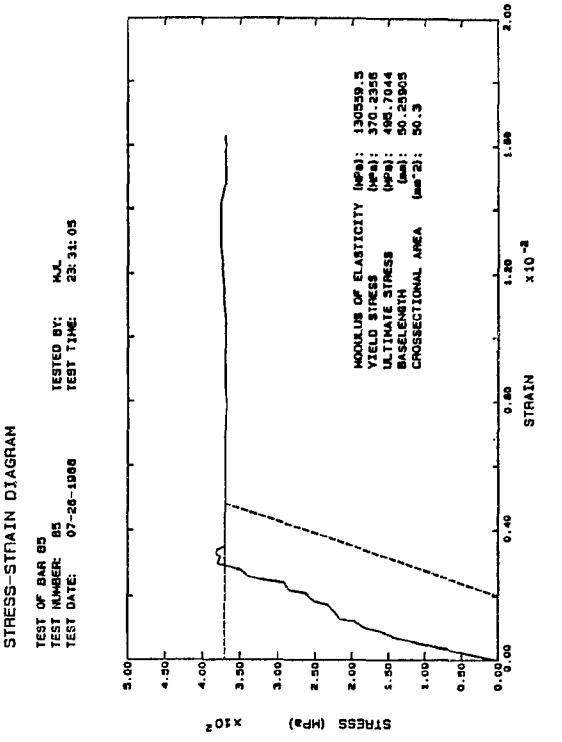

Fig.B.896: Sample B5

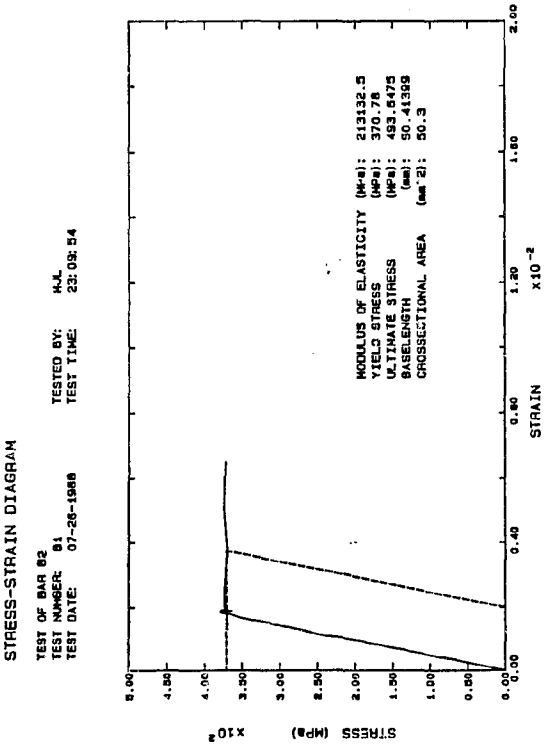

Fig.B.897: Sample B2

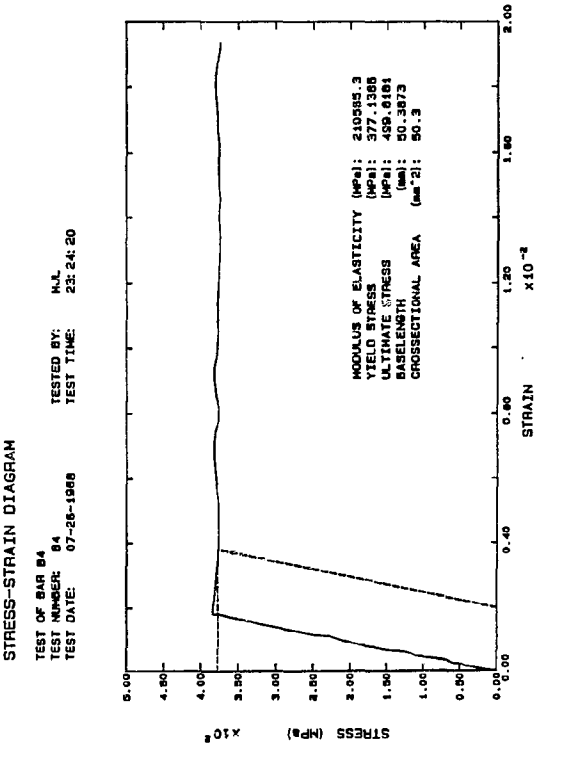

Fig. B.898: Sample B4

Stellenbosch University http://scholar.sun.ac.za

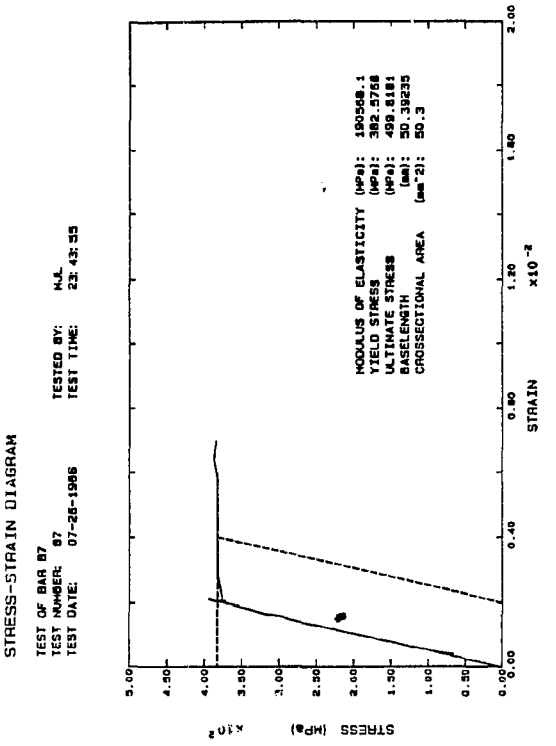

Fig.B.899: Sample B7

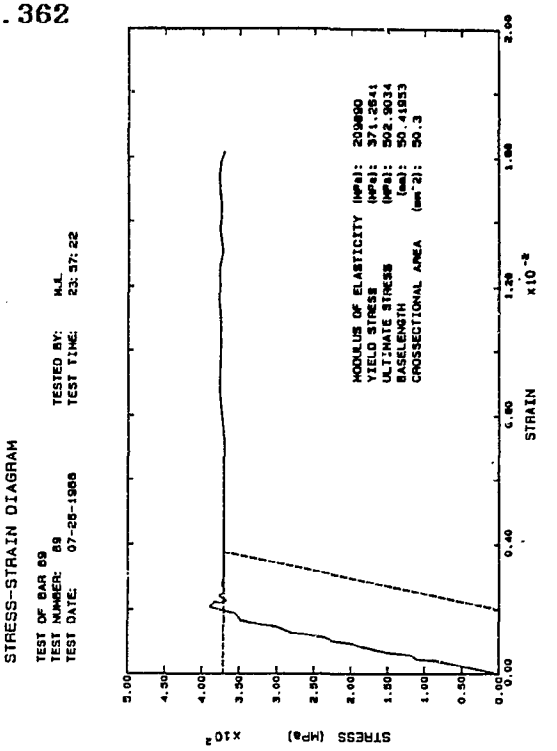

Fig.B.900: Sample B9

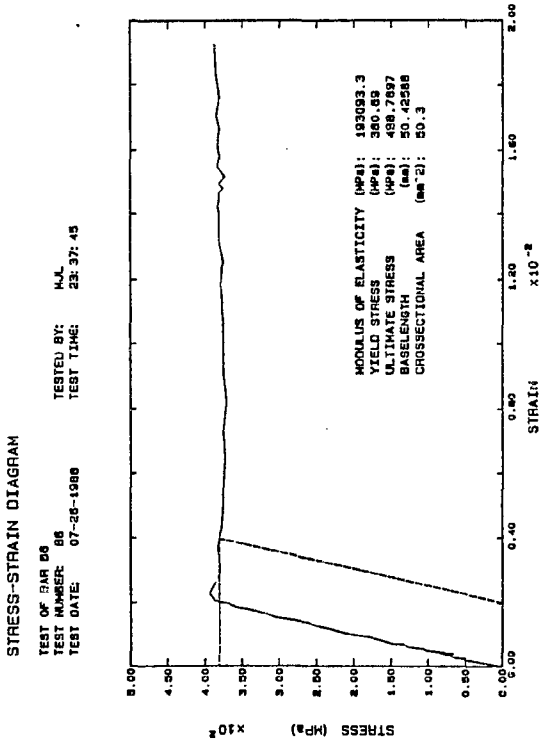

Fig.B.901: Sample B6

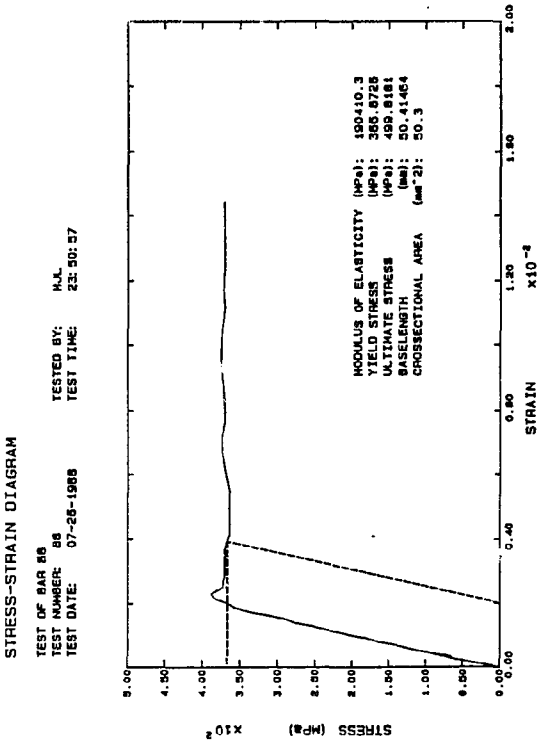

Fig. B.902: Sample B8

Stellenbosch University http://scholar.sun.ac.za

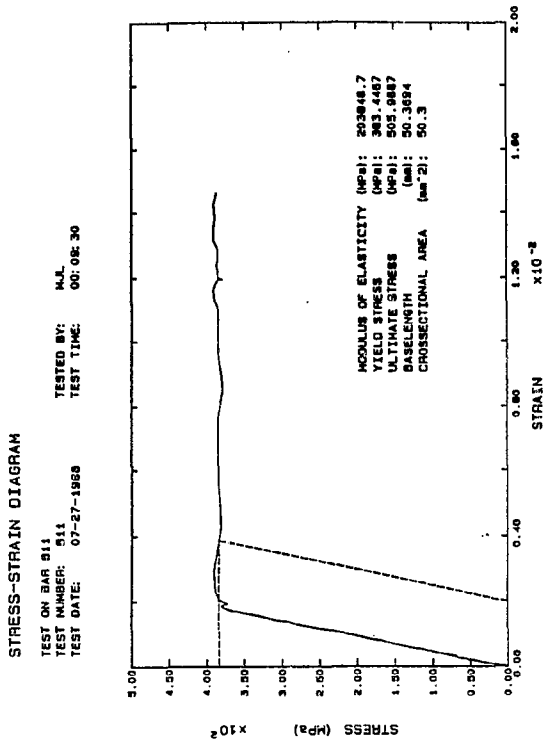

Fig.B.903: Sample B11

STIRRUPS

BAR No.	ELASTICITY MODULUS	YIELD STRESS	ULTIMATE STRESS
B12		382.4045	501.8750
B11	203848.7000	383.4467	505.9887
B10	196517.9000	378.3771	499.8181
B9	209890.0000	371.2641	502.9034
B8	190410.3000	366.8728	499.8181
B7	190568.1000	382.5768	499.8181
B6	193093.3000	380.8900	498.7897
B5		370.2356	495.7044
B4	210565.3000	377.1388	499.8181
B3	216212.2000	374.5809	495.7044
B2	213132.5000	370.7800	493.6475
AVERAGES	202693.1444	376.2334	499.4441

Fig.B.904: Summary of R8-Bars

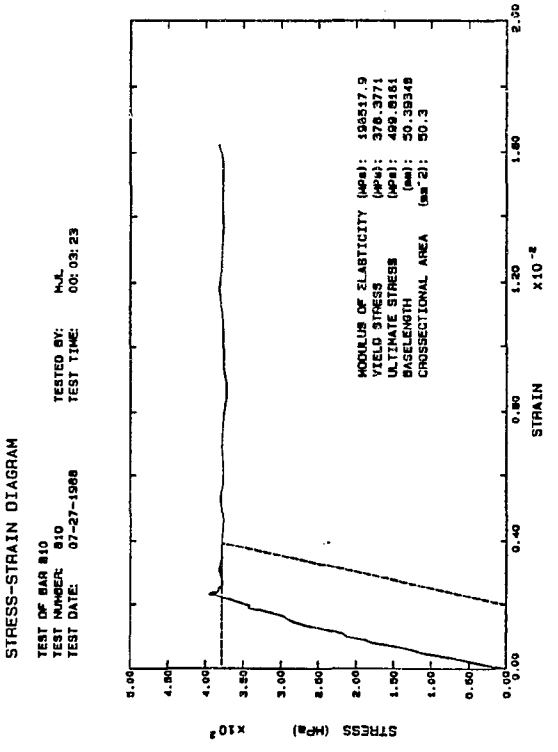

Fig.B.905: Sample B10

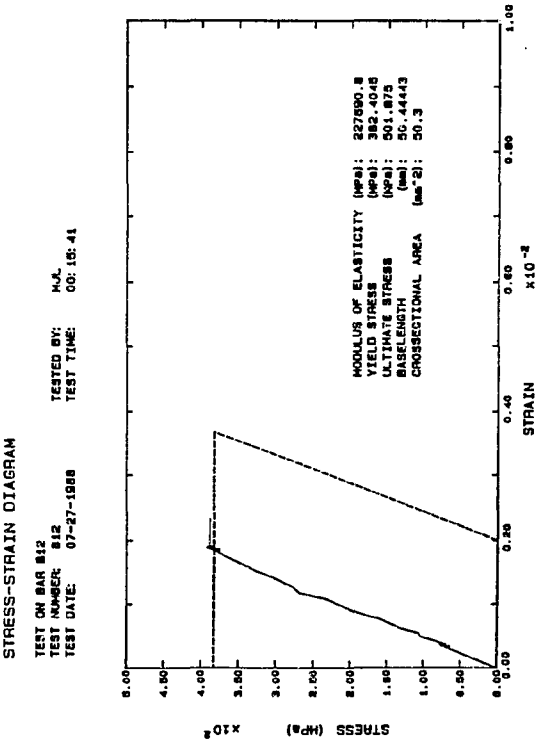

Fig. B.906: Sample B12

Stellenbosch University http://scholar.sun.ac.za

C. ENERGY ABSORPTION CHARACTERISTICS OF TUBES

The individual tubes in the energy absorbing system are assumed to be loaded as shown in Figure C.1, resulting in a collapsing mode that is assumed to be associated with the formation of four plastic hinges, 90° removed from one another. Applying the theorem of virtual work and equating the internal and external work done yields:

$$2P_c(R\alpha/2) = 4M_y\alpha \qquad (C.1)$$

Where: P_c = Small deflection static collapse load

R = Radius of tube

α = Virtual angle change

M_y = Yield moment

It follows that the collapse load is:

$$P_c = 4M_y/R \qquad (C.2)$$

But the yield moment at plastic collapse may be written as:

$$M_y = (\sigma_o W t^2)/4 \qquad (C.3)$$

Where: σ_o = Static yield stress

W = Depth of the tube

t = Thickness of the tube

This leads to:

$$P_c = (\sigma_o W t^2)/R \qquad (C.4)$$

Noting that the collapsing force increases to approximately $2P_c$ as the deformation of the ring increases, Perrone (123, 124), has proposed the force deflection curve shown in Figure C.1. The energy absorbed in the tube would then be:

$$\text{Energy} = 1,5\ P_c\ (2R) = 3\sigma_o W t^2 \qquad (C.5)$$

Stellenbosch University http://scholar.sun.ac.za

According to Carney and Sazinsky (21) this approximation of Perrone is overly conservative and a more accurate expression for the area under the load-deflection curve, equal to the energy absorbed, will take the form of:

$$\text{Energy} = 1,14(3\sigma_o Wt^2) = 3,42\sigma_o Wt^2 \qquad (C.6)$$

Equation (C.6) are valid only under static loading conditions. For the range of strains and strain rates that will be encountered in this application, Perrone suggested an overall rate sensitivity factor of 1,6. By replacing σ_o in equation (C.6) with $1,6\sigma_o$, the equivalent dynamic energy absorbed can be written as:

$$\text{Dynamic energy absorbed} = 5,47\sigma_o Wt^2 \qquad (C.7)$$

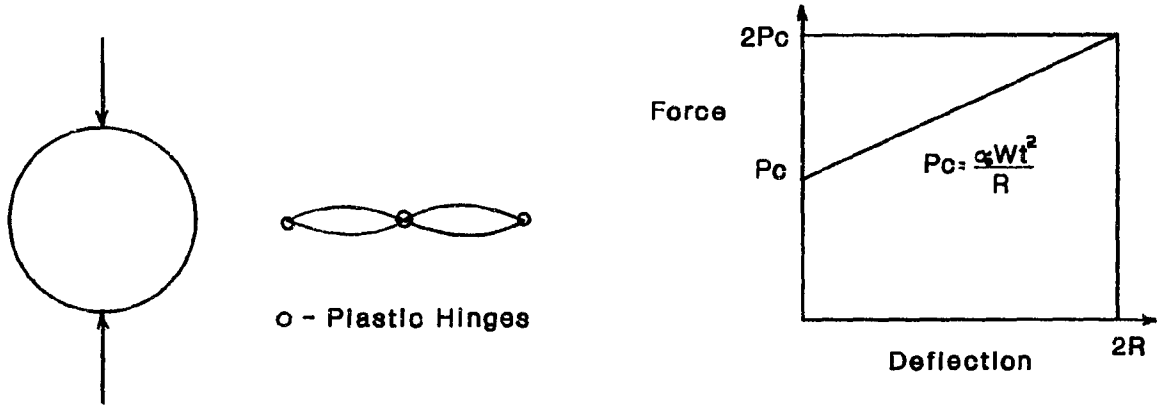

Figure C.3: Loaded tube and collapse pattern for a perfectly plastic material and an approximate force deflection curve for rings according to Perrone (123, 124).